

WOODHEAD PUBLISHING IN TEXTILES



Physical properties of textile fibres

Fourth edition

W. E. Morton and J. W. S. Hearle



The Textile Institute

WP

Physical properties of textile fibres

The Textile Institute and Woodhead Publishing

The Textile Institute is a unique organisation in textiles, clothing and footwear. Incorporated in England by a Royal Charter granted in 1925, the Institute has individual and corporate members in over 90 countries. The aim of the Institute is to facilitate learning, recognise achievement, reward excellence and disseminate information within the global textiles, clothing and footwear industries.

Historically, The Textile Institute has published books of interest to its members and the textile industry. To maintain this policy, the Institute has entered into partnership with Woodhead Publishing Limited to ensure that Institute members and the textile industry continue to have access to high calibre titles on textile science and technology.

Most Woodhead titles on textiles are now published in collaboration with The Textile Institute. Through this arrangement, the Institute provides an Editorial Board which advises Woodhead on appropriate titles for future publication and suggests possible editors and authors for these books. Each book published under this arrangement carries the Institute's logo.

Woodhead books published in collaboration with The Textile Institute are offered to Textile Institute members at a substantial discount. These books, together with those published by The Textile Institute that are still in print, are offered on the Woodhead web site at: www.woodheadpublishing.com. Textile Institute books still in print are also available directly from the Institute's web site at: www.textileinstitutebooks.com.

A list of Woodhead books on textile science and technology, most of which have been published in collaboration with The Textile Institute, can be found on pages xv-xix.

Woodhead Publishing in Textiles: Number 68

Physical properties of textile fibres

Fourth edition

W. E. Morton and J. W. S. Hearle

WPTF2005



The Textile Institute



CRC Press

Boca Raton Boston New York Washington, DC

WOODHEAD PUBLISHING LIMITED

Cambridge, England

Published by Woodhead Publishing Limited in association with The Textile Institute
 Woodhead Publishing Limited, Abington Hall, Granta Park,
 Great Abington, Cambridge CB21 6AH, England
www.woodheadpublishing.com

Published in North America by CRC Press LLC, 6000 Broken Sound Parkway, NW,
 Suite 300, Boca Raton, FL 33487, USA

First edition © The Textile Institute and Butterworth and Co. (Publishers) Ltd, 1962

Second edition © The Textile Institute, 1975

Third edition © The Textile Institute, 1993

Fourth edition published 2008, Woodhead Publishing Limited and CRC Press LLC

© Woodhead Publishing Limited, 2008

The authors have asserted their moral rights.

This book contains information obtained from authentic and highly regarded sources. Reprinted material is quoted with permission, and sources are indicated. Reasonable efforts have been made to publish reliable data and information, but the authors and the publishers cannot assume responsibility for the validity of all materials. Neither the authors nor the publishers, nor anyone else associated with this publication, shall be liable for any loss, damage or liability directly or indirectly caused or alleged to be caused by this book.

Neither this book nor any part may be reproduced or transmitted in any form or by any means, electronic or mechanical, including photocopying, microfilming and recording, or by any information storage or retrieval system, without permission in writing from Woodhead Publishing Limited.

The consent of Woodhead Publishing Limited does not extend to copying for general distribution, for promotion, for creating new works, or for resale. Specific permission must be obtained in writing from Woodhead Publishing Limited for such copying.

Trademark notice: Product or corporate names may be trademarks or registered trademarks, and are used only for identification and explanation, without intent to infringe.

British Library Cataloguing in Publication Data

A catalogue record for this book is available from the British Library.

Library of Congress Cataloging in Publication Data

A catalog record for this book is available from the Library of Congress.

Woodhead Publishing ISBN 978-1-84569-220-9 (book)

Woodhead Publishing ISBN 978-1-84569-442-5 (e-book)

CRC Press ISBN 978-1-4200-7958-6

CRC Press order number: WP7958

The publishers' policy is to use permanent paper from mills that operate a sustainable forestry policy, and which has been manufactured from pulp which is processed using acid-free and elementary chlorine-free practices. Furthermore, the publishers ensure that the text paper and cover board used have met acceptable environmental accreditation standards.

Project managed by Macfarlane Book Production Services, Dunstable, Bedfordshire, England
 (e-mail: macfarl@aol.com)

Typeset by Replika Press Pvt Ltd, India

Printed by TJ International Limited, Padstow, Cornwall, England

Contents

<i>Preface to the first edition</i>	<i>xi</i>
<i>Preface to the fourth edition</i>	<i>xiii</i>
<i>Woodhead Publishing in Textiles</i>	<i>xv</i>
1 An Introduction to fibre structure	1
1.1 General introduction	1
1.2 Methods of investigation of structure	4
1.3 Approaches to polymer fibre structure	21
1.4 Cellulose fibres	33
1.5 Regenerated and modified celluloses	43
1.6 Protein fibres	48
1.7 Synthetic fibres for general use	57
1.8 High-performance fibres	68
1.9 Specialist fibres	75
1.10 Some concluding views	77
1.11 References	78
2 Testing and sampling	82
2.1 Test procedures	82
2.2 Variability and sampling	83
2.3 Numerical and biased samples	86
2.4 Sampling techniques	90
2.5 Zoning	93
2.6 References	95
3 Fibre fineness and transverse dimensions	97
3.1 Fibre dimensions	97
3.2 Terms and definitions	99
3.3 The technical significance of fibre fineness	103
3.4 Variation in fineness	105
3.5 Measurement of linear density	107
3.6 Direct measurement of transverse dimensions	109

3.7	Optical technology for high-speed testing	111
3.8	Air-flow methods	115
3.9	The vibroscope method	122
3.10	Fibre shape and cotton maturity	123
3.11	References	131
4	Fibre length	134
4.1	Fibre lengths	134
4.2	Technical significance of fibre length	136
4.3	Length distributions and fibre diagrams	137
4.4	Wool and cotton	144
4.5	Crimp	146
4.6	Individual fibre length measurement	147
4.7	Comb-sorter methods	149
4.8	The Balls sledge sorter	152
4.9	Cutting-and-weighing methods	153
4.10	Automated scanning of fibre tufts	156
4.11	Scanning individual fibres	161
4.12	References	162
5	Fibre density	163
5.1	Introduction	163
5.2	Measurement	163
5.3	Results	165
5.4	Density and order	165
5.5	References	167
6	Thermal properties	168
6.1	Introduction	168
6.2	Thermal parameters	168
6.3	References	176
7	Equilibrium absorption of water	178
7.1	Introduction	178
7.2	Definitions	178
7.3	Measurement of regain	180
7.4	Relation between regain and relative humidity	184
7.5	References	193
8	Heats of sorption	195
8.1	Definitions	195
8.2	Measurement	196
8.3	Results	198
8.4	Effects of evolution of heat	201
8.5	References	201

9	Rate of absorption of moisture	202
9.1	Introduction	202
9.2	Diffusion of moisture	202
9.3	The interaction of moisture and heat	212
9.4	Practical effects	223
9.5	References	228
10	The retention of liquid water	229
10.1	Introduction	229
10.2	Centrifuging of wet fibres	229
10.3	Suction	232
10.4	Interactions	235
10.5	References	236
11	Swelling	237
11.1	Introduction	237
11.2	Measurement of swelling	238
11.3	Results	240
11.4	References	242
12	Theories of moisture sorption	243
12.1	The general view	243
12.2	Quantitative theories of absorption	251
12.3	The relations between absorption, swelling and elastic properties	261
12.4	Surface adsorption	270
12.5	The effect of temperature	271
12.6	References	272
13	Tensile properties	274
13.1	General introduction	274
13.2	Factors determining the results of tensile experiments	274
13.3	Expressing the results: quantities and units	276
13.4	Experimental methods	283
13.5	Fibre properties	289
13.6	Other factors	309
13.7	References	319
14	The effects of variability	322
14.1	Introduction	322
14.2	Variability, specimen length and strength	322
14.3	Variability and other quantities	330
14.4	Composite-specimen effects	332
14.5	Variability in practice	335
14.6	Changes in specimen during test	335
14.7	References	337

15	Elastic recovery	338
15.1	Introduction	338
15.2	Definitions	339
15.3	Experimental methods	340
15.4	Results	341
15.5	Change of properties as a result of straining: mechanical conditioning	346
15.6	Swelling recovery	348
15.7	Simple recovery models	349
15.8	References	356
16	Rheology	357
16.1	The study of time dependence	357
16.2	Creep	358
16.3	Stress relaxation	370
16.4	Time and tensile testing	376
16.5	Dynamic tests	390
16.6	References	411
17	Directional effects	414
17.1	Introduction	414
17.2	Bending of fibres	414
17.3	Twisting of fibres and the shear modulus	430
17.4	Shear strength	440
17.5	General elastic deformation	441
17.6	Compression stresses on fibre masses	455
17.7	References	455
18	Thermomechanical responses	458
18.1	Introduction	458
18.2	Melting	462
18.3	Dynamic mechanical responses	469
18.4	Transitions in keratin fibres	478
18.5	Thermomechanical responses	483
18.6	Setting	490
18.7	References	506
19	Fibre breakage and fatigue	509
19.1	Fibre-fracture morphology	509
19.2	Monotonic breaks	509
19.3	Tensile fatigue	525
19.4	Torsional fatigue	529
19.5	Flex fatigue	530
19.6	Combined bending and twisting: biaxial rotation	540
19.7	Surface wear and peeling	553

19.8	Abrasion and wear	554
19.9	References	557
20	Theories of mechanical properties	559
20.1	Introduction	559
20.2	Structural effects in rayon fibres	564
20.3	Nylon, polyester and similar fibres	574
20.4	High-performance fibres	580
20.5	A general theory of orientation	588
20.6	Structural effects in natural fibres	592
20.7	Theories of time dependence	604
20.8	Thermodynamic effects	618
20.9	References	622
21	Dielectric properties	625
21.1	General introduction	625
21.2	Definitions of dielectric properties	625
21.3	Measurement	628
21.4	The effect of frequency	631
21.5	The effect of moisture	634
21.6	The effect of temperature	635
21.7	The effect of other factors	638
21.8	Summary of results for various materials	640
21.9	References	642
22	Electrical resistance	643
22.1	Introduction	643
22.2	Definitions	643
22.3	Methods of measurement	644
22.4	Results of experiments	645
22.5	Theoretical	657
22.6	References	664
23	Static electricity	665
23.1	Introduction	665
23.2	Measurement of static	667
23.3	Results	669
23.4	Generation of charge	676
23.5	Leakage of charge	679
23.6	References	689
24	Optical properties	690
24.1	Introduction	690
24.2	Refraction	690
24.3	Absorption and dichroism	704

x	Contents	
24.4	Reflection and lustre	705
24.5	References	707
25	Fibre friction	709
25.1	Introduction	709
25.2	Measurement of fibre friction	710
25.3	Empirical results	716
25.4	The nature of friction	726
25.5	The friction of wool	732
25.6	References	736
	Appendix I: units	738
AI.1	Introduction	738
AI.2	Fineness	738
AI.3	Stress and specific stress	738
	Appendix II: fibre names	740
AII.1	Introduction	740
AII.2	Regenerated fibres	740
AII.3	Synthetic fibres of linear macromolecules	741
AII.4	High-modulus, high-tenacity (HM-HT) linear polymer fibres	741
AII.5	Carbon fibres	742
AII.6	Inorganic fibres	742
AII.7	Reference	742
	Appendix III: standard test methods	743

Preface to the first edition

Physics plays a large part in textile technology. But, while there are many applications to textile processing, these are diverse and cannot usefully be studied except as part of the technology of the processes themselves; however, the study of the structure and physical properties of fibres, yarns, and fabrics forms the unified subject that is legitimately called textile physics, and which is an essential part of the education of any textile technologist. The present book deals only with the fibre properties, augmented by an introductory chapter on fibre structure. While it was conceived as the first part of a trilogy, it remains to be seen whether it will be possible to write the companion volumes on yarns and fabrics.

This book is primarily a text book, based on our teaching experience, and intended for textile students in universities and colleges. While a full understanding of the whole of the text demands a wide knowledge of physics and mathematics, much of it is suitable for those who have not studied physics far beyond Ordinary G.C.E. level*. With this point in mind, the subject matter has been subdivided and arranged so that the more advanced theoretical treatments may be omitted without detriment to an understanding of the rest of the book.

We also hope that the book will prove useful to those preparing for the Associateship examinations of the Textile Institute; to graduates in science entering direct into the industry; and to the large body of technologists, already following a career in the industry, who wish to have available a survey of this particular part of textile technology.

We would like to emphasize that this book is not intended to be a comprehensive treatise, including a reference to every relevant research publication; on the contrary, our aim has been to provide a background of knowledge and understanding of the subject, much of which is unlikely to change radically with the passage of time, and which will therefore serve as a basis for more detailed study by reference to current literature.

We wish to take this opportunity of gratefully acknowledging the invaluable help that we have received from Miss Shirley Smith in the preparation of the illustrations; and from Professor R. Meredith, Mr. G. E. Cusick, and Dr. D. W. Saunders in reading and criticizing sections of the manuscript.

Manchester College of Science and Technology

W. E. M.

J. W. S. H.

* Now GCSE, a British school examination taken at age 15–16.

Preface to the fourth edition

It is 50 years since I started writing my contribution to the first edition of this book. By then, the ancient craft of manufacturing textiles from wool, cotton, flax and other natural fibres had been supplemented by 50 years of scientific research into their physical properties. Rayon had been around for 50 years and new synthetic fibres were entering the market. Nylon and polyester were expensive ‘miracle fibres’. Now polyester has replaced cotton as the cheap, general-purpose fibre. The high-performance fibres were not to come for another 20 years.

The 1960s saw the high-water mark of fibre research. Changes were rapid and a revised edition was needed in the 1970s. The third edition in 1993 was a reprint of the second edition with two extra chapters on ‘High Performance Fibres’ and ‘Flex Fatigue and other Forms of Failure’. A full revision was overdue. In this fourth edition, I have followed the approach described in the preface to the second edition.

We need to add little to our previous preface: the general character and aims of the book are unchanged, and the continuing demand shows that our approach has, as we hoped, stood the test of time. There is, indeed, a body of knowledge of fibre physical properties which is basic in the education of a textile technologist, and this is what we aim to present.

The changes in this edition result, in part, from a closer adherence to the essential character of the book: some of the details of theories and experimental techniques, which seemed important at the time, have been omitted [since then, developments in electronics and digital processing have transformed experimental methods]. The book is now more concentrated on the fundamentals of the subject; some digressions on topics less directly concerned with physical properties have been dropped.

The other source of change is new knowledge. When the first edition was published, ideas of fibre structure were in a state of disturbance and controversy, partly reflected in what we wrote. Now, it is possible to take a more stable view of the subject, and the first chapter contains substantial changes. Theories of mechanical properties, as related to structure, have also developed considerably in recent years. In experimental work, much has been published on time-dependent properties, though this has not radically changed the picture, and some valiant studies of the anisotropy of fibre mechanical properties have been made. However, the topic which has been most advanced is the study of thermal properties: this has

made it possible to write a much more useful and coherent account of experimental results, their interpretation, and their relation to the technology of heat-setting.

The general pattern of the book in this fourth edition is as it has been, but there has been some reorganisation. Partly this results from the increasing dominance of manufactured fibres. Fibre fineness is now a more important quality than fibre length. Thermomechanical responses and fibre failure now have their own chapters. High-performance fibres take their place through the book, instead of being Band-Aid at the end.

In the preface to the third edition, I wrote the following:

Since the second edition was published, my co-author, W.E. Morton, has died. During over forty years as a Professor of Textile Technology in Manchester, he did a great deal to advance the scientific study of fibres and textiles. He also gave great encouragement and help to those of us who joined him as young men on the staff or as research students. I remember with great affection his many kindnesses, not least by inviting me to join him in writing the first edition of this book 35 years ago.

After 60 years of research in fibres and textiles, I owe a debt to too many people to name. My introduction to textile fibres started in 1946 with the distinguished scientists at the Shirley Institute. Since then I have interacted with researchers in many universities, research institutes and industrial companies. Without them this book could not have been written. Finally, the writing and publication of this edition has been made much easier by the generous professional help of the staff of Woodhead Publishing and Macfarlane Book Production Services.

Mellor, Greater Manchester
John W. S. Hearle

Woodhead Publishing in Textiles

- 1 **Watson's textile design and colour (Seventh edition)**
Edited by Z. Grosicki
- 2 **Watson's advanced textile design**
Edited by Z. Grosicki
- 3 **Weaving (Second edition)**
P. R. Lord and M. H. Mohamed
- 4 **Handbook of textile fibres Vol 1: Natural fibres**
J. Gordon Cook
- 5 **Handbook of textile fibres Vol 2: Man-made fibres**
J. Gordon Cook
- 6 **Recycling textile and plastic waste**
Edited by A. R. Horrocks
- 7 **New fibers (Second edition)**
T. Hongu and G. O. Phillips
- 8 **Atlas of fibre fracture and damage to textiles (Second edition)**
J. W. S. Hearle, B. Lomas and W. D. Cooke
- 9 **Ecotextile '98**
Edited by A. R. Horrocks
- 10 **Physical testing of textiles**
B. P. Saville
- 11 **Geometric symmetry in patterns and tilings**
C. E. Horne
- 12 **Handbook of technical textiles**
Edited by A. R. Horrocks and S. C. Anand
- 13 **Textiles in automotive engineering**
W. Fung and J. M. Hardcastle
- 14 **Handbook of textile design**
J. Wilson

- 15 **High-performance fibres**
Edited by J. W. S. Hearle
- 16 **Knitting technology (Third edition)**
D. J. Spencer
- 17 **Medical textiles**
Edited by S. C. Anand
- 18 **Regenerated cellulose fibres**
Edited by C. Woodings
- 19 **Silk, mohair, cashmere and other luxury fibres**
Edited by R. R. Franck
- 20 **Smart fibres, fabrics and clothing**
Edited by X. M. Tao
- 21 **Yarn texturing technology**
J. W. S. Hearle, L. Hollick and D. K. Wilson
- 22 **Encyclopedia of textile finishing**
H-K. Rouette
- 23 **Coated and laminated textiles**
W. Fung
- 24 **Fancy yarns**
R. H. Gong and R. M. Wright
- 25 **Wool: Science and technology**
Edited by W. S. Simpson and G. Crawshaw
- 26 **Dictionary of textile finishing**
H-K. Rouette
- 27 **Environmental impact of textiles**
K. Slater
- 28 **Handbook of yarn production**
P. R. Lord
- 29 **Textile processing with enzymes**
Edited by A. Cavaco-Paulo and G. Gübitz
- 30 **The China and Hong Kong denim industry**
Y. Li, L. Yao and K. W. Yeung
- 31 **The World Trade Organization and international denim trading**
Y. Li, Y. Shen, L. Yao and E. Newton
- 32 **Chemical finishing of textiles**
W. D. Schindler and P. J. Hauser

- 33 **Clothing appearance and fit**
J. Fan, W. Yu and L. Hunter
- 34 **Handbook of fibre rope technology**
H. A. McKenna, J. W. S. Hearle and N. O'Hear
- 35 **Structure and mechanics of woven fabrics**
J. Hu
- 36 **Synthetic fibres: nylon, polyester, acrylic, polyolefin**
Edited by J. E. McIntyre
- 37 **Woollen and worsted woven fabric design**
E. G. Gilligan
- 38 **Analytical electrochemistry in textiles**
P. Westbroek, G. Priniotakis and P. Kiekens
- 39 **Bast and other plant fibres**
R. R. Franck
- 40 **Chemical testing of textiles**
Edited by Q. Fan
- 41 **Design and manufacture of textile composites**
Edited by A. C. Long
- 42 **Effect of mechanical and physical properties on fabric hand**
Edited by Hassan M. Behery
- 43 **New millennium fibers**
T. Hongu, M. Takigami and G. O. Phillips
- 44 **Textiles for protection**
Edited by R. A. Scott
- 45 **Textiles in sport**
Edited by R. Shishoo
- 46 **Wearable electronics and photonics**
Edited by X. M. Tao
- 47 **Biodegradable and sustainable fibres**
Edited by R. S. Blackburn
- 48 **Medical textiles and biomaterials for healthcare**
Edited by S. C. Anand, M. MirafTAB, S. Rajendran and J. F. Kennedy
- 49 **Total colour management in textiles**
Edited by J. Xin
- 50 **Recycling in textiles**
Edited by Y. Wang

- 51 **Clothing biosensory engineering**
Y. Li and A. S. W. Wong
- 52 **Biomechanical engineering of textiles and clothing**
Edited by Y. Li and D. X-Q. Dai
- 53 **Digital printing of textiles**
Edited by H. Ujiie
- 54 **Intelligent textiles and clothing**
Edited by H. Mattila
- 55 **Innovation and technology of women's intimate apparel**
W. Yu, J. Fan, S. C. Harlock and S. P. Ng
- 56 **Thermal and moisture transport in fibrous materials**
Edited by N. Pan and P. Gibson
- 57 **Geosynthetics in civil engineering**
Edited by R. W. Sarsby
- 58 **Handbook of nonwovens**
Edited by S. Russell
- 59 **Cotton: Science and technology**
Edited by S. Gordon and Y-L. Hsieh
- 60 **Ecotextiles**
Edited by M. MirafTAB and A. Horrocks
- 61 **Composite forming technologies**
Edited by A. C. Long
- 62 **Plasma technology for textiles**
Edited by R. Shishoo
- 63 **Smart textiles for medicine and healthcare**
Edited by L. Van Langenhove
- 64 **Sizing in clothing**
Edited by S. Ashdown
- 65 **Shape memory polymers and textiles**
J. Hu
- 66 **Environmental aspects of textile dyeing**
R. Christie
- 67 **Nanofibers and nanotechnology in textiles**
Edited by P. Brown and K. Stevens
- 68 **Physical properties of textile fibres Fourth edition**
W. E. Morton and J. W. S. Hearle
- 69 **Advances in apparel production**
Edited by C. Fairhurst

- 70 **Advances in fire retardant materials**
Edited by A. R. Horrocks and D. Price
- 71 **Polyesters and polyamides**
Edited by B. L. Deopora, R. Alagirusamy, M. Joshi and B. S. Gupta
- 72 **Advances in wool technology**
Edited by N. A. G. Johnson and I. Russell
- 73 **Military textiles**
Edited by E. Wilusz
- 74 **3-D fibrous assemblies: Properties, applications and modelling of three-dimensional textile structures**
J. Hu
- 75 **Medical textiles 2007**
Edited by J. Kennedy, A. Anand, M. MirafTAB and S. Rajendran
- 76 **Fabric testing**
Edited by J. Hu
- 77 **Biologically inspired textiles**
Edited by A. Abbott and M. Ellison
- 78 **Friction in textiles**
Edited by B .S. Gupta
- 79 **Textile advances in the automotive industry**
Edited by R. Shishoo
- 80 **Structure and mechanics of textile fibre assemblies**
Edited by P. Schwartz
- 81 **Engineering textiles: Integrating the design and manufacture of textile products**
Edited by Y. E. El-Mogahzy
- 82 **Polyolefin fibres: industrial and medical applications**
Edited by S. C. O. UgboLue
- 83 **Smart clothes and wearable technology**
Edited by J. McCann and D. Bryson
- 84 **Identification of textile fibres**
Edited by M. Houck
- 85 **Advanced textiles for wound care**
Edited by S. Rajendran
- 86 **Fatigue failure of textile fibres**
Edited by M. MirafTAB
- 87 **Advances in carpet technology**
Edited by K. Goswami

1.1 General introduction

1.1.1 The nature of matter

Fibre physics is the study of the structure and physical properties of fibres. These two aspects are not, however, independent: the properties must be explained by the structure, which they also help to elucidate. Because of this connection, it is appropriate to start this book on the physical properties of fibres with a review of what is known about their structure. There is much detail, only partly superseded by more recent work, in the book edited by Hearle and Peters [1] and the review by Hearle and Greer [2]. Other information is in the general references given at the end of the chapter.

Matter is composed of atoms linked together by bonds of varying strength. It is the arrangement of these atoms and the strength of the bonds between them that determine the physical properties of materials. Thus with light atoms, such as those of helium, attracted to one another by very weak forces, the energy of the atoms is sufficient (except at very low temperatures) to cause them to move about independently, and the material is a gas. The material will also be a gas (though with a higher liquefaction point) if it is made up of heavier atoms, or of molecules composed of two or three atoms held together by strong forces (valency bonds), provided that the forces between the individual molecules are weak. These weak forces are often called van der Waals forces, since they are the cause of one of the deviations of a real gas from an ideal gas, which were considered by van der Waals in his modification of the gas laws. If the molecules are heavy enough, and the attractive forces strong enough, then the atoms will not have sufficient energy at room temperature to move freely away from one another, and the substance will be a liquid or a solid.

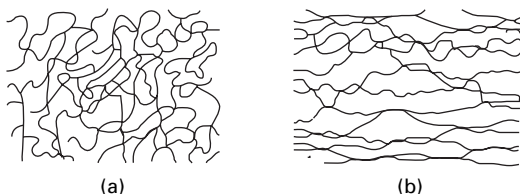
Some materials are made up of giant molecules. For example, in a crystal of diamond, all the atoms are linked to one another by valency bonds in a regular three-dimensional network. This gives a very hard, non-fusible material. In graphite, which is also pure carbon, the atoms are linked only in single planes by valency bonds; the forces between the planes are weak, so the material is one that easily splits up into sheets, and these will slide over one another, giving a lubricating action. In linear polymers, the linking is in only one dimension. If there is flexibility in the main-chain covalent bonds and only weak bonding between the long-chain molecules, there is nothing to prevent thermal energy from causing the chains to take up a

disordered, random, tangled arrangement, as suggested in Fig. 1.1(a). When the material is tensioned, the molecules straighten out, giving a large extension, Fig. 1.1(b). This extension is reversible, since on releasing the tension the molecules return to the random tangle. This is the rubbery state, though some crosslinks are introduced in vulcanisation to give cohesion to the material. At lower temperatures or with stronger bonding, such an amorphous polymer material is a glassy plastic. Other linear polymers can crystallise into regular lattices to give plastics such as polyethylene of intermediate stiffness. From these examples, we see that the characteristics of matter are determined by its molecular arrangement.

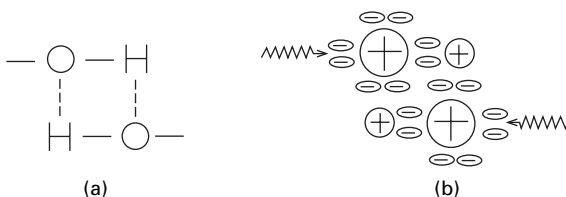
1.1.2 Intermediate bonds: hydrogen bonding

In addition to the ordinary covalent bonds that link atoms in a molecule and the usual weak van der Waals interactions between molecules, there is another class of bonds of intermediate strength, which are very important in influencing fibre properties. The best-known example is the hydrogen bond, which forms between hydroxyl (—OH) groups. Figure 1.2(a) gives a schematic representation of this bond, and Fig. 1.2(b) illustrates, in a very inexact manner, the way in which it might arise by a sharing of electrons from the outer rings of the hydrogen and oxygen atoms.

Water illustrates the importance of hydrogen bonding, both in its own properties and in its occurrence as the commonest ‘fibre plasticiser’. Below 0°C , the hydrogen bonds are strong enough to hold the water molecules together as a crystalline solid, although the mass of the molecules is less than that of many substances (propane, butane, hydrogen sulphide, chlorine, nitrogen, oxygen, to name but a few) that are gases at this temperature. At atmospheric pressure, between 0 and 100°C , water is a liquid of limited volume in equilibrium with water vapour. The water molecules are



1.1 (a) Disordered arrangement of long-chain molecules in rubber. (b) Oriented arrangement of molecules in stretched rubber.



1.2 Two schematic representations of a hydrogen bond: (a) bonding; (b) electron arrangement in outer rings.

in a mobile dynamic equilibrium, with hydrogen bonds continually breaking and re-forming. Above 100 °C (at atmospheric pressure), all the molecules disperse into a gas. At ordinary temperatures, therefore, hydrogen bonds are in a very sensitive state: they are on the verge of breaking and thus are easily affected by changes of temperature, by applied stresses and by chemical and structural changes. Deliberately or inevitably, this results in considerable effects in some fibre materials, such as cellulose and nylon. This affects fibre behaviour, processing and usage; the fibre molecules under various conditions may be held rigidly together, be free to move in a dynamic equilibrium or be completely free of one another, except for chain entanglements.

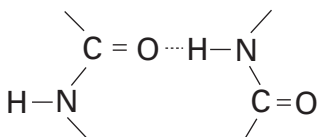
Hydrogen bonds can also form, as illustrated in Fig. 1.3, between —CO·NH— groups, which are found in polyamide and protein fibres.

In some fibres, there may be other bonds of intermediate strength. Thus, in the acrylic fibres, the asymmetry of electron arrangement in the —C≡N group, illustrated in Fig. 1.4, results in a moderately strong electrical interaction. In polyester fibres, and others based on aromatic polymers, there is an interaction between benzene rings.

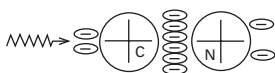
1.1.3 The nature of fibres

Fibres have been defined by the Textile Institute [3] as units of matter characterised by flexibility, fineness and a high ratio of length to thickness. To these characteristics might be added, if the fibre is to be of any use for general textile purposes, a sufficiently high temperature stability and a certain minimum strength and moderate extensibility.

The characteristic dimensions of fibres are the basis of their use and need to be stressed: individual fibres (or elements of a continuous filament) weigh only a few micrograms, and their length/width ratio is at least 1000:1, so that a single cotton fibre scaled up to be as thick as a thumb would be 100 m long. In addition to the need to be made of materials that can be produced in this special form with adequate stability for use, ordinary textile fibres must be, at least partly, elastic up to breaking extensions between 5 and 50%. This is an unusual intermediate range of extensibility, since glasses and crystalline solids are less extensible, whereas rubbers are much more extensible. The materials that meet these needs are almost all partially oriented,



1.3 Schematic indication of hydrogen bonds between —CO · NH— groups.



1.4 Electric dipoles in the acrylonitrile side group.

partially crystalline, linear polymers. A remarkable fact is that almost all the general textile fibre market is met by six polymer types: the natural polymers, *cellulose* and *proteins*, and the synthetic (manufactured) polymers, *polyamide*, *polyester*, *polyolefin* and *vinyl* (including acrylic).

The above comments relate to fibres for the traditional textile uses. More recently, a second generation of high-performance fibres has been introduced for functional applications. They have high strength and low extensibility. Some of these are linear polymer fibres. Others are inorganic networks, which, provided that they are fine enough, have the necessary flexibility. Glass and asbestos (which is no longer used because it is a health hazard) are the two older fibres in this group. At the other extreme, elastomeric fibres are used where a high stretch is specially needed.

There are other sorts of fibres, which fall outside the main theme of the book. There are fibres in living organisms, of interest to biologists: these include wood fibres, used in paper but too short for textiles, and a variety of connective tissues. Of commercial interest, there are fibres with special properties for particular uses. Metal fibres may be used for decorative purposes or for special purposes, such as reducing static electricity. Other fibres are used medically, for example to assist wound-healing. Finally, there are 'smart fibres', which can be used as transducers or change with the environment.

1.2 Methods of investigation of structure

1.2.1 Sources of evidence

The elucidation of fibre structure has been based on many sources of information, which include:

- the chemistry of the fibre material – its preparation, composition, molecular formula and reactions;
- the absorption of infrared radiation;
- Raman scattering of light;
- optical and X-ray diffraction studies;
- optical microscopy;
- electron microscopy and electron diffraction;
- nuclear magnetic resonance;
- optical properties;
- thermal analysis;
- density;
- general physical properties.

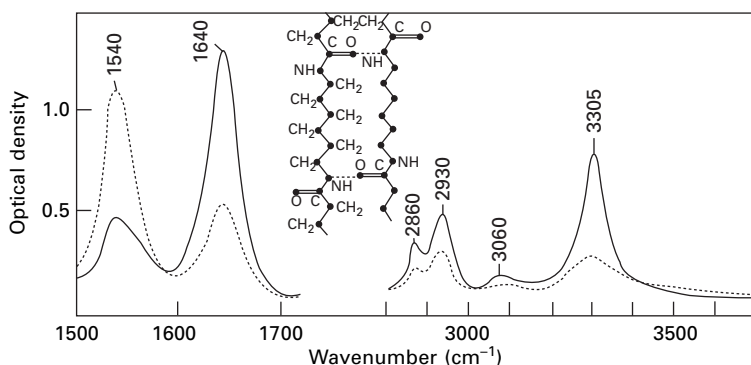
Of these, the chemistry is a subject of its own, of which the results will be assumed here; the optical, thermal, density and general physical properties are the subject of the remaining chapters of this book; and optical microscopy is a subject of which the general principles are well known and the techniques are covered in specialised textbooks. The remaining sources are specialised techniques, which it may be useful to describe briefly here.

A general comment should first be made. All the techniques are subject to errors and artefacts, and a direct unambiguous interpretation of experimental results is rarely possible. Indeed, there is a danger of a vicious circle: detailed calculations based on a particular model of structure may unjustifiably be taken as evidence in support of the model. Views on fibre structure have therefore to be built up from a collection of largely circumstantial, possibly unreliable, evidence. Unfortunately, no individual is an expert in evaluating all the techniques; and it is easy to place most reliance on the stated results of techniques with which one is less familiar and so less aware of the difficulties of interpretation. However, despite these difficulties, there is a general consensus on many aspects of fibre structure.

1.2.2 Absorption of infrared radiation and Raman scattering

When electromagnetic waves interact with matter, they are scattered and absorbed. In infrared spectroscopy, radiation with wavelengths between 1 and 15 μm is absorbed at certain characteristic frequencies, which yield structural information. Elastic scattering does not give molecular information, though light scattering does give larger-scale information. Raman spectroscopy results from the few photons that are inelastically scattered.

By using an infrared spectrometer, the variation in absorption can be found and plotted against wavelength, or, more commonly, its reciprocal, the wavenumber. This is illustrated in Fig. 1.5, which is the absorption spectrum of nylon. The peaks occur where the frequency of the electromagnetic waves corresponds with the natural frequency of vibration between two atoms in the material. If these are associated with



The peaks are due to:

3305 cm^{-1} stretching of N—H

2930 and 2860 cm^{-1} stretching of $\text{C}-\text{H}$

1640 cm^{-1} stretching of C=O

1540 cm^{-1} uncertain, involves —NH and neighbouring bonds

1.5 Infrared absorption spectrum of nylon: Full-line: electric vector perpendicular to fibre axis. Broken line: electric vector parallel to fibre axis. Inset: Crystal structure of nylon 6.6 (Bunn and Garner [5]). (After Bamford, *et al.* [4]).

an electric dipole, then the variations in the electric field set up the vibration, and energy is absorbed from the radiation. The fundamental oscillations occur at wavenumbers less than 4000 cm^{-1} . These give strong absorptions and so can be studied only in very thin films or fibres. At higher wavenumbers, nearer optical frequencies, absorptions will occur that are due to harmonics of the fundamental frequencies. The absorption spectrum in this range is more complex and less used, but, since the absorptions are weaker, thicker specimens, such as fibre bundles, can be studied.

The wavenumber at which absorption takes place depends primarily on the nature of the two atoms and of the bond between them. Thus there will be absorption frequencies characteristic of such groupings as >C—H , >C=O , >C—O— , —O—H , >N—H , >C—C< , >C=C< and so on. To a smaller extent, the absorption frequency is influenced by the other groups in the neighbourhood: for example, the absorption frequency for a carbon–hydrogen bond in a terminal group, —CH_3 , is different from that for the same bond in a chain, $\text{—CH}_2\text{—}$.

The first use of infrared absorption is therefore as an aid to the identification of the presence of certain groups in the molecule, leading to the determination of its chemical formula. The method can also be used in routine analysis to identify and estimate quantitatively the presence of given substances, even in small quantities in a mixture, by observation of their characteristic spectrum. For instance, it can be used to determine the amount of water in fibres.

Other structural information can also be obtained. If the infrared radiation is polarised, then the oscillation of the atoms will vary from a maximum for one orientation to a minimum for an orientation at right angles. The variation in the absorption spectrum with the direction of polarisation can therefore be used to investigate the degree of orientation of the molecules in a fibre. For example, in nylon, the >N—H , >CH_2 and >C=O absorption bands all show weak absorption when the vibration direction of the electric vector is along the molecular chain and strong absorption when it is vibrating perpendicular to the chain axis. The curves in Fig. 1.5 demonstrate the high molecular orientation of drawn nylon.

In addition to determining the degree of orientation of the molecules as a whole, polarised infrared may also be used to find the direction in which a particular group points in a molecule of unknown form. For example, two different forms, α and β , of the synthetic polypeptide poly-L-alanine show a difference. It is deduced that the >C=O and >N—H bonds move from a transverse direction between molecules in β towards a direction parallel to the chain axis between coils within α molecules. This is useful in determining the molecular configuration in polypeptides and proteins (see Section 1.6.3).

An advantage of the infrared absorption method is that it is influenced by all the molecules in the fibre, in both the crystalline and non-crystalline regions, whereas the X-ray diffraction method gives detailed information only about the crystalline regions of the fibre. For example, the infrared spectrum gives evidence of the presence of α - and β -forms of protein molecules in the non-crystalline regions of protein fibres.

In some materials, owing to the influence of the surroundings, an absorption will occur in the crystalline regions but not in the non-crystalline regions. Polyethylene, for example, shows a strong double peak at 725 cm^{-1} . In shorter-chain paraffin hydrocarbons, this double peak is found in the solid (crystalline) state, but only one component is present in the liquid (non-crystalline) state. The presence of a doublet is thus evidence of crystalline material. From an examination of the relative magnitudes of the two peaks, the proportion of crystalline material can be estimated. Furthermore, by using polarised infrared, the orientation in the two regions could be separately determined.

In a similar way, Sandeman and Keller [6] have found absorption bands in the infrared spectrum of nylon that are characteristic of crystalline order, and these may be used to determine the degree of crystallinity. Other bands are characteristic of chain folds [7].

One special technique that may be useful is the exposure of a material to the vapour of heavy water, D_2O . This may lead to the replacement of hydrogen atoms in the material by deuterium atoms, which can be detected by the change in the infrared absorption, consequent on the greater weight of the deuterium atom. This technique has been applied to viscose rayon and other forms of cellulose [8], in which the —OH groups in the cellulose molecule are replaced by —OD groups. Only the non-crystalline regions are accessible to the heavy water, and consequently the infrared absorption spectra of the hydroxyl groups in the crystalline and non-crystalline regions are separated and can be studied independently.

In Raman spectroscopy, the incidence of the photons shifts electrons from one state to another. The energy of the change comes from the photon. Consequently the scattered photon has a different energy and hence a different frequency. The effects are manifested in the visible region. Broadly speaking, Raman spectra are influenced by material structure in a way similar to that described for infrared absorption spectra, but the greater complication of the interaction yields more directional information. Raman spectroscopy has become a powerful tool for investigating fibre structure as a result of the development of Raman microscopes. With a spot size less than a fibre diameter, spectra can be obtained from single fibres. If the fibre is mounted on an extension stage in the microscope, it is possible to observe the shift in the spectral lines with fibre extension [9]. In this way it is possible to show which parts of the structure are changing. An account of the use of Raman spectroscopy in various ways in the study of aramid, polyester and carbon fibres is given by Young [10].

1.2.3 Optical and X-ray diffraction studies

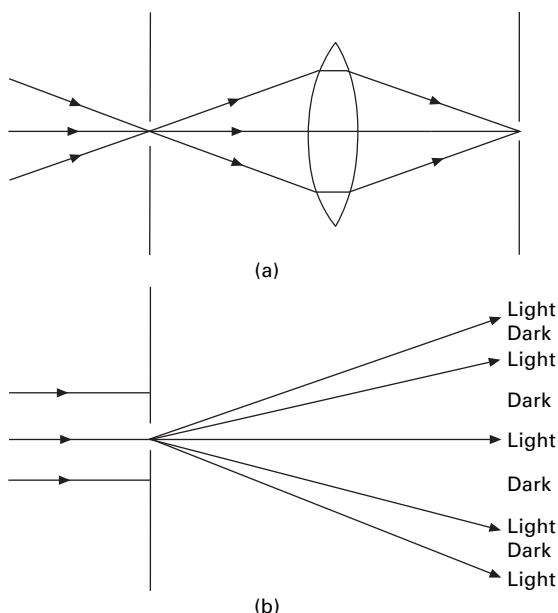
Diffraction may be viewed as a problem in information theory. For example, when a beam of light is passed through a photographic slide, the light is scattered in many directions. By using a lens in the right place, we can recombine this scattered information about the picture into an image on a screen. But the information is there before it is recombined, and diffraction is the science of understanding and using this information in all sorts of ways. Image formation is thus merely one branch of diffraction in its most general sense, and there are many circumstances in which images cannot be

formed or are not the most useful means of obtaining the required information about the object.

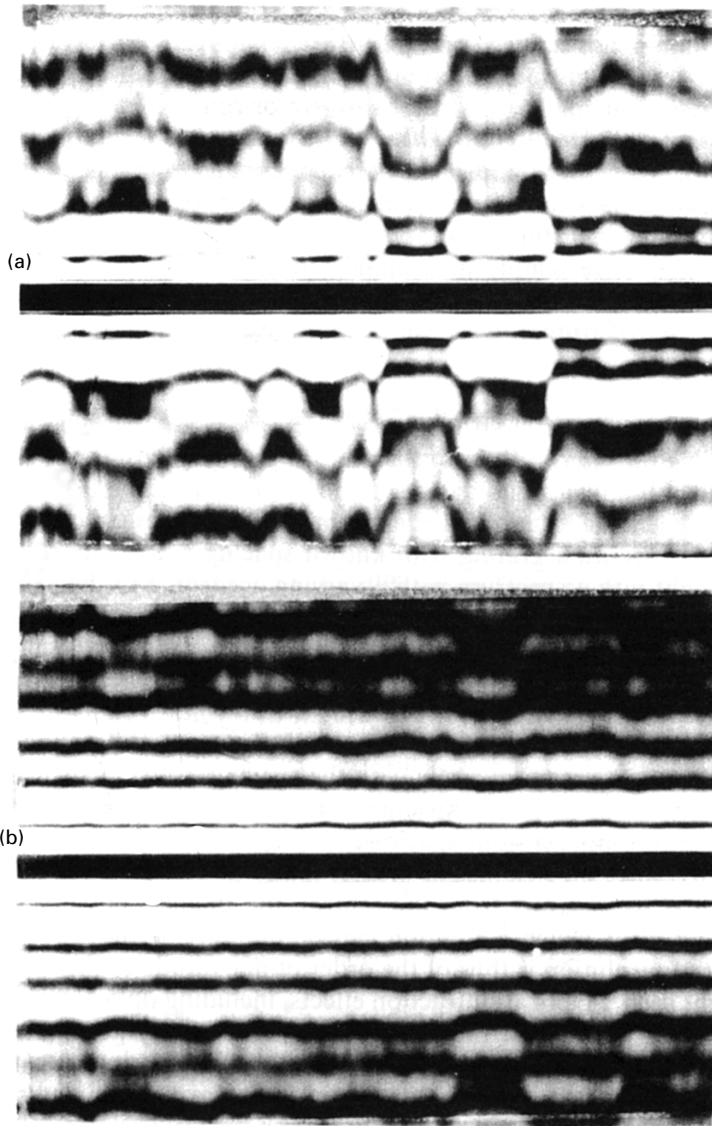
In a narrower sense, diffraction is the study of the particular patterns that may be found when waves pass through or round objects (or holes) of particular shape. For example, there is a characteristic diffraction pattern from a single slit. The difference between the image that must be focused at a particular place and the angular diffraction pattern that can be intercepted anywhere is shown in Fig. 1.6.

An example of the use of optical diffraction in fibre physics is shown in Fig. 1.7 taken from work by Lynch and Thomas [11]. A single fibre will diffract a parallel beam of light into a pattern of fringes that gives a means of measuring its diameter accurately or of showing up changes in diameter. If the fibre is gold-coated, as in Fig. 1.7(a), the pattern is relatively simple, since all the scattering is from the edge of the fibre; but if light also passes through the fibre and is scattered internally, a much more complicated pattern (Fig. 1.7(b)), is found. In this pattern, there must be a great deal of useful information on internal fibre structure. The problem is how to understand the phenomenon in sufficient detail to extract this information.

The scattering of a fine beam of light is another diffraction phenomenon that can be used to obtain information about the internal structure of polymer films [12], which may be related to fibre structure. This is analogous to the formation of a halo round the moon when it is seen through a cloud. The radius and breadth of the halo give some information about the distribution of spacings between the particles that scatter the light, for example, the crystallites within a fibre. More complicated patterns can also be made to yield information about the shape of the scattering particles and differences in spacing in different directions.



1.6 (a) Formation of image of a slit. (b) Diffraction pattern of slit.



1.7 Diffraction pattern of a nylon fibre: (a) as received; (b) coated with gold to minimise effects of internal structure. From Lynch and Thomas [11].

The use of polarised light in either of the above two techniques changes the pattern and thus, in principle, increases the available information about structure if it can be interpreted.

The diffraction patterns from objects with some regular repetitive structure are more simple and immediately useful. Thus a diffraction grating of regularly spaced lines, illuminated normally by parallel light, will give a set of fringes, with the maxima of the bright bands at angles ϕ defined by the relation:

$$n\lambda = a \sin \phi \quad (1.1)$$

where n is an integer, λ the wavelength of light and a the spacing of the lines in the grating.

Measurements of ϕ enable values of a to be found (though, more usually, in ordinary physics a grating with known spacing is used to find λ or to disperse light into a spectrum with ϕ varying according to the value of λ). Any distortion in the grating will cause a disturbance in the diffraction pattern. In the extreme, an irregular grating would give a very complicated pattern: but the structural information would still be there if it could be extracted.

Equation (1.1) illustrates two general features of diffraction effects. Firstly, the angle varies inversely with the spacing, so wide-angle patterns give information on close spacings, and narrow-angle patterns give information on more distant spacings. Secondly, since $\sin \phi$ cannot be greater than 1 and n cannot be less than 1 (for the first fringe away from the centre), the smallest possible value of the spacing a for which a solution can be obtained is the wavelength λ . The limit of resolution is thus of the order of magnitude of the wavelength of the light used¹. Optical-diffraction effects, including optical microscopy, even by using ultraviolet radiation, will therefore give information only on relatively coarse features of fibre structure with spacings greater than about 0.1 μm . Indeed, optical microscopy becomes very difficult as soon as one approaches 1 μm , which is not much less than typical fibre diameters.

Atomic and molecular spacings are more than a thousand times smaller than this: typical values lie between 0.1 and 0.5 nm. Consequently, in order to obtain information about the fine structure of fibres, we need to use much shorter electromagnetic waves, namely X-rays. X-ray diffraction is a most important tool for the study of fibre structure, firstly because it gives information at the most important level of fine structure, and secondly because focusing of X-rays is not possible, so that diffraction methods have to be used.

As before, wide-angle diffraction will give information on the finest inter-atomic spacings, and narrow-angle diffraction will give information on longer spacings, of the order of 10–100 nm. As before, an irregular structure will give a complicated pattern, which is difficult to interpret from the image on a photographic plate. However, three advances have made the technique more powerful than was available to the pioneers of X-ray diffraction: arrays of detectors give enhanced quantitative information on the diffraction pattern; computer software then enables the data to be analysed and interpreted; and the increased power of synchrotron radiation reduces exposure times and allows small spot sizes to be used. Dynamic X-ray diffraction is possible, for example on a moving threadline.

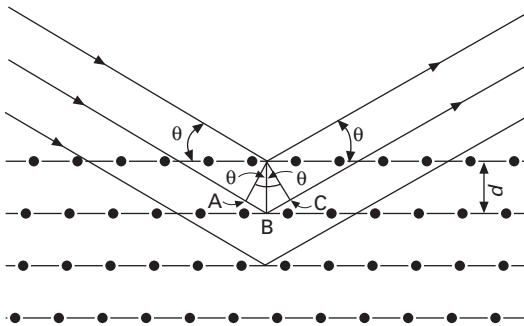
As with optical diffraction, the simplest diffraction patterns arise when the X-rays are scattered from a regular, repetitive lattice. This is the subject of X-ray diffraction by crystals, which has proved an immensely powerful tool since the first patterns were observed by von Laue in 1912.

¹A detailed plot of intensity variation over the central fringe will bring the limit down a little below λ . The limit of resolution of an optical microscope at its best is usually taken to be 0.6λ .

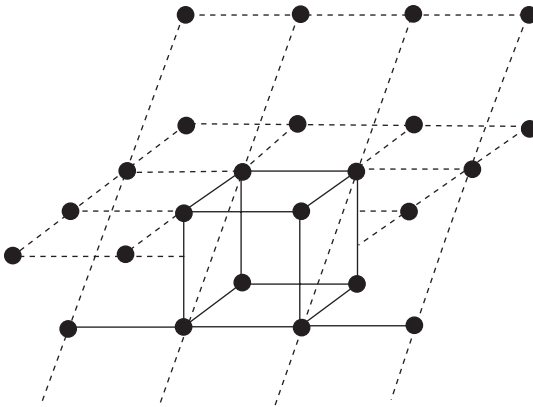
A crystal can be regarded as made up of layers of atoms, themselves regular in their two-dimensional plan, stacked regularly on top of one another². Although analysis of the diffraction from such a three-dimensional lattice is more complicated than for a simple grating, it does result in a very similar equation; for it can be shown that, if a beam of X-rays is directed at a crystal, it is strongly reflected whenever it strikes layers of atoms at an angle θ , shown in Fig. 1.8, such that:

$$n\lambda = 2d \sin \theta \quad (1.2)$$

where n is an integer, λ the wavelength of the X-rays and d the distance between the atomic layers. Under these conditions, the reflections from the individual layers reinforce one another: at other angles, they interfere with one another. Since, as is illustrated in Fig. 1.9, one can find many layers of atoms of varying density in



1.8 Reflection of X-rays from a crystal lattice. Retardation of rays reflected from successive layers = $AB + BC = 2d \sin \theta$.



1.9 Planes of atoms in a cubic crystal.

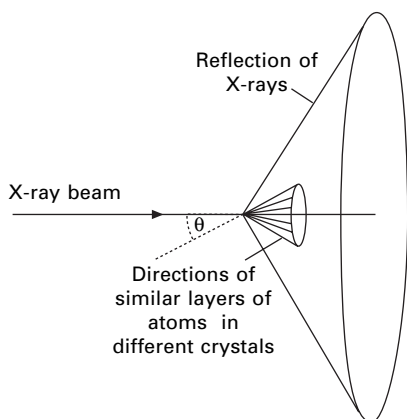
²The concept of atomic layers must not be interpreted too literally. Except in special cases, it does not mean that there are sheets of matter separated by spaces: it is merely a means of describing a repetitive structure, in which the atoms will be fairly uniformly distributed in three-dimensional space.

different directions, there will be a series of characteristic angles of incidence (relative to the crystal axes) at which strong reflections will be obtained. From these angles and from the variation in intensity of the reflections, the general crystal structure can be worked out, and particular atoms can be identified in position. The details of the diffraction pattern will be influenced by the whole form of the atomic arrangement in three dimensions; and there are a variety of methods available to help in the difficult problem of deducing the crystal lattice structure from the diffraction pattern.

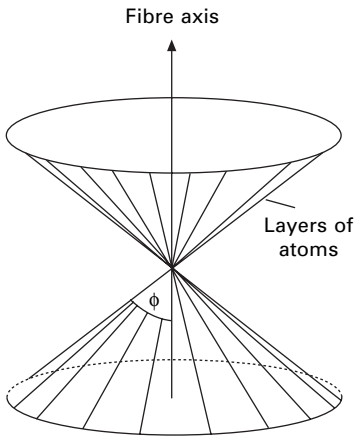
In fibres, however, we are not dealing with single crystals: we have a mass of small crystallites. These will usually be oriented parallel to the fibre axis, but it is simpler to consider first the diffraction pattern that is found when there is no preferred orientation. This is what we get if we pass an X-ray beam through powdered crystals and is called a powder photograph.

The condition that a particular reflection should occur is that the layer of atoms should make the required angle with the X-ray beam. This will happen for a series of orientations of the crystals distributed around a cone. The X-rays will be reflected around a cone of twice this angle, as shown in Fig. 1.10. Furthermore, since all orientations of the crystals are present, all the other reflections will occur, with the appropriate layers of atoms distributed round cones giving the characteristic angles of incidence. The powder photograph is given by the intersection of a photographic plate with these cones and will be a series of circles, subtending angles determined by the distances between layers of atoms in the structure. An example is the X-ray diffraction photograph of *Ardil*, a regenerated protein fibre of a type no longer produced (shown later in [Figure 1.13\(a\)](#)).

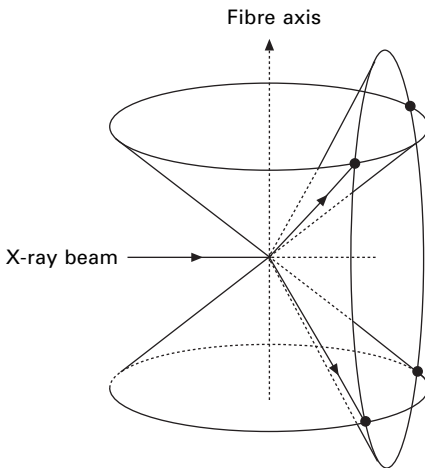
If there is a preferred orientation of the crystals, then the pattern is different. We may suppose that all the crystals are lined up with one of the crystal axes parallel to the fibre axis. Now, layers of atoms giving rise to a particular reflection will make a constant angle, ϕ , with this crystal axis, but, if there is no preferred orientation perpendicular to the fibre axis, the layers can occur at a series of positions distributed around the fibre axis on a cone, as shown in [Fig. 1.11](#). If an X-ray beam is directed



1.10 Reflection of X-rays from powdered crystals. Atomic layers giving a characteristic reflection angle are distributed around a cone.



1.11 Distribution of a particular layer of atoms at angles on a cone round the fibre axis.



1.12 Intersection of the two cones, giving fibre diagram of four spots.

at right angles to the fibre axis, the reflections will now occur, not round a whole cone, but only at those four angles at which the cone of Fig. 1.10 (defining the characteristic angles of reflection) intersects with the cone of Fig. 1.11 (defining the angles at which the particular layers of atoms occur). This is illustrated in Fig. 1.12. The restriction on the angles at which the crystals lie has reduced the X-ray diffraction pattern from the full circles of the powder photograph to the sets of four spots occurring symmetrically in each of the four quadrants of the fibre photograph. Each of the layers of atoms will contribute different sets of four spots, and these will be repeated at different spacings for different values of n in equation (1.2). There are two special cases: if $\phi = \pi/2$, then the cone of Fig. 1.11 becomes a plane cutting the other cone in only two places, and the reflections occur as two spots on the equator of the photograph; and, if $\phi = (\pi/2 - \theta)$, the two cones just touch, and the four spots

coalesce into two, this time at the poles. If $\phi < (\pi/2 - \theta)$, no reflections occur.

Although they were made around 50 years ago, the various X-ray diffraction patterns found in fibres are well illustrated in Fig. 1.13 by a set of comparative pictures. Figure 1.13 (n) is an example of a pattern of a completely crystalline, completely oriented fibre, namely, asbestos. The symmetrical pattern of sharp spots is clearly apparent. The other patterns in Fig. 1.13 are much less sharp, but the way in which they deviate from the idealised pattern yields extremely valuable information about fibre structure. For example, if the orientation is not completely perfect, one can get reflections over a range of angles, and the spots broaden out into arcs. The transition from a fibre with no preferred orientation of the crystals, through a moderately oriented fibre, to a highly oriented one is shown in Figs 1.13(a), (b) and (c) for a regenerated-protein fibre, wool and silk, respectively.

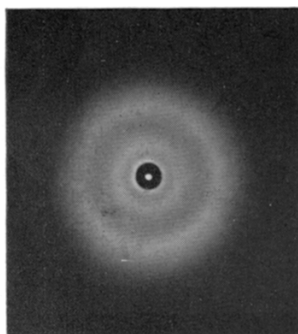
The X-ray diffraction photographs of fibres may be used for various purposes. Since the patterns for each type of fibre are different, as illustrated in Fig. 1.13, they may be used for identification, but their main use is to give information about fibre structure. If the position of a large enough number of spots is known with sufficient accuracy, then the exact crystal structure in which the molecules are packed can be worked out, and this has been done for several fibres. Even when there is not sufficient information to do this, one can deduce much that is useful. If the patterns are different, then the crystal structure must be different. For example, there is a slight difference in the spacing of the spots in Figs 1.13(d) and (e) for hemp and Fortisan³, respectively. This shows up the difference in the crystal structures of native and regenerated celluloses.

The broadening of the spots into arcs shows a decrease in the degree of orientation. This is illustrated in Figs 1.13(e), (f), and (g) for Fortisan, high-tenacity viscose rayon and ordinary viscose rayon. The arcs in these photographs gradually diminish in intensity as the distance from the middle of the arc increases. But, in the photograph for cotton (Fig. 1.13(h)), the arcs end sharply: this is due to the fact that the crystals are arranged on spirals round the fibre axis, so the range of orientations relative to the fibre axis is sharply defined. From the angles subtended by the arcs, one can calculate the spiral angle in the fibre.

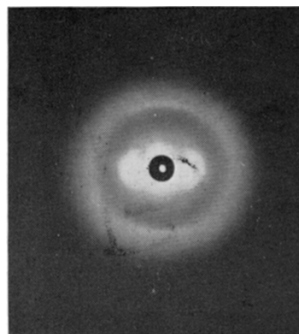
Mercerised cotton (Fig. 1.13(i)) is interesting because it shows a double pattern with the spacings characteristic of both natural and regenerated cellulose. Similarly, in delustred viscose rayon (Fig. 1.13(j)), there is a faint ring outside the main pattern, which is due to reflection from the titanium dioxide present. Another circumstance in which a double pattern is obtained occurs with almost all fibres; this is the superposition on the characteristic crystal-diffraction pattern of a diffuse background due to scattering from non-crystalline regions of the fibre. From a study of the relative intensities of the two effects, estimates of the degree of crystallinity can be made.

Broadening of the spots into arcs is characteristic of poor orientation, but a broadening along a radius of the pattern is characteristic of crystallites that are either very small or very imperfect, so that the characteristic angle of reflection from a layer of atoms

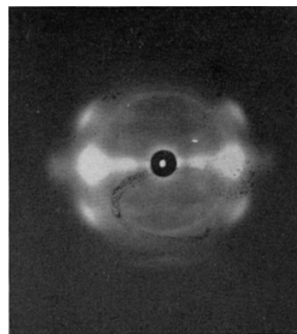
³Fortisan, which is no longer produced, was a highly oriented cellulose fibre, produced by regeneration from cellulose acetate.



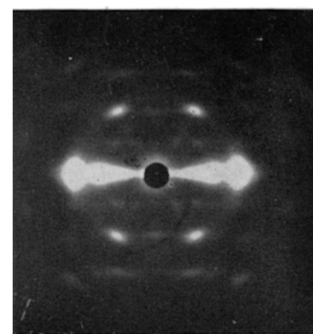
(a) Regenerated protein fibre
(*Ardil*)



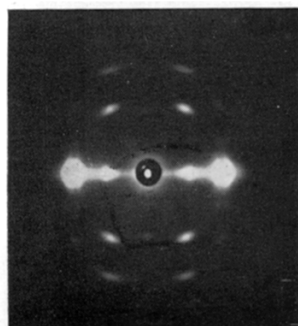
(b) Wool



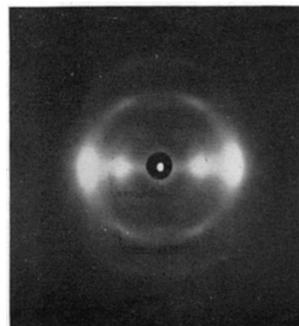
(c) Silk



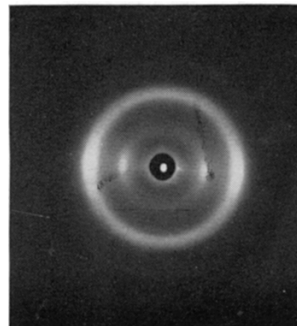
(d) Hemp



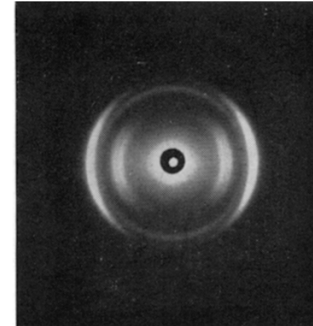
(e) *Fortisan* (regenerated
cellulose)



(f) High-tenacity viscose
rayon

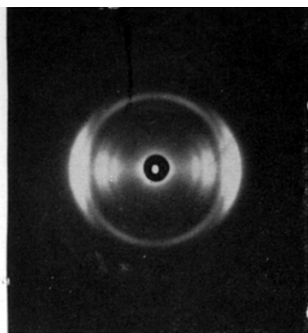


(g) Standard viscose rayon

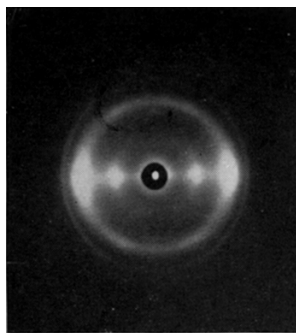


(h) Cotton

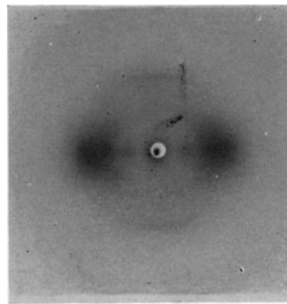
1.13 X-ray-diffraction photographs of fibres (photographs by J. A. Howsmon, American Viscose Corporation).



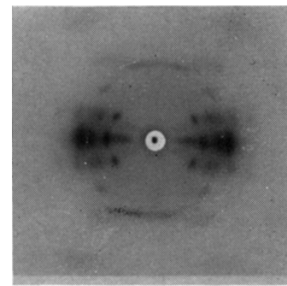
(i) Mercerised cotton



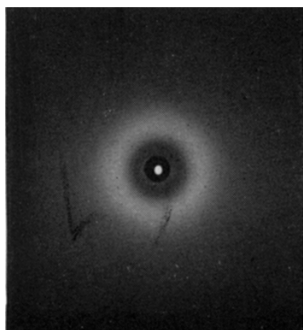
(j) Dull viscose rayon



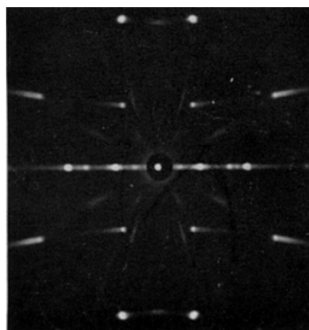
(k) Unannealed Dacron polyester fibre



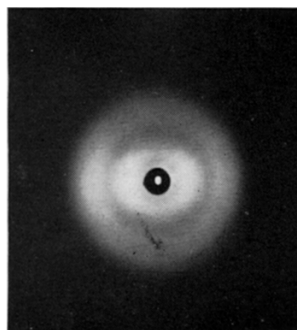
(l) Annealed Dacron polyester fibre



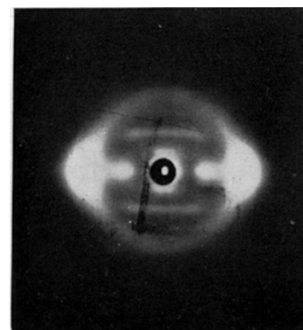
(m) Glass fibre



(n) Asbestos

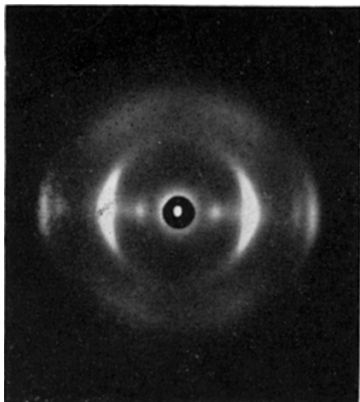


(o) Acetate

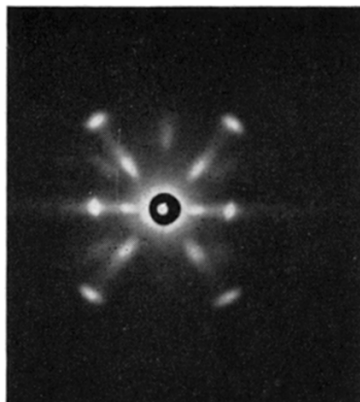


(p) Nylon

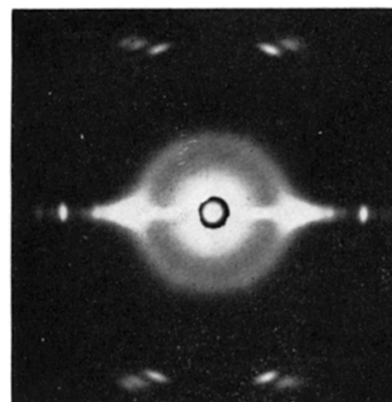
1.13 (Continued)



(q) *Orlon* acrylic fibre



(r) *Saran* copolymer fibre



(s) Polyethylene

1.13 (Continued)

is less sharply defined. An example is the X-ray diffraction pattern of unannealed polyester fibre (Fig. 1.13(k)): after annealing, the spots are sharper (Fig. 1.13(l)). We may similarly compare the photographs for two mineral fibres, glass and asbestos (Figs 1.13(m) and (n)); the first is a single halo, characteristic of a completely amorphous material, and the second contains a large number of sharp spots, characteristic of a highly crystalline material.

The reflections giving the patterns discussed above occur at angles up to about 10° , but one can obtain other useful information from the reflections that occur at very small angles, close to the X-ray beam. It follows from equation (1.2) that, since $\sin \theta$ will be nearly zero, these must be due to the occurrence of much larger values of d . Studies have been made with θ as small as 10 seconds, corresponding to $d = 2000 \text{ nm}$. In a few special materials, such as porcupine quills, sharp reflections have been obtained, indicating the presence of some repeat in the structure at a large spacing, but usually a diffuse halo is found. This is due to the scattering of X-rays by small crystallites in the fibre. A detailed study of these narrow-angle photographs can therefore lead to information about the size, shape and arrangement of the crystallites.

1.2.4 Electron microscopy and related techniques

Electrons, although usually regarded as particles, can act as if they were waves with a wavelength of the order of 0.005 nm . They can be focused by bending their paths in electric and magnetic fields in the same way that light rays are bent by lenses. Electron microscopes can form an image with a limit of resolution that is far smaller than is possible with an optical microscope. A limitation is that the specimens must be in a vacuum.

Obtaining sufficient contrast is one of the many technical difficulties in electron microscopy, and fibres are not the easiest specimens to deal with. The specimens used in ordinary transmission electron microscopy must be very thin (less than $0.1 \mu\text{m}$ thick), both to allow the passage of electrons and to avoid confusion arising from the great depth of focus. With some difficulty, it is possible to cut fibre sections of this thickness in order to make direct observations of the internal fine structure. Staining with heavy-metal compounds may be used to enhance contrast. A danger in this work is that some of the features that are observed may be caused by the section-cutting itself.

A great deal of useful information has come from the study of replicas, either of a cut face of the fibre or of the fibre surface, made in some suitable material. The contrast is often emphasised by a technique that consists of depositing heavy-metal atoms on the specimen from a given angle to give the appearance of shadows. Internal detail may also be shown by peeling a layer off the fibre to expose a new internal surface for replication. Another technique that may be used is to examine the fragments that are left behind after mechanical or chemical degradation of fibres. The polymers of which fibres are composed may also be examined as thin films.

As well as focusing an image, the electron-diffraction pattern of crystal lattices can be obtained. In general, this gives much the same sort of information about orientation and crystallinity as comes from X-ray diffraction, but with the advantage

that it can be obtained from a particular area of an electron microscope picture, rather than from the whole of a bulky specimen. In dark-field electron microscopy, an image is formed from a particular selected band of diffracted electrons. This technique can therefore be used to show up the presence of crystalline regions, which will diffract in the selected direction and appear light against a dark background (or the reverse in negative contrast).

As an alternative to the method of viewing thin specimens in transmission, it is possible to form an image from electrons reflected from a surface. However, this cannot be done very effectively in a conventional, direct electron microscope, although some interesting studies of surface damage were made in the 1950s. A much better method for examining surface detail is *scanning electron microscopy* (SEM). The principle of this method is that a fine spot of electrons is traversed across the specimen and some response is used to form an image on what is, essentially, a television screen scanned synchronously with the spot. In the usual mode of operation, where the scattered electrons picked up by a collector are used to generate the image, the picture looks like an ordinary enlarged image of the specimen as viewed along the column followed by the electrons forming the spot. There are other modes of use that give further information. The main use of scanning electron microscopy in fibre science has been in the range of medium to high magnification, which is near or beyond the limit of the optical microscope. The scanning electron microscope has the great advantage of a much larger depth of focus.

The early applications of electron microscopy to fibres are discussed by Chapman [13], Hearle and Greer [2], Hearle and Simmens [14] and Hearle *et al.* [15]. Since then there have been important advances in techniques. Some of these come from the general developments in electronics, digital processing and information technology. Spot sizes have been reduced in scanning electron microscopy and scanning has been applied to the transmission mode. Resolution has been improved, so that, in appropriate samples, individual atoms in a crystal can be seen. Increased sensitivity reduces exposure times and limits radiation damage.

An order of magnitude increase in voltage has enabled high-voltage electron microscopes to be used with thicker specimens. Bryson *et al.* [16] have used tomography to make a quantitative determination of the twist angles in the helical assembly of the intermediate filaments (microfibrils) in the macrofibrils of the ortho-cortex of wool, as shown later in Figs 1.45 and 1.46. If a specimen is observed at a series of tilt positions, a three-dimensional tomographic reconstruction can be produced. Computer graphics then enables this to be viewed at any angle and measurements to be made.

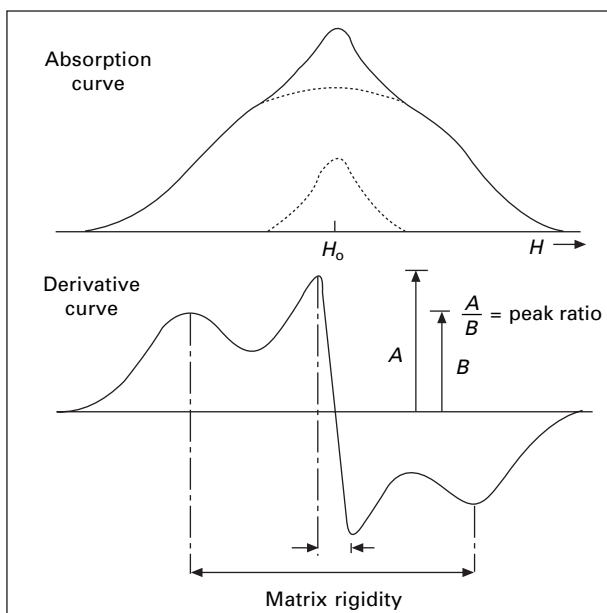
Scanning allows images to be formed from other signals. Atomic force microscopy is a useful way of examining fibres. In its simplest form, a probe with a minute tip mounted on a cantilever arm rests on the surface of the specimen. As it moves across the surface, the tip rises and falls and the deflection of the cantilever is a measure of force. This can be viewed as a line showing the surface profile or scanning over an area and conversion of the response to a grey scale gives an image of the surface topography. Atomic force microscopy can be used in other modes. For example the tapping mode gives a measure of the stiffness of the material. This can be used to show differences in elastic modulus in different parts of a fibre cross-section [17]. An

example of the use of the atomic force microscope is a study of the morphology, nano-mechanical properties and effects of moisture absorption in cotton by Maxwell *et al.* [18].

1.2.5 Nuclear magnetic resonance (NMR)

The nuclei of many atoms possess a magnetic moment. As a result, the nucleus can be caused to resonate if it is put into an appropriate alternating magnetic field. Typical values would be a field of 1.5 tesla oscillating at 60 MHz. Structural information comes from the influence of the fields of neighbouring atoms on the resonance. When the atoms can resonate independently, as in a liquid, they all do so at the same frequency, though high resolution shows that there is really a set of separate finely spaced frequencies, which give information on the structure of the molecules themselves. In a solid, however, the rigidity of the system causes a strong interaction between neighbouring molecules, and this results in a broadening of the frequency response. This effect will be greatest in a crystalline region and less in a non-crystalline region.

As usual in resonance phenomena, the energy absorbed can be caused to vary in two ways: in this system, either by scanning through a range of frequencies, with a maximum at the resonant frequency, or by running through a change of magnetic field at constant frequency. The latter procedure is usually adopted, and a typical response for a solid polymer is shown in Fig. 1.14. Differentiation of the curve aids interpretation. The ratio of the intensity of the broad band to the intensity of the narrow band gives a measure of the crystalline/non-crystalline ratio in the material.



1.14 Nuclear magnetic resonance curve for a solid polymer. From Statton [19].

What is even more interesting is the fact that the width of the broad band gives a measure of the rigidity of the more highly ordered material. Statton [19] has shown that this decreases with temperature owing to the increasing thermal oscillation in the crystal lattice, but it is also interesting that it increases on drawing nylon and increases still more on hot stretching.

Statton, as indicated in Fig. 1.14, terms the parameter derived from the broadband width the *matrix rigidity*, since the width depends on how firmly the resonating atom is held within the surrounding matrix of highly ordered material. In a perfect crystal, the width would be great; in a small or defective crystal, it would be less. In a similar way, the width of the narrow band could indicate how firmly individual atoms are held within their matrix of less ordered regions.

1.3 Approaches to polymer fibre structure

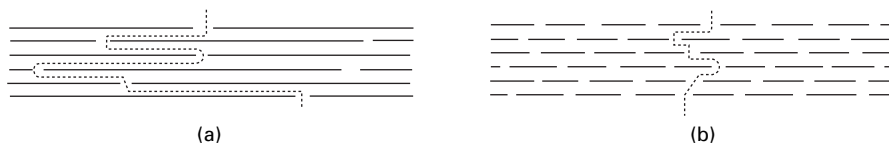
1.3.1 Requirements for fibre formation from linear polymers

An essential requirement in fibre structure is some means of ensuring continuity, and strength, along the length of the fibre. Because of the fineness of fibres, transverse strength is of much less importance. In the linear polymer fibres, it is the long-chain molecules that provide this continuity. In considering what type of molecular arrangement of linear macromolecules will be necessary in a fibre-forming structure, we can be helped by considering the larger-scale problem of how a textile yarn is made up.

A mass of raw cotton consists of a large number of long, fine fibres, arranged irregularly and tangled up, just like the molecules in rubber (Fig. 1.1(a)). In order to make this into a yarn, we must cause the fibres to line up more or less parallel to one another and then insert twist, which leads to lateral compression in the yarn and so causes frictional forces to hold the parallel fibres together. However, the twist must not bind the fibres together into a solid rod, which would destroy the flexibility and porosity required in the textile yarn.

From this, we can see by analogy that the basic requirements for fibre formation would be:

- long-chain molecules, corresponding to the long fibres that make up yarns: if the molecules or fibres are too short, there will be a loss of strength as illustrated in Fig. 1.15;
- a more or less parallel arrangement of the molecules;
- lateral forces to hold the molecules together and give cohesion to the structure;



1.15 Effect of length of fibres (or molecules) on strength: (a) long fibres showing a cohesion; (b) short fibres, showing possibility of easy breakage.

- some measure of freedom of molecular movement in order to give the necessary extensibility to the fibre and some openness to give room for moisture absorption and uptake of dyes.

It will be noted that twist is not included, since it is not a fundamental requirement but only a means of bringing lateral frictional forces into play in yarns.

In fibres, the lateral forces serve a second purpose, that of maintaining the oriented arrangements of the molecules. Without them, there would be a return to the disordered arrangement characteristic of rubbers.

1.3.2 Order and disorder in fibre structure

Fibres, as well as sheets or blocks of the same polymers, do not have the macroscopic form of crystals, but the X-ray diffraction patterns of most fibres show sharp spots in a four-point diagram, which is characteristic of an oriented crystal lattice, accompanied by an amorphous halo. This indicates that the fibres consist of *partially oriented, partially crystalline, linear polymers*. There is no problem in understanding partial orientation as a structure in which the chain molecules approach but do not fully achieve an alignment parallel to the fibre axis. However, there are many different ways in which crystallinity can be incomplete. The literature contains a great diversity of pictures. To some extent, these are interpretations that differ for different fibres. However, they are all two-dimensional or quasi-two-dimensional views of three-dimensional structures; few have a quantitative basis; and all reflect the ideas and graphical skills of the authors.

The diffraction evidence that the structure was a mixture of order and disorder was supported by values of density and moisture uptake and by other analytical techniques. However estimates of the relative amounts of order and disorder differ according to method used, as shown in Table 1.1. What is fairly consistent is that there is twice as much disorder in regenerated cellulose as in cotton. Another measure is accessibility

Table 1.1 Percentage of disordered material in various celluloses (approximate average values from published literature†)

Technique	Cotton	Wood pulp	Mercerised cotton	Regenerated cellulose
X-ray diffracton	27	40	49	65
Density	36	50	64	65
Deuteration	42	55	59	72
Moisture regain (sorption ratio)	42	49	62	77
Hailwood Horrobin	33	45	50	65
Non-freezing water	16	—	23	48
Acid hydrolysis	10	14	20	28
Alcoholysis	10	15	25	—
Periodate oxidation	8	8	10	20
Dinitrogen tetroxide oxidation	23–43	—	—	40–57
Formylation	21	31	35	63
Iodine sorption	13	27	32	52

†Values summarised by Jeffries *et al.* [20].

(Table 1.2), which indicates the availability of internal surfaces, volumes or —OH groups in cellulose. Again there is uncertainty because values differ according to the agent used (Table 1.3).

The dimensions of the crystalline regions, deduced from the diffraction data, are of the order of 10 nm, which is around 1000 times less than the length of the molecules. This suggested a *fringed-micelle* model of fibre structure. Figure 1.16(a) shows an early view of the structure after crystallisation from a melt. One can see how this sort of structure would arise if one considers a large pile of beads on strings arranged in a tangled mass. If the beads have hooks on them and several people start fastening them together, each person will build up a compact region of strings of beads fastened together in regular order. But, after a time, the actions of one person will begin to interfere with those of another: it will not be possible for some chains to be fastened

Table 1.2 Percentage accessibilities of celluloses measured by exchange of hydroxyl hydrogens for deuterium†

Celulose	Accessibility	Cellulose	Accessibility
Bleached cotton	44	Kenaf	49
Mercedised cotton	66	Flax	50
Finely ground cotton	87	Cotton linters	50
Sulphite pulp	57	Ramie	53
Mercedised sulphite pulp	70	Rayon	78
Jute	48	Potato starch‡	97
		Birch xylan‡	99

†From results of Skachkov and Sharkov [21] by a modified method of Sepal and Mason [22].

‡Soaked to the point of no more swelling in the H₂O–D₂O mixture. These highly accessible non-cellulosic polysaccharides are included for comparison.

Table 1.3 Accessibility and molecular weight

Measurement	Purified cotton (%)	Mercedised cotton (%)
Periodate oxidation: potential accessibility without crystal disruption†	40	–
Water (D ₂ ¹⁸ O): some crystal penetration‡	48.8	63.9
Water (D ₂ O): readily accessible§	36.0–37.2	48.1
<i>N,N</i> -Diethylaziridinium chloride: readily accessible¶	19–21	32–33
Diphenyl Fast Red 5BL: readily accessible	2.5 (5.4 m ² /g ^{††})	4.5 (9.9 m ² /g ^{††})

† Rowland and Cousins [23].

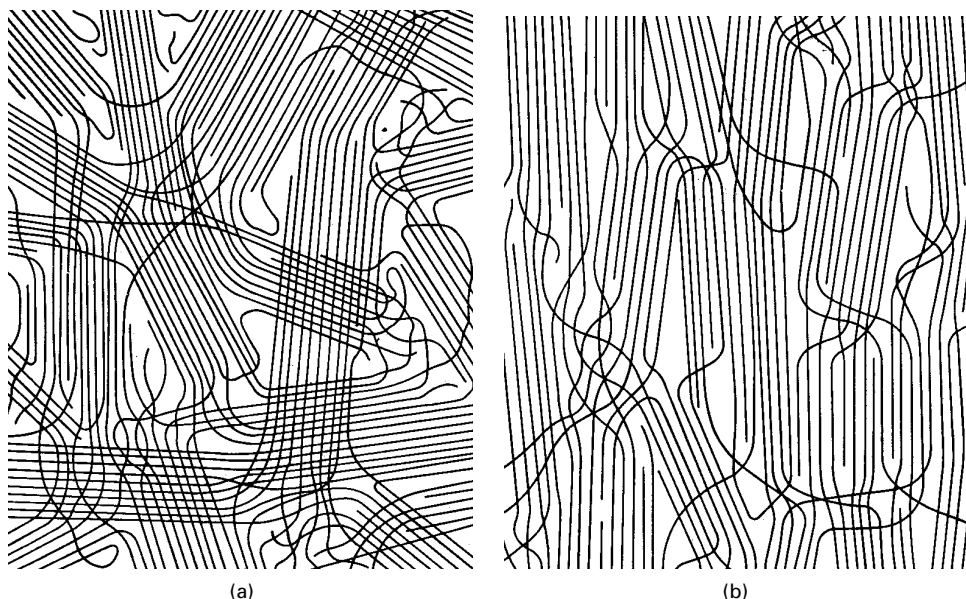
‡ Guthrie and Heinzelman [24].

§ Rousselle and Nelson [25].

¶ Bose *et al.* [26].

|| Johnson *et al.* [27].

†† Percentages calculated from an estimated 220 m²/g of surface for completely accessible cellulose chains.

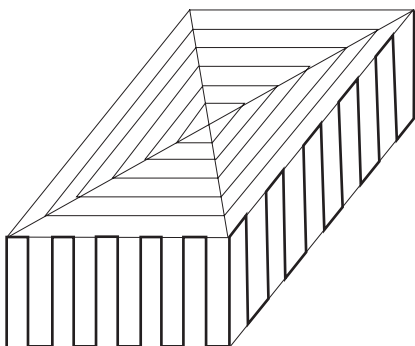


1.16 Fringed micelle structures: (a) in unoriented (undrawn) fibre; (b) in oriented (drawn) fibre. From Bunn [28].

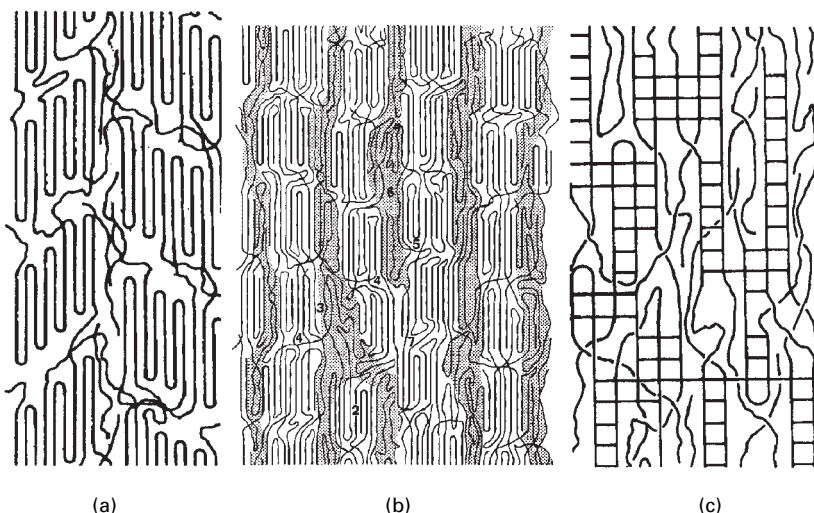
up any further because they are already fixed elsewhere. The hooking-together of the strings continues until finally there are several regions of beads fastened together, whereas between them the strings go off in various directions and can be fastened together only where two beads happen to pass close to one another. This is an exactly analogous arrangement to that shown in Fig. 1.16(a). There are the crystalline regions of regular order and the non-crystalline region, where the molecules can only be linked together in a few places. The process of formation is also analogous for, if an irregular mass of chain molecules is crystallising, crystallites will form at various places and continue to grow until they interfere with one another. The drawing process for melt-spun fibres would lead to orientation, as indicated in Fig. 1.16(b).

Figure 1.16 was proposed in the context of nylon and polyester fibres, but is now directly relevant only to stiffer molecules such as cellulose. Note that all the molecules fringe off at the edge of the crystallites to continue as tie-molecules to other crystallites. Chain folding occurs only in the amorphous regions between the crystallites. Academic studies of slow crystallisation in laboratory conditions showed other forms.

It was found that polymers, including those used in fibres, could be crystallised from dilute solution so as to give single crystals. In these lamellar crystals, the chain molecules are folded back and forth as illustrated schematically in Fig. 1.17. Similar folding may occur in fibres, and this has led to the suggestion of a modified fringed-micelle structure, in which there is a mixture of fringing and folding at the end of each micelle. Figure 1.18(a) illustrates this form of structure, but was drawn with angled ends to the crystallites in order to explain a feature of the crystal lattice of nylon 6.6 (see Fig. 1.47). Typically, Fig. 1.18(a) is too uniform a structure. There



1.17 Schematic illustration of chain-folding in a single crystal.



1.18 Views of fine structure of nylon fibres. (a) A common working model proposed by Hearle and Greer [29]. Angled ends are based on small angle X-ray diffraction pattern of nylon 66. (b) From Murthy *et al.* [30], based on X-ray diffraction studies of nylon 6. (c) An alternative form, from Hearle [31].

would be some variation in crystal size and packing as indicated in Fig. 1.18(b), which is based on X-ray diffraction studies of nylon 6 [30].

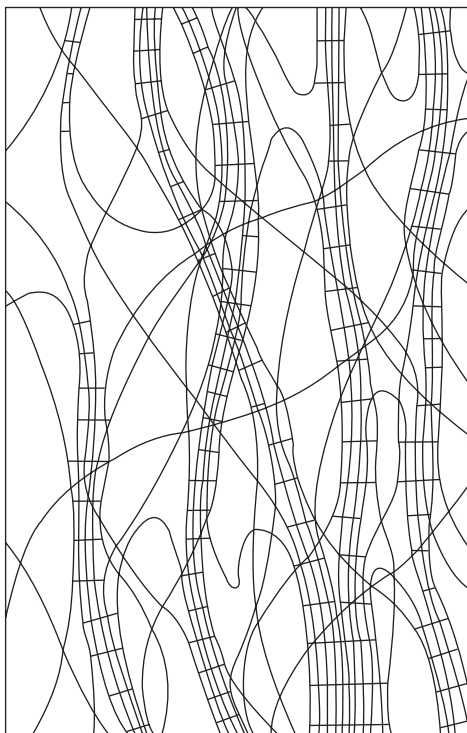
Two general points should be made. Firstly, because the structure consists of blocks within a matrix, a typical crystallinity of 50% requires that the spacing between crystallites averages one-third of the crystallite dimensions. Such tight packing is not compatible with a random placing of crystallites and leads to the quasi-fibrillar form shown in Fig. 1.18(a,b). The driving force to crystallisation will lead to the tie-molecules being somewhat extended and not random coils. Secondly, as discussed in [Chapter 18](#), rapid quenching may lead to a more uniform structure as illustrated in Fig. 1.18(c) [31]. Large crystals have a lower internal energy than small crystals, so that annealing tends to give a growth in crystal size. For polymers, in contrast to metals, where defects can move and eliminate boundaries between crystals, this

requires the small crystals to melt and reform as new larger crystals. This major change is not possible when the crystals have grown to a certain size. Consequently, the crystal size, which depends on processing conditions, is limited to a maximum of about 10 nm.

Bulk crystallisation of polymers from the melt or from more concentrated solution leads to a spherulitic structure. Such a structure starts from crystallisation as folded-chain lamellae on separate nuclei; the crystals then grow with successive branching, until the spherical region is established. Ultimately, the separately growing spherulites meet. Fringed-micelle structures are the limiting form of spherulitic crystallisation when the number of nuclei becomes so large that they are very close together and there is no room for the spherulitic branching to develop. This is typical in fibre production, with rapid solidification, but there are circumstances in which occluded spherulites occur in nylon fibres. After drawing, they become ellipsoids.

With stiffer molecules, fibrillar textures are observed in electron microscopy. For low crystallinity fibres, as in cellulose, Hearle [32, 33] proposed a fringed-fibril structure, as illustrated in Fig. 1.19. This combines (a) a fibrillar form and (b) the ideas inherent in the fringed-micelle structure of distinct crystalline and non-crystalline regions with chain molecules running continuously through each type of region. The highly crystalline high-performance fibres have a more tightly packed fibrillar structure.

Polymers such as polyethylene have been found to crystallise in lamellar forms linked by tie-molecules.



1.19 Fringed-fibril structure.

In natural fibres, genetic control leads to the lay-down of specific fibrillar forms. As discussed later, cotton may be completely crystalline, with disorder coming from imperfect register between fibrils, and wool contains fibrils separated by a chemically different matrix.

A more radical difference in views of fibre structure results from a questioning of the concept of well-defined crystalline and non-crystalline regions. Even in 1930, there had been those who regarded the structure as uniformly partly ordered. This view was revived by Kargin [34], who suggested an amorphous structure with some correlation between the positions of neighbouring chains. Hosemann [35, 36], on the other hand, suggested a paracrystalline structure in which the lattice parameters are subject to a more-or-less random disturbance. This leaves the crystal lattice locally somewhat distorted, and certainly without any long-range order.

Others have taken over ideas from metal physics and suggested that the disorder is due to crystal defects (vacancies, folds, chain ends, extra units, crossing of and twisting chains, and so on) at particular points within the crystal. These last two models substitute internal imperfections in the crystallites as a source of disorder instead of separate non-crystalline regions. Reneker and Mazur [37] have proposed explicit models for defects in polyethylene. An additional $-\text{CH}_2-$ group or a switch between neighbouring chains would be local disturbances within a continuous distorted crystal lattice. However the molecules in most textile fibres have much longer repeats (38 atoms in 14 groups in nylon 66), so that an additional repeat unit could not be incorporated without destroying the crystal.

The above comments briefly describe the diverse forms of polymer crystallisation. The experimental evidence on disorder could also be explained by the size of crystalline regions. Small crystals imperfectly packed together would give a poor X-ray diffraction pattern, a lower density and accessibility to the surfaces of the crystallites or crystalline fibrils. It is now recognised that because different fibres are made of different polymers and are produced in different ways, there may be major structural differences, and one should not look for a single form of structure. In particular, there will be differences between natural fibres, which grow very slowly as living cells or are slowly extruded as silks, and manufactured fibres, formed by high-speed extrusion and drawing.

1.3.3 A general view

A more general approach to the problem can be made by considering what parameters are needed to give a reasonable specification of fibre structure. Because the structure is intermediate between one that can be specified by a unit cell and one that can be specified by statistical parameters, a complete description would need the position of almost all the atoms to be individually stated, namely, around 10^{16} parameters per fibre. This is obviously impossible. Fortunately, we can select a limited number of parameters, which characterise the most important features. The list proposed by Hearle and coworkers [2, 38–40] is:

- degree of order;
- degree of localisation of order;
- length/width ratio of localised units;

- degree of orientation;
- size of localised units;
- molecular extent.

The first three can be taken together in a triaxial plot, as shown in Fig. 1.20(a), and the other three then regarded as applying to any structure defined by the first three. The various forms of structure already discussed are indicated by their positions on the plot. In Fig. 1.20(b), the likely positions of various fibres are marked.

Degree of order would be theoretically defined as the mean value of some correlation function relating the position of neighbouring chains. Practically, it could be defined in terms of density by the expression:

$$\text{degree of order} = \frac{\rho - \rho_{\text{am}}}{\rho_{\text{cr}} - \rho_{\text{am}}} \quad (1.3)$$

where ρ is the fibre density, ρ_{am} the density of amorphous (non-crystalline) material and ρ_{cr} the density of crystalline material.

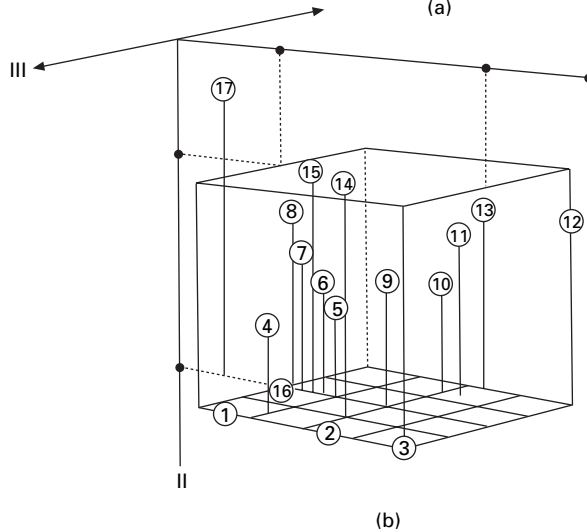
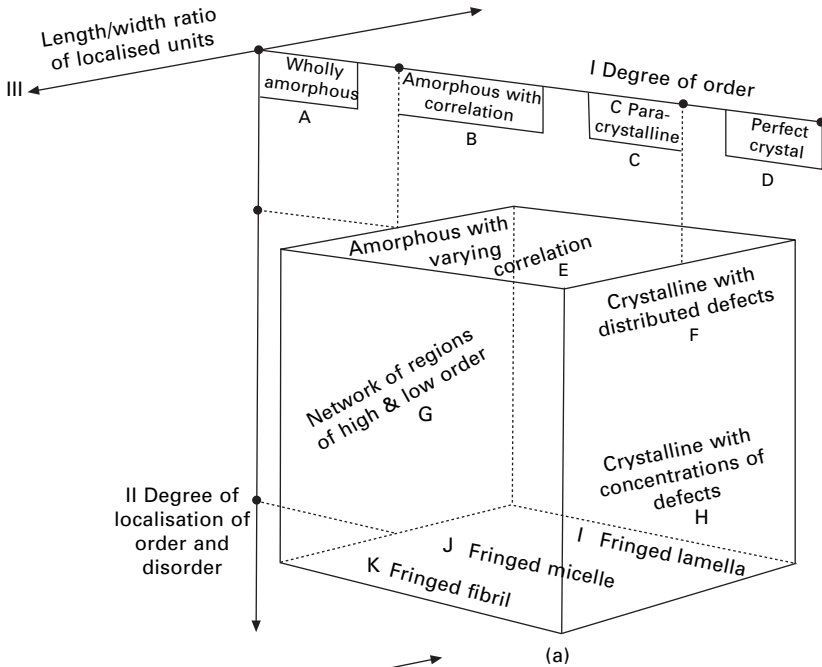
The values of degree of order would range from zero for a completely amorphous fibre to unity for a perfectly crystalline fibre. The experimental methods of density determination will be discussed in Chapter 5. Alternatively, estimates of degree of order could be obtained by other methods, such as X-ray diffraction, accessibility, infrared absorption or NMR studies.

Figure 1.21 illustrates a range of degrees of order. In a continuous structure, the whole material would be of the same degree. However, a given average value, say 50%, could correspond to many other different combinations, as indicated by the three distributions of local degree of order shown in Fig. 1.22.

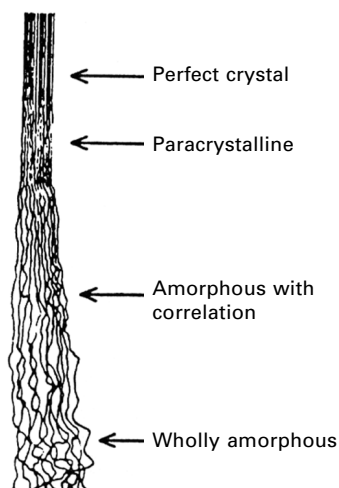
Degree of localisation of order would be theoretically defined by some measure of the spread of values of degree of order taken over zones a few molecules wide. The uniform distribution A in Fig. 1.22, would have a low value, B would be larger, and C would have the largest value, since it represents a split into separate ordered and disordered regions. Experimentally, values of the degree of localisation of order must be estimated from indirect evidence, such as electron microscope views of the fine structure.

The *length/width ratio* of the units is a more straightforward parameter, ranging from infinity for very long fibrils down to unity for cubic micelles and to zero (or minus infinity on a logarithmic scale) for extensive flat sheets. It is tacitly assumed here that the 'length' refers to the direction of the chain axis. In lamellar crystals, the ratio would be more commonly regarded as thickness/width.

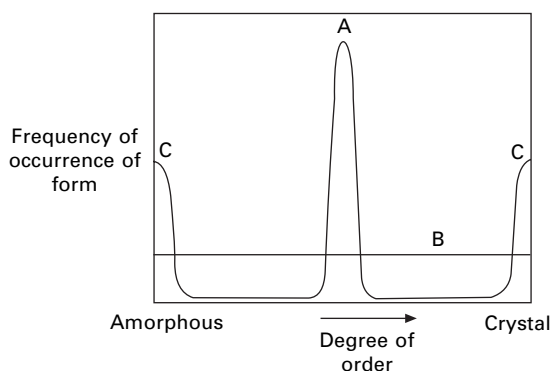
An important point to stress is that all the parameters can vary continuously and there are no sharp boundaries between the various forms of structure indicated in Fig. 1.20(a). One form merges into another. At some point, the disorder in a paracrystalline structure becomes too great to pick out the regular lattice and the structure is better regarded as amorphous with correlation. As correlation varies from place to place, it may become distinct enough to discern separate regions of high and low order, which will eventually be so distinct that they are to be regarded as crystalline and amorphous. The uniform disorder of the paracrystal can be replaced by distributed point defects; and then, if these defects come together, they may eventually be so large that they are



1.20 (a) Schematic representation of fibre structure in terms of three major variables. (b) Possible location of various materials on the plot: (1) wool and other hair fibres; (2) silk; (3) cotton and other plant fibres; (4) model rayon and lyocell; (5) ordinary rayon; (6) triacetate; (7) secondary acetate; (8) regenerated-protein fibres; (9) polyester fibre; (10) polyamide fibre; (11) polypropylene fibre; (12) linear polyethylene fibre; (13) branched polyethylene fibre; (14) acrylic fibre; (15) polyvinyl chloride fibre; (16) spandex fibre; (17) rubber, atactic polystyrene. From Hearle [38]. The newer high-modulus fibres would be further out along the line ①-②-③.



1.21 Range of degrees of order of packing of chain molecules, as drawn by Howsmon and Sisson [41], with identification of forms by Hearle [38].



1.22 Three of many possible distributions of degree of order in a 50% crystalline fibre: A, uniform intermediate order; B, all degrees of order equally represented in different regions; C, mixture of highly ordered and highly disordered regions. From Hearle and Greer [2].

better regarded as amorphous regions. As fibrils become shorter, they are eventually better regarded as elongated micelles; and then flattened micelles merge into small lamellae.

The two parameters, *degree of orientation*, defined theoretically by a mean angle between the chain molecules and the fibre axis, and *size of localised units*, indicating the difference between a coarse and a fine texture, do not give rise to any basic conceptual difficulties of definition and experimental estimates can be made.

Molecular extent is more difficult. Direct measurement is not possible and it is not included in drawings of structure, except for simple examples such as Fig. 1.15. As shown by an analogous example at a larger scale, it has a major effect on strength. The strength of a textile yarn depends not only on fibre length but also on the extent to which the fibre is folded back on itself. Drafting is used to remove folds. In highly

folded forms, as shown in Fig. 1.23, molecular extent approximates to fold length. With few folds, fibre length is more important.

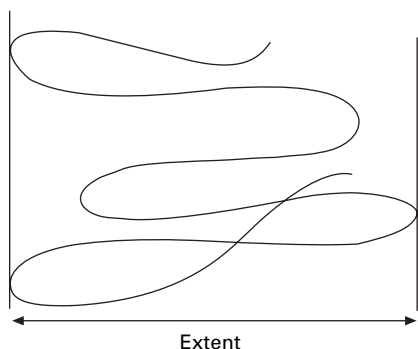
In addition to the six listed, there are other aspects of fine structure that could be specified and that may be important in some circumstances. There are other features of the shape of localised units. Fibrils may be cylindrical or ribbon-like. There are fine details of packing, such as the relative extent of fringing and folding. There are the details of interconnection between crystalline regions. There may be distributions of values of the length/width ratio, degree of orientation and size of localised units parameters; and so on. However, with adequate means of theoretical analysis, it becomes possible to predict many fibre properties from a knowledge of the chemistry of the chain molecule, of the six parameters of fine structure, and of any special larger-scale structural features.

1.3.4 Order, orientation and extent

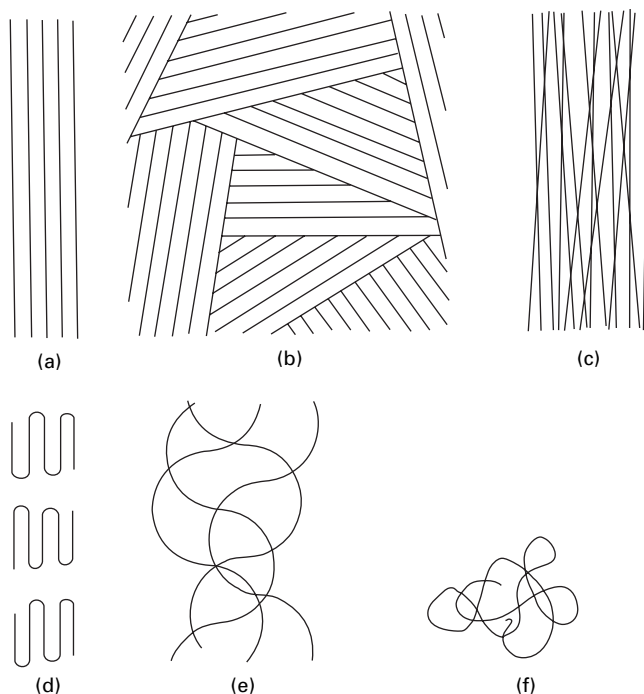
Degree of order, degree of orientation and molecular extent are often confused. This is because, at the extremes, they do come together as high or low values (Fig. 1.24(a), (f)). A perfectly ordered structure must be perfectly oriented with fully extended chains, and a completely disordered structure must be completely disoriented with short fold lengths. But these are not practical cases. In intermediate situations the three parameters are unrelated. Figure 1.24(b–e) illustrates this. A very highly ordered structure may be completely disoriented because it is composed of separate crystals pointing in all directions. A very low degree of order can occur owing to chain entanglement and lack of register with very little angular deviation from perfect orientation. A highly oriented structure may have short chain folds. A sequence of semicircular folds can give high extent and zero orientation. Other conflicting combinations can be found.

1.3.5 Limiting values of parameters

In ordinary substances composed of small molecules, it is possible to work disorder out of the system. If faults come to the edge of the crystal, they disappear. A large



1.23 Extent of a long chain in a structure.



1.24 (a) Maximum order, orientation and extent. (b) Higher order, zero orientation. (c) Low order, high orientation. (d) High orientation, low extent. (e) Zero orientation, high extent. (f) Minimum order, orientation and extent.

crystal grain can grow by rearrangement of atoms near its boundary until it eliminates a smaller grain. This is not possible in polymer systems, since, if one crystallite is caused to grow, then the connections along the polymer chains cause a disturbance elsewhere. It is easy to imagine this if one thinks of packing a tangle of string into aligned regions corresponding to crystals. Once the initial stage of ordering is over, an improvement in one place can only come with an upset somewhere else.

As a result, once fibres have crystallised with a given degree of order, it is very difficult to make more than marginal improvements (say, from 50 to 60%) in the degree of order by any treatment. On thermodynamic grounds, it is clear that there will be (below the melting point) a driving force towards increased order, which brings the structure closer to the ideal of a single crystal, and that this will continue until further progress is blocked by the complexity of molecular entanglement. Nevertheless, significant rearrangements, such as an increase in size of crystalline regions and of the space between them, or the pushing out of defects from inside a crystal into non-crystalline regions, or major mechanical deformation of the structure, can be made without much change in the overall degree of order.

With the polymers that are used for most fibres (although not necessarily with polyethylene), it also seems likely that there will be a driving force towards localisation of order. The reasons for this were discussed by Hearle and Greer [2]. The argument is that a uniform intermediate degree of order is not very favourable in either entropy

S or internal energy U . Given the above restriction that the average degree of order cannot increase, there would probably be a lowering of free energy ($U - TS$) by part of the material becoming more highly ordered, with much lower internal energy and not too large a decrease in entropy, and the other half becoming more disordered, with a large increase in entropy and with very little change in internal energy. Mechanistically, we can imagine crystalline regions growing and pushing the disorder out ahead to pile up in larger amorphous regions.

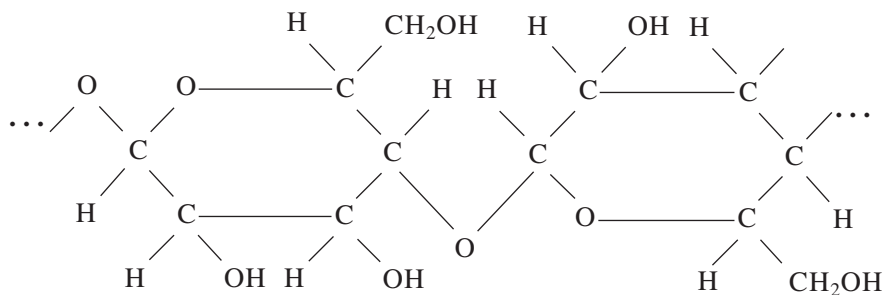
The requirements listed are satisfied in the common textile fibres. But, in specialised fibres, there are differences: for example, in the high-modulus inorganic fibres, continuity is achieved in other ways, and, in elastomeric fibres, orientation is not required.

1.4 Cellulose fibres

1.4.1 Cellulose

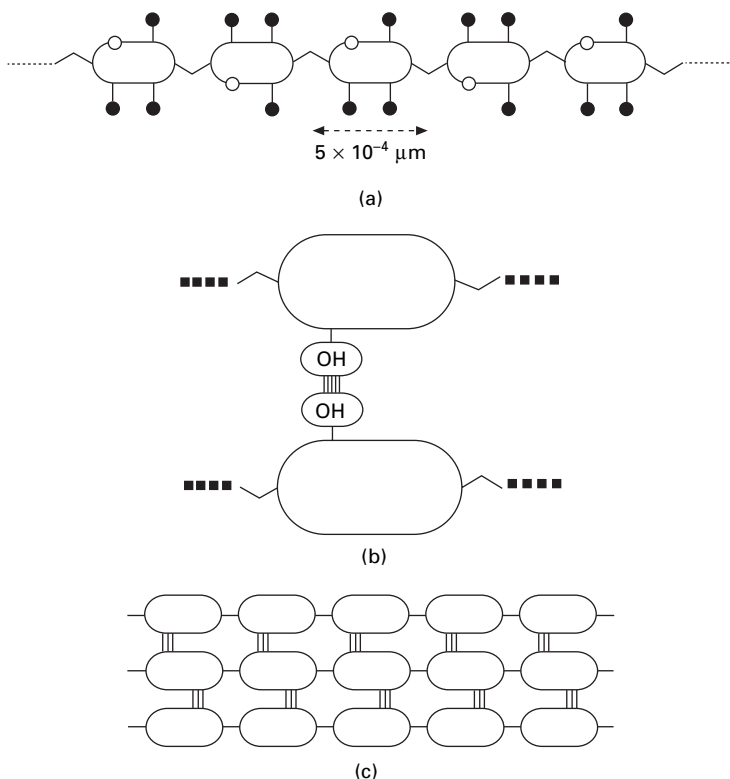
We now turn to individual fibre types and discuss their chemical constitution, fine structure and larger-scale morphology. Cellulose fibres, particularly cotton since it continues to account for a major share of the world's fibre usage, will be covered first.

The cellulose molecule consists of a series of glucose rings joined together, with the formula:



It is instructive to consider a simple schematic representation of its essential features. It is a long-chain molecule (Fig. 1.25(a)), made up of groups that are linked together by valency bonds. The strength of these bonds is such that, if the whole strength of the chain could be utilised, it would have a strength more than ten times as great as that of the strongest commercial cellulose fibre. The chain can be extended in length indefinitely. A minor feature that is worth noting is that the chain has direction, owing to the asymmetry of the atoms in the glucose rings. Protruding from the chain are —OH (hydroxyl) groups, which can link up with other hydroxyl groups by means of hydrogen bonds (see Section 1.1.2). This results in the linking together of neighbouring chains as shown in Fig. 1.25(b). Water molecules can also be attached by the same sort of bond. The chains have a strong preference to assemble into crystals (Fig. 1.25(c)). In non-crystalline regions, hydrogen bonds will form within the disordered assembly of chain segments.

The cellulose molecule is ribbon-like in form. Although stiff in comparison with

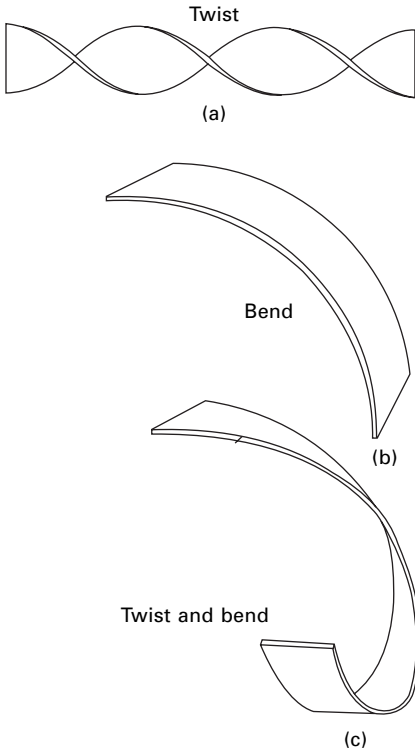


1.25 Essential features of the cellulose molecule: (a) the chain; (b) crosslinking by hydrogen bonds; (c) schematic representation of a crystal.

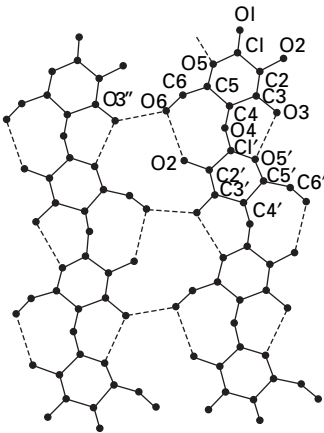
a molecule such as polyethylene, the ribbon does have considerable freedom to bend and twist in the way indicated in Fig. 1.26. As shown in Fig. 1.27, the hydrogen bonding is partly intramolecular and partly intermolecular. An important feature is that the bonding is only in one plane, which gives sheets of molecules only weakly linked between the sheets by van der Waals forces.

Because of the problems of dissolving cellulose, exact determination of the distribution of molecular weights is difficult [43]. In native cellulose fibres, the chains are estimated to contain about 10^4 glucose rings. The complete chain is, therefore, about $5\text{ }\mu\text{m}$ long by $8 \times 10^{-4}\text{ }\mu\text{m}$ wide. This ratio of length to width is about the same as that in a cotton fibre ($3 \times 10^4\text{ }\mu\text{m}$ long by $15\text{ }\mu\text{m}$ wide). In making a viscose solution for spinning into rayon, the chain length is considerably reduced. This demonstrates a general dilemma in manufactured fibre production. Increased chain length in the fibre would give better properties, but if the molecules are too long, extrusion into fibres is not possible.

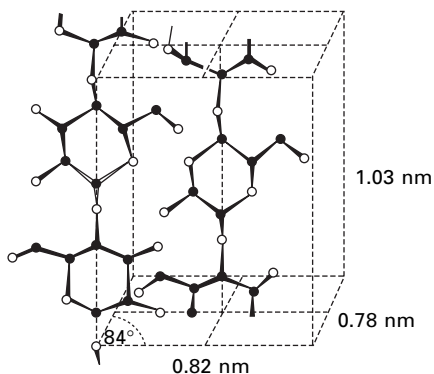
The crystal structure of native cellulose is known as cellulose I, but there is still some uncertainty about its exact form. A slightly modified version of the structure proposed by Meyer and Misch [44] is shown in Fig. 1.28 and gives the features needed to understand structure–property relations. Different studies give the following



1.26 Ways in which a ribbon-like molecule can be deformed by twisting and bending.



1.27 Hydrogen bonding between cellulose molecules. C1, O1, etc., are positions of carbon and oxygen atoms; hydrogen atoms complete the valencies; hydrogen bonds are shown by dotted lines. From French (42).



1.28 A schematic view of the crystal lattice of cellulose I, adapted from the drawing by Meyer and Misch [44], which has anti-parallel chains. Hydrogen bonded sheets are in the plane of the paper. The sheets in the middle of the cell are staggered with respect to those on the front and back faces.

ranges for the cell dimensions [42]: a , 0.814–0.825; b , 0.778–0.786; c , 1.033–1.038 nm. When these fibres are mercerised, by treatment with strong caustic soda, a second X-ray diffraction pattern appears superimposed on the original one, replacing it as mercerisation becomes complete. This corresponds to a structure known as cellulose II. The a and b dimensions are close to those for cellulose I, but the c value is 0.914 nm and the angle between b and c is 62° compared with 84° for cellulose I. Regenerated-cellulose fibres also contain cellulose II. It is generally thought that cellulose I is a parallel structure with chains pointing in the same direction but cellulose II is anti-parallel. Other crystal forms are found after some treatments [42].

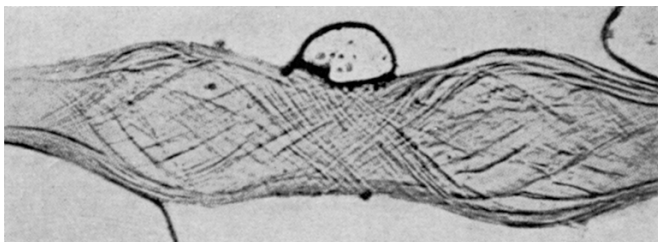
Mercerisation also results in a reduction in the proportion of crystalline material present in the fibres. In addition to mercerisation, which is a fairly old process, there are other forms of modification of cellulose fibres, particularly cotton, that are of commercial importance. Various chemical treatments replace the hydroxyl groups in the non-crystalline regions by other groups in order to modify such properties as electrical resistance, moisture absorption and rot resistance. However, the most important treatments are those that cause a resin to polymerise and react with the hydroxyl groups inside the cotton. This results in chemical crosslinks (sequences of covalent bonds) between the cellulose molecules. This stabilises the structure, gives it a set and, in fabric form, reduces the likelihood of creasing and wrinkling. Resin-treated crosslinked cottons of this type are now of great importance.

1.4.2 An integrated view of the fine structure of cotton

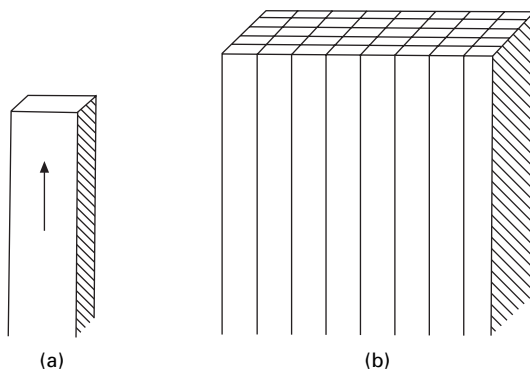
The evidence from many sources that cotton and other natural cellulose fibres are ‘two-thirds crystalline, one-third non-crystalline’ is somewhat misleading. One should really say that the X-ray-diffraction pattern (density, accessibility, etc.) is such that it is equivalent to that of a mixture of large crystalline regions and large amorphous regions in the ratio 2:1. Other interpretations are possible. Hearle [38] has pointed out that the X-ray diffraction results could be explained by the small size of the

crystalline fibrils, the density by imperfect packing and the accessibility by the fibril surfaces. The current consensus is that natural cellulose fibres are essentially 100% crystalline and that the disorder is mainly due to the fact that very small crystalline units are imperfectly packed together. The amount of actual material in any region that is not part of a crystal lattice is probably small.

An important feature of natural cellulose is that it is aggregated into fine microfibrils. A coarse fibrillar structure was observed many years ago under the optical microscope, as shown in Fig. 1.29, and is rather clearly shown in SEM pictures, such as the fibre fracture shown in Fig. 19.14 on page 517. The examination of surface replicas or disintegrated material showed up the presence of the ultimate microfibrillar texture. The biological evidence is that, in growing cells, enzyme complexes join glucose molecules into long-chain cellulose molecules. These naturally form microfibrils with thicknesses of about 4 nm. All the molecules will point in the same direction in the parallel crystal lattice of cellulose I without chain folding. The fine structure is an assembly of fine microfibrils without amorphous regions as proposed by Manley [45]. The crystallisation is driven by minimisation of the free energy. Since the strongest attractions are at the edges of the molecules, as indicated in Fig. 1.30(a), the minimum energy form is likely to be a ribbon-like crystal of the type shown in Fig. 1.30(b). At this scale, the proposed units can be identified with the observed microfibrils.



1.29 Fibrillar structure of cotton, as shown by an optical microscope. Photograph by W. L. Balls.



1.30 (a) Schematic representation of single cellulose molecule. (b) Assembly in microfibril.

The fibrils themselves have many of the characteristics of molecules. They are relatively small in cross-section (less than an order of magnitude greater than a single molecule), they are relatively flexible, and they are attracted to one another strongly by the possibility of hydrogen bonding at the edges and more weakly by van der Waals forces between the faces. The fibrils can thus be expected to 'crystallise' into flat sheets or lamellae, which will then stack in parallel layers. There is evidence of long standing of coarse concentric lamellae observed in the optical microscope, and a lamellar association of fibrils on a finer scale is also found in electron microscope studies.

The model described above is one that commands confidence because it can be derived either from a theoretical consideration of how the system would be expected to behave or by deduction from experimental observations of real cellulose fibres. But the model is too simple and tidy. It omits the disorder that is known to be present.

As it stands, the whole assembly of molecules would be regarded as coalescing into one single crystal, in which the identity of the original fibrils was lost. Remembering that the crystal lattice has not been settled, one is tempted to speculate whether, as in some other systems, such as asbestos, there is some special feature of the cellulose crystal lattice that gives an identity to the fibrils. The problem has an analogy in the behaviour of yarns. If two zero-twist continuous filament yarns are brought together, they merge, and it becomes impossible to say to which yarn a given fibre belongs. However, if the individual yarns have some twist, they retain their separate identities.

Detailed experimental evidence on disorder comes from the electron diffraction studies of Ingram [46], which show that, whereas there is often crystallographic register between adjacent fibrils, this does break down in places, and also that, at intervals along the fibres, there are positions in which the crystal lattice is defective. It remains a matter of speculation whether these discontinuities are due to chance fluctuations in the system, to some structural feature such as is hinted at in the last paragraph, or to an occasional chemical discontinuity in the cellulose molecules.

There is one source of disturbance of the simple model that is clearer. The fibrils are laid down on the inner surface of cell walls in a helical orientation. Even in a single layer, this must give rise to some strain and possible splitting between fibrils. In some plant cells, the successive layers run in different directions, so that the register between layers would be lost. Even when a similar helical orientation persists through the thickness, as in the secondary wall of cotton, complete crystallographic register is impossible between successive layers, since each layer must contain fewer chains and fibrils as the circumference is reduced. Splitting between lamellae will be relatively easy.

Finally, but perhaps most important of all, the influence of water in leading to disorder must be considered. In the presence of water, the minimisation of free energy by crystallisation is always in competition with minimisation by forming hydrogen bonds by association with water, in other words by swelling, by the attempt to go into solution.

The formation of the fibre occurs in the wet state, and it is thus highly swollen. When drying does occur, the fibrils will associate, as already suggested, but, like any crystallisation of long-chain units, appreciable disorder might be introduced owing to

some entanglement or mismatching of fibrils. Subject to these limitations, the material would be expected to collapse down to a somewhat disordered modification of the model already discussed, which, in its idealised form without any disorder, would be the presumed minimum energy state for dry natural cellulose.

What happens on re-exposure to water? Experimentally, it is known that there is a progressive increase in absorption as humidity increases and that in liquid water there is limited swelling but not solution of the material. One can suggest three reasons why the fibrillar network does not dissociate completely in water:

1. Once strain is relieved by some opening up of the structure, regions where fibrils are in crystallographic register with one another may remain as stable entities.
2. There may be that a dynamic equilibrium, in which there are always some fibrils associated together, although the actual groups are continually changing.
3. There may be some tie-molecules linking separate fibrils together.

At any ordinary relative humidity, the network would be partly opened up, whereas in water, where much chemical processing is done, the fibre would be much more highly swollen. Crosslinking reactions will serve to stabilise the structure by linking the fibrils together permanently: this gives rise to increased resistance to plastic deformation.

1.4.3 The gross morphology of cotton

The cotton fibre appears as a long, irregular, twisted, and flattened tube, tapering somewhat at its tip. [Figure 1.31\(a\)](#) is a typical illustration of the middle portion of a cotton fibre, showing the presence of convolutions. These are more strikingly shown in an SEM picture ([Fig. 1.31\(b\)](#)). Hearle and Sparrow [47] showed, by comparison with observations of a rubber tube, that the formation of convolutions was a natural consequence of the collapse of a helical structure. For American Upland cottons, measurements with an opto-electronic sensor show 11 to 13 crimps/cm [48].

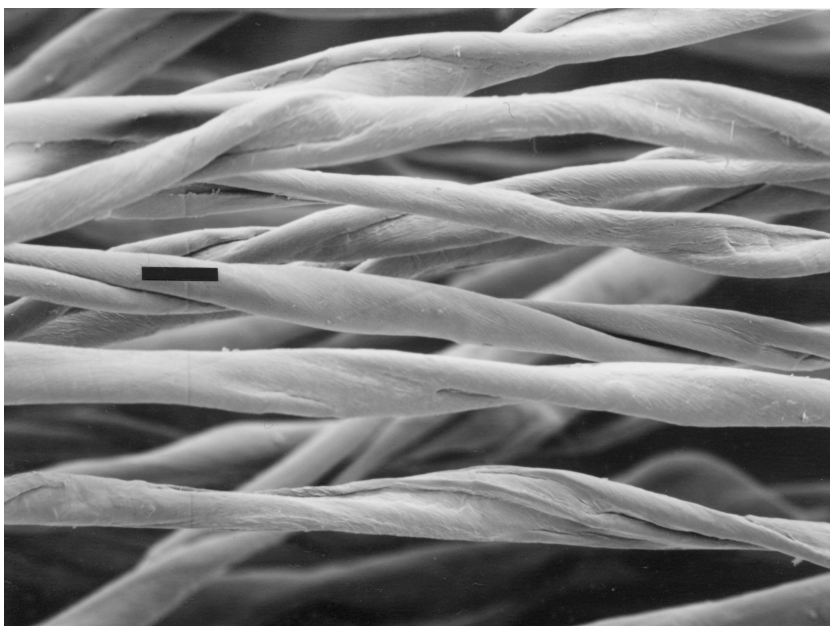
In cross-section, mature fibres have the form shown in [Fig. 1.32](#). On the outside there are a thin cuticle and primary cell wall and in the centre there is a narrow collapsed lumen, but the bulk of the fibre is made up of the secondary cell wall. During growth, this is deposited on the inside of the primary cell wall, in a series of daily growth-rings as shown in [Fig. 1.33](#). [Figure 1.34](#) shows a schematic representation of the various layers of which the fibre is composed. The layers themselves will be made up of stacks of the lamellae described in the last section.

Hebert [50] reports that the primary wall has a 'basket-weave orientation or alignment of the fibrils'. Studies of fibres at two weeks post-anthesis (after flowering) indicate that the primary wall has a crystallinity index of 30% and a fibril diameter of 2.98 nm, compared with 70% and 4.22 nm for mature fibres at seven weeks post-anthesis [51].

In the thick secondary wall (S_2 layer), there is a helical orientation of molecules and fibrils. It may be noted that the helical orientation can be shown up in various ways: optical birefringence, for direction of the chain molecules; X-ray diffraction, for the axis of the crystal lattice; electron microscopy, for the microfibrils; optical microscopy, for the coarse fibrils. There has been some uncertainty as to whether the



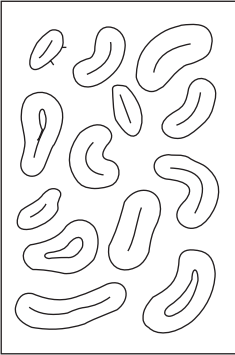
(a)



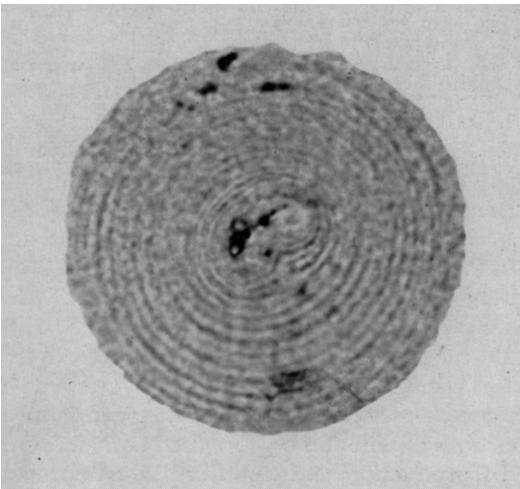
(b)

1.31 Cotton fibre: (a) portion of cotton fibre (photograph by E. Slattery); (b) scanning electron micrograph of convolutions in mature cotton fibre, bar = 18.9 μm .

pitch or the angle of the helix remains constant: the evidence now indicates that the angle is almost constant through the fibre. At intervals along the fibre, the sense of the helix reverses, as shown in Fig. 1.35. It was once thought that the helix angle varied with fibre variety, but Hebert *et al.* [52] and Morosoff and Ingram [53] indicated that, if a correction is made for the effect of convolutions, the helix angle is always the same, independent of genetic variety, and through most of the thickness a value in the range 20–23°, though it may be up to 35° in the outer layers. On drying, the fibre collapses to give the typical cross-sectional shape shown in Fig. 1.36. Kassenbeck [54] has pointed out that, after collapse, the different regions of the cotton fibre, indicated in Fig. 1.37, have important differences in structure. As can be expected from the collapse of a cylinder composed of concentric lamellae, and is easily



1.32 Typical cross-sections of mature cotton fibres.

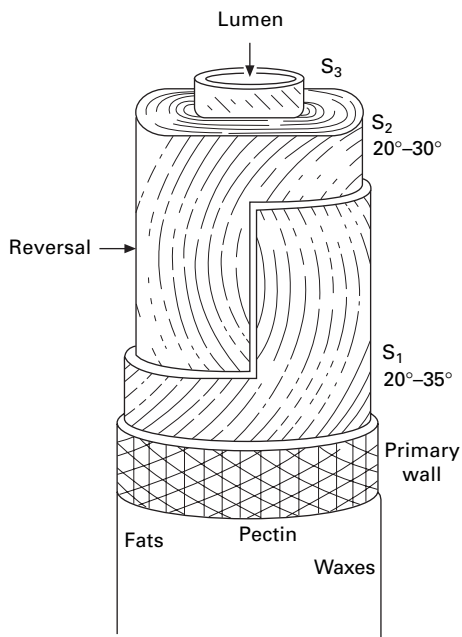


1.33 Cross-section of swollen cotton fibre showing daily growth rings. Photograph by US Department of Agriculture, after Kerr [49].

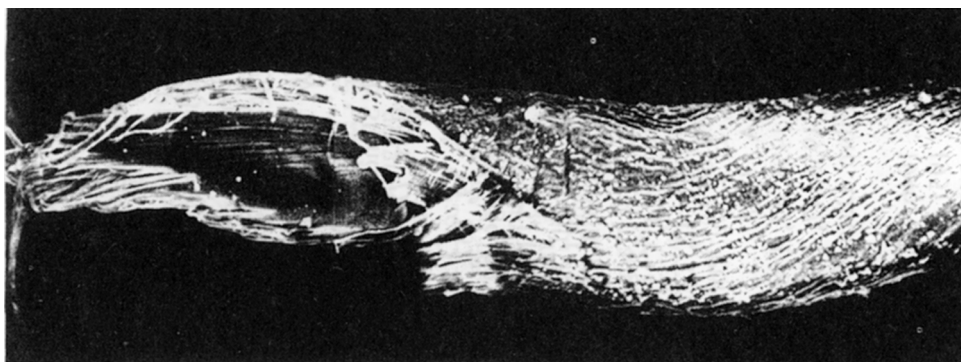
demonstrated by collapsing a roll of adhesive tape, there will be: (a) an appreciable opening up of structure in the regions C and N, where there is reversal of curvature, and thus an excess circumferential length; (b) a tightening in region A, where there is an intensification of curvature; and (c) little change in tightness in region B. Kassenbeck has shown that regions C and N are the most susceptible to chemical reaction and that A is the least susceptible.

1.4.4 Other natural cellulose fibres

Other cellulose fibres, such as flax, hemp, jute and sisal, differ from cotton in several ways. They often contain a larger proportion of non-cellulosic impurities. They are all multicellular fibres, with very small individual cells bonded together into long strands in the plant stem or leaf. During the preparation of the material for processing,

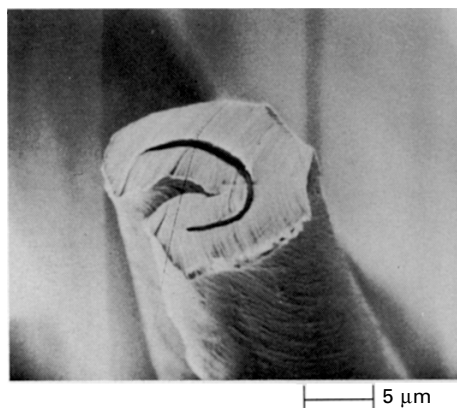


1.34 Morphological structure of the cotton fibre. From Jeffries *et al.* [20].

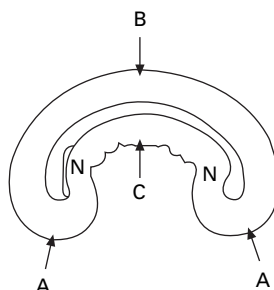


1.35 Scanning electron micrograph showing reversal adjacent to back of a cotton fibre.

the strands are broken down into shorter fibres. The fibre dimensions are, however, somewhat indeterminate, since the extent of breakdown may vary. In all natural cellulose fibres, the molecules are highly oriented parallel to one another in fibrils, but they spiral round the fibre, thus reducing the degree of orientation parallel to the fibre axis. In flax, ramie, hemp and other bast fibres, the spiral angle is small, less than 6° , so that these fibres are highly oriented and give high strength and low extensibility.



1.36 Scanning electron micrograph of cotton fibre cross-section. Picture by J. T. Sparrow.



1.37 Zones A, B, C and N in a mature cotton fibre. From Kassenbeck [54].

Table 1.4 Different forms of regenerated cellulose and modified cellulose fibres

Type	Process and structure-determining factors
Nitrocellulose ^a	Regeneration of cellulose nitrate
Cuprammonium	Solution in cuprammonium hydroxide; coagulation in water
First viscose rayon	Sodium cellulose xanthate in caustic soda into acid bath
Viscose, regular ^b	Zinc salt added to acid bath, giving skin-core structure
Lilienfeld ^a	Viscose into 65% sulphuric acid with concurrent stretch
Fortisan ^a	Regenerated from highly stretched acetate fibres
High-tenacity (HT) viscose ^b	High zinc and modifiers in solution; 'all skin'
Modal staple ^c	Modifications to viscose and weak acid bath
Polynosic ^c	High-viscosity viscose allowing gel formation
Crimped staple	Viscose modifications cause skin bursting
Cordenka HT yarn	Addition of formaldehyde to viscose process
Lyocell, e.g. Tencel	Regeneration from solution in an amine oxide
Liquid-crystal routes ^d	Cellulose derivatives in organic solvents or inorganic acids
Fibre B ^e	Liquid crystal solution in phosphoric acid into acetone
Acetate	Secondary cellulose acetate dry spun from acetone solution
Triacetate	Cellulose triacetate dry spun from CH ₂ -CCl ₂ solution

^aNot now commercial.

^bCoagulation + regeneration → stretch.

^cCoagulation + stretch → regeneration

^dVarious patented processes, not commercialised.

^eLaboratory process by Boerstel [55].

1.5 Regenerated and modified celluloses

1.5.1 Manufactured cellulosic fibres

Since the first production of regenerated cellulose fibres at the end of the 19th century, many different forms have been produced, as shown in Table 1.4. The degree

of polymerisation in ordinary rayon is of the order of 500, which is less than one-tenth of the length of the molecules in native cellulose, but may be higher in improved forms. The crystal structure of regenerated-celluloses is cellulose II. The proportion of crystalline material present is low, being about one-third of the total, except for the experimental liquid-crystal fibres. The degree of orientation of regenerated-cellulose fibres depends on the extent to which they have been stretched during spinning. Values of the optical orientation factor (that is, the ratio of the birefringence of the fibre to the birefringence of a fibre with perfect axial orientation of the molecules) are given in Table 1.5, together with those of some natural fibres for comparison. With fibres of such a low degree of order, there must be substantial non-crystalline regions, and the most likely view of the fine structure of ordinary viscose rayon is the fringed-micelle structure, as discussed in Section 1.3.2 and shown in Fig. 1.16. The stiffness of the cellulose molecule would inhibit chain folding at the ends of crystallites. The disorder in the solution will result in chains folding back on themselves in non-crystalline regions. There are other forms of viscose rayon, and we must consider the diversity.

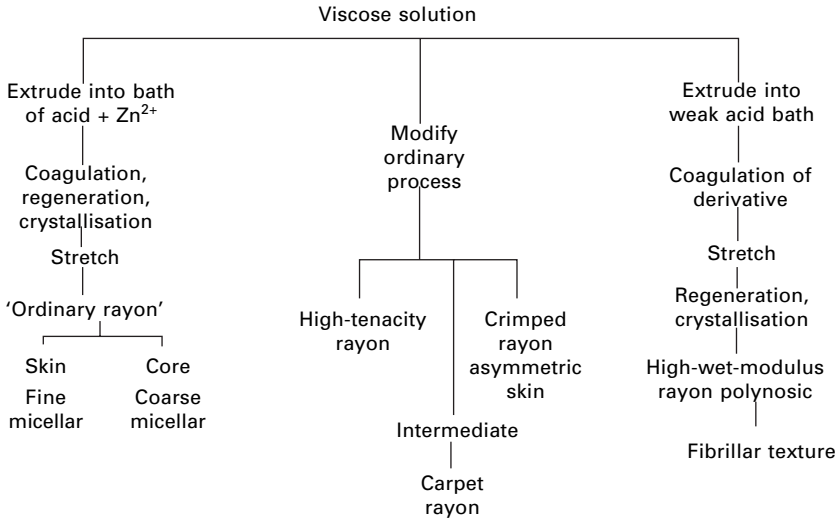
1.5.2 The diverse forms of viscose rayon

Figure 1.38 shows various routes of regeneration of fibres from a viscose solution. In the ordinary process, the resulting fibre has an irregular cross-section with a marked difference between skin and core, as shown in Fig. 1.39. The skin forms immediately after extrusion and then collapses as solvent is removed. The lateral pressures push the ribbon-like molecules into what starts as radial orientation in the plane of the cross-section, though this swings round to a perpendicular direction in the cusps of the serrations. The orientation effects are shown up by examination in polarised light, as in Fig. 1.39.

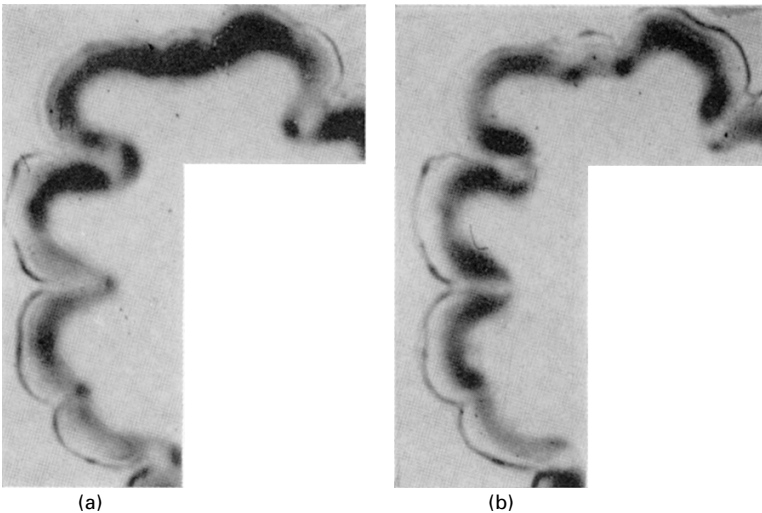
The skin is believed to have a finer texture than the core and to be stronger. It is formed by regeneration through the intermediate zinc cellulose xanthate. The rates of the alternative reactions are such as to favour this route over direct regeneration of the sodium salt by the acid, but it is prevented in the core because the low mobility of the zinc ions prevents them from getting in fast enough. The finer texture of the material regenerated indirectly is probably due to the fact that the bivalent zinc ions will attract the molecules into a network before regeneration.

Table 1.5 Optical orientation factors of cellulose fibres, (after Hermans [56])

Fibre	Orientation factor
Viscose rayon, low stretch	0.54
Viscose rayon, high stretch	0.88
Cuprammonium rayon	0.74
Ramie	0.97
Sea Island cotton	0.72
American cotton	0.62

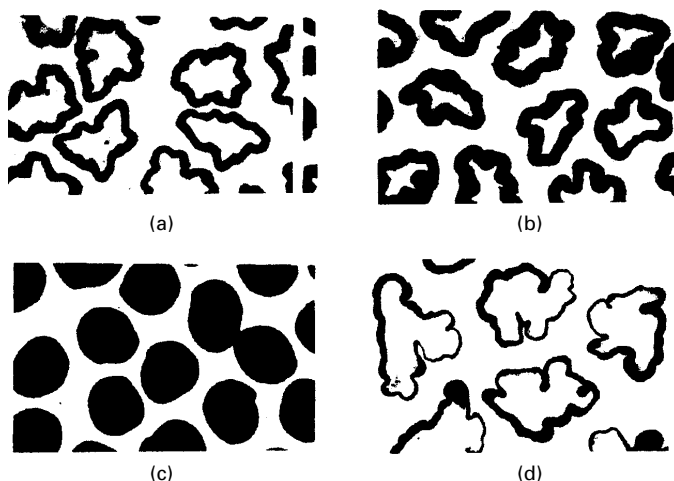


1.38 Schematic representation of fibres produced by the viscose process.



1.39 Section of viscose rayon fibre, dyed with Sky-Blue FF, showing optical dichroism when viewed in polarised light. The dark patches in the skin correspond to orientation of the crystallites parallel to the direction of polarisation: (a) plane of polarisation is N-S; (b) plane of polarisation is E-W. After Joshi and Preston [57].

As shown in Fig. 1.40, various modifications of the process have led to an increase in skin thickness and, ultimately, to all-skin fibres with a round cross-section. These are the high-tenacity rayons, introduced first for tyre cords but now also used for other textile purposes. There is also attention to other details, such as the distribution of chain lengths, in the later high-tenacity rayons. In another modification, an



1.40 Cross-sectional shapes of viscose fibres with differential dyeing of skin: (a) regular viscose rayon; (b) *Tenasco*, early high-tenacity rayon with thicker skin; (c) *Tenasco* Super 108, an 'all-skin' fibre; (d) crimped staple viscose rayon with asymmetric skin. From Woodings [58].

asymmetrical skin, caused by the first skin bursting open, is produced; these are the crimped rayons.

A greater difference occurs in the production of high-wet-modulus (modal or polynosic) rayons. A solid fibre of a cellulose derivative is first formed and oriented by stretching. Regeneration of cellulose and crystallisation then occur in what is already a solid, oriented fibre. The resulting structure is fibrillar in texture, and the fringed-fibril structure (Fig. 1.19), is probably the best model. Lyocell fibres such as *Tencel* [59], which are directly regenerated from an organic solvent of cellulose, are fibrillar in texture. The bonding between fibrils is weak, so that fibrillation occurs easily. This can be a defect, but can also be exploited to make a soft fabric.

In all these forms of rayon, the degree of orientation can be varied by altering the amount of stretch, though there are limits to the extent to which this is possible. A higher orientation can be produced in the more weakly bonded acetate fibres, and regeneration of cellulose was then used to make *Fortisan*, which was a highly oriented, high-modulus fibre that is no longer made. High crystallinity and high orientation can be achieved by liquid crystal routes, similar to those used for aramid fibres, but the side groups on the cellulose molecule mean that the achievable mechanical properties are less good.

Cellulose fibres may also be modified by additives, e.g. delustring by titanium dioxide, or by chemical reactions used to crosslink the cellulose molecules.

1.5.3 Cellulose acetate

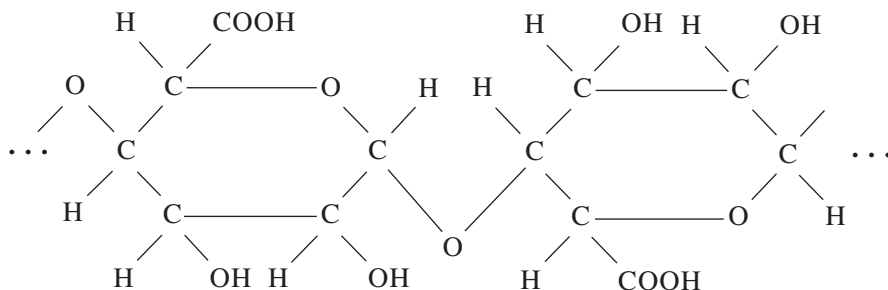
In acetate fibres, the most important of the chemically modified cellulose fibres, the cellulose is chemically treated in solution so that the hydroxyl groups are replaced by

acetyl ($\text{CH}_3\cdot\text{CO}\cdot\text{O}-$) groups. In ordinary commercial acetate (more exactly known as secondary cellulose acetate), about five out of six of the hydroxyl groups are replaced in this way. Fibres made of this material contain a smaller proportion of crystalline material than do regenerated celluloses. There are three reasons for this reduction in crystallinity: (a) the acetyl groups are comparatively inert, hydrogen bonding is not possible, and thus the attractive forces between the molecules are weaker; (b) the acetyl groups are bulky, preventing the close approach of the chain molecules; and (c) the structure is irregular, with some acetyl and some hydroxyl groups protruding from the chain, so preventing the formation of a regular crystalline order. As a consequence of these effects, acetate fibres are weaker, more extensible, and less dense and absorb less water than cellulose fibres. They also have a low softening point, whereas unmodified cellulose fibres cannot be melted and decompose first.

The large-scale production of secondary cellulose acetate was largely a historical accident arising from difficulties in the early processing of a fully acetylated cellulose. These difficulties have been overcome, and triacetate fibres, in which all the hydroxyl groups are replaced by acetyl groups, have been produced. Because of the greater regularity of structure, these fibres are more highly crystalline than ordinary acetate fibres. They also absorb less water because of the removal of all the hydrophilic hydroxyl groups. Their practical advantages are a higher softening point, greater dimensional stability, and the fact that materials made from them are crease-resistant and can be heat-set.

1.5.4 Alginate and other fibres

Alginic acid, which can be obtained from seaweed, has the formula:



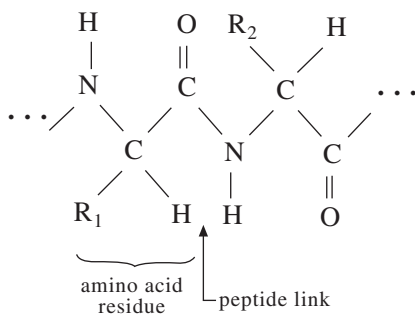
Highly oriented and highly crystalline alginic acid fibres can be obtained, but they are subject to degradation because of their acidity. The acid may be neutralised to give metallic salts, which will also form fibres. Calcium alginate is soluble in soap and water and can be exploited as removable scaffolding threads in fabrics. Crosslinking is needed to give stability for ordinary use.

Various other polysaccharides, such as chitin and its derivative chitosan, are made into fibres for medical uses.

1.6 Protein fibres

1.6.1 Protein chemistry

Proteins are formed by the polymerisation of amino acids (with the general formula $\text{NH}_2\cdot\text{CHR}\cdot\text{COOH}$) by means of peptide links ($\text{—CO}\cdot\text{NH—}$) to give long-chain molecules with the general formula:



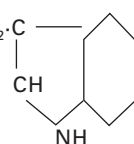
Twenty amino acids are named and represented by three or one letter designations. They contain different side groups (R_1 , R_2 , etc.). It is the variation in the order and amount of these groups that determines the properties of the material and gives rise to the large number of natural proteins that play a vital part in animal and plant life. In effect, there is an 'alphabet' of side groups. Advances in proteomics and the link to DNA have enabled the amino acid sequences in proteins to be accurately determined. An old estimate in [Table 1.6](#), which is adequate for our purposes, gives comparative proportions occurring in the raw materials of various protein fibres. This is a list of 18 amino acids because the amides asparagine and glutamine are included with aspartic and glutamic acids. It should be noted that these figures are approximate, since the chemical constitution of the protein may vary from fibre to fibre, or even from one part of a fibre to another. More recent figures for wool are given by Höcker [61].

Two forms differ from the simple formula. Proline has a ring of three $\text{—CH}_2\text{—}$ groups, which join on to replace —H in the neighbouring —NH group and distort the form that the molecule can take. Cystine, which links neighbouring chains, is derived from cysteine, $\text{R} = \text{—CH}_2\cdot\text{SH}$, which is the amino acid, by a subsequent reaction.

There are various sorts of crosslinks that can form between neighbouring protein molecules.

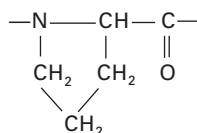
- Hydrogen bonds can form between the —NH— and —CO— groups, linking neighbouring main chains together:

Table 1.6 Side groups in protein fibres (after Harris [60])

Type	Side group	Amino acid	Proportion (g amino acid per 100 g protein) in:		
			Silk fibroin	Wool keratin	Casein
Inert	—H	Glycine	43.8	6.5	1.9
	—CH ₃	Alanine	26.4	4.1	3.5
	—CH(CH ₃) ₂	Valine	3.2	5.5	6.02
	—CH ₂ ·CH(CH ₃) ₂	Leucine	0.8	9.7	10.55
	—CH(CH ₃)·CH ₂ ·CH ₃	Isoleucine	1.37	—	5.27
	—CH ₂ ·C ₆ H ₅	Phenylalanine	1.5	1.6	6.46
Acidict	—CH ₂ ·COOH	Aspartic acid	3.0	7.27	6.70
	—CH ₂ ·CH ₂ ·COOH	Glutamic acid	2.03	16.0	22.03
Basic†	—CH ₂ ·CH ₂ ·CH ₂ ·CH ₂ ·NH ₂	Lysine	0.88	2.5	8.25
	—(CH ₂) ₃ ·NH·C(NH)NH ₂	Arginine	1.05	8.6	3.94
	$ \begin{array}{c} \text{N:CH} \\ \\ \text{—CH}_2\text{—} \diagdown \text{C:CH} \diagup \text{NH} \end{array} $	Histidine	0.47	0.7	3.24
Hydroxyl	—CH ₂ OH	Serine	12.6	9.5	5.87
	—CH(OH)·CH ₃	Threonine	1.5	6.6	4.53
	—CH ₂ ·C ₆ H ₄ OH	Tyrosine	10.6	6.1	6.28
Ring‡	$ \begin{array}{c} \text{—CH}_2\text{—} \diagup \text{CH}_2 \\ \diagdown \\ \text{—CH}_2\text{—} \end{array} $	Proline	1.5	7.2	10.54
Double§	—CH ₂ ·S·S·CH ₂ —	Cystine	—	11.8	0.40
Miscellaneous	—CH ₂ ·CH ₂ ·S·CH ₃	Methionine	—	0.35	3.50
	$ \begin{array}{c} \text{—CH}_2\text{—C—} \\ \\ \text{CH} \\ \\ \text{NH} \end{array} $ 	Tryptophane	—	0.7	1.37

†May be present in ionised forms, e.g. —CH₂·COO and —(CH₂)₄·NH₃⁺. The acids may also be present as acid amides, e.g. —CH₂·CONH₂.

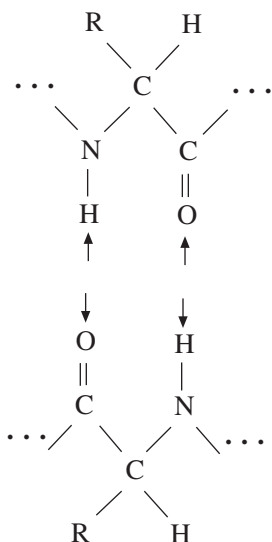
‡Fits into the chain molecule as:



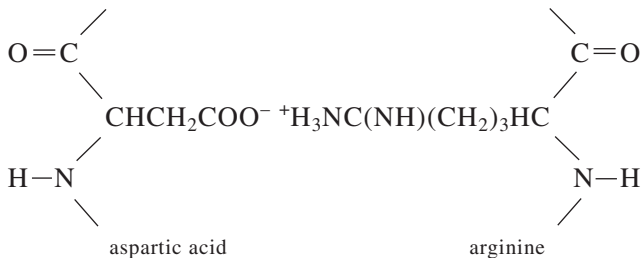
This results in some distortion and loss of flexibility in the chain.

§Joins on between two protein chain molecules or between two positions in the chain.

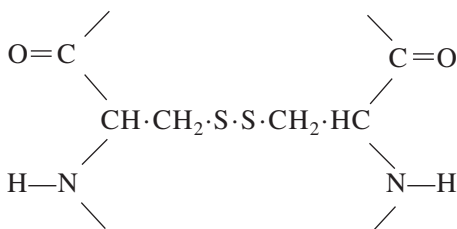
There may also be small amounts of the related cysteine, cysteinic acid, lanthionine and thiocysteine groups.



- Hydrogen bonds may form between hydroxyl groups present in the side chains.
- Since there are both acidic and basic side chains, salts may form between them, holding the side chains together by electrovalent forces. A typical example would be:



- The cystine linkage is a covalent crosslink between adjacent chains, which turns the many chain molecules into a single network molecule. The linkage is:



All these crosslinks play an important part in determining the form of the protein. For example, single long-chain molecules may fold up into a compact ball held together by internal crosslinks; these are known as *globular proteins*, and their large molecules will crystallise in the same way as inorganic molecules. Alternatively, the molecules

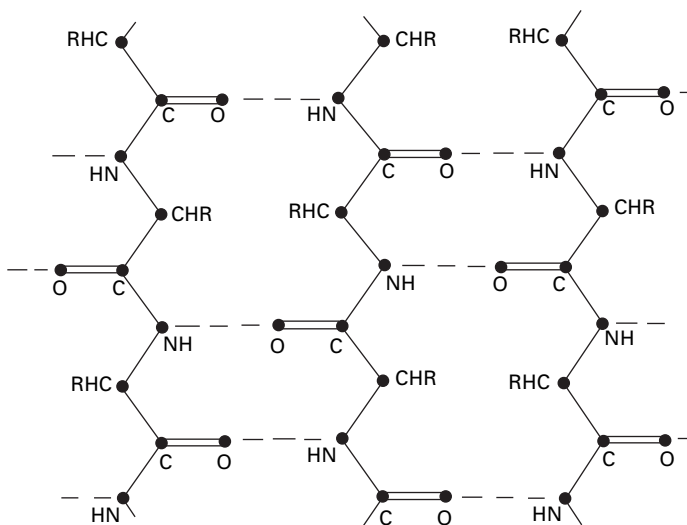
may be more or less extended and linked to their neighbours; these are the *fibrous proteins*. Globular proteins may be unfolded, or denatured, by heat or other chemical treatments and can then be drawn into fibres.

1.6.2 Silk

The two most important protein fibres for textile uses are silk and wool. The main constituent of silk is one of the simpler proteins, *fibroin*. The figures in Table 1.6 show that almost all the side groups are of four simple types: —H , —CH_3 , $\text{—CH}_2\text{OH}$ and $\text{—CH}_2\text{C}_6\text{H}_5\text{OH}$. The sulphur-containing side groups are almost completely absent, and the others are present only in small quantities. The links between molecules will therefore be mostly main-chain hydrogen bonds, with a few hydrogen bonds and salt linkages between side chains.

Examination of the X-ray diffraction pattern of silk shows that molecules in the crystalline regions must be present as fully extended chains of the sort shown in Fig. 1.41. This is a zigzag form because of the limitation on the angles between adjacent valency bonds. There is an axial repeat of 0.7 nm, corresponding to two amino acid residues. The molecules in silk are fairly highly oriented parallel to the fibre axis, and the material is moderately highly crystalline. The general structure is believed to be composed of crystalline and non-crystalline regions in the same way as cellulose, though the mode of formation may mean that there is little or no folding of chains back on themselves.

It has been suggested [62] that in the fibroin molecule, which is about 140 nm long, there are two segments, about 17 nm long, in which all the tyrosine and other bulky side groups are concentrated, the rest of the molecule being entirely of glycine, alanine and serine side groups. The segments with bulky side groups would not



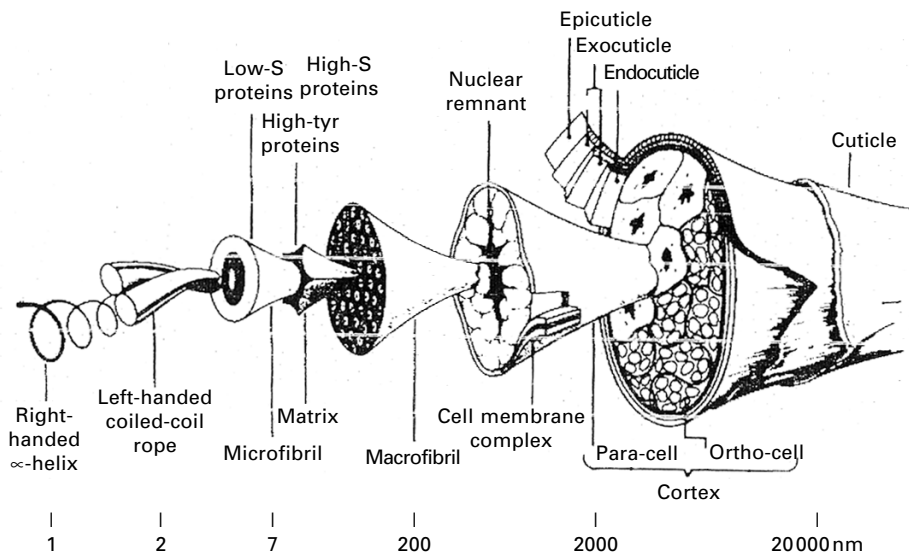
1.41 Extended-chain molecules of silk fibroin and β -keratin, packed in sheets in crystal.

crystallise so easily and would therefore form the major part of the non-crystalline regions, while the crystalline regions would be made up from the parts of the molecules with simple, easily and regularly packed side groups. This would make silk a natural block copolymer (see [Section 1.7.1](#)), composed partly of crystallisable and partly of non-crystallisable segments. Thus, in considering effects occurring mainly in the non-crystalline regions (for example, moisture absorption), the presence of certain side groups in much higher proportions than in the silk as a whole must be taken into account.

The silk fibre, as it is spun by the silkworm, consists of two triangular filaments of fibroin, stuck together with a gum called sericin.

1.6.3 Molecular form and assembly in wool (levels 2 to 6)

Wool and hair have the most complicated structures of any textile fibres (Fig. 1.42), with ten levels of structure from fundamental particles to the whole fibre ([Fig. 1.43](#)) [63]. The specific features start at level 2, the molecular constitution. [Table 1.6](#) shows that almost all possible side groups are present in appreciable proportions. Many of these contain active groups so that side-chain linkages are important. The values in [Table 1.6](#) for wool keratin are for whole fibres, which actually consist of many proteins in different parts of the fibres. In particular, there are differences of composition between the crystalline microfibrils (intermediate filaments, IFs)⁴, which make up about 40% of the fibre, and the amorphous matrix [61].



1.42 Structure of wool fibre, as drawn by Robert C. Marshall, CSIRO, Melbourne.

⁴Microfibril, often abbreviated to fibril, is the term used in describing fibre structures and is most appropriate when discussing the relation to properties. Intermediate filaments is a term used in biology to describe a category of protein structures with many functions in living organisms. Hard keratins, such as hair, and soft keratins, as in skin, constitute one group of intermediate filaments.

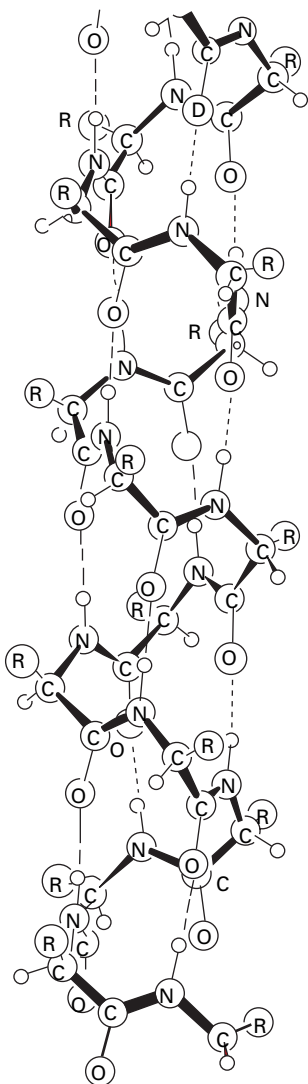
Level		Fibre structure						
9 20 cm × 20 μm		Whole fibre: length, area, shape, scales, crimp, variability						
8	Med- ulla	Cortex				Cuticle		
		Ortho	Para	Meso				
7 2 μm		Cells: major part + nuclear remnants			CMC	Endo	Exo	Epi
6 0.2 μm		Macrofibrils + matrix			Lipids, proteins etc.			
5		Whorls	Parallel array					
4		Composite of: Microfibril + Matrix				Protein etc.	Protein etc.	Lipid etc.
3 7 nm		Intermediate filaments	Matrix detail		Surface chemistry			
2 1 nm	Keratin proteins	Keratin-associated proteins						
1 0.5 nm	Atoms							
0	Fundamental particles: quantum theory							

1.43 Levels of structure in wool and hair (CMC = cell membrane complex).

The protein families in wool are (a) two low-sulphur IF keratins, which contain relatively simple, crystallisable sections, joined to terminal domains with a more complex chemistry, containing cystine and making up part of the non-crystalline material; (b) high-sulphur and high-glycine/tyrosine keratin-associated proteins, which contribute the remainder of the non-crystalline regions. Because of the high concentration of crosslinking cystine, the non-crystalline material acts as a rather highly crosslinked amorphous polymer.

Two different crystal structures, with different X-ray diffraction diagrams, can occur in keratin (and in many other similar proteins). In wool as grown and used, there is a structure known as α -keratin, but, if the fibre is stretched (and it can be extended up to 50% in water, or a maximum of 100% in steam), there is a gradual and reversible transformation to another form known as β -keratin, which has an X-ray diffraction pattern similar to that of silk fibroin (Fig. 1.41). This is, therefore, an extended chain, but the axial repeat in β -keratin is only 0.68 nm, indicating that there is some slight distortion.

The crystal structure of α -keratin is a slightly distorted form of the helical structure proved for simple synthetic polypeptides by Pauling and coworkers [64, 65]. In earlier models, such as that proposed by Astbury and Bell [66], it had been taken for granted that chemical and fold repeats must coincide, but, in fact, this is unnecessary. In Pauling's α -helix, there are 3.6 amino acid residues per turn, with the length of one turn giving the axial repeat of 0.55 nm. An impression of the model is given in Fig. 1.44. In keratin, the axial repeat is only 0.51 nm. There may be some crumpling of the helix in order to fit in bulky side groups. However, the shortening can mostly be

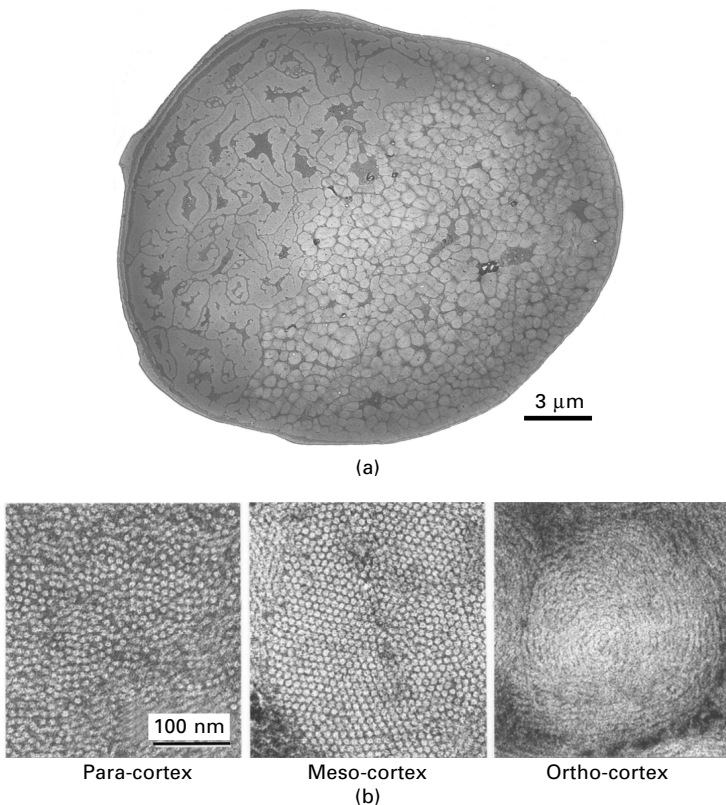


1.44 α -Helix structure for polypeptides and proteins suggested by Pauling.

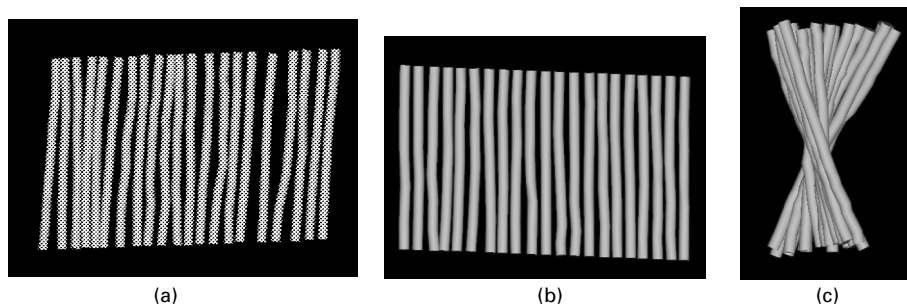
attributed to the multiple twisting of the molecules: two chains form a dimer, two dimers a protofilament, two protofilaments a protofibril, two protofibrils a half-filament, and two half-filaments giving an intermediate filament with 32 molecules in the cross-section [61].

In considering the physical properties, however, the exact details of the molecular folding are of less importance than the fact that the helical form of α -keratin molecules allows them to be opened out to extended chain β -keratin, giving a high extensibility. It is also possible, by appropriate relaxation treatments in steam, to contract the fibres to a length about 30% less than the original unstretched length. In these *supercontracted* fibres, the molecules must be still more highly folded, or randomly coiled, or recrystallised without axial orientation.

The microfibrils in wool are about 7 nm in diameter, packed at spacings of about 10 nm and separated by a matrix. However, there is a difference in structure in cells in different parts of the fibre, as shown by the transverse section in Fig. 1.45. In the meso-cortex, which is not always easily differentiated from the para-cortex, long microfibrils are packed in a hexagonal array, which is perpendicular to the section, so that the fibrils run parallel to the fibre axis. In the para-cortex, the fibrils are also parallel to the fibre axis, but are not as tightly and regularly packed as in the meso-cortex. A poorly defined macrofibrillar structure with more matrix between macrofibrils can be seen in the meso- and para-cortex. In the ortho-cortex, the macrofibrils appear as whorls. At the centre the fibrils appear circular, indicating that they are perpendicular to the section, but there is increasing ellipticity at increasing distance from the centre. This indicates that the fibrils are twisting round at increasing angles. As in a twisted continuous filament yarn, the length of one turn of twist is constant across the macrofibril. Electron microscope tomography by Bryson *et al.* [16] enables the structures to be seen more clearly and quantitative estimates of the fibril angles to be made (Fig. 1.46). In the para-cortex, the fibrils are slightly wavy but generally parallel to the



1.45 Electron microscope picture of transverse section of a high-crimp wool: (a) whole fibre; (b) macrofibrils. From Bryson *et al.* [16].



1.46 Reconstructed tomograms of macrofibrils in wool showing orientation of microfibrils: (a) in para-cortex; (b) in meso-cortex; (c) in ortho-cortex. From Bryson *et al.* [16].

fibre axis; in the meso-cortex, the fibrils are straighter; in the ortho-cortex, there is the changing angular orientations of a helical assembly.

1.6.4 The gross structure of wool

The wool fibre consists of a roughly circular cylinder, tapering from the root to the tip, and with the complex structure illustrated in Fig. 1.42. It is a multicellular and multicomponent fibre. The major component is the cortex, which leads to a simple view that wool is a bicomponent fibre divided into ortho- and para-cortex. As described in Section 20.6.2, this leads to the helical crimp of wool with the para-cortex on the inside, unless the fibre is swollen in alkali when the curvature is reversed. Crimp formation depends on the distribution of ortho- and para-cortex in wool and hair. An asymmetric distribution gives crimp; a symmetric distribution does not. In addition to the difference in fibril orientation described above, the para-cortex is reported to contain more cystine groups, crosslinking the chain molecules (see Section 1.6.1) and is more stable and less accessible to dyes than the ortho-cortex, which contains more glycine/tyrosine proteins. In some wools, a meso-cortex can be observed as distinct from the para-cortex. In coarse wools, there may be a medulla at the centre made up of a different type of cell, but in fine wools this is absent.

Between the cells, there is a cell membrane complex containing a mixture of lipids, proteins and small amounts of other compounds [67].

At the surface of the fibre, there are cuticle cells or scales. These scales face towards the tip of the fibres and cause a directional effect, which is important in the frictional behaviour of wool (see Section 25.5). On the surface of the scales, or possibly as a continuous sheath around them, there is a membrane called the *epicuticle*, which may influence the surface properties of the fibre and act as a barrier to diffusion. Between the cuticle and the cortex is another thin layer, called the sub-cuticle membrane.

1.6.5 Regenerated-protein fibres

The regenerated-protein fibres such as those made from casein, which are no longer commercial, have X-ray diffraction patterns which show that most of the material in

the fibres is non-crystalline. Such crystallites as are present are more or less imperfect and are made up of protein chains in an extended form, that is, a structure similar to β -keratin. The constitution of casein is given in [Table 1.6](#). It contains a wide variety of side groups.

Proteins have been produced from bioengineered goat's milk in an attempt to mimic the high strength of spider silk. However, when these are spun from solution, they give low-strength fibres with a poorly ordered structure. The means of forming the fibre is more important than the protein composition.

1.7 Synthetic fibres for general use

1.7.1 Chemical constitution

The synthetic fibres in major use for general textiles since the 1950s are the polyamides, nylon-6 and 6,6, the polyester, polyethylene terephthalate (PET), acrylic polyacrylonitrile (PAN) and polypropylene (PP). They are all linear polymers. In addition to the basic repeat unit, there may be small proportions of other groups inserted, within chains, at chain ends, or as chain branches, in order to modify such fibre properties as dyeability. This is particularly true of acrylic fibres, in which up to 15% of a minor component, which is usually another vinyl monomer with some other side group, $-R$, is present. Some other polyamides and polyesters are used as fibres. There are also modacrylic fibres with less acrylonitrile, usually about 50%, in the chain. Other vinyl and vinylidene copolymers are or have been used for some fibres of limited use. Polyethylene has limited use as a general texture fibre. Most recently, polylactic acid (PLA) has been introduced as a textile fibre. The chemical formulae of the polymers are given in [Table 1.7](#).

It is worth noting the features that make synthetic polymers suitable for fibres by causing them to be partly crystalline. First, the chains must be regular, so that a favourable packing at one point is repeated all along the chains. Secondly, the chains must have a shape that enables them to pack closely together and so cause the attractive forces between chains to be effective. Thirdly, the attractive forces should, inherently, be relatively strong. Fourthly, there must be some flexibility. These features work together, so that some deficiency in one can be compensated by another, but generally they are all satisfied in the best fibre-forming polymers.

Copolymerisation, as a means of mixing components, may occur in several ways. Because of the need for regularity of repeat, random copolymers, $-ABBAABAABABBBABA-$, are unlikely to be suitable. Block copolymers, $-AAAAAAAAABBBBBBBB-$, on the other hand, will contain separate sequences that are long enough to crystallise. Alternatively, the second component may be grafted on as a branch of the main chain.

Another general point should be noted. Natural fibres, which are laid down slowly under genetic control, have a well-defined structure that is not easily changed. To a slightly less extent, fibres formed from solution, especially if chemically regenerated as in viscose rayon, are locked in structures that are distinctly separated from the liquid state. In contrast to this in the melt-spun synthetic fibres, polyamides, polyesters and polypropylene, the solid and liquid states are only weakly separated by

Table 1.7 Synthetic fibre constitution

Fibre type	Chemical formula of principal repeat unit
Polyamide:	
nylon 6,6	$-\text{NH}\cdot\text{CH}_2\cdot\text{CH}_2\cdot\text{CH}_2\cdot\text{CH}_2\cdot\text{CH}_2\cdot\text{CH}_2\cdot\text{NH}\cdot\text{CO}\cdot\text{CH}_2\cdot\text{CH}_2\cdot\text{CH}_2\cdot\text{CH}_2\cdot\text{CO}-$
nylon-6	$-\text{NH}\cdot\text{CH}_2\cdot\text{CH}_2\cdot\text{CH}_2\cdot\text{CH}_2\cdot\text{CH}_2\cdot\text{CO}-$
Polyester:	
polyethylene terephthalate	$-\text{O}\cdot\text{CO}\cdot\text{C}_6\text{H}_4\cdot\text{CO}\cdot\text{O}\cdot\text{CH}_2\cdot\text{CH}_2-$
Acrylic:	
polyacrylonitrile	$-\text{CH}_2-\underset{\text{C}\equiv\text{N}}{\text{CH}}-$
Polyolefin:	
polyethylene	$-\text{CH}_2-$
polypropylene	$-\text{CH}_2-\underset{\text{CH}_3}{\text{CH}}-$
Polylactic acid	$-\text{CO}\cdot\text{CH}(\text{CH}_3)\cdot\text{O}-$
Other addition-polymer fibres:	
polyvinyl chloride	$-\text{CH}_2\cdot\text{CHCl}-$
polyvinyl alcohol	$-\text{CH}_2-\underset{\text{OH}}{\text{CH}}-$
other vinyl monomers	$-\text{CH}_2-\underset{\text{R}}{\text{CH}}-$
vinylidene monomers	$-\text{CH}_2\cdot\text{CR}_2-$

comparatively small temperature differences, with some structural mobility occurring well below the melting point. The nature of the cooling process and subsequent heat treatments leads to differences in structure. Whereas, we can describe *the structure* of a cotton fibre, we can give only broad indications of the sorts of structure that occur in melt-spun fibres. The evidence in the literature from analytical studies is strictly applicable only to the particular sample being studied and often the provenance is not well specified.

1.7.2 The structure of polyamide fibres

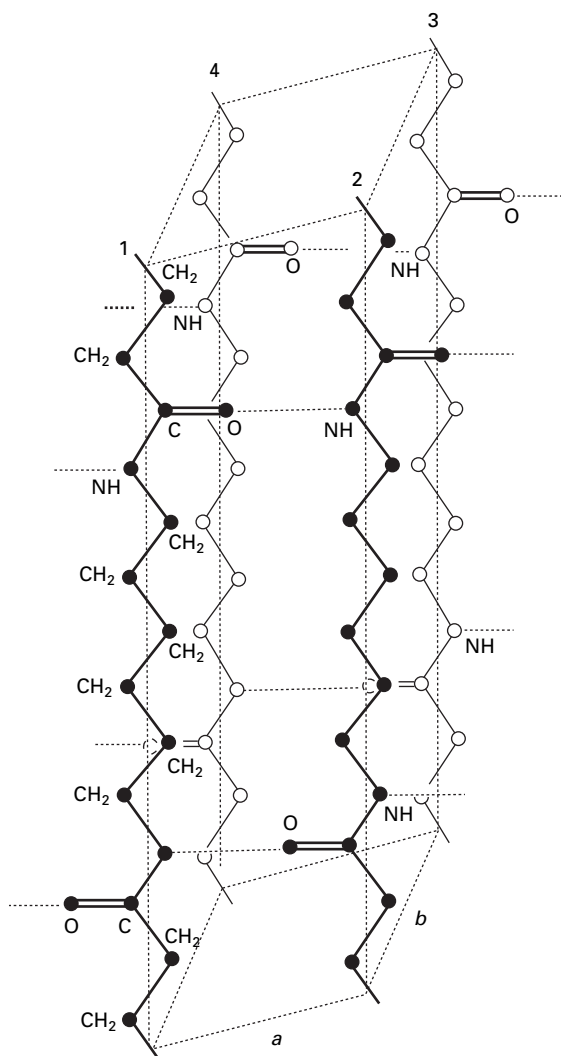
The two most important polyamide fibres, nylon 6 and nylon 6,6, contain the same groups in the same proportions along the chain. The only difference is a reversal in the order of alternate $-\text{CO}\cdot\text{NH}\cdot\text{CH}_2-$ sequences. As a result, there will be small differences in shape and packing. In addition, the nylon 6 repeat is half the length of the nylon 6,6 repeat; and the nylon 6 molecule, but not that of nylon 6,6, has a directional character:



These differences cause some not very well understood differences in structure, and some consequent slight differences in properties.

From a physical point of view, the important features of these molecules are the length of the repeat and the occurrence of alternate sequences of $\text{—CH}_2\text{—}$ and —CO·NH— groups. The long repeat unit, 1.7 nm, in nylon 6-6 with 38 atoms means that any mismatch in crystal packing will result in a substantial region of disorder and not a localised defect. Individual crystals can occur only in a limited range of sizes: 1.7, 3.4, 5.1, 6.8, 8.5, 10.2 ... nm.

The $\text{—CH}_2\text{—}$ sequences will be flexible at room temperature, with only a weak attraction for their neighbours. On the other hand, the —CO·NH— groups will attract one another strongly by hydrogen bonding. Under the action of these forces, the polyamides crystallise, and the usual crystal lattice of nylon 6.6 is shown in Fig. 1.47. However, owing to the difficulties of sorting out chains, crystallisation will not be

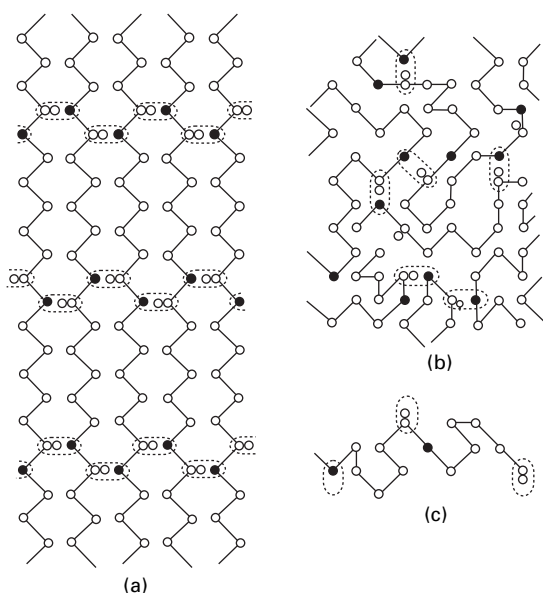


1.47 Crystal structure of α -nylon 6.6 [5].

complete, and we can also expect to find disordered regions within the fibre. Fig. 1.48 illustrates schematically the nature of the packing of nylon 6 in a crystalline region and in an amorphous structure that would occur if molten nylon was so rapidly quenched that crystallisation was prevented. The disordered region would be a rather highly crosslinked rubber with sequences of five $\text{—CH}_2\text{—}$ groups between the linked —CO·NH— groups. Many important properties derive from this structure and from the fact that the hydrogen bonds between the —CO·NH— groups are rather easily ruptured. Absorption of water plasticises disordered regions, since some direct hydrogen bonding is lost.

Both nylon 6 and nylon 6.6 do have more than one crystal lattice form, and transitions between these can occur. The structural effects of these changes are not clear.

The experimental evidence indicates that nylon fibres have a *degree of order* equivalent to about 50% crystalline, but this covers a variety of forms and dimensional parameters. The *degree of localisation of order* will depend on the fibre history. A common working model, drawn in slightly different ways by different authors, is a modified fringed-micelle structure with chain folding at the ends of the crystallites and tie-molecules linking the crystallites. One interesting feature of the nylon 6.6 crystal unit cell is that the cross-face (1234 in Fig. 1.47) makes an angle of 48° with the chain axis. This led Hearle and Greer [29] to propose the type of modified fringed-micelle structure shown in Fig. 1.18(a). This fits in with various experimental observations on fibre structure and is probably a reasonable representation of the structure of annealed nylon fibres, though the real structure is likely to be less neat



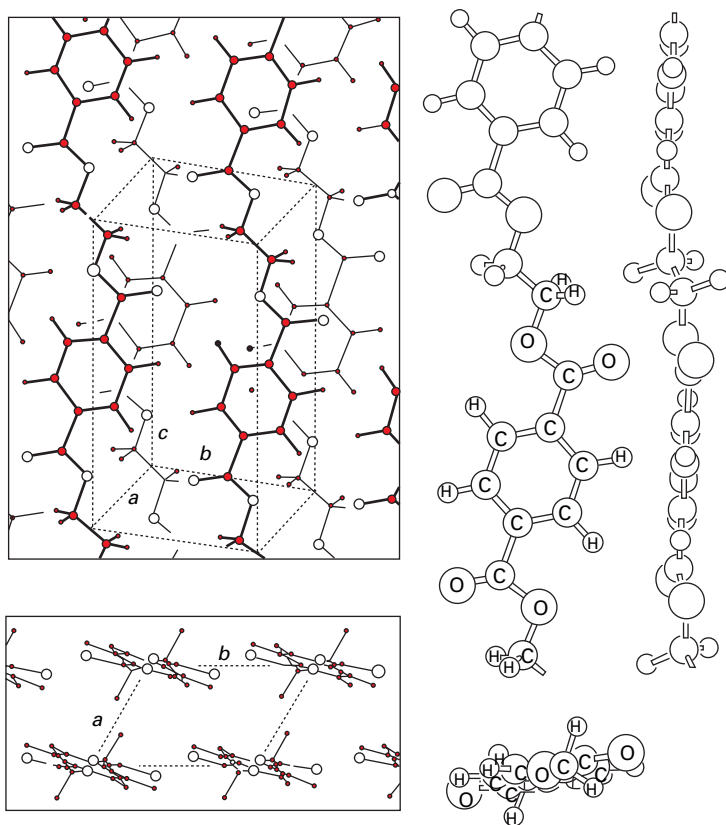
1.48 (a) Schematic representation of nylon crystal lattice. (b) Disordered region. (c) Sections of chains between crosslinks. (For convenience, the repeat is that of nylon 6).

than the diagram and must be transformed by the viewer into a three-dimensional assembly. Figure 1.18(b) is an attempt by Murthy *et al.* [30] to show a structure of nylon 6 related to X-ray diffraction observations.

The characteristic *size of localised units* is about 15 nm, with a *length/width ratio of localised units* not much greater than one. As noted in Section 1.3.2 the pseudo-fibrillar form results from the fairly close packing of the crystallites and the tie-molecules will be somewhat extended. The separation into distinct regions is probably not as complete in rapidly quenched material. In these circumstances, the possible structure shown in Fig. 1.18(c) has a lower degree of localisation of order with an intimate mixture of crystallographically registered chain segments and disorganised chain segments. Thermomechanical influences on structure will be followed up in Chapters 18 and 20.

As with all synthetic fibres, the *degree of orientation* can vary over a wide range, depending on the conditions of drawing and relaxation during fibre manufacture. The tightness of structure, shown in Fig. 1.18, means that the crystallites must be locally well oriented in zones. There is electron diffraction evidence that the orientation is close to the fibre axis direction, but differs slightly in different zones [68]. Most of the disorientation will be in the disordered regions. Owing to the high flexibility of an aliphatic chain, with about two bonds per random link, the molecules will be fairly tightly coiled and entangled in the melt, so that the *molecular extent* will be small, though it may be elongated somewhat by intermolecular attractions. Drawing will lead to an increase in molecular extent, but will still leave appreciable chain folding either at the ends of crystals or among tie-molecules. The entanglements of the chains eventually lock the structure, which leads to rupture. There is a maximum draw ratio, which limits the degree of orientation and molecular extent. Further thermal processing under appropriate tensions will give more highly oriented, high-tenacity yarns, used in tyre cords and other industrial products.

The original process for making nylon fibres started with a polymerisation operation, which produced polymer chips. The chips were melted and extruded at 1000 m/min or less into a cooling zone and wind-up of a solid undrawn fibre. Some structure may persist in the melt or be imposed by the viscous forces in the thread-line. Once the thread cools sufficiently below its melting point, crystallisation starts from a few nuclei. The crystal growth rate would be relatively rapid, though slow in comparison with extrusion rates. If crystallisation were to continue at this temperature, a coarse spherulitic structure would result. But, in reality, rapid cooling inhibits the growth of spherulites and greatly increases the number of nuclei. The subsequent crystallisation on these nuclei, either in the threadline or on the package, will give rise to unoriented variants of the micellar or more uniform structures shown in Fig. 1.18. It is not uncommon for steam to be inserted at this stage to speed up the crystallisation on the nuclei. In the next operation, the structure is transformed by drawing, which causes a length increase of about four times, with a corresponding reduction in diameter. Drawing is a plastic (irrecoverable) process, which makes the oriented fibres suitable for use as textiles. The details of the structural changes in drawing are obscure, but must involve disruption of crystallites and re-formation in the oriented structures of the type shown in Fig. 1.18 and discussed above. At various stages during or subsequent



1.49 Crystal structure of polyester fibre (Terylene), viewed from side and above, and (right) configuration of molecules in the crystal [70].

to the formation operations, heat and mechanical treatments may cause further changes in structure. In some circumstances, occluded spherulites, which after drawing are ellipsoids, remain and have been used as a way of delustring nylon.

Since nylon was first manufactured, there has been an increasing continuity of processing. Direct polymerisation feeds molten polymer to extrusion and the unoriented solid fibre can be fed directly to the rollers that impose drawing. Usable fibre is produced in a single operation. The structural changes are not very different from what happens in a discontinuous process. High-speed spinning gives bigger differences. When fibre is wound up directly, without the drawing stage, there is an increase in orientation as wind-up speeds increase to 2000 m/min, and then a transition in structure formation between 2000 and 3000 m/min. Changes in crystal form, size and orientation in nylon 6 are described by Heuvel and Huisman [69].

1.7.3 Polyester (PET) fibres

Polyester fibres are very similar to polyamide fibres: both are made in the same way, by melt-spinning and drawing, from linear condensation polymers. The PET

molecule contains two sorts of group. There is an aliphatic sequence, $\text{—CO}\cdot\text{O}\cdot\text{CH}_2\cdot\text{CH}_2\cdot\text{O}\cdot\text{CO—}$, containing about the same number of chain links as the $\text{—CH}_2\text{—}$ sequences in nylon; this aliphatic sequence would be flexible at room temperature and would give rise only to weak van der Waals interactions with neighbouring chains. The differences from polyamides are mostly due to the benzene ring. This will give some stiffness to the chain and, in particular, will impede deformation of disordered regions. Furthermore, there is an appreciable electronic interaction between neighbouring benzene rings, which gives intermolecular bonding with a function similar to the hydrogen bonding in polyamides. The crystal lattice of PET is shown in Fig. 1.49.

Two interesting comments on polymer constitution can be made in connection with polyesters. Firstly, aliphatic polyesters, which were originally studied by Carothers along with polyamides, are unsuitable for use as textile fibres. The influence of the benzene ring is needed to give firmness to the structure. Secondly, it is only when the benzene ring lies on the chain axis, because it is joined at opposite ends, that the molecular shape leads to close enough packing for easy crystallisation. If the ring is off axis, as in the chemically similar phthalate and isophthalate forms, with the ring joined at adjacent or next-but-one positions, then the shape impedes crystallisation.

PET does not crystallise as readily as nylon. The rapidly quenched, undrawn fibre from slow-speed spinning is amorphous. However, as the chains are pulled into alignment during drawing of the fibre, they lock into crystalline register. This can be demonstrated by the fact that, during drawing, the optical orientation factor, giving the overall orientation, increases continuously; but the X-ray diffraction orientation factor indicates axial orientation of the crystals as soon as the crystallisation is sufficient to give the diffraction pattern. The crystallinity of drawn fibre is about 50%. The crystallites are more elongated than in nylon, with a probable length/width ratio of 2 or more. Subject to the above comments, the structure of polyester fibres is micellar with chain folding or more uniform order/disorder, which is similar to that described for polyamide fibres and shown in Fig. 1.18.

The engineering development of high-speed spinning had important consequences for polyester fibre production. The amorphous undrawn fibre is not very stable. Its structure changes with time, especially if ambient temperatures are high. Consequently, drawing must take place at a controlled time after wind-up of the undrawn fibre. As wind-up speeds increase, there is competition between the rate of orientation as the filament is elongated and the rate of relaxation of the molecules within the attenuated filament. Above about 3000 m/min, thread-line orientation is high enough to cause crystallisation on cooling. This enables the wind-up of a partially oriented yarn (POY), which is stable and suitable for supply to yarn texturing companies. The development of orientation is then completed by drawing due to the difference of input and output speeds on a draw-texturing machine. There is an economic advantage related to production rates in dividing the orientation process in this way. For untextured yarns, drawing of POY can be combined with other processes, such as warping.

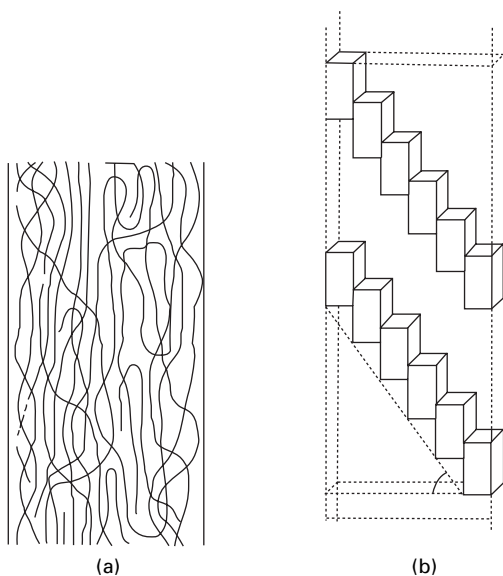
As wind-up speeds are further increased, crystallinity increases. Above about 5000 m/min, it is possible to produce polyester yarns that can be used in textiles without further processing, though they are more extensible than conventional polyester

yarns. Information on the effect of spinning speed on polyester fibre formation, structure and properties is given in a number of research studies by several authors in the book edited by Ziabicki and Kawai [71]. The uncertainty about the structure of the melt-spun polyester fibres is illustrated by Fig. 1.50, which shows two views of a polyester fibre spun at 5000 m/min by different authors in this book. Admittedly, these were drawn to refer to particular ideas, but nevertheless they give very different impressions of the nature of the structure.

As with nylon, additional thermal processing gives more highly oriented, high-tenacity polyester yarns.

1.7.4 Other polyesters

Fibres can be made from polyesters with different numbers of $\text{—CH}_2\text{—}$ groups. One now in commercial production is polytrimethylene terephthalate (PMT)⁵ with three $\text{—CH}_2\text{—}$ groups. The added flexibility of the molecule leads to properties more like those of nylon. A stiffer chain, which gives higher modulus fibres, occurs in polyethylene naphthalate (PEN), in which the benzene ring is replaced by the double naphthalate ring. These other polyester fibres are melt-spun and can be expected to have structures similar to those described for nylon and PET.



1.50 Two views of the structure of PET filaments spun at 5000 m/min, both from the same book: drawn by (a) Heuvel and Huisman [69] and (b) Shimizu *et al.* [71].

⁵An alternative terminology refers to the number of $\text{—CH}_2\text{—}$ groups: 2GT for PET, 3GT for PTT, etc.

1.7.5 Polyolefin fibres

Polyethylene is not a particularly good material for textile fibres⁶. For reasons that will be made clearer in Section 18.3.3, it is too soft and extensible. It does, however, have some usage. Polypropylene is more widely used.

Both these polymers have a fairly simple repeat, and there are not the alternating sequences of the polyamide and polyester fibres. Linear polyethylene (made by the low-pressure route, with Ziegler catalysts) readily takes up a very highly ordered form, of high density, equivalent to about 80% crystalline. This is probably best regarded as an assembly of lamellar crystals, separated by narrow crystal-defect zones. The older, branched polyethylene (made at high pressure) is somewhat less ordered.

Polypropylene, because of the side groups, cannot achieve as high a crystallinity as linear polyethylene. The bulky —CH_3 side group also causes polypropylene molecules to take up a helical form in the crystal lattice, with three repeats in one turn of the helix. The helical crystal lattice is rather easier to stretch than the extended-chain lattice of polyethylene.

Polypropylene demonstrates an interesting example of the need for regularity of structure to secure crystallisation in a polymer. During polymerisation, the successive $\text{—CH}_2\text{—CH(CH}_3\text{)—}$ sequences can be added in either a right-handed or a left-handed screw direction, owing to the stereochemistry of the chain. If these forms occur at random, the chain will have an irregular shape, impossible to remove by subsequent manipulation, and will not crystallise. This is atactic polypropylene, which is unsuitable for making fibres. But, if units are added on in the same sense, to give the isotactic form, the molecule is regular and will crystallise. It was the discovery of a means of controlling the polymerisation that led to the production of isotactic polypropylene fibres. By causing some atactic sequences to be present, the degree of order can be reduced if necessary.

Another regular form, syndiotactic, has a regular alternation of right- and left-handed groups.

1.7.6 Polylactic acid (PLA) fibres

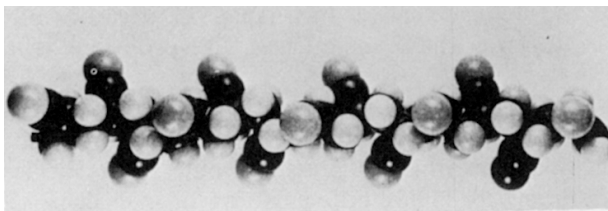
Polylactic acid, which is made from corn starch and not from oil, is a condensation polymer that is melt-spun into fibres. The structure can be expected to be similar to other melt-spun fibres.

1.7.7 Acrylic and related fibres

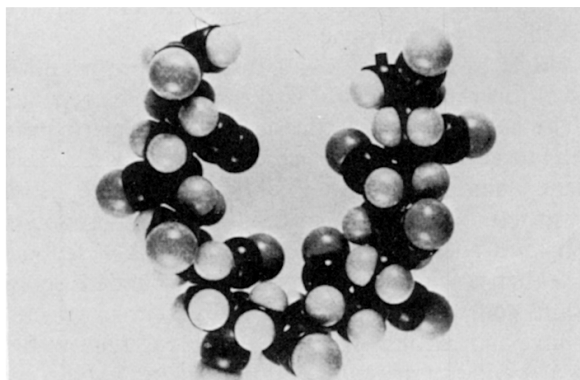
The acrylic fibres are very different from the melt-spun synthetic polymer fibres; they also differ more among themselves. The variations in the nature and means of incorporation of the minor component cause some differences; the nature of the method of production from solution, by either dry or wet spinning, causes others. But even pure polyacrylonitrile is rather unlike most other polymers.

⁶High-modulus polyethylene (HMPE) is covered in the next section on high-performance fibres.

Figure 1.51(a) shows a model of the polyacrylonitrile molecule. Because of the influence of the $\text{—C}\equiv\text{N}$ side group, it normally coils into a three-fold helix, to take up a cylindrical form, which, as indicated in Fig. 1.51(b), is only moderately flexible. The interactions between the $\text{—C}\equiv\text{N}$ groups, while strong because of the electric dipoles, are not very specifically directed. As a result, the cylinders tend to pack together in a regular hexagonal array, like sticks of chalk in a box, but without being in register along their length. This is a pseudocrystalline order, illustrated in Fig. 1.52.

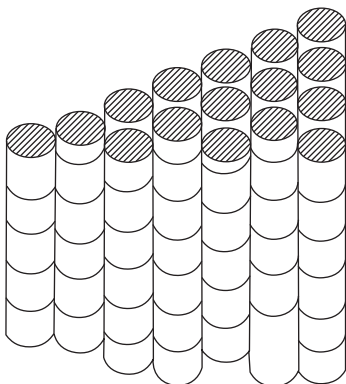


(a)



(b)

1.51 (a) Model of polyacrylonitrile molecule. (b) Bending of model.



1.52 Pseudo-crystalline packing of cylinders, typical of polyacrylonitrile.

Owing to the usual problem of sorting out long polymer chains, the highly ordered, pseudocrystalline material will make up only about half of the total material. In the other regions, there will be a more disordered structure, with the cylindrical chains crossing one another, though still held rather firmly together by the electrostatic forces. Internally, acrylic fibres have a coarse fibrillar form. This is due to the occurrence, early in the process of fibre formation, of voids containing solvent; the voids later collapse and are then drawn out during stretching of the fibre. The spongy solid incorporating the voids becomes the fibrillar network.

There are also modacrylic fibres with less acrylonitrile, usually about 50%, in the chain. Other vinyl and vinylidene copolymers are used for some fibres of limited use.

1.7.8 Elastomeric fibres

Coarse elastomeric fibres can be made from natural rubber. The structure is a network of flexible chains, which are cross-linked by covalent bonds in vulcanisation.

Spandex fibres, of which *Lycra* is a notable example, are more important. They are defined as having at least 85% of a segmented polyurethane. The molecules are alternating block copolymers of soft and hard segments. The soft segments, which make up 60–90% of the polymer, are randomly coiled aliphatic polyethers or copolyesters; the hard segments are crystallisable aromatic di-isocyanates. The result is a fringed micelle structure. The low crystallinity means that the crystalline blocks can be randomly oriented and linked together by highly coiled, flexible tie-molecules. Alternatively, the association of hard segments can be regarded as providing domains that crosslink the elastomeric network.

1.7.9 Some gross features of synthetic-fibre structure

In general, synthetic fibres are lacking in large-scale structural features. There is evidence for the presence of a skin, or of a radial variation in structure, in some fibres.

Melt-spun synthetic fibres extruded through circular spinnerets have a circular cross-section. However, shaped spinnerets lead to shaped fibres, with the sharp forms of the spinneret somewhat rounded as the molten polymer in the thread-line reduces in surface area under the forces of surface tension, tending towards the circular form. Trilobal and multilobal fibres are typical examples.

In solution-spun fibres, loss of solvent after the formation of a skin can give other shapes. Acrylic fibres often have a dumb-bell shape.

A more striking form of gross structure occurs in bicomponent fibres. A variety of forms is possible. Two streams of polymer may be extruded together from the same spinneret: a side-by-side arrangement gives an asymmetric structure with built-in crimp; a radial arrangement gives a core-sheath form for surface character or bonding. Alternatively, small zones of a second polymer may be dispersed within the main polymer fibre.

Other inclusions, delustrant, pigments, anti-static conductors, and so on, may be added to synthetic fibres to give required properties.

1.8 High-performance fibres

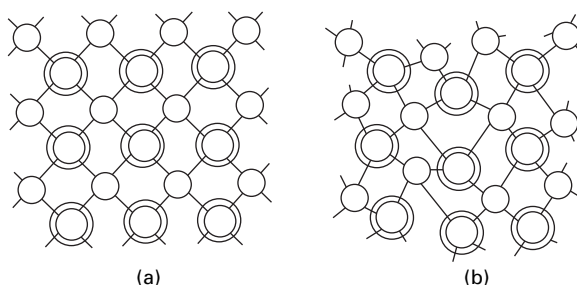
1.8.1 Fibres for engineering uses

In the final quarter of the 20th century, a new generation of manufactured fibres with high-performance properties were produced for engineering end uses. Their precursors were glass and asbestos fibres, though asbestos is no longer used for health and safety reasons. Unlike textile materials for clothing and household uses, which require a high fibre extensibility (in the range of 5–50% or, more often, 10–30%) and where strength is less important, so that moduli are relatively low, most of the textiles for engineering uses require maximum stiffness, usually accompanied by high strength. In addition to glass, which is on the borderline of general textile acceptability, the high-modulus, high-tenacity (HM–HT) fibres include: ceramics, such as alumina and silicon carbide; carbon or graphite fibres; and highly oriented polymeric fibres, such as the para-aramids, *Kevlar*, *Technora* and *Twaron*, other liquid-crystal polymer fibres, such as *Vectran*, PBO and M5, and the high-modulus polyethylenes *Spectra* and *Dyneema*.

There are also some HM–HT materials that are often referred to as fibres, but do not have the dimensions characteristic of textile fibres. Boron fibres and others made by vacuum deposition on a substrate are too thick; and single crystal whiskers are usually too thin and short. Both of these types may also be regarded as excluded from the textile category because of their extremely high cost.

1.8.2 Inorganic fibres

High mechanical and thermal resistance requires strong chemical bonding. In the ceramic fibres, this results from an array of covalent bonds in three dimensions, which holds the atoms together in the material. In the perfect crystal, the geometry will be a regular lattice, as represented schematically for a material such as silicon carbide, SiC, in Fig. 1.53(a). In fibre form, as single crystal whiskers, a particular direction will be aligned along the fibre axis. Commercial fibres, produced by heat treatment of a precursor, will not have such a regular structure. The most likely form



1.53 Schematic two-dimensional representation of the structure of a material such as silicon carbide: (a) crystalline; (b) amorphous. In the actual material, the atoms are distributed over three dimensions, to give a more complicated network.

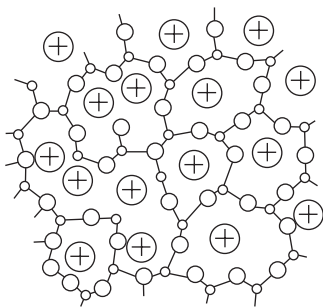
is a polycrystalline collection of variously oriented microcrystals. An alternative possibility is an amorphous structure, with distorted bonding between atoms, as illustrated in Fig. 1.53(b). It must be remembered that the real structures, whether crystalline or amorphous, are three dimensional, and the viewer must use imagination to transform the picture from the two-dimensional form, which is easier to represent. In silicon carbide, the geometry of the linkage is relatively simple, because both carbon and silicon have valencies of four, and so fit into a tetrahedral lattice with the C and Si atoms in equivalent positions. Oxide fibres, such as X_2O_3 , are more complicated because of the valency differences.

The alumina fibre FP is reported to be almost pure polycrystalline α - Al_2O_3 with a grain size of about $0.5\ \mu m$ [72]. *Nicalon* silicon carbide fibre is reported to contain ultra-fine β -SiC crystals [73].

Ceramic fibres may contain a mixture of components. For example, *Nicalon* may contain up to 30% of silica, SiO_2 , and carbon; and *Nextel* is a 70/28/2 mixture of $Al_2O_3/SiO_2/B_2O_3$. *Tyranno* is a ceramic fibre composed of silicon, titanium, carbon and oxygen (Si-Ti-C-O), which is reported to have a non-crystalline microstructure [24]. A development from FP fibre, called PRD-166, consists of α -alumina with 20% of zirconia.

In glass, the amorphous bonded network of silica, SiO_2 , is opened up by the presence of electrovalently bonded metal ions, which come from the metal oxides in the formulation. A schematic representation is shown in Fig. 1.54. The mechanical, chemical, thermal and electrical performance depends on the composition used in glass manufacture. For low-grade staple fibre, used, for example, as thermal insulation in buildings, this will be determined mainly by price, and the glass would be about 75% silica, the other main constituents being the oxides of sodium, Na_2O , and calcium, CaO . Continuous filaments for more demanding applications may be made of E-glass, containing only small amounts of alkali, Na_2O and K_2O , more CaO , and also oxides of boron, B_2O_3 , aluminium, Al_2O_3 , iron, Fe_2O_3 , and magnesium, MgO . The high-strength S-2 glass is also a magnesium oxide, aluminosilicate type, low in alkali and high in magnesium [74].

Asbestos, although no longer used, is interesting in the way in which it forms fibres [75]. The crystal lattice is naturally curved and so bends round to form a



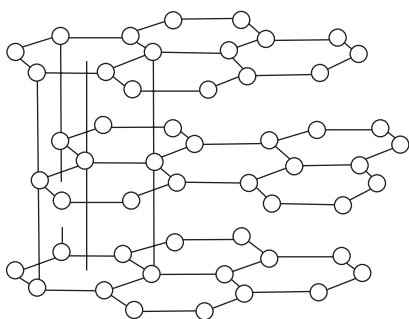
1.54 Schematic representation of the structure of glass, composed of silica, SiO_2 and metal oxides.

cylinder with a diameter in the chrysotile form of asbestos of 17.5 nm. Crystallisation can continue to a limited extent on inner and outer layers before the distortion becomes too great. Hollow cylindrical crystallites have peak diameters of 10 nm inside and 25 nm outside. When the rock is broken down, the resulting fibres are bundles of these cylindrical crystallites.

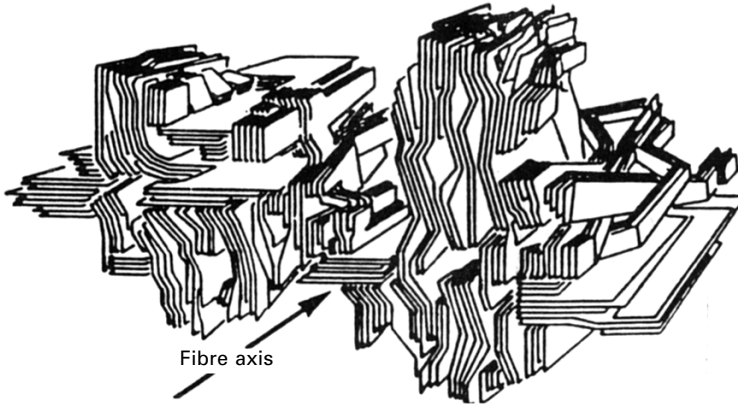
1.8.3 Carbon fibres

High-strength carbon fibres have a structure based on the graphite crystal lattice, shown in Fig. 1.55. This consists of two-dimensional sheets (planar polymer molecules) of carbon atoms, which are held together strongly by covalent bonds and are arranged in parallel layers, 0.335 nm apart, with much weaker van der Waals forces between the layers. In turbostratic graphite, the individual layers are not aligned but are irregularly rotated relative to one another, and the spacing between layers is increased to 0.344 nm. The perfect crystalline form of graphite very easily splits into microscopically thin sheets, which slide over one another in graphite lubricants.

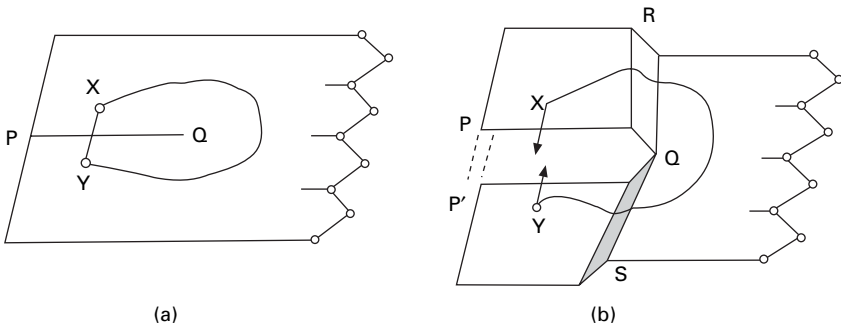
In carbon fibres, this degree of perfection is not achieved. Electron microscope examination of thin sections shows clear lattice fringe images, but also appreciable disorder [76]. The exact forms of structural disorder are not well understood, and carbon fibres from different precursors, or with different processing histories, will have different types and degrees of disorder. It is known that the orientation of the graphite sheets in high-strength and high-modulus carbon fibres is predominantly in planes parallel to the fibre axis, but with varying orientation in the direction perpendicular to the fibre axis. A schematic representation of the sort of complication that may be present is shown in Fig. 1.56, but many other variant sketches have been drawn. At a first level of comprehension, it is possible to imagine a structure composed of microcrystals of graphite, each perfect or turbostratic and oriented in a particular direction, but with the microcrystals differing in orientation in separate zones, which make up the total solid. The shapes and interconnections of the zones would be important structural parameters. At the next level, one can imagine distortion and curvature of the sheets as they pass through the structure. Different authors have drawn a variety of arrangements of whorls and interweaving of sheets and ribbons



1.55 Crystal lattice of graphite. Note staggering of layers indicated by vertical lines.



1.56 Schematic representation of the structure of a carbon fibre. Courtesy of D. J. Johnson [77].



1.57 Possible interconnection defect in graphitic structure: (a) single sheet with two connecting routes between X and Y; (b) split of sheet along PQ, giving a connecting route outside Q but with the direct route on separate planes.

within the fibre, and the real forms will vary with the precursor and the process used to make the carbon fibre. The one common feature is that the planes are predominantly aligned with one direction parallel to the fibre axis.

The most important type of disorder may be at the level of molecular perfection. The carbon atoms in the intermediate low-strength carbon fibres, which are used as thermally resistant fibres, are much more irregularly bonded together, and the subsequent transformation to planar graphite molecules may not be complete. It is possible to imagine defects that connect graphite layers together. For example, instead of the perfect sheet of Fig. 1.57(a), there might be a cut along the line PQ, and lines of dislocations upwards along RQ and downwards along QS, as suggested in Fig. 1.57(b). Although molecular continuity remains between X and Y along a route outside Q, the direct connexion is to separate neighbouring layers containing P and P'. Such a defect would form part of a network of dislocations, with the total structure being an assembly of interconnected planar molecules, arranged with the planes parallel to the fibre axis.

An ironical feature of the production of carbon fibres is that, although the ultimate goal of the heat treatment under tension appears to be the formation of a perfectly oriented structure of perfect sheets in order to maximise tensile strength and stiffness, such a perfect fibre would have serious faults in other ways. Some disorder is needed to hold the sheets together and optimise performance.

1.8.4 HM–HT polymer fibres

In order to achieve high stiffness and high strength in linear polymer fibres, it is necessary that the chains should be highly oriented and highly chain extended, as shown ideally in Fig. 1.58. This type of structure can be produced from polymers at the opposite ends of the spectrum. Very stiff chains with strong interactions easily self-assemble. Very flexible chains with weak interactions can be highly drawn. With polymers such as polyamides and polyesters, there is no self-assembly into the required form, and entanglements and interactions cause the fibre to break at lower draw-ratios.

The para-aramid fibres *Kevlar* and *Twaron* are manufactured by dry-jet wet spinning in which the extruded solution passes through an air-gap before entering a coagulation bath. They are composed of the aromatic polyamide, poly(p-phenylene terephthalamide) or PPTA:



This is a stiff molecule with strong interactions to neighbouring molecules, both at the benzene rings and by hydrogen bonding at the —CO·NH— groups. In solution, the self-attracting rod-like molecules form elongated liquid crystals, like logs in a stream. High shear at the point of fibre formation then lines up the crystals parallel to the fibre axis. The resulting fibre structure consists of fully extended chains, packed together with a very high degree of crystallinity and a very high orientation. There is some disorder, originating from boundaries between liquid crystals and imperfections of packing within crystals, and some departure from perfect orientation. Heat treatment under tension improves the structural perfection, and there are both less well-ordered, lower-modulus forms, such as *Kevlar* 29, and better-ordered, higher-modulus forms, such as *Kevlar* 49 and 149, on the market.

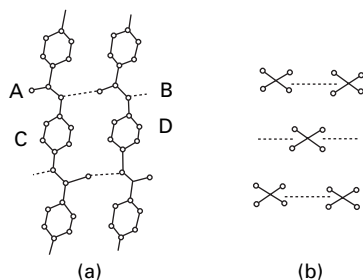


1.58 A diagram drawn by Staudinger [78] in 1932, which shows the ideal form for a linear polymer fibre with high strength and stiffness.

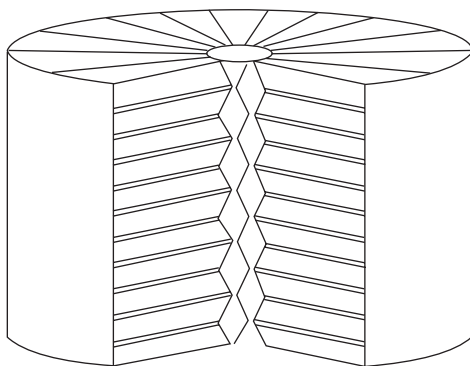
The crystal lattice of PPTA is illustrated in Fig. 1.59. Several features are noteworthy. Firstly, because of the alternation of ring and linear forms, it follows that the transverse planes, AB, containing the —CO—NH— groups have a lower density of covalent bonds than those containing rings, CD. Secondly, there are planes, shown in Fig. 1.59(a), in which neighbouring molecules are hydrogen bonded and thus more firmly held together than between the layers in the perpendicular direction, above and below the paper. This gives rise to anisotropy in the directions normal to the fibre axis, with the possibility of preferred orientation. The geometrical effects, as distinct from the intermolecular bonding, are less marked than they might be because the benzene rings in the acid and amine components are angled as shown in Fig. 1.59(b). At the level of fine structure, though the fibres are highly crystalline and highly oriented, there is an axial pleating of the crystalline sheets, which are radially oriented, as illustrated in Fig. 1.60.

There are a number of other HM-HT polymer fibres produced by dry-jet wet spinning with structures generally similar to that described above, but without the special feature of pleating.

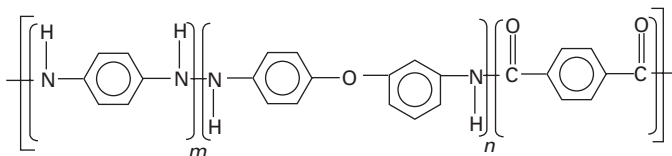
Technora [79] is an aromatic copolyamide with the chemical structure:



1.59 Molecular packing in PPTA crystal: (a) set of hydrogen bonds in a sheet; (b) view along the chains showing separate sheets and different directions of benzene rings.

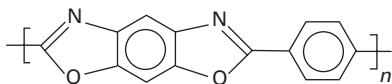


1.60 Radial pleated structure of a para-aramid fibre (Kevlar).

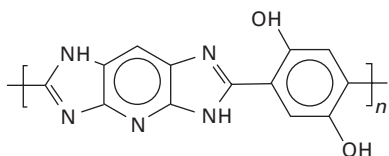


Unusually, *Technora* is spun from an isotropic, not a liquid-crystal, solution.

Poly(*p*-phenylene benzobisoxazole), usually referred to as polybenzoxazole or PBO, in *Zylon* fibres, is a stiffer molecule with triple rings in the chain:



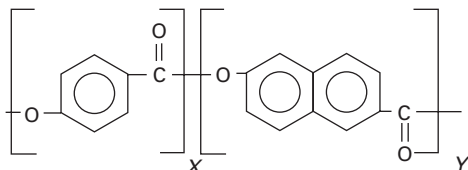
As mentioned above, PPTA has weak connections between planes and PBO similarly lacks strong interactions in all transverse directions. This led Sikkema [80] to synthesise poly {2,6-diimidazo[4,5-b:4', 5' -e]-pyridinylene-1,4(2,5-dihydroxy)phenylene} (PIPD):



The hydroxyl groups lead to hydrogen bonding in all transverse directions, which improves shear and axial compression resistance in the 'M5' fibre.

Other variants of the stiff chain scenario were investigated by Perepelkin [81] in Russia. As mentioned above, cellulose fibres can also be produced by a similar liquid-crystal route [55].

All the above fibres are made from solutions in strong acids by dry-jet wet spinning. Fully aromatic polyesters are another type of stiff chain. With limited co-polymerisation, they form thermotropic liquid crystals, which can be melt-spun to produce highly oriented, chain-extended fibres. However, the molecular weight cannot be too high in melt-spinning, so that subsequent solid-state polymerisation is needed to give the chain length required for high performance. This offsets the economic benefit of melt-spinning. The commercial fibre of this type is *Vectran* [82], with the formula:



The alternative route towards the idealised structure shown in Fig. 1.58 is to use flexible molecules with weak interactions, which can be 'combed out' to give chains that are highly extended and highly oriented, and packed with a high crystalline

order. Examples are the gel-spun, HMPE fibres *Dyneema* and *Spectra*, made from very high molecular weight polyethylene. The crystal lattice consists of extended chains of carbon atoms, with attached hydrogen atoms. This gives very efficient bonding along the polymer molecules, with a high density of covalent bonds across all planes, but very weak van der Waals bonding between chains.

Highly oriented fibres can also be made by super-drawing of melt-spun polyethylene fibres with lower molecular weight or by solid-state extrusion of high molecular weight polyethylene, but the strength is less than gel-spun fibres.

HM-HT fibres, which are perfect single crystals of linear polymer molecules, can be made by solid-state polymerisation of diacetylenes [83]. These are interesting academically in terms of their mechanical properties, because of their structural perfection and, more practically, for their electrical properties.

1.8.5 Gross features

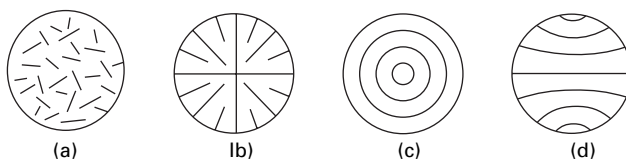
Larger-scale structural features, such as voids or packing differences, can result from the structure of precursor fibres or from effects in fibre manufacture. This is certainly true for carbon fibres, where there are differences among fibres made from acrylic, rayon and pitch precursors.

Where, as in carbon and para-aramid fibres, the crystal lattice contains sheets, there are varying possibilities of orientation in the plane perpendicular to the fibre axis. This may be random, radial, circumferential or across the fibre, as indicated in Fig. 1.61. Random arrangements are likely when there is no stress field generated by thermal or other shrinkage effects, but it is easy to envisage that stress can bias the structure into radial or circumferential arrangements. The form may not be the same over the whole cross-section; for example, there may be different orientations in core and sheath. The transverse arrangement of Fig. 1.61(d) develops in pitch-based carbon fibres.

1.9 Specialist fibres

1.9.1 Diverse functions

In addition to the common textile fibres and the high-performance fibres, there is now a great variety of fibres with special properties that match a wide range of specialist applications. These fibres are largely beyond the scope of this book, but they will be mentioned here with some comments on structure.



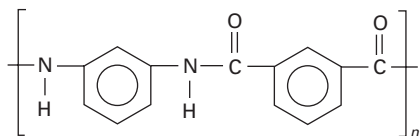
1.61 Orientation in the fibre cross-section: (a) random; (b) radial; (c) circumferential; (d) across the fibre.

1.9.2 Thermal and chemical resistance

Another engineering requirement is for high-temperature applications, which may be combined with good mechanical performance. The HM-HT ceramic and carbon fibres considered above have high thermal resistance. Glass and the polymer fibres, except HMPE, can be used for moderately high temperatures.

For other uses, moderate or poor mechanical performance is adequate. Some are weak and brittle fibres. For insulation, rock and slag wools, which are low-grade materials with a glassy structure, are used. Somewhat better textile properties are given by partially carbonised fibres, which can be made from acrylic or rayon precursors. The current commercial processes involve heat treatments of acrylic fibres, which are similar to the initial stages of carbon fibre production. The polyacrylonitrile molecule is first cyclised into a ladder-like chain, which is then oxidised. Further heat treatment displaces oxygen and nitrogen and develops three-dimensional bonding in the final black fibres. There are also three-dimensional networks in the thermoset resin fibres, *Basofil* from melamine-formaldehyde and *Kynol* from phenol-formaldehyde.

There are other applications, such as aircraft interiors and protective clothing, where good textile qualities are required as well as thermal resistance. The meta-aramid fibre *Nomex* is made of poly(*m*-phenylene terephthalamide):



The shape of the molecule prevents liquid-crystal formation, and the fibres have a partially oriented, partially crystalline structure, which is generally similar to that of other synthetic textile fibres, such as nylon and polyester. PBO, which is described above, has very high thermal stability and flame resistance. Fibres from other polymers, which include five-membered and benzene rings, but with shapes that give partially crystalline structures, are the aramid and poly(aramide-imide) fibres, such as *P84* and *Kermel* [84], and polybenzimidazole (PBI) [85].

Many of the fibres described above have good resistance to particular chemicals, but there are some fibres introduced particularly for chemical resistance [86]. They include polytetrafluoroethylene, *Teflon*, $(-\text{CF}_2\text{CF}_2-)_n$, which also has good thermal resistance and low friction, and a number of chlorinated and fluorinated hydrocarbons. Other chemically resistant polymers are polyetheretherketone (PEEK), polyphenylenesulphide (PPS), and polyetherimide (PEI).

1.9.3 Fibres with other properties

Other types of fibre have the particular physical properties needed for special applications, but their details are outside the scope of this book. Non-woven fabrics of lead fibres are used for sound absorption. Metal threads, including *Lurex*, which sandwiches metal foil between plastic films, are used for decorative purposes. Optical

fibres, either from glass or from transparent amorphous plastics, now have a major role in communication. Fibres for medical uses must have biological compatability and may be required to degrade after new growth of tissue. Hollow fibres are used for drug release.

‘Smart fibres’ [87, 88] have special electrical, magnetic, radiation-absorbing, diffusion, biological or other properties. They may be used as transducers, as wearable electronics, as actuators, or for thermal regulation and other adaptive responses. Some of these fibres depend on additives, such as carbon for electrical conduction. Others are made from particular polymers, such as the piezoelectric material, polyvinylidene fluoride, $-(CH_2 \cdot CF_2)_n-$.

1.10 Some concluding views

1.10.1 Levels of structure

The complexity of fibre structure, and of the means of achieving particular properties, comes in large measure from the number of levels of structure. To bring these various levels into relation, Table 1.8 indicates the dimensions of typical fibre features.

Wool is the extreme example of complexity, with structure at a large number of levels, as shown in Figs 1.42 and 1.43. Other fibres are less complex. At the level of fine structure, states intermediate between a perfect crystal and random disorder are difficult to define and often easy to manipulate into other forms.

1.10.2 Thermodynamic stability

The ultimate state of lowest free energy for most fibre-forming polymers would be a single crystal of extended polymer chains, but the barriers that stand in the way of reaching that state are insurmountable. The fibre states with which we are concerned are metastable states, with a local minimum of free energy. With all the possible arrangements of polymer chains, there are a vast number of local minima defining

Table 1.8 Dimensions of fibre features (approximate levels)

10 cm	Fibre lengths
1 cm	
1 mm	Spacing of crimps in wool
0.1 mm	Spacing of convolutions in cotton
10 μm	Fibre diameters
1 μm (10 ⁻⁴ cm)	Major structural features
	Molecular length
0.1 μm	Laminae
10 nm	Micro-fibrils
	Crystalline and non-crystalline regions
1 nm	Molecular width
1 Å (10 ⁻⁸ cm)	Atoms <div>C,N,O H</div>

different, reasonably stable, but metastable states. The minimum free-energy states are defined by many parameters, and could be regarded as represented by troughs in a multidimensional landscape. By the action of heat, stress and chemical changes, it is possible to shift from one metastable state to another. This is another reason for the complexity of fibre structure problems. It also has the effect that care needs to be taken in applying thermodynamics, because the thermodynamic equalities apply strictly only to reversible changes between true equilibrium states.

The situation can be illustrated by considering nylon fibres. On cooling from the melt, a partly crystalline structure will form, but important details of the structure, such as the extent of spherulitic material, will depend on the temperature at which crystallisation occurred because of its influence on the number of nuclei present. There is thus a collection of possible states of the undrawn fibre; storage may lead to further changes as thermal vibrations shake the structure down to a slightly lower energy state. Drawing causes a major rearrangement to another collection of metastable states. Subsequent heat-setting and mechanical treatments cause further changes. If the fibre has been partially or fully oriented by high-speed spinning, there will be other structures. In many important respects, these different metastable forms will have different properties; and thus the mode of formation and history of the fibre, which determine the fibre structure, in turn determine the physical properties of fibres and hence their practical utility.

1.11 References

1. J. W. S. Hearle and R. H. Peters (Editors). *Fibre Structure*, The Textile Institute and Butterworths, Manchester and London, 1963.
2. J. W. S. Hearle and R. Greer. *Text. Prog.*, 1970, **2**, No. 4.
3. M. J. Denton and P. N. Daniels (Editors). *Textile Terms and Definitions*, 11th edition, The Textile Institute, Manchester, 2002.
4. C. H. Bamford, A. Elliott, and W. E. Hanby. *Synthetic Polypeptides*, Academic Press, New York, 1956, p. 147.
5. C. W. Bunn and E. V. Garner. *Proc. Roy. Soc.*, 1947, **A189**, 39.
6. I. Sandeman and A. Keller. *J. Polymer Sci.*, 1956, **19**, 401.
7. J. L. Koenig and M. C. Aboatwalla. *J. Macromol. Sci.*, 1968, **B2**, 391.
8. H. J. Marrinan and J. J. Mann. *J. Polymer Sci.*, 1956, **21**, 301.
9. W-Y. Yeh and R. J. Young. *Polymer*, 1999, **40**, 857.
10. R. J. Young. *J. Textile Inst.*, 1995, **86**, 360.
11. L. J. Lynch and N. Thomas. *Text. Res. J.*, 1971, **41**, 568.
12. R. S. Stein. *J. Polymer Sci. C*, 1967, No. **20**, 185.
13. J. A. Chapman. In *Physical Methods of Investigating Textiles*, R. Meredith and J. W. S. Hearle (Editors), Interscience, New York, 1959, Chapter 3.
14. J. W. S. Hearle and S. C. Simmens. *Polymer*, 1973, **14**, 273.
15. J. W. S. Hearle, J. T. Sparrow and P. M. Cross (Editors). *The Use of the Scanning Electron Microscope*, Pergamon Press, Oxford, 1972.
16. W. G. Bryson, D. N. Mastronarde, J. P. Caldwell, W. G. Nelson and J. L. Woods. *Proc. 10th Int. Wool Textile Res. Conf.*, ST-P3, Aachen, 2000.
17. W. G. Bryson and J. P. Caldwell. *Proc. 11th Int. Wool Textile Res. Conf.*, Leeds, 2005.
18. J. M. Maxwell, S. G. Gordon and M. G. Huson. *Textile Res. J.*, 2003, **73**, 1005.
19. W. O. Statton. *J. Polymer Sci. C*, 1963, No. **3**, 3.

20. R. Jeffries, D. M. Jones, J. G. Roberts, K. Selby, S. C. Simmens and J. O. Warwicker. *Cell. Chem. Technol.*, 1969, **3**, 255.
21. V. M. Skachkov and V. I. Sharkov. *Izv. Vyssh. Ucheb. Zaved.. Les. Zh.*, 1967, **10**, 127 (*Chem. Abs.*, **68**, 96906c).
22. O. Sepal and S. G. Mason. *Canadian J. Res.*, 1961, **39**, 1934.
23. S. P. Rowland and E. R. Cousins. *J. Polymer Sci.*, 1966, **4**, 793.
24. J. D. Guthrie and D. C. Heinzelman. *Textile Res. J.*, 1974, **44**, 981.
25. M. A. Rouselle and M. L. Nelson. *Textile Res. J.*, 1971, **41**, 599.
26. J. L. Bose, E. J. Roberts and S. P. Rowland. *J. Appl. Polymer Sci.*, 1971, **15**, 2999.
27. A. Johnson, K. Z. Maheshwari and L. W. C. Miles. *Premier Symp. Int. de la Recherche Textile Colonnienne*, Paris, 1969, p. 557.
28. C. W. Bunn. In *Fibres from Synthetic Polymers*, R. Hill (Editor), Elsevier, Amsterdam, 1953.
29. J. W. S. Hearle and R. Greer. *J. Text. Inst.*, 1970, **61**, 243.
30. N. S. Murthy, A. C. Reimschuessel and V. J. Kramer. *J. Appl. Polymer Sci.*, 1990, **40**, 249.
31. J. W. S. Hearle. *J. Appl. Polymer Sci.*, *Appl. Polymer Symp.*, 1978, **31**, 137.
32. J. W. S. Hearle. *J. Polymer Sci.*, 1958, **28**, 432.
33. J. W. S. Hearle. *J. Appl. Polymer Sci.*, 1963, **7**, 1175.
34. V. A. Kargin. *J. Polymer Sci.*, 1958, **30**, 247.
35. R. Hosemann. *Polymer*, 1962, **3**, 349.
36. R. Hosemann. *J. Polymer Sci. C*, 1967, No. **20**, 1.
37. D. H. Reneker and J. Mazur. *Polymer*, 1983, **24**, 1387.
38. J. W. S. Hearle. *J. Polymer Sci. C*, 1967, No. **20**, 215.
39. J. W. S. Hearle and E. A. Vaughn. In *Polymer Science*, A. D. Jenkins (Editor), North-Holland Publishing Co., Amsterdam, Netherlands, 1972, Chapter 12.
40. J. W. S. Hearle. *Polymers and their Properties*, Ellis Horwood, Chichester, 1982.
41. J. A. Howsmon and W. A. Sisson. In *Cellulose and Cellulose Derivatives*, Part I, E. Ott, H. M. Spurlin and M. W. Grafen (Editors), Interscience, New York, 2nd edition, 1954, p. 251.
42. A. D. French. In *Cellulose Chemistry and its Applications*, T. P. Nevell and S. H. Zeronian (Editors), Ellis Horwood, Chichester, 1985.
43. M-A. Rouselle. *Textile Res. J.*, 2002, **72**, 131.
44. K. H. Meyer and L. Misch. *Helv. Chim. Acta*, 1937, **20**, 232.
45. R. St. J. Manley. *J. Polymer Sci. B*, 1965, **3**, 691.
46. P. Ingram. *Symp. Int. Rech. Text. Cot., Paris*, 1969, 519.
47. J. W. S. Hearle and J. T. Sparrow. *J. Appl Polymer Sci.*, 1979, **24**, 1465.
48. J. A. Foulk and D. D. McAlister. *Textile Res. J.*, 2002, **72**, 8895.
49. T. Kerr. *Protoplasma*, 1937, **27**, 229.
50. J. J. Hebert. *Textile Res. J.*, 1993, **63**, 695.
51. E. K. Boylston and J. J. Hebert. *Textile Res. J.*, 1995, **65**, 429.
52. J. J. Hebert, R. Geardina, D. Mitcham and M. L. Robbins. *Text. Res. J.*, 1970, **40**, 126.
53. N. Morosoff and P. Ingram. *Text. Res. J.*, 1970, **40**, 250.
54. P. Kassenbeck. *Text. Res. J.*, 1970, **40**, 330.
55. H. Boerstel, Doctoral thesis, Rijksuniversiteit, Groningen, 1998.
56. P. H. Hermans. *Contributions to the Physics of Cellulose Fibres*, Elsevier, Amsterdam, Netherlands, 1946, p. 171.
57. G. D. Joshi and J. M. Preston. *Text. Res. J.*, 1954, **24**, 971.
58. N. S. Woodings. In *Fibre Structure*, J. W. S. Hearle and R. H. Peters (Editors), The Textile Institute, Manchester, 1963, 455.
59. H. A. Coulsey and S. B. Smith. Dornbirn Conference, 1995.
60. M. Harris (Editor). *Handbook of Textile Fibres*, Harris Research Laboratories, Washington, DC, 1954, p. 60.
61. H. Höcker. In *Wool: Science and Technology*, W. S. Simpson and G. H. Crawshaw (Editors),

- Woodhead Publishing, Cambridge, 2002, p. 60.
62. D. Coleman and F. O. Howitt. *Proc. Roy. Soc.*, 1947, **A190**, 145.
 63. J. W. S. Hearle. *Wool Tech. Sheep Breeding*, 2003, **51**, 95.
 64. L. Pauling and R. B. Corey. *Proc. Nat. Acad. Sci., USA*, 1951, **37**, 251, 261.
 65. L. Pauling, R. B. Corey and H. R. Branson. *Proc. Nat. Acad. Sci., USA*, 1951, **37**, 205.
 66. W. T. Astbury and F. O. Bell. *Nature*, 1941, **147**, 696.
 67. J. D. Leeder. *Wool Sci. Rev.*, 1986, **63**, 3.
 68. E. M. O. Bebbington. PhD thesis, 1969, University of Manchester, UK.
 69. H. M. Heuvel and R. Huisman. In *High-speed Fibre Spinning*, A. Ziabicki and H. Kawai (Editors), Wiley, New York, 1985, p. 295.
 70. R. P. Daubeney, C. W. Bunn, and C. J. Brown. *Proc. Roy. Soc.*, 1954, **A226**, 531.
 71. J. Shimizu, N. Okui and T. Kikutani. In *High-Speed Fibre Spinning*, A. Ziabicki and H. Kawai (editors). Wiley, New York, 1985 429.
 72. A. K. Dhingra. *Phil. Trans. Roy. Soc.*, 1980, **A294**, 411.
 73. Nippon Carbon Co. Nicalon Silicon Carbide Continuous Fibre (manufacturer's leaflet), 1985.
 74. F. R. Jones. In *High-performance Fibres*, J. W. S. Hearle (Editor), Woodhead Publishing, Cambridge, 2001, p. 191.
 75. E. J. W. Whittaker. In *Fibre Structure*, J. W. S. Hearle and R. H. Peters (Editors), The Textile Institute, Manchester, 1963, p. 594.
 76. W. Johnson. *Nature*, 1979, **279**, 142.
 77. D. J. Johnson, In *Strong Fibres Handbook of Composites*, Volume 1, W. Watt and B. V. Perov (Editors), North-Holland, Amsterdam, 1985.
 78. H. Staudinger. *Die hochmolekularen organischen Verbindungen*, Springer-Verlag, Berlin, 1932.
 79. S. Ozawa. *Polymer J.*, 1987, **19**, 119.
 80. D. J. Sikkema. In *High-performance Fibres*, J. W. S. Hearle (Editor), Woodhead Publishing, Cambridge, 2001, p. 108.
 81. K. E. Perepelkin. In *High-performance Fibres* J. W. S. Hearle (Editor), Woodhead Publishing, Cambridge, 2001, p. 115.
 82. D. Beers. In *High-performance Fibres*, J. W. S. Hearle (Editor), Woodhead Publishing, Cambridge, England, 2001, 93.
 83. R. J. Young in 'Developments in Oriented Polymers – 2' I. M. Ward (Editor), Elsevier Applied Science, 1987, Chapter 1.
 84. A. R. Horrocks. In *High-performance Fibres*, J. W. S. Hearle (Editor), Woodhead Publishing, Cambridge, 2001, p. 292.
 85. C. Thomas. In *High-performance Fibres*, J. W. S. Hearle (Editor), Woodhead Publishing, Cambridge, 2001, p. 310.
 86. A. R. Horrocks and B. McIntosh. In *High-performance Fibres*, J. W. S. Hearle (editor), Woodhead Publishing, Cambridge, 2001, p. 259.
 87. X. Tao (editor). *Smart Fibres, Fabrics and Clothing*, Woodhead Publishing, Cambridge, 2001.
 88. X. Tao (editor). *Wearable electronics and photonics*, Woodhead Publishing, Cambridge, 2005.

Additional general references

- P. H. Hermans. *Physics and Chemistry of Cellulose Fibres*, Elsevier, Amsterdam, Netherlands, 1949.
- H. R. Mauersberger (Editor). *Matthews Textile Fibers*, Wiley, New York, 6th edition, 1954.
- J. G. Cook. *Handbook of Textile Fibres*, Volumes 1 and 2, Merrow Publishing Co., Watford, 4th edition, 1968.
- R. R. Franck (Editor) *Silk, Mohair, Cashmere and Other Luxury Fibres*, Woodhead Publishing, Cambridge, 2001.
- C. Woodings (Editor) *Regenerated Cellulose Fibres*, Woodhead Publishing, Cambridge, 2001.

- J. W. S. Hearle (Editor). *High Performance Fibres*, Woodhead Publishing, Cambridge, 2001.
- D. R. Salem (Editor). *Structure Formation in Polymeric Fibers*, Hanser, Munich, 2001.
- W. S. Simpson and G. Crawshaw (Editors) *Wool: Science and Technology*, Woodhead Publishing, Cambridge, 2002.
- J. E. McIntyre (Editor). *Synthetic Fibres: Nylon, Polyester, Acrylic, Polyolefin*, Woodhead Publishing, Cambridge, 2004.
- T. Hongu (editor). *New Millennium Fibers*, Woodhead Publishing, Cambridge, 2005.
- R. R. Franck (Editor). *Bast and Other Plant Fibres*, Woodhead Publishing, Cambridge, 2005.
- S. Gordon and Y. L. Hsieh (Editors). *Cotton: Science and Technology*, Woodhead Publishing, Cambridge, 2006.
- R. S. Blackburn (Editor). *Biodegradable and Sustainable Fibres*, Woodhead Publishing, Cambridge, 2006.
- S. Eichhorn, M. Jaffe and T. Kikutani (Editors), *Handbook of Fibre Structure*, Woodhead Publishing, Cambridge, due in 2009.

2.1 Test procedures

2.1.1 Evolution

The development of electronics in the middle of the 20th century and of digital processing at the end of the century led to major changes in the methods and instruments used for testing the physical properties of fibres. This is particularly important in the evolution of procedures for evaluating (classing or grading) natural fibres, which has gone through three main stages, though these are not totally distinct from one another.

At first, there was subjective evaluation by sellers and buyers viewing and handling the material. For cotton, this became somewhat more objective by skilled classers estimating fibre length on hand-stapled fibre tufts and comparing quality against sets of standard samples [1]. The cotton was described by terminology such as American middling, 5/16 inch (8 mm), with added information on colour and trash content. With the growth of fibre research in the first half of the 20th century, painstaking slow direct methods for measuring fibre dimensions were developed.

In the 1950s, there was a move to develop new test procedures, which were semi-automatic and gave objective measurements, even though these were not always directly related to specific fibre properties. Air-flow methods, which, for cotton, gave a *micronaire* value dependent on both fineness and maturity (fibre shape), are a typical example. These methods reflected the electromechanical and electronic technology of the time. After 1980, developments in robotics, sensors and computers enabled these methods to be combined with automatic handling, which fed samples through a series of tests. For cotton, HVI (high-volume instrumentation) is ‘an integrated, automatic or semi-automatic system of cotton fibre measurement hardware, software and calibration for the rapid estimation of several fibre properties in a single sample’ [2]. Typically, HVI covers micronaire, fibre length and length distribution, fibre bundle strength and elongation, colour (reflectance and yellowness), and trash content. One HVI line can test over 800 samples for length, length uniformity, short fibre content, strength, extension, micronaire and colour in a single shift [3]. Another method in current use is the Uster Advanced Fibre Information System (AFIS), which reports length and length distribution, fineness and maturity, neps, trash and dust. A 0.5 gram sample is hand-drawn into a 25 cm sliver. The results are influenced

by operator technique and a test takes 3 minutes, so that the method is not suitable for routine commercial testing, but can be used in laboratory testing [4].

By the end of the century, the IT revolution had led to further advances in digital imaging and information processing. New methods, which were faster and gave more direct information on fibre dimensions, have been introduced. As the 21st century continues, these methods are likely to replace older methods. Because the move to *sale-by-specification* came later to wool than to cotton and because the fineness of the near-circular fibres was the major defining quality parameter, digital techniques, such as the *CSIRO Laserscan* and the OFDA technology described in the next chapter, have been adopted sooner.

The commercial practices are designed to provide sufficient information at minimum cost. The test methods for dimensions, strength and other properties will be described in later chapters. It is beyond the scope of this book to give full instructions on test methods, but the basic principles will be presented. Further information on procedures can be obtained in publications of the International Committee for Cotton Test Methods, the International Wool Textile Organisation, and national and international standards. A selection of these standards is included in [Appendix III](#).

2.1.2 Material for testing

For research purposes, individual fibres can be selected and mounted for examination or testing. However, each operation is time-consuming and, with the variability of natural fibres, a very large number of fibres must be examined to get statistically useful results. In order to get the benefit of automated high-speed testing, provision of the test sample is as challenging a problem as the test method itself. After the initial preparation of a suitably aligned tuft of material, a way must be found of selecting a representative selection of the fibres. For transverse dimensions, this has been solved by cutting snippets, which can be dispersed on a slide for microscopic examination. For fibre length measurement and for tensile testing, the problem is more difficult and tufts of fibres are examined. The data may then need processing to obtain the required information.

Account must also be taken of variability in fibre dimensions and physical properties, which means that appropriate sampling procedures from the bale or other source are needed, particularly for natural fibres.

2.2 Variability and sampling

2.2.1 Quality control in manufactured fibres

With a few exceptions, such as melt-blown non-wovens and stretch-broken tows, manufactured fibres are made to controlled specifications. Chemical composition and manufacturing operations are controlled to give constant dimensions and physical properties. Standard deviations are small, though they may be significant. The scientific researcher has no difficulty in taking test samples from a package. However, it is important to specify the source and designation. One manufacturer's nylon or polyester is not the same as another's.

Nevertheless, faults can occur in manufacturing, so that quality control is needed to maintain standards. This can be done by a programme of sampling production at intervals and sending material to the test laboratory. However, there is an increasing use of on-line testing.

2.2.2 Natural fibres

For natural fibres, the situation is different. There is always appreciable variability and often great variability. Even the product of a single farm in a single season will show variations along fibres, between fibres in a cotton boll or a lock of wool, between neighbouring bolls on a cotton plant or parts of a fleece, and between different plants or animals. A typical example of variability in a consignment of cotton is shown in Table 2.1. Sources of variation are discussed by Steadman [6]. There are similar variations in other natural fibres.

The value of a source of fibre depends on the dimensions and other qualities, which have to be evaluated. There have been major changes since the mid-20th century and the evolution from subjective to objective assessment is described in Section 2.1. However, sampling is always necessary. As an example, before about 1960 the commercial procedure was for skilled buyers to view wool in bales, which had been opened up in a wool-broker's store before an auction [7]. Although the whole lot was available to them, inevitably the buyers only looked at small portions of opened bales. This was subjective sampling. Now, representative *grab samples* are displayed in viewing boxes and *core samples*, produced by punching a sharp tube into the bale, are sent to a test-house for objective testing. In the cotton industry, samples of cotton were taken from the bale after ginning for cotton classing. This procedure is still widely used, but there is a move towards samples being taken for objective testing [4]. For sampling at a later stage, Steadman [6] comments: 'As cotton is the most homogeneous of the natural fibres, when the fibre reaches the mill the usual practice is simply to cut off a sample from each side of the bale and discard the cut edges.' For routine evaluation of the wool and cotton crop, speed and cheapness of sampling are important factors, provided the information generated is adequate to determine price and expected performance. For research studies, more care may be

Table 2.1 Coefficient of variation (%) in a consignment of cotton [5.0].

Property	Between bales	Within bales
Micronaire	14.2	2.6
Upper half mean length	1.3	1.1
Strength	4.6	4.6
Extensibility	5.7	6.2
Reflectance	1.1	4.4
Yellowness	5.7	4.9
Colour grade	34	41
Trash area	99	112
Short fibre content	15.5	15

needed to obtain representative samples for detailed testing, which may be used to calibrate or validate quicker test methods or for scientific investigations.

With little alteration, the account written by W. E. Morton for the 1st and 2nd editions of this book brings out the principles and problems of sampling. Practical information on sampling is given by Saville [8].

2.2.3 Sampling requirements

Practically every measurement made on textile materials must of necessity be restricted to only a small fraction of the bulk. Where testing is carried out for commercial purposes, and especially when it is destructive, as in strength-testing, the reason for this is obvious, but in the general case the bulk is nearly always so large that to test it completely would be quite impracticable, even if any material advantage were to be gained by doing so. It is therefore almost invariably the practice to measure a sample only.

Whether and how far the results obtained from a sample may be relied upon to characterise the bulk, or, in statistical parlance, the 'population', from which it is drawn, depends on two things: the size of the sample and the manner in which it is taken.

As regards the size of the sample, little need be said here. Naturally, the larger the sample, i.e. the greater the number of individuals it contains, the more closely do the results obtained from it agree with those which would be obtained from the entire population. How large the sample should be to raise the confidence in the results to any desired level can be readily determined by the application of elementary statistical method. All that is needed is an estimate of the variability of the character measured, and this may be obtained from the sample itself or assumed as a result of past experience¹. Unfortunately, the properties of textile materials are generally characterised by such great variability that samples must nearly always be relatively large if useful reliability is to be assured. Except in special circumstances, which will be noted later, no matter how large a sample may be, it is useless unless it is also representative.

In any attempt to take a truly representative sample, or what is termed a 'numerical' sample, the guiding principle is simple to state: the technique should be such that every individual in the parent population has the same chance of being included in the sample. It is not so simple, however, to follow this precept in practice. The requirement would be met completely if we were free to take, absolutely at random and without conscious selection, any individual whatsoever, regardless of where it is to be found in the population. In fact, our freedom to do this is commonly limited, and sometimes severely limited, either by the amount of labour that would be involved or because of other, and even more practical, considerations. In commercial yarn- and cloth-testing, for example, a perfectly random sample is never possible because the bulk to be characterised would be spoilt by the taking of the individuals. The sampling of fibrous raw materials in bulk form may also suffer from limitations of a

¹Useful data are included in BS EN 12751:1999.

similar kind, though not so acutely. In all cases where such limitations apply, it must be recognised that, to the extent that a sample is not a perfectly random one, so will the results from it be less reliable than as indicated by the experimentally determined standard errors.

In fibre testing, however, uncertainty arising from restrictions on random selection can generally be reduced to small proportions without much difficulty. On the other hand, unless special precautions are taken, a much greater source of error may be introduced, which arises from the essential nature of a fibre, namely, that it is very much longer than it is thick. Because of this, it is only too easy to take a sample in such a way that it contains far more long fibres than it should; this is true whatever form the population of fibres may take, whether bale, top, roving, yarn or cloth. The nature and avoidance of this bias in favour of the longer fibres will be discussed in succeeding sections, but at this point two observations should be made.

The first is that length bias is not only of importance when fibre length is the quantity to be measured. It is also important when the test is for any fibre property associated with length. Thus with wool, for example, where there is a strong correlation between fibre length and fibre diameter, any sample biased in favour of length will also be biased in favour of coarseness. Again, in cotton, bias for length may be accompanied by a bias for strength [9] (see [Section 13.5.2](#)).

The second is that there are some circumstances in which the taking of a biased sample is convenient and desirable, or even essential. In such cases, it almost goes without saying that the quantitative nature of the bias must be known. If not, the results of any measurements made can never tell us anything useful about the population we desire to characterise. For the relation between biased and numerical samples to be known, certain conditions must be satisfied. These will be discussed in the sections that follow.

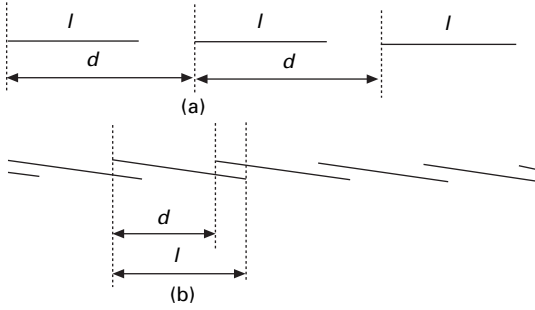
2.3 Numerical and biased samples

2.3.1 Numerical proportions

Consider first a highly idealised, homogeneous strand of overlapping straight, and parallel fibres. Since it is homogeneous, its composition is the same at all parts along its length. There are no concentrations of long fibres in some parts or short fibres in others; the short fibres are spread out evenly throughout its length, and so also are the long fibres or fibres of any other designated length. The different lengths of fibres present may, in fact, be mixed thoroughly together, but no invalid assumptions are involved if, for our present purpose, we imagine the strand to be made up of a large number of superimposed streams of fibres, each stream consisting of fibres all of a particular length.

If we take any one of these streams characterised by a length l , then, since the fibres composing it are spread out evenly, the displacement of one with respect to the next is constant, as shown in [Fig. 2.1](#).

Let the displacement be denoted by d , the number of fibres in the stream by n , and the length of the strand by L . If n is small, then d is large compared with l and there are gaps between the individuals, as at (a). If, on the other hand, n is large enough,



2.1 Fibre displacement.

d is less than l and there is overlapping, as shown at (b). In either event and in the general case, the number of whole fibres in any stream is given by:

$$n = \frac{L}{d} \quad (2.1)$$

Let the quantities referring to the several streams be denoted by the suffixes 1, 2, 3 ... etc. Then the total number of fibres in the complete strand is:

$$n_1 + n_2 + n_3 + \dots = \sum n$$

and the numbers of fibres in the several streams, expressed as fractions of the total for the strand, are

$$\frac{n_1}{\sum n}, \frac{n_2}{\sum n}, \frac{n_3}{\sum n}, \dots \quad (2.2)$$

This, then, is the pattern of the numerical proportions (frequencies) of the various fibre lengths present in the strand as a whole.

2.3.2 Length bias

In taking a sample from such a strand, the most natural procedure would be to take a pair of tweezers and pick out a few fibres here and there at random all over the strand until a sample of sufficient size has been obtained. Let us examine the consequences of such action.

Consider first the stream of fibres at (a). Since the points of the tweezers are applied entirely at random, it is by no means certain that any fibre at all will be taken from the stream. The probability of one being taken at each attempt is obviously l/d . If k attempts are made, then in the long run of experience the number taken will be $kl/d = knl/L$, since $n = L/d$, from equation (2.1).

Consider next the stream at (b). The probability of taking a fibre here is greater than 1, i.e. at least one will be taken every time and sometimes two. If $l = 2d$, it is a certainty that two would be taken every time. Thus, in k attempts, the number taken is still $kl/d = knl/L$. This relationship, in fact, holds good whatever the values of l or d , and the numbers of fibres taken from the various streams are:

$$\frac{kn_1l_1}{L}, \frac{kn_2l_2}{L}, \frac{kn_3l_3}{L}, \dots \quad (2.3)$$

or, expressed as fractions of the number of fibres in the entire sample:

$$\frac{n_1l_1}{\sum nl}, \frac{n_2l_2}{\sum nl}, \frac{n_3l_3}{\sum nl}, \dots \quad (2.4)$$

It is thus seen that, in the sample, the proportionate frequency of occurrence of fibres of any particular length is determined, not only by n , the number of them occurring in the strand as a whole, but also by how long they are. For example, if equal numbers of 50 mm and 25 mm fibres are present in the strand, the 50 mm fibres will be twice as numerous in the sample as the 25 mm fibres. Every fibre does not have an equal chance of being included in the sample, and we have not, therefore, obtained a representative, or numerical, sample. What we have instead is a length-biased sample, sometimes referred to as a Wilkinson tuft [10, 11].

2.3.3 Frequencies, length proportions and mass proportions

It will be noted that the quantities, n_1l_1 , n_2l_2 , n_3l_3 , etc., give the total lengths of fibre of lengths, l_1 , l_2 , l_3 , etc., respectively, in a numerical sample and that $\sum nl$ is the total length of fibre in a numerical sample as a whole. Thus the terms in equation (2.4) above, which represent the *frequencies* in a length-biased sample, also represent the proportions by length, or *length proportions*, in a numerical sample.

Furthermore, if the fibre mass per unit length is the same for all lengths, length proportions are equivalent to mass proportions (often referred to as weight proportions). Hence, under these conditions, the frequencies in a length-biased sample are also equivalent to the mass proportions in a numerical sample.

In practice, there are some circumstances in which the proportions by length or the proportions by mass are the quantities in which we are really interested, for example, in studies of fibre breakage in carding or of length fractionating in combing. In such cases, if a numerical sample is taken, the desired quantities must be calculated from the frequencies by multiplying the latter by the corresponding lengths. If, on the other hand, a length-biased sample is taken, the frequencies obtained from it give the desired quantities directly.

Length-biased samples have their uses also in other contexts. For example, suppose that we wish to determine the mean diameter of a sample of wool by a method in which the diameter is measured at one point only on each fibre examined. If the sample taken were a numerical one, long fibres would be given no greater weight than short fibres, and, the relation between length and fineness of wool being what it is, the resultant mean would be too low. Clearly, in such a case, the results should be weighted for length, and the only way of doing this is to work with a length-biased sample. It cannot be too strongly emphasised, however, that, in taking a sample of this kind, the population to be sampled must consist of fibres that are straight and parallel: otherwise the bias, or weighting, for length is indeterminate (see [Section 3.5](#)). Length-biased sampling is therefore only practicable when the material to be examined is in the form of well-drawn slivers, tops, rovings or yarns.

2.3.4 Tong sampling for length bias

In the procedure already described, which resulted in a length-biased sample, it will have been noted that, at each application of the tweezers, only those fibres were taken that *passed through a cross-sectional area* of the strand, the section being that normal to the fibres and lying in the plane between the points of the tweezers. This basic principle of sampling for length bias is utilised in the tong-sampling method [12], where two pairs of narrow clamps or surgical tongs with leather-lined jaws are used for defining the section.

A portion of the top, sliver, roving or yarn is clamped at right angles by one pair of tongs, and the fibres at one side are combed so as to remove those not gripped. The resulting combed tuft projecting from the side of the tongs is now clamped by the second pair of tongs, which are placed parallel to, and in contact with, the first pair. The first pair is then removed and the fibres not gripped by the second pair combed out on the side not hitherto combed. The fibres retained in the second pair are thus all those that crossed a plane perpendicular to the length of the sliver, and these constitute the sample.

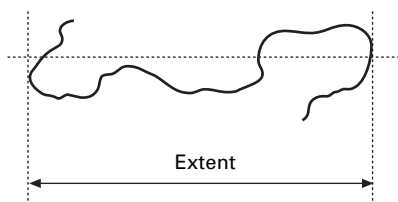
This method has been found satisfactory for wool materials [13], but according to Hertel [14] it is not very suitable for cotton because fibre breakage is excessive if the combing is to be effective.

2.3.5 Extent bias

In the foregoing, we have considered only the special case where all the fibres are assumed to lie straight and parallel in the strand, and where those fibres are taken that pass through a plane at right angles to the axis of the strand. In card webs and card slivers, and especially in bulk samples of unprocessed raw materials, however, the arrangement of the fibres is anything but regular. The fibres may be crimped and distorted, they may be bent over into a hooked form at one or both ends, and they may vary very greatly in their orientation. Even in uncombed, but otherwise well-drafted, slivers, perfect straightness and orientation of the fibres cannot be assumed with certainty. It is, therefore, necessary to introduce the notion of *fibre extent*.

Fibre extent may be defined as the length of the projection of a fibre on any chosen axis of orientation. With slivers, rovings and yarns, the direction in which extent is measured is usually parallel to the axis of the strand. With card webs, it is usually parallel to the card sides. With samples of loose raw materials, it may be anything one chooses. As will be clear from [Fig. 2.2](#), the extremities of the projection are not necessarily determined by the ends of the fibre under consideration.

Under conditions such as these, if fibres are taken which pass through a given cross-section, the sample is biased for extent, and, unless the ratio of fibre extent to fibre length is constant for all fibres, the degree of bias is indeterminate. Apart from bast and leaf fibres, nearly all fibres are crimped in some degree, and it could thus be argued that, in practice, a length-biased sample is an impossibility. However, provided that the population to be sampled is not a blend of materials having different crimp characteristics, and provided that, except for the crimp, the fibres are straight, the



2.2 Fibre extent.

extent/length ratio can be assumed to be constant. Under any other conditions, an extent-biased sample is of no use whatever.

2.3.6 Avoidance of extent bias

The object is to take fibres of the different lengths present in numerical proportions determined solely by their several frequencies of occurrence in the entire population.

We have seen from equation (2.1) that, in a strand of length L , the number of fibres n of any length l is inversely proportional to d . What we have to ensure is that this also holds good for the sample.

From Fig. 2.1, it is evident that the probability of any chosen *point* on a fibre occurring within any short length δL of the strand is strictly proportional to the ratio $\delta L/d$. If, then, we take one or other of the fibre ends as our chosen point, we see that the solution of our problem is to take *all fibres that terminate within a given volume*, i.e. within any chosen length δL of the strand, since δL is the same for all fibres.

The size of the sample taken depends on what we choose for our δL , but the composition of the sample reflects truly, on a reduced scale, the composition of the entire population, and we have an unbiased sample. Selection is made according to the occurrence of fibre ends, of which every fibre has two, whatever its length. Length therefore plays no part in the selection. This remains true whether we are dealing with fibres that are straight or fibres that are crimped and disarranged, as is clearly demonstrated in Section 2.4.2.

2.4 Sampling techniques

2.4.1 Squaring and cut-squaring

Squaring and cut-squaring are two related methods that are applicable to slivers, rovings or yarns in which the fibres are in a reasonably ordered state and give a numerical sample. In what follows, it will be assumed that the material to be sampled is in the form of a sliver.

In the simplest form of this operation [15], the sliver is opened out, without disturbing the fibres, into a flat ribbon, and one end is roughly squared by hand. It is then placed on a black velvet-covered board, and a sheet of glass, of suitable size and weight, is laid on top of it, leaving a short fringe projecting. The projecting fibres are now removed in *small* groups with tweezers until the edge of the glass is reached, whereupon the glass plate is moved back a short distance to expose a new fringe,

which is similarly treated. This is repeated until a succession of fringes have been squared back a distance at least equal to the length of the longest fibre present. Only then is the actual sample taken for measurement by moving the plate back a further short distance and withdrawing *all* the fibres that now project beyond its edge. These fibres are those that terminated in a given volume and so constitute an unbiased sample provided that the precautions mentioned are observed.

The succession of preparatory squarings, before the sample is taken, is absolutely essential because the fringe formed at the broken edge of any fibrous strand naturally contains a predominance of longer fibres, and this initial bias can be eliminated only in the manner described.

The pressure of the glass plate on the velvet board effectively controls the fibres during squaring and during the taking of the sample, while the thickness of the glass can be chosen so as to give optimum control without breakage. Since the control is by friction, and not by positive grip, looped and even slightly tangled fibres can be withdrawn, though, with cotton fibres at least, the possibility of the breakage of some fibres is always present.

In the withdrawal of fibres from the fringes, long or somewhat tangled fibres sometimes drag out with them other fibres initially lying wholly behind the edge of the glass. This is minimised by drawing the fibres almost singly, but, in any case, no bias is introduced provided this form of disturbance occurs equally in the final drawing of the sample as during the preparatory squarings. Hence the manner of withdrawal must be the same at all stages, and so also must the distance by which the plate is moved. The latter, of course, determines the size of the sample taken.

Cut-squaring is a modification of the squaring technique, designed to minimise the labour of preparatory squaring [12, 15]. Here the strand is cut to a straight edge instead of being broken and is then covered with a glass plate, as before. In theory, only one preparatory squaring of the fringe is now necessary because all the cut fibres are removed at this one stage, and the fibres whose ends project beyond the glass, when next moved back a short distance, should constitute a numerical sample. It has been shown [16], however, that in practice this is not the case and that a series of at least three preparatory squarings is necessary. The reason for this is probably to be found in the fact that the conditions under which the cut fibres are withdrawn in the first stage are not the same as those prevailing when the fibres forming the second fringe are extracted to form the sample. In the first stage, the fringe is dense, and it is inevitable that the fibres must be drawn in rather large bunches, thus giving rise to a greater degree of fibre disturbance than when the much thinner second fringe is dealt with. Hence errors due to disturbance during the taking of the sample are not cancelled out by corresponding errors during the preparatory squaring. In general, short fibres are the ones that are most easily dragged forward out of turn, and consequently, with only one preparatory 'fringing', the observed mean length is too high, the sample being deficient in short fibres.

The reason why *all* projecting fibres in the final fringe must be taken is that, if any attempt at random selection is made, bias is almost certain to be introduced by an unconscious preference for thick fibres. Thickness may be, and with wool certainly is, correlated with length.

2.4.2 Dye-sampling

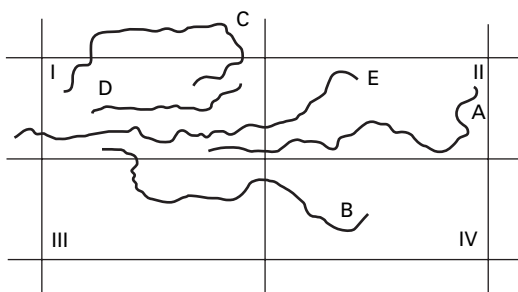
This method was evolved [16] primarily for the sampling of wool fibres in the form of card web with the object of reducing to negligible proportions the risk of fibre breakage, which is considerable if a card sliver is sampled by the squaring method. In general, it is applicable only to thin layers of fibre, as in card or comber webs, or to tops or slivers that can be opened out into thin-web form.

As required for the taking of a numerical sample, the fibres are to be identified by the occurrence of their ends in a given volume. Accordingly, the web is coloured over a small rectangular area by means of a brass or wooden block covered on one face with filter paper uniformly wetted with a suitable dye. Fibres passing through the coloured patch, and therefore having undyed ends, are neglected. Those terminating within the patch, and thus having one or both ends stained, are taken as the sample. The only proviso is that, in the final computations, fibres having only one end stained should be accorded half the weight of those having both ends stained. Thus the lengths of those with one end dyed and with two ends dyed are recorded separately. The true fibre-length distribution is then given by adding half the number of one-enders to the number of two-enders in each length group.

The necessity for this is readily seen by noting the requirement that taking fibres from the stained patch should not alter the composition of any possible adjoining patch. Let rectangle I in Fig. 2.3 be the dyed patch. Fibre E has neither end stained and is neglected. Taking A and B for patch I deprives patches II and IV of fibres to which they have an equal claim. Fibres C and D, on the other hand, cannot be claimed by any other patch, and hence, if these are given a weight of unity, A and B must each be counted as half-fibres.

There is an optimum size and shape of patch for each material to be sampled. If the patch is too small, or too long and narrow and placed transversely to the general orientation of the fibres, a large number of them pass right through the defined area and have to be handled even though they do not contribute to the sample. There is thus waste of time and effort.

For wool card webs, a patch 1.5 cm square is recommended [13], but for shorter fibres a somewhat smaller area would probably be more suitable. As regards shape, there are some circumstances in which the patch should preferably be oblong and lie



2.3 Dye-sampling.

along the direction of general fibre orientation. The more oriented the fibres, the longer and thinner the oblong should be [16].

In taking the fibres for measurement, the portion of web containing the dyed patch (when dry) is covered with a microscope slide, which has rounded edges. The fibres are then removed with forceps by drawing them one by one from under the slide, which the operator is free to move about at his or her convenience. It will be observed that the method is only suitable in cases in which the fibres are to be measured individually.

2.5 Zoning

2.5.1 The problem of heterogeneity

An individual sample obtained by any of the methods so far described represents the population under examination only if the composition of the population is the same at every point. In fact, this is very rarely, if ever, true of textile populations, and, in the absence of definite knowledge to the contrary, it should be assumed that the population is heterogeneous, i.e. that its composition varies from one part to another. This being the case, a sample draw taken from any one part must be regarded as no more than a sub-sample; the sample representative of the entire population should consist of several such sub-samples taken at random from different parts in such a way that all the elements of heterogeneity are represented in due proportion. Such an operation is referred to as zoning.

The extent to which a population must be zoned depends, of course, on how and to what extent it varies in composition from place to place, which must be found from experiment if it is not known from experience. Considering the sampling technique as a whole, including zoning, the method adopted should satisfy the requirement that replicate samples should all yield results between which the differences are statistically insignificant.

Quoting from a standard:

When carried to the limit, zoning consists in taking the required number of individuals singly from the same number of selected parts or zones. Due representation with any desired degree of accuracy is then obtained with the minimum number of individuals. However, the saving in time secured by reducing to a minimum the number of measurements that have to be made may be more than offset by the extra time required to prepare the extra zones.

If the between-zone variance is small by comparison with the within-zone variance,

it is common practice to take a relatively large number of individuals from a relatively small number of zones, even if in so doing it is necessary to maintain the accuracy by taking a rather larger number of individuals all told [17].

Sampling from slivers, rovings and yarns is comparatively simple because the fibres have been fairly well mixed in the processes through which they have passed, and the material is reasonably homogeneous. Zoning on a modest scale is therefore

all that is required. In dealing with masses of fibre in a loose state, however, it is quite otherwise, and, furthermore, special difficulties are encountered.

2.5.2 Sampling from raw materials in a loose state

Ideally, as already indicated, the required number of fibres should be taken one at a time from a corresponding number of places distributed at random all over the bale, bag or whatever other form the population assumes. This, of course, would be impracticable because of the amount of labour involved. Of greater importance is the fact that it would be impossible in this way to obtain a sample free from extent bias. The reason is that each fibre would have to be extracted with tweezers and would therefore be a fibre passing through a selected cross-sectional area.

The same objection would still hold good if a wisp of, say, ten or a dozen fibres at a time were taken. Extent bias can, in fact, only be avoided if we take, not small wisps, but quite large tufts of fibre from each zone. Preferably, these tufts should be natural units. In cotton, for example, they might be discrete clusters of fibre from single seeds, while in wool they might be natural locks.

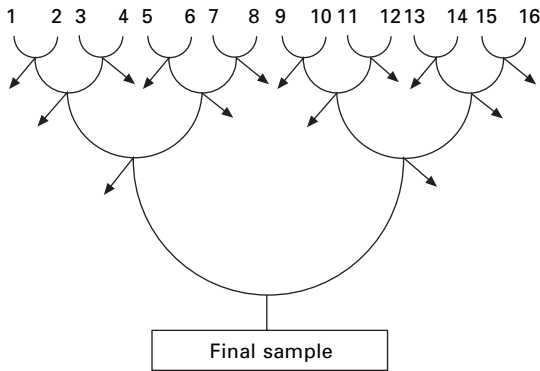
In any event, if zoning is to be carried out on any reasonable scale commensurate with the heterogeneity present, we are faced with an initial sample of very considerable size, in most cases, far greater than can be used for subsequent measurement. For some purposes, the final sample has to be of 1000 fibres or fewer, a mere fraction of the quantity, for instance, that is to be found on a single cotton seed. If m tufts have been taken, averaging w grams each, then somehow the whole mw grams of material must be reduced in size so that the final sample of the required size contains, in due proportion, representative fibres from all the original m tufts.

One method is to proceed by a process of successive halvings. Each of the m tufts is divided into two approximately equal parts, care being taken to avoid fibre breakage, and one half discarded. The retained half is again divided into two and one half discarded. This is repeated until the remnants of all the tufts taken together provide a sample of the required size.

If the fibres in the portions being divided are substantially parallel, the portions should be split lengthwise. This is important because, if the projecting fibres at the two ends of such a tuft are held, and the tuft is drawn into two parts by separating the hands, it is almost certain that one part will be greater than the other. The smaller part will be deficient in short fibres, and the larger in long; whichever part is discarded, that remaining will no longer represent the original tuft. The plane of cleavage should therefore be parallel to the fibres.

In order to reduce still further the possibility of introducing any systematic bias, it was at one time thought desirable that the choice of which half should be discarded should be made at random, but in practice this is not easy to do. An alternative procedure therefore commonly employed is to discard with the right hand and left hand alternately [18]. However, so long as lengthwise splitting is resorted to when conditions require it, the question is probably unimportant.

A somewhat different procedure, suitable for manufactured staple fibres, is as follows. The initial sample obtained by zoning is formed into 16 tufts, and, by a



2.4 Zoning.

process of doubling, drawing, halving and discarding, these are reduced to the representative sample for measurement as indicated in Fig. 2.4. Here, the tufts are taken in pairs and repeatedly drafted by hand and recombined before being divided into two parts. Since the fibres are thereby not only thoroughly mixed together but also effectively parallelised, lengthwise splitting is essential.

For cotton and other fibres of similar length, mechanical blenders are available, capable of reducing an aggregation of zonal tufts to a homogeneous batt or sliver from which the final test sample can be taken by any of the methods appropriate to material in that form.

The earliest of such mechanical devices was the Balls drawbox [19], a miniature drawframe consisting of two pairs of rollers and a special collecting device. A zoned sample weighing about 0.5 g is roughly formed by hand into a sliver about 20 cm long. This is then drafted between the drawbox rollers, which are set at a distance apart appropriate to the length of the fibres. On emerging from the delivery rollers, the fibres are deposited on a small revolving drum covered with 'one-way' hatter's plush, where they form a lap. The lapping of the fibres in successive layers on the drum mixes them effectively, and the lap may be split off and redrawn as often as desired².

Later machines, which are useful in preparing samples for fineness testing by air-flow methods or for other tests, are the SDL *Shirley Analyser*, developed for measuring trash content in cotton, and the SDL *Fibreblender*. Samples prepared by this and other such devices are thoroughly well mixed, but there is always danger of fibre breakage unless great care is taken to adjust the settings of the instrument in accordance with the maker's instructions.

2.6 References

1. J. L. Knowlton, *Proc. Cotton Council Int. Cotton Symp.*, Turkey, 2005.
2. M. J. Denton and P. N. Daniels (Editors). *Textile Terms And Definitions*, 11th edition, The Textile Institute, Manchester, 2002.

²Balls recommends four times for cotton.

3. H. Ghorashi. Report to ITMF HVI Working Group Meeting, Bremen, 2006.
4. S. Gordon. In *Cotton: Science and Technology*, S. Gordon and Y. L. Hsieh (Editors), Woodhead Publishing, Cambridge, 2006, p. 68.
5. P. R. Lord *7th Engineered Fiber Selection Conference*, 1994, 159.
6. R. G. Steadman, *Cotton Testing, Textile Progress*, 1997, **27**, Number 1.
7. W. S. Simpson In *Wool: Science and Technology*, W. S. Simpson and G. H. Crawshaw (Editors), Woodhead Publishing, Cambridge, 2002, p. 1.
8. B. P. Saville, *Physical Testing Of Textiles*, Woodhead Publishing, Cambridge, 1999.
9. O. W. Morlier, R. S. Orr and J. N. Grant. *Text. Res. J.*, 1951, **21**, 6.
10. H. Wilkinson. *J. Text. Sci.*, 1928, **2**, 104.
11. S. Townend. *J. Text. Inst.*, 1935, **26**, T130.
12. BS 2545: 1965.
13. S. Townend. *J. Text. Inst.*, 1938, **29**, T55.
14. K. L. Hertel. *Text. Res.*, 1940, **10**, 510.
15. H. E. Daniels. *J. Text. Inst.*, 1942, **33**, T137.
16. R. C. Palmer. *J. Text. Inst.*, 1948, **39**, T8.
17. T.T.S. No. 18. *J. Text. Inst.*, 1950, **41**, S1.
18. BISFA *Rules for Rayon Staple Fibre*, 1953 edition.
19. W. L. Balls. *A Method of Measuring the Length of Cotton Fibres*, Macmillan, London, 1921.

3.1 Fibre dimensions

The essential dimensional features of fibres are their fineness and length. Flexibility comes from fineness and length provides coherence. A fabric is a discontinuous solid, which is held together by friction and utilises the strength of the millions of separate fibres. Whereas two-dimensional assemblies of one-dimensional particles (powders) are just loose coatings and three-dimensional assemblies will flow, integrated two-dimensional assemblies of fibres are strong flexible sheets and three-dimensional assemblies are solid blocks.

The three 'ones' in bold type in Table 3.1 are a convenient order of magnitude of fibre dimensions, though they are at the low ends of fineness, length and density. The table includes calculated values for other quantities. Approximate ranges from these values are also indicated. Fineness is best expressed by linear density (mass/length).

Table 3.1 Fibre dimensions

	'Typical'	Approximate range
Linear density	1 dtex	to 20 dtex
Length	1 cm	staple fibres to 10 cm; filament to infinity
Density	1 g/cm³	polymer fibres to 1.5 g/cm ³ ; others to 10 g/cm ³
Mass	1 µg	20 dtex, 10 cm, 1.5 g/cm ³ → 300 µg
Diameter	11.3 µm	20 dtex, 1 g/cm ³ → 50 µm
Aspect ratio	1000:1	to ~ 10 000:1 for staple → infinity for filament
Specific surface	355 m ² /kg	20 dtex, 1 g/cm ³ → 80 m ² /kg
Assembly	10 ⁹ fibres/kg	
1 square metre at 100 g/m ²	10 ⁸ fibres	
Fibre elements	10 ¹² per kg	

tex = g/km dtex = decitex = g/10 km

Although the use of tex (g/km), which was adopted in 1960 and is recognised for use in the SI system, and millitex (mtex) are preferred for scientific orthodoxy, the decitex (dtex) value is commonly used because it is close to the value for denier (g/9000 m), which was the standard measure for silk¹, was adopted by the manufactured fibre industry and was used for most of the 20th century². When the linear density exceeds about 20 dtex (circa 50 μm diameter), the ‘fibres’ are commonly regarded as bristles or monofilaments and generally lie outside the scope of this book. At the other extreme *microfibres* were produced later in the 20th century and are now important in textiles. Even more recently, *nanofibres*, produced by electrospinning and in other ways, are entering the industry.

As shown in [Table 3.1](#), fibres have an enormous specific surface and a fibre assembly contains vast numbers of fibres. Even a small piece of a lightweight fabric might contain 100 million fibres. Interactions of fibre elements, as illustrated in [Fig. 3.1](#), may occur over lengths comparable to the diameter. Hence the number of interactions may be of the order of 10^{12} . These facts have a major influence on the performance of textiles and the study of the mechanics of fibre yarns and fabrics.

Historically, the overwhelming importance of fineness in determining quality and commercial value was recognised in the worsted industry, where a short fine wool is known to be much more valuable than a long coarse one. Synthetic fibre producers also appreciate the value of fineness, with microfibres commanding a premium price. With cotton, particularly before the worldwide adoption of improved varieties, length was a more important quantity than fineness in giving strength to yarns. Furthermore, fineness mostly correlated with length. Consequently, length, which was easily estimated by cotton classers by preparing a *staple*³, was given much of the credit that should more properly have been accorded to the fineness. Since W. E. Morton was a Professor in Manchester, the heart of the cotton industry, it was therefore natural for fibre length to precede transverse dimensions in the first edition of this book. Now fineness is recognised as a more important indicator of fibre quality.

Some standard test methods for measuring fineness are listed in [Appendix III](#).



3.1 Interaction of fibre elements.

¹The origin of the word *denier* is interesting. It is the name of an old French coin (Latin *denarius*). The fineness of silk yarns was specified by the weight (number of coins) in denier of a standard hank. This gives a direct measure of linear density. In the cotton and wool industries, various indirect measures (counts) were used based on the number of standard hanks making up a given consignment weight.

²An approach to rational units in the 1950s adopted the name *grex* for g/10 000 m, but this was displaced by *dtex* and is only found in some older literature, such as the book by Kaswell [1].

³A lock or tuft of fibre, characteristic of a bulk sample, prepared to demonstrate fibre length [2].

3.2 Terms and definitions

3.2.1 Linear density

The accurate measurement of very small lengths requires considerable expertise and care and, for fibres with irregular shapes, *thickness* defined as the apparent width of a fibre is an ill-defined quantity. Consequently, the most useful and unambiguous measure of *fibre fineness* is the *linear density*, namely mass per unit length, sometimes called *titre*. As mentioned above, the preferred unit is tex = g/km. This has the advantage that it is applicable with appropriate prefixes to all the one-dimensional structures from polymer molecules to yarns, cords and ropes. The linear density is additive in terms of the number of units in the cross-section, making allowance for any obliquity. There is no uncertainty associated with density of packing, as occurs when fineness is expressed as thickness.

The widespread use of *denier* has been mentioned and micrograms per inch has also been used for cotton. For staple yarns, the indirect term *count* (length/mass) was based on the number of skeins with a given number of turns making up a given weight. Many different systems were used for different fibres in different places. Fibre fineness was sometimes expressed by the finest count that could be spun from a given sample.

3.2.2 Transverse dimensions

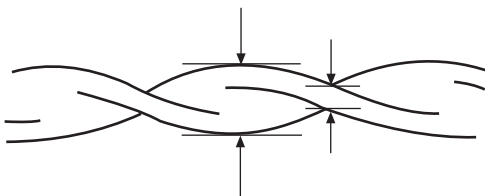
For continuous filament yarns and the tows cut to make staple fibre, the total linear density is easily measured by weighing a given length, and the fibre linear density is given by dividing by the number of fibres in the cross-section. For natural fibres, it is necessary to measure the length and mass of many individual fibres, in order to determine the average linear density. This is difficult and time-consuming. Other measures of linear dimensions are therefore used. For cotton the *micronaire value*, which is an arbitrary measure of fibre specific surface, discussed below, is used. For wool the apparent diameter in micrometre (μm), often referred to by the old name of *micron*, is used. In addition, there are many problems in fibre and textile research and performance evaluation where other linear dimensions have to be taken into account. We must therefore consider the various quantities, their meanings and definitions. For circular fibres, area, circumference, diameter (or radius) are the only parameters. For other fibres, there are more complicated descriptions.

- *Diameter*. In the early literature of textile science, the quantity invariably used for defining the fineness or coarseness of a fibre was the diameter. For wool, which is not so very far from circular and which, except for lamb's wool, does not vary in thickness systematically along its length, this was reasonable enough. For many synthetic fibres, which are even more perfectly cylindrical, fibre diameter is clearly defined. For other fibres, however, which are of irregular cross-sectional shape or which taper towards one or both ends, the term diameter has no real meaning.
- *Width*. What was frequently referred to as fibre diameter in early books about

cotton was really the maximum width as viewed under the microscope. The convoluted fibre varies in apparent width over a wide range throughout the length of each convolution, and either the maximum or the minimum may be measured (Fig. 3.2). If the cross-sectional shape were elliptical, these dimensions would correspond to the major and minor axes of the ellipse. In the general case, for the purpose of characterising a raw material, mean fibre width suffers from the disadvantage that it is too dependent on fibre shape.

- *Perimeter* is a quantity that is perhaps familiar only to the technologist and is important mainly as a link between other dimensions. For circular or oval fibres, it is usually called the *circumference*.
- *Area of cross-section* is the most clearly defined transverse dimension. For a given type of fibre, area is proportional to the linear density, and, if the fibre density is known, the one may be calculated from the other. It is important to note, however, that, whereas the former is usually, and more easily, measured somewhere around the middle of the fibre, the latter has to be measured over an appreciable length of the fibre, maybe over its entire length, so that the relationship between the two is upset if taper is present. For hollow fibres it is necessary to distinguish between the area within the outer perimeter and the area of fibre material.
- *Specific surface* may be defined in two ways: either as the surface area per unit volume or the surface area per unit mass of the fibre. The former is the more useful from the technical point of view and is the more commonly encountered. Defined in this way, provided that there is no major variation in area, specific surface is given by the area of cross-section divided by the perimeter.
- *Fibre shape* takes a variety of forms, discussed in Section 3.10. As the shape departs from circular, the specific surface increases. A *modification ratio* can be defined as the ratio of the perimeter to the circumference of a circle of the same area.
- *Hollow fibres* are characterised by the ratio of the void area to the whole area of the fibre.
- *Wall thickness* is a dimension that has relevance only to hollow fibres.
- *Maturity* (see Section 3.10.2), which is a term only relevant to cotton, is not a direct measure of a transverse dimension, but is relevant because the wall thickness of cotton increases as the fibre grows to maturity.

Relations between these quantities are presented in the next three sections in consistent units, which eliminate the need for numerical factors. In particular, they



3.2 Cotton fibre major and minor axes.

apply in strict SI units, namely linear density in kg/m, length in m, area in m², density in kg/m³, specific surface on volume basis in m⁻¹, specific surface on mass basis in m²/kg. Alternative relations with more convenient units are also included; some equations are unchanged, others contain numerical factors.

3.2.3 Solid fibres of circular cross-section

Area A is related to diameter D and radius r by the equations:

$$A = \pi r^2 = \pi \frac{D^2}{4} \quad (3.1)$$

also valid with A in 10⁻¹² m², pico(metre)², r and D in μm .

Linear density c can be related to area A and density ρ or specific volume v but is more usefully related to radius or diameter:

$$c = A\rho = \frac{A}{v} \quad (3.2)$$

$$c = \pi r^2 \rho = \frac{\pi D^2 \rho}{4} \quad (3.3)$$

or with c in dtex, r and D in μm and ρ in g/cm³.

$$c = \frac{\pi r^2 \rho}{100} = \frac{\pi D^2 \rho}{400} \quad (3.4)$$

The inverse relations are:

$$r = \left(\frac{c}{\pi \rho} \right)^{1/2} \quad (3.5)$$

$$D = 2 \left(\frac{c}{\pi \rho} \right)^{1/2} \quad (3.6)$$

or with c in tex, r and D in μm and ρ in g/cm³:

$$r = 10 \left(\frac{c}{\pi \rho} \right)^{1/2} \quad (3.7)$$

$$D = 20 \left(\frac{c}{\pi \rho} \right)^{1/2} \quad (3.8)$$

The perimeter (circumference) P is given by:

$$P = 2 \pi r = \pi D \quad (3.9)$$

also valid with P , r and D in μm .

For a length L , surface area = PL and volume = AL . Hence, on a volume basis, specific surface S_v is given by:

$$S_v = P/A = 2/r = 4/D \quad (3.10)$$

also valid with S_v in $(\mu\text{m})^{-1}$ and r and D in μm .

It follows that, other things being equal, the finer the fibre, the greater is the specific surface.

For the length L , the mass is cL . Hence on a mass basis, specific surface is S_m is given by:

$$S_m = \frac{P}{c} = \frac{2\pi r}{c} = \frac{\pi D}{c} = 2 \left(\frac{\pi}{\rho c} \right)^{1/2} \quad (3.11)$$

or with S_m in m^2/kg , r and D in μm , c in dtex and ρ in g/cm^3 :

$$S_m = 10^5 \frac{P}{c} = (2 \times 10^5) \frac{\pi r}{c} = 10^5 \frac{\pi D}{c} = 20 \left(\frac{\pi}{\rho c} \right)^{1/2} \quad (3.12)$$

3.2.4 Solid fibres with cross-sections other than circular

The volume enclosed by a given surface diminishes according to the degree of departure from circularity of section. It is still correct to write $S_v = P/A$ and $S_m = P/c$, but the value for S_m given by equation (3.12) must be multiplied by a shape factor k greater than one. Thus the greater the ellipticity of section, as in wool, or the greater the extent of indentation in the sectional shape, as in viscose rayon, the greater is the specific surface for a given linear density.

The equations above in r and D are meaningless for non-circular fibres, except when equivalent values are used to match the area. Relations for elliptical cross-sections are given in mathematical textbooks.

3.2.5 Hollow fibres

For hollow fibres of circular cross-section, denote the outer edge by a subscript $[_o]$, the inner edge by $[_i]$, and the wall by $[_w]$. With A for area and r for radius, we have:

$$A_o = \pi r_o^2 \quad (3.13a)$$

$$A_i = \pi r_i^2 \quad (3.13b)$$

$$A_w = A_o - A_i = \pi r_o^2 - \pi r_i^2 \quad (3.13c)$$

$$\text{Void percentage} = 100 \left(\frac{A_i}{A_o} \right) \% \quad (3.14)$$

$$\text{Wall thickness} = (r_o - r_i) \quad (3.15)$$

The value of A_w should be substituted in equation (3.2) to give the linear density. Outer values should be used for perimeter and specific surface values. The effective fibre density = $(A_w/A_o) \rho = [(r_o^2 - r_i^2)/r_o^2] \rho$, where ρ is the density of the fibre

material. These relations may be used for hollow manufactured fibres, which are used for bulky fillings and for liquid separation.

Cotton fibres as grown are hollow tubes, but they collapse on drying, as discussed in Section 1.4.3. Geometrically, maturity⁴ has been defined by Peirce [3] as the ratio θ of the cross-sectional area, A_w , of the cell wall to the area, A_o , of a circle of the same perimeter P . Note that A_o is the area of the fibre before collapse, though the change in material area due to drying must be taken into account. Hertel and Craven [4] prefer the reciprocal of this, which they call the *immaturity ratio*, I . Thus:

$$\theta = \frac{1}{I} = \frac{A_w}{A_o} = \frac{4\pi A_w}{P^2} \quad (3.16)$$

For the fully collapsed fibre, the total fibre area A equals the wall area A_w . Hence:

$$S = \frac{P}{A} = \left(\frac{4\pi}{A} \right)^{1/2} = 2 \left(\frac{\pi\rho}{\theta c} \right)^{1/2} \quad (3.17)$$

$$\theta = \left(\frac{S^2}{4} \right) \left(\frac{c}{\pi\rho} \right) \quad (3.18)$$

3.3 The technical significance of fibre fineness

3.3.1 Stiffness, handle and drape of fabrics

For cylindrical rods or wires of homogeneous and isotropic materials, the resistance to bending varies as the square of the cross-sectional area. Textile fibres are rarely homogeneous, never isotropic and only in certain cases circular in cross-section. Even so, it still remains true that, as fineness varies and other things are equal, resistance to bending increases more rapidly than fibre linear density (see [Section 17.2.1](#)).

From this it follows that, for a yarn of given count or a fabric of given mass per unit area, made from a given type of raw material, the resistance to bending diminishes as the fineness of the fibre increases. Fibre fineness is thus an important factor in determining the stiffness of a fabric or, alternatively, its softness of handle and its draping quality.

3.3.2 Torsional rigidity

From similar considerations, it can be shown that, as fineness varies and other things are equal, resistance to torsion increases more rapidly than fibre linear density (see [Section 17.3.1](#)). Hence fineness plays a part in determining the ease with which fibres can be twisted together during yarn formation.

Considering the situation from another angle, it can be shown that the torque generated in a yarn of given count by a given amount of twist increases as the linear density of the fibres increases. Thus internal stresses capable of producing kinks and

⁴Referred to by Peirce and Lord [5] as the *degree of thickening*.

snarls in a yarn are greater when the constituent fibres are coarse than when they are fine. This is obviously a matter of considerable importance in the design of crêpe fabrics and in twist texturing.

3.3.3 Reflection of light

The finer the fibres incorporated in a fabric, the greater is the number of individual reflecting surfaces per unit area of the fabric. Fibre fineness therefore affects the character of the lustre of the fabric. In descriptive terms, fine fibres produce a soft 'sheen', whereas coarse fibres give rise to a hard 'glitter'.

Practically all textile materials are, however, translucent to a greater or lesser degree. A substantial part of the light reflected from a fabric is therefore reflected from internal surfaces, and in dyed fabrics the intensity of the light so reflected, i.e. the apparent depth of shade, depends on the mean path length of the light rays through the coloured substance. This in turn depends on the number of fibre surfaces, both internal and external, per unit depth of the structure. Hence, other things being equal, the finer the fibre, the lighter is the apparent shade [6–8], and fibres having central canals or medullary cavities will appear lighter than those that are solid.

3.3.4 Absorption of liquids and vapours

The rate at which dyes are absorbed into a fibre obviously depends on how much surface is accessible to the dye liquor for a given volume of the fibre substance, i.e. it depends on the specific surface [9, 10]. It therefore follows that the time required to exhaust a dye bath is shorter for fine fibres than for coarse and for fibres with strongly indented cross-sections than for those which are smoothly cylindrical.

It might be expected that, in a similar way, specific surface would also influence the rate of sorption of water vapour, but, except where fibres are exposed almost singly, the effect is negligible, since the rate of conditioning is overwhelmingly determined by the rate of diffusion of the vapour through the air bounded by the fibre mass and by the associated heat effects (see [Sections 9.2](#) and [9.3](#)).

3.3.5 Fibre cohesion and twist

In a spun yarn, fibre cohesion depends on interfibre friction developed as a result of twist. It has been shown by Gurney [11] that the critical tension, above which slippage takes place, depends on $p\mu S$, where p is the pressure normal to the fibre surface and depends on the degree of twist, μ is the coefficient of friction between the fibre surfaces, and S is the fibre specific surface. Fuller analyses and experimental data for fibre slippage in twisted yarns are given by Hearle [12].

It follows from this that the finer the fibres, the less is the amount of twist necessary to prevent the occurrence of slippage. It should be added, however, that this is only strictly true provided that the shape of the fibre surface remains substantially invariant. Much depends on the extent to which intimate interfibre surface contacts can be established. Fibre length plays its part here too.

3.3.6 Yarn uniformity

More important to the spinner than any of the aspects of fineness mentioned above is the fact that the uniformity of a yarn is very largely determined by the average number of fibres in the cross-section [13–15]. For a given yarn count, therefore, the finer the fibres, the more uniform is the yarn. Improved yarn uniformity is a desirable characteristic in its own right on the score of appearance, but it brings in its train also a number of other second-order consequences of great importance: greater strength, extensibility and lustre; fewer end-breakages in spinning, winding, warping, and weaving; and greater resistance to surface abrasion.

It also follows that the finer the fibre, the finer is the count that can be spun before the irregularity becomes so great that neither acceptable strength nor reasonable end-breakage can be maintained. Fineness is therefore seen as the dominating factor in determining the limiting count to which a raw material can be spun⁵.

3.3.7 Shaped and hollow fibres

Shape influences fibre performance in a number of ways. Light is transmitted and reflected in different ways, altering fabric appearance. Flatter surfaces, as in triangular fibres, have a higher lustre. Indentations in fibres act as capillaries and give good wicking behaviour. Ribbon-like fibres bend more easily than their circular equivalents and so give softer fabrics. The *scroop* of silk is partly due to the triangular shape and similar effects can be achieved in manufactured fibres. Other forms lead to soil hiding in carpet fibres.

Hollow fibres provide more bulk at lower weight and so are used in fillings. They can also be used for filtration or to hold chemicals for release.

3.3.8 Fibre end diameter

Thick fibre ends have been shown to be a cause of prickles in wool fabrics [16]. Mahar and O'Keefe report on the relation between comfort factor and fibre end diameter [17].

3.4 Variation in fineness

3.4.1 Variation within and between fibre types

The most convenient basis of comparison between different samples is the mean linear density, which among the natural fibres can often be used to distinguish between raw materials obtained from different sources. Some breeds of sheep invariably bear coarse wool whereas others bear fine. Some types and strains of cotton produce fine

⁵The results of certain experiments, notably with short Indian cottons, suggested that in some cases fibre length is more important, but it may reasonably be argued that this arises from the increasing mechanical difficulty, as staple length is reduced, of maintaining satisfactory drafting conditions and effective fibre control.

fibres whereas others produce coarse. The mean linear density of the fibres from even a pure strain of plant or animal is not, however, always exactly the same. It varies to some extent from time to time and place to place according to environment and so cannot be used as a precise means of identification. Some strains that are recognisably different are capable of producing fibres that in fineness are the same. Nevertheless, measurements of linear density, in association with other tests, can often be used to identify the origin of a sample with a fair degree of confidence.

Fibre fineness is a major factor in determining the value of wool [18]. Fine Merino wools are mostly in the 18–21 μm range (3.4–4.6 dtex), with superfine wools from 14 to 17 μm (2.0–3.0 dtex) and small amounts of expensive ultra-fine wools down to 12 μm (1.5 dtex). New Zealand carpet wools are typically in the 30–38 μm range (9–15 dtex). Asiatic carpet wools may be as coarse as 20 dtex. Cashmere ranges from 12 to 20 μm (1.5–4.1 dtex). In a similar way, the figures for cottons range from about 1.0 dtex for a St. Vincent Sea Island to about 3.4 dtex for a coarse native Indian cotton, with the dominant American-type cottons around 2 dtex. The mean linear density of the single filament of silk ranges from about 0.95 dtex for Canton to about 1.6 dtex for Japanese.

Nearly all the manufactured fibres can be made to cover a very wide range indeed according to requirements. For many years, 100 mtex (1 dtex) represented about the lower limit. Microfibres have reduced the limit. Development of direct spinning methods have taken polyester filaments to 0.1 dtex [19]. Conjugate spinning of two components, which then split into finer fibres, and islands-in-a-sea fibres, which have ultrafine components in a soluble matrix, give even finer fibres [20]. There is no strict upper limit, but 15 denier nylon (1.67 tex), which can be knitted singly as a monofil, is about the coarsest before there is a step jump to bristles and plastic monofilaments with diameters of the order of a millimetre.

3.4.2 Variation of fineness within a sample

In 1956, Morton [21] determined the between-fibre variation in 18 different samples of fibre using a vibroscope method (see [Section 3.9](#)) on 2 cm specimens. Several of the fibre types are no longer made. Wool samples showed coefficients of variation of 29 and 36%. Most manufactured fibres had coefficients of variation between 11 and 14%, but *Fibro* (viscose rayon staple) was more uniform at 8.9% and *Terylene* (polyester) was more variable at 21.4%. Improved quality control will have reduced the variability since then. The dry-spun manufactured fibres had near normal distributions, the melt-spun and wet-spun materials mostly had distributions that were positively skewed.

It has already been shown that different samples of the same kind of natural fibre can differ widely in their mean linear densities (see [Section 3.4.1](#)). This is also true as regards the variation among the fibres within a sample. The above figures should not therefore be taken as anything more than an indication of the order of variability that might be encountered. Another set of values, which were measured in 1945 in connection with mechanical tests, is given in [Table 14.6](#) on page 335.

3.4.3 Within-fibre variation

Only with manufactured fibres is it reasonably safe to assume that the cross-sectional dimensions remain constant throughout their length. Even then, although variations are negligibly small over the comparatively short lengths of staple fibres, they may in some cases be quite appreciable over the much longer lengths represented by filaments. Thus, for example, over a 1.83 m (6 foot) length of a 4.4 dtex (4 denier) acetate filament, Lord [22] found the linear density to vary from 407 to 460 mtex. Again the degree of variability depends on the standard of quality control of the manufacturer.

Silk filaments show long-range variations throughout the length on the cocoon. In the part that can be reeled for use, the linear density increases to a maximum of about 1.75 dtex some 300 m after reeling has commenced and then falls off to about 1.0 dtex before the cocoon has to be replaced. But variations over short lengths can also be considerable. Thus Goodings and Turl [23] reported variations in cross-sectional area of up to 20% of the mean and in a particular instance noted a change from 81 to 108 μm^2 within an interval of only 180 μm .

The ultimate fibres of flax invariably show a marked tapering from the middle to the two extremities, and to this is due, in very large measure, the great variation in cross-sectional area seen in the transverse section of a flax fibre bundle. It is therefore to be expected in tensile tests that, unless the test specimens are very short, they will tend to break mostly at the grips.

With wools, systematic tapering from the root towards the tips is only evident in lamb's wool, but appreciable random variations in cross-sectional area are liable to be found in any sample [24], as shown in Fig. 3.6 on page 113, depending on the changing vigour and health of the sheep while the wool is growing. For example wool from Western Australia shows thin places from the time of dry summer growth.

The cotton fibre has a tapered tip extending over about 15% of its total length, tapers more sharply near the root end, and frequently also shows considerable variation elsewhere [25–28]. The extent and the pattern of variation evidently differ from one sample to another. Thus, apart from the tapered extremities, Turner [26] found comparatively little variation in a sample of Cambodia 295, whereas in a sample of Surat 1027 ALF he found the mean linear density to change from 215 to 318 mtex in adjacent 6–4 mm ($\frac{1}{4}$ in), lengths. From evidence at present available, it would seem that in most cases, though not in all, there is a tendency for the area of cross-section to be a maximum about one-quarter or one-third of the distance along the fibre from the base. In the region of the tip of the fibre, the area of cross-section may in some cases be as little as one-half of what it averages elsewhere.

3.5 Measurement of linear density

3.5.1 Conditioning the specimen

Measurements of the dimensions of any moisture-absorbing fibre must take account of its state. A dry fibre has a lower linear density and a smaller diameter than a wet

one. The normal procedure is to condition the fibre in a standard atmosphere of 65% relative humidity (r.h.), 20 °C (see [Section 7.2.1](#)).

3.5.2 Continuous filament yarns

The fibre linear density in continuous filament yarns is easily measured, although the manufacturer's specification is usually accepted as correct. A controlled length is obtained by winding a given number of turns on a reel of given diameter and then the skein is weighed on a standard balance. Dividing by the number of turns and by the number of filaments gives the fibre linear density.

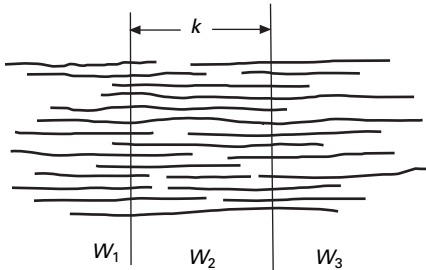
3.5.3 Staple fibres

When fibre length is determined by an individual-fibre method (see [Section 4.6](#)) the linear density of a sample of fibres is readily determined. One has only to preserve all the fibres measured for length and weigh them. The mass divided by the total length then gives the required information with a minimum expenditure of time and effort. This is the standard method prescribed by BISFA for all manufactured staple fibres [29], and, since the contribution that each fibre makes to the final result is proportional to its length, it gives a length-biased mean.

In the ASTM standard method for cotton [30], the procedure is essentially the same, though the necessity for individual fibre measurement is avoided by the use of a comb sorter. As described in [Section 4.7](#), the sorter is used to fractionate the sample into groups of known length ranges. From each group, except the two shortest and any of which the weight of fibre is less than 2 mg, a bunch of approximately 100 fibres is taken, weighed and counted. The length of every fibre in the bundle is assumed to be the mid-length of the group from which it is taken, so that if L = the group mid-length, n = the number of fibres in the bunch and M = the mass of the bunch, the linear density of the bunch is nL/M . From the values so obtained, the linear density of the sample as a whole is calculated in such a way as to give here also what is, for all practical purposes, a length-biased mean.

Yet another method giving a length-biased mean is that based on the cutting-and-weighing method of length determination described in [Section 4.9](#). For obtaining the mean fibre length, sections I and III of the tuft ([Fig. 3.3](#)) are weighed. To get the whole-fibre linear density in addition, it is only necessary to weigh section II of length k between the clamps, giving a mass M_2 , and to count the number of fibres N in section I. Then the total weight of the tuft $M_1 + M_2 + M_3$ divided by the total length NL gives the desired result. Neither this method nor the ASTM method described above is suitable for fibres that are strongly crimped because of the error thereby introduced into the length measurement. It is scarcely necessary to add that, with all hydrophilic materials, the fibres should be conditioned in a standard atmosphere before being weighed.

The CSIRO Cottonscan measures length on a weighed sample of snippets and so gives a direct measure of linear density [31].



3.3 Müller's method for fibre length measurement.

3.5.4 Cut-middles method

The earliest [32] form of gravimetric fineness test involves cutting known lengths from the middle of bundles of parallelised fibres, counting out a suitable number of those lengths, and weighing them. Alternatively, the desired number of fibres can be counted first and their middles then cut out for weighing.

In either event, the operation is most readily carried out by straightening the parallel bundle over a piece of cork linoleum or similar material and slicing through its middle with a cutter consisting of two parallel razor blades, set the desired distance apart in a holder. The lengths cut should be as long as possible, but not so long that an appreciable number of short fibres has to be rejected.

With cotton, for which this technique is most commonly employed, a length of 1 cm is the most suitable for general use, and it is better to cut before counting because short cuts can then be readily seen and discarded. In the Shirley Combined Stapling Test, where the fibres are sorted for length on a comb sorter, the mean weight per centimetre is obtained by weighing 100 lengths of 1 cm taken from each of five different places, evenly distributed over the Baer diagram. In this way, the variation of linear density with length is satisfactorily allowed for. By weighing only the middle (thickest) parts of the fibres, this method gives for cotton a result that is too great by an amount varying according to the mean profile of the fibres concerned. On the average, the cut-middles linear density is about 8% greater than that of whole fibres, though in some cases it is considerably more than this. Maximum differences ranging from 15 to 26% have been recorded by various workers [33–35]. It is to be expected, therefore, that from time to time appreciable divergences will be found between the results given by this form of test and those obtained by the rapid, whole fibre methods described in the following section.

3.6 Direct measurement of transverse dimensions

3.6.1 Width and diameter

For all fibres of cylindrical shape, and especially if the between fibre variation is small, so that only a comparatively modest number of observations is called for, the mean diameter is a very satisfactory measure of fineness. The technique of measurement is simple and straightforward involving the use of a microscope, with a micrometer

eyepiece, or a projection microscope with a scale. The scanning electron microscope (SEM) gives greater precision. If the density of the fibres under examination is known, all other transverse dimensions and quantities can be readily calculated; in addition, since individual readings are recorded, the variability of the sample can be obtained, which is sometimes an important consideration.

Provided that suitable precautions are taken, the same method can also be used for measuring the fineness of fibres of somewhat oval or flattened section. The width of a fibre of oval section can assume any value from a minimum across the minor axis to a maximum across the major axis, according to the orientation of the fibre with respect to the observer. If things are so arranged that the mean of all possible widths can be obtained, the result is a quantity that is virtually equal to the diameter of a cylinder of the same cross-sectional area and therefore proportional to the mean linear density [36].

In the projection microscope method [37], this objective is achieved by cutting the sample of fibres into 0.8 mm lengths, dispersing them in a suitable mounting medium on a microscope slide, and observing the width at one point selected at random along the length of each piece examined. If the pieces are too short, they tend to lie on their flat sides so that only their major axes are presented for measurement, but if they are 0.8 mm long or more, the position they assume is determined by the general curvature along the length of the fibre piece, and this has been shown to have no particular orientation with respect to the axis of cross-section [36].

Errors due to swelling must also be avoided. Fibre pieces should therefore first be conditioned in a standard atmosphere and then mounted for measurement in a medium that does not change their moisture content on immersion. Liquid paraffin and cedarwood oil are suitable for this purpose.

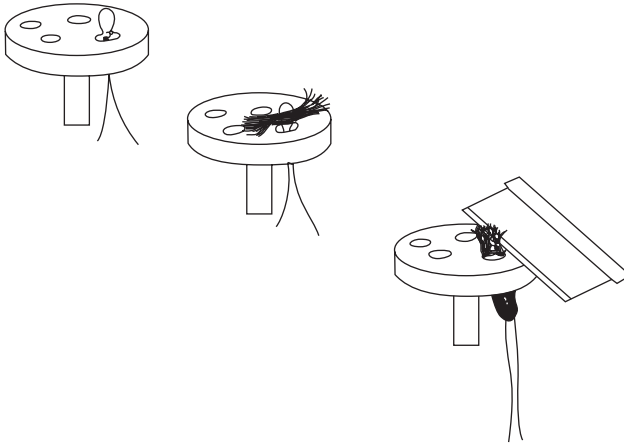
When the short pieces are obtained direct from a section of top, sliver or yarn, the sample is, of course, biased for length. This, however, is an advantage in most contexts, because the length-biased mean width gives an estimate of the fineness of the mass of fibre as a whole, each fibre contributing to the width measurement according to its length. In this respect, the method is then comparable with the more rapid methods of fineness-testing described in Sections 3.7 and 3.8.

For measurements of the width of microfibrils and nanofibrils, SEM would be used. Digital processing would compute values of diameter from the image.

3.6.2 Measurements on fibre sections

Measurements made with optical microscopes on transverse sections were used for special research purposes to obtain maximum information on the transverse dimensions of a sample of fibres. They are, however, laborious and time-consuming, call for considerable skill in section-cutting and subsequent measurement, and, unless carried out by someone of experience, can lead to misleading results.

The use of the SEM simplifies the problem with the adaptation of the method of preparation described by Ford and Simmens [38], using small holes cut in a standard specimen holder. As illustrated in Fig. 3.4 a bundle of fibres is pulled through a hole by a loop of thread and cut across with a razor blade. The specimen holder can then



3.4 Preparation of fibre cross-sections for viewing in SEM [39].

be placed in the SEM and directly observed. Originally, prints were made and measurements made, but digital processing would now allow computerised determination of the transverse dimensions.

3.7 Optical technology for high-speed testing

3.7.1 Laser scanning and digital optical analysis

The use of microscopic methods is laborious and has been mainly used in research. Advances in lasers, optical sensors, and digital detection and processing have changed the methodology.

Computerised optical analysers speed up the operation and enable large amounts of data to be collected with minimum time and effort. The underlying optics is discussed by Glass *et al.* [40]. The technology is particularly suitable for circular or near-circular fibres and was developed for rapid wool testing. It was readily extended to manufactured fibres. The first step in determining fibre diameter by these rapid methods is to guillotine a test sample of snippets of about 2 mm length.

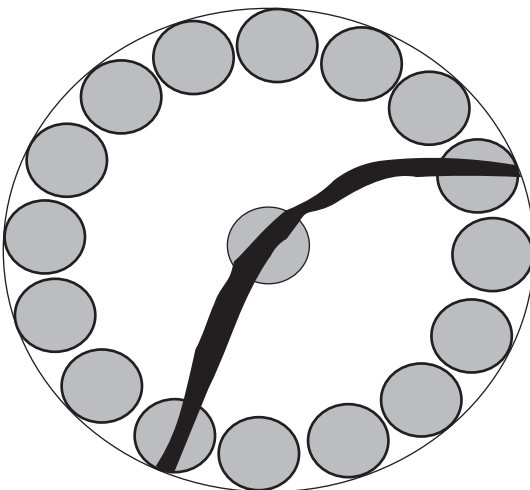
In the Laserscan [41], developed by CSIRO, the snippets are dispersed in an isopropanol–water mixture and then flow through a measurement cell, where they intersect a thin beam of light from a laser. The signal received by an optical detector is reduced in proportion to the width of the intersecting fibre, and is calibrated in diameter values by comparison with samples measured on a projection microscope. It is necessary that snippets fully intersect the beam and that only one snippet at a time is included in the measurements. An optic discriminator, consisting of a ring of detectors round a central detector, ensures that signals that do not meet the criteria are rejected. The information passes to a computer, so that mean and variability of diameter can be calculated. In addition to the usual statistical parameters, a ‘comfort factor’ is given by the percentage of wool fibres greater than $30.5\mu\text{m}$ in diameter. The effect of medullation is discussed by Butler and Glass [42]. The discriminator

also enables curvature to be determined, as indicated in Fig. 3.5, which gives a measure of crimp (see [Section 4.5](#)). Some 1000 fibres can be measured in 40 seconds.

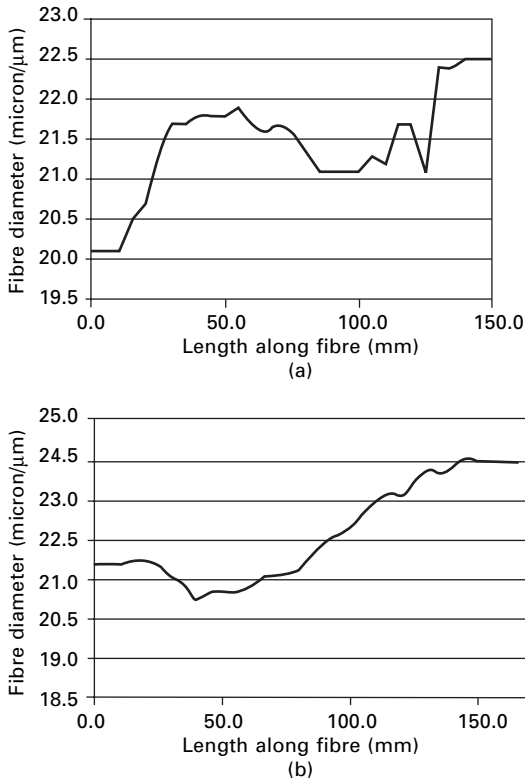
Although Laserscan is still widely used, advances in information technology (IT) are so rapid that the technology is becoming obsolescent. Detectors with multiple pixels, as in digital cameras, are used in the video-microscopes of the optical fibre diameter analyser, first introduced as OFDA100. Fibre snippets are imaged and analysed [43]. In contrast to Laserscan and to the indirect methods described later, digital imaging gives absolute values of linear dimensions, and so does not need to be calibrated by older microscopic methods. More information can be used in research studies. The OFDA100 measures fibre diameters and curvatures on 2 mm snippets of wool scattered on a glass slide [44]. The later OFDA 4000 [45], which is discussed in [Section 4.11.2](#), was primarily developed to measure length by scanning across a beard of fibres. The digital image can be processed to give fibre diameters, curvatures, diameter distributions, diameter profiles, as illustrated in [Fig. 3.6](#), and comfort factors (see [Section 3.3.8](#)). The OFDA 5000 [46], which is designed for synthetic fibres, makes 20 000 measurements per minute on fibre snippets in a diameter range of 0.5–60 μm , with a typical standard deviation of less than 0.05 μm . Mean and coefficient of variation are automatically calculated, histograms can be saved in a spreadsheet, and images saved in Windows format. The process of preparing slides by cutting snippets on a guillotine, automatic spreading and insertion in the microscope takes 1–2 minutes.

An interlaboratory comparison of measurements of wool fibre diameters was presented to IWTO [47]. This compared Laserscan and OFDA with projection microscope and air-flow methods. Butter and Glass [42] report that medollation does not affect the accuracy of *Laserscan* diameter measurements.

SIFAN [48] monitors cross-sections of fibres and produces profiles of fibre diameter. It was adapted to be mounted on a tensile tester. The width is measured from several directions at intervals along the fibre, so that three-dimensional models of fibres at



3.5 Fibre-optic discriminator in Laserscan.



3.6 OFDA 4000 fibre diameter profiles from two wool tops: (a) autumn shorn; (b) spring shorn.

increasing strain can be produced. Image processing gives cross-sectional area and maximum and minimum diameters at each point along the fibre. Mean fibre diameter in μm and, knowing fibre density, linear density in dtex can be computed, together with variability.

3.7.2 Application to cotton testing

For cotton, the complicated shape and its variation with maturity make the digital techniques more difficult to interpret. The industrial acceptance of air-flow methods in HVI testing, which give micronaire values, means that there has been less incentive to change. However, the dependence of micronaire on both fineness and maturity gives misleading information, with negative effects on the control of breeding and choice of fibres for spinning. As Gordon and Naylor point out: ‘varieties of fine, mature cotton have been wrongly discounted because low micronaire values were taken as indicating immature cotton’ [49].

The advances in affordable digital imaging and algorithms for rapid image processing have led CSIRO to adapt the testing of snippets of wool to the development of *Cottonscan* as a rapid method for the determination of the linear density of cotton

fibres [31, 49, 50]. A measured mass of snippets is placed on a slide and digitally imaged. The total length is then computed. Division of the mass by the length gives the average linear density of the cotton sample. If a micronaire value is also known, an estimate of maturity is then given by the use of the relation found by Lord [51]:

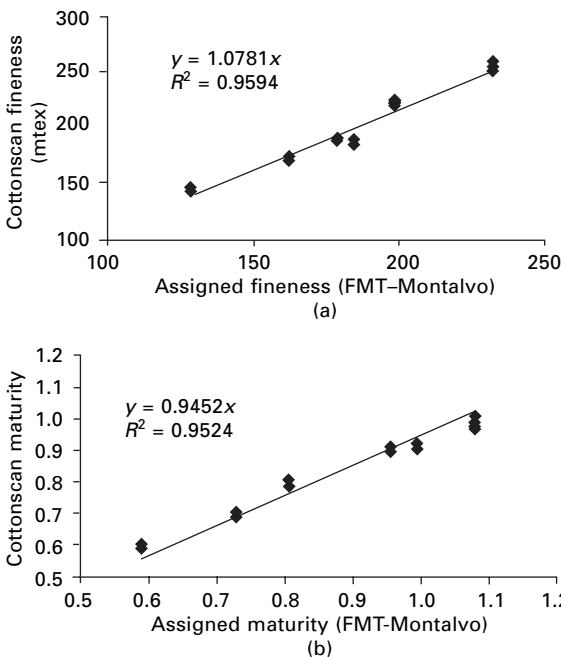
$$\theta_c = 3.86 X^2 + 18.16 X + 13 \quad (3.19)$$

where θ = maturity, i.e. degree of thickening as defined by Peirce and Lord [5] (see Section 3.2.5), c = linear density in mtex and X = micronaire value.

With a knowledge of the fibre density, the area of the fibre wall could be computed. If the maturity is also known, either from the empirical link to micronaire value or from other measurements, algorithms could be developed to determine other transverse dimensions, such as perimeter and fibre shape, if these are needed.

Figure 3.7 shows that Cottonscan gives good agreement with other methods of measuring fineness and maturity. The early tests of Cottonscan were carried out on sliver samples, but an automated method now enables samples of ginned cotton to be tested [50]. Cottonscan is a fast test method, which could be incorporated in HVI lines.

Although it is not a direct method of measuring maturity as a geometrical feature, it is convenient to mention here another CSIRO development, *Siromat* [49, 53, 54]. This estimates maturity from the interference colours produced when the fibre is viewed in polarised light. This is an old technique, which is discussed in Sections 3.10.6, but colour digital cameras and colour analysis have made it possible to have an automated computerised test. The test involves placing a collection of fibre snippets



3.7 Comparison of values obtained by Cottonscan and from Montalvo's upgrade of the FMT test [52]: (a) fineness; (b) maturity [31].

on a glass slide and immersion in castor oil. The image in a polarisation microscope is digitally recorded and the snippet colours analysed to give a distribution of maturity values. Test times are of the order of two minutes per sample, which is not fast enough for an HVI line, but is useful in quality assurance laboratories and for research purposes.

Finally, developments in sample preparation and digital imaging, together with advances in computer hardware or software, may lead to new direct methods of determining the transverse dimensions of cotton and other non-circular fibres. If fibre sections could be rapidly produced and deployed on a slide, then image analysis would give a full statement of the transverse dimensions. Alternatively, tomography might give a way of obtaining the information from observations of snippets or whole fibres.

3.7.3 Advanced fibre information system

Although air-flow methods dominate routine, high-speed testing of cotton, fineness is measured as one part of the comprehensive Uster Advanced Fibre Information System, (AFIS), which also provides information on fibre length (see [Section 4.11.1](#)), neps, trash and dust. Fibres from a tuft are transported individually in a fast air stream past a beam of light, which falls on an electro-optical sensor. Measurement of the direct intensity indicates the amount of attenuation, which is related to the linear density of the fibre. Measurement of the light scattered at 40° is related to the shape of the fibre. Calibration against known cottons enables values of micronaire, maturity ratio and per cent immature fibre content to be recorded. Gordon *et al.* [55] compare AFIS measurements with those by other methods and note that there are differences in predicted distributions of transverse dimensions. Bradow *et al.* [56] compare AFIS measurements with X-ray fluorescence spectroscopy.

3.8 Air-flow methods

3.8.1 Indirect methods

The older direct methods of measuring transverse dimensions suffer from the objection that a great deal of time and labour, as well as eye-strain, is involved. Only with the advent of digital imaging and computer software is that changing. In the second half of the 20th century, indirect methods were developed to get the desired results more quickly and with less trouble. The most successful of these endeavours has been the development of air-flow fineness testers, which contain a suitably prepared porous plug. It is important to note, however, that the quantity measured is the specific surface, not the linear density. The first use of this principle for measurements on fibres was in the Porometer devised by Balls in the late 1920s [57].

3.8.2 Flow relations

An analysis of air-flow through fibre plugs was given by Lord [58]. Kozeny's equation for the laminar flow of air through a porous plug under a small pressure gradient is usually written as:

$$Q = \left(\frac{1}{k} \right) \left(\frac{A \Delta P}{S^2 \mu L} \right) \left[\frac{\epsilon^3}{1 - \epsilon^3} \right] \quad (3.20)$$

where Q = volume rate of flow through the plug, k is a proportionality factor depending on the shape of the voids and fibres and on their orientation with respect to the direction of air-flow, A = cross-sectional area of the plug, ΔP = pressure difference between the ends of the plug, S = specific surface of the fibres constituting the plug (surface area per unit volume of material), μ = coefficient of viscosity of air, L = length of the plug, and ϵ = porosity of the plug (volume of voids/total volume of the plug).

The porosity of the plug of fibres is given by:

$$\epsilon = 1 - \frac{m}{\rho AL} \quad (3.21)$$

where m = total mass of the plug and ρ = density of the fibre.

The flow equation can therefore be rewritten to give a resistance to flow R as:

$$R = \frac{\Delta P}{Q} = \frac{k \mu m^2 \rho S^2 L^2}{(\rho AL - m)^3} \quad (3.22)$$

If the plug consists of a fixed mass of fibre uniformly compressed in a cylinder of fixed dimensions, then, for a given type of fibre, A , L , m and ρ are constant, and the coefficient of viscosity of the air, μ , is also sensibly constant over the range of normal room temperatures. Thus, if a fixed pressure drop, ΔP , is part of the experimental conditions, and provided that k can also be maintained constant, the rate of flow of air through the plug, Q , is inversely proportional to the square of the specific surface, S . This is the basis of the design of two of the air-flow instruments described briefly below, namely, the Micronaire Cotton Fibre Fineness tester and the WIRA Fibre Fineness Meter.

Alternatively, ΔP can be measured at constant Q or, as in the Arealometer⁶, measurements can be made by adjusting the length, L , of the plug so that it offers a fixed resistance, R , to the flow of air.

It is a simple matter to control all the conditions of the experiment save one. The factor k depends on the shape, orientation and distribution of the sizes of the channels through which the air flows, on the porosity of the plug, and possibly also on the character of the fibre surfaces. Thus the value to be assigned to k can only effectively be obtained by empirical means. The relation between specific surface and L , ΔP or Q , as the case may be, will differ according to the type of fibre being examined, e.g. wool, cotton, viscose rayon, and also according to the manner in which the fibres are prepared and arranged in forming the plug. Thus, when the technique of sample preparation has been determined, it is necessary to make experimental calibration of the flow-meter, by using a range of tested samples of varying fineness for each class

⁶The Arealometer, developed by Hertel and Craven [4] is no longer manufactured, but is still used in some research studies [59, 60].

of fibre [58]. The dependence on fibre shape is particularly important for cotton, since it means that the value of R depends on cotton maturity as well as fineness.

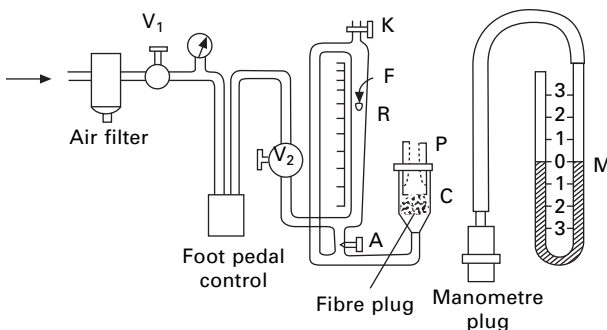
3.8.3 The Micronaire

The Sheffield Micronaire [51], the first commercial instrument to be marketed for the measurement of fibre fineness by air-flow methods, is now a standard method for evaluating cotton. Indeed, although it depends on fineness and maturity, the word ‘micronaire’ is now used as a term to characterise a cotton sample, along with length and other grading features. Micronaire values influence price. Too much attention to selecting for high yield, neglecting selection for micronaire, has been counter-productive by reducing the return to cotton growers for fibres with lower micronaire [61]. However, as discussed below, the interpretation of micronaire values is not a simple one. Low micronaire indicates fineness, which is good, but also immaturity, which is bad.

The operation of the Micronaire is illustrated in Fig. 3.8. In this instrument, air at a pressure of 41.3 kPa (6 lbf/in²) is made to flow through a plug of fibre, of mass 3.24 g, enclosed in a chamber, C, (25.4 mm (1 in.) long and 25.4 mm (1 in.) in diameter. The floor of the chamber and the bottom of the annular plunger, P, are perforated so that, although the sample is confined within a space of fixed dimensions, L and A in equation (3.19), the air can flow freely through it. The rate of air-flow is indicated by the rotometer, R, which consists of a tapered tube, wider at the top than at the bottom, in which a light metal float, F, is airborne at a level depending on the airvelocity.

The standardised air pressure is controlled and adjusted by inserting the manometer plug shown in place of the plunger P in the otherwise empty chamber C and making adjustments at V_1 and V_2 until the manometer, M, registers 41.3 kPa (6 lbf/in²). Calibration of the flowmeter at the top and bottom of its range is effected by adjustments at A and K when the outflow of air from the chamber is restricted by standardised orifices.

On the mistaken assumption that the resistance offered by the plug to the flow of air could be regarded as a unique function of the linear density of the fibres, the flowmeter scale was calibrated against a set of Upland American cotton, the linear



3.8 Micronaire.

densities of which had been determined by the standard ASTM gravimetric method, to give a reading in the mixed units of micrograms per inch. It is a matter of great regret that, when this instrument was first introduced, it was calibrated in gravimetric units. It is not surprising, therefore, that, when the instrument came to be used for testing Egyptian and other types of cottons, the results failed to agree with those of the gravimetric test. Now the micronaire value is regarded as a measure of cotton quality in its own right, loosely and inversely related to fineness, but also affected by maturity.

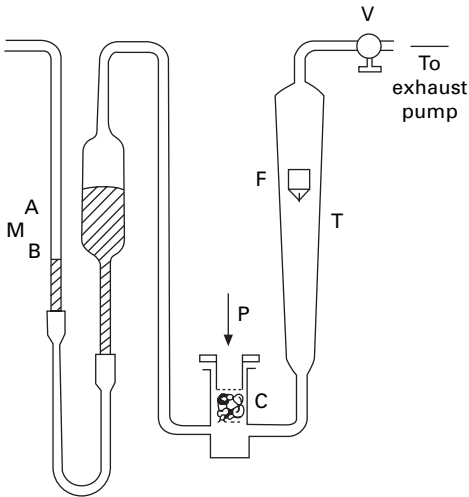
Being extremely rapid in operation, the micronaire test was quickly taken up by the American cotton spinning industry, where it was found to be extremely useful for the purpose of quality control in blending. So long as only Upland cotton was used, it was the general experience that, if the micronaire reading fell below about 3.3, neppy yarn and excessive ends down were to be expected, and that mixing bales so as to give a blend of constant micronaire led to more consistent and better running conditions in the mill. This gave rise to the quite widely held but completely false notion that the finer the cotton (low micronaire), the poorer was the performance. As has been shown, the rate of air-flow depends on the specific surface, which can be expressed as the ratio of the perimeter to the cross-sectional area. If the perimeter remains constant, changes in the rate of air-flow will reflect changes in the area of cross-section or linear density, which arise from changes in the thickness of the wall, namely the maturity. All American Upland cottons have roughly the same perimeter and what was being shown by a low micronaire was poor maturity, which caused poor spinning performance.

To obtain consistent and reliable results, the method of preparing the specimen must be standardised. Any pieces of stalk, seed or other major impurities must be removed, and, after the standard amount of cotton has been weighed out, the fibres must be well teased and fluffed with the fingers while being packed into the sample chamber. The conditions to aim at are uniform density of packing but random arrangement of fibres.

The Micronaire can also be used for testing wool, in which case the standard mass of the sample is 5.9 g and the air-pressure is 31.0 kPa (4.5 lbf/in²). Removal of oil or grease by means of a suitable solvent is necessary before the sample is conditioned, weighed, fluffed up and packed into the chamber. The flow meter is empirically calibrated for direct reading in diameter in μm , and, although different wools vary somewhat in their ellipticity, the results obtained for non-medullated samples are nearly always found to agree very closely with the mean diameter as measured by the method described in Section 3.6.1.

3.8.4 The WIRA Fibre Fineness Meter

The WIRA Fibre Fineness Meter [62], which was developed for wool testing and is shown in [Fig. 3.9](#), operates on the same principle as the Micronaire and incorporates the same simple flowmeter-tube method of measuring the rate of air-flow. It has, however, certain advantages over the Micronaire; in particular, it is simpler in design, and the air, instead of being pumped through the system by a compressor, is drawn



3.9 WIRA Fibre Fineness Meter.

through it by a suction pump. By this means is avoided the difficulty of controlling the temperature and humidity of the air passing through the specimen and consequently the errors that could arise owing to swelling of hydrophilic fibres. Although superseded by the automated optical methods described in Section 3.7, the air-flow method is still used in textile mills.

There are two models, one for wool and one for cotton, differing in the dimensions of the sample chambers and the weight of the sample. As with the Micronaire, the sample is required to be well teased out and fluffed up, so that the fibres are in a substantially random condition, and for cotton it is convenient to use a Shirley Analyser for this purpose. Both models can be obtained with the tube graduated in flow units, litres per minute, in which case there can be no misunderstanding about what the instrument is really measuring. To give results in terms of more commonly recognised textile units, the instrument should be calibrated by means of specimens of the kind for which the instrument is to be used and of which the required fineness characteristics have already been determined by independent methods. Either a calibration chart can be used or a calibrated scale may be fixed alongside the flowmeter tube T for direct reading. If the material to be tested is wool, the calibration will naturally depend on whether the fibres are in the greasy, oil-combed or scoured (or extracted) condition, and the presence of sand, dust or other foreign matter could be a source of error.

As with the Micronaire, it is convenient to calibrate the wool instrument in terms of mean fibre diameter. With cotton, the calibration can be in terms of specific surface or, regrettably, in maturity ratio or micronaire scale units. For the latter purpose, physical standards consisting of samples of cotton of known fibre properties are available.

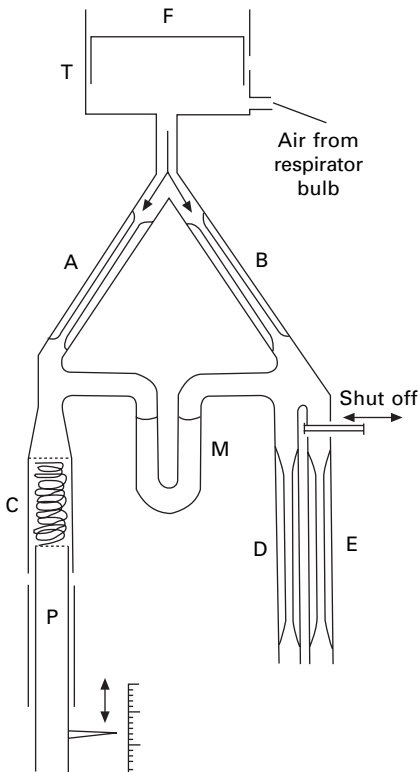
Operation is extremely simple. With the instrument levelled so that, with no air flowing, the level of liquid in the manometer tube M is at A, and with the perforated lid P placed on the weighed and uniformly packed specimen in the chamber C, the

valve V is gradually opened until the pump suction lowers the liquid level to B. Then, at the standard pressure represented by the difference in liquid levels in the manometer, the rate of air-flow (or the corresponding measure of fineness) is given by the height of the float F.

With slight modifications to the size of the sample chamber, to the weight of the sample, and to the range of the flowmeter, the wool model can also be used at a constant rate of air-flow. In that case, the valve V is opened until the flowmeter registers a fixed rate of flow, and the fineness is then measured in terms of the pressure drop indicated by the manometer M. In this case, it is, of course, the latter that has to be calibrated in the required fineness units.

3.8.5 The Arealometer

The Arealometer [4, 34], shown schematically in Fig. 3.10, works essentially on the principle of the Wheatstone bridge. Air at a low constant pressure is made to flow through a branched pair of resistance tubes, A and B, as shown. The air in branch A flows into the atmosphere through the sample chamber C in which the plug of fibres is inserted, while the air in branch B also escapes into the atmosphere through the standard resistance tubes, D and E. The tubes A and B offer equal resistance to air-



3.10 Arealometer.

flow. In operation, it is the object, by suitable compression of the fibre plug in C, to adjust its resistance to air-flow so that the pressure drop across C is equal to that across D and E combined, as recorded by the manometer M. The length to which the fibre plug has to be compressed to achieve this balance is then a measure of the specific surface of the fibres.

The desired degree of compression of the fibre plug is obtained by advancing the hollow piston P into the chamber, the crown of the piston and the inlet end of the chamber being perforated to permit the necessary flow of air. Advancement of the piston is by means of a handle on the end of a micrometer screw carrying a scale on which direct readings of specific surface can be read off in units of square millimetres per cubic millimetre.

The pressure of the air admitted to the system is determined by the weight of the freely floating piston F in the pressure tank T. This arrangement has the advantage of enabling the instrument to be small, compact and completely self-contained.

The sample chamber is only 0.8 cm in diameter, and the instrument has been so designed that the correct size of sample is one in which the volume of the fibre substance is 0.1 cm^3 . This is obtained by taking a quantity of fibre of mass (in grams) equal to one-tenth of the density of the material in g/cm^3 . Thus, for cotton, the correct test-sample mass is 152 mg, and, instead of the aim being a random orientation of the fibre, the sample is prepared by a special technique such that the fibres are made to lie in coils transverse to the direction of air-flow, and the instrument is calibrated accordingly. Unfortunately, with this technique, the time required per test is appreciably longer than with the Micronaire and WIRA instruments, and it is rather more difficult to secure concordance among different operators. For these reasons, in a later and portable version of the Arealometer, known as the Port-Ar, the makers reverted to a teased and randomised sample of much larger size, of mass 8 g. With this change and the inclusion of a built-in weighing device, specially designed for rapid weighing, it is claimed that an experienced operator can easily run 60 samples an hour, provided that the samples are accessible. With the Arealometer, the corresponding time required per test is approximately 10 minutes, but it is also possible at the same time to obtain a measure of maturity by making a measurement at another level of compression (see [Section 3.10.7](#)).

3.8.6 SDL Micromat

The SDL Micromat is a stand-alone, high-speed tester, which includes an electronic balance, a computer and a monitor to display results. It operates on the double compression principle (see Section 3.10.7) to measure fineness and maturity. The SDL operating procedure specifies a mass of 3.8 to 4.2 g, which has been opened and cleaned in a Fibreblender or Shirley Analyser, but Gordon *et al.* [54] recommend a consistent weight of $4 \pm 0.005 \text{ g}$. The specimen is compressed to two different volumes in the test chamber. It is subject to a flow of 4 litre/minute at low compression, and 1 litre/minute at high compression, giving pressure differences P_L and P_H respectively. Fineness (mtex), micronaire, maturity ratio and percentage maturity values are computed from P_L and P_H by a set of empirical equations, with constants

derived from calibrations.

3.9 The vibroscope method

The vibroscope method, originally put forward by Gonsalves [63], is a non-destructive test, which can be used in combination with a tensile test on the same specimen. Although not too suitable for measurements on cotton or wool because of the within specimen variability, it is useful for manufactured fibres.

For a perfectly flexible string of linear density c and length l , under tension T , the natural frequency of transverse vibration f is given by:

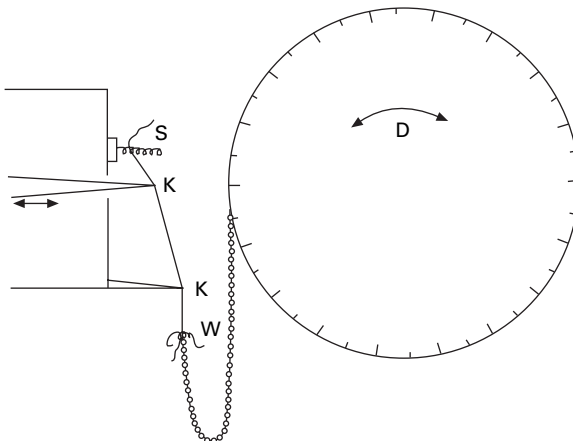
$$f = \frac{1}{2} \left(\frac{T}{c} \right)^{1/2} (1 + a) \quad (3.23)$$

whence:

$$c = T \left(\frac{1}{2} l f \right)^2 (1 + a)^2 \quad (3.24)$$

where a is a correction factor involving the elastic modulus of the material. If a can be made negligibly small as compared with unity (see below), then m can evidently be found for a specimen of fixed length l in one of two ways: either by finding what frequency of vibration f corresponds to a given tension T , or by varying T until a given natural frequency f is obtained.

In the apparatus used by Morton [21] (see Fig. 3.11), the fibre specimen is clamped between two springs S and W and stretched across two knife-edges KK under a chainomatic tension adjustable by rotation of the drum D. The knife-edges are 2 cm apart, and one of them is caused to vibrate in a direction normal to the fibre axis with a fixed frequency of 1.640 kHz. When the natural frequency of the specimen coincides with this applied frequency, resonance occurs. The fibre is therefore observed through



3.11 Vibroscope.

a low-power microscope, and the tension T is adjusted until the fibre is seen to vibrate with maximum amplitude. Since d and T are linearly related, the drum readings may be calibrated directly in the units of linear density desired. The specific stress on the fibre T/c depends only on the value of l and f , which were chosen to give a value of 8.83 mN/tex (0.1 g/den).

For fibres of circular cross-section, the correction factor a is given by:

$$a = \left(\frac{r^2}{l} \right) \left(\frac{\pi E}{T} \right)^{1/2} \quad (3.25)$$

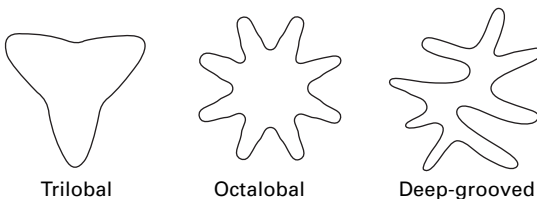
where r is the fibre radius and E the Young's modulus.

In most cases, a does not exceed 0.03 and can be neglected, but, if necessary, it can be calculated with sufficient accuracy from an approximate value of E . An alternative method suggested by Gonsalves is to compare, for a single specimen, the value of m given by the vibroscope with that determined by direct weighing on a delicate torsion balance. The percentage difference is then taken as the correction to be applied to all other specimens from the same sample.

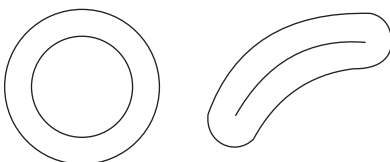
3.10 Fibre shape and cotton maturity

3.10.1 A variety of shapes

The simplest melt-spun fibres, which are extruded through a circular spinneret, are circular in cross-section. The use of shaped spinnerets has enabled fibres of different shapes to be made. Sharp edges are rounded to an extent dependent on time in the thread-line and melt viscosity. Typical examples of fibre shape are shown in Fig. 3.12. As discussed in [Chapter 1](#), solution-spun fibres, such as rayon and acrylic fibres, have shapes that result from the formation of a skin and then the loss of solvent from the core. Wool only slightly departs from being circular, though some hairs are more elliptical, but at higher resolution surface scales determine the shape of the perimeter. Silk has a triangular cross-section.



3.12 Examples of melt-spun fibre shapes.



3.13 A cotton fibre, which is not fully mature, before and after collapse.

Fibre shape has a major effect on cotton quality. As shown in [Fig. 3.13](#), cotton grows as a circular hollow tube, but collapses on drying to a ribbon or, when mature, kidney-shaped fibre (see also [Section 1.4.3](#)).

3.10.2 Cotton maturity

Whereas the mean perimeter of a raw cotton is mainly a hereditary characteristic, the degree of development of the cell wall is very largely determined by environment. If a fibre has a thick and well-developed wall, it is said to be mature. If, on the other hand, its wall is thin and poorly developed, it is said to be immature. Correspondingly, if a cotton, because of unfavourable growing conditions, contains a considerable proportion of immature fibres, it is referred to as an immature cotton. As stated in [Section 3.2.5](#), the degree of thickening, which is a measure of maturity, is given by the ratio of wall area A_w to total fibre area, which equals $4\pi A_w/P^2$, where P is the fibre perimeter. For a solid fibre, $\theta = 1$. A *maturity ratio* is defined as the ratio of the actual degree of thickening to a standard degree of thickening equal to 0.577. Mature cottons have average values of θ greater than this, but immature cottons may have average values below 0.3. In any given sample of cotton, there will be a range of maturities, which, for a mature cotton might go from 0.15 to 0.96 [64].

There is an optimum degree of maturity for a cotton fibre, above which it tends to be too stiff and bristly for ease of processing, and below which it tends to be too flabby and unresilient. It is not very certain just where this optimum lies, though it is probably somewhere between $\theta = 0.8$ and 0.9. Spinners, however, are not usually worried about fibres that have abnormal wall thickening: they are much more concerned about those that have little or none. Cottons that are classed as immature are objectionable mainly because of their liability to the formation of neps, which are small, tightly rolled-up entanglements of fibre and which, unless removed by combing, survive all processes through to the yarn, when they appear as unsightly specks. Neps are not of natural occurrence: they are artefacts [65] produced by excessive rubbing against or between surfaces, which tends to roll the fibres into minute knots, and they have been repeatedly shown to consist mainly of very thin-walled, or so-called ‘dead’, fibres [66].

In the spinning of fine yarns from fine cottons, nep formation is at once both more frequent and more deleterious in its consequences. With fine cottons, even the fully matured fibres are more delicate than with coarse cottons, and dead fibres are more delicate still so that neppiness is less easily avoided; the neps that are formed are much more noticeable because in fine yarns their size is comparable to the yarn diameter. On account of the very poor wall thickening of the fibres involved, neps when dyed appear much lighter in shade than a normal sample of fibres given the same treatment, and hence appear as light, or even almost white, specks on the surface of the fabric. Calendering increases their prominence because the knot of flabby fibres is easily flattened and given a bright, glazed appearance. In printed fabrics, somewhat similar faults are produced. If surface neps are removed or dislodged, the underlying normal yarn is relatively unstained over the small area that has been covered by the nep. From the same argument, it will be evident that similar yarns

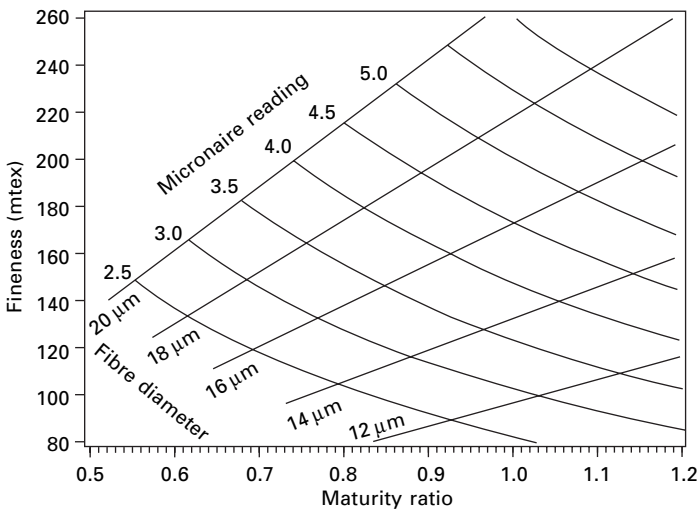
made from cottons differing in average maturity will also give different overall apparent shades and that imperfect mixing of the immature elements in a blend may give rise to streaky dyeing.

3.10.3 Measured maturity

The degree of thickening θ can be directly measured on fibre cross-sections, now made much easier by digital processing. Alternatively, as shown in equation (3.15), θ can be calculated from the mean specific surface S and the mean linear density⁷ c of a sample of cotton. In accepting such calculated values, however, while a considerable amount of labour may be saved, it must be remembered that the results are subject to two independent sources of experimental and sampling error. In particular, it should be noted that errors in S are squared in the evaluation of θ . The value of such a procedure therefore depends largely on the reliance that can be placed on the data. Experience suggests that, if the linear density is determined by duplicate tests on each of 500 well-sampled fibres and the specific surface from four air-flow tests, then the calculated maturity is as accurate as is needed for practical purposes and no less reliable than if obtained directly by other means.

3.10.4 Micronaire, fineness and maturity

As already indicated, the micronaire value depends on specific surface and is therefore



3.14 Relations between micronaire, fineness (linear density) and maturity ratio. Diameter values are for an equivalent circular fibre [68].

⁷To be consistent, of course, the linear density should be measured by a whole fibre method.

influenced by both fineness and maturity. A detailed discussion of the relations is given by Montalvo [67]. Figure 3.14 shows relations between micronaire, fineness and maturity for US cottons [68].

3.10.5 Maturity counts

For all except highly specialised research purposes, micrometric methods of measuring maturity are unsuitable, not only because of the technical difficulties referred to in Section 3.6, but also because of the amount of time consumed by comparison with other methods that are available. Among these, by far the most commonly used is that in which the fibres are examined in longitudinal view under the microscope and classified according to the apparent thickness of the cell wall relative to the width of the fibre. In the U.S.S.R., the observations were made on untreated fibres [69], but in most other countries the fibres are first swollen in caustic soda. How thin the wall has to be before it is regarded as potentially nep-forming or otherwise undesirable is impossible to define precisely: hence the criteria by which the fibres are classified are decided to some extent arbitrarily.

In the British version of the maturity count, the test is carried out on the five tufts of fibre that are left from the Baer diagram after the fibre linear density has been determined. Each tuft is laid on a microscope slide so that the fibres are parallel but separated, a cover-slip is placed over the middle of the fibres, and they are then irrigated with an 18% solution of caustic soda until swelling is complete. The dangerous fibres are considered to be those in which, after this treatment, the wall thickness is one-third or less of the apparent lumen width: these are called 'dead' fibres. 'Normal' fibres are considered to be those which have become deconvoluted and rod-like and in which swelling of the wall has virtually obliterated the lumen. Between these two is the third class of fibres, referred to as 'thin-walled'. Classification is carried out with the microscope condenser so adjusted as to give maximum definition of the boundaries of the wall. Observations are made at one place only on each fibre, somewhere about its middle and, where convolutions are still perceptible, at a point where the width is a maximum between two reversals. The slide is first traversed to count the total number of fibres in the mount. It is then traversed again to count the rod-like normal fibres. Finally, it is traversed a third time to count the number of dead fibres. The number of thin-walled fibres, if required, may be obtained by subtraction.

The percentage occurrences of normal N and dead D fibres are calculated, and the means for all the slides are obtained. The sample is then characterised as to maturity by a quantity called the *maturity ratio* M , defined as:

$$M = \left(\frac{N-D}{200} \right) + 0.7 \quad (3.26)$$

The more or less arbitrarily chosen constants⁸ are such that a value of unity is commonly obtained for high grades of Egyptian and Sudan Egyptian cottons, irrigation-

⁸For details of how this formula was arrived at, see the work of Peirce and Lord [5].

grown under generally favourable conditions. If the value of M is below about 0.8, the cotton is one which, as a whole, would be regarded as immature. Few samples of commercial crops have values for M of less than 0.7 [70].

The empirical relation between maturity ratio and degree of thickening θ has been given by Peirce and Lord [5] as:

$$\theta = 0.577M \quad (3.27)$$

The ASTM standard maturity count is carried out in a similar way on fibres that have been comb-sorted for length and fineness determinations, but, instead of three levels of maturity, only two are recognised, mature and immature. A fibre is taken to be immature if the wall thickness is equal to or less than half the maximum width of the lumen. The fibres (approximately 100) that have been taken from each length group in the sorter array and weighed for fineness determination are mounted and swollen substantially as in the British test, and then traversed once under the microscope to count the two classes, which thus gives the percentage number of mature fibres M on each slide. Since both the number N' and weight W' of fibres on each slide are also known, as well as the weight of fibre W that each slide represents, the number of fibres N in each length group can be calculated as $N = N'W/W'$. The duly weighted mean percentage of mature fibre present in the entire sample is then given by

$$P_M = \sum NM / \sum N \quad (3.28)$$

As in all tests of this kind, doubtful classification may be decided with the aid of a filar micrometer or by means of a wedge-shaped line template. It is to the advantage of the ASTM method that there is only one boundary where doubts may be entertained, and in general it is easier to recognise quickly that one dimension is more than twice another than that it is more than three times another⁹.

Although the British and American criteria of maturity are different, the results obtained by the two methods are highly correlated [71], and Lord [70] has given the following conversion formulae:

$$P_M = (M - 0.2) (1.5652 - 0.471M) \quad (3.29)$$

$$M = 1.762 - \sqrt{(2.439 - 2.123P_M)} \quad (3.30)$$

and, by combining equations (3.27) and (3.30),

$$\theta = 1.017 - \sqrt{(0.812 - 0.707P_M)} \quad (3.31)$$

It is, of course, possible to carry out a reliable maturity count without the necessity of first sorting the fibres for length, but, however conducted, the test is unfortunately tedious and time-consuming. The minimum time in which it is possible to obtain worthwhile results is about $1\frac{1}{2}$ hours [72].

3.10.6 Interference colours in polarised light

⁹Herein lies one of the main advantages of swelling the fibres with caustic soda. The ratios of lumen width to wall thickness that are of interest are smaller.

Another attempt to measure maturity, which was suggested by Grimes in 1945 [73] is examination of colours seen in polarised light [53], as used in the automated *Siromat* test described in Section 3.7.2. When cotton fibres are examined by means of a polarising microscope, they exhibit different interference colours that are dependent largely on the thickness of the cell walls. A first-order red selinite plate is used to obtain the brighter second-order additive colours and also to permit an additional check by observation of the subtractive colours when the stage is rotated. The fibres are examined at $100\times$ magnification and classified into four, three or two classes, depending on how fine a differentiation is required, as follows.

Fibres that appear purple or indigo throughout their entire length in the field of the microscope and turn orange on rotation of the stage through 90° are immature. On removal of the selinite, they show parallel extinction. Fibres that appear deep blue or alternatively blue and purple, turn orange-yellow upon rotation of the stage, and show some parallel extinction on removal of the selinite are also classed as immature. Fibres that appear blue-green or alternatively blue and yellow, turn yellow-white on rotation of the stage, and show only slight dimming on removal of the selinite are partially mature. Fibres that appear yellow or yellow-green throughout their entire length and show practically no change of colour on rotation to the subtractive position nor parallel extinction on removal of the selinite are fully mature fibres.

Approximately 1000 fibres are examined, and the whole operation, excluding sampling, takes between 2 and 3 hours, so that in the matter of time it has no advantage over the maturity count and, depending as it does on the colour judgement of the operator, it is, if anything, more subjective. Any attempt to classify a continuous variate (as maturity is) on the basis of colour judgement must inevitably give rise to uncertainties at the class boundaries. Furthermore, a question has been raised as to how far the test is one of maturity and how far it is mainly one of wall thickness. With American Upland cottons, where there is comparatively little variation in cell girth, this would not be a problem, but for world cottons as a whole, it was suggested that the correlation with a maturity count was weaker.

In more recent studies related to the development of *Siromat*, an examination of the interference colours of different cottons by Gordon and Phair [74] showed no differences dependent on genetic origin or intrinsic fineness. The fibres were classified according to the scheme of Grimes, namely blue to orange for fibres with varying degrees of immaturity and bright yellow for mature fibres.

3.10.7 Other indirect methods

Differential compression

The use of differential compression was first noticed by Hertel and Craven [4] in the course of developing the Arealometer instrument, and is now more widely used in the Shirley Fineness and Maturity Tester (FMT). It was found that, if a sample of cotton was subjected to an air-flow test at two widely differing compressions, the highly compressed condition produced an apparently greater specific surface, and the increase was greater for immature samples than for mature. This led to the idea that the difference in the results obtained at two different porosities might be made to serve

as a measure of immaturity, and for this purpose the Arealometer was designed in its present form. On referring to Fig. 3.10, it will be observed that the standard resistance tube E is provided with a cut-off switch. If, after a normal test has been made, tube E is cut off by this switch, the resistance to air-flow down limb B increases, and the sample has to be further compressed in order to restore the pressure balance as indicated by the manometer M. A second, and spurious, reading of specific surface is therefore taken on a different calibrated scale, which is automatically brought into use by the throwing over of the cut-off switch. The difference D between the two readings is then used to calculate the immaturity ratio I by using the empirical relation¹⁰:

$$I^2 = 0.0625D + 1 \quad (3.32)$$

Hertel and Craven explain the apparent increase in specific surface by supposing that, when the plug of fibre is subjected to the higher compression, the contact between the fibres is increased considerably and, as a result, the immature fibres are flattened and constrained to rotate about their own axes so that their broad sides are presented, or more effectively presented, to the direction of air-flow. The result is an increased resistance, which the Arealometer reflects by registering an apparent increase in specific surface. In other words, the factor k in the flow equation is changed.

Agreement between the results of the Arealometer test and those of the maturity count is quite good. Webb and Burley [75] found the correlation coefficient to be +0.889 as against +0.752 for the Causticaire test. Morton and Radhakrishnan [34], comparing the Arealometer immaturity with the immaturity calculated from the whole-fibre linear density and the Arealometer specific surface, found the correlation coefficient to be +0.978. The test has much to commend it. Of all the 'bulk' tests proposed, it appeared to be the most reliable and is certainly by far the quickest. Unfortunately, however, for a reason that has not yet been satisfactorily explained, it cannot be used for testing material, such as sliver, that has been mechanically processed.

Differential compression is also the principle adopted in the Shirley FMT [76], which is used in quality control laboratories in spinning mills and some test houses. Values for maturity are calibrated by swelling in caustic soda and for fineness by cutting and weighing. An upgrade of FMT has been made by Montalvo *et al.* [51].

The Causticaire test

This is an adaptation of the Micronaire test by means of which it is possible to obtain a measure of maturity. The underlying idea is that treatment with 18% caustic soda, by swelling the fibre walls, reduces the specific surface. The changes so brought about are more pronounced with immature than with mature fibres, and consequently the difference in the air-flow readings for a sample before and after caustic treatment should be a reflection of its average maturity.

Lord [77] has investigated this test in considerable detail with results that can only

¹⁰In a later publication, Hertel proposed an increase in the constant from 0.0625 to 0.070, but Morton and Radhakrishnan [34] and Webb and Burley [75] found that this led to immaturity values that were too high for agreement with standard maturity counts.

be regarded as unfavourable. He found that the 'Causticaire maturity index' was biased to an extent partly depending on the fibre fineness but that, even after correction for this bias, the method yielded estimates of maturity that were of low accuracy. Webb and Burley [75], in an investigation involving tests on 319 American Upland samples of the 1951 crop, found the correlation between Causticaire maturity index and percentage of mature fibres, as determined by the ASTM standard maturity count, to be no higher than +0.752. As Lord remarks, the Causticaire estimates for fibre maturity can, at best, only be regarded as providing a rough approximation to the real values.

The differential-dyeing test

This test, originally put forward by Goldthwait *et al.* [78], was used by workers in Ghent and Delft, in the following way. A 3 g sample is introduced into a boiling dye-bath consisting of Diphenyl Fast Red and Chlorantine Fast Green. After 15 minutes, 4% (calculated on weight of fibre) of NaCl is added and, after a further 15 minutes, a further 4% of NaCl. When the sample has been in the bath for 45 minutes, it is taken out and rinsed three times in distilled water. After draining off, the sample is immersed and continually stirred for 30 seconds in a beaker of vigorously boiling distilled water, after which it is centrifuged. The cotton is then rinsed in cold distilled water and carefully dried. The sample is now ground to powder in a mill, thoroughly mixed, and pressed into the form of a pad. The pads are then compared visually with pads prepared from Standard American cottons of known maturity as measured by the standard ASTM maturity count. Mature samples appear predominantly red and immature samples predominantly green.

According to Boulton and Armfield [7], the test depends on two circumstances: (1) that, of the two dyes used, the red diffuses into, and also washes out of, the cellulose of the cell wall much more rapidly than the green; and (2) that immature fibres have a greater specific surface than the mature and so take up dye more rapidly. Thus, because of their greater specific surface, the immature fibres take up more green dye than the mature fibres do and, because of the slow diffusion rate of the green dye, the difference between the two is not greatly affected by the subsequent boiling wash. With the rapidly diffusing red dye, on the other hand, a period of 45 minutes is long enough to cause both mature and immature to take up much the same amount of dye, but, in the 30 second boiling wash, the immature fibres lose much more of what they take up because of their greater specific surface.

From the foregoing, it will be evident that, if the test is to have any success at all, the procedure for dyeing and washing must be precisely defined and rigidly adhered to. It will be equally evident, however, that the test is essentially one of specific surface. It is a test of maturity only in the special circumstances of the American Uplands cottons already noted, namely, that mean perimeter can be assumed substantially constant. It could be used for other types only if in each case a special set of reference pads were prepared for each type. In the matter of time, the test has no advantages at all, and, bearing in mind that it is the specific surface that, in fact, is measured, the same results can be obtained far more quickly and with much less mess by means of an air-flow instrument.

Near infra-red reflectance

This is a fast test method, which has been investigated in connection with HVI testing. The radiation is scattered from the fibre surface and so correlates well with micronaire values and other methods of measuring surface area. Published work on this method of measuring cotton fineness and maturity has been reviewed by Montalvo and Von Hoven [79].

X-ray fluorescence analysis

This is another fast method, which measures the calcium content of the fibres, which can be related to maturity parameters [55, 80].

3.11 References

1. E. R. Kaswell, *Textile Fibers, yarns and Fabrics*, Reinhold, New York, 1953.
2. M. J. Denton and P. N. Daniels (Editors). *Textile Terms and Definitions*, 11th edition, The Textile Institute, Manchester, 2002.
3. F. T. Peirce. *Report of 3rd E.C.G.C. Conference*, 1938, p. 138.
4. K. L. Hertel and C. J. Craven. *Text. Res. J.*, 1951, **21**, 765.
5. F. T. Peirce and E. Lord. *J. Text. Inst.*, 1939, **30**, T173.
6. W. von Bergen. *Fibres*, 1952, **13**, January, 32.
7. J. Boulton and W. Armfield. *J. Text. Inst.*, 1949, **40**, T445.
8. F. Fothergill. *J. Soc. Dyers Col.*, 1944, **60**, 93.
9. M. V. Forward and S. T. Smith. *J. Text. Inst.*, 1955, **46**, T158.
10. J. M. Preston and P. Pal. *J. Soc. Dyers Col.*, 1947, **63**, 430.
11. H. P. Gurney. *J. Text. Inst.*, 1925, **16**, T269.
12. J. W. S. Hearle. In *Structural Mechanics of Fibres, Yarns and Fabrics*, J. W. S. Hearle, P. Grosberg and S. Backer, (Editors), Wiley-Interscience, New York, 1969, pp. 255–322.
13. J. L. Spencer-Smith and H. A. C. Todd. *Suppl. J. Roy. Stat. Soc.*, 1941, **7**, 131.
14. J. G. Martindale. *J. Text. Inst.*, 1945, **36**, T35.
15. J. L. Spencer-Smith. *J. Text. Inst.*, 1947, **38**, P237.
16. R. Garnsworthy, R. Mayfield, R. Gully, R. Westerman and P. Kenins, *7th Int. Wool Conf.*, Tokyo, 1985, **III**, 190.
17. T. J. Mahar and J. M. A. O'Keefe. *Proc. Wool Industry Sci. Tech. Conf.*, Hamilton, Victoria, Australia, 2002.
18. W. S. Simpson. In *Wool: Science and Technology*, W. S. Simpson and G. H. Crawshaw (Editors), Woodhead Publishing, Cambridge, England, 2002, p. 1.
19. R. Bianchi and R. Maglione. In *Polyester: 50 Years of Achievement*, David Brunnschweiler and John Hearle (Editors), The Textile Institute, Manchester, 1993, p. 196.
20. M. Okamoto. In *Polyester: 50 Years of Achievement*, David Brunnschweiler and John Hearle (Editors), The Textile Institute, Manchester, 1993, p. 108.
21. D. H. Morton. *J. Text. Inst.*, 1956, **47**, T422.
22. E. Lord. *J. Text. Inst.*, 1947, **38**, T84.
23. A. C. Goodings and L. H. Turl. *J. Text. Inst.*, 1940, **31**, T207.
24. J. E. Ford, G. Pearson and R. M. Smith (Editors). *Identification of Textile Materials*, The Textile Institute, Manchester, 6th edition, 1970, Figures 1 and 3.
25. N. L. Pearson. *Text. Res. J.*, 1950, **20**, 152.
26. A. J. Turner. *J. Text. Inst.*, 1929, **20**, T233.
27. W. L. Balls. *Studies of Quality in Cotton*, Macmillan, London, 1928, p. 20.

28. E. Honegger. *J. Text. Inst.*, 1951, **42**, P51.
29. BISFA Rules for Rayon Staple Fibre, 1953, and Rules for Synthetic Fibres Based on Polyamides, 1954.
30. ASTM Standards on Textile Materials *D* 1769–73.
31. G. R. N. Naylor and M. M. Purmalis. *Proc. Beltwide Cotton Conf.*, 2005, p. 2302.
32. W. L. Balls. *The Development and Properties of Raw Cotton*, Black, London, 1915, p. 187.
33. C. Nanjundayya. *Indian Cotton Gr. Rev.*, 1952, **6**, 171.
34. W. E. Morton and N. Radhakrishnan. *J. Text. Inst.*, 1954, **45**, T774.
35. N. Ahmad. *ICCC Bull., Series A*, 1933, No. 25.
36. *Wool Sci. Rev.*, 1952, No. **8**, 33.
37. International Wool Textile Organization. Method published by the British Standards Institution as BS 2043: 1968.
38. J. E. Ford and S. C. Simmens. *Shirley Institute Memoirs*, 1958, **31**, 289.
39. J. T. Sparrow. In *The Use of the Scanning Electron Microscope*, Pergamon Press, Oxford, 1972.
40. M. Glass, T. P. Dabbs and P. W. Chudleigh. *Textile Res. J.*, 1995, **65**, 85.
41. <http://www.tft.csiro.au/achievements/sirolaser.html>.
42. D. J. Butler and M. Glass. *J. Textile Inst.*, 1999, **90**, Part 1, 500.
43. B. P. Baxter, M. A. Brims and T. B. Taylor. *J. Textile Inst.*, 1992, **83**, 507.
44. B. P. Baxter, M. A. Brims and T. Taylor. *J. Textile Inst.*, 1992, **83**, 507.
45. M. A. Brims: *Report No: SG 02*, IWTO Barcelona Meeting, 2002.
46. ofda.htm on www.ofda.com, 2006.
47. INTERWOOLLABS Management Committee, IWTO Report No: SG01, 2003.
48. A. D. Peterson, A. Brims, M. A. Brims and S. G. Gherardi. *J. Textile Inst.*, 1998, **89**, Part 1, 441.
49. S. G. Gordon and G. R. N. Naylor. *Proc. Beltwide Cotton Conf.*, 2004, p. 2350.
50. G. R. N. Naylor and M. M. Purmalis. *Proc. Beltwide Cotton Conf.*, 2006, p. 1947.
51. E. Lord. *J. Text. Inst.*, 1956, **47**, T16.
52. J. G. Montalvo, S. E. Faught and S. M. Buco. *J. Cotton Sci.*, 2002, **6**, 133.
53. S. G. Gordon and N. L. Phair. *Proc. Beltwide Cotton Conf.*, 2005, p. 2284.
54. S. G. Gordon, R. Long, M. Bange, S. Lucas and N. L. Phair-Sorensen. *Proc. Beltwide Cotton Conf.*, 2007, 1305.
55. S. G. Gordon, J. G. Montalvo, S. E. Faught and R. T. Grimbail. *Textile Res. J.*, 1997, **67**, 545.
56. J. M. Bradow, O. Hinojosa, L. H. Wartelle and G. Davidson, *Textile Res. J.*, 1996, **66**, 545.
57. W. L. Balls. *Studies of Quality in Cotton*, Macmillan, London, 1928.
58. E. Lord. *J. Text. Inst.*, 1955, **46**, T191.
59. J. G. Montalvo Jr. and B. T. Vinyard. *Textile Res. J.*, 1993, **63**, 267.
60. J. Jenkins, J. Wu, J. McCarty, U. Reddy and J. Zhu *World Cotton Res. Conf.*, 2004, p. 352.
61. J. B. Worsham. *Cotton Growers*, April 2003.
62. S. L. Anderson. *J. Text. Inst.*, 1954, **45**, P312.
63. V. E. Gonsalves. *Text. Res. J.*, 1947, **17**, 369.
64. S. G. Gordon. Doctoral dissertation, Latrobe University, Melbourne, Australia, 1994.
65. W. L. Balls. *Studies of Quality in Cotton*, Macmillan, London, 1928, p. 19.
66. A. N. Gulati. *Indian Cotton Gr. Rev.*, 1947, **1**, 60.
67. J. G. Montalvo. *J. Cotton Sci.*, 2005, **88**, 81.
68. www.cottoninc.com/CottonFiberChart/?Pg=6.
69. H.-P. Hartenhauer. *Dtsch. Textiltech.*, 1958, **8**, 330.
70. E. Lord. *J. Text. Inst.*, 1956, **47**, T209.
71. F. Carpenter. *An Evaluation of Various Ratios for the Classification of Cotton Fibres for Maturity*, US Dept. of Agric. Prod. and Mark. Admn, March, 1953.
72. 'A modified technique for making cotton fibre maturity tests', *USDA Bulletin*, April, 1950.

73. M. A. Grimes. *Textile World*, 1945, February, 161.
74. S. G. Gordon and N. L. Phair. Unpublished data referred to in [48].
75. R. W. Webb and S. T. Burley. US Dept. of Agric. Marketing Res. Rep. No. 57, Dec., 1953.
76. B. P. Saville, 'Physical testing of textiles' Woodhead Publishing, Cambridge, UK, 1999, 55.
77. E. Lord. *J. Text. Inst.*, 1956, **47**, T635.
78. E. F. Goldthwait, H. O. Smith and M. P. Barnett. *Text. World*, 1947, **97**, No. 7, 105.
79. J. G. Montalvo Jr and T. Von Hoven. In *Near Infrared Spectroscopy in Agriculture*, C. A. Roberts, J. Workman Jr. and J. B. Reeves (Editors), Crop Science Society of America, Modison, Wisrovisin, USA 2004.
80. L. H. Wartelle, J. M. Bradow, O. Hinojosa, A. B. Pepperman, G. F. Sassenrath-Cole and P. Dastoor. *J. Agric. Food Chem.*, 1995, **43**, 1219.

4.1 Fibre lengths

In continuous filament yarns, the fibres are infinite in length. In the literal sense of the word, it is always possible to increase the length by adding another turn on the package. From a practical viewpoint, the fibre length in a 1 kilogram package of 100 dtex yarn is 10 kilometres, which gives an aspect ratio of 10^9 for a 1 dtex fibre and a negligible number of free ends in any product.

Manufactured staple fibres are mostly cut to a controlled length, so that the length is part of the specification, and the fibres are much more uniform in length than natural fibres, though not perfectly so. A reference from 1950 gives a coefficient of variability of 10% as indicating the degree of length variation likely to be encountered [1]. A part of this is due to imperfections in the stapling machine, which may have been reduced with improved quality control, but a part is caused by fibre breakage. All fibres are liable to breakage during handling and processing, and it follows that length measurements made on the same material in successive stages of manufacture will disclose the presence of a progressively increasing amount of short fibre, except where combing is introduced for the express purpose of removing the short fibres. In principle, manufactured staple fibres may be produced in any length, but since most manufactured staple fibre is blended with natural fibres, or, if used alone, is processed on machinery designed for natural fibres, the lengths available are selected to meet these needs. In nearly every case, the length is intended to be uniform, but it has been suggested that there are advantages for rayon staple in varied lengths when it is intended for blending with natural fibres [2]. In contrast to the genetic associations in natural fibres, length and fineness can be varied independently in manufactured fibres, and, incidentally, without affecting the cost.

An exception to the directly controlled length of manufactured staple fibres is in stretch-breaking of tows. A length distribution then depends on the quasi-random location of breaks in the filaments trapped between rollers running at increasing speeds.

For natural fibres, the length and the length distribution are critical properties, which influence processing, performance and price. In common with most of the physical properties of the natural textile raw materials, fibre length varies very greatly within any one sample. Thus, for example, the coefficient of length variation, itself differing appreciably from sample to sample, is of the order of 40% for cotton and

50% for wool [1]. This variability is biological in origin, and there is no practicable way of avoiding it, mainly because the major component of variance is to be found in the single seed of cotton or the single lock of wool. Some marginal improvement may still be possible by breeding for greater length uniformity, but, for the rest, the most that can be done is to adopt such farming, harvesting and marketing methods as will keep the other components of variance down to a minimum.

An impression of the magnitude of length variation in the natural fibres may be obtained from the fibre array shown in Fig. 4.1(a), while a comparison of (b) and (c) shows an increased tail of short fibres in a lot of $1\frac{7}{16}$ inch (3.7 mm)¹ *Fibro* viscose rayon staple as a result of breakage during processing.

In wool and cotton, length and fineness are correlated, negatively in the case of wool and positively in the case of cotton. Thus, among the wools of the world, the longer types are generally also the coarser, and the same kind of association between length and fineness is also found among the individual fibres of a given sample. Among cottons, the longer types are generally the finer, but there is no corresponding correlation for the fibres within a sample. Fineness does vary throughout the length range within a sample, but not systematically. Sometimes the longest fibres are the coarsest, sometimes the shortest, and sometimes those of intermediate length, as illustrated in the data by Clegg [3] in Table 4.1. Variations greater than those shown in Table 4.1 are not likely to be encountered very often. Sometimes, as shown by the figures for the Maarad sample, fineness is practically independent of length.

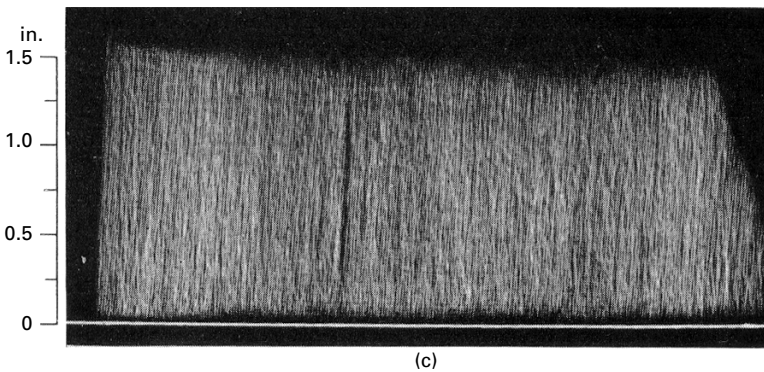
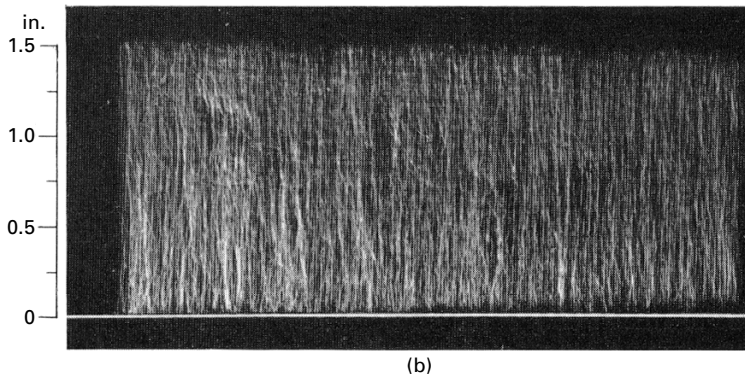
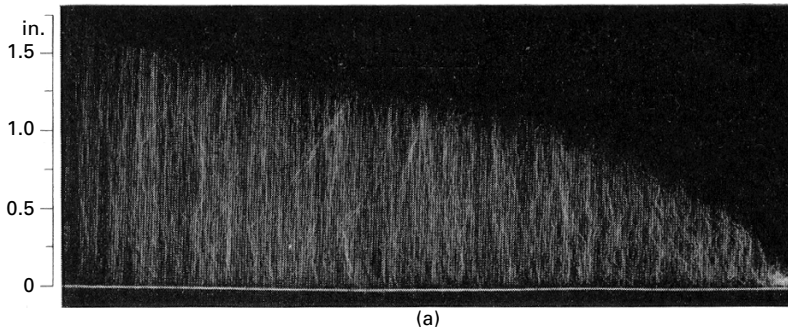
The lengths of wools and cottons are usually referred to in terms of staple length, a quantity which, so far as cotton is concerned, is discussed in some detail in Section 4.4.2. For present purposes, it is sufficient to say that the staple length of a wool is the average overall length of the natural locks in their normal crimped condition, whereas that of a cotton is somewhere between the mean length and the maximum.

Rough guides to the range of fibre lengths are given by the following examples. Coarse Indian cottons had staple lengths as low as $\frac{1}{2}$ – $\frac{5}{8}$ inch, (13–16 mm) but short fibres below 1 inch (25 mm) have mostly been replaced by improved varieties. American Upland varieties (*G. hirsutum*), which now account for 90% of world cotton production, are 1 – $1\frac{1}{4}$ inch (25–32 mm) *G. barbadense*, which has 8% of world production and includes Sea Island and long-staple Egyptian cottons, are $1\frac{1}{4}$ –2 inches (32–50 mm). Australian Merino wool is typically 65–75 mm ($2\frac{1}{2}$ to 3 inches) but a coarse Lincoln

Table 4.1 Cotton length and fineness

Type of cotton	Linear density of fibre group millitex				
	Longest				Shortest
Brazilian São Paulo	194	225	236	256	283
Egyptian, white	158	160	166	180	173
Sea Island	138	124	131	117	108
Sudan Sakel	131	132	148	132	116
Egyptian, Maarad	141	134	131	137	134

1. Inches are given as the primary unit because that is cotton industry practice. The wool industry now uses mm.



4.1 Fibre arrays (Baer diagrams): (a) cotton; (b) raw Fibro viscose rayon staple; (c) Fibro from card sliver (1 inch = 25.4 mm).

wool would be 250–300 mm (10–12 inches). Strands of flax, hemp and jute may be between 15 and 90 mm (5 and 35 inches) in length.

4.2 Technical significance of fibre length

Fibre-processing machines, and especially those incorporating roller-drafting, are designed to operate efficiently only on a comparatively narrow range of staple lengths.

Furthermore, within that range, adjustments have to be made with some care to suit the material being processed if the best results are to be obtained. Therefore, once the machinery has been set up and adjusted, to avoid repeated and costly alteration, it is desirable to maintain optimum processing conditions by ensuring that raw material supplies do not vary by more than minimal amounts from some established length standard.

Where combing is involved, it is necessary, too, to control not only the length but also the variation in length of the material put into process. The amount of short fibre present influences the amount of 'noil' or waste extracted and thus has an important bearing on the economics of manufacture.

In rovings and yarns, the longer the fibre, the longer is the overlap among the fibres over which they can be made to cohere by means of twist. It follows, therefore, that the twist can be less without sacrificing essential strength and that, as a corollary, the longer the fibre length, the lower is the end breakage rate, other things being equal.

It should be mentioned that, when the material to be processed is short, the machine designer is presented with special problems inasmuch as roller settings must be correspondingly close. Consequently, smaller, high-speed, and less robust rollers must be used and less space is available for accommodating devices capable of controlling the motions of the short fibres present. It is therefore not surprising that the longer the fibres, the finer and the more uniform is the yarn that can be spun, other things again being equal.

Hence, for most purposes, longer fibres are preferable. From the point of view of cloth characteristics, however, short fibres have the advantage where it is desirable to produce a soft, hairy and warm-handling surface. Here a large number of projecting fibre ends are desired, and, although the number of ends can be strongly influenced by the method of spinning employed, under any given set of conditions it must obviously vary inversely as the mean fibre length.

4.3 Length distributions and fibre diagrams

4.3.1 Frequency diagrams

Table 4.2 relates to a hypothetical sample of fibrous material on which 100 length measurements have been made and the results arranged in the usual way for statistical calculation. For the sake of simplicity and to avoid the compilation of a cumbrous table, it is here assumed that 100 observations are enough to make a sufficiently reliable test, though in practice so small a sample would be quite inadequate. The overall range is 20 length units, divided at equal intervals of 2 units into ten classes, the mid-points l of which are given in column (1). The frequencies f given in column (2) relate to a numerical sample, and, when these are plotted as ordinates against the corresponding values of l , the usual form of frequency diagram is obtained as a histogram, polygon or curve (see Fig. 4.2). It is evident that the smooth curve derived from the frequencies represents the probability p that any fibre taken at random will have a length lying between l and $(l + \delta l)$ (see Fig. 4.3).

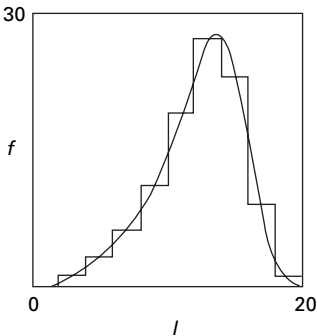
Table 4.2 Hypothetical fibre length distribution

(1)	(2)	(3)	(4)	(5)	(6)	(7)
Class mean l	f	$\sum_i l_m f$	$lf = f'$	$l^2 f = lf'$	$\sum_i l_m f'$	$\sum_i l_m \sum_i f'$
1	0	100	0	0	1236	8692
3	1	100	3	9	1236	7456
5	3	99	15	75	1233	6220
7	6	96	42	294	1218	4987
9	11	90	99	891	1176	3769
11	19	79	209	2299	1077	2569
13	27	60	351	4563	868	1516
15	23	33	345	5175	517	708
17	9	10	153	2601	172	191
19	1	1	19	361	19	19
Totals	100	–	1236	16 268	–	–

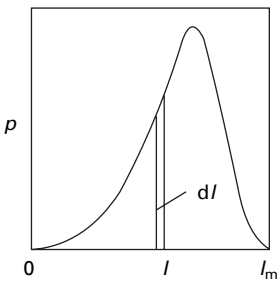
Mean length = $\bar{L} = \frac{\sum (lf)}{\sum f} = \frac{1236}{100} = 12.36$

Standard deviation = $\sigma^2 = \frac{\sum (l^2 f)}{N} - \bar{L}^2 = \frac{16\,268}{100} - 12.36^2 = 9.92$

Length biased mean length = $\bar{L}' = \frac{\sum (lf')}{\sum f'} = \frac{16\,268}{1236} = 13.16$



4.2 Frequency histogram.



4.3 Frequency curve.

To calculate the mean length, \bar{L} , we proceed in the usual way to find, by column (4), the total length of fibre $\sum(lf)$ whence

$$\bar{L} = \frac{\sum (lf)}{\sum f} = \frac{\sum (lf)}{N} \tag{4.1}$$

where N is the total number of fibres.

The standard deviation σ is conveniently calculated by working with deviations from the arbitrary value zero, in which case the values of l are treated as deviations, squared and multiplied by the corresponding values of f , giving $l^2 f$ in column (5). The total variance is given by $\sum(l^2 f) - N\bar{L}^2$, and the standard deviation by:

$$\sigma = \left(\frac{\sum l^2 f}{N} - \bar{L}^2 \right)^{1/2} \quad (4.2)$$

from which the standard error of the mean and the coefficient of variation are readily calculated. The maximum and the mode, with equal numbers shorter and longer, of the distribution can usually be estimated with reasonable accuracy from the frequency curve.

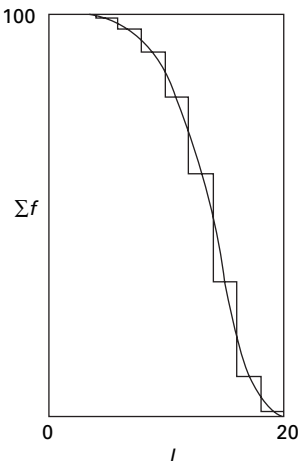
4.3.2 Survivor diagrams

An alternative way of graphically representing the fibre length distribution is to construct a survivor diagram, in which, for a numerical sample, the ordinates represent the number of fibres, expressed as a percentage or any other suitable basis, whose lengths exceed any given length, l . The most convenient way of obtaining such a diagram from frequency data is to find the cumulative totals of f , from the maximum, l_m , to zero, l_0 , as shown in column (3) of Table 4.2, and plot these totals in histogram form against l . The survivor curve can then be obtained by drawing a smooth curve through the mid-points of the horizontal steps as shown in Fig. 4.4.

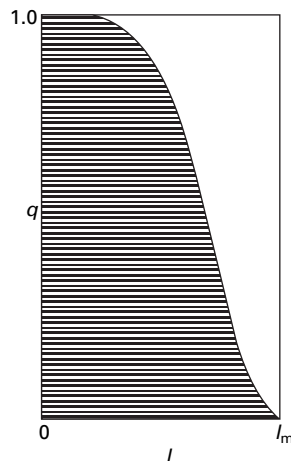
Another form of survivor curve is that given by the outline of a Baer diagram (see Section 4.7.2). In this case, the sorted fibres extend vertically from a common base-line, the longest on the left and the shortest on the right, as in Fig. 4.1(a). If, instead, they were arranged horizontally with the longest at the bottom and the shortest at the top (Fig. 4.5), the outline of the survivor curve of Fig. 4.4 would be obtained.

It is obvious that the curves of Figs 4.4 and 4.5 represent the probability q that any fibre taken at random will be longer than any given length l , and further that:

$$q = \int_l^{l_m} p \cdot dl \quad (4.3)$$



4.4 Survivor diagram.



4.5 Baer diagram.

4.3.3 Distribution for length-biased samples

It is possible, and sometimes most convenient, to take as the sample for measurement a length-biased Wilkinson tuft. The length distribution of such a sample can be related to that of a numerical sample.

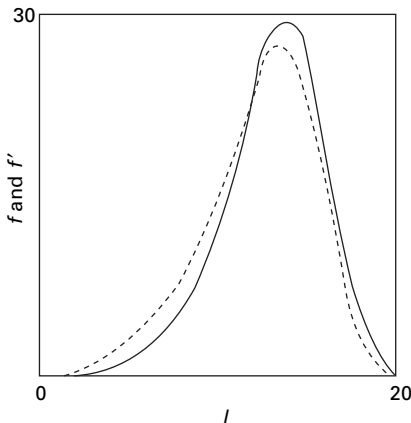
Consider a length-biased sample taken from the same population as in Table 4.2. In that case, as we have already seen, the probability of the occurrence of a fibre of length l is proportional to the product of its length and the frequency with which that length occurs in the population, or in the numerical sample, which we here assume accurately represents the population. Hence the relative length-biased frequencies, f' , are given by $f' = lf$.

These quantities are given in column (4) of Table 4.2. With suitable adjustment of scale, they can be plotted as in Fig. 4.6 to show how a length-biased distribution compares with its numerical counterpart. Similarly, by taking cumulative totals of f' from l_m to l_0 , we can obtain, as in column (6), the ordinates for a survivor curve for the length-biased sample. This is shown in full line in Fig. 4.7. Such is the curve that would be obtained if a Baer Sorter test (see Section 4.7.2) were made on a length-biased sample. For the infinite population, the equation corresponding to equation (4.3) is:

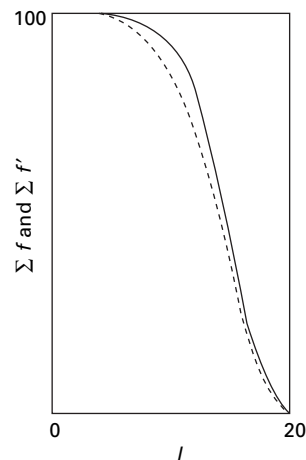
$$q' = \int_l^{l_m} p' \cdot dl \quad (4.4)$$

To calculate the mean length, \bar{L}' , of the length-biased sample, we treat the values of f' as frequencies and proceed as usual to find $\Sigma(lf')$. But, since $f' = lf$, this quantity is the same as $\Sigma(l^2f)$, which has already been found by column (5) of the table. Hence:

$$\bar{L}' = \frac{\Sigma(l^2f)}{\Sigma(lf)} \quad (4.5)$$



4.6 Length-biased (full line) and numerical distributions (dashed line).



4.7 Cumulative length-biased (full line) and numerical distributions (dashed line).

But $\Sigma(lf) = LN$ and, from equation (4.2), $\Sigma(l^2f) = (L^2 + \sigma^2)N$.

We have, therefore:

$$\bar{L}' = \frac{(\bar{L}^2 + \sigma^2)N}{\bar{L}N} = \bar{L} + \frac{\sigma^2}{\bar{L}} \quad (4.6)$$

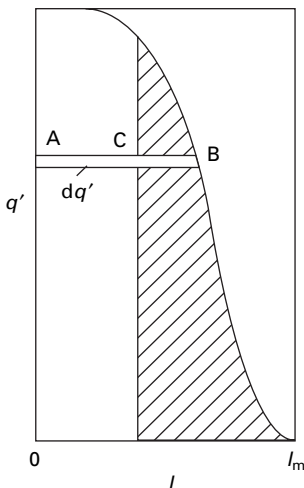
Thus, if the mean and standard deviation of a numerical sample are known, the mean of the corresponding length-biased sample can be calculated [4].

4.3.4 Beard diagrams

If a sliver of straight and randomly overlapping fibres is clamped across a section and all loose fibres are combed away on one side, a beard of fibres is left projecting. The distribution of lengths of the fibres in the beard will be the same as the distribution of distances from fibre ends to points randomly selected along the fibres. The length characteristics of the beard are of great technical importance [4, 5]. It is such a beard, for instance, that is held by a pair of drafting rollers or by the nippers of a rectilinear comb. The fibres held by the clamp, including the lengths on the other side, which have not been combed away, constitute a Wilkinson tuft, the nature of which has been discussed in Section 2.3.2, but here we are concerned with a semi-Wilkinson tuft, the composition of which is quite different.

Consider a beard formed by the left-hand ends of a length-biased population of fibres represented by the survivor diagram shown in full line in Fig. 4.7, and reproduced in Fig. 4.8. For convenience, let us refer to that part of a fibre that contributes to the beard as a beard element, or simply an element.

In the formation of the beard, every fibre that is held at all may be held at any point along its length with equal probability; so fibres of length l will contribute to the beard every length of element from zero to l in equal proportions. From the population



4.8 Clamp diagram.

as a whole, therefore, beard elements can arise varying in length from zero to l_m , the maximum length of fibre present.

Consider the probability r' that a beard element will be longer than l . For this to happen, it is clear that a fibre must be clamped at a distance $> l$ from its left-hand end. Hence no fibre shorter than l makes any contribution. On the other hand, every fibre longer than l contributes to r' in a measure depending on how greatly its length exceeds l .

Take, for example, the fibre AB in Fig. 4.8, the probability of whose occurrence in the length-biased population is dq' . The probability that it will form a beard element longer than l is the probability that it will occur at all multiplied by the probability that the point where it is clamped will fall between B and C.

Since it is equally likely that the clamping point will be anywhere between A and B, the probability that it will fall between B and C is obviously BC/AB , and a similar condition holds for every other fibre longer than l . The total probability of an element longer than l occurring in the beard is therefore the ratio of the shaded area to the entire area under the curve, i.e.:

$$r' = \int_l^{l_m} q' \cdot dl \bigg/ \int_0^{l_m} q' \cdot dl \quad (4.7)$$

But, since, substituting from equation (4.4), and noting that $\int_0^{l_m} q' \cdot dl$ is a constant for a sample, we have:

$$r' = \int_l^{l_m} dl \int_l^{l_m} p' \cdot dl \quad (4.8)$$

From this it is evident that all we have to do to obtain the distribution of beard elements from the length frequencies of a numerical sample of fibres is first to find the length-biased frequencies, $f' = lf$, and then to obtain the second successive cumulative

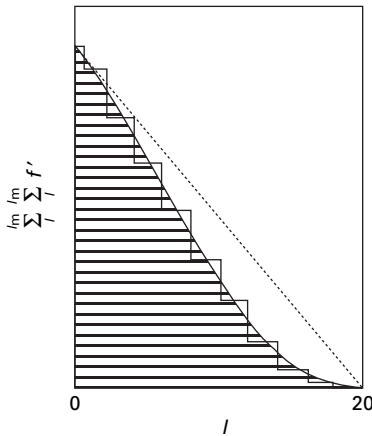
totals of these frequencies, i.e.: $\sum_l^{l_m} \sum_l^{l_m} f'$. This is done in column (7) of Table 4.2.

When these values are plotted against l , the diagram shown in Fig. 4.9 is obtained. Horizontal and closely spaced lines are here drawn in to convey more graphically what the composition of a beard diagram is really like and to emphasise the striking difference between it and the corresponding Baer diagram. The dotted line shows what the beard diagram would have been if all the fibres had been of the same length l_m .

4.3.5 Distributions by mass

In some of the techniques of fibre-length measurement, the fibres of a sample are sorted into length groups; and the fibres in each group, instead of being counted to enable the frequencies to be obtained, are weighed.

Referring to Table 4.2, it is evident that, if f is the number of fibres in a group having a length l , then $(f l)$ is the total length of fibre in that group. If the linear



4.9 Beard diagram.

density of all the fibres is c , then $(c f l)$ is the mass of the fibres in the group. Thus, since c is a constant factor, the figures in column (4) also represent the proportions by mass of the different lengths.

For this to be true, it is not necessary that every individual fibre should have the same linear density: it is sufficient if c varies randomly so that its mean value shows no appreciable variation over the entire length range. Given these conditions, it is possible to transform a numerical distribution into a mass distribution, or vice versa, simply by multiplying or dividing by l , as the case may be. It is further evident that, given these conditions, the proportions by mass of a sample are the same as the proportions by number (i.e. proportionate frequencies) of a length-biased sample.

The necessary conditions can be assumed to hold good for all manufactured staple fibres, but not for wool or cotton, since fineness varies between fibres usually with length bias (see [Section 4.1](#)). When, therefore, as a result of using certain measuring techniques, mass distributions of length are obtained directly, they are best left and interpreted as such, without any attempt at transformation, unless c is actually measured for each group and the values so found are used in the computations (see [Section 3.5.3](#)).

A distribution can also be given in terms of the proportion biased by fineness (linear density or titre). This is mass-based in the sense that it depends on mass per unit length, but is not biased by the mass of the whole long fibre.

4.3.6 Measures of fibre length

The frequency distributions described above give a full picture of the fibre lengths in a sample. However it is also useful to give values for particular parameters. *Mean fibre length*, *variance*, *standard deviation* and *coefficient of variation*, whether on a numerical or a biased basis, are standard statistical parameters. A number of other terms have particular connotations [6]. *Staple length* is a characteristic length, usually estimated by subjective visual assessment. For cotton, it corresponds closely with the

modal (most frequent) length when the fibres are straightened; for wool it is usually taken as the length (extent) of the longer fibres in the crimped state in a hand-prepared tuft. *Short fibre content* is the percentage by number or weight of fibres shorter than a specified length, $\frac{1}{2}$ inch (13 mm) for cotton, typically 25 or 40 mm for wool.

For cotton, *effective length* is given by a series of approximations, usually two, to the upper-quartile length with elimination of short fibres by a procedure described below. The *fibrogram* is a particular form of length distribution obtained on modern automated instruments. Statistically, it is the second summation of the numerical distribution, which is column (7) of Table 4.2. *Upper-half mean (UHM) length* is the mean length by number of fibres in the longest half by weight of the fibres in a cotton sample, usually measured from the fibrogram. *Uniformity index* is then the ratio of mean length to UHM length expressed as a percentage. *Span length* is the length exceeded by a stated percentage of cotton fibres in the fibrogram. *Uniformity ratio* is the ratio of the 50% span length to the 2.5% span length, expressed as a percentage.

For wool, *hauteur* is defined as the mean length in sliver or roving from a titre (linear density)-biased distribution; *barbe* is the equivalent quantity from a mass (whole fibre) biased distribution. Because of the greater influence of longer fibres, *barbe B* is always greater than *hauteur H*. If the coefficient of variation of *hauteur* is *V*:

$$B = H \left(\frac{1 + V}{100} \right) \quad (4.9)$$

4.4 Wool and cotton

4.4.1 Wool fibre length

Because wool fibres are relatively long, length is a less important property. The twists needed in yarns are less and, in woollen yarns, entanglement is effective in giving strength. The low twist preserves yarn bulk, though sometimes at the expense of a propensity to pilling. Length was not a factor in traditional wool grading. However as Simpson [7] notes: ‘Objective testing of fine Merino wools [which are shorter] has come to include measurement of wool staple length and strength (IWTO-30 test method) applied to greasy wool samples.’ For long staple New Zealand wools, the reduction in length in carding of wool that has become entangled in scouring is a more important consideration. Data on short fibre percentage, mean fibre length and coefficient of variation of *hauteur* for *length after carding* can be provided for *sale-by-sample*.

4.4.2 Cotton staple length

From the earliest inception of roller drafting, it must have been recognised that there was a very strong association between the optimum spacing of the rollers and the length characteristics of the cotton being processed. It is therefore not unreasonable to assume that the values assigned to the so-called ‘staple lengths’ of the different cottons in use corresponded fairly closely with the roller settings that each demanded. But the concept of staple length came into use long before satisfactory methods of

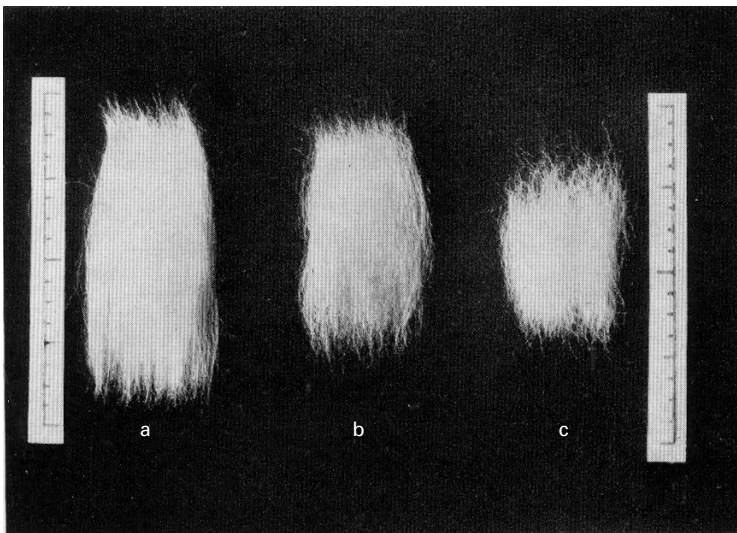
measuring fibres had been developed, so that merchants, spinners or graders in doing business with one another, had to be content with estimates of length made by personal judgement of the appearance of a hand-prepared staple such as is shown in Fig. 4.10. Thus, being arrived at by judgement and not by measurement, staple length was never formally defined in terms of any statistic of length distribution.

Continuous commercial intercourse has naturally resulted in a substantial measure of agreement throughout a business community as to what the staple length of any particular sample of cotton is, and, in the United States, at least, stability in the standards of judgement of Upland staples was greatly helped by the setting-up of physical reference standards, in the form of actual cotton samples, by the Department of Agriculture in 1918. Nevertheless, individuals differed in extreme cases by as much as 3 mm in their judgement, and furthermore, there is evidence to show that in Britain, if not also elsewhere, the whole level of judgement shifted with the passage of time. Whereas, in the 1920s, Lancashire estimates of Uplands staple tended to be about 10% over the American, by 1950 they had changed so as to fall into line. It was obviously desirable to give greater definition to this somewhat elusive quantity.

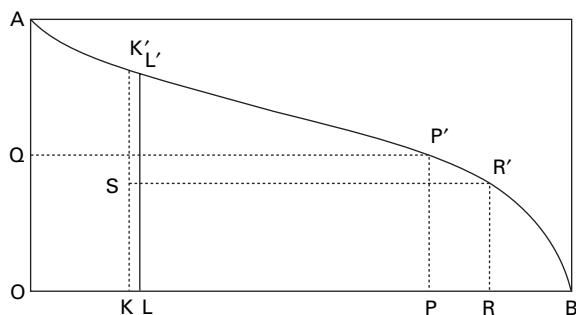
The earliest attempt to do this was that made by Clegg [3], who, starting with the outline of the Baer Sorter diagram (see Section 4.7.2), devised a geometric construction to give a quantity that she called the *effective length*. She found this to agree fairly well with the grader's estimate of staple length as judged on the Liverpool raw-cotton market at that time (1930). The construction is as follows (see Fig. 4.11):

$$OQ = \frac{1}{2} OA = PP'$$

$$OK = \frac{1}{4} OP$$



4.10 Hand staples from around 1960: (a) Egyptian cotton of $1\frac{7}{16}$ inch (37 mm) staple; (b) American cotton of $1\frac{1}{8}$ inch (29 mm) staple; (c) Indian cotton of $\frac{7}{8}$ inch (22 mm) staple.



4.11 Baer diagram analysis.

$$KS = \frac{1}{2}KK' = \frac{1}{2}RR$$

$$OL = \frac{1}{4}OR$$

and LL' is the effective length.

It will thus be seen that the effective length is the upper quartile of a numerical length-distribution from which some of the shortest fibres (to the right of R) have been eliminated by an arbitrary construction. As has been remarked above, however, Lancashire judgement of Upland staples changed. Hence, so far as American cottons are concerned, the effective length must be divided by 1.1 in order to obtain the staple length. For Egyptian-type cottons, the effective length still corresponded fairly closely to the grader's estimate of staple according to Morton in the first edition of this book in 1962.

With the standard American methods of testing, the staple length is claimed to be given by the UHM length of the distribution by weight, though unfortunately there are no extensive data available by which the closeness of the agreement can be judged. If Egyptian-type cotton is tested with the Balls Sorter (see [Section 4.7.2](#)) to give a weight distribution, the staple length is said to be given by the 71st percentile [8].

An extensive investigation of this subject was carried out by Lord [9], who subjected a large number of samples of cotton from all over the world both to repeated judgement and to measurement. His results showed that, except for Egyptian cottons, the best measure of staple length for general application is that given by the modal, or most frequent, length of a numerical distribution, and he designed an instrument to measure this quantity rapidly and accurately (see [Section 4.10.4](#)). For Egyptian cottons, the modal length must be multiplied by 1.1 to obtain the commercial staple length.

4.5 Crimp

A characteristic feature of practically all staple fibres, which cannot be neglected in any discussion of fibre length, is crimp. Crimp, which in general terms may be defined as the waviness of a fibre, is of technological importance in several contexts. In brief, it determines the capacity of the fibres to cohere under light pressure and so in turn determines the cohesiveness of card webs, the amount of fly liberated during

processing, and the hairiness of the resultant yarn. It is also the principal feature governing the bulk of a textile material and so influences the specific volume of yarns and fabrics, through the dependence on packing factor.

It may be measured in terms of either the number of crimps or waves per unit length or the percentage increase in extent of the fibre on removal of the crimp. With strongly crimped fibres, the force necessary to straighten a fibre may be enough to cause some actual elongation of its axial length, but this is not likely to be of any moment unless the fibre is exceptionally extensible. Cotton has a relatively low crimp associated with the convolutions. In wool, the bicomponent structure gives rise to a helical crimp, which if lost in processing is regenerated on wetting. Crimp can also result from asymmetric forms in manufactured fibres, either in the skin of viscose rayon or in bicomponent synthetic fibres. In manufactured staple fibres, crimp is imposed by serrated rollers as an aid to processing, which may or may not survive into the final product.

For continuous filament yarns, a number of texturing processes lead to the filaments taking up forms, which may be pig-tail snarls in high-stretch yarns or alternating helices or other forms in low-stretch yarns [10]. However, detailed discussion of this type of crimp is outside the scope of this book, though the discussion of setting in [Chapter 18](#) is highly relevant to the processes.

4.6 Individual fibre length measurement

4.6.1 Direct methods

The most obvious and most reliable method of fibre length measurement is to straighten the fibres from the sample, one by one, over a suitable scale and to measure their lengths directly. It is tedious and involves a certain amount of eye-strain. On the other hand, the results it yields are completely comprehensive, and it is superior to any other for accuracy, especially where the short-fibre components of a sample have to be accurately delineated, as in studies of fibre breakage, for example. It is essentially a research worker's method and is that by which the accuracy of other methods may be tested. By suitable illumination of the working plane, combined with a contrasting background and the use of a large lens when necessary, eye-strain may be reduced to a minimum; with practice, especially where it is possible to use a semi-automatic device such as is described in Section 4.6.3, measurements may be made surprisingly quickly.

If individual fibres can be selected, optical analysis of digitised images speeds up the direct measurement of length. However, automated methods are not as easy to develop as the use of snippets for fineness measurements. Recent advances are described in Section 4.11.

4.6.2 Oiled plate method

For cotton and short manufactured staple fibres, a convenient form of scale to use is a sheet of glass, of about quarter-plate size, which has a centimetre scale photographed or etched on its underside. The surface of the glass is smeared with liquid paraffin,

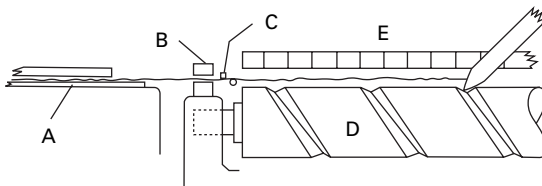
and a bunch of about a dozen fibres from the sample is placed on the far left-hand corner. Then, with the tips of the little fingers of each hand, the fibres are drawn one at a time over the scale and smoothed out straight, and their lengths are noted. The paraffin serves to keep the fibres from blowing about and assists in making them lie flat and straight on the scale when brought into position. As each fibre is measured, it is drawn off into a bunch at the right-hand side of the slide and its length is recorded. The measurements may be written down in columns in the ordinary way, or, more conveniently, the readings may be entered as individuals directly into the appropriate length groups of a frequency table.

If the scale is placed on a dark grey background of matt card and the whole is suitably illuminated, both the fibres and the graduations of the scale may be clearly observed without any difficulty. Up to 300 fibres per hour may be measured in this way, so that, even with cotton, a test may be completed in $2-2\frac{1}{2}$ hours. It is worth noting, too, that, if it is required to know also the mean linear density of the fibres, this may be obtained with very little extra work. All that is necessary is to weigh the entire sample before bringing the oiled plate into use. If one knows the total weight and the total length, a short calculation provides the answer, which would otherwise have to be found separately at the expense of considerable labour.

4.6.3 Semi-automatic single-fibre testers

For measurements on wool and manufactured fibres of comparable length, a purely manual procedure similar to the foregoing may be used, in which a black velvet-covered board is used instead of the oiled plate. To speed up the operation for wool tops, Anderson and Palmer [11] devised the semi-automatic WIRA Fibre Length Machine, and a special cotton version for measuring lengths down to 5 mm (0.2 in.) has been described by Wakelin, *et al.* [12].

The WIRA instrument [13, 14] is illustrated in Fig. 4.12, where the material under test is shown in the form of a 'squared' top spread out under a glass plate resting on a cloth A, ready for sampling. Each fibre to be measured is gripped at its extremity with forceps and drawn to the right successively under the light tensioning arm C, and the point of the forceps is pressed gently into the groove of the revolving screw shaft D. This causes the forceps to traverse smoothly sideways and draw the tensioned fibre after it until the tail end emerges through B. Thereupon the detector wire drops and makes an electric contact, which stops the revolving shaft and indicates by the position of the forceps the length of the fibre being measured. The operator then raises the forceps vertically, thus lifting one of the keys E, which in turn registers the



4.12 WIRA fibre length machine.

observation on the appropriate one of a drum of frequency counters at the back. The counters are spaced at 5 mm intervals, so that, by reading off the numbers on the counters at the end of the test, the frequency distribution of the results is obtained, classified in 5 mm groups. An experienced operator using this instrument can measure wool fibres at the rate of 500 per hour. Here again, by collecting the measured fibres and weighing them, the average linear density may be obtained with very little extra labour.

The drag of the fibre through the tensioning arm B is such as effectively to remove the crimp without stretching the fibre. There is a small consistent error of about 1 mm in the mean, owing to the fact that each fibre can be gripped not at, but only near, its end. This may be neglected in measuring wools but assumes some importance in dealing with short fibre materials.

4.7 Comb-sorter methods

4.7.1 Fibre sorters

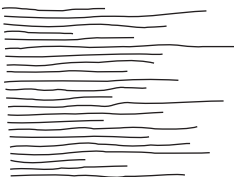
In order to avoid what was regarded as the too laborious measurement of individual fibres, and to expedite the handling of larger and therefore ostensibly more representative samples, a variety of mechanical or semi-mechanical 'sorters' were devised for the purpose of fractionating the sample into a suitable number of groups or of grading the fibres in the order of their lengths.

In all cases, the operation involves two steps: (i) the preparation of a fringe or tuft of fibres, all of which are aligned at one end as shown in Fig. 4.13 and (ii) the withdrawal of the fibres from the fringe in the order of either their increasing or their decreasing length.

4.7.2 Comb sorters

The commonest type of sorter in use is the comb sorter, which, in a variety of forms, can be used for measurements of most kinds of fibres. Only where strong crimp presents difficulties are comb sorters unsuitable.

The principle of operation is the same for all, though there are differences in matters of detail. The essential element is a bed of upright and parallel steel combs in which the fibres are embedded for control during manipulation. The pitch and fineness of the needles and the spacing of the combs vary according to the kind of fibre for which the instrument is designed. For cotton, the comb spacing is usually 5 mm, while for

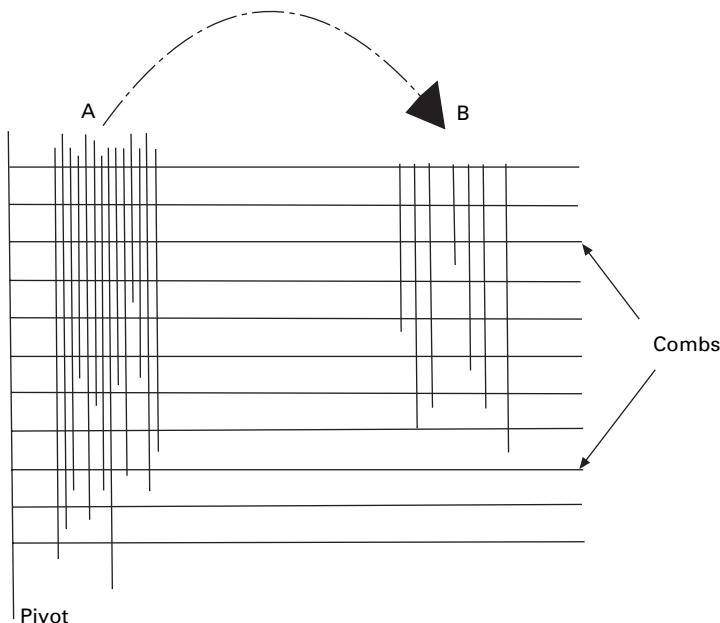


4.13 Fibres aligned for sorting.

wool it may be 1 cm or $\frac{1}{2}$ inch (1.25 cm). The following is a brief description of the manipulation of the Baer Sorter as used for raw-cotton testing [15, 16].

A sample weighing approximately 15 mg is first prepared by one of the zoning methods described in Section 2.5.2, and, by repeated drawing and doubling, it is formed into a narrow bundle of fibres, which are as straight and parallel as possible. This bundle is impaled in the combs with a short fringe protruding, as illustrated in the left-hand side of Fig. 4.14. With the aid of special tweezers, the fibres are taken successively in small groups by their extreme ends, withdrawn from the bundle, and transferred to the right-hand side of the needle bed, so that they lie straight and parallel with their near ends almost flush with the rearmost comb. When the entire sample has been thus transferred, the sorter is turned round and a set of hinged intersecting top combs is swung over into position to aid in controlling the fibres during the final, sorting, stage. In this, again by using the special tweezers to grip the fibres only at their extremities, the fibres are withdrawn in small groups in the order of their diminishing lengths, the combs being successively dropped or lifted out of the way as required.

From this point onwards, the procedure varies according to the method of analysis that it is proposed to adopt. In the United Kingdom, the usual practice is to prepare what is known as a Baer diagram (Fig. 4.1). To do this, the succession of small groups of fibres withdrawn from the tuft in the combs is deposited on a black velvet pad so that all their ends are conterminous with a base-line, which may conveniently take the form of a piece of white thread tied round the pad. When complete, the 'diagram' consists of an array of all the fibres in the tuft, arranged in order of their lengths; the longest, drawn first, is on the left and the shortest, drawn last, on the right, with any



4.14 Operation of a comb sorter.

neppy remnants from the first stage of manipulation gathered in a cluster on one side. The outline of the fibre array may then be traced on suitably graduated transparent paper to give a survivor, or cumulative-frequency, curve, which can be analysed to obtain any of the desired length parameters.

If, however, the results are to be at all reliable, considerable skill is required on the part of the operator in preparing the fibre array. In the analysis of the traced outline, two things must be assumed: (i) that, at any point on the trace, the vertical distance between the curve and the base-line represents the straightened length of the fibre at that point and (ii) that distances measured along the base-line are proportional to the number of fibres present. It is unnecessary to elaborate on the care and precautions that must be taken to justify these assumptions. Failure to straighten the fibres properly in preparing the array can alone give rise to an error of as much as $\frac{1}{16}$ inch (1.6 mm) [16], and errors of similar magnitude can also arise from failure to space the fibres along the base-line with uniform density. Appreciable subjective errors are thus involved, and, even with only one operator, it is usually thought desirable to make two diagrams to obtain a sufficiently reliable result. The time taken by an experienced worker in making a single Baer Sorter test, excluding sampling and analysis of data, ranges from about $\frac{3}{4}$ hour for a short-stapled Indian cotton to $1\frac{1}{2}$ hours for long-stapled Egyptian or Sea Island cotton. It will be seen, therefore, that, although it may be less of a strain, the Baer Sorter method has by no means a great advantage over the oiled plate method described in Section 4.6.2 as far as time is concerned.

An alternative and less subjective method of using comb sorters is to sort the fibres into groups at predetermined length intervals, weigh the groups, and so obtain a mass distribution for the sample (see [Section 4.3.5](#)). One way of doing this [17] is to withdraw, a few at a time, all the fibres whose proximal ends lie between each comb and the next, form them into convenient bundles, and weigh them on a micro-balance of suitable capacity. In this procedure, the group intervals are determined by the spacing of the combs, which must therefore be such as to provide at least ten groups from the sample of material under examination and must extend over at least the length of the longest fibre. For this reason, the Baer Sorter, with its nine combs spaced 5 mm apart, would be unsuitable for cotton. Accuracy depends on the thorough straightening of the fibres as they lie in the comb-bed, and appropriate allowances must be made for the facts that (a) the distal, conterminous ends of the fibres inevitably project a short distance behind the rearmost comb, and (b) it may not be possible, according to the type of gripping tweezers used, to withdraw all the fibres right up to the edge of each comb.

With the Schlumberger Analyser [18], which is designed for the sorting of wool and other long fibre materials, the operations just described are carried out semi-automatically, and a complete test on a wool top can be made in $1\frac{1}{4} - 1\frac{1}{2}$ hours. The fibres are laid in the combs in a crimped condition, however, and results for wool are consequently some 10% too low, though consistently so.

For cotton, which presents the greatest difficulties owing to its shortness, the most accurate method of obtaining the length characteristics directly from a distribution by weight is by the Suter-Webb Comb Sorter [19]. Here, the weight of the test specimen is standardised at 75 ± 2 mg, and a three-stage process of combing is prescribed

which ensures that, in the final tuft to be sorted, all the fibres are as straight as possible, with no displaced or straggling fibres breaking the alignment of the more distant fringe. By using the special tweezers, a long succession of small 'pulls' of fibres is now carefully withdrawn from the forward projecting fringe (combs being dropped out of the way as required) and deposited *separately* on plush-covered boards, each capable of holding about ten pulls. If the successive pulls diminish in length by only very small amounts (which is ensured by the requirement that their number should be in the range of 65–100), and if the depositing of the pulls on the plush is carried out meticulously as specified, then it may be assumed with negligible error that each one consists of straightened fibres, all of the same length. It then becomes a simple matter to measure each pull and assign it to its appropriate length group for weighing. A suitable interval between the length groups is $\frac{1}{8}$ inch (3 mm) and the mid-point of the group range is taken to be its mean. From the weights of the groups and their respective lengths, a reliable distribution by weight is obtained, but it is perhaps desirable to repeat that the 'mean' length and other characteristics of the material are derived from what is, in effect, a length-biased sample.

When the material to be examined is in the form of a random sliver of well-straightened and parallelised fibres as, for example, a wool top or a finisher-drawframe cotton sliver, the early stages of manipulating the sorter are modified [17] so that one may obtain a cut-square sample directly. This is done very simply by cutting the top or sliver, impaling it on the comb-bed with the cut end projecting slightly, and squaring back by the removal of all cut fibres.

Comb sorters cannot, of course, be used for card slivers. Even when the fibres are highly oriented, a certain amount of fibre breakage takes place, a fact that should be borne in mind in contemplating the use of comb sorters in experimental work on fibre breakage in processing or length fractionation in combing.

As already explained in Section 4.3.5, distributions by mass can only be transformed into frequency distributions if, within the sample, the linear density of the fibres is independent of, or bears a known relation to, length. With this in mind, it has been suggested in reference to both wool [20] and cotton [21] that the linear density of each length group can be determined by the method described in Section 3.5 and the transformation thus made possible. It should be pointed out, however, that, in some technical contexts, the proportionate weight of the different length groups is the information that is really required and transformation is unnecessary.

Sometimes, the sole interest lies in the amount of short fibre present in the sample. Comb sorters can be used to yield this information in terms of weight proportions quickly and without the necessity for making fibre arrays. All that is needed is to know the weight of the original sample and the weight of the fibres remaining after those longer than the desired length limit have been withdrawn and discarded.

4.8 The Balls sledge sorter

This ingenious semi-automatic instrument was devised by the first great cotton scientist, W. L. Balls, for use in cotton-breeding field stations where electricity was not available [22]. Since it is now very rarely used and is somewhat complex in design and operation,

it will not be described in detail here¹, but it is worthy of brief mention if only to show how far ahead of his time Balls was in recognising the pitfall of length bias.

The sample to be tested was first made up into the form of a short sliver of parallelised fibres, prepared with the miniature drawbox referred to in Section 2.5.2. This was then fed into the machine, which could be comfortably held in the hand and with which, by suitable manipulation, the following operations were carried out.

- The leading end of the sliver was subjected mechanically to a series of squarings in order to eliminate length bias (see [Section 2.4.1](#)).
- From the squared fringe, a small tuft, similar to that shown in [Fig. 4.13](#) but containing about 500 fibres, was withdrawn and passed slowly downwards through a pair of delivery rollers. Since the leading ends of the fibres in the tuft were aligned, the rotation of the rollers released the fibres in succession according to their length, the shortest first and the longest last.
- Meanwhile, by manually traversing the sorter on its road wheels over a 180 cm (6 foot) long strip of one-way hatter's plush, the fibres were deposited as they were released, each to its appointed place on the plush according to its length. This was repeated for 20 tufts, the deposit at each traverse being superimposed on those preceding it.
- Finally, the elongated deposit on the plush strip was gathered up into bunches representing 3.2 mm (1/8 in.) intervals of fibre length and weighed on a torsion micro-balance.

The sample, then, was a numerical sample, but the result was a mean length determined from mass proportions (see [Section 4.3.5](#)). Results were very consistent, it being rare for differences of as much as 0.8 mm (1/32 in.) between repeat tests to be encountered. The time taken, however, was what would now be regarded as unacceptably long.

4.9 Cutting-and-weighing methods

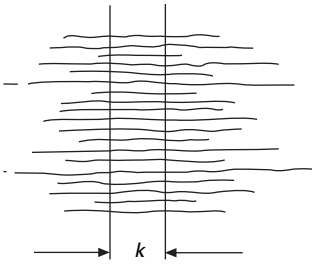
4.9.1 Method 1 (Chandler)

From a representative sample of fibres, a tuft or staple is prepared by repeated drawing and doubling and building it up by successive draws of small quantities, so that the fibres lie straight and parallel and extend approximately equally on either side of the middle of the tuft. The tuft is placed on a surface of fine cork linoleum, or similar material, and clamped across its middle at right angles to the fibres by a metal bar of width k ([Fig. 4.15](#)). The projecting fringes are cut off close to the edges of the bar and their combined mass, expressed as a ratio, r , of the mass of the middle portion, is then determined.

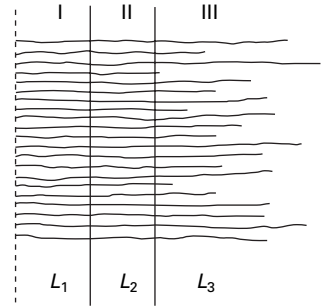
If L = mean fibre length, n = number of fibres in the tuft and c = mean linear density, then the total mass of fibre = Lcn , the mass of the middle portion = kcn , the

mass of the fringes = $cn(L - k)$, and the ratio, $r = \frac{cn(L - k)}{kcn} = \frac{L}{k - 1}$, whence:

¹ A fuller description is given in the first edition of this book.



4.15 Chandler's method.



4.16 Ahmad and Nanjundayya's method.

$$L = k(r + 1) \quad (4.10)$$

It should be noted that in this method a number of assumptions are made: (1) that all fibres are at least as long as k and extend wholly across the middle portion; (2) that they lie straight and free from crimp; (3) that the fibre linear density is the same for all lengths; and (4) that the fibres are not tapered towards either end. Because of this last assumption, the results for cotton are invariably on the low side. Ahmad and Nanjundayya [23] show that for Indian cottons, if k is approximately $l/2$ as recommended by Chandler [24], the results are too low by about 0.1 inch (2.5 mm). Even if, because of (1) above, k is reduced to $\frac{1}{8}$ inch (3.2 mm), the results are still about 5% too low according to Lord [25].

4.9.2 Method 2 (Ahmed and Nanjundaya)

The following method was devised by Ahmad and Nanjundayya [23] with the object of allowing for tapering fibre tips in measurements on cotton.

A representative sample is first made into a sliver by means of a Balls drawbox. This is placed on a set of four combs, and one end is squared-back as required in the squaring method of sampling (see Section 2.4.1). With a Baer-type tweezer, a numerical-sample tuft is withdrawn and combed free of any stray fibres. The tuft is then cut, as indicated in Fig. 4.16, into three sections, of which the lengths L_1 and L_2 are predetermined and can be varied to suit the cotton under examination. Sections I and III are next weighed, which gives masses M_1 and M_3 . L_3 is the mean length of the fibres in section III.

Assuming the fibre linear density in sections I and III to be the same, then $M_1/L_1 = M_3/L_3$, i.e. $L_3 = M_3/M_1 \times L_1$. Hence the mean length of the tuft, L , is given by:

$$\bar{L} = L_1 + L_2 + \left(\frac{L_1 M_3}{M_1} \right) \quad (4.11)$$

The principal assumption, namely that the fibre linear density in section I is the same as that in section III, is justified on the grounds that, since the tuft is drawn from a random sliver, the number of basal and apical ends should be equal in both sections. How far this is true depends to some extent on the dimensions chosen for L_1 and

L_2 . In general, since section I contains a length L_1 of all the fibres in the tuft, the fibre linear density in section I might be expected to be slightly greater than that in section III. Hence $L_1 M_3 / M_1$ will tend to be too small and \bar{L} will be slightly under-estimated.

The other assumption is that all the fibres are at least as long as $L_1 + L_2$. To the extent that fibres terminate within sections I or II, so will \bar{L} be over-estimated. The two errors tend, therefore, to cancel one another, and it is claimed that for Indian cottons the results obtained are not likely to exceed the true value by more than 0.01 inch (0.3 mm).

As regards the dimensions L_1 , L_2 and L_3 , it is recommended that the weight ratio, M_3 / M_1 , should be approximately unity, since otherwise the cut fibres in one section may weigh appreciably more per unit length than those in the other. The middle section should be neither too narrow nor too wide, because in the former case the effect of the tapering ends will be magnified, whereas in the latter it will be diminished.

4.9.3 Method 3 (Muller)

This method, due to Müller [26], can be used only for measurements on slivers, tops, rovings or yarns and gives the mean length of a length-biased sample.

A length of the strand, longer than the length of the longest fibre present, is cut, measured and weighed to determine its linear density C . It is then held near its middle by a suitable clamp, and all loose fibres on one side of the clamp are combed away. The projecting beard that remains is cut off and its mass M determined.

Since the beard is half a Wilkinson tuft, it is evident that, using the symbols n and w as before, we obtain

$$M = \frac{nc\bar{L}'}{2} \quad (4.12)$$

where \bar{L}' is the length-biased mean length. Hence

$$\bar{L}' = \frac{2M}{nw} \quad (4.13)$$

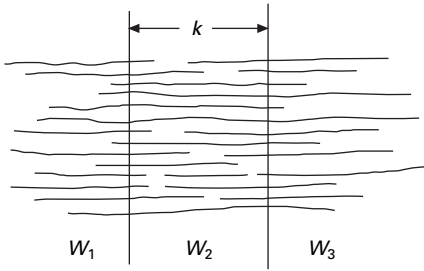
But, assuming uniformity of the strand specimen, $C = nc$. Hence

$$\bar{L}' = \frac{2M}{C} \quad (4.14)$$

Because the fibres in the strand specimen are not stretched out straight, W is over-estimated, and \bar{L}' is given as less than it should be (see Section 4.9.4).

4.9.4 Method 4

This is a refinement of Müller's method and is again applicable only to strands of parallel fibres. Here the strand is held under a clamp of width k , and, after all loose fibres have been combed away on either side, the two projecting fringes are cut off. The combined masses of these, $M_1 + M_3$, and also that of the middle portion, M_2 , are then determined (Fig. 4.17).



4.17 Müller's method.

$$M_1 + M_3 = n \bar{L}' c \quad (4.15a)$$

It follows that

$$\bar{L}' = \frac{M_1 + M_3}{nc} \quad (4.15b)$$

But $M_2 = nkc$; i.e. $nc = M_2/k$. Hence:

$$\bar{L}' = k \frac{M_1 + M_3}{M_2} \quad (4.16)$$

According to Lord [25], the results obtained for cotton are about 10% too low because the fibres in the mid-section are not straight, and, in fact, they agree fairly well with the mean lengths of the corresponding numerical samples. In other words, the error is approximately balanced by the bias in sampling. For cotton, it is recommended that k should be $\frac{1}{2}$ inch (12.7 mm), but for worsted tops Huberty [27] recommends 5 cm.

4.10 Automated scanning of fibre tufts

4.10.1 Automated procedures

The physical sorting of fibres into their various lengths is, in general, tedious and slow. To obtain quicker results, numerous devices have been introduced in which a representative tuft of a standard form is prepared and then scanned from end to end for some property more or less linearly related to number of fibres reaching each position. From results obtained in this way, and with suitable calibration, various length characteristics of the material may be derived.

4.10.2 Thickness scanning

Thickness is one way of determining the amount of material at each position in the tuft, but has now been superseded by other methods described below. In the 1960s, the Uster Stapling Apparatus², designed for the testing of cotton, is the most notable

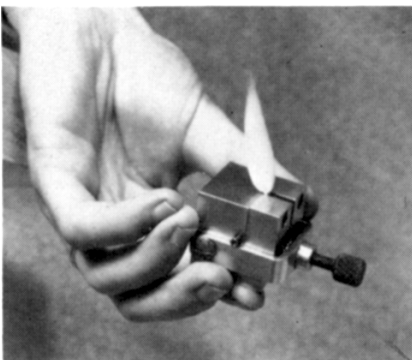
² More details are given in 2nd and 3rd editions of this book.

of the devices that operated on the thickness principle. It consists essentially of three parts: (1) an intersecting comb sorter of the semiautomatic Schlumberger type, by means of which a fringe of fibres having the characteristics of that shown in [Fig. 4.13](#) may be rapidly prepared; (2) a tufting apparatus for converting the flattened fibre fringe into a tuft of the form shown in [Fig. 4.18](#); (3) a dial gauge with which the thickness of the tuft can be measured from end to end.

4.10.3 Capacitance scanning

Suitably prepared fibre fringes or 'draws' may also be scanned by traversing them slowly between the plates of a condenser and recording the changes in its capacity. The latter quantity may be assumed with negligible error to be proportional to the weight of the fibres lying between the electrodes, i.e. $\text{length} \times \text{linear density} \times \text{number of fibres}$. Therefore, if the mean linear density of the fibres can be assumed constant over all parts of the draw, and if the fibres lie straight and normal to the width of the condenser, then successive readings of capacity lead directly to a cumulative-frequency distribution based on a numerical sample. From this, the various parameters of length may be calculated. The method is particularly useful for measuring fibre length in combed slivers or rovings of wool and other fibres of similar length. The fringe to be examined is of the type illustrated in [Fig. 4.13](#) and is obtained from the top or sliver by the squaring technique, essentially as described in [Section 2.4.1](#).

The Almeter was introduced in the 1960s [28–30], but has since been additionally automated and linked to a computer. An end-aligned sample is produced by a comb device built on the lines of the Schlumberger Analyser (see [Section 4.7.2](#)) and is fed at constant speed through the plates of a condenser. The signal is processed by a computer to show a cumulative length diagram and values of hauteur and barbe, their coefficients of variation, percentages of fibres longer or shorter than given lengths and length exceeded by a given percentage of fibres, both of the latter biased by cross-section or weight. Twisting of slivers is necessary to obtain accurate results.

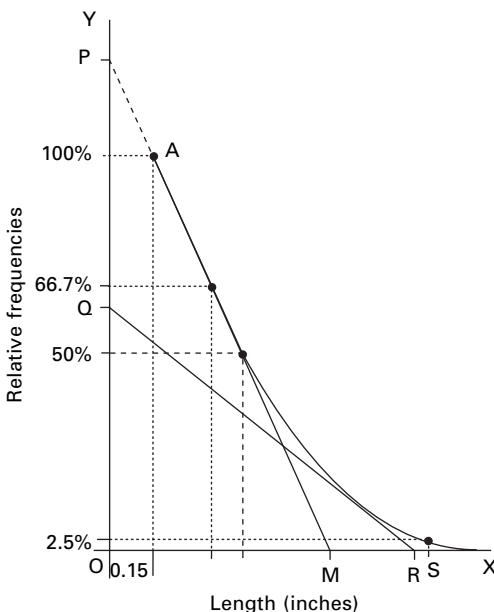


4.18 Uster clamping block with fibre tuft.

4.10.4 Photo-electric scanning

Photo-electric scanning was first developed in the early days of electronics by Hertel in 1940 for the testing of lint cotton [4]. Developments of his method are still the main way of testing cotton lengths. The basic principle is that carefully prepared fringes of cotton are passed through photo-electric scanning, in which the reduction in signal depends on the number of fibres in the cross-section. Current instrumentation for HVI testing of cotton uses automatic preparation and feeding of fringes through photo-electric sensing, with the signal passed to a computer for analysis. The principles of the method can be explained by reference to Hertel's original Fibrograph test.

The sample to be examined is presented for scanning in the form of a pair of fibre fringes, the composition of which is intended to be closely similar to that indicated by the beard diagram in Fig. 4.9. In manual testing, the preparation of the fringes is all-important for consistency of results and inter-laboratory agreement [31], and the makers put considerable stress on the need for a careful following of instructions, repeated checks and the exercise of judgement based on experience. In its original form, the Fibrograph made provision for the changes in the photo-electric current to be recorded graphically by hand against the distance of the slit from the roots of the fringes. The resulting graph, called a Fibrogram (Fig. 4.19), thus shows by an indirect measure the number of fibres surviving in the fringes as they are traversed from root to tip. However, because of the thickness of the lens at the light source, scanning cannot be carried out right at the very roots of the fringes and must start a short distance away. The instrument is consequently insensitive to the presence of very short fibres, and in practice the Fibrogram has its origin at a point representing a length of 0.15 inch (3.8 mm).



4.19 Fibrogram diagram (1 inch = 25.4 mm).

The Fibrogram may be analysed graphically to yield various length parameters of interest to the producers and users of cotton [4]. The tangent to the curve at its starting point A cuts OY at P and OX at M. Then OM is the mean length of the fibres in the original population longer than 0.15 inch (3.8 mm). If OP is bisected at Q and the tangent to the curve from Q cuts OX at R, then OR is the upper-half mean length, UHM (see [Section 4.3.6](#)), and the ratio of OM to OR is a valid index of uniformity.

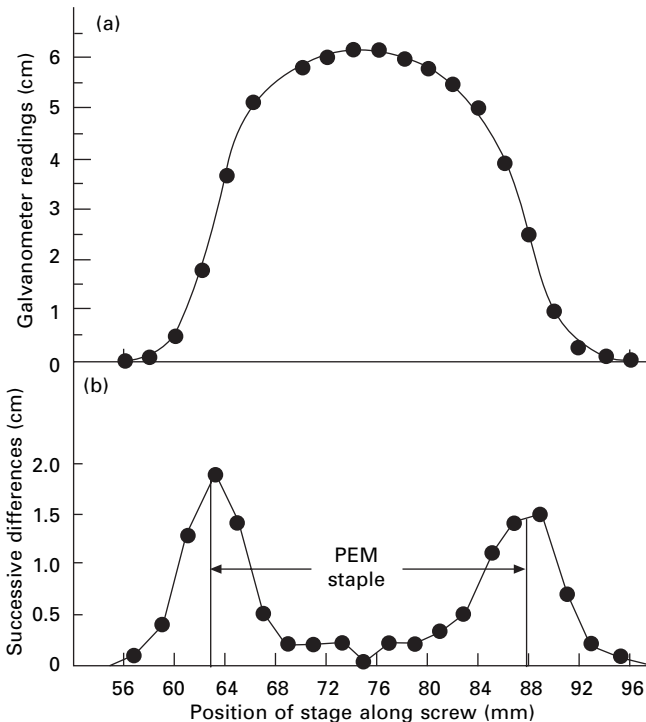
Another significant quantity introduced by Hertel is the ‘span length’. As noted in [Section 4.3.4](#), the fibre beard represented by the Fibrogram shows the distribution of fibre lengths that would project on one side of the nip of a pair of drafting rollers. The curve can therefore be used to determine the span or setting between successive pairs of drafting rollers to avoid more than any given proportion of the fibres being clamped in both pairs of rollers simultaneously. A span length found useful in this connection is the 2.5% span length, i.e. the length that is exceeded by only 2.5% of the beard fibres scanned by the instrument. This is shown by OS in [Fig. 4.19](#).

The curve itself is the locus of the various span lengths (abscissae) for the beard scanned, and in computerised versions of the Fibrograph the span lengths are automatically recorded on digital counters throughout the scanning operation. From the span lengths read off at suitably chosen intervals, the curve can be constructed if desired and the mean, UHM, and other quantities determined graphically. Alternatively, it may be considered that the sample is sufficiently characterised by the span lengths at, say, 66.7, 50 and 2.5%, in which case tests may be made extremely rapidly, several in a minute. With the original Fibrograph, the time required to make a complete test, including preparation of the fringes and analysis of the Fibrogram, is about 10 minutes. In the automated HVI tests, the analysis is computerised and testing is rapid.

The following are possible sources of error:

- The analysis of the Fibrogram is based on the assumption that, in the fringes prepared in the manner described, all points along the length of each fibre have an equal chance of coinciding with the line of the comb teeth. This is not strictly true because the frictional drag of combing tends to displace the fibres outwards somewhat and so leads to an over-estimate of length.
- The fibres in the fringe are assumed to be straight, whereas in fact they are crimped, and length is therefore likely to be under-estimated. This is a source of error held in common with most other methods.
- The tapering of the fibre ends also leads to some under-estimation of fibre length.
- So also does fibre breakage incurred in the preparation of the sample, which must, of course, at all times be minimised, perhaps especially if any mechanical aid to expedite the operation is used.
- Because of personal errors in the drawing of the tangent PM, the estimate of the mean length, OM, is not too reliable, though the UHM length is comparatively little affected. So far as this latter quantity is concerned, it has been found that, for cottons of staple length up to about $\frac{1}{8}$ inch (29 mm), the result given by the Fibrograph is correct to within $\frac{1}{32}$ inch (0.8 mm) but that above that length accuracy falls off considerably [25].

Another early photo-electric tester was the Shirley PEM Stapler [32]. This scanned a hand-prepared tuft, similar to those shown in Fig. 4.10. The measured boundaries are taken to lie where the visual density shows the greatest rate of change³. Consequently, the test gave only one statistic of length, namely, the modal length. It did this very rapidly (as regarded in the 1940s), and the quantity so measured agreed very closely with the standard American staple lengths from $\frac{3}{4}$ to $\frac{15}{16}$ inch (19 to 33 mm). The difficulty with hand-stapling lies in the fact that the boundaries of the tuft or staple are ill defined: over a large part of the middle, the visual density of the fibres is fairly uniform, but near the extremities it falls off until the tips of the longest fibres are reached. The light reflected from the surface was focused on a photo-cell, and the current generated was measured with a sensitive galvanometer. In this way, determinations of visual density were made at equal intervals along the length of the tuft, and, when these were plotted, a graph such as that shown in Fig. 4.20(a) was obtained. If, then, the differences between successive readings were plotted, a graph such as (b) was obtained, which indicated by its peaks the positions where the greatest rates of change occurred. These peaks located the boundaries of the tuft, and the distance separating these boundaries corresponded to the modal length of fibres as they lay in the tuft.



4.20 PEM test.

³ This is evidently also true of the subjective judgement of the hand stapler.

4.11 Scanning individual fibres

4.11.1 Advanced fibre information system

The Uster Advanced Fibre Information System (AFIS), which was described for fineness testing in Section 3.7.3, also provides data on fibre lengths. A fibre individualiser unit opens the sample, typically 0.5 gram, separates individual fibres and transfers them to an air-stream. As each fibre is carried past the photo-electric sensor, its presence is detected. Hence the length of each fibre can be recorded. Computer software analyses the data and provides numerical and mass-biased length distributions, short fibre content, upper quartile length, 5.0% length and coefficients of variation.

Cui *et al.* [33] compare measurements of length by AFIS with those by Spinlab HVI and Suter-Webb array (Table 4.3). Values of mean length are reasonably consistent, but there are appreciable differences in short fibre content. Accuracy of prediction may be affected by natural fibre length variation in sampling, number of fibres in each test, number of repeats and accuracy of the length measurement. A major factor is the length calibration level for short fibres. A shift of 0.01 inch (0.25 mm) would change the short fibre content percentage by about 0.4%. There is high variability in the short fibre contents, so that sample non-uniformity is another source of differences. There is reasonable correlation between the different methods, so that users of a given method can assess the relative incidence of short fibres in different consignments of cotton.

4.11.2 Digital imaging

The application of digital imaging, which is the technology of the 21st century, to length testing is a severe challenge. Whereas snippets can be used for diameter measurement, whole fibres must be presented for length measurements.

The OFDA 4000 [34] prepares wool on a moving needle bed to form an end-aligned beard of fibres, like that in Fig. 4.16. A moving gripper transports the beard along a guide past a digital video-microscope in 5 mm steps. At each step, a digital image across the beard is recorded and the sequence is continued until the longest fibre has been scanned. The images are processed to count the number of fibres in the cross-section and their diameters are saved on the computer. A minimum number of fibres, typically 4000, are included in the count. The OFDA software analyses the data to provide distributions of fibre length and compute values of hauteur and barbe.

Table 4.3 Fibre length measurements for 45 cottons by three methods. From Cui *et al.* [33]

	Mean length (inches*)			Short fibre content (%)		
	Array	AFIS	HVI	array	AFIS	HVI
Average	0.92	0.96	0.89	11.41	7.41	9.56
Minimum	0.66	0.73	0.72	6.48	3.50	5.50
Maximum	1.13	1.19	1.13	26.13	17.40	23.20

* 1 inch = 25.4 mm.

As described in Section 3.7.1, the data are also processed for diameter and curvature. A draft test method for diameter and length measurements by OFDA4000 has been reported by Carroll [35].

4.12 References

1. TTS No. 18. *J. Text. Inst.*, 1950, **41**, S1.
2. H. R. Mauersberger (Editor). '*Matthews' Textile Fibers*, Wiley, New York, 6th edition, 1954, p. 841.
3. G. G. Clegg. *J. Text. Inst.*, 1932, **23**, T35.
4. K. L. Hertel. *Text. Res.*, 1940, **10**, 510.
5. E. Honegger. *J. Text. Inst.*, 1951, **42**, P57.
6. M. J. Denton and P. N. Daniels (Editors). *Textile Terms and Definitions*, 11th edition, The Textile Institute, Manchester, 2002, p. 130.
7. W. S. Simpson. In *Wool: Science and Technology*, W. S. Simpson and G. H. Crawshaw (Editors), Woodhead Publishing, Cambridge, 2002, p. 1.
8. E. R. Goshawk. Private communication.
9. E. Lord. *J. Text. Inst.*, 1942, **33**, T205.
10. J. W. S. Hearle. L. Hollick and D. K. Wilson. *Yarn Texturing Technology*, Woodhead Publishing, Cambridge, 2001.
11. S. L. Anderson and R. C. Palmer. *J. Text. Inst.*, 1953, **44**, T95.
12. J. H. Wakelin, H. W. Lambert and D. J. Montgomery. *Text. Res. J.*, 1956, **46**, 665.
13. *Wool Research*, Vol. 3, Testing and Control, WIRA, Leeds, 1955, p. 41.
14. *Wool Sci. Rev.*, 1952, No. 9, 23.
15. BS Handbook No. 11, *Methods of Test for Textiles*, 3rd edition, 1963, p. 33.
16. G. G. Clegg. *J. Text. Inst.*, 1932, **23**, T35.
17. *Wool Sci. Rev.*, 1952, No. 9, 24.
18. *Wool Sci. Rev.*, 1952, No. 9, 25.
19. R. W. Webb. *Proc. ASTM*, 1932, **32**, Part II, 764.
20. R. Maillard and O. Roehrich. *Proc. IWTO Tech. Comm.*, 1947, p. 35.
21. H. Richardson, B. Bailey and O. M. Conrad. *US Dept. Agr. Tech. Bull.*, No. 545, 1937.
22. W. L. Balls. *A Method of Measuring the Length of Cotton Fibres*, Macmillan, London, 1921.
23. N. Ahmad and C. Nanjundayya. *J. Text. Inst.*, 1936, **27**, T253.
24. E. E. Chandler. *Text. Rec.*, 1926, **44**, Nov., 40.
25. E. Lord, Lecture, Manchester College of Science and Technology, 1954.
26. E. Müller. *Zeitsch. des Vereins Deut. Ing.* 1894, S. 997.
27. A. Huberty. *J. Text. Inst.*, 1952, **43**, P153.
28. *Wool Sci. Rev.*, 1965, No. 28, 22.
29. J. Grignet. *Ann. Sci. Text. Belges*, 1962, No. 3, 70.
30. F. Monfort. *Ann. Sci. Text. Belges.*, 1964, No. 1, 35.
31. K. L. Hertel and R. Lawson. *Text. Res. J.*, 1964, **34**, 866.
32. E. Lord. *J. Text. Inst.*, 1946, **37**, T237.
33. X. Cui, T. A. Calamari, K. Q. Robert and J. B. Price. *Textile Res. J.*, 2003, **73**, 891.
34. M. Brims, IWTO Barcelona Meeting, May 2002, Report No: SG 02.
35. D. R. Carroll, IWTO Sliver Group, Biella Meeting, November 2005, submission No: SG 02.

5.1 Introduction

Fibre density plays a direct part in affecting the weight of fabrics, so that glass fabrics, with a fibre density of 2.56 g/cm^3 , will tend to be heavy, whereas those of polyethylene, with a density of 0.92 g/cm^3 , will be light. It is also a useful parameter in fibre identification and occurs incidentally in many parts of textile physics.

The definitions are straightforward: density is the mass of unit volume and is usually expressed in grams per cubic centimetre (g/cm^3)¹. For some purposes, it is more convenient to use specific volume, which is the reciprocal of density and is expressed in cubic centimetres per gram (cm^3/g).

5.2 Measurement

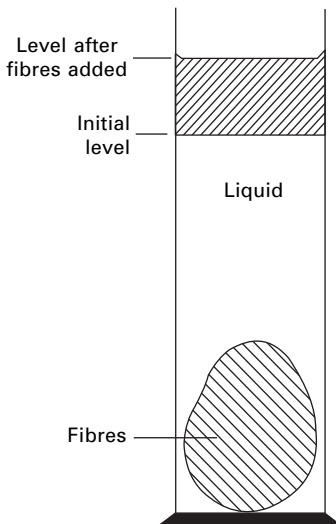
The mass of a specimen is easily determined by weighing it on a balance, but the determination of volume involves difficulties of definition and experimental problems. Any mass of fibres, whether disorganised raw material or organised into yarn or fabric, includes a large proportion of air as well as the fibres. Consequently, measurement of its overall volume gives no information on fibre volume. There is an additional complication with hollow fibres.

All measurements of volume, or of density directly, therefore depend on immersing the material in a fluid that will displace all the air from around the fibres. The simplest form of this method is shown in [Fig. 5.1](#). The displacement of the level of liquid in a measuring cylinder equals the volume of the added fibres.

Two fundamental sources of error are immediately obvious. Firstly, the liquid may not displace all the air, particularly from crevices in the fibre surface. This means that the measured volume will be too high and the density too low. Secondly, the liquid may be absorbed by the fibres, which results in a smaller displacement of the liquid level. This would give too low a volume and too high a density.

It is now generally accepted that the best values of density are obtained with a large number of organic liquids (such as nitrobenzene, olive oil, toluene, benzene and

¹The consistent SI unit is kg/m^3 ; $1 \text{ g/cm}^3 = 10^3 \text{ kg/m}^3$ (i.e. 1 tonne per cubic metre).



5.1 Fibre volume by displacement of liquid.

carbon tetrachloride), which give the same results. Hermans [1] has put forward the arguments in favour of this and pointed out that it is extremely unlikely that the same values would be obtained if errors were involved. He has confirmed that these liquids do not penetrate into the fibre material but do envelop the fibre and fill any lumens or other true pores in native fibres. The earlier preference of Davidson [2] for the higher value of density obtained on immersion in helium was rejected, partly because of the evidence in favour of other values, but also because there was some evidence that helium was absorbed by the cellulose.

The experimental method indicated above, although sound in principle, would not be very accurate in practice. Some of the other standard methods, such as the use of a density bottle, or weighing a specimen immersed in a liquid, need a fairly large mass of material, from which it is difficult to exclude air completely. For single fibres, or small bundles of fibres, flotation methods are preferred. For example, Abbott and Goodings [3] found that, if chopped-up fibres were placed in a liquid (or a mixture of liquids) of the same density as the fibres, and then centrifuged in a tube, they remained as a uniform cloud; if the densities were different, they accumulated into a single group, which floated if the fibre density was the lower and sank if it was the greater. By a process of trial and error, the correct density can be found.

A more rapid adaptation of this method is the density gradient tube. This is a long tube containing a heavy liquid (e.g. pentachlorethane, 1.7 g/cm^3) at the bottom, a light liquid (e.g. xylol, 0.9 g/cm^3) at the top, and a continuously varying mixture of the two between them. If fibres are dropped in, they sink to the point at which the fibre density equals the liquid density and remain suspended there. Calibration of the tube may be provided either by means of pieces of different materials of known densities floating at their appropriate levels or by hollow glass spheres of varying mean density. The fibre density can be found by interpolation between the known densities on either side of the position at which the fibres come to rest. Methods of

setting up density gradient tubes and precautions to be adopted in their use are described by Preston and Nimkar [4], Stock and Scofield [5] and Austin and Roberts [6].

De Vries and Weijland [7] have described a method of measuring density by weighing fibres on a cantilever microbalance, first in air and then submerged in a suitable liquid. Neelakantan and Patel [8] have described improvements on the displacement and flotation methods.

5.3 Results

Typical values of the densities and specific volumes of fibres used in general textiles, dry and at 65% r.h., are given in Table 5.1. It will be seen that most of these fibres have a density slightly greater than that of water. Table 5.2 gives densities of some high-modulus fibres, used in composites and specialist applications, and Table 5.3 gives densities of some chemically and thermally resistant fibres. Some fibres, such as cotton and to a much greater extent kapok, do contain internal void spaces, which will lower the overall density to a value of about 1.35 g/cm^3 in cotton.

The density of fibres varies when they absorb water, as is shown in Fig. 5.2. The increase in density on the addition of water, which has a density less than that of the fibres, means that there is a net contraction. The reasons for this are discussed later in connection with the swelling of fibres (see Section 12.1.6).

5.4 Density and order

Density measurement is commonly used as a means of estimating the degree of order, or crystallinity, of fibres. The necessary relation was given earlier as equation (1.3):

Table 5.1 Densities of some general-purpose textile fibres [4, 9–11]

Fibre	Density (g/cm^3 , Mg/m^3)		Specific volume (cm^3/g)	
	dry	65% r.h.	dry	65% r.h.
Cotton (lumen filled)	1.55	1.52	0.64	0.66
Viscose rayon	1.52	1.49	0.66	0.67
Secondary acetate, triacetate	1.31	1.32	0.76	0.76
Wool	1.30	1.31	0.77	0.76
Silk	1.34	1.34	0.75	0.75
Regenerated protein (casein)	1.30	1.30	0.77	0.77
Alginate		1.75		0.57
Nylon 6.6, nylon 6	1.14	1.14	0.88	0.88
Polyester (PET)	1.39	1.39	0.72	0.72
Acrylic (PAN)	1.19	1.19	0.84	0.84
Polyethylene (high density)	0.95	0.95	1.05	1.05
Polypropylene	0.91	0.91	1.09	1.09
Modacrylic (<i>Dynel</i>)	1.29	1.29	0.78	0.78
Modacrylic (<i>Teklan</i>)		1.34		0.75
Polyvinyl chloride (PVC)		1.40		0.71
Polylactic acid (PLA)		1.25		0.80
Glass	2.5	2.5	0.40	0.40

Table 5.2 Densities of some high-modulus fibres [12]

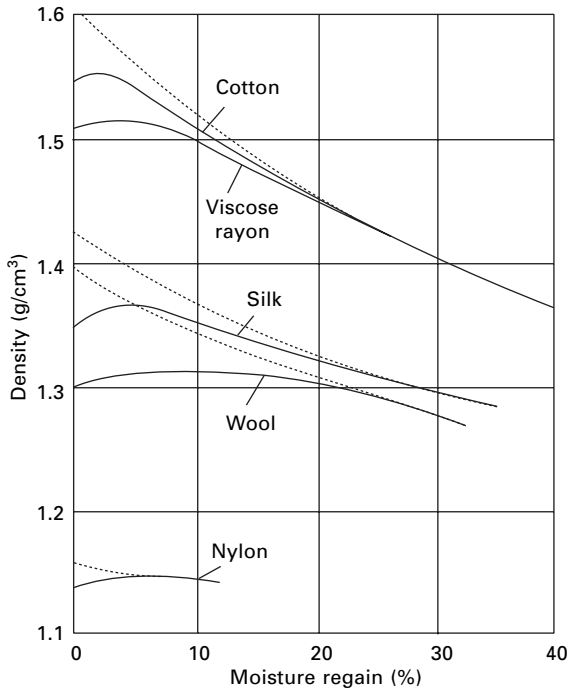
Fibre	Density (g/cm ³ , Mg/m ³)	Specific volume (cm ³ /g)
Para-aramid (<i>Kevlar</i> , <i>Twaron</i>)	1.44	0.69
Aramid (<i>Technora</i>)	1.39	0.72
High-modulus polyethylene (HMPE)	0.97	1.03
LCP fibre (<i>Vectran</i>)	1.40	0.71
PBO (<i>Zylon</i>)	1.56	0.64
PIPD (<i>M5</i>)	1.70	0.59
Carbon	1.8–2.0	0.56–0.55
Silicon carbide based	2.4–2.75	0.42–0.36
Silicon carbide near stoichiometric	3.0	0.33
Alumina	3.6–3.9	0.28–0.26
Alumina/silica	2.7–3.4	0.37–0.29
Alumina/zirconia	4.1	0.24
Steel	7.85	0.13

Table 5.3 Densities of some chemically and thermally resistant fibres [12]

Fibre	Density (g/cm ³ , Mg/m ³)	Specific volume (cm ³ /g)
Polyvinylidene chloride (PVDC)	1.60	0.63
Polytetrafluorethylene (PTFE)	2.2	0.45
Polyetheretherketone (PEEK)	1.30	0.77
Polyphenylene sulphide (PPS)	1.37	0.73
Meta-aramid (<i>Nomex</i>)	1.46	0.68
Melamine-formaldehyde (<i>Basofil</i>)	1.4	0.71
Novoloid, phenol-aldehyde (<i>Kynol</i>)	1.27	0.79
Polyimide (<i>P84</i>)	1.41	0.71
Polyamide-imide (<i>Kermel</i>)	1.34	0.75
Polybenzimidazole (PBI)	1.43	0.70
Semi-carbon (oxidised acrylic)	1.35–1.4	0.74–0.71

$$\text{degree of order} = \frac{\rho - \rho_{\text{am}}}{\rho_{\text{cr}} - \rho_{\text{am}}} \quad (5.1)$$

The fibre density, ρ , is measured by the methods described above. The crystal density, ρ_{cr} , can be calculated from the dimensions of the unit cell, determined from the X-ray-diffraction pattern, and the molecular weight. Difficulty arises in the estimation of the amorphous density, ρ_{am} . In some instances, the material can be obtained in the amorphous state, for example, by the rapid quenching of undrawn polyester fibres. In other cases, the value must be obtained by extrapolation or by estimation from analogous compounds or the contribution of the constituent groups [18].



5.2 Variation of density with moisture regain for cotton [13], viscose rayon [14], silk [15], wool [16] and nylon [17].

5.5 References

1. P. H. Hermans. *Physics and Chemistry of Cellulose Fibres*, Elsevier, Amsterdam, Netherlands, 1949, pp. 197 *et seq.*
2. G. F. Davidson. *J. Text. Inst.*, 1927, **18**, T175.
3. N. J. Abbott and A. C. Goodings. *J. Text. Inst.*, 1949, **40**, T232.
4. J. M. Preston and M. V. Nimkar. *J. Text. Inst.*, 1950, **41**, T446.
5. C. R. Stock and E. R. Scofield. *Text. Res. J.*, 1951, **21**, 521.
6. J. C. Austin and J. S. Roberts. *Text. Res. J.*, 1956, **26**, 303.
7. H. de Vries and H. G. Weijland, *Text. Res. J.*, 1958, **28**, 183.
8. P. Neelakantan and N. C. Patel. *J. Text. Inst.*, 1967, **58**, 137.
9. J. F. Ford. *Fibre Data Summaries*, Shirley Institute, Manchester, 1966.
10. W. J. Roff and J. R. Scott. *Fibres, Films, Plastics, and Rubbers*, Butterworths, London, 1971.
11. R. S. Blackburn. In *Biodegradable and Sustainable Fibres*, R. S. Blackburn (Editor), Woodhead Publishing, Cambridge, p. 191.
12. J. W. S. Hearle (Editor). *High-performance Fibres*, Woodhead Publishing, Cambridge, 2001.
13. G. F. Davidson. Quoted by F. T. Peirce and E. Lord. *J. Text. Inst.*, 1939, **30**, T173.
14. P. H. Hermans. *Contributions to the Physics and Chemistry of Cellulose Fibres*, Elsevier, Amsterdam, Netherlands, 1946, p. 75.
15. A. C. Goodings and L. H. Turl. *J. Text. Inst.*, 1940, **31**, T69.
16. F. L. Warburton. *J. Text. Inst.*, 1947, **38**, T65.
17. J. B. Speakman and A. K. Saville. *J. Text. Inst.*, 1946, **37**, P271.
18. D. W. van Krevelen. *Properties of Polymers: Correlations with Chemical Structure*, Elsevier, Amsterdam, Netherlands, 1972.

6.1 Introduction

This chapter deals with basic thermal properties of fibres. Thermal transitions and the associated changes in structure and properties are covered in [Chapter 18](#), which includes an account of heat setting of fibres. For simple solid materials, the thermal properties consist of the thermal conductivity, specific heat and its variation with temperature, the coefficient of thermal expansion, the melting point, and the latent heat of melting. In fibres, many of these properties have not been studied in great detail because the relevant practical effects are influenced much more by other factors. The thermal conductivity of a textile fabric depends to a much greater extent on the air entrapped within it than on the fibre conductivity. Dimensional changes in fabrics due to reversible swelling on moisture absorption are much larger than those due to reversible thermal expansion. For moisture-absorbing fibres, the heat of absorption resulting from changes in moisture regain, rather than the thermal capacity, contributes the largest share of the uptake or loss of heat by a textile material when the ambient conditions change.

6.2 Thermal parameters

6.2.1 Specific heat of fibres

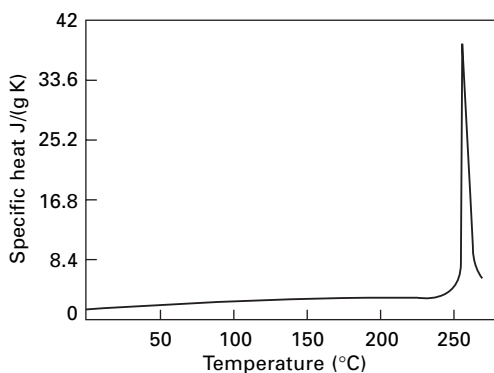
Various workers have measured the specific heat of dry fibres at room temperature, and some typical values are given in [Table 6.1](#).

Dole and his associates [3–8] have measured the variation of specific heats of several polymers with temperature, in a search for transition effects in the structure. [Figure 6.1](#) shows results for nylon. The high values of specific heat found at about 260 °C are due to the melting of the nylon. Since this is spread over a range of temperature, the heat does not appear as a latent heat of fusion at a single temperature but contributes to the heat change over the whole melting range. By integration of the area under the peak, values of latent heat of fusion of about 150 J/g are found, though the values vary with the history of the fibre. This gives rise to high values of the apparent specific heat. Some evidence was also found of a small latent heat associated with a change in structure at about 165 °C.

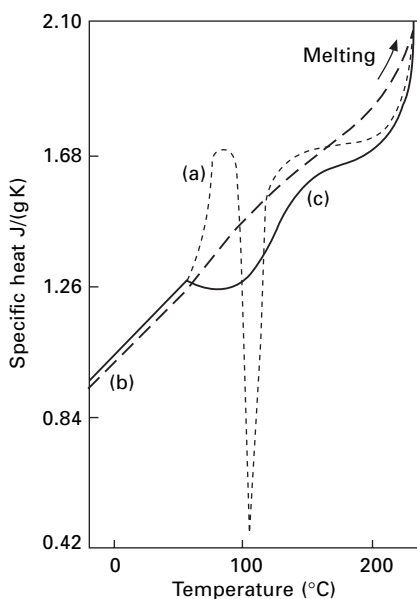
[Figure 6.2](#) shows some results for polyethylene terephthalate (*Dacron*) in various forms. The sharp rise at about 70 °C is associated with a second-order transition in

Table 6.1 Specific heat of dry fibres

Fibre	Specific heat J/(g K)
Cotton [1]	1.22–1.35
Rayon [1]	1.35–1.59
Wool [2]	1.36
Silk [2]	1.38
Nylon 6 [3]	1.43
Nylon 6.6 [1]	1.46
Polyester (PET) [1]	1.03
Asbestos [2]	1.05
Glass [2]	0.80



6.1 Specific heat of drawn nylon filament [4].



6.2 Specific heat of *Dacron* polyester [5]: (a) undrawn; (b) annealed undrawn; (c) commercially drawn fibres.

the structure, and the minimum at about 100 °C with increasing crystallisation, resulting in an evolution of heat. Both of these effects can be eliminated by annealing the fibres. A maximum, occurring at about 250 °C, is associated with melting accompanied by the absorption of the latent heat of fusion.

Teflon (polytetrafluoroethylene) is interesting, since there are two first-order transitions, with latent heats estimated to be 8.4 and 1.7 J/g, at 20 and 28 °C, respectively. This means that the specific heat apparently rises to very high values near room temperature, as is shown in Fig. 6.3. The transition at 20 °C is believed to be due to a change from a fully crystalline form with three-dimensional order to a structure with a lower degree of order [9].

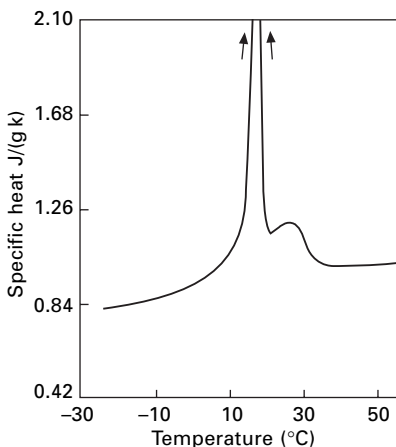
The absorption of water, which as a liquid has a specific heat of 4.2 J/(g K), would be expected to increase the specific heat of fibres. For changes in temperature at constant regain, a simple mixture law would give the relation:

$$\text{mixture specific heat} = C' = \frac{C_0 + 4.2r}{1 + r} \quad (6.1)$$

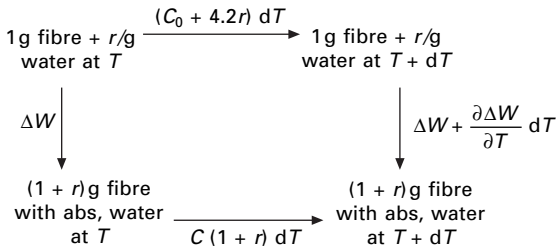
where C_0 = specific heat when dry and r = fractional regain.

Changes at constant relative humidity will, as discussed in [Chapter 8](#), have a very much larger effective specific heat because of the contribution from the heat of sorption associated with the regain changes.

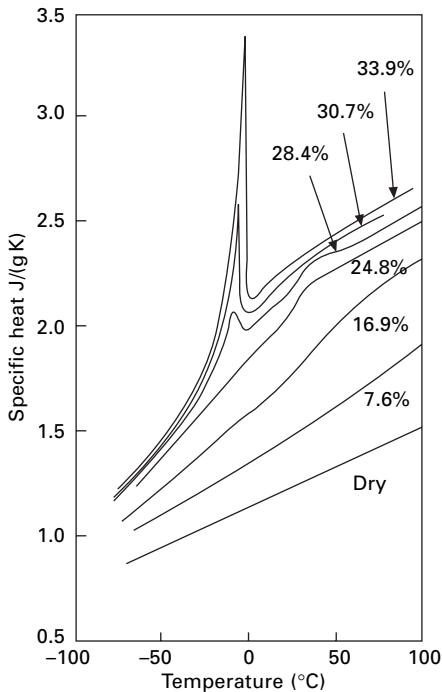
Even at constant regain, however, equation (6.1) will not predict actual specific heats, for two reasons. Firstly, the absorbed water may not be behaving like liquid water: it may be more like ice with a specific heat of about 2 J/(g K). Secondly, the absorption of water, which loosens up the fibre structure, may change the effective specific heat of the polymer molecules. A correction term, ΔC , will therefore be added to C' to give the actual specific heat, C . The term ΔC can be related to changes in the heat of wetting with temperature. If ΔW is the difference between the heat of wetting from zero regain and the heat of wetting from regain r , it follows from the First Law of Thermodynamics that the changes in heat along either of the two alternative routes shown in [Fig. 6.4](#) must be the same. Hence:



6.3 Specific heat of PTFE (Teflon) near room temperature [8].



6.4 Alternative routes for moisture absorption and temperature change.



6.5 Variation of specific heat of wool with regain. From Haly and Snaith [11].

$$\Delta W + C(1 + r) dT = (C_0 + 4.2r) dT + \Delta W + (\partial \Delta W / \partial T) dT \quad (6.2)$$

from which:

$$C = \frac{C_0 + 4.2r}{1 + r} + \frac{\partial \Delta W / \partial T}{1 + r} \quad (6.3)$$

Hearmon and Burcham [10] found agreement, within the limits of experimental error, between values of ΔC and $(\partial \Delta W / \partial T) / (1 + r)$ for wood cellulose. The values of the ΔC term ranged from about 0.1 J/(g K) at medium regains and room temperature to 0.4 J/(g K) at high regains and 60 °C, so that the correction is small but appreciable.

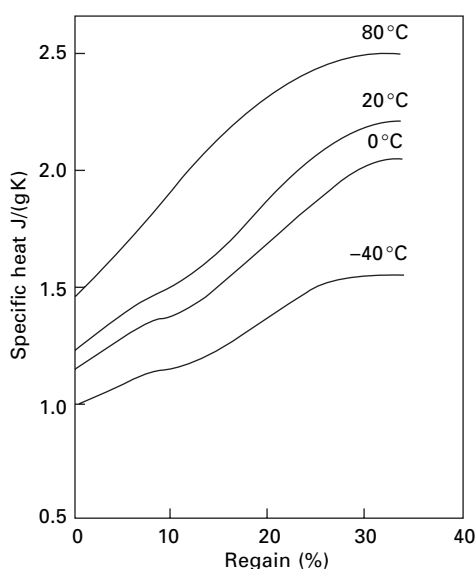
Figure 6.5 shows how the specific heat of wool varied with moisture regain in some studies by Haly and Snaith [11], using an adiabatic calorimeter. Examples of

particular plots of variation of specific heat with temperature are shown in Fig. 6.6. Very careful experimental work is needed, and various corrections have to be applied: for example, in addition to the usual need to minimise energy losses, a correction is required for the influence of evaporation into the small void space in the sample container. On the first heating, a small dip in the curve was often found at about 50 °C: this is probably due to the release of elastic energy set in the fibres during its compression into the container.

The specific heats generally show a linear variation with temperature, with a higher slope at higher regains. However, in the samples at all regains above zero, there is a definite upturn at about 50 °C: it becomes more pronounced at higher regains and may be a latent heat from a small, diffuse, first-order transition.

A much more distinct peak appears at low temperatures at regains greater than 25%. At a regain of 34%, this effect is large and sharp and has its peak just below 0 °C: it is obviously associated with a change in loosely held water from an ice-like to a liquid-like form. The latent heat of fusion of this transition is 200 J/g of water at 34% regain. At lower regains, the peak is less marked, and its maximum occurs at lower temperatures. In all cases, the rise to the peak starts at -30 °C, which indicates that this is the temperature at which the first absorbed water to be involved in the effect goes through the transition: the further absorbed water will have an effect at successively higher temperatures.

These results for wool are of interest not only in themselves, but also as being indicative of effects that may occur in other fibres.



6.6 Individual plots of variation of specific heat of wool samples with regain at various temperatures. From Haly and Snaith [11].

6.2.2 Thermal conductivity

Until the 1980s, there are no records of direct measurement of the thermal conductivity of fibres. However, an estimate of relative values can be obtained by comparing the results of measurements of thermal conductivity of pads of different fibres packed to the same density [12, 13]. Some values are given in Table 6.2. The protein fibres have a lower conductivity than the cellulosic fibres. Experiments can also be made with materials in the solid form. Figure 6.7 shows the variation of thermal conductivity of horn, which is a similar material to wool, with regain, and Table 6.3 gives values for the thermal conductivity of some solid polymers.

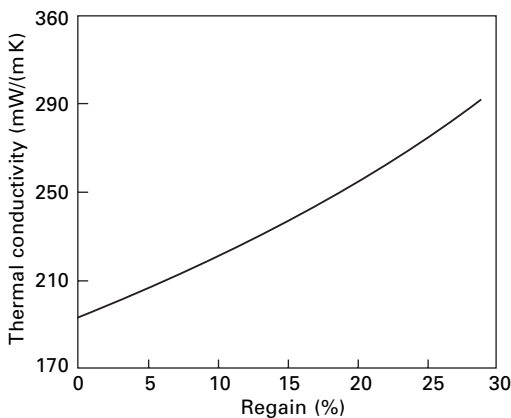
Table 6.2 Thermal conductivity of pads of fibres with a bulk density of 0.5 g/cm^3 [12, 13]

Fibre	Thermal conductivity (mW/(m K))
Cotton	71
Wool	54
Silk	50

Note: Still air has a thermal conductivity of 25 mW/(m K)

Table 6.3 Thermal conductivity of polymers [1, 12]

	Thermal conductivity (mW/(m K))
Cellulose acetate	230
Nylon	250
Polyester (PET)	140
Polyethylene	340
Polypropylene	120
Polyvinyl chloride (PVC)	160



6.7 Variation of thermal conductivity of horn with moisture regain [12].

Kawabata [14, 15] has measured the longitudinal conductivity of fibres, using the apparatus shown in Fig. 6.8(a). About 10 000 fibres are clamped at 20 mm width with 3 mm between the clamps. Since the heat flow is very small, about 20 mW, great care has to be taken to avoid errors. The conductivity K_L is given by:

$$K_L = \frac{qL}{A\Delta T} \quad (6.4)$$

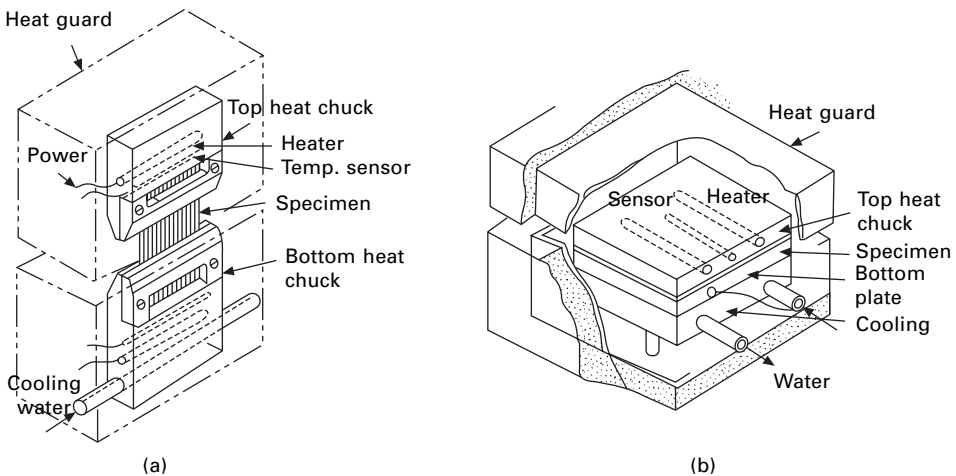
where q = heat flow rate, L = specimen length, A = total area of fibre cross-sections and ΔT = temperature difference between ends.

In order to determine the anisotropy of thermal conductivity, Kawabata used a composite film of aligned fibres with an epoxy matrix at a fibre volume fraction of about 80%. An area of film, $50 \times 50 \text{ mm}^2$ and between 0.5 and 1 mm in thickness, was clamped between plates as shown in Fig. 6.8(b). The transverse conductivity K_T was calculated from a series mixture law, though this is not strictly valid for an assembly of cylinders in matrix. Owing to the high volume content, the error may be small.

$$K_T = \frac{qV_F}{[A\Delta T/L] - \left[\frac{q(1 - V_R)}{K_R} \right]} \quad (6.5)$$

where V_F = fibre volume fraction and K_R = thermal conductivity of resin.

Table 6.4 shows the measured thermal conductivities. The high values for carbon fibres reflect the continuous ring structure and for aramids the close sequence of benzene rings. The values for the different aramid and carbon fibres shows the importance of molecular arrangement and orientation, which would also account for the differences between filament and staple. The conductivities of these fibres increase by about 25% between 20 and 200 °C. There is a high degree of anisotropy, though



6.8 Thermal conductivity measurement units: (a) axial; (b) transverse. From Kawabata [14].

Table 6.4 Thermal conductivities of fibres. From Kawabata [14, 15]

Fibre	Thermal conductivity (W/(m K))		Anisotropy K_L/K_T
	Longitudinal K_L	Transverse K_T	
Aramid			
<i>Kevlar</i> 29	3.05	0.192	15.9
<i>Kevlar</i> 49	3.34	0.212	15.8
<i>Kevlar</i> 149	4.74	0.230	20.6
Carbon			
<i>Torayca</i> T-300	6.69	0.530	12.6
<i>Torayca</i> M-308	18.33	0.667	27.5
<i>Torayca</i> M-408	58.81	1.215	48.4
E-glass	2.250	0.509	4.42
Nylon	1.43	0.171	8.38
Polyester filament	1.26	0.157	8.01
Polyester staple	1.18	0.127	9.25
Polypropylene	1.241	0.111	11.18
Acrylic	1.028	0.172	5.93
Rayon filament	1.89	—	—
Rayon staple	1.41	0.237	5.97
Cotton	2.88	0.243	11.85
Flax	2.851	0.344	8.23
Wool	0.48	0.165	2.91
Silk	1.49	0.118	12.64

the results for glass fibre, which is expected to be isotropic, suggest that the composite mixture equation underestimates the transverse fibre conductivity. The increasing anisotropy in the aramid and carbon fibres correlates with the increasing anisotropy of their moduli.

Lavin [16] confirms the correlations of thermal and electrical conductivities with moduli of carbon fibres. In PAN-based fibres there was an almost exponential increase in thermal conductivity from 5 to 100 W/(m K) with an increase in moduli from 250 to 600 GPa. In pitch-based fibres, the thermal conductivity reached almost 900 W/(m K) at 950 GPa.

6.2.3 Thermal expansion and contraction

Only a limited amount of work on the reversible thermal expansion of fibres has been done. Some values of the coefficients of expansion are given in Table 6.5. It will be noticed that the coefficient for nylon and polyester fibres is negative. This anomalous contraction may also occur with other fibres. The thermodynamic arguments discussed in Section 20.8.1 may be applied to thermal expansion and contraction. Equation (20.62) is:

$$\left(\frac{\partial S}{\partial l}\right)_T = -\left(\frac{\partial F}{\partial T}\right)_l \quad (6.6)$$

where S = entropy, l = length of fibre, F = tension of fibre and T = temperature.

Table 6.5 Coefficient of linear expansion of fibres (axial)

Fibre	Coefficient of expansion per degree C
Cotton [17]	4×10^{-4}
Cellulose acetate [18]	$0.8\text{--}1.6 \times 10^{-4}$
Nylon fibre [17]	-3×10^{-4}
Polyester (PET) [17]	-10×10^{-4} above 80°C
Polyethylene [18]	2×10^{-4}
Polyacrylonitrile (PAN) [19]	10×10^{-4}

Since

$$\left(\frac{\partial F}{\partial T}\right)_l = -\left(\frac{\partial F}{\partial l}\right)_T \left(\frac{\partial l}{\partial T}\right)_F \quad (6.7)$$

$$\text{the coefficient of linear expansion} = \left(\frac{1}{l}\right) \left(\frac{\partial l}{\partial T}\right)_F$$

$$= \left(\frac{1}{l}\right) \frac{(\partial S / \partial l)_T}{(\partial F / \partial l)_T} = \left(\frac{1}{l}\right) \left(\frac{\partial S}{\partial F}\right)_T \quad (6.8)$$

This means that the expansion is positive when stretching the fibre causes an increase of entropy, i.e. a greater degree of disorder due to increasing thermal vibrations. It is negative when the entropy decreases on stretching, i.e. the material becomes more highly ordered, as it does in a rubber when the molecules are straightened (see Section 20.1.2). This is more commonly observed as an increase in tension, indicating that the fibre wants to contract, on heating. Superimposed on the above effect there is the usual volume expansion due to the fact that the molecules take up more space at higher temperatures when they are vibrating more strongly. In rubber, this leads to the thermoelastic inversion: at zero tension, a rubber expands on heating because of the volume change, but a rubber specimen held at constant tension will contract axially if its extension is greater than about 10%. As shown in Section 20.3.2, the tie-molecules, which link the crystallites in nylon and polyester fibres, are in an extended rubbery state. Consequently, the coefficients of expansion can be negative as shown in Table 6.5.

A useful property of carbon fibres is their low coefficient of thermal expansion.

6.3 References

1. J. Brandrup and E. H. Immergut. *Polymer Handbook*, Interscience, New York, 1966.
2. *International Critical Tables*, Vol. II, McGraw-Hill, New York, 1900, p. 237.
3. P. Marx, C. W. Smith, A. E. Worthington and M. Dole. *J. Phys. Chem.*, 1955, **59**, 1015.
4. R. C. Wilhoit and M. Dole. *J. Phys. Chem.*, 1953, **57**, 14.
5. C. W. Smith and M. Dole. *J. Polymer Sci.*, 1956, **20**, 37.
6. S. Alford and M. Dole. *J. Amer. Chem. Soc.*, 1955, **77**, 4774.
7. M. Dole, W. P. Hettinger, N. R. Larson and J. A. Wethington. *J. Chem. Phys.*, 1952, **20**, 781.

8. P. Marx and M. Dole. *J. Amer. Chem. Soc.*, 1955, **77**, 4771.
9. H. A. Rigby and C. W. Bunn. *Nature*, 1949, **164**, 583.
10. R. F. S. Hearmon and J. N. Burcham. *Nature*, 1955, **176**, 978.
11. A. R. Haly and J. W. Snaith. *Biopolymers*, 1968, **6**, 1355.
12. S. Baxter. *Proc. Phys. Soc.*, 1946, **58**, 105.
13. W. H. Rees. *J. Text. Inst.*, 1946, **37**, P132.
14. S. Kawabata. *Proc. 4th Japan-U.S. Conf. Composite Materials*, 1988, p. 253.
15. S. Kawabata. *J. Textile Machinery Soc. Japan*, 1986, **39**, 184.
16. J. G. Lavin. In *High-performance Fibres*, J. W. S. Hearle (Editor), Woodhead Publishing, Cambridge, 2001, p. 156.
17. J. F. Clark and J. M. Preston. *J. Text. Inst.*, 1953, **44**, T596.
18. W. J. Roff and J. R. Scott. *Fibres, Films, Plastics, and Rubbers*, Butterworths, London, 1971.
19. S. Rosenbaum. *J. Appl. Polymer Sci.*, 1965, **9**, 2071, 2085.

7.1 Introduction

It has been known for a long time that fibres take up moisture from the air. Leonardo da Vinci (1452–1519) has, in his notebooks, two drawings of self-indicating balances with cotton on one pan and wax on the other; the increased weight of the cotton in a damp atmosphere alters the setting of the balance so that it can be used ‘for knowing the quality and density of the air and when it will rain’. Earlier, Nicholas of Cusa (1401–1463) had measured the increase in weight of wool for the same purpose. The first detailed investigation of the subject was carried out by Schloesing [1] in 1893. Between 1924 and 1932, Urquhart and his collaborators conducted an investigation of the absorption of cotton, rayons and acetate that will remain a classic of painstaking experiment.

The property of absorbing moisture is a valuable feature of clothing materials. Apart from its direct utility in keeping the skin dry, the absorption of water causes the fabric to act as a heat reservoir, protecting the body from sudden changes of external conditions. However, it may be a disadvantage in drying the hygroscopic fibres that it is necessary to remove the absorbed moisture that is not present in the non-hygroscopic synthetic fibres.

The absorption changes the properties of fibres. It causes swelling to occur, which alters the dimensions of the fibre, and this, in turn, will cause changes in the size, shape, stiffness and permeability of yarns and fabrics. The mechanical properties and the frictional properties are altered, so affecting the behaviour of the fibres in processing and in use. Wetting and drying may lead to permanent set or creasing. The moisture condition of the material is one of the most important factors in determining its electrical properties; ‘static’ is much less likely to occur in damp conditions.

The above examples show the technological importance of moisture absorption in fibres. There is also a direct commercial interest. In 100 kg of raw cotton, for example, there may be up to 12 kg of water. Since it is expensive to pay for this at the price of raw cotton, it must be allowed for in calculating the weight to be charged.

7.2 Definitions

7.2.1 Humidity

The *absolute humidity* h of an atmosphere is defined as the mass of water in unit volume of air. The dampness of the air is also indicated by the *vapour pressure* p that

is, the partial pressure of the water vapour in the atmosphere. The most convenient term is the relative humidity H , given by:

$$H = 100 \left(\frac{h}{h_s} \right) \quad (7.1)$$

where h_s is the absolute humidity of saturated air at the same temperature. At ordinary air temperatures, this ratio differs inappreciably from the corresponding ratio of vapour pressures.

Since the properties of fibres vary with the moisture condition, testing should be done under controlled conditions. For this purpose, a *standard temperate atmosphere* is defined as one of 65% r.h. and 20 °C¹. The permitted tolerances for testing are $\pm 2\%$ r.h. and $\pm 2^\circ\text{C}$. An uncontrolled indoor atmosphere is usually drier than this.

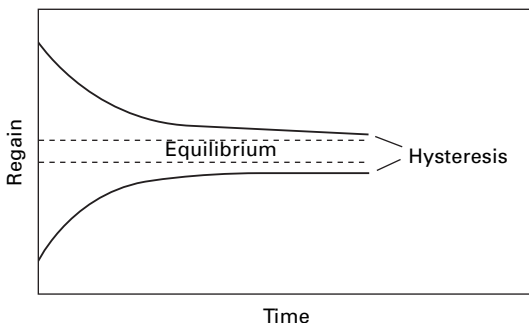
7.2.2 Equilibrium

When a textile material is placed in a given atmosphere, it takes up or loses water at a gradually decreasing rate (Fig. 7.1) until it reaches equilibrium, when no further change takes place. This is a dynamic equilibrium, which occurs when the number of water molecules evaporating from the specimen in a given time becomes equal to the number condensing and being absorbed.

7.2.3 Regain and moisture content

The amount of water in a specimen may be expressed in terms of either the regain or the moisture content:

$$\text{regain} = \frac{\text{mass of absorbed water in specimen}}{\text{mass of dry specimen}} \times 100\% = R \quad (7.2)$$



7.1 The approach to moisture equilibrium, with hysteresis depending on whether sample is gaining or losing water.

¹ In tropical and sub-tropical countries, 27 °C may be used as a secondary standard.

$$\text{moisture content} = \frac{\text{mass of absorbed water in specimen}}{\text{mass of undried specimen}} \times 100\% = M \quad (7.3)$$

The two are simply related, for, if the dry mass = D and the mass of absorbed water = W , we have:

$$R = \frac{100 W}{D} \quad (7.4)$$

$$M = \frac{100 W}{D + W} = \frac{100 W/D}{1 + W/D} = R \frac{1 + R}{100} \quad (7.5)$$

7.2.4 Recommended allowance

For commercial transactions, a set of values of recommended allowance² has been agreed on. The mass of a consignment of a textile material on which the charge is to be based is known as the *correct invoice mass* and is equal to the mass that the consignment would have if its regain were the recommended allowance.

It should be noted that the values of the recommended allowances are chosen purely for convenience, since they are near the values found in practice and are not the regains in a standard atmosphere. The values of the recommended allowances are included in [Table 7.3](#).

7.3 Measurement of regain

7.3.1 The gravimetric method

The gravimetric method is the basic method of measuring regain or moisture content, and any indirect method must be calibrated by it. The sample to be tested is weighed, dried and then weighed again. The regain R is calculated as follows:

$$\text{mass of undried specimen} = W + D = m_1$$

$$\text{mass of dried specimen} = D = m_2$$

$$R = \frac{100 W}{D} = 100 \frac{(m_1 - m_2)}{m_2} \% \quad (7.6)$$

No difficulty is involved in the first weighing, except that care should be taken that the regain of the sample does not change before or during the weighing. The determination of the dry weight does involve certain difficulties.

7.3.2 Difficulties involved in drying the specimen

To obtain the most accurate results, the sample should be dried by exposing it in an enclosed space containing an efficient drying agent, such as phosphorus pentoxide,

²Commercial regain in the United States

at room temperature. The high affinity of the drying agent for water results in complete drying of the specimen, and, since the temperature is not raised, other changes in the specimen are not likely to occur. This method, however, has the disadvantage that it is extremely slow. Davidson and Shorter [2] found that a period of from 4 to 6 weeks was necessary to dry 8 g specimens of cotton. This slowness renders the method impracticable except for very special investigations.

The usual method in practice is to dry the specimen in an oven at about 110 °C. The raising of the temperature of the air lowers its relative humidity, since, although the absolute humidity of the air changes very little, the saturation humidity increases enormously. Water must then evaporate from the specimen until it reaches equilibrium. Since all chemical processes are more rapid at higher temperatures, this does not take long.

However, the relative humidity in the oven is not zero. If the air outside the oven has a relative humidity of 50% at 20 °C, when it is heated to 110 °C its relative humidity will be 0.8%. The moisture that is left in equilibrium with this humidity is known as the *residual regain* and is the first inherent source of error in the oven method. It results in a measured value of the regain that is too low, since the loss of weight on drying is not as great as it should be.

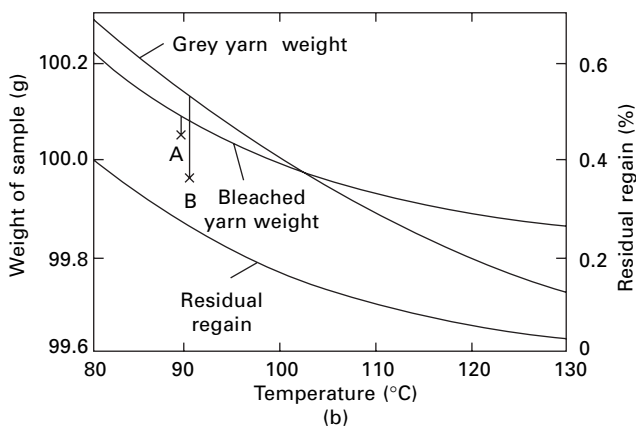
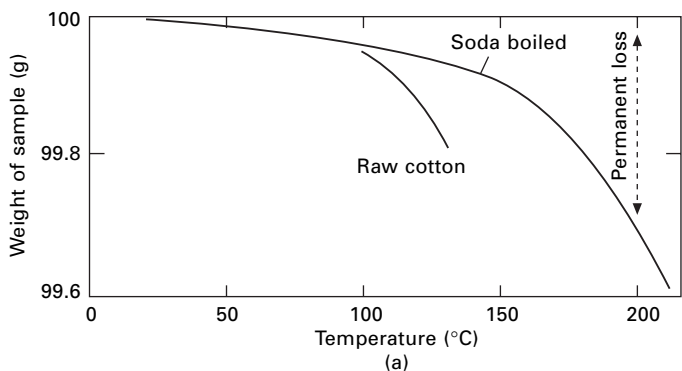
The heating of the specimen may cause substances other than water, for example, oils and waxes present as impurities, to be driven off from the sample. This is known as *permanent loss* and is the second inherent source of error in the oven method. It causes the measured loss of weight to be greater than it should be and thus gives a high value of the regain. Figure 7.2 illustrates the two sources of error. Figure 7.2(a) shows the permanent loss of soda-boiled and unbleached cotton after 3 h heating, dry, in a vacuum. Figure 7.2(b) shows the residual regain in cotton due to a water vapour pressure of 8 mm of mercury (1.07 kPa) at various temperatures. The change of weight of bleached cotton follows this curve closely, but the raw cotton shows a greater change in weight owing to the permanent loss. The amount of permanent loss can be shown by allowing the specimen to reabsorb water and then drying again at 90 °C; for bleached cotton, this shows little difference from the previous value, but the value for raw cotton is almost 0.2% lower than the previous value owing to the permanent loss in the first drying to 130 °C.

The amounts of error due to these causes will vary with the conditions but they may both be of the order of 0.2% in the value of the regain. The true dry weight is given by:

$$\text{true dry weight} = \text{oven-dry weight} - \text{residual regain} + \text{permanent loss}$$

7.3.3 Experimental practice

For commercial and routine testing, a special oven is usually used. It contains a basket in which about 1 kg of material can be placed and weighed *in situ*. The material is then dried until its weight becomes constant in a current of heated air. The dry sample is weighed with the air current switched off. Stephenson [3] has described the experimental errors that may occur:



7.2 (a) Permanent loss on heating 100 g of dry cotton for 3 h *in vacuo*. (b) Change in weight of samples of cotton dried at water vapour pressure of 8 mm of mercury (1.07 kPa). Points A and B are for material dried at 130 °C, allowed to reabsorb water at room temperature, and then dried at 90 °C. From Davidson and Shorter [2].

- The differing density of hot and cold air will affect the buoyancy of the specimen.
- Convection currents may affect the balance, but this can be minimised by a well-designed oven.
- Absorption may occur during weighing, after the air current has been switched off.

The errors should not total more than 0.1% in the value of the regain. Balls [4] found that random errors in routine oven-testing amounted to $\pm 0.2\%$ in the regain value for cotton at 10% regain.

More rapid tests may be made by using an apparatus in which a stream of hot air is blown through a container holding the specimen. The container can be removed and closed for weighing. In another instrument, a standard weight of material is used, and, after drying, the regain is directly indicated on a scale.

Laboratory tests are usually made on smaller samples, which are placed in weighing bottles. For the most accurate work, they are dried in a desiccator with a drying agent.

A more rapid method is to dry them in a small chemical oven at 110 °C. The bottles are removed from the oven, stoppered up and cooled before being weighed. The errors liable to occur in this method are:

- absorption of moisture before the stopper is replaced;
- enclosure of hot air in the container, giving it added buoyancy (the amount of the error due to this cause will depend on the relative size of container and sample);
- convection errors, which should be negligible if the bottle is cooled;
- diffusion of moisture into the bottle, which can be prevented by a good seal.

Stephenson [3] estimates that the errors due to these causes may be between 0.2 and 0.8% in the value of the regain.

Table 7.1 gives a comparison of results obtained by LeCompte and Lipp [5] when using various methods for determining moisture in wool. They conclude that toluene distillation (Section 7.3.4) is the most accurate method in this case. Impurities accounted for less than 0.01% in the water distilled over.

The techniques involved in obtaining accurate relations between equilibrium regain and relative humidity have been reviewed by McLaren and Rowen [6].

7.3.4 Other direct methods

Another method of determining the water in the material is by heating the sample with toluene (boiling point 111 °C) and measuring the amount of water that distils over and is collected in a receiver. The toluene used should be saturated with water. The method is not open to the error of residual regain, since a fresh atmosphere of toluene is continually being supplied. Errors due to permanent loss can be checked by analysis of the water collected.

Van Lamoen and Borsten [7] have described a method for the titration of water, which they consider to be superior to the use of drying ovens, though the reagents are relatively expensive.

7.3.5 Indirect methods

Methods based on the variation of the electrical properties of fibres have been used to indicate their moisture condition.

Table 7.1 Regain determination for wool [5]

Method	Average	Range of values of regain % in three tests
Vacuum oven over P ₂ O ₅	7.13*	0.22
Conditioning oven 110 °C	7.16	0.19
USDA suction drier 150 °C	7.27	0.15
Forced-draught drier	7.33	0.16
Toluene distillation	7.77	0.17

*Still falling at 0.05% per day at end of test.

The Shirley Moisture Meter [8] was, at one time, widely used for the measurement of electrical resistance of cotton, and, although it is no longer manufactured, its essential features could be reproduced in other equipment. As illustrated in Fig. 7.3, an electronic circuit measures the resistance between the inner and outer electrodes of the cone, which is pressed onto the sample of fibre. Other types of electrode may be used for material in other forms. Because of the rapid variation of electrical resistance with moisture content, the method is sensitive. The resistance values depend on fibre type and are sensitive to temperature, additives, contact pressure and material form, but, if a resistance meter is properly calibrated for the test, it gives an accurate measure of resistance. Instruments based on the variation of dielectric constant are also available, but they suffer from the disadvantages that the weight and distribution of material between the plates of the condenser must be controlled and that the variation of dielectric constant with moisture content is much less than the variation of resistance. The capacity method has been extensively used in process-control applications, but, where it can be applied, a resistance method is better.

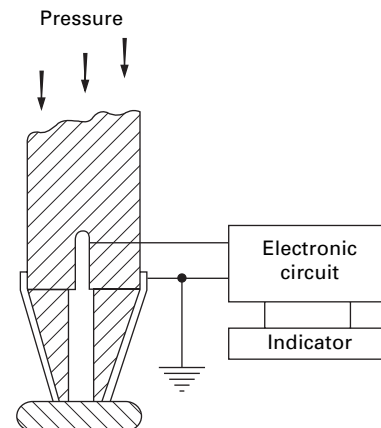
Another indirect method of measuring regain is to shake up a known weight of the sample with calcium carbide in a closed container. This reacts with the water and generates acetylene; measurement of the pressure indicates the regain.

The Shirley Moisture Regain Indicator may also be mentioned. A prepared sample of material is hung on a balance, and, as the relative humidity changes, its weight changes, and the regain is directly indicated on a scale. This may be placed in a spinning room and used for calculating the dry or standard weights of the material being processed.

7.4 Relation between regain and relative humidity

7.4.1 General

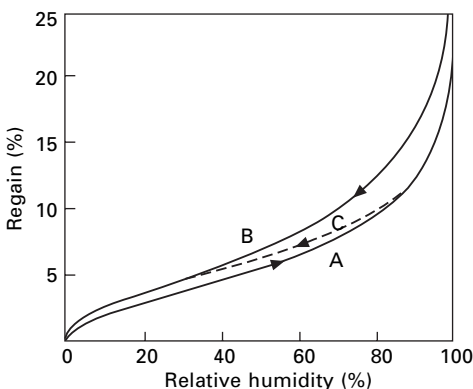
There is hysteresis in the relation between the regain of a textile material and the relative humidity of the atmosphere with which it is in equilibrium. This is illustrated



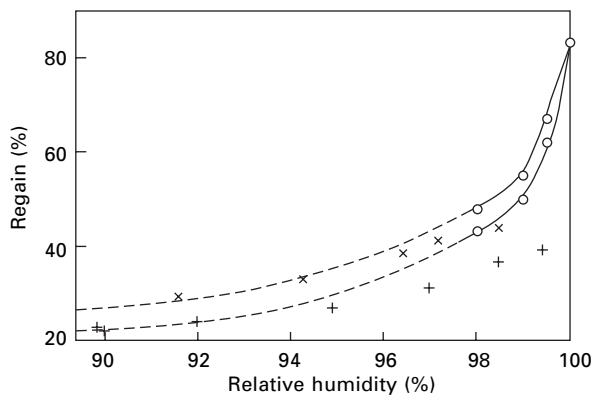
7.3 Basic features of Shirley Moisture Meter.

in Fig. 7.1, which shows the approach to equilibrium in the same atmosphere of two specimens initially at different regains. The specimen that originally had the higher regain also has the higher regain at equilibrium. Depending on its previous history, the specimen may come to equilibrium anywhere in a range of metastable states and does not come to a true thermodynamic equilibrium. In relating regain to relative humidity, it is usual to plot two curves (Fig. 7.4). The first curve A, commonly called the absorption isotherm, is a plot of equilibrium regains at successively higher humidities of a specimen initially bone-dry; the second curve B, the desorption isotherm, is a plot for a specimen initially wet, at successively lower humidities. The nomenclature is unfortunately in confusion. *Desorption* always refers to the loss of water, but the terms *sorption*, *absorption* and *adsorption* are used variously by different authors for the uptake of water or for the whole general phenomenon. Adsorption is, however, best reserved for a specialised meaning implying a particular mechanism of attachment of the water molecules.

The curves usually have the sigmoidal shape shown in Fig. 7.4: a rapidly increasing regain at low humidities, followed by an almost linear portion, and then a more rapid rise at high humidities. The two curves must join at the origin, but Urquhart and Eckersall's experiments [9] indicated that they were separate at 100% r.h. Wetting the specimen caused the values to lie on a higher curve than could be reached by exposure in a saturated atmosphere. Ashpole [10] has disputed this view and produced experimental results indicating that there is a rapid rise in the absorption curve near the saturation point (Fig. 7.5). Experiments are difficult near saturation, since the rapid rise in the absorption means that a large amount of water has to be taken up under a small vapour pressure gradient when conditioning is very slow, while, if there are any temperature fluctuations, it is easy for supersaturation and condensation to occur. Ashpole devised the technique of enclosing the specimen in waxed gauze surrounded by a cellophane membrane and placing this in a solution of sugar of the concentration needed to give the required humidity. This reduces the distance over which diffusion has to occur and so hastens the attainment of equilibrium. By special precautions, temperature fluctuations were kept below 10^{-4} °C. At the highest humidities,



7.4 Typical curves of regain of soda-boiled cotton against relative humidity: A, absorption; B, desorption; C, intermediate [9].



7.5 Hysteresis loop for viscose rayon near saturation. o Ashpole’s experimental values [10]; + absorption; × desorption values found by Urquhart and Eckersall [9].

Ashpole found that the regain varied continuously with time, and, to allow for this, he extrapolated back to zero time. This effect casts some doubt on the validity of his results, and the exact form of the curves near saturation remains uncertain.

The two curves are the limiting equilibrium values. Equilibrium can be attained at any point between them by taking the specimen through a suitable chain of humidities. The curve C in Fig. 7.4 shows a typical result for the desorption of a specimen that had previously been absorbing. The intermediate curves are also sigmoidal in shape.

Taylor [11, 12] has shown that hysteresis occurs even in cycles at low relative humidities. The results given in Table 7.2 show that at about 1% r.h. the hysteresis due to desorption from 4% r.h. may be only a little less than half the hysteresis due to desorption from saturation.

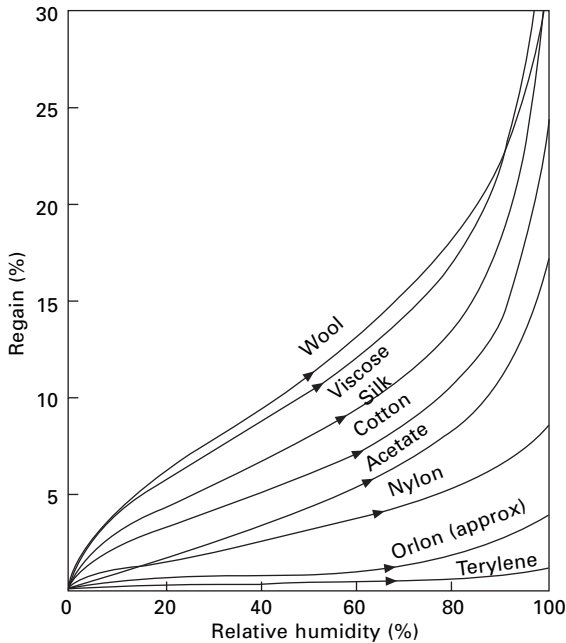
7.4.2 Comparison of various materials

Figure 7.6 shows the relations between regain and relative humidity for various textile fibres, and Table 7.3 gives values of regains at 65% r.h. and the widths of the hysteresis loops.

Cotton shows the typical behaviour. There are small differences between cottons of different origins, for example, at 57.6% r.h. Urquhart and Williams [25] found

Table 7.2 Hysteresis in cycles at low regains [11, 12]

Material	r.h. (%)	Absorption regain (%)	(Desorption regain – absorption regain) (%)	
			cycle 0–4% r.h.	Cycle 0% r.h. to saturation
Viscose rayon (Fibro)	0.85	0.95	0.23	0.49
	1.7	1.38	0.14	0.69
	4	2.19	–	0.69
Cotton	1.7	0.66	0.036	0.095
	4	1.07	–	0.159



7.6 Regain versus relative humidity for cotton [13], viscose rayon [14], acetate [14], silk [15], wool [16], nylon [17], *Terylene* polyester (PET) [18] and *Orlon* acrylic [18].

absorption regains ranging from 6.76% for a Texas cotton to 7.19% for a Peruvian cotton. After soda-boiling to remove impurities, the difference between these two cottons decreased to 0.12%. Processing, especially wet processing, may cause large changes in the amount of moisture absorbed. There are two principal effects: a removal of highly absorbing non-cellulosic impurities; and a change in the internal arrangement of the cellulose molecules. Heating the sample dry lowers the curve of regain against relative humidity, but wet heating raises it. Mercerisation without tension can increase the regain at a given relative humidity to 1.5 times its previous value; mercerisation under tension does not cause such a large increase [19].

A sample of cotton straight from the boll of the cotton plant or immediately after hot-wet processing shows a desorption curve higher than the usual one (Fig. 7.7). This is known as the *primary desorption curve*. Once the material has been dried below 50% r.h., it follows the usual curves. The intermediate curves for cotton are very long, as shown in Fig. 7.8. For example, if absorption is started from 10% r.h. on the desorption curve, the absorption curve will not be joined below 80% r.h. To be sure of getting on either the absorption or the desorption curve, it is necessary to start from almost complete dryness or wetness, respectively.

The effects of processing were shown to a marked extent by experiments by Gu [26] on naturally coloured green cotton, which contained 14.19% of fat, lignin and pectin, compared with 1.8% in white cotton. The moisture regain of the green cotton was 3.87% and of white was 8.6%. After treatments in NaOH solutions of varying

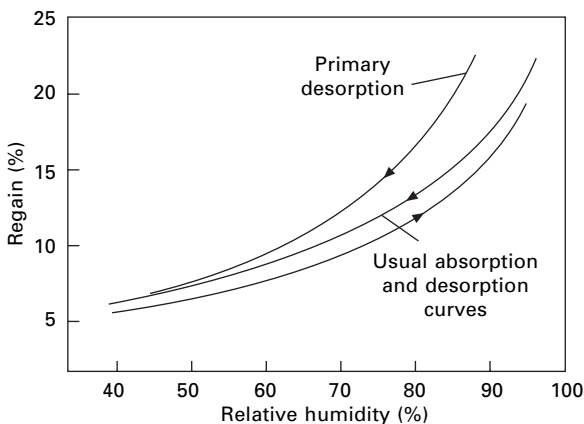
Table 7.3 Moisture absorption of fibres. Based on data by Ford [19] and other workers

Material	Recommended allowance or commercial regain or conventional allowance* (%)	Absorption regain at 65% r.h. 20 °C** (%)	Desorption regain <i>minus</i> absorption regain at 65% r.h. 20 °C** (%)
Cotton [13]	8.5	7–8	0.9
Mercedised cotton [20]	–	up to 12	1.5
Hemp [21]	12	8	–
Flax [21]	12	7	–
Jute [22]	13.75	12	1.5
Viscose rayon [14]	13	12–14	1.8
Secondary acetate [14]	9	6, 6.9	2.6
Triacetate	–	4.5	–
Silk [15]	11	10	1.2
Wool [16]	14–19	14, 16–18	2.0
Casein [23]	–	14	1.0
Nylon 6.6, Nylon 6 [17]	5 ³ / ₄ or 6 ¹ / ₄	4.1	0.25
Polyester [18]	1.5 or 3	0.4	–
Acrylic	–	1–2	–
Modacrylic	–	0.5–1	–
Polyvinyl alcohol [18]	–	4.5–5.0	–
Polylactic acid [24]	–	0.4–0.6	–
Para-aramid (Kevlar, Twaron)		low modulus 7 to high modulus 1.2	–
Meta-aramid (Nomex)	–	5	–

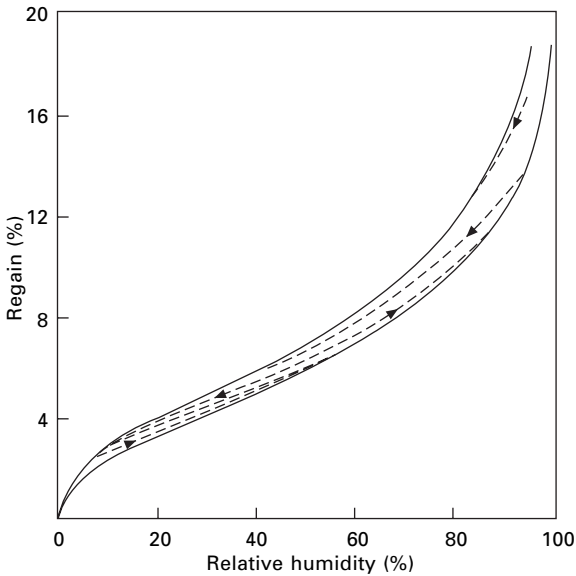
Polyethylene, polypropylene, polyvinyl chloride, carbon, glass and ceramic fibres have zero moisture absorption.

*As given in BS 4784:1973; other standardising organisations may quote different values.

**The earlier measurements were at 70 °F (21.1 °C).



7.7 Primary desorption curve of raw cotton from boll. From Urquhart and Eckersall [9].



7.8 Intermediate curves for raw cotton. The outer full lines are for absorption and sorption between 0 and 100% rh; The inner dashed lines are for absorption and addesorption between intermediate humidities. From Urquhart and Eckersall [9].

strengths at different temperatures and for different times, the regain of the green cotton increased to 7.53–8.69%.

Viscose rayon has regain values that can be obtained by multiplying the regain values for cotton at the same humidity by an almost constant factor. For a particular specimen of viscose rayon, the figures were [14]:

r.h. (%)	5	20	40	60	80
Regain of viscose rayon/regain of cotton	1.99	2.13	2.08	2.03	1.98

For other specimens of viscose rayon, this ratio, which is often called the *sorption ratio* of the material, may not be as close to 2 as the values quoted, but it is a general feature of cellulosic fibres that their sorption ratios remain almost constant over the whole range of humidity.

Taylor's results [11] (Table 7.2) show that, although the absorption regain of viscose rayon is twice that of cotton, the difference between the desorption and absorption regains at low humidities is four times that of cotton. Above 30% r.h., this behaviour is reversed and cotton shows the greater hysteresis, in proportion to its regain.

Acetate has a curve of a different shape and does not show a rapid rise of regain at low humidities. The regains are lower than those of cotton, but the rate of change of regain with r.h. in the practical range above 20% r.h. is about the same.

Wool has a regain curve close to that of viscose rayon but of slightly different

shape. In particular, at high humidities the regain of wool is lower. The type of wool and its processing also affect the regain values. For example, Speakman [16] found regains at 63.3% r.h. ranging from 13.97% for a merino wool to 14.54% for a Wensleydale. Nicholls and Speakman [27] have shown that acid-treated wool has a lower equilibrium regain; thus, at 53.8% r.h., untreated wool had a regain of 12.68%, but wool containing 40 milliequivalents of acid per gram of wool had regains ranging from 11.89% for sulphuric acid to 9.79% for picric acid.

Figure 7.9, from Speakman and Cooper [28], shows that the intermediate hysteresis curves for wool are shorter than those for cotton, a change of 18% r.h. being sufficient to pass between the main absorption and the main desorption curves. This range is independent of the value of the regain.

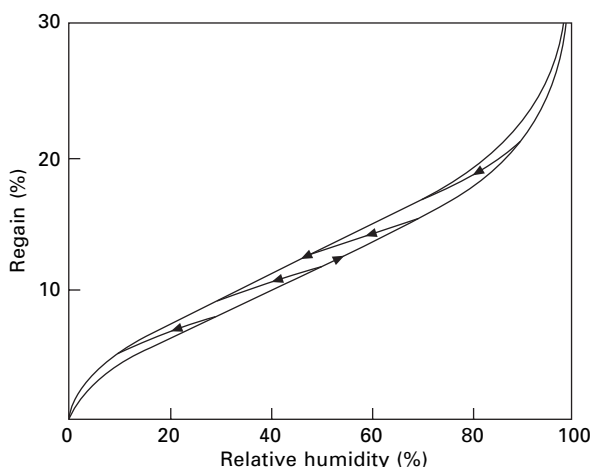
Casein fibres have regains very close to those of wool at the same humidity but show a rather large difference between absorption and desorption values [23].

Silk has a regain intermediate between cotton and wool. Silk gum has a high regain, and the degumming causes a reduction in regain at 65 r.h. from 10.65 to 9.9% [15].

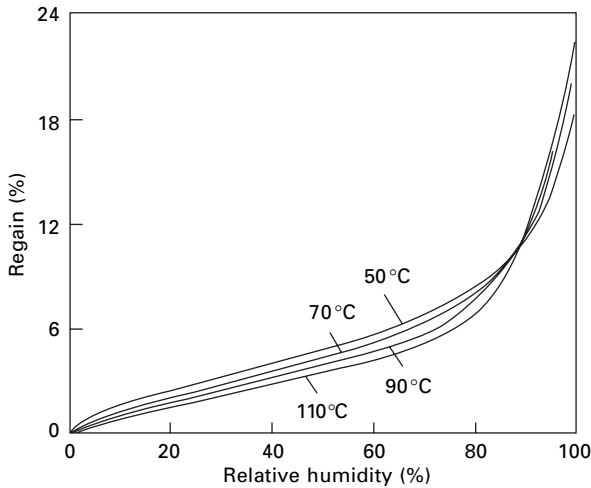
The synthetic fibres have low regains. Nylon has about half the regain of cotton. Some workers have suggested that hysteresis is absent, but Hutton and Gartside [17] showed that a small hysteresis definitely existed. At 80% r.h., they obtained regain values of 5.48% in absorption and 5.64% in desorption. Forward and Smith [29] have shown that the moisture absorption of undrawn nylon yarn can be appreciably altered by chemical treatment. Polyester (PET) fibres have a small regain. Many other polymer fibres have zero moisture absorption, as do inorganic fibres.

7.4.3 Influence of temperature

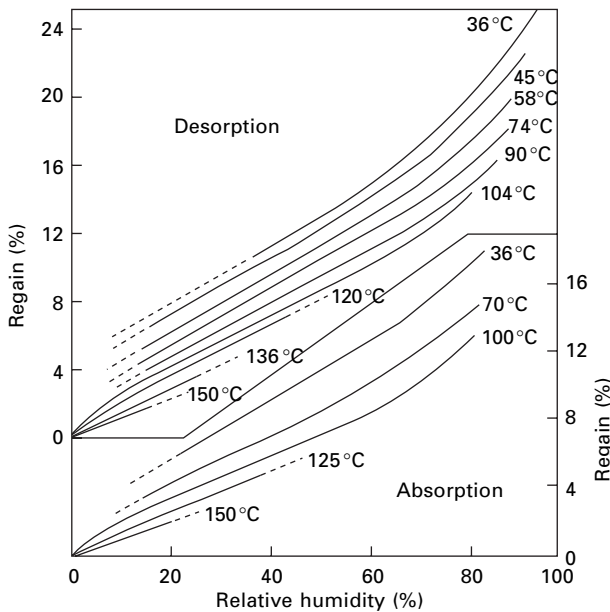
The curves of regain against relative humidity depend to a slight extent on temperature, the result being a family of isothermals. Figure 7.10 shows data for cotton. Except at



7.9 Intermediate curves for wool. The outer full lines are for absorption and sorption between 0 and 100% rh; the crossing lines are for absorption and sorption between intermediate humidifier From Speakman and Cooper [28].



7.10 Effect of temperature on absorption of cotton. From Urquhart and Williams [30].



7.11 Effect of temperature on absorption of wool. From Wiegerink [31].

high temperatures and humidities, the regain decreases as the temperature increases. This is the expected thermodynamic behaviour for an exothermic reaction such as absorption. The increase above 50 °C at high humidities is due to a change in the internal structure and is associated with the irreversible hysteresis effects.

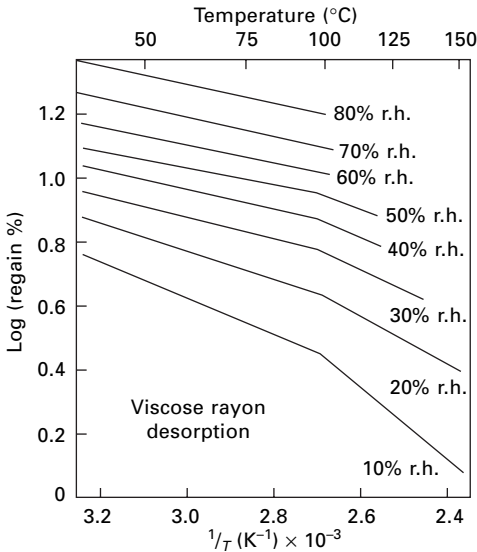
Wiegerink [31] tested a variety of fibres between 35 and 150 °C, and the curves for wool, shown in Fig. 7.11, are typical of his results. He found that when the logarithms

of the regains were plotted against the reciprocal of temperature, straight lines were obtained, with a change of slope at about 100 °C. Figure 7.12 illustrates this for viscose rayon. Darling and Belding [32] tested the same materials at low temperatures, but, owing to the slowness of conditioning, they were able to test only at a limited set of conditions. Their results indicate that the linear relations cease to apply below 20 °C. Below about 0 °C, the regain decreases. Values for the regain at 70% r.h. are given in Table 7.4.

7.4.4 Effect of stresses

The swelling of fibres during absorption means that the application of stresses will change the regain. Table 7.5 shows the increases in regain due to the application of a tension to filaments that were reported by Treloar [33, 34].

By contrast, the lateral compression of fibres, such as would come from applying tension to a twisted yarn, would lower the regain. For example, Nickerson [35] states



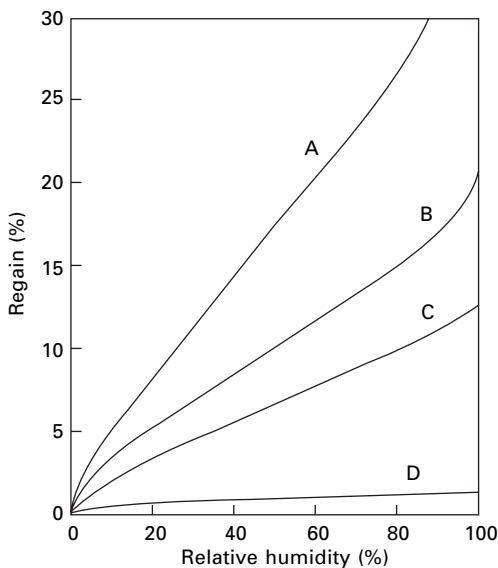
7.12 Effect of temperature on absorption of viscose rayon. T is absolute temperature in Kelvin (K). From Wiegerink [31].

Table 7.4 Change of regain with temperature [32]

Temperature (°C)	Regain at 70% r.h.			
	Cotton	Wool	Viscose rayon	Secondary acetate
–29	8.5	17	16	7.9
–18	9.8	18	17	9.6
4	9.7	17.5	17	9.0
35	7.8	15	14	7.1
71	6.7	13	12	6.2

Table 7.5 Effect of axial applied stress on moisture absorption at 75.5% r.h., 25 °C. From Treloar [33, 34]

Isotropic cellulose		Oriented cellulose		Horsehair	
Stress (MPa)	Increase in regain (%)	Stress (MPa)	Increase in regain (%)	Stress (MPa)	Increase in regain (%)
5.7	0.2	10.2	0.1	25.8	0.14
10.2	0.4	17.7	0.4	47.3	0.28
13.6	0.6	35.6	1.1		
27.4	1.5				
40.5	1.1				



7.13 Absorption of spruce wood under stress: (A) material completely free of stress; (B) natural sorption, including internal restraints on swelling of block of wood; (C) volume of block of wood held constant, but allowing swelling into void spaces in wood cells; (D) wood cell walls (internal and external) held at constant volume.

Curve B is experimental; remainder are calculated. From Barkas [36].

that the application of 60% of its breaking load to a cotton yarn lowered the regain from 8.78 to 8.19%. Barkas [36] has studied this effect in wood, and the curves in Figure 7.13 show the large changes that can occur when severe restraints are applied.

7.5 References

1. T. Schloesing. *Compt. Rend.*, 1893, **116**, 808.
2. G. F. Davidson and S. A. Shorter. *J. Text. Inst.*, 1930, **21**, T165.
3. M. Stephenson. *J. Text. Inst.*, 1938, **29**, T297.

4. W. L. Balls. *J. Text. Inst.*, 1950, **41**, T127.
5. G. LeCompte and H. H. Lipp. *Amer. Dyest. Rep.*, 1949, **38**, 484.
6. A. D. McLaren and J. W. Rowen. *J. Polymer Sci.*, 1951, **7**, 289.
7. F. L. J. van Lamoen and H. Borsten. *Tex.*, 1953, **12**, 861.
8. E. H. Jones. *J. Sci. Instrum.*, 1940, **17**, 55.
9. A. R. Urquhart and N. Eckersall. *J. Text. Inst.*, 1930, **21**, T499.
10. D. K. Ashpole. *Proc. Roy. Soc.*, 1952, **A212**, 112.
11. J. B. Taylor. *J. Text. Inst.*, 1952, **43**, T489.
12. J. B. Taylor. *J. Text. Inst.*, 1954, **45**, T642.
13. A. R. Urquhart and A. M. Williams. *J. Text. Inst.*, 1924, **15**, T138.
14. A. R. Urquhart and N. Eckersall. *J. Text. Inst.*, 1932, **23**, T163.
15. E. A. Hutton and J. Gartside. *J. Text. Inst.*, 1949, **40**, T161.
16. J. B. Speakman. *J. Soc. Chem. Industr.*, 1930, **49**, 209T.
17. E. A. Hutton and J. Gartside. *J. Text. Inst.*, 1949, **40**, T170.
18. R. Hill (Editor). *Fibres from Synthetic Polymers*, Elsevier, Amsterdam, Netherlands, 1953.
19. J. E. Ford. *Fibre Data Summaries*, Shirley Institute, Manchester, 1966.
20. A. R. Urquhart and A. M. Williams. *J. Text. Inst.*, 1925, **16**, T155.
21. F. Howlett. *J. Text. Inst.*, 1942, **33**, T102.
22. A. Powrie and J. B. Speakman. *J. Text. Inst.*, 1943, **34**, T77.
23. R. L. Wormell. *New Fibres from Proteins*, Butterworths, London, 1954, p. 129.
24. D. W. Farrington, J. Lunt, S. Davies and R. S. Blackburn. in *Biodegradable and Sustainable Fibres*, R. S. Blackburn (Editor), Woodhead Publish Cambridge, 2055, p. 191.
25. A. R. Urquhart and A. M. Williams. *J. Text. Inst.*, 1926, **17**, T38.
26. H. Gu. *J. Textile Inst.* 2006, **96**, 247.
27. C. H. Nicholls and J. B. Speakman. *J. Text. Inst.*, 1954, **45**, T267.
28. J. B. Speakman and C. A. Cooper. *J. Text. Inst.*, 1936, **27**, T183.
29. M. V. Forward and S. T. Smith. *J. Text. Inst.*, 1955, **46**, T158.
30. A. R. Urquhart and A. M. Williams. *J. Text. Inst.*, 1924, **15**, T559.
31. J. G. Wiegerink. *Text. Res.*, 1940, **10**, 357.
32. R. C. Darling and H. S. Belding. *Industr. Engng Chem.*, 1946, **38**, 524.
33. L. R. G. Treloar. *Trans. Faraday Soc.*, 1952, **48**, 567.
34. L. R. G. Treloar. *Trans. Faraday Soc.*, 1953, **49**, 816.
35. R. F. Nickerson in *Matthews' Textile Fibers* H. R. Mauersberger (Editor), 6th edition, Wiley, New York, 1954, p. 212.
36. W. W. Barkas. *The Swelling of Wood under Stress*, Svenska Träforskningsinstitutet Meddelande 61, Stockholm, 1950, p. 35. (See also: W. W. Barkas. *The Swelling of Wood under Stress*, HMSO, London, 1949.)

8.1 Definitions

When a fibre absorbs water, heat is evolved. If liquid water is taken up, this is similar to the heat of solution that occurs, for instance, when sulphuric acid and water are mixed. It results from the attractive forces between the fibre molecules and water molecules. If water vapour is absorbed, there is also heat similar to latent heat of condensation. The heat evolved may be expressed in various ways.

The *differential heat of sorption* Q (sometimes called the heat of absorption) is the heat evolved when 1 g of water is absorbed by an infinite mass of the material at a given moisture regain. It is expressed in joules per gram (of water absorbed).

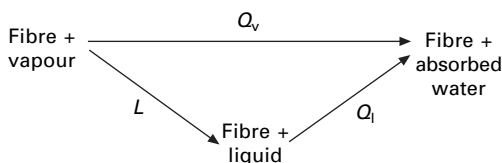
The water may be absorbed from water vapour, to give a value Q_v , or from liquid water, to give a value Q_l . The relation between the two quantities is illustrated in Fig. 8.1. It follows from the First Law of Thermodynamics that the total heat evolved must be the same along each path, and therefore:

$$Q_v = Q_l + L \quad (8.1)$$

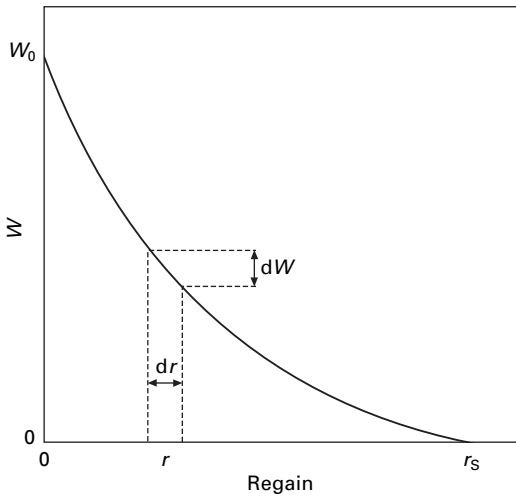
where L is the latent heat of condensation of water in J/g at the temperature concerned. The quantity Q_l is sometimes called the heat of swelling.

The *integral heat of sorption* W (sometimes called the *heat of wetting*) is the heat evolved when a specimen of the material at a given regain, whose dry mass is 1 g, is completely wetted. It is expressed in joules per gram (of dry material) and is almost always given in terms of absorption from the liquid state.

The relation between the differential and integral heats can be seen by considering the graph of integral heat of sorption against regain (Fig. 8.2). The increase of the regain by dr causes an amount of heat equal to $Q_l dr/100$ to be evolved. If this is



8.1 Relation between heats of sorption from vapour and liquid.



8.2 Variation of integral heat of sorption with regain.

integrated from a regain r to the saturation regain, r_s , it will give the total amount of heat evolved when the specimen is wetted, that is, the heat of wetting for the regain r . Thus:

$$W = \int_r^{r_s} \frac{Q_1 \cdot dr}{100} \quad (8.2)$$

Conversely, the heat $Q_1 \cdot dr/100$ equals the decrease in the heat of wetting for the regain change dr , giving:

$$Q_1 = -100 \frac{dW}{dr} \quad (8.3)$$

An integral heat of sorption defined as the heat evolved when 1 g of dry material is raised to the given regain is sometimes used. If we call this quantity W' and let W_0 be the heat of wetting from dryness to saturation, we have:

$$W' = W_0 - W \quad (8.4)$$

8.2 Measurement

Heats of wetting may be measured calorimetrically. A known mass of the material at the required regain is placed in a calorimeter, and an excess of water is added. From the rise in temperature and the thermal capacity of the system, the heat evolved can be calculated and the heat of wetting determined. Because a large amount of water is needed to secure satisfactory wetting of the fibres, the temperature rise will be small, and careful experimental technique and sensitive temperature measurement are necessary. Several workers have described methods in detail [1–3].

The differential heats of sorption, which are of more practical and theoretical importance, may be obtained from the experimental values of the heats of wetting by

using equation (8.3). They may also be determined by calculation from the absorption isotherms. The Clausius–Clapeyron equation for water vapour, if the specific volume of liquid water is neglected in comparison with that of water vapour, is:

$$\frac{dp_s}{dT} = \frac{L}{TV_s} \quad (8.5)$$

where p_s = saturation vapour pressure of water, T = absolute temperature and V_s = specific volume of vapour at saturation vapour pressure.

Application of the equation to a textile system at constant regain r gives:

$$\left(\frac{\partial p}{\partial T} \right)_r = \frac{Q_v}{TV} \quad (8.6)$$

where p = vapour pressure in equilibrium with the textile and V = specific volume of vapour at this vapour pressure.

But relative humidity = $H = (p/p_s \times 100)\%$. Thus

$$\log_e H = \log_e p - \log_e p_s + \log_e 100 \quad (8.7)$$

Differentiating with respect to temperature at constant regain, we have:

$$\begin{aligned} \left(\frac{\partial \log_e H}{\partial T} \right)_r &= \frac{1}{p} \left(\frac{\partial p}{\partial T} \right)_r - \frac{1}{p_s} \left(\frac{dp_s}{dT} \right) \\ &= \frac{Q_v}{pTV} - \frac{L}{p_s TV_s} \end{aligned} \quad (8.8)$$

If we assume the ideal gas laws, $pV = p_s V_s = RT$, this gives:

$$\left(\frac{\partial \log_e H}{\partial T} \right)_r = \frac{1}{RT^2} (Q_v - L) = \left(\frac{1}{RT^2} \right) Q_1 \quad (8.9)$$

$$Q_1 = RT^2 \left(\frac{\partial \log_e H}{\partial T} \right)_r = -R \left[\frac{\partial \log_e H}{\partial (1/T)} \right]_r \quad (8.10)$$

Thus the differential heat of sorption can be obtained from the slope of the curve of $\log_e H$ against $1/T$ at constant regain. This relation, based on thermodynamics, only holds when one is dealing with a system in effective thermodynamic equilibrium. The results in Fig. 7.11 (see p. 191), which show that at high humidities, moisture regain increases with rise in temperature, so that $(\delta \log_e H / \delta T)_r$ becomes negative though Q_1 remains positive, indicate that this is not always so for textile fibres. Where hysteresis exists, there can only be metastable equilibrium. Different results will be obtained depending on whether absorption or desorption values are used. It has also been pointed out by Rees [1] that the results obtained by this method depend to a great extent on the care with which the curves are drawn, and different workers calculate widely different results from the same data.

8.3 Results

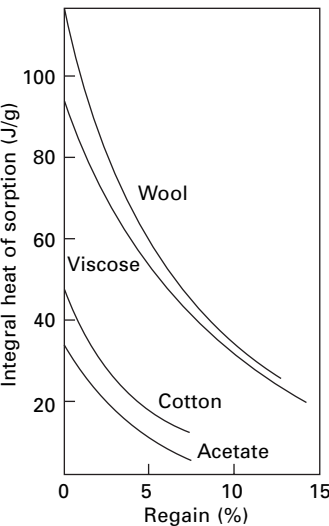
Table 8.1 shows values of the heat of wetting of dry fibres, and Fig. 8.3 indicates how the heats of wetting decrease to zero at saturation regain. As would be expected, the heat of wetting is greatest for the most highly absorbing fibres and is very small in the non-hygroscopic fibres. Figure 8.4 shows that the heat evolved in going from 0% to 65% r.h. is proportional to the regain of the fibre at 65% r.h. Plotting these particular values eliminates the effect of loosely held water near saturation, which contributes little to the heat evolved.

Bright *et al.* [3] found that, for three specimens of polyester fibre of the same draw-ratio but different linear density, the heat of wetting was proportional to the external surface area, a value of $16 \times 10^{-4} \text{ J/cm}^2$ being obtained.

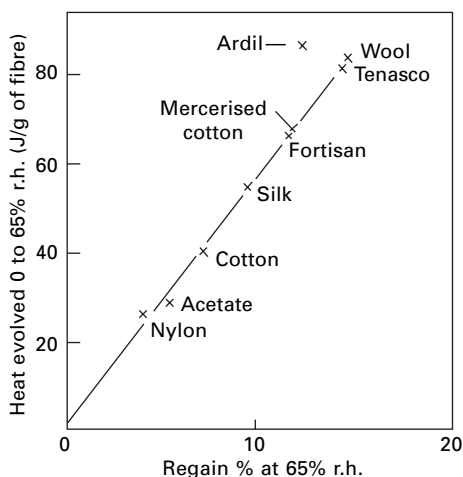
Figure 8.5 shows the decrease in the differential heat of sorption as the regain increases. At zero regain, the differential heat of sorption of the cellulosic fibres is of

Table 8.1 Heats of wetting from zero regain W_0 (J/g)

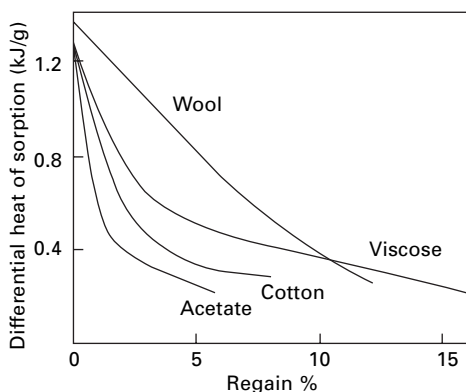
Cotton [1]	46
Mercerised cotton [1]	73
Flax [2]	55
Viscose rayon [2]	106
Secondary acetate [2]	34
Wool [3]	113
Silk [4]	69
Nylon [3]	31
Polyester (PET) 2.4 dtex [3]	5
Acrylic (PAN) [3]	7



8.3 Variation of integral heats of sorption of cotton, viscose rayon, secondary acetate [2] and wool [3] with regain.



8.4 Relation between evolution of heat and regain [5].



8.5 Variation of differential heats of sorption of cotton, viscose rayon, secondary acetate [2] and wool [3] with regain.

the order of 1250 J/g, which is about the same as the heat of hydration of hydroxyl ions. As absorption continues, the water is more loosely attached, and consequently less heat is evolved. Owing to the similarity in the nature of the absorption, all cellulosic fibres have differential heats of sorption that are close together at a given relative humidity. This is shown by the results in Table 8.2, which also includes values for other fibres. Wool and nylon have values that are close together, which indicates absorption on similar sites. The results given in Table 8.2 are typical values; there will be slight variations from these according to the particular specimen tested, as shown in Table 8.3.

Values of the differential heat of sorption found by calculation from sorption isotherms are usually somewhat lower than those obtained by direct measurement. Some examples of this are given in Table 8.4.

The values of the differential heat of sorption given here have been for absorption

Table 8.2 Differential heats of sorption Q_i (kJ/g)

Fibre	Relative humidity (%)					
	0	15	30	45	60	75
Cotton [2]	1.24	0.50	0.39	0.32	0.29	–
Mercerised cotton [1]	1.17	0.61	0.44	0.33	0.23	–
Viscose rayon [2]	1.17	0.55	0.46	0.39	0.32	0.24
Secondary acetate [2]	1.24	0.56	0.38	0.31	0.24	–
Wool [3]	1.34	0.75	0.55	0.42	–	–
Nylon [6]	1.05	0.75	0.55	0.42	–	–

Table 8.3 Integral and differential heats of sorption

Fibre	At zero regain		At 65% r.h.
	W (kJ/g)	Q_i (kJ/g)	Q_i (kJ/g)
Cotton			
Bengals [2]	47.3	1.33	0.25
Texas [1]	46.1	1.19	0.20
Sea Island [2]	46.9	1.24	0.28
various sorts and methods [1, 7]	41–54	–	–
Viscose rayon			
continuous filament [2]	106	1.17	0.30
staple fibre [2]	97	1.22	0.27
various sorts and methods [1, 7]	84–105	–	–

Table 8.4 Direct and calculated differential heats of sorption

Material	Regain (%)	Differential heat of sorption (kJ/g)	
		Calorimetric method	From sorption isotherms
Viscose rayon [2]	0	1.17	1.09 [8]
	5	0.53	0.44
	10	0.39	0.25
Acetate [2]	5	0.27	0.21
Cotton [1]	5	0.32	0.27
Wool [9]	6	0.59	0.54
	12	0.40	0.40
	18	0.17	0.26

Table 8.5 Heat evolved (in kJ) by 1 kg of material in going from 40 to 70% r.h.

Wool	159
Cotton	84
Viscose rayon	168
Acetate	50
Nylon	42
Terylene	4

from the liquid. Values for absorption from the vapour can be obtained by adding the latent heat of vaporisation of water (2.45 kJ/g at 20 °C). This is several times as great as most values of differential heat of sorption from liquid, and its addition reduces the proportional difference between the various fibres. At low humidities, the differential heat of sorption from the vapour will be about 4000 J/g, but, over the middle range of humidities, it will lie between 2500 and 3000 J/g, depending on the particular fibre and humidity.

8.4 Effects of evolution of heat

The evolution of heat has a considerable effect on the rate of conditioning of textile materials, as will be described in the next chapter. It is also an important feature of clothing materials. For example, on going from an atmosphere of 18 °C, 45% r.h., indoors to one of 5 °C, 95% r.h., outdoors, the regain of wool would change from 10 to 27%. A man's suit, weighing 1.5 kg, would give out 6000 kJ owing to this change, that is, as much heat as the body metabolism produces in 12 h. This evolution of heat is of physiological advantage, since it gives the body time to adjust itself to the new conditions. The greater the moisture absorption of the fibre, the greater will be the amount of heat evolved. Comparative values are given in [Table 8.5](#).

8.5 References

1. W. H. Rees. *J. Text. Inst.*, 1948, **39**, T351.
2. J. C. Guthrie. *J. Text. Inst.*, 1949, **40**, T489.
3. N. F. H. Bright, T. Carson and G. M. Duff. *J. Text. Inst.*, 1953, **44**, T587.
4. J. J. Hedges. *Trans. Faraday Soc.*, 1926, **22**, 178.
5. R. Meredith. In *Fibre Science* J. M. Preston (Editor), The Textile Institute, Manchester, 1953, p. 243.
6. J. B. Speakman and A. K. Saville. *J. Text. Inst.*, 1946, **37**, P271.
7. P. H. Hermans. *Contributions to the Physics of Cellulose Fibres*, Elsevier, Amsterdam, Netherlands, 1946, p. 35.
8. J. B. Taylor. *J. Text. Inst.*, 1952, **43**, T489.
9. P. Alexander and R. F. Hudson. *Wool: Its Chemistry and Physics*, Chapman & Hall, London, 2nd edition (revised by C. Earland), 1963, p. 116.

9.1 Introduction

Textile materials take a long time to come into equilibrium with their surroundings. The drying of washing is a simple example of this and shows that the rate depends on a variety of factors: temperature, air humidity, wind velocity, surrounding space, thickness of material, density of material, nature of the fibre, and so on. The slowness of conditioning may be a nuisance technically, since textiles often have to be conditioned before further processing or sale. On the other hand, a slow process may act as a valuable stabilising influence, for example absorbent fibrous materials in a room will prevent rapid changes of humidity or temperature.

In this chapter, we shall be considering the factors that play a part in the change of conditions in textile materials. To avoid the tedious repetition of alternatives, it will usually be written on the assumption that the material is *taking up* water. In general, drying follows the reverse procedure.

9.2 Diffusion of moisture

9.2.1 The diffusion equation and its solution

The most obvious way of explaining the slowness of conditioning is to assume that it is due to the slowness with which water molecules diffuse through the fibre and through the air to the fibre.

If the concentration of water molecules (or of any other substance with which one is concerned) varies from place to place in a given medium (e.g. air or fibre substance), the molecules will diffuse from regions of high concentration to regions of low concentration until their distribution becomes uniform. The rate of transport, dm/dt , of the diffusing substance across an area A of a plane perpendicular to the concentration gradient $\partial c/\partial x$ is given by Fick's equation:

$$\frac{dm}{dt} = -DA \frac{\partial c}{\partial x} \quad (9.1)$$

where D is called the diffusion coefficient.

From this equation, we can derive a differential equation giving the relation between concentration, position and time. If we consider an element of unit area and of

thickness dx , as shown in Fig. 9.1, then in a time dt the mass diffusing across the left-hand face into the element is $[-D(\partial c/\partial x) dt]$, and the mass diffusing out of the element across the right-hand face is

$$\left[- \left\{ D \frac{\partial c}{\partial x} + \frac{\partial}{\partial x} \left(D \frac{\partial c}{\partial x} \right) dx \right\} dt \right]$$

The difference in these two amounts gives the increase of mass of the diffusing substance in the element, that is, the change of concentration multiplied by the volume of the element. Hence:

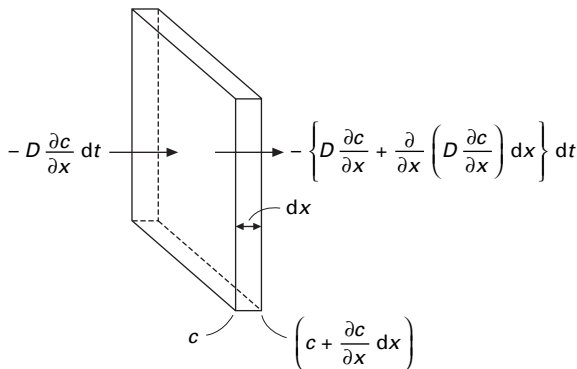
$$\begin{aligned} \frac{\partial c}{\partial t} dt \cdot dx &= -D \frac{\partial c}{\partial x} dt + \left[D \frac{\partial c}{\partial x} + \frac{\partial}{\partial x} \left(D \frac{\partial c}{\partial x} \right) dx \right] dt \\ \frac{\partial c}{\partial t} &= \frac{\partial}{\partial x} \left(D \frac{\partial c}{\partial x} \right) \end{aligned} \quad (9.2)$$

This is the diffusion equation in one dimension. It may be generalised to apply to three dimensions. In the simplest, and fairly common, case, the diffusion coefficient D is constant, and the equation becomes:

$$\frac{\partial c}{\partial t} = D \frac{\partial^2 c}{\partial x^2} \quad (9.3)$$

This equation can be solved for appropriate initial and boundary conditions, but the solutions are of a complexity beyond the scope of this book. They have been discussed in detail for many systems by Crank [1].

In more complicated systems, such as fibres, the diffusion coefficient may vary with concentration. Equation (9.2) cannot then be solved analytically unless some relation between D and c can be substituted in it. Other complications arise when absorption takes place, because this removes molecules from the diffusion process. If there is swelling, the medium is moving as well as the diffusing substance. Crank [1] discusses ways of dealing mathematically with these problems.



9.1 Diffusion across unit area perpendicular to concentration gradient.

However, avoiding the mathematical complexity of exact solutions, we can often obtain useful approximate results by simpler methods. A special case of the equation gives the effect of diffusion from an infinite source of concentration c_0 to a receiver whose mean concentration is c at a time t . This is illustrated in Fig. 9.2. Under these conditions, we have:

$$\frac{dc}{dt} \propto \frac{dm}{dt} \propto \left(-\frac{dc}{dx} \right) \propto [-(c - c_0)]$$

$$\frac{dc}{c - c_0} = \frac{dt}{\tau} \quad (9.4)$$

where τ is a time constant.

On integrating, and assuming as initial conditions that $c = 0$ at $t = 0$, this gives:

$$-\log(c_0 - c) = \frac{t}{\tau} - \log c_0 \quad (9.5)$$

which leads to

$$c = c_0(1 - e^{-t/\tau}) \quad (9.6)$$

At $t = \tau$, we have

$$c = c_0 \left(1 - \frac{1}{e} \right) \quad (9.7)$$

and thus τ is the time taken for 63% of the total change to be completed, as shown in Fig. 9.3.

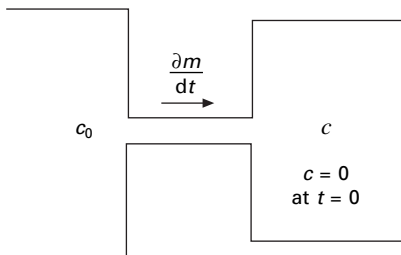
Differentiating Equation (9.6), we have:

$$\frac{dc}{dt} = \frac{c_0}{\tau} e^{-t/\tau} \quad (9.8)$$

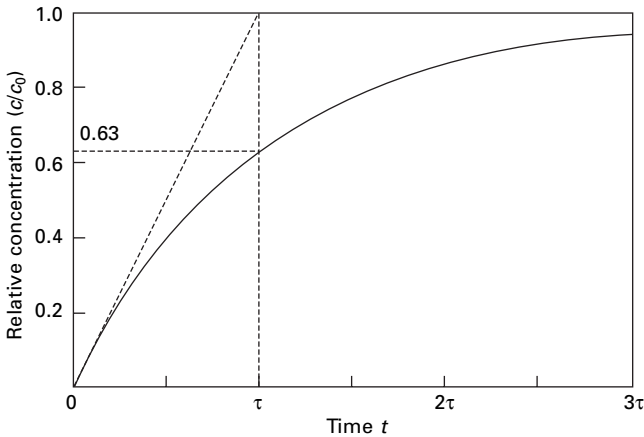
At $t = 0$ this becomes:

$$\frac{dc}{dt} = \frac{c_0}{\tau} \quad (9.9)$$

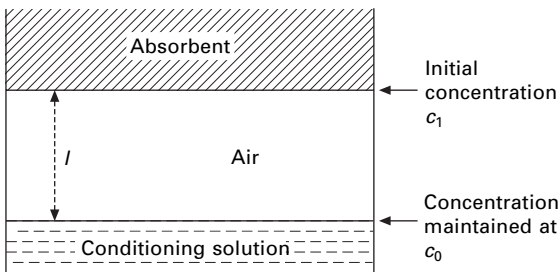
and thus it follows that τ is also the time that the whole process would take if carried out at the initial rate.



9.2 Diffusion into a receiver from an infinite source of concentration c_0 .



9.3 Change of relative concentration c/c_0 in receiver, following diffusion from an infinite source of concentration c_0 . The parameter τ is a time constant depending on the particular diffusion conditions.



9.4 Diffusion across an air space to an absorbent.

If we consider the system shown in Fig. 9.4, where moisture is diffusing across a length l of air to the absorbing substance, we see that time for whole process at initial rate

$$\tau = \frac{M}{dm/dt}$$

mass needed to bring the absorbent into equilibrium. Applying equation (9.1), this becomes:

$$\tau = \frac{Ml}{D(c_0 - c_1)A} \quad (9.10)$$

where c_1 = initial concentration at surface of absorbent and c_0 = concentration at surface of conditioning solution.

For a homogeneous cylinder of length L and radius r in which there is a change of conditions at the surface, such as to cause a change in the equilibrium concentration in the cylinder from c_1 to c_0 , the mass absorbed will be given by the product of the volume of the cylinder and the change in concentration and the diffusion length is of

the order of the radius r . We can apply equation (9.10) to obtain the order of magnitude of τ .

$$\tau \approx \frac{\pi r^2 L (c_0 - c_1) r}{D (c_0 - c_1) 2 \pi r L} \approx \frac{r^2}{2D} \quad (9.11)$$

This is one example of a general result, suggested by dimensional analysis, that in a single medium the order of magnitude of time involved in a diffusion process equals l^2/D , where l is the length along which diffusion has to take place.

9.2.2 Diffusion coefficients of fibre materials

Application of the theory of diffusion would enable one to work out diffusion coefficients in fibres from observations of the rate of uptake of water or of the movement of water into a fibre. However, a much simpler method may be applied when the same materials can be obtained in the form of thin films. Constant concentrations may then be maintained on either side of the film, and the rate of transport of water across the film may be measured when a steady state has been reached.

In a typical experimental arrangement, shown in Fig. 9.5, water vapour is continually pumped away from one side so that $c = 0$, and the other side is maintained at a constant value c_1 . By repeating this for various values of c , one can obtain a series of values of the average diffusion coefficient over ranges from 0 to c_1 . Since the system is in a steady state, the rate of flow dm/dt across unit area is independent of x , the position in the film, and we must therefore have:

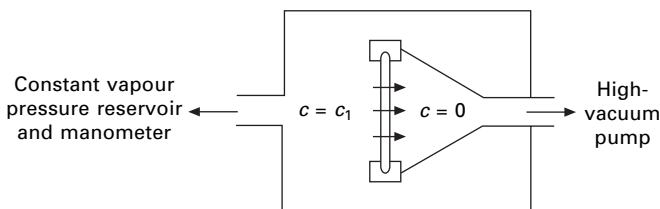
$$\int_0^l \frac{dm}{dt} dx = \frac{dm}{dt} \int_0^l dx = l \frac{dm}{dt} \quad (9.12)$$

Substituting from Equation (9.1), we then obtain:

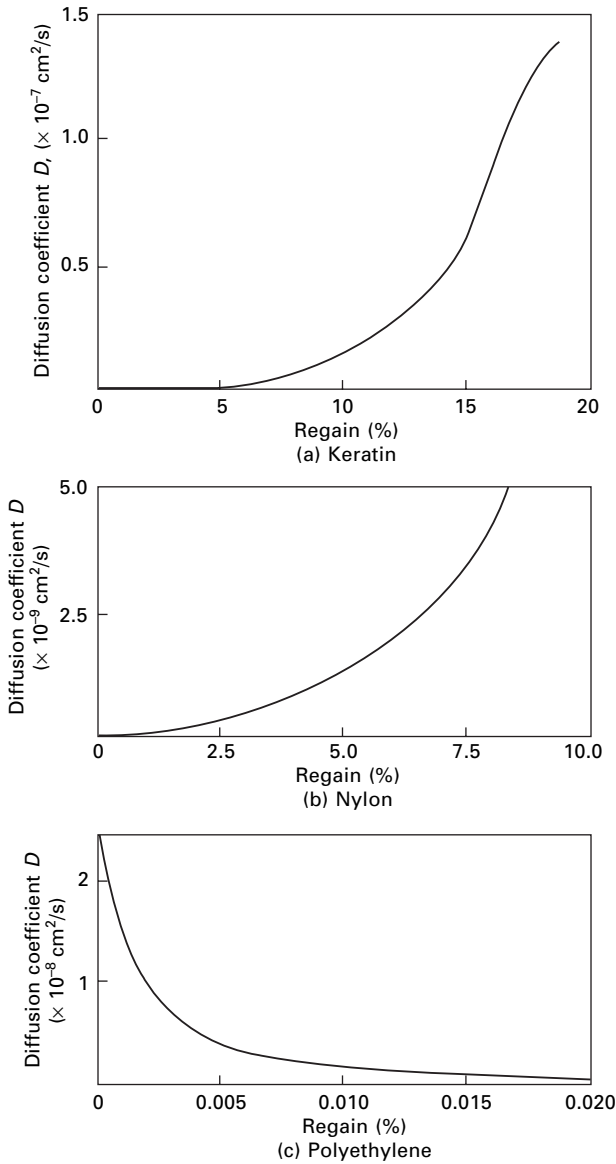
$$\frac{dm}{dt} = \frac{1}{l} \int_0^l -D \frac{dc}{dx} dx = -\frac{1}{l} \int_0^l -D dc \quad (9.13)$$

By a numerical process of successive approximations, the experimental results giving values of dm/dt for various values of c_1 may be fitted to this equation, and the diffusion coefficients at the various concentrations may be determined.

Some results of measurements of this sort are given in Fig. 9.6. The wide range of values, from 10^{-7} to less than 10^{-9} cm²/s, should be noted. Diffusion is very slow in the dry state, but it becomes much more rapid at moderate or high regains. This



9.5 Flow through a thin film under steady conditions.



9.6 Variation of diffusion coefficients with regain: (a) keratin, after King [2]; (b) nylon, after Rouse [3]; (c) polyethylene, after Rouse [3]. Note differences in scales, especially different powers of 10 in values of D .

explains the extreme difficulty of removing the last traces of water from a fibre. An exception to this behaviour is polyethylene, which absorbs little water and in which diffusion becomes slower at higher regains.

From studies on the initial rate of absorption by fibres, Watt [4] and Mackay and Downes [5] report values of about $2 \times 10^{-10} \text{ cm}^2/\text{s}$ for dry wool, and values in agreement with those shown in Fig. 9.6(a) for wool at higher regains.

Fukuda and Kawai [6] measured the rate of diffusion of water into para-aramid fibres by following the rate of uptake of water in by 200 mg of yarn. Values of diffusion coefficients are shown in Table 9.1.

9.2.3 Penetration into a dry fibre

Because the diffusion coefficient increases so rapidly with increasing concentration of water in fibres, it follows that the variation in moisture content through a fibre that is absorbing water will show a sharp boundary. The initial diffusion through the dry fibre is slow and determines the position of the advancing front, but, once some absorption has occurred, the diffusion becomes faster, and so one has a rapid build-up to the final value of the moisture content.

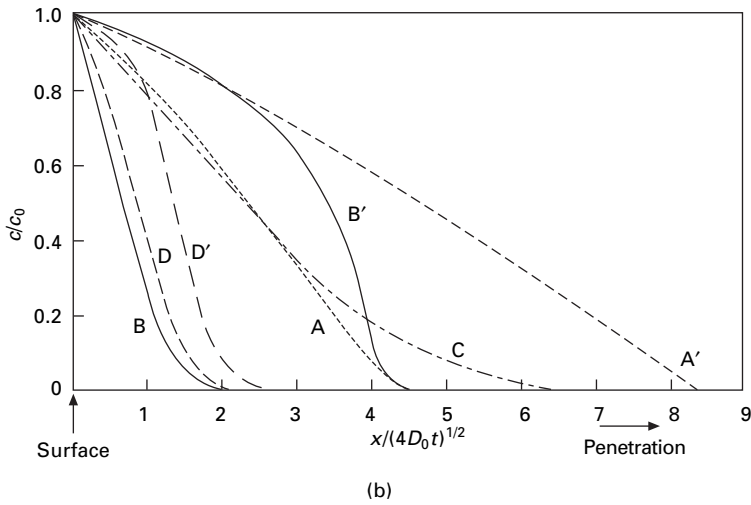
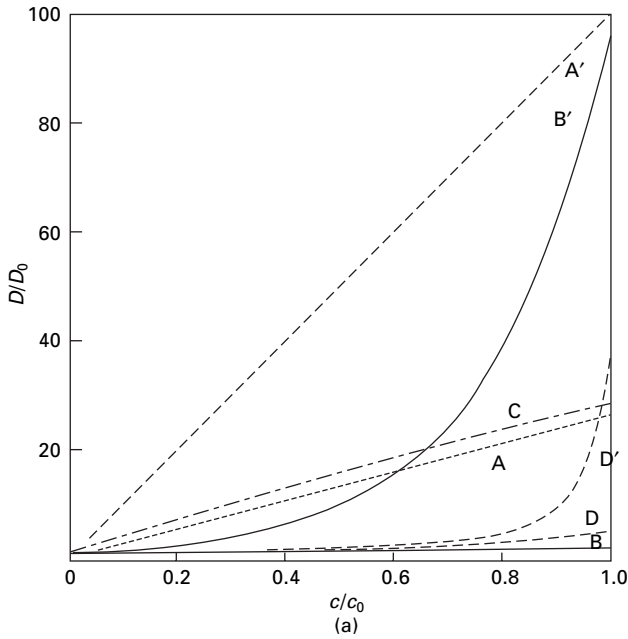
Crank [1] has calculated the variation of concentration with distance for diffusion coefficients related in various ways to the concentration. Examples with differing degrees of sharpness of the advancing front are shown in Fig. 9.7.

Hermans and Vermaas [7] have shown that this advancing front may be observed in thick filaments under the microscope because of the change in refractive index associated with it. Photographs of this effect are shown in Fig. 9.8. Observation of this rate of advance of the boundary is another method of determining the diffusion coefficient in fibres.

There is another effect that may slow down the approach to the final equilibrium moisture absorption. When water is absorbed by the fibre, swelling stresses are set up. Newns [8] has suggested that after the initial diffusion process, there is a second stage in which these stresses relax (see Section 16.3). This relaxation of stress in the fibres will, in effect, alter the equilibrium moisture condition towards which the diffusion is proceeding. It will thus delay the attainment of a final steady state.

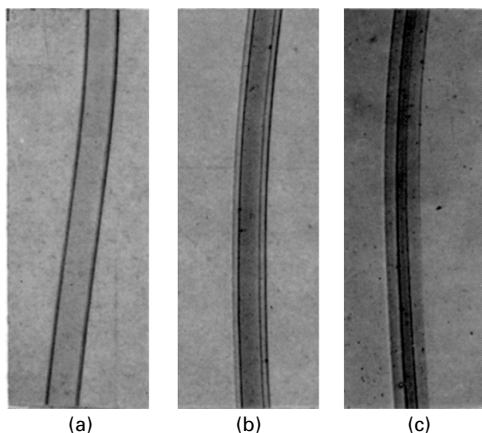
Table 9.1 Diffusion coefficients of para-aramid fibres. From Fukuda and Kawai [6]

Fibre	p/p_s	D_{skin} ($\text{cm}^2/\text{s} \times 10^{-12}$)	D_{core} ($\text{cm}^2/\text{s} \times 10^{-12}$)
Regular Kevlar	0.140	2.38	3.56
	0.213	3.97	5.96
	0.303	4.10	6.15
	0.482	5.01	10.0
	0.668	5.40	21.6
	0.896	6.51	26.0
Kevlar 49	0.144	1.39	2.77
	0.264	1.45	2.90
	0.396	1.36	5.42
	0.652	1.54	6.18
	0.800	1.76	12.4
Kevlar 149	0.343	2.52	1.61
	0.464	3.15	2.02
	0.583	4.03	2.62
	0.825	6.18	2.61
	0.934	—	—



9.7 (a) Relations between diffusion coefficients, D and D_0 , and concentrations, c and c_0 . (b) Concentration-distance curves for penetration into materials with different relations between diffusion coefficient and concentration. D = diffusion coefficient at concentration c , D_0 = diffusion coefficient at concentration c_0 , x = distance into material, t = time. After Crank [1].

Relation between D and c	Ratio of D at $c = c_0$ to D at $c = 0$	
$D/D_0 = 1 + ac/c_0$	A: 26	A': 101
$D/D_0 = \exp(kc/c_0)$	B: 2	B': 95
$D/D_0 = 1 + 50 \log_e(1 + kc/c_0)$	C: 28	
$D/D_0 = 1/(1 - \alpha c/c_0)$	D: 5	D': 50



9.8 Micrographs showing boundary gradually penetrating into filament. After Hermans and Vermaas [7].

Newns has derived a mathematical analysis for a process in which diffusion and stress relaxation are coupled together.

9.2.4 Conditioning of a mass of fibres

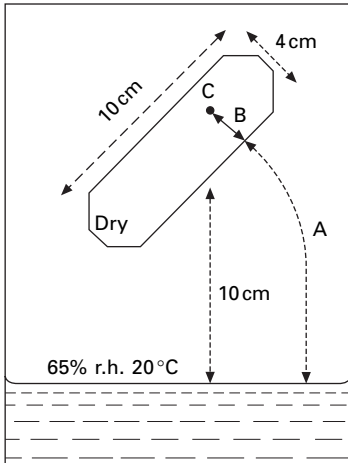
During the conditioning of a mass of fibres, diffusion must take place in three stages. First, there will be diffusion (or convection) in the air from the source of water vapour to the surface of the mass of fibres. Secondly, there will be diffusion in the air in the interstices between fibres, from the surface of the mass to the surface of a fibre. Thirdly, there will be diffusion from the surface of a fibre to its interior.

A value of $10^{-7} \text{ cm}^2/\text{s}$ may be taken for the diffusion coefficient within a hygroscopic fibre at medium humidities and, with a fibre radius of 10^{-3} cm , equation (9.11) would give $\tau = (10^{-3})^2 / (2 \times 10^{-7}) = 5$ seconds.

The time taken for diffusion in the air, whether inside or outside the specimen, will depend on the size, shape and density of the specimen; that for the diffusion outside will also depend on the ease of access to a source of moisture. The result for diffusion outside the specimen is calculated here for a typical case illustrated in Fig. 9.9. Suppose we have 100 g of dry cotton in a package 10 cm long and 2 cm in radius, placed in a close container, 10 cm from a solution giving a relative humidity of 65% at its surface, that is, a concentration of water vapour of 10^{-5} g/cm^3 at 20°C . The mass of water to be absorbed for equilibrium is about 7 g. In still air at 20°C , D is about $0.25 \text{ cm}^2/\text{s}$. The area across which diffusion is occurring varies with the distance from the package, but we may take as the approximate area the surface of a sphere of radius 10 cm, that is, $400\pi \text{ cm}^2$. Applying equation (9.10), we then have:

$$\tau = \frac{7 \times 10}{0.25 \times 10^{-5} \times 400\pi} = 20 \times 10^3 \text{ s (5 hours)}$$

It is difficult to calculate the time taken for diffusion in the air within the specimen,



9.9 Diffusion into a mass of fibres in three stages: A, in outside air; B, in air spaces between fibres; C, within the fibre.

but, since the area and length are both less than they are outside, we should expect the times to be of the same order of magnitude.

The two effects would take place to some extent concurrently. We note that the times for diffusion in the air are much greater than the time for diffusion in a fibre. The latter is very rapid because of the small diameter of a fibre. Consequently, in calculations concerning a mass of fibres, the individual fibres may usually be taken to be in equilibrium with the air at their surfaces; this also applies in the more complicated mechanism discussed later.

9.2.5 Comparison with experimental results

From the considerations discussed above, diffusion times can be estimated. These are found to be much shorter than the times needed in practice for conditioning specimens. For example, Clayton and Peirce [9] report that 90% of the total change in a single cotton hair takes about 32 minutes, and not 5 seconds as the diffusion calculation indicates; Roberts and Haly [10] obtained values of about 1 minute for single wool fibres. A cop takes about 5 days, compared with the value of 5 hours calculated above; a bale, in which diffusion calculations indicate a few weeks, takes years.

It is thus clear that other factors, besides the diffusion of moisture, are involved. The heat that is evolved when the fibres absorb water, and which must be dissipated during conditioning, plays a dominant role in fibre assemblies.

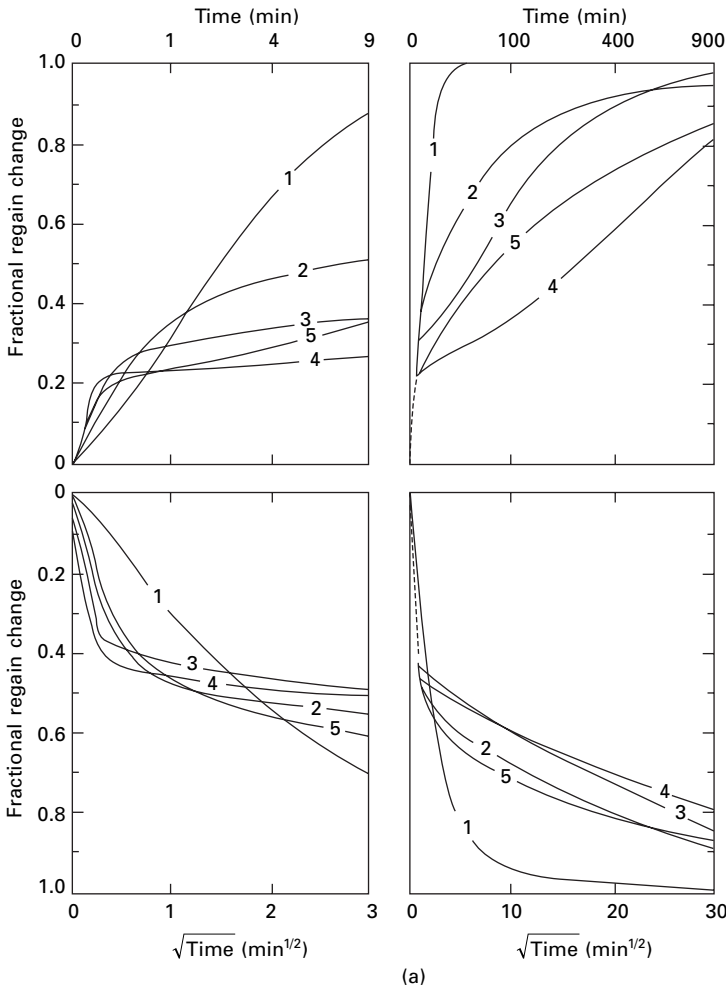
However, in single fibres, there may be delays due to other causes. Mackay and Downes [5], using a vibroscope system, found very slow rates of change of regain in single wool fibres under conditions of forced convection, where the temperature changes due to heat of sorption were believed to be small. They investigated a variety of steps in both absorption and desorption. Some typical results are shown in Fig. 9.10. In many circumstances, there was an initial rapid change, followed by a slower change: the first stage is slowed down by an increase in fibre thickness, but the

second-stage rate is unaffected, which suggests that it is not controlled by diffusion but is a structural relaxation. The length changes of fibres as the absorption proceeds are complicated, and this also indicates structural changes.

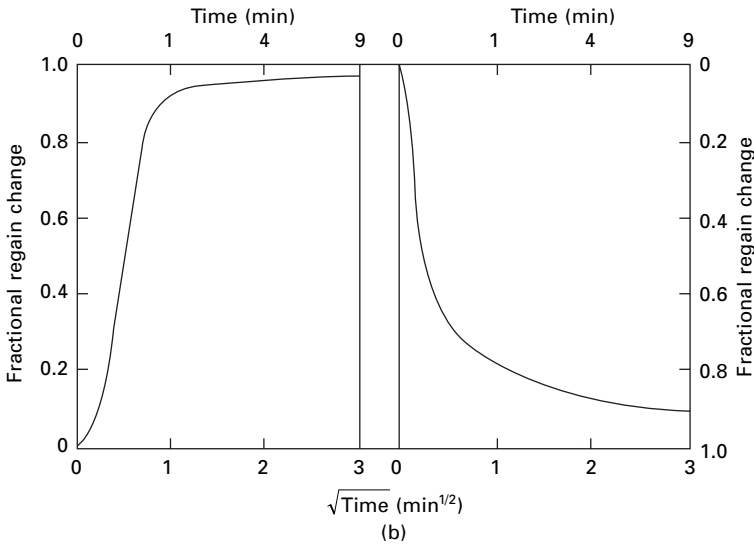
9.3 The interaction of moisture and heat

9.3.1 The conditioning process

When textile fibres absorb moisture, they generate heat, as was described in [Chapter 8](#). The evolution of heat raises the temperature of the fibres and increases their water



9.10 Examples of the rate of absorption and desorption of a 16.9 μm diameter merino wool fibre at 20 °C from the studies of Mackay and Downes [5]. (a) Small changes (about 2% regain) in steps between the following values of r.h. %: (1) 0 and 12; (2) 23 and 35; (3) 46 and 58; (4) 68 and 74; (5) 95.0 and 96.4. (b) Changes between 0 and 100% r.h. (on facing page)



9.10 (Continued)

vapour pressure, consequently reducing the vapour pressure gradient and slowing down the rate of absorption.

The nature of the changes occurring during conditioning may be seen in the diagrams (Fig. 9.11). Owing to the higher vapour pressure in the atmosphere at the start of the process, moisture will pass into the specimen, which gives an increase in regain, generation of heat and a rise in temperature. The vapour pressure of the fibres will therefore increase, partly because of the increased regain but to a greater extent because of the rise in temperature. This process will continue until the vapour pressure of the fibres has become almost equal to that outside. This is a state of transient equilibrium in which further absorption is impossible until heat has been lost by the specimen. As heat is lost to the surrounding atmosphere, the temperature decreases, which allows a further increase in regain to occur and maintains the vapour pressure close to that of the atmosphere. This continues until final equilibrium is reached with both temperature and vapour pressure equal in fibre and atmosphere. It must be remembered that, throughout this cooling process, the absorption that occurs is generating heat which must also be lost to the surroundings.

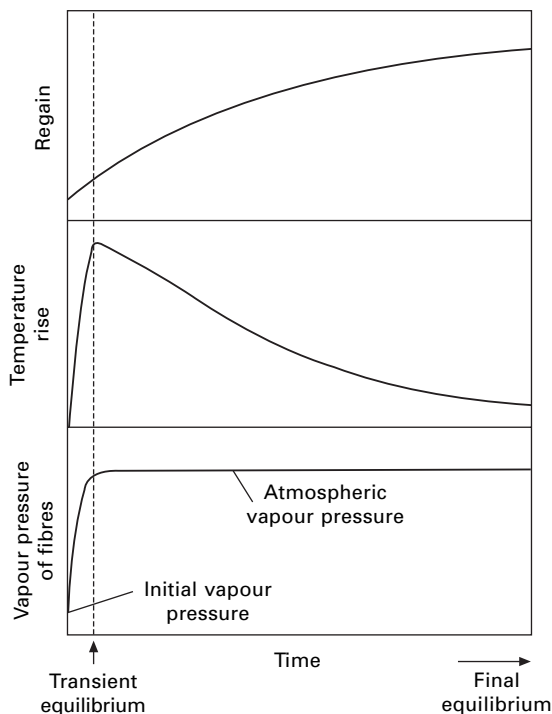
For a change of regain ΔR in a specimen of 100 g dry weight, the heat evolved will be $Q_v \Delta R$, where Q_v is the differential heat of sorption, and hence, if no heat is lost to the surroundings, we must have:

$$Q_v \Delta R = (100 + R) (\Delta T) C$$

$$\frac{\Delta T}{\Delta R} = \frac{Q_v}{(100 + R) C} \quad (9.14)$$

where ΔT = rise in temperature and C = specific heat.

This equation governs the change of temperature during the approach to transient



9.11 Changes in regain, temperature and vapour pressure during conditioning.

equilibrium. We may use it to calculate the position of transient equilibrium in a particular case on the assumption that no heat is lost during the initial stage.

Suppose 100 g of cotton are taken from an atmosphere of 28% r.h., 20 °C, in which the cotton would have an equilibrium regain of 3.7%, to an atmosphere of 70% r.h., 20 °C, giving an equilibrium regain of 7.7%. Trials with different final regains show that transient equilibrium occurs at a regain of 4.3%, as confirmed by the following calculation. The saturation vapour pressure at 20 °C is 17.5 mm of mercury. At 70% r.h., the vapour pressure is $0.7 \times 17.5 = 12.25$ mm. The rise in temperature for an increase of 0.6% in regain is given by the above equation:

$$\Delta T = \frac{2600}{104 \times 1.45} \times 0.6 = 10.3 \text{ }^{\circ}\text{C}$$

The temperature is therefore 30.3 °C, for which the saturation vapour pressure is 31.8 mm. Experimental data show that the relative humidity corresponding to 4.3% regain at 30.3 °C is 38.6%, and thus the vapour pressure over the specimen is $0.318 \times 38.6 = 12.27$ mm. Thus the vapour pressure over the specimen equals that in the conditioning atmosphere and there is transient equilibrium at 4.3% regain at 30.3 °C. Final equilibrium involves a rise in the regain to 7.7%.

The calculation shows that transient equilibrium results from only a small change of regain. Its attainment is thus a comparatively rapid process, and the main factor in determining the time for the whole process is the rate at which the heat being generated

by the absorption can be dissipated. The lower rise in temperature given later in Fig. 9.16 indicates that the above rise in temperature is a maximum value on the assumption that the heat is generated throughout the fibre mass with no external heat loss.

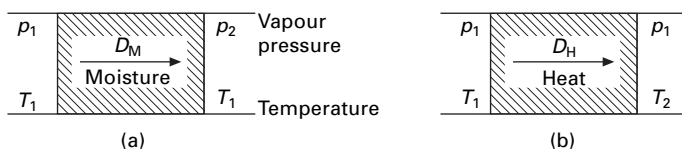
Heat transfer by conduction follows the same law as diffusion, with heat replacing mass, temperature replacing concentration, and thermal capacity replacing volume in the equations. The heat diffusion constant is the thermal conductivity divided by the specific heat per unit volume. The changes thus follow the diffusion equations, already discussed, but with the complications arising from the interaction of two diffusion processes, which are discussed in the next section. One result of this is that final equilibrium is delayed.

Experiments on clumps of wool by King and Cassie [11] and Watt and McMahon [12] confirmed the above behaviour.

9.3.2 Penetration of a change into a mass of fibres

Heat effects and moisture absorption in hygroscopic materials, such as fibres, are inseparably interrelated: it is impossible to change one without affecting the other, and final equilibrium is impossible in one without the other. A complete description of changing conditions requires both the diffusion of moisture and the conduction of heat to be taken into account. Both are transfer phenomena following differential equations of the same form but with different constants, and they are linked by the heat of absorption and the change of moisture content with temperature at constant absolute humidity. Henry [13] carried out a mathematical analysis of the system for a simplified linearised model. Other studies, taking advantage of advances in computation, have treated more realistic models [14]. The general conclusion of the analysis is that, when a mass of fibres is exposed to new conditions, the change passes through the mass in two waves of diffusion, with different diffusion constants, D_1 and D_2 . To the parts of the change associated with each wave, we may apply the methods discussed in Section 9.2.1, the appropriate diffusion constant being used.

By steady-state methods, in which constant conditions are maintained on either side of the material, as in Fig. 9.12, the diffusion coefficient, D_M , for moisture in a system involving no temperature changes and the diffusion coefficient, D_H , for heat in a system involving no moisture changes can be found. If the moisture and heat effects were independent of one another or only weakly coupled, then, in a system in which both were changing, each would diffuse independently, and we should have $D_1 = D_M$ and $D_2 = D_H$.



9.12 Steady-state conditions: (a) vapour pressure gradient at constant temperature; (b) temperature gradient at constant vapour pressure.

In most textile systems, however, the coupling between the two is strong, since the heats of absorption are high, and the moisture content changes rapidly with temperature at constant vapour pressure. In Henry's analysis, the strength of the coupling is given by a quantity which he refers to as $(1 - \lambda\nu)$ and which would be one if the two were independent but tends to zero as the coupling becomes stronger. He has shown that, for hygroscopic fibres under most circumstances, it is reasonable to take:

$$(1 - \lambda\nu) = \frac{1}{1 + \frac{Q_v}{C} \left(-\frac{\partial M}{\partial T} \right)_c} \quad (9.15)$$

where Q_v = differential heat of sorption of the vapour in J/g (of water), C = specific heat of the material in J/(gK) of dry material, and $(-\delta M/\delta T)_c$ = rate of decrease of moisture content as temperature increases, the concentration of water vapour remaining constant.

For cotton at room temperature, the values of $(1 - \lambda\nu)$ are as follows:

r.h. (%)	10	30	50	70	90
$(1 - \lambda\nu)$	0.35	0.22	0.15	0.08	0.025

The value of $(1 - \lambda\nu)$ increases slightly as the temperature increases and reaches 0.6 at 110 °C at 10% r.h.

Henry has shown that, when $(1 - \lambda\nu)$ is small compared with 1, as would be the case in many textile applications, the following approximations hold¹:

$$D_1 = \frac{D_M D_H}{D_M + D_H} \quad (9.16)$$

$$D_2 = \frac{D_M + D_H}{1 - \lambda\nu} \quad (9.17)$$

If the two diffusion coefficients D_M and D_H have the same values, it follows that D_1 is equal to half that value; if they are different, D_1 is less than either but tends to equal the lower value as the difference becomes greater. Thus one wave travels through the material at a rate that is slower than would be expected from independent moisture or heat diffusion and may be as slow as half the rate of the slower of the two processes. Since $(1 - \lambda\nu)$ is small, it follows from equation (9.17) that D_2 is large. Consequently, the other wave passes through the material at a rate that is much faster than either of the two independent processes.

Table 9.2 gives values of the diffusion coefficients worked out by Henry for cotton under various conditions. These figures show how the diffusion rates decrease as the humidity increases; increase as the temperature increases; and decrease as the density of packing increases. They show that under some conditions D_M is greater than D_H , but under other conditions this is reversed. The values of D_1 and D_2 are related to them as described above.

¹Henry [15] also gives more exact expressions for the diffusion coefficients and provides nomograms to assist in their calculation.

Table 9.2 Coupled diffusion for cotton assemblies [15]

Density (g/cm ³)	Temperature (°C)	r.h. (%)	Diffusion coefficients $\times 10^{-5}$ cm ² /s				p	n
			D_M	D_H	D_1	D_2		
0.2	70	20	4.5	34	4.1	130	0.094	0.0037
		65	3.1	12	2.5	140	0.192	0.0040
		90	0.93	3.2	0.72	160	0.22	0.0013
	50	65	21	16	9.3	230	0.39	0.041
	80	65	90	20	17	690	0.17	0.11
0.5	20	20	1.4	16	1.3	63	0.050	0.0016
		65	0.92	5.7	0.80	66	0.13	0.0019
		90	0.28	1.5	0.24	62	0.15	0.0006
	50	65	5.7	7.7	3.4	99	0.38	0.023
	80	65	27	9.8	7.4	210	0.24	0.087

In addition to the speed of the two waves, the magnitudes of the changes they carry are also important. Henry has shown that, if f_1 and f_2 are functions of position and time, being the appropriate solutions of the diffusion equation for the particular problem and differing only in their timescale (owing to the different diffusion constants, D_1 and D_2), then, for a change of temperature at the outside of a mass of material without change of vapour pressure:

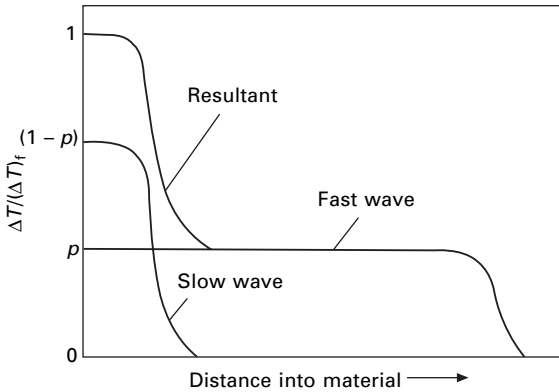
$$\frac{\Delta T}{(\Delta T)_f} = (1 - p)f_1 + pf_2 \quad (9.18)$$

where ΔT is the change in temperature at a given time at a given position in the material, $(\Delta T)_f$ is the final change of temperature and p is the fraction determining the relative magnitudes of the two waves.

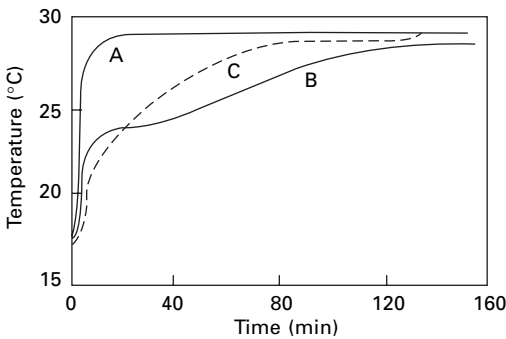
This means that a change of temperature $p(\Delta T)_f$ passes through the material with the velocity of the fast wave, defined by f_2 and D_2 , while the remainder of the change $(1 - p)(\Delta T)_f$ is transmitted with the velocity of the slow wave. The shape of the waves varies with circumstances but is indicated in Fig. 9.13 most of the change takes place over a narrow interval and tails off at a distance from the main wave front. Values of p are given in Table 9.2, and they show that an appreciable proportion of a temperature change may be carried on the fast wave. For a change of humidity at the outside of the material without change of temperature, the vapour concentration, or absolute humidity, in the air over the fibres passes through the specimen according to the same relation with the same value of p .

It is more convenient in following the conditioning process to consider changes ΔM in the moisture content of the material, owing to a change in external circumstances, such as a change in vapour pressure at constant temperature or a change in temperature at constant vapour pressure. The change in moisture content does not follow the same equation as the changes in temperature or vapour concentration but follows approximately the equation:

$$\frac{\Delta M}{(\Delta M)_f} = (1 + n)f_1 - nf_2 \quad (9.19)$$



9.13 Fast and slow waves in diffusion into a material.



9.14 Transmission of temperature change through a cotton cylinder by diffusion. A, outer air temperature; B, observed temperature at centre of cylinder; C, theoretical temperature at centre of cylinder. After Cassie and Baxter [16].

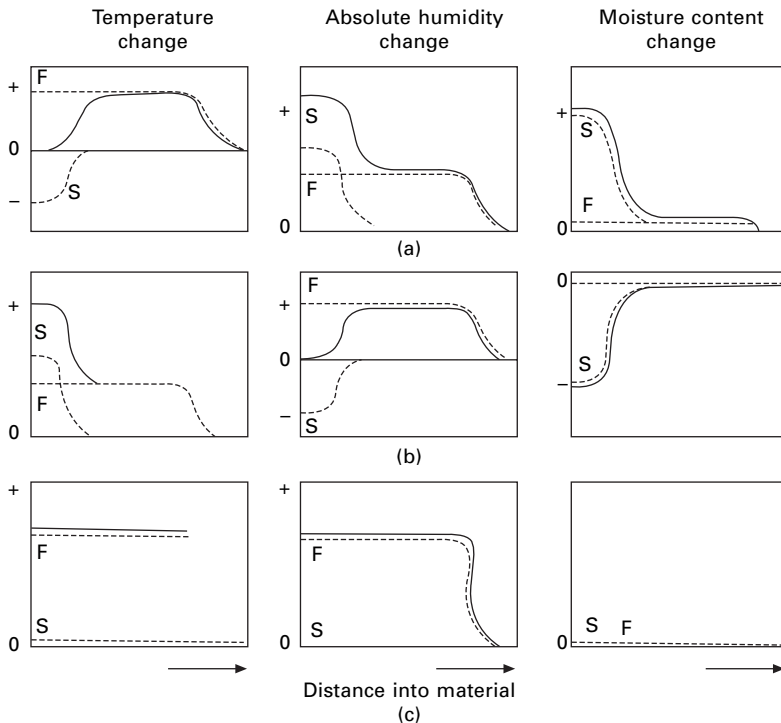
where n is the fraction defining the relative magnitude of the two waves. The negative sign of the fast wave means that it is carrying a change in the opposite direction to the main change. However, values of n are small, as shown in Table 9.2, and the magnitude of the fast wave is less than that of the forward part of the slow wave. Consequently, the resultant disturbance is never negative. Almost the whole change is carried on the slow wave. The effect of the fast wave is to cause a slowing down of the first part of the change in moisture content, but it has little effect on the major part of the change.

Figure 9.14 shows experimental results obtained by Cassie and Baxter [16] for the transmission by diffusion alone of a temperature change through the wall of a cylinder made of cotton of density 0.12 g/cm^3 in a linen cover. The external air was suddenly changed in temperature from 17 to 29°C , without change of vapour pressure. The change in temperature at the inside of the cylinder was measured, and the graph clearly shows the division of the change into two parts corresponding to two waves. The agreement with theory is fairly good, part of the divergence being due to the effect of the linen cover.

To summarise the work of Henry, and Cassie and Baxter, changes of temperature and absolute humidity, transmitted by diffusion through a mass of hygroscopic fibres, are divided roughly equally between fast and slow waves. Even where there are no final changes in temperature or vapour concentration, there may be transient changes transmitted on the fast wave, with the slow wave restoring the original condition. Several examples of the changes, which are of obvious importance in clothing materials, are given in Fig. 9.15. Changes of moisture content are transmitted almost entirely by the slow wave. In fibres that absorb no water, moisture and heat will diffuse independently at their own rates. The water vapour will pass solely through the spaces between the fibres.

9.3.3 Experimental confirmation of a computational model

Approximations in Henry's analysis were reduced in a computational model by Li and Luo [14]. The predictions were verified by experiments on double jersey fabrics



9.15 Changes in temperature, absolute humidity (or vapour pressure) in air in contact with fibres, and moisture content during diffusion, for (a) rise in humidity at constant temperature; (b) rise in temperature at constant absolute humidity; and (c) rise in temperature at constant relative humidity. Dotted lines: F, fast wave; S, slow wave. Full lines: total change. Left-hand end of lines (surface of material) shows final condition. Right-hand end of lines (interior of fibre) shows initial conditions. For falls in humidity and temperature, the curves will be the negative of those shown here.

of wool, cotton, an acrylic with micropores and polypropylene [17]. Fabric samples, 3 cm × 15 cm, were suspended in a cell at 20 °C and the relative humidity was changed in a single step from 0 to 99% with an air-flow of 1.7 m s⁻¹ over the fabric surface. Table 9.3 gives details of the fabrics. For the moisture-absorbing fibres the first and second-stage diffusion coefficients D_1 and D_2 have a complicated non-linear dependence on moisture content M .

Figure 9.16 shows the changes in moisture uptake and temperature. The predictions, based on the arbitrary constants in the expressions for diffusion coefficients, are in good agreement with experimental results. The very small change in the polypropylene fabric takes place rapidly. The changes are increasingly slower and the temperature increases greater with increasing moisture absorption of the materials. Figure 9.17 shows 3D plots of changes through the thickness of the fabric with time. The water vapour pressure quickly reaches a constant equilibrium value through the whole thickness. The trough in the plots of moisture content and the inverted trough for temperature reflect the faster changes at the two fabric surfaces and the slower changes within the fabric.

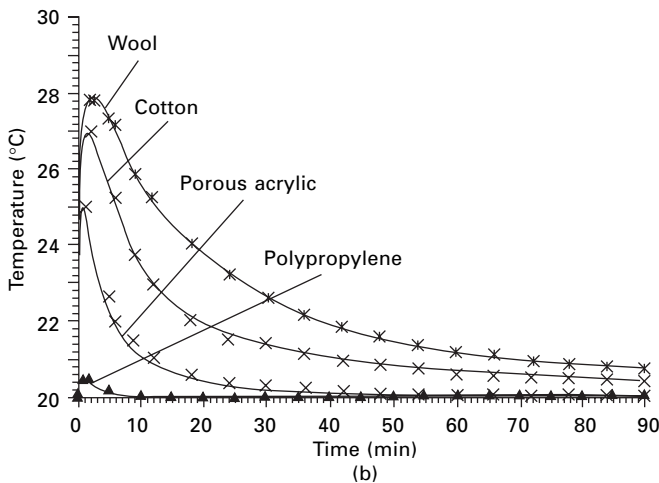
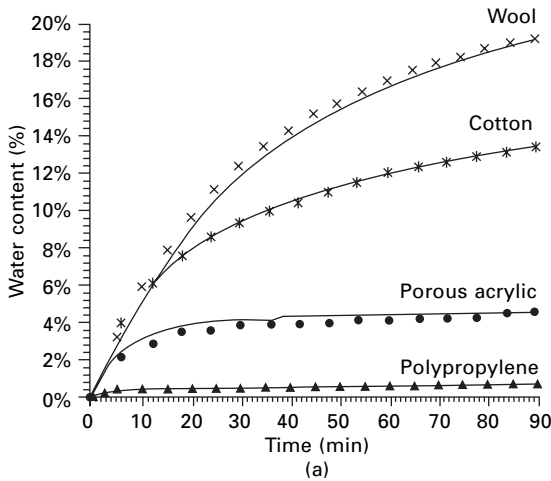
9.3.4 Changes under forced draught

So far we have been considering changes due to diffusion processes, but changes due to blowing air through the material are also of interest. This subject has been studied by Cassie and his coworkers [16, 18, 20] and Daniels [19].

If air is forced through a mass of hygroscopic fibres, theory indicates that the change in conditions will be transmitted in two waves, similar to the two waves found in the diffusion process. The first wave passes through with the same velocity as the air-stream, and the second wave lags behind. If diffusion effects are neglected and it is assumed that the air velocity is constant at all places (which it will not be, owing to variations in the resistance to air-flow), theory shows that the waves should both be sharp changes, as in Fig. 9.18, if there is a sudden change in conditions. In fact, the slow wave is so slow that diffusion is not negligible, and a more exact theory enables its shape to be calculated. As in diffusion, temperature and vapour concentration

Table 9.3 Double jersey fabrics tested by Li and Luo [17]

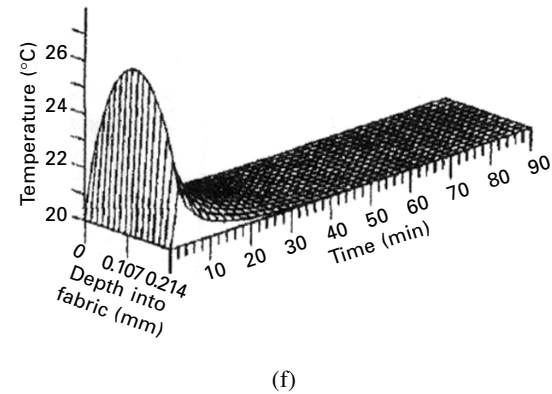
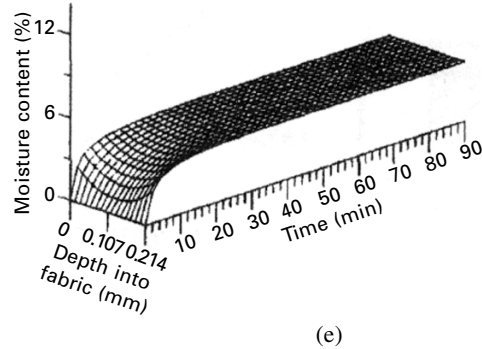
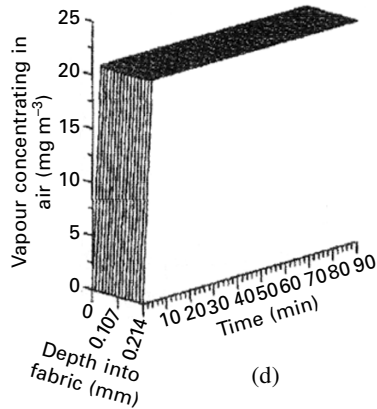
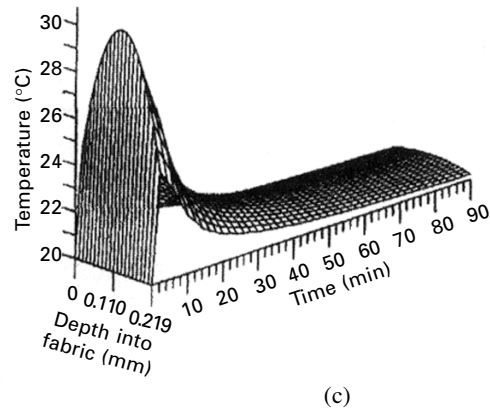
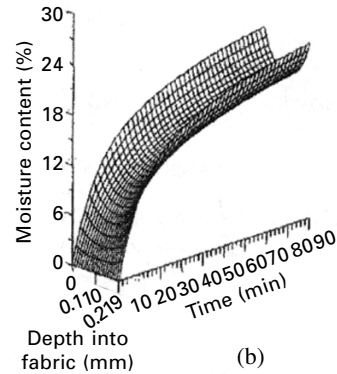
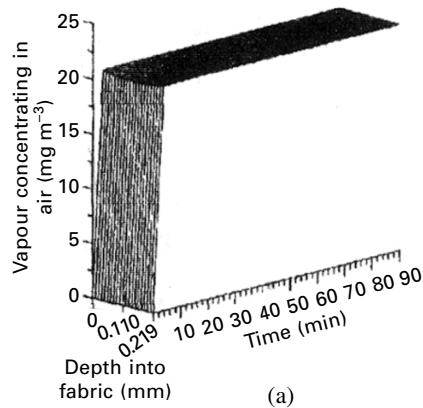
	Wool	Cotton	Acrylic	Polypropylene
Fibre diameter (μm)	20.6	13.3	18.4	20.0
Yarn tex	20	20	21	18
Fabric g/m ²	272	275	287	279
Thickness (mm)	2.96	2.19	2.14	2.42
D_1 (m ² /s × 10 ¹⁴)	1.04 + 68.2 M -1342.59 M^2	0.8481 + 50.6 M -1100 M^2	11.2 + 4100 M -82 000 M^2	13
D_2 (m ² /s × 10 ¹⁴)	1.614{1-exp[-18.163 × exp(-28.0 M)]}	2.5{1-exp[-3.5385 × exp(-45 M)]}	62.3	13



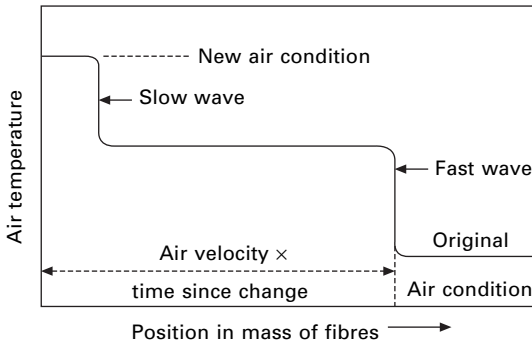
9.16 Diffusion into fabrics in change from 0 to 99% r.h. Theoretical lines and experimental points: (a) moisture uptake; (b) temperature change at surface of fabric. From Li and Luo [17].

changes are roughly equally divided between the two waves, and there may be transient changes on the fast wave, whereas moisture content changes occur mainly on the slow wave.

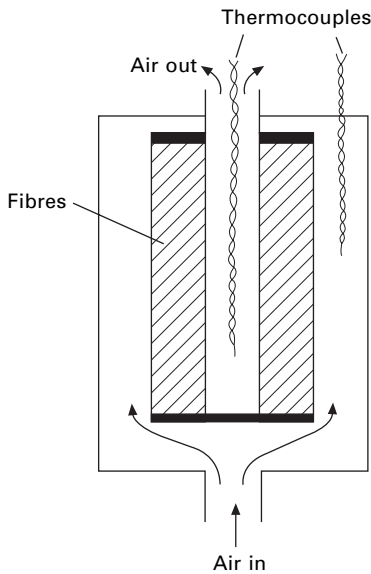
The theory has been tested experimentally by blowing air through the walls of a hollow cylinder as shown in Fig. 9.19. The walls of the cylinder were 1 cm thick, and the fibres were packed to a density of 0.147 g/cm^3 ; the air velocity was 1.75 cm/s . When steady conditions had been attained at one temperature, the temperature of the incoming air was suddenly changed, without change of vapour pressure, and the change in temperature of the outgoing air was measured. Figure 9.20 shows the good agreement between experiment and theory. Results for various fibres are given in Fig. 9.21 and Table 9.4. It is found that the time taken for the slow wave to pass



9.17 Change in fabrics from 0 to 99% r.h. with time and depth into fabric: (a)–(c) cotton; (d), (e) acrylic; (a), (d) vapour concentration; (b), (e) moisture content; (c) (f) temperature. From Li and Luo [17].



9.18 Ideal transmission of change by a forced draught.



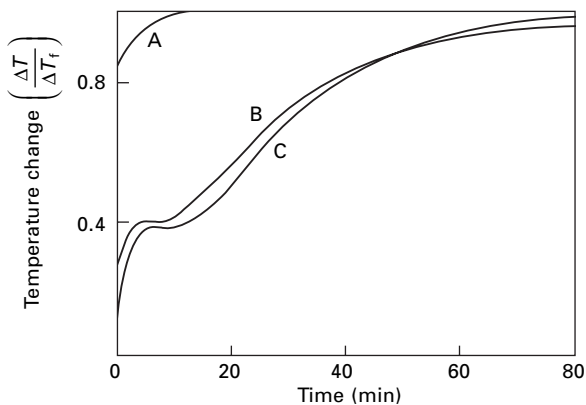
9.19 Textile cylinder for testing change of condition on blowing air through a mass of fibres. After Cassie and Baxter [16].

through increases as the steepness of the curve of regain against relative humidity increases. Consequently, the more absorbent the fibres, the slower is the change. In addition to the results given by Baxter and Cassie, some values have been calculated for synthetic fibres and are included in [Table 9.4](#). These are only very approximate, since such factors as the specific heat of the material, which can be neglected for hygroscopic fibres, will be important for hydrophobic fibres.

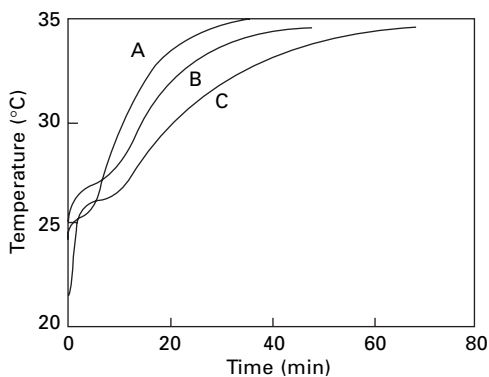
9.4 Practical effects

9.4.1 Conditioning

The above discussion has shown that the rate of conditioning (meaning the change of regain) of fibres will depend on the slow wave resulting from the combination of heat



9.20 Transmission of temperature change through a textile cylinder by forced draught: A, ingoing air temperature; B, temperature after passing through cylinder, experimental; C, temperature after passing through cylinder, theoretical. After Daniels [19].



9.21 Transmission of temperature change from 20 to 35 °C through various fibres in textile cylinder. The curves show temperature of air after passing through cylinder: A, acetate; B, cotton; C, wool. After Baxter and Cassie [20].

Table 9.4 Transmission of temperature changes under forced draught through apparatus shown in Fig. 9.19 with dimensions in text [16]

Material	Time for slow wave		Amplitude (°C)	
	Calculated	Observed	Fast wave	Slow wave
Cotton	15.7	13.8	5.7	9.3
Flax	20.5	19.5	5.9	9.1
Kapok	19.9	23.6	6.0	9.0
Viscose rayon	26.6	30.0	5.9	9.1
Acetate	16.1	19.6	6.5	8.5
Wool	22.1	28.4	5.9	9.1
Silk	19.0	19.8	6.4	8.6
Nylon	8			
Polyester (PET)	4			
Acrylic (PAN)	2			

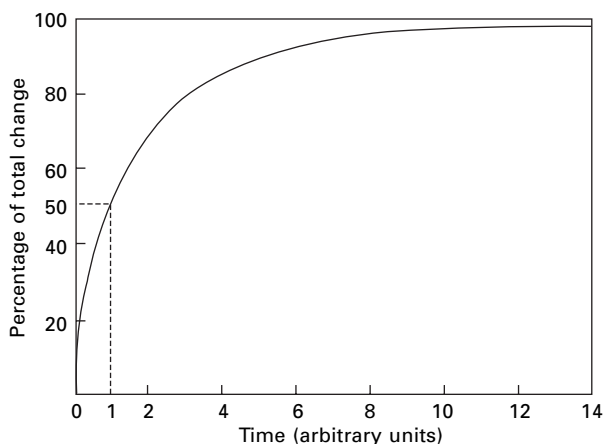
and moisture diffusion. The change will take place roughly exponentially, as is shown in Fig. 9.22. For a given set of conditions, a given proportion of the total change will always take the same time irrespective of the magnitude of the total change. For example, three-quarters of the change from 8 to 10% regain will take the same time as three-quarters of the change from 9 to 9.1%. The actual time taken for a change to occur will depend on the ease with which heat and moisture can be dissipated from the specimen. This is influenced by many factors: the size, shape and density of packing of the mass of fibres; the type of fibre; the temperature; and the general level of regain at which the change occurs.

The numerical values for the effect of these factors can be based on a standard half-change period of 12 hours for a slab of cotton fibres 2.5 cm thick, with a density of 0.5 g/cm^3 when dry, at a regain of 7%, and at a temperature of 18°C . The time for other percentages of the total change may be obtained by multiplying the basic half-change period of 12 hours by the factors given in Table 9.5².

The effects of the principal factors that influence the rate of conditioning are as follows.

- *Size and shape of package.* The greater the distance for which heat has to be transferred through the mass of fibres (which is an effective heat insulator), the slower will be the rate of conditioning. Heat generated in the centre of a bale will take a long time to escape. It will escape more rapidly from a smaller package or from the same mass of material spread out in a thin layer.

The total amount of heat that has to be lost is proportional to the volume of the package. The rate of loss of heat will depend partly on the time taken for the heat to reach the surface, decreasing as the distance to the surface increases, and partly on the rate of loss of heat from the surface, increasing as the surface area increases. In fact, mathematical analysis shows that:



9.22 Rate of conditioning in practice.

²Based on information from the Cotton Silk and Man-made Fibres Research Association.

Table 9.5 Time for conditioning. Basic half-change period of 12 hours has to be multiplied by appropriate factors for other conditions

Percentage of total change	5	10	20	30	40	50	60	70	80	90	95	99
Factor	$\frac{1}{80}$	$\frac{1}{20}$	$\frac{1}{6}$	$\frac{1}{3}$	$\frac{2}{3}$	1	$1\frac{1}{2}$	2	3	6	8	14
							Density (g/cm ³)	Factor				
Size and shape of package:							0.09	$\frac{1}{6}$				
Factor = $\left(\frac{0.8 \times \text{volume of package}}{\text{surface area}}\right)^2$							0.17	$\frac{1}{3}$				
(measured in cm)							0.35	$\frac{2}{3}$				
							0.5	1				
							0.7	$1\frac{1}{2}$				
Material	Factor	Average regain		Factor		Temperature (°C)		Factor				
Cotton	1	0		6		5		$2\frac{3}{8}$				
Mercerised cotton	$1\frac{1}{4}$	1		2		10		$1\frac{3}{4}$				
Viscose rayon	2	2		1		15		$1\frac{1}{4}$				
Cuprammonium rayon	$1\frac{3}{4}$	4		$\frac{2}{3}$		20		$\frac{7}{8}$				
Fortisan	$1\frac{2}{3}$	6		$\frac{3}{4}$		25		$\frac{5}{8}$				
Acetate	$1\frac{1}{4}$	7		1		30		$\frac{3}{8}$				
Silk	$1\frac{1}{2}$	8		$1\frac{1}{4}$								
Nylon	$\frac{2}{3}$	10		2								
		12		3								
		14		5								

$$\text{conditioning time} \propto \left(\frac{\text{volume}}{\text{surface area}} \right)^2$$

For packages of the same shape, this reduces to:

$$\text{conditioning time} \propto (\text{linear dimension})^2$$

Different specimens will have values of these quantities differing by at least a million times, and this is the most important factor in determining whether the time taken in conditioning is seconds or years. The other factors to be considered have smaller effects, though they may be more easily changed.

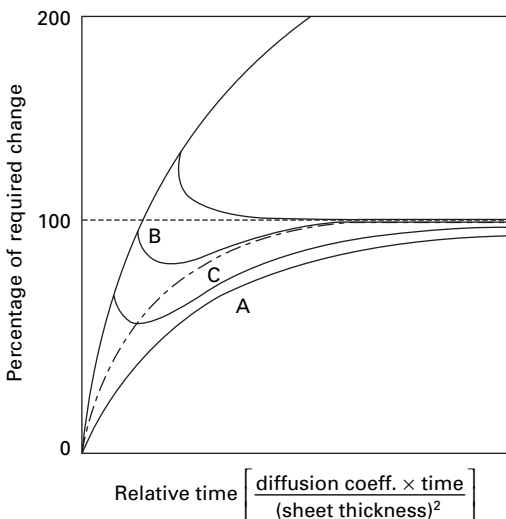
- *Bulk density.* The mass of moisture absorbed, and so the amount of heat evolved, for a given change of regain is proportional to the density of packing of the material. It is therefore found that:

$$\text{conditioning time} \propto \text{density}$$

- *Material.* There are some variations depending on the nature of the material. The numerical values are given in Table 9.5.
- *Regain.* The rate of conditioning is slower at the extreme values, as shown in Table 9.5. This results from differences in the diffusion constants.
- *Temperature.* Conditioning is more rapid at higher temperatures, since the heat transfer, in common with most other processes, occurs more rapidly at higher temperatures. At low temperatures, conditioning is slow. Darling and Belding [21] found the following times for 80% of the change in wool yarn: 5 °C, 10 hours; -18 °C, 95 hours; -30 °C, 260 hours.
- *Air circulation.* The ventilation around a mass of fibres is important in affecting the rate of loss of heat from the surface of the specimen and thus the rate of conditioning.

Quantitative values for the influences of the above factors are summarised in Table 9.5.

Conditioning may be speeded up by carrying it out in two stages. The theory has been worked out by Crank and Henry [22] for sheet and cylindrical specimens. Figure 9.23 shows the theoretical behaviour during conditioning of an initially dry plane sheet. The conditioning is more rapid when the specimen is first placed in an atmosphere much damper than is required, for the final state and then, after a period, transferred to an atmosphere, giving the required equilibrium condition. Since the outer layers will have come into equilibrium with the damper atmosphere, there is a fall in the amount of moisture in the specimen after the transfer, and thus the optimum procedure involves allowing the specimen to absorb somewhat more moisture than is finally required. Another procedure that may be adopted is to place the material in a



9.23 Methods of conditioning in practice: A, infinite atmosphere of required condition; B, two-stage processes; C, closed systems containing correct total amount of water. After Crank and Henry [22].

closed system containing the required total amount of water: this gives more rapid conditioning than the use of an infinite atmosphere of the required condition but is less rapid than the shortest two-stage process.

9.4.2 Influence in clothing

The value of the heat of absorption in clothing was mentioned in the last chapter. The discussion in this chapter shows that, in a hygroscopic material, a considerable part (the fraction carried on the slow wave) of an external temperature change is delayed in its passage through the material.

This happens even if air is being blown through the material. Thus only a part of the total change reaches the body immediately, and the body is given time to adapt itself to the remainder of the change. Under almost all conditions, this will be beneficial in clothing materials. The best fibres from this point of view will be the most hygroscopic fibres. In non-absorbing fibres, the delay in the transmission of temperature change will be only that due to the insulating power of the material.

Farnworth [23] extended the treatment to multilayer clothing and also took account of condensation and wet insulation. An extensive account of thermal and moisture transport in fibrous materials, with particular reference to clothing is given in the book edited by Pan and Gibson [24].

9.5 References

1. J. Crank. *The Mathematics of Diffusion*, Oxford University Press, London, 1956.
2. G. King. *Trans. Faraday Soc.*, 1945, **41**, 479.
3. P. E. Rouse. *J. Amer. Chem. Soc.*, 1947, **69**, 1068.
4. I. C. Watt. *Text. Res. J.*, 1960, **30**, 644.
5. B. H. Mackay and J. G. Downes. *J. Text. Inst.*, 1969, **60**, 378.
6. M. Fukuda and H. Kawai. *Textile Res. J.*, 1993, **63**, 185.
7. P. H. Hermans and D. Vermaas. *J. Polymer Sci.*, 1946, **1**, 149.
8. A. C. Newns. *Trans. Faraday Soc.*, 1956, **52**, 1533.
9. F. H. Clayton and F. T. Peirce. *J. Text. Inst.*, 1929, **20**, T315.
10. N. F. Roberts and A. R. Haly. *Text. Res. J.*, 1954, **24**, 261.
11. G. King and A. B. D. Cassie. *Trans. Faraday Soc.*, 1940, **36**, 445.
12. I. C. Watt and G. B. McMahon. *Text. Res. J.*, 1966, **36**, 738.
13. P. S. H. Henry. *Proc. Roy. Soc.*, 1939, **A171**, 215.
14. Y. Li and Z. Luo. *Textile Res. J.*, 1999, **69**, 760.
15. P. S. H. Henry. *Disc. Faraday Soc.*, 1948, No. **3**, 243.
16. A. B. D. Cassie and S. Baxter. *Trans. Faraday Soc.*, 1940, **36**, 458.
17. Y. Li and Z. Luo. *J. Textile Inst.*, 2000, **91**, Part 1, 302.
18. A. B. D. Cassie. *Trans. Faraday Soc.*, 1940, **36**, 453.
19. H. E. Daniels. *Trans. Faraday Soc.*, 1941, **37**, 506.
20. S. Baxter and A. B. D. Cassie. *Trans. Faraday Soc.*, 1941, **37**, 517.
21. R. C. Darling and H. S. Belding. *Industr. Engng Chem.*, 1946, **38**, 524.
22. J. Crank and M. E. Henry. *Proc. Phys. Soc.*, 1949, **B62**, 257.
23. B. Farnworth. *Textile Res. J.*, 1986, **56**, 653.
24. N. Pan and P. Gibson (Editors). *Thermal and Moisture Transport in Fibrous Materials*, Woodhead Publishing, Cambridge, 2006.

10.1 Introduction

The account of moisture absorption given in the last three chapters has been concerned with the behaviour of fibres exposed to atmospheric humidity, but the interactions of fibres with liquid water are also important. The removal of water from masses of fibres has practical application in the drying of textiles, where the initial surplus water may be removed by squeezing, by centrifuging, or merely by gravity, as in ‘drip-dry’ materials.

Fundamental experimental investigations have made use of two methods: centrifuging and suction. The latter is particularly useful, since it can easily be related to the behaviour at high relative humidities.

10.2 Centrifuging of wet fibres

10.2.1 Experimental method

The centrifugal method has been used by Preston and his colleagues [1, 2]. It is basically simple. The mass of fibres is swung round in a centrifuge, so that it is subject to a high field of force, which in Preston’s experiments ranged from 1000 to 5000 times the gravitational field. Under the action of this force, the water rapidly drains out of the fibre mass.

The method of supporting the fibres in the centrifuge influences the results. If they are placed in a hollow container, so that the centrifugal field presses them against a porous plate, then this will tend to compact the fibre mass and reduce the space that can be filled with water, but if the material is in the form of yarn wound in small hanks and placed on hooks, this compacting will not occur.

10.2.2 Theoretical estimate of water retention

In a waterlogged state, all the spaces between the fibres will be filled with water. Under the action of gravity, and to a much greater extent under high centrifugal fields, this water will drain out. Finally a stage will be reached in which the water that remains is held by surface tension in capillary spaces between the fibres, just as a

column of water will remain suspended in a fine capillary tube. The exact form of these spaces will depend on the way in which the fibres are packed together. The retention of water will also be affected by the alignment of the spaces with respect to the centrifugal field.

For the simple case, illustrated in Fig. 10.1, in which circular fibres are close-packed parallel to the direction of the centrifugal field, it is possible to work out the equation for the equilibrium condition. We shall also make the simplifying assumption that the curvature of the meniscus is negligible at the end of the tube from which the water empties.

The spaces between the fibres will be roughly triangular tubes, and these hold the capillary water. If p is the length of the perimeter formed by the three sides of one of these tubes, then the force due to surface tension will be $\sigma p \cos \theta$, where σ is the surface tension and θ is the contact angle. The centrifugal pull on the water in a tube is mg , where m is the mass of water in the tube and g is the acceleration due to the centrifugal field. At equilibrium, these two forces must balance, and we have

$$mg = \sigma p \cos \theta \quad (10.1)$$

It is clear from this equation that as the centrifugal field increases, the mass of water that can be retained in a tube of a given perimeter decreases.

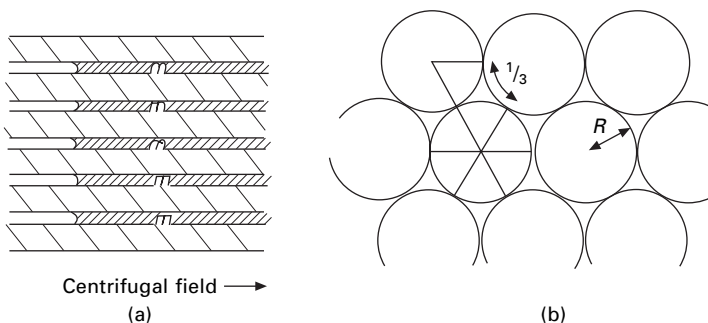
As can be seen from the plan view of the close packing, Fig. 10.1(b), the length of each side of the tube is equal to one-sixth of the circumference of a fibre. This can be related to the linear density (mass/unit length), c , of the fibre and its density, ρ , for, if R is the fibre radius, we have:

$$\pi R^2 \rho = c \quad (10.2)$$

$$p = 3 \left(\frac{2\pi R}{6} \right) = \pi R = \sqrt{\left(\frac{\pi c}{\rho} \right)} \quad (10.3)$$

It is also clear from the plan that there are twice as many spaces between fibres as there are fibres (since each fibre can be regarded as having one-third share in six spaces), and the mass M of fibre associated with one tube is therefore given by:

$$M = \frac{1}{2} ch \quad (10.4)$$



10.1 (a) Capillary spaces between fibres filled with water, in centrifugal field.
(b) Plan of close-packed fibres, showing spaces between them.

where h is the total height of the fibre mass parallel to the centrifugal field.

The fractional water retention r of the specimen is given by:

$$r = \frac{\text{mass of water}}{\text{mass of fibre}} = \frac{m}{M} \quad (10.5)$$

Substituting from equations (10.1), (10.3) and (10.4), we obtain:

$$r = \frac{2\sigma \cos\theta \sqrt{\pi}}{gh\sqrt{(cp)}} \quad (10.6)$$

This equation will only apply exactly to the simple example that we have described, but it is reasonable to suppose that an equation of the same form, though with different numerical constants, would apply in the more complex cases that occur in reality. For a given system, it may be expected that:

$$r \propto \frac{\sigma \cos\theta}{gh\sqrt{(cp)}} \quad (10.7)$$

A more detailed analysis has been given by Koppers [3].

10.2.3 Experimental results

In experiments in which they varied the surface tension, the centrifugal field, and the contact angle, Preston *et al.* [2] obtained good agreement with the theoretical relation (10.7). As would be expected, they found that the nature of the packing influenced the amount of water retained. For example, less water was held by randomly oriented viscose rayon fibres than by parallel ones. In addition, any compacting of the specimen, reducing the size of the spaces, increases the amount of water retained.

Table 10.1 shows the amount of water retained by various fibre masses after centrifuging. It should be noted that centrifuging will never remove all the water held

Table 10.1 Water retained in centrifuging and suction. After Preston and Nimkar [4]

Material	Regain (%)	
	Suction – 30 cm Hg, 40 kpa	Centrifuging 1000g, 5 min
Cotton yarn	52	48
Viscose rayon yarn	106	103
<i>Fortisan</i> yarn*		
0.11 dtex per filament	70	63
1.1 dtex per filament	48	48
Acetate yarn	31	31
Loose wool	133	45
Silk yarn	55	52
Nylon yarn	14	16

**Fortisan*, which was an industrial rayon, is no longer made, but is included here to show the effect of fibre fineness.

in capillary spaces but will only reduce it to the amount given by equation (10.1). The method will not therefore give a reliable estimate of the water held in the fibre material itself at saturation.

10.3 Suction

10.3.1 Experimental method

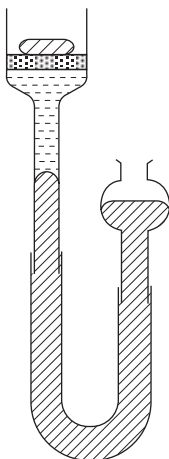
An alternative method of investigation is to apply a hydrostatic tension to the waterlogged mass of fibres. A simple apparatus for doing this is shown in Fig. 10.2 and has been used by Preston and Nimkar [4]. The fibres are placed on a porous plate, below which there is a column of water leading to a mercury manometer. It is essential that there should be a continuous water-path between the mercury and the water surrounding the fibres. Lowering the right arm of the manometer puts the water into a state of hydrostatic tension, which will tend to pull the water away from the fibre mass. This will be resisted by the forces of surface tension.

10.3.2 Relation between suction, capillary size and humidity

The force exerted by surface tension depends on the curvature of the water meniscus. If the curvature is great, there will be a high capillary force, which will resist the hydrostatic tension, but, if it is low, the force will be small and the hydrostatic tension will empty the capillary space. The critical condition, when the two forces just balance, is given by the usual equation:

$$P = \sigma \left(\frac{1}{r_1} + \frac{1}{r_2} \right) \quad (10.8)$$

where P = hydrostatic pressure, and r_1 and r_2 are the principal radii of curvature.



10.2 Apparatus for removal of water from a mass of fibres by suction.

If the spaces are circular and the contact angle is zero, this relation reduces to $P = 2\sigma/r$, where r is the radius of the capillary. If the spaces have plane parallel walls, separated by a width $2w$, it reduces to $P = \sigma/w$. The spaces between fibres will vary in shape and will lie somewhere between these two conditions. The re-entrant spaces in some rayon fibres will approximate to the second case.

The use of Kelvin's equation [5] enables the relative humidity corresponding to any hydrostatic tension to be calculated. The relation is:

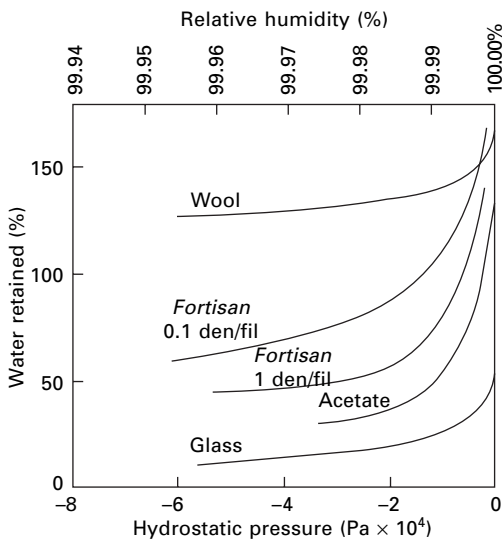
$$\log_e H = \frac{PM}{\rho RT} \quad (10.9)$$

where H = relative humidity (fractional), M = molecular weight of water, ρ = density of water, R = gas constant and T = absolute temperature. Consequently, the results of suction experiments may be related to experiments in which the specimen attains equilibrium with a given relative humidity.

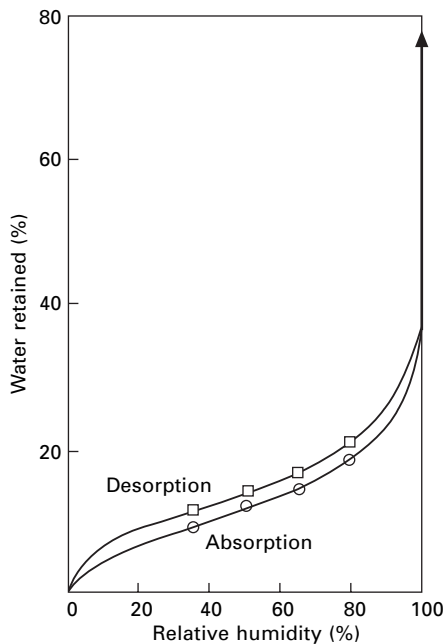
10.3.3 Experimental results

Figure 10.3 shows some values of the moisture retained in the mass of fibres plotted against the hydrostatic tension (negative values of hydrostatic pressure). The corresponding values of humidity are also shown. Figure 10.4 shows the way in which data obtained by the suction method join on to normal absorption data.

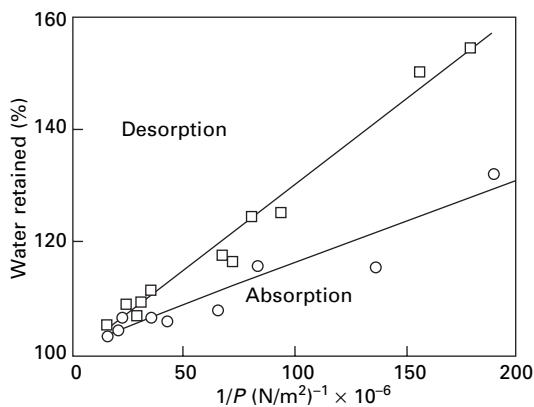
It will be noticed that there is a very rapid rise near saturation. This is when water held in capillary spaces becomes important. The filling of capillary spaces does not cause any increase in volume. Hence, if the water causing volume swelling (plus that filling the void space between the fibre molecules, discussed in Section 12.1.6) is subtracted from the total water retained, we can get a figure for the amount of



10.3 Removal of water from fibres by suction. After Preston and Nimkar [4].



10.4 Combination of suction data with normal sorption isotherms of viscose rayon. After Preston and Nimkar [4].



10.5 Hysteresis in removal of water by suction: viscose rayon. After Preston and Nimkar [4].

capillary water present. Preston and Nimkar [4] state that this is a significant amount only at relative humidities greater than 99%.

Hysteresis is found to persist even at the very high humidities corresponding to suction experiments. This is shown by Fig. 10.5, in which the water retained is plotted against the reciprocal of the hydrostatic tension, which is a more convenient way of presenting the results.

Comparative values for the water retained by various fibres after a suction experiment are given in [Table 10.1](#). In the suction method, the force tending to remove the water is independent of the amount of water in the capillary space (if this is assumed to be constant in size). The space will consequently either be emptied completely if it is larger than the critical value given by equation (10.8), or left completely full if it is smaller. By contrast, in the centrifugal method, the force decreases as the space empties, and thus any spaces may be emptied to some extent, but none will be completely emptied unless the field is infinite. We should not therefore necessarily expect a close correlation between the results of suction and centrifugal experiments. However, the values given in [Table 10.1](#) show that, for many fibre materials, a hydrostatic tension of 30 cm of mercury (corresponding to 99.97% r.h.) gives very similar results to the application of a centrifugal field of 1000g for 5 min. Capillary-sorption cycles in a variety of fibre assemblies have been studied by Burgeni and Kanpur [6].

Another method of estimating the amount of water retained as capillary water is to freeze the sample. Any free liquid water freezes at 0 °C, and thus its amount can be calculated from the latent heat at 0 °C. Absorbed water has an influence over a range of temperatures. Haly [7] used this method and found that the saturation regain of wool was 33.9% at 0 °C. Any excess over this amount is free water.

A practical example of the removal of water by means of hydrostatic tension occurs when a wet textile material is hung up vertically. The water at any point will be under a hydrostatic tension determined by the length of the continuous column of water below it. If evaporation is prevented, one would expect an equilibrium to be obtained in which there would be a gradient of wetness from top to bottom. Preston and Nimkar [1] have confirmed that this is so.

10.4 Interactions

If capillary water is present in the spaces between fibres, the fibres will be attracted to one another by the hydrostatic tension in the water. Consequently, when a waterlogged mass of fibres is dried, the individual fibres will be drawn together and there will be forces of adhesion wherever they cross. This adhesion will persist down to any humidities at which capillary water is present, even if it is only in amounts that are insignificant by comparison with the total water absorption.

Preston and Nimkar [4] have both calculated and measured the force of adhesion between fibres due to this cause, and [Table 10.2](#) gives examples of their results. The agreement between experiment and theory is good for the glass fibres. The low experimental values obtained with the cellulosic fibres are probably due to surface irregularities.

Wettability is another response related to surface tension and contact angles, Lee and Michielsen [8] review aspects of surface tension, contact angles and contact angle hysteresis in the context of super-hydrophobicity and the Lotus effect, which leads to water drops rolling off a tilted surface.

Table 10.2 Force of adhesion between fibres due to surface tension of water. After Preston and Nimkar [4]

Fibre	Radius (μm)	r.h. (%)	Force (μN)	
			Calculated	Measured
Viscose rayon	16	93	15	1
Cuprammonium rayon	158	93	145	6
Glass	41	0	0	0
		31	37	34
		64	37	26
		93	37	32
		Wet	0	0
Glass	54	31	49	48
		64	49	34
		93	49	37

10.5 References

1. J. M. Preston and M. V. Nimkar. *J. Text. Inst.*, 1949, **40**, P674.
2. J. M. Preston, M. V. Nimkar and S. P. Gundava. *J. Text. Inst.*, 1951, **42**, T79.
3. J. R. Koppers. *Text. Res. J.*, 1961, **31**, 490.
4. J. M. Preston and M. V. Nimkar. *J. Text. Inst.*, 1952, **43**, T402.
5. W. Thomson. *Phil. Mag.*, 1871, 42, No. **4**, 148.
6. A. A. Burgeni and C. Kanpur. *Text. Res. J.*, 1967, **37**, 356.
7. A. R. Haly. *J. Text. Inst.*, 1969, **60**, 403.
8. H. J. Lee and S. Michielsen. *J. Text. Inst.*, 2006, **97**, 455.

11.1 Introduction

11.1.1 Technical significance

When fibres absorb water, they change in dimensions, swelling transversely and axially. This has technical consequences in the dimensional stability of fabrics, the predominant transverse swelling usually resulting in a shrinkage of twisted or interlaced structures. It also means that the pores of closely woven fabrics will be completely blocked when the fibres are swollen, and they may then be impermeable to water. This principle is utilised in hosepipe materials and the *Ventile* fabrics, which were developed in the 1940s for showerproof garments. Swelling is also an important factor in crêpeing, due to the increased twist angle in a swollen yarn, and in drying and dyeing.

Swelling is akin to solution in that there is an interchange of position between fibre molecules and water molecules, but in swelling this occurs only to a limited extent, whereas in solution it continues until there is a uniform mixture of the two substances.

11.1.2 Definitions

The swelling may be expressed in terms of the increase in diameter, area, length or volume as illustrated in Fig. 11.1. This leads to the following quantities:

transverse diameter swelling = fractional increase in diameter

$$= S_D = \frac{\Delta D}{D} \quad (11.1)$$

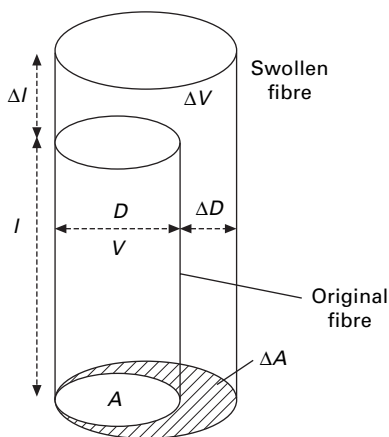
transverse area swelling = fractional increase in area of cross-section

$$= S_A = \frac{\Delta A}{A} \quad (11.2)$$

$$\text{axial swelling} = \text{fractional increase in length} = S_l = \frac{\Delta l}{l} \quad (11.3)$$

$$\text{volume swelling} = \text{fractional increase in volume} = S_v = \frac{\Delta V}{V} \quad (11.4)$$

In practice, these quantities are often expressed as percentages rather than fractions.



11.1 Changes in fibre dimensions on swelling.

Relations between them reduce the number of independent parameters to two, though these relations may be affected by the fibre shape. For instance, in a fibre that is uniform along its length, we have

$$V = Al \quad (11.5)$$

$$V + \Delta V = (A + \Delta A)(l + \Delta l) \quad (11.6)$$

$$S_v = \frac{\Delta V}{V} = \left(\frac{A + \Delta A l}{Al} \right) = \frac{\Delta l}{l} + \frac{\Delta A}{A} + \frac{\Delta A \Delta l}{Al} = S_l + S_A + S_l S_A \quad (11.7)$$

where V = volume, A = area of cross-section and l = length.

It can be similarly shown that, for a fibre of circular cross-section

$$S_A = 2S_D + S_D^2 \quad (11.8)$$

Another quantity that is a useful expression of the swelling behaviour is the swelling anisotropy $K = S_D/S_l$. This is related to the orientation of the molecules in the fibre, which cause it to range from infinity for a perfectly oriented arrangement, with no length swelling, to unity for a completely random one.

11.2 Measurement of swelling

11.2.1 Volume swelling

If we consider a specimen of mass 1 g when dry, we have

$$V = \frac{1}{\rho_0} \quad (11.9)$$

$$V + \Delta V = \frac{1 + m}{\rho_s} = \frac{1 + r/100}{\rho_s} \quad (11.10)$$

where ρ_0 = density when dry, ρ_s = density when swollen, m = mass of water absorbed, and r = regain %. Hence:

$$S_v = \frac{\Delta V}{V} = \frac{\left(\frac{1 + r/100}{\rho_s - 1/\rho_0} \right)}{1/\rho_0} = \frac{\rho_0}{\rho_s} \left/ \left(\frac{1 + r}{100} \right) \right. - 1 \quad (11.11)$$

Thus the volume swelling may be found from measurements of density (by using the methods described in Section 5.2) and regain.

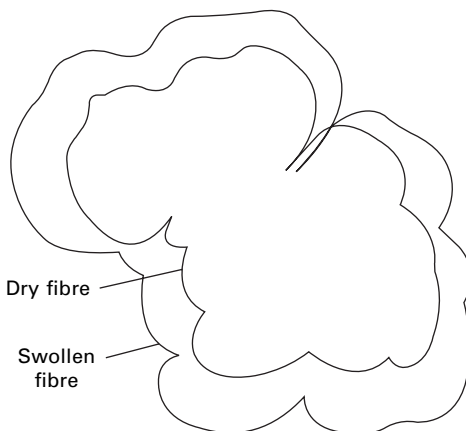
11.2.2 Axial swelling

The axial swelling of a continuous filament may be found by hanging up a length under a low tension and measuring the change in length with a cathetometer or some form of extension gauge. Observations of the change in length of short fibres may be made with a travelling microscope by using the procedure described by White and Stam [1].

11.2.3 Transverse swelling

Because fibres have such a small diameter, measurements of changes in transverse dimensions are not easy to make. The accuracy of a microscopical method is limited by the resolution of the microscope, which is of the order of magnitude of the wavelength of light used, say, $0.5 \mu\text{m}$. If a fibre of $20 \mu\text{m}$ diameter is examined, it will be possible to distinguish detail down to one-fortieth of the fibre diameter, but, if the diameter swelling is 10%, it will be possible to measure this to an accuracy of only 0.5 in 2. This means that there may be an error of 25%.

However, microscopy methods are used, either for examining the fibre profile and measuring the apparent diameter or for examining sections and measuring the diameter, or the area of cross-section, with a planimeter. Figure 11.2 shows the outlines of a viscose rayon fibre, swollen and unswollen, as observed by Morehead [2]. This



11.2 Outlines of cross-section of viscose rayon filament, dry and swollen in water. After Morehead [2].

makes clear the fact that diameter swelling is not a sound way of expressing the transverse swelling of a fibre with an irregular cross-section, since it will vary according to the position in which the 'diameter' is drawn. For irregular fibres, area swelling must be used.

Denton [3] has described an optical-interference method, and other workers have measured the change in air-flow along a tube containing a fibre [4] or the conductance in a tube with the fibre surrounded by a conducting liquid [5].

11.2.4 Digital imaging

The use of modern digital imaging, as described for fibre diameter and length measurements in Sections 3.7.1 and 4.11.2 would simplify the measurement of both axial and transverse swelling.

11.3 Results

11.3.1 The swelling of fibres in water

Table 11.1 gives a collection of values of swelling observed by several workers when fibres are immersed in water. It is immediately obvious that there are considerable discrepancies in the values of a given quantity obtained by different people. There are also several cases in which the relations between the results are widely different from equations (11.7) and (11.8). To some extent, these divergencies are a reflection of experimental difficulties, but there will also be real differences between different specimens of a given type of fibre.

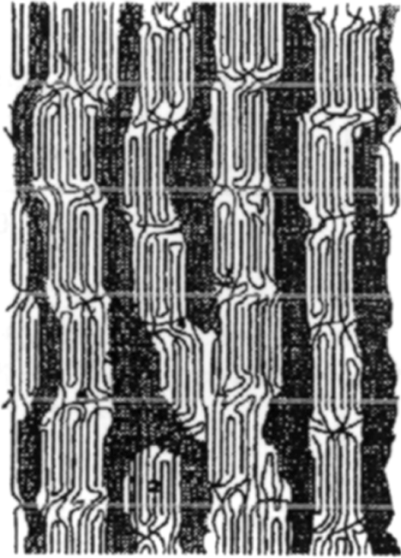
As would be expected, the values of volume swelling vary between different fibres in much the same way as values of regain: those fibres that absorb most water swell to the greatest extent.

Most moisture-absorbing fibres show a large transverse swelling, with a smaller axial swelling, so that the swelling anisotropy is high.

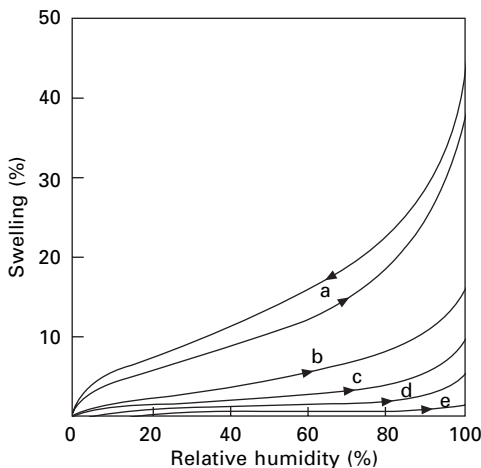
Table 11.1 Swelling of fibres in water. Values reported by various authors, collected by Preston and Nimkar [6]

Fibre	Transverse swelling (%)		Axial swelling (%)	Volume swelling (%)
	Diameter	Area		
Cotton	20, 23, 7	40, 42, 21		
Mercerised cotton	17	46, 24	0.1	
Flax		47	0.1, 0.2	
Jute	20, 21	40		
Viscose rayon	25, 35, 52	50, 65, 67, 66, 113, 114	3.7, 4.8	109, 117, 115, 119, 123, 126, 74, 122, 127
Acetate	9, 11, 14	6, 8	0.1, 0.3	
Wool	14, 8, 17	25, 26		36, 37, 41
Silk	16.5, 16.3, 18.7	19	1.6, 1.3	30, 32
Nylon	1.9, 2.6	1.6, 3.2	2.7, 2.9	8.1, 11.0

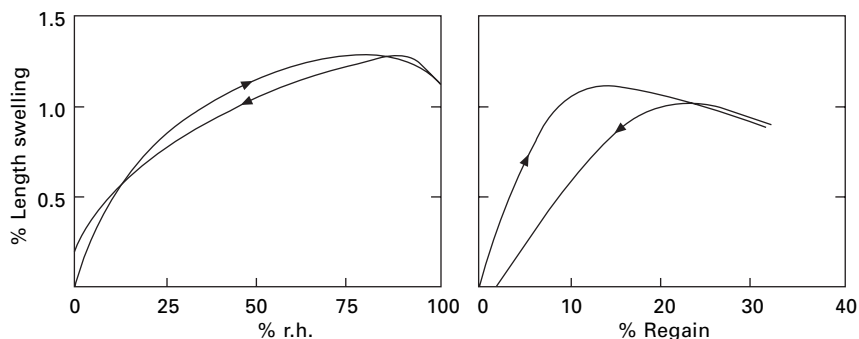
Nylon is exceptional in having a value of the anisotropy that is close to or less than unity. There has been some controversy about the cause of this; it has been suggested that the nylon fibre is surrounded by a skin or sheath, which restricts the transverse swelling. However, it is more likely that it results from the micellar form shown in Fig. 11.3. The swelling of amorphous regions between crystallites in the quasi-fibrils will have a larger effect than the swelling between the fibrils. An interesting consequence of the axial swelling is that carpet tiles expand when humidity increases and this leads to buckling [8].



11.3 Micellar structure of nylon, as proposed by Murthy *et al.* [7].



11.4 Swelling of fibres between dryness and saturation: a, cotton, area swelling in absorption and desorption [9]; b, wool, diameter swelling [4]; c, nylon, area swelling [10]; d, nylon, diameter swelling [10]; e cotton, length swelling [9].



11.5 Length changes in merino wool fibres, observed by Mackay and Downes [11]; (a) variation of length in absorption and desorption; (b) hysteresis between length change and regain.

11.3.2 Swelling at various humidities

The variation of swelling with humidity usually follows the change of regain, with hysteresis showing between swelling and humidity. Typical curves are shown in Fig. 11.4.

However, Mackay and Downes [11] found that single wool fibres can show a maximum length between 75 and 85% r.h., as in Fig. 11.5(a). This was not observed in other studies by Speakman [12], Haly [13] and Watt [14]. Mackay and Downes also found hysteresis between length swelling and regain, as shown in Figure 11.4(b); Treloar [15] found a similar result for horsehair.

11.4 References

1. H. J. White and P. B. Stam. *Text. Res. J.*, 1949, **19**, 136.
2. F. F. Morehead. *Text. Res. J.*, 1947, **17**, 96; 1952, **22**, 535.
3. P. Denton. *J. Sci. Instrum.*, 1952, **29**, 55.
4. F. L. Warburton. *J. Text. Inst.*, 1947, **38**, T65.
5. J. M. Preston. *Trans. Faraday Soc.*, 1946, **42B**, 131.
6. J. M. Preston and M. V. Nimkar. *J. Text. Inst.*, 1949, **40**, P674.
7. N. S. Murthy, A. C. Reimschuessel and V. J. Kramer, *J. Appl. Polymer Sci.*, 1990, **40** 249.
8. E Tan. PhD thesis, University of Manchester, 1970.
9. G. E. Collins. *J. Text. Inst.*, 1930, **21**, T311.
10. J. B. Speakman and A. K. Saville. *J. Text. Inst.*, 1946, **37**, P271.
11. B. H. Mackay and J. G. Downes. *J. Text. Inst.*, 1969, **60**, 378.
12. J. B. Speakman. *Trans. Faraday Soc.*, 1929, **25**, 92.
13. A. R. Haly. *Text. Res. J.*, 1961, **31**, 189.
14. I. C. Watt. *Text. Res. J.*, 1965, **35**, 1072.
15. L. R. G. Treloar. *Trans. Faraday Soc.*, 1952, **48**, 567.

12.1 The general view

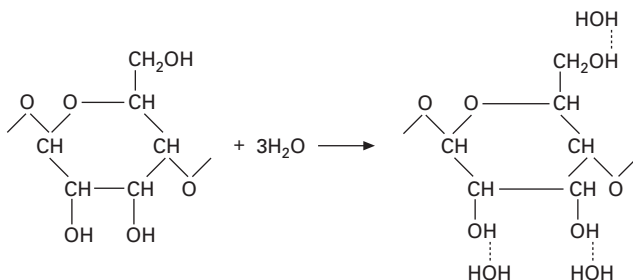
12.1.1 Introduction

Adsorption in a non-swelling medium, for example, the adsorption of gases on charcoal, is a comparatively simple process, and so is the solution of one substance in another, for example the solution of sugar in water, but the absorption of water by fibres is an example of a process that comes midway between these two and partakes of some features of each. It encompasses not only the relation between regain and humidity but also associated phenomena, such as hysteresis, heat effects, the variation of regain with temperature, the influence of moisture on physical properties, and all the complicated factors arising from the interaction of moisture and mechanical effects owing to the limited swelling of fibres. All this cannot be explained by a single theory. A general qualitative view of the whole subject shows the action of several mechanisms of absorption, and there are quantitative theories associated with every possible mechanism. These theories shed light on the subject from a variety of points of view, and a quantitative understanding of the whole process must be built up from them. Although some of the ideas are conflicting, they are mainly complementary to one another.

In this chapter, we shall first give a broad description of the way in which water is absorbed and then go on to discuss some particular theories. For convenience, the theories will usually be discussed in terms of the particular type of fibre for which they were first proposed, but the ideas will usually be applicable to other fibres as well.

12.1.2 The effect of hydrophilic groups

In considering absorption, we must take account of the interaction between the water molecules and the molecules of the fibre substance. All the natural animal and vegetable fibres (and the fibres regenerated from natural materials) have groups in their molecules that attract water: indeed, this is probably a necessary result of the fact that the molecules were first formed in the presence of water. For example, the cellulose molecule contains three hydroxyl groups for each glucose residue, and hydrogen bonds can be formed between water molecules and the hydroxyl groups (see [Fig. 12.1](#)).



12.1 Absorption of water by hydrogen bonding to hydroxyl groups in a cellulose molecule.

The molecular weight of water is 18, and that of the glucose residue is 162, so that if one water molecule were attached to each hydroxyl group the regain would be 33.1%. In fact, as is discussed in later sections, not all the hydroxyl groups are involved, and there may be more than one water molecule per hydroxyl group.

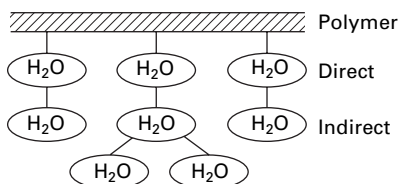
In cellulose acetate, all or most of the hydroxyl groups have been replaced by the comparatively inert acetyl (CH_3COO —) groups. These groups do not attract water strongly, so the absorption of water by acetate is low. In particular, there is no rapid rise at low humidities owing to the initial absorption on strongly attractive groups.

The protein fibres contain amide groups (—NH—) in the main chain, to which water can be hydrogen bonded, and other water-attracting groups such as —OH , —NH_3^+ , —COO^- , —CO-NH_2 , in the side chains. Wool contains many active groups in the side chains, but silk contains only a few. By blocking off certain groups, Watt and Leeder [1] have attempted to divide up the water absorbed by wool according to the various amino-acid residues responsible.

All the synthetic fibres so far produced contain few if any water-attractive groups, and this accounts for their low moisture absorption. The polyamide fibres, nylon 6.6 and 6 and aramids, contain one amide (—NH—) group for every six carbon atoms in the chain, which would give a regain of 16% of each amide group held one water molecule. The polyester fibres, polyethylene terephthalate, are composed only of benzene rings, $\text{—CH}_2\text{—}$ groups, and —COO— groups, none of which attracts water strongly. Polyethylene is simply a $\text{—CH}_2\text{—}$ chain, polypropylene has additional —CH_3 side groups, and the vinyl fibres are similar except for the substitution of —Cl , —O-CO-CH_3 , or other comparatively inert groups for some of the hydrogen atoms, and consequently these fibres absorb little water. Acrylic fibres, containing —CN groups and other groups from the minor components, absorb slightly more than the other vinyl fibres, and polyvinyl alcohol, containing some —OH groups, absorbs still more. Inorganic fibres, including carbon, do not attract water absorption.

12.1.3 Directly and indirectly attached water

The first water molecules must be absorbed directly onto the hydrophilic groups, but, there is a choice for those absorbed after the first. They may be attracted to other hydrophilic groups, or they may form further layers on top of the water molecules already absorbed. The resulting effect is illustrated in Fig. 12.2.



12.2 Direct and indirect absorption of water molecules by a polymer molecule.

The directly attached water molecules will be firmly fixed, fitting closely to the structure of the molecules. They will be limited in their movement. The indirectly attached water molecules will be more loosely held. Their arrangement is uncertain, but the dielectric properties of fibres (see [Section 21.5](#)) suggest that they are not as free as the molecules in liquid water and are probably restrained to about the same extent as the water molecules in ice. This is not incompatible with values of the heat of sorption (see [Section 8.3](#)), which for most fibres at 50% r.h. are of the order of magnitude of the latent heat of freezing of water (330 J/g). At high humidities, the heat of sorption falls to about half the value of the latent heat. It may also be noted that Kolkmeier and Heyn [2] observed lines characteristic of ice in the X-ray diffraction pattern of cellulose. Nuclear magnetic resonance (NMR) studies on keratin by Lynch and Marsden [3] suggest a more complicated situation, with relaxation times one-thousandth of those for water molecules in ice, but 100 times as long as those in the liquid state.

Quantitative estimates of the division between the two types of absorbed water are given in [Section 12.2](#). Boesen [4] reviewed the evidence on the amount of directly bound water in cellulose.

12.1.4 Absorption in crystalline and non-crystalline regions

In crystalline regions, the fibre molecules are closely packed together in a regular pattern. The active groups form crosslinks between the molecules, for example by hydrogen bonding in cellulose and keratin. Thus it will not be easy for water molecules to penetrate into a crystalline region, and, for absorption to take place, the active groups would have to be freed by the breaking of crosslinks.

In native cellulose, with the crystalline arrangement known as cellulose I, the X-ray diffraction pattern is unchanged during the absorption of water by the fibre, which indicates that no water is absorbed in the crystalline regions. In regenerated cellulose, with a slightly less compact crystal structure known as cellulose II, there is a change of crystal structure on absorption. This is due to the formation of a hydrate, which probably contains one water molecule to every three glucose residues. This would correspond to a regain of about 3.7% in the crystalline region (about 1% regain in the whole fibre). When the regenerated cellulose is wet, there is a further modification of the crystal structure owing to the formation of a hydrate with about three water molecules to every two glucose residues.

The material easily accessible to moisture will be either the non-crystalline regions

or the surfaces of crystalline regions. As was stated in [Chapter 1](#), it is very difficult to separate the disorder in a fibre that is due to extensive disordered regions from that which is due to the imperfect packing of small crystallites or crystalline fibrils. It is therefore simplest, for the present discussion, to lump both categories of accessible material together as effectively non-crystalline.

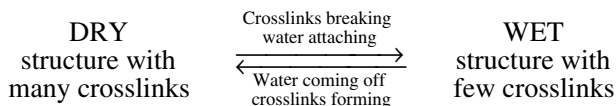
It would then be expected that the regain at any particular relative humidity would be proportional to the amount of this effectively non-crystalline material. Consequently, the ratios of regain at the same relative humidity for any two cellulosic fibres should be independent of the relative humidity, that is, the curves of regain against relative humidity should be the same shape and differ only in scale. This has been proved experimentally (see [Section 7.4.2](#)). In addition, the differential heat of sorption should be the same for all cellulosic fibres at the same relative humidity, since it must be the heat evolved when 1 g of water reacts with non-crystalline cellulose. This has also been demonstrated experimentally (see [Section 8.3](#)). On the other hand, other fibres, having different absorbing substances, give curves of different shapes and have different heats of sorption.

The moisture absorption thus offers one way of estimating the effective crystalline/non-crystalline ratio in cellulosic fibres. Marsden [5] gives values of approximately 60% crystalline material for native cellulose and 25% for regenerated cellulose. Results by different methods do not agree exactly, probably because the distinction between non-crystalline and crystalline regions is not precise and different methods would have different limits. Jeffries *et al.* [6], collecting data from the literature, have values for percentage of disordered material ranging from 8 to 42% for cotton and from 20 to 77% for regenerated cellulose.

In nylon, the amount of crystalline material has been estimated to be 50–60% of the whole.

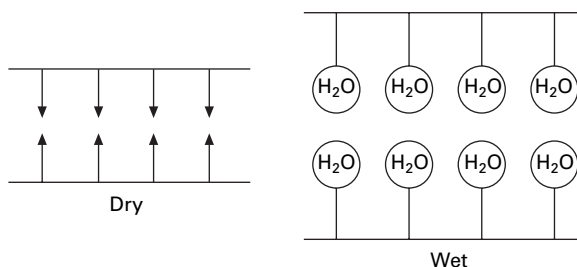
12.1.5 Hysteresis: a molecular explanation

Urquhart [7] put forward a theory of hysteresis based on molecular effects, and this has been restated, in the light of later views of cellulose structure, by Hermans [8]. In non-crystalline cellulose, there are some crosslinks, formed where molecules pass near to one another, and these crosslinks reduce the amount of absorption, both by providing mechanical restraint (the influence of which is discussed in [Section 12.3](#)) and by reducing the number of available hydroxyl groups. As absorption increases, the crosslinks will tend to be broken and replaced by water absorption on the hydroxyl groups. Thus there is the following change:



Owing to the tendency of the structure to remain unchanged, there will be a hysteresis in the breaking and re-forming of crosslinks, and consequently in the moisture absorption.

In the more highly ordered, fibrillar, natural cellulose fibres, the crosslinks and



12.3 Schematic view of dry and wet structures.

water attachment will be between and on the surfaces of the fibrils. Figure 12.3 can thus be regarded as showing a small part of these surfaces.

The structure in extensive non-crystalline regions is a three-dimensional network and is more difficult to visualise. However, the two-dimensional analogy (which must not be taken too literally) shown in Fig. 12.3 may be used to lead to an understanding of what happens. The figure shows a dry structure with crosslinks and a wet structure with water absorption. Suppose that the two structures are both put in the same atmosphere. Owing to the natural energy of the system, causing the continual motion of atoms and molecules, active groups will at intervals become free because of the breaking of crosslinks or the evaporation of water. A free active group will not remain free indefinitely, since either a water molecule will be absorbed on it or a crosslink will form. If these two possibilities are considered independently, the chance of water absorption depends on the number and velocity of the water molecules present in the atmosphere, and this is the same in both cases. The chance of a crosslink forming depends on the nearness of another active group. It is thus more likely to occur in the dry structure, where the other crosslinks are holding the molecules close together, than in the wet structure, where the molecules are far apart. Consequently, when the two possibilities are in competition, the net chance of water absorption is greater in the wet structure, so there will be hysteresis in the moisture absorption.

Translating the above ideas into three-dimensional terms, we may say that the presence of other crosslinks in a dry structure tends to hold the molecules together in the network and makes crosslink formation easier than in a structure with few crosslinks. Thus an initially dry specimen will always retain a higher number of crosslinks and less water absorption than an initially wet specimen in the same atmosphere. Similar arguments apply to the fibrillar network in the natural fibres.

When cellulose is first formed in the cotton plant, it is laid down in the presence of water. This favours the absorption of water, and the resulting structure has few crosslinks, giving rise to the high primary desorption curve (see [Section 7.4.2](#)). Once it has been dried below a certain humidity, crosslinks will form. Some of these will remain permanently and prevent such high regains from being obtained again. Heating a fibre wet is also a process that favours moisture absorption, destroys crosslinks, and gives rise to a high primary-desorption curve. On the other hand, heating a substance dry increases the number of crosslinks and lowers the curve of regain against relative humidity.

12.1.6 Limited swelling

Although glucose and cellulose are chemically very similar, they behave differently when placed in water. Glucose dissolves, but cellulose swells to only a limited extent. The limited swelling is due to the penetration of water into the non-crystalline regions or between fibrils and its failure to penetrate into crystalline regions. The non-crystalline regions tend to dissolve as glucose does, the cellulose molecules moving apart and so giving room for the water to enter, but the cellulose molecules cannot break away completely, since they are held firmly in the crystalline regions. The fibrils in natural cellulose fibres must also be molecularly interconnected in a way that prevents complete solution or alternatively held together in a state of dynamic equilibrium, which prevents any fibre from becoming completely free at any instant.

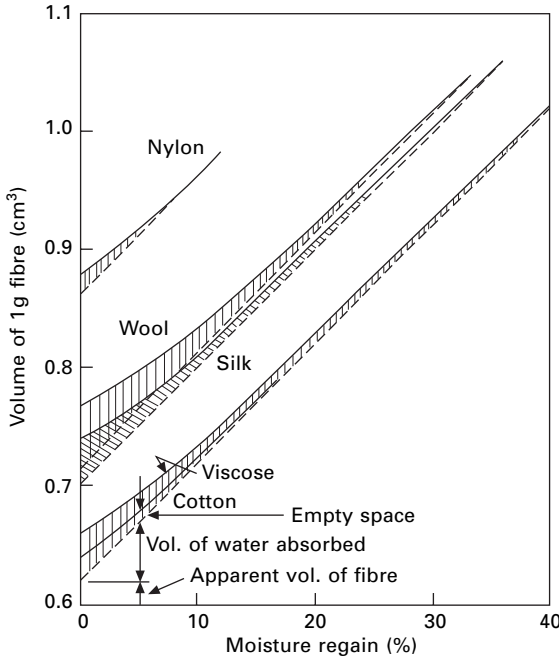
Since it is a necessary condition for the stability of fibres in water, the reason why the crystalline regions do not dissolve is worth a closer study. It is due to the cumulative action of all the active groups in forming crosslinks. Whereas in glucose, or non-crystalline cellulose, one active group can be attacked by water at a time, in order to penetrate the crystalline regions of cellulose it would be necessary to attack a large number of active groups at the same time. This is inherently unlikely to occur, since the water molecules act at random and not together. The situation may be compared to a war between irregular forces and a large army. If the army is spread out, the irregular forces can harry and destroy it by isolated raids, although they could not organise and win a single pitched battle with the army in close formation.

Swelling occurs because the fibre molecules are pushed apart by the absorbed water molecules. The resulting distortion of the fibre sets up internal stresses, which influence the moisture absorption. This aspect of the subject, which can be treated mathematically by thermodynamics, has been particularly studied by Barkas and is discussed in Section 12.3. It leads to an alternative explanation of hysteresis, for if there is mechanical hysteresis in the fibres, it must necessarily cause moisture hysteresis.

The density changes during swelling (see [Section 6.3](#)) are also of interest. Initially, as shown in [Fig. 12.4](#), the change is such that the increase in volume is less than the volume of the added water. Apart from the improbable suggestion that the absorbed water is compressed, this must mean that the water molecules are fitted closely into the structure, with a more complete use of the space available. This is analogous to filling the spaces between tennis balls in a box with marbles. The close fitting is in accord with the view that the first water molecules are directly attached to the active groups in the fibre molecule. As absorption proceeds, the increase in volume becomes equal to the volume of water added, which indicates that the water is packed in much the same way as in liquid water or ice and is merely spreading out the polymer structure. A change in moisture content with little change in volume will again occur at high moisture contents if void spaces are filled with water by capillary sorption.

12.1.7 Capillary water

At very high humidities, liquid water may be held by the forces of surface tension in capillary spaces between fibres or in crevices in the fibre surface. The equilibrium vapour pressure, p_a over a concave curved surface of radius a is lower than that over



12.4 Change in fibre specific volume with regain. From Meredith [9].

a plane surface p_{∞} , owing to the surface tension of the water. This is given by Kelvin's equation:

$$\log_e \frac{p_a}{p_{\infty}} = - \frac{2\sigma M}{\rho R T a} \quad (12.1)$$

where σ = surface tension, M = molecular weight of water, i.e. 18, ρ = density of water, R = gas constant, and T = absolute temperature.

Now, p_{∞} is equal to the saturation vapour pressure, and thus the relative humidity over the curved surface will be given by:

$$\text{relative humidity} = H = 100 \left(\frac{p_a}{p_{\infty}} \right) \% \quad (12.2)$$

$$\log_e \frac{H}{100} = - \frac{2\sigma M}{\rho R T a} \quad (12.3)$$

For water at 20 °C,

$$a = \frac{0.47}{2 - \log_{10} H} \text{ nm} \quad (12.4)$$

Consequently, for a specimen in an atmosphere of given relative humidity, there will be no tendency for water to evaporate from capillaries in which the radius of the water meniscus is less than that given by the above equation. At higher relative humidities, water will remain in larger capillaries, and so the regain will increase.

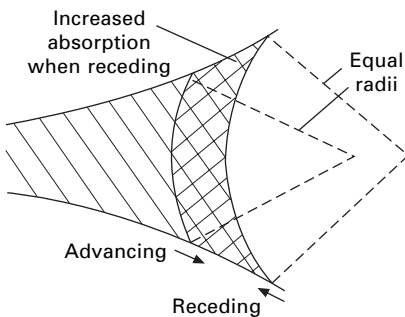
Hysteresis may be explained as being due to a change of contact angle, depending on whether the meniscus is advancing or receding. Thus a given radius of meniscus (i.e. a given relative humidity) will occur at a wider portion of the capillary when it is receding, and there will be a greater amount of water present, as shown in Fig. 12.5.

The capillary theory was, indeed, first proposed as a general explanation of moisture absorption over a wide range of humidities. It is worth examining why it is not valid in this way, apart from the fact that capillary spaces within the fibre are purely hypothetical.

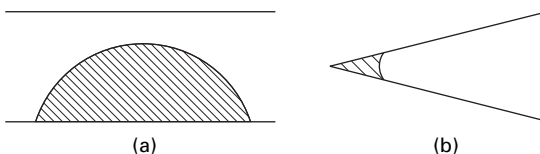
The first difficulty with the theory is that it does not explain how condensation could occur initially in an open capillary. As is shown in Fig. 12.6(a), this would have to pass through a phase in which the surface is convex and would thus be formed only in a supersaturated atmosphere. A possible answer to this difficulty is that the condensation starts at the end of a wedge-shaped capillary (Fig. 12.6(b)), where the radius would be very small and the surface concave.

The second difficulty is more important. Table 12.1 shows the radii of the menisci at various humidities, given by Equation (12.4). The diameter of a water molecule is 0.4 nm, which enables us to calculate the number of water molecules that would fit across a capillary. At 60% r.h., this is only ten, or fewer if the contact angle is greater than zero. Surface tension is, however, an average property based on summation over a large number of molecules, and thus it is not a concept that can be applied to capillaries that are only a few molecules wide. Indeed, unless there is a large number of molecules in the surface, it is not possible to define a radius of curvature.

This means that the capillary water can play a part only at very high humidities. In fact, the experimental results, discussed in Section 10.3.3, suggest that there is a



12.5 Hysteresis in capillaries.



12.6 Initial condensation in capillaries: (a) open capillary; (b) wedge-shaped capillary.

Table 12.1 Meniscus dimensions

r.h. (%)	Radius of meniscus (nm) from equation (12.4)	Diameter of meniscus
		Diameter of water molecule
50	1.6	5
60	2.1	10
70	3.0	15
80	4.8	24
90	10	50
95	21	104
99	110	500
99.9	1200 (1.2 μm)	5000

significant amount of capillary water present only at relative humidities greater than 99%.

12.2 Quantitative theories of absorption

12.2.1 Mechanistic molecular theories

The calculation of the division between directly and indirectly attached water, and its relation to relative humidity, have been the subject of much theoretical speculation. These theories have been reviewed by McLaren and Rowen [10] and subjected to critical comment by various other authors [11, 12]. Some of them will be described here, but others will be mentioned only briefly. More recent reviews [13–15] relate to moisture absorption in foods.

In 1929, Peirce [16] put forward a theory which, despite arbitrary assumptions, still bears comparison with the more sophisticated theories proposed later. He first developed an argument for calculating the division between directly and indirectly attached water molecules, as follows. Let C = total number of water molecules/absorption site, C_a = number of directly absorbed water molecules/absorption site, C_b = number of indirectly absorbed water molecules/absorption site, so that

$$C = C_a + C_b \quad (12.5)$$

If C increases by dC , then the fraction of molecules directly absorbed will be proportional to the number of unoccupied sites ($1 - C_a$):

$$\frac{dC_a}{dC} = q(1 - C_a) \quad (12.6)$$

where q is a factor of proportionality. Integrating, we obtain

$$-\log_e (1 - C_a) = qC \quad (12.7)$$

$$C_a = 1 - e^{-qC} \quad (12.8)$$

Peirce assumes that the constant q is equal to 1 and puts forward some arguments in support of this. It must, however, be regarded as an arbitrary assumption, which is

open to criticism on the grounds that it does not correctly represent the different attractions of the vacant and covered sites. With this assumption, we have

$$C_a = 1 - e^{-C} \quad (12.9)$$

and, from equation (12.5):

$$C_b = C - 1 + e^{-C} \quad (12.10)$$

We can express C in terms of the regain of the material r since we have:

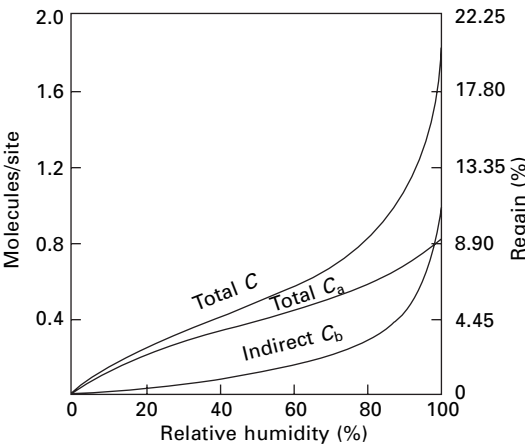
$$r = 100 \left(\frac{\text{mass of absorbed water}}{\text{mass of material}} \right) \% = 100 \frac{M_w C}{\gamma M_0} \quad (12.11)$$

where M_w = molecular weight of water = 18; M_0 = molecular weight per absorption site = $1/3$ molecular weight of glucose residue = 54; γ = total mass of material/mass of absorbing (non-crystalline) material¹. Hence

$$C = \frac{3\gamma r}{100} \quad (12.12)$$

Figure 12.7 shows the division of the experimental curve for regain against relative humidity into the two phases. This shows the combination of two curves of different shapes to give a resultant sigmoidal curve. Most of the initial absorption is directly attached, whereas the absorption at higher humidities is mainly indirectly attached.

It is the directly attached water that changes the forces between molecules and breaks crosslinks, so that it should have a greater effect than the indirectly attached



12.7 Division of regain of cotton between two phases on Peirce's theory.

¹In his original argument for cotton, Peirce assumed that all the material was accessible but that only one hydroxyl group per glucose residue was effective in absorption, but Hearle [17] has pointed out that, since only about one-third of the material in cotton is effectively non-crystalline and so accessible to water molecules, the same numerical result would be obtained by assuming that all the hydroxyl groups in the non-crystalline regions, but none in the crystalline regions, are effective in absorption. This also enables the analysis to be applied to other cellulosic fibres.

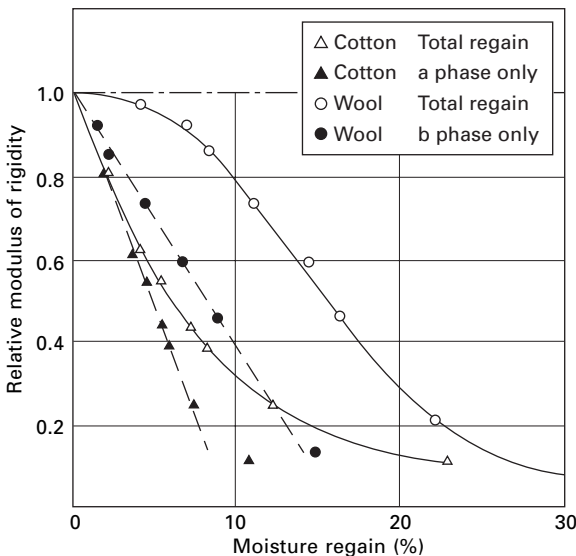
water on the physical properties of the fibre. Figure 12.8 shows a plot of relative torsional rigidity against moisture absorption that confirms this view. There is a linear relation between rigidity and C_a .

On the other hand, it will be the indirectly attached water molecules that will be the first to evaporate, so these would be expected to have the greatest effect on the vapour pressure. This enables a relation between regain and relative humidity to be calculated. Peirce assumes that only a fraction $1/\beta$ of the sites is effective in indirect absorption and that when these are filled there is saturation. The reason given for assuming that not all sites are effective is that one indirectly attached water molecule can seal off a number of sites, as in Fig. 12.9.

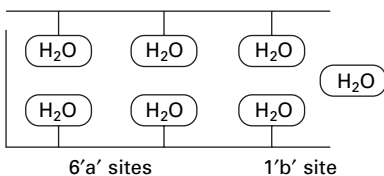
We then have:

$$\begin{aligned} \text{vapour pressure} &= p = \text{saturation vapour pressure } p_0 \\ &\times \text{fraction of these sites occupied} \end{aligned}$$

Thus the fraction of sites occupied by one or more water molecules equals p/p_0 .



12.8 Modulus of rigidity (relative to value when dry) plotted against regain.



12.9 Suggested mechanism for limitation of number of sites for indirect absorption.

If C_b increases by dC_b , the added water molecules divide between previously occupied and unoccupied sites, and we have:

$$\begin{aligned}
 \text{increase in fraction of occupied sites} &= d(p/p_0) \\
 &= (1/p_0) dp \\
 &= \frac{\text{fraction of previously unoccupied sites} \times \text{number of molecules added}}{\text{total number of sites}} \\
 &= \frac{(1 - p/p_0) dC_b}{1/\beta} \quad (12.13)
 \end{aligned}$$

Thus,

$$\frac{dp}{1 - p/p_0} = \beta p_0 dC_0 \quad (12.14)$$

which on integration gives:

$$\frac{p}{p_0} = 1 - \exp(-\beta C_b) \quad (12.15)$$

This gives a relation between relative humidity and moisture absorption, but a correction term should be added for evaporation from sites with directly absorbed water that is not covered by indirectly absorbed water. The number of these is $(1 - p/p_0)C_a$, which equals $C_a \exp(-\beta C_b)$. Assuming that they have K times the effect of indirectly attached water molecules, we get:

$$\frac{p}{p_0} = 1 - \exp(-\beta C_b) + K C_a \exp(-\beta C_b) \quad (12.16)$$

which gives

$$1 - \frac{p}{p_0} = (1 - K C_a) \exp(-\beta C_b) \quad (12.17)$$

or, substituting from equations (12.9), (12.10) and (12.12)

$$1 - \frac{p}{p_0} = \{1 - K(1 - e^{-3\gamma r/100})\} e^{-\beta(e^{(-3\gamma r/100)} - 1 + 3\gamma r/100)} \quad (12.18)$$

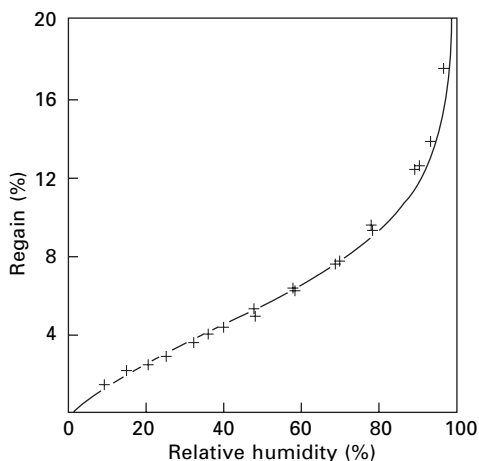
This is the equation for the curve of regain against relative humidity. A comparison with experiment is shown in [Fig. 12.10](#).

Cooper [18] has shown that, at very low humidities, Peirce's equation reduces to the form

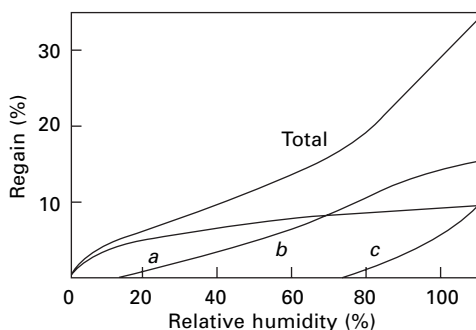
$$-\log_e (1 - p/P) = b_1 r + b_2 r^2 \quad (12.19)$$

where b_1 and b_2 are constants. This equation fits experimental results for cellulosic fibres reasonably well.

Speakman [19] developed for wool a theory similar to Peirce's. He divided the water up into three phases, as shown in [Fig. 12.11](#). The first phase to be absorbed is



12.10 Comparison of Peirce's equation with experimental data for soda-boiled cotton at 110 °C [12]. Equation for curve is: $1 - p/P = (1 - 0.40 C_a) e^{-5.4C_b}$.



12.11 Division of water into three phases on Speakman's theory for wool [19].

tightly bound to hydrophilic groups in the side chains of the keratin molecule, and has little effect on the rigidity of the structure. Hearle [20] has pointed out that it has little effect on the permittivity and electrical resistance of wool. The second phase is attached to groups in the main chain and replaces crosslinks between molecules. It thus has the main effect on the rigidity, as shown in Fig. 12.8. The third phase is more loosely attached and is appreciable only at high humidities. Speakman suggested that it is due to capillary condensation, though it would probably be more correct to regard it as similar to Peirce's indirectly attached water.

12.2.2 Multilayer adsorption: the Brunauer, Emmett and Teller (BET) equation

Another theory derives from Langmuir's [21] classical adsorption isotherm for gases and vapours adsorbed in a monomolecular layer on the surface of a material.

This was extended by Brunauer Emmett, and Teller [22] to cover multilayer adsorption².

The analysis is based on the equilibrium between the rate of evaporation and the rate of condensation on the surface. The analysis involves two constants: r_1 , the regain corresponding to a monomolecular layer, and α , which is approximately equal to $\exp[(E_1 - E_L)/RT]$, where E_1 is the heat of absorption on the first and E_L that on the succeeding layers. It yields an equation that may be written in the following forms:

$$\frac{r}{r_1} = \frac{\alpha p}{(p_0 - p) [1 + (\alpha - 1) p/p_0]} \quad (12.20)$$

$$\frac{p}{r(p_0 - p)} = \frac{1}{\alpha r_1} + \frac{\alpha - 1}{\alpha r_1} \frac{p}{p_0} \quad (12.21)$$

The latter is a convenient form for testing the relation, since it means that a plot of $p/r(p_0 - p)$ against p/p_0 should give a straight line from which the values α and r_1 can be determined.

The BET equation gives a sigmoidal isotherm, which shows a good fit with several practical examples of absorption. However, its application to absorption by fibres may be criticised on several grounds: (1) that the idea of adsorption on a surface, even an internal surface, is not valid for the mixing of fibre molecules and water molecules that actually occurs; (2) that it neglects the interaction between neighbouring molecules in a layer; (3) that it takes no account of effects due to swelling and mechanical restraint. The first objection does not apply to the derivations of the same equation on the basis of modern theories of statistical thermodynamics that have been put forward by Cassie³ [23] and by Hill [24]. In this method, it is necessary to assume that the adsorption takes place on localised sites, but these may be either spread throughout the volume of the material or concentrated on a surface.

The BET equation fits the experimental results for cotton, viscose rayon, secondary acetate, wool, silk and nylon between about 5 and 50% r.h. It breaks down at high humidities, as would be expected, since it assumes that the regain tends to infinity at saturation. Bull [25] gives values of α , r_1 and $(E_1 - E_L)$ for these fibres Taylor's experiments [26, 27] on the absorption of viscose rayon and cotton below 5% r.h. also show that the BET equation does not fit the results in this range. He finds a good fit in this region with the Freundlich relation ($r = Kp^{1/n}$, where K and n are constants, $n > 1$) though this relation lacks a sound theoretical basis.

Cassie [28] has attempted to take account of swelling by applying the BET equation to his reduced regain–relative humidity curve (see [Section 12.3.5](#)). There is improved agreement at high humidities when the reduced vapour pressure, p_F , is substituted for the actual vapour pressure.

Windle [29] has modified Cassie's theory, in an application to wool, by assuming that the absorbed water molecules may be divided into three types: localised water,

²A more detailed discussion of the BET equation is given in earlier editions of this book, but, since its predictive value for fibres is limited, a shorter version is included here.

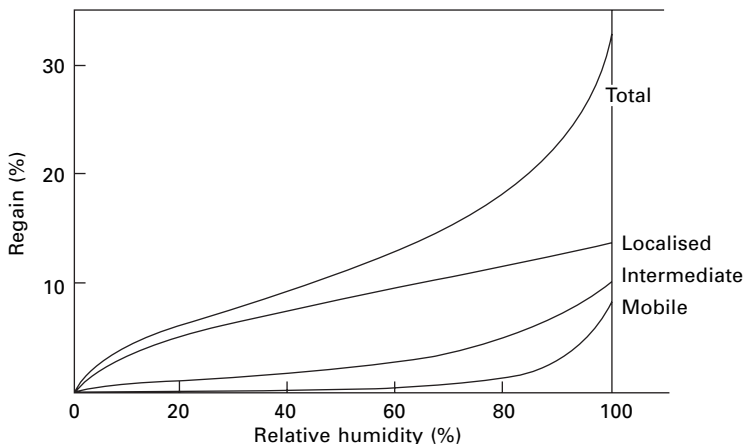
³Cassie's derivation has been criticised [12], and Hill's differs from it in certain details.

directly absorbed onto absorption sites and limited to one per site; intermediate water, absorbed onto localised water molecules and limited to one on each localised water molecule; and mobile water, absorbed on intermediate water molecules, with no restriction on numbers. There are three arbitrary constants to be fitted and, when this is done, the theory shows good agreement with experimental data on absorption and heat of wetting. The number of absorption sites is what would be expected from the molecular structure, and the energies of absorption are reasonable. The theory has been used to explain the dielectric data at very high frequencies (see [Section 19.5](#)). The division between the three phases is shown in Fig. 12.12.

This theory differs from Speakman's three-phase theory [19] in that the three types of water are absorbed on top of each other, whereas in Speakman's theory the first two phases were absorbed in parallel on different types of absorption site. It is likely that there ought to be a division of the localised water on Windle's theory in the same way, for the torsional rigidity is found to have a linear relation with the sum of the localised and intermediate water only when this is greater than 4%. This suggests that the first 4% is absorbed on different positions in the molecules.

Another version of this line of approach, due to Feughelman and Haly [30], is based on the assumption that each water molecule has four associations with its neighbours. The water is thus split up into five types, depending on whether the water molecules have zero, one, two, three or four associations with a keratin molecule. The first group, with four associations with other water molecules, is completely free; the fifth group is the most strongly bound.

A number of modifications [31–35] have been applied to Hill's derivation [31] of the BET equation; these take into account such factors as swelling, the presence of more than one type of absorption site, interaction between layers, varying heats of absorption, and so on, but none of them shows a marked improvement in the agreement with experiment.



12.12 Division of water into three phases on Windle's theory for wool [29].

12.2.3 Solution theories

Adsorption theories are based on the attachment of water molecules to particular sites (localised on the surface or at definite positions in the volume of the material), but there is an alternative view, which considers the mixing of molecules of different types with no limitation on the positions of the molecules. Such a mixture of molecules is a solid solution, and solution theory can be applied to it.

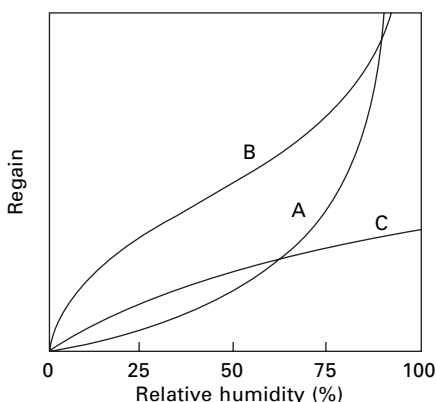
Barrer [36] has derived a solution theory for absorption by using statistical thermodynamics, which fit the practical results for the absorption of gases in rubber-like polymers. This solution theory gives a curve that is concave to the regain axis, in contrast to the convex Langmuir isotherm and the sigmoidal BET isotherm, as shown in Fig. 12.13. This type of theory is thus unlikely to fit the results at low humidities.

Extending the current thermodynamic theories of solution to take account of the energy involved in elastic deformation of the polymer, Rowen and Simha [37] obtained the following isotherm:

$$\log_e \frac{H}{100} = \log_e v_1 + v_2 + \mu v_2^2 + \frac{KV}{RT} \left(\frac{1}{-v_2^{1/2}} - 1 \right) \left(\frac{5}{3v_2^{1/2}} - 1 \right) \quad (12.22)$$

where H = relative humidity %, v_1 = volume fraction of the material, v_2 = volume fraction of the absorbed water, V = partial molal volume of liquid, μ = a constant, determined by the heat and entropy of mixing, and K = a constant, depending on the mechanical reaction of the polymer to sorption.

This equation gives a better fit above 50% r.h. than the BET isotherm, but shows the failure of a simple solution theory at low humidities⁴.



12.13 Comparison of plots of regain against relative humidity on: A solution theory, B BET isotherm and C Langmuir isotherm.

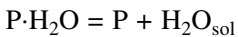
⁴A comparative plot for cotton was included in earlier editions of this book.

12.2.4 Hailwood and Horrobin's theory

In one of the most interesting theoretical treatments, Hailwood and Horrobin [38] have combined an attachment of the first water molecules onto particular sites in the polymer molecule with a solution theory for the further absorption of water by the material.

They consider that some of the water is present as hydrates formed with definite units of the polymer molecule and that the remainder forms an ideal solid solution in the polymer. By consideration of the chemical equilibrium, they derive an equation relating the amount of water absorbed to the relative humidity. Their derivation is a general one, allowing for a variety of different hydrates to be formed but, in fitting the results, they find that it is sufficient to assume that only one type of hydrate is involved. To simplify the working, this assumption is made at the beginning of the derivation of the equation given here, and consequently there are only two chemical equilibria involved.

It is assumed that the dissolved water, the unhydrated polymer and the polymer hydrate form a single solid phase. In this phase, there will be an equilibrium between water combined with a unit, P of the polymer molecule to form the hydrate, and water present as dissolved water

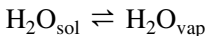


By the Law of Mass Action, we have

$$[P \cdot H_2O] = K_1 [H_2O_{\text{sol}}] [P] \quad (12.23)$$

where K_1 is the equilibrium constant.

There is also an equilibrium between the dissolved water and the water vapour in the atmosphere:



giving:

$$[H_2O_{\text{sol}}] = K_2 [H_2O_{\text{vap}}] \quad (12.24)$$

The activity of the water vapour, at the low water vapour concentration involved, is given by the fractional humidity. If the relative humidity is $H\%$, we thus have

$$[H_2O_{\text{vap}}] = H/100 \quad (12.25)$$

and hence from equation (12.24)

$$[H_2O_{\text{sol}}] = KH \quad (12.26)$$

where $K = K_2/100$.

The activities of the three types of molecule present in what is assumed to be an ideal solid solution are given by the mole fractions of each type of molecule present, that is:

$$[H_2O_{\text{sol}}] = \frac{n_w}{n_w + n_0 + n_1} \quad (12.27)$$

$$[P] = \frac{n_0}{n_w + n_0 + n_1} \quad (12.28)$$

$$[P \cdot H_2O] = \frac{n_1}{n_w + n_0 + n_1} \quad (12.29)$$

where n_w = number of moles of water in solution in polymer, n_0 = number of moles of the unhydrated polymer units and n_1 = number of moles of polymer hydrate.

It follows from equations (12.26) and (12.27) that:

$$n_w = \frac{n_0 + n_1}{1 - [H_2O_{sol}]} [H_2O_{sol}] = \frac{(n_0 + n_1) KH}{1 - KH} \quad (12.30)$$

and from equations (12.23), (12.26), (12.28) and (12.29) that:

$$n_1 = \frac{n_0 [P \cdot H_2O]}{[P]} = n_0 K K_1 H \quad (12.31)$$

The number of moles of water taken up by the material (whether dissolved or as hydrate) is equal to $(n_w + n_1)$, and the number of moles of the polymer unit present (whether hydrated or not) is equal to $(n_0 + n_1)$. The percentage regain r is therefore given by:

$$r = \frac{1800 (n_w + n_1)}{(n_0 + n_1) M} \quad (12.32)$$

where M = molecular weight of the polymer unit, and 18 = molecular weight of water. Thus:

$$\frac{Mr}{1800} = \frac{n_w}{n_0 + n_1} + \frac{n_1}{n_0 + n_1} \quad (12.33)$$

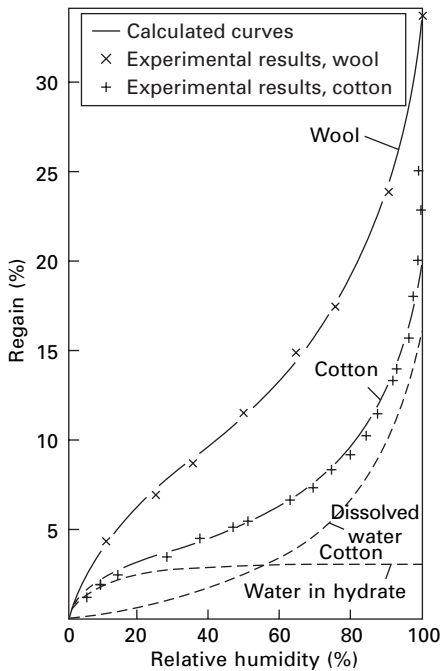
and from equations (12.30) and (12.31):

$$\frac{Mr}{1800} = \frac{KH}{1 - KH} + \frac{KK_1H}{1 + KK_1H} \quad (12.34)$$

which is the equation relating regain and relative humidity derived by Hailwood and Horrobin [38].

This equation contains three constants M , K and K_1 which can be chosen to give the best fit with the experimental data. Figure 12.14 gives a comparison of the observed and calculated results for cotton and wool at 25 °C and shows the division of the water taken up by cotton between the hydrate and the solution. Hailwood and Horrobin also found a good fit between the calculated and observed results for hair, silk and nylon. It has, however, been pointed out that any equation of this form must give a sigmoidal curve with a suitable choice of the three constants, and thus the significance of the fit is reduced.

From the equilibrium constants chosen, the heats of the reaction can be calculated, and a reasonable agreement with results from calorimetric measurements is found for wool. The theory also leads to a prediction of the variation of specific volume with



12.14 Comparison of Hailwood and Horrobin's equation [38] with experimental results for wool and cotton.

regain, which is in fair agreement with the experimental results for wool, except at the higher humidities.

The values of M that are found are all greater than the molecular weight corresponding to a single polar group in the fibre molecule. It is assumed that this is due to the fact that the crystalline material is not accessible to moisture and adds to the mass of polymer present. Consequently, the value of M can be used to estimate the amount of inaccessible material present, and the values obtained are in reasonable agreement with values obtained by other methods.

Hailwood and Horrobin's theory has been criticised mainly because of the assumption that an ideal solid solution is formed, whereas mixtures of large and small molecules usually depart from the ideal.

12.3 The relations between absorption, swelling and elastic properties

12.3.1 Swelling and osmosis

Quite a different approach to moisture sorption has been developed by Barkas [39], starting from the analogy between swelling and osmotic phenomena. In osmosis, water passes through a semipermeable membrane from a region of low solute concentration to a region of high solute concentration until a pressure sufficient to prevent the flow of water is built up. The same sort of thing happens in swelling.

Water passes into the region of high polymer concentration, and the polymer swells. This continues until the stresses generated by the deformation of the polymer are sufficient to prevent more water from flowing in.

Consequently, the moisture absorption will be very dependent on the stresses developed in the fibre owing to internal or external effects, and thermodynamic relations similar to those applicable in osmosis can be applied to swelling.

12.3.2 Qualitative view of influence of mechanical forces on absorption

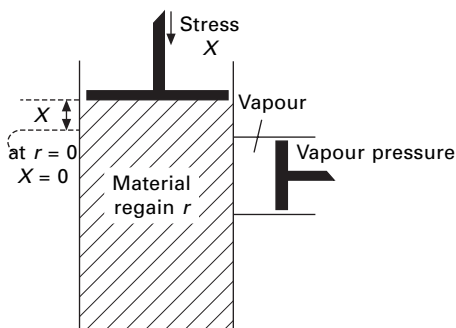
We can consider a substance absorbing from an atmosphere of given vapour pressure and subject to a stress. The exact form of the specimen is unimportant for the qualitative argument: one simple form is illustrated in Fig. 12.15. Let vapour pressure = p , regain of material = r , stress applied to material = X , with a compression, i.e. a force reducing swelling, taken as positive, and strain, or swelling = x , with an increase in size taken as positive. The origin $x = 0$ is taken at $r = 0$, $X = 0$.

Figure 12.16 (a) shows the curves of regain against vapour pressure that would be obtained at various values of the applied stress X . As the stress increases, the regain decreases. Figure 12.16(b) shows stress–strain curves for various values of the regain of the material. Owing to swelling, the position of the origin of the stress–strain curves (i.e., the value of x at $X = 0$) varies with the regain.

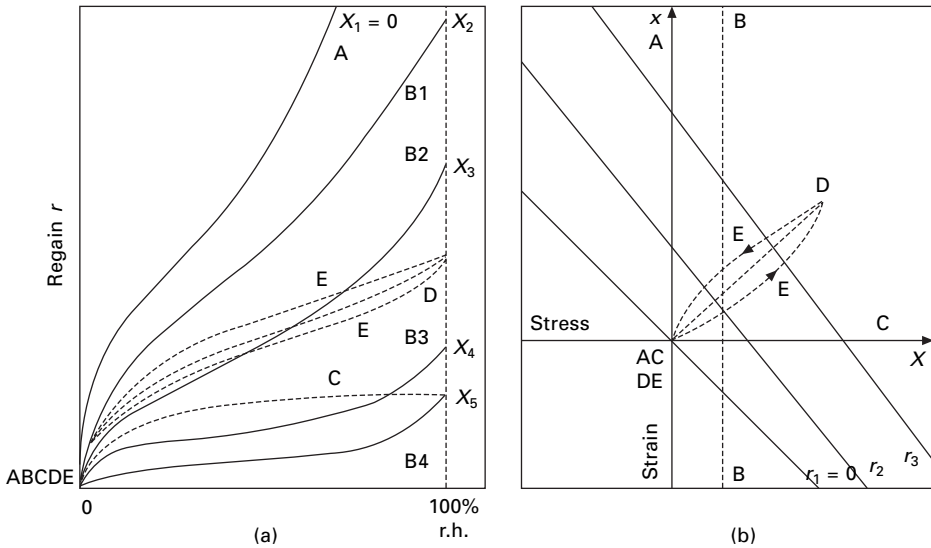
The system being considered has two degrees of freedom (at constant temperature) for, when any two of the quantities considered are specified (for example, the stress and vapour pressure), the other quantities involved are necessarily determined. This means that any given point on the stress–strain curve corresponds to a particular point on the regain vs vapour pressure curve, and vice versa.

It is interesting to see what happens under various conditions that might occur in practice.

- (A) Free swelling. There will be zero applied stress, so the line AA will be followed.
- (B) Swelling under constant stress, X_2 . The line BB will be followed. The lower full lines are at increasing values of stress X_3 , X_4 , X_5 .
- (C) Moisture absorption at constant volume. In this case, x does not vary, so the



12.15 Model for absorption under stress.



12.16 (a) Absorption curves (full lines at constant stress). (b) Stress-strain curves (full lines at constant regain). Practical cases: A, free swelling; B1–B4, swelling under stress; C, swelling at constant volume; D, swelling restrained by ideal spring; E, swelling restrained by internal restraint, with mechanical hysteresis.

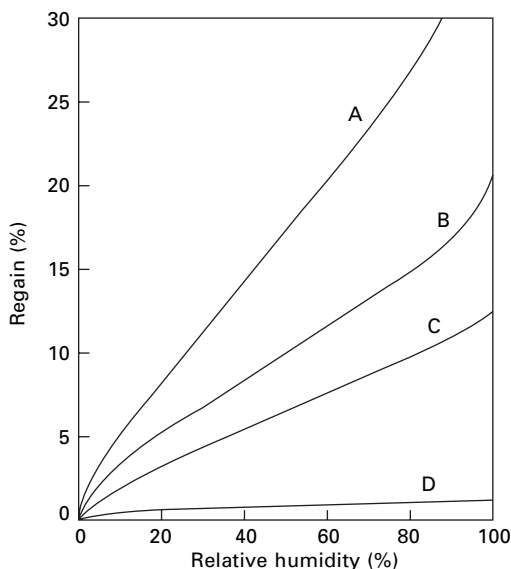
stress increases as the swelling proceeds. This gives the curve CC, showing a reduced moisture absorption.

- (D) Swelling restrained by an ideal spring. In this case, the stress will increase in proportion to the strain x and the absorption will be reduced, but not as much as in the previous case. The curves DD will be followed.
- (E) Swelling restrained by a spring showing hysteresis. There will be hysteresis in the X/x relation, and this will be transferred to the relation between regain and vapour pressure. The curves EE result.

Figure 12.17 illustrates a practical example of these effects. It shows the reduction of moisture absorption that would occur in wood under two restraining conditions, namely, when the volume of a block of wood is held constant, and when the volume of the wood cell walls is constant.

12.3.3 Internal restraints; plasticity and hysteresis

The above discussion has been concerned with external forces, and it is also these to which thermodynamics is immediately applicable. However, the swelling of a fibre is limited by restraints arising from the arrangement of the molecules in a three-dimensional network. There will be stresses acting on a small element of an amorphous region that is absorbing water, because the molecules are held firmly fixed elsewhere in crystalline regions. On a larger scale, there may be forces arising from the interference from one part of the fibre with the swelling of another part. This will occur when the



12.17 Absorption of spruce wood under stress: A, material completely free of stress; B, natural sorption, including internal restraints on swelling of block of wood; C, volume of block of wood held constant, but allowing swelling into void spaces in wood cells; D, wood cell walls (internal and external) held at constant volume. Curve B is experimental; remainder are calculated. From Barkas [39].

swelling is non-uniform, for example, when there is a skin on the fibre. All these internal forces in a fibre will thus be important in determining its moisture absorption. For example, Fig. 12.17 shows the increased absorption that would occur in stress-free wood with the internal restraints removed, except for those in the molecular structure itself.

Fibres are not perfectly elastic, however. There is plasticity. When a stress is removed, recovery is incomplete. The internal stress-strain curve would be a loop similar to the curve EE in Fig. 12.16(b) and would thus cause hysteresis in the moisture absorption as well. In other words, wherever there is mechanical hysteresis in a fibre, there must also be moisture hysteresis. Experimentally it is found that in natural and regenerated fibres both forms of hysteresis occur to a marked extent. In nylon, where the elastic recovery is good, there is also very little moisture hysteresis.

12.3.4 Thermodynamic relations

By the use of thermodynamics, quantitative relations between swelling, moisture absorption and mechanical properties can be derived. It should be remembered that thermodynamic equations (as distinct from inequalities) apply only to reversible changes, and they break down when there is hysteresis.

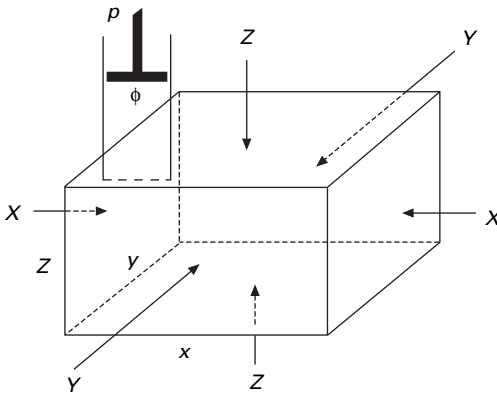
The general equation may conveniently be derived, in the method proposed by Hearle [40], by considering a rectangular parallelepiped under stresses normal to its

faces and swelling in directions parallel to its sides. This can be modified for other shapes and for other types of stress and deformation.

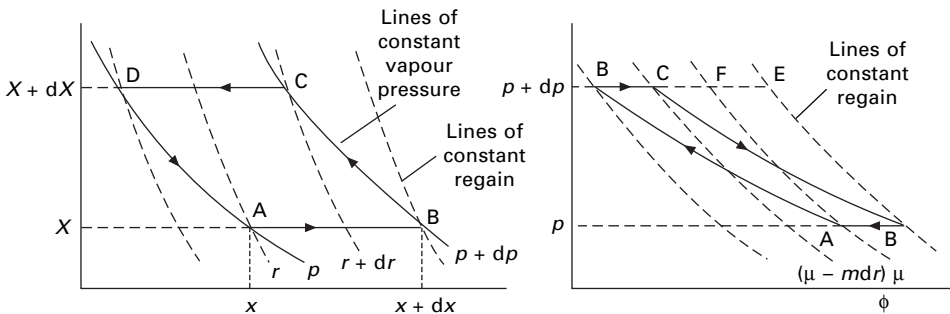
Figure 12.18 illustrates a specimen of mass m (when dry); of volume mV (i.e. V is the volume of a specimen having unit mass when dry); with sides x, y, z ; at a fractional regain ρ (i.e. containing a mass $m\rho$ of water); and having compressive stresses, X, Y, Z , normal to its faces. It is assumed that water can only be lost to or gained from a container of volume ϕ containing a mass μ of vapour at a vapour pressure p . Let the specific volume of the vapour be v .

We consider a general isothermal change in condition of this specimen, in which the stresses change from X to $X + dX$, Y to $Y + dY$, and Z to $Z + dZ$; the lengths of the sides change from x to $x + dx$, y to $y + dy$, and z to $z + dz$; the regain changes from ρ to $\rho + d\rho$; and the vapour pressure changes from p to $p + dp$. The mass of vapour in the container will change from μ to $(\mu - md)\rho$.

In order to find the relations between these changes, we can take the specimen through a suitable cycle. Since this will be a reversible isothermal cycle, it follows from the Second Law of Thermodynamics that the total work done is zero. The cycle chosen, and illustrated for the x -direction in Figure 12.19, is as follows:



12.18 Parallelepiped model.



12.19 X, x and p, ϕ cycles.

- a → b: an increase in vapour pressure from p to $p + dp$ at constant applied stress. Specimen absorbing moisture from container.
- b → c: an increase in applied stress by dX , dY and dZ , at constant vapour pressure. Moisture evaporating into container.
- c → d: a decrease in vapour pressure to p at constant applied stress. Moisture evaporating.
- d → a: a decrease in stress to X , Y , Z . Moisture being absorbed.

The work done may be evaluated as follows:

- by force on the X-face:

$$\begin{aligned}
 \text{work} &= \oint (\text{force} \times \text{displacement}) \\
 &= \text{area of X-face} \times \text{area enclosed by X, } x \text{ cycle} \\
 &= \frac{mV}{x} \left(\frac{\partial x}{\partial p} \right)_{X,Y,Z} dp \cdot dX \quad (12.35)
 \end{aligned}$$

- similarly for the Y- and Z-faces;
- by force on the vapour container:

$$\begin{aligned}
 \text{work} &= \oint (\text{pressure} \times \text{volume}) \\
 &= -\text{area of } p, \phi \text{ cycle}
 \end{aligned}$$

The negative sign is introduced because the cycle is enclosed in the reverse direction to that of the stress cycles.

$$\text{Area of } p, \phi \text{ cycle} = dp \text{ (increase in } \phi_{a \rightarrow d}) \quad (12.36)$$

This change in ϕ may be expressed in one of two ways. Either:

increase in $\phi_{a \rightarrow d}$ = increase in mass of vapour in container \times specific volume

$$= -m \left[\left(\frac{\partial \rho}{\partial X} \right)_{p,Y,Z} + \left(\frac{\partial \rho}{\partial Y} \right)_{p,Z,X} + \left(\frac{\partial \rho}{\partial Z} \right)_{p,X,Y} \right] v \quad (12.37a)$$

The negative sign is introduced because an increase of mass of vapour in the container corresponds to a decrease of regain in the material.

Or:

$$\begin{aligned}
 \text{increase in } \phi_{a \rightarrow d} &= \text{increase in } \phi_{c \rightarrow e} - \text{increase in } \phi_{c \rightarrow f} \\
 &= -mv (\text{increase in regain}_{c \rightarrow d} - \text{increase in regain}_{c \rightarrow a}) \\
 &= -mv \left[\left(\frac{\partial \rho}{\partial p} \right)_{X,Y,Z} (-dp) - (-dp) \right] \quad (12.37b)
 \end{aligned}$$

Hence, from equations (12.36) and (12.37):

$$\text{work} = mv \, dp \left[\left(\frac{\partial p}{\partial X} \right)_{p,Y,Z} + \left(\frac{\partial p}{\partial Y} \right)_{p,Z,X} + \left(\frac{\partial p}{\partial Z} \right)_{p,X,Y} \right] \quad (12.38a)$$

or

$$= -mv \, dp \left[\left(\frac{\partial p}{\partial p} \right)_{X,Y,Z} dp - dp \right] \quad (12.38b)$$

Summing the work done, and equating it to zero, we then have, from equations (12.35) and (12.38a), by cancelling m and dp throughout:

$$\begin{aligned} \frac{V}{x} dX + \frac{V}{y} \left(\frac{\partial y}{\partial p} \right)_{X,Y,Z} dY + \frac{V}{z} \left(\frac{\partial z}{\partial p} \right)_{X,Y,Z} dZ \\ + v \left[\left(\frac{\partial p}{\partial X} \right)_{p,Y,Z} dX + \left(\frac{\partial p}{\partial Y} \right)_{p,Z,X} dY + \left(\frac{\partial p}{\partial Z} \right)_{p,X,Y} dZ \right] = 0 \end{aligned} \quad (12.39)$$

Collecting the coefficients of dX , dY and dZ , we obtain the series of useful relations:

$$\frac{V}{x} \left(\frac{\partial x}{\partial p} \right)_{X,Y,Z} = - \left(\frac{\partial p}{\partial X} \right)_{p,Z,X} \quad (12.40)$$

and similarly for the other two directions.

Alternatively, from equations (12.35) and (12.38b), we obtain:

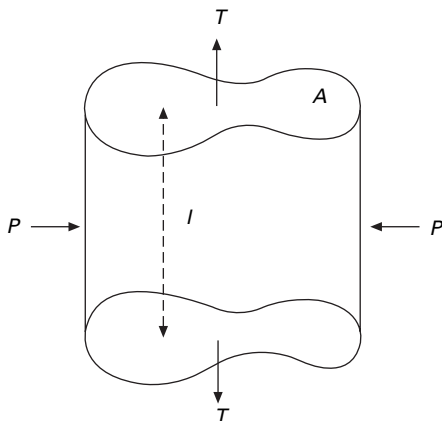
$$\begin{aligned} \frac{V}{x} \left(\frac{\partial x}{\partial p} \right)_{X,Y,Z} dX + \frac{V}{y} \left(\frac{\partial y}{\partial p} \right)_{X,Y,Z} dY + \frac{V}{z} \left(\frac{\partial z}{\partial p} \right)_{X,Y,Z} dZ \\ = v \left(\frac{\partial p}{\partial p} \right)_{X,Y,Z} dp - v dp \end{aligned} \quad (12.41)$$

which, on multiplying through by $(\delta p / \delta p)_{XYZ}$, gives:

$$\begin{aligned} \frac{V}{x} \left(\frac{\partial x}{\partial p} \right)_{X,Y,Z} dX + \frac{V}{y} \left(\frac{\partial y}{\partial p} \right)_{X,Y,Z} dY + \frac{V}{z} \left(\frac{\partial z}{\partial p} \right)_{X,Y,Z} dZ \\ = v \, dp - v \left(\frac{\partial p}{\partial p} \right) dp \end{aligned} \quad (12.42)$$

Equations (12.41) and (12.42) are alternative forms of the general equation relating the changes dX , dY , dZ , dp and dp . If other forces, such as shear forces, are involved, the appropriate work terms must be added to the equations.

It is convenient to modify the equations to apply them to single fibres. If we consider a fibre to be a cylinder of irregular cross-section, as shown in [Fig. 12.20](#), with area A and length l , the forces on the fibre to be a tensile stress T (being a



12.20 Stresses on a fibre.

tension, this will have the opposite sign to the forces so far considered) and a uniform transverse pressure P the equations become

$$\frac{1}{l} \left(\frac{\partial l}{\partial p} \right)_{T,P} = \frac{v}{V} \left(\frac{\partial p}{\partial T} \right)_{p,P} \quad (12.43)$$

$$\frac{1}{A} \left(\frac{\partial A}{\partial p} \right)_{T,P} = - \frac{v}{V} \left(\frac{\partial p}{\partial P} \right)_{p,T} \quad (12.44)$$

$$- \frac{1}{l} \left(\frac{\partial l}{\partial p} \right)_{T,P} dT + \frac{1}{A} \left(\frac{\partial A}{\partial p} \right)_{T,P} dP = \frac{v}{V} \left[\left(\frac{\partial p}{\partial p} \right)_{T,P} dp - dp \right] \quad (12.45)$$

and, for the change in regain

$$- \frac{1}{l} \left(\frac{\partial l}{\partial p} \right)_{T,P} dT + \frac{1}{A} \left(\frac{\partial A}{\partial p} \right)_{T,P} dP = \frac{v}{V} \left[dp - \left(\frac{\partial p}{\partial p} \right)_{T,P} dp \right] \quad (12.46)$$

It may be noted that, for a fibre under constant transverse pressure, for example, a single fibre in air, $dP = 0$, and thus the second term drops out of equations (12.45) and (12.46).

In applying these equations, two points must be remembered. First, they apply exactly only to reversible changes. Secondly, they are all differential equations, and direct integration is not possible, since the quantities involved vary with one another in ways that have not been analytically expressed, for example, v will be a function of p , and V will be a function of p , T , and P .

However, the equations may be used to obtain valuable approximate results that could not be obtained by direct experiment. For example, equation (12.44) would enable transverse pressures on fibres to be calculated approximately from the change in regain if the area-swelling behaviour of the fibre is known.

Figure 12.21 shows an experimental test of equation (12.43) made by Treloar [41]. The agreement between experiment and theory is quite good. Measurements of the converse effect, the stress ('hygrostress') that develops when wool fibres are taken from 100 to 0% r.h. at various extension levels, are reported by Haly [42].

12.3.5 Cassie's reduced regain–relative humidity curve

Cassie [28] has proposed another method of dealing with the influence of mechanical effects. He assumes that the water absorbed in wool is under a hydrostatic pressure P , which can be calculated from the swelling and the elastic properties. If the volume-swelling is dV/V , the pressure P is given by:

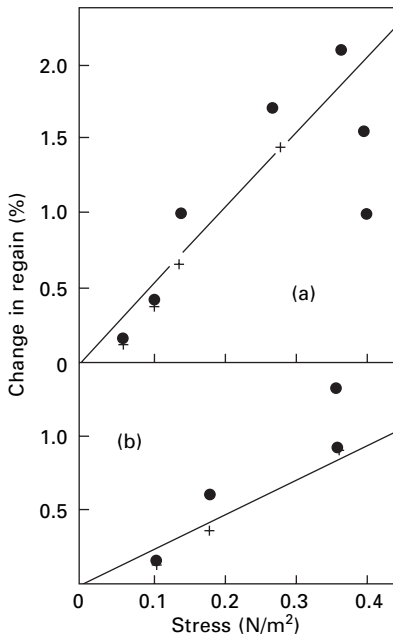
$$P = k \frac{\Delta V}{V} \quad (12.47)$$

where k is the bulk modulus of elasticity.

If the fibres are assumed to be isotropic in elastic properties, this becomes

$$P = \frac{E}{3(1 - 2\sigma)} \frac{\Delta V}{V} = \frac{E}{1 - 2\sigma} \frac{\Delta D}{D} \quad (12.48)$$

where E is the Young modulus, σ is the Poisson ratio, and is taken as 0.25, and $\Delta D/D$ is the diameter-swelling, which equals $\frac{1}{3}\Delta V/V$ if the swelling is isotropic.



12.21 Variation of regain of cellulose fibres with tension: (a) isotropic; (b) oriented. Experimental points compared with lines from equation (12.43). After Treloar [41].

The term $\Delta D/D$ is equivalent to a strain, and the values of $E \cdot \Delta D/D$ were assumed to be equal to the stress at the corresponding strain on Speakman's tensile stress-strain curves [43] at the appropriate humidity. Hence values of P at each relative humidity were obtained.

The variation of the vapour pressure of water with hydrostatic pressure is given by the thermodynamic relation

$$P = \frac{RT}{V_M} \log_e \frac{p}{p_F} \quad (12.49)$$

where R = gas constant, T = absolute temperature, V_M = molar volume, p = observed vapour pressure and, p_F = vapour pressure at zero hydrostatic pressure.

Putting in the appropriate numerical values, namely, $R = 8.31 \text{ J K}^{-1} \text{ mol}^{-1}$, $T = 298 \text{ K}$ (20°C) and $V_M = 18 \times 10^{-6} \text{ m}^3 \text{ mol}^{-1}$ ($18 \text{ cm}^3/\text{mol}$), gives the pressure in pascals (N/m^2) as:

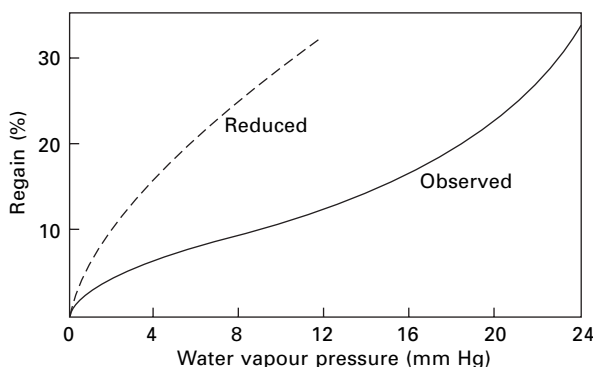
$$P = 3.16 \times 10^8 \log_{10}(p/p_F) \quad (12.50)$$

Thus, by using the values of P calculated as above, the values of p_F , the vapour pressure reduced to zero hydrostatic pressure, can be obtained. The reduced relative humidity is the ratio of this reduced vapour pressure to the saturation vapour pressure of water.

Figure 12.22 shows a plot of regain against actual and reduced vapour pressure. The use of reduced values gives a simpler curve and, as has been mentioned earlier (Section 12.2.2), gives a good fit with the BET isotherm. However, the initial assumption that the water acts in a manner similar to liquid water, and that it may be regarded as being under a hydrostatic pressure, may be doubted. The assumptions with regard to the elastic properties of the fibre are drastic and may not be very near the truth.

12.4 Surface adsorption

The idea of adsorption on internal surfaces has already been discussed and has been shown to be of doubtful validity for fibres. There may, however, be adsorption on the



12.22 Cassie's reduced curve of regain against vapour pressure for wool [23].

external surface of fibres. In hygroscopic fibres, this would be a negligible proportion of the total regain, but in a non-hygroscopic fibre it may contribute most or all of the small moisture absorption.

Table 12.2 shows results obtained by Bright *et al.* [44] for the heat of wetting of similar specimens of polyester fibre. The heat of wetting is proportional to (linear density)^{-1/2}. In other words, the amount of heat evolved is proportional to the surface area (per unit mass), which suggests that the moisture taken up by polyester fibres is present on the surface of the fibre.

12.5 The effect of temperature

In order to correlate the relations between regain and relative humidity at various temperatures, Whitwell and his associates [45] analysed Wiegerink's data [46] on the basis of Othmer's method [47]. This depends on the application of the Clausius–Clapeyron equation, which for a pure substance is:

$$\frac{dp_0}{dT} = \frac{p_0 L}{RT^2} \quad (12.51)$$

where p_0 = vapour pressure, T = absolute temperature, L = latent heat of condensation and R = gas constant. For a fibre at a given regain, this becomes:

$$\frac{dp}{dT} = \frac{pQ_v}{RT^2} \quad (12.52)$$

where p = vapour pressure over the fibre, Q_v = heat of absorption of the fibre.

Combining the two equations, we obtain:

$$\frac{dp}{dp_0} = \frac{pQ_v}{p_0 L}$$

or

$$\frac{dp/p}{dp_0/p_0} = \frac{Q_v}{L} \quad (12.53)$$

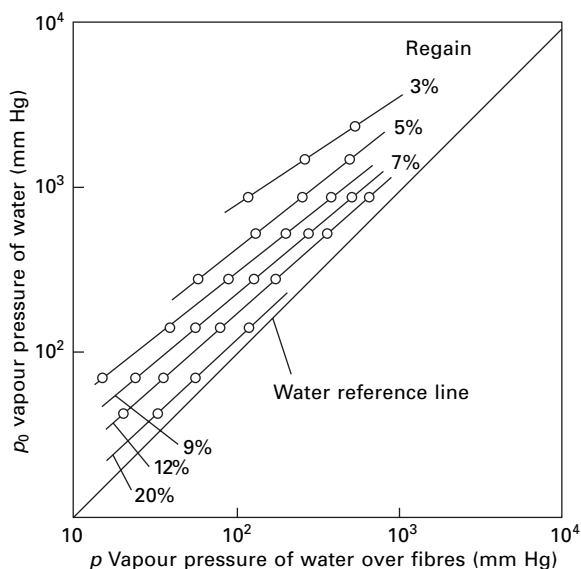
which on integration gives:

$$\log p = \frac{Q_v}{L} \log p_0 + \text{constant} \quad (12.54)$$

Thus if values of $\log p$ for various temperatures at constant regain are plotted against the corresponding values of $\log p_0$, straight lines should be obtained. This is illustrated

Table 12.2 Heat of wetting of polyester fibre at constant draw-ratio [44]

Linear density (dtex)	Heat of wetting	Heat of wetting $\times \text{tex}^{1/2}$
2.2	0.85	0.401
4.4	0.56	0.373
8.9	0.39	0.368



12.23 Whitwell's plot of $\log p$ against $\log p_0$ for cuprammonium rayon on desorption [45].

in Fig. 12.23. It has been further found that for most fibres the lines for various regains intercept in a common point.

Plotting results in this way enables them to be extrapolated beyond the experimental range of temperatures and, by making use of the common point, allows a line to be drawn for other values of the regain if a single point is known. At low temperatures, other effects must be involved, since the values obtained by Darling and Belding [48] at low temperatures do not agree with this theory.

12.6 References

1. I. C. Watt and J. D. Leeder. *J. Text., Inst.* 1968, **59**, 353.
2. N. H. Kolkmeier and A. N. J. Heyn. *Proc. Konink. Nederland Akad. Wetenschap.*, 1934, **37**, 92.
3. L. J. Lynch and K. H. Marsden. *J. Chem. Phys.*, 1969, **51**, 5681.
4. C. E. Boesen. *Cell. Chem. Technol.*, 1970, **4**, 149.
5. R. J. B. Marsden. In *Fibre Science* J. M. Preston (Editor), The Textile Institute, Manchester, 2nd edition, 1953, p. 229.
6. Jeffries, D. M. Jones, J. G. Roberts, K. Selby, S.C. Simmens and J. O. Warwick. *Cellulose Chem. Tech.*, 1969, **3**, 255.
7. A. R. Urquhart. *J. Text. Inst.*, 1929, **20**, T125.
8. P. H. Hermans. *Physics and Chemistry of Cellulose Fibres*, Elsevier, Amsterdam, Netherlands, 1949.
9. R. Meredith. In *Fibre Science* J. M. Preston (Editor), The Textile Institute, Manchester, 2nd edition, 1953, p. 246.
10. A. D. McLaren and J. W. Rowen. *J. Polymer Sci.*, 1951, **7**, 289.
11. A. B. D. Cassie. In *Fibrous Proteins Symposium*, Society of Dyers and Colourists, Bradford, 1946, p. 86.

12. G. A. Gilbert. In *Fibrous Proteins Symposium*, Society of Dyers and Colourists, Bradford, 1946, p. 96.
13. T. P. Labuza *Moisture Absorption: Practical Aspects of Isotherm Measurement and Use*, Amer. Association of Cereal Chemists, St Paul, Minnesota, 1984.
14. C. Van den Berg and S. Bruin. In *Water Activity: Influences on Food Quality*, L. B. Rockland and G. F. Stewart (Editors), Academic Press, New York, 1981, p. 147.
15. M. J. Sabchez-Montero, C. Herdes, F. Salvador and L. F. Vega. *Appl. Surface Sci.*, 2005, **25**, 519.
16. F. T. Peirce. *J. Text. Inst.*, 1929, **20**, T133.
17. J. W. S. Hearle. *J. Text. Inst.*, 1952, **43**, T354.
18. D. N. E. Cooper. *J. Text. Inst.*, 1961, **52**, T433.
19. J. B. Speakman. *Trans. Faraday Soc.*, 1944, **40**, 6.
20. J. W. S. Hearle. *Text. Res. J.*, 1954, **24**, 307.
21. I. Langmuir. *J. Amer. Chem. Soc.*, 1918, **40**, 1361.
22. S. Brunauer, P. H. Emmett, and E. Teller. *J. Amer. Chem. Soc.*, 1938, **60**, 309.
23. A. B. D. Cassie. *Trans. Faraday Soc.*, 1945, **41**, 450.
24. T. L. Hill. *J. Chem. Phys.*, 1946, **14**, 263.
25. H. B. Bull. *J. Amer. Chem. Soc.*, 1944, **66**, 1499.
26. J. B. Taylor. *J. Text. Inst.*, 1952, **43**, T489.
27. J. B. Taylor. *J. Text. Inst.*, 1954, **45**, T642.
28. A. B. D. Cassie. *Trans. Faraday Soc.*, 1945, **41**, 458.
29. J. J. Windle. *J. Polymer Sci.*, 1956, **21**, 103.
30. M. Feughelman and A. R. Haly. *Text. Res. J.*, 1962, **32**, 1966.
31. T. L. Hill. *J. Chem. Phys.*, 1946–50, ‘Statistical Mechanics of Adsorption’, I–X.
32. H. J. White and H. Eyring. *Text. Res. J.*, 1947, **17**, 523.
33. H. J. White and P. B. Stam. *Text. Res. J.*, 1949, **19**, 136.
34. A. D. McLaren and M. Ottesen. *Compt. Rend. Trav. Lab. Carlsberg, Ser. Chim.*, 1950, **27**, 325.
35. M. Dole. *J. Chem. Phys.*, 1948, **16**, 25.
36. R. M. Barrer. *Trans. Faraday Soc.*, 1947, **43**, 3.
37. J. W. Rowen and R. Simha. *J. Phys. Colloid Chem.*, 1949, **53**, 921.
38. A. J. Hailwood and S. Horrobin. *Trans. Faraday Soc.*, 1946, **42B**, 84.
39. W. W. Barkas. *The Swelling of Wood under Stress*, HMSO, London, 1949.
40. J. W. S. Hearle. *Text. Res. J.*, 1957, **27**, 940.
41. L. R. G. Treloar. *Trans. Faraday Soc.*, 1953, **49**, 816.
42. A. R. Haly. *Text. Res. J.*, 1965, **35**, 889.
43. J. B. Speakman. *J. Text. Inst.*, 1927, **18**, T431.
44. N. F. H. Bright, T. Carson and G. M. Duff. *J. Text. Inst.*, 1953, **44**, T587.
45. J. C. Whitwell *et al.* *Text. Res. J.*, 1946, **16**, 255, 307; 1947, **17**, 7, 99, 664.
46. J. G. Wiegerink. *Text. Res.*, 1940, **10**, 357.
47. D. F. Othmer. *Industr. Engng Chem.*, 1940, **32**, 841.
48. R. C. Darling and H. S. Belding. *Industr. Engng Chem.*, 1946, **38**, 527.

13.1 General introduction

The mechanical properties of textile fibres, the responses to applied forces and deformations, are probably their most important properties technically, contributing both to the behaviour of fibres in processing and to the performance of the final product. The properties of a textile structure such as a yarn or a fabric depend on a complex interrelation between fibre arrangement and fibre properties, so that, although a knowledge of fibre properties is essential to an understanding of the properties of yarns and fabrics, it is not in itself sufficient. There will be some effects that are due to the inherent properties of the structural arrangement, and the fibre properties may be modified by the presence of neighbouring fibres. The fibre properties in themselves do, however, give a limit to what is possible in a yarn or fabric. For example, except for minor effects due to mutual support of variable fibres, the strength of a yarn cannot be greater than the sum of the strengths of its component fibres.

The mechanical properties of a fibre cover a large number of effects, all of which combine to determine the particular character of the fibre. In using fibres, it is necessary to find that fibre whose character best suits the needs of the particular job. These needs vary widely in the manifold applications of textile materials.

Because of their shape, the most studied and, in many applications, the most important mechanical properties of fibres are their tensile properties, namely their behaviour under forces and deformations applied along the fibre axis. Of these, the simplest to study experimentally is the elongation, and finally the break, under a gradually increasing load. Experiments of this sort form the subject of the present chapter, but, to avoid giving a false impression, it will first be necessary to describe the various factors that affect the results of such experiments. These factors will be considered in greater detail later.

13.2 Factors determining the results of tensile experiments

13.2.1 The material and its condition

The behaviour of a material depends on the nature and arrangement of the molecules of which it is composed, and these will vary not only from one type of fibre to

another, but also from one fibre to another in a given sample, and from one condition of the material to another. These latter effects must be taken into account in considering the results of a test. The different behaviour of individual fibres must be investigated. On some occasions, the variability of the results may be more important than the mean value, as, for example, it would be if we wished to know the chance that the strength of a fibre would fall below a certain critical value. The condition of the material depends on its previous history, including the processes to which it has been subjected and the mechanical treatment that it has received, on the amount of moisture that it contains, and on the temperature. All of these must be specified if the results of tests are to be of value.

13.2.2 The arrangement and dimensions of the specimen

The dimensions of the specimen will, of course, have a direct effect on the results of tests. For example, other things being equal, the breaking load of a fibre will increase in proportion to its area of cross-section, and its elongation will increase in proportion to its length. It is, however, with the indirect effects that we are more concerned here.

In a variable material, there is a greater chance of the occurrence of a very weak place in a long length than in a short one, and, since a fibre breaks at its weakest place, the mean breaking load of long lengths will be less than that of short ones (see [Section 14.2.1](#)). For this reason, the length tested should be stated.

If composite specimens, made up of a number of fibres, are used in a test, then not all the fibres will necessarily bear the same proportion of the load, and they may not all break at the same time. For these reasons, the properties of a composite specimen are affected by the particular arrangement of fibres in the specimen and are not given by a simple combination of the properties of the individual fibres.

13.2.3 The nature and timing of the test

The elongation of a textile fibre is not a single-valued function of the applied load, for it depends on the length of time for which the load and any previous loads have been applied. If a constant load is applied to a fibre, it will, after its instantaneous extension, continue to extend for a considerable time and, if the load is great enough, it will eventually break. The load necessary to cause breakage will vary with the speed of the test, a rapid test requiring a greater breaking load than a slow one. Thus the results of experiments will be affected by the time allowed and by the way in which the load is applied, whether it is by constant rate of loading, constant rate of elongation, reduction from a higher load or any other sequence of events.

A limitation on the value of experimental results may be noted here. In use, textile fibres are subject to complex, variable and probably unknown loading histories. In assessing the practical behaviour of fibres, therefore, attempts must be made to predict the results under the actual conditions of use from experimental results obtained under different conditions. This can best be done if the experimental conditions are as simple as possible.

13.3 Expressing the results: quantities and units

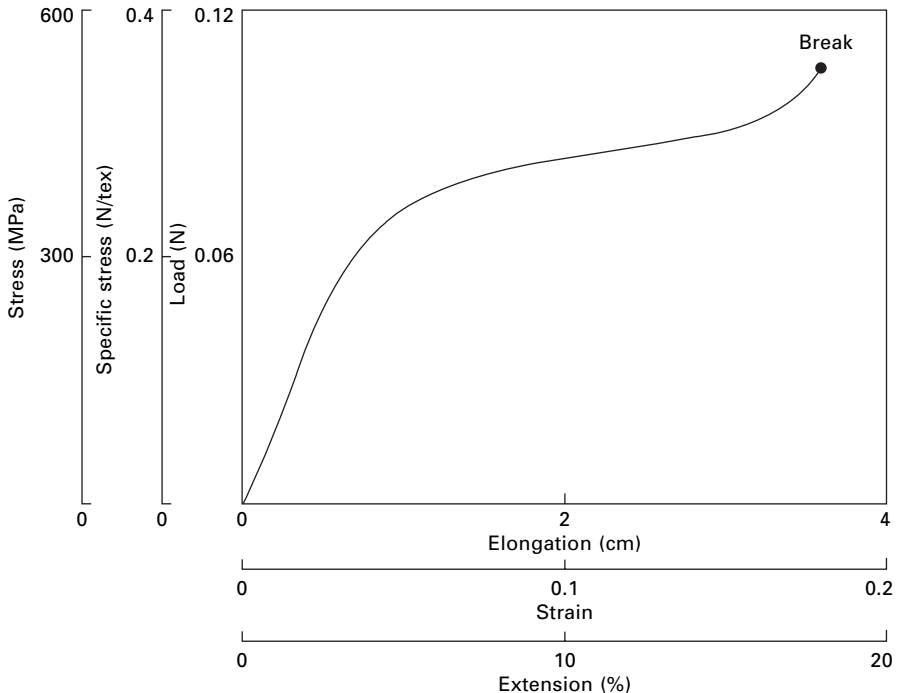
13.3.1 Load–elongation and stress–strain curves

The behaviour of an individual fibre under a gradually increasing applied force is completely expressed by the load–elongation curve with its end-point breakage, as is shown in Fig. 13.1. The load may be measured in newtons or grams force and the elongation in centimetres, but, if we wish to compare different types of fibre, independently of the direct effect of their dimensions, we must use other quantities. Elongation is easily normalised as fractional strain or percentage extension. However, as described in [Appendix I](#), which contains a conversion table, the normalisation of force has produced great diversity dependent on the choice of quantity and units.

In most physical and engineering applications, load is replaced by *stress*, defined as:

$$\text{stress} = \frac{\text{load}}{\text{area of cross-section}}$$

The SI unit of stress is newton per square metre (N/m^2), which is also called a pascal (Pa). The convenient units for strength and modulus are megapascal (MPa) or gigapascal (GPa). Other commonly found units are kg/mm^2 and pounds per square inch (psi).



13.1 Hypothetical load–elongation curve for 20 cm specimen of 0.3 tex fibre with density of 1.5 g/cm^3 .

In textile technology, however, we are more often interested in materials in terms of their weight, rather than in terms of their bulk. In addition, the area of cross-section of textile yarns and fabrics is not well defined, since it is confused by the space between fibres. For single fibres, the area is definitive, but is more easily obtained indirectly from the mass and density of the specimen than by direct measurement. The primary definition of fineness is the linear density (mass per unit length). It is therefore more convenient to use mass-based quantities based on the linear density, which give consistent information from the molecular to the macroscopic level. The normalised force is termed the *specific stress*¹ and is defined as:

$$\text{specific stress} = \frac{\text{load}}{\text{linear density}}$$

The consistent SI unit for specific stress would be N m/kg. However, in order to fit in with the tex system for linear density, it is better to use newton per tex (N/tex), which is 10⁶ times as large as N m/kg. For smaller stresses, millinewton per tex (mN/tex) may be a more convenient size. When manufactured fibres were introduced in the first half of the 20th century, the unit chosen was gram force per denier, usually written as g/den, and this unit is still widely used. In order to get a unit of similar size to g/den, cN/dtex is often found.

In consistent units, we have the following relation between stress f , specific stress σ and density ρ :

$$f = \rho \sigma \quad (13.1)$$

The same equation is correct with f in GPa, σ in N/tex and ρ in g/cm³. Conversion relations in other units are given in [Appendix I](#). When engineers who are used to working with conventional stress wish to change to a mass basis, they often think of specific stress as (f/ρ) and use units such as GPa/(g/cm³), which is equal to N/tex, or even the hybrid unit psi/(g/cm³).

The distinction between stress and specific stress becomes significant only when we wish to compare materials of different density, for example silk and nylon, and more particularly between organic and inorganic high-performance fibres. Usually, we should want to do this on the basis of equal weights, but in some special cases, for example if material had to be packed into a small space, bulk might be important, and the conventional stress should be used. In composites, linear dimensions are used in engineering design, though weight can be important, and stresses are commonly used.

There are other related quantities. Specific stress is dimensionally equivalent to energy per unit mass, which is relevant to some applications. N/tex equals kJ/g. Another quantity, which was often quoted as a measure of strength, is the breaking length in kilometres, or more correctly kilometre-force. This is the length of material that would break under its own weight. 1 kmf equals 1 gf/tex or 9.8 mN/tex. The usage of older units is more common in the United States than in the rest of the world, and an extreme example was the uses of inches, strictly inch-force, for strength in manufacturer's literature for the Spectra HMPE fibre.

¹When the context is clear, *stress* is often used.

To take account of the length of the specimen, the elongation is expressed as *tensile strain* or *percentage extension*:

$$\text{tensile strain} = \frac{\text{elongation}}{\text{initial length}}$$

Load–elongation curves become stress–strain curves by a change of units, without affecting the shape of the curve, as is indicated in Fig. 13.1.

Although stress–extension curves completely express the results of this type of test, there are some features of the curve that it is useful to define separately. These refer either to the shape of the curve or to the position of its end point, that is, breakage.

13.3.2 Strength

We first consider strength, which is a measure of the steady force necessary to break a fibre and is given experimentally by the maximum load developed in a tensile test. (See Section 14.6 for a discussion of some complications.) For an individual fibre, the strength is given by the breaking load. For comparing different fibres, the value of the specific stress at break is used and is called *tenacity* or *specific strength*. As noted above, *breaking length* may also be used. For use in comparing strengths on the basis of area of cross-section, the stress at break is termed the *ultimate tensile stress*.

13.3.3 Elongation at break

The elongation necessary to break a fibre is a useful quantity. It may be expressed by the actual, the fractional or the percentage increase in length, and is termed the *breaking extension* or *break extension*.

13.3.4 Work of rupture

For an individual fibre, the work of rupture, sometimes called the *toughness*, is defined as the energy needed to break the fibre. The units for this are joules. If we consider a fibre under a load F , increasing in length by an amount dl , we have:

$$\text{work done} = \text{force} \times \text{displacement} = F \cdot dl \quad (13.2)$$

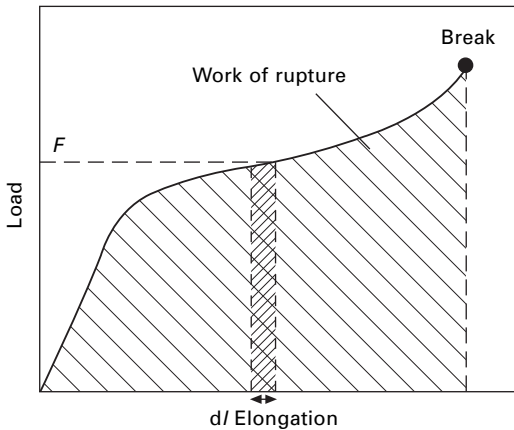
$$\text{total work done in breaking the fibre} = \text{work of rupture}$$

$$= \int_0^{\text{break}} F \cdot dl \quad (13.3)$$

This equals the area under the load–elongation curve, as shown in Fig. 13.2.

Other things being equal, the work of rupture of a fibre will be proportional to its linear density (because of the effect on the load needed) and to its length (because of the effect on the elongation). To compare different materials, we may use the term, *specific work of rupture*², defined as:

²*Specific* may be dropped when the context is clear.



13.2 Work of rupture.

$$\text{specific work of rupture} = \frac{\text{work of rupture}}{\text{linear density} \times \text{initial length}}$$

As indicated above, specific work of rupture may be expressed in units of N/tex or kJ/g, and is given by the area under the curve of specific stress against strain. This represents the energy in joules needed to break a 1 tex filament, 1 m long. The total work of rupture of any particular specimen is proportional to its mass, independent of the actual values of linear density and length which determine that mass.

13.3.5 Comparison of methods of specifying breakage

We have now described three ways of specifying breakage, or resistance to breakage: by the force, elongation or energy necessary. Whenever breakage occurs, the values of each of these appropriate to the conditions of test must be reached, but usually the limiting value of only one of the three will be inherent in the conditions causing breakage, while the other two follow automatically. It is useful to compare the three quantities from this point of view.

Strength, or tenacity, gives a measure of the resistance to steady forces. It will thus be the correct quantity to consider when a specimen is subject to a steady pull, as, for example, in a rope used for slow hoisting of heavy weights.

The breaking elongation gives a measure of the resistance of the material to elongation. It is thus important when a specimen is subject to stretching, for example the neck of a garment being pulled over the head, or the warp extension in weaving.

The work of rupture, which is the energy needed to break a fibre, gives a measure of the ability of the material to withstand sudden shocks of given energy. When a mass m , attached to a textile specimen, is dropped from a height h , it acquires a kinetic energy, equal to mgh , and, if this energy is greater than the work of rupture, breakage will occur, whereas if it is less the specimen will withstand the shock. Thus the work of rupture is the appropriate quantity to consider in such events as the opening of a parachute, a falling climber being stopped by a rope and all the occasions

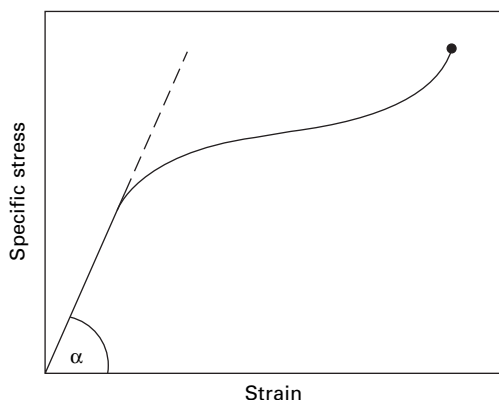
when sudden shocks are liable to cause breakage. It should be noted that the significant feature in the application of the work of rupture is that the shock contains a given amount of energy; the fact that it occurs rapidly is not directly relevant, though the rate of loading will affect the value of the work of rupture.

In comparing materials to see which is least likely to break, it is important to consider the conditions under which breakage would occur and then to decide which quantity is the appropriate one to use. For instance, it is no use for a climbing rope to have a high tenacity if its work of rupture is low. In actual practice, more complicated tensile conditions may occur, for example a sudden shock may be applied to a specimen already carrying a steady load. It should also be remembered that breakage may occur as a result of the repeated applications of forces, not necessarily along the fibre axis, as discussed in [Chapter 19](#).

13.3.6 Initial modulus and other moduli

The first of several quantities related to the shape of the tensile stress–strain curve is the *initial modulus*, which is equal to the slope of the stress–strain curve at the origin (after the removal of any crimp). This slope usually remains constant over the initial portion of the curve, as in Fig. 13.3. The modulus is measured in units of stress or specific stress. Note that fractional strain is always used, even though the data may be given in percentage extension. The corresponding absolute quantity is the spring constant, equal to force/elongation.

It may be noted that the value of the initial modulus equals the value of the stress that would be necessary to double the length of the specimen if the conditions at the origin persisted. It is a measure of the resistance to extension for small extensions. An easily extensible fibre will have a low modulus. The modulus is important in situations where the amount of extension has to be limited, for example in the magnitude of offset allowable for an oilrig subject to environmental forces. It also gives a measure of force developed when a given displacement is imposed, as when an oilrig rises and falls under wave action.



13.3 Initial modulus = $\tan \alpha$.

Two other moduli may be reported. The *tangent modulus* is the slope of the stress–strain curve at any given position. It is relevant when materials are subject to cyclic loading. Plots of tangent modulus against strain are another useful way of showing the changes in extensibility as fibres are increasingly strained, as described by van Miltenburg [1]. The *secant modulus* is stress/strain at any position on the stress–strain curve. Dynamic moduli are covered in [Chapters 16](#) and [18](#). The reciprocal of modulus is called the *compliance*.

13.3.7 Work factor

If the fibre obeyed Hooke's law, the load–elongation curve would be a straight line, and the work of rupture would be given by:

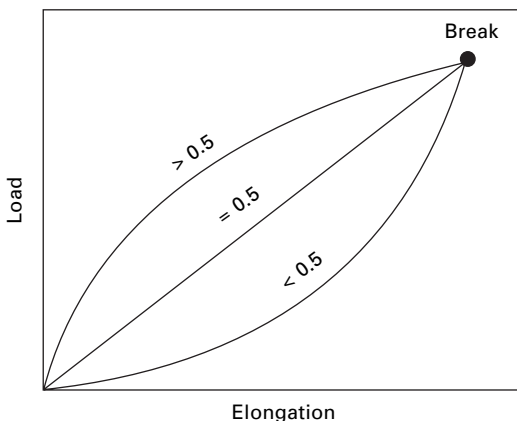
$$\text{work of rupture} = \frac{1}{2} (\text{breaking load} \times \text{breaking elongation})$$

It is convenient to define a quantity, the work factor, dependent on the difference from this ideal state:

$$\text{work factor} = \frac{\text{work of rupture}}{\text{breaking load} \times \text{breaking elongation}}$$

In the ideal state, the work factor will be 0.5. If the load–elongation curve lies mainly above the straight line, the work factor will be more than 0.5; if below, it will be less than 0.5. This is illustrated in Fig. 13.4.

For materials breaking at the same point, the work of rupture will be greater the higher the work factor. Since the work factor will not vary much in different specimens of the same material, the values given later (in [Table 13.1](#)) or other available values may be used to estimate the work of rupture from measurements of the breaking load and elongation.

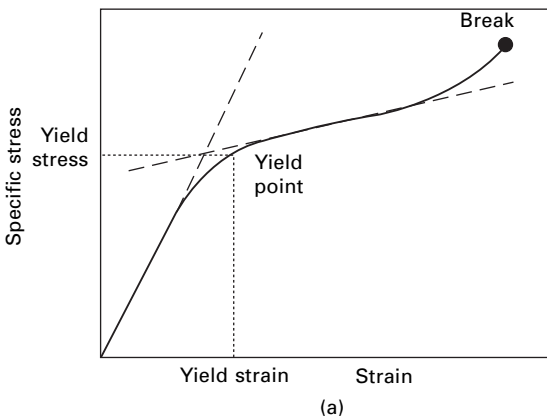
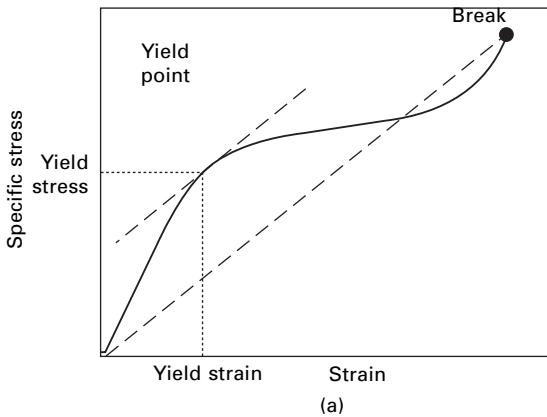


13.4 Work factor.

13.3.8 Yield point

Many stress–strain curves have a shape similar to that in Fig. 13.5. After an initial period with a steep slope, extension suddenly becomes much easier. It is in this region that the *yield point* occurs. In order to locate a precise position, Meredith [2] has suggested defining the yield point as the point at which the tangent to the curve is parallel to the line joining the origin to the breaking point, as in Fig. 13.5(a). This point is then characterised by its stress and strain as the *yield stress* and *yield strain*. Coplan [3] used a different construction and defined the yield point as occurring at the stress given by the intersection of the tangent at the origin with the tangent having the least slope. This is shown in Fig. 13.5(b). Alternatively, particularly when there are considerable linear regions both above and below the yield region, the point of intersection of the tangents may be taken as the yield point. Since the stress–strain curve is approximately linear up to the yield point, the work to the yield point will be almost equal to $\frac{1}{2}$ (yield stress \times yield strain).

Apart from its indication of the shape of the curve, the yield point is important because for most materials, elastic recovery, which is good up to the yield point,



13.5 Yield point: (a) Meredith's construction; (b) Coplan's construction.

becomes less complete for higher strains. In practice, the point at which permanent deformation starts to take place may be just as important as the point at which breakage occurs. Recovery behaviour is discussed in greater detail in [Chapter 15](#).

The actual amount of bending over of the stress–strain curve may be important. Where there is a marked flattening of the curve, it means that the fibre will firmly resist small loads but will yield under high loads. This will have an influence on the handle of fabrics made from the fibres.

13.3.9 Crimp

In the discussion so far, it has tacitly been assumed that the fibre is initially straight. However, many fibres are crimped. The crimp is normally pulled out by a suitable small tension in measuring linear density, and it can be removed by a pre-tension at the start of a tensile test.

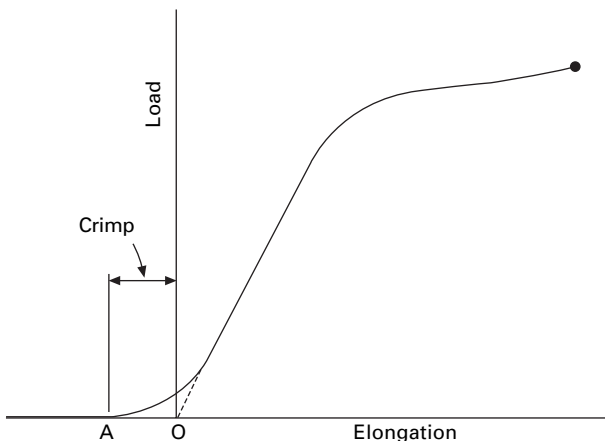
If a crimped fibre is inserted in the tester without any initial tension, the load–elongation curve will have the form shown in Fig. 13.6. The origin of the curve may be put at A, where it diverges from the zero line, but this point is difficult to locate precisely. A better procedure is to put the origin at O, the extrapolated point corresponding to a hypothetical straight fibre. The crimp is given by AO and may be expressed as a percentage of the initial length, again probably best taken as at O, though the value based on the crimped state at A may be used.

Studies of the methods of measuring and defining crimp have been made by Alexander *et al.* [4–6] and more recently by Bauer-Kurz *et al.* [7].

13.4 Experimental methods

13.4.1 General

The load–elongation curve of a textile fibre may be obtained by gradually extending it and measuring the tension corresponding to each increase in length. The essential

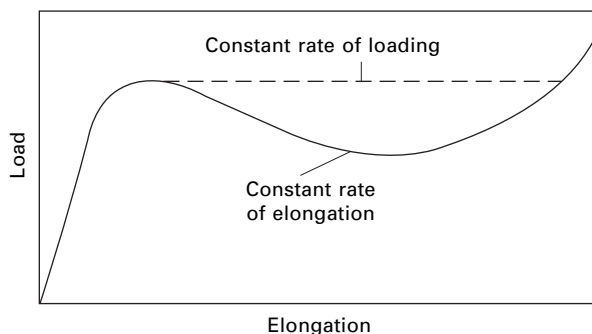


13.6 Load–elongation curve of a crimped fibre.

features of any method consist of the jaws in which the ends of the specimen are held, the type of specimen used, the method of varying the load and elongation, and the means of recording their values to give the load–elongation curve. Prior to the middle of the 20th century, a variety of mechanical testers were used for this purpose and were followed by early electronic testers. However since the research of Hindman and Burr [8] at MIT, which led to commercialisation of Instron³ testers, the almost universal method has been the imposition of a controlled elongation with force measured on a load cell. The next section describes this type of tester. Brief comments follow on other testers. More information is given in books on textile testing [9–11] and in manufacturers' literature. Some relevant standards for test methods are listed in [Appendix III](#). Special methods for high-speed testing are covered in [Chapter 16](#).

For continuous filament materials, tests are usually carried out on yarns. A small amount of twist may be inserted to cause all fibres to break at the same point. Single fibre tests and individual yarn tests are appropriate for research purposes, but are time-consuming. For routine testing of cotton, either in laboratory testers or in HVI lines, bundle tests are used. Because of the influence of variability, these are discussed in [Chapter 14](#). For yarns, automated testers can pull yarn off a package and make a large number of repeated tests.

Because of the way in which the elongation and the breaking point of textile fibres vary with time, the method of extending the specimen is a factor in determining the results of the test. In *constant rate of elongation* (CRE) tests, the specimen is extended at a constant rate and the force is a dependent quantity; in *constant rate of loading* (CRL) tests, the specimen is loaded at a constant rate and the elongation is a dependent quantity. For the usual non-linear fibre stress–strain relations, the load–time relation is different in the two procedures. Hence differences in creep will cause differences in the shape of the curve. Another consequence is that in a constant rate of elongation test it is possible for the load to decrease while the elongation increases, but this is not possible in constant rate of loading tests, where the load must increase throughout the test, giving the difference shown in Fig. 13.7. The pendulum tester⁴, which was



13.7 Constant rate of elongation and constant rate of loading results.

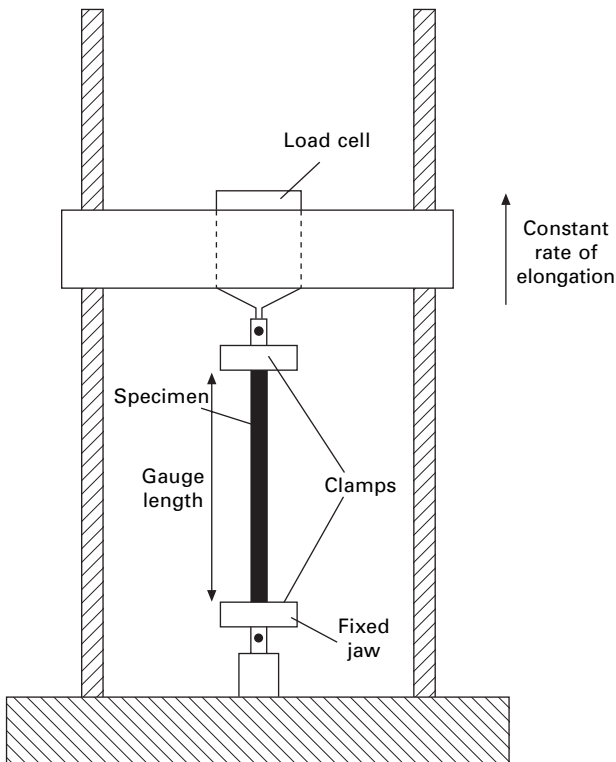
³Like Hoover and Google, Instron is often used as a generic description.

⁴The pendulum tester was extensively described in the first edition of this book.

once widely used for strength tests, is described as constant rate of traverse; the controlled jaw moves at a constant rate, as in CRE; the dependent jaw is attached to the pendulum, which rises to record the load. It is not CRE, because there is a substantial displacement of the dependent jaw as the pendulum rises, which influences the elongation; it is not CRL, because the movement of the pendulum depends on the non-linearity of increase of tension with elongation.

13.4.2 Instron-type tests

The Instron tensile tester and others acting on the same principles are constant rate of elongation instruments. The essential feature of these instruments, illustrated in Fig. 13.8, is that one end of the specimen is clamped in jaws, which are mounted on a cross-head that is traversed at a constant rate by a mechanical drive. The drive may come from a constant speed motor, with interchangeable gears to vary rate of elongation, or from a computer-controlled stepper motor. The other end is clamped in jaws, which are mounted on a stiff load cell containing a strain-gauge or other form of transducer. In early versions of the testers, the drive is connected to the recorder drive, and the electronic circuits of the load cell lead to deflection of the recorder pen. A paper record of the load–elongation curve is thus obtained. In modern versions, the



13.8 Instron-type tester.

load and elongation are digitally transferred to a computer, so that the data can be plotted or analysed as required. Instruments of this type are usually very versatile in load ranges, traverse rates, chart-drive rates, testing sequences and auxiliary facilities. Stress relaxation can be measured by holding the elongation constant. Servo-control is used to give constant rate of loading or to hold load constant for creep testing.

A finite, but small, deflection is, of course, necessary in order to measure load. For reasonable lengths of most fibres, the resulting error in elongation values is negligible. For stiff high-performance fibres or when it is necessary to test short lengths, corrections must be applied. If an inextensible specimen, e.g. a thick strip of metal, is tested, the extension will solely be due to the deformation of the load cell and can be used as a correction. Alternatively, specimens of different length can be tested and one elongation subtracted from the other to give the elongation of the difference in length.

Another type of Instron tester employs pneumatic loading, which enables higher-speed and cyclic tests to be carried out under electronic control.

Medium and large Instron-type testers cater for a wide range of specimens, from single fibres and yarns to large cords, but smaller instruments have been introduced for specialist investigations of single fibres or fine yarns. The tensile fatigue tester [12], described in Section 19.3, can be used as a tensile tester if the vibrator is not activated. It has been redesigned as a Universal Fibre Tester (UFT) [13]. Mwaisengela [14] discusses its operation in detail, and describes the addition of a temperature-controlled chamber. An updated version of the UFT also allows for temperature control [15]. Sikorski *et al.* [16] describe a flexible thermomechanical analyser, which treats elongation and tension as described above. The instrument, which is computer controlled, has facilities for twist insertion and torque measurement, but its most notable feature is that the test specimen is enclosed in a chamber which can subject to rapid programmes of temperature change [17]. Fudge *et al.* [18], in a paper on hagfish slime threads, describe a micromechanical tester, which measures tension by the deflection of a fine glass micro-beam. The test thread was extended by a constant speed motor and the deflection of the beam was monitored by a video-camera mounted on a low-power microscope. Data was recorded and analysed by LabView collection software. Kawabata [19] describes a sensitive tester for single fibres.

The SIFAN tester (see [Section 3.7.1](#)) enables tensile tests to be combined with observations of fineness along the length of a fibre, thus enabling the stress at the point of break to be found.

13.4.3 Other testers

In the mechanical era, there were several ingenious methods for securing constant rate of loading. The simplest method is direct loading, which was used, for example, by Leonardo da Vinci in the 15th century in measuring the strength of wire. Water or shot can be fed into a bucket attached to the specimen. The load on the specimen is controlled by the flow of water in the Krais instrument [20]. Alternatively load can be increased by the movement of a rider on a balance, as described by Saxl [21], or by electromagnetic methods, as described by Barratt [22]. Unwinding a chain does

not, in its simplest form give constant rate of loading, since the elongation of the specimen alters the load. However, de Meulemeester and Nicoloff [23, 24] described an ingenious way of overcoming the difficulty in a chainomatic tester. A widely used method was the inclined-plane tester. The test specimen is fixed to a carriage on a planar track. As the track is inclined the load on the specimen increases at a constant rate. Since the loading is by dead weight, inertia errors may occur and lead to an oscillation, with the elongation lagging initially behind the load. There may also be an error due to centrifugal force if the carriage moves down too rapidly. The Scott IP testers were examples of this type of instrument. Raes, *et al.* [25] have described an inclined-plane instrument that is mounted on the stage of a polarising microscope in order to permit cotton fibres to be mounted at positions related to reversals.

One old form of tester is worth mention because it was used by Meredith in his classical researches (see [Table 13.1](#)), which provide the most comprehensive comparative data on a variety of fibres. The tester designed by Cliff [26] secures constant rate of loading by the use of a very soft loading system, which can be activated by a suitable drive with a negligible error due to extension of the specimen. The tester uses a spring in torsion, as shown in Fig. 13.9. The rotation of the free end of the spring through an angle ϕ applies a load F to the specimen, given by:

$$FR = K(\phi - \theta) \quad (13.4)$$

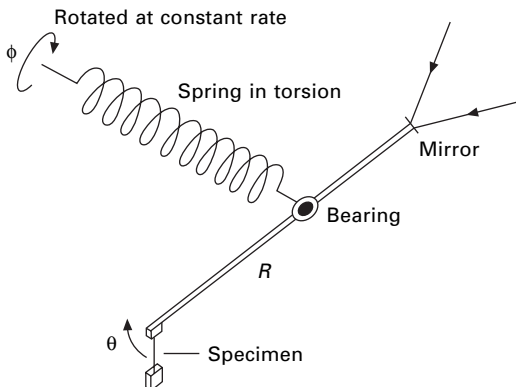
where R = radius of arm connected to specimen, K = torque per unit angle of rotation of spring, and θ = angle of rotation of rod due to elongation of specimen.

With a weak spring and a long rod, $\theta \ll \phi$, so that we can put:

$$F = \frac{K\phi}{R} \quad (13.5)$$

A constant rate of rotation gives a constant rate of loading.

Another tester which was widely used before Instron testers became available was the Cambridge Textile Extensometer, which could be used for constant rate of loading or constant rate of elongation tests. This type of tester was used for another set of comparative tests (see [Table 13.1](#)). The test specimen is mounted between a spring,



13.9 Cliff tester.

which can be extended at a controlled rate to apply tension, and a drive to give controlled elongation. Between the spring and the specimen, an electrode is located between two other fixed electrodes. For CRL tests, the spring is driven at a constant rate which causes contact with the electrode on the spring side; the elongation motor is then driven to maintain a balance of tensions. Conversely, for CRE, the elongation motor is driven at a constant and the spring motor is activated by the electrical contacts. The two motors are linked to a paper recorder to provide a load–elongation curve. Creep and stress relaxation tests can be made by holding one side or the other constant.

13.4.4 Direct measurement of work of rupture

The work of rupture may be obtained from the load–elongation curve, but it can also be measured directly by the ballistic test. A pendulum (Fig. 13.10) is released from a given angle to the vertical and on its swing engages with one of the specimen jaws and breaks the specimen. The energy necessary to break the specimen is lost by the pendulum, and thus we have:

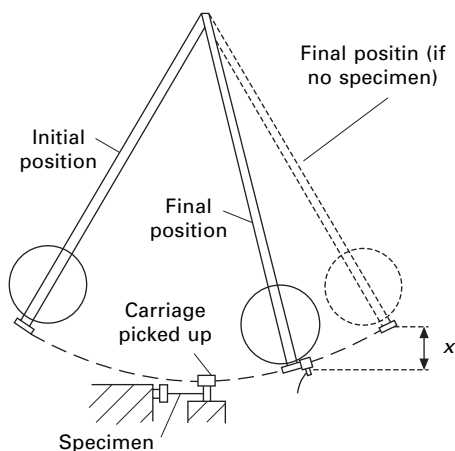
$$\text{work of rupture} = \text{loss of potential energy} = M g x \quad (13.6)$$

where M = mass of pendulum and x = difference in height of final positions of pendulum, with and without the specimen.

This method is more rapid than a normal load–elongation test, but the variation of load with time will depend on the properties of the specimen and the conditions of the experiment. The method has been discussed in detail by Lang [27].

13.4.5 Other experimental features

Some other experimental features that are common to the above methods may be mentioned here. Single-fibre specimens are best if it is required to investigate the



13.10 Ballistic tester.

properties of the fibres themselves, since the results for bundles of fibres will be affected by the form of the specimen and the variability of the material, as described in more detail later (see [Section 14.4](#)). The clamps holding the specimen must not damage it. If this happens, there will be an undue proportion of breaks at the jaw. But undue extension or slippage within the jaws must also be avoided. Care must be taken not to stretch the fibres during the operations preliminary to the test, since this will change the fibre properties. An adequate system of sampling must be used, to take account of the variation in behaviour from one fibre to another. Moisture-absorbing fibres should be in equilibrium with an atmosphere of controlled humidity and temperature, which should always be approached from the same side, preferably the dry side.

13.4.6 Meredith's experimental procedure

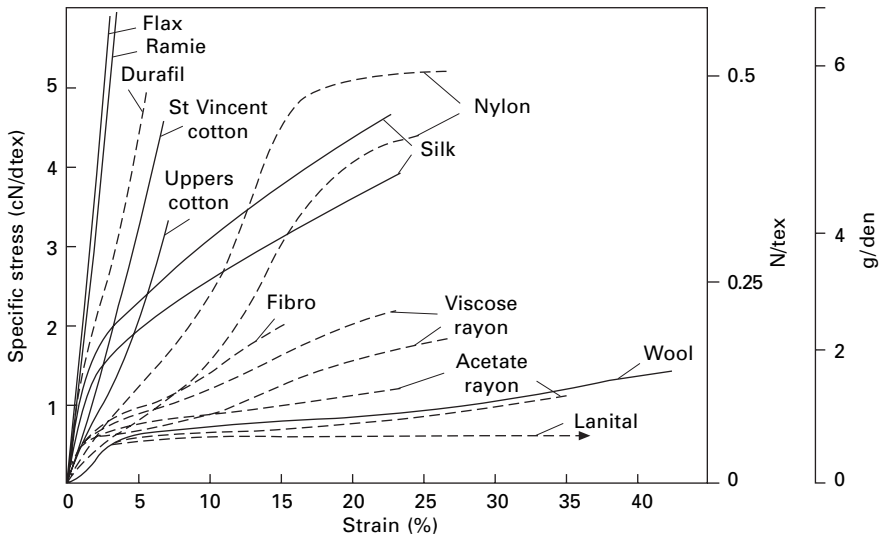
It is useful to study one particular experimental procedure in more detail, and the methods used by Meredith [2] have been chosen, since he made the best early comprehensive set of measurements of load–elongation curves of textile fibres. He tested single fibres, 1 cm long, at $65 \pm 2\%$ r.h. and $20 \pm 2^\circ\text{C}$. Unbiased samples of 25 or 50 fibres of each material were selected, and the fineness of each fibre was measured by weighing a 2 cm length on a micro-balance. The load–elongation curve was then obtained on a Cliff load–elongation recorder, at a constant rate of loading of $10 \text{ gf den}^{-1} \text{ min}^{-1}$ ($0.15 \text{ mN tex}^{-1} \text{ s}^{-1}$).

The method of drawing an average or typical stress–strain curve for a given material is interesting. It is important that the characteristic shape of the curves should be preserved, but straightforward averaging of all the curves would result in the transformation of a sharp bend to a smooth curve if it occurred in somewhat different points in different specimens. Meredith chose the five curves whose strength, breaking extension and yield point were nearest to the mean values of these quantities. From these curves, he took the loads corresponding to 20, 40, 60, 80 and 100% of the breaking elongation of the specimen and expressed them as percentages of the breaking load of the specimen. These percentages were then averaged for the five curves. Thus a series of related percentages of breaking load and breaking elongation was obtained. The mean breaking stress and breaking extension were then used to convert the percentages to absolute values of stress and extension. The typical stress–strain curve was drawn through these points, the yield point being put in at its average value.

13.5 Fibre properties

13.5.1 General

Meredith [2] carried out an extensive set of tests to give comparative data on the fibres available in the 1940s as described in [Section 13.4.6](#). A selection of the results is given in [Fig. 13.11](#) and [Table 13.1](#). It should be remembered that these values apply only to the particular types of material tested and to the particular conditions of test. A later set of comparative data for manufactured fibres of the 1950s is given in [Fig.](#)



13.11 Stress-strain curves of various fibres tested at 65% r.h., 20 °C, 0.15 mN tex⁻¹ s⁻¹. From Meredith's [2] 1945 data. Note: *Durafile* is Lilienfeld rayon; *Fibro* is staple viscose rayon; *Lanital* is a casein fibre; acetate rayon is secondary acetate.

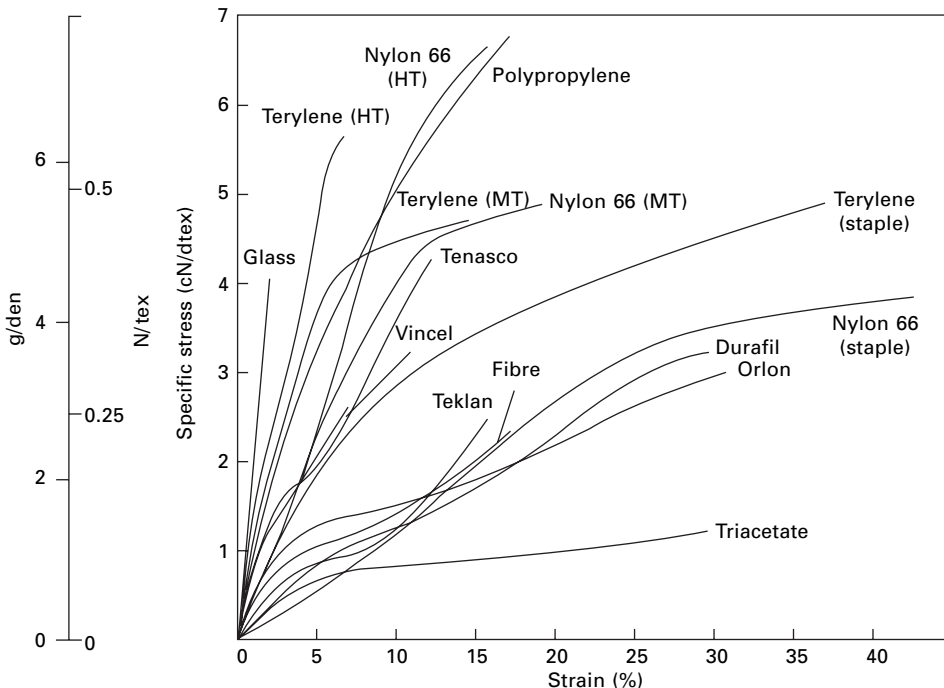
Table 13.1 Tensile properties of fibres at 65% r.h., 20 °C, 1 cm test length, 0.15 mN tex⁻¹ s⁻¹ [2]

Fibre	Tenacity (N/tex)	Breaking extension (%)	Work of rupture (mN/tex)	Initial modulus (N/tex)	Yield stress (mN/tex)	Yield strain (%)	Work factor
Cotton							
St Vincent	0.45	6.8	14.9	7.3	—	—	0.49
Upper	0.32	7.1	10.7	5.0	—	—	0.46
Bengals	0.19	5.6	5.1	3.9	—	—	0.49
Flax	0.54	3.0	8.0	18.0	—	—	0.50
Jute	0.31	1.8	2.7	17.2	—	—	0.50
Hemp	0.47	2.2	5.3	21.7	—	—	0.50
Ramie	0.59	3.7	10.6	14.6	—	—	0.47
Viscose rayon	0.18	27.2	30.6	4.8	57	2.0	0.62
Courtaulds continuous- filament							
Fibro	0.21	15.7	18.8	6.5	68	1.9	0.59
Tenasco	0.27	16.9	19.7	6.0	66	1.6	0.50
Acetate (Celanese)	0.13	23.7	21.6	3.6	75	3.2	0.72
Fortisan (cellulose)	0.59	6.4	19.1	16.1	113	0.8	0.51
Silk	0.38	23.4	59.7	7.3	156	3.3	0.66
Nylon	0.47	26.0	76.0	2.6	407	16.0	0.61
Wool							
Botany 64s	0.11	42.5	30.9	2.3	57	5.0	0.64
Crossbred 56s	0.14	42.9	37.5	2.1	62	5.1	0.62
Crossbred 36s	0.12	29.8	26.6	3.0	74	3.6	0.78
Glass	0.75	2.5	9.8	29.4	—	—	—
Steel wire	0.26	8.0	17.7	28.5	—	—	—

13.12 and Table 13.2. Another useful set of comparative data was published by du Pont [31] at this time.

For the second generation of synthetic fibres, the high-modulus, high-tenacity fibres (HM-HT), there is no comparative data for fibres tested in a single investigation. It is necessary to take data from a variety of sources, for which test conditions may not be the same. A set of stress-strain curves is shown in Fig. 13.13(a) and another set, which gives a comparison with nylon and polyester (PET) fibres in Fig. 13.13(b). Table 13.3 lists the tensile properties of a selection of HM-HT fibres. Table 13.4 gives values for some chemically and thermally resistant fibres.

The complete collection of fibres can be roughly divided mechanically into five groups, which are illustrated in Fig. 13.14. The weak inextensible fibres such as rock wool are of little interest. The natural and regenerated fibres and some synthetics have moderate strength and extensibility. The tough synthetic fibres have higher strength combined with extensibility. The HM-HT fibres have high strength and low extensibility. The elastomeric fibres have low tenacity, when related to their unstrained dimensions, and high extensibility.



13.12 Stress-strain curves of various fibres. From Farrow [28, 29] and Ford [30]. Note: viscose rayon variants are *Fibro* (regular staple), *Vincel* (high-wet modulus) and *Tenasco* (high-tenacity, industrial); *Terylene* is polyester fibre; *Orlon* is acrylic fibre.

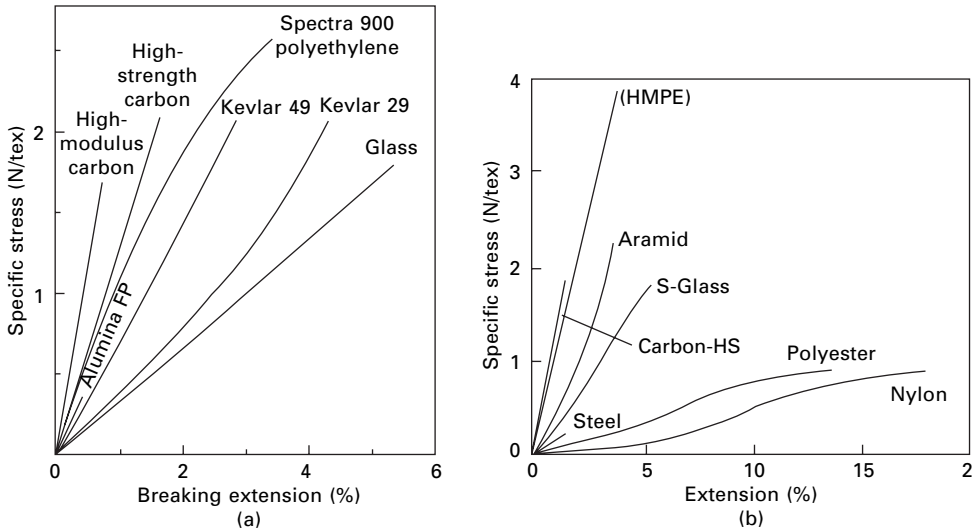
Table 13.2 Tensile properties of fibres at 65% r.h., 20 °C [28–30]

Fibre	Tenacity (N/tex)	Breaking extension (%)	Work of rupture (mN/tex)	Initial modulus (N/tex)
Viscose rayon				
high-tenacity	0.41	12	28	8.8
polynosic	0.26	7	11	13.2
Triacetate	0.12	30	18	3.1
Casein	0.10	63	44	3.5
Nylon 6.6				
medium-tenacity	0.48	20	63	3.0
high-tenacity	0.66	16	58	4.4
staple fibre	0.37	43	101	1.0
Nylon 6 (<i>Perlon</i>)	0.29	46	77	0.6
Polyester fibre (<i>Terylene</i>)				
medium-tenacity	0.47	15	53	10.6
high-tenacity	0.56	7	22	13.2
staple fibre	0.47	37	119	8.8
Acrylic (<i>Orlon</i> 42 staple-fibre)	0.27	25	47	6.2
Modacrylic (<i>Dynel</i>)	0.34	34	63	8.8
Poly(vinyl alcohol)	0.17	26	24	2.2
Poly(vinyl chloride)	0.24	17	23	3.5
Polyethylene				
<i>Courlene</i> (low-density)	0.08	20–40	11–26	0.9
<i>Courlene</i> X3 (high-density)	0.34	10	19	4.4
Polypropylene (<i>Ulstron</i>)	0.65	17	71	7.1
Glass	0.40	1.9	3.9	21.2
Elastomer				
polyurethane	0.0309	540	65	0.0071
rubber	0.008	520	14	0.0026

13.5.2 Cotton and the other natural cellulose fibres

The stress–strain curve for cotton is slightly concave to the extension axis, and there is no obvious yield point. Meredith [2] found considerable variation between different varieties of cotton. In general, the finer cottons showed a higher tenacity and a higher initial modulus than the coarser cottons. The breaking extension ranged from 5 to 10% but was not related to fineness. Figure 13.15 shows stress–strain curves of five cottons from the 1970s. The Punjab–American cotton is much stronger than the 1940s Bengals cotton in Table 13.1.

Meredith [34] later showed that there was a better correlation between tenacity and molecular orientation than there was between tenacity and fineness. The orientation may be measured by the birefringence of the fibre, that is, the difference ($n_{\parallel} - n_{\perp}$) between the refractive indices for light polarised parallel and perpendicular to the fibre axis. The orientation value decreases as the spiral angle in the cotton fibre increases (see Section 1.4.3). Figure 13.16 shows the correlation between tenacity and the difference in the refractive indices for 36 different samples of cotton of 26



13.13 Typical stress-strain curves of HM-HT fibres.

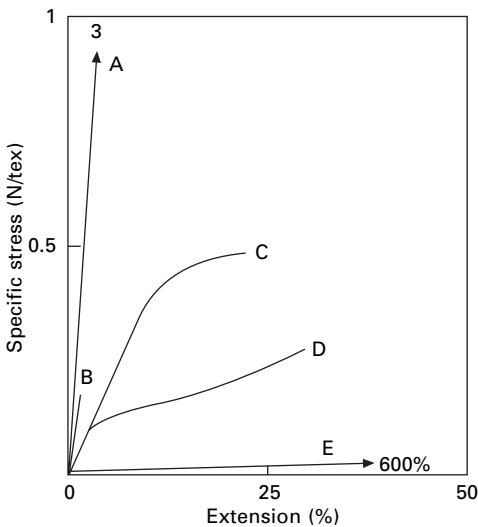
Table 13.3 Illustrative values of tensile properties of HM-HT fibres from manufacturers' literature

Fibre	Tenacity (N/tex)	Initial modulus (N/tex)	Breaking extension (%)	Tensile strength (GPa)	Initial modulus (GPa)
HMPE					
Spectra 900	2.6	124	3.5	2.5	120
Spectra 1000	3.1	177	2.7	3.0	172
Aramid					
Kevlar 29	2.1	58	4.4	3.0	83
Kevlar 49	2.1	80	2.9	3.0	115
Kevlar 149	1.6	98	2.5	2.3	141
Carbon (Hysil Grafil)					
XA	1.8	128	1.4	3.2	230
High-strain	2.1	128	1.7	3.7	230
High-modulus	1.3	183	0.7	2.5	340
Ultra-HM	1.7	218	0.8	3.1	405
Silica					
Enka LT	0.14	7	2.0	0.25	13
Enka HT	0.40	28	1.4	0.8	56
Tyranno	1.2	83	1.5	2.8	200
Glass-E	1.4	2.9	4.8	3.5	72
-S	1.8	35	5.4	4.6	87
Silicon carbide					
Nicalon	1.0	81	1.5	2.7	210
Whisker	3.2	220	1.2	8.4	580
Nextel	0.63	56	1.1	1.7	150
Alumina - FP	0.36	97	0.4	1.4	380
Alumina-zirconia					
PRD-166	0.50	90	0.6	2.1	380

These are illustrative examples, taken from manufacturers' literature.

Table 13.4 Tensile properties of chemically and thermally resistant fibres [32]

Fibre	Tenacity (N/tex)	Break extension (%)	Initial modulus (N tex)
Polyvinylidene chloride (PVDC)	0.20	15–30	0.44–0.68
Polytetrafluorethylene (PTFE) (<i>Teflon</i>)	0.14	20	–
Polyetheretherketone (PEEK)	0.65	20	4–5
Polyphenylenesulphide (PPS)	0.27–0.47	25–35	2.7–3.7
Melamine-formaldehyde (<i>Basofil</i>)	0.2–0.4	15–20	6
Novoloid phenolic resin (<i>Kynol</i>)	0.12–0.16	30–50	2.6–3.5
meta-Aramid (<i>Nomex</i>)	0.485	20	7.5
Polyimide (P84)	0.35–0.38	33–38	3–4
Polyamide-imide (<i>Kermel</i>)	0.25–0.59	8–20	4.9–9.4
Semi-carbon oxidised acrylic	0.14–0.21	15–21	5–8
Polybenzimidazole (PBI)	0.24	28.5	2.8

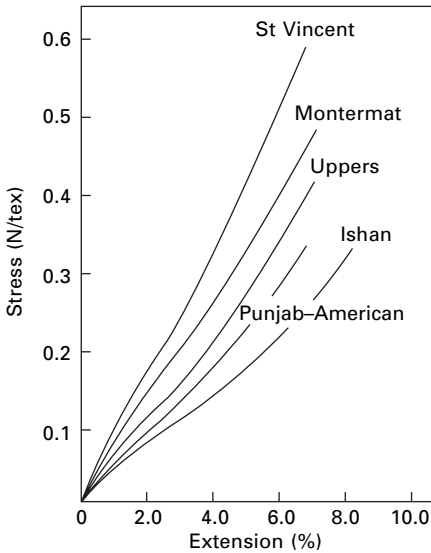


13.14 Mechanical classification of the fibre types: A, HM-HT fibre; B, weak inorganic fibre, e.g. rock wool; C, tough synthetic fibre; D, weaker textile fibre; E, elastomeric fibre.

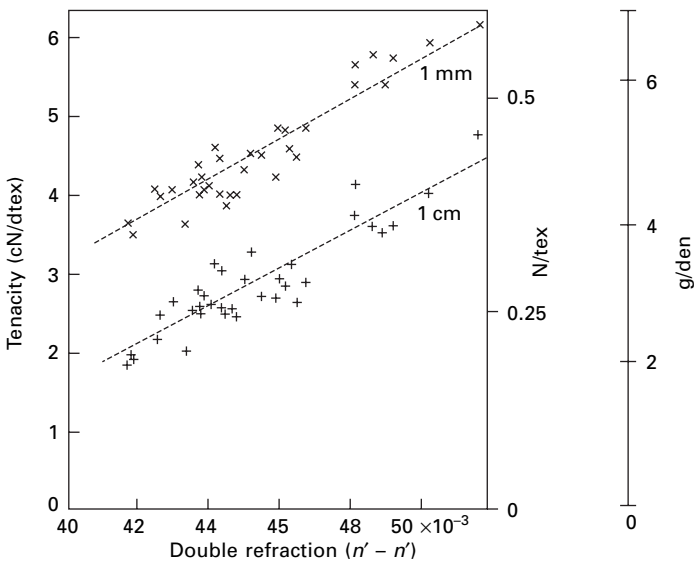
different varieties. Similar results are obtained by using X-ray methods to measure molecular orientation [35], and a correlation is also found between initial modulus and orientation. It must, however, be noted that it has been reported [36, 37] that the spiral angle of cotton fibres is constant within the range 20–23° and that the apparent differences are really due to the effect of convolutions.

Hessler *et al.* [38] investigated the effect of the length of chain molecules in the cotton and found that this also gave a good correlation with the tenacity of different types of cotton. Thus it is not clear which is the effective factor in determining the tenacity of different varieties of cotton.

Morlier *et al.* [39] investigated the difference between fibres *within* a given sample of cotton for six different varieties of cotton. In most cases, they found that tenacity

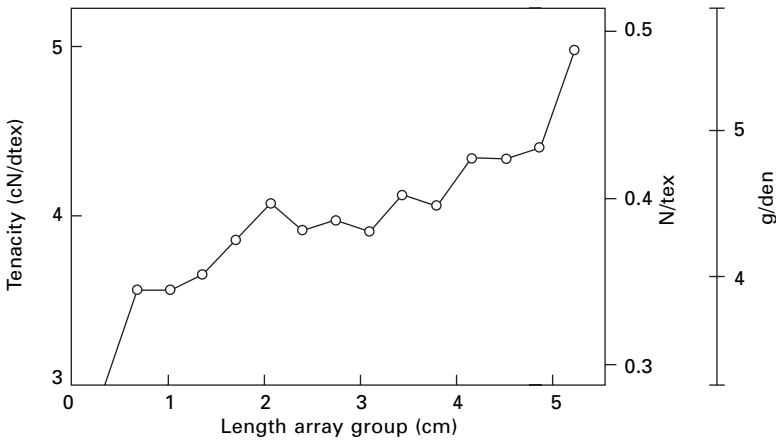


13.15 Stress-strain curves for various cottons. After Sparrow [33].



13.16 Correlation between tenacity and birefringence of cotton at test lengths of 1 mm and 1 cm. From Meredith [34].

and breaking extension increased with increasing length of fibre. An example of their results is given in Fig. 13.17. Meredith found no correlation between strength and fineness within a sample of cotton. Timpa and Ramey [40] found an increase of strength, measured in four laboratories according to HVI standards, from 0.2 to 0.3 N/tex with increasing length from 21.2 mm (staple length code: 26) to 32 mm (code: 40); they also found a significant increase of strength with molecular weight, albeit



13.17 Correlation between tenacity and length for a Sea Island cotton. From Morlier *et al.* [39].

Table 13.5 USDA descriptive designations for HVI tenacity values of cotton

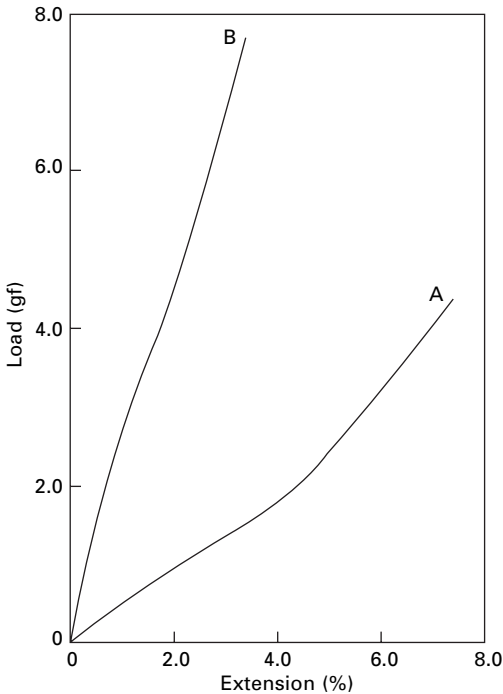
Designation	HVI tenacity	
	Specified grams per tex	Equivalent N/tex
Very weak	<20	<0.196
Weak	21–23	0.206–0.226
Average	24–26	0.235–0.255
Strong	27–29	0.265–0.284
Very strong	>30	>0.294

with considerable scatter. Foulk and McAlister [41] report an extensive study of the tensile properties of cottons with three micronaire values, each subdivided into seven length groups.

With the advent of HVI testing of cotton, the US Department of Agriculture (USDA) has given the designations of tenacity values in Table 13.5 as an indication of cotton fibre quality. The values are lower than those from Meredith's single fibre tests, reflecting the influence of bundle testing discussed in [Chapter 14](#).

Hearle and Sparrow studied the effect of convolutions on the behaviour of cotton fibres [42]. If a fibre is stretched, the convolutions are pulled out. If the fibre is extended in the wet state and dried while held under tension, the extended form is temporarily set. [Figure 13.18\(a\)](#) shows the effect on the stress–strain curve at 65% r.h. The treated fibre is stiffer, and shows a higher tenacity and lower break extension.

The bast fibres, in which the molecules are very nearly parallel to the fibre axis, show a greater tenacity, a higher modulus, a lower breaking extension and a lower work of rupture. They constitute the strongest but least extensible of natural fibres. The jute tested by Meredith gave lower values of tenacity than the other bast fibres, but it has been shown by Mukherjee *et al.* [43] that a better-quality jute has a tenacity



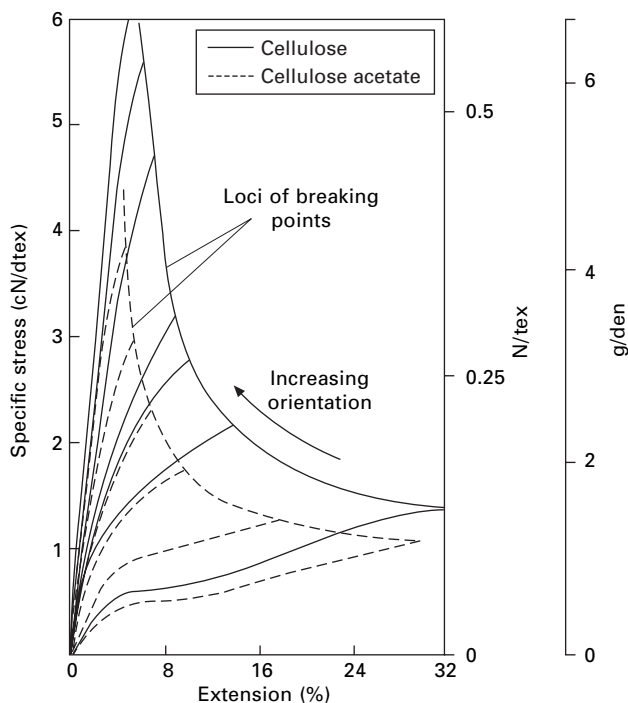
13.18 Load–extension curves of Acala cotton: A, normal fibre; B, after stretching wet and drying.

of 0.56 N/tex under similar conditions; this is as strong as flax or hemp. Franck [44] includes a large collection of reported values of mechanical properties of bast and other plant fibres. The values are generally similar to those for flax, jute, hemp and ramie in [Table 13.1](#).

13.5.3 Regenerated cellulose and related fibres

The stress–strain curves of rayon and acetate fibres show an initial rapid rise with a marked yield point, followed by a nearly flat portion and a rise again as breakage approaches. The curves vary widely for different types of rayon and different manufacturing methods. Differences are due to the spinning method and the degree of stretch imposed. A highly stretched fibre, such as the formerly produced *Durafil*, has high molecular orientation, which gives high strength and low extensibility, similar to the bast fibres. Rayons used for apparel are weaker and more extensible. Tyre-cord rayons, such as *Tenasco*, are intermediate in value.

The effect of orientation is clearly shown in the set of curves in [Fig. 13.19](#), for acetate of varying degrees of orientation. If cellulose yarns are regenerated from the acetate, as they were in *Fortisan*, the locus of strengths is somewhat higher. Acetate fibres are, in general, weaker and more extensible than viscose rayon fibres. The load–elongation curves of acetate fibres, measured at constant rate of elongation, often show a drop after the yield point.

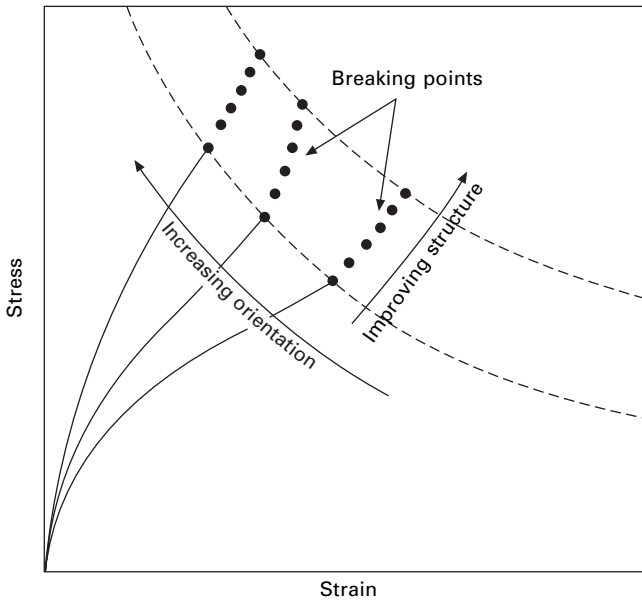


13.19 Stress-strain curves of filaments of varying degrees of orientation. The dotted curves are secondary cellulose acetate and the full curves are cellulose fibres regenerated from acetate. The lowest curve in each set is for unoriented material. From Work [45].

There are also important differences in the tensile properties of viscose rayon, depending on their fine structure. An improvement in structure will cause the whole locus of breaking points to be moved farther from the origin, so that strength is increased without the loss of extensibility that occurs when orientation is increased. This is illustrated in Fig. 13.20, and the great advances that were made in high-tenacity rayon tyre yarns in the 1950s are shown in Table 13.6. More extensible analogues of these fibres are used as high-strength staple fibres. Rayons made until the 1950s had a micellar structure, which results in a low-wet-modulus and a low strength as shown later in Fig. 13.26.

The modal rayons, which include polynosic fibres, are fibrillar in texture, and are stiffer, and closer to cotton in properties, than earlier rayon fibres (see Fig. 13.21). They have a high-wet-modulus and better wet strength. The reasons for this are discussed in Section 20.2.2. Lyocell fibres, such as *Tencel*, are similar in tensile properties, but somewhat stronger and stiffer. White *et al.* [47] give dry tenacities and break extensions of 0.38–0.42 N/tex at 14–16% dry and 0.34–0.38 N/tex at 16–18%.

Chamberlain and Khera [48] investigated the variation in the properties as the outer layers of viscose and cuprammonium rayon filaments are removed chemically. A typical result for viscose rayon is shown in Fig. 13.22. It appears from these results that the outermost layers are less extensible than the layers below the surface, but the



13.20 Load–extension curves for viscose rayon, showing changes produced by increasing orientation and improving structure.

Table 13.6 Properties of viscose rayon tyre cords.
From Wilkinson [46]

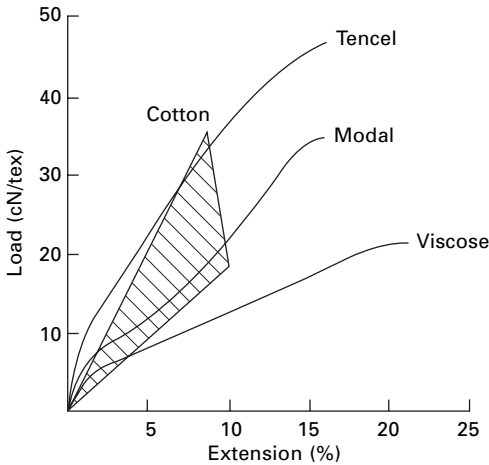
Type	Tenacity (N/tex)	Breaking extension (%)
Textile rayon	0.19	20
Tenasco	0.30	10
Tenasco 35	0.35	10.5
Tenasco 70	0.36	13.5
Tenasco Super 105	0.47	12.5

variation in tenacity cannot be worked out, since the stress would concentrate in the least extensible parts of the fibre. The results for cuprammonium rayon were different for the two samples of fibre tested.

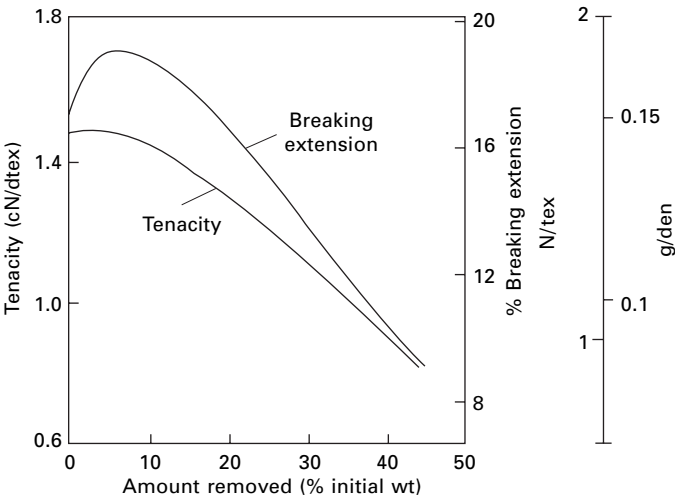
From reports by different workers, Muri and Brown include tenacities N/tex and break extensions of 0.154/14.5% and 0.183/ 6% for calcium alginate fibres and 0.204/10% for zinc alginate [49].

13.5.4 Protein fibres

Silk, like nylon, is characterised by fairly high strength and breaking extension, which combine to give a work of rupture very much greater than that of the other fibres tested by Meredith. The wide range of spider silks include fibres of very high



13.21 Stress-strain curves of lyocell (*Tencel*), modal and regular viscose rayon compared with cotton. From Courtaulds Lyocell Overview.



13.22 Change of tenacity and braking extension of viscose rayon as outer layers are removed. From Chamberlain and Khera [48].

strength combined with high extensibility, which leads to very high work of rupture [50, 51].

Wool and other hair fibres are characterised by low strength but great extensibility. Owing to the high breaking extension, and to the shape of the curve, the work of rupture is not low despite the low strength. Different types of wool give slightly different curves, but these are always characterised by an initial linear Hookean region up to 2% extension, a yield region of very low slope from 2 to 30% extension, and finally a post-yield region of greater slope, up to a breaking extension around 45%.

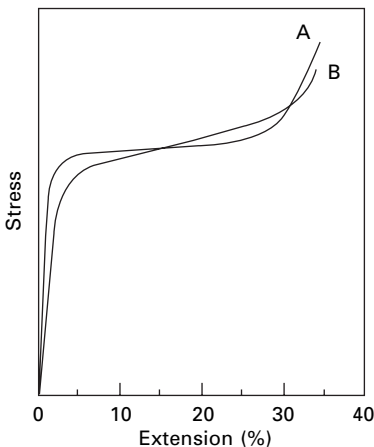
The very extensive experimental studies that have been carried out on wool have been reviewed by Chapman [52] and Feughelman [53]. Much of the work has been done on wet fibres, and Collins and Chaikin [54] have found, as illustrated in Fig. 13.23, that, if the effects of fibre irregularity are eliminated, the separate regions become even more distinct, with sharp turning points between them, and the yield slope becomes very small.

Anderson and Cox [55] have shown that although there was a very wide scatter of the results, the tenacity of wool fibres from a given lock of wool increased with the fibre diameter. There was a slight positive correlation between breaking extension and fibre diameter.

Regenerated protein fibres are weak and extensible and even weaker when wet. In addition to the fibres manufactured in the 1950s, this also applies to the attempts to produce fibres from spider silk proteins derived from genetically engineered sources.

13.5.5 Synthetic fibres

The general tendency in melt-spun synthetic fibres, as shown by Figs 13.11 and 13.12 and Tables 13.1 and 13.2, is for moderately high strength to be combined with moderately high breaking extension, which results in a tough fibre, though this is open to modification through the amount of drawing. The lower part of the stress–strain curve is very sensitive to the treatment of the fibre and may or may not show a yield point. There is commonly another yield point at a high stress, close to the breaking stress, though this may be cut off by premature rupture. Although their breaking points lie close together, polyester fibres have a markedly higher initial modulus than nylon and polypropylene fibres. This has a practical effect on the handle of fabrics. Differences in the shape of the stress–strain curves of commercial polyamide and polyester fibres can be attributed to changes in the annealing and drawing processes during manufacture.

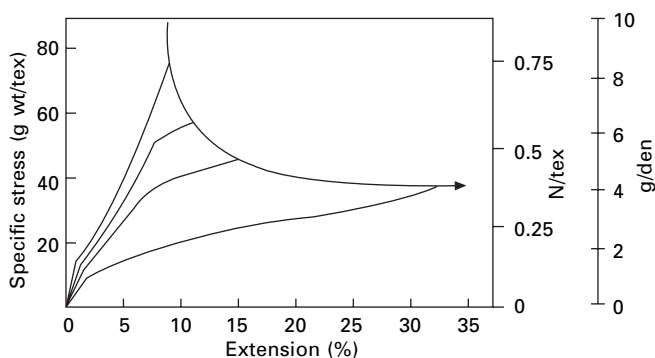


13.23 Stress–strain curves of wool fibres: A, with good uniformity; B, more irregular fibre. From Collins and Chaikin [54].

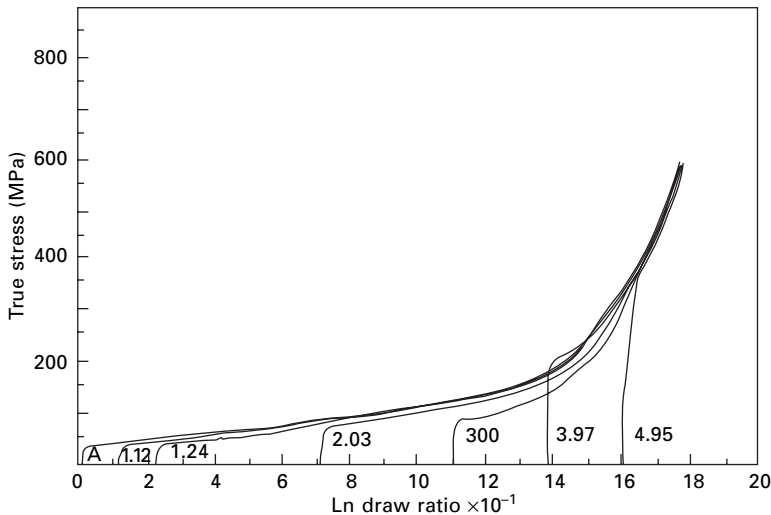
The tensile properties of synthetic fibres depend to a considerable extent on the molecular weight of the polymer and on the conditions of spinning and drawing. A good example of this is polyester fibre, which can have a variety of stress–strain curves, as shown in Fig. 13.24. As the degree of orientation is increased by drawing, strength and stiffness increase and breaking extension decreases. If the molecular weight increases, the locus of breaking points moves upwards, but the initial parts of the stress–strain curve are little altered.

The results in Fig. 13.24 are for an early *Terylene* polyester fibre produced by winding up an undrawn, low orientation fibre and then drawing it under different conditions. Ward [57], and Long and Ward, [58] have studied the drawing behaviour of polyester fibres, previously drawn to different degrees. After an initial stiff region, the fibre yields and joins a common curve to the break point (Fig. 13.25). Recovery from any point on the draw curves is approximately along lines parallel to the elongation curve of the fibre with the highest draw ratio. The yield at the end of the stress–strain curve of a drawn fibre is the final stage of the draw process. For practical operation, the maximum draw cannot be imposed, because a certain margin has to be left or there would be a risk of breakage during the drawing operation. In polybutylene terephthalate (PBT, 3GT) a crystalline phase transition and in polyethylene naphthalate (PEN) crystallisation effects complicate the relation between drawing and properties [57].

The early separation of spinning and drawing gave way to a continuous spin-draw operation, but this did not appreciably change the mechanical behaviour. A greater change when spinning at higher speed, *c.* 3000 m/min, gave partially oriented yarns (POY), for which drawing could be completed in subsequent draw-texturing or other processes. Figure 13.26 shows stress–strain curves for polyester fibres spun at different speeds. If the curves are translated to an equivalent draw ratio, then after the initial elongation, they fall on a master curve similar to Fig. 13.25. Polyester fibres spun at around 6000 m/min are sometimes referred to as fully oriented fibres (FOY). What this means is that they are oriented to a degree that allows them to be used directly in some textile fabrics without additional drawing. However, it can be seen from Fig.



13.24 Stress–strain curves of polyester fibre (Terylene) at varying orientations [56].



13.25 Stress–strain curves of polyester fibres previously drawn to different degrees. Note that the stress is a true stress, based on the changing area of cross-section. The numbers attached to the curves are the initial draw ratios. From Ward *et al.* [59].

13.26(a) that they are more extensible than conventional drawn fibres and they will have a lower tenacity based on the as-spun linear density.

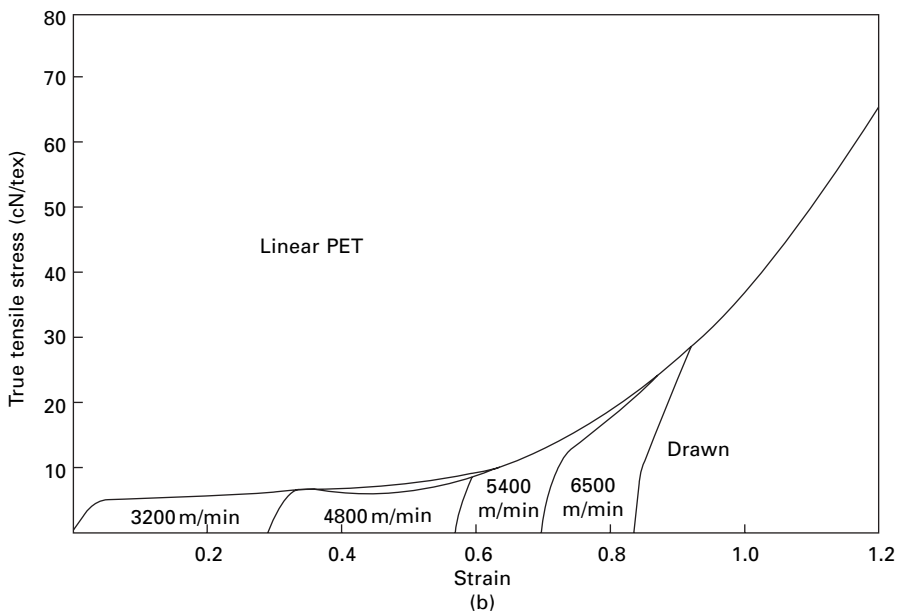
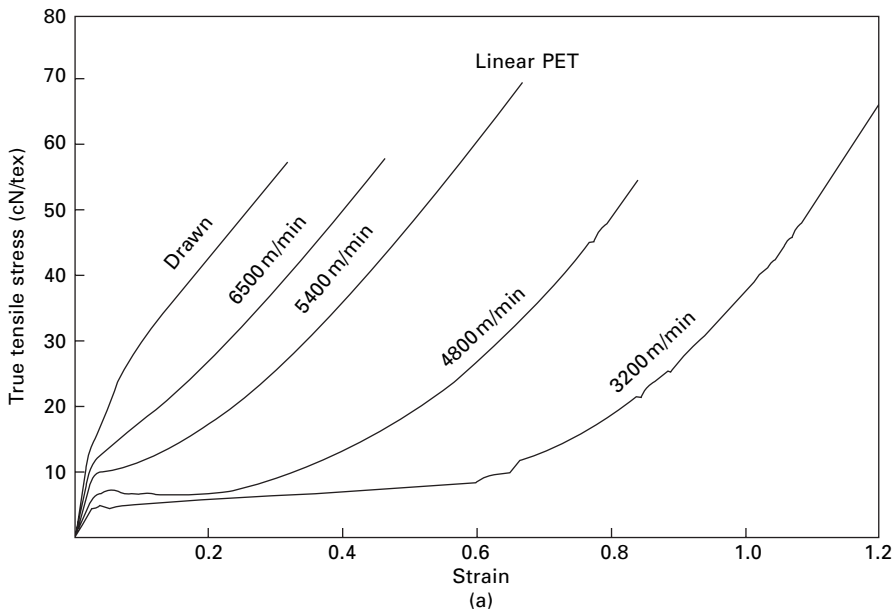
For maximum stiffness and strength, which naturally combine with low breaking extension, polyester fibres are subject to additional heat treatments under tension. These high-tenacity yarns were initially developed for tyre cords, but are also used in other technical textiles. Typical properties of a high-tenacity polyester yarn would be a tenacity of 0.8–0.85 N/tex with a breaking extension of 13–18%. This is considerably stronger than the early high-tenacity polyester listed in Table 13.1. The fact that both strength and break extension have increased means that the stress-strain curve has been extended to a higher locus without much change in stiffness.

PEN fibres have a higher modulus than PET fibres. Polytrimethylene terephthalate fibres have a lower modulus and are more similar to nylon in tensile properties.

The effect of draw ratio and spinning speed for nylon is broadly similar to that for polyester. Figure 13.27 shows stress–strain curves for nylon 66 fibres spun at different speeds. High-tenacity nylon yarns reach about 0.85 N/tex in tenacity, but have a breaking extension of 20%, which makes them tougher and more extensible than polyester yarns.

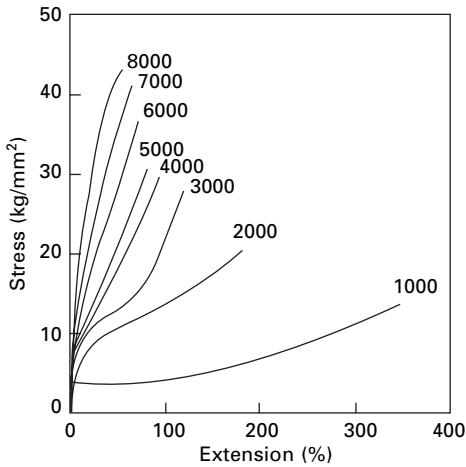
Much detailed information on the effect of spinning speed on mechanical properties and structure of polyester, nylon and polyolefin fibres is included in the book edited by Ziabicki and Kawai [62].

The shape of the stress–strain curve of both nylon and polyester fibres can be considerably altered by heat treatments under tension. Figure 13.28 shows a set of stress–strain curves, related to the original fibre dimensions, for nylon fibres subjected to heat treatments by Hearle *et al.* [63]. Another example of the influence of subsequent

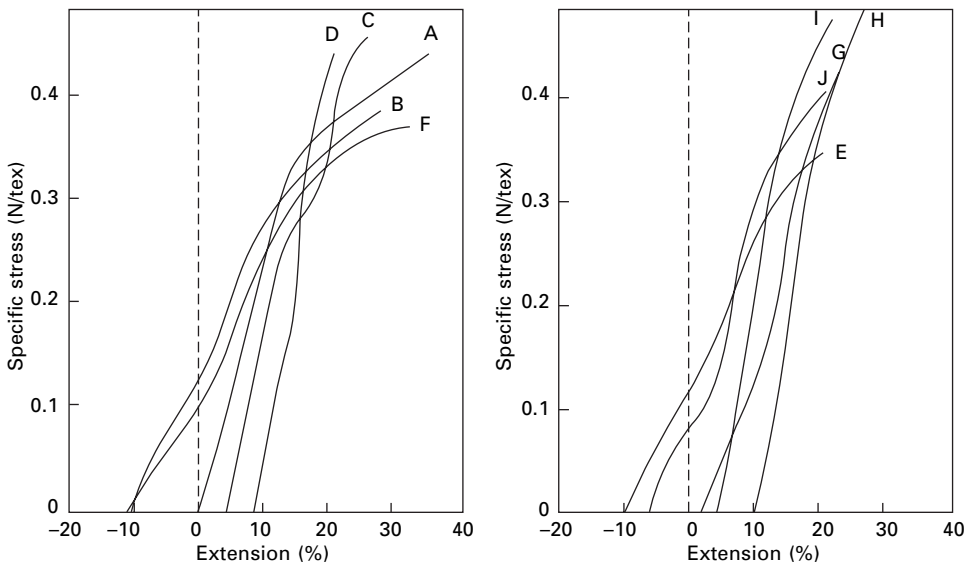


13.26 True stress–strain curves for polyester fibres spun at different speeds: (a) with strain based on as-spun length, (b) with curves translated to an equivalent initial draw-ratio. From Perez [60].

heat treatments is shown by [Figure 13.29](#) for polyester fibres tested at 20 °C and 65% r.h. as received, and under the same conditions after exposure to water at 95 °C: the shape of the curve is markedly different in the two cases. [Figure 13.30\(a\)](#), from an extensive study by Mwaisengela [14] shows stress–strain curves after free annealing

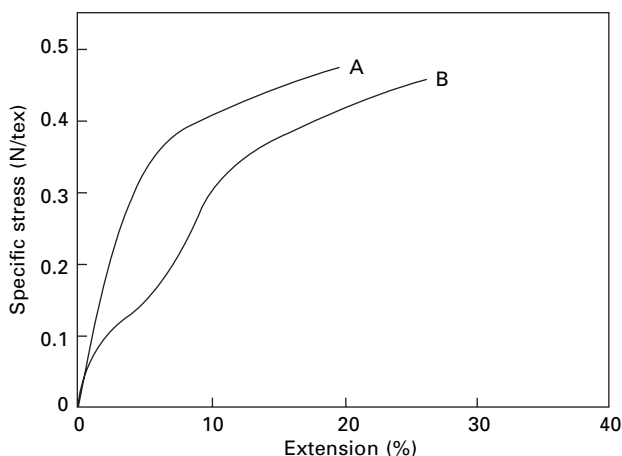


13.27 Stress-strain curves of nylon 66 fibres spun at different speeds. From Shimizu *et al.* [61].



13.28 Stress-strain curves of 70 denier (78 dtex) nylon yarns after various heat treatments: A, as received; B, 200 °C, zero tension; C, 200 °C, 0.3 N; D 200 °C, 0.75 N; E, relaxed in boiling water; F, 200 °C, zero tension, then relaxed; G, 200 °C, 0.75 N, then relaxed; H, 200 °C, 0.1 N, then 240 °C, 0.5 N; I, 200 °C, 0.5 N, then 160 °C, 0.1 N; J, 200 °C, 0.1 N, then 160 °C, 0.5 N, then relaxed [63].

for a moderately high-tenacity polyester yarn spun at 800 m/min, but drawn 4× and heat-set at 160 °C, as used for sewing thread. The low-stress yield has been eliminated by the heat setting, but reappears after annealing. When re-plotted using original dimensions, Fig. 13.30(b), the fibre shows shrinkage of up to 18% and all the curves come together at about 0.3 N/tex and 8% extension. The heat treatment causes a



13.29 Stress–strain curve of polyester fibre under standard conditions: A as received; B, after treatment in water at 95 °C [30].

small loss in strength. Commercially provided polyester yarns may be similar to this yarn in showing no low yield point and having low shrinkage or, if they have been processed differently, may have stress–strain curves with a low yield point like the stress–strain curve in Fig. 13.30(a) at 120 °C. Mwaisengela [14] found a similar behaviour in a high-tenacity nylon 66 yarn, as shown by the tangent modulus plot in Fig. 13.31. The initial stiff region leads to the low yield point, represented by the minimum in the modulus, which is followed by a gradual stiffening and then a lower modulus as break is approached.

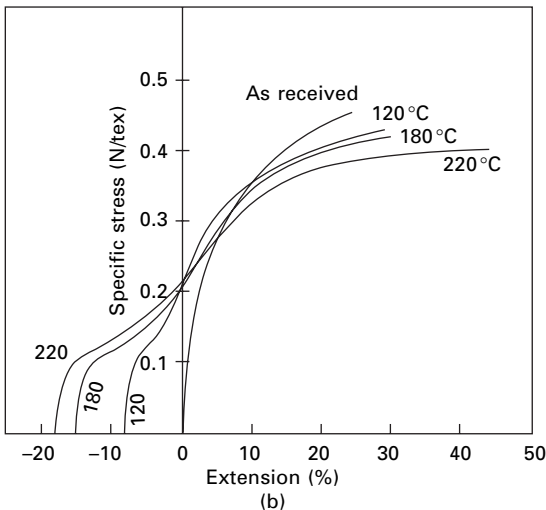
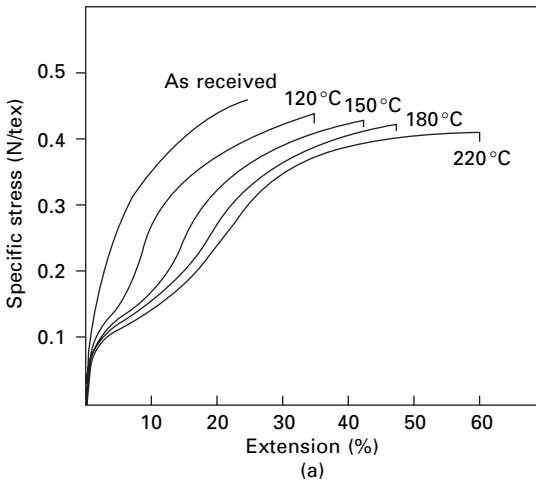
Wang *et al.* [64] report that the strength of polypropylene can be increased to 0.88 N/tex by a second stage drawing process at 140 °C, but some whitening of the fibre is observed. This is an indication of defects in the fibre and the breaking extension is 18.4%, compared with 22% for fibres drawn at lower temperatures.

Figure 13.32 shows the stress–strain curve of an acrylic fibre under standard conditions. As in all acrylic fibres, there is a yield point at around 2% extension. Although treatments can give higher strength and lower breaking extension, commercial acrylic fibres are usually at the lower strength and higher extension range for synthetic fibres. Acrylic fibres are not quite as tough as nylon, polyester or polypropylene fibres.

Staple polylactic acid (PLA) fibres have stress–strain curves in extension similar to wool, with tenacities of 0.32–0.36 N/tex and a break extension of 55% [65]. Elastic recovery is 99.2% from 2% extension and 92.6% from 5% extension, but is not as good as wool from higher extensions.

13.5.6 High-performance fibres

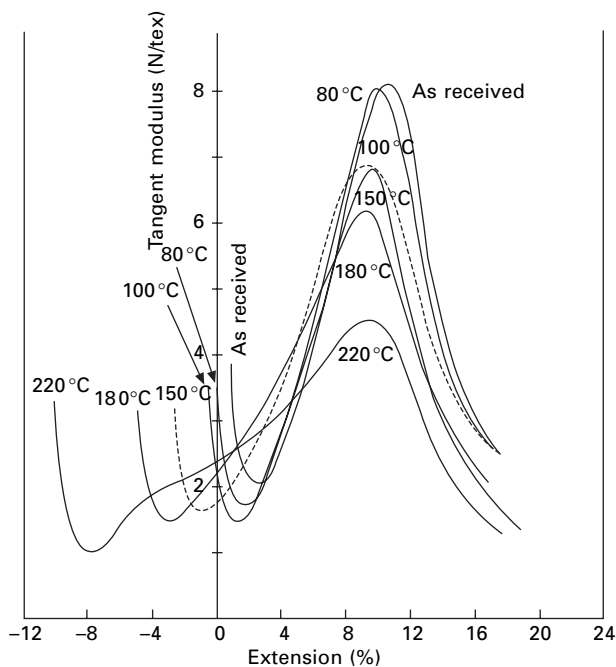
For the characterisation of the tensile stress–strain properties of HM–HT fibres, two aspects merit special mention. Experimentally, the high strength of the fibres makes the problem of securing a grip that holds but does not weaken the specimen more



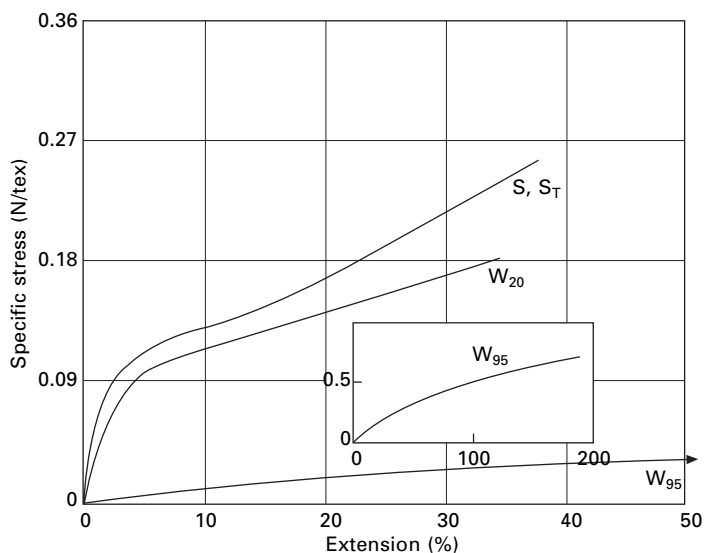
13.30 Stress-strain curves of polyester yarn annealed under zero tension at different temperatures: (a) based on length after annealing; (b) based on original length. From Mwaisengela [14].

acute; and, because of the high stiffness, any softness of the gripping system, including deformation of the jaws and the load cell, will cause greater errors in determination of fibre extension, especially for short samples. In interpretation, the large density differences cause large changes in relative values of strength and stiffness for different fibres, depending on whether specific stresses, normalised by linear density, or stresses, normalised by area, are quoted.

Some typical stress-strain curves of HM-HT fibres were shown in [Fig. 13.13](#). Numerical data in [Table 13.3](#) were given on both a mass and volume basis. It must be stressed: (1) that these are not like the data in [Tables 13.1](#) and [13.2](#), obtained in single scientific comparisons of many fibre types, but are mostly from manufacturers'



13.31 Tangent modulus plot for nylon 66 yarn free annealed at different temperatures. From Mwaisengela [14].



13.32 Stress-strain curves of Courttelle acrylic fibre: S: 65% r.h., 20°C, as received; S_T , 65% r.h., 20°C, after water at 95°C, W_{20} , in water at 20°C, as received; W_{95} , in water at 95°C, as received.

literature; (2) that process differences can cause substantial differences in properties; (3) that most of these fibres are in the first or second generation of development, and improved performance can be expected in future. The examples quoted in [Table 13.3](#) are typical of the range found, but variants and fibres from other manufacturers may have somewhat different properties. For improved forms of HMPE fibres, van Dingenen [66] quotes values up to 3.7 N/tex at a break extension of 3.8% for *Dyneema* SK76. For its *Tenax* carbon fibres, Enka quoted moduli from 238 to 440 GPa, strengths from 2.15 to 4.7 GPa, and breaking extensions from 0.4 to 1.8%. Test methods can also cause differences: for example, Simon and Bunsell [67] report a reduction in mean strength of *Nicalon* SiC fibres from 2.04 GPa at a 15 mm test length to 1.29 GPa at a 220 mm length owing to coefficients of variation of around 30%; and similar effects would occur in other fibres.

To a first approximation, HM–HT fibres follow Hooke’s Law, with stress proportional to strain, and break is sharp without any yield. There is no appreciable deviation from linearity in ceramic, glass and carbon fibres. The lower-modulus aramids, like *Kevlar* 29, show a stiffening with extension, but this is reduced in the higher-modulus forms, *Kevlar* 49 and 149, which have been subject to further processing. The HMPE fibres show a softening at high extension. The concave deviation of the aramids is most marked at low stresses, but the convex deviation of HMPE is most marked at high stresses.

A rough guide to comparative values of strength, stiffness (average modulus), and extensibility that can be expected from different sorts of HM–HT fibre is shown in [Fig. 13.33](#), but, for any purposes needing precision, the actual properties should be checked or measured.

[Table 13.4](#) listed tensile properties of fibres that are used for their thermal or chemical properties. Their mechanical properties are generally somewhat inferior to the corresponding general-purpose textile fibres.

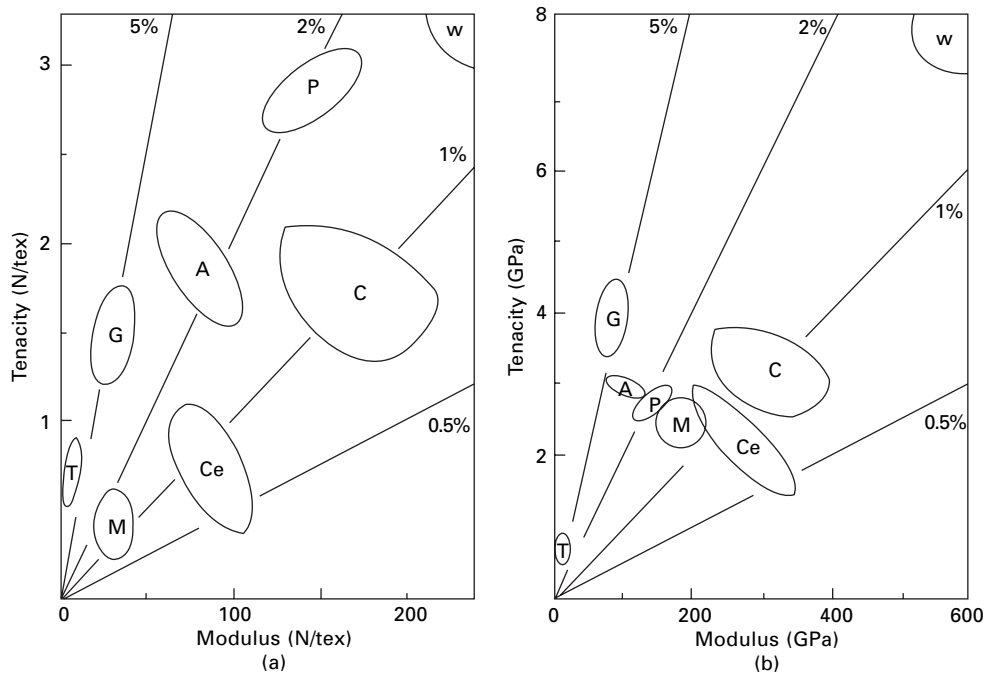
13.5.7 Elastomeric fibres

At the other end of the performance limits from HM–HT fibres, there are elastomeric fibres, which show good elastic recovery up to high extension. Natural rubber can be used, but the most important fine fibres are spandex, with *Lycra* as one example. [Figure 13.34](#) shows a comparison of spandex and rubber fibres: their extensibilities are similar, but the spandex fibre is twice as strong. Based on the initial linear density, the strength appears low; but the true stress at break is about 0.5 N/tex, which is similar to that of nylon and polyester fibres.

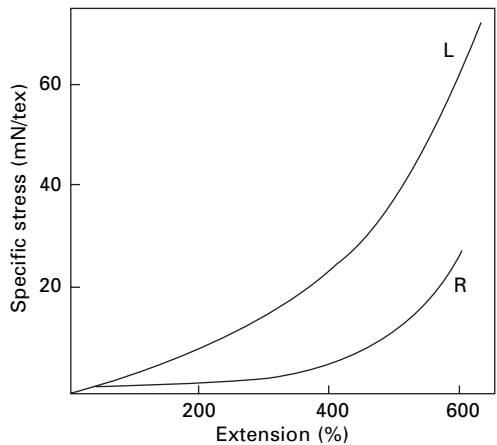
13.6 Other factors

13.6.1 Variability and time dependence

As discussed in the next chapter, particularly for natural fibres, variability must be taken into account in studying tensile properties. The weak link effect means that strengths may be much lower than expected.



13.33 Comparison of regions of mechanical properties approximately covered by different classes of fibres: (a) on weight basis; (b) on volume basis: A, aramid; C, carbon; Ce, ceramic; G, glass; M, metals; P, polyethylene (HMPE); T, textile fibres such as nylon or polyester; W, single-crystal whiskers. The radiating lines show breaking extensions, assuming Hooke's Law.



13.34 Stress-strain curves of *Lycra* spandex fibre (L) and natural rubber (R) [68].

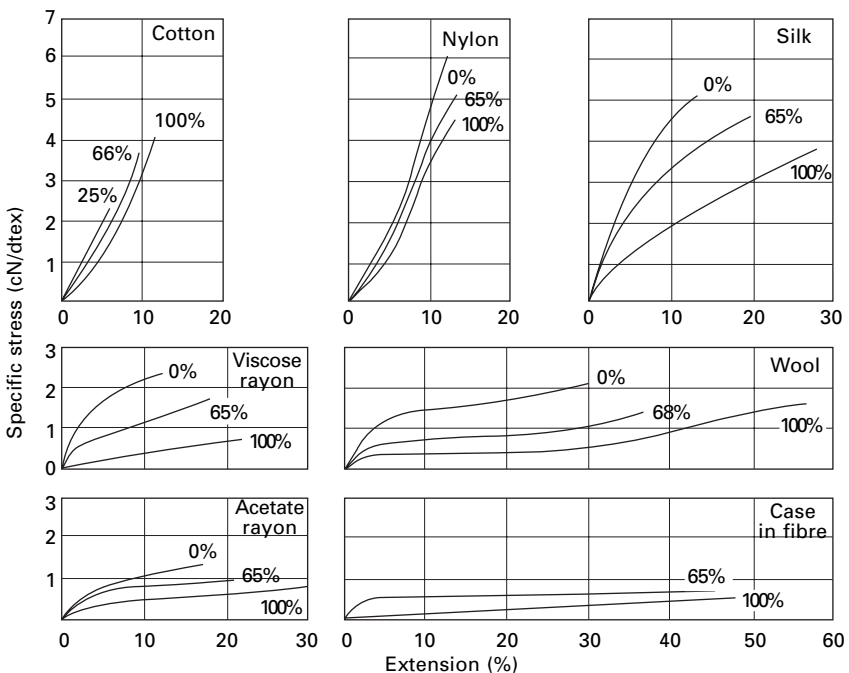
The rate of extension is another factor influencing tensile properties, but this is included in the consideration of rheology in [Chapter 16](#). Generally an increase in rate of testing, often expressed as reduced time to break, leads to lower extensibility and greater strength.

13.6.2 Effect of moisture and temperature

Figure 13.35 shows stress–extension curves for various fibres at different relative humidities. All the fibres become more extensible at higher humidities, the modulus becoming smaller and the breaking extension greater, but, whereas cotton and other natural cellulose fibres become stronger, the rest of the fibres become weaker. [Table 13.7](#) gives values of the tensile properties of a number of fibres expressed as a percentage of the values under standard conditions. The properties of those synthetic fibres which absorb little or no water would not be expected to vary with humidity.

As an example of a set of very detailed results, [Fig. 13.36](#) shows the effect of relative humidity on the stress–strain curves of wool fibres. It will be noted that the major effect is to raise the yield point. This behaviour is also found in other fibres.

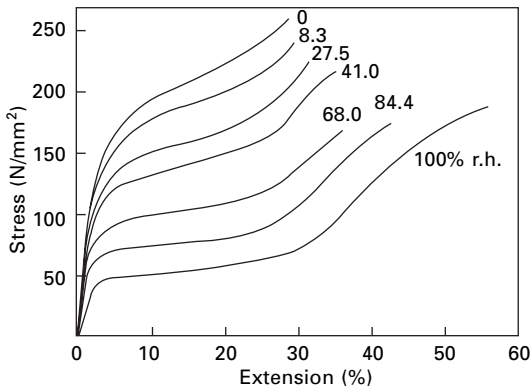
The mechanical properties of fibres also change with temperature. [Table 13.7](#) illustrates the differences between the behaviour at 20 °C and that at 95 °C when wet. The tenacity and stiffness are lower at the higher temperature, but the breaking extension is usually higher. Prolonged exposure to high temperatures can lead to permanent degradation of fibres.



13.35 Stress–strain curves at various humidities [69].

Table 13.7 Effect of moisture and temperature on tensile properties [28, 30]

Fibre	Ratio of values: wet/65% r.h				Ratio of values: wet, 95 °C/wet, 20 °C			
	Tenacity	Breaking extension	Work of rupture	Initial modulus	Tenacity	Breaking extension	Work of rupture	Initial modulus
Cotton, Uppers	1.11	1.11	0.92	0.33	1.00	1.00	1.00	1.00
Viscose rayon								
high-tenacity	0.64	2.00	0.78	0.02	0.90	1.25	1.25	0.75
polynosic	0.70	1.21	0.62	0.08	0.95	1.06	1.00	0.83
normal	0.50	1.58	0.69	0.03	0.90	1.03	0.89	0.80
Acetate	0.54	1.41	0.63	0.17	0.43	1.98	0.75	0.07
Triacetate	0.62	1.27	1.10	0.57	0.56	1.79	0.91	0.30
Silk	0.92	1.63	1.31	0.25	0.71	0.96	0.67	0.67
Wool, merino	0.69	1.33	0.65	0.40	0.55	1.37	0.82	0.50
<i>Fibrolane</i> (casein)	0.32	0.95	0.18	0.05	0.29	0.67	0.33	1.00
Nylon	0.80	1.05	0.87	0.82	0.79	1.76	1.19	0.21
<i>Terylene</i> (polyester fibre)	1.00	1.00	1.00	1.00	0.72	1.40	0.85	0.42
<i>Orlon</i> (acrylic fibre)	0.84	1.08	0.98	1.00	0.35	4.26	1.04	0.02
Polypropylene fibre	1.00	1.00	1.00	1.00	0.45	2.47	1.13	0.21
Fibreglass	0.80	0.78	0.63	1.00	0.68	0.78	0.53	0.86



13.36 Effect of relative humidity on stress–strain curves of wool at room temperature [52].

Du Pont [31] published data on the influence of temperature on the stress–strain curves of various fibres. Tests in water (Fig. 13.37) illustrate the effect of temperature alone; but those in air combine an effect of moisture, since at -57°C the humidity would be close to 100 r.h., at 21°C it was 65% r.h., and at the high temperatures it would be close to 0% r.h. The influence of temperature on the stress–strain properties of wet wool is shown in Fig. 13.38.

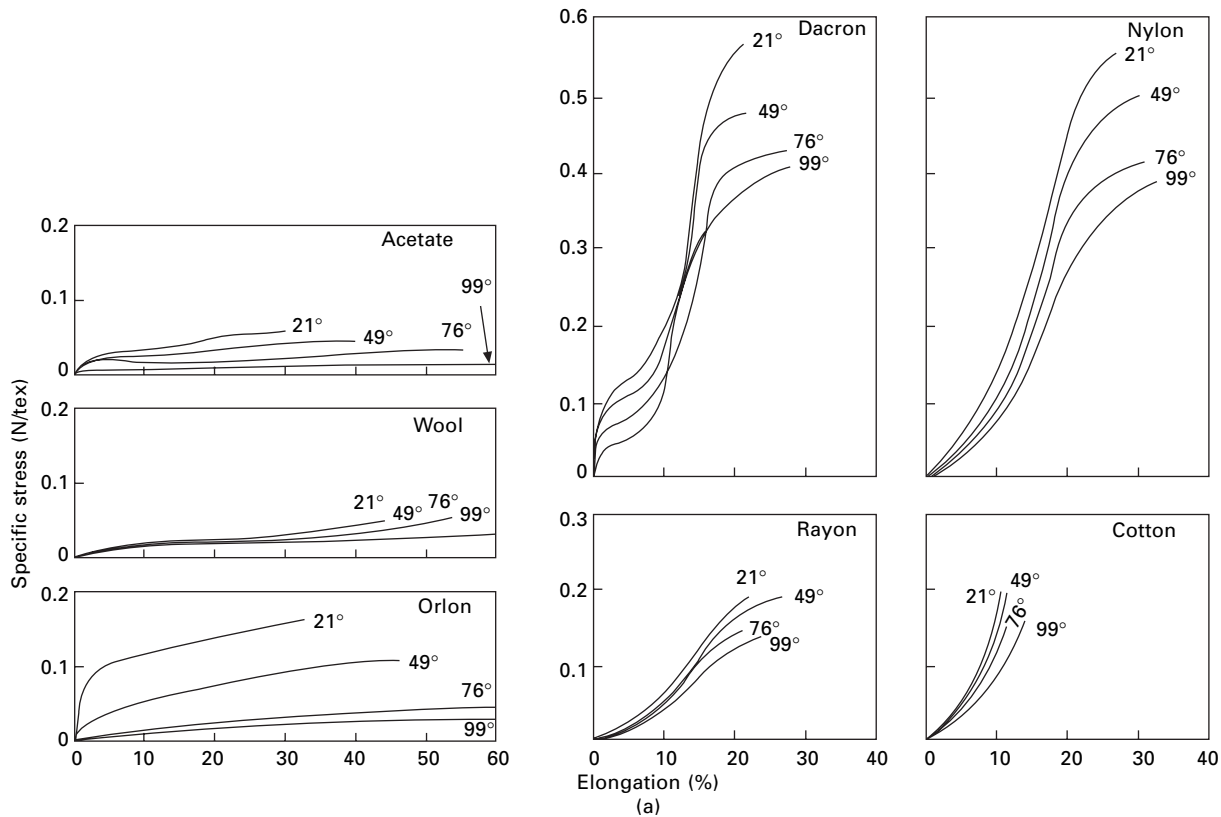
Daniels [71] has shown that the breaking extension of undrawn nylon fibres at -196°C is only about 12%, but the value increases abruptly to 70% at a draw ratio of 2. The breaking extension then progressively decreases to a value of about 20% at a draw ratio of 4. Hall [72] found that, in drawn polypropylene monofilaments, the breaking extension decreased rapidly from 75% at 35°C to 50% at 10°C and 20% at -16°C the final long yield region of the stress-strain curve was missing at lower temperatures.

Rosenbaum [73] gives stress–strain curves of acrylic fibres at various temperatures and shows that the resistance to extension at 100°C or more is very small. The low resistance to extension of an acrylic fibre is also shown in Fig. 13.32.

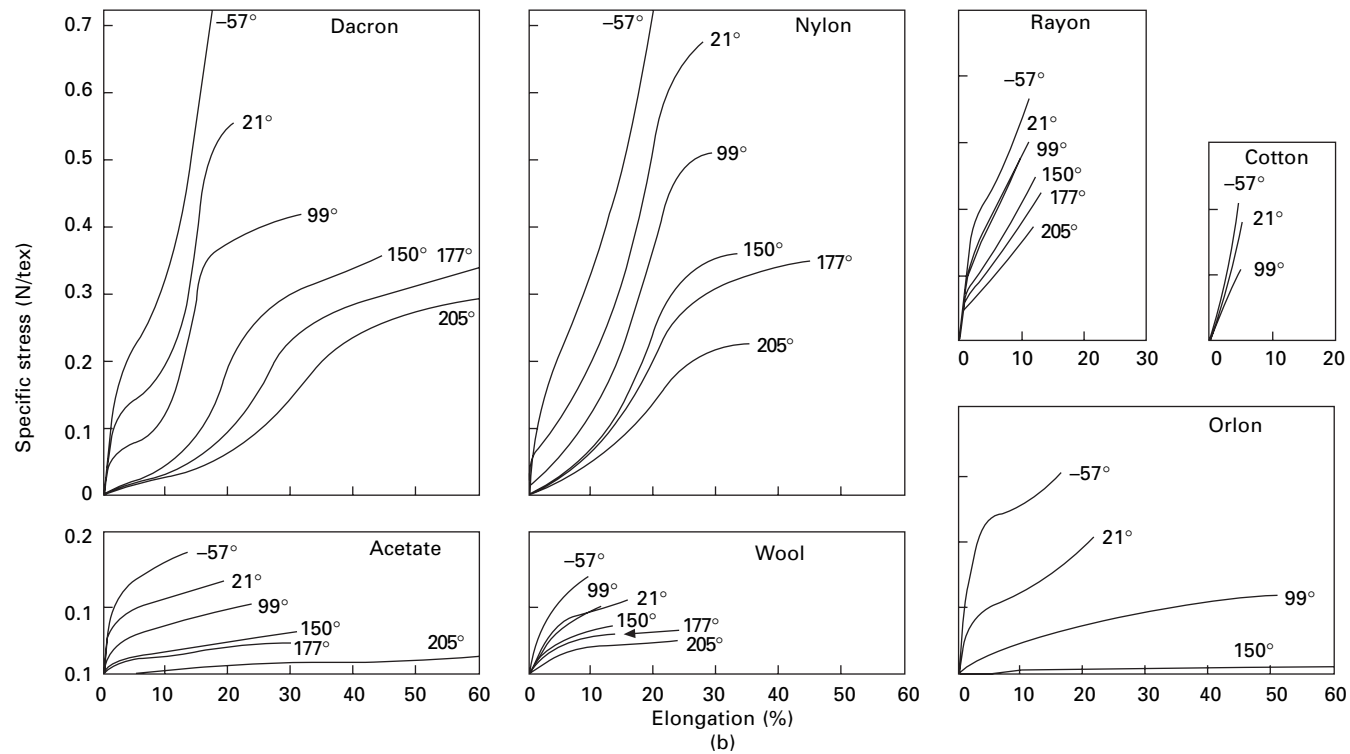
Measurements of the initial modulus of wet fibres at temperatures between 20 and 100°C have been made by Guthrie [74], and some of his results are shown in Fig. 13.39. The presence of water reduces the modulus of viscose rayon to a low value, and temperature has little further effect; nylon is also little affected. Polyester, triacetate and acrylic fibres all show a very marked fall in modulus as the temperature is raised. This has technical consequences in dyeing, and other forms of hot wet processing, of these materials.

Other data on the effect of temperature on modulus are reported by Ross [75].

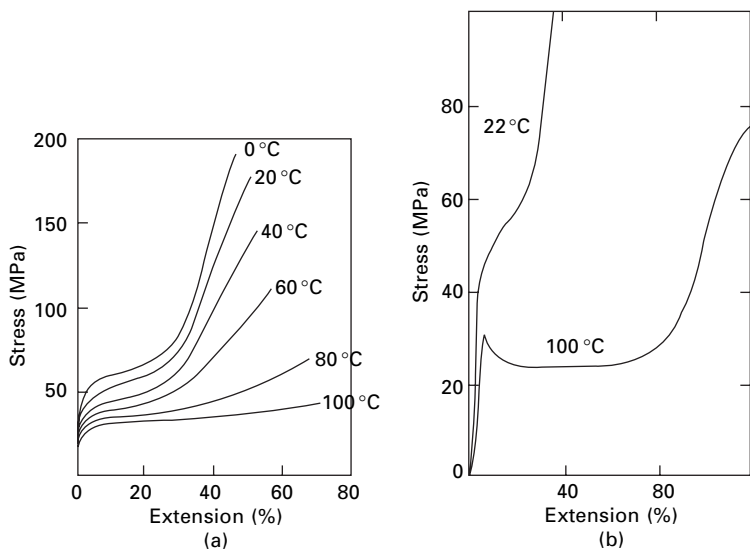
Ceramic and carbon fibres retain their strength well up to high temperatures; but glass will lose strength, especially for long times under load, as its softening point is approached. Para-aramid and other liquid crystal fibres retain their strength up to moderately high temperatures, *c.* 400°C . HMPE suffers considerable strength loss when the temperature increases above about 50°C , as shown in Fig. 13.40. Since the effect of an increase in temperature is to speed up deformation mechanisms, the



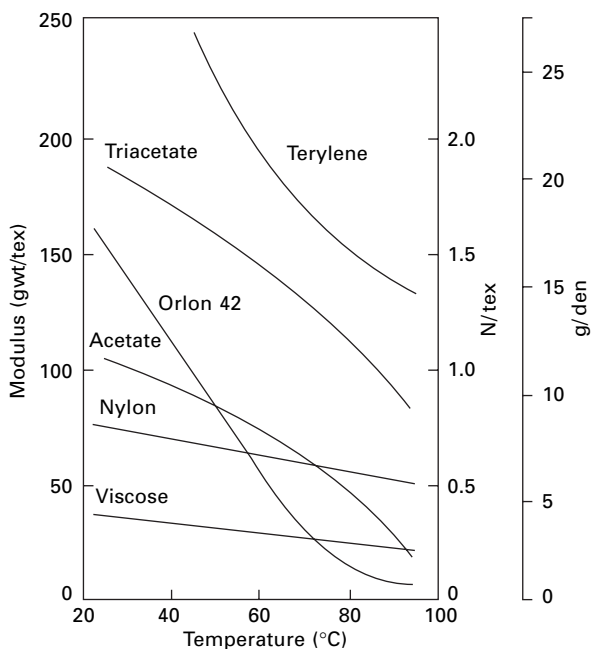
13.37 Comparative stress-strain curves of fibres at various temperatures: (a) in water; (b) in air [31]. *Dacron* is polyester; *Orlon* is acrylic.



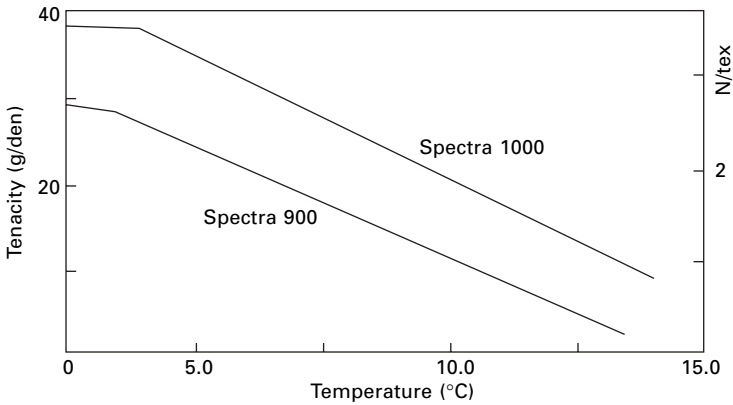
13.37 (Continued)



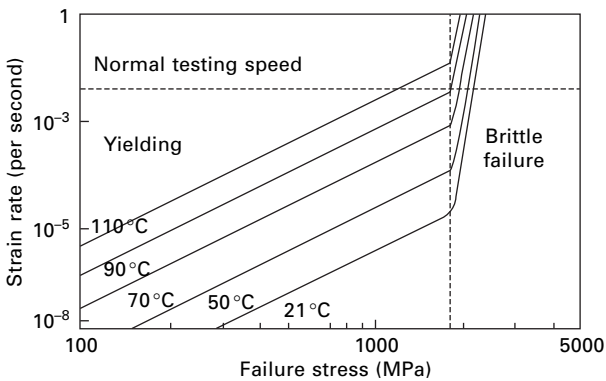
13.38 (a) Effect of temperature on stress–strain curves of wet wool [52]. (b) Stress–strain curves at 22 °C and 100 °C. From Peters and Woods [70].



13.39 Change in initial modulus of wet fibres with temperature. *Terylene* is *Polyester*; *Orlon* is acrylic. After Guthrie [74].



13.40 Effect of temperature on strength of Spectra 900 and 1000 [76].



13.41 Effect of strain rate and temperature on breakage of HMPE (Dyneema) yarn. From van Dingenen [66].

counterpart to this is strength loss with time, as shown in Fig. 13.41. Later improved forms of HMPE fibre have improved creep resistance, which implies lower strength loss with temperature.

13.6.3 Effect of light

When exposed to light, or to ultraviolet or infrared radiation, textile fibres may deteriorate and show a decrease in strength and breaking extension. The degree of deterioration depends on the type of fibre; on the fibre fineness, and the extent to which the fibres are protected by other neighbouring fibres; on whether any dyes, finishes or other agents are present on the fibre; and on the type and intensity of the radiation. The last-named factors are in turn affected by the type of exposure, for example, whether it is in full sunlight, partly shaded, behind glass, or in artificial light; and, for daylight exposure, by the geographical location and the time of year.

In testing materials for light resistance, it must be remembered that other factors, such as mildew, moulds, fungi, industrial fumes, smoke, flexing, abrasion and sand carried in the wind, may cause more deterioration than the sunlight.

Although there have been many *ad hoc* tests, little fundamental information is available. Table 13.8 gives the relative order of resistance to deterioration. Table 13.9 gives values for the loss in strength of undyed cotton and nylon fabrics exposed to sunlight and shows that if ultraviolet radiation is excluded, the damage is considerably reduced.

13.6.4 Effect of chemical environment

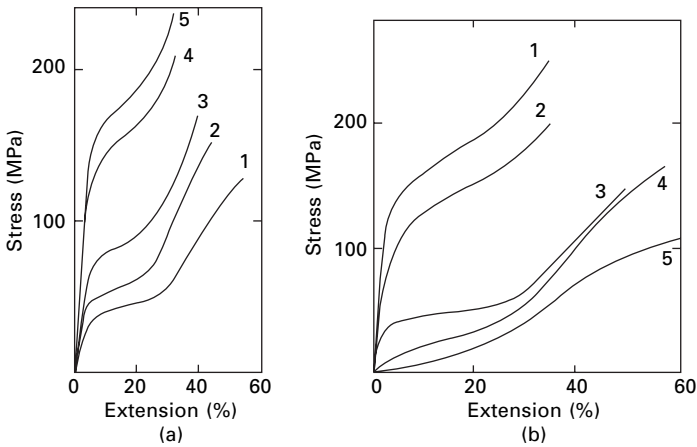
The tensile properties of fibres may also change with the chemical environment. For example, the properties of wool change remarkably in alcohol and in acid conditions, as illustrated in Fig. 13.42. and in salt solutions. Wool supercontracts in a first stage in a cold lithium bromide solution and in a second stage in a stronger hot solution. The resulting stress–strain curves are shown in Fig. 13.43. After the first stage, the initial Hookean and yield regions have been lost. After the second stage, the post-yield stress is lost. Other fibres are affected by different chemicals. More severe chemical treatments lead to permanent changes in mechanical properties.

Table 13.8 Relative loss in strength due to sunlight [77]

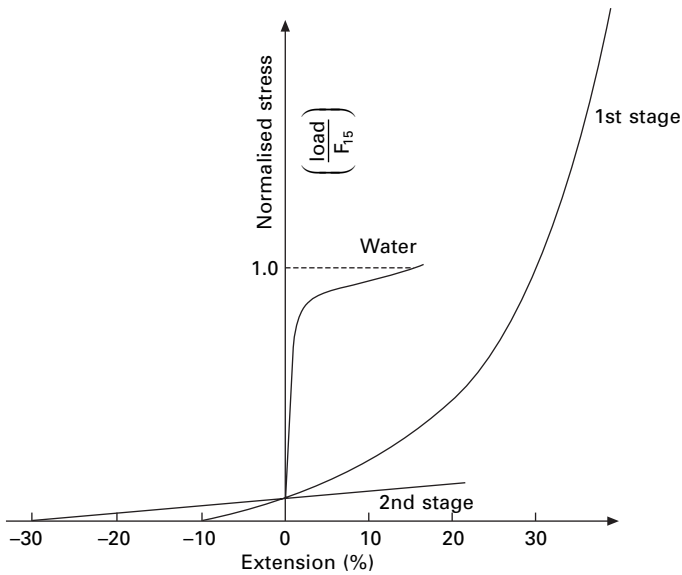
Exposed behind glass		Exposed outdoors
Bright <i>Orlon</i> acrylic	Decreasing resistance ↓	Bright <i>Orlon</i> acrylic
Semi-dull <i>Orlon</i> acrylic		Semi-dull <i>Orlon</i> acrylic
Bright <i>Dacron</i> polyester		Bright acetate, bright <i>Dacron</i> , bright nylon, type 680 dull nylon, bright rayon, cotton
Semi-dull <i>Dacron</i> polyester		Semi-dull <i>Dacron</i> polyester
Bright acetate, bright nylon, type 680 dull nylon, bright rayon, cotton		Silk, and most other semi-dull fibres
Silk, and most other semi-dull fibres		Most dull fibres; excluding dull <i>Dacron</i> , or those with a light-degradation inhibitor, such as type 680 nylon
Most dull fibres; excluding dull <i>Dacron</i> , or those with a light-degradation inhibitor, such as type 680 nylon		

Table 13.9 Loss in strength of nylon and cotton fabrics [78]

	Residual tensile strength (%)	
	Behind untreated film	Behind ultraviolet absorbing film
Cotton, after 4 months, in		
Florida	64	92
Arizona	48	85
Nylon, after 2 months, in		
Florida	15	60
Arizona	13	39



13.42 Effect of chemical environment on stress-strain curves of wool. (a) 1 water and alcohols, 2 methyl, 3 ethyl, 4 *n*-propyl, 5 *n*-butyl or *n*-amyl; (b) 3 water and acids, 1 *n* butyric, 2 propionic, 4 acetic, 5 formic. From Peters and Woods [70].



13.43 Stress-strain curves of wool after first and second stage supercontraction with stress normalised by stress at 15% extension in water. From Chapman [79].

13.7 References

1. J. G. M. van Miltenburg. *Textile Res. J.*, 1991, **61**, 363.
2. R. Meredith. *J. Text. Inst.*, 1945, **36**, T107.
3. M. J. Coplan. WADC Technical Report, 53–21, United States Air Force.
4. E. Alexander, M. Lewin, H. V. Musham and M. Shiloh. *Text. Res. J.*, 1956, **26**, 606.

5. M. Shiloh, J. Goldstein, D. Mejzler and E. Alexander. *Text. Res. J.*, 1961, **31**, 999.
6. E. Alexander, M. Lewin, Y. Litav, H. Peres and M. Shiloh. *Text. Res. J.*, 1962, **32**, 898.
7. I. Bauer-Kurz, W. Oxenham and D. A. Shiffler. *Textile Res. J.*, 2004, **74**, 343.
8. H. Hindman and G. S. Burr. *Trans. Amer. Soc. Mech. Engrs*, 1949, **71**, 789.
9. J. E. Booth. *Principles of Textile Testing*, Heywood, London, 3rd edition, 1968.
10. R. Meredith and J. W. S. Hearle (Editors). *Physical Methods of Investigating Textiles*, Interscience, New York, 1959.
11. B. P. Saville. *Physical Testing of Textiles*, Woodhead Publishing, Cambridge, 1999.
12. A. R. Bunsell, J. W. S. Hearle and R. D. Hunter. *J. Physics E, Sci. Instruments*, 1971, **4**, 868.
13. A. R. Oudet, A. R. Bunsell, R. Hagege and M. Sotton. *J. Appl. Polymer Sci.*, 1984, **29**, 4363.
14. D. J. Mwaisengela. PhD thesis, University of Manchester, 1987.
15. C. Le Clerc, A. R. Bunsell and A. Plant. *J. Materials Sci.*, 2006, **41**, 7509.
16. M. E. Sikorski, C. P. Buckley, J. W. S. Hearle and S. K. Mukhopadhyay. *Rev. Sci. Instrum.*, 1993, **64**, 1947.
17. C. P. Buckley and M. E. Sikorski. *J. Textile Inst.*, 1991, **82**, 25.
18. D. S. Fudge, K. H. Gardner, V. T. Forsyth, C. Riekel and J. M. Gosline. *Biophys. J.*, 2003, **85**, 2015.
19. S. Kawabata. *Proc. 4th Japan–USA Conf. Composite Materials*, 1988, p. 253.
20. P. Krais. *J. Text. Inst.*, 1928, **19**, T32.
21. E. J. Saxl. *Amer. Dyest. Rep.*, 1939, **28**, 615.
22. T. Barratt. *J. Text. Inst.*, 1922, **13**, T17.
23. D. de Meulemeester and I. Nicoloff. *J. Text. Inst.*, 1935, **26**, T147.
24. D. de Meulemeester and I. Nicoloff. *J. Text. Inst.*, 1936, **27**, T84.
25. G. Raes, T. Franssen and L. Verschraege. *Text. Res. J.*, 1968, **38**, 182.
26. H. S. Cliff. *J. Text. Inst.*, 1933, **24**, T351.
27. W. R. Lang. *J. Text. Inst.*, 1951, **42**, T314.
28. B. Farrow. *J. Text. Inst.*, 1956, **47**, T58.
29. B. Farrow. *J. Text. Inst.*, 1956, **47**, T650.
30. J. E. Ford (Editor). *Fibre Data Summaries*, Shirley Institute, Manchester, 1966.
31. Technical Bulletin X–82, E. I. du Pont de Nemours & Co. Inc., Wilmington, DE, 1958.
32. J. W. S. Hearle (Editor). *High-performance Fibres*, Woodhead Publishing, Cambridge, 2001, pp. 259, 281.
33. J. T. Sparrow. The fracture of cotton, PhD thesis, University of Manchester, 1973.
34. R. Meredith. *J. Text. Inst.*, 1946, **37**, T205.
35. R. Meredith. *J. Text. Inst.*, 1951, **42**, T291.
36. J. J. Hebert, R. Giardina, D. Mitcham and M. L. Rollins. *Text. Res. J.*, 1970, **40**, 126.
37. N. Morosoff and P. Ingram. *Text. Res. J.*, 1970, **40**, 250.
38. L. E. Hessler, M. E. Simpson and E. E. Berkley. *Text. Res. J.*, 1948, **18**, 679.
39. O. W. Morlier, R. S. Orr and J. N. Grant. *Text. Res. J.*, 1951, **21**, 6.
40. J. D. Timpa and H. H. Ramey. *Textile Res. J.*, 1994, **64**, 537.
41. J. A. Foulk and D. D. McAlister. *Textile Res. J.*, 2002, **72**, 885.
42. J. W. S. Hearle and J. T. Sparrow. *J. Appl. Polymer Sci.*, 1979, **24**, 1465.
43. R. R. Mukherjee, M. K. Sen and H. J. Woods. *J. Text. Inst.*, 1948, **39**, P241.
44. R. R. Franck (Editor). *Bast and other Plant Fibres*, Woodhead Publishing, Cambridge, 2005.
45. R. W. Work. *Text. Res. J.*, 1949, **19**, 381.
46. J. W. Wilkinson. *J. Text. Inst.*, 1962, **53**, P191.
47. P. White, M. Hayhurst, J. Taylor and A. Slater. In *Biodegradable and Sustainable Fibres*, R. S. Blackburn (Editor), Woodhead Publishing, Cambridge, 2005, p. 157.
48. N. H. Chamberlain and M. P. Khera. *J. Text. Inst.*, 1952, **43**, T123.
49. J. M. Muri and P. J. Brown. In *Biodegradable and Sustainable Fibres*, R. S. Blackburn (Editor), Woodhead Publishing, Cambridge, 2005, p. 89.

50. F. Vollrath. *Int. J. Biol. Macromol.*, 1999, **24**, 81.
51. C. Viney. *J. Textile Inst.*, 2000, **91**, 2.
52. B. M. Chapman. *J. Text. Inst.*, 1969, **60**, 181.
53. M. Feughelman. *Mechanical Properties and Structure of Alpha-Keratin Fibres*, UNSW Press, Sydney, Australia, 1997.
54. J. D. Collins and M. Chaikin. *J. Text. Inst.*, 1968, **59**, 379.
55. S. L. Anderson and D. R. Cox. *J. Text. Inst.*, 1950, **41**, T481.
56. I. Marshall and J. R. Whinfield. In *Fibres from Synthetic Polymers*, R. Hill (Editor), Elsevier, Amsterdam, Netherlands, 1953, p. 437.
57. I. M. Ward. *J. Textile Inst.*, 1995, **86**, 289.
58. S. M. Long and I. M. Ward. *J. Appl. Polymer Sci.*, 1991, **42**, 1911.
59. I. M. Ward, D. L. M. Cansfield and P. L. Carr. In *Polyester: 50 Years of Achievement*, D. Brunnschweiler and J. W. S. Hearle (Editors), The Textile Institute, Manchester, 1993, p. 192.
60. G. Perez. In *High-speed Fiber Spinning*, A. Ziabicki and H. Kawai (Editors), Wiley-Interscience, New York, 1985, p. 333.
61. J. Shimizu, N. Okui and T. Kikutani. In *High-speed Fiber Spinning*, A. Ziabicki and H. Kawai (Editors), Wiley-Interscience, New York, 1985, p. 429.
62. A. Ziabicki and H. Kawai (Editors). *High-speed Fiber Spinning*, Wiley-Interscience, New York, 1985.
63. J. W. S. Hearle, P. K. Sen Gupta and A. Matthews. *Fibre Sci. Technol.*, 1971, **3**, 167.
64. I. C. Wang, M. G. Dobb and J. G. Tomka. *J. Textile Inst.*, 1996, **87**, 1.
65. D. W. Farrington, J. Lunt, S. Davies and R. S. Blackburn. In *Biodegradable and Sustainable Fibres*, R. S. Blackburn (Editor), Woodhead Publishing, Cambridge, 2005, p. 191.
66. J. L. J. van Dingenen. In *High-performance Fibres*, J. W. S. Hearle (Editor), Woodhead Publishing, Cambridge, 2001, p. 62.
67. G. Simon and A. R. Bunsell. *J. Mater. Sci.*, 1984, **19**, 3649.
68. N. Wilson. *J. Text. Inst.*, 1967, **58**, 611; 1968, **59**, 296.
69. R. Meredith. In *Fibre Science*, J. M. Preston (Editor), The Textile Institute, Manchester, 2nd edition, 1953, p. 252.
70. L. Peters and H. J. Woods. In *Protein Fibres*, R. Meredith (Editor), North-Holland, Amsterdam, 1956.
71. B. K. Daniels. *J. Appl. Polymer Sci.*, 1971, **15**, 3109.
72. I. H. Hall. *J. Polymer Sci.*, 1961, **54**, 505.
73. S. Rosenbaum. *J. Appl. Polymer Sci.*, 1965, **9**, 2071.
74. J. C. Guthrie. *J. Text. Inst.*, 1957, **48**, T193.
75. S. E. Ross. *Text. Res. J.*, 1965, **35**, 958.
76. Allied Fibers. Manufacturer's leaflet.
77. *The Light Resistance of Textile Fibres*, Bulletin X-43, E. I. du Pont de Nemours & Co. Inc., Wilmington, DE Nov., 1955.
78. R. A. Coleman and W. H. Peacock. *Text. Res. J.*, 1958, **28**, 784.
79. B. M. Chapman. *J. Textile Inst.*, 1970, **61**, 448.

14.1 Introduction

Textile fibres are not uniform: their composition and fineness vary both from one fibre to another in a sample and along the length of each fibre (see Fig. 3.6(a)). Consequently, their tensile properties are also variable. The variability is of direct interest, since it is just as important to know the range of values of a given quantity in a specimen that is being tested as it is to know the mean value. For example, the variation of properties from one fibre to another influences the distribution of load on fibres in a textile structure, so that a material may be more valuable if it is more uniform, even though it appears to be less satisfactory in terms of its average properties.

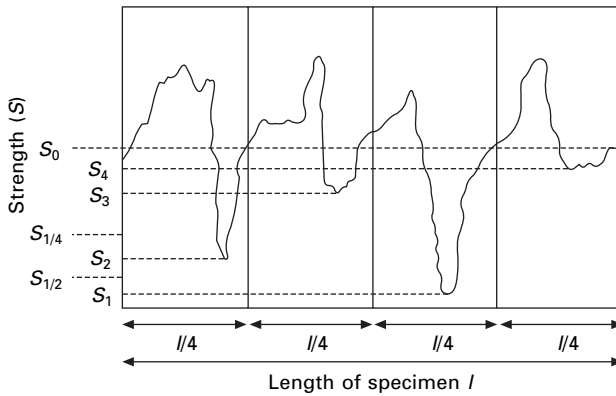
The variability also has important indirect effects on the results of measurements of mechanical properties. These may even result in a change in the order of ranking of specimens when the test conditions are changed.

The dimensions of a fibre also vary as a test is made. When a fibre is extended, it will become narrower. The extension and narrowing may not be uniform along the specimen. These changes during a test must not be neglected in the fundamental study of the behaviour of fibres.

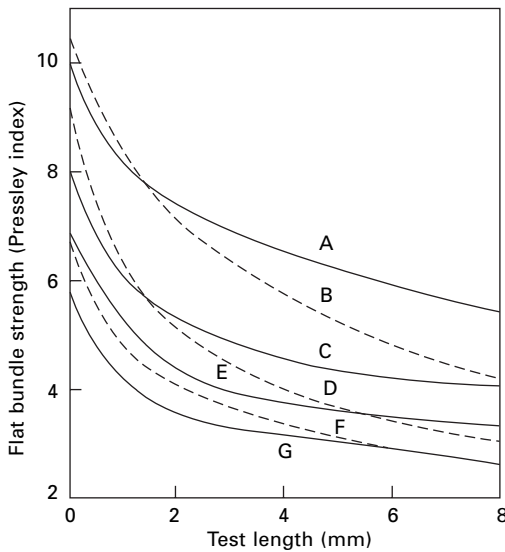
14.2 Variability, specimen length and strength

14.2.1 The weak-link effect

The weak-link effect in its simple form can be expressed as follows. Suppose that we could determine the strength at every point along the length of a fibre. We should find that it varied from point to point, as shown in Fig. 14.1. If a gradually increasing load is applied to this whole specimen, it will break at its weakest point, giving a strength S_1 , but if the specimen is tested in two half-lengths, each will break at its own weakest place, one giving the value S_1 , and the other a value S_2 , which is necessarily greater than S_1 . The mean strength $S_{1/2}$, measured on half-lengths, is the mean of S_1 and S_2 , and must therefore be greater than the strength measured on the whole length. Similarly, going to quarter-lengths, we get the four values, S_1, S_2, S_3, S_4 , and the mean strength $S_{1/4}$ is greater still. This increase will continue until at very short lengths the mean strength tends to the value S_0 , which gives equal areas of the curve above and below the line $S = S_0$, since each small element will break at its own value of strength.



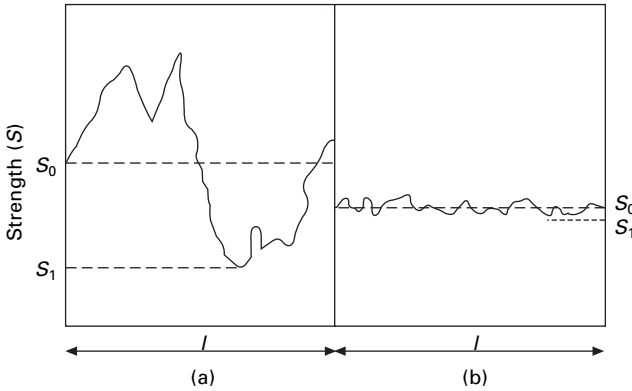
14.1 Weak-link effect.



14.2 Effect of specimen length on strength of cotton in flat bundle test [1]: A, Pima 32; B, THD-27; C, St Vincent; D, Bolshaw 1A; E, Deltapine; F, D and PL Fox; G, Watson Meban.

The weak-link effect described above has the following results:

- The mean measured strength of a specimen decreases as the test-length is increased. A typical example is shown in Fig. 14.2, which shows results from a commonly used bundle-breaking test, the Pressley test (see [Section 14.4.2](#)).
- The decrease in mean measured strength will be more rapid the more irregular the fibre is.
- The order of ranking of specimens may alter if the test-length is altered. [Figure 14.3](#) illustrates this. At very short lengths, the fibre shown in (a) appears stronger, but at the length l the more uniform fibre in (b), appears stronger. As an example



14.3 Change in order of ranking of materials. S_0 is greater for (a) than for (b), but S_1 is greater for (b).

Table 14.1 Tenacity and length [2]

	Tenacity (N/tex) for test length of:		
	1 cm	1 mm	0.1 mm
Cotton	0.31	0.43	0.59
Nylon	0.47	0.50	0.54

Table 14.2 Estimating strength value

Strength values obtained with 1 cm length	4	5	3	4	6	4	5	3	6	4	Mean
Strength values selected for 2 cm lengths	4		3		4		3		4		3.6

of such a reversal in ranking, Meredith [2] quotes the values in Table 14.1 for cotton and nylon fibres.

The same effects occur in yarns as in fibres, and it is in relation to yarns that the weak-link effect has been most studied. In the absence of detailed results for fibres, some results for yarns will be included here, since the same ideas should be applicable to fibres.

If one wishes to estimate the strength that would be obtained at some greater test length than that actually used, the simplest method in principle is to group the results together in the appropriate numbers and to take the mean of the lowest value in each group. An example is given in Table 14.2. This method was tedious in practice, and several attempts at mathematical analysis have been made. However, with computers available, there is now no reason to avoid the direct numerical methods.

14.2.2 Peirce's theory [3]

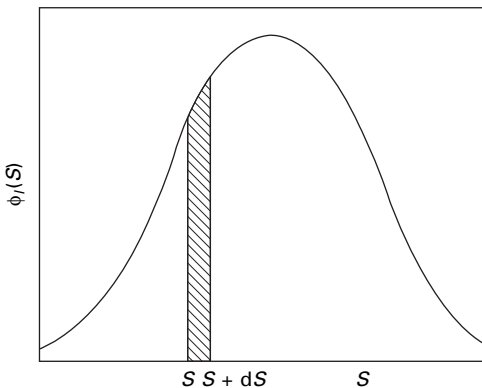
Let $\phi_l(S) \cdot dS$ be the probability that the strength of a specimen of length l should lie between S and $(S + dS)$. The function $\phi_l(S)$, shown in Fig. 14.4, thus gives the distributions of breaking loads. It is assumed that this function does not vary significantly from one part of the batch of specimens to another. From the values of the distribution $\phi_l(S)$, one can work out the mean value S_l and the standard deviation σ_l by the usual methods.

We now wish to find the distribution of breaking loads for specimens of length nl , that is, the probability, $\phi_{nl}(S) \cdot dS$, that the strength of a specimen of length nl lies between S and $(S + dS)$. The condition for this to occur is that the weakest of the n portions of length l of which the complete specimen of length nl is made up should have a strength lying between S and $(S + dS)$. In other words, any one of the n portions must have a strength between S and $(S + dS)$, and the other $(n - 1)$ portions must have a strength greater than S . The probability that any one of n lengths l has a strength between S and $(S + dS)$ is $n \cdot \phi_l(S) \cdot dS$. The probability that the strength of a length l shall be greater than S is $\int_S^\infty \phi_l(S) \cdot dS$; and thus the probability that all

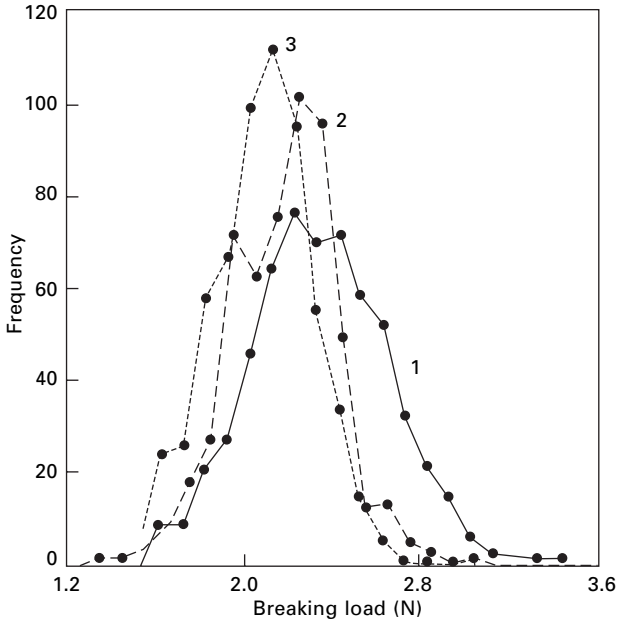
$(n - 1)$ lengths shall have a strength greater than S is $\left[\int_S^\infty \phi_l(S) \cdot dS \right]^{(n-1)}$. The probability that the strength of a specimen of length nl lies between S and $(S + dS)$ will therefore be given by the product of these two terms, that is:

$$\phi_{nl}(S) = n\phi_l(S) \left[\int_S^\infty \phi_l(S) \cdot dS \right]^{(n-1)} \quad (14.1)$$

By using this relation, the frequency distribution can be worked out for any length of specimen. The relation is valid whether n is less than or greater than unity. [Figure 14.5](#) shows an example of the application of this formula to cotton yarns.



14.4 Distribution of strengths.



14.5 Application of Peirce's theory to cotton yarn. Curves 1 and 2 are experimental curves for test-lengths of 9 and 27 inch (230 and 690 mm), respectively; curve 3 is the calculated curve for 686 mm (27 in.) test-lengths from the data in curve 1.

For further mathematical development, it is necessary to assume a form for the function $\phi_l(S)$. It is simplest to assume a normal distribution. This gives:

$$\phi_l(S) = \frac{1}{2\sigma_l\sqrt{\pi}} e^{-(S_l - \bar{S}_l)^2/4\sigma_l^2} \quad (14.2)$$

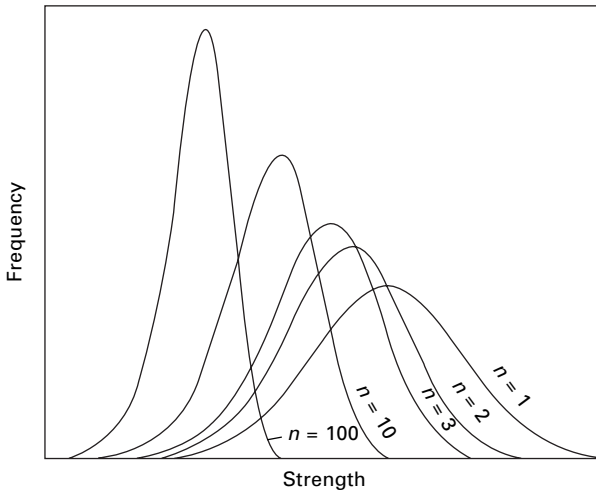
where \bar{S}_l is the mean value of S_l , and σ_l is the standard deviation of S_l . This relation can be substituted in equation (14.1), and the new distribution is then defined. [Figure 14.6](#) shows an example of this. It will be noticed that, even though we start with a symmetrical normal distribution, the derived distributions at other lengths are skew.

The distribution $\phi_{nl}(S)$ is thus known in terms of S_l , σ_l and n . Analysing this expression, and making some mathematical approximations, Peirce obtained equations giving the mean strength \bar{S}_{nl} and standard deviation σ_{nl} for specimens of length nl . The relations are:

$$\bar{S}_l - \bar{S}_{nl} = 4.2(1 - n^{-1/5})\sigma_l \quad (14.3)$$

$$\frac{\sigma_{nl}}{\sigma_l} = n^{-1/5} \quad (14.4)$$

[Table 14.3](#) shows a comparison of values obtained by using these relations with experimental results for cotton fibres. It will be seen that Peirce's relation gives too high a value for the shorter length. This is also found with results for yarns. It is



14.6 Application of Peirce's theory to a normal distribution. Curves for various test-lengths nl , calculated from the normal distribution at $n = 1$.

Table 14.3 Tenacity in N/tex and test-length, cotton [4]

Cotton variety	S 1 cm	σ 1 cm	S 1 mm calc.	S 1 mm expt
St Vincent	0.473	0.136	0.688	0.609
Sakel	0.405	0.180	0.688	0.535
Uppers	0.288	0.136	0.503	0.477
Ishan	0.324	0.093	0.467	0.446

useful to summarise here the approximations in Peirce's theory that cause these deviations. They are:

- the assumption that the distribution of strength is independent of the part of the sample considered;
- the assumption of a normal frequency distribution;
- the mathematical approximations.

14.2.3 Other treatments

An improvement on Peirce's theory has been worked out and applied to yarns by Spencer-Smith [5]. It is first necessary to clear away the assumption, which has been implicit in the previous discussion, that breakage occurs at a point. In fact, the disturbance involved in a break will be spread over a certain length, which Spencer-Smith called the *fracture zone*. Any theory of the weak-link effect should therefore consider a succession of fracture zones.

Spencer-Smith further pointed out that the strengths of neighbouring fracture zones in yarns are related to one another. This will also hold for fibres, since the same

molecules will be passing through neighbouring zones, and the dimensions and composition of neighbouring zones cannot be very different. There will thus be a tendency for strong zones to group together and for weak zones to group together. This means that, in testing a number of specimens, most of the weak places will be concentrated in a few of them, and thus only a few will give breaking values. Instead, some higher values will be included, and the mean strength will appear higher. Table 14.4 shows a numerical example of this effect. It is in this respect that Spencer-Smith's theory is an advance on that of Peirce, where the values were, in effect, redistributed at random.

Spencer-Smith has worked out the theory in detail and obtained the relation

$$\bar{S}_f - \bar{S}_{nf} = W(n) \cdot F(n) \cdot \sigma_f \quad (14.5)$$

where f is the fracture-zone length, S_f and S_{nf} are the mean values for lengths f and nf , respectively, σ_f is the standard deviation for length f , $W(n)$ is a statistical function, tabulated by Tippett [6] for values of n , and $F(n)$ is the serial correlation function.

$$F(n) = \left\{ \frac{1}{n^2} [n(n-1) - 2(n-1)r_1 - 2(n-2)r_2 \dots - 2(n-m)r_m \dots 2r_{n-1}] \right\}^{1/2} \quad (14.6)$$

where r_m = correlation coefficient for the strengths of zones a length mf apart. In this expression, $W(n)$ is a numerical factor, $F(n)$ is a factor taking account of the correlation of strengths of neighbouring zones, and σ_f brings in the variability. The product $W(n) \cdot F(n)$ replaces $4.2 (1 - n^{-1/5})$ in Peirce's expression.

Spencer-Smith's theory has been applied only to yarns, and examples are given in Fig. 14.7. The agreement with experiment is still not perfect.

In many studies of fracture, a Weibull distribution is found to give the best statistics and has been applied to weak link theory. The basic two and three parameter equations for the Weibull distribution and the change of mean strength with length are as

Table 14.4 Four-zone lengths with zones (a) perfectly grouped and at random

(a)

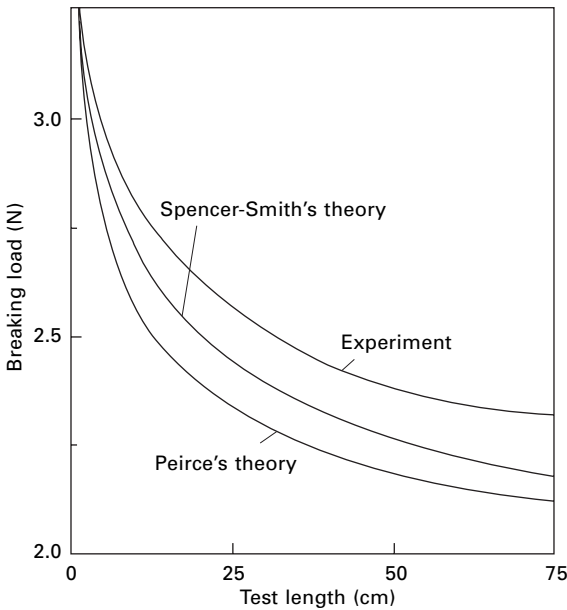
Zone strength	4	4	4	4	3	3	3	3	2	2	2	2	1	1	1	1
Four-zone strength	4				3				2				1			

Mean for four-zone length = 2.5

(b)

Zone strength	4	1	2	1	2	3	1	2	4	4	2	1	3	2	3	4
Four-zone strength	1				1				1				2			

Mean for four-zone length = 1.25



14.7 Comparison of theory and experiment for a spun-rayon yarn [7].

follows.

$$\phi_l(S) = 1 - \exp \left[-N \left(\frac{S}{S_0} \right)^m \right] \quad (14.7a)$$

$$\phi_l(S) = 1 - \exp \left[-N^\beta \left(\frac{S}{S_0} \right)^m \right] \quad (14.7b)$$

$$\frac{\bar{S}_{nl}}{\bar{S}_l} = n^{-1/m} \quad (14.8a)$$

$$\frac{\bar{S}_{nl}}{\bar{S}_l} = n^{-\beta/m} \quad (14.8b)$$

$$\log \bar{S}_{nl} - \log \bar{S}_l = -(1/m) \log n \quad (14.9a)$$

$$\log \bar{S}_{nl} - \log \bar{S}_l = -(\beta/m) \log n \quad (14.9b)$$

where N is the number of independent segments with strength S_0 , m is the Weibull shape parameter and β was proposed by Watson and Smith [8] to account for diameter variations, though its physical meaning is not clear.

Pickering and Murray [9] measured the variation of strength of a high-strength carbon fibre and found a linear plot corresponding to equation (14.9a) with $(1/m) =$

0.126. The Weibull distribution itself should give a linear plot when $\log\{\log[1/(1-\phi)]\}$ is plotted against $\log(S)$. Their results showed up a basic problem in weak-link modelling. There was good linearity in the Weibull plots for the major part of the distribution, but points at the extremes diverged from the line. Unfortunately the extreme low values have most effect on failure at weak links. This is probably why Pickering and Murray found errors of 8–25% in predicting strengths at 2 to 500 mm from values at 1 mm test length. Amaniampong and Burgoyne [10] found that the two-parameter Weibull distribution fitted polyester strengths but the three-parameter was better for breaking strain. For aramid fibres the Gumbel distribution gave a better fit. They also found the problem of extreme values lying off the straight line. Zhang *et al.* [11] discuss the application of Weibull and modified Weibull distributions to gauge length effects on wool strength. Yu *et al.* [12] combined SIFAN (see [Sections 3.7.1](#) and [13.4.2](#)) and optical microscope studies of wool to differentiate between breaks at thin places and breaks due to weaknesses in internal structure. They conclude that about 40–50% of breaks occur at the position of minimum diameter, with the remainder being associated with defects.

14.2.4 Difficulties in weak-link theory

Theories of the weak-link effect continue to be developed, though Peirce's theory is a useful approximation, and Spencer-Smith's a better one. Spencer-Smith's relation is open to criticism on the grounds that it must be based on experimental results for the fracture-zone length. Apart from the fact that this length is not known and may be very ill defined, it is very likely that when jaws are clamped on the specimens at a distance apart equal to the estimated fracture-zone length, the nature of the break will be different from that at much shorter or much longer lengths. When the jaws are close together, they will restrain deformation of the fibre, and the distribution of strain, giving rise eventually to rupture, will be different. The effect of changes in the mechanism of breakage cannot be included in any statistical theory, and it seems likely that different relations would apply for lengths much greater than, and much less than, the fracture-zone length. The variations for lengths near the fracture-zone length would depend on the particular properties of the fibre.

These difficulties also apply to yarns, and the redistribution of twist is another source of error there. Together these must account for the deviation of experiment and theory shown in [Fig. 14.7](#).

14.3 Variability and other quantities

14.3.1 Variation of stress and strain

The weak-link effect is concerned with the effect of variability on strength, and we must also consider the influence of variability on other quantities. For a fibre under a given tension, the stress will vary from place to place and will follow the variations of cross-section. At each point, the specific stress will be given by the tension divided by the linear density at that point.

As a consequence of the variation of stress, the strain will also vary from place to

Table 14.5 Variation along successive sections (5 mm lengths) of a wool fibre [13]

Fibre No. 1					Fibre No. 2	
Diameter of section (μm)	Extension (%) of section with overall extension (%) of:				Diameter (μm)	Extension (%) (overall = 13.9%)
	5.2	15.5	24.2	32.9		
30.0	2.0	6.0	20.0	28.0	29.8	4.0
29.9	0.0	5.9	19.6	29.4	30.2	10.2
28.0	3.9	21.6	27.4	35.3	28.2	17.6
28.0	9.6	21.2	25.0	34.6	26.4	22.0
26.6	10.4	22.9	29.2	37.5	24.8	15.5
				(break)		(break)

place. The thin places will extend more than the thick ones. Table 14.5 shows the variation in diameter and extension along 5 mm lengths of a wool fibre. Provided that all the lengths in a particular set of tests are equal, the average of the strain values for each length will be the same whether the lengths are long or short.

The effect of variability on the shape of the stress–strain curve of wool fibres has been extensively examined by Collins and Chaikin [14–17]. He *et al.* [18, 19] have reported simulations of the stress–strain behaviour of fibres with variable thickness for linear elastic and non-linear tensile properties.

14.3.2 Tensile modulus

Owing to variation in composition, the modulus may vary from place to place in a fibre or between the fibres in a given sample. With an irregular specimen, there will also be an effect due to specimen length. This arises because of a difference in the averaging. Suppose the specimen consists of n sections, each of length x , and the extensions of the sections are represented by δx , varying from section to section. Then, if the modulus is measured on a specimen of length nx , we have:

$$\text{modulus} = \frac{S}{\Sigma(\delta x)/nx} = Sx(1/\bar{\delta x}) \quad (14.10)$$

where S = stress, and $\bar{\delta x}$ = mean value of δx . But, if the modulus were measured on the lengths x and then averaged, we should have:

$$\text{modulus} = \frac{1}{n} \Sigma \left(\frac{S}{(\delta x)/x} \right) = \frac{Sx}{n} \Sigma \left(\frac{1}{\delta x} \right) = Sx \left(\frac{\bar{1}}{\bar{\delta x}} \right) \quad (14.11)$$

where $\left(\frac{\bar{1}}{\bar{\delta x}} \right)$ is the mean value of $\frac{1}{\delta x}$.

There is a difference between $(1/\bar{\delta x})$ and $\left(\frac{\bar{1}}{\bar{\delta x}} \right)$ and thus the mean value of the modulus may vary with the length tested.

It is obvious that an apparently lower value of modulus results from softness of the

tester load cell and deformation within the gripped region of the fibre. There will be a more serious error if there is slippage of the fibre in the grips. These effects mean that the apparent modulus will increase as the test length increases. Pan *et al.* [20] report substantial increases in initial modulus of fibres as gauge length increases from 10 to 100 mm and regard this as a change in fibre properties and not just a testing artefact. However, it is difficult to see how, except for the immediate vicinity of clamps, the stiffness of a length of fibre could be influenced by distance from the gripped points.

14.3.3 Breaking extension

The weak-link effect also affects breaking extension. If a fibre breaks under a low load owing to the presence of a weak place, the rest of the specimen will have a comparatively small extension and the breaking extension will be low. The mean breaking extension will decrease as the specimen length increases.

14.4 Composite-specimen effects

14.4.1 Theoretical

If, instead of testing a single fibre, one tests a number of fibres together, the form of the specimen has a considerable influence on the result of the test. Practical cases are usually complicated and difficult to formulate mathematically, but the simple examples given by Peirce [3] may be used as approximations. It is assumed that the fibres are free to act independently.

- *Fibres gripped at the ends, of equal original length, and of uniform breaking extension.* All the fibres will break together and therefore, however variable the breaking loads may be, each fibre will have developed the maximum possible load, and the breaking load of the composite specimen will be equal to the sum of the breaking loads of the fibres.
- *Variable fibres gripped at the ends, of equal original length, in a constant rate of extension test (CRE).* The fibres with the lowest breaking extension will break first. Let the fraction of fibres having a breaking extension between e and $(e + de)$ be $\phi(e) \cdot de$. Then, when the extension is e , the fraction f of the total number of fibres remaining unbroken will be:

$$f = \int_e^{\infty} \phi(e) \cdot de \quad (14.12)$$

The force on the specimen will be influenced by any correlation between modulus and breaking extension but, if we assume a constant modulus, E , the stress will be given by:

$$\text{stress} = S = f \cdot Ee = Ee = \int_e^{\infty} \phi(e) \cdot de \quad (14.13)$$

The stress will be a maximum when $dS/de = 0$, that is, when:

$$E \int_e^{\infty} \phi(e) de - Ee\phi(e) = 0 \quad (14.14)$$

$$\int_e^{\infty} \phi(e) de = e\phi(e) \quad (14.15)$$

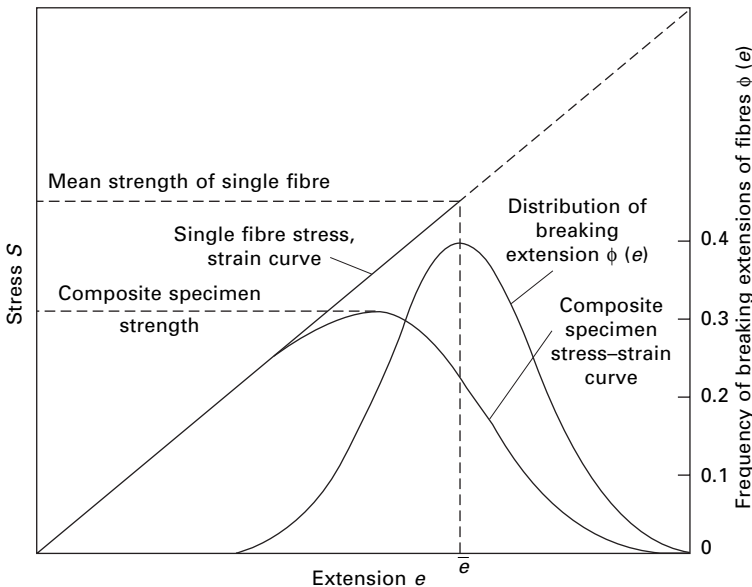
Writing \hat{e} for this value of e , and substituting in equation (14.9), we get:

$$\text{maximum stress} = E\hat{e}^2 \cdot \phi(\hat{e}) \quad (14.16)$$

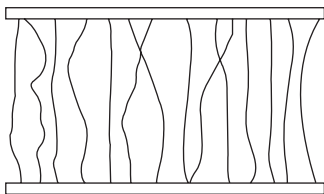
The mean breaking stress of the single fibres would be $E\bar{e}$, so that the ratio of the breaking stress of the composite specimen to the mean breaking stress of the fibres is $(\hat{e}^2 \bar{e}) \cdot \phi(\hat{e})$.

Figure 14.8 gives an example of this behaviour for a linear stress–strain curve and a normal frequency distribution. This clearly shows the reduction in strength resulting from the early breakdown of some of the fibres.

- *Variable fibres gripped at the ends, of equal original length in a constant rate of loading test (CRL).* Below the maximum load, the relation will be the same as in the previous case, Fig. 14.8, but then the specimen will fail completely because a decreasing load is not allowable.
- *Fibres gripped at the ends, of variable original length.* When a specimen is arranged between jaws, some of the fibres may not lie straight. This is illustrated in Fig. 14.9. The effect of this is to cause a much greater unevenness in the



14.8 Composite-specimen stress–strain curve, calculated for constant rate of extension of fibres with identical linear stress–strain curves but normal distribution of breaking extensions.



14.9 Fibres of varying length between jaws.

sharing of the load. When the fibres that are initially straight start to break, the fibres in which there was some 'slack' to take up will be less extended or may even not be contributing to the load at all. Consequently, the maximum load that can be developed will be much less.

- *Filaments under uniform tension, all slipping when one breaks.* This would be the case if the filaments were taken over a number of light pulleys. It is exactly the same as a single long specimen.
- *Filaments uniformly extended, all slipping when one breaks.* The lea test for yarns approximates to this condition. It is similar to the last case except that there will not be the same tension in each end of the specimen, owing to variations in the extensibility of the fibres.

There is a tacit assumption that a smooth stress–strain curve is found as in Fig. 14.8. This would be valid for an infinite number of fibres in the bundle. In practice there will be discontinuities. As the load increases and the jaws separate, a point is reached at which the first fibre breaks. The load is then taken by fewer fibres. In CRE, there would be a drop in tension; in CRL, there would be an increase of extension.

The mechanism of rupture is different when the fibres interact with one another. This is shown by the behaviour of twisted continuous filament yarns, as described by Hearle *et al.* [21]. A zero-twist yarn has a lower strength than one with a small amount of twist. Transverse compressive forces in the twisted yarn cause weak places in one fibre to be supported by neighbours. This will continue, with more fibres breaking, until the situation is reached in which the increase of load due to the breaking of a fibre is sufficient to cause another fibre to break and so on. The process is thus cumulative and the whole specimen ruptures. This happens at a load that is less than the sum of the breaking loads of the individual fibres. In twisted yarns, strength increases up to a twist angle of about 7° , when the effect of obliquity leads to a reduction in strength.

There is an extensive literature on the statistics of strength of interactive bundles of fibres, which is particularly important for composites, but also relevant to yarns and cables. An account of the chain of bundles model with load sharing is given by Phoenix [22], who also contributes a more recent review [23]. However, apart from bundle tests, the subject is of marginal relevance to the properties of fibres and will not be pursued here.

14.4.2 Practical bundle tests

Bundle tests are used extensively for rapid testing of cotton fibres. The earlier Chandler test was replaced by the Pressley test [24], a version of which is included in HVI test lines for cotton.

In the Chandler test, the combed bundle of fibres is wrapped with two spirals of sewing thread. At the centre, where the two spirals meet, the specimen is free to break. From the length of thread for ten revolutions, the circumference of the bundle is obtained, and consequently the breaking load per unit area can be calculated.

In the Pressley test, a bundle of fibres is combed straight and then clamped between jaws and broken. The fibre bundles are cut to a standard length and weighed, so that the breaking stress can be calculated. The results may vary considerably according to the width of the bundle, the tightness of clamping, the skill and technique of the operative, and the particular jaws used. However, provided that frequent checks are made with standard samples, reproducible results can be obtained. The original Pressley test had nominally a zero gauge length¹, but since then gauge lengths of a few millimetres have been proposed.

An advantage of a bundle test is that it automatically takes account of variability, which is a factor with a practical influence on yarn strength. The disadvantage is the more limited information and the lack of reproducibility.

14.5 Variability in practice

Table 14.6 shows values of the coefficient of variation of various quantities among 1 cm specimens tested by Meredith. It will be seen that the natural vegetable fibres show a large coefficient of variation; the natural protein fibres and rayon are rather more regular, and synthetic fibres such as nylon show only a small variability.

14.6 Changes in specimen during test

When fibres are extended, they usually contract in diameter. Consequently, the true stress increases more rapidly than does the stress based on the original dimensions of the fibre. This is important in fundamental studies of the subject, since what appears

Table 14.6 Variation within a sample of fibres [25]

	Coefficient of variation (%)			
	Fineness	Breaking load	Tenacity	Breaking extension
Cotton	24	46	43	40
Bast fibres	24	45	40	31
Rayon	12	20	17	23
Silk	17	19	20	15
Nylon	9	8	7	18
Wool	21	34	28	32

¹The gauge length is the length of specimen between the jaws of the tester.

to be a basic property of the material may be a function of the conditions of test.

If σ is the true stress, and σ' is the nominal stress based on the original dimensions, we have:

$$\text{load} = F = \sigma A = \sigma' A' \quad (14.17)$$

$$\sigma = \sigma' \cdot \left(\frac{A'}{A} \right) \quad (14.18)$$

where A is the true area of cross-section and A' is the original area of cross-section.

If the specimen extends uniformly and the volume remains constant, we have:

$$Al = A' l' \quad (14.19)$$

$$\frac{A'}{A} = \frac{l}{l'} = 1 + \epsilon \quad (14.20)$$

$$\sigma = (1 + \epsilon)\sigma' \quad (14.21)$$

where l = length of specimen, l' = original length of specimen and ϵ = strain.

The maximum load will occur when

$$\frac{dF}{d\epsilon} = \sigma \frac{dA}{d\epsilon} + A \frac{d\sigma}{d\epsilon} = 0 \quad (14.22)$$

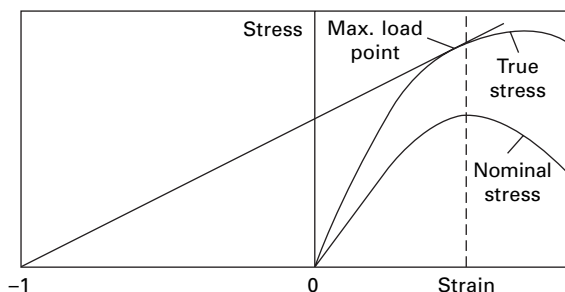
But, from equation (14.20):

$$\frac{dA}{d\epsilon} = -A' \frac{1}{(1 + \epsilon)^2} \quad (14.23)$$

$$-A' \frac{\sigma}{(1 + \epsilon)^2} + \frac{A'}{(1 + \epsilon)} \frac{d\sigma}{d\epsilon} = 0 \quad (14.24)$$

$$\frac{d\sigma}{d\epsilon} = \frac{\sigma}{(1 + \epsilon)} \quad (14.25)$$

This condition is satisfied at the point where a line from (-1) on the strain axis is a tangent to the curve, as in Fig. 14.10. This shows that the breaking load corresponds to a rather arbitrary condition in terms of true stress and thus has little fundamental significance.



14.10 True and nominal stress-strain curves.

However, the specimen will probably not extend uniformly and the weaker places will extend more than the stronger ones. This results in a further increase of stress on the weak places, so that the process is cumulative and breaking may occur. This means that the true stress near the point of break will increase even more rapidly than appears from Fig. 14.10.

It will be clear from this, and other parts of this chapter, that, in an investigation of the behaviour of a material (with a view to understanding it, rather than to using it), the mean stress–strain curve for the whole specimen gives only a rough idea of what is actually taking place. Exact stress–strain relations at particular points in the specimen would be much more valuable.

14.7 References

1. H. M. Brown. *Text. Res. J.*, 1954, **24**, 251.
2. R. Meredith. *J. Text. Inst.*, 1952, **43**, P755.
3. F. T. Peirce. *J. Text. Inst.*, 1926, **17**, T355.
4. R. Meredith. *J. Text. Inst.*, 1946, **37**, T205.
5. J. L. Spencer-Smith. *J. Text. Inst.*, 1947, **38**, P257.
6. L. H. C. Tippett. *Biometrika*, 1925, **17**, 364.
7. C. Nanjundayya. PhD Thesis. University of Manchester, May, 1949.
8. A. S. Watson and R. L. Smith. *J. Materials Sci.*, 1985, **20**, 3260.
9. K. L. Pickering and T. L. Murray, Composites, Part A-Applied Science and Manufacturing, 1999, **30** 1017.
10. G. Amaniampong and C. J. Burgoyne. *J. Materials Sci.*, 1994, **29**, 5141.
11. Y. Zhang, X. Wang, N. Pan and R. Postle. *J. Materials Sci.*, 2002, **37**, 401.
12. W. Yu, R. Postle and H. Yan. *J. Appl. Polymer Sci.*, 2003, **90**, 1206.
13. E. C. Banky and S. B. Slen. *Text. Res. J.*, 1955, **25**, 358.
14. J. D. Collins and M. Chaikin. *Text. Res. J.*, 1965, **35**, 679.
15. J. D. Collins and M. Chaikin. *Text. Res. J.*, 1965, **35**, 777.
16. J. D. Collins and M. Chaikin. *Text. Res. J.*, 1969, **39**, 121.
17. J. D. Collins and M. Chaikin. *J. Text. Inst.*, 1968, **59**, 379.
18. W. He, X. Wang and S. Zhang. *Textile Res. J.*, 2001, **71**, 556.
19. W. He, X. Wang and S. Zhang. *Textile Res. J.*, 2001, **71**, 939.
20. N. Pan, C. Chen, M. K. Inglesby, S. Khatua, X. S. Zhang and S. H. Zeronian. *J. Materials Sci.*, 1997, **32**, 2677.
21. J. W. S. Hearle, P. Grosberg and S. Backer. *Structural Mechanics of Fibers, Yarns and Fabrics*, Wiley-Interscience, New York, 1969, p. 222.
22. S. L. Phoenix. In *Mechanics of Flexible Fibre Assemblies*, J. W. S. Hearle, J. J. Thwaites and J. Amirbayat (Editors), Sijthoff and Noordoff, Alphen aan den Rijn, Netherlands, 1980, p. 113.
23. S. L. Phoenix and I. J. Beyerlein. In *Comprehensive Composite Materials*, Vol. 1, T. W. Chou (Editor), Elsevier Science, Oxford, 2000, p. 559.
24. S. Williams and E. V. Painter. *Text. Res. J.*, 1945, **15**, 403.
25. R. Meredith. *J. Text. Inst.*, 1945, **36**, T107.

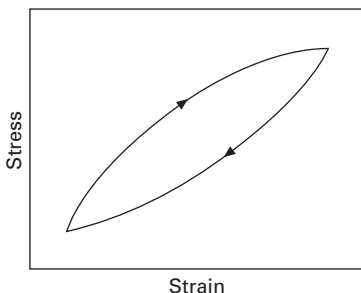
15.1 Introduction

The extent to which a fibre becomes permanently deformed when it is stretched is of great technical importance. It may be just as serious a form of damage as actual breakage of the fibre. The values of stress and strain above which permanent deformation occurs may well be the limiting values in use. In some specialised applications, such as ropes used in rock-climbing, the fibres may safely be taken beyond their yield point once, but their properties will then be so altered that they are unfit for further use.

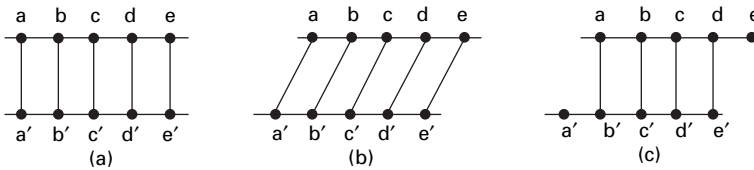
Elastic recovery, that is, the behaviour on removal of stress, is only a special case of the general phenomenon of hysteresis. In a cyclic change of stress or strain, the results will not fall on a single line. After a few initial cycles, the fibre will become conditioned and the results will tend to fall on a loop, as in Fig. 15.1. This means that energy is used up by internal friction, and consequently the material will heat up and may tend to dry out. This is important where fibres are subject to repeated loading, as in tyres, and the heating will affect their properties. In these uses, fibres showing little hysteresis are desirable.

On a molecular scale, recoverable or elastic deformation is due to a stretching of inter-atomic and intermolecular bonds, as in Fig. 15.2(b), while non-recoverable or plastic deformations result from a breaking of bonds and their re-forming in new positions, Fig. 15.2(c), or to the stabilisation of new chain conformations.

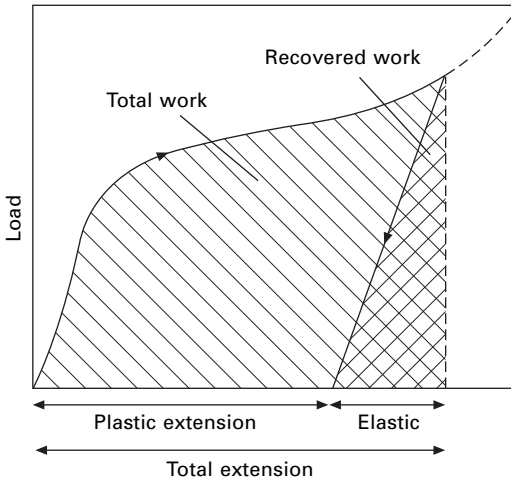
As with other tensile properties, recovery is time dependent. This leads to hysteresis, even if, after time, the recovery is complete. Although creep is defined as elongation



15.1 Hysteresis loop.



15.2 Schematic illustration of elastic and plastic deformations: (a) initial configuration; (b) elastic deformation with straining of links; (c) plastic deformation with re-forming of links in new positions.



15.3 Elastic and plastic extension.

under constant load, part of the elongation under increasing load can be regarded as slow ‘creep’, which is followed by slow ‘creep recovery’.

15.2 Definitions

Elasticity, a much misused word, has been defined by the American Society for Testing and Materials as ‘that property of a body by virtue of which it tends to recover its original size and shape after deformation’. Its opposite is plasticity. It should not be used as synonymous with extensibility.

A deformation may be divided up, as shown in Fig. 15.3, into an elastic part, which is recovered when the stress is removed, and a plastic or permanent part. Quantitatively, it is convenient to use the following definition:

$$\text{elastic recovery} = \frac{\text{elastic extension}}{\text{total extension}}$$

Complete recovery will then have the value 1 (or 100%), incomplete recovery will have a proportionately lower fraction, and no recovery at all will have the value zero.

Instead of studying dimensional recovery, one may study and define work recovery in a similar manner:

$$\text{work recovery} = \frac{\text{work returned during recovery}}{\text{total work done in extension}}$$

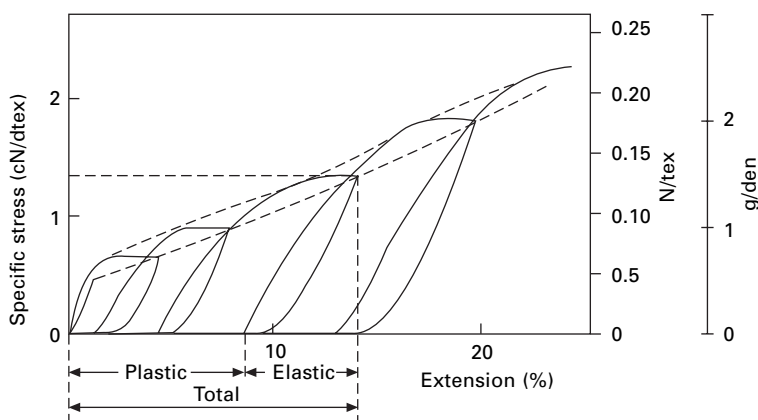
It should be noted that $(1 - \text{work recovery})$ gives the proportion of the total work that is dissipated as heat.

15.3 Experimental methods

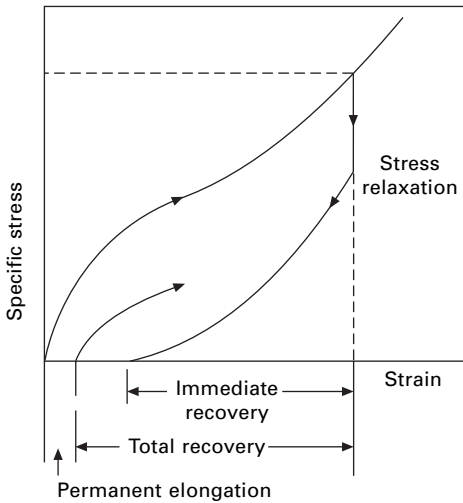
The method used by Meredith [1] in his classic series of comparative tests, is typical of experiments on elastic recovery, though Instron-type testers would now be used. He studied the same fibres as he had used in tests of their tensile properties.

In measurements of recovery, the particular programme of application and removal of stress is important. Meredith used the Cliff constant-rate-of-loading tester and applied the load at a rate of 10 gf/(den min) (0.15 mN/(tex s)). When the required load had been reached, it was left on the specimen for 2 min. The load was taken off at the same rate and left off until 1 min after the start of unloading. The procedure was then repeated for higher loads. Preliminary experiments had shown that this timing was the minimum that would give a reasonable approach to equilibrium. Tests were made at stresses of 0.3, 0.5, 1, 2, 2.5, 3, 4 and 5 gf/den (26.7, 44.5, 89, 198, 222.5, 267, 396, 445 mN/tex) (up to break) and at the yield stress. The results were found to be little affected by test-length. A 1.5 cm length was used for short fibres and a 5 cm length for long fibres. The relative humidity was 65% and the temperature 20 °C.

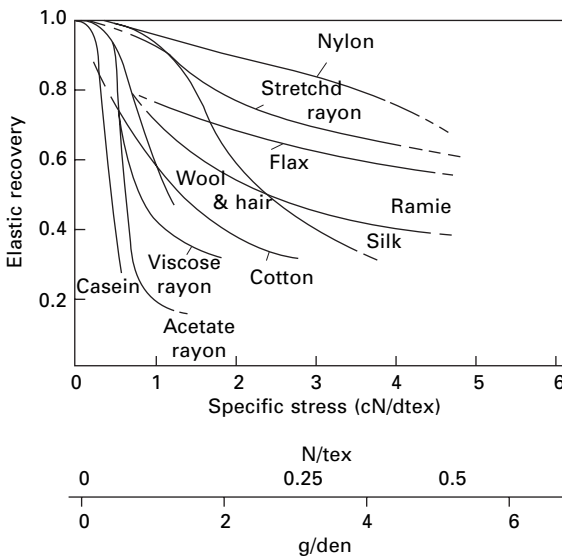
Figure 15.4 gives a typical record obtained in the tests and shows the division into elastic and permanent extensions. From this, the elastic recovery can be calculated. Note the extension and recovery at constant stress due to creep during the dwell periods. In an Instron test at constant rate of extension, there would be a decrease of stress at constant extension due to stress relaxation, as shown in Figure 15.5.



15.4 Stress-strain curves of viscose rayon in loading and unloading. After Meredith [1].



15.5 Test procedure used by Hockenberger *et al.* [2].

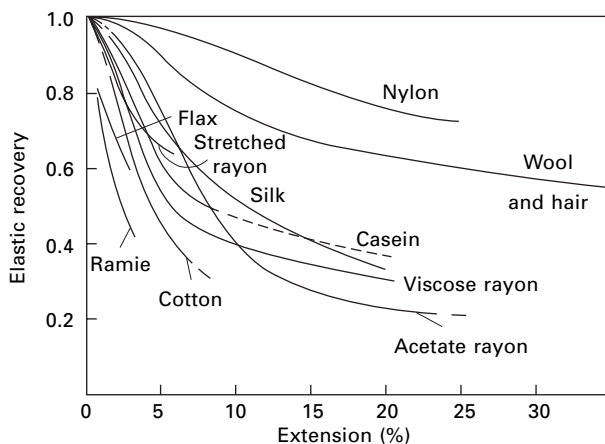


15.6 Elastic recovery plotted against stress. After Meredith [1].

15.4 Results

15.4.1 Comparative values

Elastic recovery may be plotted against stress or strain. The first shows the extent to which a given force will cause permanent damage to a fibre. The second shows what proportion of a given extension will be recovered and the amount of the permanent deformation. Figs 15.6 and 15.7 show Meredith's results.



15.7 Elastic recovery plotted against strain. After Meredith [1].

In cotton, the elastic recovery from a given strain is almost independent of the variety, but, since coarse cottons have a lower modulus, it follows that they will show less recovery from a given stress. Cotton shows no yield point (or it may be more correct to say that the yield point is at zero stress and zero strain). The elastic recovery falls steadily to about 0.3. Compared with that of other fibres, the recovery of cotton is only moderate. In particular, even small strains leave an appreciable proportion of permanent deformation.

The bast fibres show poor recovery from strain but can withstand large stress without great permanent damage.

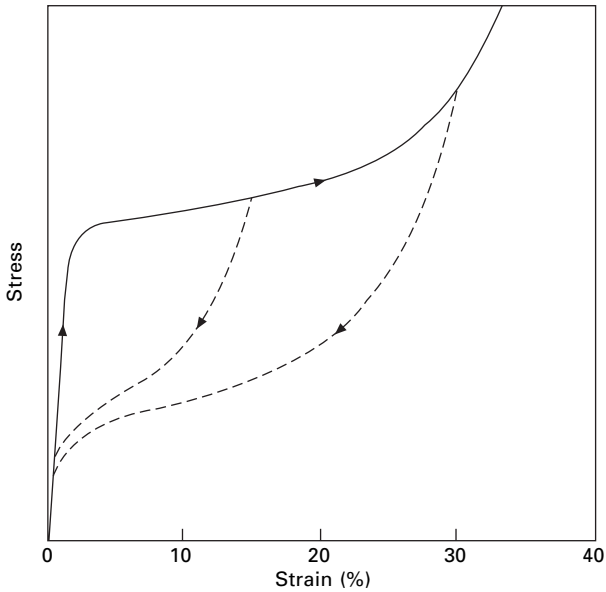
Viscose rayon and acetate show a marked yield point. Below this point, the recovery is good, but above it the curve drops rapidly, and the recovery is poor. The stretched rayons can stand higher stresses without suffering permanent deformation.

Wool and hair also show a yield point, but the drop in the curve is less rapid, and even near break there is still considerable recovery. These fibres are not good under high stresses but can recover from large strains. Thus they show 60% recovery from an extension of 35%. By contrast, in the casein fibre tested, the curve drops rapidly above the yield point, and the large additional extension that can occur before break is almost entirely non-recoverable. Thus, though the stress-strain curves of wool and casein are similar, their recovery behaviour is quite different, and this is one of the reasons why the regenerated-protein fibres of the 1950s did not last.

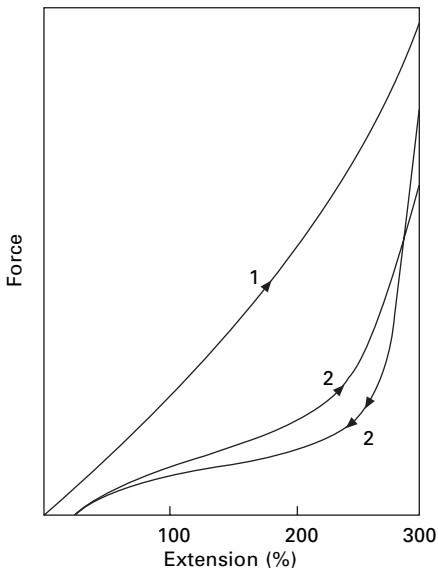
Wet wool fibres show complete recovery up to the end of the yield region (30% extension) and very good recovery from higher strains. However, the path of the recovery curve is different from that of the extension curve, as shown in Fig. 15.8, and thus there is energy loss in cyclic deformation.

Silk shows fairly good elastic recovery from both stress and strain.

Nylon shows the best elastic recovery of any of the fibres tested by Meredith, whether considered on the basis of stress or on that of strain. Even near break, its recovery falls only to 0.7. Although, in strength and extension at break, nylon is surpassed by some other fibres, these curves show its superiority in resisting permanent damage as a result of undue stress or strain.



15.8 Stress–strain behaviour of wool in extension and recovery. The stress is in arbitrary units.



15.9 Cycling response of spandex fibre: 1, first elongation; 2, 6th cycle loading and unloading [3].

After some time on a package, spandex fibres such as *Lycra* acquire a temporary set, and the first elongation shows a high stiffness. As shown in Fig. 15.9, a small amount of the initial extension is not recovered; in subsequent elongations, a steady hysteresis cycle with good reversible behaviour is established [3].

It is interesting to compare values of the yield point obtained from stress–strain curves (see [Section 13.5](#)) with those from recovery curves (arbitrarily defined as the point of 95% recovery). This is done in Table 15.1. It will be seen that there is qualitative agreement, though the values from the stress–strain curves are generally higher than those from the recovery curves.

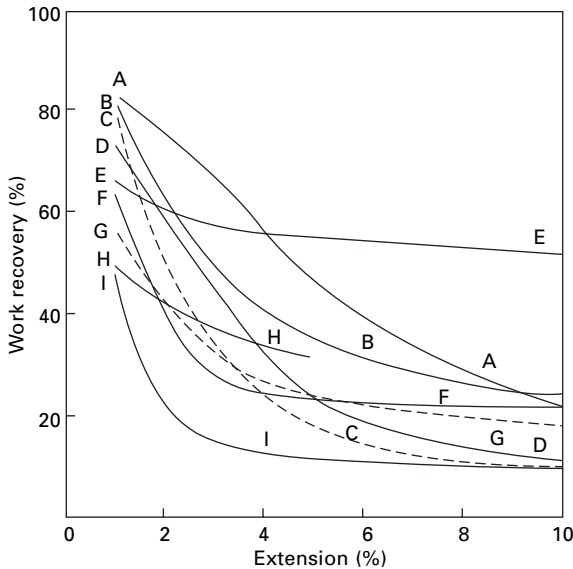
Beste and Hoffman [4] measured the elastic recovery of fibres, by means of a slightly different experimental procedure, and obtained results in general agreement with those of Meredith. They made tests at relative humidities of 60 and 90%, and examples of their results are given in Table 15.2. It will be seen that at small strains the elastic recovery is less at the higher humidity, but at larger strains it is greater for a number of the materials. They also measured work recovery, and some of their results are shown in [Fig. 15.10](#). This shows that, at large strains, the energy dissipated by nylon is considerably less than that by other fibres.

Table 15.1 Yield point

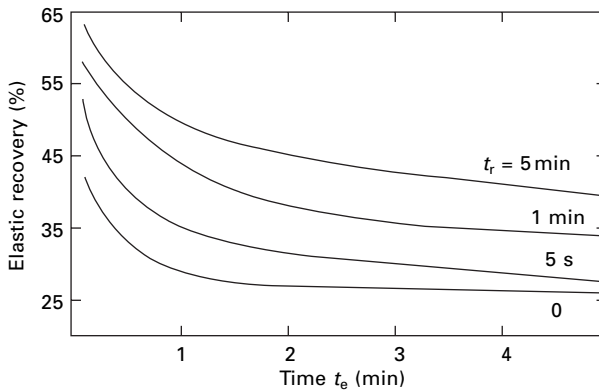
Fibre	From stress–strain curves		From recovery curves	
	Stress (mN/tex)	Strain (%)	Stress (mN/tex)	Strain (%)
Cotton	–	–	9	1
Viscose rayon	59	2	39	1
Acetate	69	3	39	2
Stretched rayon	118	0.8	88	1
Wool	59	5	39	4
Casein	49	5	29	1
Silk	156	3.3	98	4
Nylon	402	16	127	8

Table 15.2 Effect of humidity on elastic recovery [4]

Material	Elastic recovery (%) from:					
	1% extension		5% extension		10% extension	
	60% r.h.	90% r.h.	60% r.h.	90% r.h.	60% r.h.	90% r.h.
Cotton	91	83	52	59	–	–
Viscose rayon	67	60	32	28	23	27
Acetate	96	75	46	37	24	22
Wool	99	94	69	82	51	56
Silk	84	78	52	58	34	45
Nylon	90	92	89	90	89	–
Polyethylene terephthalate (Dacron)	98	92	65	60	51	47
Polyacrylonitrile (Orlon)	92	90	50	48	43	39
Casein	90	76	47	43	30	25



15.10 Work recovery of fibres After Beste and Hoffman [4]: A, wool; B, Dacron polyester fibre; C, acetate; D, casein; E, nylon; F, Orlon acrylic fibre; G, silk; H, cotton; I viscose rayon.



15.11 Elastic recovery of viscose rayon, showing variation with time extended, t_e , and recovery time, t_r .

15.4.2 Influence of test conditions on recovery

Values obtained for elastic recovery are very sensitive to conditions. Guthrie and Norman [5] studied the influence of the time t_e for which viscose rayon fibres were held at constant strain and the time t_r of recovery at zero stress. The rate of extension and contraction was 100%/min. Figure 15.11 shows their results and indicates that any value between 25 and 65% could be obtained, depending on the test procedure. Even if, as is often done, the two times were made equal, the values would range

from 50 to 38%. Similar behaviour in other fibres has been described by Guthrie and Wibberley [6], and the problem has also been discussed by Hadley [7].

Temperature will also influence recovery behaviour, as described for acrylic fibres by Beevers and Heap [8]. Ford [9] lists the elastic recoveries, wet and dry, at 20 °C and 95 °C, for many types of fibre. Figure 15.12 shows values for continuous filament nylon 66 and polyester fibres, both of which have tenacities of about 0.45 N tex and breaking extensions of 20%. Polyester fibres show better recovery than nylon at low stresses, but fall off more at high stresses. For glass fibres the elastic recovery was 85% for all conditions and strains.

A comparative set of work recovery values from a comprehensive study of recovery reported by du Pont [10] is given in Table 15.3. The comparatively poor work recovery of nylon is due to 'creep' and 'creep recovery', which leads to substantial hysteresis. Polyester shows better recovery from small strains than nylon, but poorer from large strains.

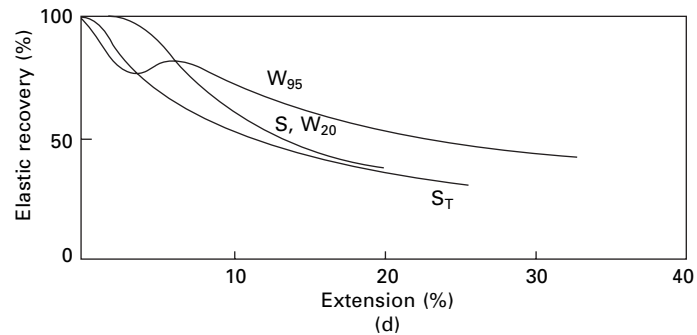
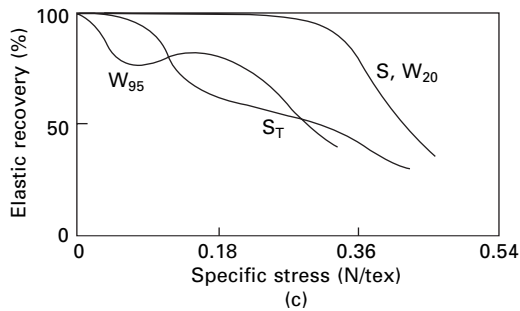
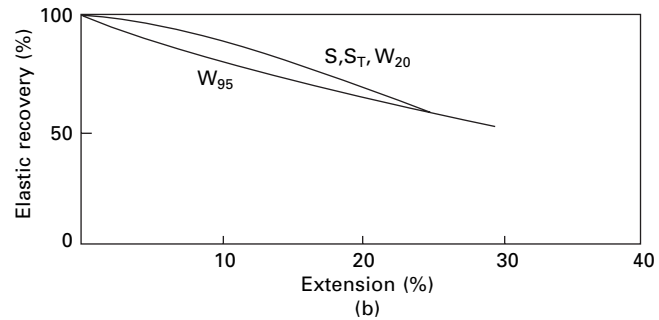
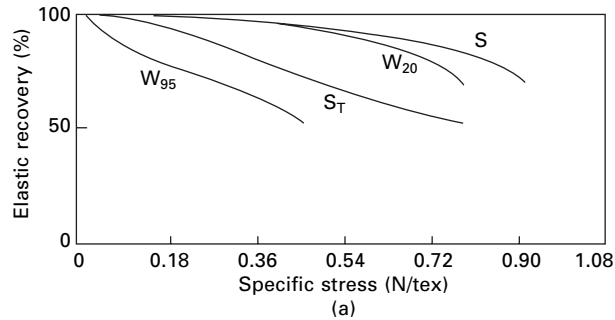
15.5 Change of properties as a result of straining: mechanical conditioning

Stretching a fibre far enough to leave it with a permanent set causes other changes in the properties of the fibre. This is illustrated in the idealised model of Fig. 15.13. When the fibre is first strained, the stress–strain curve OA is followed, but, on removal of the load, recovery takes place along AB, the permanent extension OB being left. If the fibre is again stressed, the curve BAC is followed. Re-plotting this as a new stress–strain curve (Fig 15.13(b)), we see that the effect of the first straining has been to raise the yield stress and reduce the breaking extension (and consequently the work of rupture). This has practical implications, since it means that the properties of fibres may be changed by high forces during processing. It also means that if a structure is highly strained in use, even though it is not broken, its properties will be altered, and it may no longer serve its proper function.

The rise in the yield stress means that the application of a given stress to a fibre for some time usually results in almost perfect recovery from subsequent stresses below this value. This treatment is known as mechanical conditioning. Table 15.4 gives values of elastic recovery from near the breaking point before and after mechanical conditioning at 80% of the breaking elongation. It will be seen that there is little permanent deformation in the tests after mechanical conditioning, even though this is taken to a greater extension.

Averett *et al.* [12] studied a partially oriented nylon fibre (draw ratio of 2.5×), which shows a large plastic extension beyond the yield point. Figure 15.14 shows its response to cyclic loading at increasing loads. The initial modulus is appreciably lower than in the initial elongation. Figure 15.15 shows the division between elastic and plastic extension.

If a fibre is repeatedly taken through a given cycle of stress, the loading and unloading curves in successive cycles will gradually come closer together until they form a continuously repeated loop. This is illustrated in Fig. 15.16. The area within the loop will be a measure of the energy dissipated in each cycle.



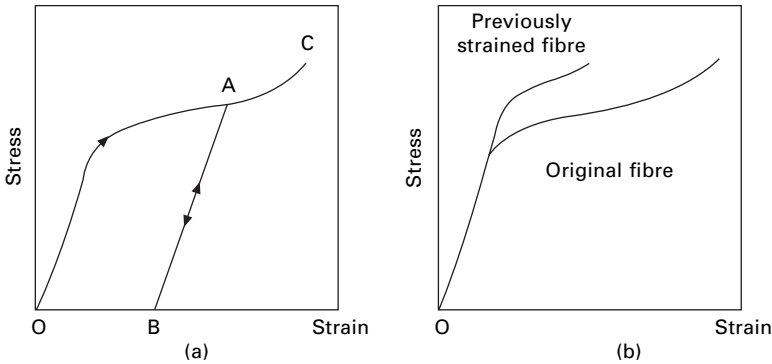
15.12 Elastic recovery under various conditions. S, as received tested at 65% r.h., 20 °C; S_T , 65% r.h., 20 °C after water at 95 °C; W_{20} , in water at 20 °C; W_{95} , in water at 95 °C: (a), (b) nylon 66; (c), (d) polyester. (a) and (c) From given stress; (b) and (d) from given strain.

Table 15.3 Percentage work-recovery values [10]

	Acetate	Polyester fibre	Nylon	Acrylic fibre	Rayon	Wool
From 1% extension	60	81	51	55	32	80
3% extension	32	34	42	28	18	43
5% extension	17	22	47	14	13	27
15% extension	7	19	43	10	11	15
At 8% r.h.	42	38	38	31	22	50
92% r.h.	21	28	78	26	16	58
In water at 21 °C	20	41	73	22	58	43
76 °C	7	21	95	13	80	61
				at 50 °C		
In air at – 70 °C	55	57	45	56	25	68
177 °C	5	33	54	29	12	25
After holding 1 s	47	49	60	40	27	66
900 s	13	23	24	10	8	25

Standard conditions (except as indicated above): 21 °C, 65% r.h.; 3% extension; 30 s holding time.

Cotton had a work recover of 67% under standard conditions.



15.13 Change in fibre properties on straining.

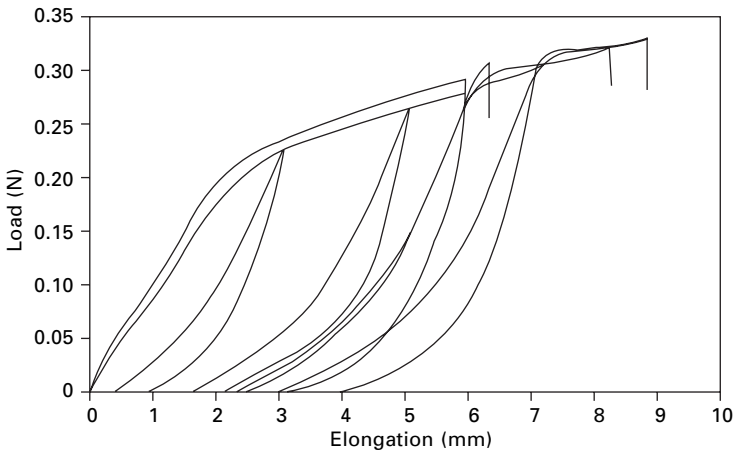
15.6 Swelling recovery

For fibres that absorb water, the ‘permanent’ (plastic) extension as defined in [Figs 15.3](#) and [15.5](#) is partly recovered on immersion in water or treatment in steam. The fibre will revert almost to its original form on subsequent drying. When a fibre is wetted, it usually extends owing to swelling, but the swelling recovery may cause a net contraction. Swelling recovery may be useful as a means of restoring the original fibre properties, but it also means that fibres that have been stretched in processing will shrink on wetting. [Table 15.5](#) shows values of swelling recovery obtained by Leaderman [14]. Viscose rayon shows almost complete recovery in water, as does silk in steam, but acetate shows only partial recovery.

Immersion of ‘permanently’ strained wool fibres in water for 24 hours serves to restore their properties to a standard state. This procedure was used by Feughelman [15] to make repeated tests on the same wool fibres.

Table 15.4 Effect of mechanical conditioning on elastic recovery [11]

Material	Elastic recovery % near breaking point	
	Before mechanical Conditioning	After mechanical conditioning
Cotton yarn	56	80
Fortisan (stretched cellulose)	72	94
Acetate	30	92
Silk	36	93
Viscose rayon	39	74
Dacron polyester fibre	55	92
Orlon acrylic fibre	58	92
Vicara (zein protein)	43	97
Casein	39	80
Nylon	72	92
Wool	59	88

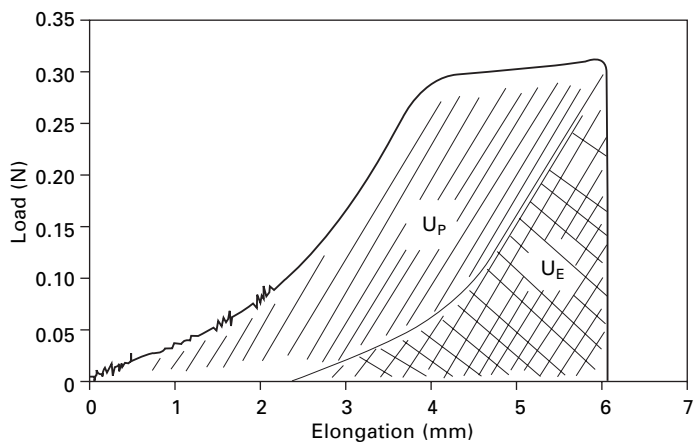


15.14 Cyclic responses of a partially orientated, 33 μm diameter nylon fibre at increasing loads. Gauge length of 25.4 mm means that 10 mm elongation = 40% extension. From Averett *et al.* [12].

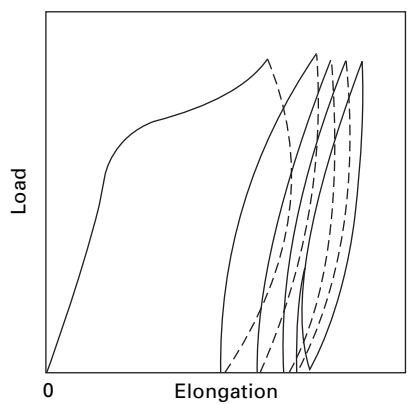
15.7 Simple recovery models

15.7.1 Idealised fibre stress–strain relations

In dealing with other materials, ideal elasticity (Hooke's Law) or ideal plasticity (a Hooke's Law region leading to a constant plastic-yield stress) is often assumed. Neither of these is very suitable for representing fibre behaviour. Instead, a form that gives a reasonable approximation to the behaviour of many fibres is shown in Fig. 15.17. It is often helpful to use this form in studying the response of fibres to complicated loading sequences, though some fibres, of which wool is a notable example, deviate markedly from the idealised behaviour. The idealised model is characterised by four parameters: two slopes, yield strain and breaking strain.



15.15 Elastic energy U_E and plastic energy U_P after load-cycling for the partially oriented nylon fibre. From Averett *et al.* [12].



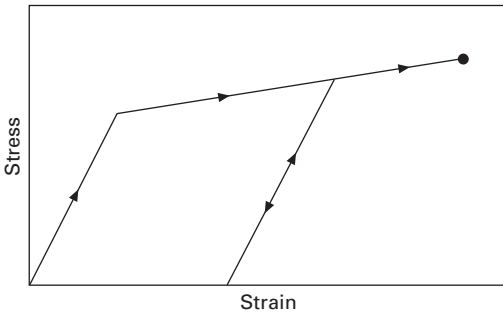
15.16 Load – elongation curves for acetate under repeated stressing to 90% of breaking load. After Hamburger [13].

Table 15.5 Swelling recovery [14]

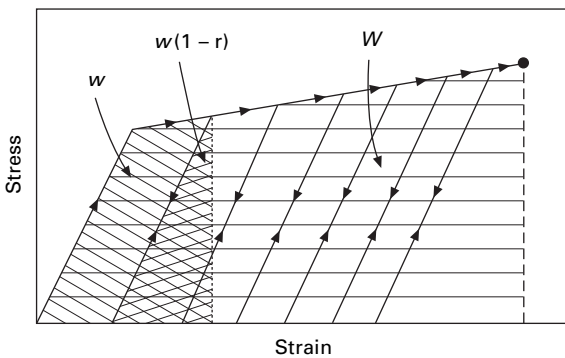
Material	Permanent extension (%)	Permanent extension (%) after recovery in:	
		Water	Steam
Viscose rayon	1.7	0.08	–
Silk	1.2	0.7	(–0.02)
Acetate	4.1	3.3	1.6

15.7.2 Recovery, work of rupture and durability

In use, fibres are frequently subjected to shocks of given energy, well below their work of rupture. Failure does not occur initially, but a succession of repeated shocks can lead up the stress–strain curve to the point of break, as shown in Fig. 15.18.



15.17 Simple idealised fibre stress-strain curve.



15.18 Behaviour of idealised fibre subject to repeated shocks of energy (w).

If the imposed shock has an energy w , and if the work recovery in a given cycle is r , then the amount of energy used up in the cycle is $w(1 - r)$. If the additional elastic energy in the final cycle is ignored, it follows that failure will occur when the total energy used up equals the work of rupture W of the fibre. This means that the life of the fibres, expressed in terms of the number N of shocks that it will resist, is given by:

$$\sum_{i=1}^N w(1 - r) = W \quad (15.1)$$

If, to show up the nature of the relation more clearly, we take w and r as constants, we find that:

$$N = \frac{W}{(1 - r)w} \quad (15.2)$$

Long life therefore results, rather obviously, from gentle use, giving a low value of w , and more importantly, from the use of fibres with high work of rupture W and good recovery properties, namely, values of r close to 1.

15.7.3 A simple model of cyclic testing

Hearle and Plonsker [16] have explained some of the features of cumulative-extension and other forms of cyclic testing on the basis of a simple model of recovery behaviour

with the essential features shown in the stress–strain curve, Fig. 15.19, which is not quite as restricted as Fig. 15.17. The assumptions are as follows:

- The stress–strain curve in simple extension is ABE. If a specimen is strained to any point B and allowed to recover to C, it is assumed that, on re-straining, the original stress–strain curve will be rejoined at B and then followed towards E.
- It is assumed that, on first reaching any strain level, such as B, the elastic recovery r , defined as the ratio of elastic strain R to total strain ϵ , will be a function only of strain ϵ . In particular, r will be independent of the previous history at lower strain levels.

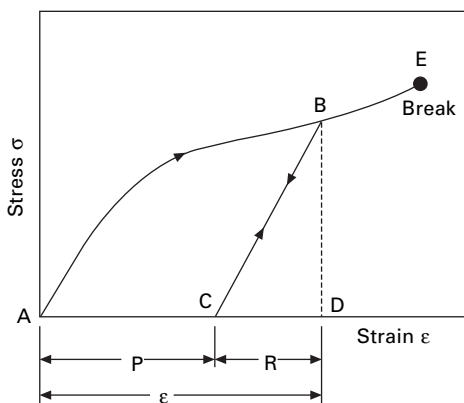
These are the two basic assumptions, but we can add three others, as follows:

- Repeated application of the same level of strain B does not lead to any change in the elastic-recovery value.
- Viscoelastic time-dependent effects are ignored.
- Break occurs at the same point E irrespective of the previous history, so that any true ‘fatigue’ effects are not taken into account.

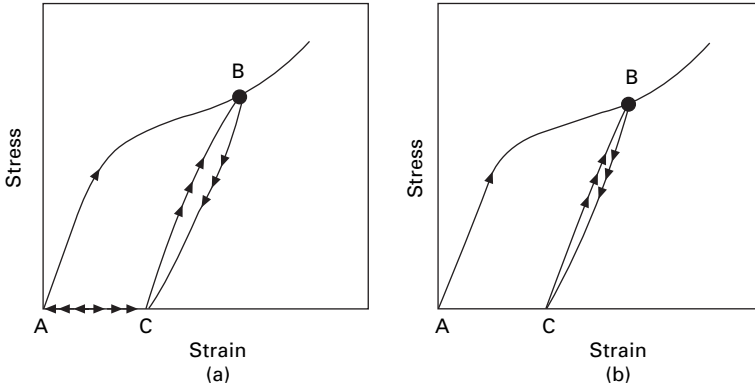
We can now note the behaviour in simple cycling procedures. Simple extension-cycling between fixed limits of imposed strain without the removal of slack is shown in Fig. 15.20(a). Initially, the stress–strain curve is followed from A to B; recovery to zero strain goes along BCA; and then re-straining to B reverses the path ACB. The strain level B cannot be exceeded, and the path BCACB is followed in all succeeding cycles. It will be noted that the return path from C to B has been shown here as different from the path from B to C: this, while it is avoided in the simpler model shown in Figure 15.19, is not incompatible with the basic assumptions.

Simple load-cycling, as in Figure 15.20(b) between the levels A and B, is almost identical, except that there is an immediate reversal at C, without traversing the region of slack fibre back to the original length at A.

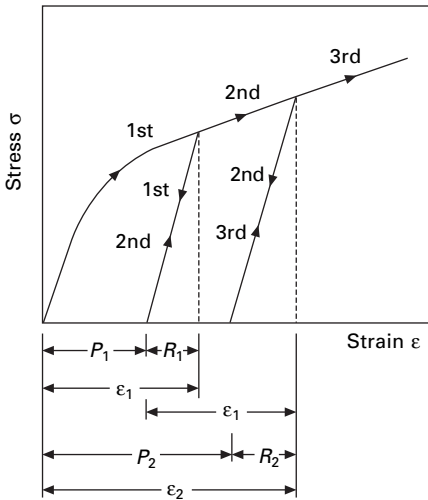
Figure 15.21 illustrates the behaviour of the basic model in cumulative-extension cycling. An imposed strain ϵ_1 is applied to the material and then released; the material



15.19 Idealised model of recovery behaviour.



15.20 Model in (a) simple extension-cycling and (b) load-cycling.



15.21 Model in cumulative extension-cycling.

has a permanent strain P_1 after this first cycle. The slack P_1 is removed, and then the imposed strain ϵ_1 is again applied. The strain on the material in the second cycle is now $\epsilon_2 = P_1 + \epsilon_1$; after the second cycle, the permanent strain is P_2 , and this is removed before applying ϵ_1 ; and so on. The gradual increase of strain is given by noting that, in the $(n - 1)$ th cycle:

$$\text{permanent strain} = P_{n-1} = (1 - r_{n-1})\epsilon_{n-1} \quad (15.3)$$

in the n th cycle:

$$\text{total strain} = \epsilon_n = P_{n-1} + \epsilon_1 = (1 - r_{n-1}) \epsilon_{n-1} + \epsilon_1 \quad (15.4)$$

$$\text{permanent strain} = (1 - r_n) \epsilon_n \quad (15.5)$$

in the $(n + 1)$ th cycle:

$$\text{total strain} = \epsilon_{n+1} = P_n + \epsilon_1 = (1 - r_n) \epsilon_n + \epsilon_1 \quad (15.6)$$

The strain will have reached a limiting value when the total strain in successive cycles remains unaltered, that is, when:

$$\epsilon_n = \epsilon_{n+1} \quad (15.7)$$

$$\epsilon_n = (1 - r_n) \epsilon_n + \epsilon_1 \quad (15.8)$$

$$\epsilon_n r_n = \epsilon_1 \quad (15.9)$$

In general, the condition for the limiting extension is thus:

$$\epsilon r = \epsilon_1 \quad (15.10)$$

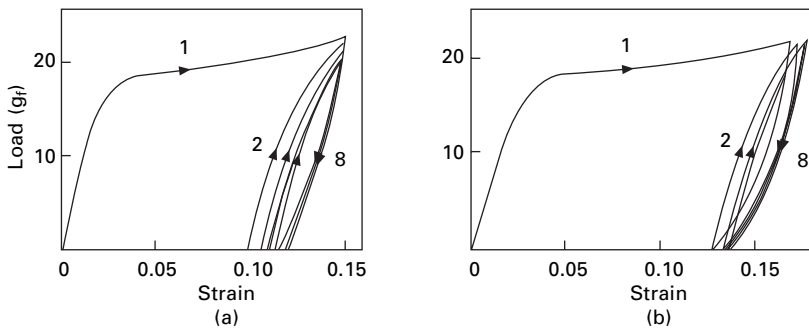
where ϵ_1 is the constant strain imposed in each cycle. This condition states that, at the limit, the strain recovered after a cycle just equals the imposed strain, so that there is no additional straining in the next cycle.

If elastic-recovery values are known as a function of ϵ_1 , then equations (15.3) to (15.6) can be used to compute the total elastic and permanent strains in each successive cycle.

Three different types of behaviour are predicted during cumulative extension cycling: (1) if the limiting extension is less than the breaking extension, the specimen will steadily increase in length until it reaches the stable limiting value; (2) if the limiting extension is greater than the breaking extension, the specimen will fail before it reaches the limit; and (3) there may be no limiting extension, and hence the specimen will extend indefinitely and finally fail by breaking. The distinction between (2) and (3) is, in a way, artificial, since both describe a steady increase in extension up to the breaking point. However, in some instances, extrapolated recovery curves would lead to a limit, whereas in other instances they lead away from a limit. In using the recovery values for nylon, there is a rather sharp change at a level of imposed extension of 10.7% from a stable limit to an indefinite increase in length.

15.7.4 Experimental behaviour in cyclic testing

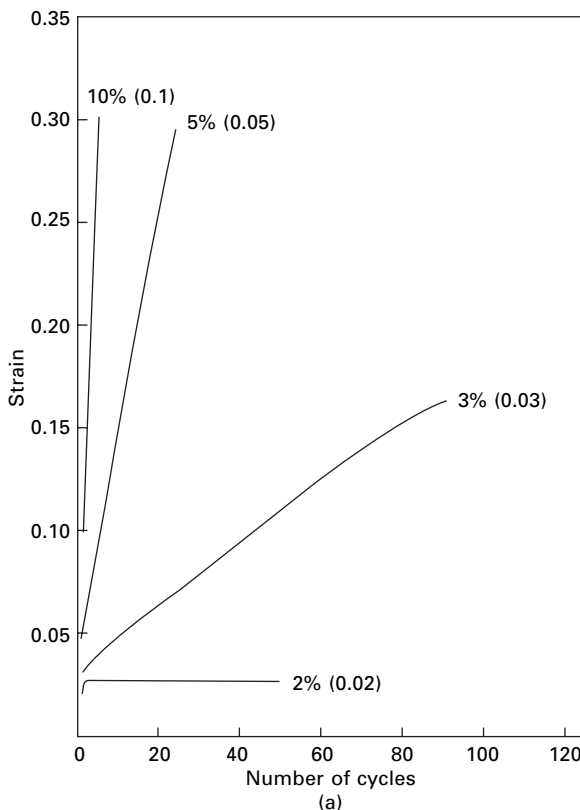
For comparison with the predictions given in Fig. 15.20, Fig. 15.22 shows the behaviour of an acetate fibre in simple extension and load cycling. Contrary to the behaviour of



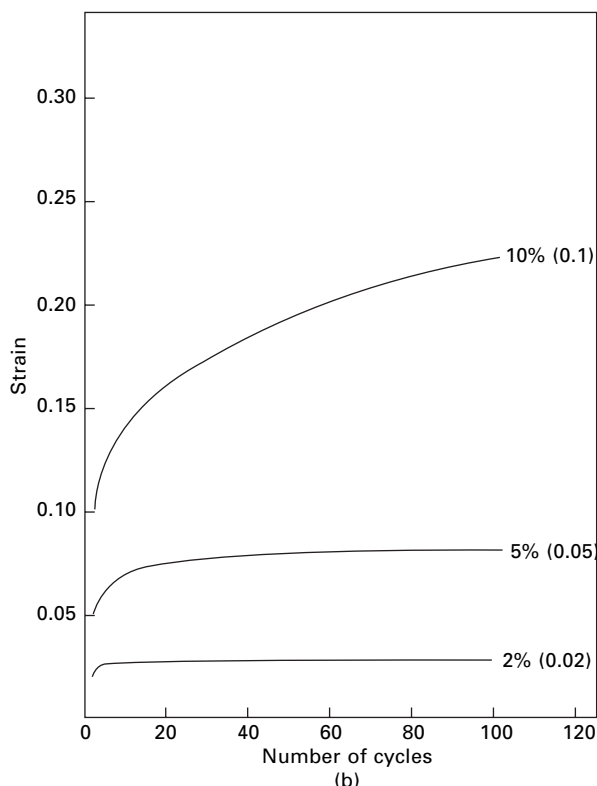
15.22 Behaviour of 2.5 tex acetate in (a) simple extension-cycling and (b) load-cycling.

the model, there is a gradual reduction of peak stress and increase of permanent extension (decrease of elastic recovery) in successive cycles of simple extension cycling; and there is a corresponding increase of total and permanent extension in load cycling. These effects correspond to the occurrence of some secondary creep (non-recoverable time-dependent extension) as the test proceeds.

In cumulative-extension cycling, the experimental results as illustrated in Fig. 15.23 for acetate and nylon do show that, at low imposed strains, a limiting extension is reached, whereas at high imposed strains the extension continues until break occurs. The computed values based on recovery values predict appreciably less permanent extension than is observed in practice, which is due to deviation of the behaviour of real fibres from that of the simple model. Time-dependent aspects of cumulative-extension are discussed in Section 16.2.5 and in relation to fatigue in Section 19.3.



15.23 Behaviour of (a) acetate and (b) nylon at various levels of imposed extension in cumulative-extension tests.



15.23 (Continued)

15.8 References

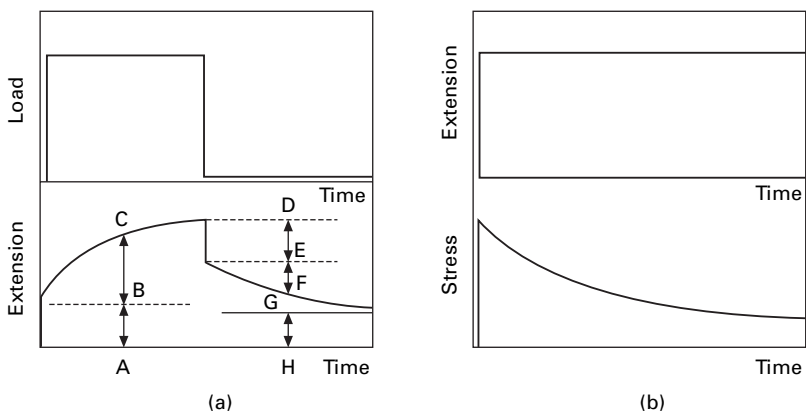
1. R. Meredith. *J. Text. Inst.*, 1945, **36**, T147.
2. A. R. Hockenberger, S. Koral and M. A. Wilding. *Textile Res. J.*, 2005, **75**, 111.
3. A. J. Hughes and J. E. McIntyre (Coordinators). *Textile Progress*, 1976, **8**, No. 1.
4. L. F. Beste and R. M. Hoffman. *Text. Res. J.*, 1950, **20**, 441.
5. J. C. Guthrie and S. Norman. *J. Text. Inst.*, 1961, **52**, T503.
6. J. C. Guthrie and J. Wibberley. *J. Text. Inst.*, 1965, **56**, T97.
7. D. W. Hadley. *J. Text. Inst.*, 1969, **60**, 301, 312.
8. R. B. Beevers and S. A. Heap. *J. Text. Inst.*, 1966, **57**, T191.
9. J. E. Ford (Editor). *Fibre Data Summaries*, Shirley Institute, Manchester, 1966.
10. Bulletin X-142, E. I. du Pont de Nemours & Co. Inc., Wilmington, DE, 1961.
11. L. Susich, *Text. Res. J.*, 1953, **23**, 545.
12. R. D. Averett, M. L. Realff, S. Michielsen and R. W. Neu. *Composites Sci. Tech.*, 2006, **66**, 1671.
13. W. J. Hamburger. *Text. Res. J.*, 1948, **18**, 102.
14. H. Leaderman. *Elastic and Creep Properties of Filamentous Materials and Other High Polymers*, The Textile Foundation, Washington, DC, 1943, p. 128.
15. M. Feughelman. *Mechanical Properties and Structure of alpha-Keratin Fibres*, UNSW Press, Sydney, 1997.
16. J. W. S. Hearle and H. R. Plonsker. *J. Appl. Polymer Sci.*, 1966, **10**, 1949.

16.1 The study of time dependence

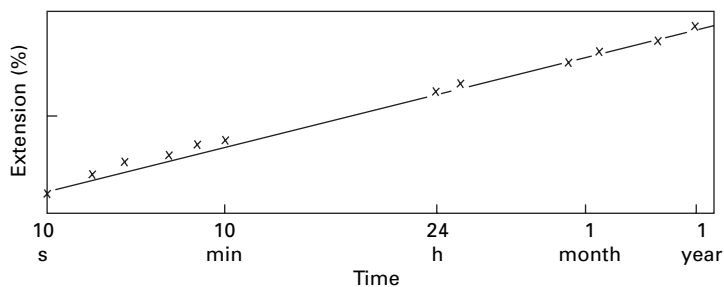
So far, we have been discussing the mechanical properties of fibres, with only a brief mention of one of the main characters: time. The extension caused by a given applied force, or the stress resulting from a given strain in the fibre, depends on how long the force or the strain has been present and on the earlier mechanical history of the fibre.

On the application of a load to a fibre, it will, after an instantaneous extension, continue to extend as time goes on. On removal of the load, the recovery will not be limited to the instantaneous recovery but will continue to take place. This behaviour is illustrated in Fig. 16.1(a) and is known as creep and creep recovery. It may continue for a very long time, as illustrated in Fig. 16.2. Creep is extension with time under an applied load: the complementary effect is stress relaxation, the reduction of tension with time under a given extension. This is illustrated in Fig. 16.1(b): when the fibre is stretched, an instantaneous stress is set up, but this gradually decreases as time passes.

The continued deformation and possible rupture of the specimen when a load is applied for some time have important consequences in the testing of mechanical



16.1 (a) Creep under constant load and recovery under zero load, showing instantaneous extension, A-B and D-E; total creep, B-C; primary creep, E-F; and secondary creep, G-H. (b) Relaxation of stress under constant extension.



16.2 Creep of 16.5 den (1.8 tex) nylon under a load of 30 gf (0.29 N) continuing for one year [1].

properties, since it means that the results of a test, for example the stress–strain curve obtained, will depend on the timing. This in turn creates interest in the high-speed properties of fibres, the study of which needs special experimental techniques, since conventional methods of testing have time-scales that cannot be shorter than a few seconds. With very rapid tests, there is the further complication that they may be more nearly adiabatic than isothermal.

An alternative means of studying time dependence is to subject the fibre to an oscillating load: dynamic testing.

The four methods suggested are the simplest of the infinite variety of time sequences of stress and strain that a fibre might experience. Between them, they conveniently cover a wide range of times. The timescales for which the methods are easily used are as follows:

- creep: long times, from 1 minute to 1 month
- stress relaxation: medium to long times, from 1 second to 1 hour
- stress–strain curves, including impact methods: short to medium times, from 1/100 second to 10 minutes
- dynamic testing: short times, from 0.1 millisecond to 1 second.

These time ranges can be increased somewhat by more elaborate or difficult experimental methods.

Effects in the processing or use of fibres are liable to cover all the time ranges and to involve more complicated variations of stress and strain with time. One aim of the development of the academic subject of fibre rheology should be to provide means of predicting behaviour in real situations.

16.2 Creep

16.2.1 Primary and secondary creep

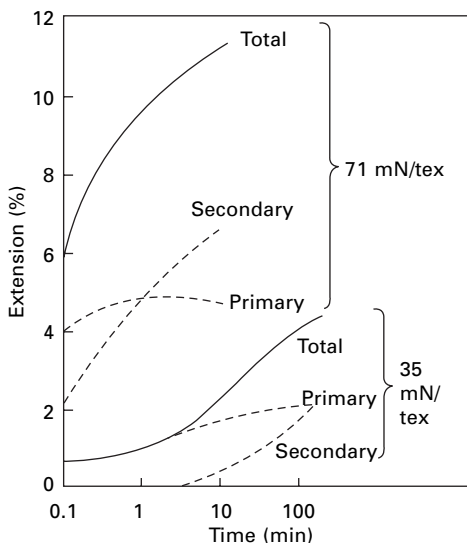
Figure 16.1(a) indicates the effect of applying a constant load to a fibre for a given time and then removing it. The instantaneous extension is followed by creep. The removal of load gives rise to an instantaneous recovery, usually equal to the instantaneous extension, followed by a further partial recovery with time, which still leaves some unrecovered extension. The total extension may therefore be divided into three parts:

the *immediate elastic deformation*, which is instantaneous and recoverable; the *primary creep*, which is recoverable in time; and the secondary creep, which is non-recoverable. The mechanisms of creep will be discussed in [Chapter 20](#), but it is worth noting here that there are two main effects. At low stress, creep is due to localised molecular rearrangement, which may or may not be recoverable. At high stress, molecules slide past one another in non-recoverable deformation.

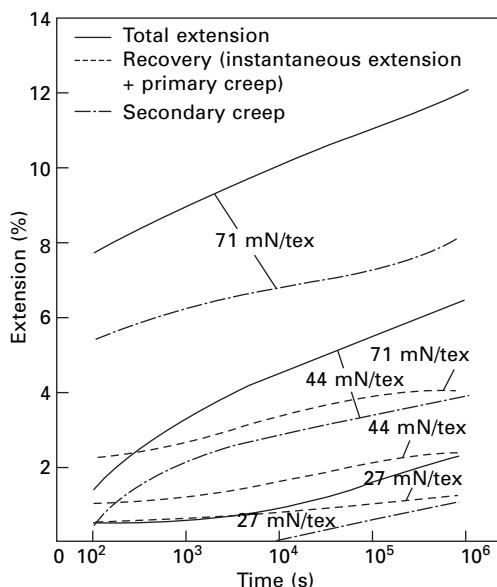
O'Shaughnessy [2] has studied the division of the total extension of viscose rayon yarn into its three parts. He measured the creep under a constant load and the recovery after various times of loading. Figure 16.3 gives examples of his results plotted on a logarithmic scale, and it will be seen that the secondary creep continues after the primary creep has ceased.

[Figure 16.4](#) shows results calculated from experiments by Press [3] at longer times. In these experiments, recovery was measured only after the full time for creep, and the division between primary and secondary creep depends on the assumption, derived from the superposition principle (see [Section 20.7.7](#)), that the time-dependent part of the recovery curve is identical with the primary creep curve.

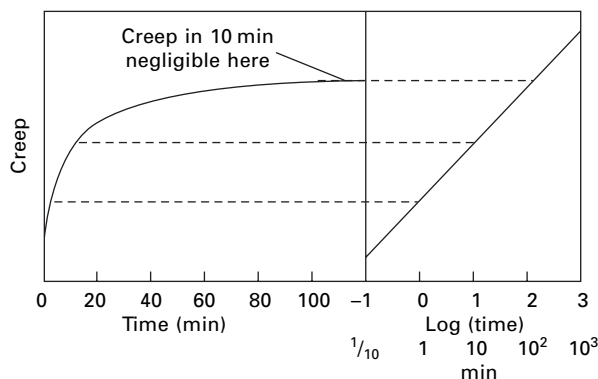
If, after recovery, the same load is applied again, the rate of creep is less than that in the first test on the specimen. The primary creep takes place at its initial rate, as before, but the secondary resumes at the rate at which it left off. The mechanical conditioning effect is a special case of this, since it means that if the load has been applied for long enough for the rate of secondary creep to become negligible, then there will not be any appreciable secondary creep in later experiments unless the load is further increased. The recovery will therefore be complete. The use of logarithmic timescales may cause some confusion here. The important practical point in mechanical conditioning is that there should be negligible secondary creep on the timescale of



16.3 Primary and secondary creep of viscose rayon at 60% r.h. [2].



16.4 Creep of viscose rayon at 21 °C, 65% r.h. [3]. 10² s \approx 2 minutes; 10⁴ s \approx 3 hours; 10⁶ s \approx 12 days.



16.5 Comparison of linear and logarithmic timescales.

the experiments; this may be so even when a plot on a logarithmic scale shows that secondary creep has not ceased, and this is illustrated in Fig. 16.5.

The secondary creep gives rise to the major part of the permanent extension of a fibre and is usually negligible below the yield point. Thus a comparison of the amounts of secondary creep that occur in various fibres after particular loading histories is given by the figures for inelastic extension in [Chapter 15](#).

16.2.2 Leaderman's experiments on primary creep

Leaderman [4] carried out a classical investigation of primary creep in viscose rayon, acetate, silk and nylon. In his experiments, 280 mm (11 in.) specimens were mounted

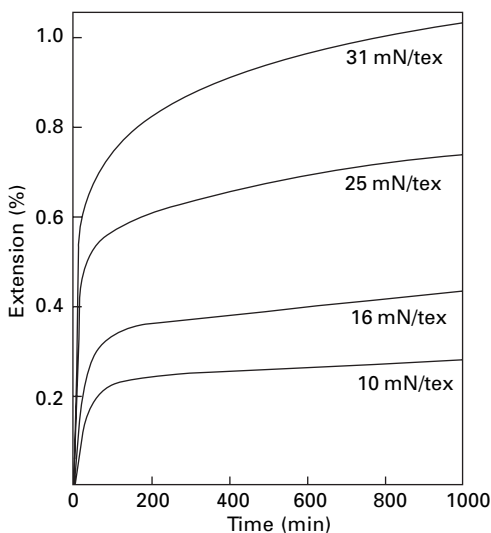
on one arm of a balance. At zero time, the other arm of the balance was released so that a given load was applied to the filament, whose extension was followed by a cathetometer. Measurements were made every 15 seconds for the first minute and thereafter at longer intervals up to 24 hours after the application of the load. Most of Leaderman's tests were made at 65% r.h. and 21 °C, but there were also arrangements for testing dry fibres over a range of temperatures.

To ensure that only primary creep was involved, the stresses employed were small and the specimen was first mechanically conditioned, since it was found that the first application of a load resulted in some permanent deformation but that subsequent applications showed perfect recovery.

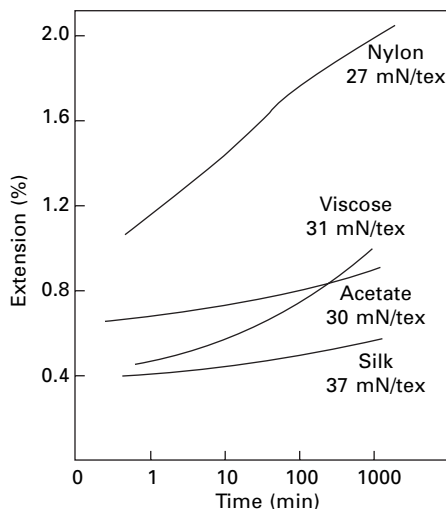
When extension is plotted against time, curves such as the one in Fig. 16.6 are obtained. To show the behaviour over a long time, it is more useful to plot the results on a logarithmic scale of time. This is done in Fig. 16.7, which shows the results obtained by Leaderman for various fibres. It is clear from these graphs that the amount of extension occurring as primary creep is comparable to that occurring instantaneously.

In viscose rayon and acetate, the recovery curves are identical with the creep curves inverted, as is shown in Fig. 16.8(b). In silk, the recovery curves are the same shape as the creep curves but lie slightly higher than those in Figure 16.8(b). This means that the instantaneous contraction on removing the load is less than the instantaneous extension found on applying it.

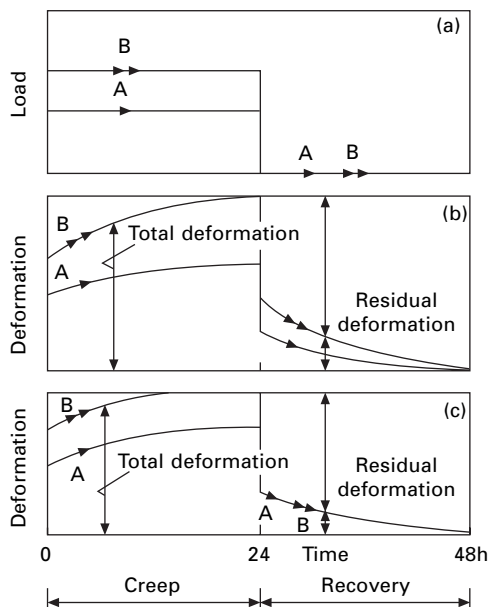
In nylon at low loads, the recovery curve is the same as the creep curve, but at high loads the behaviour is that shown in Fig. 16.8(c). It will be seen that the instantaneous contraction is less than the instantaneous extension, but the rate of recovery is greater than the rate of creep, so that after a long time recovery is complete. The rate of recovery is, in fact, found to be the same for all loads above a certain level.



16.6 Primary creep of viscose rayon [4].

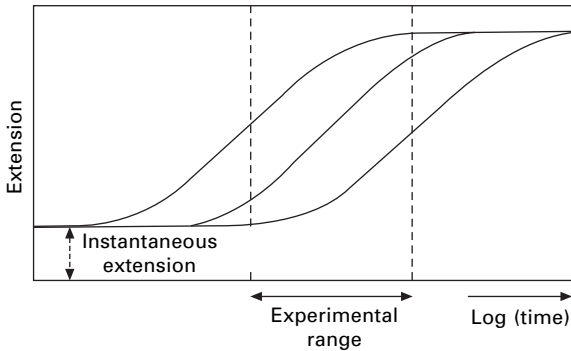


16.7 Primary creep of various fibres [4].

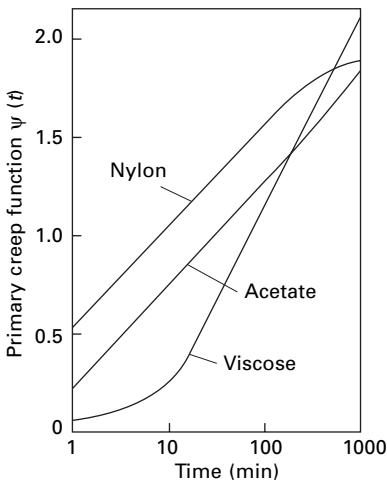


16.8 Creep and recovery of fibres [4]: (a) Load-time diagram; (b) behaviour of viscose rayon and acetate; and of nylon at low loads; (c) behaviour of nylon at high loads.

The shape of the creep curves appears to be different for the different fibres. This is largely a result of the limits on the times for which tests can be made. It is not possible to make measurements at very short time intervals, and it is not practicable to make them at very long time intervals. If this could be done, we should expect all the curves to be sigmoidal, as in Fig. 16.9. It will be seen from this diagram that the



16.9 Creep curves over a wide range of times.

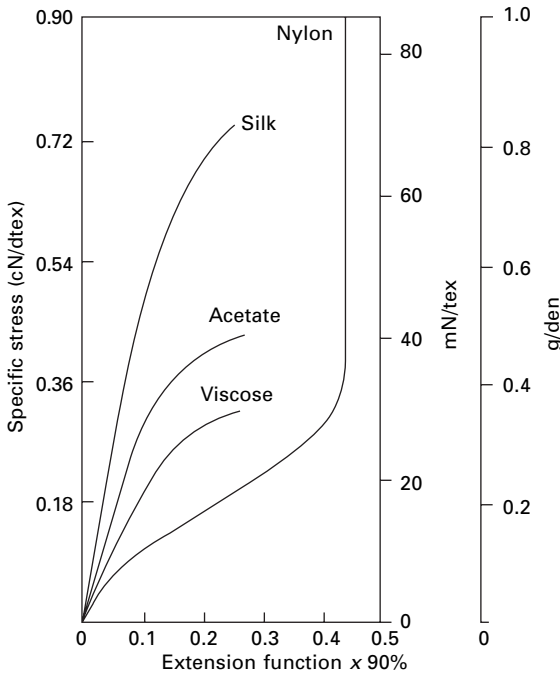


16.10 Values of $\Psi(t)$, calculated from Leaderman's data [4], plotted against time. The value of instantaneous extension has been estimated, so that intercepts of graphs are approximate. Slopes that give creep during a given time interval are correct.

shape of curve found experimentally depends on which portion of the curve lies within the experimental time range. The effect of time may be summarised by a function $\Psi(t)$, which equals the ratio of the primary creep (excluding the instantaneous extension) at a time t to the primary creep occurring between 1 and 90 min under the same load. Values obtained from Leaderman's data are plotted in Fig. 16.10.

The effect of load may be summarised by the quantity $x(90)$, which equals the extension occurring between 1 and 90 min. Values are given in Fig. 16.11, which is analogous to a stress–strain diagram. One notable feature is that for nylon at high loads the amount of creep becomes independent of the load.

It follows from the application of the superposition principle, which is discussed later in Section 20.7.7, and is confirmed by Leaderman's experiments, that the total extension x_t occurring after a time t is then given by:



16.11 Values of $x(90)$, calculated from Leaderman's data, plotted against stress [4].

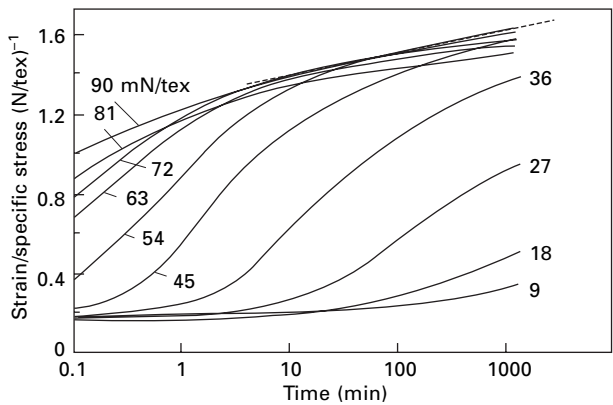
$$x_t = x_0 + x(90) \cdot \Psi(t) \quad (16.1)$$

where x_0 = instantaneous extension. This means that, in addition to its special definition (which refers to its absolute magnitude), $x(90)$ gives the relative amount of primary creep at different loads after the same time, in the same way that $\Psi(t)$ gives the relative amount of primary creep at different times under the same load. An interesting result of Leaderman's work, confirmed by many later studies, is the very high level of primary creep in nylon. This has important technical consequences.

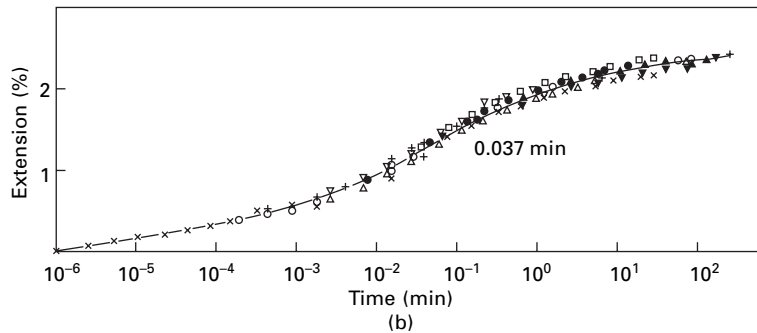
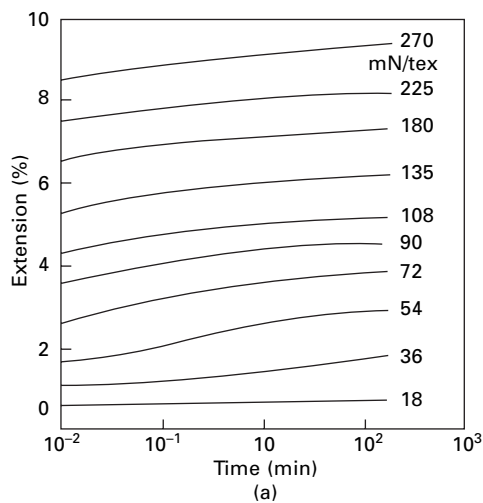
16.2.3 Generalised creep curves

O'Shaughnessy [2] showed that the creep of viscose rayon at various loads showed a certain regularity when the elongation divided by the stress was plotted against the time, as shown in Fig. 16.12. It will be seen that, at long and short times, the results for all the loads appear to come together, though for many of the loads this would be at times beyond the experimental range. Thus the creep curves can be regarded as lying between two loci, crossing from one to the other with a characteristic sigmoidal curve (when plotted on a logarithmic time scale) at times that depend on the load.

In a later paper concerned with the creep of nylon, Catsiff *et al.* [5] carried the generalisation of the curves a stage further. The creep curves obtained at various loads, shown in Fig. 16.13, have been fitted to a single master curve by vertical and lateral shift and by multiplying the elongation scale by an appropriate factor. The



16.12 Generalised creep curves for viscose rayon at 6% r.h. [2].



16.13 (a) Creep curves for nylon at 36 °C and 30% r.h. under various stresses [5]. (b) Master creep curve.

experimental results for the various loads group closely round the master curve, and thus, in view of the considerable overlap, it would appear that the agreement is something more than an inevitable result of the procedure for obtaining the master curve.

16.2.4 Influence of various factors on creep

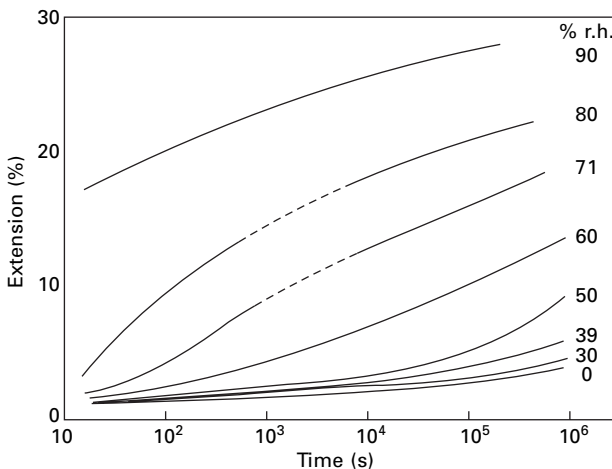
Steinberger [6] found that the creep of acetate increased with the humidity, as is shown in Fig. 16.14. The change was small below 40% r.h. but was considerable at higher humidities. With cuprammonium rayon, Steinberger found that the creep increased at high humidities, but at low humidities he obtained irregular results. Catsiff *et al.* [5] found a similar irregular behaviour in the effect of humidity on the primary and secondary creep of nylon over the whole range of moisture conditions, although the instantaneous elongation increased regularly with humidity.

Leaderman [4] found that the creep of acetate fibre increased as the temperature increased. This was also observed by Feughelman [7], who measured the creep of wool fibres in water at various loads and temperatures, with the results shown in Fig. 16.15. His results were found to fit relations of the form:

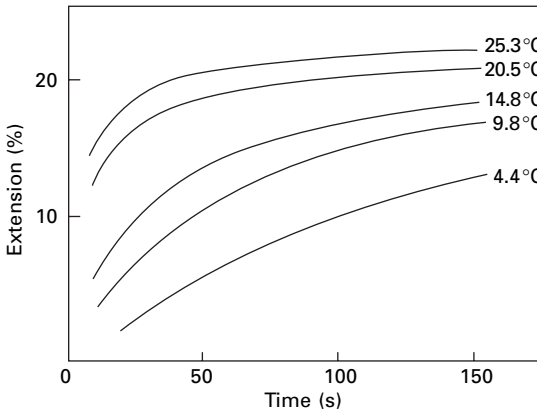
$$\frac{1}{\epsilon_t} = \frac{a}{t} + b \quad (16.2)$$

where ϵ_t is the strain at time t , and a and b are constants at constant temperature and load.

Ripa and Speakman [8] found a wide variation in creep rates in individual wool fibres, with a few fibres showing an abnormally high rate of creep. A fibre with a high rate of creep follows a normal creep curve for the first 60 min and then turns steeply upwards to give the rapid creep, which suggests that some primary resistance to extension has been broken down. Ripa and Speakman showed that the fibres with a



16.14 Effect of humidity on creep of acetate [6].



16.15 Effect of temperature on creep of a wool fibre under load of 58.8 mN in water [7].

high rate of creep had a low sulphur content, which suggested that the high rate was associated with a breakdown of cystine crosslinks.

16.2.5 A cumulative-extension test

A set of experiments that involves secondary creep is the cumulative-extension test used by Meredith and Peirce [9]. This test is also interesting as an example of a type involving a cycle of stresses and strains, and to some extent it simulates the repeated loading of fibres in use. This may show up behaviour different from that under a constant or steadily increasing stress or strain. As is indicated in Section 15.7.3, a pure recovery model would indicate a rapid approach either to break or to a limiting extension. The continuing effects are due to the viscoelastic behaviour of the fibre.

The method used was to apply cyclically to the specimen a simple harmonic extension followed by a period of dwell, during which any permanent extension was taken up. The time sequence is shown in Fig. 16.16. The extension was controlled by an eccentric cam and the dwell period with take-up of slack by the release of pawls on a ratchet. Because of the taking-up of the permanent extension, the stress would increase in each cycle, so that mechanical conditioning would not be effective.

The cumulative extension E_n after n cycles was defined by the relation

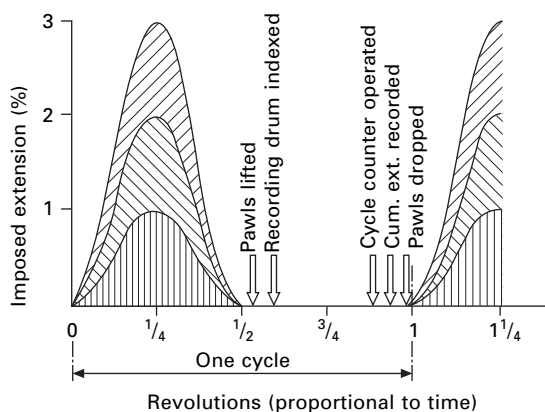
$$E_n = 100 \log \frac{l_n}{l_0} \quad (16.3)$$

where l_0 = initial length and l_n = length after n cycles. The advantage of this definition is that it is additive, for we have:

$$E_{0 \rightarrow 1} + E_{1 \rightarrow 2} = 100 \left(\log \frac{l_1}{l_0} \right) + \log \frac{l_2}{l_1} = 100 \log \frac{l_2}{l_0} = E_{0 \rightarrow 2} \quad (16.4)$$

For small strains, E_n is approximately equal to the simple strain, $100(l_n - l_0)/l_{0\%}$.

The samples tested were cords of 2000–20 000 den (222–2222 tex). Although they



16.16 Time sequence in cumulative-extension test.

were fibre bundles, they indicated comparative fibre behaviour. The tests were made at 65% r.h. and 21 °C. It was found that the residual tension had a considerable effect, since it determined the part of the stress–strain curve at which the test was operating. The standard value used was 10 mN/tex. The cumulative extension decreases as the frequency is increased; the standard tests were made at 1 cycle/second (1 Hz).

In expressing the results, one could give the cumulative-extension (1) after a given number of cycles of a certain imposed extension, (2) after a number of cycles of the same stress pattern, or (3) after the same amount of energy has been imposed in a given number of cycles. Each of these has some significance, and the difference between them is analogous to the difference between breaking extension, breaking load and work of rupture.

Table 16.1 gives examples of the results obtained in these tests. Fibres showing a high value of the cumulative-extension are those which suffer most permanent deformation as a result of repeated straining. Nylon and linen show the least cumulative-extension, though their properties differ in that linen breaks at a lower extension than does nylon. Wool stands up well to extension but extends permanently for large inputs of energy. Casein and viscose rayon show the largest cumulative-extensions.

The type of information given by tests such as this should be added to that given by simpler tests so that a ‘personality’ for each fibre can be built up.

Some of the fatigue testing described in Chapter 19 has used cumulative-extension testing; the simple recovery aspects of the problem are discussed in Sections 15.7.3 and 15.7.4.

16.2.6 Comparative creep behaviour

Except when cumulative-extension keeps imposing higher strains, creep is comparatively small in cellulosic and protein fibres, except at high loads. In nylon, primary creep is higher. The creep of nylon is also shown when it is used as a matrix in composites [10]. Table 16.2 shows results of tests made on yarns used in high-performance ropes. Polyester and aramid fibres show a small amount of creep. The creep of *Kevlar*

Table 16.1 Cumulative-extension results [9]

Material	Imposed extension of 2%				Cycles to break	Cumulative-extension (%) after imposed energy per unit mass of:	
	$E_n - E_1$		Stress in n th cycle (mN/tex)			0.1 J/g in 100 cycles	1 J/g in 1000 cycles
	$n = 10$	$n = 1000$	$n = 10$	$n = 1000$			
Cotton	1.98	—	68	—	331	5.2	breaks
Linen	0.66*	—	263	—	75*	1.0	1.1
Viscose rayon	1.79	10..8	51	80	1420	11.7	16.0
<i>Durafilt</i>	1.14	—	177	—	224	1.8	1.9
Acetate	0.35	2.48	37	49	>5000	18.5	breaks
Silk	0.36	1.92	108	144	>5000	1.0	1.6
Nylon	0.28	1.03	51	63	>5000	1.0	1.4
Wool	0.48	1.44	25	29	>2000	5.1	9.2
Casein	1.33	7.12	21	26	>2000	breaks	breaks

*Imposed extension of $1\frac{1}{2}\%$.

†Lilienfeld rayon, from 1948.

Table 16.2 Creep in one decade of log-time as quoted in *Deepwater Moorings: An Engineer's Guide*, TTI and Noble Denton [11]

	15% break load		30% break load	
	1–10 days	10–100 days	1–10 days	10–100 days
<i>Polyester</i>				
Diolen 855TN	0.240%	0.166%	0.093%	0.034%
Trevira 785	0.119%	0.069%	0.165%	0.009%
<i>Aramid</i>				
Kevlar 29	0.023%	0.066%	0.046%	0.021%
Kevlar 49	0.011%	0.030%	0.041%	0.009%
<i>HMPE</i>				
Spectra 900	1.7%	13%	broken	broken
	7/182 days*		0.7/4 days*	
Spectra 1000	1.1%	6.3%	8%	broken
	11/321 days*		1/28 days*	
Dyneema SK60	0.16%	0.47%	0.98%	8%
	70/>354 days*		7/123 days*	

*The figures in days for HMPE fibres are (time to start of rapid creep)/(time to break).

is due to the removal of misorientation at low stresses. Other liquid-crystal fibres, Vectran (melt-spun aromatic copolyester), PBO and M5, have little or no creep. Creep of HMPE fibres is covered in the next section.

16.2.7 Creep of high-modulus polyethylene (HMPE) fibres

The high creep of HMPE is a factor that has to be taken into account in using the fibre. It is not a problem for ballistic protection but would be for mooring oil-rigs for

long periods. The amount of creep varies with the type of HMPE fibre. The first commercial HMPE fibre, *Spectra* 900, had very severe creep as shown in Table 16.2. Adoption of a second heat treatment under tension in *Spectra* 1000 and *Dyneema* SK60 reduced the creep, and it was further reduced in *Dyneema* SK65 and SK75. Alternatively *Dyneema* SK76 is optimised for ballistic protection with high energy absorption.

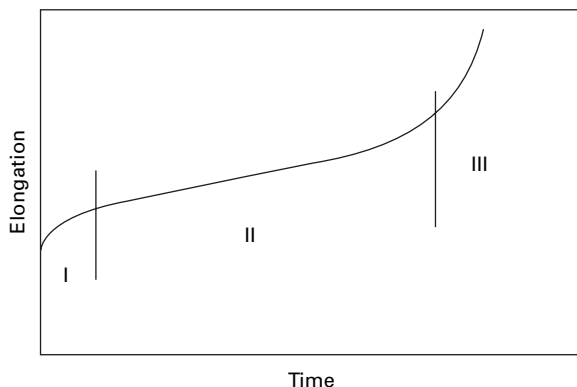
Extensive studies of creep of HMPE fibres have been reported by Govaert [12] and Jacobs [13]. The creep follows three regimes, as shown in Fig. 16.17: I creep rate decreasing with time (primary creep); II creep rate nearly constant (secondary creep); III increasing creep rate leading to fracture (tertiary creep). Creep increases under increasing load (Fig. 16.18(a)), and increasing temperature (Fig. 16.18(b)). Two other ways of showing creep data are given in Fig. 16.19. Plotting creep compliance (strain/stress) in Fig. 16.19(a) shows the extensibility increasing with time, stress and temperature. A Sherby-Dorn graph, introduced by Wilding and Ward [15, 16], is a log–log plot of creep rate against elongation. Figure 16.19(b) shows creep rate falling to a constant value at high elongations. Measurements of creep recovery by Govaert *et al.* [17] indicated that the creep could be divided into reversible and irreversible elongations (Fig. 16.20). Linearity of the log–log plot shows that each from can be represented by a power law, $\epsilon(t) \propto t^n$.

Jacobs [13] gives additional information on the effects of molecular weight and draw-ratio on creep of HMPE fibres. Increasing either will reduce creep, but makes fibre production processes more difficult. Creep can be reduced by using branched polyethylene or by crosslinking, but both have other disadvantages.

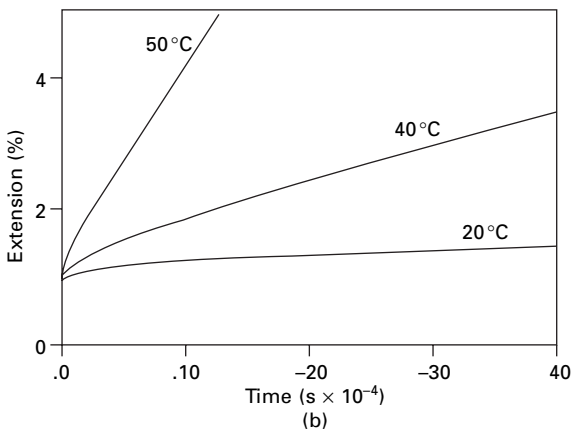
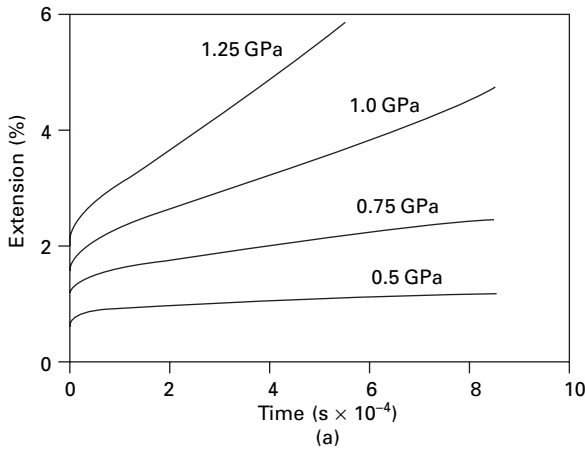
16.3 Stress relaxation

When a fibre is held stretched, its stress gradually decays. It may drop to a limiting value or may disappear completely. This phenomenon is known as relaxation.

Meredith [18] described an experimental procedure for investigating this. Attached to one end of the specimen, which was usually 20 cm long, was a strong spring. On the release of a catch, the spring extended the specimen to a stop fixed at a known



16.17 Three regimes in creep of HMPE fibre [13].

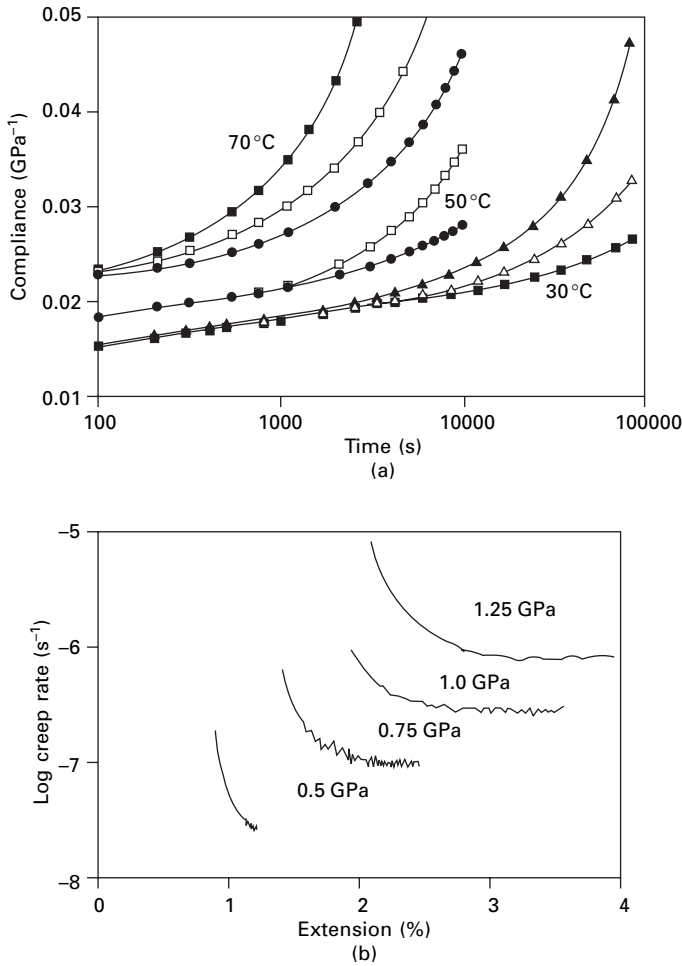


16.18 (a) Creep of *Dyneema* SK66 at 30°C under various loads. (b) Creep of *Dyneema* SK75 under 0.6 GPa at various temperatures [12].

extension. The extension of the specimen took less than 10 milliseconds, and thus the relaxation of the stress, indicated by a cantilever and mirror system, could be recorded from very short times up to a day.

Figure 16.21 shows a typical result for stress plotted against time. From this it appears that, after a rapid initial decay of stress, the rate of decay drops to zero. In fact, on plotting on a logarithmic scale, as in Fig. 16.22, it becomes clear that the stress is still decreasing after 24 hours. Meredith stated that the stress had not reached a constant value after 2 weeks. It will be seen that, between $1/10$ and 10^5 s, the decrease in stress is of the order of 50%, the exact percentage varying with the fibre and the extension.

The curious behaviour of acetate yarn, in which the stress in the first part of the test decays more rapidly at the higher extensions, so that after 1 s the stress is greater for a 2% extension than it is for larger extensions, is believed to be due to a temperature effect. A rapid extension beyond the yield point, with a large energy loss, causes a

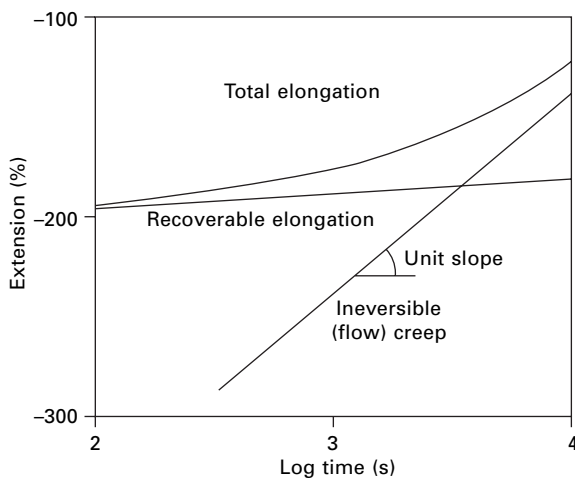


16.19 (a) Creep compliance of *Dyneema* SK66 at different temperatures and stresses. • 0.25 GPa; □ 0.4 GPa; ■ 0.5 GPa; △ 0.75 GPa; ▲ 1 GPa. From Jacobs [13] replotted from [14]. (b) Sherby-Dorn plot for creep of *Dyneema* SK66 in Figure 16.18 (a). From Jacobs [13] replotted from [14].

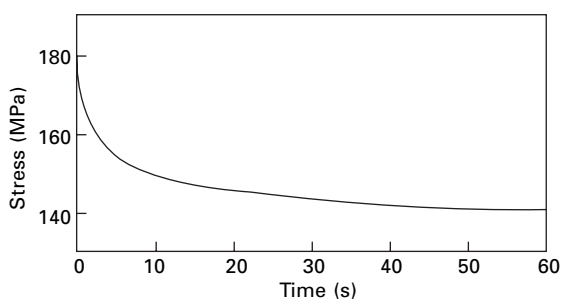
rise in temperature of the order of 11 °C for a 20% extension. It takes several seconds for the excess heat to be lost from the specimen, so that the initial part of the relaxation curve could be considerably affected.

Figure 16.23 illustrates the relaxation of wool fibres in water at various temperatures by plotting the ratio of the stress at a given time to the stress after 1 h against time on a logarithmic scale. There is considerable scatter in the results obtained on different fibres. The rate of relaxation increases as the temperature increases.

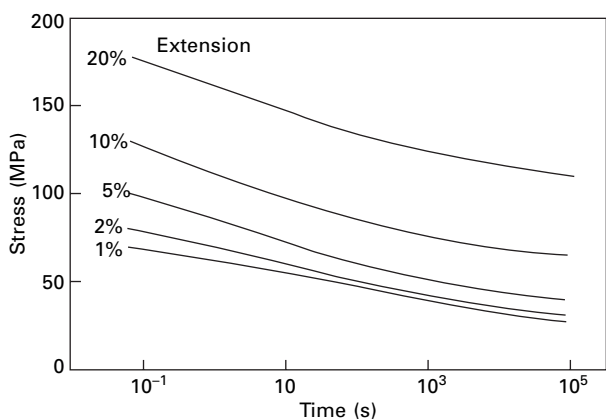
Feughelman [20] has pointed out that the effective initial modulus lies between high and low values, depending on the amount of time allowed for relaxation. The limiting values are the same for all humidities, but the relaxation time is about 500 min at 0% r.h., 100 min at 65% r.h 40 min at 90 r.h., and less than 1 min at 100% r.h.



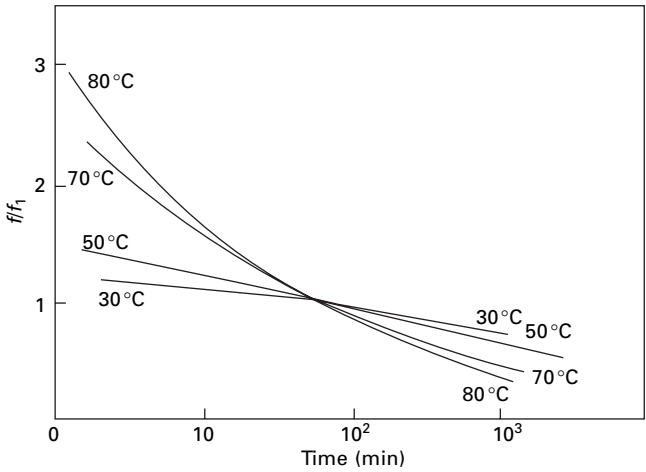
16.20 Recoverable and non-recoverable creep of HMPE fibres. From Jacobs [13].



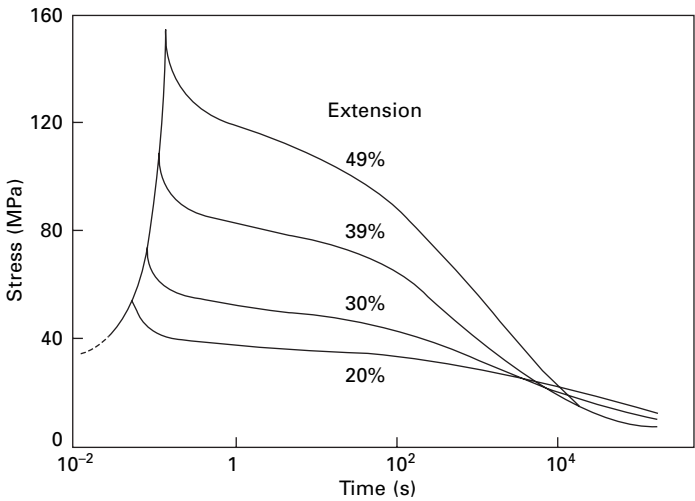
16.21 Stress relaxation in viscose rayon [18].



16.22 Stress relaxation in viscose rayon plotted against time on a logarithmic scale [18].



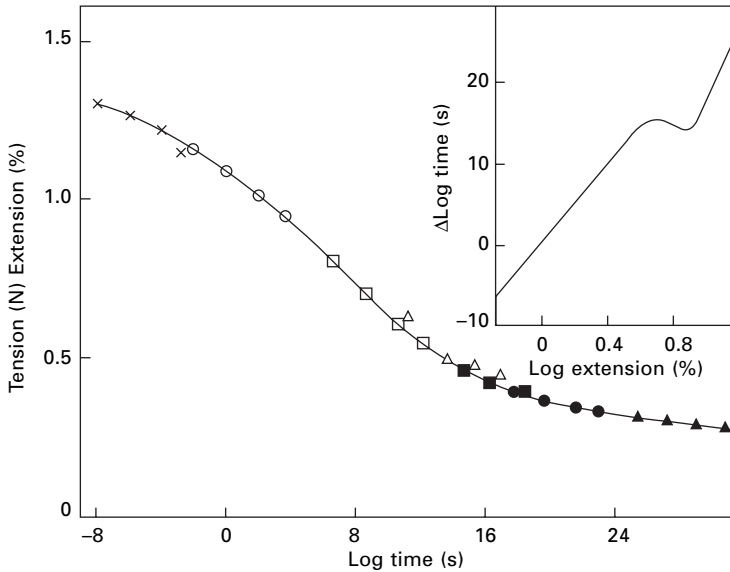
16.23 Relaxation of wool fibres in water with 15% extension at various temperatures [11] (f/f_1 is the ratio of the stress after the given time to the stress after 1 h).



16.24 Relaxation of human hair in water at 35 °C [21].

Figure 16.24 is an example of the relaxation behaviour of human hair in water, as studied by Wood [21]. It will be seen that the curves have a rather complicated shape, with two points of inflection –one between 1 and 10 s, and one between 1000 and 10 000 s.

The stress relaxation of nylon and polyester fibres at a range of temperatures and humidities has been studied by Meredith and Hsu [22]. The data for the polyester fibre relaxing at different strain levels may be presented as a composite sigmoidal curve as shown in Fig. 16.25. The curve as drawn is correct for relaxation at 1% extension, but for other extension values it must be shifted along the time-axis by an

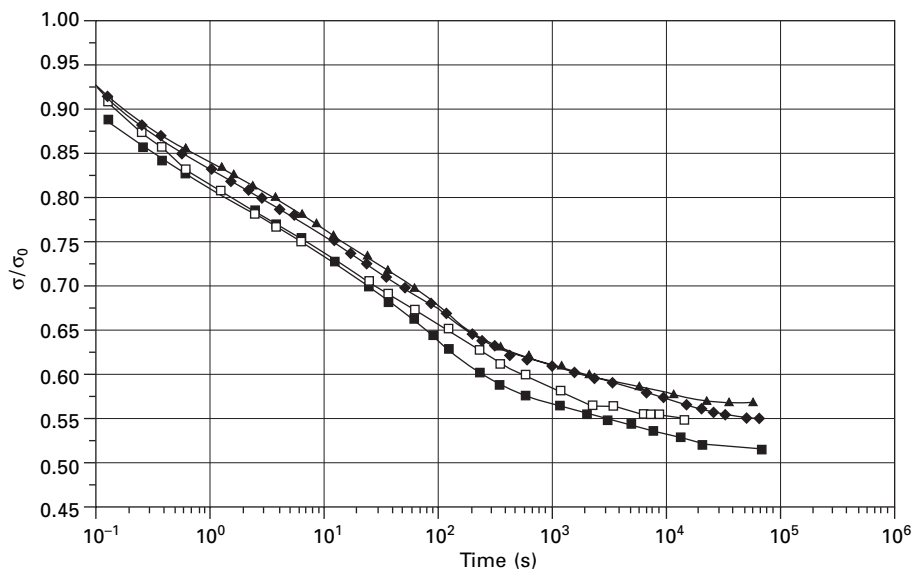


16.25 Composite stress-relaxation curve for a mechanically conditioned 150 den (17 tex) Terylene polyester fibre yarn at 65% r.h. and 25°C. The separate points are for tests for relaxation from different extensions. From Meredith and Hsu [22].

amount ($\Delta \log t$) shown in the inset graph. Superposition was not possible in this way for the nylon data, but Murayama *et al.* [23] were able to superpose stress relaxation curves for nylon for a constant extension of 2% at different temperatures. Both Murayama *et al.* [24] and Pinnock and Ward [25] have used time-temperature superposition on polyester fibre data. Figure 16.26 shows stress relaxation of nylon 6 [26]. A fast rate of elongation was used, so that measurement started at 0.1 seconds and continued for 1 day. The percentage decrease in stress is almost constant from different starting stresses and is almost the same for stress relaxation in water.

Figure 16.27 shows stress relaxation on polyester (PET) and nylon 6 fibres reported by van Miltenburg [27]. At various imposed elongations, stresses were monitored at 1 second intervals over 100 minutes and are shown as percentages of the stress at the start of the relaxation. In both fibres, the rate of stress relaxation increases rapidly to a maximum value (minimum in the residual stress plot) at around 2% extension. The changes correlate with values of the tangent moduli shown in the lower plots. A similar correlation was found for viscose rayon. Plots of the stress relaxation of HMPE and aramid fibres are shown in Figure 16.28. There was no correlation with tangent modulus, but these fibres have a different structure so that different mechanisms can be expected.

As described in Section 13.5.6 and shown in Fig. 13.29 and others, the stress-strain curves of nylon and polyester fibres may or may not show a minimum in the tangent modulus, depending on the prior treatment of the fibre. The nylon 6 fibre in Figure 16.26 has an almost constant tangent modulus, which would correlate with the lack of change of stress relaxation with starting stress.



16.26 Stress relaxation of nylon 6 in air at 65% r.h., 20 °C. From 0.96 cN/dtex □; 2.25 cN/dtex ▲; 2.99 cN/dtex ◆; 4.13 cN/dtex. After Selden and Dartman [26].

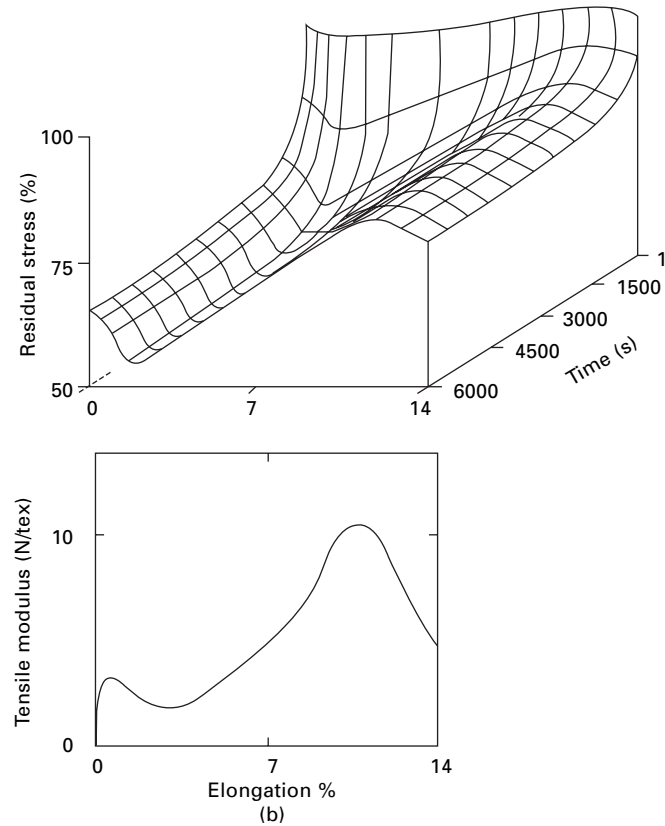
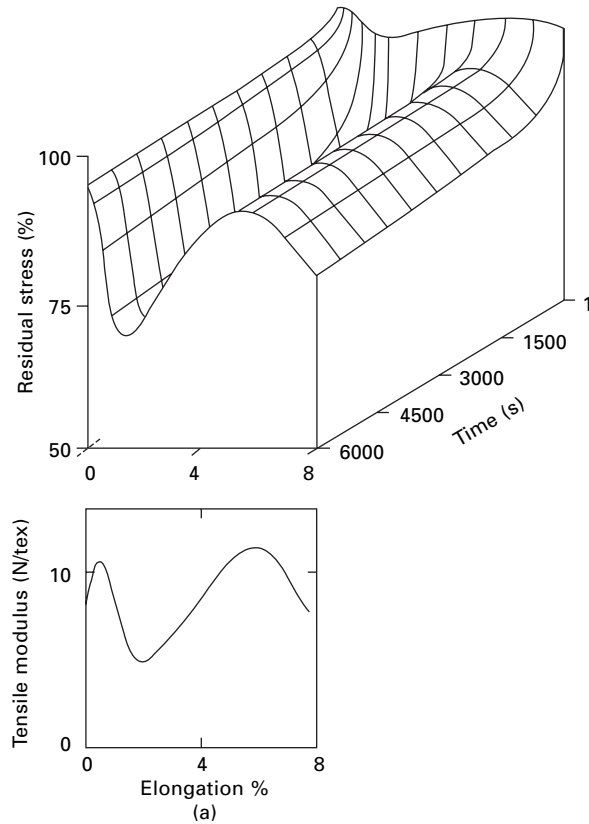
As demonstrated in Fig. 16.29, when a fibre is extended (OA) and immediately retracted (A→B→.....→G→H→I) at the same rate, it may show *inverse relaxation*. When retraction is stopped between A to P, the stress decreases as usual in stress relaxation. From P to Q, the stress first increases and then decreases. Beyond Q, there is only inverse relaxation. In the final section from G back to the original length at I, the fibre will buckle under zero tension. Nachane and Sundaram [28, 29] report on relaxation and inverse relaxation in polyester fibres and represent the behaviour by empirical equations with exponential terms. Whereas in extension the molecular structure is pulled into a less favourable state, from which it can relax towards equilibrium at a lower stress state, in substantial retraction it goes back beyond the equilibrium state and so the stress increases in inverse relaxation. The actual molecular mechanisms may be quite complicated.

16.4 Time and tensile testing

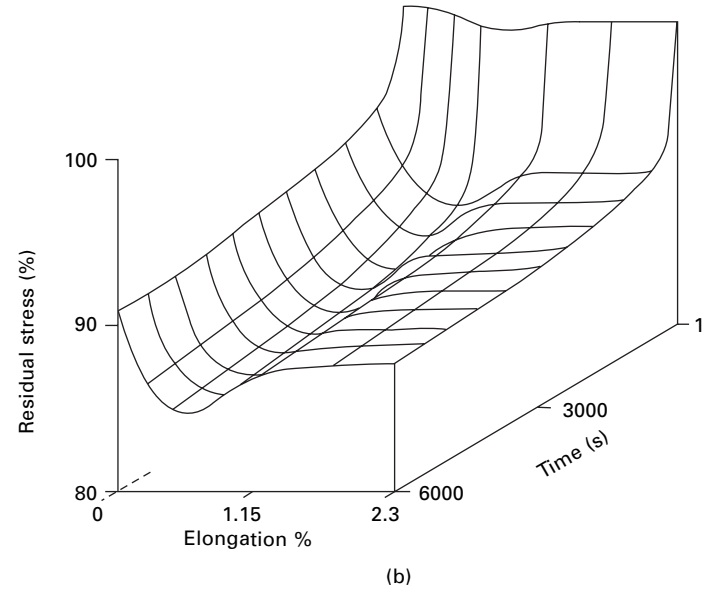
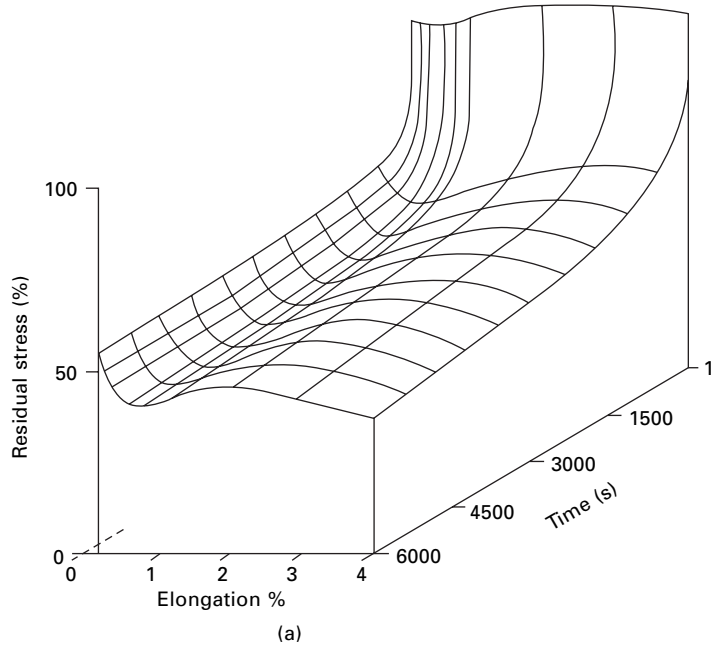
16.4.1 High-speed tests

At low speeds, that is, for tests lasting more than a few seconds, the conventional methods described in Chapter 13 can be used. At higher speeds, other methods must be adopted.

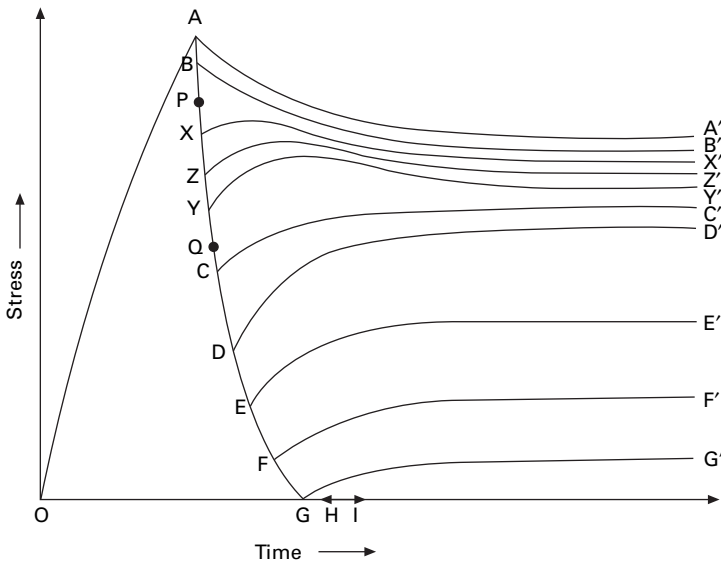
One way is to use an impact test. In this method, a moving large mass is engaged with one end of the specimen, while the other end is held fixed and connected to a load-measuring device. There must be appropriate mechanical arrangements to ensure that the free jaw is engaged only after the mass has attained its required speed. The moving mass may be a rotating flywheel [30], the bob of a pendulum [31], a falling



16.27 Upper diagrams: stress relaxation plotted against elongation and time to 100 minutes. Lower diagrams: tangent modulus plotted against elongation: (a) polyester (PET) yarn; (b) nylon 6 yarn. From van Miltenburg [27].



16.28 Stress relaxation plots over 100 minutes for: (a) gel-spun HMPE fibre; (b) aramid fibre. Note the scale difference: HMPE drops to a low of 40%, but aramid only to 85%. From van Miltenburg [27].

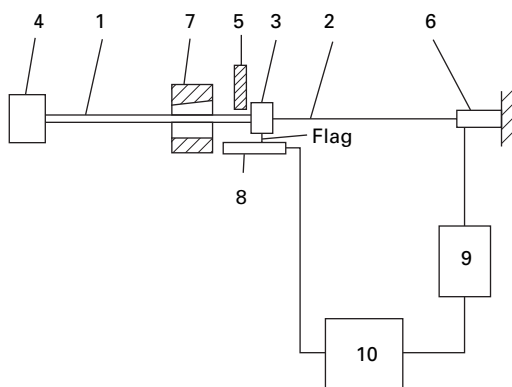


16.29 Inverse relaxation of polyester. From Nachane and Sundaram [28].

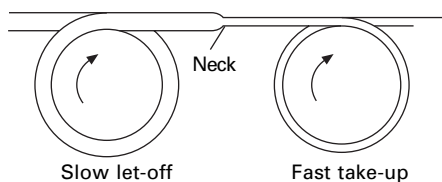
weight [32] or a rifle bullet [33–36]. In the past, the load measurement could be by means of a cantilever arm and mirror, recording on photographic paper, or by a resistance strain-gauge, a capacitive or inductive pick-up, or a piezo-electric crystal, connected through an appropriate circuit to an oscilloscope. Nowadays, digital recording would be used. If the weight is massive, its speed will not change on breaking the specimen, and thus there will be a constant rate of extension. If the recorder or oscilloscope has a linear time-base, it will record the load–elongation curve directly. In this way, rates of extension of from 10 to 3000% per second can be obtained.

At still higher rates of straining, the velocity of transmission of the strain along the specimen becomes important, and more complicated experimental arrangements are necessary. Schiefer and his colleagues [37–40] have been able to work out stress–strain curves at rates of straining of 1000–15 000% per second from successive photographs of the configurations of a clamped length of yarn subjected to a transverse impact. They had made earlier investigations at similar rates of straining by determining the lowest velocity of impact at which a yarn would break when one end was impacted, the other end being either free or attached to a small free mass.

Mi [41] adapted a catapult method, originally developed by Stevens and coworkers [42, 43] for heavy duty testing, for a study of wave propagation in twisted yarns. The essential principles of the method, which could be used to determine stress–strain relations, are shown in Fig. 16.30. A driving member (*Kevlar* cord), which is highly stretched, is joined to the test specimen by a clamped connector. When the clamp is released, the driving member rapidly contracts, thus extending the test specimen at a high rate. Force and displacement are recorded. The elongation velocity can be varied by altering the pre-strain of the driving member, but is limited by the mass of the connector. The deformation of the much lighter test specimen has little effect on the rate. The typical time for the connector to reach the stop was 1 millisecond. The



16.30 Catapult test method. 1, driving member; 2, test specimen; 3, connector; 4, stretching device; 5, quick release clamp; 6, force transducer; 7, stop device; 8, displacement detector (optical switches); 9, charge amplifier; 10, oscilloscope. From Mi [41].



16.31 Drawing of synthetic fibre.

initial rise in force and elongation is followed by a damped oscillation due to the impact of the clamp on the stop. If the stop was not present, elongation could proceed to break, but safety precautions would be needed.

16.4.2 Temperature and time: isothermal and adiabatic changes

In an imperfectly elastic material, energy will be dissipated in internal friction when the material is extended. This energy is represented by the area inside a hysteresis loop and is turned into heat. In a slow test, this heat will be given off to the surroundings and there will be no appreciable change of temperature of the specimen, but in a rapid test there will be less opportunity for loss of heat and the specimen will rise in temperature. Experiments thus range between two limiting cases: the isothermal, with no change of temperature, and the adiabatic, with no loss of heat. Since the properties of a fibre vary with temperature, the results obtained in the two types of test will be different, and this must be remembered in interpreting the effect of time.

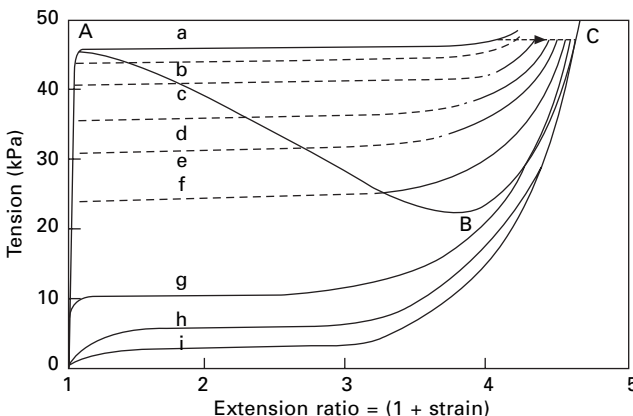
An interesting example of adiabatic (or nearly adiabatic) conditions occurs in the drawing of fibres. Marshall and Thompson [44] have shown that it offers an explanation of the occurrence of characteristic draw-ratios. The process is illustrated in Fig. 16.31. Any attempt to alter the draw-ratio by changing the relative speeds of the rollers merely results in the neck's moving backwards or forwards, the actual draw-ratio remaining constant. If the neck reaches the back roller, the filament breaks, and,

if it reaches the front roller, intermittent portions of undrawn material pass through. In either case, the technical consequences are serious.

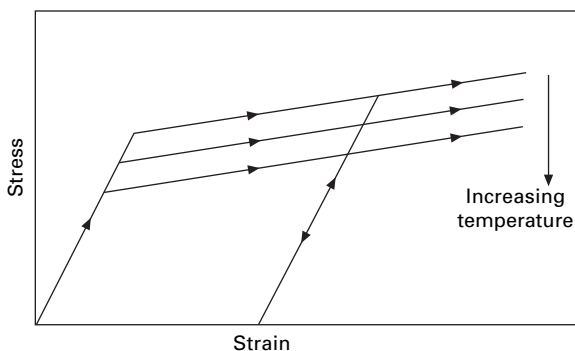
Figure 16.32 shows the isothermal stress–strain curves for (undrawn) polyester fibre. If extension takes place adiabatically, however, the temperature rises and the path OABC should be followed. But, under actual drawing conditions, a decreasing load is an unstable condition, so that the line AC is followed. It is this sudden increase in length past the unstable region ABC that results in the formation of a neck and determines the characteristic draw-ratio. If the whole process is slowed down, there will be some loss of heat, the temperature rise will be smaller, and thus the draw-ratio will be reduced. This is found in practice. The draw-ratio is also affected by the mean temperature at which the drawing is carried out.

Godfrey [45] examined the effect of heat dissipation during plastic deformation, taking account of heat transfer to the surroundings. The model assumes that the fibre behaves in the idealised elastic/plastic way shown in Fig. 16.33, with the plastic stress line decreasing linearly with increase of temperature. Figure 16.34(a) shows that, for a 7.2 dtex nylon fibre, the deformation is close to isothermal at a rate of extension of 10% per second and close to adiabatic at 500% per second. Figure 16.34(b) shows the reduction in tension as the specimen heats up. Godfrey's numerical data is expressed in terms of a dimensionless temperature rise, $\Delta T/T$, and a dimensionless time, t^* , which is proportional to imposed strain and depends on fibre dimensions, thermal and mechanical properties, and ambient conditions. For a thick (195 tex) nylon yarn, there is appreciable heating at a strain rate of 10% per second.

There may also be a difference, analogous to the difference between adiabatic and isothermal changes, due to the influence of moisture. As was discussed in Section 12.3.2, the equilibrium regain of a fibre at a given vapour pressure depends on the stress in the fibre. On the application of a tension to a fibre, its equilibrium regain increases. Consequently, there will be a difference between tests made rapidly, which



16.32 Isothermal and adiabatic load–extension curves of *Terylene* polyester fibre. Isothermals: a, 20 °C; b, 30 °C; c, 40 °C; d, 50 °C; e, 60 °C; f, 70 °C; g, 80 °C; h, 100 °C; i, 140 °C. Adiabatic: (A) from 20 °C. (Dotted portions obtained by interpolation).



16.33 Idealised fibre stress–strain curve with yield stress decreasing linearly with temperature.

will be at constant regain, and those made slowly, which will be at constant vapour pressure. Since the change in regain with tension is very small, the difference between the two will be small in tensile tests. A loss of moisture due to adiabatic heating would have a larger effect.

16.4.3 Influence of rate of loading on breakage

The breaking load of a fibre depends on the rate at which the load is applied. As a first approximation, we can say that the breaking extension is independent of the rate of loading. If we apply a constant load to a fibre, we get the behaviour shown in Fig. 16.35, that is, instantaneous extension followed by creep and then, when the critical extension is reached, breakage. The time for this to happen will be shorter the greater the load. Thus the time to break decreases with increasing load.

There is a similar effect in testing when the load is increased throughout the test. If the rate of increase of load is slow, there is more time for creep to occur, and consequently the breaking extension is reached at a lower load. The breaking load therefore increases as the rate of loading increases.

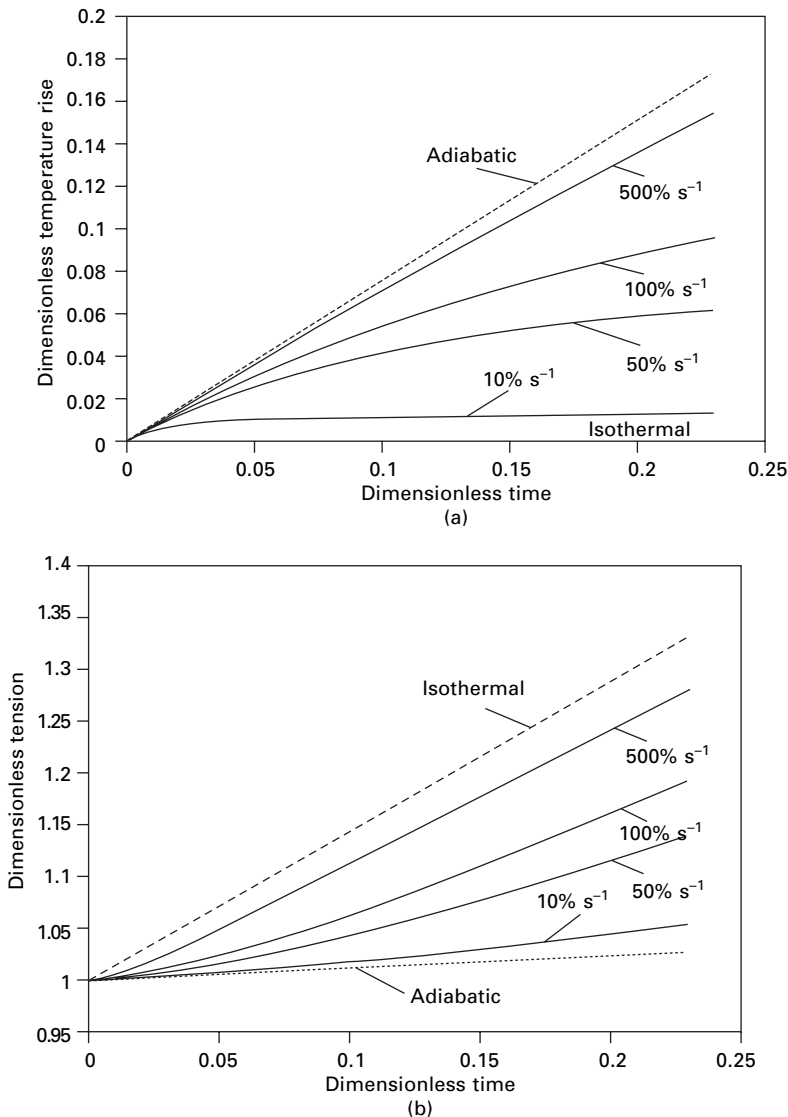
Meredith [30] tested yarns over a millionfold range of rates of extension and found that the relation between tenacity and rate of extension was approximately linear (actually slightly concave to the tenacity axis) for most fibres. For breaking times ranging between a second and an hour, the following formula may be used without much error:

$$F_1 - F_2 = kF_1 \log_{10}(t_2/t_1) \quad (16.5)$$

where F_1 is breaking load in a time t_1 , F_2 is breaking load in a time t_2 , and k is the *strength–time coefficient*.

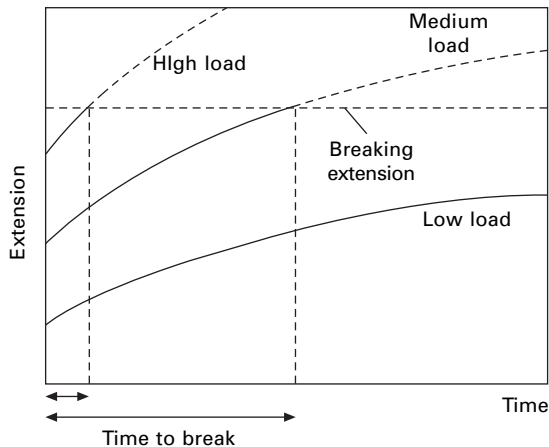
Values of the strength–time coefficient are given in Table 16.3. They show that the strength of these textile fibres increases by 6–9% for each tenfold increase of rate of extension. Meredith stated that the same formula applies to constant rate of loading and constant rate of extension tests.

Some values of tenacity and other tensile properties obtained in Schiefer's very



16.34 Simulated response of 7.2 dtex nylon fibre extended at various strain rates. Adapted from Godfrey [45].

high-speed tests are given in Table 16.4, together with comparative values obtained in ordinary tests. The increase in strength and modulus means that performance in ballistic testing is better than expected from low-speed tests, though the reduction in breaking extension will act in the opposite way. The counterpart to this is that performance will be worse for long-term loading as in mooring oil-rigs. Table 16.5 shows expected time to break under various percentages of the 1 minute break load. It is estimated that k is less than 0.05 for aramid yarns and slightly more for polyester. Since safety factors are below 50%, creep rupture is not significant for this application.



16.35 Breakage of fibre under various loads.

Table 16.3 Strength–time coefficients [46]

Material	<i>k</i>
Cotton	0.088
Viscose rayon	0.083
Acetate	0.060
Flax	0.079
Silk	0.079
Nylon	0.080
Wool	0.073

Table 16.4 Results of high-speed tests [32]

Material	Rate of straining (% per second)	Tenacity (N/tex)	Breaking extension (%)	Initial modulus (N/tex)
High-tenacity nylon	1/60	0.55	16.7	3
	5000	0.67	14.7	5
<i>Fortisan</i> (highly oriented)	1/60	0.56	5.4	14
cellulose)	2000	0.80	5.2	22
<i>Fiberglas</i>	1/60	0.42	2.8	22
	1000	0.54	1.8	28

Table 16.5 Creep rupture. From TTI and Noble Denton [11]

<i>k</i>	Time to fail at percentage of 1 minute break load			
	20%	30%	50%	80%
0.05	2×10^{10} years	2×10^8 years	2×10^5 years	200 hours
0.08	2×10^4 years	1000 years	3 years	5 hours
0.1	200 years	19 years	60 days	100 minutes

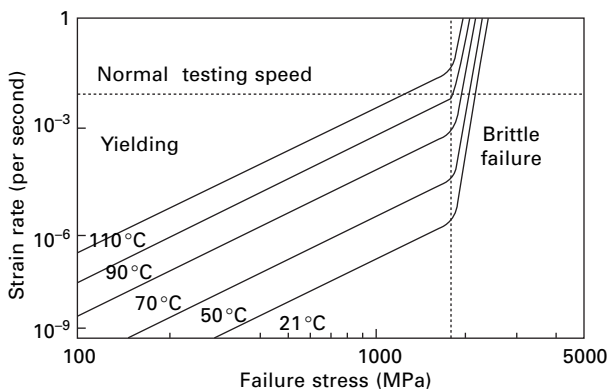
In a fatigue test, when some fibres in an assembly have broken, the increased stress on the remaining fibres leads to creep rupture as the final failure mechanism. For nylon, the loss of strength is marginal.

HMPE fibres do not follow equation (16.5), but fail more rapidly than a value of $k = 0.1$ would indicate. Creep rupture in long-term loading is a serious concern. Figure 16.36 shows how the strength of HMPE fibres at 21 °C has a tenfold decrease in strength between normal testing speeds and a rate of strain of $10^{-7}\%$ per second, which corresponds to a time to break of about 1 year. Figure 16.36 also shows the large influence of temperature. At lower temperatures in the sea, break would take longer, but in warm conditions it would occur sooner. Schwartz *et al.* [48] found that the strength of *Spectra* 900 increased from 2.13 GPa at a strain rate of 0.4% per minute to 3.34 GPa at 100% per minute. They express the results by a Weibull distributions associated with a power law breakdown rule.

The rate of extension affects the breaking extension in different ways for different fibres. Thus, in an acetate yarn, the breaking extension, which was about 30%, varied by less than 0.5% for rates of extension between 0001 and 1000% per second, but in a viscose rayon yarn the breaking extension increased from 20.6 to 26.6%, and in a silk yarn it increased from 15.3 to 23.1%, over the same range. In a nylon yarn, the breaking extension increased from 15.9% at 0.0013% per second to 20.7% at 22% per second and then decreased to 14.5% at 1096% per second. Where the strength increases with the rate of extension and the breaking extension is constant or increases, then the work of rupture will be greater in the more rapid breaks, but, in nylon at high speeds, the decrease in the breaking extension has a greater effect than the increase in breaking load, and the work of rupture decreases. This must be considered where fibres are used under impact conditions.

16.4.4 Stress–strain curves

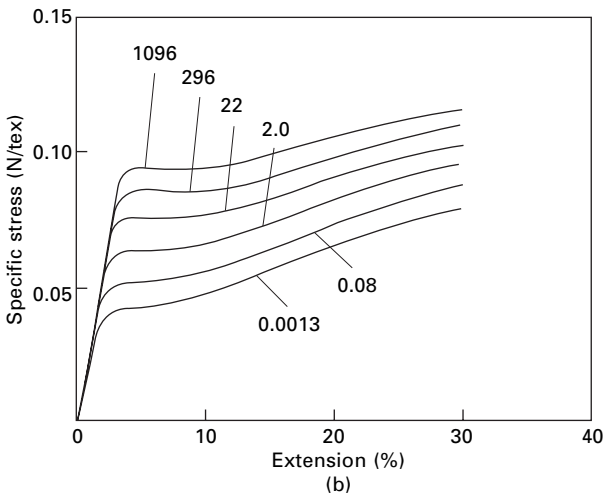
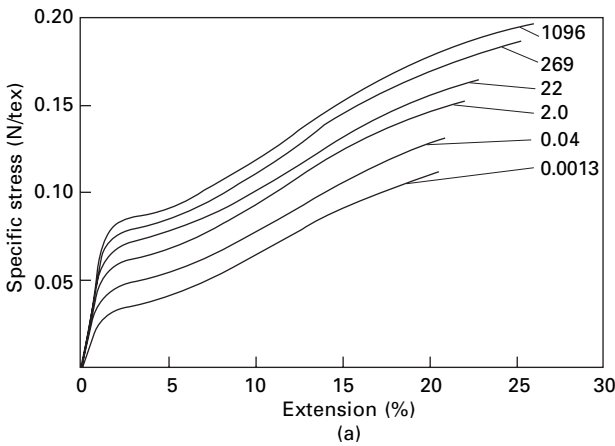
Stress–strain tests take some time, and consequently there is an opportunity for creep to occur. The slower the test, the more time there is available, and thus the greater the



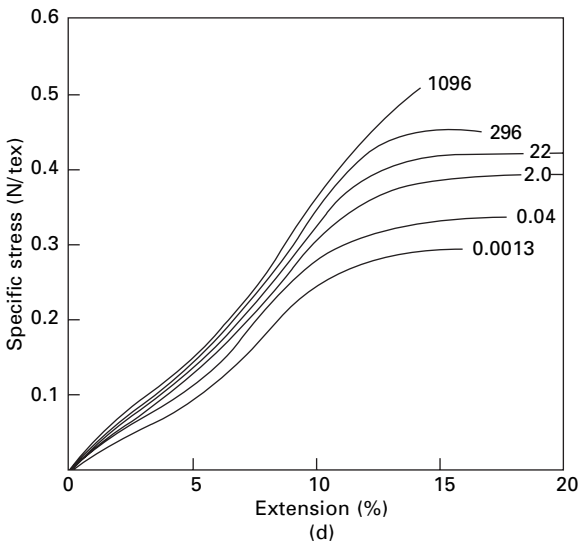
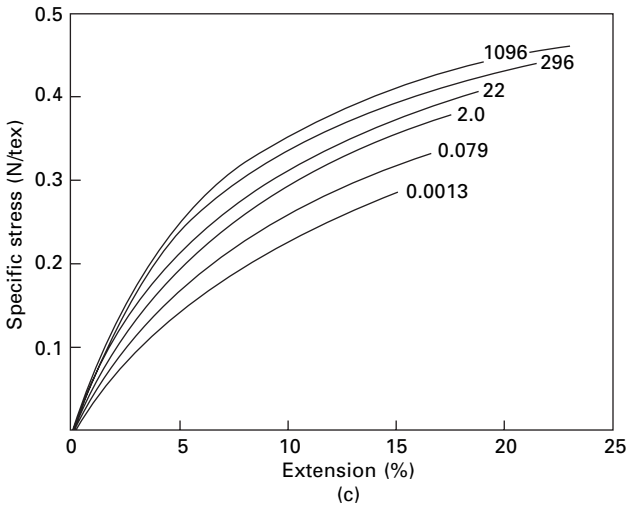
16.36 Effect of strain rate and temperature on breakage of HMPE (Dyneema) yarn. From van Dingenen [47].

extension at a given load. This is illustrated in Fig. 16.37, which shows results for viscose rayon, acetate, silk and nylon. Because of creep, the slower curves are nearer to the strain axis than the faster curves. This effect is particularly marked at the higher loads. There are two reasons for this. Near the end of the test, there has been more time for creep, and above the yield point the rate of creep is greater.

If the stress–strain curves are non-linear, there will also be a difference between constant rate of loading and constant rate of extension tests, owing to the different proportions of time spent on different parts of the curves. For a stress–strain curve that bends towards the strain axis, as in Fig. 16.38(a), we see that a greater proportion of the time is spent on the part of the curve at high loads in a constant rate of extension test than is the case in a constant rate of loading test. In the example shown, three-quarters of the time is spent above the point A and one-quarter below it, compared



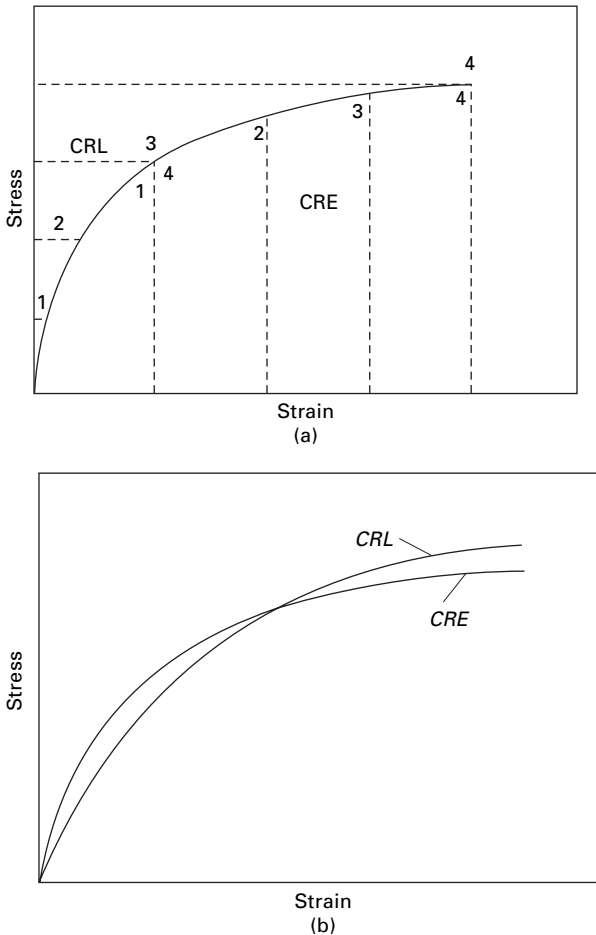
16.37 Stress–strain curves at various rates of extension [30]: (a) viscose rayon; (b) acetate; (c) silk; (d) nylon. The figures against the curves refer to the percentage rates of extension per second.



16.37 (Continued)

with the reverse proportions in a constant rate of loading test. The result of this is that, in a constant rate of extension test, whereas there will be slightly less creep in the early stages, there will be a greater total amount of creep at the end of the test, since the rate of creep is greater at high loads. The two curves will therefore differ as shown in Fig. 16.38(b).

The stress-strain curves obtained for a fibre thus depend on the time taken in the test and on the way in which the time is distributed. There will be consequent effects on the quantities, such as modulus and yield point, derived from the curve. An example of the change in Young's modulus (up to 1% extension) of wet wool with rate of extension is shown in Fig. 16.39. Meredith [30] also found that the initial



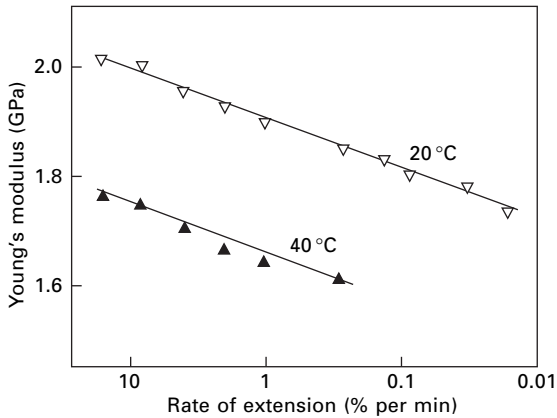
16.38 (a) Stress–strain curve showing equal intervals of time at constant rate of loading (CRL) and constant rate of elongation (CRE). (b) Difference between CRL and CRE curves.

modulus increased almost linearly with log (rate of extension). Values of the initial modulus obtained by Schiefer *et al.* [32] are included in Table 16.4. In viscose rayon and acetate, the yield points occur at increasingly higher stresses as the rate of extension increases, but the parts of the curves beyond the yield point are almost parallel.

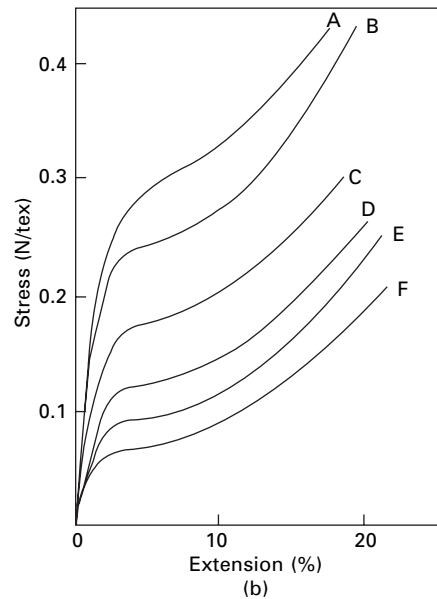
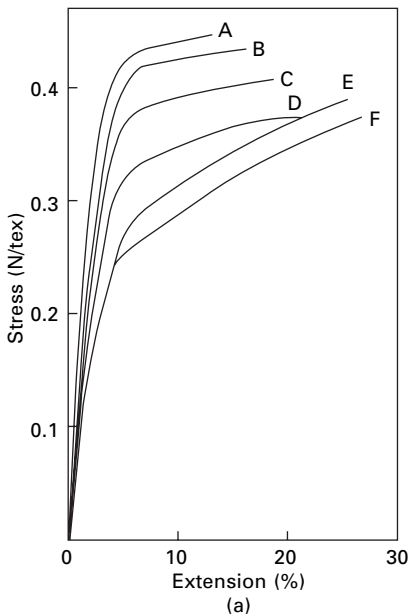
Hall [35] found that it was possible to express the stress–strain curves of rayon, nylon, polyester, acrylic and polypropylene fibres, at 12 rates of strain between 10^{-2} and 50 000% per second, by equations of the form:

$$\frac{\sigma}{\epsilon} = \frac{f_2(\epsilon) + f(t)}{f_1(\epsilon)} \quad (16.6)$$

where σ , ϵ and t are stress, strain and time, respectively. Hall's experimental results [50] for polyester and acrylic fibres are shown in Fig. 16.40.



16.39 Change of modulus of wet wool with rate of extension [49]: note that x-axis is for decreasing rate.



16.40 Stress–strain curves at various rates [50]: (a) polyester fibre: A, 23 000; B, 6400; C, 120; D, 7.7; E, 1.3; F, 0.018 % per second; (b) acrylic fibre: A, 60 000; B, 7500; C, 420; D, 7.7; E, 0.99; F, 0.001 % per second.

Determinations of stress–strain curves at high rates have also been reported by Holden [36], Smith *et al.* [34, 51] and Skelton *et al.* [52]. Smith *et al.* [51] found that, at a rate of extension of 4100% per second, polyester fibre yarn broke at 8% extension, without any yield region and at a higher strength level than in the fracture at low speed with breakage at 20% extension. The change in mode of fracture of nylon and polyester fibres is described in Section 19.2.1.

16.5 Dynamic tests

16.5.1 Static and dynamic testing

In the conventional methods of testing described in Section 13.4 and most of the high-speed tests described in Section 16.4.1, although the time of application has influenced the result, it has been possible to observe directly the stress–strain relation without considering the equation of motion of the system. Consequently, these tests may be described as static (or quasi-static) tests. There are, however, other tests in which the equation of motion must be considered, and these are one type of dynamic test. However, if there is a monotonic increase of stress, they are considered with the static tests. The high-speed impact tests described in Section 16.4.5 are examples of this situation. It is necessary to take account of the dynamic effects when the inertia, either of part of the apparatus or of the specimen, cannot be neglected. Thus the inertia effects involved in old-fashioned pendulum testers or in inclined-plane testers (Section 13.4.3) are examples of the occurrence of dynamic effects as sources of error in what are intended to be static tests. The dynamic tests dealt with in this section are of two types: (1) cyclic loading and (2) tests in such a short time that the propagation of the stress wave means that the stress cannot be regarded as constant along the specimen.

16.5.2 Characterisation of viscoelastic behaviour

It is now necessary to consider how the results of dynamic tests may be expressed. Let stress = f and strain = e at time t . If we apply a sinusoidal extension to the fibre (the converse argument will apply for sinusoidal loading), starting at time $t = 0$, we have:

$$e = e_m \sin \omega t \text{ for } t \geq 0 \quad (16.7)$$

where e_m is the strain amplitude, and ω is the angular frequency in radians/second (equal to $2\pi \times$ frequency in Hz).

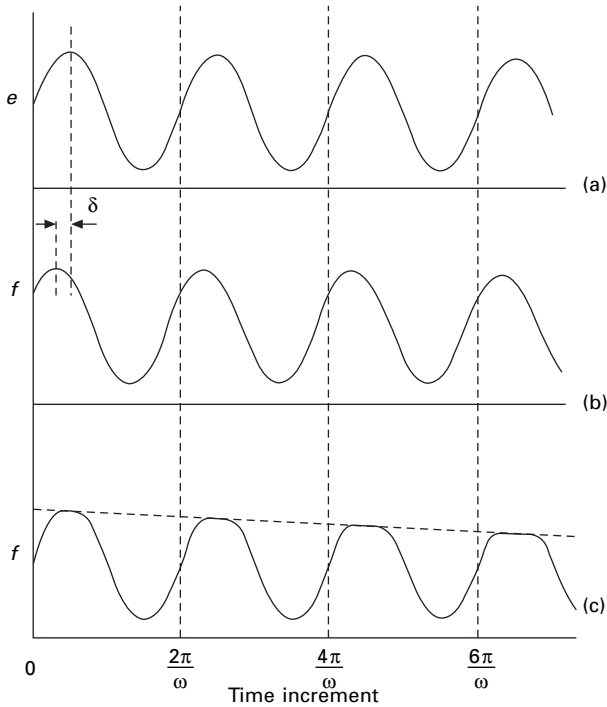
In general, the fibre will respond so that the stress f shows (1) an initial transient response; and (2) an ultimate ‘steady-state’ response, which may have a complex shape and which may change slowly with time owing to the effects of creep and stress relaxation.

The steady-state stress variation will certainly have an amplitude and be related in phase to the imposed extension. In the simplest situation, we can therefore put:

$$f = f_m \sin (\omega t + \delta) \quad (16.8)$$

where f_m is the stress amplitude and δ is the angular phase difference.

Equation (16.8) is only strictly valid for materials that obey the laws of *linear viscoelasticity*. For these materials, the interrelations between the various parameters discussed below will apply correctly, but for non-linear materials, including most fibres except at very small strain, the relations will be only approximately true. It is common practice to interpret the data from dynamic tests as if equation (16.8) were valid, the more complicated functional relation between stress and time being ignored. The differences are indicated in Fig. 16.41.



16.41 Dynamic structures and steady-state response: (a) imposed sinusoidal strain variation; (b) stress variation for linear viscoelastic material; (c) stress variation for a non-linear material, showing also a longer-term trend.

Another simplification is to separate the static and dynamic components of the stress and strain. Thus, when a sinusoidal extension is imposed on a constant extension, we have:

$$e = e_0 + e_m \sin \omega t \quad (16.9)$$

$$f = f_0 + f_m \sin (\omega t + \delta) \quad (16.10)$$

In the consideration of dynamic behaviour, the constant parts e_0 and f_0 can be ignored and equations (16.7) and (16.8) used instead of equations (16.9) and (16.10). This is particularly important in fibres, where the whole nature of the deformation changes owing to buckling if the stress f becomes negative. The dynamic variation must therefore always be superimposed on a static loading.

The subject is complicated by the number of ways in which the dynamic behaviour can be represented. We note that, with the above simplification, the response will be given by two parameters, but there are several possible pairs.

Representation (1):

The most direct method of expressing experimentally observed results is by quoting:

$$\text{modulus from ratio of amplitudes} = f_m/e_m$$

phase angle or loss angle = δ

However, these quantities are less convenient in other ways.

The phase lag is shown up as a hysteresis loop in the stress–strain relation.

Representation (2)

Equation (16.8) transforms to:

$$f = f_m (\cos \delta \sin \omega t + \sin \delta \cos \omega t) \quad (16.11)$$

Thus the stress response can be regarded as the addition of a component $f_m \cos \delta$, in-phase with the strain, and a component $f_m \sin \delta$, which is 90° out of phase.

This leads to a definition of the two quantities:

‘in-phase’ modulus (usually termed *dynamic modulus*)

$$= \frac{\text{in-phase stress amplitude}}{\text{strain amplitude}} = \frac{f_m \cos \delta}{e_m} = E \quad (16.12)$$

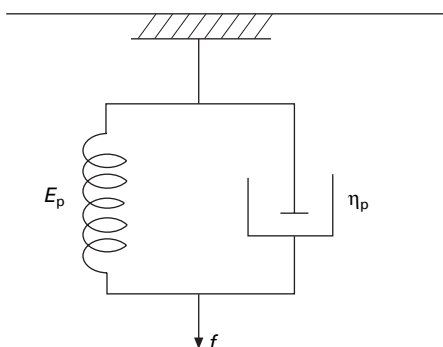
ratio of out-of-phase stress amplitude to in-phase stress amplitude
(usually termed *loss factor* or *dissipation factor*)

$$= \frac{\sin \delta}{\cos \delta} = \tan \delta \quad (16.13)$$

We may note that, in the analogous situation in alternating-current electricity, the quantity usually used is power factor = $\cos \phi = \sin \delta$, where $\phi = (\pi/2) - \delta$.

Representation (3): Voight model

A system that obeys equations (16.7) and (16.8) can be physically represented at any given frequency by an ideal (Hookean) spring, with stress proportional to strain, in parallel with an ideal (Newtonian) dashpot, with stress proportional to rate of strain, as shown in Fig. 16.42. The stress is given additively as:



16.42 Parallel combination of spring and dashpot (Voigt model).

$$f = E_p + \eta_p \frac{de}{dt} \quad (16.14)$$

where E_p is the spring modulus and η_p is the viscous coefficient of the dashpot.

Substitution from equation (16.7) gives:

$$\begin{aligned} f &= E_p e_m \sin \omega t + \eta_p \omega e_m \cos \omega t \\ &= (E_p^2 + \eta_p^2 \omega^2)^{\frac{1}{2}} e_m \left\{ \frac{E_p}{(E_p^2 + \eta_p^2 \omega^2)^{\frac{1}{2}}} \sin \omega t + \frac{\eta_p \omega}{(E_p^2 + \eta_p^2 \omega^2)^{\frac{1}{2}}} \cos \omega t \right\} \end{aligned} \quad (16.15)$$

We see that this is the sum of in-phase and out-of-phase components and is similar in form to equation (16.11), which thus proves the equivalence of the representation. The relations between the quantities are:

$$f_m = (E_p^2 + \eta_p^2 \omega^2)^{1/2} e_m \quad (16.16)$$

$$\tan \delta = \frac{\eta_p \omega}{E_p} \quad (16.17)$$

$$E_p = E \quad (16.18)$$

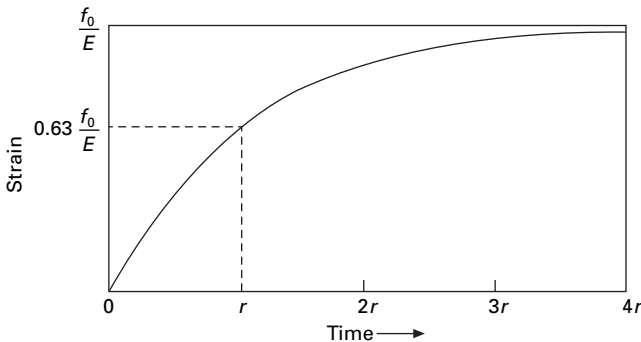
The parameter $\eta_p \omega$ is often used as an alternative to $\tan \delta$ to express the loss properties.

It may be noted that in a creep test, with constant f_0 , the basic equation (16.14) of the parallel model has the solution by integration:

$$e = \left(\frac{f_0}{E_p} \right) \left[1 - \exp \left(\frac{-E_p t}{\eta_p} \right) \right] = \left(\frac{f_0}{E_p} \right) \left[1 - \exp \left(\frac{-t}{\tau_p} \right) \right] \quad (16.19)$$

where $\tau_p = \eta_p / E_p =$ creep time constant. There is thus a link between this expression of the dynamic properties and exponential creep behaviour, illustrated in Fig. 16.43.

It must be remembered, however, that this will apply in this simple form if the parallel model is a complete representation of the system at all frequencies. But the



16.43 Behaviour of ideal specimen under constant load.

model was introduced here only to represent behaviour at a particular frequency. In general, the parameters E_p and η will vary with frequency.

Representation (4): Maxwell model

The behaviour at any given frequency can also be represented by an ideal spring in series with an ideal dashpot, as in Fig. 16.44. The basic equation of this model is given by the addition of strains in an infinitesimal increment of time:

$$\frac{de}{dt} = \frac{1}{E_s} \frac{df}{dt} + \frac{f}{\eta_s} \quad (16.20)$$

Substitution of equation (16.7) and rearrangement lead once again to an expression that is similar in form to equation (16.11). The parameters are related by the equations:

$$E_s = E \sec^2 \delta \quad (16.21)$$

$$\tan \delta = E_s / \eta_s \omega \quad (16.22)$$

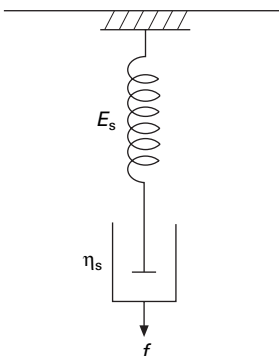
These quantities are less simply related to the other parameters and so are less useful. They do, however, provide a link to stress–relaxation behaviour because, with constant strain τ_0 , the solution of equation (16.20) is:

$$f = (E_s e_0) \exp(-E_s t / \eta_s) = (E_s e_0) \exp(-t / \tau_s) \quad (16.23)$$

where $\tau_s = \eta_s / E_s$ = relaxation time constant. But it must again be stressed that, in a real system, the parameters E_s and η_s would vary with frequency, so that the simple relations would not apply.

Representation (5)

In a single cycle, the energy loss per unit volume (or per unit mass, if f is a specific stress and the moduli are in corresponding units) is given, with the notation of equation (16.15), by:



16.44 Series combination of spring and dashpot (Maxwell model).

$$\begin{aligned}
\oint f \, d\epsilon &= \int_t^{(t+2\pi/\omega)} e_m (E_p \sin \omega t + \eta_p \omega \cos \omega t) e_m \omega \cos \omega t \cdot dt \\
&= e_m^2 \left[\frac{E_p}{2} \sin^2 \omega t + \eta_p \omega \left(\frac{1}{2} \omega t + \frac{1}{4} \sin 2 \omega t \right) \right]_t^{(t+2\pi/\omega)} \\
&= \frac{1}{2} e_m^2 \cdot 2\pi \eta_p \omega
\end{aligned} \tag{16.24}$$

The expression may be rearranged to give alternative forms

(energy loss/radian) per unit volume

$$= \frac{1}{2} e_m^2 \eta_p \omega = \frac{1}{2} f_m^2 \frac{\eta_p \omega}{(E_p^2 + \eta_p^2 \omega^2)} = \frac{1}{2} f_m e_m \sin \delta \tag{16.25}$$

This indicates why δ is referred to as a loss angle. The representation in this form is important because it shows that, when the out-of-phase component is large (high values of $\tan \delta$ or $\eta_p \omega$), then there will be considerable energy dissipation, with consequent heating, if the material is subject to cyclic loading.

Representation (6)

For further mathematical development of the subject, the use of complex number notation is useful, just as it is in alternating current electricity.

With $i = \sqrt{(-1)}$, we can put:

$$e = e_m \exp(i\omega t) = e_m (\cos \omega t + i \sin \omega t) \tag{16.26}$$

Our earlier basic relation, $e = e_m \sin \omega t$, thus corresponds to the imaginary part of the above expression. If we follow through the analysis, and, at the end, take the imaginary part, this will therefore represent the behaviour of the system¹.

We now introduce a complex modulus E with a real part E' and an imaginary part E'' : $E = E' + i E''$. By the usual definition of a modulus, we have:

$$\begin{aligned}
f &= Ee = (E' + iE'') e_m \exp(i\omega t) \\
&= e_m (E' \cos \omega t - E'' \sin \omega t) + ie_m (E' \sin \omega t + E'' \cos \omega t)
\end{aligned} \tag{16.27}$$

The imaginary part of this expression, $e_m (E' \sin \omega t + E'' \cos \omega t)$, is identical in form to the expression for f in equations (16.11) and (16.15), so that the equivalence of the representation is proved. The parameters of this representation, which is very widely used, are:

¹For this representation, though not for the others, it would have been simpler to shift the time origin, which is immaterial in the steady-state situation, and to use $e = e_m \cos \omega t$. The real part of the complex quantities would then correspond to the actual ('real') behaviour. But, since the $\exp(i\omega t)$ factor is dropped anyway in analysis, there is no great harm in the other notation.

real part of modulus (often termed real modulus)

$$= E' = E_p = E \text{ as defined above} \quad (16.28)$$

imaginary part of modulus (often termed imaginary modulus or loss modulus)

$$= E'' = \eta_p \omega = E' \tan \delta \quad (16.29)$$

The advantage of this approach for mathematical purposes is that the factor $\exp(i\omega t)$ can be omitted and the analysis performed with the modulus in either the vector or the complex form:

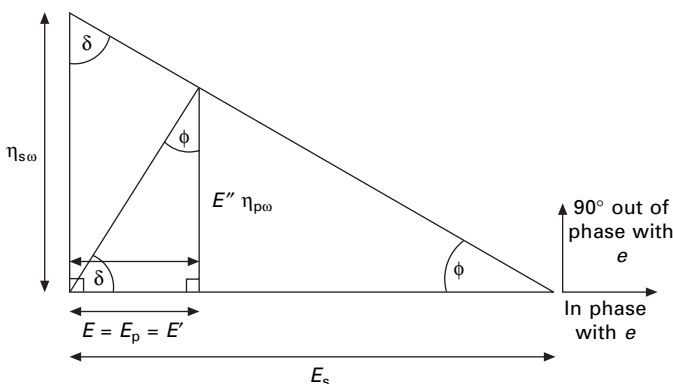
$$\mathbf{F} = \mathbf{E} \mathbf{e} = (E' + i E'') \mathbf{e} \quad (16.30)$$

At the end of the analysis, the real part gives the in-phase component and the imaginary part the out-of-phase component. This is particularly valuable in dealing with composite systems or complex geometries. The same rules apply as in Hookean elasticity.

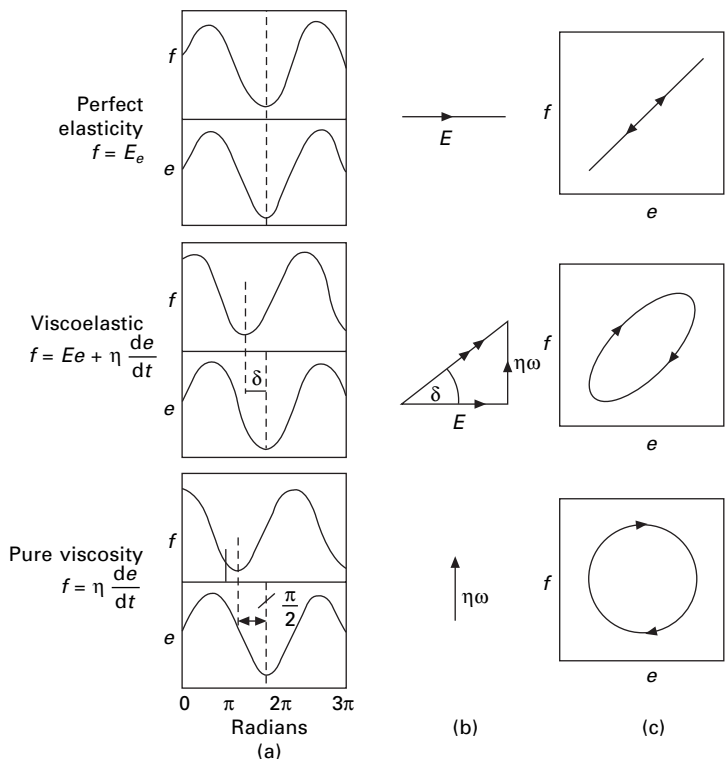
Summary of representations

The interrelations of the various representations are conveniently summarised by the vector diagram (Fig. 16.45). We note the identity of E , E_p and E' , which are often referred to as the *storage modulus* because they define energy stored and recovered, and the identity of E'' and $\eta_p \omega$, referred to as the *loss modulus* representing dissipated energy, and their close relation to $\tan \delta$. One extreme situation occurs when there is ideal elasticity, $\eta_p \omega = 0$; the stress is in phase with strain, and there is no energy loss. The other extreme occurs with pure viscosity, with $E_p = 0$, the stress 90° out of phase, and a large energy loss. The relations, together with the intermediate situation, are illustrated in Fig. 16.46.

The use of more complicated spring and dashpot models in an attempt to represent the complete behaviour of fibres, as distinct from a response at a single frequency, is discussed in Section 20.7.1.



16.45 Summary of representations of linear viscoelasticity.



16.46 Representation of perfectly elastic, purely viscous and viscoelastic materials: (a) relations between sinusoidal stress and strain; (b) vector diagram; (c) stress–strain curve.

Table 16.6 Frequency range of dynamic tests

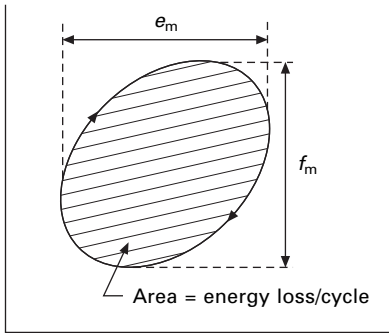
Method	Frequency range
Direct observation of stress–strain loop	up to 10 Hz
Free vibrations	1–50 Hz
Forced resonant vibration	1–300 Hz
Direct observation of forced vibrations	1–200 Hz
Flexural resonance of specimen (see Section 17.2.3)	20 Hz–10 kHz
Velocity of sound waves – continuous	500 Hz–30 kHz
Pulse velocity	10–100 kHz

16.5.3 Methods of dynamic testing

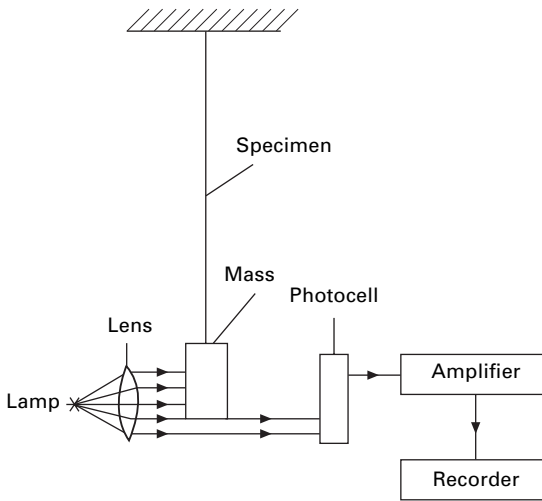
A variety of methods may be used in dynamic testing. The frequencies for which the methods described below have been used are given in Table 16.6.

Direct observation of stress–strain loop

At low frequencies (up to about 10 Hz), the methods described in Section 13.4 may be adapted to impose cyclic loading or extension and to record the stress–strain loop



16.47 Hysteresis loop obtained in stress-strain test.



16.48 Oscillations of a free mass attached to a fibre.

directly. The values of f_m , e_m and the energy loss are simply found from the loop as shown in Fig. 16.47, and hence the other parameters can be calculated. As has been stated, this is really a quasi-static method.

Free vibrations

A truly dynamic method available over much the same frequency range is the study of the free vibrations of a mass suspended by a filament. Figure 16.48 illustrates the method used by Ballou and Smith [53]. The vibrations of the mass modulate the amount of light received by the photocell, and thus the frequency and damping of the oscillation may be followed on the recorder. A linear variable differential transformer (LVDT) or laser measurement of displacement could now be used in this method.

If A is the area of cross-section, l the length of the specimen and x its extension beyond its rest position, the restoring force will be given by substituting $x = el$ in equation (16.14) and multiplying the stress f by A . The equation of motion of the system is therefore:

$$m \frac{d^2 x}{dt^2} - \eta_p A \frac{1}{l} \frac{dx}{dt} - E_p A \frac{x}{l} = 0 \quad (16.31)$$

where m is the suspended mass.

This is a damped simple harmonic motion, which will have a frequency given by:

$$\omega = \left(\frac{E_p A}{ml} - \frac{\eta_p^2 A^2}{4m^2 l^2} \right)^{1/2} \quad (16.32)$$

and a logarithmic decrement² given by

$$\lambda = \frac{\pi \eta_p A}{\omega ml} \quad (16.33)$$

From these expressions, E_p and η_p can be calculated. If the damping is small, the following approximate relations hold:

$$E_p = \frac{ml}{A} \omega^2 \quad (16.34)$$

$$\eta_p = \frac{\omega ml \lambda}{A} \quad (16.35)$$

In a similar method, Lincoln [54] recorded photographically the oscillations of an out-of-balance beam, one arm of which was connected to the specimen.

Van der Meer [55, 56] has used the free vibration of a torsion pendulum restrained by a pair of yarns, as illustrated in Fig. 16.49, to measure dynamic properties in air and water. At any instant, two yarn sections are extending and two are contracting, so that they are subject to a dynamic tensile loading.

Forced resonant vibrations

Alternatively, the specimen may be subjected to forced oscillations by means of an electromagnetic drive, as illustrated in Fig. 16.50. The equation of motion will then be:

$$m \frac{d^2 x}{dt^2} - \eta_p A \frac{1}{l} \frac{dx}{dt} - E_p A \frac{x}{l} = F \cos \omega t \quad (16.36)$$

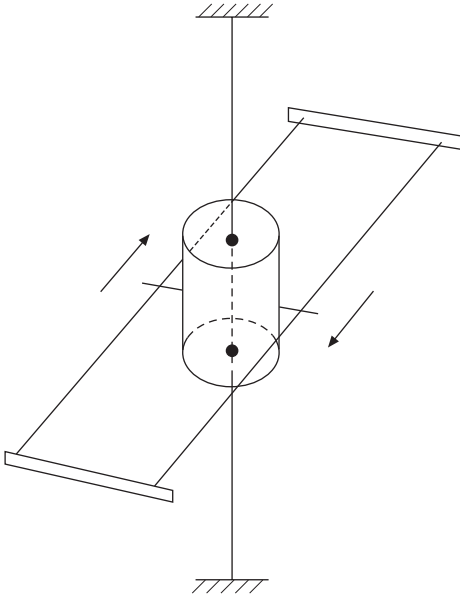
where F = amplitude of the applied force and ω = frequency of the forced vibration.

If the amplitude of the vibration is plotted against the frequency, it will give a resonance curve. The resonant frequency is given by:

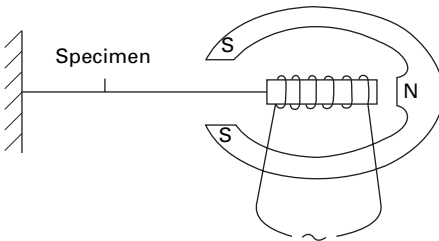
$$\omega_0^2 = \frac{E_p A}{ml} \quad (16.37)$$

and the width of the resonance curve, when the amplitude of the vibration is $1/\sqrt{2}$ times its maximum value, by:

²If x_1 and x_2 are successive maxima of the vibration in the same direction, the logarithmic decrement is defined by the relation $x_1/x_2 = e^\lambda$.



16.49 Torsion pendulum as used for tensile dynamic oscillation by van der Meer [55, 56].



16.50 Forced oscillations with electromagnetic drive.

$$\Delta\omega = \frac{\eta_p A}{2ml} \quad (16.38)$$

Thus the parameters E_p and η_p can be calculated. If the damping is large, slightly more complicated expressions must be used to find E_p and η_p .

A method suitable for use with single filaments between 1 and 100 Hz has been described in detail by Dunell and Dillon [57], and a similar method has been used by Tipton [58].

The vibrator consists of a solenoid of fine wire wound on a paper core and mounted in a magnetic field. Dunell and Dillon also discussed the corrections needed to take account of the frictional resistance and elastic reaction of parts of the vibrator itself. The use of this method is limited to conditions in which the length of the specimen is much less than the wavelength of the propagated wave. At high frequencies, the specimen must be short.

Direct observation of forced vibrations

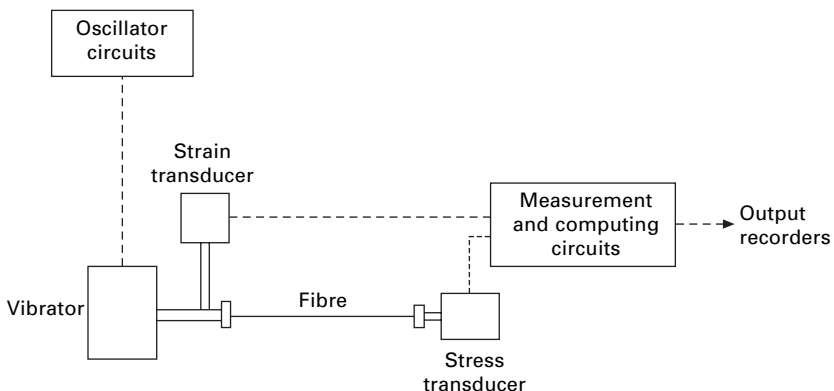
Probably the most widely used method is the direct observation of forced vibrations by means of the apparatus developed by Takayanagi [59, 60] (marketed as the *Rheovibron* tester) or similar procedures with newer transducers and digital recording and analysis. These instruments are often referred to as dynamic mechanical analysers (DMA). The *Universal Fibre Tester* [61, 62], which was derived from a fatigue tester described in Section 19.3, is an instrument that can be used in the same way.

The principle of the method is illustrated in Fig. 16.51. An oscillator, which can be set at various frequencies, typically 110 Hz, excites a vibrator, which subjects the fibre to a cyclic strain. A transducer at the other end of the fibre detects the resulting tension variation. The outputs from the load transducer and a strain transducer are fed to appropriate electronic circuits; and the values of the ratio of load to elongation and of $\tan \delta$ are directly indicated or recorded. Means of varying temperature are incorporated in the *Rheovibron* tester.

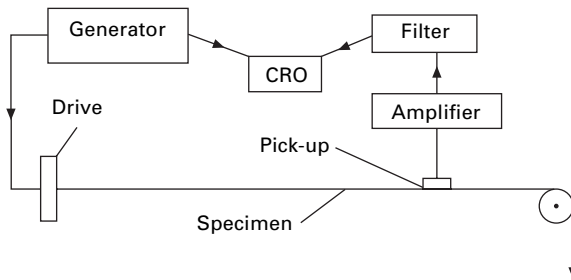
Velocity of sound: continuous transmission

At higher frequencies, the inertia of the specimen itself cannot be neglected, and the methods used must take account of this. The problem is essentially one of measuring the velocity of longitudinal (sound) waves in the specimen. The method was first applied by Lotmar [63], who excited the specimen by friction and matched the note produced with that of a standard specimen. Later, Ballou and Silverman [64] investigated the standing waves set up for certain positions of a reflecting pickup when one end of a filament was excited with a known frequency.

Probably the best method is the interference method adopted by Ballou and Smith [53], which could now be modified by analogue to digital conversion and signal processing. As illustrated in Fig. 16.52, one end of the specimen is excited electromagnetically, and consequently sound waves travel along the specimen and can be picked up by a piezo-electric crystal detector. The signal from the detector is amplified and filtered and fed into a cathode-ray oscilloscope (CRO), together with



16.51 Principle of *Rheovibron* tester.



16.52 Interference method for finding velocity of sound waves.

a signal direct from the generator. The resultant trace on the oscilloscope will depend on the difference in phase of the two signals and will be a maximum whenever the two are in phase. Thus, as the pick-up is moved along the specimen, an interference pattern of maxima and minima will be observed. The time taken for the waves to travel the distance between successive maxima must be equal to the period of the oscillation. Therefore:

$$c = L \left(\frac{\omega}{2\pi} \right) \quad (16.39)$$

where c = velocity of sound waves in cm/s, L = distance moved by pick-up between successive maxima and $(\omega/2\pi)$ = frequency in Hz.

If the damping is small, the velocity of sound in a medium is given by:

$$c^2 = \frac{E}{\rho} \quad (16.40)$$

where ρ = density. Thus the value of the dynamic modulus may be calculated. The specific modulus is equal to c^2 .

From the attenuation of sound along the specimen, which will be given by the reduction in amplitude of the interference pattern on the oscilloscope, we get:

$$\eta = \frac{2\rho\alpha c^3}{\omega^2} \quad (16.41)$$

where α = attenuation in nepers/cm.³

If the damping is appreciable, these expressions must be modified. Corrections must also be included for the effect of standing waves owing to reflection from the end of the specimen. The full expressions are given in the paper by Ballou and Smith [53].

A similar method was used by Hillier and Kolsky [65, 66], but they compared the transmitter and receiver signals connected to separate beams of a double-beam oscilloscope.

³Neper (Np) = $\log_e (x_1/x_2)$, where x_1 and x_2 are successive values of amplitude (in this case at 1 cm intervals). The neper is analogous to the decibel, which is based on \log_{10} . 1 Np = 8.686 decibel.

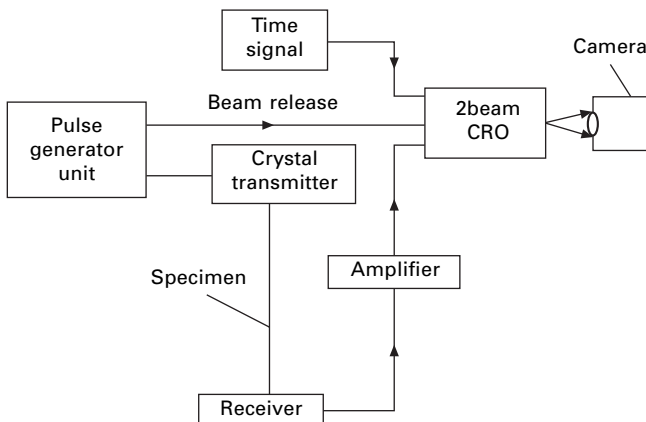
Pulse-velocity methods

Instead of exciting the whole specimen into continuous vibration, one may measure the velocity of a train of waves of known frequency by determining the time taken for a short pulse to travel along the specimen. This method has been used by Chaikin and Chamberlain [67] at 100 kHz. The circuit arrangements indicated in Fig. 16.53 illustrate the basic principles, but later instruments use other transducers, electronics and information technology.

A brief pulse of the required frequency is transmitted along the specimen from a crystal of Rochelle salt and eventually arrives at the receiver, which is a condenser microphone. The time of travel is measured by a method similar to that used in recording echo pulses in radar systems. At the instant that the pulse is transmitted, the two beams of a cathode-ray oscilloscope are released and start to travel at constant speed across the screen. The receiver is connected to one of the beams and a mark appears on the trace at the instant at which the pulse arrives. A timing unit is connected to the other beam to give a series of time marks. Thus the time taken for the pulse to travel can be found from a photograph of the traces.

In order to avoid errors due to delays in the circuit, the time taken for travel along specimens of varying length is determined. The slope of the graph of time against length, determined by the method of least squares, then gives the velocity of travel of the pulse. Young's modulus is given by equation (16.40): $E = \rho c^2$. The method is not suited to the measurement of attenuation, so the viscous parameter η cannot be found.

Another apparatus, incorporating two transducers, transmitter and receiver, that touch the specimen and an electronic circuit to measure the time interval for the pulse to travel from one to the other, has been described by Hamburger [68] and used by Moseley [69, 70]. It is commercially available as a pulse propagation meter (PPM). Some care is needed in the interpretation of results of pulse propagation tests, since at 10 kHz, as used by Moseley, and a typical recorded sonic velocity of 1 km/s, the wavelength will be 10 cm. This is about the distance apart of the transducers, so that



16.53 Pulse-velocity method.

the measurement is one not of a short pulse of waves travelling along the specimen, but of the times between the triggering of the transducers by the transient at the beginning of the pulse. This is a complex situation, which makes the true test frequency unknown and can lead to error if the pulse changes in shape during transmission. At higher frequencies, as used by Chaikin and Chamberlain [67], the error will be less. Mi [41] modified the PPM to have receivers at different distances on either side of the transmitter, which eliminated any errors associated with time detection differences at transmitter and receiver and allowed attenuation to be determined.

16.5.4 Cyclic dynamic modulus

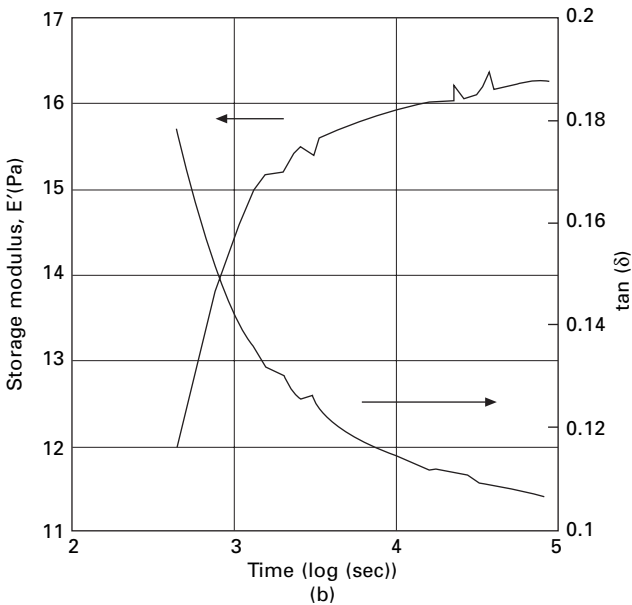
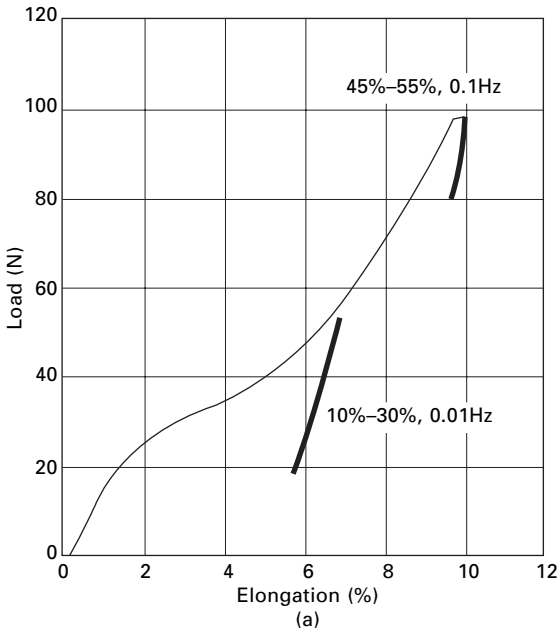
The fact that the dynamic storage and loss moduli are not the constant values of the simple model is shown in studies by Bosman [71]. Figure 16.54(a) shows cyclic loading plots at different positions on the load–elongation curve of a high-tenacity polyester yarn. The continuing shift of the hysteresis loops is due to creep. Other tests were carried out at constant strain amplitudes. Figure 16.54(b) shows that the moduli change with number of cycles, the storage modulus increasing and the loss factor ($\tan \delta$) decreasing. Figure 16.55(a) shows that the dynamic modulus E' increases with increasing mean load and decreases with increasing strain amplitude. Figure 16.55(b) shows that the loss modulus E'' is independent of mean load but increases with strain amplitude. The latter effect has important consequences for heating when large fibre assemblies, such as ropes, are cyclically loaded. Not only is there a direct effect of the increased amplitude but the rise in E'' , which is also shown in a plot of $\tan \delta$, means that a larger fraction of the input energy is dissipated as heat. $\tan \delta$ increases from 0.006 at 0.25% strain amplitude to 0.15 at 2%, a 25-fold increase.

Selden and Dartman [26] report the values for nylon 6 given in Table 16.7. The most consistent effects are an increase in both E' and E'' with pre-load, a decrease in E' and an increase in E'' with dynamic strain. Values of $\tan \delta$ are only slightly higher at the higher dynamic strain.

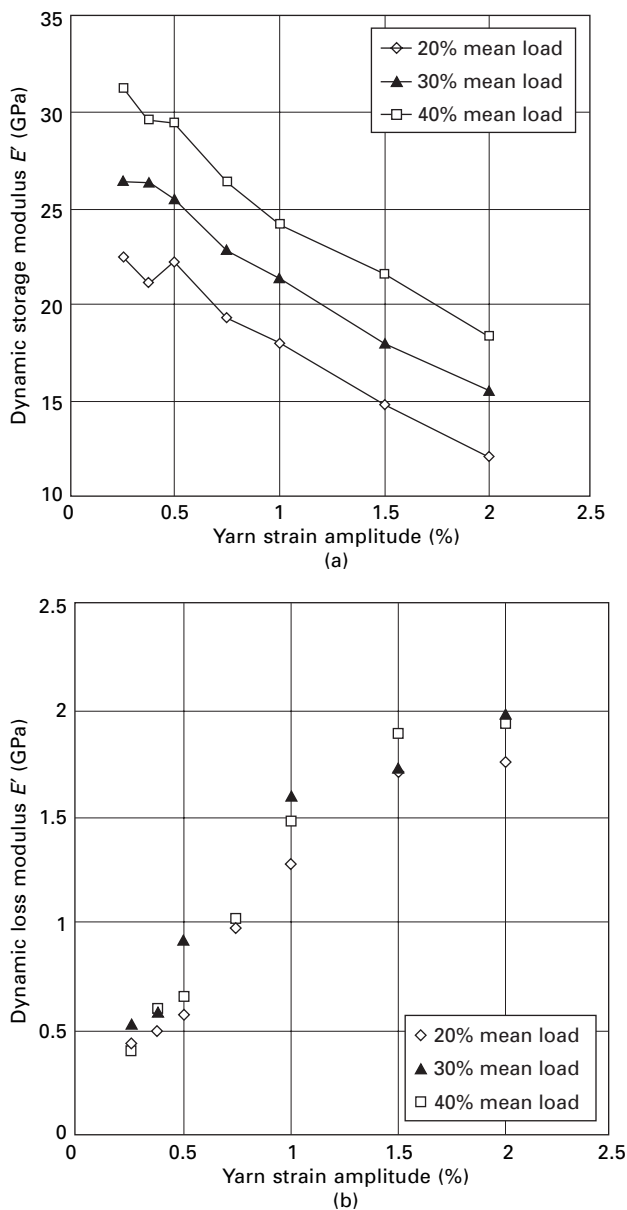
16.5.5 Values of dynamic modulus

The relation of the dynamic modulus (sonic modulus) to the moduli determined by a stress–strain test is illustrated by the results of Charch and Moseley [69], shown in Fig. 16.56. For an *Orlon* acrylic fibre yarn, the dynamic modulus, measured with a 10 kHz pulse, had a value of 14.7 N/tex, which was somewhat larger than the value of 12.4 N/tex observed for the initial modulus in a stress–strain test at 1700% per second, and considerably larger than the value of 7.9 N/tex found at 1/60% per second (1% per minute). Similar results were obtained for other fibres.

In continuing extension, the incremental modulus given by the slope of the curve decreases markedly at the yield point. By contrast, the dynamic modulus, which shows up the response to a superimposed oscillation, usually increases. Even up to strains as small as 1%, Chaikin and Chamberlain [67] found a small but significant increase in the dynamic modulus of nylon, though the values for wool and hair were constant.



16.54 (a) Cyclic loading at percentage of break load and frequency indicated at different parts of the stress-strain curve of high-tenacity polyester yarn showing also some creep in successive cycles. (b) Change in dynamic modulus E and $\tan \delta$ with time at 0.1 Hz, 30% of mean break load and 2% strain amplitude. From Bosman [71].

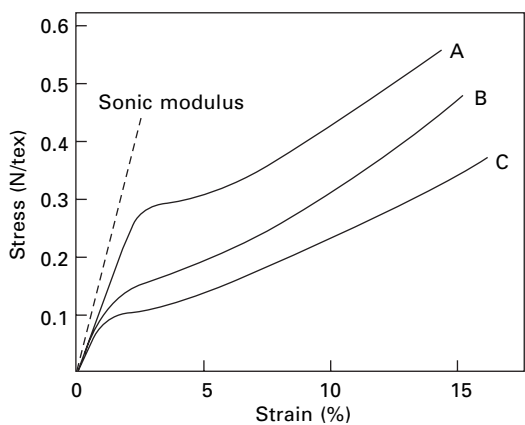


16.55 Change in (a) dynamic modulus E' and (b) loss modulus E'' of high-tenacity polyester yarn after 10 000 cycles at various mean loads and strain amplitudes.

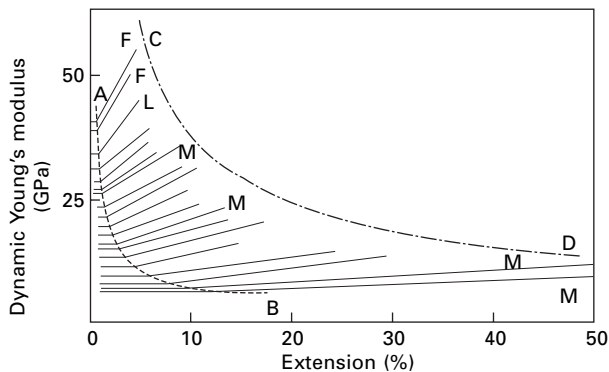
Figure 16.57 shows results obtained by de Vries [72] for a variety of regenerated-cellulose fibres. The variation of dynamic modulus with extension falls into two parts: up to a critical strain, e_c , the modulus is constant, with a value E , but above this value it increases linearly with strain. The critical values for the various fibres fall on a curve given by:

Table 16.7 Dynamic moduli of nylon 6 fibres. Based on Selden and Dartman [26]

Pre-load (mN/tex)	E' (GPa)			E'' (GPa)			$\tan\delta$		
	0.1 Hz	1 Hz	10 Hz	0.1 Hz	1 Hz	10 Hz	0.1 Hz	1 Hz	10 Hz
Dynamic strain = $\pm 1\%$									
27	1.39	1.69	1.97	0.32	0.37	0.34	0.23	0.22	0.17
45	2.56	2.71	3.14	0.54	0.64	0.58	0.21	0.24	0.18
91	2.58	3.55	4.14	0.82	0.77	0.59	0.32	0.22	0.14
182	5.14	7.28	8.19	1.15	0.96	0.75	0.22	0.12	0.09
Dynamic strain = $\pm 2\%$									
27	1.08	1.56	1.78	0.27	0.40	0.40	0.25	0.26	0.22
45	1.45	2.00	2.25	0.37	0.51	0.49	0.26	0.26	0.22
91	1.77	2.63	3.08	0.58	0.54	0.51	0.33	0.19	0.11



16.56 Stress–strain curves of *Orlon* acrylic fibre yarn at rates of strain of: A, 1700; B, 1.7; C, 0.017% per second, showing relation of initial slope to dynamic modulus [69].



16.57 Dynamic modulus of cellulose fibres. AB is locus of e_c . CD is locus of breaking extensions in tensile tests. F, saponified acetate; L, Lilienfield rayon; M, model filament; remainder are viscose rayon [72].

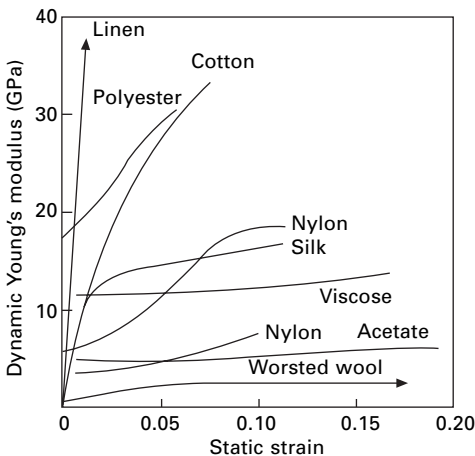
$$E_c \cdot e_c^{0.63} = 1.73 \text{ kN/mm}^2 \quad (16.42)$$

The critical strain e_c is found to be more nearly equal to the yield point given by recovery experiments than to that given by the shape of the stress–strain curve. De Vries also found that, during relaxation of stress at constant extension, the dynamic modulus changed very little, and not at all after the first 30 s, even though the stress decreased by as much as 30%. Measurements of dynamic modulus during load–extension tests carried out at various rates also indicate that the dynamic modulus reaches equilibrium in less than a minute as a single-valued function of the strain. This value is independent both of the particular stress-history of the specimen leading to the given strain and of the value of the stress in the specimen at the time of measurement. It was, however, found that only values of E above the critical strain were reversible; once a specimen had been extended into the range of increasing E , the initial constant portion of the curve was not repeated.

Figure 16.58 shows values obtained by Tipton [58] for a variety of textile yarns. He also found that the dynamic modulus fell slightly and that the loss factor increased as the amplitude of the dynamic strain was increased.

The orientation and crystallinity of the specimen will have a considerable influence on the dynamic modulus. Table 16.8 shows the various types of regenerated-cellulose filaments studied by de Vries, together with the values of the dynamic modulus at low strain. The modulus is much greater in the more highly oriented specimens. The effects of both crystallinity and orientation in *Dacron* polyester are shown in Table 16.9, which presents data obtained by Ballou and Smith [53]. Other values, obtained by the pulse propagation technique, have been reported by Dumbleton [73].

If other factors are unchanged, the dynamic modulus can be used as a measure of orientation; but care must be taken, since many treatments, for example, the effect of annealing or hot stretching of synthetic fibres, change the structure in other ways, which also influence the modulus. It must be remembered that all one is measuring



16.58 Dynamic modulus with static strain for various textile yarns [58].

Table 16.8 Dynamic modulus of regenerated-cellulose filaments at 8.8 kHz [72]

Material	E_c (GPa)
Nearly isotropic model filaments	5.4
Stretched model filaments	5.4–23
Viscose rayons of low, medium and high tenacity	8–20
Very high-tenacity viscose rayon	20–30
Lilienfeld rayon	35
Fortisan	40

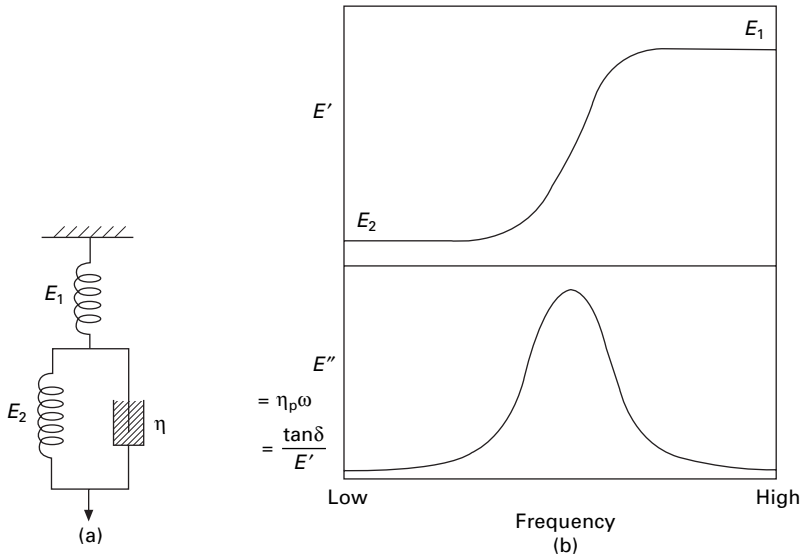
Table 16.9 Viscoelastic constants of poly(ethylene terephthalate) [53]

Frequency	Orientation	Crystallinity	E (GPa)	η (N s/mm ²)	$\tau = \eta/E$ (μ s)
8 Hz	None	None	2.3	1.11	480
8 Hz	None	High	0.95	0.53	560
8 Hz	High	None	11.4	4.67	410
8 Hz	High	Low	12.0	6.48	540
8 kHz	High	Low	15.3	0.020	1.3
12 kHz	High	Low	15.3	0.012	0.8
16 kHz	High	Low	15.3	0.008	0.55
34 kHz	High	Low	16.3	0.007	0.45

in determining the dynamic modulus is the response of the fibre as a whole to a rapid cyclic extension.

16.5.6 Transitions in dynamic moduli

There are many mechanisms by which a fibre can deform. Some of these, such as the stretching of atomic bonds, are characterised by large stresses and small strains but occur at very high speed; others, such as the uncoiling of chains, lead to large strains under low stresses but take a long time owing to viscous drag. The typical effect of one of these mechanisms on the dynamic moduli is illustrated by the simple model shown in Fig. 16.59(a). At high frequencies, only the stiff mechanism operates and the modulus is high, but at low frequencies the soft mechanism can operate and the modulus is low. At the extremes, there is little energy loss: at high frequencies, there is little viscous displacement; at low frequencies, there is little viscous resistance. But near the transition, when the structure is just becoming mobile, the viscous resistance is very important in causing a large energy loss, or, what comes to the same, in causing a large phase lag. The ‘loss’ quantities (E'' , $\eta_p\omega$, $\tan \delta$) will therefore go through a maximum, as shown in Fig. 16.59(b). With a variety of mechanisms, a sequence of drops in E' and peaks in E'' can be expected. Unfortunately, there are no studies of fibres over a wide enough range of frequencies to enable one to plot experimental data analogous to Fig. 16.59(b). However, it is found that the modulus increases with frequency; for example, Chaikin and Chamberlain [67] obtained the comparative values given in Table 16.10. This table also includes some data from other sources.



16.59 (a) Simple model of viscoelastic behaviour. (b) Real and imaginary moduli of model.

Table 16.10 Dynamic modulus values

Fibre	E' (GPa)				E'' (GPa)
	Static [67]	1.5–100 Hz [57]	10 kHz [68]	100 kHz [67]	1.5–100 Hz [57]
Viscose rayon	4.2	10.6	17.1	19.5	0.48
Wool	3.1			8.6	
Nylon	2.9	5.8	8.5	7.0	0.38
Steel	1.93			1.98	

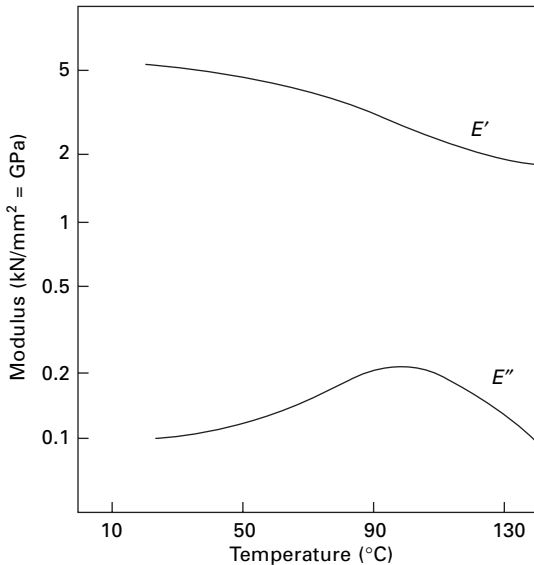
It is possible, however, to observe the transitions by causing the structure to loosen up, to become mobile, for oscillations of a given frequency. This can be achieved by raising the temperature, so that thermal vibrations become more effective, or by plasticising the structure, most easily with water, so that the intermolecular forces are reduced.

The thermal transitions will be discussed in detail in [Chapter 18](#), but one example is given here. [Figure 16.60](#) shows the changes in the real and imaginary (loss) modulus of nylon 6.6 fibres with a transition at about 90 °C.

The transitions in dynamic properties can also be studied in bending or torsion, as will be described in the next chapter.

16.5.7 Strain-wave propagation: limiting impact velocity

At very high rates of extension, or impact, the tension wave (or stress wave) and the associated strain wave take a significant time to travel along the fibre. Smith *et al.*



16.60 Real and imaginary dynamic moduli of nylon 6.6 fibres. From Murayama *et al.* [23].

[33] have studied the propagation of strain waves along yarns. The theory and the interpretation of data are complicated, but the order of magnitude of the effects can be indicated by noting that the strain wave front velocity is about 3900 m/s in a polyester fibre yarn and 2800 m/s in a nylon yarn. A comparison of experimental results with a theoretical prediction suggested that appreciable creep and stress relaxation occurred within 50 μ s of impact but that there was no creep or stress relaxation between 50 and 300 μ s. The very rapid effects will, of course, be due to different mechanisms from the slow creep and relaxation discussed previously. Mi [41], using the PPM found similar values for the wave velocity in polyester and nylon and 7500 m/s in aramid (*Kevlar*). Attenuation of the signal was as $\exp(-\eta L)$, where η is the attenuation coefficient and L is the length travelled, so that there is a decrease of 0.37 times in a length $1/\eta$. The values of $1/\eta$ were: nylon, 2.3 m; polyester, 3.4 m; aramid 20 m.

As the speed of impact is increased, a point is reached at which the material is unable to accommodate the rapid displacement of the end of the specimen by propagating strain along the specimen. There is thus a critical velocity at which the specimen breaks on impact. Smith *et al.* [74] have shown how the critical velocity may be estimated from stress-strain curves. The estimated values lie between 100 and 300 m/s for different yarns and are generally greater in fibres with an appreciable region of low modulus at the high level of extension before break.

16.6 References

1. N. J. Abbott. *Text. Res. J.*, 1951, **21**, 227.
2. M. T. O'Shaughnessy. *Text. Res. J.*, 1948, **18**, 263.

3. J. J. Press. *J. Appl. Phys.*, 1943, **14**, 224.
4. H. Leaderman. *Elastic and Creep Properties of Filamentous Materials and Other High Polymers*, the Textile Foundation, Washington, DC, 1943.
5. E. Catsiff, T. Alfrey and M. T. O'Shaughnessy. *Text. Res. J.*, 1953, **23**, 808.
6. R. L. Steinberger. *Text. Res.*, 1936, **6**, 191, 267.
7. M. Feughelman. *J. Text. Inst.*, 1954, **45**, T630.
8. O. Ripa and J. B. Speakman. *Text. Res. J.*, 1951, **21**, 215.
9. R. Meredith and F. T. Peirce. *J. Text. Inst.*, 1948, **39**, T159.
10. W. J. Lou and C. I. Tseng., *Polymer Composites*, 1997, **18**, 492.
11. TTI and Noble Denton. *Deepwater Moorings: An Engineer's Guide*, Oilfield Publications, Ledbury, 1999.
12. L.E. Govaert. PhD thesis, Eindhoven University of Technology, 1990.
13. M. J. N. Jacobs. PhD thesis, Eindhoven University of Technology, 1999.
14. D. J. Dijkstra and A. J. Pennings. *Polymer Bulletin*, 1988, **19**, 75.
15. M. A. Wilding and I. M. Ward., *Polymer*, 1978, **19**, 919.
16. I. M. Ward. *Polymer Eng. Sci.*, 1984, **24**, 724.
17. L. E. Govaert, C. W. M. Bastaansen and P. J. R. Libland. *Polymer*, 1993, **34**, 534.
18. R. Meredith. *J. Text. Inst.*, 1954, **45**, T438.
19. S. M. Katz and A. V. Tobolsky. *Text. Res. J.*, 1950, **20**, 87.
20. M. Feughelman. *Appl. Polymer Symp.*, 1971, No. **18**, 757.
21. G. C. Wood. *J. Text. Inst.*, 1954, **45**, T462.
22. R. Meredith and B. Hsu. *J. Polymer Sci.*, 1962, **61**, 253.
23. T. Murayama, J. H. Dumbleton and M. L. Williams. *J. Macromol. Sci. (Phys.) B*, 1967, **1**, 1.
24. T. Murayama, J. H. Dumbleton and M. L. Williams. *J. Polymer Sci. A-2*, 1968, **6**, 787.
25. P. R. Pinnock and I. M. Ward. *Polymer*, 1966, **7**, 255.
26. R. Selden and T. Dartman. *Textile Res. J.*, 1998, **68**, 264.
27. J. G. M. van Miltenburg. *Textile Res. J.*, 1991, **61**, 363.
28. R. P. Nachane and V. Sundaram. *J. Textile Inst.*, 1995, **86**, 10.
29. R. P. Nachane and V. Sundaram. *J. Textile Inst.*, 1995, **86**, 20.
30. R. Meredith. *J. Text. Inst.*, 1954, **45**, T30.
31. W. J. Lyons and I. B. Prettyman. *Text. Res. J.*, 1953, **23**, 917.
32. H. F. Schiefer, W. D. Appel, J. F. Krasny and G. G. Richey. *Text. Res. J.*, 1953, **23**, 489.
33. J. C. Smith, C. A. Fenstermaker and P. J. Shouse. *Text. Res. J.*, 1965, **35**, 743.
34. J. C. Smith, C. A. Fenstermaker and P. J. Shouse. *Text. Res. J.*, 1963, **33**, 919.
35. I. H. Hall, *J. Polymer Sci. A-2*, 1967, **5**, 1119.
36. G. Holden. *J. Text. Inst.*, 1959, **50**, T41.
37. J. C. Smith, F. L. McCrackin, H. F. Schiefer, W. K. Stone, and K. M. Towne. *Text. Res. J.*, 1956, **26**, 281.
38. W. K. Stone, H. F. Schiefer and G. Fox. *Text. Res. J.*, 1955, **25**, 520.
39. F. L. McCrackin, H. F. Schiefer, J. C. Smith, and W. K. Stone. *Text. Res. J.*, 1955, **25**, 529.
40. J. C. Smith, F. L. McCrackin, and H. F. Schiefer. *Text. Res. J.*, 1955, **25**, 701.
41. Z. X. Mi. PhD thesis, University of Manchester, 1983.
42. G. W. H. Stevens and F. C. Bluett. Aeronautical Research Council, Current Papers, No. 1061, 1969.
43. G. W. H. Stevens and J. C. H. Longrigg. RAE Technical Report, No. 69108, 1969.
44. I. Marshall and A. B. Thompson. *Proc. Roy. Soc.*, 1954, **A221**, 541.
45. T. A. Godfrey. *J. Textile Inst.*, 2001, **92**, 16.
46. R. Meredith. In *Fibre Science*, J. M. Preston (Editor), The Textile Institute, Manchester, 2nd edition, 1953, p. 260.
47. J. L. J. van Dingenen. In *High-performance Fibres*, J. W. S. Hearle (Editor), Woodhead Publishing, Cambridge, 2001, p. 62.

48. P. Schwartz, A. Netravali and S. Sembach. *Textile Res. J.*, 1986, **56**, 502.
49. J. Sikorski and H. J. Woods. *Proc. Leeds Phil. Soc.*, 1950, **5**, 313.
50. I. H. Hall. *J. Appl. Polymer Sci.*, 1968, **12**, 731, 739.
51. J. C. Smith, P. J. Shouse, J. M. Blandford and K. M. Towne. *Text. Res. J.*, 1961, **31**, 721.
52. J. Skelton, W. D. Freeston and H. K. Ford. *Appl. Polymer Symp.*, 1969, No. **12**, 111.
53. J. W. Ballou and J. C. Smith. *J. Appl. Phys.*, 1949, **20**, 493.
54. B. Lincoln. *J. Text. Inst.*, 1952, **43**, T158.
55. S. J. van der Meer. Doctoral Thesis, Delft, Netherlands, 1970.
56. S. J. van der Meer. *J. Text. Inst.*, 1974, **65**, 288.
57. B. A. Dunell and J. H. Dillon. *Text. Res. J.*, 1951, **21**, 393.
58. H. Tipton. *J. Text. Inst.*, 1955, **46**, T322.
59. M. Takayanagi. *Mem. Fac. Engng Kyushu Univ.*, 1963, **23**, No. 1.
60. M. Takayanagi. In *Proceedings of Fourth International Congress of Rheology* E. H. Lee and A. L. Copley (Editors), Interscience, New York, 1965, Part I, p. 161.
61. A. R. Oudet, A. R. Bunsell, R. Hagege and M. Sotton. *J. Appl. Polymer Sci.*, 1984, **29**, 4363.
62. C. Le Clerc, A. R. Bunsell and A. Plant, *J. Materials Sci.*, 2006, **41**, 750.
63. W. Lotmar. *Helv. Chim. Acta*, 1936, **19**, 68.
64. J. W. Ballou and S. Silverman, *Text. Res.*, 1944, **14**, 289.
65. K. W. Hillier and H. Kolsky. *Proc. Phys. Soc.*, 1949, **B62**, 111.
66. K. W. Hillier. *Proc. Phys. Soc.*, 1949, **B62**, 701.
67. M. Chaikin and N. H. Chamberlain. *J. Text. Inst.*, 1955, **46**, T25, T44.
68. W. J. Hamburger. *Text. Res. J.*, 1948, **18**, 705.
69. W. H. Charch and W. W. Moseley, jr. *Text. Res. J.*, 1959, **29**, 525.
70. W. W. Moseley, jr. *J. Appl. Polymer Sci.*, 1960, **3**, 266.
71. R. L. Bosman. OCEANS 96 conference Institution of Electrical and Electronics Engineers and Marine Technology Society, Fort Laoderdale, Florida, OSA, 1996, September 23–26.
72. H. de Vries. *Appl. Sci. Res.*, 1952, **A3**, 111.
73. J. H. Dumbleton. *J. Polymer Sci. A-2*, 1968, **6**, 795.
74. J. C. Smith, J. M. Blandford, and K. M. Towne. *Text. Res. J.*, 1962, **32**, 67.

17.1 Introduction

The last four chapters have been concerned with tensile properties, the extension of fibres under loads applied along the fibre axis. The influence of forces in other directions is also interesting and of practical importance. The bending and twisting of fibres influence the behaviour of bulked yarn filaments and the drape and handle of fabrics. Recovery from bending is a factor in creasing. Twisting and bending both play a part in the arrangement of fibres in a yarn, and transverse compressive forces are involved when tension is applied to a twisted yarn. Bending strength and shear strength may be important in wear. It is these properties that will be considered in this chapter.

17.2 Bending of fibres

17.2.1 Flexural rigidity for small curvature

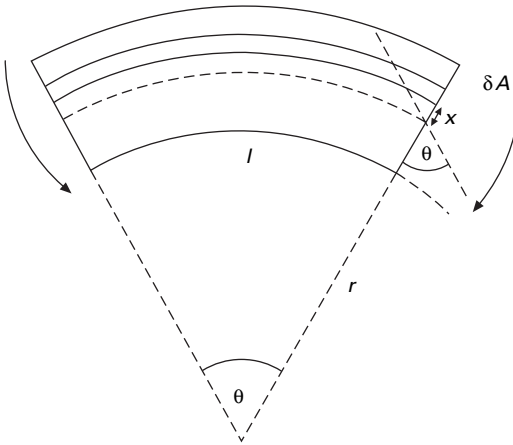
The flexural rigidity (or stiffness) of a fibre is defined as the couple required to bend the fibre to unit curvature. Curvature is the reciprocal of radius of curvature. By this definition, the direct effect of the length of the specimen is eliminated. The flexural rigidity may be calculated in terms of other fibre properties. The problem is similar to that of the bending of beams. Suppose we have a specimen of length l , bent through an angle θ to a radius of curvature r , as shown in Fig. 17.1. Its outer layers will be extended and its inner layers compressed, but a plane in the centre, known as the neutral plane, will be unchanged in length. As a result of the extension and compression, stresses will be set up that give an internal couple to balance the applied couple.

Consider an element of area of cross-section δA , at a perpendicular distance x from the neutral plane:

$$\text{elongation of element} = x \theta = \frac{xl}{r} \quad (17.1)$$

$$\text{tension in element} = \frac{xl/r}{lE \delta A} \quad (17.2)$$

where E = Young's modulus,



17.1 Bending of a fibre.

the moment about an axis in the neutral plane

$$= \frac{x}{r} E \delta A x = \frac{E}{r} x^2 \delta A \quad (17.3)$$

$$\text{total internal couple} = \frac{E}{r} \sum (x^2 \delta A) = \frac{E A k^2}{r} \quad (17.4)$$

$$\text{where } A = \sum \delta A = \text{area of cross-section and } k^2 = \sum (x^2 \delta A) / \sum \delta A. \quad (17.5)$$

$E A k^2$ is often referred to as EI , where I is the moment of inertia of the cross-section. The parameter k is analogous to a radius of gyration, taken about the neutral plane. It may be related to a shape factor η , which is 1 for a circular fibre, by the expression:

$$k^2 = \frac{1}{4\pi} \eta A \quad (17.6)$$

$$\text{Since } A = \frac{c}{\rho} \quad (17.7)$$

where ρ = density and c = linear density of filament,

$$\text{and } E = \rho E_s \quad (17.8)$$

where E_s = specific modulus

$$\text{total couple} = \frac{1}{4\pi} \frac{\eta E_s c^2}{r \rho} \quad (17.9)$$

$$\text{flexural rigidity}^1 = \frac{1}{4\pi} \frac{\eta E_s c^2}{\rho} \quad (17.10)$$

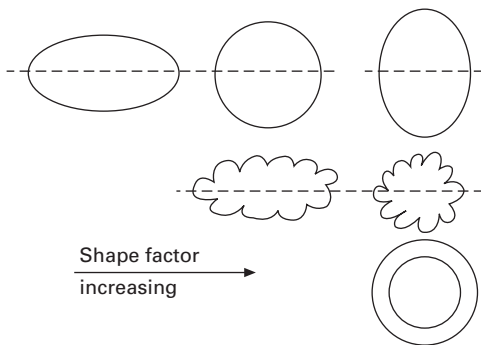
¹It should be noted that this equation is in a consistent set of units. In SI: E_s in N/kg m; c in kg/m; ρ in kg/m³; and flexural rigidity in N m². In likely practical units, with E_s in N/tex, c in tex, and ρ in g/cm³, the equation becomes: flexural rigidity = $(1/4\pi) (\eta E_s c^2) / \rho \times 10^{-3}$ N mm².

It follows from this relation that the flexibility of a fibre depends on its shape, its tensile modulus, its density and, most of all, its thickness.

The densities of the ordinary textile fibres range only between 1.1 and 1.6 g/cm³, so that this is not a very large factor. Values of the modulus obtained in tensile tests have been given in Chapter 13. They range from over 200 N/tex for HM–HT fibres to about 10 N/tex for polyester fibre and as low as 2 N/tex for wool. The shape factor becomes greater, and the rigidity increases, the more distant the material is from the centre. This is illustrated in Fig. 17.2. It will be seen that with an asymmetrical shape there may be a difference according to the direction of bending. In practice, the fibres will usually twist so as to bend about the easiest direction. For simple shapes, values of η may be obtained by integration from a relation derived from equations (17.5) and (17.6). For more complicated shapes, either numerical computation or experiment will be necessary. Table 17.1 gives some typical values.

Since the fineness comes in as a squared term, and in view of the range of values occurring in practice, from around 0.01 tex for microfibres and smaller for nanofibres to 1 tex for a coarse wool and higher for some hair fibres and manufactured monofilaments, it will be the most important factor in determining the flexural rigidity. The choice of fibre linear density is thus important in deciding flexibility.

In order to compare material properties, it is convenient to introduce a quantity that is independent of the fineness of the specimen. We may call this quantity the



17.2 Shape factors.

Table 17.1 Flexural rigidity (after Finlayson [1])

Fibre	Shape factor η	Specific flexural rigidity R_1 (mN mm ² /tex ²)
Viscose	0.74	0.19
Acetate	0.67	0.08
Wool	0.80	0.20
Silk	0.59	0.19
Nylon	0.91	0.14
Glass	1.0	0.89

specific flexural rigidity R_f , which is the flexural rigidity of a fibre of unit linear density². It equals (couple/curvature)/(linear density)² and is given by:

$$R_f = \frac{1}{4\pi} \frac{\eta E_s}{\rho} \quad (17.11)$$

Values of R_f obtained by using values of the modulus obtained in tensile tests are given in Table 17.1. They show the great flexibility of acetate filaments and the stiffness of glass.

The above analysis assumes that the fibre modulus E (or E_s) is constant. In reality, fibre stress–strain curves are mostly non-linear, so that the analysis applies only to small strains, namely to the relation between the initial flexural rigidity and the initial tensile modulus. For a neutral plane in the centre of the fibre, the maximum tensile strain, which will be positive on the outside and negative on the inside of the bend, equals r/R in a circular fibre, where r = fibre radius and R = radius of curvature of bend. Since fibres are so fine, quite small values of R (high curvature) result in fairly small strains, so that, in many practical situations, though not in severe creasing, it is only the initial flexural rigidity that is relevant.

17.2.2 Non-linearity at large curvatures

For more severe bending, the behaviour is represented by a moment–curvature relation. Non-linearity of stress–strain relations must then be taken into account. For most fibres, yield occurs at a lower stress in compression than in tension. This means that resistance to deformation will be less on the inside of a bend than on the outside. Consequently, in order to minimise strain energy, the neutral plane will move towards the outside. If the fibre shape and the stress–strain curves in tension and compression are known, the position of the neutral axis and the resistance to bending can be calculated.

A common procedure is to calculate an effective bending modulus E_B (or E_{Bs}) from the above equations. The difference from the modulus measured in tension gives an indication of the difference between compressive and extensional resistance.

Chapman [2] developed this approach by presenting his results as bending ‘stress–strain’ curves. This is a convenient way of normalising the information to eliminate the direct effect of fibre dimensions. He defined the bending strain as b/R , where b is half the thickness in the plane of bending. If the neutral plane is in the mid-way position, this is the maximum strain in the fibre. However, there will be lower strains in other parts of the fibre, with a complicated distribution if the fibre is irregular in shape. If the neutral plane shifts from the mid-position, the maximum strain (at the greater distance from the neutral plane) will be larger.

Equation (17.4) may be written as:

²The consistent SI units for specific flexural rigidity are $\text{N m} \times \text{m}/(\text{kg m}^{-1})^2$ or $\text{N m}^4 \text{kg}^{-2}$. If E is in N/tex and ρ in g/cm^3 , then $R_f = (1/4 \pi) (\eta E_s/\rho) \times 10^{-3} \text{ N mm}^2/\text{tex}^2$.

$$\text{moment} = M = \left(\frac{E A k^2}{b} \right) \left(\frac{b}{R} \right) \text{ or } \left(\frac{M b}{A k^2} \right) = E \left(\frac{b}{R} \right) \quad (17.12)$$

This equation is analogous to Hooke's law, and (Mb/Ak^2) has the dimensions of stress. Chapman therefore terms it the 'bending stress' and uses it in the more general non-linear situation.

Lee [3] has modified the standard analysis and derived the bending moment versus curvature relation for rectangular, elliptical and hollow cross-sections with a power law relation for the stress-strain properties of the material. In a later paper [4], he treats a greater variety of cross-sections. Jung and Kang [5] also analyse the large deflection of fibres with non-linear elastic properties. He and Wang [6] treat the buckling of fibres with irregular cross-sections.

17.2.3 Measurement of bending

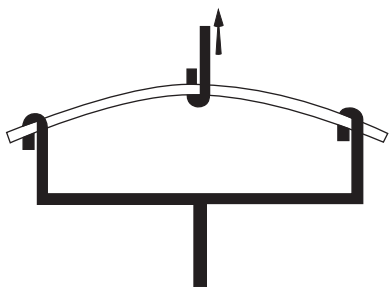
The flexural rigidity of coarse monofilaments may be measured by supporting the specimen at either end and finding the deformation due to a load at the centre. A tensile tester may be modified as shown in Fig. 17.3 [7].

Peirce [8] suggested studying the deformation of loops under an applied load. Carlene [9] used this method for viscose rayon filaments. A circular ring was suspended and loaded by a rider, as shown in Fig. 17.4. Peirce showed that:

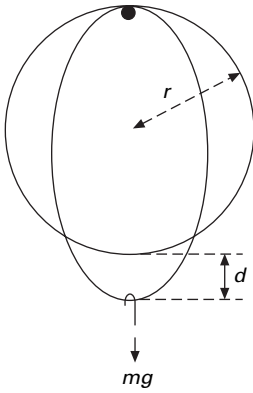
$$\text{flexural rigidity} = 0.0047 mg (2\pi r)^2 \frac{\cos \theta}{\tan \theta} \quad (17.13)$$

where mg = weight of rider, r = radius of ring, $\theta = 493d/2\pi r$ and d = deflection of lower end of ring.

Guthrie *et al.* [10], following a method devised by Khayatt and Chamberlain [11], measured the deflection of short lengths (from a fraction of 1 mm to 2.5 mm) of filaments clamped at one end and loaded at the other. The loading was applied by pressing the specimen against a razor edge attached to the arm of a torsion-balance. The deflection could be measured by a microscope with a micrometer eyepiece. If the deflection was small, it could be shown that:



17.3 Adaptation of tensile tester for measurement of flexural rigidity of coarse fibres.



17.4 Measurement of flexural rigidity by a loop.

$$\text{flexural rigidity} = \frac{Fl^3}{3d} \quad (17.14)$$

where F = force applied to specimen, l = length of specimen from clamp to razor-edge and d = deflection of specimen.

The flexural rigidity may also be measured dynamically [12, 13]. One end of a specimen is vibrated transversely, and the frequency is varied until the position of resonance, at which the amplitude of vibration of the specimen is a maximum, is reached. At least 0.5 cm of straight fibre is required for a test, and it may be observed with a microscope. The method may be used at frequencies between about 20 Hz and 10 kHz. The air damping may usually be neglected, and the rigidity is then given by:

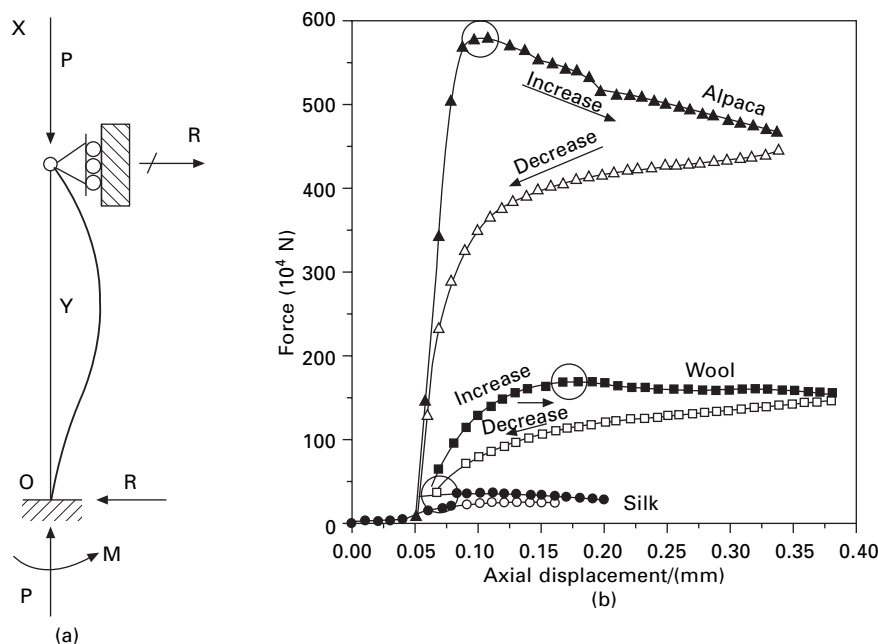
$$\text{flexural rigidity} = \frac{4\pi^2 A \rho l^4 f^2}{h^4} \quad (17.15)$$

where A = area of cross-section of specimen, ρ = density of specimen, l = length of specimen, f = resonant frequency and m depends on the harmonic that is being excited and is a solution of the equation $\cos h \times \cosh h = -1$ (for the fundamental $m = 1.8751$).

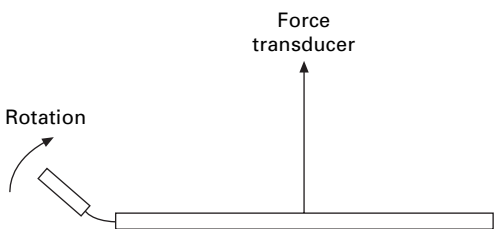
The loss modulus or $\tan \delta$ may be determined from the width of the resonance peak, as described in Section 16.5.3.

Yu and Liu [14] used a buckling test shown in Fig. 17.5(a) to measure bending resistance. Figure 17.5(b) shows the variation of displacement with axial compressive force. The force rises to a maximum, which is the critical value at which buckling occurs. Yu and Liu solve the differential equations for the bending mechanics and show that the effective bending modulus can be determined from the linear plot of critical stress against (D^4/L^2) , where D = fibre diameter and L = fibre length.

There are three experimental difficulties in measuring the full bending moment versus curvature relations: the manipulation of fine fibres at small radii of curvature; the measurement of small moments; and the maintenance of a uniform curvature in the specimen (most simple methods of bending lead to a variable curvature, as is apparent for example, from Figs 17.3, 17.4 and 17.5). Chapman [15] has described



17.5 (a) Axial buckling test. (b) Force displacement plots with critical condition circled. From Yu and Liu [14].



17.6 Principle of Chapman's fibre-bending tester [15].

an apparatus that overcomes these difficulties. It is based on a principle introduced in a fabric-bending test by Livesey and Owen [16]. The essential features of Chapman's method are shown in Fig. 17.6. Curvature is applied by rotation of one fibre mount, and the couple is determined by using a sensitive electronic microbalance to measure the force on a lever arm attached to the other mount. Provided that the lever arm is long, the errors due to non-uniform curvature are negligible.

17.2.4 Experimental results

Table 17.2 gives examples of the results of experiments on bending obtained by Owen [17], using a double-pendulum method. If the fibre is non-uniform, one would expect a difference between the moduli found in bending tests and those found in tensile tests, since the outer layers play a larger part in bending than do the centres

Table 17.2 Flexural and torsional properties of fibres 65% r.h.20 °C [18]

Fibre	Specific flexural rigidity (mN mm ² /tex ²)	Modulus GPa		Specific torsional rigidity (mN mm ² /tex ²)	Shear modulus (kN/mm ²)
		bending	tension		
Cotton	0.53		7.7	0.16	
Viscose rayon					
<i>Fibro</i> (staple)	0.35	10	8.7	0.058–0.083	0.84–1.2
<i>Vincel</i> (high wet modulus)	0.69	20		0.097	1.4
Secondary acetate	0.25		4.2	0.064	
Triacetate	0.25		3.8	0.091	
Wool	0.24	3.9	5.2	0.12	1.3
Silk	0.60		14	0.16	
Casein					
<i>Fibrolane</i>	0.18		2.3	0.11	
Nylon 6.6 (3 types)	0.15–0.22	2.5–3.6	1.9–3.8	0.041–0.060	0.033–0.48
Polyester fibre					
<i>Terylene</i>	0.30	7.7	6.2	0.067	0.85
Acrylic fibre (3 types)	0.33–0.48	6.0–8.1	4.9–7.0	0.12–0.18	1.0–1.6
Polypropylene	0.51	5.2	2.4	0.14	0.75

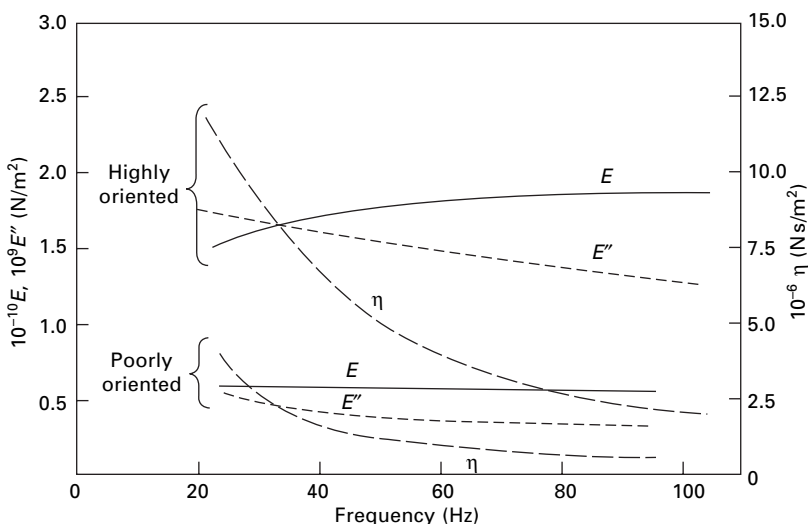
of the fibre. In practice, Guthrie *et al.* [10] found that the modulus in bending tests was greater than that in tensile tests at similar rates of loading for acrylic, polyamide and polyester fibres. K  rrholm and Schr  der [19] obtained the same results for viscose rayon, but Khayatt and Chamberlain [11] found the bending moduli in wool to be lower than the tensile moduli. Yu and Liu [14], using the buckling test, found bending moduli of 1.47 GPa for wool, 2.15 for alpaca and 4.58 for silk.

In dynamic tests, Guthrie *et al.* [10] found that the modulus of viscose rayon was constant between 40 Hz and 7 kHz; but Horio *et al.* [20] observed a drop in the modulus near 20 Hz. This is shown in Fig. 17.7, together with values of E'' and η (see Section 16.5.2). This suggests that there is a peak in the absorption and a drop in the modulus at a low frequency.

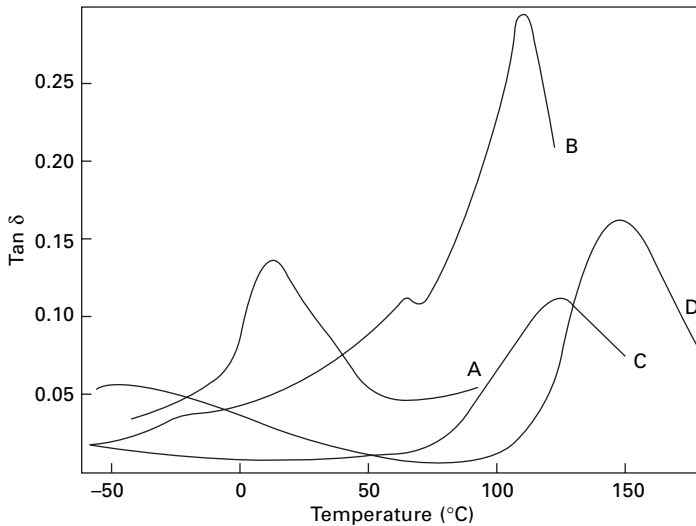
Meredith [18] reported dynamic-bending measurements of $\tan \delta$, as shown in Fig. 17.8 for four synthetic fibres, with peaks in the important range between 0 and 150 °C. He also reported rather complicated results for cellulosic and protein fibres. Other results have been given by Meredith and Hsu [13].

Elder [21] reported on the effect of temperature and humidity on the bending modulus of some synthetic monofilaments. It is interesting to note that nylon 6 and 6.6, polyethylene, and polypropylene are on the lower part of a sigmoidal curve between 20 and 80 °C, but polyester fibres are on the upper part. For example, at 65% r.h., the bending modulus of nylon 6 falls from 3 GPa at 15 °C to 1.3 GPa at 40 °C but then changes less, whereas *Terylene* polyester fibre is close to 13 GPa between 20 and 40 °C but falls to 10.3 GPa at 80 °C. A change in relative humidity of from 30 to 85% at 20 °C causes the bending modulus of nylon to fall from 5.5 to 1.5 GPa.

Experimentally, for viscose rayon, the flexural rigidity has been found to be proportional to $(\text{tex})^n$, where the index n is slightly less than the theoretical value of 2. Guthrie *et al.* [10] found $n = 1.96$ for Fibro staple fibre, and Carlene [9] found $n = 1.80$ and 1.82 for other specimens of viscose rayon.



17.7 Values of E , E'' and η in in bending of two viscose rayon monofilaments [20].



17.8 Tan δ measured in dynamic bending of fibres at 0% r.h at frequencies of 200–300 Hz: A polypropylene; B, acrylic fibre; C, nylon; D polyester fibre.

Skelton [22] reported that the bending recovery of 15 denier (1.67 tex) nylon fell steadily from close to 100 % for small curvature to about 20 % at high curvature.

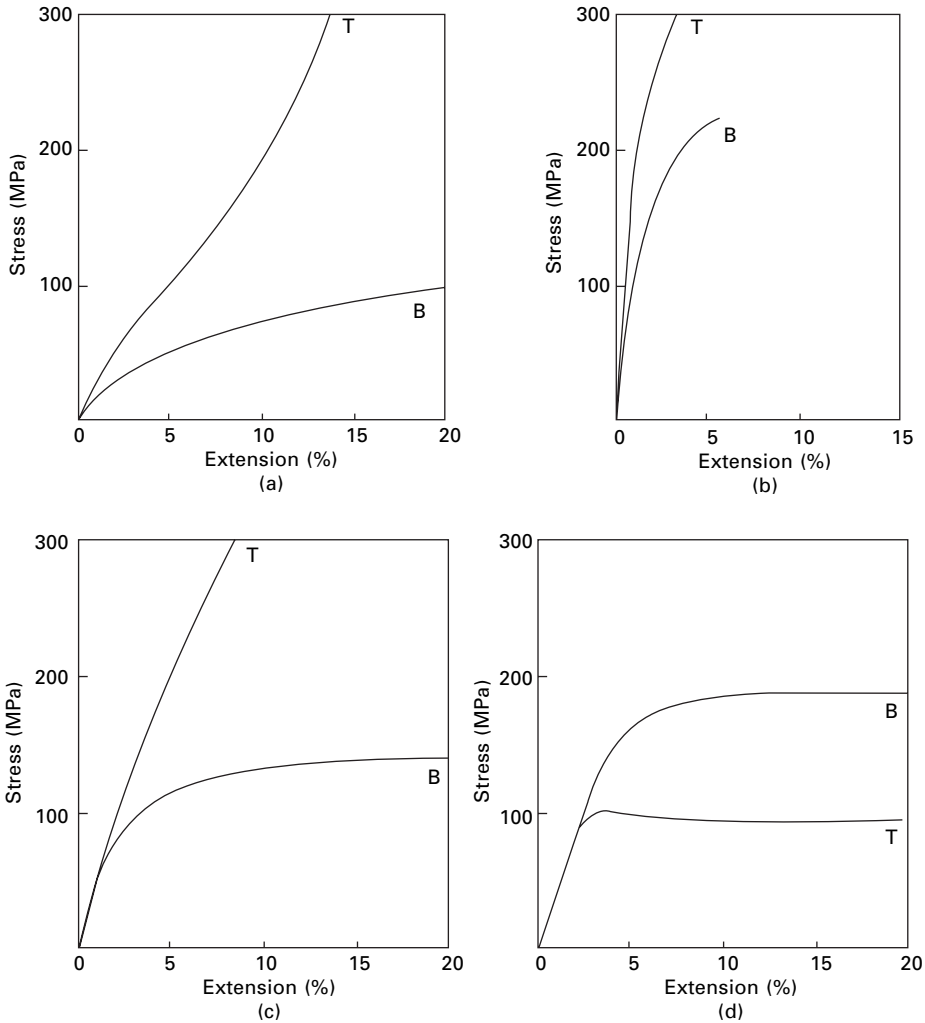
17.2.5 Bending stress–strain relations

Love [23] showed from elasticity theory that a modulus defined as the ratio of bending stress to bending strain is identical with the tensile modulus for a uniform, transversely isotropic beam. In the absence of other complications, the bending and tensile stress–strain curves should coincide near the origin.

If the fibres being tested are elliptical, with semi-axis a perpendicular to the plane of bending and semi-axis b in the plane of bending, then the bending strain is (b/R) as defined above, and the bending stress is $(4M/\pi b^2 a)$.

A comparison of bending stress–strain curves with tensile stress–strain curves is shown in Fig. 17.9. Generally similar results were found by Chapman with finer fibres, though it was not possible to carry the tests to such large bending strains.

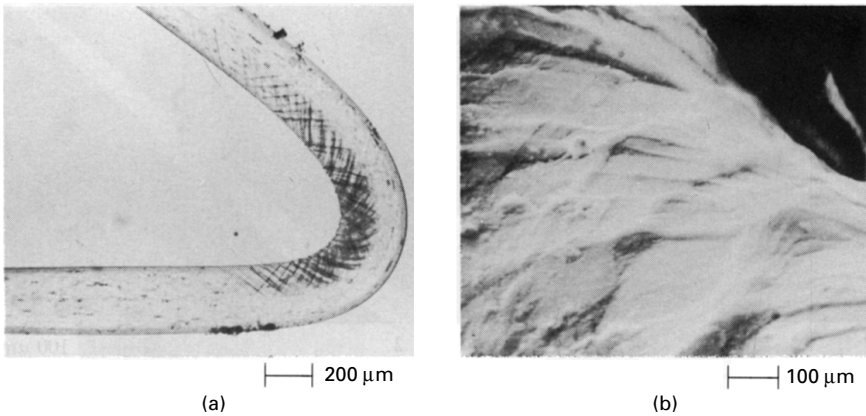
In all the manufactured fibres, the bending stress–strain curves lay below the tensile curves and indicated that yield in bending, due to yield on the compression side of the bend, occurred more easily than yield in tension. This was accompanied by the development of kink-bands on the inside of the bend. Observations of these kink-bands were described by Bosley [24] and Jariwala [25, 26]. Typical examples are shown in Fig. 17.10. Application of tension after a single bend removes the visible kink-bands and there is no loss of strength. The occurrence of kink-bands depends on test conditions. In polyester fibres, kink-bands develop in a single bend at 20 °C but not at 100 °C, whereas in nylon they appear at 100 °C but not at 20 °C. The development of kink-bands into flex fatigue failure, including the effect of temperature and humidity, is discussed in Section 19.5.2.



17.9 Bending (B) and tensile (T) stress–strain curves from Chapman [2]: (a) nylon 6 fishing line; (b) high-tenacity polyester fibre filament; (c) polypropylene monofil; (d) horse hair.

However, in horsehair (and wool), the bending curve is higher. If the yield behaviour were the same in compression as in tension, Chapman showed that the bending yield stress would be about 1.7 times as great as the yield stress in a tensile test. In fact, the bending yield stress in horsehair is twice the tensile value, and this indicates that the yield stress in compression is larger than the yield stress in tension. In this situation, the neutral plane will move towards the outside of the bend, whereas in the synthetic fibres it will move towards the inside.

Chapman [2] also studied the influence of ambient conditions in bending modulus and found, as would be expected, a decrease in stiffness with increase in temperature and humidity. In another paper, Chapman [27] described studies of bending-stress



7.10 Kink-bands in bent polyester fibres: (a) shown by polarised light microscopy; (b) visible on the surface in scanning electron microscopy.

Table 17.3 Loop and knot strengths

Fibre	$\frac{\text{Loop strength}}{\text{Tensile strength}} \times 100$	$\frac{\text{Knot strength}}{\text{Tensile strength}} \times 100$
Cotton		91
Viscose rayon		58
High-tenacity viscose rayon	96.5	90
Acetate		63
Wool		95
Silk		85
Nylon	82.5	88
Orlon acrylic fibre	80.9	86
Dacron polyester fibre	72.8	98,88
Fibreglas	8.4	5
	(from Coplan [28])	(from Bohringer and Schieber [29])
		(from Berry [30])

relaxation and recovery. Whereas wool and nylon usually did show complete recovery in time, polyester fibres were left with a permanent set, probably as a result of the compressive yielding.

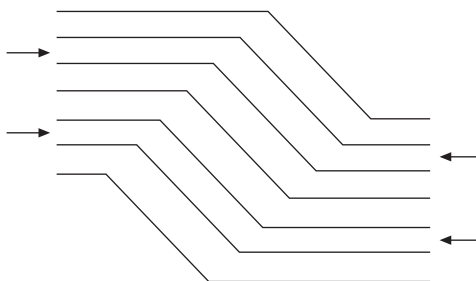
17.2.6 Loop strength and knot strength

If a filament is loaded in a bent state, it will break more easily than when it is straight. This is due to the initiation of breakage by the high extension of the outside layers. The reduction in strength, of which some values are given in Table 17.3, is greatest in fibres with the lowest elongation at break. A similar effect is observed when there is a knot in the filament, and values for the decrease in strength due to this cause are also given in Table 17.3.

17.2.7 Compression and bending in high-performance fibres

There is a major difference between different types of HM–HT fibres in their resistance to bending, which is related to their resistance to axial compressive stresses. Yielding in compression with the formation of kink-bands, which is described above for nylon and polyester fibres, is a more severe problem in highly oriented linear-polymer fibres. Yielding occurs by internal buckling of cylindrical elements. This is really a manifestation of the Euler buckling of a column, which occurs under a low stress when the aspect ratio L/D of the element is long. The simple Euler treatment is for a single element, but analogous effects occur in multiple assemblies provided that the interaction between the elements is not so high that shear between elements is prevented. For single rods or bundles without any lateral cohesion, the buckling will be into a smooth bending curve; but, where there is some interaction between neighbouring elements, it is more likely to occur as sharp kinks of the form indicated in Fig. 17.11. Details of the occurrence of kink-bands in aramid fibre filaments have been discussed by van der Zwaag *et al.* [31]. Such effects can occur at any structural level: fibres in a yarn or a composite; fibrils or other elements within a fibre; or the linear molecules themselves. Sometimes, the forms may be biased by particular structural features, such as crystal twinning or particular molecular conformations; but this is essentially a secondary effect and merely reflects that the yield will occur in the easiest of various possible ways.

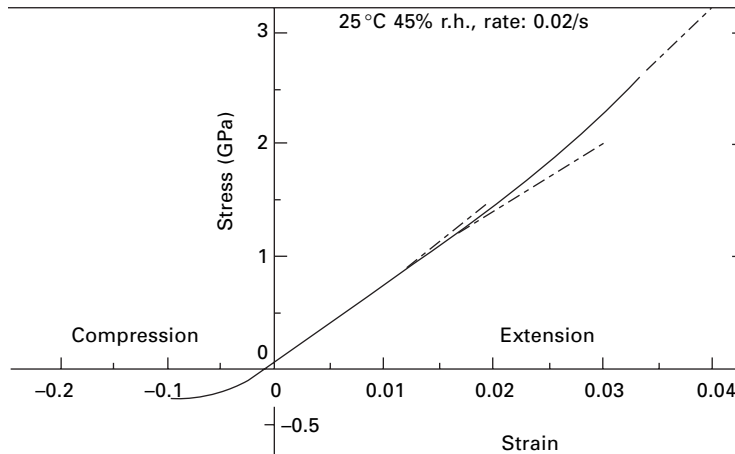
It is, of course, difficult to study single fibres in compression because, except at impossibly short test lengths, they buckle as a whole before the internal yielding occurs. However, the formation of kink-bands in compression can be demonstrated by the dynamic effects of snap-back after breakage. Quantitative estimates of compressive strength can be obtained from tensile recoil measurements [32], and some experimental results are listed in Table 17.4. Values of compressive strength can also be inferred from loop tests, and van der Zwaag and Kampschoer [33] found that the compressive strength of aramid fibres ranged from 0.5 GPa for a low-modulus type to 0.9 GPa for a high-modulus type. The values for HMPE were much lower. Compressive yield can also be shown in composites. For example, although the initial moduli in tension and compression of a *Kevlar* 49/epoxy unidirectional composite are almost the same, there is yield in compression at a strain of about 0.3% at a stress of about one-fifth of the tensile breaking stress. The yield determines the



17.11 Compressive deformation to a kink-band.

Table 17.4 Comparison of tensile strength and compressive strength measured in recoil [32]

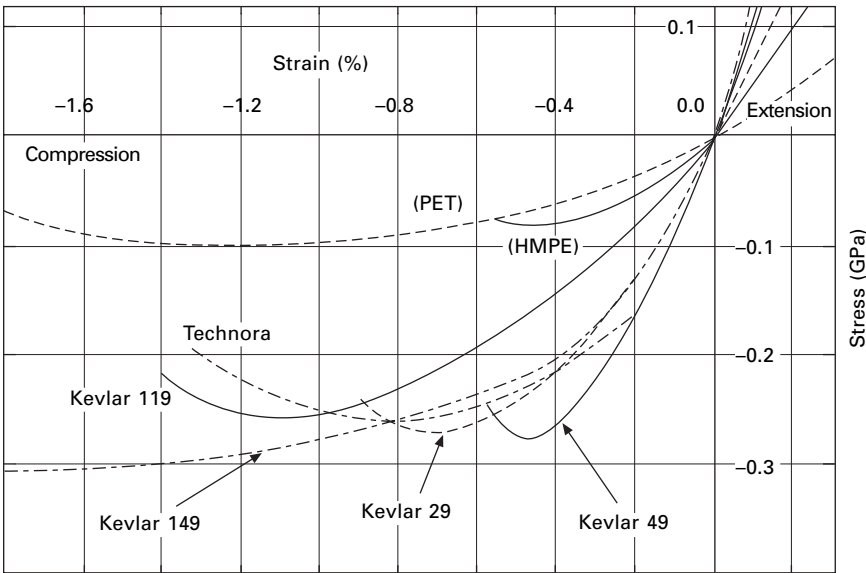
Fibre	Tensile strength (GPa)	Compressive strength (GPa)
<i>Kevlar 29,49</i>	3.4	0.37
Polyethylene, gel-spun	2.7	0.07
Carbon, <i>Magnamite AS4</i>	3.6	1.4
<i>Thornel P-55</i>	2.1	0.4



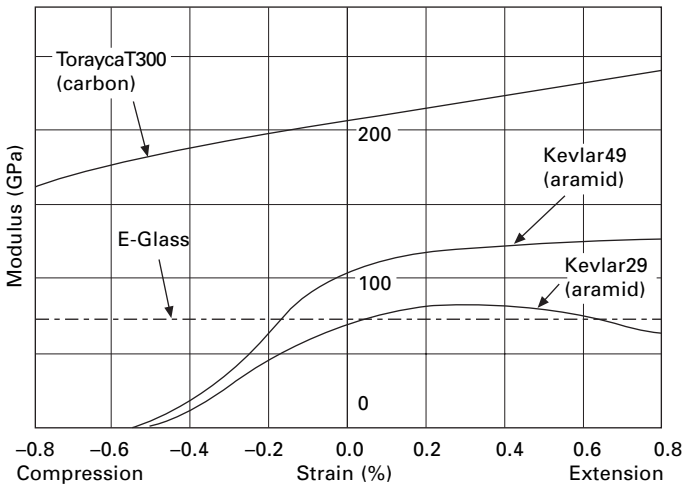
17.12 Aramid (*Kevlar 29*) fibre in axial extension and compression. From Kawabata [35].

maximum stress that an oriented linear polymer fibre can sustain. Consequently, the compressive strength is the same low value as the compressive yield stress.

Kawabata [34] developed a microcomposite method for measuring axial compression of fibres. A fibre bundle, which has been dipped in liquid epoxy resin is pulled into a *Teflon* tube with an inner diameter of 1 mm. After curing, the composite, which has a fibre volume fraction of 0.8 to 0.85, is extracted and cut into 5 mm lengths. Compression forces up to 2 kN are applied through a steel plunger giving deformations of less than 2 μm , which can be measured on an LDVT. The fibre stress is calculated from a simple mixture law. Figure 17.12, which includes axial extension, shows the low yield stress in axial compression. Results for a number of fibres are shown in Figure 17.13. HMPE and polyester fibres have a lower compressive yield stress than aramids. Another way of presenting the data by plotting the tangent modulus against strain is shown in Fig. 17.14. The low compressive modulus of the *Kevlar* fibres corresponds to the approach to the minima in Fig. 17.13. Glass shows a constant modulus, indicating linearity in extension and compression. The ceramic fibre *Tyranno* is also linear in extension and compression. The carbon fibre shows an increasing modulus, indicating a constant upward curvature in the stress–strain curve from compression to extension.



17.13 Axial compression behaviour of aramid fibres compared with HMPE and polyester. From Kawabata [34].



17.14 Longitudinal modulus as a function of strain. From Kawabata [34].

In contrast to the easy compressive yield of the one-dimensional structures, the three-dimensional bonding in ceramic and glass fibres allows no mechanism for compressive yield. If there is a high degree of three-dimensional interlocking in carbon fibres, there will be no mechanism for yield in compression, and the compressive strength will be high. But, in more perfect graphitic structures, the compressive strength will be lower.

The counterpart to the low compressive strength of the oriented linear polymer

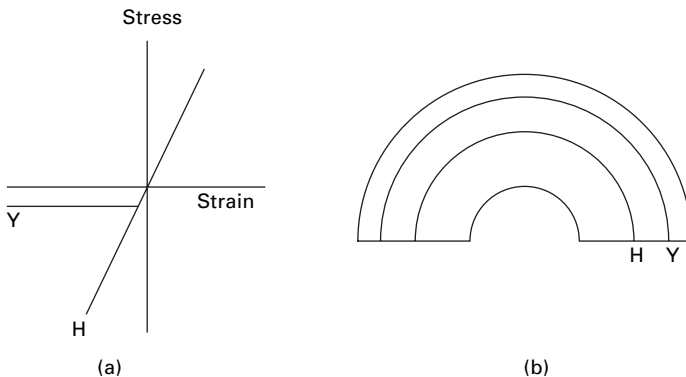
fibres is that they can suffer severe bending without breaking, whereas the three-dimensionally bonded fibres cannot do so.

Materials such as carbon, glass and ceramic fibres, which are linear elastic in tension and compression, follow the classical behaviour in bending, as shown in Fig. 17.1. The neutral plane remains central and leads to equal and opposite tensile and compressive strains on the outside and inside of the bend. If the radius of curvature of the bend is R and the fibre radius is r , the maximum strain present is r/R , and, when this equals the breaking strain, rupture will occur. Consequently, DuPont's alumina FP fibre with a breaking extension of 0.4% cannot be bent into a curvature tighter than 250 fibre diameters without breaking.

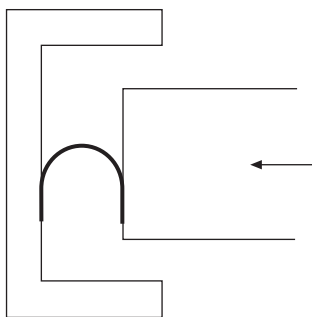
In contrast to this, when there is yield in compression, the neutral plane will move out to allow most of the deformation to occur by the easier compression mode. The situation is illustrated in Fig. 17.15. Mathematically, equation (17.2) has to be modified because the compressive force on an element on the inside of the bend, beyond the small region of elastic deformation, will be given by $f_y \delta A$, instead of $(x/R) Y \delta A$, where f_y is the yield stress and Y is Young's modulus. The division of area between the tension side, δA_t , and the compression side, δA_c , will be given by a minimisation of the deformation energy, U_b , where:

$$U_b = \sum 1/2 (x/r)^2 Y \delta A_t + \sum f_y (x/r) \delta A_c \quad (17.16)$$

Schoppee and Skelton [36] have developed the bending-breakage test shown in Fig. 17.16, and this confirms that *Kevlar* fibres can be bent back on themselves without breaking. If the neutral plane had remained central, this would have implied a tensile strain of 100%. Values for various fibres are shown in Table 17.5. The fibres that do not yield in compression break at curvature levels close to those that would be predicted from the tensile breaking extensions. It is reasonable that the breaking strains calculated from bending tests should be larger than those from tensile tests, since they are effectively made on a very short test length, comparable with the fibre diameter.



17.15 (a) Stress-strain relations for Hookean material (H) and material yielding in compression (Y). (b) Bending response: H, neutral plane central; Y, neutral plane moving out.



17.16 The bending test developed by Schoppee and Skelton [36].

Table 17.5 Rupture in bending [36]

Fibre	Breaking strain in tensile test (%)	Maximum apparent strain in bending (%)
Glass	6.2	7.3
Graphite HM-S	0.8	1.4
HT-S	1.4	2.8
Kevlar 49	3.0	100

17.3 Twisting of fibres and the shear modulus

17.3.1 Torsional rigidity

The torsional rigidity of a fibre, its resistance to twisting, is defined as the couple needed to put in unit twist, that is, unit angular deflection between the ends of a specimen of unit length. The shear modulus is defined as the ratio of shear stress to shear strain, the shear strain being measured in radians.

The torsional rigidity can be obtained in terms of the shear modulus (or modulus of rigidity) in the same way that the flexural rigidity can be obtained in terms of the tensile modulus, since twisting bears the same relation to shearing as bending does to stretching.

We consider the twisting of a cylinder of length l , as shown in Fig. 17.17. After it has been twisted through an angle θ , a line AB has been sheared through an angle ϕ to the new position AC. The shear stresses set up give an internal couple opposed to the applied torque. The shear angle, which is zero at the centre, increases in proportion to the distance from the centre, x . Consider an element of area δA at a distance x from the centre:

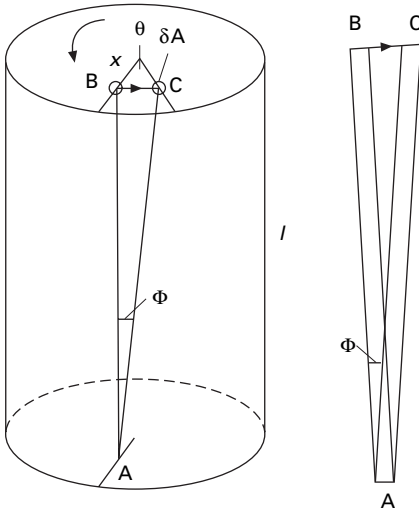
$$\text{shearing force} = v\phi\delta A = v(\theta x/l)\delta A \tag{17.17}$$

where v = shear modulus (force/unit area). Therefore:

$$\text{moment about the centre line} = v(\theta x/l)\delta A \cdot x = v\theta x^2\delta A/l \tag{17.18}$$

$$\text{total torque} = (v \theta / l) \sum x^2\delta A = vAk^2\theta/l \tag{17.19}$$

$$\text{where } Ak^2 = \sum x^2\delta A \tag{17.20}$$



17.17 Twisting of a fibre.

We can define a shape factor, ϵ , by the relation:

$$k^2 = \frac{\epsilon A}{2\pi} \quad (17.21)$$

This gives $\epsilon = 1$ for a circular fibre. The shape factor ϵ is different from η in bending, since, in equation (17.19), x is the distance from the centre line, whereas in equation (17.5), x is the distance from the neutral plane.

When equation (17.18) is converted to a relation involving specific shear modulus n , linear density c , density ρ and twist per unit length τ , it becomes:

$$\text{total torque} = \left(\frac{\epsilon n c^2}{\rho} \right) \tau \quad (17.22)$$

The torsional rigidity may be defined *either* as the torque to produce unit twist in radians per unit length, when it will equal $(\epsilon n c^2 / 2\pi \rho)$, or as the torque to produce one turn per unit length, when it will equal $(\epsilon n c^2 / \rho)$. The expression shows the effect of shape, density, modulus and fineness on the torsional rigidity of a fibre. As in bending, since fineness comes in as a squared term, it is the most important factor. It is convenient to introduce a quantity, the torsional rigidity of a specimen of unit linear density (in tex), independent of the fineness of the particular specimen, and this may be called the specific torsional rigidity³, R_t . It is given by:

$$R_t = \left(\frac{\epsilon n}{\rho} \right) \quad (17.23)$$

We have no direct values of the shear modulus, since these are found by torsional measurements, as described in the next section.

³See footnotes 1 and 2 on pages 415 and 417 for notes on units.

The determination of shape factor has been discussed by Meredith [37]. For simple shapes, the value of the shape factor may be obtained theoretically by integration, no measurement on the fibre being necessary. For slightly more complicated shapes, there are expressions for the shape factor that require the substitution of certain parameters of the fibre cross-section, for example, the major and minor axes of elliptic cross-section, or the relative areas of wall and void in hollow fibres.

For very complicated shapes, such as that of rayon, an experimental analogy may be used. If a membrane is formed across a hole having the same shape as the cross-section of the fibre and is then distended by air pressure, the shape factor will be proportional to the volume between the film and the plane of the plate containing the hole. This analogy depends on the fact that both problems are governed by equations of the same form. The experiment may be carried out by having a burette communicating with a vessel fitted with two plates, one having a hole of circular cross-section and the other a hole of the shape of the cross-section that is being investigated. The holes are covered with a soap film, and the volume needed to raise the circular membrane to a given height (and thus to a given air pressure) is measured first with both soap films being distended, and then with the irregular hole sealed off. Thus the volumes contained under the two membranes can be determined. The areas of the holes are also measured, and the shape factor is given by:

$$\epsilon = \left(\frac{V_1}{V_2} \right) \left(\frac{A_2}{A_1} \right)^2 \quad (17.24)$$

where V_1 and A_1 are the volume and area for the irregular hole, and V_2 and A_2 are the volume and area for the circular hole.

Table 17.6 gives expressions for the shape factor for various cross-sections and shows the values given by Meredith [37]. Lee [38] provides a more detailed analysis of the torsional rigidity of fibres with a generalised elliptical cross-section.

The above analysis is only valid for small twist. In Figure 17.17, $AC = AB \sec \phi$, which causes a tensile strain of $(\sec \phi - 1)$, increasing from the centre to the outside, where ϕ equals the twist angle α . Table 17.7 compares the shear strain, equal to $\tan \alpha$, with the tensile strain. At low twists, tensile strain can be neglected, but it must be taken into account at high twists, particularly as tensile modulus is greater than shear modulus. The tensile strains will be strongest for twisting at constant length. Figure 17.18 shows the development of torque and tension in a nylon monofilament twisted at constant length. At zero tension, the fibre will contract on twisting, reducing the tensile strain at the outside but giving a compressive strain at the centre.

17.3.2 Experimental methods

A method used by Morton and Permanyer [40] for measuring torque–twist relations is indicated in Fig. 17.19. The specimen is mounted between a rotating head A and a torsion-wire of known properties, which is connected to another rotating head C. The principle of the method is that, as the specimen is twisted by the rotation of A, the other head, C, is rotated so as to maintain the pointer B freely in a constant position, marked by the indicating pointer D. Owing to the absence of rotation of B,

Table 17.6 Shape factors for torsion (after Meredith [37])

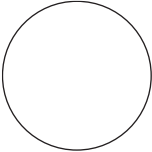
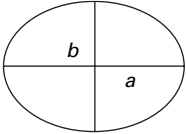
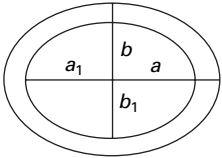
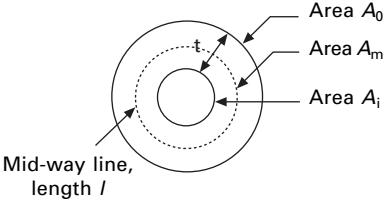
Cross-section	Expression for shape factor ϵ	Fibres approximating to the cross-section	Shape factor ϵ
Circular 	1	Cuprammonium rayon, nylon, casein, Ardil, Terylene, Saran, glass, polythene, etc.	1
Elliptical, $l = b/a$ 	$\frac{2}{e + 1/e}$	Wool	>0.977
Thin elliptical tube of constant thickness $a/a_1 = x, b_1/a_1 = e$ 	$\frac{(2e - 1 + x)^2 (1 + x)^2}{2(e + x)^3 (1 - x)}$	Kapok	5.07 (mean of 10 values)
Thick tube, constant wall thickness 	Approximately $\frac{4 \pi A_m / l}{(A_o - A_i) / l}$	Cotton Flax Ramie	0.71 0.96, 0.92 0.77 (mean values)

Table 17.6 (Continued)

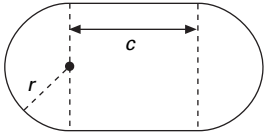
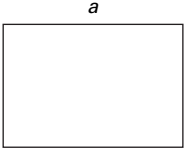

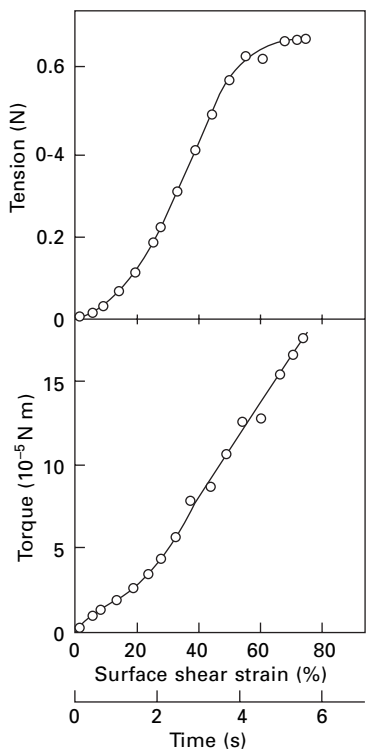
Cross-section	Expression for shape factor ϵ	Fibres approximating to the cross-section	Shape factor ϵ
Irregular, determined by soap-film method		Viscose <i>Fibro</i> 0.95 Rayon <i>viscose rayon</i> 0.93 <i>Tenasco</i> 0.94 Fortisan 0.97 Acetate <i>Celanese</i> 0.73 <i>Seraceta</i> 0.69	
Race-rack, $e = c/2r$	 $\frac{3(4e + \pi)^2}{\pi[3\pi(1 + 2e^2) + 8e(e^2 + 3)]}$	<i>Orlon</i> 0.57 <i>Vinylnon</i> 0.66 <i>Vinyon</i> 0.67	
Rectangular, $e = b/a$	 $\frac{2\pi e(1 - 0.63e)}{3}$	Tussah silk 0.35 Calcium alginate 0.51	
Quadrant of circle	 0.84	Silk 0.84	

Table 17.7 Comparison of shear and tensile strains at surface of a circular fibre

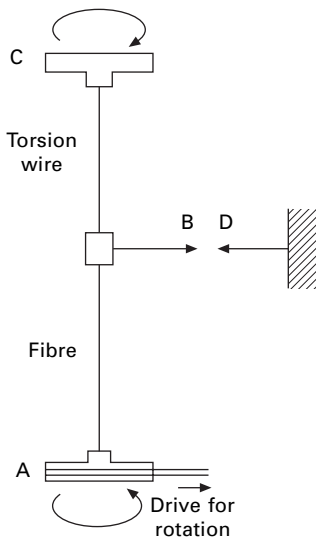
Twist angle α	Shear strain (%) $\tan \alpha$	Tensile strain (%) $\sec \alpha - 1$
1°	0.17	0.015
5°	8.7	0.4
10°	18	1.5
45°	100	41



17.18 Development of tension and torque in an 80 µm diameter nylon monofilament twisted at 5 turns/second. From Sikorski *et al.* [39].

the twist in the specimen is given by the number of turns taken by A, which may be rotated at a constant rate. The torque is obtained from the twist of the torsion wire, which is calculated from the angle turned through by C. Values are noted at intervals as the test is in progress. The same apparatus can be used for measuring the relaxation of torque. With sensitive transducers, the method could be automated [41].

A torque transducer suitable for fibres is described by Sikorski [42, 43] as part of the flexible thermomechanical analyser (FTMA) described in Section 18.5.2. It incorporates semiconductor strain gauges in a commercially available flexible pivot. Twist is directly inserted. The instrument is computer controlled to give programmed changes in two independent variables selected from tension, torque, elongation and twist together with temperature control. Another sensitive torsion tester is described by Kawabata [44].



17.19 Measurement of torque–twist relation [40].

Values of the torsional rigidity can also be found dynamically, by observing the oscillations of a torsion pendulum, which consists of a bar suspended by the fibre. It may be shown that:

$$\text{torsional rigidity of fibre} = \frac{8\pi^3 Il}{t^2} \quad (17.25)$$

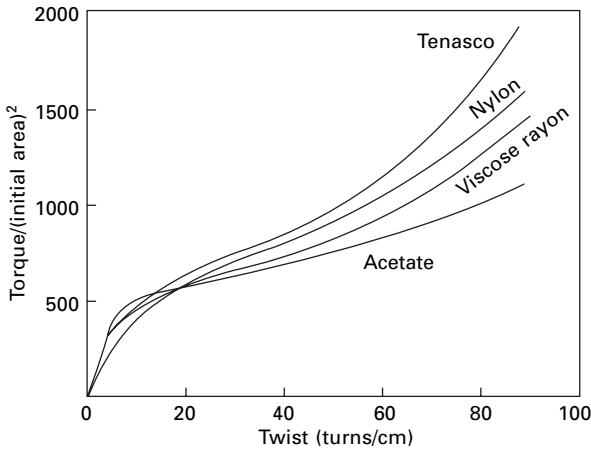
where I = moment of inertia of the bar about the fibre axis, l = length of fibre and t = period of the oscillation, corrected, if necessary, for the damping.

Meredith [37] used 1.5 cm lengths of fibre with light-alloy inertia-bars, ranging in mass from 16 to 110 mg and in length from 1.3 to 2.6 cm. By a suitable choice of bar, the tension on the filament could be kept between 0.49 and 1.96 mN/tex, and the period of oscillation between 4 and 10 s. Under these conditions, the damping was negligible. Owen [17] used a double-pendulum method.

17.3.3 Results of torsional experiments

Figure 17.20 shows torque-twist relations obtained by Morton and Permanyer [41]. They are similar to tensile stress–strain curves. Table 17.2 includes values of the specific torsional rigidity and shear modulus of fibres determined in Owen's dynamic tests [17], in which the strain was small. The results are directly comparable with Owen's bending results in Table 17.2. The specific torsional rigidities range from 0.05 to 2 mN mm²/tex².

Meredith [37] found a very low value for specific torsional rigidity of polyethylene (0.054 mN mm²/tex²) and high values for glass (6.4 mN mm²/tex²), as expected from its material properties, and kapok (73 mN mm²/tex²), due to its hollow form. Shear moduli are typically five to ten times lower than tensile moduli, but in the ratio is



17.20 Torque–twist relations for various fibres at 65% r.h. and 20 °C [41].

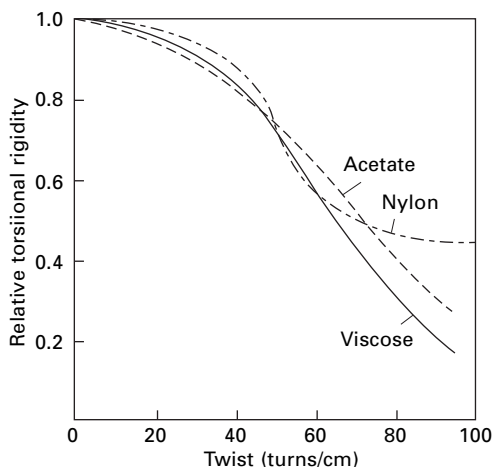
Table 17.8 Tensile and torsional properties. From Zeronian *et al.* [46]

Fibre	Tensile modulus– E (GPa)	Torsional (shear) modulus– ν (GPa)	E/ν	Breaking twist angle (°)
Polyester (PET) experimental filament	9.01	0.85	10.5	44
Polyester (PET) high-speed spun (POY)	1.98	0.65	3.05	77
Polyester (PET) drawn POY	8.81	0.85	10.4	32
Nylon 6 filament	3.41	0.49	6.96	48
Polypropylene filament	2.09	0.57	3.67	60
Gel-spun polyethylene (HMPE)	93.7	0.84	111	22
Polybenzimidazole (PBI) staple fibre	6.78	1.37	4.95	25
Aramid (PPTA) <i>Kevlar</i> 49 filament	94.2	1.60	58.9	17
Polyphenylenesulphide (PPS) staple	4.62	1.39	3.32	46
<i>Vectran</i> M filament	62.2	0.56	111	18
<i>Vectran</i> HS heat-set filament	69.5	0.56	124	20

greater in highly oriented fibres, such as flax and *Tenasco* (28). Muraki *et al.* [45] found shear moduli of 1.28 to 1.42 GPa for wool compared with tensile moduli of 3.55 to 3.73 GPa.

Table 17.8 gives values of tensile and shear moduli of fibres measured with a torsion pendulum by Zeronian *et al.* [46]. Values of the shear moduli cover a three-fold range from 0.5 to 1.6 GPa, but the tensile moduli cover a 50-fold range, reflecting the much higher orientation of the HM–HT fibres.

Torsional rigidity is very much affected by moisture, fibres being easier to twist as their regain increases. This is shown by the results in Fig. 17.21, in which the torsional rigidity, compared to a value of 1 when dry, is plotted against the relative humidity. Clayton and Peirce [48] found that the rigidity of cotton fibres decreased as the temperature increased; the temperature coefficient was 0.28% per °C in the dry state, rising to 1.48% per °C at 8.3% regain.



17.21 Variation of torsional rigidity with twist [47].

Meredith [37] found that the torsional rigidity was independent of tension for the acrylic fibre *Orlon* between 0.98 and 9.80 mN/tex, increased slightly for nylon; and increased by 1.3% for an increase of tension of 0.98 mN/tex in crimpy wool, where the configuration of the fibre would be altered.

Guthrie *et al.* [10] found that the torsional rigidity of viscose staple *Fibro* was proportional to $(\text{tex})^{1.9}$. The difference from the theoretical index of 2 can be accounted for by a difference of shape in fibres of different fineness.

Chamberlain and Khera [49] found that the specific torsional rigidity increased as the outer layers of viscose rayon filaments were removed. Meredith [18] found that the average coefficient of variation of shear modulus was 22% for cellulosic fibres, 15% for protein fibres, and 12 for synthetic fibres.

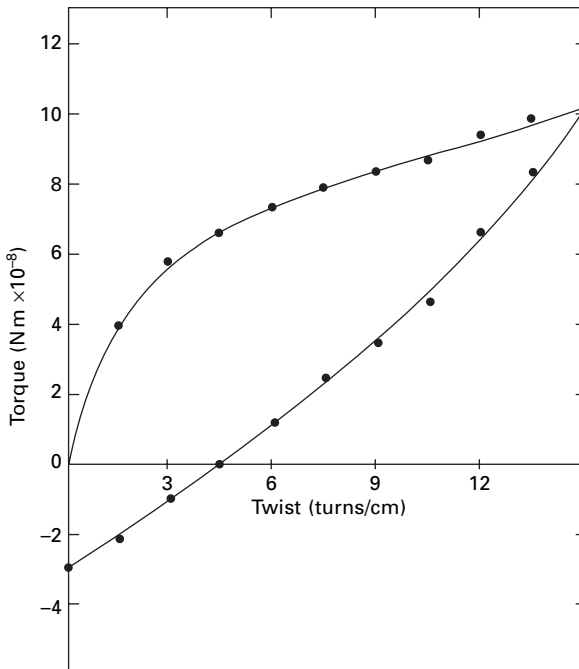
Skelton [50] reported that the torsional recovery of nylon falls from 100% for low strains to 60% for high strains. Figure 17.22 shows torque–twist and recovery response of a polypropylene fibre.

17.3.4 Torsion and time

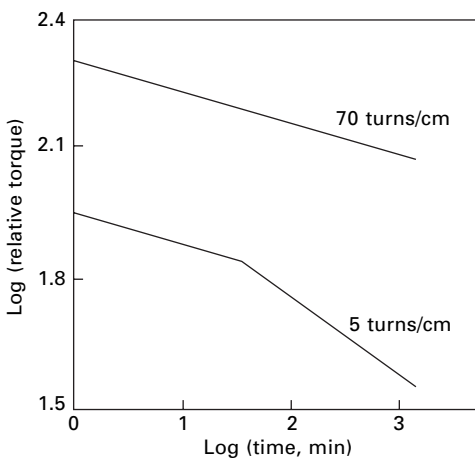
Creep and relaxation will occur in twisting just as they do in extension. Fig. 17.23 gives examples of the relaxation of torque found by Permanyer [47]. When $\log(\text{torque})$ is plotted against $\log(\text{time})$, straight lines are found. At low twists, there is a change of slope at about 30 minutes. Figure 17.24 shows stress relaxation and inverse relaxation after recovery in a nylon monofilament.

If determined in tests made over a wide frequency range, the dynamic modulus would also be expected to vary, but Meredith [37] found no change in nylon for periods of oscillation between 5 and 16 seconds. He also found that the damping of the oscillations was very small when the period of oscillation was long.

Kawabata *et al.* [51] found torsional creep compliance of *Kevlar* 29 to be about 300 times greater than the longitudinal compliance.



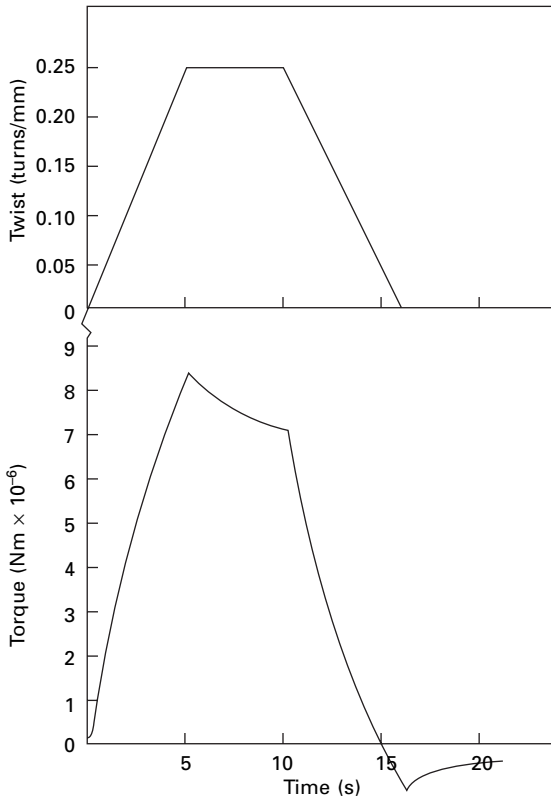
17.22 Torque–twist and recovery of 0.54 tex polypropylene fibre. From Sikorski *et al.* [39].



17.23 Relaxation of torque [47].

17.3.5 Breaking twist

If a fibre is twisted far enough, it will eventually rupture. The twist for which this occurs may be called the breaking twist. It has been confirmed experimentally by Schwab [52] and Koch [53] that, as would be expected theoretically, the number of turns to rupture is inversely proportional to the fibre diameter. To obtain a characteristic



17.24 Torque–twist behaviour for a 75 μm diameter nylon monofilament, followed by stress relaxation, recovery and inverse relaxation. From Sikorski *et al.* [39].

property of the fibre material, one may use the breaking twist angle α . This is the angle through which the outer layers are sheared and is given by:

$$\tan \alpha = \pi d \tau_b \quad (17.26)$$

where d = diameter of fibre and τ_b = breaking twist in turns per unit length.

Typical values of breaking twist angles found by Koch [53] are given in [Table 17.9](#). The general pattern of the results is the same as that for breaking extensions. The effects of some changes of testing conditions are given in [Table 17.10](#).

[Table 17.8](#) includes breaking twist angles measured at constant length by Zeronian *et al.* [46] using an apparatus described by Ellison *et al* [55]. The breaking twist angles correlate with break extensions, which reflects the fact that break is triggered by the elongation at the fibre surface.

17.4 Shear strength

It would be difficult to measure directly the relation between shear stress and shear strain. Finlayson [56] made direct measurements of shear strength by using a bundle of fibres placed in a hole passing through both jaws of the apparatus. The jaws are

Table 17.9 Breaking twist angle [53]

Fibre	Range of α°
Casein	$58\frac{1}{2}$ –62
Polyamide fibre, staple	56–63
Polyamide fibre, continuous-filament	$47\frac{1}{2}$ – $55\frac{1}{2}$
Polyester fibre, staple	59
Polyester fibre, continuous-filament	42–50
Acetate	$40\frac{1}{2}$ –46
Wool	$38\frac{1}{2}$ – $41\frac{1}{2}$
Silk	39
Viscose rayon, normal	$39\frac{1}{2}$ – $35\frac{1}{2}$
Cotton	37–34
Polyacrylonitrile fibre	33 – $34\frac{1}{2}$
Viscose rayon, high-tenacity	$31\frac{1}{2}$ – $33\frac{1}{2}$
Flax	$29\frac{1}{2}$ – $21\frac{1}{2}$
Viscose rayon, very high-tenacity	23
Glass fibre	$2\frac{1}{2}$ –5

Test conditions 65% r.h.; room temperature; 1 cm lengths;
tensile stress of 10 N/mm²; 240 turns/min.

Table 17.10 Effect of conditions on breaking twist angle [54]

Change in condition	Change in breaking twist angle	
	Viscose rayon	Acetate
Test length, 5 → 60 mm	25.2 → 28.7°	—
Rate of twisting, 30 → 565 turns/min	Negligible	Negligible
Humidity, 65% r.h. → wet	None	28 → 36°

then pulled apart and the force required to break the bundle is measured. Breakage must occur through shear. It was found that the breaking load was proportional to the total count of the bundle, which indicated that any composite specimen effect was small. The tensile strength was measured on the same specimens, and the results are given in Table 17.11. It will be seen that shear strength is less than tensile strength, the difference being particularly great in a stretched rayon.

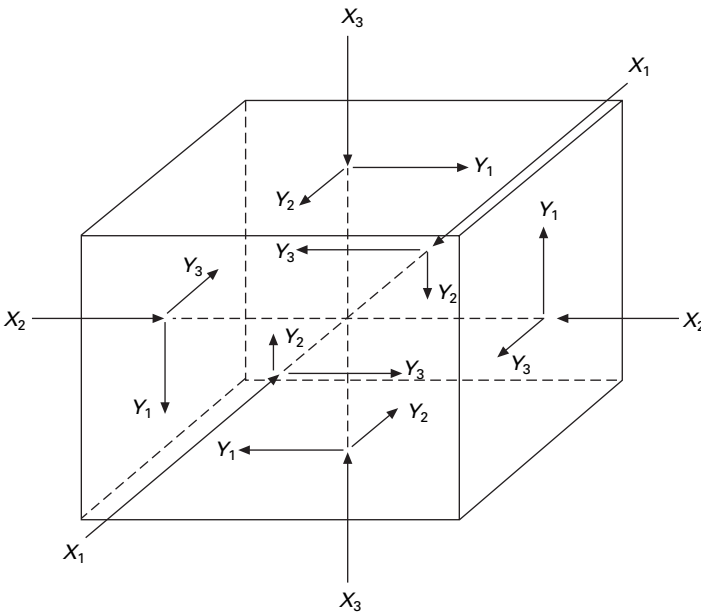
17.5 General elastic deformation

17.5.1 Elastic constants

For small strains, the properties of a homogeneous, perfectly elastic, but anisotropic material may be expressed in terms of a number of elastic constants [23, 57–59]. As indicated in Fig. 17.25, there are three tensile stresses, perpendicular to each face of a cube, and three shear stresses, paired together in two perpendicular directions in the plane of each face. These are related to six possible strains, extension in three mutually

Table 17.11 Shear strength [29]

Fibre	Shear tenacity (mN/tex)		Tensile tenacity (mN/tex)	
	65% r.h.	Wet	65% r.h.	Wet
Highly oriented cellulose	104.0	94.2	706	589
Nylon	111.8	95.2	392	353
Flax	81.4	73.6	255	284
Vinyon	98.1	94.2	275	245
Viscose rayon	63.8	31.4	177	69
Silk	115.8	88.3	314	245
Cotton	84.4	76.5	235	216
Acetate	57.9	50.0	118	78



17.25 Direction of principal stresses.

perpendicular directions and shear about three mutually perpendicular axes. Consequently, there are 36 elastic constants in the stress–strain matrix. However, the matrix is symmetrical, so that the number reduces to 21 for the most asymmetric structure. As the symmetry of the material increases, the number of constants decreases, until, in a completely isotropic material, only four constants (Young’s modulus, Poisson ratio, shear modulus and bulk modulus), of which only two are independent, are usually considered.

It is rare for fibres to be isotropic, and the simplest assumption, which is likely to hold reasonably well for many fibres, is that there is no difference in properties between different directions at right angles to the fibre axis, although these are different from the properties parallel to the fibre axis. Under these conditions, which

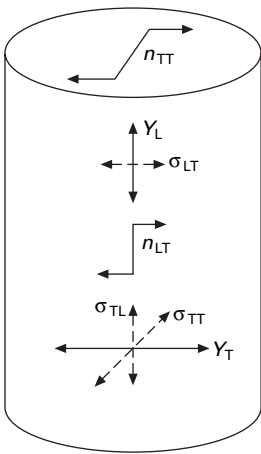
may be called transversely isotropic, the number of common constants may be reduced to seven: two Young's moduli, Y_L and Y_T ; two shear moduli, n_{LT} and n_{TT} ; and three Poisson ratios, σ_{LT} , σ_{TL} and σ_{TT} . Their directions are illustrated in Fig. 17.26. Of these, Y_L is the modulus measured in tensile or bending tests and n_{LT} the shear modulus involved in torsional rigidity. The number of independent constants is reduced to five by the relations:

$$n_{TT} = \frac{Y_T}{2(1 + \sigma_{TT})} \frac{\sigma_{LT}}{Y_L} = \frac{\sigma_{TL}}{Y_T} \quad (17.27)$$

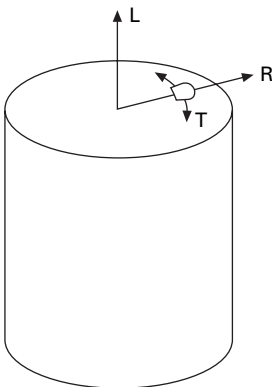
For this system, the bulk modulus, k , that is, the ratio of a hydrostatic stress to the resulting volume strain, is given by:

$$k = \frac{Y_T}{2 + (\sigma_{TL}/\sigma_{LT}) - 2(\sigma_{TT} + 2\sigma_{TL})} \quad (17.28)$$

In a fibre with radial symmetry, as illustrated in Fig. 17.27, all that is justified is the orthotropic system with three mutually perpendicular axes of symmetry. With



17.26 Elastic constants of a transversely isotropic fibre.



17.27 Directions of principal axes in a fibre with radial symmetry.

orthogonal curvilinear coordinates, the directions are taken as longitudinal, radial and tangential. There are 12 constants

$$Y_L, Y_R, Y_T; n_{LR}, n_{RT}, n_{TL}; \sigma_{LR}, \sigma_{RT}, \sigma_{TL}; \sigma_{RL}, \sigma_{TR}, \sigma_{LT}$$

with three relations between them:

$$\begin{aligned}\frac{\sigma_{LR}}{Y_L} &= \frac{\sigma_{RL}}{Y_R} \\ \frac{\sigma_{RT}}{Y_R} &= \frac{\sigma_{TR}}{Y_T} \\ \frac{\sigma_{TL}}{Y_T} &= \frac{\sigma_{LT}}{Y_L}\end{aligned}\tag{17.29}$$

A detailed account of orthotropic elasticity is given by Jayne [60].

In fibres, particularly natural fibres, with an internal structure, a simple model is not a true representation. Transversely isotropic or orthogonal symmetry may apply locally but the elastic constants vary from place to place. This gives rise to complicating effects. For example, in cotton the helical orientation of the molecules leads to an untwisting, namely a shearing, of the fibre under axial tension. In wool the properties will differ in ortho- and para-cortex and in the cuticle (and in meso-cortex and medulla, if present). However, for experiments on whole fibres, it may be convenient to present results as if the simple model was valid.

It may also be noted that the particular elastic constants mentioned are not the only ones that could be defined. It is quite common to use compliances, ratio of strain to stress, instead of moduli. The transverse deformation may be given by the ratio of transverse strain to axial stress instead of by the Poisson ratio, which is the ratio of transverse strain to axial strain. Moduli could be defined as at zero transverse strain, with another constant to give transverse stress developed, instead of at zero transverse stress, and so on. The constants also serve as surrogates for full stress-strain relations.

17.5.2 Measured properties

Tensile tests account for the overwhelming majority of studies of the mechanical properties of fibres. In addition, as already described, there have been a number of studies of torsional behaviour. Thus the only moduli (or more generally the stress-strain relations) for which information is easily available are Y_L and n_{LT} .

Bending, as described earlier, also involves Y_L , but, while tensile behaviour is averaged over the whole fibre, bending is influenced more by outer layers. Comparison of the two gives information on variations in modulus, particularly between skin and core. Bending also gives information on behaviour in compression. Marlow [61] reports that the initial moduli in tension and compression are equal: indeed, a discontinuity at the origin would be highly improbable. This result was confirmed by Elder [62], who examined various synthetic fibre monofilaments in tension, compression, and bending up to 1% strain. However, Chapman's results in Section 17.2.5 show that at larger strains the yielding behaviour is different.

Direct studies of axial compression have been made by cutting sections of fibres or monofilaments and compressing them between plates. Miles [63] found that, although nylon bristle shows the same modulus in tension and compression, the compressive stress–strain curve deviates markedly from the tensile stress–strain curve at strains greater than 1.5%. Whereas the tensile stress–strain curve is approximately linear up to a stress of 0.2 N/tex and a strain of 15%, the compression curve bends over to reach a stress level of 0.04 N/tex, which is substantially constant above 5% compression.

Compression between plates may also be used to study the transverse properties and obtain information on Y_T . Figure 17.28 shows the principles of the test.

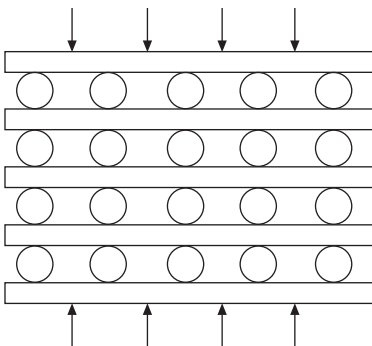
The Poisson ratio σ_{LT} (transverse contraction for imposed extension) can be studied, with some difficulty, by several methods: direct microscopical examination; diffraction methods [65]; and methods involving the insertion of a fibre in a tube and noting the change in electrical conductance [66] or fluid flow. Values of about 0.39 have been reported for nylon. Banky and Slen [67] found values between 0.42 and 0.63 for wool.

A complete study of elastic constants was made by Hadley *et al.* [68], who obtained values of the five independent elastic constants for several manufactured fibre monofilaments, with diameters of 100–300 μm . The experimental methods used were as follows:

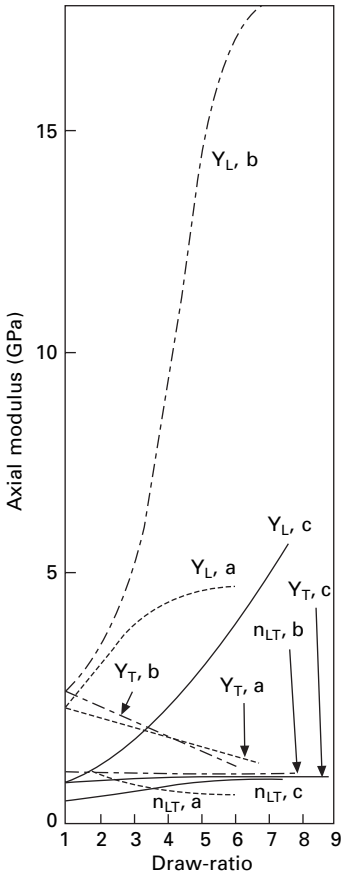
- axial extension, by applying loads and measuring length changes with a travelling microscope, 1 minute after loading, to obtain the axial modulus Y_L ;
- axial Poisson ratio σ_{LT} by measuring the change of diameter of monofilament by means of a microscope with a calibrated eyepiece;
- transverse compression to give thickness of contact between monofilament and plates and change in diameter parallel to plane of contact (the former is mainly dependent on the transverse modulus Y_T ; the latter is related to the transverse Poisson ratio σ_{TT} by an extension of Hertzian contact theory);
- torsion measurements with a vibration pendulum, giving the shear modulus n_{LT} .

By calculation from these observations, the values of all the constants can be obtained.

Figure 17.29 shows how the three moduli vary with the draw-ratio. In general, the tensile modulus changes most rapidly in the range of draw-ratio values that are



17.28 Principle of method of measurement of transverse moduli [64].



17.29 Variation of moduli with draw-ratio: a, nylon; b, polyester fibre; c, polypropylene fibre [68].

commonly found. Consequently, the ratio of tensile to shear modulus, which plays an important part in the buckling of filaments in bulked yarns, can be varied considerably. Table 17.12 collects a set of values, including all the usual constants, together with values of the moduli obtained by Morris [64] under wet and dry conditions.

In spruce wood, which has orthotropic symmetry, Barkas [57] found the values given in Table 17.13. The wood had a density of 0.5 g/cm^3 and a regain of 12%. It will be noted that $Y_T \ll Y_L$, $n_{TT} \ll n_{LT}$, and $\sigma_{TL} \ll \sigma_{LT}$ or σ_{TT} , as would be expected for a material that is highly oriented along the fibre axis.

In the highly oriented HM–HT fibres, such as aramids HMPE and PBO, the weak bonding between the molecules will give low values of the transverse modulus, Y_T , both shear moduli, n_{LT} and n_{TT} , and the Poisson ratio, σ_{TL} . The PIPD ‘M5’ fibre has the somewhat higher shear modulus of 7 GPa due to the hydrogen bonding.

In perfect graphite, there is a very high degree of anisotropy, as shown by Fig. 17.30. The maximum Young’s modulus, for extension within the planes of atoms, is estimated to be 1060 GPa, but across the planes it is only about 37 GPa [69]. The

Table 17.12 Elastic constant data for drawn nylon and drawn and undrawn polyester fibre [68] and for three other fibres [64]

Constant*	Nylon	Undrawn polyester fibre	Polyester fibre A†	Polyester fibre B‡
Y_L	3.45	2.27	9.09	14.08
Y_T	1.37	2.50	1.12	0.62
n_{LT}	0.61	0.93	0.74	0.74
n_{TT}	0.54	0.89	0.39	0.23
σ_{LT}	0.48	—	0.43	0.44
σ_{TL}	0.19	—	0.05	0.02
σ_{TT}	0.27	0.38	0.44	0.37

Constant*	Nylon	Courtelle acrylic fibre	Viscose rayon
Y_L dry	2.50	2.80	2.85
wet	0.95	2.77	0.15
Y_T dry	0.91	0.21	0.14
wet	0.74	0.20	0.0075

*Values of Y and n are expressed in GPa.

†Drawn to a birefringence of 0.153.

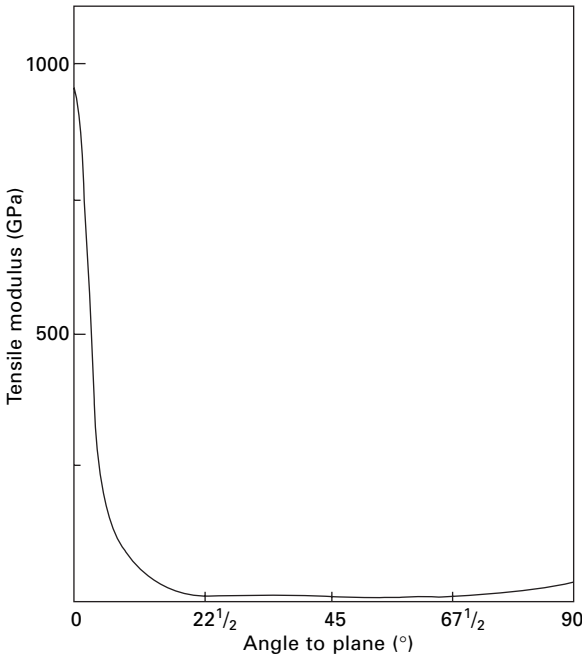
‡Drawn to a birefringence of 0.187.

Table 17.13 Elastic constants of spruce wood [57]

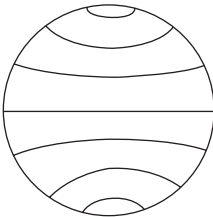
Moduli (kN/mm ²) and Poisson ratios				
Young's moduli	Y_L	$Y_L = 16.6$	Y_T	$Y_R = 0.85$; $Y_T = 0.69$
Shear moduli	n_{LT}	$n_{LT} = 0.84$; $n_{LR} = 0.63$	n_{TT}	$n_{RT} = 0.037$
Poisson ratios	σ_{LT}	$\sigma_{LR} = 0.36$; $\sigma_{LT} = 0.52$	σ_{TT}	$\sigma_{RT} = 0.43$; $\sigma_{TR} = 0.33$
		σ_{TL}	$\sigma_{RL} = 0.018$; $\sigma_{TL} = 0.023$	

shear modulus between planes is estimated to be 4 GPa, but that within planes, 180 GPa and, through planes is estimated as 15 GPa. These properties must be reflected in carbon fibres, though the exact effect will depend on the extent of disorder, disorientation, and interconnection between the planes. Good orientation of planes parallel to the fibre axis implies that the shear modulus (n_{LT} in Fig. 17.26), which determines torsional rigidity, will be low. If the overall arrangement of planes is such that the fibre is transversely isotropic, the transverse modulus Y_T and the shear modulus n_{TT} will be an average of high and low values; but, if the structure is layered, as in Fig. 17.31, which approximates to the form of pitch fibres, there will be substantial transverse anisotropy.

Glass and ceramic fibres are isotropic, so their Young's modulus Y will be the same in all directions. Poisson ratios σ have typical values of around 0.3, and, since there are only two independent elastic constants in an isotropic material, the shear modulus n will equal $Y/2(1 + \sigma)$, namely about 40% of the tensile modulus. There will be no directions of particular weakness in the structure.



17.30 Variation of modulus of perfect graphite crystal with direction [7].

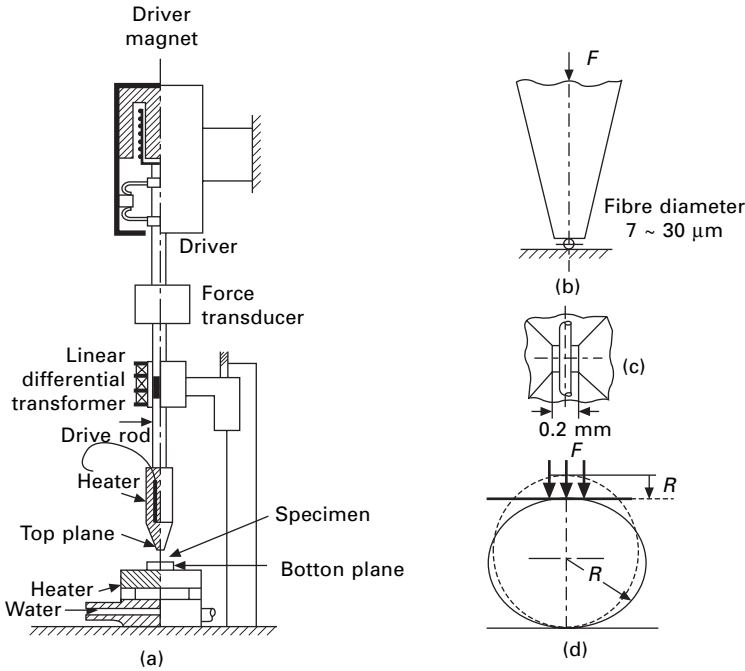


17.31 Carbon fibre oriented in layers across the fibre.

17.5.3 Transverse compression

Kawabata [70] developed the instrument shown in Fig. 17.32(a) for measuring transverse compression on single fibres. As indicated in Fig. 17.32(b) and (c), the fibre is compressed between a top plane, $0.2 \times 0.2 \text{ mm}^2$, and a bottom plane. Both surfaces are mirror finished steel. Other features of the instrument are the driver, force transducer, LDVT for deformation, and provision for heating and wetting. The displacement resolution is $0.05 \mu\text{m}$, which is adequate for testing fibres with a diameter of $5 \mu\text{m}$ or more. Figure 17.32(d) shows the deformation geometry for a fibre of radius R (diameter D) for a contraction U under a force F per unit length. Kawabata modifies the analysis used by Ward *et al.* [71, 72] to give the following equations between measures of stress $f = F/D$ and strain $u = U/D$:

$$u = \left(\frac{4f}{\pi} \right) \left[\left(\frac{1}{E_T} \right) - \left(\frac{\sigma_{LT}^2}{E_L} \right) \right] \left[0.19 + \sinh^{-1} \left(\frac{R}{b} \right) \right] \quad (17.30)$$



17.32 (a) Transverse compression instrument. (b) Section through compression zone. (c) Plan of compression zone. (d) Compression geometry. From Kawabata [70].

$$b^2 = \left(\frac{8fR^2}{\pi} \right) \left[\left(\frac{1}{E_T} \right) - \left(\frac{\sigma_{LT}^2}{E_L} \right) \right] \quad (17.31)$$

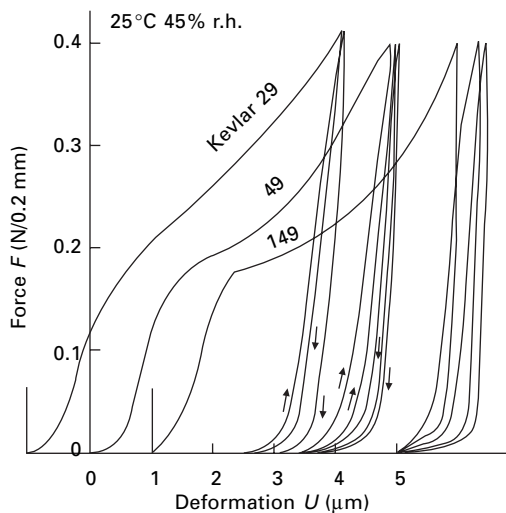
If $(\sigma_{LT}^2/E_L) \ll (1/E_T)$, i.e. when longitudinal modulus \gg transverse modulus, the equations simplify to:

$$u = \left(\frac{4f}{\pi E_T} \right) \left[0.19 + \sinh^{-1} \left(\frac{R}{b} \right) \right] \quad (17.32)$$

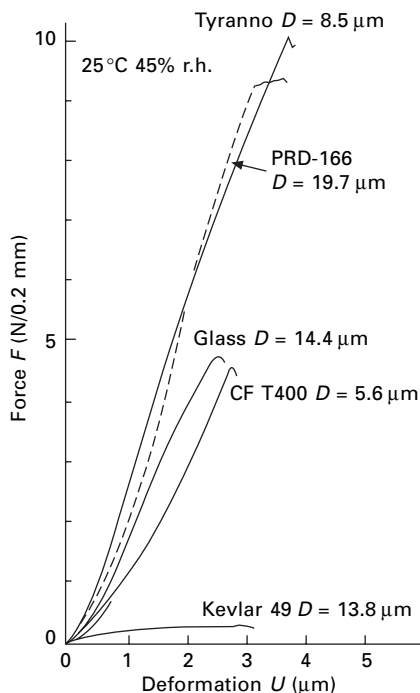
$$b^2 = \frac{8fR^2}{\pi E_T} \quad (17.33)$$

A finite element computation showed good agreement with predictions of the equations used by Kawabata [70]. The \sinh^{-1} term causes little divergence from linearity except for small values of f . The experimental results for *Kevlar 48* diverged from the relation between f and u at low stresses, probably due to an artefact of mounting the specimen, and at high stresses, which would be a change in material properties. Calculated moduli were obtained from intervals along the linear part of the experimental curve.

Figure 17.33 shows force/deformation plots for aramid fibres in transverse squashing and recovery and Fig. 17.34 shows the much larger resistance to deformation in

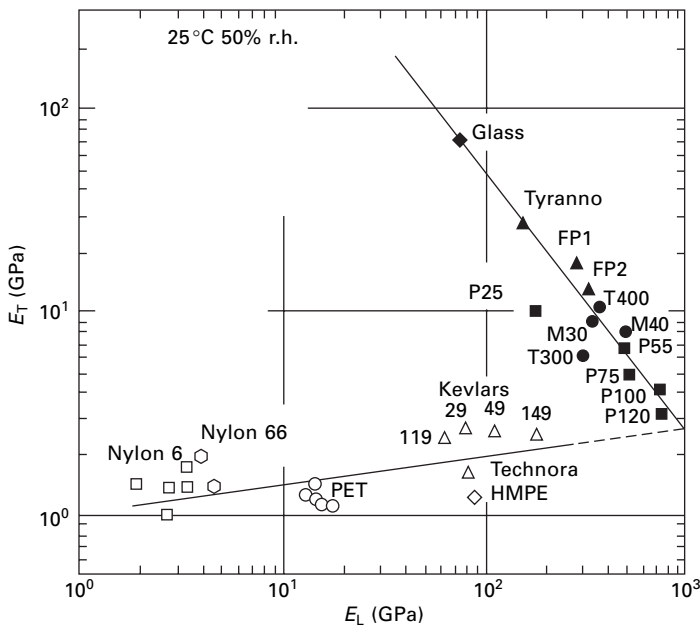


17.33 Deformation and recovery of aramid fibres in transverse compression. From Kawabata [70].



17.34 Inorganic fibres in transverse compression, with *Kevlar* for comparison. *Tyranno* is a silica fibre. PRD-166 is an alumina/zirconia fibre (not commercialised), CF 1400 is a carbon fibre. From Kawabata [70].

inorganic fibres. The log–log plot of axial and transverse moduli in Fig. 17.35 shows a comparatively small difference between the moduli in nylon, which is in agreement with earlier data. There are only small increases in transverse modulus in going to polyester and HM–HT fibres, but the axial modulus increases greatly. In the glass fibre, the moduli are almost equal, but other inorganic fibres show anisotropy with the axial moduli increasing and the transverse moduli decreasing. This is to be expected in carbon fibres where the graphitic planes are axially oriented, but is surprising in the ceramic fibres. Table 17.14 gives values of transverse and axial moduli and strengths. Transverse creep compliance was about 600 times greater than axial compliance [51].



17.35 Comparison of transverse moduli E_T and axial moduli E_L . Brittle type: • carbon (PAN), ■ carbon (pitch), ▲ ceramic, ◆ glass. Yielding type: ○ PET, □ nylon 6, ○ nylon 66, △ kevlar, ◇ HMPE From Kawabata [70].

Table 17.14 Elastic moduli measured by Kawabata [45, 70]

Fibre type	Transverse modulus (GPa)	Axial modulus (GPa)	Transverse strength (GPa)	Axial strength (GPa)
PAN-based carbon	6.03–10.08	235–343	0.95–3.34	3.08–5.19
Pitch-based carbon	3.08–9.95	126–379	0.079–0.64	2.35–4.73
Alumina	12.7	341	2.34	1.34
Silica	26.5	160	6.73	3.34
Aramid	1.59–2.59	63.4–179	0.042–0.077	2.18–3.57
Wool	0.97–1.01	3.55–3.73		

17.5.4 Interactions of stresses

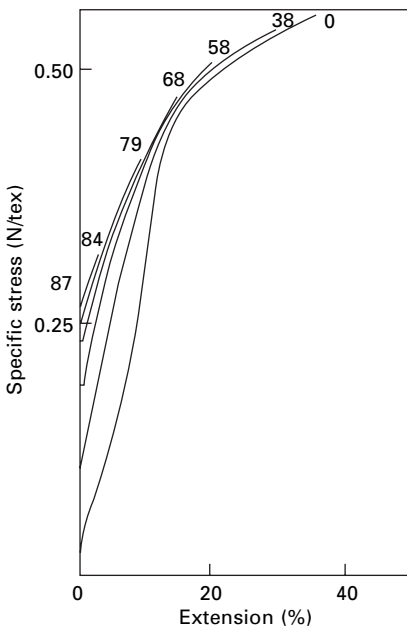
For small stresses and strains, it is assumed in elasticity theory that the effect of each stress is independent and that the total effect of a complex stress situation can be obtained by summing the separate effects of all the stresses. Thus the initial tensile modulus of a fibre would be unaffected by slight twisting. But, when the strains become large, there will be an interaction between the effects.

Dent and Hearle [73] examined the tensile properties of twisted single fibres. The experiments were performed in two ways: with constant length during twisting and with a constant low tension during twisting. Twist values are given as the twist factor $\tau\sqrt{c}$ ($\text{tex}^{1/2}\text{cm}^{-1}$), where τ is the twist in turns/cm and c is the linear density in tex. This is related to the twist angle α by the relation:

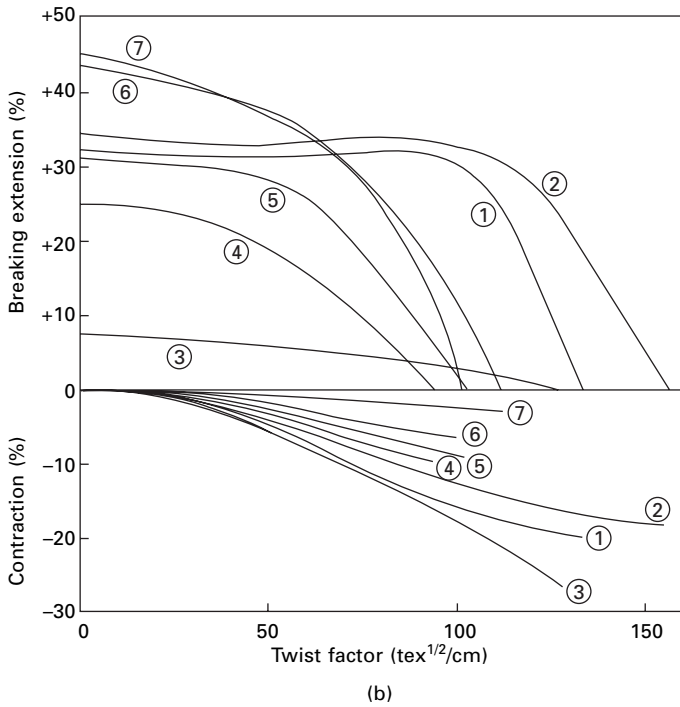
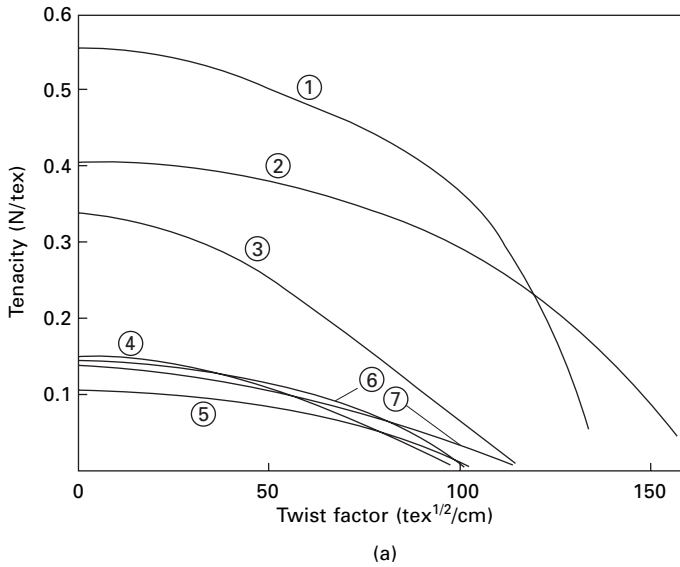
$$\sigma\sqrt{c} = \frac{1}{2}\sqrt{(10^5/\pi v)} \tan \alpha \quad (17.34)$$

where v is the fibre specific volume in cm^3/g .

Figure 17.36 illustrates the effect of twist on the stress–strain curves, with constant length twisting. The tendency to contract during twisting displaces the start of the curve up the stress axis. The initial moduli become less at high twists, and the breaking point occurs much earlier when the twist factor becomes large. A comparison of results obtained in constant tension twisting is given in Fig. 17.37. In most fibres, though not in cotton and wool, the strength is fairly constant up to twist factors of between 30 and 50 $\text{tex}^{1/2}/\text{cm}$ but then decreases rapidly. Failure due to twist alone occurs at twist factors between 50 and 120 $\text{tex}^{1/2}/\text{cm}$.



17.36 Stress–strain curves of nylon fibre twisted to various levels at constant length [73].



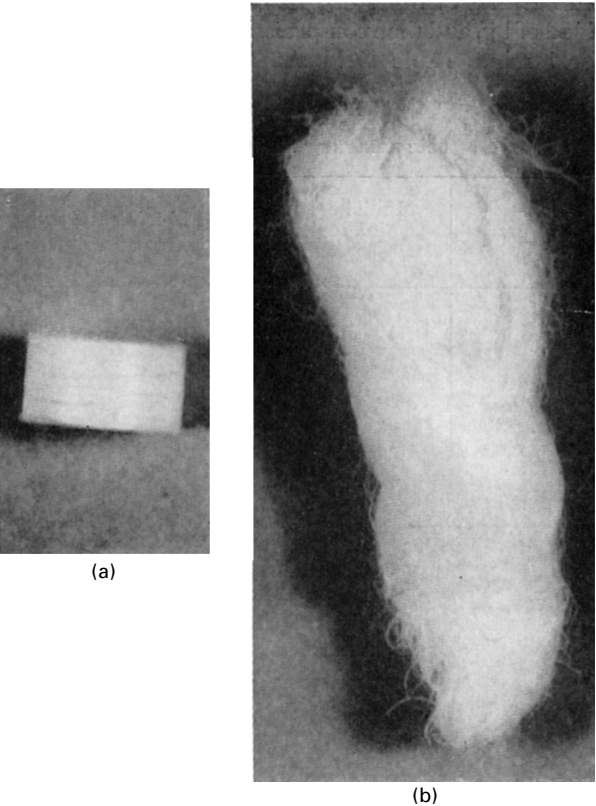
17.37 (a) Change of tenacity, based on linear density before extension, of fibres twisted at constant tension [73]. (b) Change of breaking extension, based on length in twisted state before extension, and of contraction, based on length before twisting, of fibres twisted at constant tension: 1, nylon; 2 *Terylene* polymer; 3, cotton; 4, viscose rayon; 5, acetate; 6 *Acrilan* acrylic; 7, wool [73].

Hearle and Zhou [74] have reported a study of the effect of combined torque and tension on *Kevlar*. The effects are generally similar, except that, in constant-length twisting, the strength of *Kevlar* falls to zero at a twist factor of $30 \text{ tex}^{1/2}/\text{cm}$, which is about half the value found in nylon and polyester fibres.

Table 17.15 Compression of fibre mass [76]

Fibre	Initial height, in., under 1-gf load*	15 min recovery (%)
<i>Saran</i>	0.80	100
Nylon	1.00	90
Wool	1.00	31
Casein	0.50	24
<i>Orlon</i> acrylic fibre	1.20	17
<i>Dacron</i> polyester fibre	1.10	14
Acetate	0.84	11
Viscose rayon	1.30	8

*1 gf = 9.81 mN; 1 in. = 2.54 cm.



17.38 Recovery of compressed rayon staple on wetting: (a) immediately after immersion; (b) 30 s later After Kolb *et al.* [76].

Another example of the application of combined stresses is in the observation by Wilson [75] of a change in the breaking extension of nylon under combined axial and transverse stress.

17.6 Compression stresses on fibre masses

One other type of stress that has been studied is the application of a compressive stress to a mass of staple fibres. Kolb *et al.* [76] placed 0.3 g of fibres in a cylinder of 13 mm ($1/2$ in). diameter, measured the height under a load of 1 gf, and then compressed it under a pressure of 689 MN/mm² (100 000 lbf/in²) for 1 min. Table 17.15 shows values of the initial height and of the recovery after 15 min. It will be noted that fibres that show good tensile recovery also show high recovery after compression. The fibres showed a crushed appearance where they crossed one another. By contrast, the nylon is seen to be little affected. The synthetic fibres recovered better in hot air, and viscose rayon recovered 100% in water. The photographs in Fig. 17.38 show the effect of water on the rayon staple.

17.7 References

1. D. Finlayson. *J. Text. Inst.*, 1946, **37**, P168.
2. B. M. Chapman. *J. Text. Inst.*, 1973, **64**, 312.
3. K. Lee. *J. Textile Inst.*, 2002, **93**, Part 1, 293.
4. K. W. Lee. *Textile Res. J.*, 2005, **75**, 710.
5. J. H. Jung and T. J. Kang. *Textile Res. J.*, 2005, **75**, 713.
6. W. He and X. Wang. *Textile Res. J.*, 2002, **72**, 573.
7. P. W. Carlene. *J. Text. Inst.*, 1947, **38**, T38.
8. F. T. Peirce. *J. Text. Inst.*, 1930, **21**, T377.
9. P. W. Carlene. *J. Text. Inst.*, 1950, **41**, T159.
10. J. C. Guthrie, D. H. Morton, and P. H. Oliver. *J. Text. Inst.*, 1954, **45**, T192.
11. R. Khayatt and N. H. Chamberlain. *J. Text. Inst.*, 1948, **39**, T185.
12. J. W. Ballou and J. C. Smith. *J. Appl. Phys.*, 1949, **20**, 493.
13. R. Meredith and B. S. Hsu. *J. Polymer Sci.*, 1962, **61**, 271.
14. W. Yu and Y. Liu. *J. Appl. Polymer Sci.*, 2006, **101**, 701.
15. B. M. Chapman. *Text. Res. J.*, 1971, **41**, 705.
16. R. G. Livesey and J. D. Owen. *J. Text. Inst.*, 1964, **55**, T516.
17. J. D. Owen. *J. Text. Inst.*, 1965, **56**, T329.
18. R. Meredith In *Proceedings of Fifth International Congress on Rheology*, University of Tokyo Press, Tokyo, Japan, 1969, Volume 1, p. 43.
19. E. M. K  rholm and B. Schr  der. *Text. Res. J.*, 1953, **23**, 207.
20. M. Horio, S. Onogi, C. Nakayama and K. Yamomoto. *J. Appl. Phys.*, 1951, **22**, 966.
21. H. M. Elder. *J. Text. Inst.*, 1966, **57**, T75.
22. J. Skelton. *J. Text. Inst.*, 1965, **56**, T454.
23. A. E. H. Love. *A Treatise on the Mathematical Theory of Elasticity*, Cambridge University Press, Cambridge, 4th edition, 1927.
24. D. E. Bosley. *Text. Res. J.*, 1968, **38**, 141.
25. B. C. Jariwala. MSc thesis, University of Manchester, 1971.
26. B. C. Jariwala. PhD thesis, University of Manchester, 1974
27. B. M. Chapman. *J. Appl. Polymer Sci.*, 1973, **17**, 1693.

28. M. J. Coplan. USAF Report No. 1134, Part III, March, 1952. Cited by E. R. Kaswell in *Textile Fibers, Yarns, and Fabrics*, Reinhold, New York, 1953, p. 61).
29. H. Bohringer and W. Schieber. Cited by H. F. Schiefer, L. Fourt and R. Kropf. *Text. Res. J.*, 1948, **18**, 18.
30. J. K. Berry. *Text. Rec.*, 1946, **64**, Sept., 52.
31. S. van der Zwaag, S. J. Picken and C. P. van Sluijs. Paper presented at Rolduc Polymer Conference, 1988.
32. S. R. Allen. *J. Mater Sci.*, 1987, **22**, 853.
33. S. van der Zwaag and G. Kampschoer. Paper presented at Rolduc Polymer Science Conference, 1987.
34. S. Kawabata. *J. Textile Inst.*, 1995, **86**, 347.
35. S. Kawabata. In *Modern Textile Characterization Methods*, M. Raheel (Editor), Marcel Dekker, New York, 1996, Chapter 19, 311.
36. M. M. Schoppee and J. Skelton. *Text. Res. J.*, 1974, **44**, 968.
37. R. Meredith. *J. Text. Inst.*, 1954, **45**, T489.
38. K. W. Lee. *Textile Res. J.*, 2005, **75**, 377.
39. M. E. Sikorski, C. P. Buckley, J. W. S. Hearle and S. K. Mukhopadhyay. *Rev. Sci. Instrum.*, 1993, **64**, 1947.
40. W. E. Morton and F. Permanyer. *J. Text. Inst.*, 1947, **38**, T54.
41. W. E. Morton and F. Permanyer. *J. Text. Inst.*, 1949, **40**, T371.
42. M. E. Sikorski. PhD thesis, University of Manchester, 1986.
43. M. E. Sikorski and C. P. Buckley. *Proc. 35th Int. Symp. Instrument Soc. America*, Orlando, FL, 1989.
44. S. Kawabata. *Proc. 4th Japan-USA Conf. Composite Materials*, 1988, p. 253.
45. C. Muraki, M. Niwa, N. Amino and S. Kawabata. *J. Textile Inst.*, 1994, **85**, 12.
46. S. H. Zeronian, G. Buschler-Diller, S. Holmes and M. K. Inglesby. *J. Textile Inst.*, 1994, **85**, 293.
47. F. Permanyer. Ph.D. Thesis, University of Manchester, 1947.
48. F. H. Clayton and F. T. Peirce. *J. Text. Inst.*, 1929, **20**, T315.
49. N. H. Chamberlain and M. P. Khera. *J. Text. Inst.*, 1952, **43**, T123.
50. J. Skelton. *J. Text. Inst.*, 1965, **56**, T443.
51. S. Kawabata, M. Sera, T. Kotani, K. Katsuma, M. Niwa and C. Xiaoxin. ICCM 9, 1993, **VI**, 671.
52. R. Schwab. *Kleppzig's Textil-Z.*, 1939, **42**, 397.
53. P.-A. Koch. *Textil-Rdsch.*, 1949, **4**, 199; 1951, **6**, 111.
54. K. Breuer. *Kunstseide*, 1939, **21**, 202.
55. M. S. Ellison, S. H. Zeronian, K. W. Alger, S. M. Aboul-Fadl and T. M. Soler. *Polymer Eng. Sci.*, 1989, **29**, 1738.
56. D. Finlayson. *J. Text. Inst.*, 1947, **38**, T50.
57. W. W. Barkas. *The Swelling of Wood under Stress*, HMSO, London, 1949, Chapter 2.
58. J. C. Jaeger. *Elasticity, Fracture, and Flow*, Methuen, London, 1956, pp. 63-67.
59. J. W. S. Hearle. *J. Text. Inst.*, 1958, **49**, T389.
60. B. A. Jayne. *Theory and Design of Wood and Fiber Composite Materials*, Syracuse University Press, Syracuse, NY, 1972, Chapter 2.
61. P. F. Marlow. *J. Text. Inst.*, 1958, **49**, T40.
62. H. M. Elder. *J. Text. Inst.*, 1966, **57**, T8.
63. J. B. Miles. *Text. Res. J.*, 1971, **41**, 108.
64. S. Morris. *J. Text. Inst.*, 1968, **59**, 536.
65. V. V. Davis. *J. Text. Inst.*, 1959, **50**, T688.
66. F. I. Frank and A. L. Ruoff. *Text. Res. J.*, 1958, **28**, 213.
67. E. C. Banky and S. B. Slen. *Text. Res. J.*, 1956, **26**, 204.

68. D. W. Hadley, P. R. Pinnock and I. M. Ward. *J. Mater. Sci.*, 1969, **4**, 152
69. W. N. Reynolds. *Physical Properties of Graphite*, Elsevier, Amsterdam, 1968.
70. S. Kawabata. *J. Textile Inst.*, 1990, **81**, 432.
71. D.W. Hadley, I. M. Ward and J. Ward. *Proc. Roy. Soc.*, 1965, **A285**, 275.
72. P. R. Pinnock, I. M. Ward and J. M. Wolfe. *Proc. Roy. Soc.*, 1965, **A291**, 267.
73. R. W. Dent and J. W. S. Hearle. *Text. Res. J.*, 1960, **30**, 805.
74. J. W. S. Hearle and C. Y. Zhou. *Text. Res. J.*, 1987, **57**, 7.
75. N. Wilson. *Nature*, 1963, **198**, 474.
76. H. J. Kolb, H. E. Stanley, W. F. Busse and F. W. Billmeyer. *Text. Res. J.*, 1953, **23**, 84.

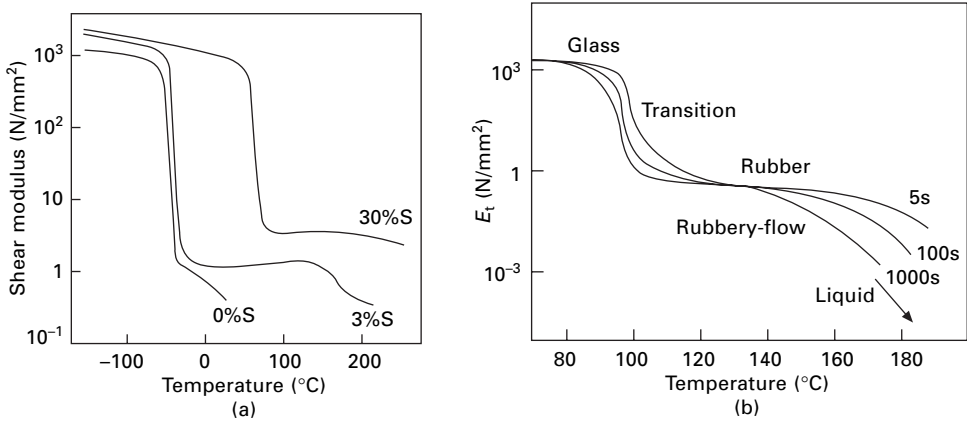
18.1 Introduction

18.1.1 Changes of state in polymers

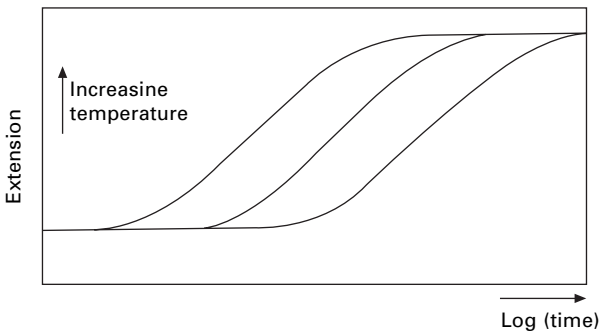
Most materials are characterised by transitions between three states: solid, liquid and gas. Melting and boiling occur so sharply that they can define the limits of temperature scales or be used to identify chemical substances. Polymers behave differently. Firstly, the molecules are so large that decomposition occurs before there could be any possibility of vaporisation. In many polymers, such as cellulose and aramids, decomposition occurs before melting can take place. Secondly, when it occurs, melting is not sharp. There is a gradual softening before a viscous melt forms. The flow properties change strongly with temperature, so that melt-spinning conditions must be carefully chosen. Thirdly, there are important transitions in the solid state. Different allotropic crystal forms are also found in many materials and are of minor importance for fibre behaviour. Transitions within amorphous regions and more subtle effects in crystalline regions play a major role in the processing and use of fibres.

Simple amorphous polymers show one important transition in the solid state. At low temperatures, they are glassy solids; at high temperatures, they are elastomeric. In natural and synthetic rubbers, the transition occurs below room temperature. In plastics, such as polystyrene or polyvinyl chloride, the transition is above room temperature. There are complications. Firstly, the transitions are time dependent as well as temperature dependent. Secondly, unless the polymer molecules are very long and entangled or are lightly crosslinked, the rubbery state merges into viscous flow. There are two other polymeric states. At high degrees of crosslinking, the materials are rigid thermoset resins. Regular polymers can form crystals. All of these features are involved in thermal transitions of fibres, many of which combine crystalline and amorphous material.

Figure 18.1 illustrates the above effects. Below -20°C , natural rubber (Fig. 18.1(a)), is a hard solid with a shear modulus over 1 GPa. It then falls sharply to a value over a thousand times smaller. If there is no crosslinking, the viscoelastic modulus continues to fall as temperature rises. However a moderate degree of vulcanisation forms crosslinks through sulphur bridges and the material has good rubbery properties from -20°C to 150°C . With more crosslinks, the transition from the glassy to the rubbery state moves to higher temperatures. In polystyrene (Fig. 18.1(b)), the transition from glass



18.1 (a) Change with temperature of shear modulus in dynamic tests at about 1 Hz for natural rubber with varying degrees of cross-linking by sulphur(s). From Schneider and Wolf [1]. (b) Tensile relaxation modulus of polystyrene after various times at different temperatures. *s* is for second From Tobolsky [2].



18.2 Creep curves over a wide range of times at different temperatures.

to rubber occurs at around 100 $^{\circ}\text{C}$. The influence of rheology is shown by the change in transition temperature and the change to rubbery flow according to the time available. For large changes in rate, from milliseconds to years, the changes in transition temperature will be much larger. The sigmoidal creep curves in Fig. 18.2 could represent the behaviour of a given polymer at different temperatures.

18.1.2 The nature of transitions

Melting of crystals and boiling of liquids are first-order transitions. The structure changes from the regular packing in crystals to the mobile disorder in a liquid and then to the dispersion into the available volume for a vapour. In addition to the transformation of mechanical state, they are characterised by latent heats and changes of volume.

A thermodynamic second-order transition involves no change of molecular

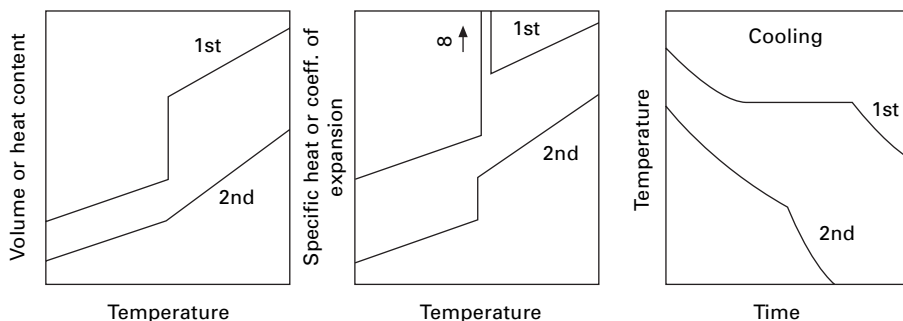
arrangement. Snapshots of the molecular arrangement above and below the transition would be virtually the same. But there is a change in response of the structure, shown up by changes in the second-order quantities, namely the rate of thermal expansion (dV/dT), the specific heat (dH/dT), and so on. The difference between first- and second-order transitions is shown graphically in Fig. 18.3.

The change in amorphous polymers from the glassy to the rubbery state has many of the characteristics of a second-order transition, but is not as sharp and is time dependent. The transition would not be obvious to anyone merely watching a polymer such as polystyrene being heated (in contrast to the clear indication of the melting of wax). It would be apparent if the material were allowed to deform, since it suddenly becomes flexible.

There is a distinction between sharp and broad transitions. This may be, and often is in polymer materials, merely a reflection of local variations in structure, for example, in crystal size or perfection or in local packing, so that the observed effect is really a collection of sharp transitions spread over a range of temperatures. Even in a uniform system, transitions vary in sharpness depending on the extent to which they are cooperative. A highly cooperative transition with a large total energy change, such as the change from crystal lattice to liquid disorder, will be sharp. It makes no sense to say that a crystal is half-melted (except in terms of a molten region progressively spreading over the crystal with sharp boundaries between the regions), since the only way of defining the crystal is by saying that a large number of neighbouring molecules are packed regularly together. However, at the other extreme, the dissociation of a molecule into two parts (e.g. $H_2 \rightarrow H + H$) is not at all cooperative: each molecule splits independently of the rest and the degree of dissociation can change steadily from 0 to 100% over a broad transition range of temperature. Some of the transitions in fibres lie between these two extremes.

18.1.3 Observation of transitions

Melting can be directly observed, for example by putting a fibre on the hot stage of a microscope and noting when it flows. However, the change may not be very sharp. Softening of the material, which leads to fibres sticking together, gives an impression of melting. Values of melting points for a given fibre vary. For example, in earlier

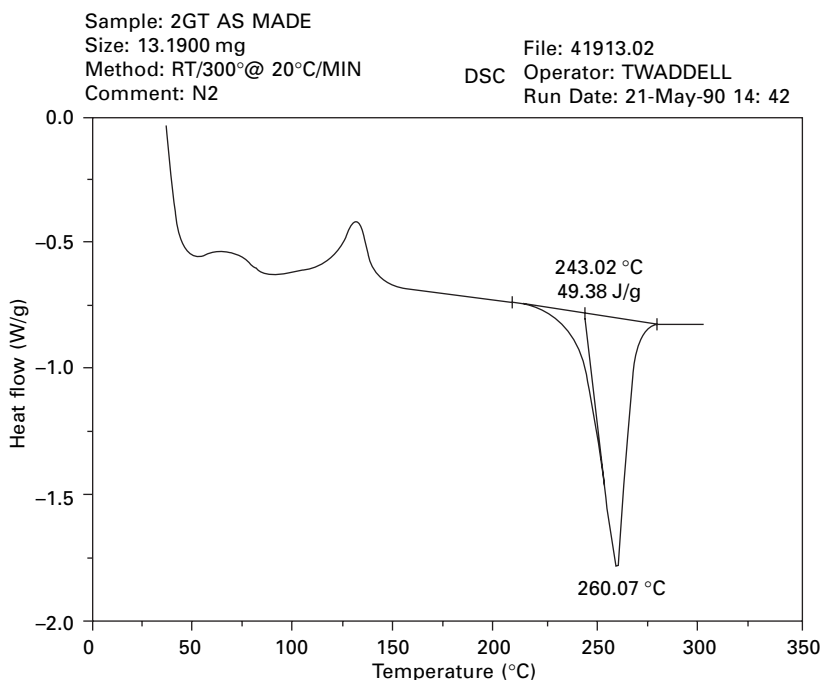


18.3 Changes occurring in first- and second-order transitions.

accounts the melting point of nylon 66 is given as 250 °C but later to values between 255 and 265 °C.

More information can be obtained from thermo-analytical techniques using commercial instruments. In differential scanning calorimetry (DSC), the heat required to increase the temperature of a sample is compared with a reference. The heat flow is controlled to maintain a constant heating rate and to keep both temperatures the same. A plot of heat flow against temperature would indicate the value of the specific heat¹. Since latent heat is ideally taken up at a constant temperature, it should show as an infinite negative spike. Experimental limitations would spread the spike to a limited extent, but in a typical fibre test as shown in Fig. 18.4 the spread is much larger, indicating the range over which melting occurs. The positive spike at about 120 °C indicates some additional crystallisation or increased crystal perfection. The broad peak above 50 °C may be due to some rearrangement of the structure to a lower energy state. The initial rapid decrease is an artefact of the start of heating. The heat flow rate between peaks and troughs gives values of specific heat and integration of the peak or trough gives values of latent heat of crystallisation or melting.

An alternative to DSC is differential thermal analysis (DTA) in which heat flow is maintained constant. Differences in temperature between sample and reference give similar information to DSC and enable specific and latent heats to be computed.



18.4 A typical print-out from a DSC scan of a polyester fibre melting around 260 °C. Courtesy of Du Pont.

¹For a given heating rate, heat flow in J/s (watt) can be converted to J/°C, and knowing the mass of the sample to specific heat in J/°C/g.

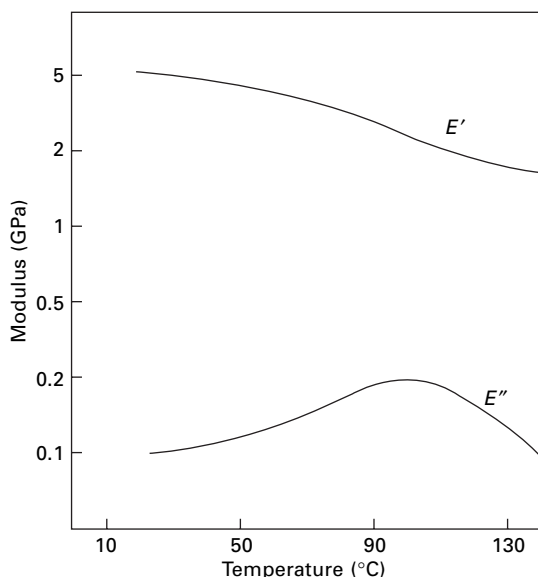
Measurements of volume or other dimensional changes with temperature are not very convenient for fibres. The most instructive way of studying the secondary transitions in the solid state is by measurement of dynamic mechanical analysis (DMA), as described in Section 16.5.3, with the typical plot in Fig. 18.5 showing the decrease in the modulus E' and paer in the modulus E'' in the transition region. Measurements of dielectric constant and dielectric loss can be made, but while these are good for polymer films or blocks, they are not well suited to fibres. Changes of dielectric properties with frequency and temperature are included in [Chapter 21](#).

Thermomechanical analysis (TMA) measures changes in length at constant tension or vice versa and has been less used on fibres than DMA. The other common thermal measurement, thermogravimetric analysis (TGA), measures chemical decomposition through loss of weight and is not relevant to this book.

18.2 Melting

18.2.1 Characteristic features

Melting is an obvious phenomenon. The fibre loses its identity and contracts to a molten globule. In bulk, the molten material is a viscous liquid, quite different from a collection of solid fibres. Melting can also be detected in other ways, though different experimental methods do give slightly different values of melting point, particularly if the heating rate changes. The fibre loses strength, so that, at the melting point, a small weight suspended by the fibre will fall. At the melting point, the fibre becomes sticky. And on melting, the material takes up its latent heat, detectable as an endotherm peak in calorimetry, as described above.



18.5 Real and imaginary dynamic moduli of nylon 6.6 fibres: plotted on a logarithmic scale. From Murayama *et al.* [3].

The melting of textile fibres is an essentially irreversible process. To some extent, this is true of all materials: a wax statuette cannot be reformed without the mould. But in fibres, it is not only the external form but also the fine structure that cannot be reproduced without repeating the manufacturing sequence of extrusion, drawing and other treatments. Typical values of fibre melting points are given in Table 18.1.

Apart from differences attributed to experimental error, there are differences between different specimens of the same type of fibre as a result of structural differences. A major source of difference is the size and perfection of crystalline regions. Thermodynamically, the melting point is the temperature at which the values of the free energy F in the crystalline and molten states are the same, so that they are in equilibrium together. We therefore have:

$$\Delta F = \Delta U - T_m \Delta S = 0 \quad (18.1)$$

$$T_m = \frac{\Delta U}{\Delta S} \quad (18.2)$$

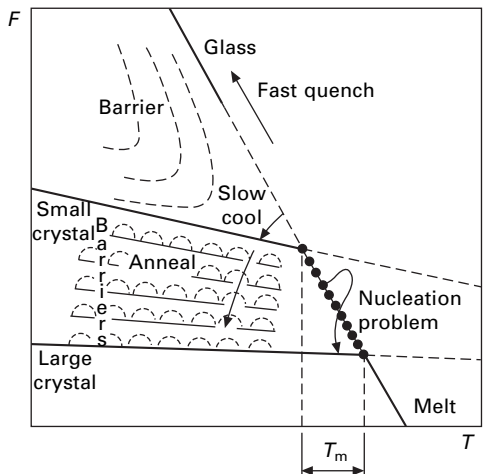
where Δ refers to the difference between the states, U is the internal energy, S is the entropy and T_m is the melting point.

The situation is shown graphically in Fig. 18.6. In a small or imperfect crystal, which forms on initial crystallisation, the internal energy is not as low as in large perfect crystals, owing to the surface or defect energy contributions. The melting point is therefore low, but increases as crystals grow and defects are eliminated on annealing. An example of this effect is shown in Fig. 18.7, in which the variation of melting point with the thickness of polyethylene single crystal lamellae is plotted. It may be noted that a value of about 140 °C is usually quoted for bulk linear polyethylene, with values of about 110 °C for branched polyethylene, where the crystals are necessarily less perfect. The extrapolated value for large perfect crystals is 146 °C.

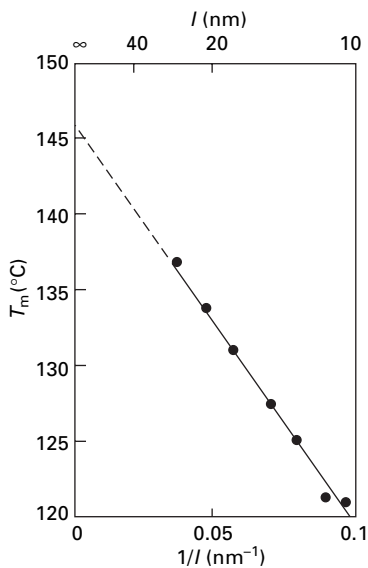
The dependence of melting point on crystal size and perfection is important in melt-spun synthetic fibres, because, as a result of their formation by rapid quenching and drawing, they will contain many small imperfect crystals. Annealing, by exposure to temperatures approaching the quoted melting point, will serve to melt the smallest and least perfect crystals and allow larger, more perfect ones to grow or, more generally, will allow a molecular rearrangement, with a removal of defects, which leads to bigger and better crystalline regions. There will also be some increase in total crystallinity, although this will be relatively small, since, to a considerable

Table 18.1 Fibre melting points (approximate values)

Polyethylene – low density 120 °C
– high density 135 °C
Polypropylene 170 °C
Secondary acetate 250 °C
Cellulose triacetate 300 °C
Nylon 6 215 °C
Nylon 6.6 260 °C
Polyester fibre 260 °C
(Cellulosic and protein fibres decompose before melting)



18.6 Classical free energy diagram for melting and annealing.



18.7 Variation of melting point of polyethylene single crystals with lamellar thickness. From Bair *et al.* [4].

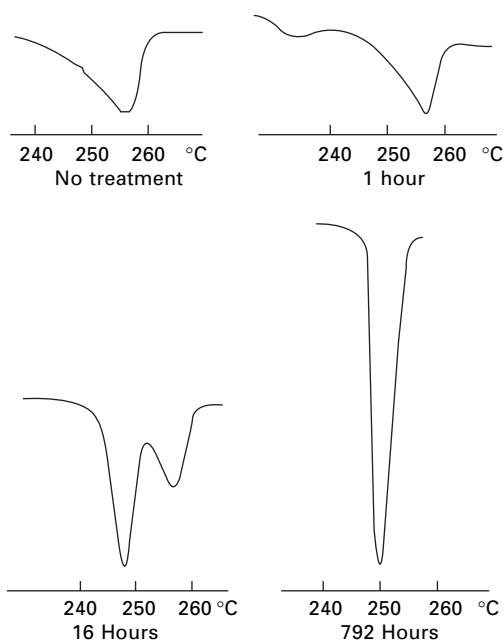
degree, an increase in ordering in one region of a structure of long chains can only be achieved by accumulating disorder in other regions.

Another well-known phenomenon is the depression of the melting point in the presence of impurities. This shows up in fibres as a lowering of the melting point in the presence of water, as is shown experimentally by observing the melting of fibres enclosed in a glass capsule full of water. In nylon, the wet melting point is 80 °C lower than the dry melting point, and even in polyester fibres it is 35 °C lower [5].

A situation that is specific to polymers is the strong dependence of melting point, particularly the internal melting during annealing, on the state of stress on the system. The cause of this is the existence of the tie-molecules that link the crystalline regions. If these are under tension, then the melting of part of the chain will relieve the tension in the tie-segment and allow its entropy to increase. There is thus not only the usual contribution to ΔS from the portion transferring from crystal to melt but also a contribution from the change in the linked segment. The latter part will be greater if the chains are under tension. Looking at it another way, one can say that stress from the tie-molecules will help to break up the smaller crystals.

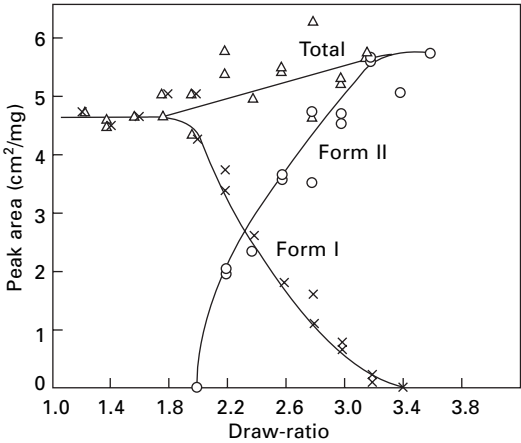
18.2.2 Multiple melting phenomena

Nylon and polyester fibres, among other polymeric materials, show interesting effects of multiple melting in differential calorimetry. When a fibre sample is heated, a negative peak is indicative of the absorption of latent heat and thus of melting. Figure 18.8 shows such data for undrawn nylon yarn as received and after annealing at 220 °C. In the untreated yarn, the peak is at 256 °C, but on annealing a second peak appears below 240 °C. With further annealing this becomes more prominent and rises in temperature level, to reach 260 °C eventually. This suggests that there are two structures with different melting behaviour. Bell [6] calls the first, produced by rapid melting, form I and the second, given by annealing, form II. There is a point at which both give a peak at 256 °C, but the two can be distinguished by seeing if annealing

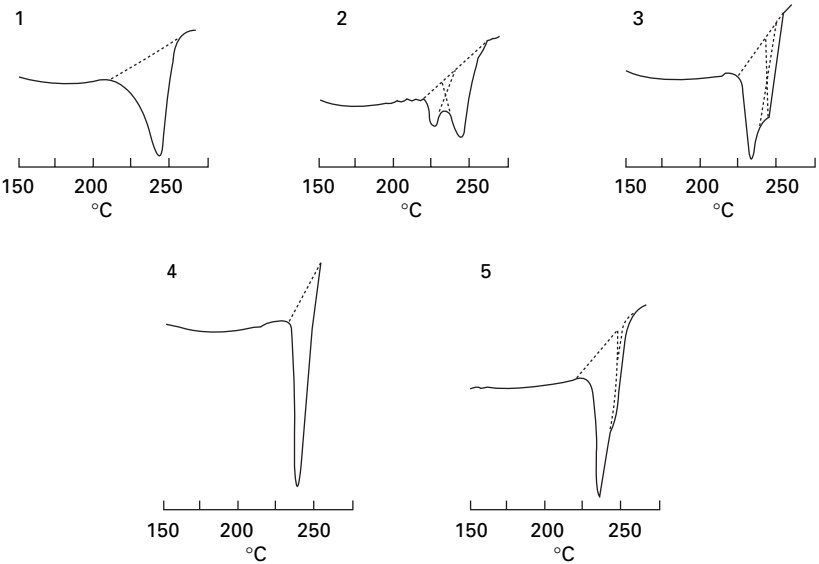


18.8 DSC data for undrawn nylon 6.6 yarn after annealing at 220 °C for various times. From Bell *et al.* [6].

causes the second peak to appear or not. The change from form I to form II also occurs on cold drawing, as shown in Fig. 18.9. Similar effects are found for polyester (PET), (Fig. 18.10). Even after a day's annealing, form II melting has only reached about 240 °C, whereas the drawn fibre in Fig. 18.4 has an endotherm at 260 °C. Presumably the higher stiffness of the polyester molecule hinders the growth of larger perfect crystals except in an oriented structure where the molecules are more nearly parallel.

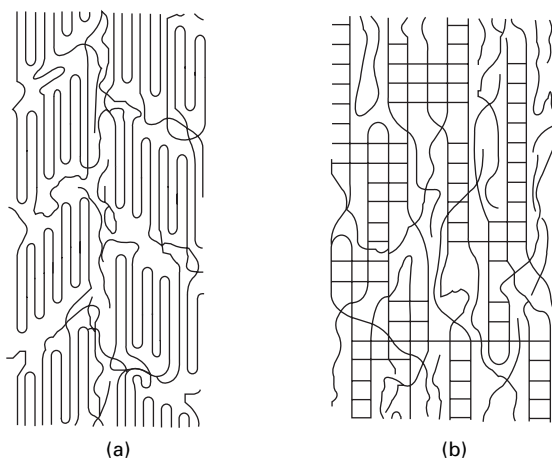


18.9 Change in areas of melting endotherms with draw ratio for nylon 66. From Bell and Murayama [7].

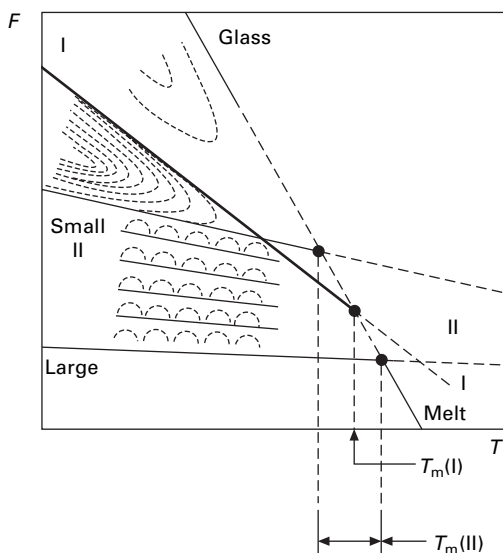


18.10 Effect of annealing time at 220 °C on DTA plots for polyester (PET) that had been crystallised for 0.5 h at 110 °C: 1, no annealing; 2, 0.25 h; 3 2 h; 4, 6.5 h; 5, 23.5 h. From Bell and Murayama [7].

The experimental evidence on the subject was reviewed by Hearle and Greer [8]. They suggested that form II consists of crystalline micelles, as in Figs 1.16 and 18.11, which become larger on annealing, whereas form I is another state of the solid polymer in which many individual chain repeat units will be in register with neighbouring units, but interspersed with disorder so that there are no separate crystalline and non-crystalline regions, as in Fig. 1.18(c). Although there are problems in applying thermodynamics to metastable states, they explained the effects in terms of changes in free-energy, $F = (U - TS)$. Hearle [10] took the argument further, as shown in Fig. 18.12. As temperature increases, $(-TS)$ becomes numerically greater leading to a

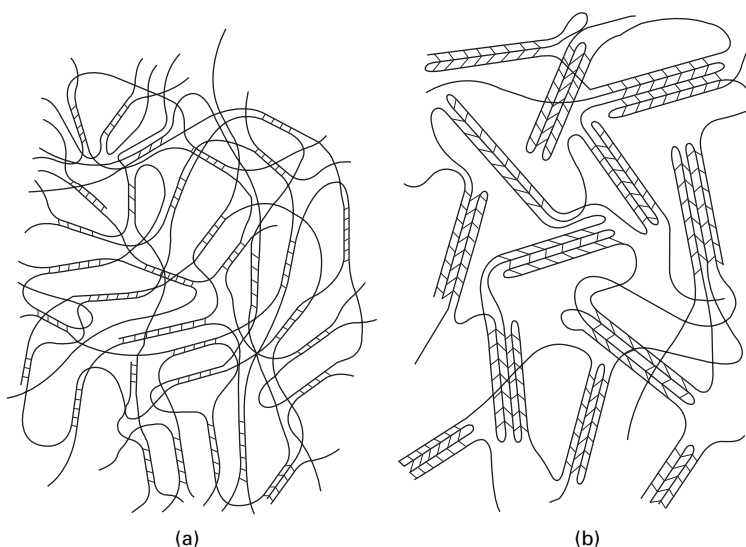


18.11 (a) A fringed micellar model proposed by Hearle and Greer [9]. (b) An alternative form, from Hearle [10].

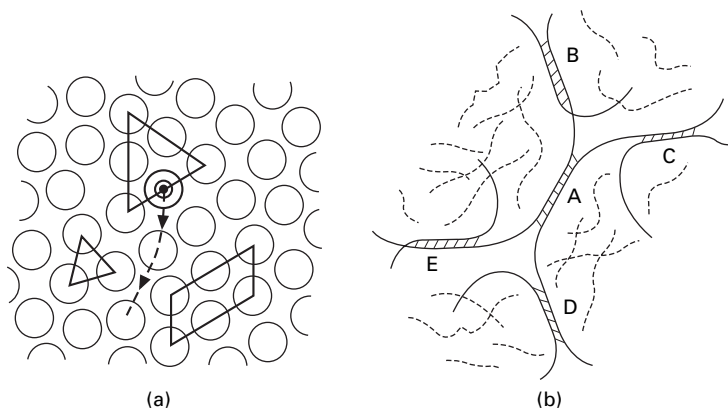


18.12 Free energy of various forms. From Hearle [10].

decrease in free energy along the glass \rightarrow liquid line. The lines for form II correspond to the effect of annealing with the melting point increasing as crystals grow and become more nearly perfect, as shown in Fig. 18.6. There is nothing remarkable in this. The question is where form I fits in. Hearle [10] made the controversial suggestion that form I is a *dynamic crystalline gel*. Figure 18.13(a) is a schematic view of a form I structure in unoriented polymer, which anneals to form II shown in Fig. 18.13(b). The dynamics are as follows. In a liquid near the melting point (Fig. 18.14(a)), molecules are locally in crystallographic register but are continually changing position in a state of dynamic equilibrium. In the polymer form II (Fig. 18.14(b)), the locally



18.13 Schematic of possible structures of (a) form I and (b) form II in unoriented polymer. For clarity, the packing is much more open than in reality. From Hearle [10].



18.14 (a) Molecules locally in crystallographic register in a liquid. (b) Chain segments locally in register in form I. From Hearle [10].

linked segments would also be in a state of dynamic equilibrium. However, when the segments (A) separated, the neighbours (B, C, D, E) would still be linked. This would be happening all over the material with links breaking and re-forming, but always maintaining the continuity of a solid. The entropy of this form would be greater than the static structure of form II, so that the slope of the free energy diagram would be steeper, as shown in Fig. 18.12 and would intersect with the liquid line to give the melting point of form I. However, annealing would allow the material to fall through the energy barriers to form II with small imperfect crystals having a lower melting point. Further annealing would give larger and better crystals with a higher melting point, eventually passing that of form I. The changes between the several structures in various circumstances are shown in Fig. 18.15(a), with the thermodynamic justification in Fig. 18.15(b).

Whether or not the above explanations are correct, the important practical point is to note the complexity of melting behaviour and the difference in forms that can occur. Commercial fibre samples may be in either form I or form II, depending on their thermomechanical history.

18.2.3 Sticking and bonding

At temperatures below the melting point as defined above, thermoplastic fibres stick together. For example, in early studies of false-twist texturing, Burnip *et al.* [11] found that nylon yarn would pass through the heater at 255 °C but emerged as solid rod. The filaments had not become liquid but they had merged together. The sticking temperature is sometimes referred to as the meting point, since it implies a degree of molecular mobility that is not normally found in a solid.

This property of fibres is utilised in thermal bonding of nonwovens. Mukhopadhyay *et al.* [12] used the flexible thermomechanical analyser described in Section 18.5.2 to measure the strength of thermal bonds. Figure 18.16 shows the experimental arrangement. Fibre loops are held together at specified tension, temperature and time.

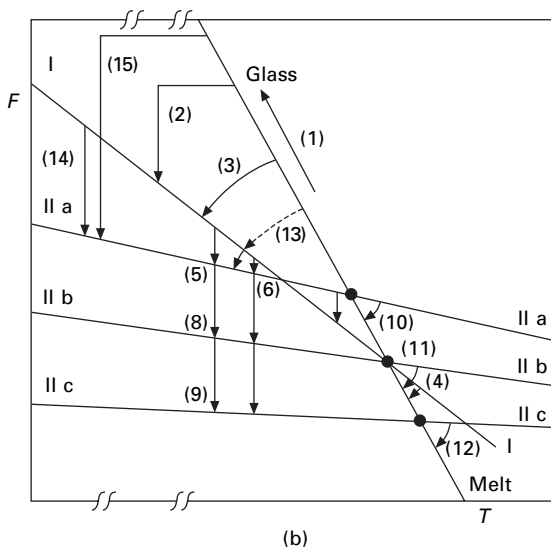
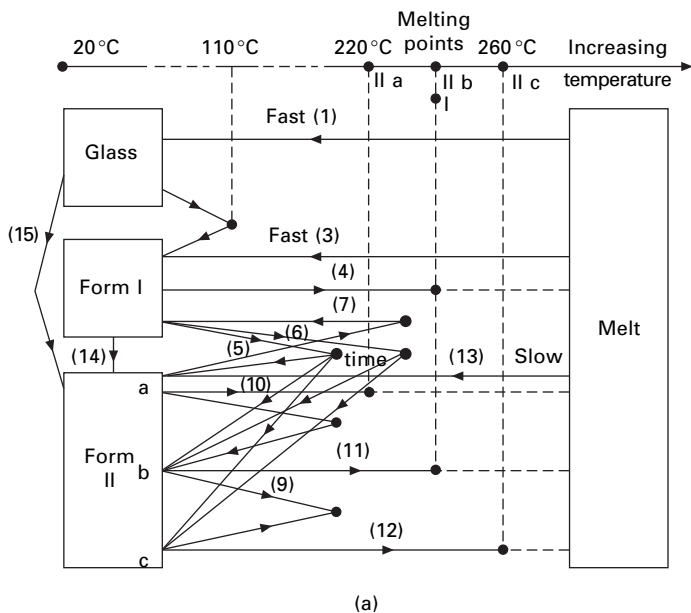
After cooling to room temperature, two arms are then cut and the force required to break the bond is measured. Table 18.2 shows measurements of bond strengths of four polypropylene fibre types and one copolyester. Except for the low bond strength for PP4, where an SEM picture shows that the material has become too nearly molten, the bond strengths correlate with commercial bonding performance. For optimum bonding, it is clearly necessary to choose the right fibre and the right bonding conditions. In a later paper, Mukhopadhyay [13] showed that pre-wetting polypropylene fibres gave good bonding at a lower temperature.

Kim *et al.* [14] present computational analysis of thermal bonding in bicomponent fibres.

18.3 Dynamic mechanical responses

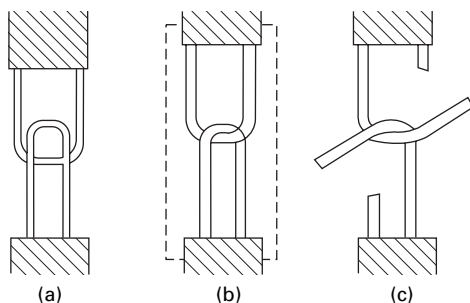
18.3.1 Dynamic moduli

As described in Section 16.5.2, the real (storage) modulus depends on the elastic part of the deformation, and the imaginary (loss) modulus or $\tan \delta$ depends on the time-



18.15 (a) Schematic of changes between various forms. (b) Changes between forms on free energy diagram. From Hearle [10].

dependent part. Above and below the transition region, the elastic deformation, with high or low modulus, is dominant. In the transition, the structural response is sluggish, so that there is substantial energy absorption, which gives the peak in loss modulus and the phase difference between stress and strain given by the peak in $\tan \delta$.



18.16 Testing bond strength: (a) fibres as mounted; (b) in heated chamber under controlled tension; (c) ready to measure bond strength. From Mukhopadhyay *et al.* [12].

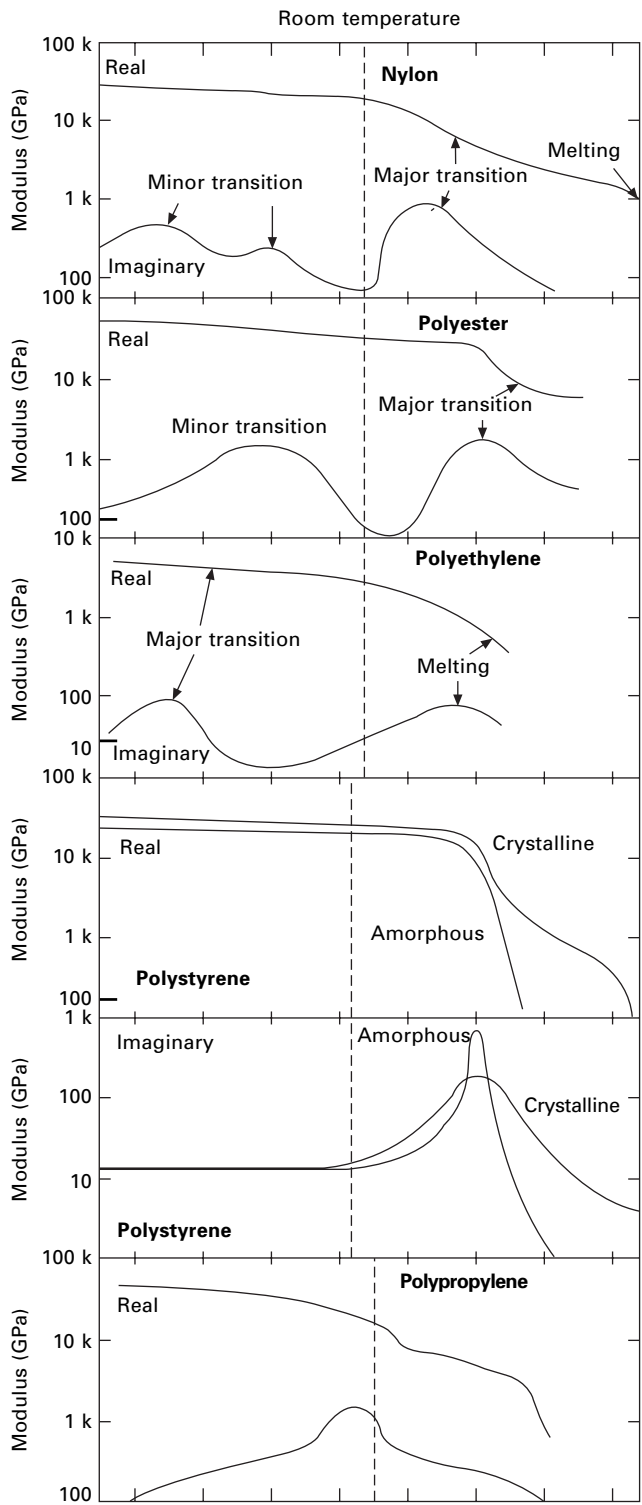
Table 18.2 Thermal bonding of four polypropylene fibres and a copolyester. 10 mN tension gives 17 mN/tex on each arm. From Mukhopadhyay *et al.* [12]

Bonding conditions					Fibre properties		Commercial thermobonding performance
Temperature (°C)	160	100	150	150	20	150	
Time (seconds)	60	60	60	60			
Tension (mN)	10	20	10	20			
Fibre type	Bond strength mN/tex				Fibre strength mN/tex		
PP1		96			391	125	Very poor
PP2		124			355	113	Poor
PP3		240	134	191	308	113	Good
PP4		161	168	224	255	101	Very good
Co-polyester	103, 132	Fibre broke			122	70	Good

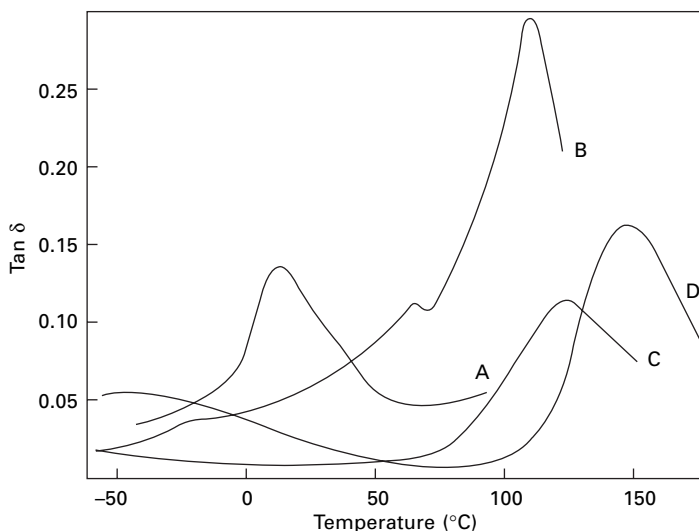
18.3.2 Observed behaviour

The dynamic and loss moduli of various polymers as measured by Takayanagi [15] are shown in Fig. 18.17. For the simplest semicrystalline polymer, polyethylene, a glass transition is shown by a sharp drop in modulus E' and peak in E'' (also shown in $\tan \delta$) around -120°C . This can be attributed to the onset of freedom of rotation around $-\text{CH}_2-$ bonds. There is then a reduction of slope of the modulus plot, which is clearer in data by Kawaguchi [17], and a trough in $\tan \delta$ before a steeper fall in modulus and increase in $\tan \delta$ over a long temperature range towards melting. In polystyrene, which is too stiff at room temperature to be useful as a textile fibre, there is a single transition at around 100°C in plots that show the major influence of crystallisation.

Polypropylene has a single transition near room temperature, which is also shown by the peak in $\tan \delta$ in dynamic bending in Fig. 18.18. This accounts for the sluggishness of its response. Any cyclic deformation is damped by the large energy absorption. The transition will be due to the onset of bond rotation, occurring at a higher temperature than in polyethylene because of the bulky side group.



18.17 Dynamic mechanical properties of various polymers. Upper lines are real (dynamic) and lower lines are imaginary (loss) moduli. From Hearle [16] based on data from Takayanagi [15].

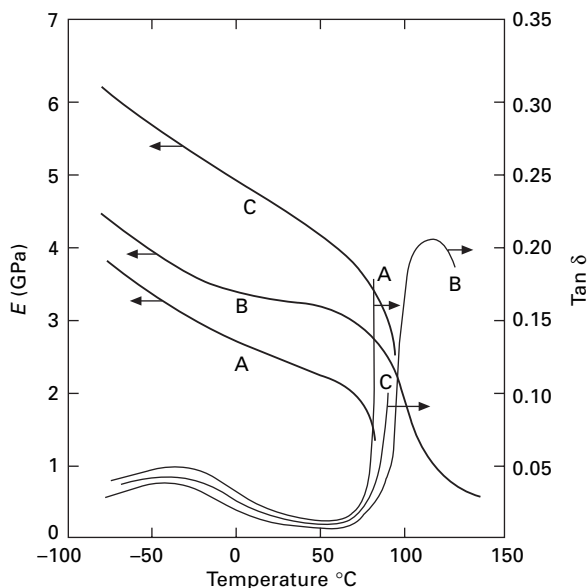


18.18 Tan δ measured in dynamic bending of fibres at 0% r.h. at frequencies of 200–300 Hz: A polypropylene; B acrylic fibre; C nylon 6.6; D polyester fibre.

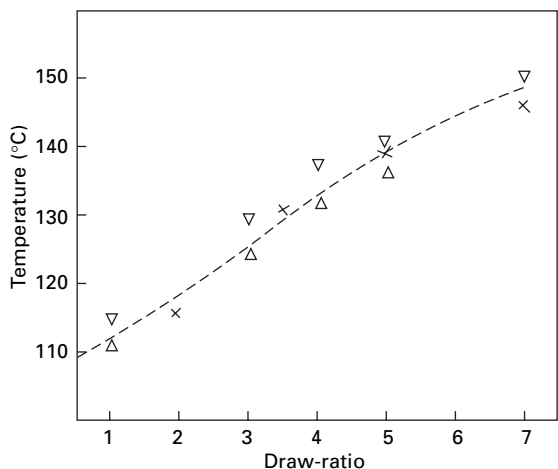
Nylon 6 shows two low-temperature peaks in E'' , which correspond to the peak in polyethylene but reflect bonds becoming free at different temperatures. Similar peaks in $\tan \delta$ are reported by Kawaguchi [17] and, in nylon 66, by Bell and Murayama [7] film at slightly lower temperatures, though this may be due to different test conditions. In rapidly quenched film, referred to in the above discussion of multiple melting as form I, the low-temperature transition was split between two peaks, but in slowly cooled film, form II, the whole transition was in the higher of the two peaks. Polyester shows a single peak in the low-temperature region.

The low-temperature peaks are of academic interest, but the peak at about 70 °C in nylon and 120 °C in polyester has great practical relevance to the behaviour of the fibres in processing and use. The transition curves are influenced by crystallinity and orientation, as shown by the results for polyester fibre in Fig. 18.19. The variation of the transition temperature (as indicated by a maximum in $\tan \delta$) with draw-ratio in polyester fibres is shown in Fig. 18.20 Davis [21] found that there was a change with time in polyester held at 150 °C at a stress of 5.5 mN/tex. The storage modulus increased and $\tan \delta$ decreased by about 10%, approaching equilibrium after 30 minutes. He also showed that the storage modulus was about 30% higher in an annealed fibre than in a direct spun fibre. In a paper on the relation between the transition and dye diffusion, Davis [22] showed that both storage and loss moduli are higher for nylon 66 in glycerol than in water and decrease as the amount of water in a glycerol/water mixture increases.

In addition to the fairly large transitions shown up by large peaks in the loss modulus, there may be minor transitions, causing small peaks or shoulders. These may be due to other deformation mechanisms, though Moseley [23] attributed a large collection of small peaks at large strain amplitudes to non-linearity of response, and Dumbleton and Murayama [24] showed that lack of uniformity in a fibre could cause



18.19 Dynamic modulus and $\tan \delta$ of PET as measured by Kawaguchi [18] at about 100 Hz: A, undrawn, 2% crystallinity; B, undrawn, 50% crystallinity; C, drawn 5×, 25% crystallinity.



18.20 Effects of draw-ratio on temperature of maximum $\tan \delta$ for polyester fibres, from data by Meredith [19] and Kondo *et al.* [20].

the appearance of extra peaks. Kveder and Rijavec [25] report dynamic modulus and loss data for partially oriented and drawn nylon 66 yarns.

The two transitions are also shown in dielectric properties of polyester film as described in Section 21.6, which includes the combined influence of temperature and frequency.

The influence of water on the transitions is shown by the work of van der Meer [26, 27], as illustrated in Fig. 18.21. In dry viscose rayon, there appears to be a transition somewhere above 200 °C, but in wet rayon it shifts to below 0 °C. In nylon 6, the transition falls from about 80 to 10 °C; and there is a slight effect even in polyester fibres. The change in the position of the $\tan \delta$ peak of nylon 6.6 with relative humidity is shown in Fig. 18.22.

Figure 18.23 demonstrates how the peak in $\tan \delta$ can be traversed by varying relative humidity, instead of temperature or time. The acrylic fibre has a large transition near 100 °C, which is shown in Fig. 18.18. The large decrease in stiffness is shown by the dramatic changes in stress–strain curves in Fig. 18.24. Experimental demonstration of the transition just below 100 °C was given by Rosenbaum [28], who found sharp changes in axial thermal expansion, breaking extension and creep rate. In this material, the mobility is mainly restricted by the intermolecular forces caused by the strong electric dipoles in the $\text{—C}\equiv\text{N}$ groups, and the transition occurs when freedom of relative movement of chains in less-ordered regions becomes possible. Another transition, at a slightly higher temperature, will be due to a similar effect in the ordered regions. However, the individual chains still remain stiff enough for the fibre to be solid, and a further increase in mobility occurs at a considerably higher temperature when the chain changes from its regularly coiled, cylindrical, rod-like form to a more flexible, random coil. Results for some natural polymer fibres are shown in Fig. 18.25.

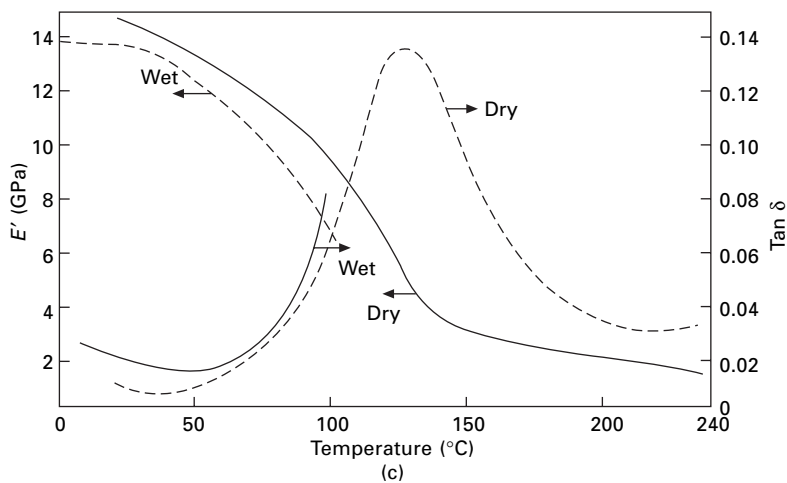
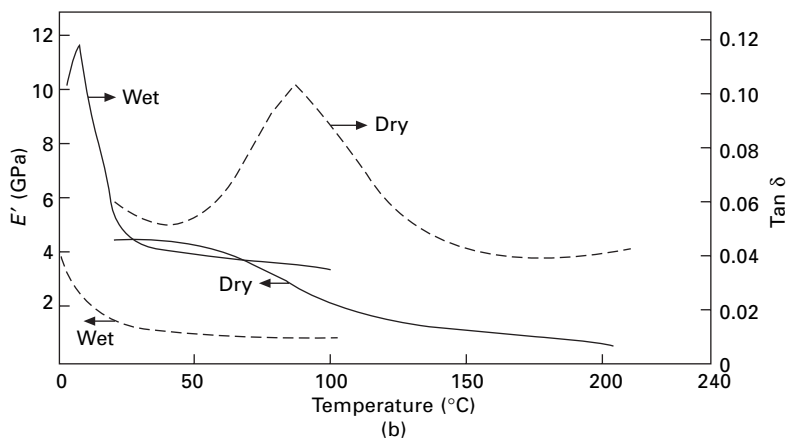
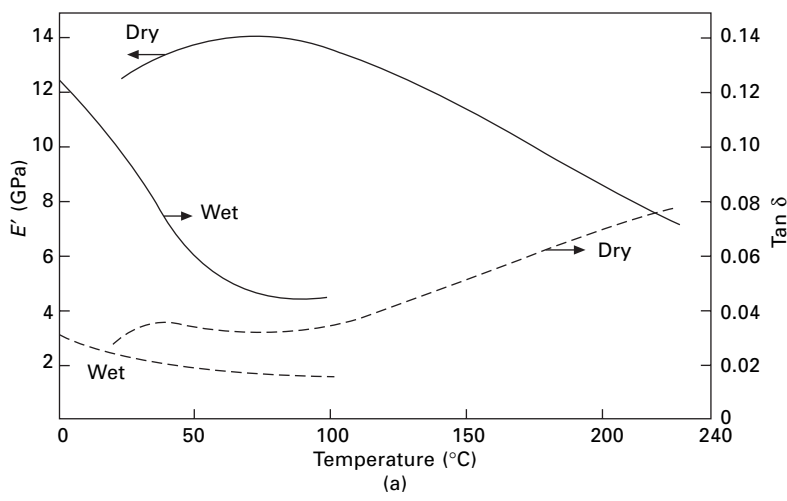
The low modulus and high extensibility of elastomeric fibres depend on their glass transition temperature being below the working temperature. Measurements of dynamic mechanical properties by Houston and Meredith [30], illustrated in Fig. 18.26, show a rather sharp transition for natural rubber between -50 and -20 °C but a more spread-out transition for the spandex fibre *Lycra* from about -80 to $+20$ °C.

18.3.3 A comparison of temperature effects

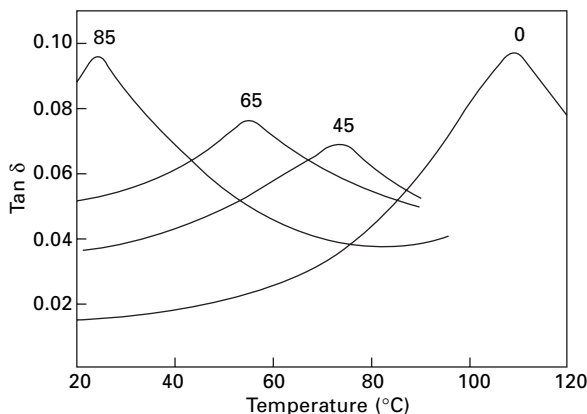
Hearle [31] suggested that an ideal set of transitions for a fibre material was of the type shown in Fig. 18.27. The low-temperature transition (A) gives some freedom to the non-crystalline regions, and thus gives moderate extensibility and high toughness to the fibre, without making it too soft and extensible. The working region near room temperature is free of transitions. The greater freedom required to allow crystallisation to occur appears at the higher transition (B). Then the melting point (C) is higher still but well below the temperature of chemical degradation.

These properties are shown, in considerable measure, by nylon and polyester fibres, except that the higher transition in wet nylon does come down to room temperature, and chemical degradation impinges on the melting point. The latter effect means that the material must not be kept in the molten state, certainly in the presence of oxygen, for any length of time. Even appreciably below the melting point, prolonged exposure can cause a loss of strength, as indicated by the results in Table 18.3.

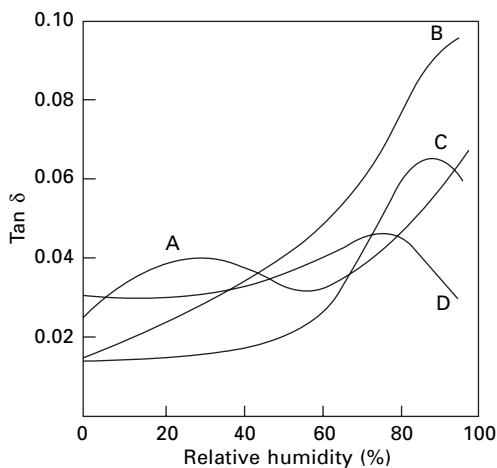
Where there is a single glass-to-rubber transition, the fibres are too soft if the transition is below room temperature, as in polyethylene, or too stiff and brittle if



18.21 Variation of E' and $\tan \delta$ with temperature wet and dry: (a) viscose rayon; (b) nylon 6; (c) polyester fibre.



18.22 Effect of temperature on $\tan \delta$ for nylon at various humidities. From Meredith [19].

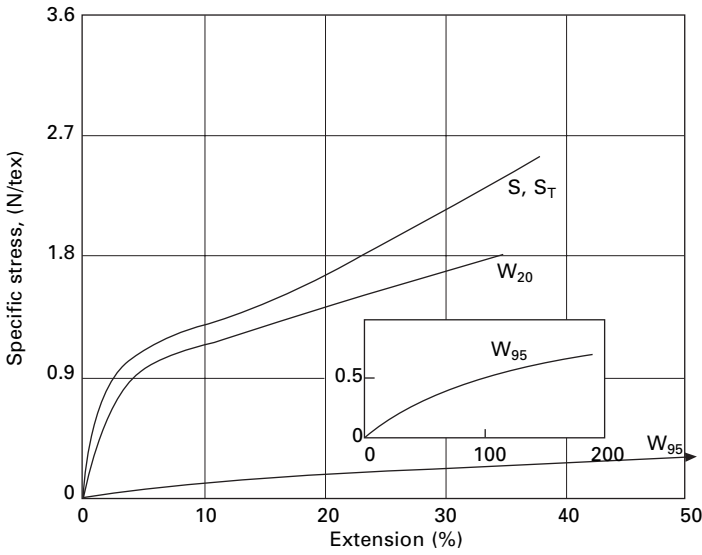


18.23 Effect of relative humidity at 20°C on $\tan \delta$: A, viscose rayon; B, nylon 6.6; C, nylon 6; D, *Acrilan* acrylic fibre.

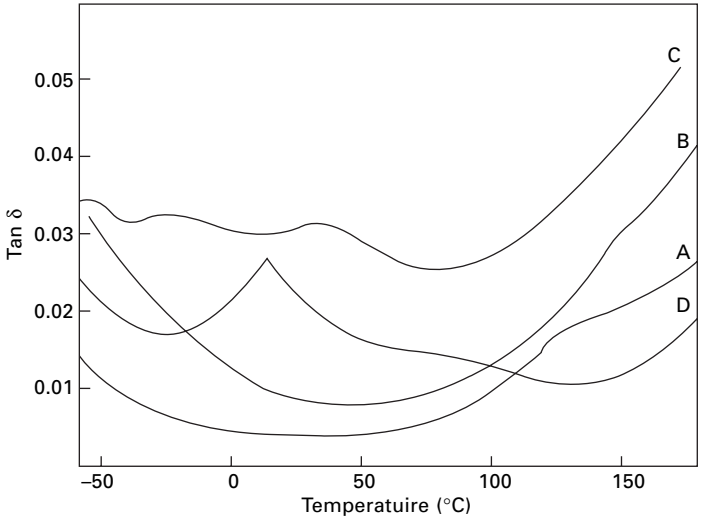
the transition is above room temperature, as in polystyrene. If the transition straddles room temperature, as in polypropylene, the properties are acceptable but not ideal.

In fibres that are not melt-spun, the above requirements are not as critical, although in one way or another there must be some freedom in the structure at room temperatures and a greater freedom at higher temperatures. Moisture often plays a part in this.

All the fibres made from linear polymers are fundamentally thermoplastic (as distinct from crosslinked polymers, which are not), but in some, such as cellulose, the thermoplastic character cannot be exhibited because chemical decomposition, leading to charring or burning, sets in first. Acrylic fibres and wool are on the borderline, where both effects occur at similar temperatures.



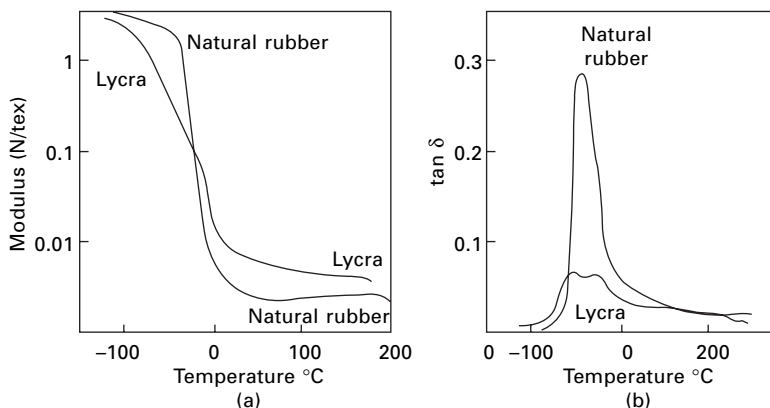
18.24 Stress–strain curves of *Courtelle* acrylic fibre. S, 65% r.h., 20 °C as received; ST, 65% r.h., 20 °C, after water at 95 °C; W₂₀, in water at 20 °C, as received; W₉₅, in water at 95 °C, as received.



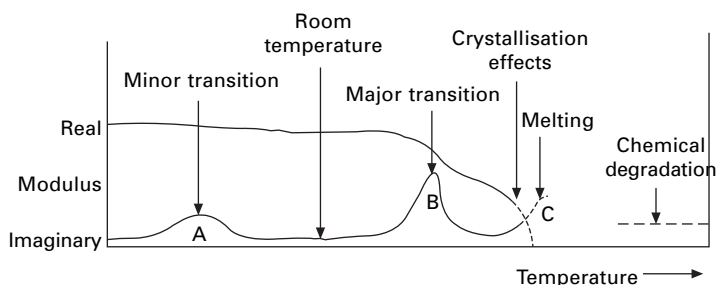
18.25 Dynamic loss of some natural polymer fibres at 0% r.h. in dynamic bending: A, mercerised cotton; B, viscose rayon; C, secondary acetate; D, wool. From Meredith [29].

18.4 Transitions in keratin fibres

As can be expected from their complex multilevel structure, the transitions in wool and other keratin fibres are complicated. There are three defined transitions, which are reviewed by Wortmann [33]. All are strongly dependent on regain as well as



18.26 Dynamic mechanical response of elastomeric fibres: (a) dynamic modulus; (b) $\tan \delta$ [30].



18.27 Transitions in an 'ideal' fibre. From Hearle [31].

Table 18.3 Loss of strength on prolonged exposure of high temperatures [32]

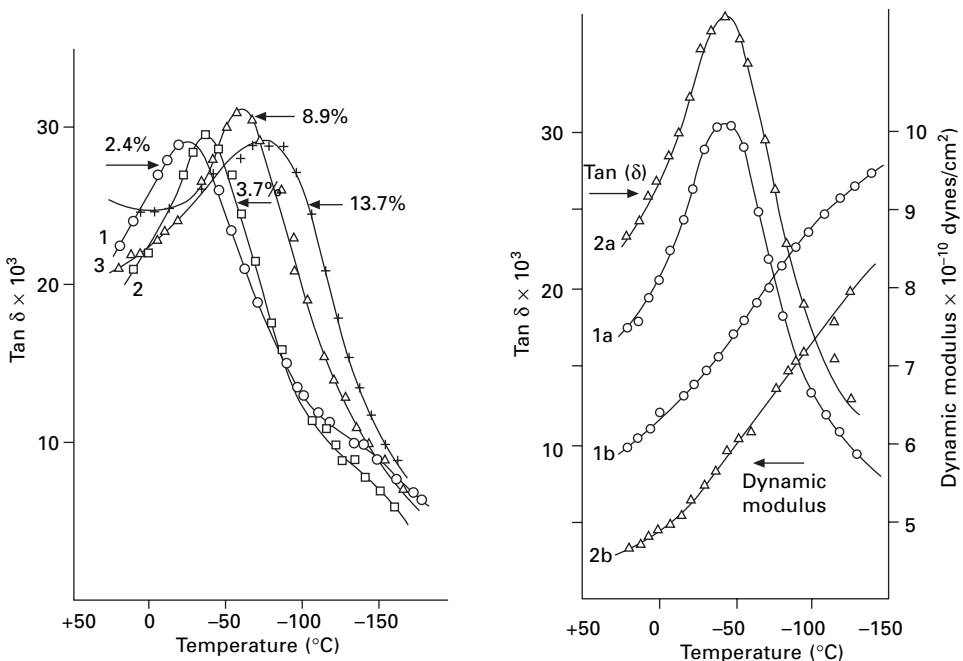
Fibre	Percentage strength retained			
	After 20 days		After 80 days	
	At 100 °C	At 130 °C	At 100 °C	At 130 °C
Viscose rayon	90	44	62	32
Cotton	92	38	68	10
Linen	70	24	41	12
Glass	100	100	100	100
Silk	73	—	39	—
Nylon	82	21	43	13
Polyester, <i>Terylene</i>	100	95	96	75
Acrylic, <i>Orlon</i>	100	91	100	55

temperature. In increasing temperature, these are referred to as β , α ¹ and denaturation transitions. The α -transition is also called the glass transition, but it is more instructive to regard the glass-to-rubber transition as occurring in two stages at the β and α transitions.

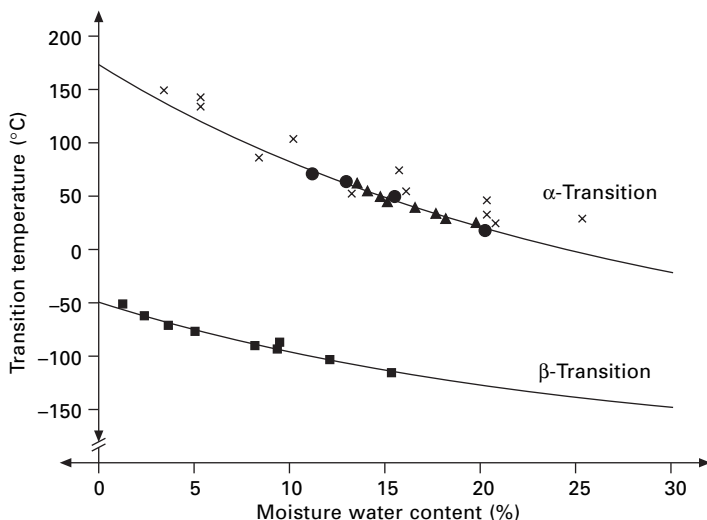
¹Not to be confused with the mechanically induced $\alpha \leftrightarrow \beta$ transition in helical crystals.

Druhala and Feughelman [34, 35] investigated the β -transition by cyclic tensile testing and found a peak in $\tan \delta$ at about -40°C in horsehair in a fairly dry state (2.4% regain), dropping to about -90°C at 13.7% regain, (Fig. 18.28(a)). This is similar to the low-temperature transition in nylon, which, as indicated in Fig. 20.15, is associated with freedom of rotation around covalent bonds. In proteins both main chain and side chain bonds are immobile below the transition region. A comparable measurement on rhinoceros horn, Fig. 18.28(b), shows the decrease in modulus at the transition. The variation in the transition temperature is shown by the lower curve in Fig. 18.29.

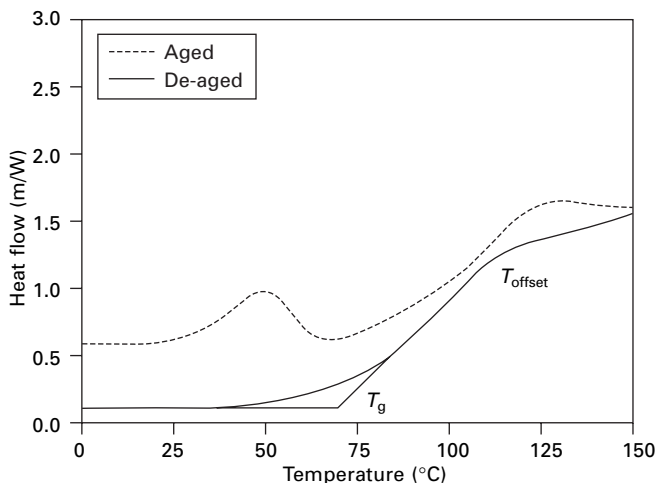
Wortmann *et al.* [37] investigated the α -transition by measuring the recovery from cohesive torsional set as mobility was induced. They found the transition at 175°C in dry wool decreasing with increasing moisture content as shown by the upper curve in Fig. 18.29. The behaviour is similar to that of nylon, which has a transition going from around 100°C when dry to near 0°C when wet. Phillips [38] and Kure *et al.* [39] studied the transition by DSC. As shown in Fig. 18.30, a sample of wool, referred to as aged, has an endothermic peak at 50°C , which presumably reflects the release of some temporary set in the amorphous matrix. This is followed by an increase in the heat flow rate, namely an increase in specific heat, between 75 and 125°C , which is interpreted as a glass transition. If the sample is heated to the final temperature and then cooled, the endotherm at 50°C is no longer present in a subsequent



18.28 (a) $\tan \delta$ for low-temperature transition in horsehair at 110 Hz at different regains. (b) Modulus and $\tan \delta$ for rhinoceros horn: 1a and 1b cut parallel to growth; 2a and 2b cut perpendicular to growth. From Druhala and Feughelman [34].



18.29 Change of transition temperatures with moisture content with lines for the Fox equation, from Wortmann [33], with data from Druhala and Feughelman ■ [34, 35], Rosenbaum ▲ [36], Wortmann *et al.* ● [37] and Phillips × [38].



18.30 DSC traces for wool. From Kure *et al.* [39].

DSC trace, but the heat flow at the glass transition is still present. In wool, the temperatures are higher in the dry material, and run into the temperatures of denaturation. Phillips [38] found that an endotherm at 60 °C was present in a fibre aged for 52 days at 20 °C, disappeared after rapid cooling, and reappeared in a trace after 15 days at 20 °C.

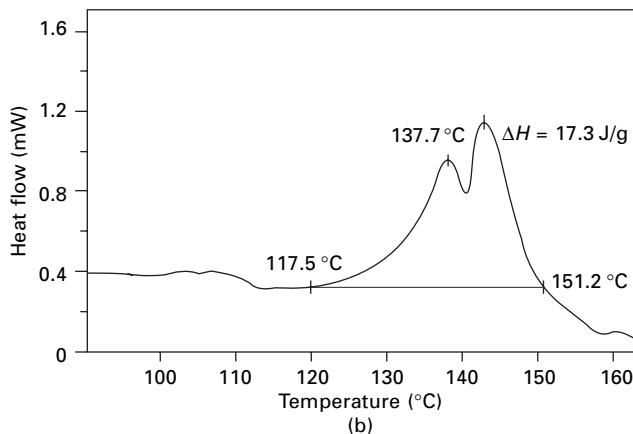
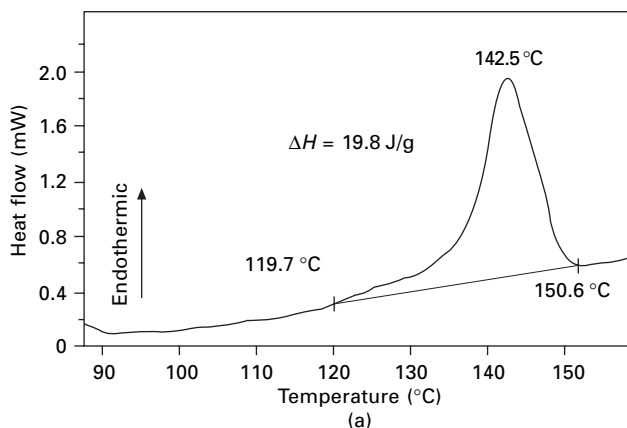
Wortmann *et al.* [33, 37, 40] has shown that for both wool and human hair the β and α transition temperatures T_i vary with moisture content according to the simple mixture equation proposed by Fox [41] as shown in Fig. 18.29:

$$\frac{1}{T_t} = \frac{m_1}{T_{t1}} + \frac{m_2}{T_{t2}}$$

where m_1 and m_2 are the mass fractions and T_{t1} and T_{t2} relate to dry and wet wool.

By fitting and extrapolating the experimental data, the α -transition in wool has $T_{\alpha1} = 174^\circ\text{C}$, which is in agreement with torsional data by Menefee and Yen [42], and $T_{\alpha2} = -148^\circ\text{C}$, which agrees with values found for ice and glassy water ($m_1 = 0$ and $m_1 = 1$) [43, 44]. For the β -transition, $T_{\beta1} = -49^\circ\text{C}$ and $T_{\beta2} = -210^\circ\text{C}$.

The highest temperature transition can be studied by high-pressure DSC in order to maintain water in the material. Wortmann and Deutz [45, 46] report measurements on eight keratinous materials. Figure 18.31 shows a single endotherm peak at 143°C in mohair and double peaks in wool at 138 and 143°C . The transition is interpreted as a ‘melting’ of the helical crystalline fibrils, though it is influenced by restraints from the amorphous matrix. It is called *denaturation*, since it is an irreversible process. The enthalpy $\Delta H = 17.1 \text{ J/g}$. If heating is stopped just past the first peak in wool and



18.31 DSC curves for (a) mohair and (b) merino wool. ΔH = denaturation enthalpy From Wortmann and Deutz [45].

the fibre is then rapidly cooled, a tightly crimped coil is formed. This indicates that the first transition occurs in the ortho-cortex, which has super-contracted, and the second transition occurs in the para-cortex, which has a higher cystine content. Differences in denaturation temperatures in different keratins are attributed to the varying cystine concentrations in the matrix.

The denaturation temperature decreases from 210 °C in the dry state to 150 °C at a moisture content of 25% [47, 48]. Wortmann [33] considers various explanations for the effect of water, but concludes that there is a gap in understanding that requires further investigation.

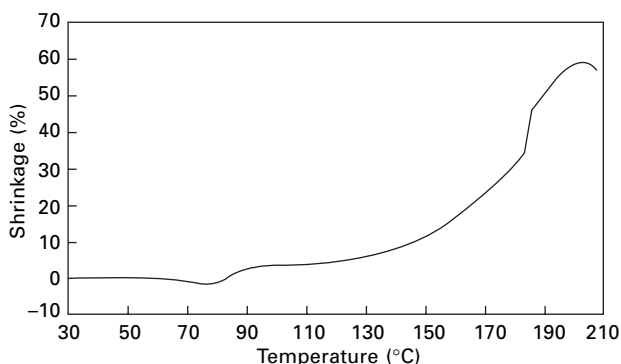
18.5 Thermomechanical responses

18.5.1 Thermomechanical analysis

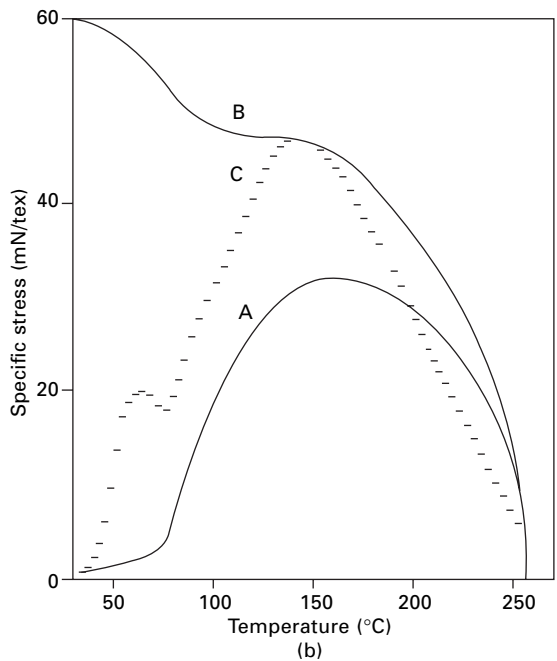
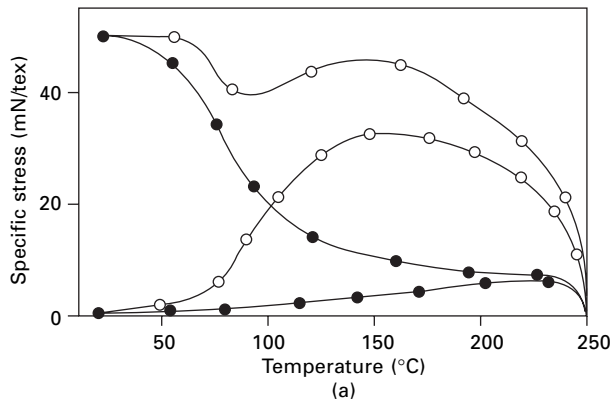
TMA is another way of studying thermal changes in materials. Specimens are held under constant tension and the length changes monitored. Commercial instruments, such as the Mettler Thermomechanical Analyser, have attachments for fibre testing. The simplest response gives a measure of the coefficient of thermal expansion. With fibres, the interest is more in reversible or irreversible shrinkage and in the step changes at transitions, though these are not as clear as the peaks in DMA. Buchanan [49] gives an extensive account of the dependence of thermal shrinkage on the prior history of nylon and polyester fibres.

Figure 18.32 is a typical TMA trace in a paper on the structural characterisation and properties of polyvinyl chloride (PVC) fibres [50]. The rise between 80 and 90 °C is a second-order transition, which is followed above 130 °C by an elastomeric thermal shrinkage as the structure loosens up. The trace terminates with a slight lengthening, which is due to the fibre extending under the applied tension as it becomes softer in the approach to melting.

The tendency to contraction, but not expansion, can be studied by the alternative procedure of measuring tension changes at constant length. Figure 18.33(a) shows shrinkage force measurements for a polyester (PET) yarn [51]. From a low pre-tension, the shrinkage force increases over the lower transition range from 75 to



18.32 TMA trace of drawn PVC fibre. From Kim and Gilbert [50].



18.33 Shrinkage force measurement of a polyester (PET) yarn (15 tex, 48 filaments). (a) Heated at 25 °C/min from pre-tensions of 0.5 mN/tex and 50 mN/tex for yarn as made ○ and for yarn pre-treated at 180 °C for 20 s at 5 mN/tex ●. (b) For fibre as received: A and B are standard shrinkage force tests; C is equilibrium shrinkage force. From Berndt and Heidemann [51].

150 °C and then falls as the fibre softens. Pre-treatment at 180 °C almost eliminates the shrinkage tension. The tension has dropped to almost zero at 250 °C, which can be taken as one measure of the melting point. A stepwise approach to the equilibrium shrinkage force (Fig. 18.33(b)), shows a maximum at 60 °C, which is attributed to a ‘classically defined glass transition’.

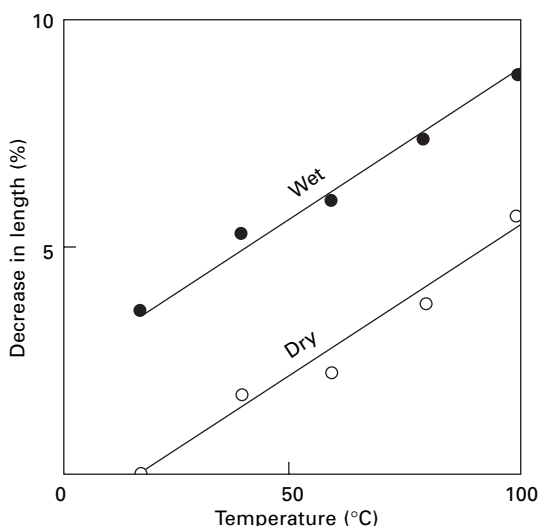
18.5.2 A flexible thermomechanical analyser for fibres

Sikorski and coworkers [52–54] describes a thermomechanical analyser that was specially developed for fibres and incorporates twisting as well as tensile changes. There were later enhancements, particularly in software for computer control, data retrieval and data processing [55]. The fibre specimen is clamped between jaws that are contained within a heating chamber and connected by rods to external functions. Temperature is controlled and can be rapidly changed by mixing streams of hot and cold air through a valve controlled by a stepper motor. Two more stepper motors control specimen length and twist. Tension is measured by a piezoelectric transducers for fast response and a strain-gauge transducer for quasi-static measurements. Torque measurement by the new transducer was described in Section 17.3.2. Twist was measured by an optical encoder and extension by an LDVT. With this tester, a great variety of test sequences can be studied.

18.5.3 Irreversible shrinkage

In addition to the reversible changes of dimensions with temperature, which occur in all materials, many fibres show an irreversible contraction or sometimes an irreversible expansion on heating. What happens depends on the prior process history of the fibre, so that manufacturers can supply nylon and polyester fibre in high- or low-shrinkage variants.

Figure 18.34 shows the irreversible changes in length of typical nylon fibres with increasing temperature. In order to achieve the same effect, the temperatures must be about 70 °C greater dry than in steam. In nylon fibres as produced, the shrinkage in boiling water is usually about 10%, but the value is very sensitive to subsequent heat



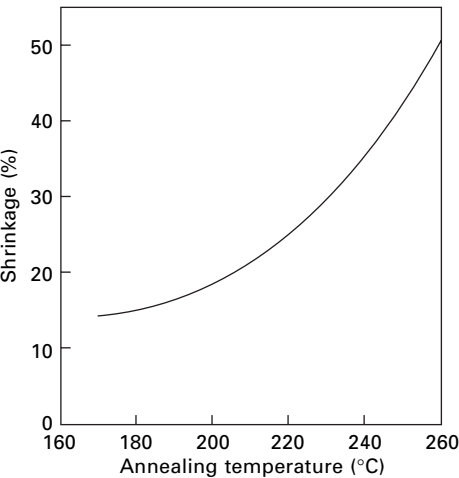
18.34 Irreversible shrinkage of nylon on heating [56].

treatments, and examples of the range of values are shown in Table 18.4. Similar effects are observed in polyester fibres, and spontaneously extensible fibres can be made by appropriate thermomechanical treatments. The more rapid shrinkage that occurs as the melting point of nylon is approached is shown in Fig. 18.35.

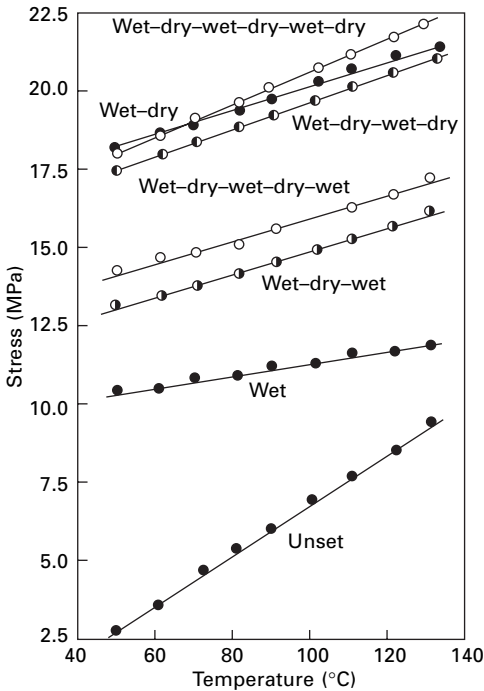
As an alternative to measuring shrinkage, the increase in tension on heating fibres at constant length may be observed. Some examples of studies on nylon 6 are shown in Fig. 18.36. The unset fibre shows a rapid build-up in tension. Corresponding to the tendency to irreversible shrinkage there is an irreversible build-up of tension, so that subsequent lines lie at a higher level. The positive slope of these lines corresponds to the reversible contraction, and is another manifestation of the occurrence of rubber elasticity in nylon. However, the results are also remarkable for the fact that successive setting treatments, wet at 120 °C and dry at 170 °C for 30 min, cause the lines to shift to progressively higher tension levels, the values always being highest when the final

Table 18.4 Shrinkage of 7.8 tex nylon 6.6 yarn in boiling water [57]

Treatment	Tension (N)	Shrinkage % in boiling water
As received		9
Dry heat (°C)		
200	0	0
200	0.1	2
200	0.3	7
200	0.5	6
200	0.75	8
160	0.1	5
240	0.1	4
160	0.5	9
240	0.5	5



18.35 Length changes in the experiments of Dismore and Statton [58] on annealing nylon 6.6.



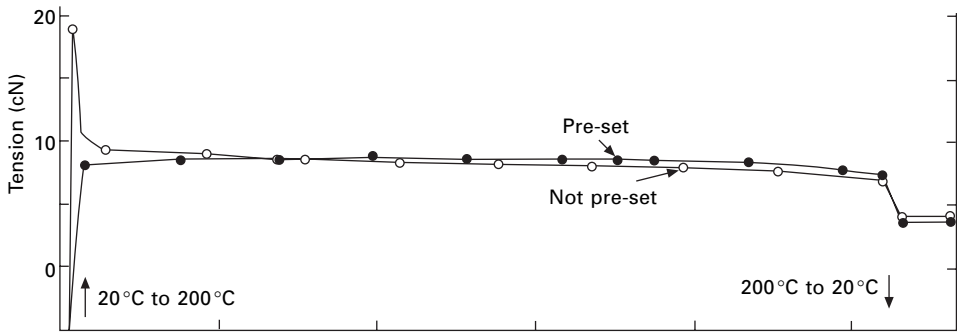
18.36 Tension-temperature curves for nylon 6 fibres, as produced and after successive setting treatments at 130 °C wet and 170 °C dry. From Koshimo [59].

treatment was wet. This demonstrates that complicated and continuing structural changes can occur in repeated treatments.

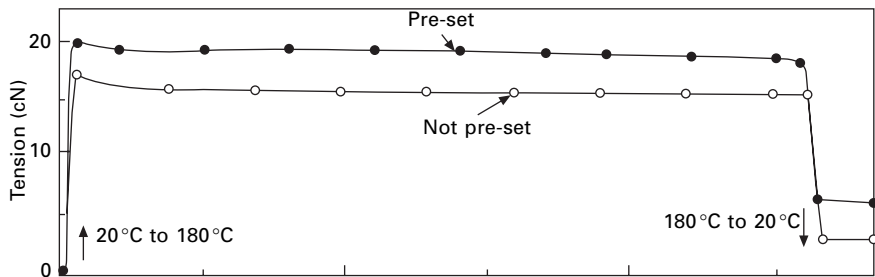
Mukhopadhyay and Hearle [60] report tests with the flexible thermomechanical analyser, which show that it is necessary to avoid artefacts due to expansion and contraction of the rods linked to the jaws. With a modified procedure, Fig. 18.37 shows shrinkage tension measurements of polyester (PET) and nylon 6. The general pattern is a rapid rise in tension followed by some stress relaxation. The fall in tension on cooling corresponds to a reversible contraction on heating. The residual tension corresponds to the irreversible shrinkage. Figure 18.38 shows that the high spike in the curve in Fig. 18.37(a) is due to the shrinkage tension in unset polyester peaking at 180 °C during the rise in temperature.

Acrylic fibres that have been stretched, for example, by stretch-breaking, and left with a 'permanent' extension, will contract severely on heating. This is the analogue of swelling recovery in rayon, which was discussed in Section 15.6. The plastic deformation of the structure is released when it is freed at the higher temperature. High-shrinkage fibres of this type are used in combination with non-contracting (or already contracted) fibres in high-bulk yarns.

The main mechanisms giving rise to an irreversible shrinkage are probably the following.

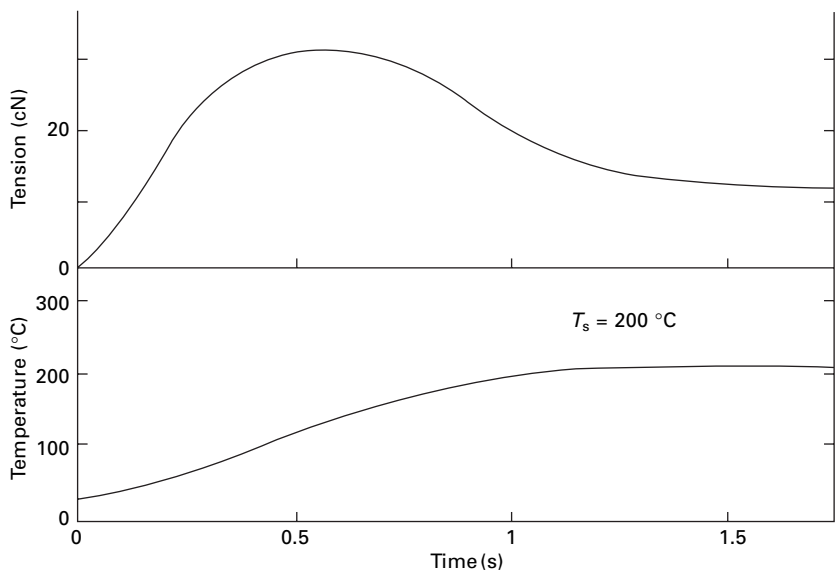


(a)



(b)

18.37 Shrinkage–tension plots for fibres rapidly heated, held at constant temperature and then cooled. (a) Polyester (PET) monofilament, 88 μm diameter, heated to 200 $^{\circ}\text{C}$, as received and pre-set at 180 $^{\circ}\text{C}$ for 30 mins. (b) Nylon 6 monofilament, 85 μm diameter, heated to 180 $^{\circ}\text{C}$, as received and pre-set at 160 $^{\circ}\text{C}$ for 30 mins. From Mukhopadhyay [61].



18.38 Expansion of the timescale in the initial part of Fig. 18.37(a). From Mukhopadhyay [61].

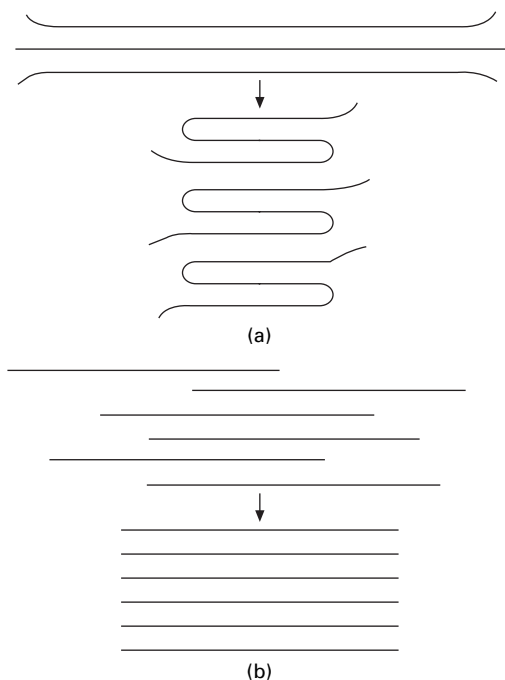
- Oriented non-crystalline material, resulting from the original drawing of the fibre or from mechanical hysteresis or from heating under tension, will revert to an unoriented or less oriented state when it is loosened by heating.
- The annealing of crystalline regions may reduce their length, as indicated in Fig. 18.39. This will certainly be true if the chain molecules fold in order to crystallise better, but it may also be true when they move relatively so as to come into better register.
- Small crystallites may melt, with the chains shrinking axially to a random coil. Recrystallisation elsewhere will tend to stabilise the shortened form.

18.5.4 Other property changes

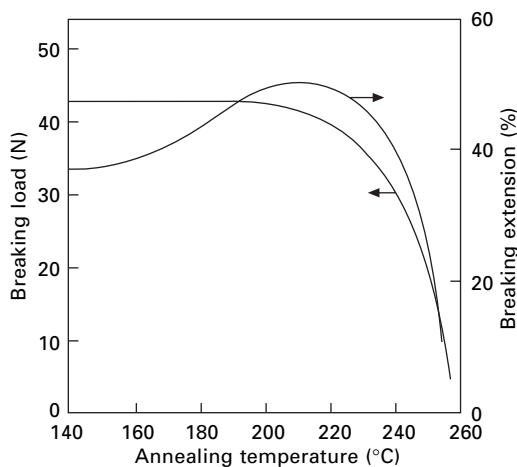
Accompanying the thermal shrinkage, there are many other changes in properties, and a full account of the effects in synthetic fibres has been given by Statton [62].

Figure 18.40, which comes from the same experimental series as Fig. 18.35, shows that, up to about 190 °C in nylon 6.6, there is little change in strength but an increase in breaking elongation, which can be accounted for as being due to the addition of the thermal shrinkage to the breaking extension. But the more rapid shrinkage above 190 °C is accompanied by a loss in strength and a corresponding reduction in breaking elongation.

The dyeing behaviour of fibres is altered in complicated ways by heat treatments.



18.39 Length changes that may occur on annealing of crystalline regions with (a) chain-folding and (b) rearrangement of chains.



18.40 Changes in strength and breaking extension in the experiments of Dismore and Statton on annealing nylon 6.6 [58].

Thus, in some experiments on nylon 6, exposure at about 120 °C causes an increase in dye uptake, but for temperatures above 190 °C there is a decrease: the rates of dye diffusion also change. This connection shows the need for great uniformity of heat treatments if dye faults are to be avoided.

The structural changes observed by Dismore and Statton [58] in the nylon samples for which observations are shown in Figs 18.35 and 18.40 included some increase in crystallinity (as indicated by the X-ray orientation index) but a reduction in dynamic modulus, an increased intensity of small-angle X-ray diffraction and an increase in long-period diffraction, and more fluid-like mobility as indicated by nuclear magnetic resonance (NMR) results. These results suggest that the crystalline regions are becoming larger and more perfect, while remaining oriented, with the non-crystalline material becoming less oriented and more mobile.

Gupta [63] summarises a number of papers on the effect of heat-setting polyester (PET) yarns at various temperatures both free to shrink and at constant length. The fibres were structurally characterised by wide- and narrow-angle X-ray diffraction, polarising optical microscopy, infrared spectroscopy and electron microscopy. The properties reported on are density, sonic modulus, boiling water shrinkage, tensile stress–strain response, recovery from elongation and uptake of disperse dye.

18.6 Setting

18.6.1 Technical importance and characteristic features

The ability to set fibres, namely to stabilise their state either in an existing form or after deformation, has major effects in processing and use. Traditionally, this was carried out on natural fibres by ironing, which combines pressure, heat and, most importantly, drying. The advent of synthetic fibres, which could be heat-set, revolutionised the technology. Fabrics could be heat set, either in a smooth form or

in sharp creases or pleats. To a considerable degree, the set was held during use and laundering, which gave 'non-iron', 'drip-dry' and 'wash-and-wear'. Processing continuous filament yarns to give bulk, stretch and texture was the most important of new fibre processing operations. The 'ease-of-care' features of synthetic fibres stimulated the natural fibre community to develop setting procedures in order to compete with synthetics.

Setting can be characterised as either *temporary* or *permanent*, though the terms are somewhat loosely used. Temporary set is commonly lost in use and certainly by going back into the setting conditions and re-setting in a new form. Permanent set cannot be undone except by going to more severe conditions, if this is possible.

Setting can also be characterised by how it is achieved. This may be by chemical action. In cotton, rayon and other cellulosic fibres, chemical crosslinks between the molecules are introduced by treatment with resins. In wool, the natural cystine crosslinks are broken and re-formed in new positions. These chemical setting treatments are outside the scope of this book, except insofar as they influence physical properties. In moisture-absorbing fibres, hydrogen bonds are broken on wetting and can re-form in new positions on drying to give a temporary set. Setting on drying is seen on drying of cotton, wool or hair. It is interesting to note that K  rholm *et al.* [64] found that a more severe wrinkling in wool fabrics occurred when the relative humidity was changed while the material was in the deformed state. Finally there are the thermal transitions, which have been described in this chapter. The observation of heat setting and its interaction with moisture raises important scientific and technical questions. The whole subject of setting was discussed in detail in the book edited by Hearle and Miles [65], but important research has been done since this was published.

Any thermal transition that causes a peak in the loss modulus must give rise to a setting effect, since it implies that part of a structure that is rigid below the transition is mobile above it. If the fibre is cooled through the transition in a deformed state, then it will become rigid and be set in the new form. The secondary transitions cause temporary setting effects, since the structure is not changed. A reference state can always be reproduced by taking the fibre above the transition and cooling it free of any restraint. The transitions below room temperature are of little practical importance for setting, but the ones above room temperature do give important temporary set to fibres. At higher temperatures, but well below the melting point (around 200 °C for nylon 66 and polyester), a permanent set is achieved. Successive setting can be achieved by successive treatments under conditions that will disturb the structure once again. In nylon, industrial experience in false-twist texturing indicates that it is necessary to go to more severe conditions of temperature or stress to re-set the fibre. In polyester, second-stage heating, which gives yarns with high bulk but low stretch, is carried out at lower temperatures than in the first heater where the yarn is set in the twist state prior to untwisting. The definition of *permanent set* appears to be weaker in polyester than in nylon.

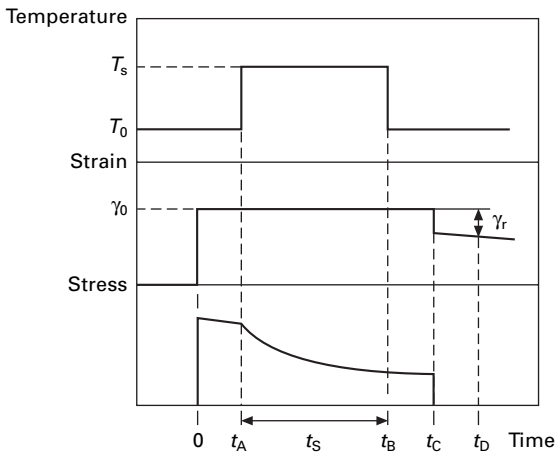
It must be remembered that any thermal treatment severe enough to cause a permanent heat-set will also cause the mechanism of temporary set to operate. A subsequent less severe treatment, for example, in boiling water, will release the temporary set but not the permanent set. Fibres set under tension will therefore show

a shrinkage when later heated. The temporary set may also act as the material cools down. On first unwinding a textured yarn from a package, it will not show any texture, but on exposure to heat, the temporary set will be released and the bulk will develop. The texture can also be developed by ‘milking’ the yarn, namely by repeated tensioning.

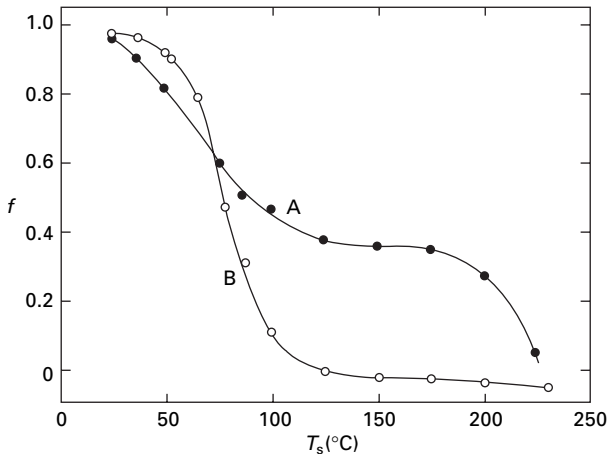
18.6.2 Heat setting of polyester and nylon

An important series of experiments on the heat setting of polyester (PET) monofilaments was reported by Salem [66] and Buckley and Salem [67, 68]. The monofilaments had been melt-extruded in the laboratory and drawn 5× to give a diameter of 51 μm (27 dtex). Any pre-setting was carried out with the fibre taut at constant length. The setting sequence is shown in Fig. 18.41. For torsional experiments, after releasing any initial twist, specimens were clamped and twisted at constant length, transferred to heating in oil or air, then removed to room temperature and released from the clamps to allow recovery. The fractional recovery f , which is a measure of the degree of set, is defined as recovered twist/imposed twist. Thus $f = 1$ indicates no setting and $f = 0$ indicates complete set. The quoted strain value is the shear strain at the surface of the monofilament. For bending experiments, specimens were wound round *Tufnol* or glass rods and clamped for the heat-setting sequence. The quoted strain value is r/R , where r is fibre radius and R is rod diameter.

Figure 18.42 shows the interaction of two setting effects. If the material is tested as produced, the setting is apparently complete in the range of 50–120 °C. Although the recovery hardly changes, a temperature around 200 °C gives some added stability,



18.41 Heat setting sequence starting from zero stress at room temperature, through imposed changes in strain and temperature with time (with assumed stress change), followed by recovery at zero stress and room temperature where T_0 is the initial temperature, T_s is the setting temperature, t_s is the setting time and t_A , t_B , t_C and t_D are times at each stage. γ_0 is the imposed shear strain on the outside of the twisted monofilament and γ_r is this strain after release. From Buckley and Salem [68].



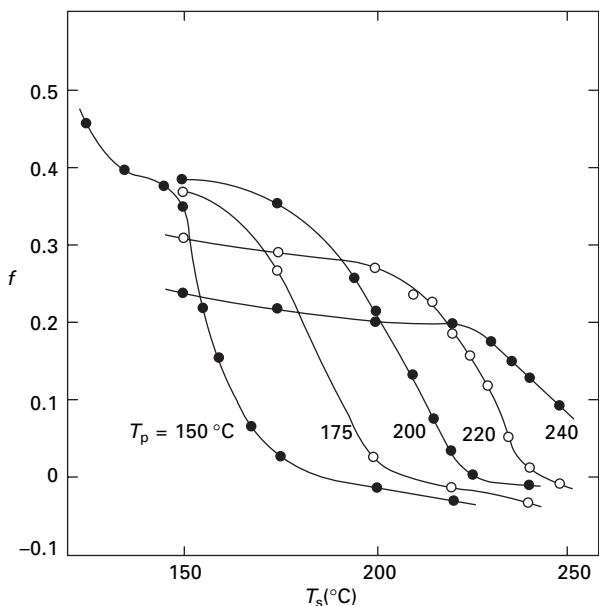
18.42 Fractional recovery of polyester monofilament in torsion plotted against setting temperature: A, pre-set at 200 °C; B, as produced. Setting time = 120 s. From Buckley and Salem [67].

which is suggested by the slight overshoot to negative values of f above 180 °C. The clear evidence comes from re-setting. A specimen that has been pre-set at 200 °C has only half the recovery in the range of 50–120 °C. The setting is completed in the range of 180–220 °C. The 50–120 °C set is associated with the transition shown in Section 18.3.2, e.g. in Fig. 18.21 or the ‘major transition’ in Fig. 18.27. It is a temporary set, which is overcome by re-heating. The ‘permanent set’, which is used in texturing and other processes, is in the 180–220 °C range. The unavoidable imposition of temporary set on any permanent setting sequence must be taken into account in interpreting the results of setting tests.

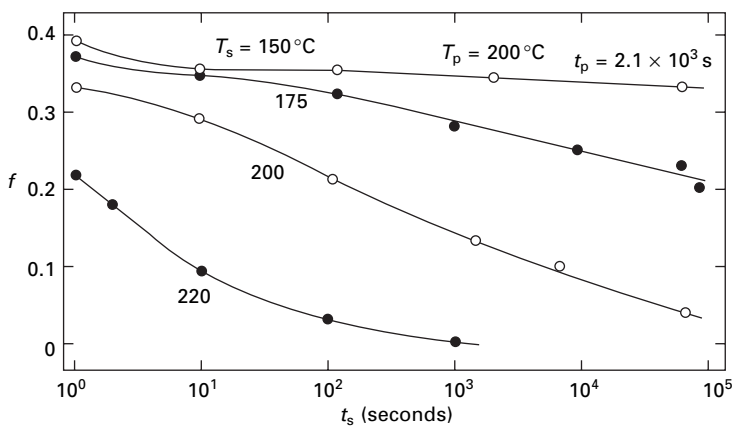
Figure 18.43 shows that the high-temperature set is moved to higher temperatures as the pre-setting temperature is increased. However, the setting starts below the pre-set temperature. Figure 18.44 shows that setting is time-dependent. A fibre pre-set at 200 °C for 35 minutes is almost fully re-set in 1 second at 220 °C, but takes one day to reach the same set at 200 °C. Re-setting occurs at 175 °C, but is much slower and still continuing after 1 day. Figure 18.45 shows that setting in bending is similar to setting in torsion. Figure 18.46 shows that setting becomes more complete as the level of deformation increases.

Mukhopadhyay [61] found a difference in clockwise and anti-clockwise heat setting of a polyester monofilament.

A more limited set of tests on nylon 66 were reported by Hearle *et al.* [69]. Figure 18.47(a) shows similar behaviour to that in Figs 18.42 and 18.43 for polyester, with a low-temperature set around 40 °C and a high-temperature set which can start at 140 °C and is complete at 180–240 °C with higher temperatures needed to overcome the pre-set. Figure 18.47(b) shows a marked difference from polyester. There is time dependence in the low-temperature set, but none in the high-temperature set. This was confirmed in tests at other setting temperatures. Some uncertainty then appears in the report. A set of tests on a different sample of nylon 66 shows time dependence in setting temperatures from 150 to 200 °C, which is similar to that of polyester.

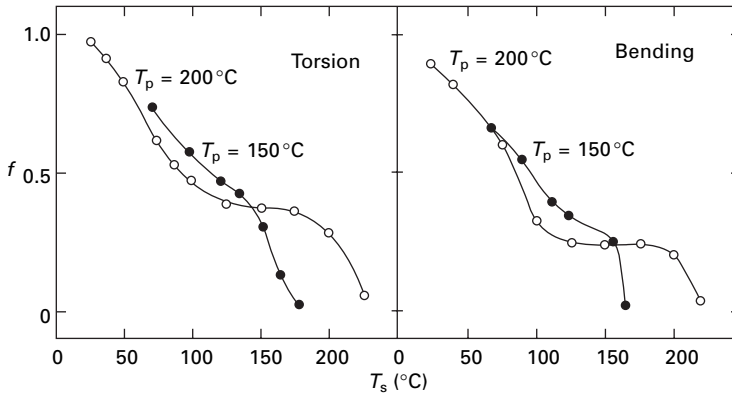


18.43 Fractional recovery of polyester monofilament in torsion plotted against setting temperature at various pre-setting temperature T_p . Pre-setting time 35 mins; setting time = 120 s. From Buckley and Salem [67].

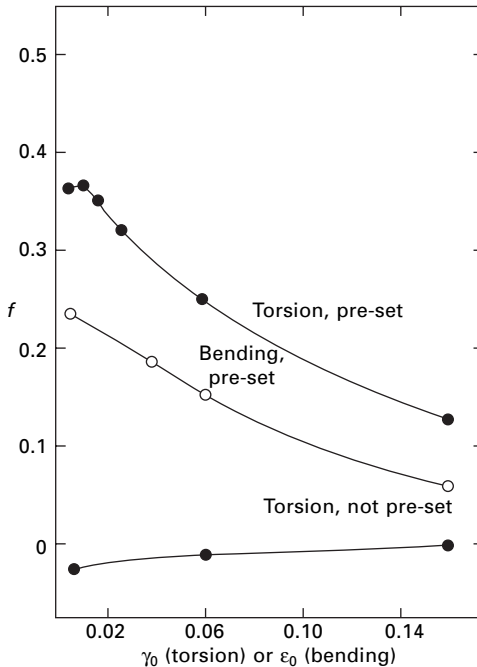


18.44 Fractional recovery of polyester monofilament in torsion plotted against setting time at various setting temperatures. Pre-set at 200 $^{\circ}\text{C}$; setting time of 35 mins. From Salem [66].

An abundance of technological experience shows that steam setting of nylon occurs at a temperature about 80 $^{\circ}\text{C}$ below that in the dry state, corresponding to the lower melting point. Most fabric setting is carried out in superheated steam at temperatures around 120 $^{\circ}\text{C}$ compared to 200 $^{\circ}\text{C}$ for dry setting. Appreciably lower temperatures are used for nylon 6, reflecting its lower melting point.



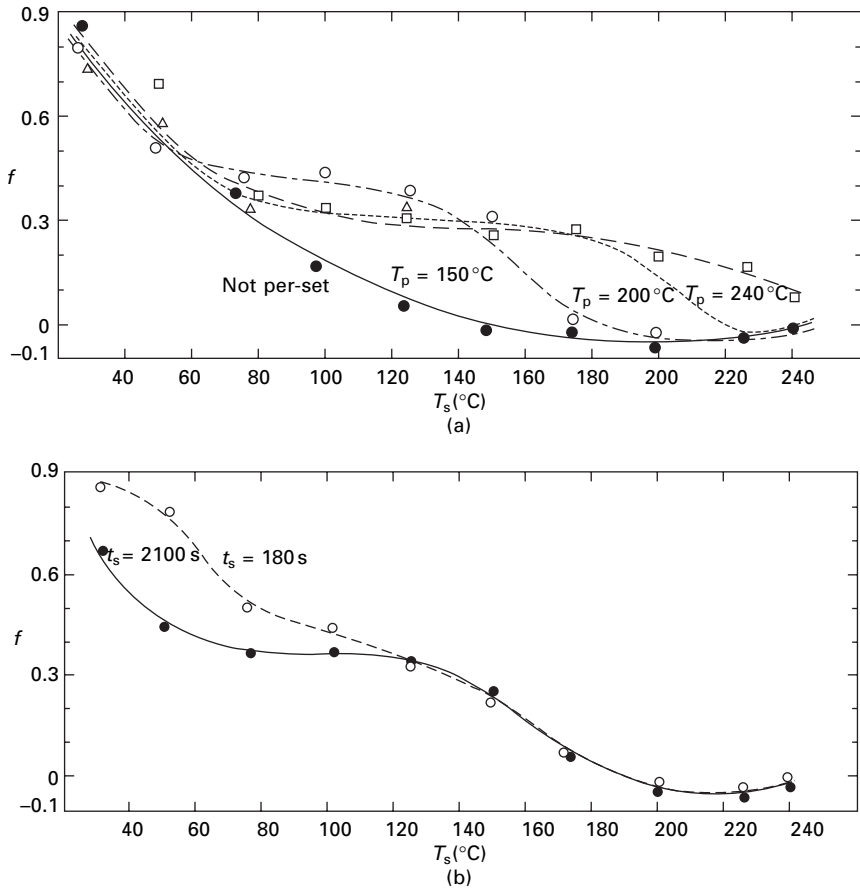
18.45 Fractional recovery of polyester monofilament plotted against setting temperature in torsion and bending at two pre-setting temperatures. Pre-set at 200°C ; setting time of 35 mins. From Buckley and Salem [68].



18.46 Strain dependence of fractional recovery in torsion and bending for polyester monofilament heat-set at 150°C for 2 mins after pre-set at 200°C and (in torsion) without pre-set. From Buckley and Salem [68].

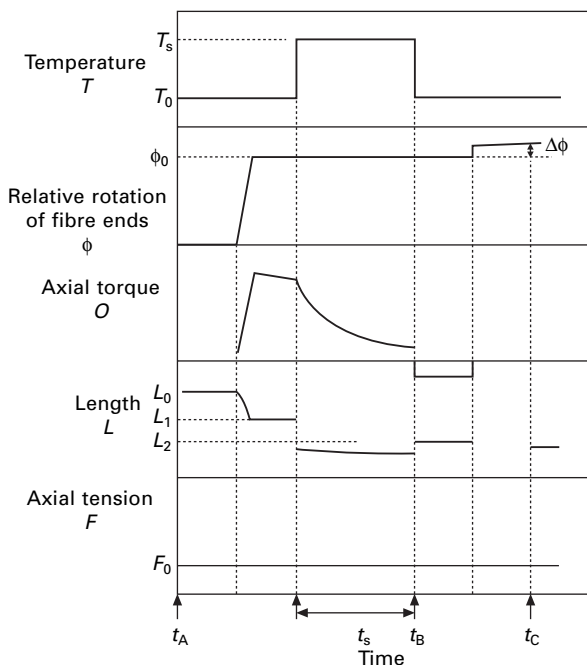
18.6.3 Overtwisting

There is a brief mention above of the occurrence of negative values of f , which implies that the set has *overtwisted* to a value greater than the imposed twist. This anomaly was reported by Arghyros and Backer [70] in their research on twist-texturing.

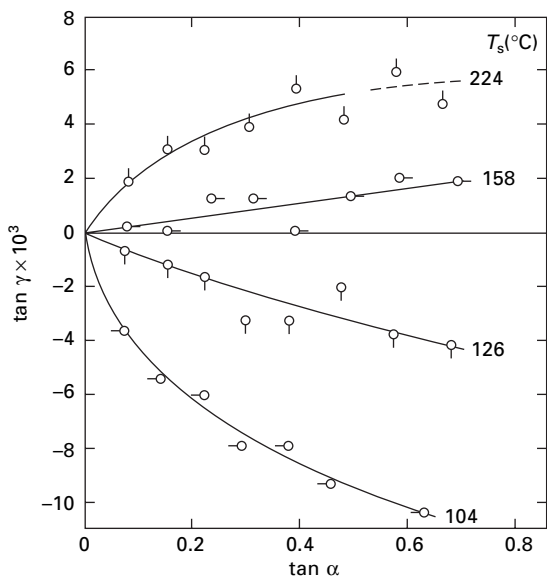


18.47 Fractional recovery in heat-setting of nylon 66. (a) Plotted against setting temperature for various pre-set temperatures. Pre-set of 2100 s; set time of 120 s. (b) Plotted against setting temperature for set times of 180 and 2100 s. Pre-set at 150°C for 2100 s.

Figure 18.48 shows a sequence of changes in twisting, heating, cooling and releasing at constant tension by Buckley *et al.* [71]. Note the contraction in length on both twisting and heating and some length recovery on release. The data were reported in terms of tangents of the shear angle α at the surface during setting and of an angle γ , which is the difference between α and the shear angle after release, namely the shear angle associated with the overtwist $\Delta\phi$ in Fig. 18.48. As shown in Fig. 18.49, there is a positive overtwist given by $\tan \gamma$ for setting above about 150°C , and a negative value of $\tan \gamma$, which implies incomplete setting, for lower temperatures. The overtwist increases with increased imposed twist. Similar results were found with other samples of polyester and nylon. The overtwist decreased with increased tension and $\tan \gamma$ became negative at higher tensions. Overtwist was decreased by pre-setting. Repetition of the setting sequence, by clamping, heating, cooling and releasing, shows *twist-climbing* with the overtwist increasing without more twist being inserted.



18.48 Sequence of changes in test of overtwisting. T , ϕ and F are independent variables; O and L are dependent variables; $\Delta\phi$ is the overtwist. From Buckley *et al.* [71].



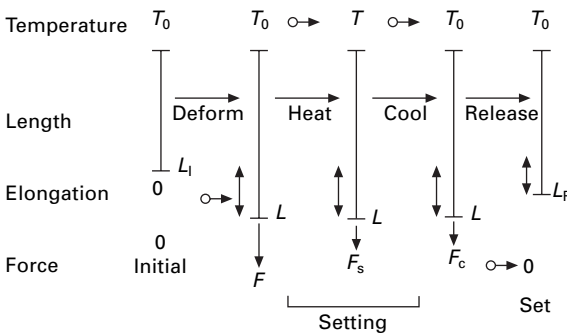
18.49 Overtwist of polyester monofilament plotted against imposed twist for various setting temperatures. α is shear angle at surface during setting; γ is difference from α after recovery (corresponding to $\Delta\phi$ in Fig. 18.48).

Buckley *et al.* [71] show that the phenomenon of overtwisting can be explained by the length changes and thermo-elasticity of an oriented polymer. A quantitative analysis follows a treatment of the thermoviscoelasticity of a twisted yarn [72].

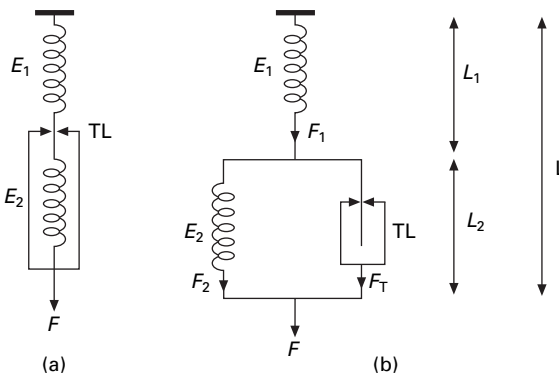
18.6.4 Phenomenological treatment of heat setting

A simplistic treatment of heat setting illuminates some of the features of an extremely complex subject. It is presented in terms of a model of force and length changes in temporary set, but other modes such as torque and twist or bending moment and curvature could be substituted. Normalised quantities, namely stress and strain, could also be used. The treatment, which predicts degree of set, is a simplification of the viscoelastic model of Buckley and Salem [67]. Other enhancements could be added to the model to take account of secondary effects, but the simple model brings out the primary features of setting.

Figure 18.50 shows a typical heat setting sequence: elongating, heating and cooling at constant length, and releasing. The terminology is as follows. F = total force; L =



18.50 Typical heat-setting sequence. F = total force, L = total length, L = total elongation. A zero subscript indicates the stress-free state, S = setting state, R = state after release.



18.51 (a) Simple model for heat-setting. (b) Expanded version showing forces and lengths.

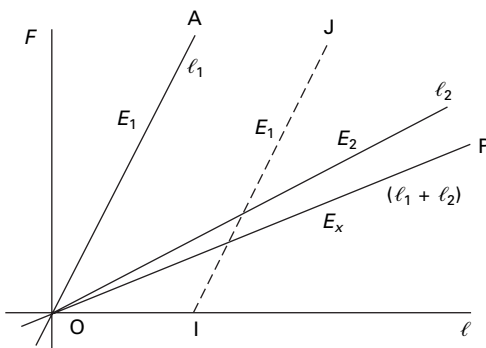
total length; l = total elongation. Subscript $[_0]$ is for stress-free state; subscript $[_S]$ is for setting state; subscript $[_c]$ is for cooled state; subscript $[_R]$ is for state after release. The degree of set is defined as set length/setting length = l_R / l_S .

The simple model, Fig. 18.51, consists of two springs, with spring constants E_1 and E_2 , in series with a thermal lock TL, which can open or close. $F_{1,2}$, $L_{1,2}$, $l_{1,2}$ are forces, lengths, and elongations for springs 1 and 2. The combined spring constant with TL open is E_x . For a series system, $E_x^{-1} = (E_1^{-1} + E_2^{-1})$. The basic assumption of the model is that setting is due to a single change between a more rigid state below a transition temperature, when TL is closed, and a more mobile state above the transition temperature, when TL is open. Setting is by release of restraint on heating and application of restraint on cooling, while the material is held at constant length. Linearity, absence of reversible expansion and contraction, time dependence, combined modes of deformation, and change in moduli except at transition are secondary features that are neglected.

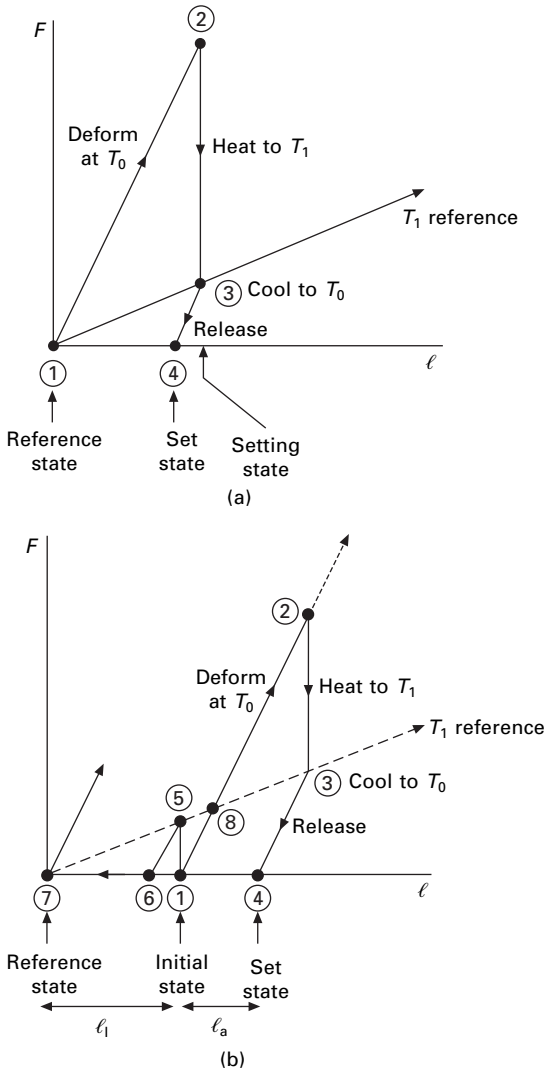
Force–elongation plots are shown in Fig. 18.52. There is a reference state at O, which is always reached if TL is opened above the transition temperature and both springs drop to zero force. With TL closed at ambient temperature, deformation would follow the line OA, or the dotted line IJ if the fibre had been set at another state. With TL open above the transition temperature, the line OP would always be followed.

A setting sequence from the reference state is shown in Fig. 18.53(a). The temperature T_0 is below the transition temperature and T_1 is above. The fibre is first extended at T_0 (1→2), and then heated to T_1 (2→3), with a consequent drop in force. (Any approach to (3) would give the same final result.) The specimen is then cooled to T_0 and released. Since TL is closed at T_0 , the recovery will be along a line with the slope E_1 . The fibre is left in the set state (4). With TL open at (3) the force is in both springs is ($E_x l_S$). When the fibre is cooled and released with TL closed, spring 2 is clamped and cannot retract, but spring 1 can recover by ($E_x l_S / E_1$). Hence:

$$\text{set length} = l_R = l_S - \left(\frac{E_x l_S}{E_1} \right) = l_S \left[1 - \left(\frac{E_x}{E_1} \right) \right] \quad (18.3)$$



18.52 Force–elongation relations. Lines from O are for initial state at temperature T_0 with TL open. Line IJ is with TL closed at intermediate state.



18.53 (a) Heat-setting sequence from initial state of model. (b) Sequences from an initial set state.

$$\text{degree of set} = \frac{l_R}{l_S} = 1 - \frac{E_x}{E_l} \quad (18.4)$$

The effectiveness of a setting operation on this simple model is determined by the ratio of the modulus above the transition temperature to the modulus below the transition temperature.

Setting from a previously set state is shown by the sequence (1→2→3→4) in Fig. 18.53(b) and finished at the same set state. The sequence (1→5→6) shows the effect of holding the specimen at its initial state, heating to T_1 , cooling and releasing. Geometric modelling, which could be programmed for computing, would be the way

to follow complicated sequences. Some experimental data [73] indicates that setting of nylon and polyester monofilaments followed the predictions for temperatures up to 190 °C provided some stress relaxation was added to the model.

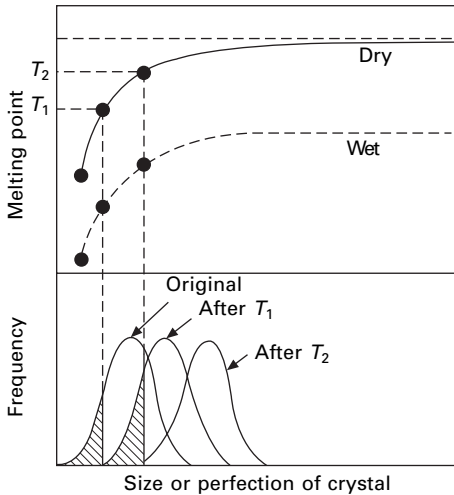
Although the model is highly simplified, it does indicate that the degree of set can be estimated from the ratio of deformability at the cool temperature to deformability at the setting temperature. For permanent setting, the model could be applied to an initial set, but the structure would then be changed and it is the deformability of the cooled structure that would be relevant. Heating again, unless it was to a higher temperature that gave full mobility, and releasing would lead back to a new reference state.

18.6.5 Setting mechanisms

Setting in cotton by introducing new bonds between molecules and in wool by switching the position of cystine bonds are clear chemical mechanisms for permanent setting of fibres in new forms, which are not changed in use. Setting by wetting and drying, with hydrogen bonds being broken and re-formed in new positions, is a clear mechanism for temporary set. The low-temperature effect in nylon and polyester fibres at *c.* 100 °C is a temporary set that can also be explained by the changed positions of hydrogen bonds or mutual attractions of benzene rings, as discussed in Section 1.1.2. The mechanism for the high-temperature ‘permanent’ setting is difficult to explain because there are so many possibilities. It is likely that various mechanisms act together, with their relative importance varying according to the type of fibre and its previous thermomechanical history. Possible mechanisms are reviewed below.

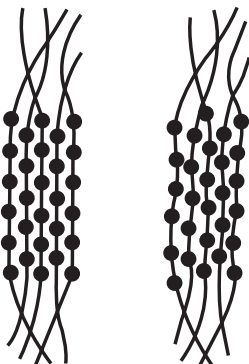
It should be re-stated that the permanent setting sequence will have the temporary set superimposed and that reversible thermal expansion or contraction will also be superimposed. Thermodynamically, permanent set must result from a transfer from one free energy minimum to another at a lower level, which is made possible by thermal vibrations. Such changes are almost always time dependent, certainly for small systems, which is another complication. It must also be remembered that it is not clear whether the high-temperature set of nylon and polyester is permanent or temporary, albeit not being overcome in normal use.

- *Larger and better crystals.* The simplest explanation is that heating leads to annealing, namely the melting of small or imperfect crystals and the growth of larger, more perfect crystals. The mechanism is illustrated in Fig. 18.54, which also shows the effect of lower melting points of wet fibres. At the start, there is a distribution of crystal sizes and perfections, which give a range of melting points. At a given temperature, the smallest crystals will melt and larger ones will be formed. The process can be repeated at successively higher temperatures, but cannot be reversed. This happens in metals, where the small crystal grains butt on to larger ones. It is more difficult to see how it would work with a distribution of polymer crystallites separated from one another without melting of the whole material. Once a fine structure of crystalline and amorphous regions is established, the pattern tends to remain. Furthermore the setting temperatures are appreciably lower than the melting temperatures.



18.54 Distributions of melting points of crystals with different sizes.

- *Defect mobility.* In metals, defects can move to the surface of crystals and disappear. This may well be a setting mechanism in polyethylene, where defects due to mis-packing of $\text{—CH}_2\text{—}$ units occur and are a cause of imperfect crystallinity. It may possibly also apply to polypropylene and other polymers with short repeats. However, as discussed in Section 1.3.2, defect models are not sensible for polymers with the long repeats found in nylon 6 or 66 and polyesters.
- *Multiple melting.* For rapidly quenched fibres, the change from form I to form II, discussed in Section 18.2.2, would certainly provide a setting mechanism. However, form II can be set, so that this cannot be a complete explanation.
- *Crystallite mobility.* A variant included in the discussion on multiple melting is that, owing to thermal vibrations, individual crystalline micelles might be able to melt and then recrystallise, as indicated in Fig. 18.55. Rather like molecules moving between liquid and vapour, most micelles would be crystalline, thus maintaining the integrity of the fibre, but a changing population would be molten.



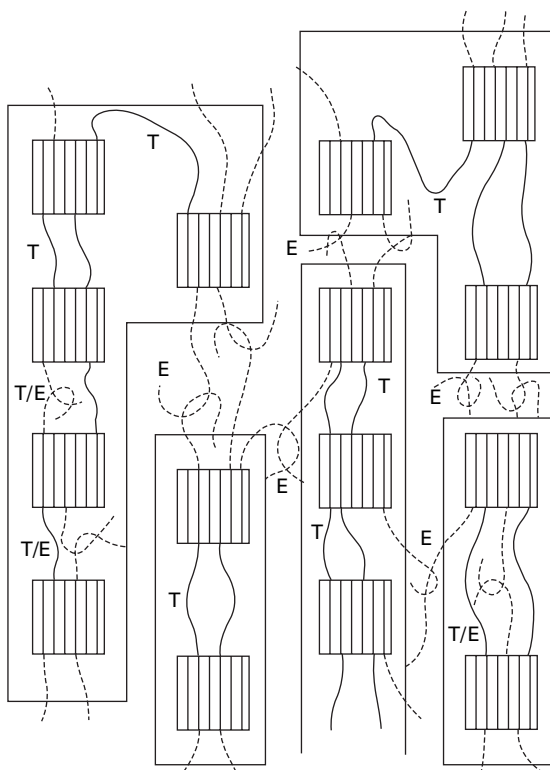
18.55 Flipping between crystalline and locally molten states.

Berry [74] has shown that small clusters of argon atoms can act in this way, flipping between the two states over a certain temperature range. If the material was deformed, the recrystallisation would take place in a slightly different form, which stabilised a new state.

- *Quantum superposition.* Hearle [75] has suggested a more speculative variant that at the setting temperature, there is a quantum superposition of ordered and disordered states. Even though the molten state was at a higher energy, the greater number of energy levels would encourage movement between the two states.
- *Movement through crystals.* Molecules passing through a crystallite will be under variable tension. The simplest case to consider is where one end is linked to the network and the other is a free end. Above a certain temperature, it is possible that thermal vibrations will give a high enough tension to pull the molecule through the crystallite. The reverse would not occur, so that a new state would be set. This effect is more likely if the fibre as a whole is under stress, though the discussion in Section 20.3.2 indicates that tie-molecules are tensioned even when there is no externally applied stress. Variants would apply if both ends are linked to the network, but in different ways, or if there is chain folding.
- *Plastic crystals.* There are more extreme options for mechanically driven setting. If a crystallite is subject to shear, layers of molecule would move relative to one another if the yield stress in shear was exceeded.
- *Drawing.* The drawing of unoriented fibres into oriented forms is a form of set induced by plastic yielding of the fine structure with rupture and re-formation of crystallites. This mechanism is obviously not applicable to drawn fibres, but it will be playing a part when partially oriented yarns are subject to draw-texturing.
- *Kink-band formation.* Another form of severe mechanical deformation is the development of kink-bands in bending or shear (see [Section 17.2.5](#)). Heating may lead to an annealing of the deformation and stabilisation in a new form.

All the above explanations relate to physical effects in the crystalline regions, with some also involving molecular segments from amorphous regions. However, there are two possible explanations that do not involve crystalline regions:

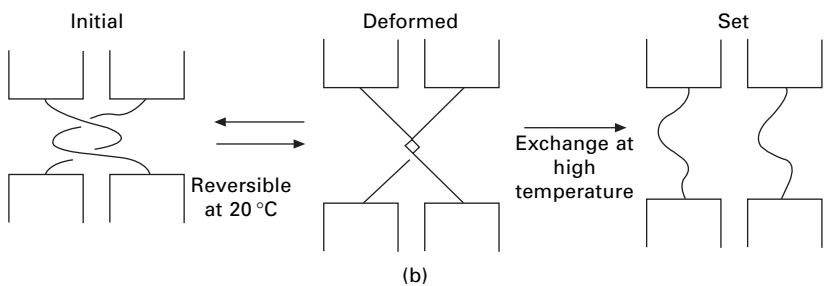
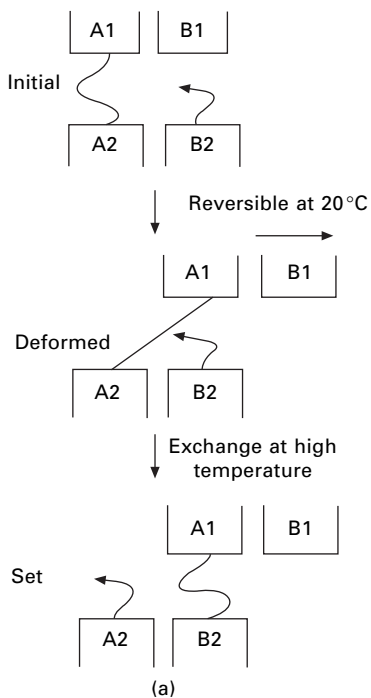
- *Entanglement reptation.* Buckley and Salem [67], citing a low molecular weight commercial polymer, propose the structure in [Fig. 18.56](#) for polyester (PET). Some crystallites are linked together by tie-molecules to form blocks. Between the blocks, there are only entangled chain ends. It is argued that the blocks can move relative to another by viscous flow by a reptation mechanism in which molecular segments progressively move through entanglements. This is accepted behaviour for wholly amorphous polymers, and provides a simple explanation of the time dependence of setting. The explanation is plausible if there is a high degree of chain folding, as implied by the limited number of molecular segments emerging from the crystallites in [Fig. 18.56](#). Alternatively, it is possible that, even if all crystallites are tied together, there could be reptation through entanglements in the amorphous region between crystallites.
- *Transesterification.* It is possible that there is chain scission and re-formation,



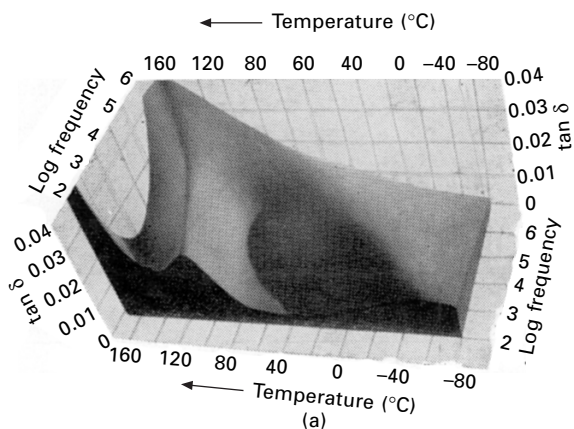
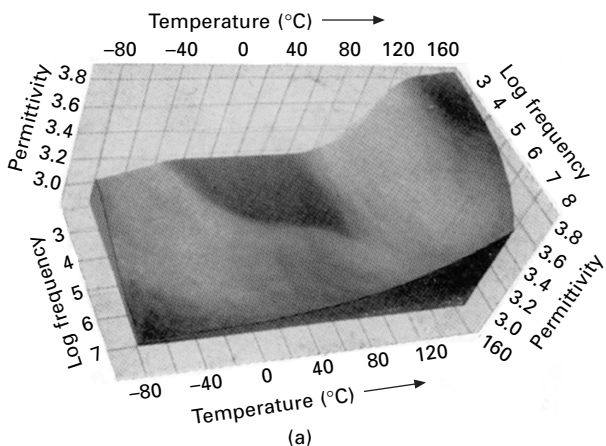
18.56 Structural model for polyester (PET) showing crystallites linked in blocks by tie-molecules (T), possibly plus entanglements (E). Separate blocks linked solely by entanglements. From Buckley and Salem [67].

which can occur in the two ways shown in Fig. 18.57. This is most likely on polyesters, where it is known as transesterification, but there would be an analogous effect in polyamides. Fakirov [76] has reviewed the solid-state reactions that would be relevant. One way of investigating the effects is by bonding together of polymer films. Quantitative information comes from studies by Kugler *et al.* [77] of the changes in length of deuterated segments of PET as measured by SANS (small-angle neutron scattering). Based on extrapolations of their data, calculations by Hearle [73] indicate that the rates of transesterification offer a plausible mechanism for heat setting of polyester.

All the mechanisms involved in heat setting of nylon 66 and polyester (PET) in the 180–220 °C region should be reflected in studies of thermal transitions. Unfortunately reported thermomechanical studies stop at about 180 °C, so that no direct observations are available. The dielectric measurements of polyester film in Fig. 18.58 do show the start of a rapid rise in $\tan \delta$ at 160 °C at low frequency. This may lead to an energy loss peak.



18.57 Two ways for changing links between crystals: (a) exchange of free end; (b) break and re-formation of tie-molecules.



18.58 Influence of temperature and frequency on dielectric properties of Terylene film (after Reddish [78]): (a) relative-permittivity solid model, (b) dissipation-factor solid model.

18.7 References

1. K. Schneider and K. Wolf. *Kolloid-Z*, 1953, **134**, 149.
2. A. V. Tobolsky. In *Rheology* F. R. Eirich, (Editor), Volume 2, Academic Press, New York, 1958.
3. T. Murayama, J. H. Dumbleton and M. L. Williams. *J. Polymer Sci. A-2*, 1968, **6**, 787.
4. H. E. Bair, T. W. Huseby and R. Salovey. *Analytical Calorimetry*, Plenum Press, New York, 1968, p. 31.
5. S. C. Simmens. Private communication.
6. J. P. Bell, P. E. Slade and J. H. Dumbleton. *J. Polymer Sci. A-2*, 1968, **6**, 1773.
7. J. P. Bell and T. K. Murayama. *J. Polymer Sci. A-2*, 1969, **7**, 1059.
8. J. W. S. Hearle and R. Greer. *Text. Prog.*, 1970, **2**, No. 4, 68.
9. J. W. S. Hearle and R. Greer. *J. Text. Inst.*, 1970, **61**, 243.
10. J. W. S. Hearle. *J. Appl. Polymer Sci., Appl. Polymer Symp.*, 1977, **31**, 137.
11. M. S. Burnip, J. W. S. Hearle and G. R. Wray. *J. Textile Inst.*, 1961, **52**, P343.

12. S. K. Mukhopadhyay, J. W. S. Hearle and P. W. Foster. *J. Textile Inst.*, 1988, **79**, 235.
13. S. K. Mukhopadhyay. *J. Textile Inst.*, 1992, **83**, 573.
14. H. S. Kim, H. Ito, T. Kikutani and N. Okui. *J. Textile Inst.*, 1999, **90**, 508.
15. M. Takayanagi. *Mem. Fac. Engng Kyushu Univ.*, 1963, **23**, No. 1.
16. J. W. S. Hearle. *J. Polymer Sci., Part C, Polymer Symposia*, 1967, **20**, 215.
17. T. Kawaguchi. *J. Appl. Polymer Sci.*, 1959, **2**, 56.
18. T. Kawaguchi. *J. Polymer Sci.*, 1958, **32**, 417.
19. R. Meredith. In *Proceedings of Fifth International Congress of Rheology*, University of Tokyo Press, Tokyo, Japan, 1969, Volume I, p. 43.
20. A. Kondo, S. Fujino and T. Agatsuma. *Bull. Text. Res. Inst. Japan*, 1964, **6**, 11.
21. H. A. Davis. *J. Textile Inst.*, 1991, **82**, 86.
22. H. A. Davis. *J. Textile Inst.*, 1995, **86**, 332.
23. W. W. Moseley, jr. *J. Appl. Polymer Sci.*, 1964, **8**, 2095.
24. J. H. Dumbleton and T. Murayama. *J. Appl. Polymer Sci.*, 1970, **14**, 2921.
25. S. M. Kveder and T. Rijavec. *Textile Res. J.*, 1994, **64**, 495.
26. S. J. van der Meer. Doctoral Thesis, Delft, Netherlands, 1970.
27. S. J. van der Meer. *J. Text. Inst.*, 1974, **65**, 288.
28. S. Rosenbaum. *J. Appl. Polymer Sci.*, 1965, **9**, 2071.
29. R. Meredith. In *Proceedings of Fifth International Congress in Rheology* S. Onogi (Editor), University of Tokyo Press, Tokyo, Japan, 1969, Vol. 1, p. 43.
30. D. J. Houston and R. Meredith. *J. Appl. Polymer Sci.*, 1973, **17**, 3259.
31. J. W. S. Hearle. *J. Polymer Sci. C*, 1967, No. 20.
32. J. W. Illingworth. *J. Text. Inst.*, 1953, **44**, P328.
33. F.-J. Wortmann. *Int. J. Sheep Wool Sci.*, 2007, **55**, 1.
34. M. Druhalá and M. Feighelman. *Colloid Polymer Sci.*, 1974, **252**, 381.
35. M. Druhalá and M. Feughelman. *Kolloid Z. Z. Polymere*, 1971, **248**, 1032.
36. S. Rosenbaum. *J. Polymer Sci.*, 1970, **C31**, 45.
37. F.-J. Wortmann, B. J. Rigby and D. G. Phillips. *Textile Res. J.*, 1984, **54**, 6.
38. D. G. Phillips. *Textile Res. J.*, 1985, **55**, 171.
39. J. M. Kure, A. P. Pierlot, I. M. Russell and R. A. Shanks. *Textile Res. J.*, 1997, **67**, 18.
40. F.-J. Wortmann, M. Stapels, R. Elliott and L. Chandra. *Biopolymers*, 2006, **81**, 371.
41. T. G. Fox. *Bull. Amer. Phys. Soc.*, 1956, **1**, 123.
42. E. Menefee and G. Yen. *Textile Res. J.*, 1965, **35**, 801.
43. M. Sugisaki, H. Suka and S. Saki. *Bull. Chem. Soc. Japan*, 1968, **41**, 2591.
44. M. T. Katchevsky, E. M. Jaroskiewics and J. M. V. Blanchard. *Int. J. Biol. Macromol.*, 1992, **14**, 257.
45. F.-J. Wortmann and H. Deutz. *J. Appl. Polymer Sci.*, 1993, **48**, 137.
46. F.-J. Wortmann and H. Deutz. *J. Appl. Polymer Sci.*, 1998, **68**, 1991.
47. A. R. Haly and J. W. Snaith. *Textile Res. J.*, 1967, **37**, 898.
48. J. Cao and F. Leroy. *Biopolymers*, 2005, **77**, 38.
49. D. R. Buchanan. In *Advances in Fibre Science*, S. K. Mukhopadhyay (Editor), The Textile Institute, Mandnester, 1992.
50. H. C. Kim and M. Gilbert. *Polymer*, 2004, **45**, 7293.
51. H. J. Berndt and G. Heidemann. *Colloid & Polymer Sci.*, 1980, **258**, 612.
52. M. E. Sikorski. PhD thesis, University of Manchester, 1986.
53. M. E. Sikorski and C. P. Buckley. *Proc. 35th Int. Symp. Instrument Soc. America*, Orlando, FL, 1989.
54. M. E. Sikorski, C. P. Buckley, J. W. S. Hearle and S. K. Mukhopadhyay. *Rev. Sci. Instrum.*, 1993, **64**, 1947.
55. S. K. Mukhopadhyay and L. Noui. Unpublished reports, 1991-93, University of Manchester Institute of Science and Technology.

56. M. V. Forward and H. J. Palmer. *J. Text. Inst.*, 1954, **45**, T510.
57. J. W. S. Hearle, P. K. Sen Gupta and A. Matthews. *Fibre Sci. Technol.*, 1971, **3**, 167.
58. P. F. Dismore and W. O. Statton. *J. Polymer Sci. C*, 1966, No. **13**, 133.
59. A. Koshimo. *J. Appl. Polymer Sci.*, 1965, **9**, 69.
60. S. K. Mukhopadhyay and J. W. S. Hearle. *J. Textile Inst.*, 1990, **81**, 156.
61. S. K. Mukhopadhyay. PhD thesis, University of Manchester, 1985.
62. W. O. Statton. In *The Setting of Fibres and Fabrics*, J. W. S. Hearle and L. W. C. Miles (Editors), Merrow, Watford, 1971, Chapter 4.
63. V. B. Gupta. *J. Textile Inst.*, 1995, **86**, 299.
64. E. M. K  rholm, C. O. Bostwick, G. Sil  n, and C. Kahlson. *Appl. Polymer Symp.*, 1971, No. **18**, 999.
65. J. W. S. Hearle and L. W. C. Miles (Editors). *The Setting of Fibres and Fabrics*, Merrow, Watford, 1971.
66. D. R. Salem. PhD Thesis, University of Manchester, 1982.
67. C. P. Buckley and D. R. Salem. *Polymer*, 1987, **28**, 69.
68. C. P. Buckley and D. R. Salem. *J. Appl. Polymer Sci.*, 1990, **41**, 1707.
69. J. W. S. Hearle, M. A. Wilding, C. Auyeung and R. Ihmayed. *J. Textile Inst.*, 1990, **81**, 214.
70. S. Arghyros and S. Backer. *Textile Res. J.*, 1982, **52**, 295.
71. C. P. Buckley, J. W. S. Hearle and R. Mandal. *J. Textile Inst.*, 1985, **76**, 264.
72. C. P. Buckley. *Int. J. Mech. Sci.*, 1981, **23**, 503.
73. J. W. S. Hearle., Unpublished experiments and calculations.
74. R. S. Berry. *Scientific American*, 1990 (August), **263**, 68.
75. J. W. S. Hearle. *Polymer Eng. Sci.*, 1994, **34**, 260.
76. S. Fakirov. In *Solid State Behaviour of Linear Polyesters and Polyamides* J. M. Schultz and S. Fakirov (Editors), Prentice Hall, Englewood Cliffs, N J, 1990.
77. J. Kugler, J. W. Gilmer, D. Wiswe, H. G. Zachmann, K. Hann and E. W. Fischer. *Macromolecules*, 1987, **20**, 1116.
78. W. Reddish. *Turns. Fowaday Soc.*, 1950, **46**, 459.

19.1 Fibre-fracture morphology

Data on the tensile strength of fibres were included in [Chapter 13](#) with its time dependence in [Chapter 16](#). Loop and knot strength and breaking twist were covered in [Chapter 17](#). This chapter is concerned with the forms of fracture and with fatigue failures due to repeated deformation. As a result of scanning electron microscope (SEM) studies since the 1970s, the appearances of fibre ends resulting from breakage by high loads, fatigue or other causes have been classified into the 18 types shown in [Fig. 19.1](#), and a comprehensive collection of pictures of the fractography has been published by Hearle *et al.* [1].

The following forms are included in [Fig. 19.1](#) for completeness and will not be discussed further: (14) the rounding of fibre ends, which develops after prolonged wear on fibres that have broken in use in a textile material; (17) melting of thermoplastic fibres; (18) the natural ends formed during the growth of fibres such as cotton.

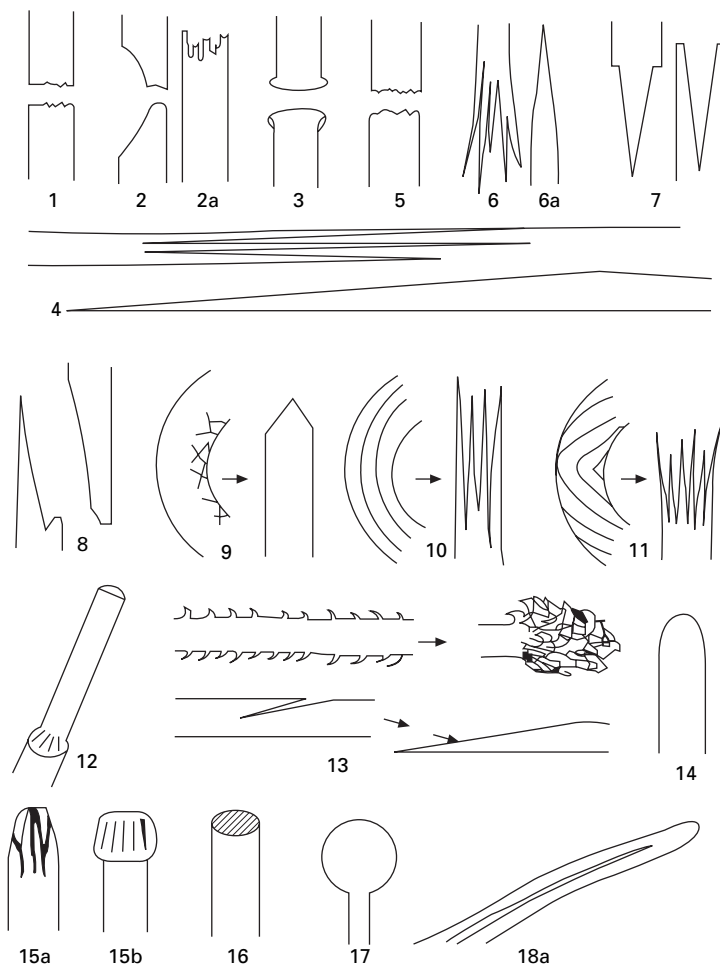
19.2 Monotonic breaks

19.2.1 Tensile failures of manufactured fibres

Depending on the nature of the fibre, different forms of tensile fracture are found. In elastic fibres, whether inextensible (glass and ceramic) fibres or highly extensible (spandex)¹, the break follows the classical mode of brittle failure described by Griffiths, as illustrated in [Fig. 19.2](#). When the load reaches a certain level, the break initiates from a flaw and propagates rapidly as a smooth crack running across the fibre under the influence of stress concentration at the tip of the crack. Usually, when the stress on the unbroken part becomes sufficiently large, multiple-fracture initiation will start and give a rougher portion to complete the break. In some cases, the crack runs at an angle on the line of maximum shear stress for all or a part of the fracture.

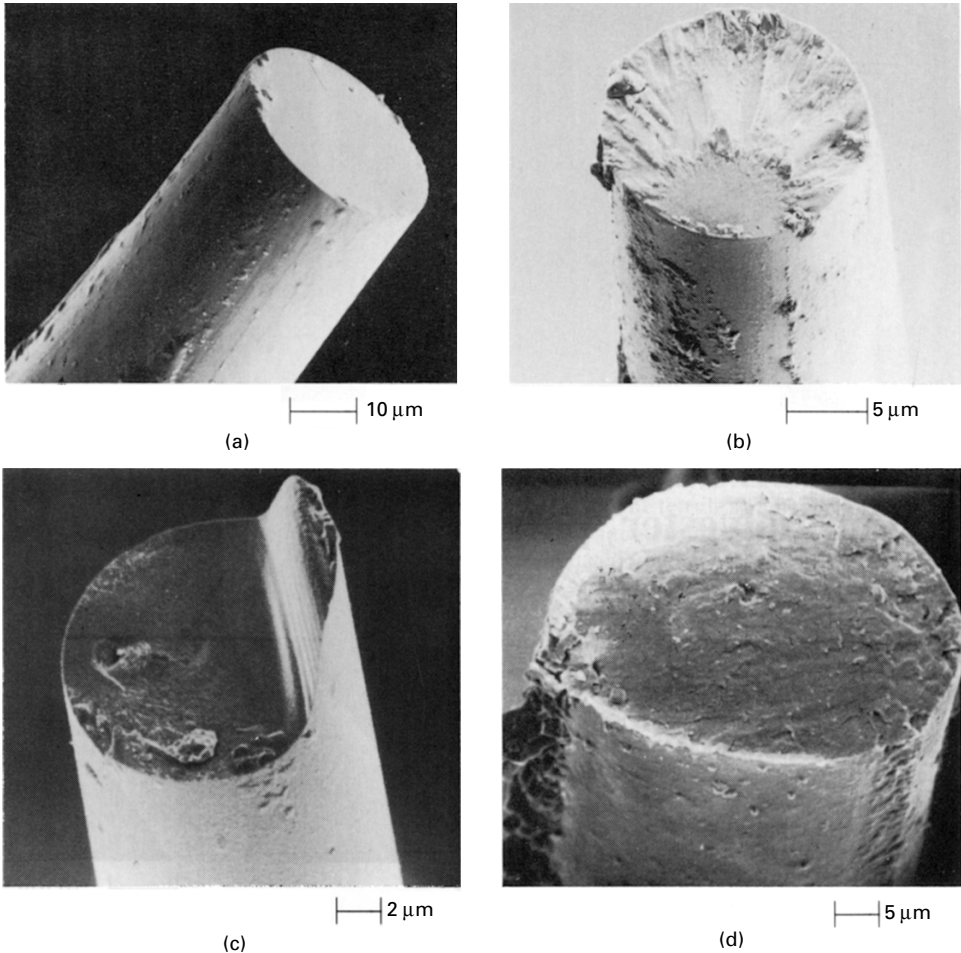
The mechanism in ductile fibres, such as nylon and polyester fibres, is not dissimilar, except that the crack propagates in a controlled manner under a gradually increasing

¹Note that although elastomeric fibres have a low initial modulus, they have a high modulus in the final stage before break.



19.1 Classification of fibre ends. *Tensile failures:* (1) brittle fracture; (2) ductile fracture, (2a) modified form (light-degraded nylon); (3) high-speed break in melt-spun fibre; (4) axial split; (5) granular failure; (6) independent fibrillar failure; (6a) fibrillar break intr fibrils collapsed onto free end; (7) stake-and-socket break. *Fatigue failures:* (8) tensile fatigue; (9) flex fatigue kink-band; (10) flex fatigue-split; (11) multiple split-bend and twist fatigue; (12) surface wear; (13) peeling and splitting; (14) rounding. *Other forms:* (15a,b) transverse pressure, (a) mangled, (b) localised; (16) sharp cut; (17) melt; (18) natural fibre ends, e.g., (18a) cotton tip.

total load and opens into a V-notch owing to the drawing (high plastic extension) of the remainder of the fibre, until a final multiple crack initiation zone completes the failure. The fracture morphology was described by Hearle and Cross [2] and is shown in Fig. 19.3 with break starting at a point. The other end of the break is a mirror image of the one shown. There are variant forms [1]. Many breaks start from an extended defect perpendicular to the fibre axis. Occasionally the defect is angled, which distorts the form of failure and may lead to multiple final stages. Rarely, cracks start from

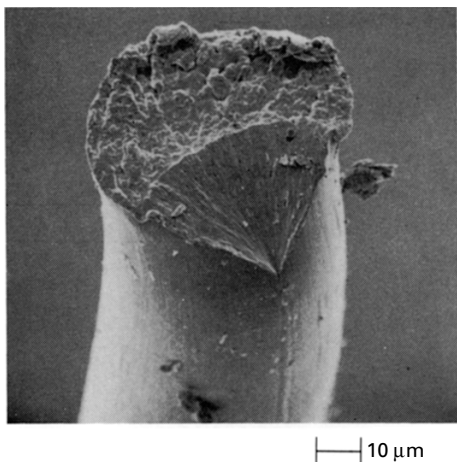


19.2 Tensile fracture of brittle fibres: (a) glass fibre with single cleavage plane; (b) glass fibre showing mirror and hackled zones; (c) ceramic fibre, Nextel 312 (silicon carbide), showing diversion at end of crack; (d) spandex, Lycra.

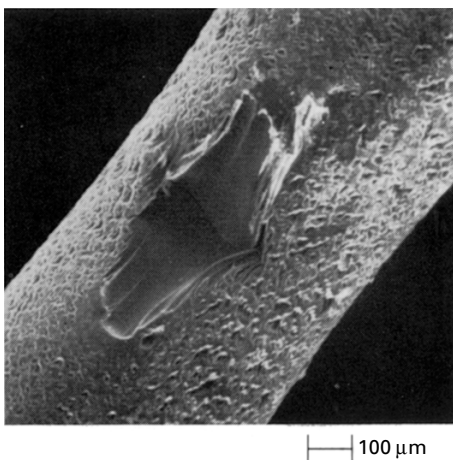
more than one place, joining for the final stage, or start at an internal defect to give a double cone leading to the final stage. In a heat-set nylon 6 fibre, there were small multiple V-notches along the fibre, one of which had propagated to form the break.

A break in progress in a coarse nylon bristle is shown in Fig. 19.4. Such a break can be detected long before the final failure. In these breaks of coarse bristles, put into the Instron Tensile Tester in the undrawn form, Hearle and Cross were able to identify five zones as shown in Fig. 19.5. These were A initiation, B controlled ductile tearing, C 'slip-stick' crack growth, D fast crack growth and, E final overall failure. In light-degraded nylon, the fracture, as shown in Fig. 19.6, appears to be very different, but, in fact, it is probably due to similar failure mechanisms of ductile crack growth, starting from many internal voids [1].

As the rate of loading increases, the size of the V-notch reduces. The final stage becomes larger and may become smooth and rounded. After ballistic impact, by



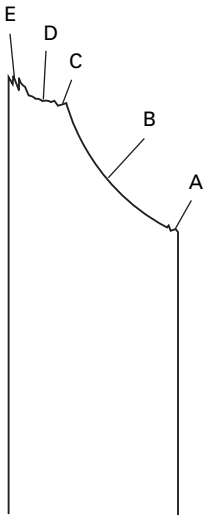
19.3 Tensile break of nylon fibre: experimental nylon 66 filament, with initiation of break at point.



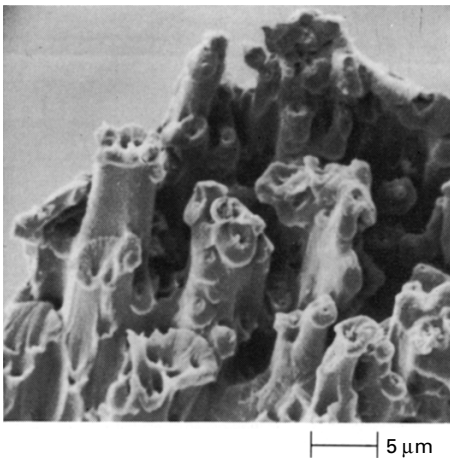
19.4 Rupture of a coarse undrawn nylon 66 bristle, 1 mm diameter, extended at a strain rate of $8 \times 10^{-4} \text{ s}^{-1}$.

release of a pendulum or a relaxation catapult, the form of break changes completely to a mushroom end, as shown in Fig. 19.7. This is due to a change from isothermal to adiabatic conditions. The rapid plastic extension, following the start of break, generates heat and softens or melts the region of the break. Snap-back after break causes a collapse to the mushroom form.

Chemical degradation attacks outer layers first and, under tension, a crack may form around the fibre. A variant of the tensile break then occurs with a circular 'V-notch' leading to a circular catastrophic failure in the centre of the fibre [1]. In other circumstances the shear stress at the tip of the circular crack may lead to an axial split penetrating into the fibre, as shown in Fig. 19.8. The final failure is a stake-and-socket break (Fig. 19.9).



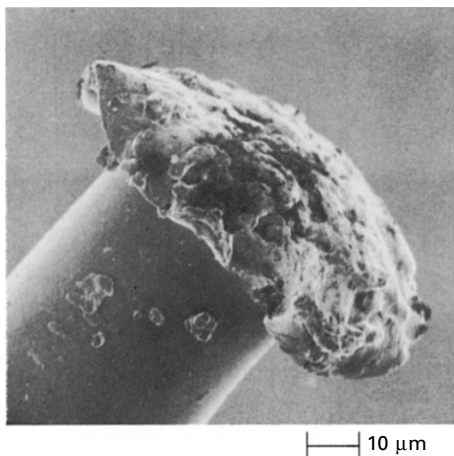
19.5 Breakage zones in nylon bristle.



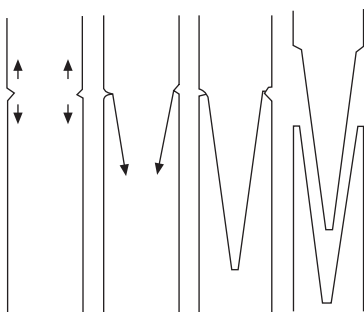
19.6 Tensile breaks of light-degraded nylon 66, 16 dtex, exposed in summer in Manchester, facing WSW: 24 weeks' exposure.

Tensile breaks of acrylic fibres are quite different [1] as shown in Fig. 19.10. The granular appearance is probably due to the independent fracture of many fibrillar sub-units. Sometimes, the final granular break is preceded by a V-notch and sometimes separate granular cracks are joined by an axial split. Granular breaks are also found in regenerated cellulose fibres, polyvinyl alcohol (PVA) and polybenzimidazole (PBI) fibres, ceramic fibres some carbon fibres, and thermally degraded nylon and polyester fibres [1].

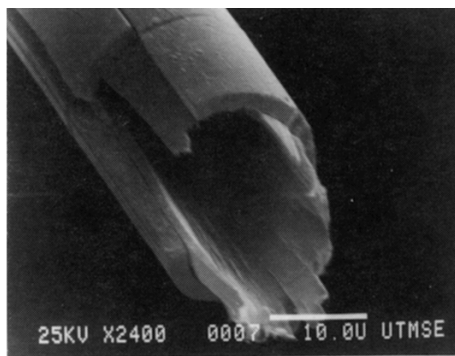
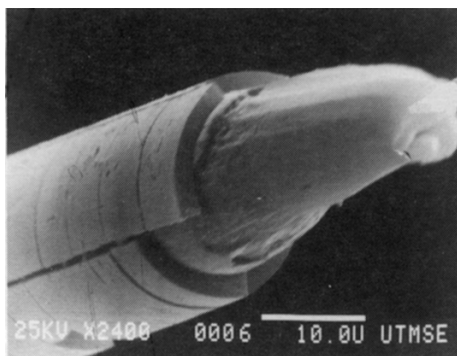
In acetate fibres, Simmens and Howlett [3] found, by optical microscopy, that many surface cracks developed in highly stressed filaments, as shown in Fig. 19.11. This can lead to multiple fracture, with the fibre finally shattering into many fragments.



19.7 High-speed tensile break of nylon 66.



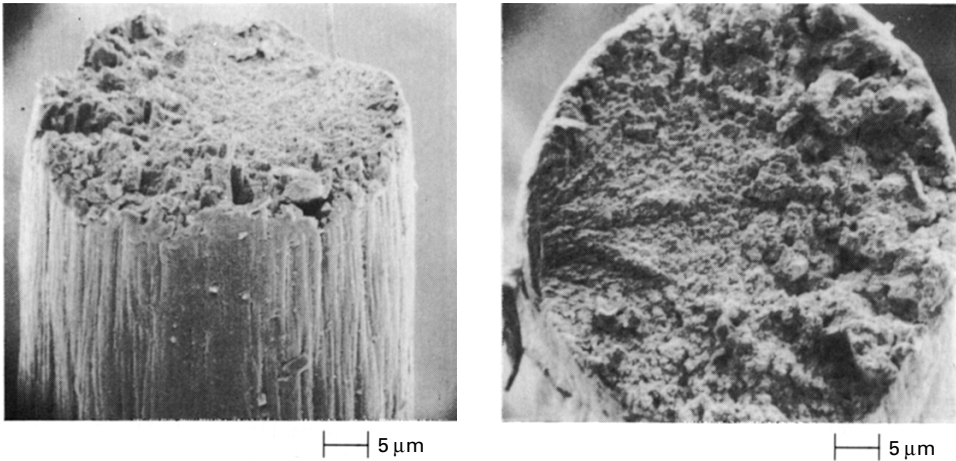
19.8 Shear cracking, following degradation round surface of fibre.



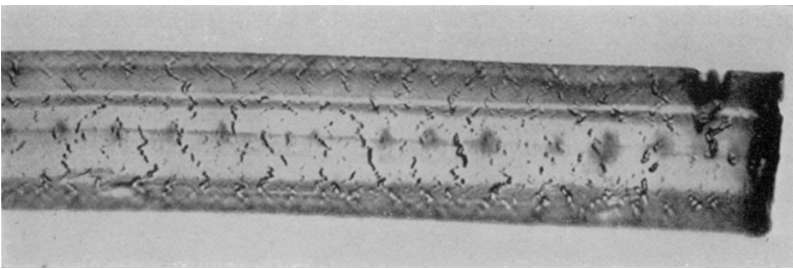
19.9 Stake-and-socket break of polyester fibre after exposure to *n*-butylamine vapour.

The occurrence of fissures during extension, but before fracture, has been observed in many fibres by Cumberbirch *et al.* [4].

In the highly oriented linear-polymer fibres, para-aramid and HMPE, tensile fracture occurs by long axial splits [5]. This is because the forces holding the molecules



19.10 Granular fractures of acrylic fibres.

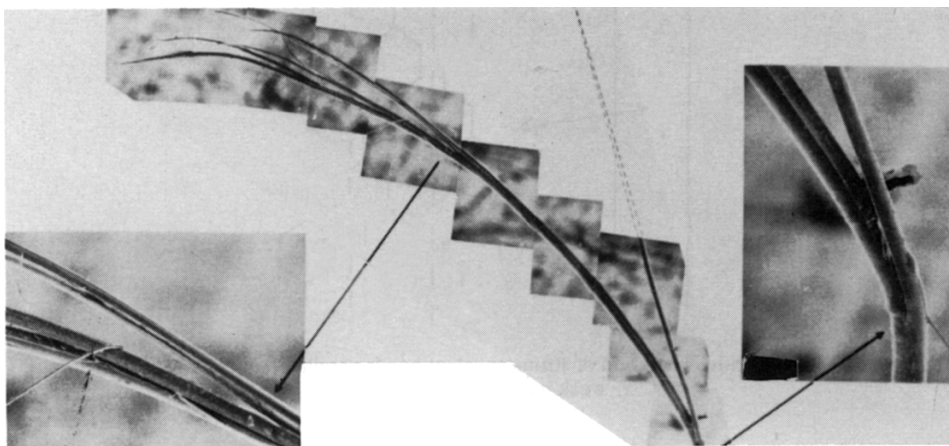


19.11 cracks in stressed acetate filaments as observed by Simmens and Howlett [3].

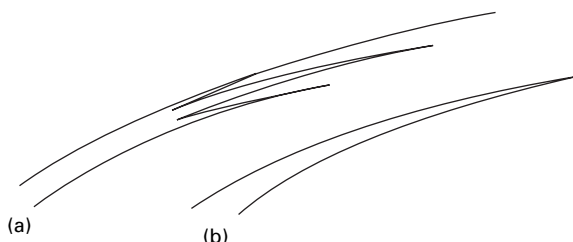
together across the fibre are much weaker than the forces acting along the molecules in the axial direction. If there are any defects or discontinuities in the structure, the resultant shear stress causes rupture by an axial split in preference to the imposed tensile stress causing a transverse crack. If the splits are slightly off-axis, they will eventually cross the fibre and so separate it into pieces, with the break extending over a length equal to many fibre diameters. An SEM picture of a break is shown in Fig. 19.12. Frequently, one end has a single split and the other end has a multiple split, as illustrated in Fig. 19.13. This is a geometrical consequence of an axial crack starting at the surface of the fibre and branching as it propagates along and across the fibre. The extensive axial splitting means that, in fibre assemblies and composites, more energy is absorbed during breakage than when fibres break sharply.

19.2.2 Tensile failures of natural fibres

Tensile breaks of natural fibres are strongly influenced by their particular internal morphologies. In cotton, the form varies according to test conditions. At 65% r.h., Hearle and Sparrow [6] showed that tensile failure is started by splitting between



19.12 Tensile break of aramid fibre, Kevlar 29.



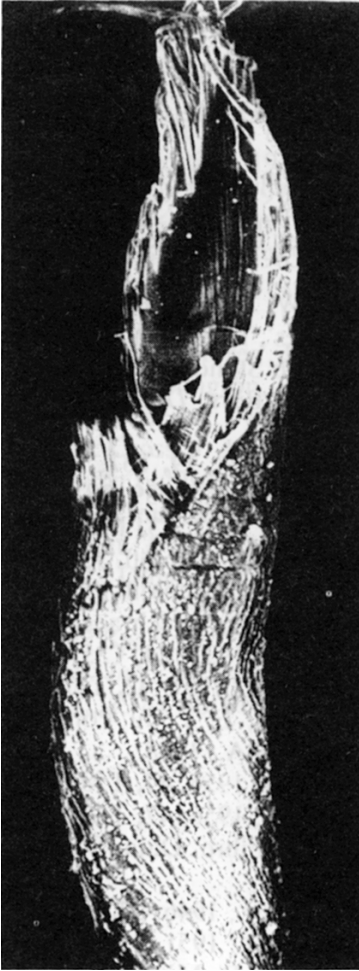
19.13 Fractures of Kevlar: (a) multiple split; (b) single split end.

fibrils (Fig. 19.14). The break occurs adjacent to a reversal, and the split, which follows the helical path of the fibrils around the fibre, is due to the untwisting forces. Eventually a tear develops along the edge of the concave region of the cross-section to join up the two ends of the helical split, as illustrated in Fig. 19.15.

The form changes as the strength of bonding between fibrils varies. When it is weak, in wet cotton, the break is fibrillar. The cause is illustrated in Fig. 19.16. Fibrils can be regarded as independent entities, which break at different weak places. Eventually all fibrils have broken over a short fibre length and the two ends separate. In the SEM, the separate fibrils may be seen (Fig. 19.17), but often the broken fibrils coalesce into a tapered end. Where the bonding is stronger, in dry cotton, the fracture runs across the fibre as a granular break with little splitting. If the fibre is clamped at a nominally zero gauge length without a reversal between the jaws, there is again usually little splitting, with the break running straight across the fibre.

In resin crosslinked cotton, the increased bonding causes the break to be straight across the fibre at 65% r.h. and has a split form, similar to Fig. 19.14, when broken in water.

In wool and hair fibres, tensile failures occur by cracks running across the fibre in a granular break, which may be coarse enough to reflect separate breaks of cells. It is fairly common for cracks at different positions along the fibre to be linked by an



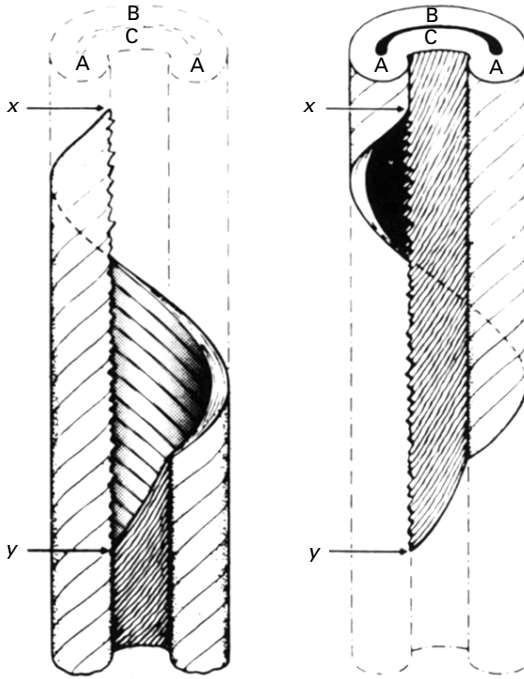
19.14 Tensile fracture of cotton fibre under standard conditions.

axial crack. Cracks in the cuticular layer of wool have been examined by Makinson [7].

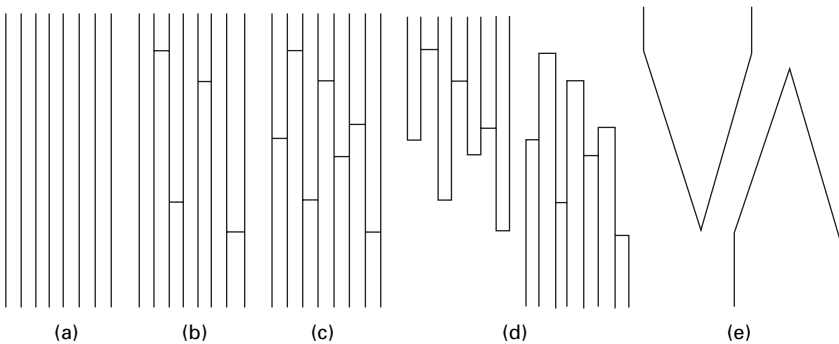
Haly [8] noted that transverse striations developed in wool between 2 and 30% extension. However, these are probably regions of high local deformation and not cracks. Crazeing in synthetic polymers is another phenomenon, in which there is some continuity of material across an apparent crack.

19.2.3 Twist, lateral cohesion and compression

As stated in Section 17.3.1, the major deformation at high twist levels is extension of the outer layers due to the longer helical path. This results in twist breaks being essentially tensile breaks, which are distorted by the twisting and may include axial splits [1].



19.15 Idealised picture of break of cotton fibre at 65% r.h. A, B and C are the separate zones shown in Fig. 1.37. The split runs from x to y.



19.16 Schematic of fibrillar break. (a) Unbroken fibrils; (b) isolated breaks; (c) all fibrils broken; (d) separated ends; (e) collapse of ends.

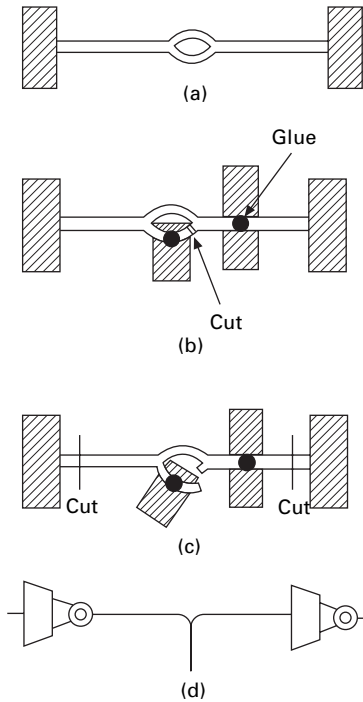
Law and Mukhopadhyay [9] describe in detail a method of measuring the lateral cohesion of fibres. Briefly stated, a fibre is mounted between tabs and a micromanipulator is used to open a split in the centre (Fig. 19.18(a)). Pieces of copper ribbon are then stuck to the fibre in the positions shown in Fig. 19.18(b) and the split is cut on one side. The test specimen is then cut away (Fig. 19.18(c)) and mounted between jaws (Fig. 19.18(d)) of a tensile tester, which incorporates a micro-balance and a micro-drive unit. The tearing force required to pull the two ends apart can then be measured.



19.17 Fibrillar break of wet mercerised cotton.

The force is divided by the width of the tear, assumed to be the fibre diameter for a central tear, and expressed in N/m ($= \text{J/m}^2$). Figure 19.19(a) shows the tearing force for an aramid filament, which has three regions as indicated in Fig. 19.19(b). SEM examination shows that the tear is in regions 1 and 2. There may be a precursor crack from the initial split formation, which reduces the tear force in region 1, or the occurrence of a hemispherical skin tear may increase the force in region 2. Although not mentioned by the authors, the energy loss in the bend at the splitting point must also contribute to the tear force. The change to region 3 is due to the onset of multiple splitting, which would increase the surface energy and hence require more force. It is estimated that the lateral cohesion or energy for crack propagation is the value in region 2, namely 160 J/m^2 . Other tests were carried out on acrylic fibres, but it was not possible to test dry fibres. Never-dried fibres impregnated with glycerol were used.

The failure properties in transverse compression have been studied by Settle and Anderson [10] by pressing metal cutting wires against fibres. The loads needed for cutting increase with the fibre and wire diameters: typical values are given in Table 19.1. With wires finer than $100 \mu\text{m}$, the cutting load decreases rapidly. Subsidiary experiments led to an estimate of the principal strains at failure, which were much larger laterally than axially. The fibre was observed to be squeezed out sideways, and



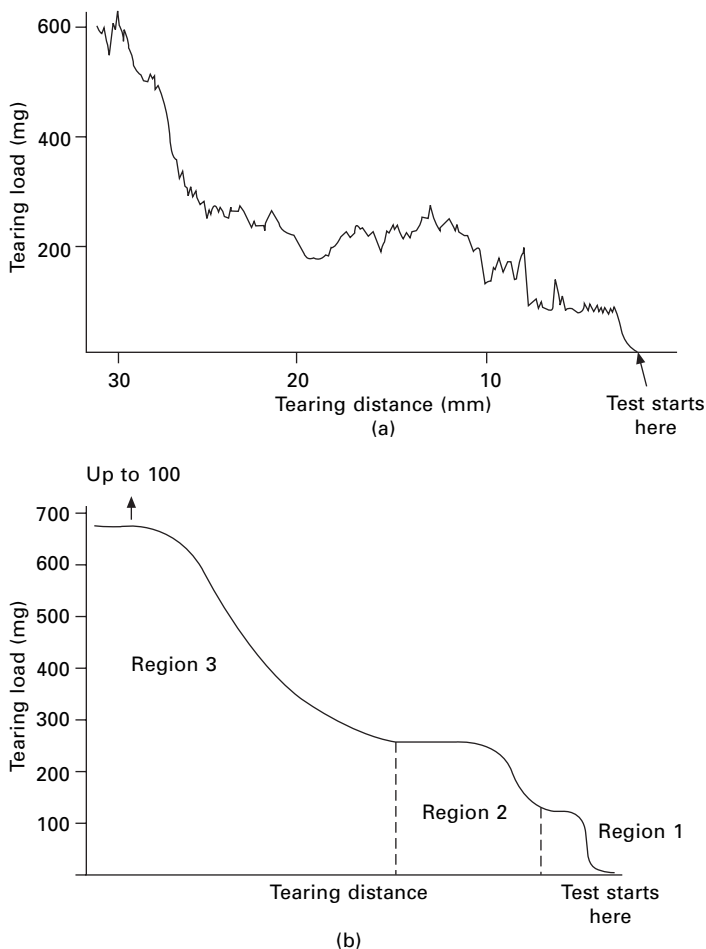
19.18 Stages in measuring lateral cohesion of fibres. From Law and Mukhopadhyay [9].

then, after a certain degree of penetration, a V-shaped cleft appeared and penetrated through the fibre. The elastic recovery was poor (about 50%) even when the applied load was only a quarter of the load needed for cutting.

Shin *et al.* [11] investigated the cut resistance of HM-HT yarns using the apparatus in Fig. 19.20. Neighbouring yarns were removed from a piece of fabric clamped on a base plate, in order to leave isolated yarns subject to the cut. The force–displacement plot is shown in Fig. 19.21(a) for aramid *Kevlar*, HMPE *Spectra* and PBO *Zylon*. The massive reduction in cut resistance when the slice angle is reduced from 90 to 80° is shown in Fig. 19.21(b). Blade sharpness has a major effect, with a 2.5-fold increase in resistance for a blade radius change from 2 to 20 μm . Some end beaks were fairly straight across the fibres, but others showed considerable squashing.

19.2.4 Fracture mechanics

Theoretical analysis of fibre strength and detailed understanding of how and why strengths fall below maximum possible values are not easy. The basic theory of the tensile strength of a perfect crystal is illustrated in Fig. 19.22. The internal energy U is a minimum at the equilibrium spacing x_0 between the atoms; but as the crystal is extended, so that x increases, U reaches a maximum and then falls asymptotically to zero. Differentiation of this curve gives the variation of force with extension ($x - x_0$).



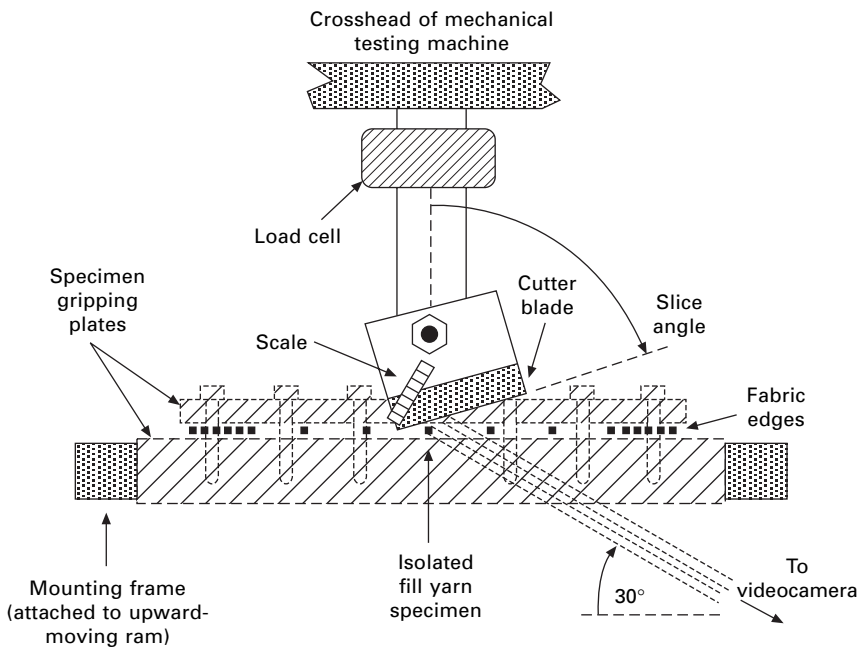
19.19 (a) Tearing force for Kevlar 49 filament, (b) Schematic representation. From Law and Mukhopadhyay [9].

The maximum value F , which is the ‘theoretical’ strength, occurs at the point of inflection on the energy curve. It will be high when there are strong covalent bonds between the atoms, weaker with intermediate attractions, such as hydrogen bonds and dipoles, and least with weak van der Waals interactions. However, the theoretical predictions of the shape of the variation of U with x are not exact, especially in terms of the precise position and slope of the inflection point. More commonly, an approximate value of F is estimated from the linear construction shown in Fig. 19.22(c), which demonstrates that the theoretical strength should equal the modulus times a strain level e_c , related to the position at which the energy curve is expected to go through its inflection. Generally, the maximum strength is expected to be about 0.1 times its modulus.

Among the factors that lower modulus, disorientation and slip at the ends of molecules will also lower strength, but the removal of crumpled disorder at low

Table 19.1 Loads required to cut fibres [12]

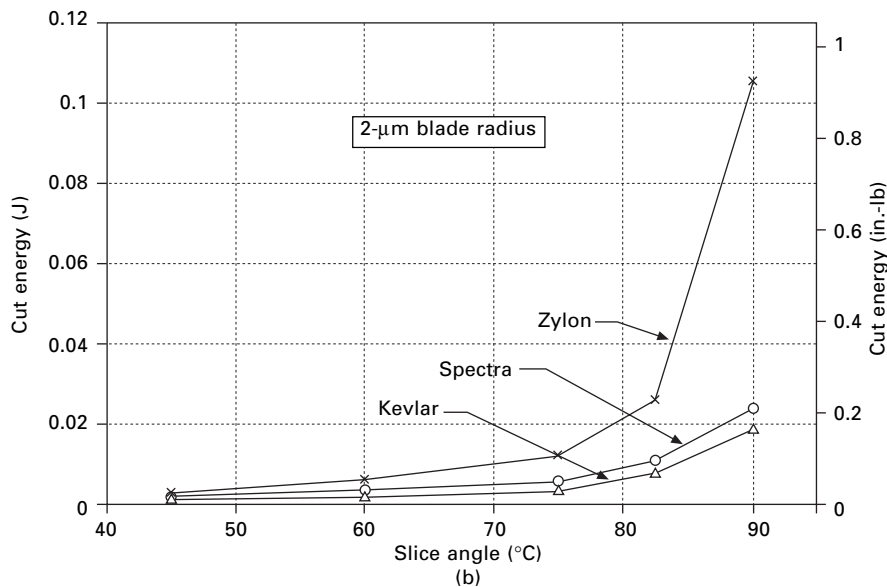
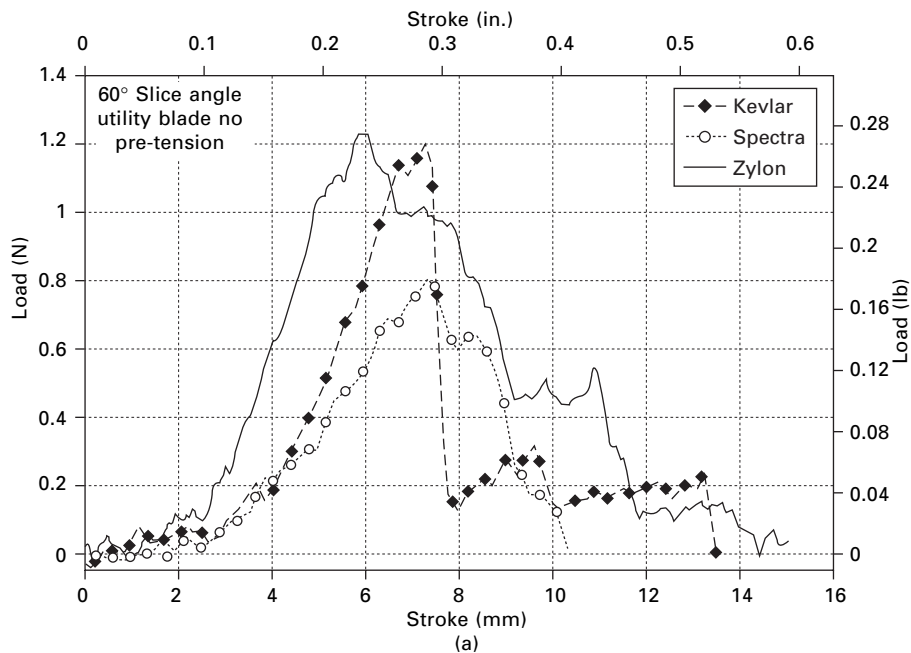
Fibre type	Fibre diameter (µm)	Wire diameter (µm)	Cutting load (N)	Estimated principal strains (%)	
				Axial	Lateral
Nylon	20	200	2.2	6	86
	20	400	3.7	–	–
	40	200	5.0	12	81
	40	400	8.0	–	–
Polyester fibre	20	200	2.0	6	114
	20	400	3.5	–	–
	40	200	4.2	15	107
	40	400	8.5	–	–
Wool	20	200	0.5	–	–
	20	400	0.7	–	–
	40	200	2.2	10	47
	40	400	3.3	–	–



19.20 Cut testing. From Shin *et al.* [13].

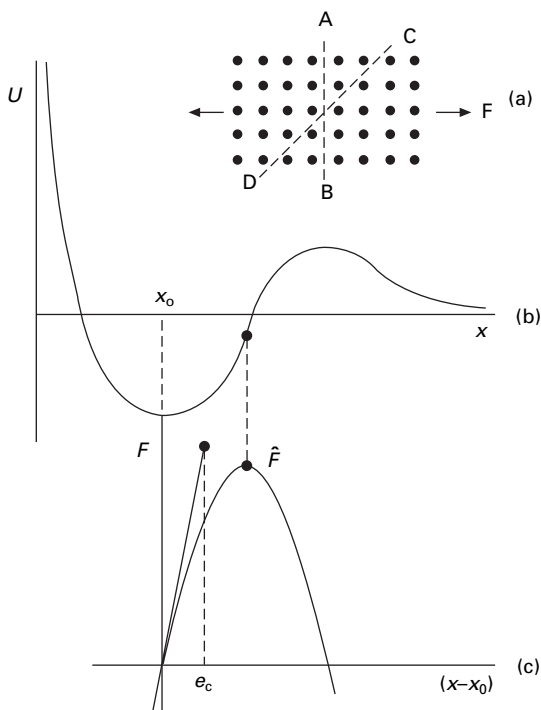
strains will not. Any non-uniformity in the distribution of stress between different parts of the structure will lower strength.

Failure is a competitive phenomenon, determined by extreme value and not central value statistics, and will always occur in whichever way is easiest. Even at the theoretical level of a perfect crystal, this means that rupture may occur not under tensile stress across the plane AB in Fig. 19.22(a) but under some other stress, such



19.21 Cut test results: (a) force-stroke plot; (b) effect of slice angle. From Shin *et al.* [11].

as the resolved shear stress across CD. At the practical level, there are all the complications of local variations in stress due to gross structural differences, of stress concentrations at microscopic defects, and of uneven sharing of load at the molecular level in an imperfect structure. As indicated above, the interaction of defects with

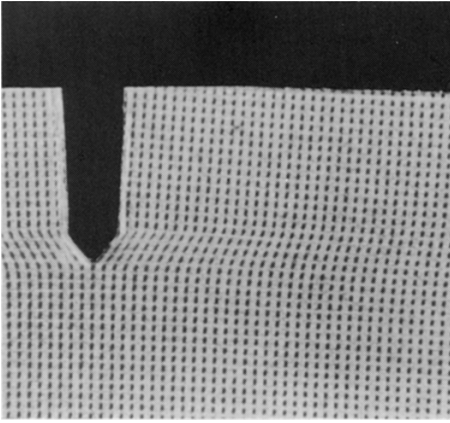


19.22 Simple theory of tensile strength: (a) perfect crystal under tensile force F ; (b) variation of internal energy U with spacing x ; (c) variation of force F with elongation $(x - x_0)$.

very high anisotropy leads to completely different modes of failure in the oriented linear polymer fibres. The simple argument also ignores the time-dependence associated with thermal vibrations, which allows jumps over the point of inflection as discussed in Sections 20.2.1 and 20.7.2.

The role of defects is critical. The foundations of fracture mechanics were laid by A. A. Griffiths in 1921. He emphasised the role of flaws either on the surface or internal, which led to stress concentrations. A direct approach models the stress distribution round a defect. The crack will propagate when the stress at its tip exceeds the fundamental value of the strength as discussed above. A more useful approach depends on the relation between the elastic energy released by crack growth and the increase in surface energy dS . The crack will propagate when $dE > dS$. The deeper the defect, the greater the stress concentration or energy release, so that once the inequality is reached the crack will continue catastrophically across the fibre.

The classical theory applies well to brittle fibres such as glass, where the deformation is purely elastic. When there is also plastic deformation, the situation is more complicated. If there is a small, localised, plastic zone, an additional energy term can be added to dS without altering the basic analysis. Modifications can be made when the plastic zone is large compared with the crack depth. The mechanics of the ductile fracture of nylon and polyester fibres raises more difficulties. As indicated by the tensile break of a polyester film in Fig. 19.23, the plastic deformation would extend



19.23 Tensile break of a marked polyester film.

right across the fibre and for a considerable length along the fibre, where it is linked to the unstressed region in line with the crack by a shear zone.

The mechanics of this complexity has not been analysed. It should be noted that the material across from the crack is under a higher stress than unaffected remote parts of the fibre length and is extended by larger amounts than the measured break extension of the fibre. The stress-strain relation at these stresses is unknown.

Michielsen [12, 13] has studied the fracture toughness of nylon 66 monofilaments. Applying fracture mechanics, he derives a value of 17 kJ/m^2 for the energy release rate at 65% r.h., rising to 31 kJ/m^2 at 0% r.h. and falling to 16 kJ/m^2 at 100% r.h.

In other forms of break, granular, axial splitting, fibrillar, the stress concentrations that lead to failure are distributed in more complex ways. However, the fundamental principle that cracks will propagate when it leads to a reduction of energy remains valid. The problem is how to calculate the energy terms.

19.3 Tensile fatigue

The classic definition of fatigue, as found, for example, in metals, is of failure under cyclic straining at a level that would not cause failure if applied as a constant strain. There has been a search for similar effects in fibres.

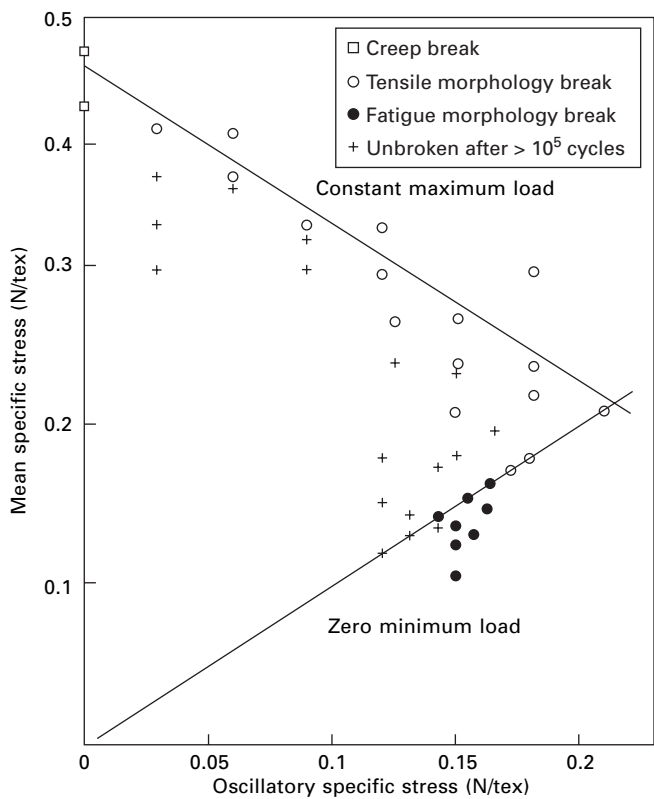
One of the problems has been that in simple extension-cycling, the load progressively decreases owing to stress relaxation: failure does not occur unless the imposed extension is very close to the usual breaking extension. Most fatigue testers therefore operate on the principle of cumulative-extension cycling, with the slack removed at the end of each cycle. This work has been reviewed by Hearle [14]. However, as shown in Section 15.7.3, a common result of such a test at larger imposed extensions is a climb up the stress-strain curve to the normal breaking point. At low imposed extensions, failure does not occur. There have been some indications that fatigue effects might be important over a narrow range of imposed extensions.

Table 19.2 gives a comparison of the behaviour of fibres in such a cumulative-extension test.

Table 19.2 Median number of cycles to break for various yarns in cumulative-extension test (from Booth and Hearle [15])

Fibre	Imposed extension (%)					
	2½	5	7½	10	12½	15
Viscose rayon	†	79		6		
Acetate	32 000	58		6		
Nylon			>5 × 10 ⁵	11 000	220	12
Polyester fibre		>5 × 10 ⁵	16 000	18	7	

†Four out of ten had failed at 5 × 10⁵ cycles.



19.24 Failure conditions in fatigue-testing of nylon [17].

More interesting results have been obtained with a controlled-load fatigue tester operating at 50 Hz [16]. The specimen is cyclically strained by a vibrator acting on one end of the fibre, and the clamp at the other end is driven through a servo-system to maintain the peak load constant.

Studies of nylon by Bunsell and Hearle [17] showed that, at high maximum loads, failure occurred in the same time and the same mode as in a creep test. This gives the failures about the line of constant maximum load in Fig. 19.24. Under these conditions,

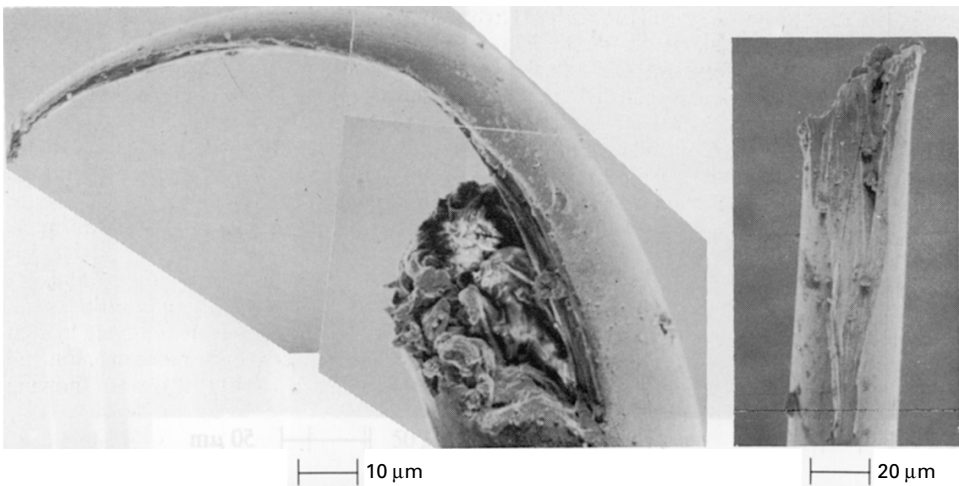
the cyclic nature of the loading has no effect, and the behaviour could be predicted from studies of creep failure.

However, at much lower maximum loads, between one-half and two-thirds of the equivalent creep breaking load, failure occurred provided that the minimum load in each cycle was zero. This gives the breaks about the line of zero minimum load in Fig. 19.24. At an intermediate state, with higher maximum and minimum loads, failure did not occur.

The fracture morphology is also different. In creep failure, and at the high maximum loads, the fracture showed the V-notch typical of tensile failure, as in Fig. 19.3. But the fatigue failures, at zero minimum load, were quite different in appearance. One end showed a long tail, which had stripped off the other end, as shown in Fig. 19.25. The sequence of events is that an initial transverse crack appears (Fig. 19.26(a)), and this then turns and runs along the fibre, to become gradually wider and deeper (Fig. 19.26(b)), until final failure occurs with a tensile break across the reduced cross-section. The angle of the crack in nylon is about 10° , so that the tail is about five fibre diameters long.

In more recent work, Oudet and Bunsell [18] have shown that zero minimum load was not an absolute criterion for tensile fatigue failure in nylon fibres. For a particular sample of nylon, fatigue failures were found with a small positive minimum load. They were still present, together with some creep failures, when the minimum load was 4% of breaking load but were absent when it was increased to 6%.

A similar tensile fatigue failure is found in polyester fibres [19, 20], though the fatigue lifetime is greater than that in nylon. Another difference is that the axial crack in polyester fibre runs almost parallel to the fibre axis and leads to extremely long tails (Fig. 19.27(a)). The other end shows where the material is stripped off (Fig. 19.27(b) and in this example the final failure has occurred where there is a weak

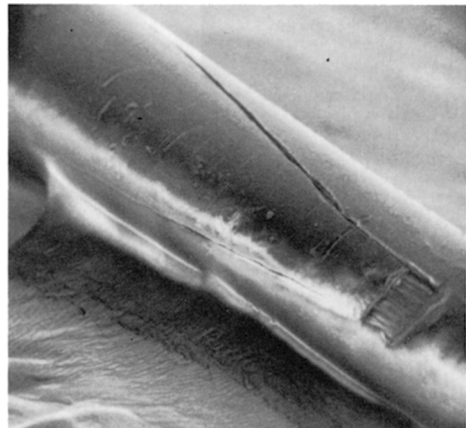


19.25 Opposite ends of break of nylon 66 fibre after 62 000 cycles at 50 Hz between zero load and 71% of normal break load.



2 μm

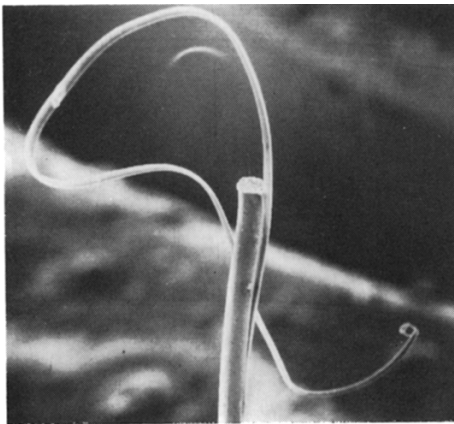
(a)



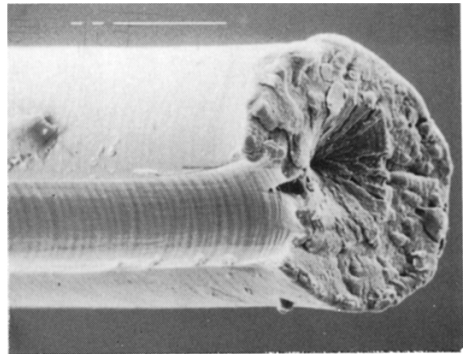
20 μm

(b)

19.26 (a) Initial transverse crack in tensile fatigue. (b) Shear crack runs along the fibre.



50 μm



5 μm

19.27 (a) Break of polyester fibre after 83 000 cycles at 50 Hz between zero load and 65% of normal break load. (b) Final break of a polyester fibre by tensile fatigue.

place due to an internal defect in the fibre. Although the long axial splits eventually lead to complete fibre rupture over the remaining cross-section in a single-fibre test, they would not necessarily do so in an assembly in which the fibres are held together by twist or other means and mutually support one another.

Bunsell and his colleagues have continued to study tensile fatigue failures in nylon and polyester fibres. In nylon 6 and 66, final rupture occurs when the crack reaches a point where the reduced cross-section leads to tensile failure, but in polyesters, PET and PEN, it is by creep at a point further back along the crack [21]. The transverse

cracks, which initiate the failure, are attributed to hard inclusions, which may be introduced as catalysts, antioxidants or flame retardants, at the interface between skin and core about 1 μm below the surface [22]. In a study of the effect of temperature on several mechanical properties, a threefold decrease in fatigue lifetime was found for polyester fibres [23].

In the meta-aramid fibre *Nomex*, tensile fatigue occurs in a similar form to that in nylon [19]. In an acrylic fibre *Courtelle*, tensile fatigue causes failure by axial splitting, but there is no requirement that the minimum load should be zero in order to promote this mode of fatigue failure. A comparison of typical tensile fatigue failure conditions is given in Table 19.3. The breaking extension in the fatigue tests is lower than that in the tensile tests. This confirms that a special fatigue mode of failure is occurring and provides a means of differentiating from a creep failure after repeated cycling, which occurs at the same breaking extension as in a tensile test.

In the para-aramid fibre *Kevlar*, tensile-load cycling causes a much greater degree of axial splitting but no appreciable loss of strength [24]. In order to achieve failure in around 10^5 cycles, it is necessary to go to at least 90% of the normal breaking load, which is within the range of normal variability.

19.4 Torsional fatigue

Twisting, as discussed in Section 17.3, is the second easiest mode of load-deformation response to study in the laboratory, provided that only a single test to break or a few cycles of deformation and recovery are needed. However, fatigue testing, which requires a large number of cycles at relatively high speeds, is not so easy. For example, a typical test on a 1 cm test length twisted to half the breaking twist might involve a million revolutions, reversing every 50 revolutions. In these circumstances, it is easy to wear out a mechanical drive. Some studies of torsional fatigue, which were carried out before SEM was available to examine fracture morphology, were reported by van der Vegt [25] but these were made under rather severe conditions, which led to failure in less than 1000 cycles, with twist angles ranging from about 11° for rayon to 45° for nylon. There have been few later investigations.

Goswami and Hearle [26], as part of a comparative study of forms of fracture, carried out some torsional fatigue on a 1 mm length of a 16.7 dtex nylon fibre, vibrated to a twist angle of 45° at 5 Hz. Rupture occurred after about 16 hours. The

Table 19.3 Tensile fatigue failure conditions [21]

Fibre type	As percentage of breaking load		Fatigue life cycles	Breaking strain (%) in:	
	Minimum load	Maximum load		tensile test	fatigue test
Nylon 6.6 (MT)	0	62	0.8×10^5	36	25
Nylon 6.6 (HT)	0	55	0.5×10^5	17	11
Polyester fibre	0	65	2×10^5	20	12
<i>Nomex</i>	0	70	0.2×10^5	20	14
<i>Courtelle</i>	20	65	$0.04\text{--}2.6 \times 10^5$	55	45

failure started with the development of several splits running along the fibre, which led to the breaking away of chunks of material. Duckett and Goswami [27] have described a multi-station torsional fatigue tester, which has been used for studies of fibre failure related to pilling in fabrics [28].

Toney and Schwartz [29] report a linear decrease $\log(\text{cycles to failure})$ with increase of surface strain.

19.5 Flex fatigue

19.5.1 Test method

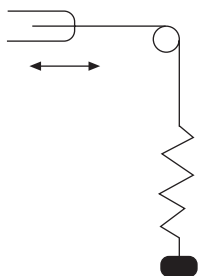
The simplest way of repeatedly bending a fibre is to pull it backwards and forwards over a pin under sufficient tension to cause the fibre to follow the curvature of the pin surface as illustrated in Fig. 19.28. If the tension is applied by a hanging weight, the fibre is free to turn round, so that the application of tension on the outside of the bend and compression on the inside occurs rather irregularly on different parts of the fibre. It is therefore preferable to apply the tension by means of an elastic string [30] and to mount a card to check that there is no rotation. A simple, approximate description of the test would then be that a length of fibre, equal to the reciprocating stroke of the drive vibrator, is subject to an alternation between a straight and a bent form.

Application of classical bending theory, as given in Section 17.2.1, predicts that, in the bent state, the fibre strain would increase from zero at the centre plane to a maximum tensile strain e_b on the outside of the bend, and a maximum compressive strain $-e_b$ on the inside. Depending on the position within the fibre, the material would oscillate between zero strain and the maxima in tension or compression. The value of e_b is given by:

$$e_b = \frac{r}{R + r} \approx \frac{r}{R} \quad (19.1)$$

where r = fibre radius and R = pin radius.

In reality, there are a number of complicating factors, which will be discussed in more detail in Section 19.5.4. Firstly, there is the additional strain due to the applied tension. Secondly, the fibre cannot change abruptly from finite curvature on the pin to zero curvature off the pin, since there must be a zone of varying curvature with resulting shear stresses. Thirdly, friction on the pin will generate surface shear stresses.



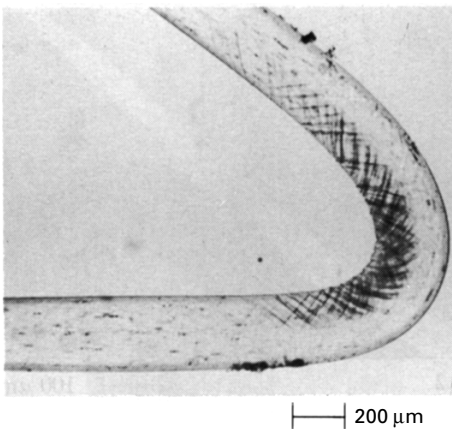
19.28 Flex fatigue over a pin.

These three effects are inherent in the mechanics of the test method and would be present even if the fibre were ideally linear elastic (Hookean). But, in fact, most fibres have non-linear stress–strain curves and, as shown in Section 17.2.4, yield more easily in compression than in tension. Consequently, a fourth complication is that the neutral plane shifts away from the geometric centre of the fibre, the maximum tensile strain is reduced, and the maximum compressive strain is increased. An exception to this rule occurs in wool and hair, which yield more easily in tension. Although the ‘bending strain’ e_b is thus not strictly a measure of maximum strain, it is a convenient quantity to quote as an indicator of the severity of bending in a flex fatigue test.

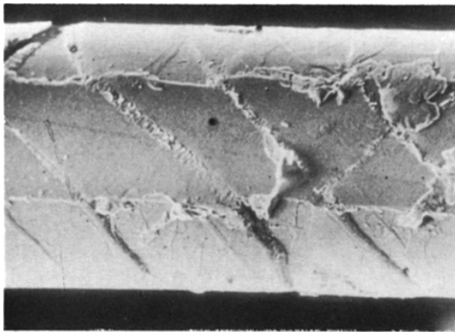
Temperature and moisture conditions are found to have a considerable influence on flex fatigue, and the apparatus has therefore been modified so that four test positions are enclosed within a box under controlled atmospheric conditions [31]. A complete statement of test conditions should include: bending strain, tension, temperature, humidity, and the state of the pin and fibre surfaces.

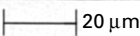
19.5.2 Modes of failure

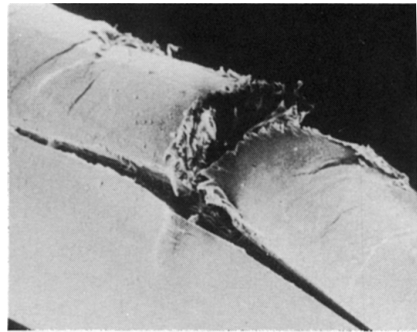
The bending of fibres with yield in compression causes the appearance of kink-bands as illustrated for polyester fibre in Fig. 19.29. A single bend causes no detectable damage to the fibre. If tension is applied, the kink-bands are pulled out, and there is no loss of strength. However, fatigue tests [1, 30, 32] show that repeated flexing leads to failure. Three forms of damage occur in cycling over a pin. Initially, Fig. 19.30(a), there is some surface wear due to rubbing on the pin. This is an artefact not directly related to flexing and is discussed in Section 19.7. In addition, there are kink-bands, which have started to break up into a fibrillar or crazed formation and some incipient cracking. A complete crack, which would be on the compression side of the fibre, is shown in Fig. 19.30(b). Shear at the tip of the transverse crack has led to an axial crack. When the compression side of the fibre has failed, it ceases to be effective, and

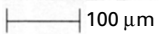


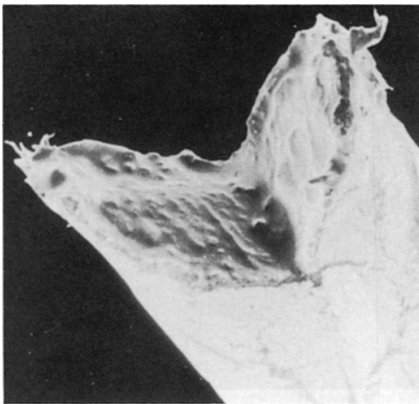
19.29 Kink-band, visible in polarised light, formed on the inside of a bent polyester fibre.

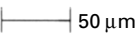


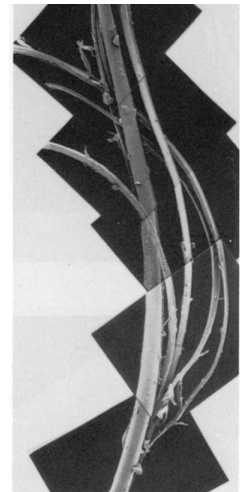
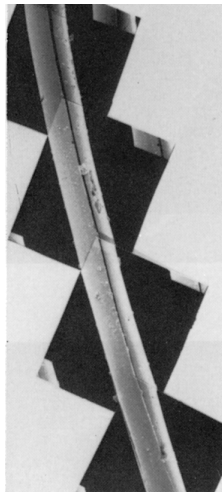
(a)  20 μm



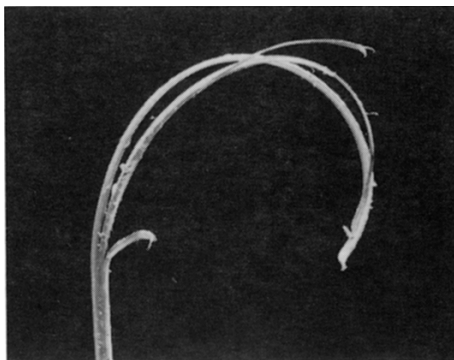
(b)  100 μm

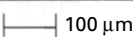


(c)  50 μm



(d)



(e)  100 μm

19.30 Forms of damage in flex fatigue over a pin: (a)–(c) polyester (PET) at 65% r.h., 20 °C; (d) nylon 66 at 60 °C, 30% r.h.; (e) polyester (PET) at 80 °C, 5% r.h.; (f) nylon 6 at 100 °C, dry air.

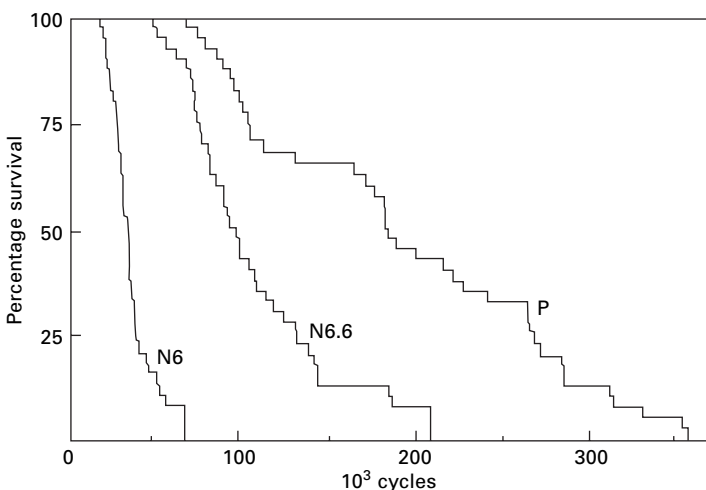
the other half of the fibre then bends independently, so that the same mechanism can repeat itself, with the formation of more angular cracks, which constitute this mode of failure in flex-fatigue tests. In tests in which the fibre is allowed to rotate, kink-bands will come in from all sides and a final break occurs along the angle of kink-bands (Fig. 19.30(c)). This mode of flex fatigue failure, which is directly related to the compression that occurs in bending, is found in some examples of wear in use [1]. However, another mode of failure can also occur. Variable curvature results in shear stresses, which lead to single or multiple splits, Fig. 19.30 (d, e). As the fibre is pulled over the pin, the region of shear stress will travel along the fibre and cause long axial splits. Failure by multiple splitting is the commonest mode of failure in use, but may result from twisting, bending or a combination of both.

Observations of the development of damage in flex fatigue testing is reported by Hearle and Miraftab [33].

19.5.3 Flex fatigue lifetimes

The statistical variability of fatigue tests of fibres is usually fairly high, and the results are most conveniently expressed by survivor diagrams. Typical examples are shown in Fig. 19.31 for nylon and polyester fibres flexed over a pin with a diameter of 0.25 mm under standard atmospheric conditions (65% r.h., 20 °C). The mechanical conditions are similar, but not identical, as indicated in Table 19.4 [31], which also includes some statistical data on lifetimes. The median is the most convenient measure to quote, since it avoids large errors due to a few abnormally large or small values.

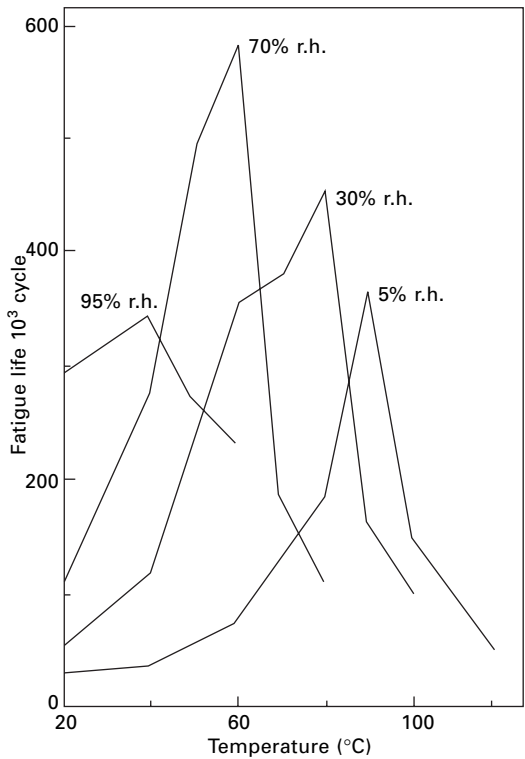
Flex fatigue has been found to be very dependent on conditions of temperature and humidity. A set of results obtained by Miraftab [32] for the 22 dtex nylon 6 fibre, under the same conditions as given in Table 19.4, are shown in Fig. 19.32. The median lifetime ranges between about 30 000 cycles at 5% r.h., 20 °C and 600 000



19.31 Survivor diagrams for nylon 6 (N6), nylon 6.6 (N6.6) and polyester (P) fibres flex-fatigued under conditions shown in Table 19.4 [32].

Table 19.4 Flex fatigue tests at 65% r.h., 20 °C [34]

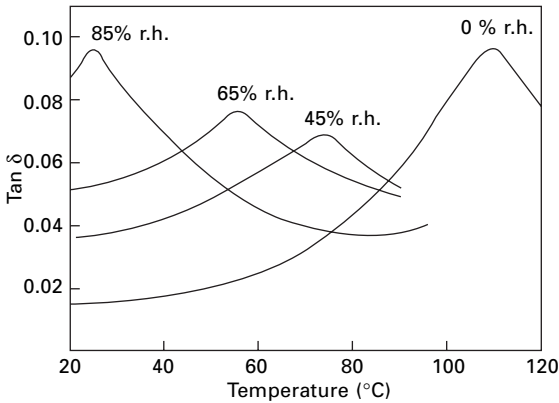
Fibre	Linear density (dtex)	Bending strain (%)	Specific stress (mN/tex)	Fatigue lifetimes in cycles		
				Mean	Median	Coefficient variance (%)
Nylon 6	22	16.1	54	35 825	34 725	32
Nylon 6.6	13.6	13.5	73	104 807	98 050	34
Polyester	13.3	12.4	75	194 616	187 825	44



19.32 Effect of temperature and humidity on median-flex fatigue life of nylon 6, with test conditions as in Table 19.4 [31].

cycles at 70% r.h., 60 °C. The peak lifetime positions are remarkably similar to the peaks in the loss modulus, as shown in [Chapter 18](#). The closest comparison in terms of temperature and humidity is with [Fig. 19.33](#), though this is for nylon 6.6, but the $\tan \delta$ peaks in nylon 6 are similarly located (see [Section 18.3.1](#)). Miraftab's flex fatigue results for nylon 6.6 show the same trends, but the curves are shallower, and the only sharp peak is at 60 °C and 70% r.h. For the polyester fibre, the peak lifetime at 5% and 30% r.h. occurs at about 65 °C. The absence of an effect of humidity is expected in this material, but the temperature is lower than for the peak in $\tan \delta$. At higher humidities, the plots of flex fatigue life against temperature are almost flat.

The reasons for the association between a high flex fatigue life and dynamic loss



19.33 Effect of temperature on $\tan \delta$ for nylon at various humidities. From Meredith [34].

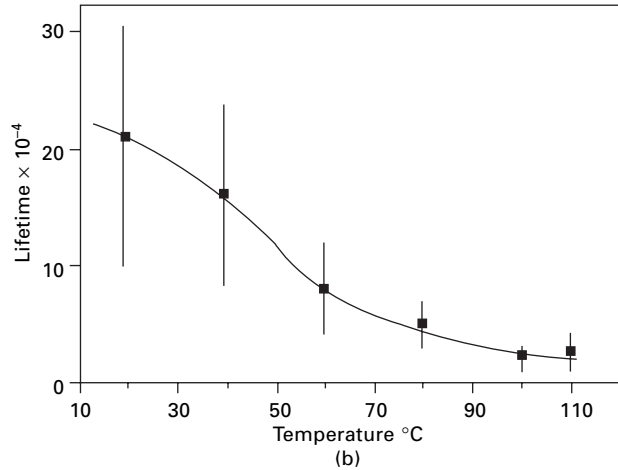
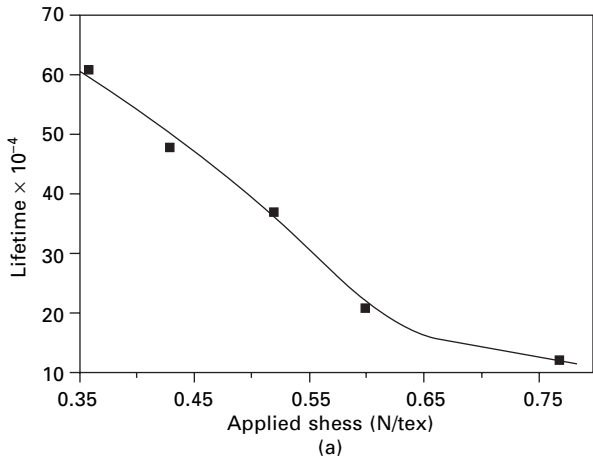
in deformation are not clear. Furthermore, the test is complicated by the fact that a number of properties of fibres are affected by temperature and humidity. In addition to the bulk mechanical properties, the fibre friction will change and so alter the stress pattern. Effects may be masked because one mode of breakdown takes over from another as the mode with the shortest life. Mirafteb [32] found that the dominant forms of failure were as follows: kink-bands, type (9) in Fig. 19.1, at lower humidities and temperatures; axial splits, type (10), at intermediate values; and surface wear, type (12), at higher values.

Sengonul and Wilding [35, 36] studied the flex fatigue of *Dyneema* gel-spun HMPE fibres. Figure 19.34 shows the fatigue life dependence on (a) tensile stress and (b) temperature. Failure is by multiple splitting.

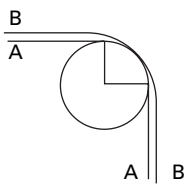
19.5.4 Mechanics of the flex test

A perfectly flexible fibre, with no resistance to bending, would follow the curvature of the pin surface and then run straight to the clamps, as shown in Fig. 19.35(a). If we ignore any deviations from this geometry, neglect the tension applied to the fibre, and assume that the material follows Hooke's law, there will be zero stress in the straight part, and the analysis given in Section 17.2.1 will apply to the bent part. On the central neutral plane, the stress and strain will be zero, but along the contact with the pin there will be a compressive strain $-e_b$ given by equation (19.1), and a corresponding specific stress $-Ee_b$, where E is the tensile modulus of the fibre, and at the opposite extremity there will be a tensile strain e_b and a stress Ee_b .

Most fibres, as discussed in Section 17.2.4, have non-linear stress-strain relations and yield more easily in compression. Consequently, the neutral plane moves out in order to balance the moments on either side (or minimise the deformation energy), the compressive strain is increased, and the tensile strain is reduced. On the basis of this model, it follows that if the fibre is not allowed to rotate, the material will oscillate between zero strain and a magnitude of tensile or compressive strain determined by the distance from the neutral plane. The compressive effect will be more damaging



19.34 Flex fatigue at 50 Hz of HMPE fibres at nominal bending strain of 4.95%: (a) effect of applied stress at 20 °C; (b) effect of temperature at 0.6 N/tex. From Sengonul and Wilding [36].



19.35 Comparison of fibre paths over a pin: A, perfectly flexible; B, real.

than the tensile in an oriented linear-polymer fibre, and thus the kink-band mode of failure can be expected. In wool and hair, the strain distribution, but not necessarily the damage, will be reversed because yield occurs more easily in tension.

In reality, the forms are not as simple as indicated above, and other stresses will also be present. Firstly, some tension is needed to hold the fibre in contact with the

pin. For the curved portion of the fibre, this superimposes a small tensile strain as a correction to the strains indicated above, and the plane of zero stress is displaced slightly inwards. However, it does mean that the straight part is under tension, and it may well be that an oscillation between compression and even a small tension will cause a greater disturbance of the fibre structure than one between compression and zero tension.

Secondly, there will be normal and frictional forces at the contact between the fibre and the pin. The most obvious effect of this is to add alternating shear stresses in the material close to the contact point, and these can promote surface-peeling and wear. However, a full analysis of contact stresses may show up other damaging features.

In well-designed experiments, these two effects can be regarded as minor corrections. The tensile stress is kept small, and, if necessary, the frictional effects can be reduced by allowing the pin to rotate. However, there is a third feature, which is more fundamental. The assumption that the fibre changes abruptly from curved to straight implies a discontinuity in bending moment, which cannot occur in practice. In reality, the length in contact with the pin is reduced and there is a zone of gradually reducing curvature, as shown in exaggerated form in Fig. 19.35(b).

Mirafatab [32] has shown that, for a fibre with flexural rigidity B , under a tension T , the contact length on the pin is reduced at either end by an amount l_0 where l_0^2 equals B/T . For the maximum curvature to be determined by the pin radius, the applied tension must be large enough to make less than the nominal contact length for a perfectly flexible fibre. Away from the ends of the contact region, the curvature is given by:

$$c = c_0 e^{-l/l_0} \quad (19.2)$$

where l is the distance from the pin contact and c_0 is the curvature of the pin surface, equal to the reciprocal of the pin radius.

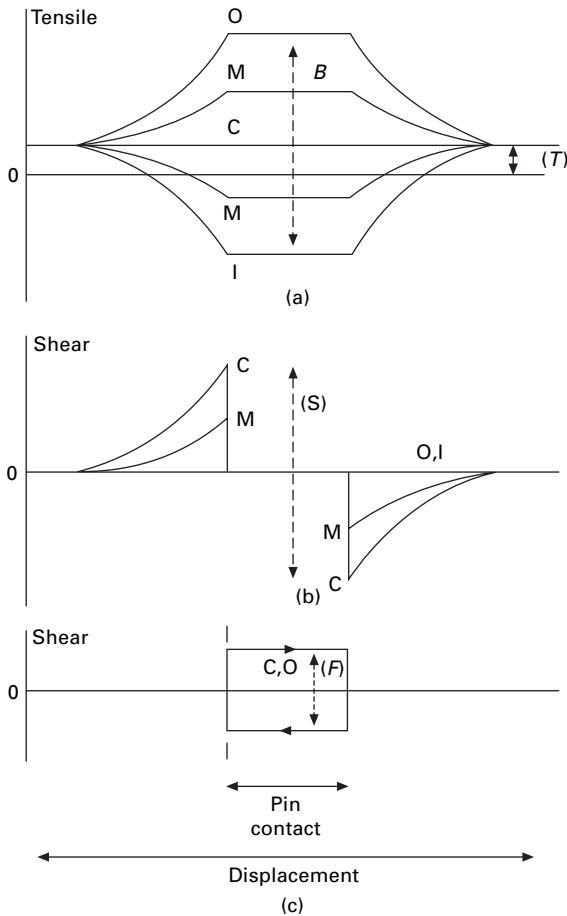
Standard textbooks on strength of materials, such as that by den Hartog [37], show that the change in bending moment in variable curvature is balanced by a shear force, S given by:

$$S = B \frac{dc}{dl} = -B \left(\frac{c_0}{l_0} \right) e^{-l/l_0} \quad (19.3)$$

The standard theory also shows that, for a Hookean material, the shear stress in a fibre of radius r is a maximum, equal to $(4S/3\pi r^2)$ at the centre plane of the fibre and reduces in proportion to $[1 - (y^2/r^2)]^{1/2}$ with the distance y from the central plane.

For the fibre over the pin, the highest shear stress will occur on the centre plane at the point at which the fibre leaves the pin and will be given by $-[4(B/T)^{1/2} c_0/3\pi r^2]$. The shear stresses will decrease with the distance from the centre plane and with the distance from the pin contact. However, it is these shear stresses that can cause the fibre to fail by splitting.

A qualitative summary of the stress pattern is presented in Fig. 19.36, which is at least a second approximation to reality, because there will be other complications arising from localised stresses and from the non-linear and inelastic properties of fibres. The lines in the diagram show how the major contributions to the stress at the

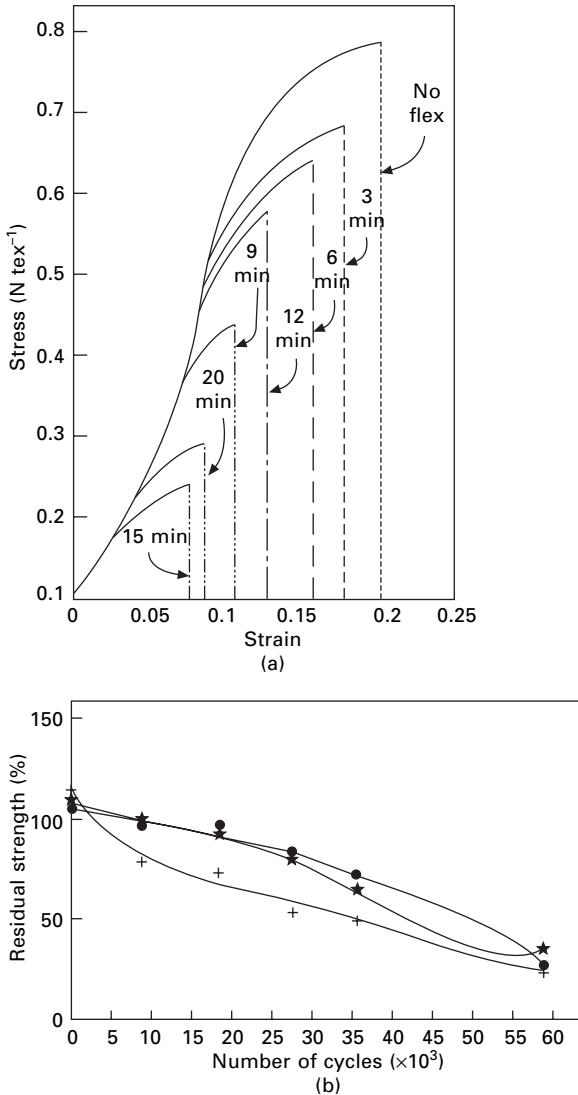


19.36 Main stresses in a flex fatigue test: C, on centre plane; I, on inner surface in contact with pin; O, on outer surface; M, intermediate positions. (a) Tensile stress due to bending (B) plus the constant tensile stress (T): note that zero-stress line will move out for a fibre that yields easily in compression. (b) Shear stress (S) due to change of curvature: there will be a shift associated with displacement of the neutral plane. (c) Frictional shear stress (F), alternating in direction as the fibre moves in opposite directions.

centre plane and extremities of the fibres vary along the fibre. Under normal test conditions, the axial displacement of the fibre by the drive mechanism will be much longer than the nominal contact length over the pin and so will be longer than the length over which the stresses are varying appreciably. Consequently, the material will move backwards and forwards through the stress field, given by summation of the components shown in Fig. 19.36, as the fibre is cycled.

19.5.5 Reduction in tensile strength after flex cycling

Hearle and Miraftab [33] report the loss of tensile strength due to flex fatigue. [Figure 19.37\(a\)](#) shows that change in the stress–strain curves of nylon 6.6 fibres after various



19.37 Tensile testing of fibres after flex fatigue cycling at 50 Hz, so 10 mins = 30 000 cycles: (a) stress–strain curves of nylon 6.6 fibres; (b) residual strength; * nylon 6.6, 6 ● nylon polyester [33].

times of flex cycling. The initial part of the stress–strain curve is unchanged, but only a fraction of the tensile test covered the part of the fibre that was subject to flexing over the pin. However, this zone provides a substantial yield section before breakage. Nylon 8 has a similar behaviour, but polyester follow an unchanged curve up to the reduced break point, except for the fibre fatigued for the longest time. Figure 19.37(b) shows that the rate of loss of strength is similar for all three fibre types. The nylon fibres typically show two V-notch breaks separated by a central split. Polyester fibres showed more multiple splitting.

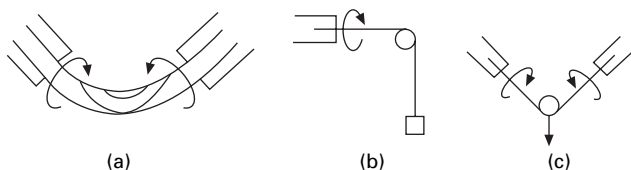
19.6 Combined bending and twisting: biaxial rotation

19.6.1 Test methods

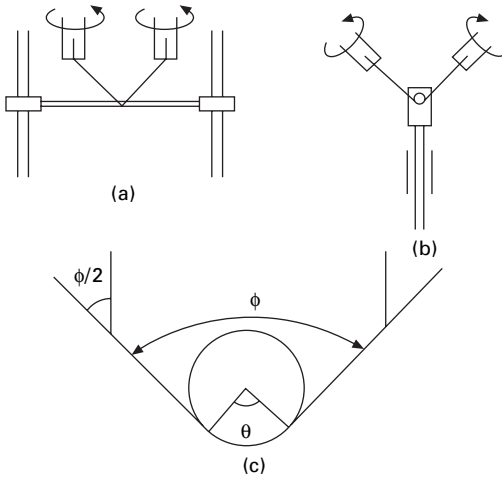
For coarse monofilaments, Lyons [38] introduced a method of studying bending fatigue by biaxial rotation, as illustrated in Fig. 19.38(a). However, this method, which was also used by Hearle and Vaughn [39] is not convenient for textile fibres because it would be necessary to miniaturise the rotating and clamping arrangements in order to achieve a high enough curvature and to control fine fibres. Nevertheless, the mode of failure by multiple splitting is very similar to that found in many examples of wear in use, so it was desirable to find a way of adapting it for testing fibres. The solution is to concentrate the curvature by passing the fibre over a pin under a small tension, as shown in Fig. 19.38(b) and (c). Surface wear, as a result of rubbing on the pin, has not proved to be a problem, except in fibres such as wool and *Kevlar*, which are highly susceptible to this form of damage. The friction will impose a drag and generate torque and twist in opposite senses in the portions of fibre on either side of the pin. Even in the tests on monofilaments without a pin, the splits followed helical lines in opposite senses in each half of the test length, which indicated false twist about the centre point, as shown in Fig. 19.38(a). As explained below, this is due to hysteresis ('internal friction'), and means that, in addition to the cyclic bending as the fibre is rotated, torque also promotes failure.

In the first version of rotation over a pin [26, 40], indicated in Fig. 19.38(b), the fibre rotation was driven from one end, with a weight hanging from the other end. Although this method gave interesting results, some of which will be quoted later, the fibre was not well controlled, and there were unwanted inertial forces from the rotation of the weight. Consequently, a change was made to driving from both ends, as shown in Fig. 19.38(c). Various different instrument designs were tried [41–44] with different drive methods to the fibre ends and different methods of applying tension to the fibre. The best method of tensioning consists of mounting the pin on a holder that is free to slide up or down a guide. The mechanical design is simplified if the drive shafts can be parallel, and the form used in one multi-station tester designed by Clark [44], which proved satisfactory for fairly coarse textile fibres, is shown in Fig. 19.39(a).

In later work [45], it was found that this apparatus was unsuitable for finer fibres. The first problem was purely mechanical. The frame holding the pin was too heavy, and, if it was made lighter, it tended to stick on the two guide bars. This problem was cured by having the pin mounted on a rod sliding in a tube, as shown in Fig. 19.39(b).



19.38 Forms of fibre biaxial rotation: (a) without a pin; (b) over a pin, driven from one end; (c) over a pin driven from both ends.

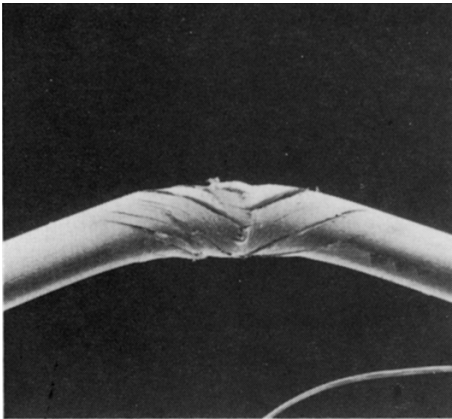


19.39 Arrangements in multi-station testers: (a) first type, with pin mounted on a beam sliding on two shafts; (b) second type, with pin mounted on holder sliding through single collar; (c) test angle, ϕ and wrap angle θ .

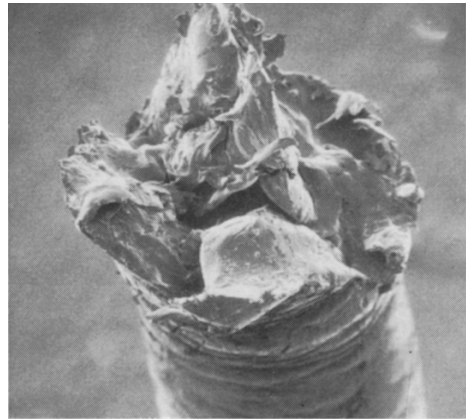
The other problem involved the mode of fibre failure and depended on the test angle, ϕ , as defined in Fig. 19.39(c). The fibre is bent through an angle $\phi/2$ where it is clamped to the drive shaft. If ϕ is too large, jaw breaks, which are not determined by conditions at the pin, can result. If ϕ is too small, the angle of wrap, $\theta = (\pi - \phi)$, round the pin becomes large. Under these conditions, it was found that anomalous failures, called 'direct breaks', could occur after a small number of cycles and before the false twist had fully developed [46]. Direct breaks appear to be associated with an irregular motion of the fibre as it rolls and slips over the pin before reaching a steady motion, with the torque fully developed and overcoming the external and internal friction. Direct breaks show evidence of the fibre softening and melting, with localised deorientation, contraction to form bulges, and the formation of voids seen in the broken fibres. The detail of how this happens is not understood. For the coarser fibres being studied by Clark and Hearle [43], it was possible to find suitable intermediate values of ϕ that avoided both direct and jaw breaks. However, this was not possible in the later work of Liolios [45] on finer fibres, and a new multi-station apparatus was made with the drives aligned, as in Fig. 19.39(b), so that there was no bend where the fibres were clamped, and jaw breaks were eliminated. With $\phi = 90^\circ$, the occurrence of direct breaks was negligible.

19.6.2 The form of failure

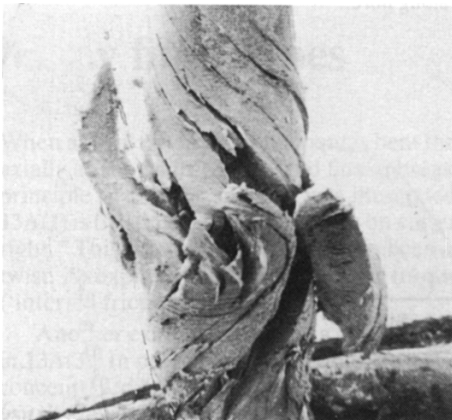
In biaxial rotation without a pin, two zones of splits, which twist in opposite direction, join in a more intense damage zone, which eventually ruptures (Fig. 19.40(a-c)). In fairly thick textile fibre, the two regions with helical splits are separated by an undamaged zone, which covers most of the length in contact with the pin (Fig. 19.40(d)). Rupture occurs at one of the positions at the end of splits. In finer fibres,



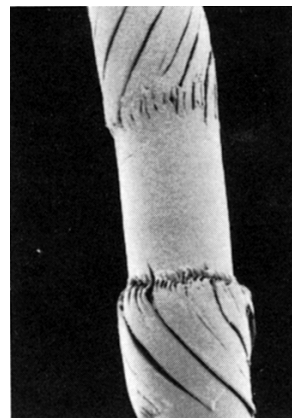
(a) 100 μm



(b) 50 μm



(c) 100 μm



(d)



(e)



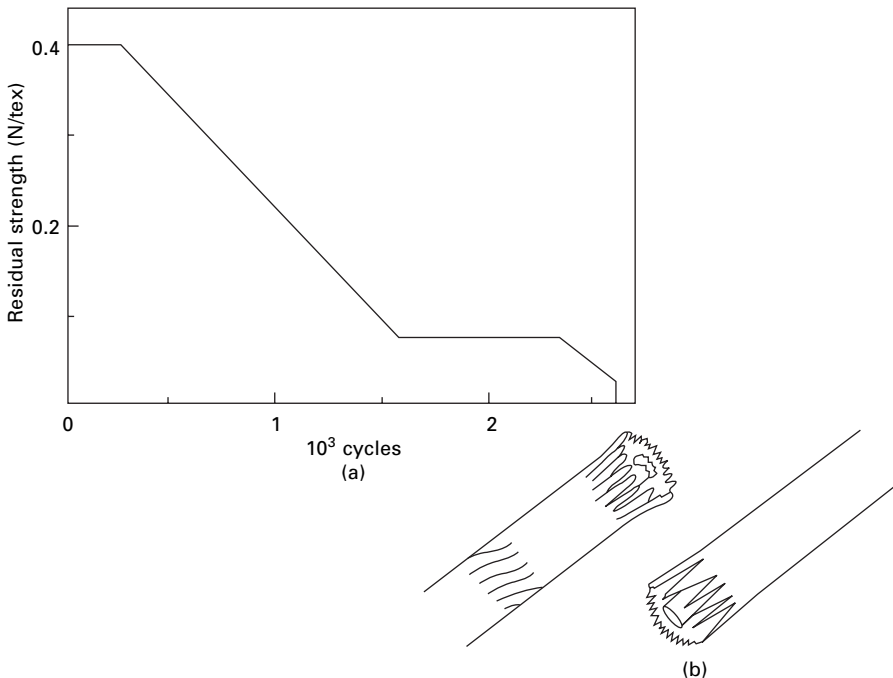
(f)

19.40 (a) Nylon monofil, 67 tex, in biaxial rotation without a pin. (b) Severe damage zone. (c) Break of the monofil. (d) Polyester fibre, 4.2 tex, after 1503 cycles in biaxial rotation over a pin. (e, f) Opposite ends of break at 2606 cycles.

the helical splits join and there is no undamaged zone [1]. In most fibres, there would be at least ten separate split portions in the final break, giving a brush-like end, but nylon gives fewer and larger pieces. This form of break by multiple splitting is also common in fibres after wear in use, though there can be confusion with splitting due to simple flex cycling or other causes [1].

The sequence of damage and loss of strength in fibres, rotated at 15 Hz over a 0.254 mm diameter stainless steel pin in water at 20 °C, has been described by Calil *et al.* [47]. For an 8.4 dtex polyester fibre, which gives a bending strain of 11%, there is no loss of strength up to about 2000 cycles, and the only visible damage consists of some kink-bands and some surface abrasion. There is then a linear loss of strength with number of cycles, accompanied by progressively increasing splitting, up to failure at about 4000 cycles. The helical splits cover the whole length of bent fibre.

In a thicker polyester fibre, of 42 dtex, with a bending strain of 20%, there were two regions of strength loss, in which the visible damage increased, preceded by two initiation regions (Fig. 19.41(a)). The final break divided into separate zones, both along and across the fibre (Fig. 19.41(b)). The axial separation is associated with the more severe stresses at the points at which the fibre leaves the pin, as discussed below. The transverse separation is due to the neutral plane moving out as indicated in Fig. 19.36. On rotation, this will cause an outer zone to suffer a damaging alternation of tension and compression, which causes splitting in the first period of strength loss. The inner zone will always be in compression in the early stages of the test and does



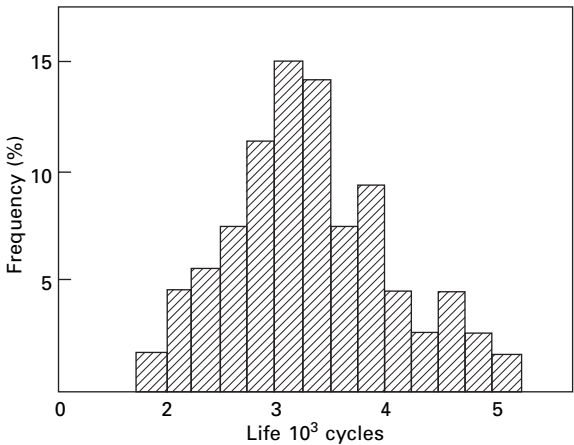
19.41 (a) Variation in retained strength for a 42 dtex polyester fibre subject to biaxial rotation in water at 20% bending strain. (b) The appearance of a fibre broken after 2600 cycles [47].

not start to break up until the outer zone is unable to resist stress and a further initiation of damage has occurred.

19.6.3 Statistics of fatigue failure

Figure 19.42 shows a histogram of the fatigue lifetimes from ten tests on each of ten stations for 17 dtex polyester fibres under typical test conditions in a laboratory atmosphere [48]. It should be noted that the biaxial rotation test operates on a very short length of fibre in contact with the pin (about eight fibre diameters for a 90° wrap at 10% strain). There was no significant difference in the results from different positions on the multi-station tester. The total range from 1878 to 9480 cycles is acceptably low for fatigue testing. The distribution is slightly skewed. The histogram for 17 dtex nylon had a similar shape, and the statistical parameters for both fibres are given in Table 19.5.

In these results reported by Clark and Hearle [48] and in earlier studies by Calil and Hearle [41] and Hearle and Wong [49], it was found that the statistics gave a reasonable fit to a Weibull distribution, as might be expected for an extreme value situation. However, from a practical viewpoint, the agreement was almost as good with a normal distribution of log(cycles to break).



19.42 Distribution of fatigue lifetimes for 17 dtex polyester fibre rotated at 2.5 Hz, with a bending strain of 10% and a tension of 58 mN/tex (0.65 gf/den), at 20 °C, 65% r.h. [48].

Table 19.5 Statistics of fatigue failure [50] (test conditions as for Fig. 19.42)

	17 dtx polyester fibre	17 dtex nylon
Number of tests	100	100
Mean cycles to break	3352	5507
Median	3293	5282
Standard deviation	736	1320
Coefficient of variation (%)	22	24

In order to investigate statistical features, at least 100 tests are needed, but, for comparative testing, about 20 tests are adequate. A survival diagram is the best way to present the results, and the most useful parameters to quote are often the median fatigue life and the coefficient of variation.

19.6.4 Effect of mechanical parameters on fatigue life

There are several geometrical and mechanical parameters that affect biaxial rotation fatigue life. The state of the pin surface is usually not critical, unless it is highly abrasive or the fibre is of a type highly prone to surface wear. Figure 19.43 shows the influence of angle of wrap, as reported for 42 dtex polyester fibre by Clark and Hearle [43]. It can be seen that there is a very sharp change from the short lifetimes ending in direct breaks at high wrap angles to the longer times for fatigue breaks. Provided that the direct break region is avoided, and the jaw break region is not entered, the angle of wrap has only a small effect on fatigue life. As discussed in Section 19.6.1, smaller wrap angles must be used to eliminate direct breaks in finer fibres, and the design of equipment must then be changed to prevent jaw breaks.

The two most important normalised controlling parameters are the bending strain, given in terms of fibre diameter and pin diameter by equation (19.1), and the specific stress in the fibre. The latter is controlled by fibre tension, which, for the preferred form of apparatus shown in Fig. 19.39 is given by:

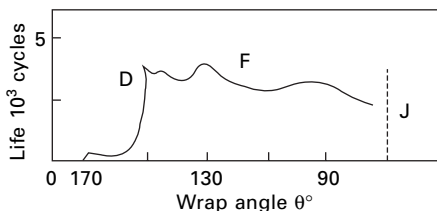
$$T = \frac{1}{2} W \sec (\phi/2) \quad (19.4)$$

where W is the total weight of the pin holder.

The effects of these two parameters are demonstrated in Table 19.6. As would be expected, the fatigue life decreases as the intensity of bending is increased and as the tension in the fibre is increased. Note that, in the second set of results, the specific stress on the fibre is decreasing, so that the effect of bending is under-estimated.

19.6.5 Environmental influences

It is easy to study the effect of different environments in biaxial rotation fatigue by immersing the fibre over the pin in liquid in a trough or by enclosing the whole



19.43 Change of mean fatigue life with wrap angle, $\theta (= \pi - \phi)$, for 42 dtex polyester fibre rotated at 5.3 Hz with bending strain of 14% and tension of 86 mN in air regions are: (D) direct breaks, (F) fatigue breaks and (J) jaw breaks [43].

*Table 19.6 Effect of bending strain and fibre tension on biaxial rotation fatigue
17 dtex nylon 6.6 rotated from one end with hanging weight [50]*

Bending strain (%)	Median life in thousand cycles							
	In air				In water			
	Fibre tension (mN)							
	58	83	96	121	*58	83	96	121*
14	31	20	9.2	5.1	14	7.3	5.0	3.0
22	8.8	4.7	3.4	1.6	2.4	1.1	1.0	–
28	4.4	2.2	1.3	–	1.7	0.8	0.7	–

*not corrected for buoyancy

Polyester fibre rotated from both ends in air over same pin at 41 mN [43]

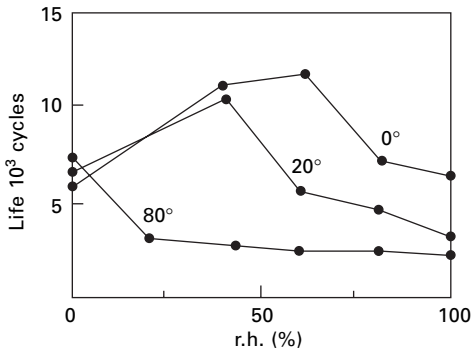
Linear density (dtex)	Bending strain (%)	Mean life (thousand cycles)
8	10	9.0
17	14	5.5
27	17	3.0
42	20	2.2

8 dtex Polyester fibre rotated from both ends in water at 10% strain [43]

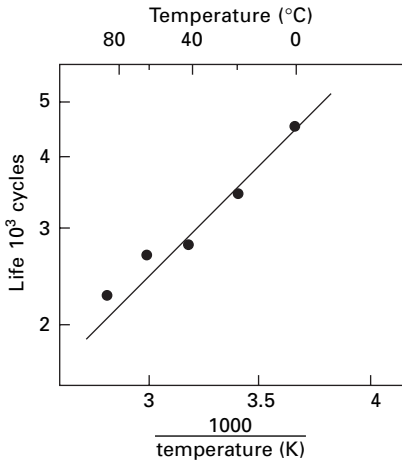
Fibre tension (mN)	Mean life (thousand cycles)
6	27
20	12
30	10
41	7.8
70	4.0

apparatus in an environmental chamber for gaseous environments. The reduction in the fatigue life of nylon in water compared with air under standard conditions has been shown in Table 19.6. The effect of buoyancy means that the tension is lower in water, so that the effect of the change of environment is slightly reduced. The effect of temperature in the same series of experiments was to reduce the median fatigue life of 17 dtex nylon 6.6, tested in water at 14.5% strain and 108 mN tension, from 4207 cycles at 20 °C to 2356 cycles at 66 °C [50].

A more extensive study of the effects of temperature has been reported by Clark and Hearle [51]. The results for nylon 6 are shown in Fig. 19.44. The trend follows the trend in dynamic loss, $\tan \delta$, with the position of the maximum fatigue life increasing in humidity as the temperature is reduced. For polyester fibre, there is little effect of humidity, but, subject to some scatter in the results, the maximum fatigue life appears to decrease as the temperature increases from 0 to 80 °C. There is a linear relation between $\log(\text{fatigue life})$ and reciprocal of absolute temperature, as shown in Fig. 19.45. In water, the fatigue lives of both nylon 6 and polyester fibre decreased with increasing temperature. In polyester fibre, the magnitude of the effect was similar to that in air, but in nylon 6 the effect was greater than that for air at 100% r.h.



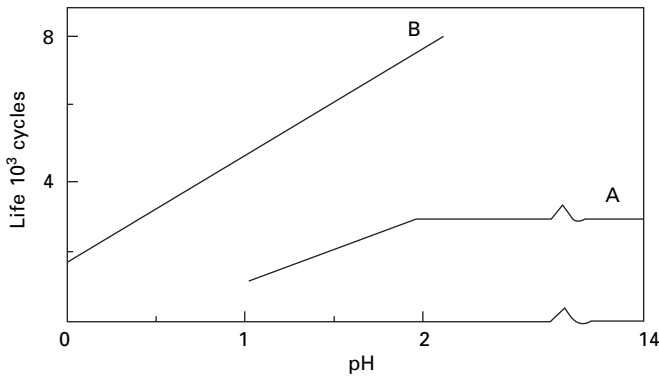
19.44 Variation of mean fatigue life with humidity at 0, 20 and 60°C for 17 dtex nylon 6 rotated at 2.5 Hz with a bending strain of 10%, a tension of 100 mN, and a wrap angle of 90°; the plots for 40 and 80°C are close to those for 60°C [51].



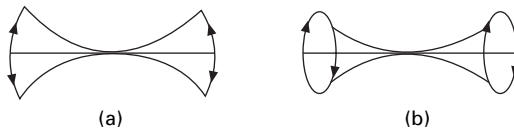
19.45 Relation between mean fatigue life on a logarithmic scale and reciprocal of absolute temperature for 17 dtex polyester fibre, tested under same conditions as for Fig. 19.44 [51].

The effect of changing pH on the biaxial-rotation fatigue of nylon 6.6 is shown in Fig. 19.46 [50]. From alkaline conditions in sodium hydroxide solution down through increasing concentrations of hydrochloric acid, there is no change in life until pH 2 is reached, but there is then a rapid linear decrease. The reduction in fatigue life is proportionately much greater than the reduction in tensile strength.

Clark [52] found that atmospheres of hydrogen, carbon monoxide and methane gave no difference from air in the fatigue life of nylon 6, but small amounts of nitrous oxide (N_2O) or sulphur dioxide (SO_2) caused an appreciable reduction in the fatigue lives of both nylon 6 and polyester fibre. Nitrogen dioxide (NO_2) reduced the fatigue life of nylon 6 to zero cycles but did not have as severe an effect on polyester fibres.



19.46 Effect of pH on median fatigue life for 17 dtex nylon 6.6 rotated from one end over a 273 μm diameter wire: A, with weight of 12 gf; B, with weight of 2 gf [50].



19.47 Cyclic bending: (a) in a plane; (b) by rotation.

19.6.6 Effects in different fibres

Unfortunately, there is not a good set of comparative data for the biaxial rotation fatigue lives of different types of fibre, though similar multiple splitting failures have been found in most general textile fibres. The study of failures in use would suggest that rayon may be an exception [1]. Hearle and Wong [50] report that, in order to obtain broadly similar fatigue lives, in the range from 300 to 8000 cycles, polypropylene fibre will stand more severe conditions than nylon, which in turn is slightly more resistant than polyester fibre, as also shown by the results in Table 19.5. However, as shown above, the results are highly dependent on temperature and humidity.

In natural fibres, comparative results are difficult to obtain because of the variability of fibre diameter. However, observations from experiments on cotton [42] and wool and hair [53] have been reported.

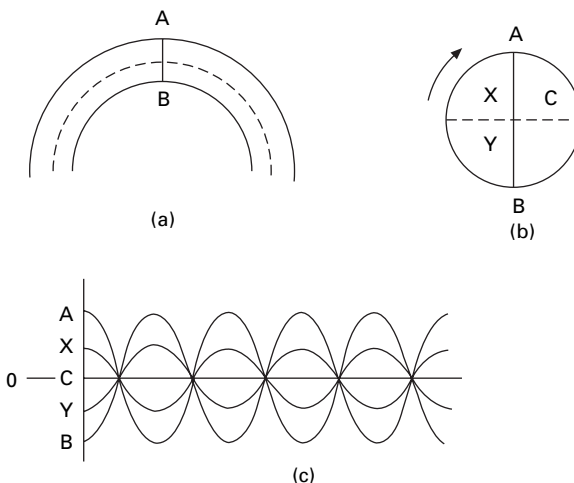
19.6.7 Mechanics of biaxial rotation

The initial rationale for the biaxial rotation test was that it was a means of applying cyclic bending to a fibre, not from straight to bent as in the flex fatigue test described in Section 19.5, but from bent in one direction to bent in the opposite direction. However, this is not done by flexing backwards and forwards in a plane as in Fig. 19.47(a). Instead, the same extreme positions are reached by rotating the fibre, as in Fig. 19.47(b).

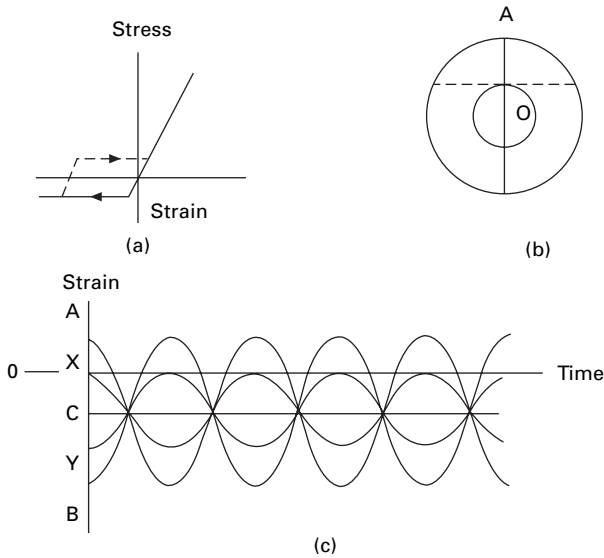
In order to understand the mechanics of the test, which is more complex than first appears, we start by considering the simpler situation without a pin, in which a length of fibre is bent into constant curvature, as in Fig. 19.48(a), and then rotated. For a material following Hooke's Law, there will be a central neutral plane, which rotates as indicated in Fig. 19.48(b): the strain variation over the fibre would then be as shown in Fig. 19.48(c), with a phase difference related to the position around the fibre cross-section. If, as is common, the fibre yields more easily in compression, with a stress-strain relation like that in Fig. 19.49(a), the neutral plane will move out, as indicated in Fig. 19.49(b), and during rotation will define a cylinder, within which the material is always in compression. The strain variation with time and position is shown in Fig. 19.49(b). The stresses during the first bending are indicated in Fig. 19.49(a), but the situation for stress, strain and the position of the neutral plane will evolve in successive cycles as the material follows the indicated hysteresis loop.

In the exceptional case of wool and hair fibres, which yield more easily in tension, the above argument will be reversed. The neutral plane will move in the opposite direction, and most of the fibre will be in tension. Effectively, the horizontal axis in Fig. 19.48(b) will be moved downwards instead of upwards.

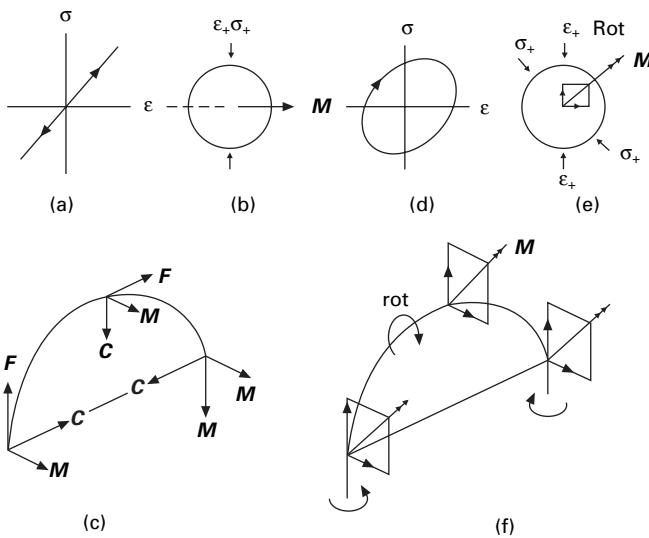
For a perfectly elastic fibre, as in Fig. 19.50(a), the bending moment will be the only force present. As indicated in Fig. 19.50(b), the maximum stresses coincide with the maximum strains at the top and bottom of the fibre, and they act normal to the plane of the paper in opposite directions on the tension and compression sides. Consequently, the bending moment vector, M , acts in the direction shown. On rotation of the fibre, M remains fixed in space, but it changes direction relative to the material. The situation is the same at all positions along a uniformly curved fibre, as indicated in Fig. 19.50(c), in which three mutually perpendicular vectors represent the fibre



19.48 (a) Linear elastic fibre deformation in uniform curvature, showing neutral plane dotted. (b) Cross-section, showing the line AOB from maximum tension to maximum compression, which rotates during the test. (c) Strain variation with time and position in the fibre.



19.49 (a) Idealised stress–strain relation with yielding in compression: the hysteresis recovery path is shown dotted. (b) Fibre cross-section showing displacement of neutral plane. (c) Strain variation in the fibre.



19.50 (a) Elastic stress–strain relation. (b) Fibre cross-section showing positions of maximum stress and strain and bending moment vector. (c) Changing directions of fibre direction F , curvature direction C , and constant direction of bending moment M . (d) Stress–strain relation with hysteresis. (e) Fibre cross-section with stress leading strain and changed direction of bending moment vector. (f) Translation of the bending-moment vector from the centre of the fibre to the ends.

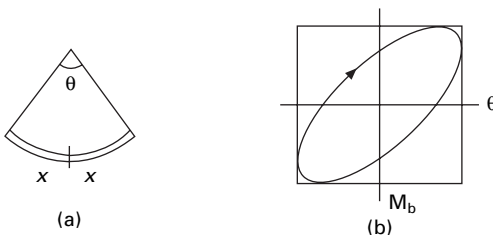
direction F , the direction to the centre of curvature C , and the bending moment M , which is always in the same direction perpendicular to the plane of the fibre.

However, if there is hysteresis, as shown in the simplest possible form in Fig. 19.50(d), energy is dissipated in each cycle. The work needed can be supplied only through the drive shafts, which must therefore apply torque to the fibre in opposite senses at either end. At the centre point, there will be zero torque, but this will increase with distance from the centre as energy has to be supplied to increasing lengths of material. The torques will cause the fibre to be false-twisted about the centre point, just as if there were an external frictional drag.

The situation, in terms of forces and moments, is explained by noting that when there is hysteresis, stress and strain are not in phase. Consequently, the position of maximum stress will lead the position of maximum strain, and the bending moment vector will change direction, as shown in Fig. 19.50(e). Considering effects along the fibre, as shown in Fig. 19.50(f), it can be seen that a component of the bending moment vector, which is in the vertical direction in the cross-sectional plane at the centre point, must be balanced by an axial component at the ends, which is the direction of a torque vector. However, Fig. 19.50(f) is oversimplified, except at the centre point, because the moment vector will really have components in all three directions, owing to the combination of in-phase and out-of-phase bending moments and increasing torque.

The energy argument is not only simpler in qualitative terms; it is also the best basis for quantitative estimates of the magnitude of the torque. An approximate analysis has been made by Calil *et al.* [54] and a more precise treatment by Waterman [55]. In the approximate treatment, we consider a length of fibre, $2x$, bent in uniform curvature through an angle θ , as in Fig. 19.51(a). If the fibre were bent backwards and forwards in a plane between $+\theta$ and $-\theta$ through $\theta = 0$, in the manner of Fig. 19.47(a), the relation between bending moment and bending angle could be represented as in Fig. 19.51(b). The energy loss per cycle would be $M_b d\theta$, and we can assume that it will be similar in value when the bending cycle is caused by rotation, as in Fig. 19.47(b). At each end, there is an energy input per cycle of $2\pi M_t$ from the drive torque, M_t . The sum of the two inputs must equal the energy loss. A generalised form of the equation for different lengths and variable bending would have the form:

$$2 \times 2\pi M_t = \int_{-x}^x \oint M_b d\theta dx \quad (19.5)$$



19.51 (a) Fibre bent through an angle θ . (b) Hysteresis loop between bending moment and bending angle.

The torque must increase from zero at the centre point to a maximum value at the ends. For constant curvature through a total angle θ , the value is given by:

$$M_t = (1/4\pi) \oint M_b d\theta \quad (19.6)$$

If f is the ratio of the area of the ellipse in Fig. 19.50(b) to the area of the circumscribing rectangle, ranging from zero for a perfectly elastic material to $\pi/4$ for a completely lossy viscous material, Calil *et al.* [54] derived the following equation by the use of the standard bending theory given in Section 17.2.1:

$$M = \frac{\eta f E c^2 \theta}{4\pi^2 \rho R} = \frac{\eta f E c^2 x}{2\pi \rho R^2} \quad (19.7)$$

where η is the shape factor (1 for a circle), E is the specific modulus, c is the linear density, ρ is the density and R is the radius of curvature.

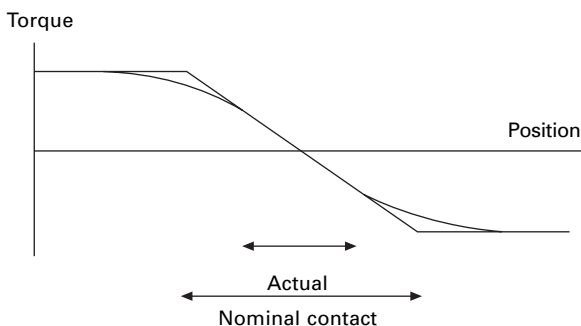
The form of stress-strain relation given above would be applicable to a linear viscoelastic material. The reality, with the more complicated non-linearity of yielding, will be somewhat different but will be similar in principle.

For rotation over a pin, the friction between the fibre and the solid surface will also contribute a torsional drag. The total torque M will be given by:

$$M = M_t + \frac{1}{2} Fr \quad (19.8)$$

where M_t is given by equation (19.7), F is the total frictional force over the whole length on both sides of the centre point and r is the fibre radius.

The variation in torque along the test length is indicated in Fig. 19.52. By putting in what seemed to be reasonable values of the various parameters, Calil *et al.* estimated that the torque due to hysteresis ('internal friction') would be at least ten times as large as the torque due to surface friction. For a 42 dtex polyester fibre with a wrap angle of 90° , the torque was estimated to be in excess of $1 \mu\text{N m}$, which would produce in excess of 1 turn/mm. This is in reasonable agreement with the angles of the helical splits found in fatigue failures by biaxial rotation. Clearly, the torque contributes in an important way to the failure of the fibres, which will have been weakened by the tension/compression action in cyclic bending.



19.52 Variation of torque along the fibre in biaxial rotation test: the line with a sharp discontinuity is for the fibre path A in Figure 19.35; the smooth curve is for an actual path like B.

The increase in torque with wrap angle is probably a cause of the change from fatigue breaks to direct breaks, described in Section 19.6.

For rotation over a pin, there will also be the complications of variable curvature, which were discussed in 19.5, since the fibre will follow the path illustrated in Fig. 19.35(b). The stresses due to bending, tension and shear will be the same as in Fig. 19.36, but the frictional force will be acting circumferentially instead of axially; and the stresses will rotate within the fibre, instead of moving along the fibre. In addition, there will be the torque shown in Fig. 19.52.

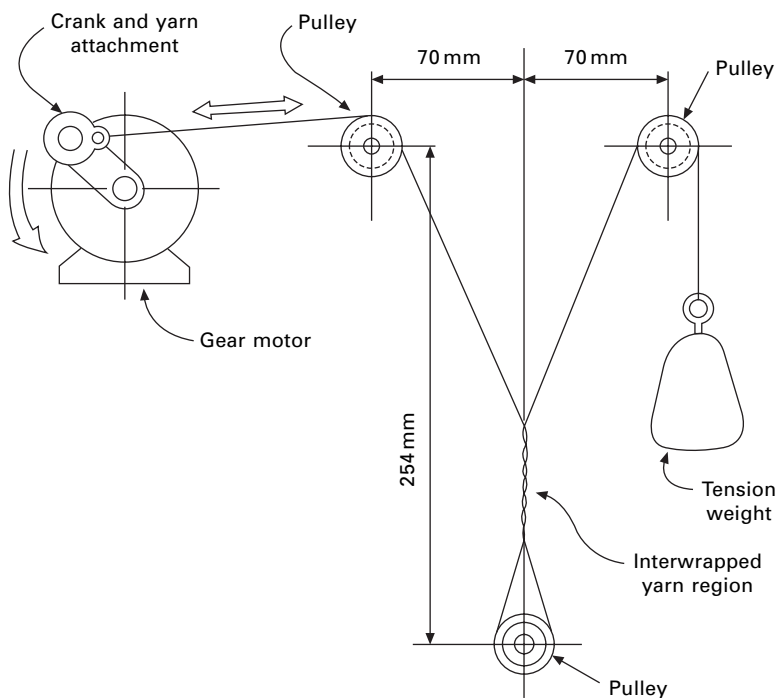
The most highly stressed part of the fibre will be where it leaves the pin because at that point the bending stresses have not reduced, the shear stresses have abruptly appeared, and the torque has reached its maximum value. As in the flex test, the normal and frictional contact stresses may also influence fibre failure, particularly in fibres that are prone to surface wear.

19.7 Surface wear and peeling

Another mode of fibre failure, which has been found to occur often in use [1], consists of splitting and peeling of fibre surfaces when they are subject to abrasion. The observed forms vary in appearance, but they are grouped in one poorly defined class, type 13 in Fig. 19.1. Unfortunately, there is little information in the literature on the experimental or theoretical fibre physics of these effects. Recent papers on yarn-on-yarn abrasion [56–58] using the apparatus shown in Fig. 19.53 give some comparative information and show that in wet conditions nylon does not last as long as polyester fibres. The nature of the fibre finish is major determining factor. But the method is complicated by the yarn structural effects. As mentioned in Section 19.5.2, the flex fatigue test, in which a fibre is pulled backwards and forwards over a pin, can lead to failure by surface wear.

In order to avoid the effects of repeated flexing, another method that has been tried is wear of fibres held under tension over a rotating pin. The commonest form of wear is a progressive peeling of the surface (Fig. 19.54(a,b)). This is eventually leads to break over a reduced cross-section (Fig. 19.54(c)). Alternatively, the break may from a long taper (Fig. 19.54(d)).

This form of failure clearly results from the contact forces. In external application, these consist of a normal load, acting at right angles to the surface, and a frictional force, acting tangentially in opposition to the relative motion. The direct effects of these forces will be a transverse compressive stress and an axial shear stress within the fibre near the surface, as shown in Fig. 19.55(a). This can lead to formation of a crack developing from the surface (Fig. 19.55(b)). However, the internal stress distribution resulting from contact stresses can become much more complicated, especially when there is hysteresis [59]. High subsurface shear stresses can be present and cause internal cracks (Fig. 19.55(c)). These cracks lead to peeling of slivers from the surface and a reduction of the cross-section until a tensile break occurs. Alternatively the shear stresses may lead to angled cracks crossing the fibre (Fig. 19.55(e)), to give a tapered end. In *Kevlar*, surface wear eventually led to a break with multiple splitting [1].



19.53 Yarn-on-yarn abrasion tester.

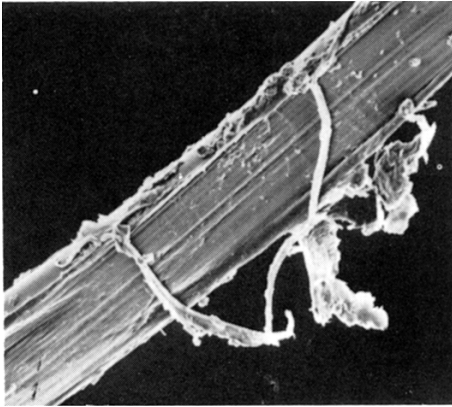
19.8 Abrasion and wear

Other information on the failure of fibres can be obtained from studies of yarn and fabric wear. Fibres in use are subject to a variety of different forces, which are repeated many times until finally the fibres wear out. The abrasive wear of materials depends to a considerable extent on the construction of the yarn or fabric, and no way has been found to eliminate the influence of these factors and calculate a basic fibre property, if indeed this exists at all. Wear resistance is more likely to be a complex of several properties, whose relative influence is different in different uses.

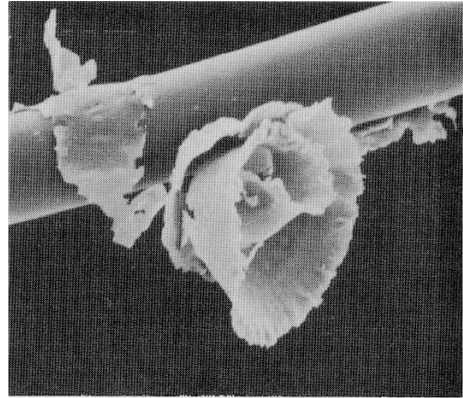
It is, however, true that simple tensile tests of fibre properties do not give an exact indication of resistance to wear. On the other hand, there is general qualitative agreement between the results of various types of abrasion test and of tests of wear in actual use. It is therefore not completely unreasonable, in the absence of further knowledge, to consider abrasion resistance as a fibre property.

Table 19.7 gives some results obtained in practice, reduced so as to give nylon the value 100 in all tests. These tests were carried out as follows:

- A Taber Abrader, in which rubber-emery wheels are rubbed over a yarn sheet. The figure gives the relative number of cycles for 60 loss in strength (Hamburger [60]).
- B As A (Hicks and Scroggie [61]).
- C As A, on fabric (Hicks and Scroggie [61]).
- D Laboratory wear test (Schiefer *et al.* [62]).
- E Yarn-on-yarn abrasion (du Pont [63]).

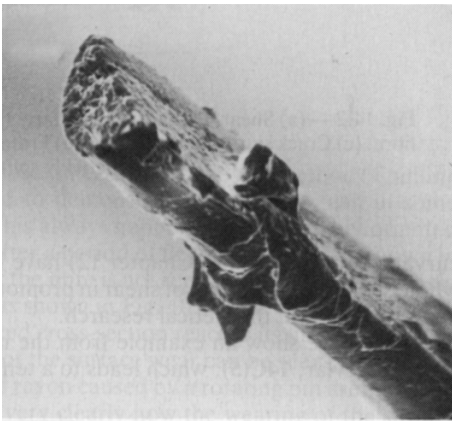


(a)

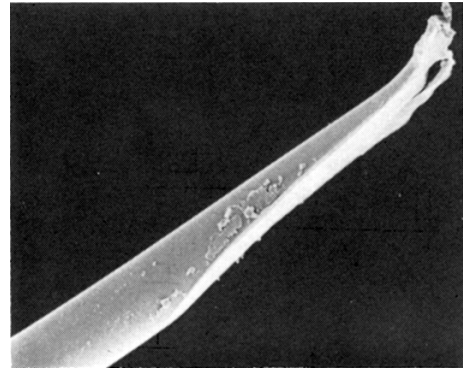


(b)

20 μm



(c)



(d)

19.54 Wear of fibres over rotating pin: (a) nylon; (b) polyester; (c) wool, (d) nylon.

F Walker Abrader, in which yarn is twisted round a guide, and then round itself—mainly yarn-on-yarn abrasion. Relative number of cycles to break. Staple-fibre yarns (Abrams and Whitten [64]).

G As F – continuous-filament yarns (Abrams and Whitten [64]).

H Stoll flex and abrasion test. Yarn folded and rubbed over a bar. Staple-fibre yarns (same as in F) (Susich [65]).

I As H – continuous-filament yarns (same as in G) (Susich [65]).

J As H – wet fabric (Dennison and Leach [66]).

K Flexing test. Cycles to break (Thomson and Traill [67]).

L Flex cycles to failure (du Pont [63]).

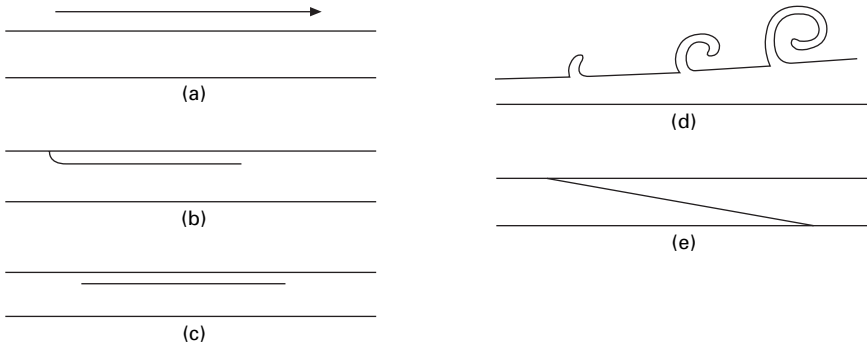
M Flex cycles to failure (Schiefer *et al.* [62]).

N Service-wear test on men's socks. Days of wear (Schiefer *et al.* [62]).

The fibres have been arranged in the order of ranking found in most tests. The exceptions are in italics, but it will be seen that there are few of these.

Table 19.7 Abrasion and wear – relative values

Fibre	Conditions													
	A	B	C	D	E	F	G	H	I	J	K	L	M	N
Nylon	100	100	100	100	100	100, 4	100	100, 73	100	100	100	100	100	100
<i>Terylene, Dacron</i>					42	696,	33	77, 57	62	62				
polyester fibres						249, 21								
Wool				20		28, 13		29, 17			100	11.6	64	33
Cotton						32, 5		44, 30			16		25.6	33
Silk							6		8.3		9, 1.8			
<i>Orlon acrylic</i>	41	28	19		3.0	18,3	2.6	14, 12	9.7	13		83		
fibre														
High-tenacity		25	17				2.7		16		4.7	1.32	31.3	
rayon														
Viscose	17	10, 15	13, 15	6	1.6	6	3.2	9.1	18	3.7	3.3, 0.7	0.66	0.28	12
rayon														
Acetate	17	7.5	9.3	4.5		3	0.31	5.3	7.2	2.2	0.5	0.053		5
Casein				1.5			0.45		1.9		0.12			1.8



19.55 (a) Shear stress in fibre over a rotating pin. (b)–(e) Various consequences.

Another form of damage occurs within twisted ropes if a component yarn cycles between tension and compression [1]. This is axial compression fatigue, with failure at kink bands, similar to those in flex fatigue. Guidance design limites are 2,000, 40,000 and 100,000 cycles for aramid, HMPE and polyester fibres respectively [68].

19.9 References

1. J. W. S. Hearle, B. Lomas and W. D. Cooke. *Atlas of Fibre Fracture and Damage to Textiles*, 2nd edition, Woodhead Publishing, Cambridge, 1998.
2. J. W. S. Hearle and P. M. Cross. *J. Mater. Sci.*, 1970, **5**, 507.
3. S. Simmens and F. Howlett. *J. Text. Inst.*, 1949, **40**, T590.
4. R. J. E. Cumberbirch, J. Długosz and J. E. Ford. *J. Text. Inst.*, 1961, **52**, T513.
5. L. Konopasek and J. W. S. Hearle. *J. Appl. Polymer Sci.*, 1977, **21**, 2791.
6. J. W. S. Hearle and J. T. Sparrow. *Text. Res. J.*, 1971, **41**, 736.
7. K. R. Makinson. *J. Text. Inst.*, 1970, **61**, 151.
8. A. R. Haly. *Text. Res. J.*, 1970, **40**, 965.
9. S. J. Law and S. K. Mukhopadhyay. *J. Textile Inst.*, 1999, **90**, 137.
10. G. E. Settle and S. L. Anderson. *J. Text. Inst.*, 1963, **54**, T28.
11. H.-S. Shin, D. E. Erlich, J. W. Simons and D. A. Shockey. *Textile Res. J.*, 2006, **76**, 607.
12. S. Michielsen. *J. Materials Sci. Letters*, 1992, **11**, 982.
13. S. Michielsen. *J. Appl. Polymer Sci.*, 1994, **52**, 1081.
14. J. W. S. Hearle. *J. Mater. Sci.*, 1967, **2**, 474.
15. A. J. Booth and J. W. S. Hearle. In 'Proceedings of Fourth International Congress of Rheology', Interscience, New York, 1965, p. 203.
16. A. R. Bunsell, J. W. S. Hearle and R. D. Hunter. *J. Phys. E*, 1971, **4**, 868.
17. A. R. Bunsell and J. W. S. Hearle. *J. Mater. Sci.*, 1971, **6**, 1303.
18. Ch. Oudet and A. R. Bunsell. *J. Mater. Sci.*, 1987, **22**, 4292.
19. J. W. S. Hearle and A. R. Bunsell. *J. Appl. Polymer Sci.*, 1974, **18**, 26.
20. Ch. Oudet and A. R. Bunsell. *J. Mater. Sci. Letters*, 1984, **3**, 295.
21. C. Lechat, A. R. Bunsell, P. Davies and A. Plant. *J. Materials Sci.*, 2006, **41**, 1745.
22. Le Clerc, A. R. Bunsell, A. Plant and B. Monasse. *J. Materials Sci.*, 2006, **41**, 6830.
23. Le Clerc, A. R. Bunsell and A. Plant. *J. Materials Sci.*, 2006, **41**, 7509.
24. L. Konopasek and J. W. S. Hearle. *J. Appl. Polymer Sci.*, 1977, **21**, 2791.

25. A. K. van der Vegt. *Rheol. Acta*, 1962, **2**, 17.
26. B. C. Goswami and J. W. S. Hearle. *Text. Res. J.*, 1976, **46**, 55.
27. K. E. Duckett and B. C. Goswami. *Text. Res. J.*, 1984, **54**, 43.
28. B. C. Goswami, K. E. Duckett and T. L. Vigo. *Text. Res. J.*, 1980, **50**, 481.
29. M. Toney and P. Schwartz. *J. Appl. Polymer Sci.*, 1992, **B46**, 2023.
30. B. C. Jariwala. PhD Thesis, University of Manchester, 1974.
31. J. W. S. Hearle and M. MirafTAB, *J. Mater. Sci.*, 1991, **26**, 2861.
32. M. MirafTAB. PhD Thesis, University of Manchester, 1986.
33. J. W. S. Hearle and M. MirafTAB. *J. Materials Sci.*, 1995, **30**, 1661.
34. R. Meredith. In *Proceedings of Fifth International Congress of Theology*, University of Tokyo Press, Tokyo, Japan, 1969, Volume 1, p. 43.
35. A. Sengonul and M. A. Wilding. *J. Textile Inst.*, 1994, **85**, 1.
36. A. Sengonul and M. A. Wilding. *J. Textile Inst.*, 1996, **87**, 13.
37. J. P. Den Hartog. *Strength of Materials*, McGraw-Hill, New York, 1949.
38. W. J. Lyons. *Text. Res. J.*, 1962, **32**, 750.
39. J. W. S. Hearle and E. A. Vaughn. *Rheol. Acta*, 1970, **9**, 76.
40. J. W. S. Hearle and B. S. Wong. *J. Phys. E: Sci. Instrum.*, 1977, **10**, 448.
41. S. F. Calil and J. W. S. Hearle. *Fracture 1977, ICF4 Conf.*, Waterloo, Canada, 2, p. 1267.
42. J. W. S. Hearle and N. Hasnain. In *Cotton in a Competitive World*, (P. W. Harrison Editor), The Textile Institute, Manchester, 1979, p. 163.
43. I. E. Clark and J. W. S. Hearle. *J. Phys. E: Sci. Instrum.*, 1979, **12**, 11.
44. I. E. Clark, J. W. S. Hearle and A. R. Taylor. *J. Phys. E: Sci. Instrum.*, 1980, **13**, 516.
45. K. Liolios. PhD Thesis, University of Manchester, 1988.
46. I. E. Clark and J. W. S. Hearle. *J. Text. Inst.*, 1980, **71**, 87.
47. S. F. Calil, I. E. Clark and J. W. S. Hearle. *J. Mater. Sci.*, 1988, **24**, 736.
48. I. E. Clark and J. W. S. Hearle. *J. Text. Inst.*, 1983, **74**, 168.
49. J. W. S. Hearle and B. S. Wong. *J. Text. Inst.*, 1977, **68**, 155.
50. J. W. S. Hearle and B. S. Wong. *J. Text. Inst.*, 1977, **68**, 127.
51. I. E. Clark and J. W. S. Hearle. *J. Text. Inst.*, 1982, **73**, 273.
52. I. E. Clark. PhD Thesis, University of Manchester, 1980.
53. J. W. S. Hearle, B. C. Jariwala, L. Konopasek and B. Lomas. *Proc. Int. Wool Text. Res. Conf.*, Aachen, 1975, II-370.
54. S. F. Calil, B. C. Goswami and J. W. S. Hearle. *J. Phys. D: Appl. Phys.*, 1980, **13**, 725.
55. H. A. Waterman. *J. Phys. D: Appl. Phys.*, 1983, **16**, 227.
56. J. F. Flory, M. Goksoy and J. W. S. Hearle. *J. Text. Inst.*, 1988, **79**, 417.
57. M. Goksoy and J. W. S. Hearle. *J. Text. Inst.*, 1988, **79**, 432.
58. M. Goksoy and J. W. S. Hearle. *J. Text. Inst.*, 1988, **79**, 443.
59. K. L. Johnson. *Contact Mechanics*, Cambridge University Press, Cambridge, 1985.
60. W. J. Hamburger. *Text. Res. J.*, 1945, **15**, 169.
61. E. M. Hicks and A. G. Scroggie. *Text. Res. J.*, 1948, **18**, 416.
62. H. F. Schiefer, L. Fourn and R. Kropf. *Text. Res. J.*, 1948, **18**, 18.
63. E. I. du Pont de Nemours and Co. Inc. Cited by E. R. Kaswell. *Textile Fibers, Yarns, and Fabrics*, Reinhold, New York, 1953.
64. E. Abrams and H. P. Whitten. *Text. Res. J.*, 1954, **24**, 980.
65. G. Susich. *Text. Res. J.*, 1954, **24**, 210.
66. R. W. Dennison and L. L. Leach. *J. Text. Inst.*, 1952, **43**, P473.
67. R. H. K. Thomson and D. Traill. *J. Text. Inst.*, 1947, **38**, T43.
68. Tension Technology International and Noble Denton, *Deepwater Fibre Moorings*, Oilfield Publications, Ledbury, 1999.

20.1 Introduction

20.1.1 A variety of approaches

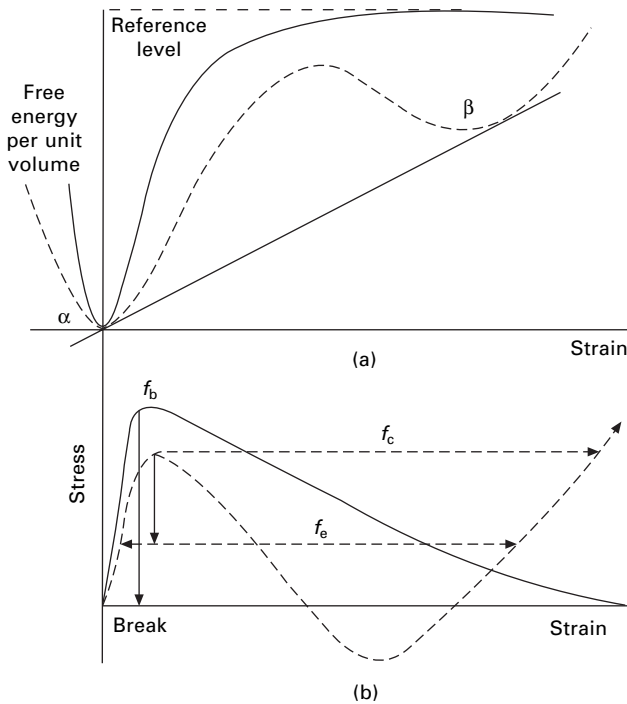
The wide range of materials and phenomena concerned in the study of the mechanical properties of fibres leads to a variety of useful theoretical approaches. A study of changes in structure at various levels gives the best general scientific understanding of the observed effects. One approach is to treat polymer fibres as composites of crystalline and amorphous regions, even though, in dealing with regions of the order of 10 nm (100 Å) in size, atomic and molecular effects must be borne in mind.

The chief technological interest is in deriving relations that will describe mathematically the macroscopic properties of the material: the stress–strain curves, recovery behaviour, creep, relaxation of stress, and so on. There are two main schools of thought: the analytical and the integral. Analytical theories aim at breaking down the behaviour into that of a combination of ideal elements. This may be done empirically, but the more sophisticated theories are based on fundamental reasoning. Integral theories aim at a single relation to fit the experimental results. An alternative mathematical approach is the application to the problem of thermodynamics, dealing with the changes of energy and entropy involved in deformation. The various theories are neither exclusive nor completely separate, and there is a crosslinking of ideas. Inorganic fibres are very different in structure and require different theoretical treatments.

20.1.2 Basic theory

Polymer fibres contain material in three main forms: crystalline; rigid amorphous below the glass transition temperature; rubbery amorphous above the glass transition. The behaviour will also be affected by the extent of secondary bonding, e.g. hydrogen bonds, in amorphous regions. It is useful to give a brief account of the basic mechanical theories for the three types of material.

Crystalline lattices are bonded by covalent, electrovalent or weaker intermolecular bonds. In the simple case, shown by the full line in [Fig. 20.1\(a\)](#), increasing strain gives a rise in energy up to a maximum value and then an asymptotic approach to a reference level. Differentiation of the free energy curve results in the stress–strain curve ([Fig. 20.1\(b\)](#)), giving Hooke's Law for small strains.



20.1 Crystal lattice deformation. Full lines: a crystal which extends to rupture. Dotted lines: a transition between different α and β forms. Note that in reality the full lines would go to much higher values of free energy and stress than the dotted lines. Following the transition, the dotted line would continue in the form of the full line to give rupture of the β -lattice. (a) Free energy versus strain. (b) Stress versus strain.

$$f = \frac{dU}{de} = Ee \quad (20.1)$$

where f = stress (or specific stress), U = free energy per unit volume (or per unit mass), e = strain and E = initial modulus.

Owing to the strength of the bonding, a crystal is a high-stiffness material. Typical moduli are of the order of 100 GPa for extended chain crystals dominated by bond stretching, but are much lower with helical lattices when bond bending and twisting can occur. The maximum stress occurs at the point of inflection on the free energy curve. For uniform straining, the stress would then fall and approach zero as the free energy reaches its asymptotic level with complete separation of parts of the crystal. In practice, a local instability will lead to a catastrophic rupture at the point of maximum stress, or earlier if there are stress concentrations or, for small crystals, thermal vibrations leading a jump over the energy barrier.

The dotted lines in Fig. 20.1 relate to materials in which there can be a transition from one crystal lattice to another, such as the $\alpha \leftrightarrow \beta$ change from helices to extended chains in keratin. For uniform deformation, the stress curves go into negative stress before increasing again, but, in practice, an instability will lead to a jump from one

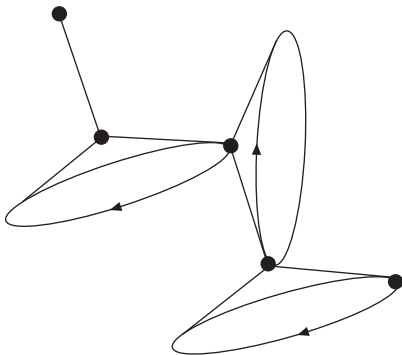
form to the other at a critical stress f_c . The stress drops to the equilibrium stress f_e , which is given by the slope of the common tangent to the two troughs in the free energy curve.

The energy and stress relations for glassy polymers are similar to the full lines in Fig. 20.1. In addition to bond stretching and bending, a major cause of the stiffness is resistance to bond rotation. Polystyrene has a modulus of 3 GPa. In the simplest case, the transition from glass to rubber is due to thermal vibrations becoming strong enough to allow free rotation around main chain bonds (Fig. 20.2). There may be secondary transitions associated with side chains or with intermolecular bonds. In particular, in nylons, there are two major transitions, one due to bond rotation and the other to mobility of hydrogen bonds. There is a similar effect in polyesters and the consequences are discussed in Section 20.3.1.

The classical theory of rubber elasticity [1] is based on the assumption that there are no changes in internal energy, so that the resistance to deformation depends only on changes in entropy. The greatest number of possible conformations of a chain of N freely orienting links, and hence the maximum entropy, occurs when the two ends of the chain are closest together. As the chain extends, the number of possible conformations decreases. The change in entropy, which can be related to the tension in the chain, depends on the change in probability of chain ends being separated by a distance r . An approximate solution, which is not valid at high extensions, for a random chain gives a Gaussian function for the probability $P(r)$:

$$P(r) = \left(\frac{4b^2}{\pi} \right)^{1/2} r^2 e^{-b^2 r^2} \quad (20.2)$$

For large extensions, getting near to a fully extended chain, it is better to follow a derivation by Flory [2, 3]. This depends on the fact that for a link of a length a at an angle ψ , the length x along the chain axis is $(a \cos \psi)$. If the tension on the chain is F , there is an associated potential energy of $(-Fx)^1$. According to the



20.2 Freedom of rotation around main chain bonds.

¹The negative sign results from an increase in x lowering a notional weight on the end of the chain and hence a reduction in potential energy.

Maxwell–Boltzmann law, the probability of a value between x and $(x + dx)$ is $\exp[-(-Fx/kT)]dx$. This leads to a mean value of x of $a[\coth(Fa/kT) - (Fa/kT)^{-1}] = a\mathcal{L}(Fa/kT)$, where \mathcal{L} is the Langevin function, which first appeared in the theory of the alignment of dipoles. The total end-to-end length l of the chain is N times the mean value of x and the fully extended chain length L is Na . Hence:

$$l = N \left[a \mathcal{L} \left(\frac{Fa}{kT} \right) \right] = L \left[a \mathcal{L} \left(\frac{Fa}{kT} \right) \right] \quad (20.3)$$

$$F = \left(\frac{kT}{a} \right) \left[\text{arc } \mathcal{L} \left(\frac{l}{L} \right) \right] = \left(\frac{kT}{a} \right) \left[3 \left(\frac{l}{L} \right) + \left(\frac{9}{5} \right) \left(\frac{l}{L} \right)^3 + \left(\frac{297}{175} \right) \left(\frac{l}{L} \right)^5 + \dots \right] \quad (20.4)$$

The first term is the Gaussian approximation in the entropic derivation and is reasonable to use up to $(l/L) = 0.4$.

Rubbers are a network of flexible polymer molecules. If the chains are long enough and sufficiently entangled, slippage of molecules past one another is inhibited to the extent that a low-modulus plateau appears below the glass transition. However, viscous flow will take place with time and, if the molecules are short, the plateau will disappear. Commercial rubbers are vulcanised to form a network that is covalently crosslinked by $(-S-)_n$ bonds or in other ways. This prevents long-term flow. Rubbers are elastic with very low hysteresis, i.e. complete recovery with very small differences between stress–strain curves in extension and recovery.

Energy minimisation provides a means of calculating stress–strain relations [1, 3]. The details are complicated and only a brief account will be given here. The dominant energy term is elongation of the flexible tie-molecules between crosslinks, which is given by integrating equation (20.4) for the changes in l from the initial to the extended lengths. There is also energy associated with change in volume, just as there is in a liquid. Except when there is a large change of hydrostatic pressure, a common procedure is to assume constant volume, which is close enough to give acceptable values of l for most deformations, although paradoxically the stresses to give exact constant volume are not small. A better procedure is to include in the analysis a volume energy term derived from the relatively high bulk modulus², and at the end to neglect negligibly small contributions to the stress [3].

Affine deformation³ relates the changes in lengths of tie-molecules between network points to the external deformation and hence, in principle, enables energy changes to be calculated. The complications arise from the need to take account of different initial lengths, extended lengths and orientations. If the Gaussian approximation is assumed, i.e. only the first term of the series in equation (20.4), an averaging procedure gives an algebraic solution for the shear modulus G :

²An advantage of this approach is that it eliminates an indeterminacy in the constant volume theory. Since there can be no volume change, any value of hydrostatic pressure gives the same result.

³Affine: the strain matrix for any small element, e.g. as defined by the distribution of network points, is the same as for the specimen as a whole.

$$G = N k T \quad (20.5)$$

where N = number of tie-molecules per unit volume, which can be related to the density of crosslinks, k = Boltzmann's constant and T = temperature.

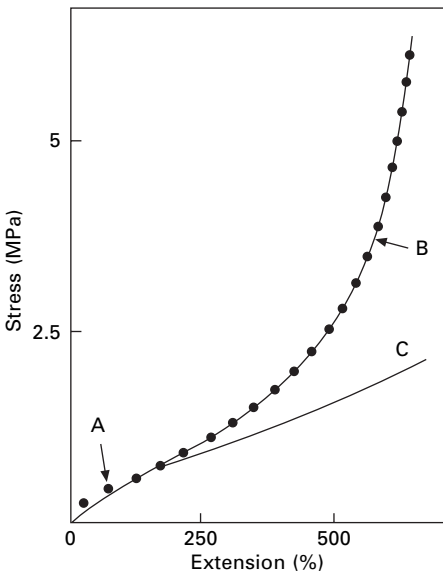
A typical value of the shear modulus G is 0.5 MPa. With a Poisson ratio close to 0.5, this gives a tensile modulus of 1.5 MPa, many orders of magnitude less than the modulus of crystals or glasses. The bulk modulus is more than 1 GPa, over 1000 times greater than the shear and tensile moduli and can clearly be neglected in most modes of deformation.

For large strains, which require use of the full equation (20.4), the averaging is more difficult, except by numerical computation. For an analytic solution, a three-chain (XYZ) model can replace the distribution of orientations. This gives the following equation for uniaxial stress f :

$$\begin{aligned} f &= \left(\frac{NkT}{3} \right) n^{1/2} \left\{ \text{arc } \mathcal{L} \left(\frac{\lambda}{n^{1/2}} \right) - \lambda^{-3/2} \text{arc } \mathcal{L} \left[\frac{1}{(\lambda n)^{1/2}} \right] \right\} \\ &= NkT \left[\lambda - \left(\frac{1}{\lambda} \right)^2 \right] \left[1 + \left(\frac{3}{25n} \right) \left(3\lambda^2 + \frac{4}{\lambda} \right) + \left(\frac{297}{6125n^2} \right) \left(5\lambda^2 + 8\lambda + \frac{8}{\lambda^2} \right) + \dots \right] \end{aligned} \quad (20.6)$$

where λ = extension ratio = (1 + axial strain) and n = number of freely orienting links in the tie-molecules between network points.

Treloar (1) quotes the series for two more terms, which go to a sum of five powers of λ . There are interesting features of equation (20.6) illustrated in Fig. 20.3, which



20.3 Stress-strain curves for a typical rubber: A, experimental data, B, inverse Langevin function form; C, Gaussian approximation.

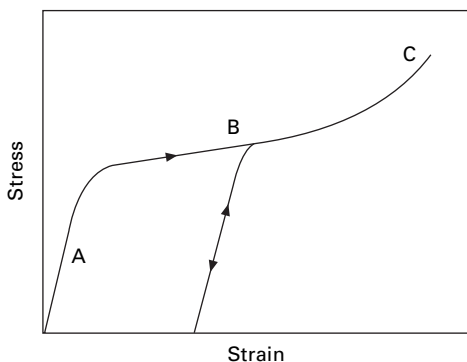
also shows the agreement between experiment and theory. The inclusion of $(1/\lambda)^2$, which also comes into the full treatment of the Gaussian approximation, means that there is some initial curvature of the stress–strain curve. The later terms of the series in λ determine the large strain behaviour with the stress rising more sharply and becoming asymptotic to infinity when the chains are fully extended. The first term in the series, which is the Gaussian approximation, does not include n . The stress depends only on the number of tie-molecules and is independent of the number of links that they contain. However the large-strain behaviour is dependent on n . It should be noted that the number of freely rotating links $n = (\text{number of repeat units in a tie-molecule}/\text{number of repeat units in a freely rotating link})$. This differentiates different polymers. For a simple polymer, which can be represented by Fig. 20.2, the freedom is limited to rotation with the angle between bonds remaining constant and a freely rotating link is equivalent to three repeats. However, for different bonds and other interactions, the number varies considerably. For polyisoprene (natural rubber), in which the monomer includes four main chain and contains a double bond, a freely rotating link corresponds to 1.73 monomer units.

Following the first edition of Treloar's classic text in 1949, there were many advances in the theory of rubber elasticity. Some of these dealt with the mathematical approximations, but others dealt with physical differences between the idealised model and real materials. In particular, there are internal energy changes as well as entropy changes. Semicrystalline polymer fibres bring in other effects, but the basic analyses described above can be used in theories for particular fibre types.

20.2 Structural effects in rayon fibres

20.2.1 The extension and recovery of ordinary rayon

Viscose rayon exhibits many features of fibre behaviour that are also shown by other fibres. It is therefore a good example to consider first in qualitative and semi-empirical quantitative theory. The stress–strain curve shown in Fig. 20.4 has three distinct regions: an initial linear portion A, in which recovery is good; a region of easier extension B, in which recovery is incomplete; and, finally, a region of increasing



20.4 Stress–strain curve of rayon.

slope C, leading to breakage. This curve may be explained in terms of the structure of the fibres.

When a small force is applied to the fibres, extension will occur for two reasons:

- a slight stretching of the chain molecules themselves;
- a straightening of the molecules in the non-crystalline regions, with a resultant straining of the hydrogen bond crosslinks between them.

The behaviour is thus analogous to that of a bundle of rods held together at irregular intervals by short lengths of elastic. On the application of a force, there may be some stretching of the rods, but there will be a greater stretching of the elastic links, allowing the rods to change position. There will also be some change in bond angles in the main chains.

The magnitude of the distortion of the molecules and crosslinks will be proportional to the applied force, so that the stress–strain curve will be linear. On removal of the force, the molecules and crosslinks will spring back to their original positions, and recovery will be complete. The straining of the bonds occurs at rates comparable to thermal vibrations of the atoms, namely, in times of the order of 10^{-13} second, so that there is no detectable time dependence except at such high rates that inertia effects are also significant.

When the applied force becomes larger, some of the most highly strained crosslinks in the amorphous region will break because they cannot support the force applied to them. This permits a much greater straightening of the molecules and, in turn, puts an increased load on other crosslinks. Consequently, extension becomes much easier. This is the region B. When the force is removed, recovery is incomplete, since many of the crosslinks are now missing and cannot spring back to their original positions or, more probably, hydrogen bonds have re-formed in new positions and are thus tending to stabilise the deformed state. Mechanical conditioning is explained, since the small elastic recovery from the deformed state will be reversible. When the specimen is extended again, no more crosslinks need to break until the original stress–strain curve is reached.

The observed time dependence of this yield region is explained by the fact that the rupture of a crosslink is a statistical phenomenon. The random thermal vibrations of the system give a certain probability that a given crosslink will break in a given time. In the absence of an applied stress, or with a low stress, the probability is almost infinitesimal, and, even when a link does break, the neighbouring links hold the structure in place and prevent any extension or recovery of the fibre. But, as the stress is increased, the most strained crosslinks become less stable and thus are more easily broken by thermal vibrations. The chances of achieving sufficient loosening of the structure to get appreciable localised deformations become significant. The interaction of these two effects, the increasing instability of bonds under stress and the chance fluctuations of thermal vibrations, causes the yield stress to be rate-dependent. At higher rates of extension, the crosslinks have to be raised to a higher level of instability before sufficient chance breaks occur within the timescale of the test; at low rates, the stress does not need to be so great for there to be a sufficient number of random breakages to cause yield.

When put in other ways, the same argument explains secondary creep and stress relaxation. Under constant stress, continued rupture of crosslinks will occur owing to chance fluctuations as time goes on and thus lead to continued deformation or creep. It will be secondary creep without recovery because, when the stress is returned to zero, the structure is so firmly held by the many hydrogen bonds in cellulose that the influence of thermal vibrations is negligible. The rate of creep will slow down with increasing time because the continued rearrangement of the structure tends to remove the most highly strained and unstable crosslinks and leads progressively towards a more uniform sharing of the load among all the chains and hydrogen bonds, with a reducing probability of breakage of crosslinks.

When the fibre is held extended at fixed length, the continued spontaneous breakage of crosslinks relieves the internal stresses in the molecular assembly and thus leads to the lowering of tension, which is termed *stress relaxation*. An oversimplified, but instructive, model of stress relaxation is a set of links that are put under tension by the imposed strain. It is assumed that there is a certain probability that a link will break in a given time and cease to contribute to the stress. The number of crosslinks breaking in a time interval dt will be proportional to the number remaining n . Thus:

$$\frac{dn}{dt} = -kn \quad (20.7)$$

where k = constant. But the stress will be proportional to n , the number of effective crosslinks (per unit area), so that:

$$\frac{df}{dt} = -kf \quad (20.8)$$

Integrating and putting $f = f_0$ at $t = 0$, we get:

$$\frac{f}{f_0} = \exp(-kt) = \exp(-t/\tau) \quad (20.9)$$

where $\tau = 1/k$ = relaxation time for the type of bond concerned.

This indicates that an exponential decay of stress is likely, though the situation is more complicated in real fibres for several reasons. There may be various sorts of bond with different relaxation times; there is a complicated distribution of stress over the links; and the effects of breaking a link in the network will not be as simple as in the model. Each break will lead to structural rearrangement.

The small positive slope of the stress-strain curve in the region B can be explained by local variations in molecular packing. The most unfavourable arrangements are disturbed first, and higher stresses are needed to cause further breakage of crosslinks, allowing the molecular chain to straighten and give more fibre extension. However, eventually a point is reached at which some of the molecules are fully straightened. Further extension then becomes more difficult, and the slope increases as at C. During this period, an increasing strain is put on the crosslinks and molecules. Finally, breakage occurs at locally highly stressed or weak points to give a granular break.

Because the yield phenomena are affected by thermal vibrations, they will be influenced by temperature. Creep and stress relaxation will occur more rapidly at the

higher temperatures. Moisture absorption will have a much greater effect. The stress–strain curve in Fig. 20.4 is typical of the behaviour of ordinary rayon at low and medium humidities. In the perfectly dry state, there will be a maximum crosslinking of the cellulose molecules by hydrogen bonds, and the yield stress will be high. As moisture is absorbed, some of these crosslinks are replaced by absorbed water molecules. This loosens the structure and makes yield easier. Consequently, as relative humidity increases, the yield stress falls.

In wet rayon fibres, there is so much moisture absorbed that the non-crystalline regions are virtually free of restrictions on relative movement. The plasticising effect is such that the molecules can be regarded as swimming in a sea of water molecules, held together only by the crystalline micelles. This is why the modulus of standard viscose rayon is so low when wet. In effect, the yield stress can be regarded as having moved down to the origin, the yield slope being left to determine the fibre stiffness.

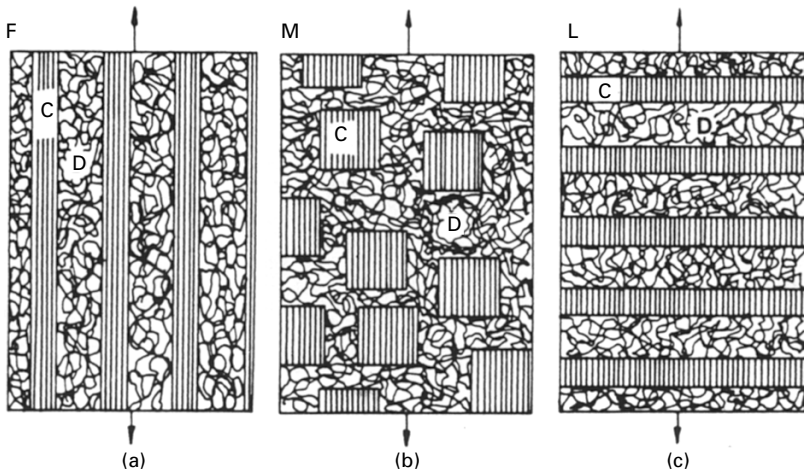
The loosening effect of absorbed water is such that, at zero stress, spontaneous structural arrangements can occur and the structure will recover to an equilibrium state. This explains swelling recovery (see Section 15.6). A structure that has been left with a ‘permanent’ extension as a result of being strained while dry will recover when it is loosened up by absorbed water or steam.

20.2.2 A comparison of regenerated cellulose fibres

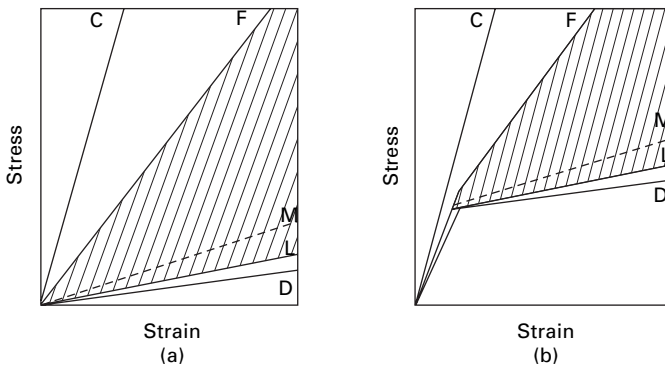
There is a great diversity of regenerated cellulose fibres with different mechanical properties due to differences in manufacturing sequences (Section 1.5.2). The influence of large-scale structural features is shown by fibres with an asymmetric skin, giving rise to a crimp that has a major influence on the initial part of the stress–strain curve. The all-skin fibres have a finer texture, which leads to lower localised stress concentrations, a more uniform sharing of load among the molecular chains, and thus to higher strengths. These are the high-tenacity rayons. Although not a rayon, cellulose acetate shows behaviour that is qualitatively similar to that of ordinary rayon, except that the weaker attractions between molecules lead to easier yield; the drop in stress that is often observed at the start of yield must be due to the development of an unstable situation once large-scale molecular movement begins.

Finally, there are the very interesting differences between ordinary and high-tenacity rayons in one group and high-wet-modulus or polynosic rayons in another. If orientation effects are ignored, the structure of the high-wet-modulus rayons may be represented by the fibrillar model of Fig. 20.5(a), whereas the ordinary rayons are micellar as in Fig. 20.5(b). If, with some exaggeration, we consider these models as made of glass embedded in rubber, the difference is obvious: the fibrillar model will have almost the stiffness of glass, but the micellar model will have almost the extensibility of rubber.

The fibrillar model (Fig. 20.5(a)), is easily analysed for any combination of material properties because the stress will be the mean stress contributed by the two components at the same strain, weighted to allow for one-third crystalline to two-thirds amorphous. The micellar model is difficult to analyse; but the more extreme lamellar structure of Figure 20.5(c) is again easy to analyse. The behaviour of the composite system is



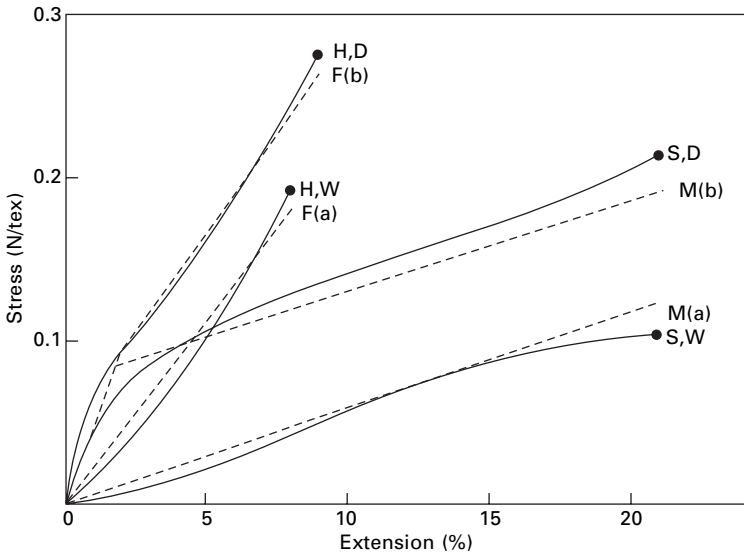
20.5 Structural models – one-third crystalline (C), two-thirds amorphous disorder (D): (a) fibrillar; (b) micellar; (c) lamellar.



20.6 Idealised stress–strain relations of rayon: C, crystal line; D, disordered; F, fibrillar; M, micellar; L, lamellar; (a) wet; (b) dry.

given by taking the weighted mean strain with the same stress on each component. The micellar structure will give a result between the two extremes and was arbitrarily placed at the mid-point between the fibrillar (F) line and lamellar (L) lines *at a given stress* [4].

Figure 20.6 shows idealised stress–strain curves for the components: a stiff, linear, elastic stress–strain curve, unaffected by water, for the crystalline material, using expected values of the modulus of cellulose crystals; a less stiff, initial linear portion followed by yield for the dry disordered material; and a single region of low slope for the wet disordered material. The arguments for the form of these relations were given in the last section. These combine to give predicted curves, which are then compared with experimental results in Fig. 20.7. The form of the relation for the disordered material was given by fitting to the results for dry standard rayon. There is then good agreement for the other three curves. It is the stiffening effect of the fibrils that causes the high-wet-modulus of polynosic fibres. Lyocell fibres follow the same pattern.



20.7 Comparison of theoretical predictions from 20.6 with experimental results: S, standard rayon; H, high-wet modulus rayon; D, dry; W, wet.

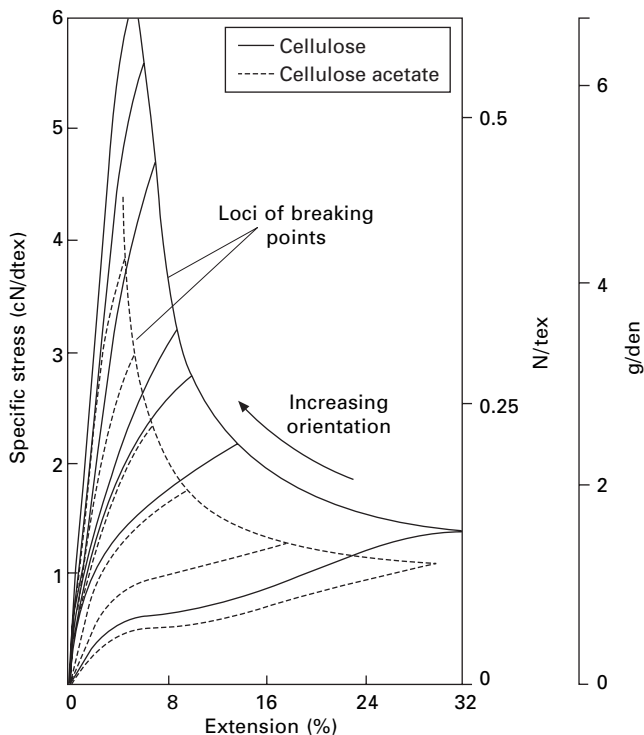
20.2.3 The effect of orientation

The stress–strain curves shown in Fig. 20.8 demonstrate the influence of molecular orientation in raising the stress–strain curve. Intuitively, this is to be expected, since a poorly oriented structure has an opportunity to extend by becoming more highly oriented, but this is not possible in a structure that is oriented to start with. The behaviour is illustrated schematically by the three pairs of diagrams in Fig. 20.9, where the structures in the left-hand pictures have low orientations and can deform to give those in the right-hand pictures. The right-hand pictures can alternatively be regarded as illustrations of the initial states of stiffer structures.

If we consider a simple network of linear elements, as in Fig. 20.9(a), those that lie in the direction of extension will resist deformation more strongly than those lying across it. This is the basis of the influence of fibre orientation on the properties of non-woven fabrics; and the same argument will explain the influence of orientation in the non-crystalline regions of a cellulose fibre. The preferred orientation is produced by stretching during fibre production and stabilised by the pattern of interconnections between crystalline regions. A fibre that has been stretched and permanently set in the dry state will show a further preferred orientation, stabilised by hydrogen bonding.

Crystalline orientation also plays a part. In the micellar structures, the crystalline regions may reasonably be regarded as rigid filler particles with all the deformation occurring in the non-crystalline regions. However, the deformation is easier if the micelles are initially poorly oriented and so are able to swing into alignment and give an added extension with less strain in the non-crystalline matrix, as indicated in Fig. 20.9(b).

In fibrillar structures, with less than perfect orientation as in Fig. 20.9(c), a

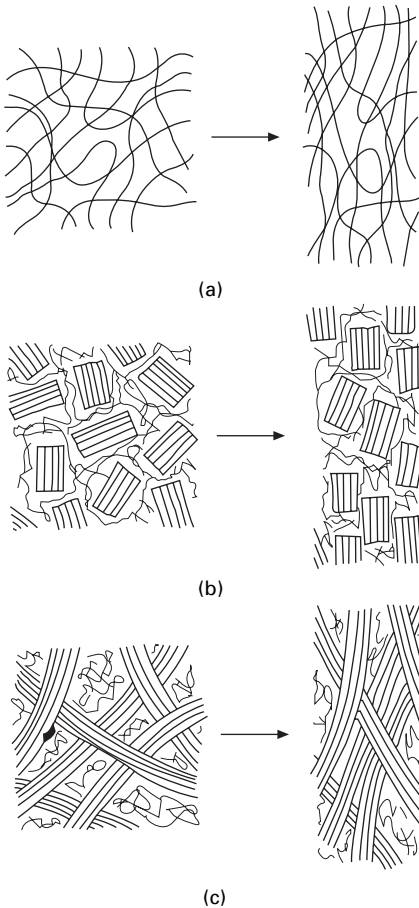


20.8 Stress-strain curves of filaments of varying degrees of orientation. The dotted curves are secondary cellulose acetate and the full curves are cellulose fibres regenerated from acetate. The lowest curve in each set is for unoriented material. From Work [5].

contribution to extension can come from straightening of fibrils, as well as the fibril extension considered in the last section. The less the degree of orientation, the greater is the contribution, and thus the stress-strain curve is at a lower level. A detailed theory of a particular model of this situation has been worked out by Hearle [6] and agrees reasonably with experimental results. It turns out that the major resistance to extension by straightening of fibrils comes not from the bending resistance of the fibrils themselves, but from the resistance to deformation of the disordered material between the curved fibrils.

20.2.4 Ultimate failure

Rupture is, in general, more difficult to explain in detail than earlier deformation behaviour because it is determined by extremes, by the concurrence of abnormal stress concentrations with abnormal structural weaknesses. There has been no special study of stress concentrations in fibres beyond the general recognition that high stresses will occur near cracks, voids and foreign particles. Places of particular weakness, which can be a nuisance in processing even when they occur only at intervals of thousands of kilometres, can probably be attributed to major defects of this sort. But

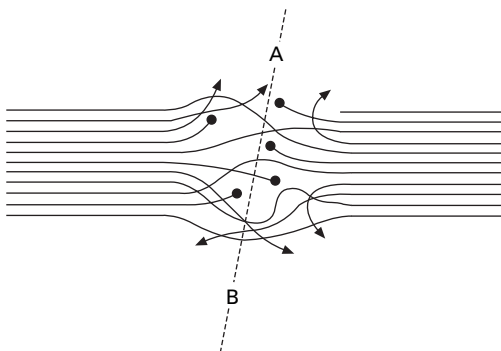


20.9 Schematic representation of effects of orientation: (a) network; (b) micelles; (c) fibrils.

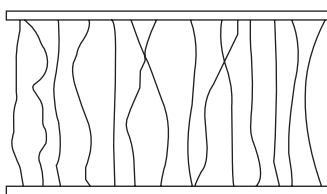
the occurrence of tensile fracture of rayon in a laboratory test, with a test length of a few centimetres, appears to involve multiple initiation and development of fracture at many places within the fibre. Thus, while there will be an influence of the statistical coincidence of points of weakness and of fibre irregularity, the fibre strength will be related to the general ultimate strength of the material structure.

It is simplest to consider first wet rayon, with a structure composed of crystalline regions, linked together by tie-molecules (strictly, better called tie-segments of molecules) passing through non-crystalline regions, as illustrated in [Fig. 20.10](#). The structure will fail and part when all the links along some line such as AB, which represents a surface in the real three-dimensional structure, are broken.

Free ends emerging from a micelle will contribute nothing to the strength. The influence of total chain length (degree of polymerisation or molecular weight) is therefore apparent, since the shorter the chains the more free ends there will be. In



20.10 Schematic representation of chain molecules emerging from micelles, showing chain ends, tie-molecules between the two micelles, and links to other micelles. The line AB continues between other micelles.



20.11 Tie-molecules of varying length between micelles.

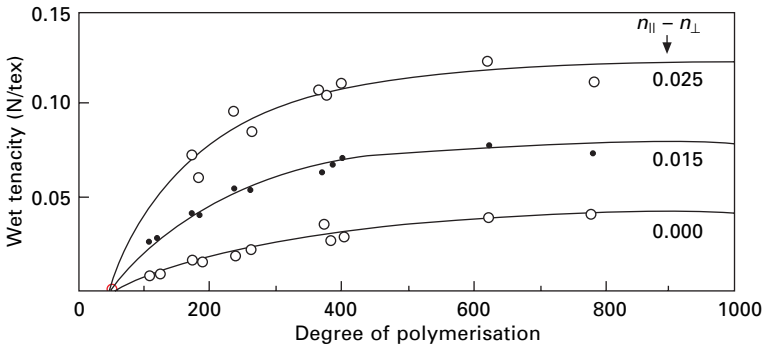
typical rayon fibres, about one-third of the chains emerging from a micelle will be free ends⁴.

The other factor that is important is the distribution of segment lengths between micelles as illustrated in Fig. 20.11. As the structure is extended, the shortest segments will break first, but there will still be enough others to take up an increased load. Eventually, however, as the peak of the distribution of segment lengths is approached, there will be insufficient segments left to support the load, and catastrophic failure will occur. The situation is similar to that of a fibre bundle discussed in Section 14.4.

A detailed theory along these lines has been worked out by Cumberbirch and Mack [7, 8], using rubber chain conformation theory to obtain the distribution of chain lengths. There is good agreement with experimental results, and Fig. 20.12 shows the variation of wet strength with degree of polymerisation and orientation.

Both the experimental and the theoretical results demonstrate that, up to a certain level, care in maintaining a high degree of polymerisation (DP) of the cellulose is valuable in improving strength. But there is little advantage to be gained by having a DP greater than about 500, since the number of free ends has then become negligible. Other work shows that it is important to pay attention to the distribution of chain lengths, as well as to the mean value. Any appreciable number of short chains is undesirable.

⁴Owing to the stiffness of cellulose molecules, it is reasonable to assume that there is no chain folding at the ends of crystallites. This is not true for more flexible polymers.



20.12 Theoretical prediction of variation of strength of wet rayon with degree of polymerisation, compared with experimental results, at varying degrees of orientation given by birefringence ($n_{\parallel} - n_{\perp}$). From Cumberbirch and Mack [8].

In dry rayon, including rayon at medium humidities, the tie segments will be linked together by hydrogen bonds. One consequence of this is that the free ends contribute to holding the structure together, so that the strength is increased. The shorter the chains, the greater will be the increase; or, conversely, the decrease in strength on wetting will be greater in ordinary rayon than it will be in better quality rayon with a higher degree of polymerisation. It is also possible that some of the weakening effect due to the range of tie-segment lengths may be mitigated in the crosslinked network.

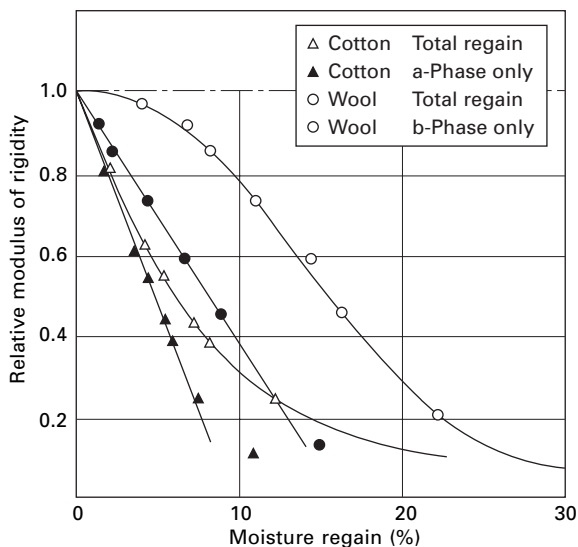
20.2.5 Torsion

In torsion, shear forces are between the molecules. Deformation in this way is much easier than in tension, just as it is easier to twist a bundle of rods than to stretch it. Consequently, the shear modulus should be less than the tensile modulus. This is found in practice (see [Section 17.3.3](#)), the difference being greatest for the most highly oriented fibres.

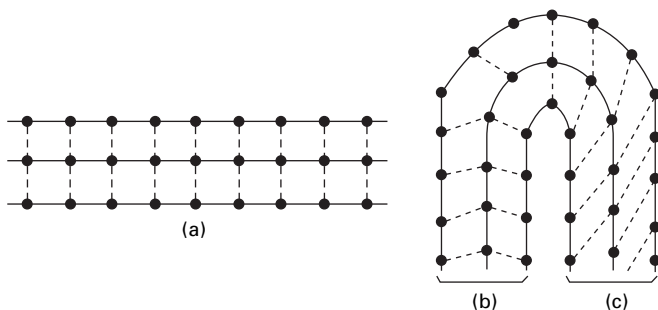
Water has a great effect on the intermolecular forces, so it is not surprising that it has a great influence on fibre torsional rigidity, as shown in [Fig. 20.13](#).

20.2.6 Creasing

Creasing and crease resistance may be explained on a molecular theory. If a structure, such as the one in [Fig. 20.14\(a\)](#), is bent into a crease, there are two possibilities. The crosslinks may break, and re-form in new positions, as in [Fig. 20.14\(b\)](#). On removal of the load, there will be no recovery, and a crease will be left. Alternatively, the crosslinks may be strained without breaking, as in [Fig. 20.14\(c\)](#). Under these conditions, there will be a recovery on removing the load, and no crease will result.



20.13 Modulus of rigidity (relative to value when dry) plotted against moisture regain.



20.14 Creasing and crease-resistance: (a) schematic representation of structure with crosslinks; (b) formation of new crosslinks, giving a crease; (c) straining of crosslinks, leading to crease recovery.

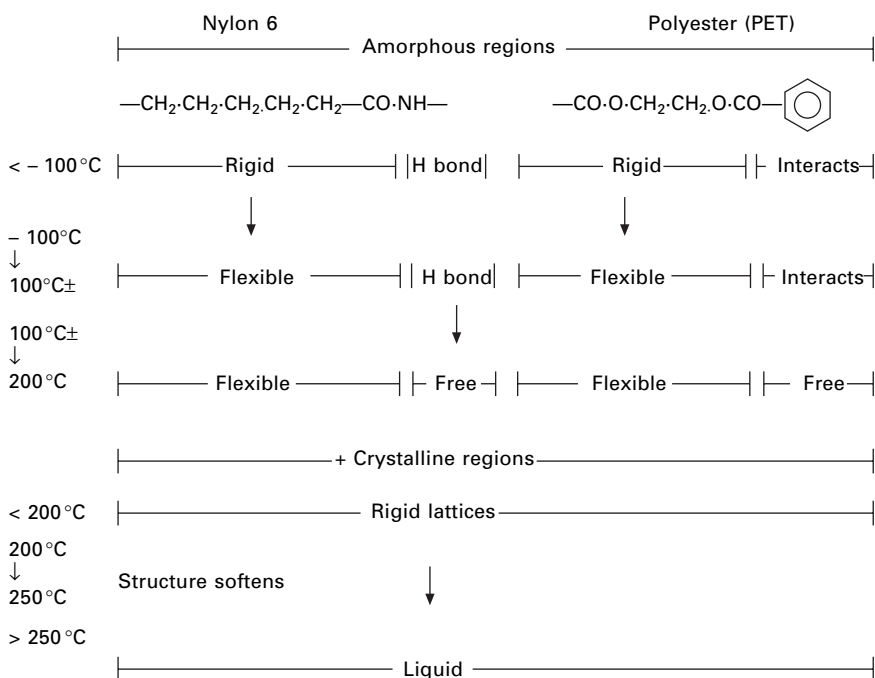
20.3 Nylon, polyester and similar fibres

20.3.1 Molecular responses and fine structure

Polyamide and polyester molecules have important differences from cellulose molecules, which contribute to their superior properties in manufactured fibres. In nylon 6, there is an alternation between five $\text{—CH}_2\text{—}$ groups and —CO·NH— groups. Nylon 66 is similar, except that the repeat is twice as long with alternately four and six $\text{—CH}_2\text{—}$ groups. Polyester (PET) has an aliphatic sequence $\text{—CO·O·CH}_2\text{·CH}_2\text{·O·CO—}$, which with six main chain bonds matches the $\text{—CH}_2\text{—}$ sequences in polyamides, alternating with benzene rings. These similar structures, or near versions of them, are ideal for synthetic fibres for general textile uses. At room temperature, the aliphatic sequences

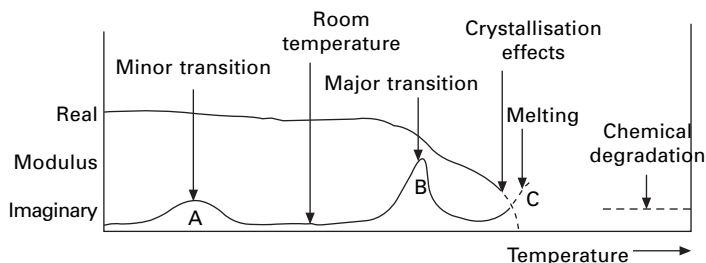
in amorphous regions provide a freedom that gives extensibility and the interactions of the —CO·NH— groups or benzene rings in amorphous and crystalline regions give stability, strength and suitable stiffness to the structure.

Figure 20.15 illustrates how the fibres respond to change in temperature. In the unimportant range below about $-100\text{ }^{\circ}\text{C}$, energy barriers prevent freedom of rotation around main chain bonds in the aliphatic sequences. The —CO·NH— groups are strongly hydrogen bonded. The material is fully glassy with high stiffness. Above $-100\text{ }^{\circ}\text{C}$, the thermal vibrations are large enough to overcome the barriers and allow free rotation, as shown in Fig. 20.2. The aliphatic sequences thus act as short rubbery links. The change at around $-100\text{ }^{\circ}\text{C}$ is the first half of a glass-to-rubber transition, as suggested in Fig. 20.16. At around $100\text{ }^{\circ}\text{C}$ ⁵, the thermal vibrations become large enough for hydrogen bonds in nylons and phenolic interactions in polyesters to become mobile. The glass-to-rubber transition is completed. There is some softening of nylon 66 and PET at temperatures near $200\text{ }^{\circ}\text{C}$ with a mechanism that is not well understood but allows for permanent heat setting. Finally, somewhere above about $250\text{ }^{\circ}\text{C}$, the crystals melt and the material becomes a spinnable liquid, which can be extruded to form fibres. Softening melting temperatures are lower in nylon 6.

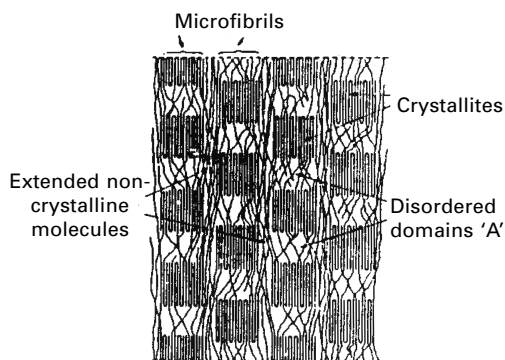


20.15 Polyamide and polyester molecular structures and their thermal transitions. Note that temperatures are approximate within $\pm 25\text{ }^{\circ}\text{C}$, and are less in nylon 6 than in polyester (PET).

⁵As discussed in Chapter 18, the transition temperature is lower in wet nylon, is a bit higher in polyesters, and is time dependent.



20.16 Transitions in an 'ideal' fibre. From Hearle [9].

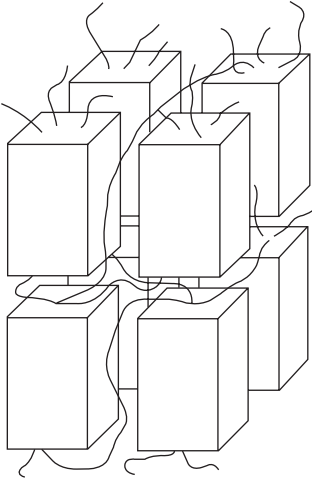


20.17 A model of the fine structure of a polyester fibre, as proposed by Prevorsek *et al.* [10].

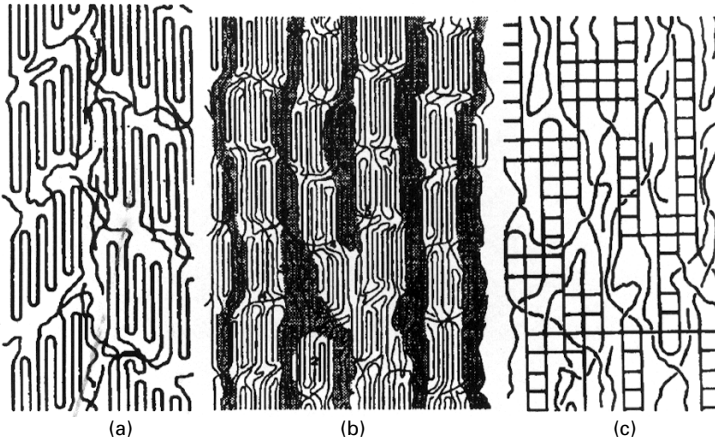
A version of a common working model, by Prevorsek *et al.* [10], for the fine structure of polyester (PET) fibres is shown in Fig. 20.17. They have a similar model for nylon 6, except that they place the crystallites in register and not staggered as in Fig. 20.17. Although such views are probably a reasonable representation of the real structure, they suffer from being 2D pictures of a 3D network and there remains much uncertainty about the details of the structure. A simplified model, which will be used in a theoretical derivation, is shown in Fig. 20.18. Other views of roughly cuboid crystals, with a mixture of chain folding and emerging tie-molecules at the ends of crystallites, are shown in Figs 20.19(a,b). Typically, there will be about 100 molecules in the cross-section of a crystallite and the width will be 5–10 nm. There is some indirect evidence suggesting that the ratio of length to width in polyester crystallites is greater than in nylon. In some circumstances the distinction between crystalline and amorphous regions may be less sharp, as indicated in Fig. 20.19(c). The crystallinity is typically about 50% when the fibre has had some exposure to heat or drawing.

20.3.2 A network model

The modelling of a fringed micelle structure in Section 20.2.2 is based on mixture laws applied to a composite of crystalline and amorphous regions. However, it is clear that the model is arbitrary. If the micellar line in Fig. 20.6 had been placed



20.18 Simplified model for theoretical analysis, showing a regular array of crystallites linked by tie-molecules, of which only a few are shown.



20.19 Views of fine structure of nylon fibres. (a) A common working model proposed by Hearle and Greer [11]. Angled ends are based on small angle X-ray diffraction pattern of nylon 66. (b) From Murthy *et al.* [12], based on X-ray diffraction studies of nylon 6. (c) An alternative form, from Hearle [13].

between the lines for fibrillar and lamellar forms at the same strain, it would have been much higher. Hearle *et al.* [14] showed that the predictions of a combined series and parallel model could be several orders of magnitude apart depending on whether modulus weighting or compliance weighting was used in combining the series and parallel parts. A simplistic approach is not quantitatively viable. It is possible that a more detailed calculation of stress distributions, e.g. by finite element computing, might give better results.

A network model is a more promising way forward and is particularly applicable above the glass transition temperature when the tie-molecules can be regarded as

flexible chains linking crystallites, which would be large-scale crosslinks in an elastomeric polymer network. A theory [15] of this type has been developed and is outlined by Hearle [16]. The quantitative predictions of stress are too low, but both the methodology and the results are instructive.

The basic premise is that the state of the material is determined by the energy per unit volume U , which is the sum of two terms: the energy of extension of tie-molecules between crystallites and the energy of volume change. The first term is the sum over all tie-molecules of the integral of equation (20.4) and the second depends on the bulk modulus k and the volume strain e_v ;

$$U = \Sigma \int_{l_0}^l \left(\frac{kT}{a} \right) \left[\operatorname{arc} \mathcal{L} \left(\frac{l}{L} \right) \right] + \frac{1}{2} k e_v^2 \quad (20.10)$$

The assumed fine structure is the regular array of orthogonal crystallites linked by tie-molecules, as indicated in Fig. 20.18. The crystallinity determines the division of polymer material between crystalline and amorphous regions. Hence the total length of tie-molecules in the set can be calculated. The length and width of the crystallites and the ratio of axial to transverse separation are geometrical parameters. The summation is over the tie-molecules in unit volume. A representative set is given by all the tie-molecules that emerge from the end of a crystallite, which equals the number of molecules in a cross-section of the crystallite minus twice the number of chain folds. This length must then be divided among the locations of the other ends of the tie-molecules, with a correction for chain ends and loops back to the same crystallite. In the absence of more structural information, arbitrary choices were made with links as far apart as next nearest neighbours. It was assumed that the ratio of actual chain length to the shortest path was constant for all tie-molecules. This gives values of l , which is the end-to-end length along the shortest path, and the fully extended chain length L for all the tie-molecules. The integral is from the initial end-to-end length l_0 of tie-molecules in the stress-free state to the extended length l in a deformed fibre. Affine deformation of the positions of the crystallites changes the spacing between crystallites and enables l to be calculated.

For uniaxial extension, the applied strain determines the change in axial spacing of crystallites, but the transverse spacing is left as a dependent variable to be determined by energy minimisation. This gives a value of the Poisson ratio. The procedure is then repeated with a small change of axial strain. The change in energy per unit volume equals the stress times the change in strain. Hence the stress–strain curve can be computed.

There is a difficulty. There is no guarantee that the parameters used to define the initial geometry relate to the stress-free state. Indeed it would be exceptional if they did. The first step in the computation is therefore to allow both axial and transverse spacing to be dependent variables and use energy minimisation to determine the actual spacings in the stress-free state. This illustrates an important insight. In drawing or looking at models of fine structure, such as those shown in Figs 20.17 and 20.19, it is natural to assume that they are static models in which, if there is no external applied stress, there are no internal stresses. In reality, the thermal vibrations mean that the tie-molecules are under tension, pulling the crystallites closer together against

the resistance of volume reduction. The structure can be likened to an array of bricks linked by stretched rubber strings.

The parameters needed to define the model for computation are listed in Table 20.1. Although some, such as molar mass of repeat unit, are known exactly, others, such as the connectivity, are almost unknown quantities. Indeed the first estimate of connectivity gave an impossible structure. The shortest paths were longer than the total chain length. More structural studies using modern techniques would give more information to test the theory, but the real advance would come from modelling the structure formation from the more-or-less random arrangement in the melt through crystallisation and drawing.

The predicted stress–strain curves are of the right form for nylon above the glass transition temperature but, unless unrealistic values of parameters are used, give too low values of stress. Although there are obvious ways of making the theory more rigorous, by eliminating approximations, major changes seem to be necessary to make valid predictions. If the fundamental approach is valid, there are various possibilities. Constant values are assumed for many features that will have statistical distributions. In particular, low values of the ratio of chain length to shortest path would have a disproportionate effect in generating high stresses. It is also likely that interactions and entanglements within the amorphous regions cause the energy of

Table 20.1 Input quantities for computation of the network model

Features of the polymer

- # Molar mass of the repeat unit
- # Length of repeat unit in crystal
- # Crystal density
- # Amorphous density, stress-free
- # Number of equivalent free links per repeat
- Degree of polymerisation

Features of fine structure

- # Fractional mass crystallinity
- # Number of repeats in crystallite length
- # Number of repeats across crystallite
- # Series fraction of amorphite
- Fraction of sites with crystallographic folds
- Fraction of sites with loose folds
- Length factor for free ends
- Length factor for loose folds
- Relative probability of connector types

Other parameters

- * Bulk modulus of amorphous material
 - * Stress at which chains break
 - * Temperature
 - * Mass of proton
 - * Boltzmann's constant
-

= required to characterise two-phase structure; ○

○ = required to characterise connectivity;

* = required to analyse mechanics.

chain extension to be greater than given by equation (20.4). Other neglected features, such as extension and rotation of misoriented crystallites, would lead to lower stresses.

For predictions of the stress–strain curve at room temperature, it would be necessary to model a network linked by hydrogen bonds or phenolic interactions. Long and Ward [17] have applied theories of crosslinked rubbers and show that this explains shrinkage forces, which increase with temperature, as expected for an entropic mechanism. In another paper, Ward [18] considers the change from *gauche* to *trans* conformations of the molecules in the drawing of polyester (PET). In PBT (3GT) the behaviour is complicated by a crystal lattice transition and in PEN by crystallisation effects.

20.3.3 A theory for dynamic mechanical properties

A purely series model, which is a simpler variant of the above theory, has been presented by Davis [19]. The crystallites are in series with tie-molecules that follow the inverse Langevin [4] for force on a flexible chain. He recognises that this only applies at higher temperatures when the chains act as freely orienting links and then uses Rouse's theory [20] to introduce viscous drag on chain segments in the transition temperature region. The predicted value of the loss factor is given by:

$$\tan \delta = \frac{N\eta\omega Z}{E} \quad (20.11)$$

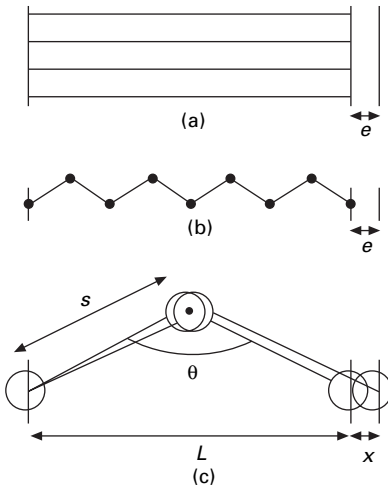
where N = number of load-bearing chains per unit area, η = a temperature-dependent viscosity, ω = frequency, Z = a temperature-dependent structural parameter and E = modulus of the amorphous material. Although the model gives useful guidance, it suffers from quantitative limitations similar to those for the network theory.

20.4 High-performance fibres

20.4.1 Simplistic theory of tensile deformation of HM–HT fibres

At a first level of approximation, theoretical understanding of the deformation of HM–HT fibres is easier than for the general textile fibres. The dominant mechanism is elastic deformation of covalent bonds. In the ceramic fibres, the network is three dimensional, so that similar effects occur in all directions. In the highly oriented linear polymer fibres, axial elongation is resisted by the covalent bond deformation, which therefore exerts the major control on tensile properties of the fibre. Transverse and shear deformations are resisted only by weaker inter molecular forces. In HM–HT carbon fibres, the orientation of the graphite planes parallel to the fibre axis causes covalent bond deformation to be the dominant effect in fibre extension; but perpendicular to the fibre axis there is a mixture of covalent bonding in the planes and weak bonding between the planes.

The simplest case to consider is the behaviour of a fibre made of infinitely long polymer molecules, with a simple —C—C— backbone like that of polyethylene, oriented parallel to one another, but not necessarily in crystalline register, as indicated in Fig. 20.20(a). Because of the perfect uniformity of the structure, a tensile strain e



20.20 (a) Perfectly oriented fibre of infinitely long molecules subject to tensile strain e ; (b) application of strain e to molecule; (c) application of strain e to repeat unit of molecule.

imposed on the fibre must also occur uniformly along the polymer molecules, as indicated in Fig. 20.20(b), and so to the individual repeat unit in Fig. 20.20(c).

If m is the mass and l is the length of the repeat unit, and U is the change in internal energy associated with an elongation x , then U must be proportional to x^2 , in order to give a minimum value at the equilibrium zero-force state with $x = 0$. This leads to the relations, given in terms of a spring constant K as:

$$U = \frac{1}{2} K x^2 \quad (20.12)$$

$$\text{force} = F = \frac{dU}{dx} = K x \quad (20.13)$$

If we normalise in terms of specific energy $u = U/m$, strain $e = x/l$ and specific stress $f = F/(m/l)$, we can express the relation in terms of a specific modulus E :

$$u = \frac{1}{2} K (l^2/m) e^2 = \frac{1}{2} E e^2 \quad f = E e \quad (20.14)$$

The simplicity of the structure and the small-strain assumption cause the extension to follow Hooke's Law, with a modulus E that is the same for the fibre as for the molecule and is given in terms of basic features of the atomic bonding by $K(l^2/m)$.

The repeat-unit mass m is known from the chemistry, and the repeat length l is given by standard atomic dimensions, or, more exactly, on allowing for some distortion due to neighbouring interactions, by theoretical calculation or measurement on the crystal lattice. The force constant K can be estimated from spectroscopic measurements, which give natural vibration frequencies, or by calculation from interatomic potentials.

In a molecule such as polyethylene, illustrated in Fig. 20.20(c), most of the elongation will come from a change in bond angle θ , with a smaller contribution from change in bond length s . If the energy changes $U(\theta)$ and $U(s)$ due to changes in θ and s are known, including any corrections due to changing interactions with other neighbouring

atoms, then K can be determined. Details of such analyses go beyond the scope of this book, but the following outline indicates the basis of the method.

The geometry is defined by:

$$l = s \sin (\theta/2) \quad (20.15)$$

$$x = dl = \sin (\theta/2)ds + \frac{1}{2}s\cos(\theta/2)d\theta \quad (20.16)$$

The energy relations are defined by:

$$U = U(s) + U(\theta) = \frac{1}{2}K_s(ds)^2 + \frac{1}{2}K_\theta(d\theta)^2 \quad (20.17)$$

where K_s and K_θ are the force constants for bond length and bond angle changes, respectively.

Equilibrium will occur at a minimum-energy state given by:

$$\left(\frac{\delta U}{\delta \theta} \right)_s = 0 \quad \left(\frac{\delta U}{\delta s} \right)_\theta = 0 \quad (20.18)$$

Hence the equations can be solved, and the division of the deformation between ds and $d\theta$ determined, together with the value of K in the expression $U = Kx^2$.

There is some uncertainty in the parameters used in the determination of the axial modulus in a perfect polyethylene crystal, and estimates range from 220 to 380 GPa [21], 300 GPa being a commonly accepted value.

Generally, in linear polymers, the modulus of the perfect structure will depend on the molecular geometry, and the calculations are more complicated when there are many atoms in the repeat unit. The most efficient system would consist of a chain of atoms in line, so that the only mode of extension was change in bond length. There is no complete occurrence of this geometry, but, where it occurs in parts of the chain, it will tend to increase the modulus. Zigzag geometry, as typified by the extended polyethylene chain, allows bond angle change to contribute to extension. Nevertheless, the polyethylene molecule is efficient, because most of the mass is in the main chain, with only light hydrogen atoms pendant to it. The modulus will be lower if there are large side groups, which contribute mass but do not help to resist elongation. Modulus will also tend to be lower if some bonds carry a higher than average load, for example, when single-bond connections carry the whole load between rings of atoms, where the load is shared. A major decrease in modulus occurs when bond rotation can contribute to elongation. This occurs in helical chains and is the reason why polypropylene has an inherently low modulus, even in a perfect structure.

On the above basis, the para-aramid molecules have the slight disadvantage from the —CO·NH— links between the benzene rings, possibly offset by the more axial orientation of some groups. The axial modulus has been estimated to be 200 GPa [22]. The influence of molecular geometry is shown by the fact that the corresponding figure for the meta-aramid is 127 GPa.

For a perfectly oriented graphitic fibre, the theoretical treatment would be similar, except that the geometrical deformation occurs in aligned planes. Values close to 1000 GPa are given for the theoretical modulus [23].

Similarly, in three-dimensional crystal structures, extension can be linked to change

in bond lengths and bond angles and the modulus calculated. But many of these materials can also be obtained as large single crystals, so that the modulus is easily measured.

Commercial fibres, of course, do not have the degree of perfection of these simplistic models. Nevertheless, in summary, we can say that, to a first approximation, all the HM-HT fibres are linear elastic, with a tensile modulus E related to the modulus E_c of an appropriately (axially) oriented single crystal by the relation:

$$E = pE_c \quad (20.19)$$

The parameter p is a measure of the efficiency of the structure in utilising the crystal properties and would be the product of a number of factors dependent on deviations from the ideal model. In special cases, such as polydiacetylene, single crystal fibres made by solid-state polymerisation, the value of p will be 1. But, in all cases, it will not be so much less than 1 that it becomes a meaningless quantity, because the deformation mechanisms are completely different, as they are, for example, in a general textile fibre such as nylon.

Some values of E_c together with typical values of E and p , are given in Table 20.2. However, in interpreting this table, it must be remembered that there is some uncertainty in the estimates of E_c and that the experimental values are for typical current fibres, selected as high-modulus variants.

20.4.2 Deviations from the simplistic theory

Table 20.2 shows that real fibres do not achieve the theoretical maximum modulus, so it is necessary to consider the factors that lead to a reduction in efficiency. In addition, the non-linearities of response of the para-aramid and HMPE fibres need explaining. There are several reasons for deviations from the ideal behaviour.

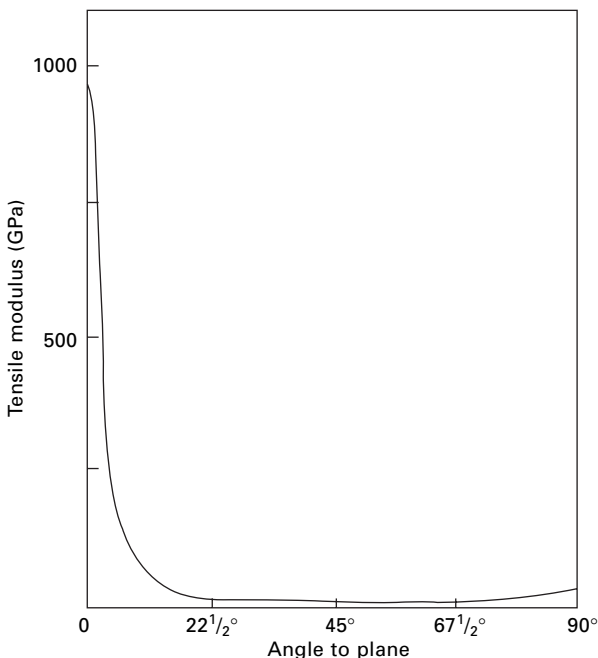
The first is disorientation. The forces between linear polymer molecules or between separate graphitic planes are much weaker than those along the covalent bonding of the chains or planes. This results in a dependence of modulus on direction. Figure

Table 20.2 Approximate tensile moduli of crystals E_c and fibres E

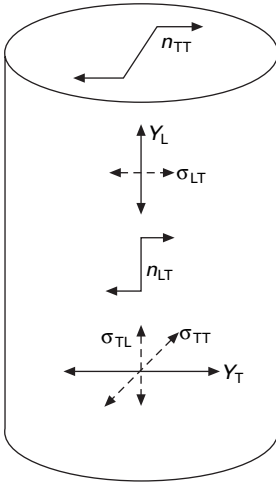
Material	Modulus (GPa)		Specific modulus (N/tex)		p
	E_c	E	E_c	E	
Polyethylene	300		310		
<i>Spectra</i> 1000		175		180	0.50
Para-aramid PPTA	200		140		
<i>Kevlar</i> 149		145		100	0.73
Graphite	1000		550		
<i>Grafil</i> HM-S/12K		400		220	0.39
Silicon carbide	700		250		
<i>Nicalon</i>		200		80	0.29
Alumina	530		130		
FP		380		100	0.72

20.21 illustrates this for the variation of Young's modulus with direction in a graphite crystal: at 8° inclination, the modulus has fallen to about one-tenth of the 0° modulus, and at 45° to almost one-hundredth. Consequently, any disorientation within carbon fibres will lead to a reduction of stiffness, the modulus being an appropriate average of the moduli at the orientations present in the fibre. In the para-aramid poly phenylene terephthalamide (PPTA), the transverse modulus of the crystal is reported to be 4.08 GPa [24], which is one-fiftieth of the axial modulus. In polyethylene, the crystal moduli have been calculated [25] to have values, given in the terminology of Fig. 20.22 as: $Y_L = 325$ GPa; $Y_T = 12\text{--}14$ GPa; $n_{TT} = 6$ GPa; $n_{LT} = 2\text{--}3$ GPa. The range of values for Y_T and n_T depend on the particular transverse direction in the crystal. A general theory of the effect of orientation is given in the next section.

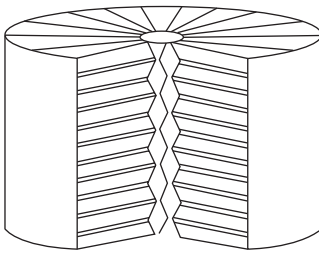
A second reason for a reduction in stiffness is what might be termed crumpled disorder of the molecules, or, on a larger scale, defects within the structure. In either case, the initial application of tension leads to a tightening-up of the structure as the buckling of the molecules is pulled out and the structure becomes more compact. This effect will be most pronounced at lower stresses and so will lead to the increasing slope of the stress–strain curve found in para-aramid fibres. The crumpling may be irregular but in the para-aramid fibres is believed to be due to the regular pleated structure shown in Fig. 20.23. As stress is increased, there is progressively less pleat to pull out. The processing that gives the higher-modulus versions changes the structure and reduces the effect. If the compacting of the structure involves the breaking of hydrogen bonds in order that molecules may slip and rearrange, then the extension will be time dependent. This explains the creep.



20.21 Variation of modulus of perfect graphite crystal with direction [6].



20.22 Elastic constants of a transversely isotropic system.



20.23 Radial pleated structure of a para-aramid fibre (Kevlar).

A third reason for the reduction in fibre modulus is slip near the ends of the molecules. At a chain end, the tensile stress must be zero, but it can build up owing to shear forces from neighbouring molecules. A simple analysis [3] shows that this would lead to a factor equal to $1 - \frac{1}{2} [(f/f_b)/AN]$ in the expression for p in equation (20.19), where f is the applied tensile stress, f_b is the bonding shear stress, A is the aspect ratio of a repeat unit, and N is the degree of polymerisation, giving AN as the aspect ratio of the molecule. The important features of this result are (1) that the reduction in modulus is less for a high molecular weight polymer and (2) that the reduction increases with stress and causes the stress–strain curve to soften at high stresses. This explains the behaviour of HMPE. The associated creep would be due to the fact that, even at room temperature, but to a greater extent at higher temperatures, a certain equilibrium concentration of defects, namely kinks of various sorts in the molecules, will be present. Under the influence of thermal vibrations, these will move through the system and allow the slow movement of chains past one another.

Computational molecular modelling is the way forward for more exact predictions of the stress–strain behaviour of HM–HT polymer fibres. Dynamic molecular modelling of thermotropic polyesters has been carried out by Johnson *et al.* [26].

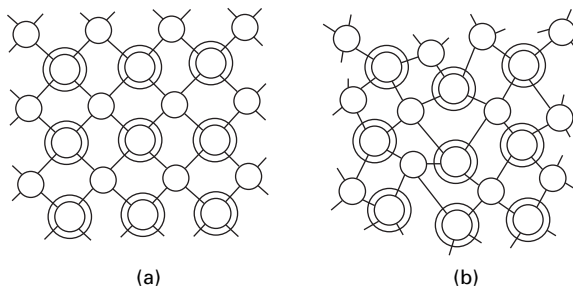
The effects so far described apply to the one- and two-dimensional molecular

materials. The situation is somewhat different in the three-dimensionally bonded ceramic fibres. Here the modulus will be reduced because there are easier modes of deformation in an irregularly bonded material such as amorphous silicon carbide (Fig. 20.24(b)) or glass (Fig. 20.25) than there are in the regular crystal of Fig. 20.24(a). Detailed analysis would require a proper description of the disordered packing of the atoms. In a polycrystalline material, deformation will be somewhat easier at grain boundaries.

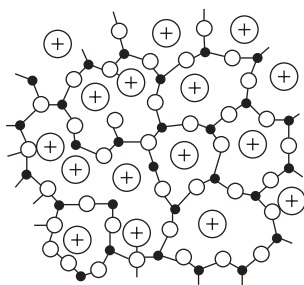
20.4.3 Strength

Theoretical analysis of fibre strength and detailed understanding of how and why strengths fall below maximum possible values are not easy. The basic theory of the tensile strength of a perfect crystal was described in Section 20.1.2 and suggests that the maximum strength should be about 0.1 times its modulus. Among the factors that lower modulus, disorientation and slip at the ends of molecules will also lower strength, but the removal of crumpled disorder at low strains will not. Any non-uniformity in the distribution of stress between different parts of the structure will lower strength.

Failure is a competitive phenomenon, determined by extreme-value and not central-



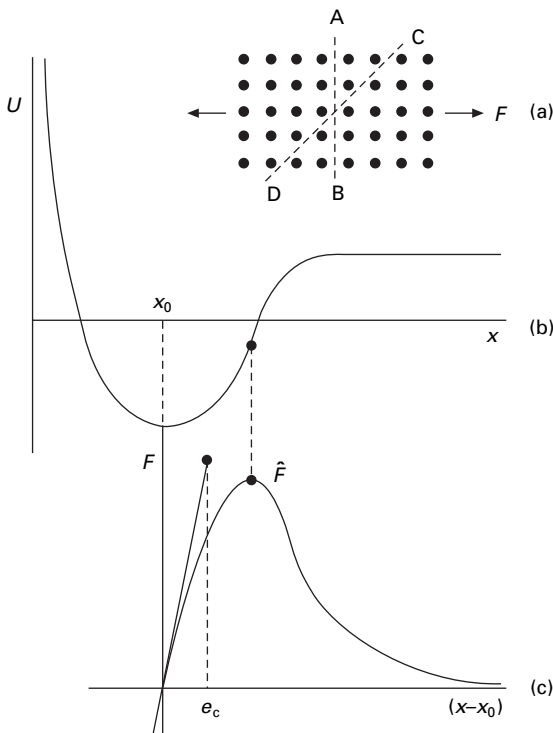
20.24 Schematic two-dimensional representation of the structure of a material such as silicon carbide: (a) crystalline; (b) amorphous. In the actual material, the atoms are distributed over three dimensions, to give a more complicated network.



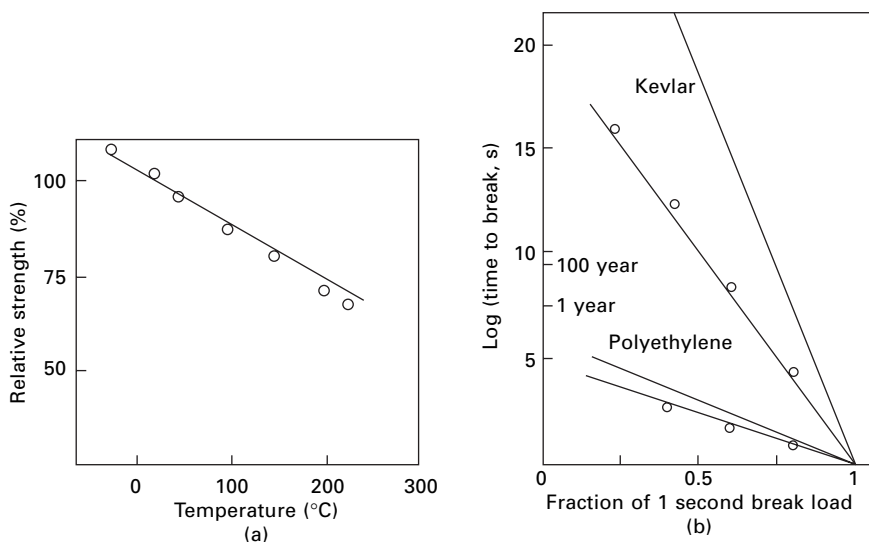
20.25 Schematic representation of the structure of glass, composed of silica, SiO_2 , and metal oxides.

value statistics, and will always occur in whichever way is easiest. Even at the theoretical level of a perfect crystal, this means that rupture may occur not under tensile stress across the plane AB in Fig. 20.26(a) but under some other stress, such as the resolved shear stress across CD. At the practical level, there are all the complications of local variations in stress due to gross structural differences, of stress concentrations at microscopic defects, and of uneven sharing of load at the molecular level in an imperfect structure.

The simple argument also ignores the time dependence associated with thermal vibrations, which allows jumps over the point of inflection as discussed in Section 20.7.2. Some detailed modelling by Termonia and Smith [24] predicts the results shown in Fig. 20.27 for the variation of strength of PPTA with temperature, compared with experimental values for *Kevlar*, and of the variation with time at room temperature predicted for PPTA and polyethylene. The predictions are, of course, very dependent on the choice of input parameter used in the computational modelling: there is a major effect of activation energies for bond breakage and a less effect for activation volume. The authors' conclusion that fracture in both PPTA and polyethylene is initiated through primary-bond breakage is not immediately compatible with the explanation of breakage that comes from the morphology.



20.26 Simple theory of tensile strength: (a) perfect crystal under tensile force F ; (b) variation of internal energy U with spacing x ; (c) variation of force F with elongation $(x - x_0)$.



20.27 Theoretical model predictions by Termonia and Smith [24], (a) change of strength of PPTA (*Kevlar*) with temperature (full lines show experimental results); (b) variation of time to break at different stress levels at room temperature for PPTA (*Kevlar*) and polyethylene (full lines indicate range of experimental results).

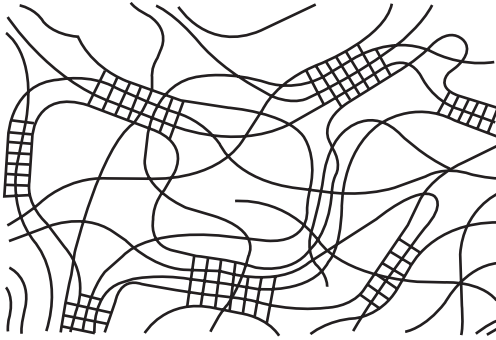
20.4.4 Elastomeric fibres

At the other end of the performance limits from HM–HT fibres, we have elastomeric fibres, which show good elastic recovery up to high extension. Natural rubber follows the standard network theory described in Section 20.1.2. Spandex fibres, with *Lycra* as one example, are composed of segmented polyurethanes in the form of block copolymers. The hard segments crystallise, and the soft segments provide rubbery linkages between the crystallites. The structure is thus an unoriented fringed-micelle form with the crystallites widely separated by amorphous regions, as suggested in Fig. 20.28. A development of the network theory in Section 20.3.2, which included crystallite rotation, may be applicable.

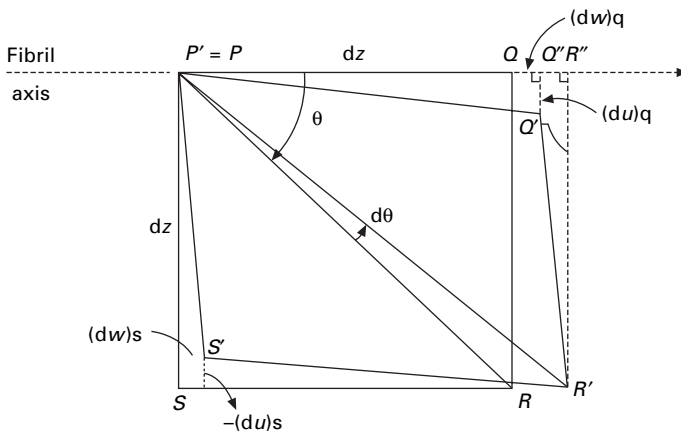
20.5 A general theory of orientation

Northolt (27) presented a theory of the effect of orientation, which was first applied to predict the modulus of highly crystalline, highly oriented polymer fibres, such as the para-aramid PPTA (*Kevlar*, *Twaron*). The theory has since been developed to be more rigorous (28), to include yield, hysteresis and creep and to be applicable to semicrystalline fibres of cellulose, nylon and polyester (29–32). The full tensor analysis is too long to be given here, but the essential principles can be explained.

The model is assumed to be made up of structural units at angles given by an orientation distribution. In the original version for PPTA, the units were long crystalline blocks, referred to as fibrils, which were variously oriented in the fibre. A particular



20.28 An unoriented fringed micelle structure with crystallites separated by coiled chains.



20.29 Deformation of a structural unit, based on a diagram by Northolt and van der Hout [28].

form would be the zigzag pleated structure shown in Fig. 20.23, where all the molecules are locally oriented in the same direction but switch from one direction to another. In other cases, it is necessary to take account of the distribution of orientation and use an appropriate mean value. For the semicrystalline fibres, the units are better viewed as blocks of material with locally parallel crystallite orientation, but different orientations in different blocks. There is evidence that nylon and polyester fibres consist of local domains varying in crystalline orientation, but with a constant orientation in each domain (see Section 1.7.2). The blocks contain quasi-fibrils with an alternation of crystalline and amorphous material. The fibrils are separated by amorphous regions in parallel with the fibrils.

For a fibre subject to uniaxial stress f giving an axial extension and a lateral contraction, Fig. 20.29 shows the deformation of a unit that is at an angle θ to the fibre axis. In addition to its axial strain and lateral strain, the rotation of the unit direction causes a shear strain of the unit. The magnitudes of the strains are expressed by the strain tensor, which depends on the geometry of the deformation. An analysis

shows that the modulus E of the fibre at any strain is given in terms of the axial modulus E_u of the unit, the shear modulus G_u and what is described as an unusual (*sic*) parameter of the orientation distribution [28] by an additive expression for compliances:

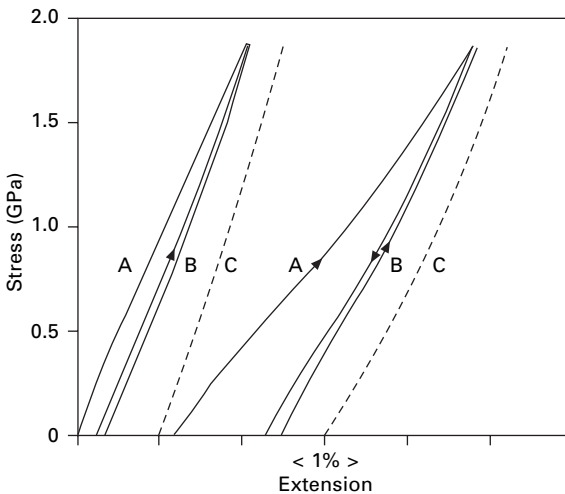
$$\frac{1}{E} = \frac{1}{E_u} + \frac{\langle \sin^2 \theta \rangle}{2 G_u} \quad (20.20)$$

$$\langle \sin^2 \theta \rangle = \frac{\int_0^{\pi/2} P(\theta) \sin^2 \theta \cos \theta \, d\theta}{\int_0^{\pi/2} P(\theta_0) \cos \theta_0 \, d\theta} \quad (20.21)$$

where $P(\theta_0)d\theta_0$ is the initial fraction of units with an orientation angle between θ_0 and $(\theta_0 + d\theta_0)$ and $P(\theta)d\theta$ and $P(\theta)d\theta_0$ gives the fractions after extension.

For highly crystalline fibres, such as the para-aramids, E_u and G_u would equal the crystal moduli E_c and G_c . This would give a contribution to p in equation (20.19) of a factor equal to $(1 + E_c \langle \sin^2 \theta \rangle / 2 G_c)^{-1}$. As stress increases, the elongation of the specimen causes $\langle \sin^2 \theta \rangle$ to increase and thus to give an increased slope of the stress-strain curve. Fig. 20.30 shows a comparison of the predictions of the theory with experimental data for high- and low-modulus PPTA fibres (*Twaron*) with $E_c = 240$ GPa, $G_c = 2$ GPa and $\langle \sin^2 \theta \rangle$ derived from sonic moduli measured before the second extension. The increasing stiffness is particularly obvious for the more extensible fibre.

In considering the application of the theory to less highly oriented fibres, it should be noted that, owing to the presence of $\cos \theta$ in equation (20.21), $\langle \sin^2 \theta \rangle$ does not



20.30 Comparison of predictions of equation (20.20) for high- and low-modulus PPTA fibres: A, first extension; B, second extension; C, theoretical prediction. The curves all start from zero extension, but are displaced for clarity. From Northolt and Hout [28].

show a simple increase with θ . Some other approximations applicable to highly oriented fibres may not be valid and the full theoretical derivation should be followed.

Figure 20.31 is a schematic representation of the yield process in polyester, cellulose and similar fibres, showing the sequence from zero to increasing stress f . The initial distribution of orientations first shows small changes in angle, but then progressively yields to an angle θ_4 . The yield theory [31] uses an affine deformation of an isotropic material dependent on draw-ratio λ to give values for $\langle \sin^2 \theta_0 \rangle$. If the analysis is simplified to a bundle of parallel units at a constant orientation angle θ_a , given by the average of the distribution, the yield strain e_y is given in terms of the shear yield stress f_g by:

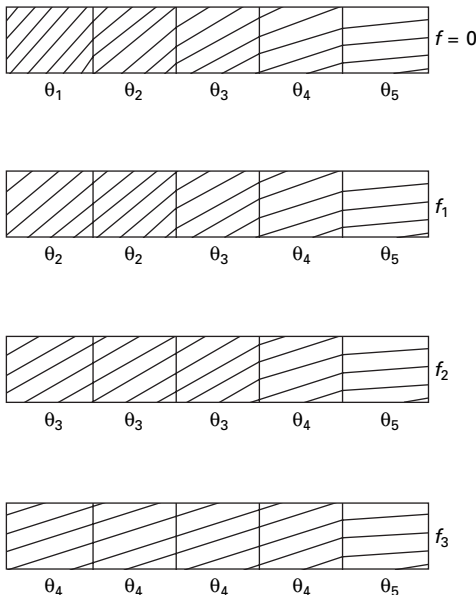
$$e_y \approx \left[\left(\frac{1}{E_u} \right) + \left(\frac{\langle \sin^2 \theta_0 \rangle}{2 G_u} \right) \right] \left(\frac{f_g}{\sin \theta_a \cos \theta_a} \right) \quad (20.22)$$

For fibres with low and medium orientation:

$$e_y \approx \frac{1}{2} f_g \tan \theta_a \quad (20.23)$$

For well-oriented fibres such as PPTA, the viscoelastic theory [32] gives the following expression for the strain $e(t)$ as a function of time t under a stress f :

$$e(t) = \frac{\frac{1}{2} k \log(t) \langle \sin^2 \theta_0 \rangle f}{[1 + (f/2G_c)]^3} \quad (20.24)$$



20.31 Schematic representation of yield. After Northolt *et al.* [31].

20.6 Structural effects in natural fibres

20.6.1 Cotton and other plant fibres

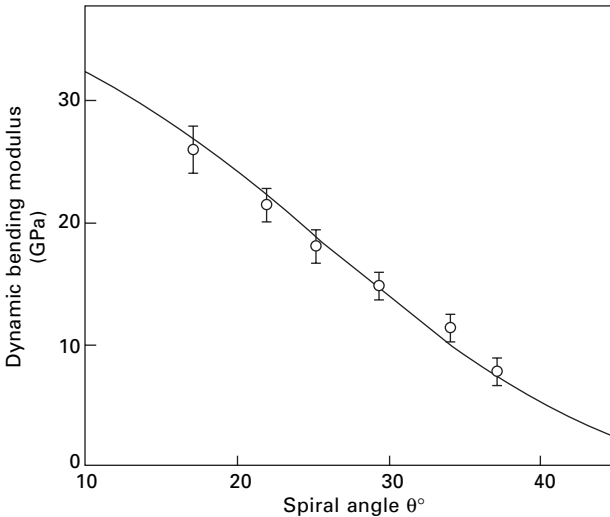
Vegetable fibres have a specialised structure of crystalline fibrils spiralling around a central axis. Analysis of the mechanics of such a system has many similarities to that of twisted-yarn mechanics [33]. In such systems, the resistance to extension decreases as the helix angle increases. There are two reasons. For a given axial strain in the system as a whole, the tensile strain in the elements is less at higher angles, and at higher angles, there is a reduced contribution to the total tension. An analysis by Hearle [4], which considers both the extension of the crystalline fibrils and the possible reduction in volume, by means of a minimum energy method, gives the following results for an assembly with a constant helix angle at all radii throughout the fibre:

$$E = E_c (\cos^2 \theta - \sigma \sin^2 \theta)^2 + K(1 - 2\sigma)^2 \quad (20.25)$$

$$\sigma = \frac{E_c \cos^2 \theta \sin^2 \theta + 2K}{E_f \sin^4 \theta + 4K} \quad (20.26)$$

where E = fibre tensile modulus, σ = fibre Poisson ratio, θ = helix angle, E_c = tensile modulus of cellulose crystal and K = bulk modulus.

Figure 20.32 shows an application of this equation to experimental results for the dynamic modulus of dry stretch mercerised cotton fibres, due to Meredith [34]. The mercerisation has caused the fibre to be a circular cylinder with a helical internal geometry in contrast to the more complicated form of natural cotton fibres discussed below. The assumed value of the moduli, 70 GPa, is of the same order as that

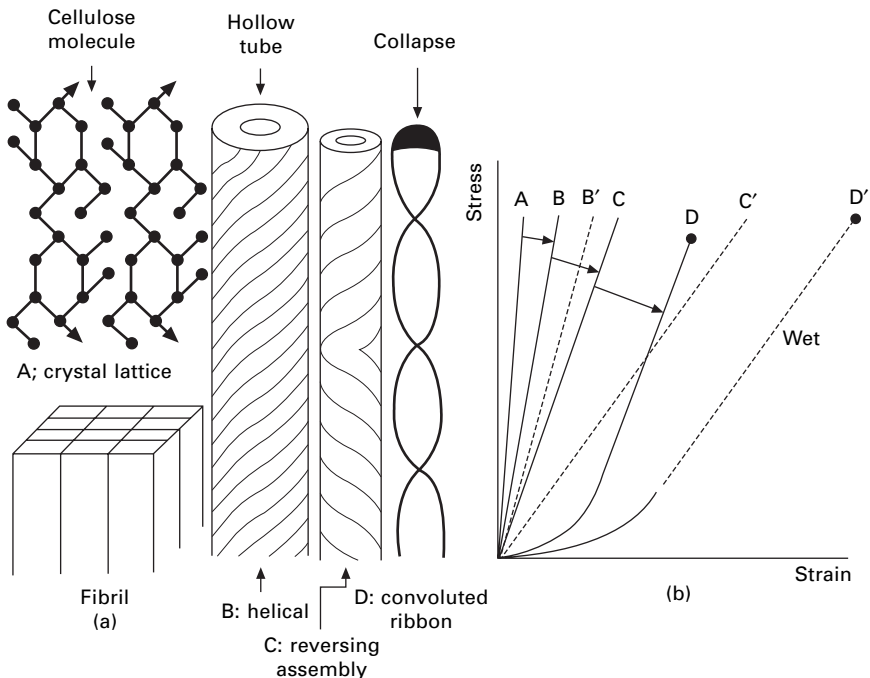


20.32 Comparison of experimental values of dynamic modulus of stretched mercerised cotton fibres at 0% r.h., 20 °C, with theoretical prediction from equation (20.25) From Meredith [34].

calculated theoretically for a crystal lattice of cellulose. Hearle [4] showed that the equation also fitted results for other plant fibres.

The complications that occur with natural cotton fibres are illustrated in Fig. 20.33, which shows how the structural features progressively modify the predicted tensile stress–strain curve. The starting point is the modulus of the crystal lattice of cellulose (A), which gives the properties of the crystalline fibrils. The helical structure in the circular hollow fibre as formed (B) leads to a lowering of modulus as described above. Although there are small changes of helix angle through the fibre, it is reasonable to take a constant value of 21° . However, in cotton, there are reversals of the helices from left-handed to right-handed helices (C). Under tension, a twisted structure will untwist, unless prevented from doing so, and lead to increased length. Free untwisting can occur at the reversals and add to the fibre extension. Finally, there are the convolutions (D), which, as shown in Section 13.5.2, are pulled out under tension. The convolutions provide another mode of extension, which leads to the curvature of the stress–strain curve of cotton. In the dry state, deformation is inhibited by hydrogen bonding between fibrils, but when wet this resistance to deformation due to shear stiffness is reduced leading to lower stresses.

A quantitative theory of the above effects, with some simplifying assumptions has been given by Hearle and Sparrow [35]⁶. The simple theory of twisted yarn mechanics



20.33 (a) Structural features of cotton fibres. (b) Development of tensile stress–strain curves. From Hearle [16].

⁶The full analysis includes a volume energy term, but surprisingly energy minimisation shows that extension is at constant volume.

[36] which is the basis for equation (20.25), neglects any resistance to shear, but this is taken into account in a more advanced treatment [37]. For a tensile strain e of the helical structure (B), the crystalline fibrils have a tensile strain e_c and a shear strain s_c , due to change of helix angle, given by:

$$e_c = e (\cos^2 \theta - \sigma \sin^2 \theta) \quad s_c = -e (1 + \sigma) \sin \theta \cos \theta \quad (20.27)$$

A fractional rotation $(-\gamma e)$ adds additional terms to the tensile and shear strains, so that the total strain energy per unit volume (or unit mass for specific quantities) is given by:

$$U = \frac{1}{2} e^2 \{ E_c [\cos^2 \theta - (\sigma + \gamma) \sin^2 \theta]^2 + G_c [(1 + \sigma + \gamma) \sin \theta \cos \theta]^2 \} \quad (20.28)$$

where G_c = relevant shear modulus of cellulose crystal.

The value of γ , which is found by energy minimisation ($dU/d\gamma = 0$), is given by:

$$\gamma = \frac{E_c - G_c \cos^2 \theta}{E_c \sin^2 \theta + G_c \cos^2 \theta} - \frac{1}{2} \quad (20.29)$$

Substitution and differentiation of equation (20.28) gives;

$$f = Ee = \frac{E_c - G_c \cos^2 \theta}{E_c \sin^2 \theta + G_c \cos^2 \theta} \quad (20.30)$$

This is the line C in Fig. 20.33(b). In the wet state, the shear modulus will be lower because fibrils can slip past one another, thus reducing the fibre modulus E . The simple expression would not apply when there is large untwisting. In the limiting state with $G_c = 0$, there would be complete untwisting, which would be determined by geometry.

As convolutions have a major influence on the stress-strain curve of cotton. Hearle and Sparrow [35] modelled the effect by using the converse of a relation given by Timoshenko [38] for the contraction of a ribbon due to twisting:

$$e = -\left(\frac{\phi^2}{2}\right)\left(\frac{b^2}{12}\right) + \frac{f}{E} \quad (20.31)$$

where e = strain, ϕ = twist in radians per unit length, b = ribbon width, f = tensile stress and E = Young's modulus of the material.

It is necessary to take account of the resistance to the untwisting. An approximate analysis of the mechanics gives the following relation between tensile stress f and the strain e_{con} due to untwisting of convolutions, which have an angle of ω :

$$f = k \left[\frac{\tan \omega}{(\tan^2 \omega - e_{\text{con}}/X)^{1/2} - 1} \right] \quad (20.32)$$

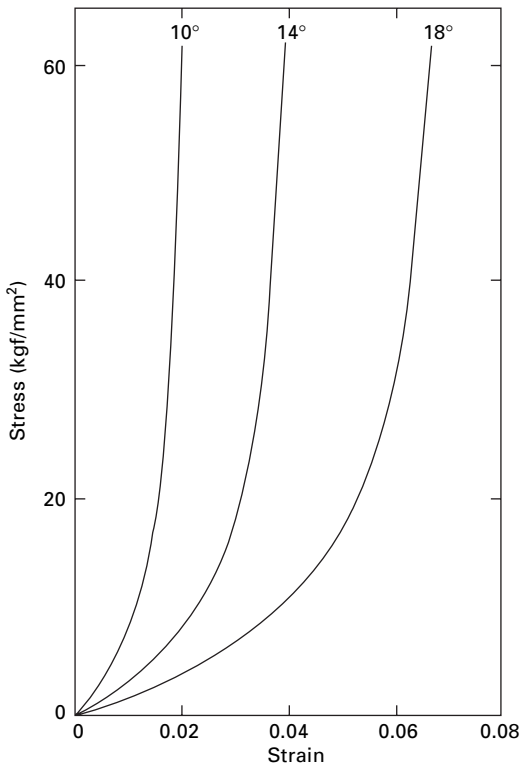
where $k = (\eta A G_c / \pi b^2 X)$ and η is a shape factor, A is area of cross-section and X is a factor taking account of differences in the shape of a cotton fibre.

Data on cross-sections by House [39] and torsion by Meredith [40] suggest that η

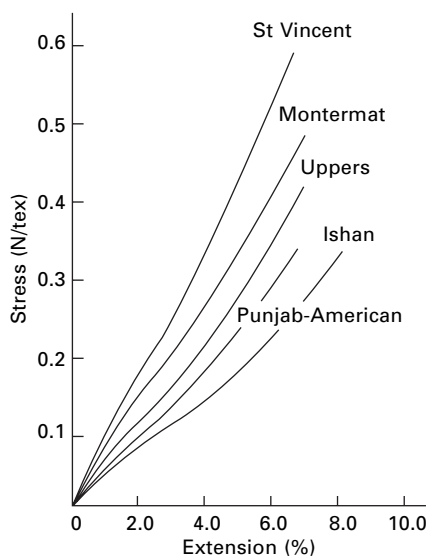
$= 0.56$, $A/b^2 = 0.27$ and $G = 250$ GPa. A plot of breaking strain against convolution angle indicates that X is about 0.67, which gives $k = 18$ GPa. Owing to differences in cotton types, there will be a wide range of values of k . With $k = 100$ there is little curvature in the stress–strain curve; with $k = 5$, the curve changes from a low slope to a high slope at around 3% extension. Figure 20.34 shows that the strain due to pulling out of convolutions for different values of ω with $k = 20$. These can be compared with the curvature in Fig. 20.35. The mechanisms for A, B and C in Fig. 20.33 all give linear plots at the small strains involved; the curvature comes from the convolutions and, as shown in Fig. 20.36 is lost when the convolutions have been removed.

For cotton fibres clamped at short lengths, untwisting at reversals would be prevented and the modulus would be higher.

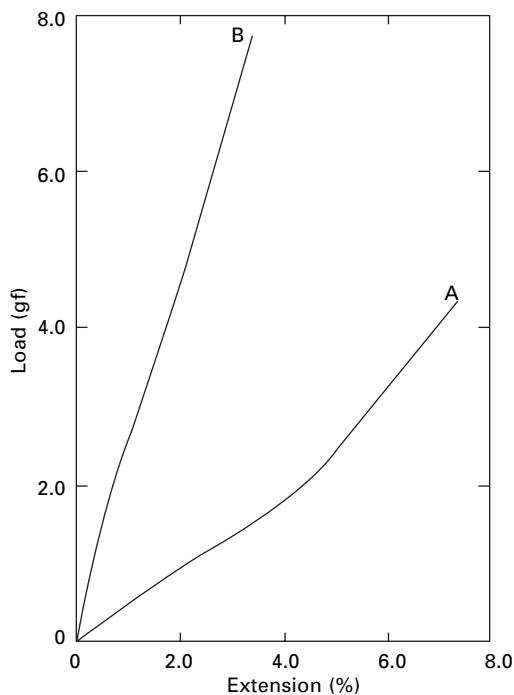
In considering the tensile failure of cotton fibres, there are three separate modes that can occur. When the fibrils are firmly bonded together, as in completely dry or resin crosslinked cotton, fracture occurs by cracks running across the fibre, which are presumably due to tensile failure of the crystalline fibrils. At medium humidities, splits develop between fibrils and the material between successive turns of the split tears. The fracture extends over a long length, influenced by the geometry of the collapsed fibre. In wet cotton, the fibrils are so separate that they break individually.



20.34 Strain due to pulling out of convolutions for different convolution angles ω . From Hearle and Sparrow [35].



20.35 Stress–strain curves for various cottons. From Sparrow [41].



20.36 Load–extension curves of Acala cotton: A Normal fibre, B after stretching wet and drying to remove convolutions.

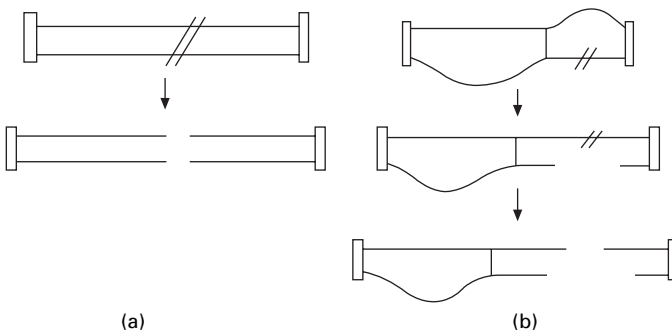
The reason why wet cotton is stronger than dry is probably mainly the relief of shear stresses that can occur by the untwisting and unbending of the fibre. When the fibrils are bonded together, the complex stresses lead to early breakdown, but when they are free to move and relieve stresses, the fibre is stronger.

Another way of regarding the situation is by considering the sharing of load between molecular chains or fibrils. An analogous system of two elements is shown in Fig. 20.37. With a crosslink present, each element breaks separately, and the strength will be half the value that it would be without the crosslink when both elements have to be broken together. Because the molecules in native cellulose are very long ($DP > 10\,000$), the effect of easier slip at chain ends will be negligible, and thus the main reason why rayon is weaker when wet will not be operative.

20.6.2 Wool and hair fibres

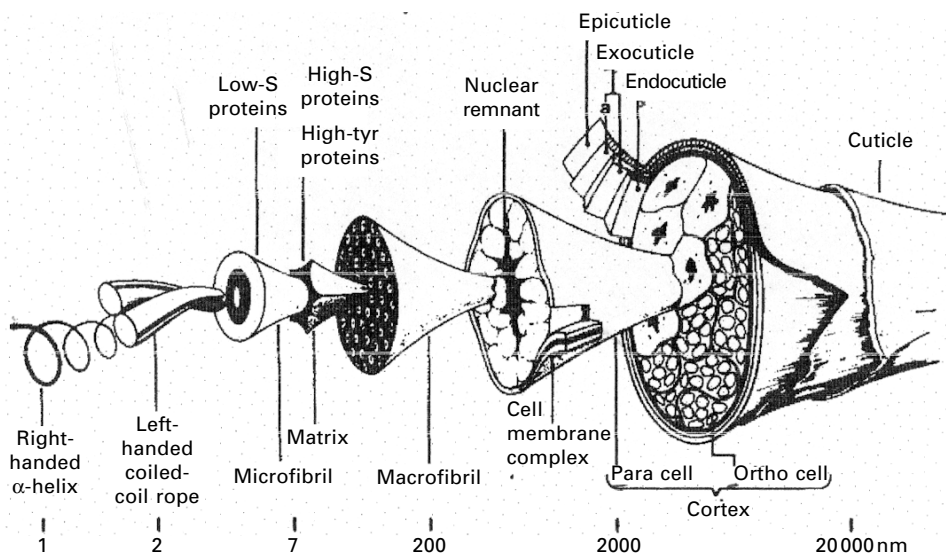
As shown in Fig. 20.38, there are many structural levels from the protein molecules to whole wool and hair fibres⁷. All of these have some influence on mechanical properties. Figure 20.39 shows a scheme for a total mechanical model of a wool fibre. Ideally, the starting point would be computational dynamic modelling of the properties of the protein molecules, but the technology is not yet sufficiently advanced to do this for the complexity of keratin and keratin-associated proteins, though small segments might be modelled. However, there is enough understanding and practical information to model all higher levels, at least to a first approximation, but the programming has not been done [42, 43].

Since the various units of the structure are in parallel, a simple mixture law can be applied in parts of the analysis. The macrofibril assembly and the cell assembly probably have only a small influence on mechanical properties, though slip between cells may be one cause of low strength in some wools [44] and is one likely cause of transverse yielding at low stress, which has been observed in rhinoceros horn and porcupine quill. Prediction of bending and twisting resistance would follow the usual

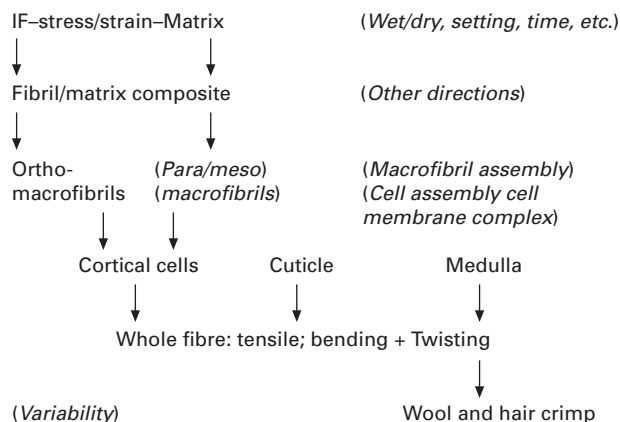


20.37 Rupture of two chains: (a) without link; (b) with a crosslink.

⁷In the remainder of this section the use of the word *wool* also covers in a general way hair fibres, including goat, camel and other hairs used in textiles and human hair.



20.38 Structure of wool fibre, as drawn by Robert C. Marshall, CSIRO, Melbourne.

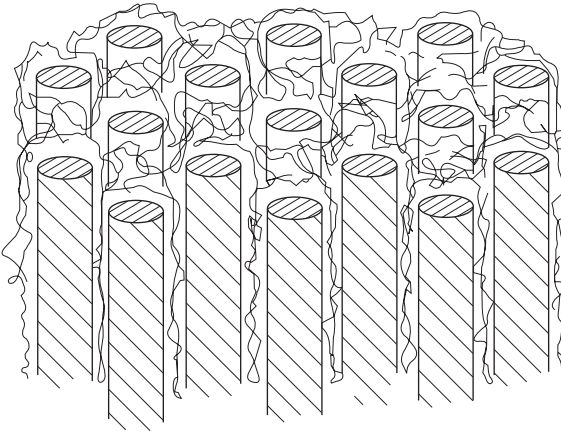


20.39 Scheme for modelling the total mechanics of a wool fibre. Entries in italics in parentheses are supplementary to the main scheme.

treatment for a multicomponent fibre with an increasing influence of outer layers. A three component model of cuticle surrounding the ortho- and para-cortex has been modelled by Liu and Bryson [45]. Unfortunately, knowledge of the properties of the cuticle is limited.

The two parts of the model that are best understood are the tensile stress-strain curve based on the behaviour of the fibril/matrix composite and the explanation of crimp in terms of the difference between the macrofibrils in the ortho- and the para-cortex.

A simple parallel two-phase model (Fig. 20.40) was first proposed by Feughelman



20.40 Simple two-phase fibril-matrix model of fine structure of wool.

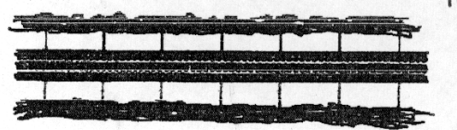
[46]. It explains the low strain behaviour, including shear having a lower modulus than extension, and the onset of yield. A model for the whole stress-strain curve in extension and recovery was derived by Chapman [47] and has been shown to be valid in a comparison with two alternative models [48, 49].

The Chapman model represents the two-phase model by crystalline fibrils in the α -helical form linked at intervals to an amorphous matrix⁸ (Fig. 20.41(a)). This zonal model was originally used to simplify the analysis, but later research showing that the heads and tails of the keratin molecules protrude into the matrix makes it a better model than one with continuous coupling. The fibrils follow the mechanics shown in Fig. 20.1 for an $\alpha \leftrightarrow \beta$ transition from a helical to an extended chain form, characterised by an initial modulus, and critical and equilibrium stresses for the transition (Fig. 20.42(a)). In wet wool, the matrix is assumed to be a moderately highly crosslinked rubber. Chapman [49] showed that the matrix stress-strain curve could be derived from the stress-strain curves of supercontracted wool in Fig. 20.42. In the first stage, the crystalline fibrils are disrupted, so that the stress-strain curve is dominated by the matrix. There is some residual stress from the fibrils, which remains after second stage, when it is assumed that the matrix contribution is lost. Subtracting the second stage curve from the first stage curve gives the matrix stress-strain curve, as shown in Fig. 20.43. Up to 35% extension, the curve follows the theoretical rubber elasticity curve given by equation (20.6). At larger extensions, the curves diverge due to breakage of cystine crosslinks, which allows greater extension and eventual break of the network. The matrix stress-strain curve is included in Fig. 20.42(a).

Initial extension is controlled by the elastic modulus of the helical crystals with a small contribution from the matrix (Fig. 20.41(a)). At 2% extension, the critical stress is reached and an $\alpha \leftrightarrow \beta$ transition starts in one of the zones (Fig. 20.41(b)). The stress in the fibril falls to the equilibrium value and the difference is taken up by an

⁸In the biological literature, the fibrils are referred to as *keratin intermediate filaments* and the matrix is composed of a collection of *keratin-associated proteins*.

From 0% to 2%: uniform extension: at 2% intermediate filaments reach critical stress



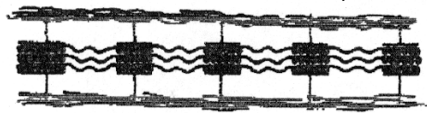
(a)

From 2 to 30%: zones open in succession: in open zone intermediate filament at equilibrium stress, matrix at 30%



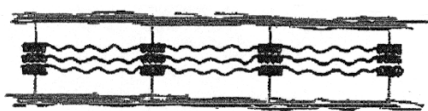
(b)

At 30% extension, all zones open



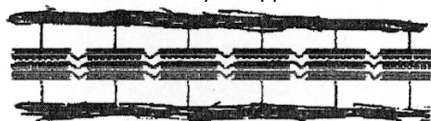
(c)

Beyond 30%, intermediate filament at equilibrium, matrix stress rises



(d)

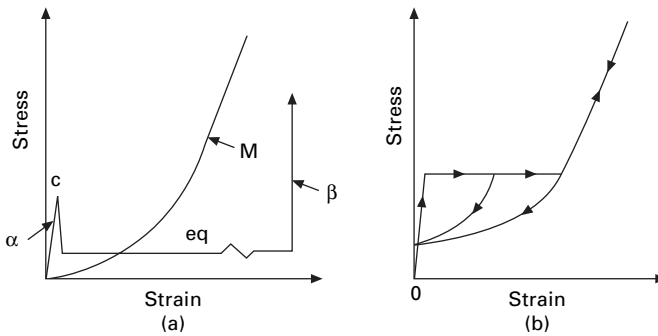
In recovery, intermediate filaments at equilibrium stress; all zones contract until they disappear



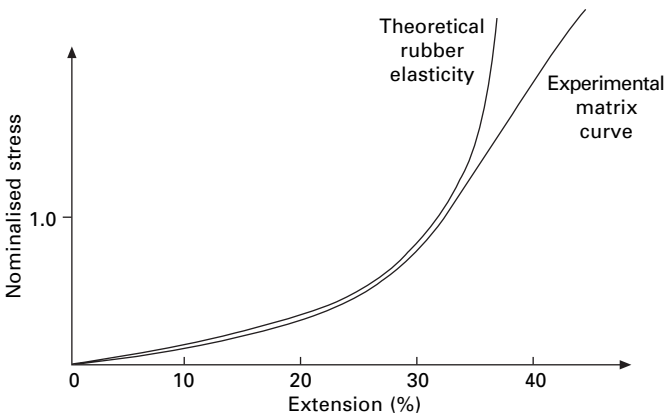
(e)

20.41 Sequence of changes in the Chapman model. From Hearle [48].

additional 28% extension of the matrix. The process continues in successive zones until all have been opened at 30% extension (Fig. 20.41(c)). Further extension then follows the line of the matrix curve plus the equilibrium stress in the fibrils (Fig. 20.41(d)). At 40–50% extension, the stress is high enough to cause rupture of the amorphous network and trigger fibre breakage. In recovery, the stress follows the matrix curve down to 2% extension, since the α and β forms remain in equilibrium (Fig. 20.41(e)). Below 2%, the initial curve is rejoined, Fig. 20.41(a). With the controlling parameters listed in Table 20.3, the predicted stress–strain relations, which



20.42 (a) Stress-strain relations: at a critical stress (c), fibril changes from helical α -crystal to extended chain β -crystal with equilibrium stress (eq); matrix (M), follows a rubber elasticity curve.



20.43 Matrix stress-strain curve derived from supercontraction experiments compared with rubber elasticity curve. Stress is normalised by stress in wet wool at 15% extension. From Chapman [49].

are shown in Fig. 20.42(b), have good agreement with the experimental results for wet wool in Fig. 20.44. The differences are in some rounding of the sharp changes and a small positive slope in the yield region. Both effects can be explained by variability in wool fibres. The simple Chapman model considers only the fibril/matrix composite and assumes that it is parallel to the fibres axis. In reality, there is a helical orientation in the macrofibrils of the ortho-cortex, which must be taken into account together with other features of the total model for wool.

Developments of the Chapman model explain other features of wool. Hearle and Susitoglu [50] showed that the addition of viscous dashpots would model time dependence. The influence of water and the setting of wool were explained by Hearle *et al.* [51]. As moisture content is reduced, the hydrogen bonds form between peptide and other groups in the matrix. By subtraction of the fibril contribution, the matrix stress-strain curves can be calculated for the initial and post-yield regions and then interpolated for the intermediate regions (Fig. 20.45). The initial stiffening up to a

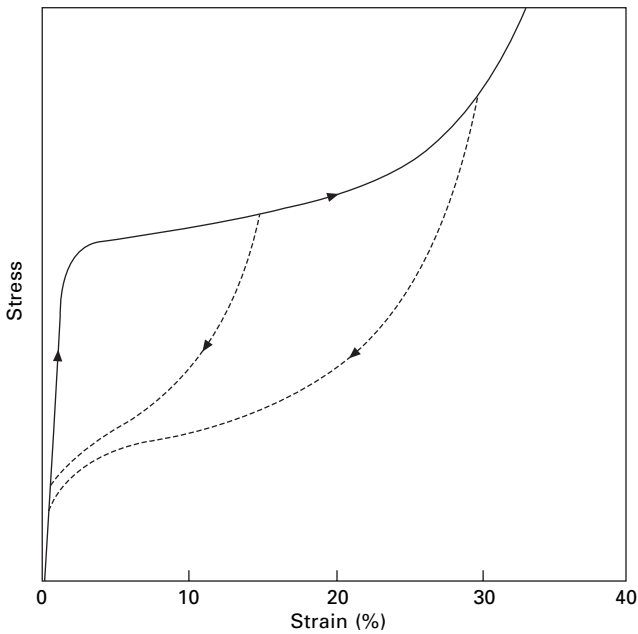
Table 20.3 Controlling parameters for the Chapman model

Parameter	Value	Determines	Notes
<i>Microfibrils</i>			
α modulus	1.75 GPa	Initial fibre modulus (plus small matrix contribution)	Similar to theoretical calculation
Critical stress $\alpha \rightarrow \beta$ transition	35 MPa	Fibre yield stress (plus small matrix contribution)	Reasonable at 2% strain
Equilibrium stress $\alpha \rightarrow \beta$ transition	7 MPa	Junction of extension and recover curves	Reasonable on basis of Fig. 13.43
β modulus	1.75 GPa	Additional microfibril extension in post-yield region	Actually higher; negligible effect
$\alpha \rightarrow \beta$ strain	80%	Extension in opened zones	From X-ray diffraction experiments; less than ideal α -helix
<i>Matrix</i>			
# Non-linear stress/strain	See Fig. 20.43	Post-yield and recovery curves (plus microfibril contribution)	From supercontraction experiments & rubber elasticity theory
Internal modulus	0.35 GPa	Addition to microfibril tension	Follows from #
Extension at critical stress	30%	End of yield region	Follows from #
Ideal maximum extension	40%	Limiting extension if no crosslink failure	Follows from #
Actual maximum extension	50%	Fibre break extension and strength	Greater than ideal maximum due to cystine bond break

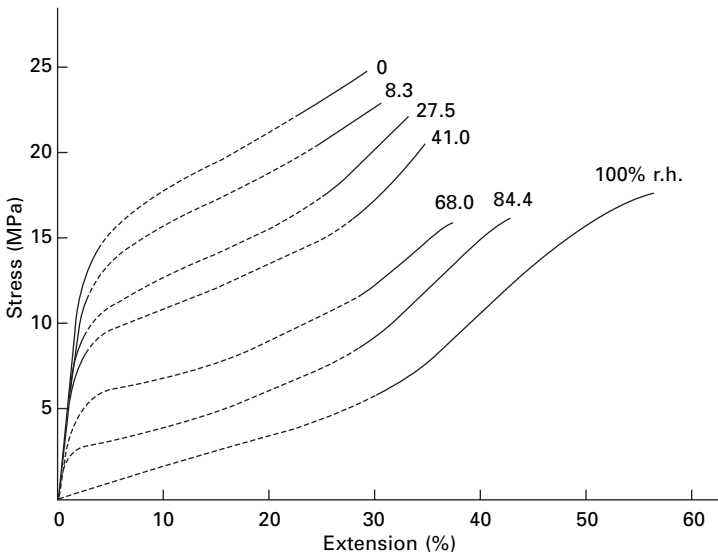
yield point and then following parallel to the curve in the wet state is typical of bonding of an amorphous polymer, as shown in Fig. 20.6 for rayon. Setting of wool depends on rupture of cystine crosslinks in the matrix and their re-formation in new places. It can be assumed to drop the matrix curve to zero stress at the setting strain. Calculated curves for set fibres then show good agreement with the positions of the beginning and end of the yield region in set fibres.

Arai *et al.* [53] presented a theoretical analysis of the rubber-like elasticity of swollen wool and hair fibres based on the inverse Langevin function. They related this to a two-phase structure and make a comparison with experimental results.

Crimp in wool results from the bi-component structure. In the para-cortex (and meso-cortex, if present) the fibril/matrix composite is oriented parallel to the fibre axis, but in the macrofibrils of the ortho-cortex, as discussed in Section 1.6.3, the fibril/matrix composite follows helical paths similar to a twisted yarn. In the wet state, the matrix is swollen by absorbed water. On drying, the fibril/matrix composite shrinks, with the fibrils coming closer together. In the para-cortex, there is no change of length, but in the ortho-cortex the macrofibrils increase in length, owing to their



20.44 Stress-strain behavior of wool in extension and recovery. The stress is in arbitrary units.



20.45 Matrix stress-strain curves at different humidities calculated by application of Chapman model to experimental data [52].

reduced radius reducing the helix angles. This means that the fibre behaves like a bimetallic strip and develops a crimp with one side increasing in length and the other staying constant. An analysis of the mechanics has been given by Munro and Carnaby [54, 55].

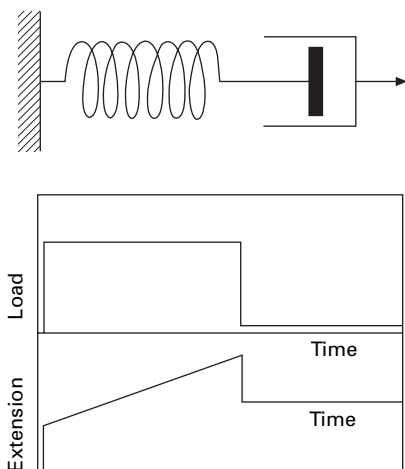
20.7 Theories of time dependence

20.7.1 Ideal springs and dashpots

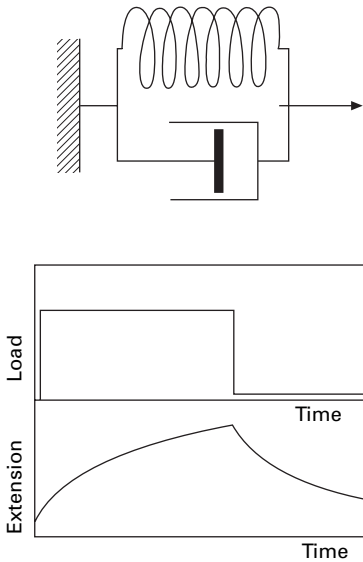
The mechanical behaviour of polymer fibres is viscoelastic, combining features of both elasticity and viscosity. The use of a parallel spring and dashpot model (or, less conveniently, a series model) in the definition of parameters to characterise experimental results has been described in Section 16.5.2. However, the numerical values obtained relate only to the particular experimental conditions and do not reflect the full complexity of the viscoelastic responses. Analysis can be carried further by the by more complicated combinations of springs and and dashpots and introducing non-linearity.

Ideal springs will follow Hooke's Law, so that stress $f = (E\varepsilon)$, where $E = \text{constant}$ and $\varepsilon = \text{strain}$, and will show perfect recovery. Ideal dashpots will follow Newton's Law, with stress $f = (\eta \, d\varepsilon/dt)$, where $\eta = \text{constant}$ and $d\varepsilon/dt = \text{rate of strain}$, and will show no recovery. If the spring and dashpot are arranged in series, as in Fig. 20.46, the model will show instantaneous extension of the spring on the application of load, followed by secondary (irrecoverable) creep of the dashpot at a constant rate; it will also show stress relaxation at constant length as the tension in the spring causes continuing elongation of the dashpot. If the units are arranged in parallel, as in Fig. 20.47, they will show primary (recoverable) creep as the extension of the spring is hindered by the dashpot; if held at constant length, there will be an instantaneous drop in tension as the viscous term ceases to contribute but the spring remains extended. The simplest model that shows qualitatively all the features of instantaneous extension, primary and secondary creep, and stress relaxation is the four-element model shown in Fig. 20.48.

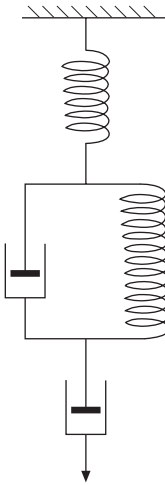
It would, however, require a very complicated arrangement of elements to give a complete representation of the behaviour of fibres, exhibiting not only the four effects mentioned, but also dynamic properties, which vary with frequency, and non-linear relations between extension, load and time. This multiplication of the number of



20.46 Spring and dashpot in series.



20.47 Spring and dashpot in parallel.



20.48 Four-element model.

elements involved is no simplification of the problem and has led Peirce [56] to say that ‘the mechanical analogy in general is an unsatisfactory substitute for direct knowledge of molecular force ... there is every reason to allow that imperfect elasticity is a proper characteristic of molecular behaviour, of more physical reality than the end-cases of ideal elasticity and viscosity’.

The use of a combination of springs and dashpots is one way of developing the theory of viscoelasticity, which can be expressed in various other forms. By combining a spectrum of elements, the theory can represent any form of variation with time. Ferry [57] describes the mathematics and its application to eight types of polymer. A

combination of ideal springs and dashpots is necessarily limited to a linear dependence on stress. If all the stress values of a given sequence are doubled, all the strain values will also be doubled. This limitation severely restricts the application of the theory to fibres.

20.7.2 Eyring's three element model: reaction-rate theory

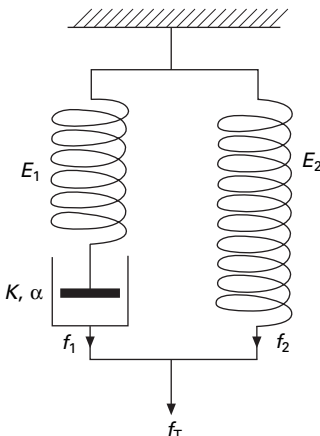
Instead of adding to the number and complexity of arrangement of ideal elastic and viscous elements, one may approach the problem by modifying the properties of the elements themselves. In the three element model put forward by Eyring and his colleagues [58, 59], Fig. 20.49, the springs follow Hooke's Law, but the dashpot shows non-Newtonian viscosity, its behaviour being represented by a hyperbolic sine law of viscous flow:

$$\frac{de}{dt} = K \sinh \alpha f \quad (20.33)$$

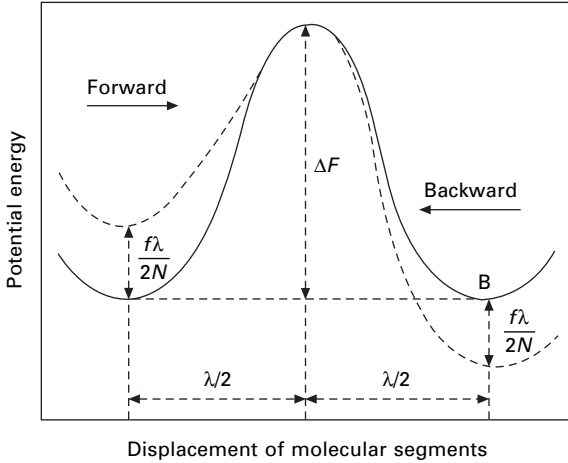
where de/dt = rate of strain, f = stress, and K and α are constants.

This means that the rate of strain increases more rapidly with increase of stress than it would do if it were proportional to stress, as in Newton's Law.

There is a justification for the use of an expression of this form in the theory of reaction rates [60]. In its application to the deformation of fibres, we assume that the strain occurs because flow units (which may be chain molecules, segments of chain molecules, or groups of segments of chain molecules) slip over one another from one equilibrium position to another when stress is applied. In order to do this, the flow unit will have to overcome a potential energy barrier, illustrated in Fig. 20.50. This barrier is called the *free energy of activation* for the flow process. In the absence of stress, let its value be ΔF . The frequency with which a flow-unit will surmount the barrier and move to a new equilibrium position is given by statistical thermodynamics as:



20.49 Eyring's three-clement model.



20.50 Potential-energy barrier for flow.

$$\text{number of moves per second} = \nu e^{-\Delta F/kT} \quad (20.34)$$

where ν is a thermal vibration frequency ($\approx 10^{13}$ Hz), k is Boltzmann's constant and T is the absolute temperature.

Since the two positions are in the same state, in contrast to the different states in Fig. 20.1, their potential energies are at the same level. In the absence of stress, there will be equal numbers of moves in opposite directions in unit time.

However, if a stress f is acting, and is distributed over N flow-units per unit area of cross-section so that the mean force applied to each unit is f/N , then it will contribute to the surmounting of the barrier an amount of work $(f/N)(\lambda/2)$, where λ is the mean distance between equilibrium positions. Conversely, for moves in the opposite direction, this amount of work must be done in addition to ΔF . Consequently, the application of stress may be regarded as equivalent to modifying the potential barrier as shown by the dotted line in Fig. 20.50. Thus we have:

$$\begin{aligned} & \text{net number of forward moves per second} \\ &= \text{number of forward moves} - \text{number of backward moves} \\ &= \nu e^{-(\Delta F - f\lambda/2kT)} - \nu e^{-(\Delta F + f\lambda/2kT)} \\ &= \nu e^{-\Delta F/kT} (e^{f\lambda/2kT} - e^{-f\lambda/2kT}) \\ &= 2\nu e^{-\Delta F/kT} \sinh f \frac{\lambda}{2NkT} \end{aligned} \quad (20.35)$$

If we multiply the net number of moves forward per second by the distance moved λ , we get the velocity of flow. In order to convert this to a rate of strain, we must divide by λ_1 , the mean distance between neighbouring flow units, measured along the direction of flow. This gives:

$$\begin{aligned} & \text{rate of strain} = d\varepsilon/dt \\ &= 2 \frac{\lambda}{\lambda_1} \nu e^{-\Delta F/kT} \sinh f \frac{\lambda}{2NkT} \end{aligned} \quad (20.36)$$

This is the full form of equation (20.33), and we see from it that:

$$K = 2 \frac{\lambda}{\lambda_1} \nu e^{-\Delta F/kT} \quad (20.37)$$

$$\alpha = \frac{\lambda}{2NkT} \quad (20.38)$$

In addition to the movement of flow units over one another, there will be an initial extension owing to the elastic deformation of the structure. If this is relieved by the flow, then it can be represented by a spring in series with the dashpot. There may also be an elastic deformation that is not relieved by the flow, which must be represented by a spring in parallel. Thus we arrive at the three element model. Various detailed structural interpretations of it are possible. One is that the dashpot represents the flow of segments of chain molecules over one another; the spring in the left-hand arm represents the elastic extension of the molecules; and the spring in the right-hand arm represents an elastic deformation of the molecular network unrelated to the viscous flow.

In the three element model, the springs will follow Hooke's Law with modulus E , so that

$$\text{strain} = \varepsilon = \frac{f}{E} \quad (20.39)$$

$$\frac{d\varepsilon}{dt} = \left(\frac{1}{E} \right) \frac{df}{dt} \quad (20.40)$$

If E_1 is the modulus of the left-hand spring and f_1 is the stress in the left-hand arm of the model, then we have:

$$\frac{d\varepsilon}{dt} = \frac{1}{E} \frac{df_1}{dt} + K \sinh \alpha f_1 \quad (20.41)$$

For the right-hand arm, with a spring of modulus E_2 , and a stress f_2 , we have

$$\varepsilon = \frac{f_2}{E_2} \quad (20.42)$$

$$\frac{d\varepsilon}{dt} = \frac{1}{E_2} \frac{df_2}{dt} \quad (20.43)$$

The total stress, f_T , is given by:

$$f_T = f_1 + f_2 \quad (20.44)$$

$$\frac{df_T}{dt} = \frac{df_1}{dt} + \frac{df_2}{dt} \quad (20.45)$$

Eliminating f_1 and f_2 from these equations, we get:

$$\frac{d}{dt} [(E_1 + E_2) \varepsilon - f_T] = E_1 K \sinh \alpha (f_T - E_2 \varepsilon) \quad (20.46)$$

This is the differential equation that gives the relation between stress, strain, and time for Eyring's three element model (incorporating a non-Newtonian dashpot) in terms of the constants E_1 , E_2 , K , and α . It may be applied to fibre deformation under any loading history. The most straightforward examples are stress relaxation, when $\epsilon = \text{constant}$; creep, when $f_T = \text{constant}$; and the stress-strain behaviour under constant rate of elongation, when $d\epsilon/dt$ is constant.

20.7.3 Stress relaxation on Eyring's model

For stress relaxation, with $\epsilon = \epsilon_c = \text{constant}$ and $d\epsilon/dt = 0$, equation (20.42) becomes:

$$\frac{df_T}{dt} = -E_1 K \sinh \alpha (f_T - E_2 \epsilon_c) \quad (20.47)$$

On integration, this gives:

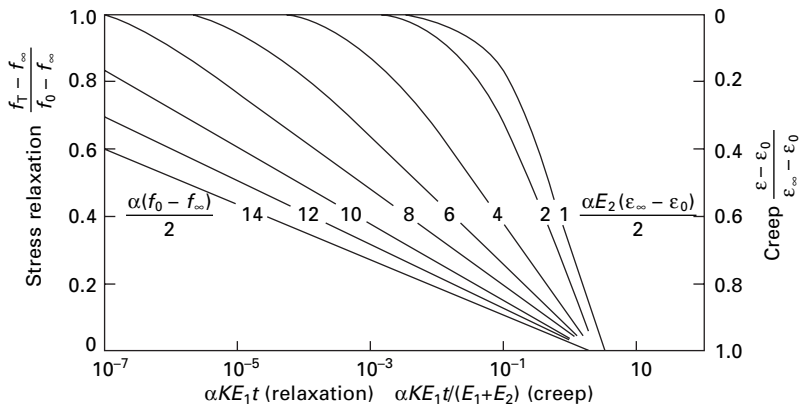
$$\frac{\tanh \{\alpha(f_T - f_\infty)/2\}}{\tanh \{\alpha(f_0 - f_\infty)/2\}} = e^{-\alpha E_1 K t} \quad (20.48)$$

where $f_0 = (E_1 + E_2) \epsilon_c = \text{initial stress at } t = 0$, and $f_\infty = E_2 \epsilon_c = \text{final stress at } t = \infty$.

It is convenient to plot this expression in terms of universal variables. The stress is expressed by $(f_T - f_\infty)/(f_0 - f_\infty)$; in other words, the final stress is subtracted from it, and the result is divided by the difference between the initial and final stresses. The time is given in terms of $\alpha K E_1 t$. Curves showing the relation between these two quantities for various values of $\alpha(f_0 - f_\infty)/2$ are given in Fig. 20.51 and are generally similar to those found experimentally. A graph from which numerical values of the constants needed to fit particular experimental curves may be calculated is given by Meredith [62].

If $f_0 \gg f_T \gg f_\infty$, equation (18.44) reduces approximately to:

$$f_T = f_\infty - \frac{1}{\alpha} \log_e \left(\frac{\alpha E_1 K t}{2} \right) \quad (20.49)$$



20.51 Graphs of equations (20.44) and (20.47) for stress relaxation and creep [61].

This means that, in the middle stages of the relaxation process, the stress decreases linearly with the logarithm of the time. This is in agreement with experimental results.

By fitting the experimental data to the theoretical equations, values of the constants α and K can be obtained, and then, if one assigns values to λ and λ/λ_1 , one can calculate N and ΔF from equations (20.37) and (20.38). Burleigh and Wakeham [63] assumed that in cellulose λ_1 was equal to the length of two glucose units, that is, 1.03 nm; they then found that, for cotton and rayon cords under an initial stress of 78 MPa, N remained fairly constant with values of 3.6×10^{11} and 4.9×10^{11} per mm^2 , respectively, over a range of temperatures and humidities. These values correspond to approximately one-eighth and one-sixth, respectively, of the total number of chain molecules per unit area of cross-section.

As the stress is increased, the values of N increase and approach the total number of cellulose chains at a stress approximating to that at which rupture occurs. Burleigh and Wakeham also found that in the wet state there was evidence of the simultaneous occurrence of a second relaxation process. This process was rapid, being completed in 30 s, and gave a value of N equal to the total number of cellulose chains. In other words, all the molecules were moving as individuals.

The values of λ/λ_1 used by different workers [59, 63, 64] range from 2 to 10, according to the assumptions made. However, even this wide range of values has only a small effect (about 6%) on the values obtained for ΔF . Andersen [64] has calculated values of activation energy, ΔF , for cotton and viscose rayon over a range of humidities and initial stresses. He obtained values of about 100 kJ/mol, which varied little with the conditions. However, as Meredith [62] has pointed out, similar values of activation energy will always be found for relaxation processes assumed to be completed in a given time range at a given temperature. To observe other activation energies, experiments must be made at a different temperature or on another timescale.

20.7.4 Creep on Eyring's model

For creep, we have stress $= f_T = \text{constant} = f_c$, and $df_T/dt = 0$, so that equation (20.46) becomes:

$$(E_1 + E_2) d\epsilon/dt = E_1 K \sinh \alpha(f_c - E_2\epsilon) \quad (20.50)$$

On integration this gives:

$$\frac{\tanh [\alpha E_2 (\epsilon_\infty - \epsilon)/2]}{\tanh [\alpha E_2 (\epsilon_\infty - \epsilon_0)/2]} = e^{-\alpha E_1 K t / (E_1 + E_2)} \quad (20.51)$$

This is similar in form to equation (20.48) for stress relaxation, so that the curves in Fig. 20.51 will also apply to creep. The abscissa will give values of $(\epsilon_\infty - \epsilon)/(\epsilon_\infty - \epsilon_0)$. It should be noted that this quantity decreases from 1 to 0 as ϵ increases from ϵ_0 to ϵ_∞ . More directly applicable to creep is the quantity $(\epsilon - \epsilon_0)/(\epsilon_\infty - \epsilon_0) = 1 - (\epsilon_\infty - \epsilon)/(\epsilon_\infty - \epsilon_0)$ shown on the right-hand scale. The ordinate will give values of $\alpha E_1 K t / (E_1 + E_2)$, and the figures on the curves will be values of $\alpha E_2 (\epsilon_\infty - \epsilon_0)/2$. As a consequence of the similarity of form, the same numerical methods may be employed to find the constants to fit the experimental data.

If the stresses involved are small, and the times concerned are less than 10^5 s, it can be shown that equation (20.51) reduces to:

$$\epsilon = \epsilon_0 + \frac{\epsilon_\infty}{\alpha f_c} \log_e(1 + At) \quad (20.52)$$

where $A = \frac{\alpha K f_c (1 - \epsilon_0/\epsilon_\infty)}{\epsilon_\infty \log_e \{ \coth[\alpha f_c (1 - \epsilon_0/\epsilon_\infty)/2] \}}$

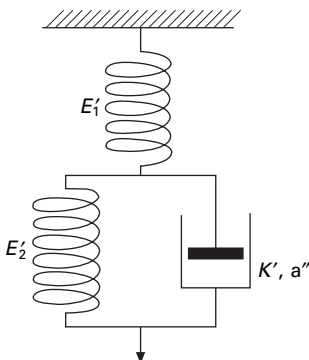
Halsey *et al.* [59] applied this equation to Leaderman's creep and creep-recovery data [65] for viscose rayon, acetate and silk and found a good fit over a 10^4 -fold range of times. A similar attempt to fit a three element model with a Newtonian viscous element gave a good fit only over a 50-fold range of times. Assuming that $\lambda = 1/2$, they calculated activation energies of the order of 100 kJ/mol.

The alternative three element model shown in Fig. 20.52 has been used by Reichardt *et al.* [66] to analyse Steinberger's data [67] on the creep of acetate. This model is simpler to apply to creep, since the upper spring has a constant extension under constant stress, and only the lower elements vary in extension with time, but it is less directly related to the structural picture. It is mathematically equivalent to the model of Fig. 20.49, though the values of E'_1 , E'_2 , K' and α' will be different from those of E_1 , E_2 , K , and α .

The three element model applies only to primary creep. There is no provision for a non-recoverable extension. Holland *et al.* [68] have tried to allow for this by putting a viscous element in series with the three element model, as in Fig. 20.48. This gives a secondary creep continuing indefinitely at a constant rate, which is not in accord with the usual experimental results. The fourth element must have a more complex response.

20.7.5 Stress-strain curve on Eyring's model

For constant rate of extension, we have $d\epsilon/dt = \text{constant}$, so that equation (20.46) becomes:



20.52 Alternative three-element model.

$$\frac{df_T}{dt} = (E_1 + E_2) \frac{d\epsilon}{dt} - E_1 K \sinh \alpha (f_T - E_2 \epsilon) \quad (20.53)$$

On integration, this gives:

$$f_T = E_2 \epsilon + \frac{1}{\alpha} \log_e \left\{ \beta + S \tanh \left[\frac{\alpha K S t}{2} + \tanh^{-1} \frac{(1 - \beta)}{S} \right] \right\} \quad (20.54)$$

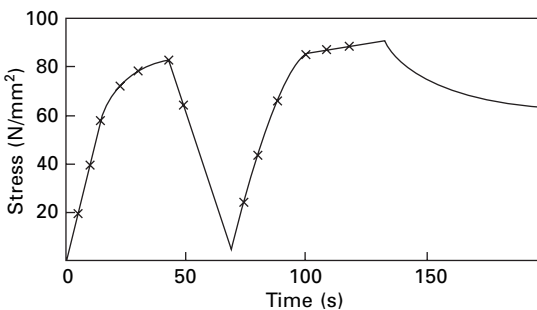
where $\beta = (d\epsilon/dt)/K$ and $S^2 = 1 + \beta^2$.

Methods of fitting this equation to the experimental data and determining the parameter β have been described by Eyring and Halsey [69], Geyer *et al.* [70] and Meredith [62]. The theoretical relations are found to give good agreement with some experimental results for viscose rayon and acetate. A typical example of the application of the theory is shown in Fig. 20.53.

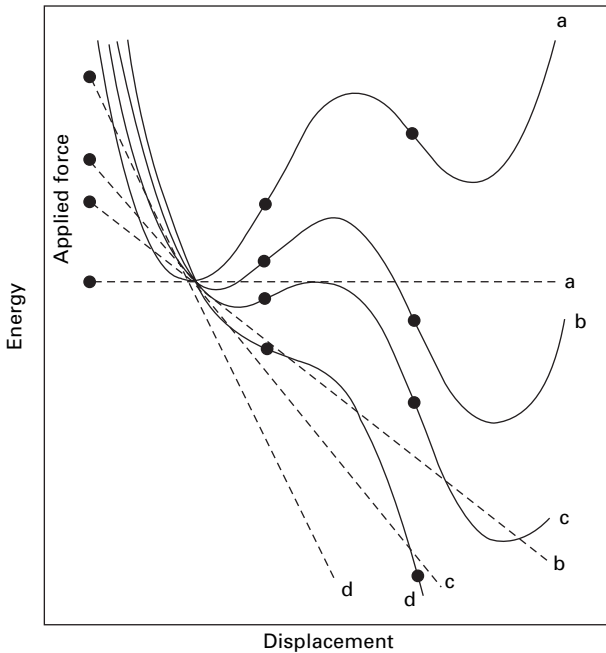
20.7.6 A generalisation of Eyring's model

There are many simplifications in Eyring's application of reaction-rate theory to deformation. One difficulty, about which little can be done, is that there are complicated interactions within a fibre, which cannot really be represented as an assembly of separate flow units.

It is also an approximation to assume that an applied stress merely changes the position of the troughs in the energy barrier, although this is valid provided that the stresses are not too large. A more realistic view of the effect of large stresses is shown in Fig. 20.54. The work done by the applied force changes the whole curve and, if it is large enough, removes the barrier; this would lead to spontaneous deformation or yield. Even before this happens, a thermal fluctuation may cause the barrier to be surmounted. Yield stresses will thus be time-dependent. Chapman [52] has shown that, with parabolic barriers, the effective yield stress $f_{c,t}$ with a time t available is given by:



20.53 Application of Eyring's three element model to the stress-strain relations of acetate at 57% r.h. and 27 °C. The full curve gives the experimental results, and the crosses are calculated from Eyring's theory with parameters derived from the first loading curve. After Reichardt and Eyring [71].



20.54 Generalised effect of stress on an energy barrier. The dotted lines show the work contribution of successively higher applied force (a–d), causing a progressive change in the energy barrier. It should be noted that the points of inflection remain in the same position, but that the maxima and minima change in position as well as height.

$$\frac{f_{c,t}}{f_{c,0}} = 1 - \left[\left(\frac{kT}{\Delta F} \right) \log_e vt \right]^{1/2} \quad (20.55)$$

A similar equation should apply to fracture stress, since fracture is merely a special case whereby the second trough in the curves is at infinity.

It may be noted that, depending on the absolute height of the energy barriers present (which will be determined by the nature of the interaction and the number of units acting cooperatively together), the following different modes of response may occur:

- very low barrier – an immediate achievement of the equilibrium state;
- low barriers – a sluggish approach to equilibrium;
- medium barriers – a rate-dependent yield, but no spontaneous recovery;
- high barriers – yield at a stress independent of rate.

An increase of temperature will increase the magnitude of thermal fluctuations, so that the barriers are easier to cross and seem less high.

20.7.7 The superposition principle in primary creep

Another form of analytical approach is found in Leaderman's study [65] of the primary creep of fibres. He found that this could be represented by the relation:

$$x_t = x_0 + \phi(F) \psi(t) \quad (20.56)$$

where x_t = extension after time t , x_0 = instantaneous extension, $\phi(F)$ is a function of force and $\psi(t)$ is a function of time.

As a special case of this relation, we can put $\phi(F) = x(90)$ and $\psi(t) = \Psi(t)$, as defined earlier in Section 16.2.2. The important feature of the relation is that, although creep is not a linear function of force, the effects of force and time can be separated into two functions. This gives a much simpler relation than a single function involving force and time.

In order to test equation (20.56), Leaderman made use of the relative delayed deformation, $x(t)$, defined as the difference between the deformation at the time t and the deformation at 1 min. This removes uncertainty about the value of the instantaneous deformation. Thus we have:

$$x(t) = x_0 + \phi(F) \psi(t) - x_0 - \phi(F) \psi(1) = \phi(F) [\psi(t) - \psi(1)] \quad (20.57)$$

$$\log x(t) = \log[\phi(F)] + \log[\psi(t) - \psi(1)] \quad (20.58)$$

Graphs of $\log x(t)$ against t or $\log t$ should therefore be parallel to one another and displaced only by the differences in $\log \phi(F)$. Leaderman found this to be so. An example is given in Fig. 20.55.

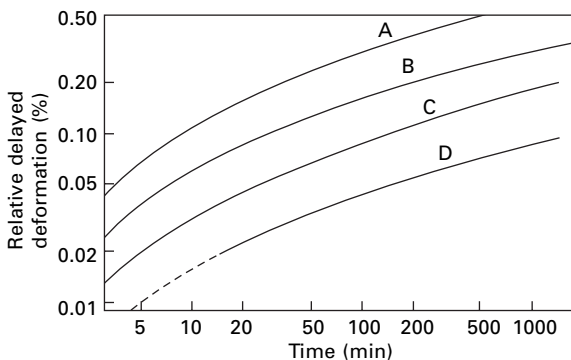
A reduced deformation can also be obtained by making use of $x(90)$, the deformation between 1 and 90 min, for we have:

$$x(t) = x(90)[\Psi(t) - \Psi(1)] \quad (20.59)$$

$$\text{reduced deformation} = x(t)/x(90) = \Psi(t) - \Psi(1) \quad (20.60)$$

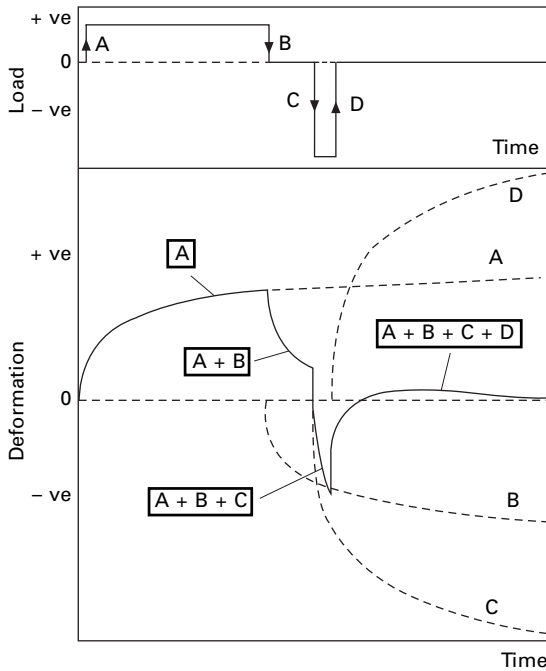
The reduced deformation should be independent of load and a function only of time. This was found to be so.

Boltzmann [72] in 1874 put forward his superposition principle, and this has since been found to apply to many materials. Leaderman decided to test it for fibres. The principle states that the deformation of a body is a function of its entire loading history and is given by a summation of the effects of every previous change of load.

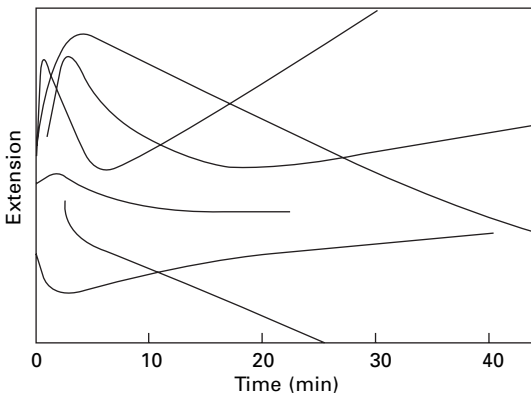


20.55 Plots of relative delayed deformations of viscose rayon for different loads [65]: A 31.0 mN/tex; B 25.2 mN/tex; C, 15.5 mN/tex; D 10.2 mN/tex.

This is illustrated in Fig. 20.56. The extension curve for each increment of load is put down, and the algebraic sum gives the resultant deformation. It is interesting to note that as a result of the superposition principle, the final creep recovery under zero load may, after a complex loading history, go past the zero position and then reverse direction before reaching equilibrium. An example of the reversal is included in Fig. 20.56, and some actual curves obtained for rubber by Kohlrausch [73] are given in Fig. 20.57. This is a remarkable phenomenon, since it means that under no load the



20.56 Application of superposition principle.



20.57 Creep-recovery of rubber after complex loading histories [73].

material is moving away from its equilibrium position. Inverse stress relaxation can also occur.

One way of testing the superposition principle is by long-duration creep and recovery tests. Suppose a load is left on for a time t_1 and then removed. The creep is given by:

$$x_t = x_0 + \phi(F) \psi(t) \quad (20.61)$$

and, by applying the superposition principle, the recovery by:

$$x_t = x_0 + \phi(F) \psi(t) - [x_0 + \phi(F) \psi(t - t_1)] = \phi(F)[\psi(t) - \psi(t - t_1)] \quad (20.62)$$

Let us call the recovery time $t' = (t - t_1)$ and the change of length during recovery t'_t , then:

$$\begin{aligned} t' &= x_0 + \phi(F)\psi(t_1) - \phi(F)[\psi(t) - \psi(t - t_1)] \\ &= x_0 + \phi(F)\psi(t') - \phi(F)[\psi(t + t') - \psi(t_1)] \end{aligned} \quad (20.63)$$

But if $t' \ll (t_1 + t')$ the last term is very small, since the initial creep has almost ceased and may be neglected in comparison with the second term. This is illustrated in Fig. 20.58. We thus get:

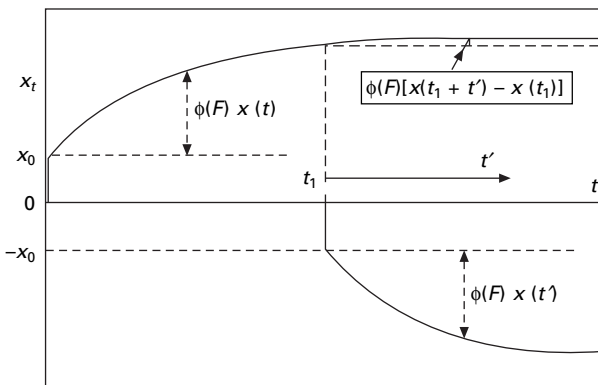
$$x'_{t'} = x_0 + \phi(F) \psi(t') \quad (20.64)$$

This equation is identical in form with Equation (20.61), which means that the changes in length during creep and recovery must follow the same curve. Leaderman showed that this was so, as mentioned earlier (Section 16.2.2).

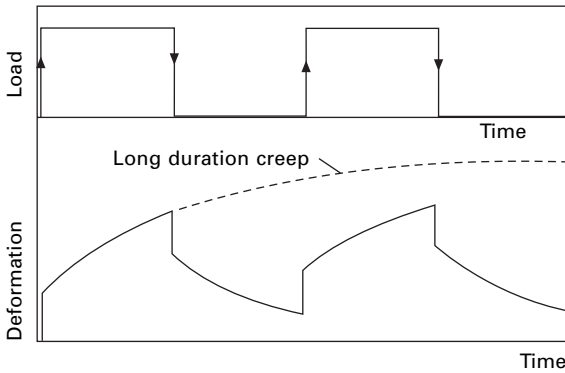
Another way of testing the superposition principle is by obtaining experimentally the deformation under repeated application and removal of load, as shown in Fig. 20.59. Suppose the first reversal occurs at a time t_1 , then at a time t , greater than t_1 , we have, writing $\chi(t)$ for x_t :

$$\chi(t) = \phi(F)[\psi(t) - \phi(F)] \quad (20.65)$$

But, if we add this to the creep for a time $(t - t_1)$, we get:



20.58 Long duration creep and recovery.



20.59 Creep under repeated applications and removal of load.

$$\begin{aligned}\chi(t) + \chi(t - t_1) &= \phi(F)[\psi(t) - \psi(t - t_1)] + x_0 + \phi(F)\psi(t - t_1) \\ &= x_0 + \phi(F)\psi(t)\end{aligned}\quad (20.66)$$

This equals the creep at a time t if there had been no reversal of load. Similar relations apply to the other reversals. From these tests, we can therefore calculate a complete creep curve and compare it with the one obtained directly. Leaderman found good agreement.

There is thus evidence that the superposition principle applies to primary creep in fibres, with the exceptions already noted (see [Section 16.2.2](#)), namely, the incomplete recovery of the instantaneous extension of silk and the behaviour of nylon at high loads. The value of the superposition principle lies in the fact that the behaviour under complex loading histories can be calculated from simple creep tests. It is another form of representation of linear viscoelasticity.

20.7.8. An integral theory

An example of an integral theory is the equation put forward by Nutting [74]:

$$x = \psi^{-1} f^\beta t^K \quad (20.67)$$

where x = strain, f = stress, t = time and ψ , β and K are constants. The constants β and K determine the type of deformation and ψ determines its magnitude. An example of its use is in the relaxation of torsional stress. The strain is constant, so that, taking logarithms, we get:

$$\log f = -\frac{K}{\beta} \log t + \text{constant} \quad (20.68)$$

Experimentally, Permyer [75] found linear relations between $\log(\text{stress})$ and $\log(\text{time})$, as shown in [Fig. 17.23](#), but at low twists the slope changed abruptly at one point. It may be noted that the equation is a special case of the creep part of Leaderman's expression [65], $\phi(F)\psi(t)$. However, Leaderman has pointed out that a power law does not always fit the experimental results well. In general, although it may be

useful in special cases, the equation is too limited to explain the complicated behaviour of fibres.

20.8 Thermodynamic effects

20.8.1 Thermodynamic equation of deformation

When a net amount of work $\sum dW$ is done on a system, it causes a change in the internal energy U and the entropy S of the system. The combined statement of the First and Second Laws of Thermodynamics for a reversibly isothermal change gives the relations between these quantities

$$\sum dW = dU - TdS \quad (20.69)$$

where T = absolute temperature.

If a fibre is extended by an amount dl through the application of a force F , then the work done on the system is $F dl$. We may therefore put:

$$F dl + \sum' dW = dU - TdS \quad (20.70)$$

In this equation, $\sum' dW$ is the sum of any other work or heat. Among other possible sources are an increase in volume dV against a pressure P , doing work ($-PdV$), and the absorption of water liberating the heat of absorption. It is usual in experimental investigations to maintain conditions (e.g. constant volume and constant water absorption) so that the other sources of work may be neglected, and we then have:

$$Fdl = dU - TdS \quad (20.71)$$

$$F = \left(\frac{\partial U}{\partial l} \right)_T - T \left(\frac{\partial S}{\partial l} \right)_T \quad (20.72)$$

This means that the stress caused by a given elastic extension may be divided into two parts, one depending on the changes in internal energy and the other on changes in the entropy. Increases in internal energy on extension come from the bonds between atoms being stretched, bent or rotated as described for crystals and glasses in Section 20.1.2. Changes in entropy come from changes in the degree of order of the system. All systems have a general tendency to take up the most random, least ordered condition, that is, the condition of highest entropy. Consequently, if the extension of a system means that it is increasing in its degree of order, a force must be applied to overcome the fall in entropy. This effect is predominant in the extension of rubbers (as it is for the volume changes of gases) as described in 20.1.2. There are thus two distinct mechanisms involved in determining the equilibrium position of a system and the forces needed to deform it. They are the tendencies, which are often opposed to one another, to achieve positions of minimum internal energy and maximum entropy (maximum randomness). On deformation of the system, there are three possibilities: (a) both the internal energy and the entropy effects may give positive contributions to the force; (b) the internal-energy contribution may be positive and numerically greater than a negative entropy contribution; or (c) the entropy contribution may be positive and numerically greater than a negative internal energy contribution.

For further mathematical development, it is convenient to introduce a quantity $A = (U - TS)$, which is known as the *Helmholtz free energy*. For a general change and substituting from equation (20.71):

$$dA = dU - TdS - SdT = Fdl - SdT \quad (20.73)$$

Thus

$$\left(\frac{\partial A}{\partial l} \right)_T = F \quad (20.74)$$

$$\left(\frac{\partial A}{\partial T} \right)_l = -S \quad (20.75)$$

However, it follows from a general property of partial differentials that:

$$\frac{\partial}{\partial l} \left(\frac{\partial A}{\partial T} \right)_l = \frac{\partial}{\partial T} \left(\frac{\partial A}{\partial l} \right)_T \quad (20.76)$$

Consequently, substituting from equations (20.74) and (20.75) we have:

$$\left(\frac{\partial S}{\partial l} \right)_T = - \left(\frac{\partial F}{\partial T} \right)_l \quad (20.77)$$

This means that the entropy contribution may be worked out from the change of force with temperature for a specimen extended by a constant amount. Equation (20.72) then gives internal energy contribution by subtraction from the force.

It has been shown experimentally that, for rubbers, $F \approx T(\delta F/\delta T)_l$, which indicates that the internal-energy contribution is negligible and that the rubber-like extension depends on entropy effects. Rubber-like elasticity is also characterised by a negative coefficient of linear expansion (see [Section 6.2.3](#)).

20.8.2 Application to fibres

There have been several investigations aimed at determining the extent of the energy and entropy effects in fibre extension. To do this, it is necessary, as we have seen, to measure the change of stress on a fibre held at constant extension. However, the stress on such a fibre will change owing to relaxation, apart from the change of temperature. This is an important experimental difficulty. It is one aspect of the general proposition that the thermodynamic equations are not applicable to irreversible effects, such as occur in the deformation of fibres. Experiments can therefore be made only on fibres in which the stress has relaxed to a fairly constant value, and even then the results must be viewed with caution.

Experiments have been made on both dry and wet fibres. In the latter case, corrections should be applied for the change of absorption on extension as described by Bryant and Wakeham [76].

The results of experiments on cellulose fibres given in [Table 20.4](#) show that for dry fibres the positive contribution to the force is derived from the internal energy

Table 20.4 Internal energy and entropy contributions in cellulose fibres

Fibre	Elongation (%)	Temp. (°C)	Total stress (mN/tex)	Energy contribution $\left(\frac{\partial U}{\partial l}\right)_T$	Entropy contribution $-T\left(\frac{\partial S}{\partial l}\right)_T$
Dry fibres					
Isotropic rayon	1	25	12.4	41.9	– 29.5
Textile rayon	1	25	29.1	60.3	– 31.2
Tyre-cord rayon	1	25	36.2	66.6	– 30.4
Stretched rayon (fibre G)	1	25	50.4	81.1	– 30.7
Wet fibres					
Cotton yarn	1	25	1.06	2.90	– 1.84
Tyre-cord rayon	1	25	1.06	3.16	– 2.10
Stretched rayon (fibre G)	1	25	7.68	23.4	– 15.8
Saponified acetate (highly oriented)	1	25	14.2	36.4	– 22.2
Textile rayon	1	25	1.15	1.84	– 0.70
	10	25	24.8	25.5	– 7.36
	1	75	1.17	0.33	+ 0.83
	10	75	24.8	24.0	+ 0.77
Acetate	1	25	0.31	0.70	– 0.38
	28	25	1.96	3.40	– 1.44
	1	75	0.11	2.05	– 1.94
	28	75	1.97	1.15	– 0.82

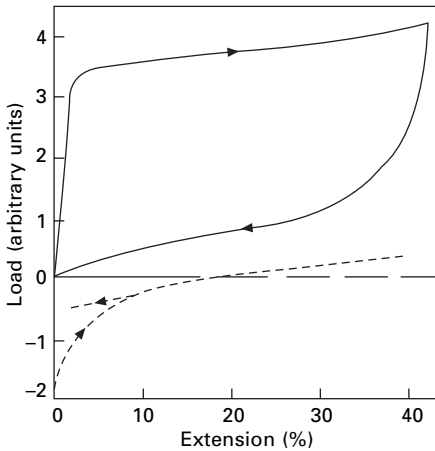
Calculations from original data [76, 77] by Wakeham [61].

effect, but this is reduced by a fairly large negative entropy term. The energy term derives from the stretching or angular deformation of the inter-atomic bonds and becomes greater the more highly oriented the fibre. The negative entropy term means that the structure is moving towards a less ordered state on deformation. For wet fibres, both the energy and the entropy terms are numerically less, and the latter becomes positive at higher temperatures.

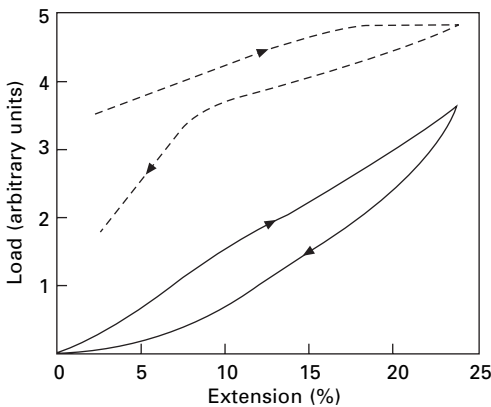
An application to wool is shown in Figure 20.60. This indicates that the energy term predominates, which was interesting at the time, because it was thought that the large extension shown by wool was due to a rubber-like type of elasticity depending on an alignment of disordered chains. The subsequent observation of the $\alpha \leftrightarrow \beta$ transition confirmed the energy change, though there is an entropic contribution from the matrix.

By contrast, Fig. 20.61 shows that in casein at low extensions the entropy effect predominates and is combined with a negative internal-energy effect. This suggests that, in this almost completely non-crystalline material, the chains are bent at random and the order increases on extension. The decrease in internal energy would derive from a more favourable interaction between the molecules.

It is well known that if stretched rubber is cooled to a low temperature, its oriented structure is ‘frozen in’, and it exhibits a stress–strain curve similar to that of a textile



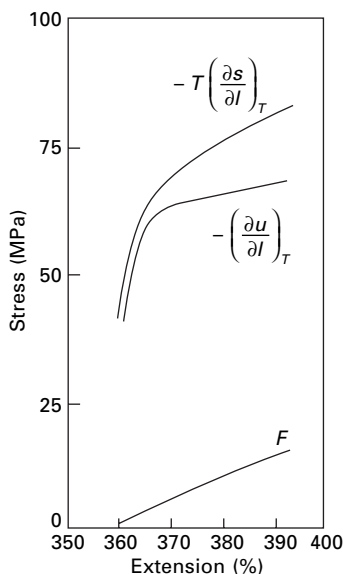
20.60 Extension and recovery curves of wool fibre in water [78]. Full line; total load. Dotted line: entropy contribution.



20.61 Extension and recovery curves of casein fibre in water [78]. Full line: total load. Dotted line: entropy contribution.

fibre. Clark and Preston [79] have observed the reverse effect with nylon and *Vinyon*. When heated above a certain temperature, these fibres contract and then show rubber-like properties, namely, a large extension and a large entropy effect as shown in Fig. 20.62. There is, however, a divergence from ideal rubber-like elasticity because the internal-energy effect is not negligible.

Rather different results were obtained by Dart [80], who found that, in nylon and polyester and acrylic fibres, the internal energy term was dominant and the entropy effects were small.



20.62 Stress-strain relations for nylon in the range 150–180 °C.

20.9 References

1. L. R. G. Treloar *The Physics of Rubber Elasticity*, 3rd edition, Clarendon Press, Oxford, 1975.
2. P. J. Flory. *Principles of Polymer Chemistry*, Cornell University Press, Ithaca, NY, 1953, p. 427–428.
3. J. W. S. Hearle. *Polymers and Their Properties*, Ellis Horwood, Chichester, 1982.
4. J. W. S. Hearle. *J. Polymer Sci. C*, 1967, No. 20, 215.
5. R. W. Work. *Text. Res. J.*, 1949, **19**, 381.
6. J. W. S. Hearle. *J. Appl. Polymer Sci.*, 1963, **7**, 1635.
7. R. J. E. Cumberbirch and C. Mack. *J. Text. Inst.*, 1960, **51**, T458.
8. R. J. E. Cumberbirch and C. Mack. *J. Text. Inst.*, 1961, **52**, T382.
9. J. W. S. Hearle. *J. Polymer Sci. C*, 1967, No. 20, 215.
10. D. C. Prevorsek, P. J. Harget, R. K. Sharma and A.C. Reimschuessel. *J. Macromol. Sci.*, 1973, **B-8**, 127.
11. J. W. S. Hearle and R. Greer. *J. Text. Inst.*, 1970, **61**, 243.
12. N. S. Murthy, A. C. Reimschuessel and V. J. Kramer. *J. Appl. Polymer Sci.*, 1990, **40**, 249.
13. J. W. S. Hearle. *J. Appl. Polymer Sci.*, *Appl. Polymer Symp.*, 1978, **31**, 137.
14. J. W. S. Hearle, R. Prakash and M. A. Wilding. *Polymer*, 1987, **28**, 441.
15. J. W. S. Hearle, M. A. Wilding and G. W. Du, unpublished reports to Du Pont, 1985–90.
16. J. W. S. Hearle. *J. Appl. Polymer Sci.: Appl. Polymer Symp.*, 1991, **47**, 1.
17. S. D. Long and I. M. Ward. *J. Appl. Polymer Sci.*, 1991, **42**, 1921.
18. I. M. Ward. *J. Textile Inst.*, 1995, **86**, 289.
19. H. A. Davis. *J. Textile Inst.*, 1991, **82**, 86.
20. P. E. Rouse. *J. Chem. Phys.*, 1953, **21**, 1272.
21. P. J. Barham and A. Keller. *J. Mater. Sci.*, 1985, **20**, 2281.
22. G. S. Fielding-Russell. *Text. Res. J.*, 1971, **41**, 861.
23. R. Meredith. *Text. Prog.*, 1975, **7**, No.4.
24. Y. Termonia and P. Smith. *Polymer*, 1986, **27**, 1845.
25. G. Wobser and S. Blasenbrey. *Kolloid-Z. Z. Polymer*, 1970, **241**, 985.

26. D. J. Johnson, L. Karacan and J. G. Tomka. *J. Textile Inst.*, 1990, **81**, 421
27. M. G. Northolt. *Polymer*, 1980, **21**, 1199.
28. M. G. Northolt and R. van der Hout. *Polymer*, 1985, **26**, 310.
29. M. G. Northolt, A. Roos and J. H. Kampschreur. *J. Polymer Sci., Physics Edition*, 1989, **27**, 1107.
30. M. G. Northolt and D. J. Sikkema. *Adv. Polymer Sci.*, 1990, **98**, 115.
31. M. G. Northolt, J. J. M. Baltussen and B. Schaffers-Korff. 1995, **36**, 3485.
32. J. J. M. Baltussen and M. G. Northolt. *Polymer*, 2001, **42**, 3835.
33. J. W. S. Hearle, P. Grosberg and S. Backer. *Structural Mechanics of Fibers, Yarns, and Fabrics*, Volume I, Wiley-Interscience, New York, 1969.
34. R. Meredith. In *Proceedings of Fifth International Congress on Rheology*, University of Tokyo Press, Tokyo, Japan, 1969, Volume 1, p. 43.
35. J. W. S. Hearle and J. T. Sparrow. *J. Appl. Polymer Sci.*, 1979, **24**, 1857.
36. J. W. S. Hearle. In *Mechanics of Flexible Fibre Assemblies*, J. W. S. Hearle, J. J. Thwaites and J. Amirbayat (Editors), Sijthoff and Noordhoff, Alphen an den Rijn, Netherlands, 1980, p. 51.
37. J. J. Thwaites. In *Mechanics of Flexible Fibre Assemblies*, J. W. S. Hearle, J. J. Thwaites and J. Amirbayat (Editors), Sijthoff and Noordhoff, Alphen an den Rijn, Netherlands, 1980, p. 87.
38. S. Timoshenko. *Strength of materials Part II*, Van Nostrand, New York, 1957, p. 259.
39. D. L. House. MSc thesis, Georgia Institute of Technology, 1966.
40. R. Meredith. *J. Textile Inst.*, 1954, **45**, T489.
41. J. T. Sparrow, The fracture of cotton, PhD thesis, University of Manchester, 1973.
42. J. W. S. Hearle. *Wool Tech. Sheep Breeding*, 2003, **35**, 95.
43. J. W. S. Hearle. 11th Int. Wool Textile Res. Conf., 2005, Leeds.
44. J. W. S. Hearle. *Textile Horizons*, 1997, August/September, 12.
45. H. Liu and W. G. Bryson. *J. Textile Inst.*, 2002, **93**, 121.
46. M. Feughelman. *Textile Res. J.*, 1959, **29**, 223.
47. B. M. Chapman. *Text. Res. J.*, 1969, **39**, 1102.
48. J. W. S. Hearle. *Int. J. Biological Macromolecules*, 2000, **27**, 123.
49. B. M. Chapman. *J. Textile Inst.*, 1970, **61**, 448.
50. J. W. S. Hearle and M. Susitoglu. *Proc. 7th Int. Wool Textile Res. Conf.*, Tokyo, Japan, 1985, **1**, 214.
51. J. W. S. Hearle, B. M. Chapman and G. S. Senior. *Appl. Polymer Symp.*, 1971, **18**, 775.
52. B. M. Chapman. PhD thesis, University of Manchester, 1968.
53. K. Arai, G. Ma and T. Hirata. *J. Appl. Polymer Sci.*, 1991, **42**, 1125.
54. W. A. Munro and G. A. Carnaby. *J. Textile Inst.*, 1999, **90**, 123.
55. W. A. Munro. *J. Textile Inst.*, 2001, **92**, 213.
56. F. T. Peirce. *J. Text. Inst.*, 1927, **18**, T486.
57. J. D. Ferry, *Viscoelastic Properties of Polymers*, 2nd edition, Wiley, New York, 1970.
58. A. V. Tobolsky and H. Eyring. *J. Chem. Phys.*, 1943, **11**, 125.
59. G. Halsey, H. J. White and H. Eyring. *Text. Res. J.*, 1945, **15**, 295.
60. S. Glasstone, K. J. Laidler and H. Eyring. *The Theory of Rate Processes*, McGraw-Hill, New York, 1941.
61. H. Wakeham. In *Cellulose and Cellulose Derivatives*, E. Ott and H. M. Spurlin (Editors), Interscience, New York, 1955, Chapter 11, p. 1302.
62. R. Meredith. *The Mechanical Properties of Textile Fibres*, North Holland Publishing Co., Amsterdam, Netherlands, 1956, pp. 87 *et seq.*
63. E. G. Burleigh and H. Wakeham. *Text. Res. J.*, 1947, **17**, 245.
64. F. Andersen. *Trans. Danish Acad. Tech. Sci.*, 1950, No. 3.
65. H. Leaderman. *Elastic and Creep Properties of Filamentous Materials and Other High Polymers*, The Textile Foundation, Washington, DC, 1943.
66. C. H. Reichardt, G. Halsey and H. Eyring. *Text. Res. J.*, 1946, **16**, 382.

67. R. L. Steinberger. *Text. Res.*, 1936, **6**, 191.
68. H. D. Holland, G. Halsey and H. Eyring. *Text. Res. J.*, 1946, **16**, 201.
69. H. Eyring and G. Halsey. In *High-polymer Physics*, Chemical Publishing Co., New York, 1948, p. 98.
70. C. J. Geyer, C. H. Reichardt and G. Halsey. *J. Appl. Phys.*, 1948, **19**, 464.
71. C. H. Reichardt and H. Eyring. *Text. Res. J.*, 1946, **16**, 635.
72. L. Boltzmann. *Pogg. Ann. Physik.*, 1876, **7**, 624.
73. F. Kohlrausch. *Pogg. Ann. Physik.*, 1876, **8**, 337.
74. P. G. Nutting. *J. Franklin Inst.*, 1943, **235**, 513.
75. F. Permanyer. PhD Thesis, University of Manchester, 1947.
76. G. M. Bryant and H. Wakeham. *Text. Res. J.*, 1955, **25**, 224.
77. W. E. Roseveare and L. Poore. *J. Polymer Sci.*, 1954, **14**, 341.
78. H. J. Woods. *J. Colloid Sci.*, 1946, **1**, 407.
79. J. F. Clark and J. M. Preston. *J. Text. Inst.*, 1953, **44**, T596.
80. S. L. Dart. *Text. Res. J.*, 1960, **30**, 372.

21.1 General introduction

The electrical properties of fibres are of less obvious technical importance than, for example, the mechanical properties. Apart from their intrinsic interest, the first stimulus for their investigation came from the use of fibres as insulating materials, and much important work was done in the Bell Telephone Laboratories. Later, the use of resistance and capacity methods for measuring the moisture condition of textile materials, and of capacity methods for measuring irregularity, increased the interest in electrical properties. With the introduction of synthetic fibres, the troubles due to static charges, both in processing and in use, became more frequent and more severe. The electrical properties are interrelated. The liability of materials to static charges is determined by their electrical resistance. The electrical resistance is, on what seems to be the most likely theory, mainly determined by the permittivity of the material. It is, therefore, most appropriate to consider first the dielectric properties, then the electrical resistance, and finally static.

21.2 Definitions of dielectric properties

The *permittivity*, ϵ , of a material may be defined either in terms of the capacitance, C , of a condenser with the material between parallel plates of area A and separation d , or in terms of the force F between two charges Q_1 and Q_2 at a distance r in the material. Expressed in SI units as $\text{kg}^{-1} \text{m}^{-3} \text{s}^4 \text{A}^2$ (A = ampere) or F/m (F = farad), the relations contain no arbitrary numerical factors and are:

$$C = \frac{\epsilon A}{d} \quad (21.1)$$

$$F = \frac{Q_1 Q_2}{4\pi \epsilon r^2} \quad (21.2)$$

This does, however, mean that *in vacuo* the equations become:

$$C = \frac{\epsilon_0 A}{d} \quad (21.3)$$

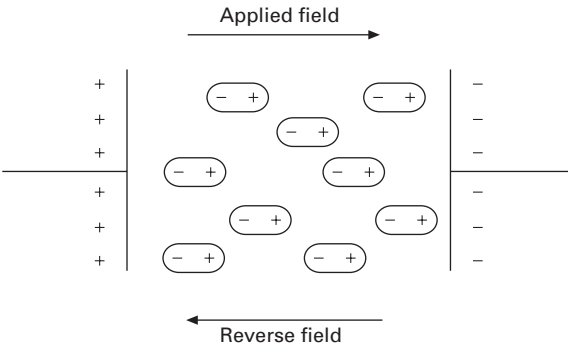
$$F = \frac{Q_1 Q_2}{4\pi \epsilon_0 r^2} \quad (21.4)$$

where ϵ_0 is the permittivity of a vacuum, which is a fundamental physical quantity with the value 8.854×10^{-12} F/m. For many purposes, it is more convenient to use the *relative permittivity*, $\epsilon_r = \epsilon/\epsilon_0$; which is also called the *dielectric constant*.

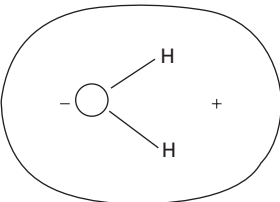
Physically, dielectric effects are due to polarisation in the medium (Fig. 21.1). This gives rise to a reverse field, which reduces the force between two charges and reduces the potential difference between the charged plates of a condenser, which thus increases its capacitance (given by charge/potential difference). The polarisation may be due either to the alignment of permanent dipoles, such as the water molecule (Fig. 21.2), or to the separation of charge, which forms induced dipoles (Fig. 21.3). Because of its influence on capacitance, the relative permittivity is important in alternating current electricity. For a pure capacitance, current is proportional to rate of change of voltage and is therefore, with a sinusoidal applied voltage, 90° out of phase with voltage. By contrast, in a pure resistance, current is in phase with voltage. In actual practice, dielectrics are imperfect, and a real condenser (Fig. 21.4(a)) acts as a combination of capacitance and resistance. The current through the condenser due to an applied voltage of frequency f Hz is made up of a current proportional to $1/R_p$ in phase with the applied voltage and a current proportional to $2\pi f C_p$ at 90° to the applied voltage, where R_p and C_p are the equivalent parallel resistance and capacitance, respectively (Fig. 21.4(b)). The current vector diagram is shown in Fig. 21.4(c).

The relative permittivity is then given by:

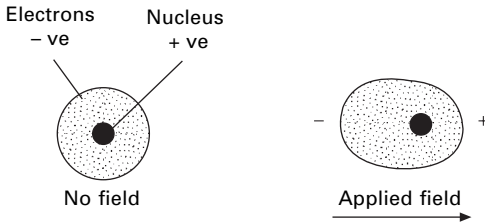
$$\epsilon_r = \frac{C_p}{C_0} \quad (21.5)$$



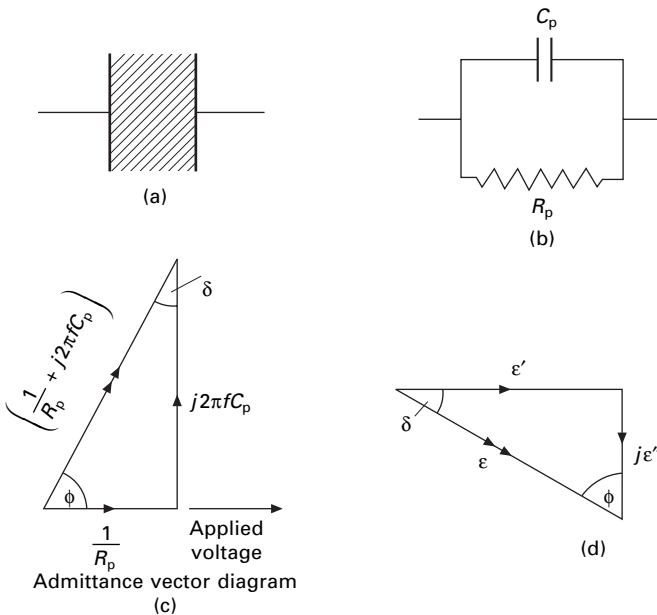
21.1 Polarisation of a medium.



21.2 A permanent dipole – the water molecule.



21.3 An induced dipole-distortion of the distribution of electrons round the nucleus of an atom.



21.4 Representation of a real dielectric: (a) condenser with dielectric; (b) equivalent parallel circuit; (c) current vector diagram for circuit; (d) vector diagram – complex dielectric constant.

where C_0 = capacitance of the condenser with a vacuum (or, in practice, air) as dielectric.

The imperfection of the dielectric may be expressed as:

$$\text{dissipation factor, or loss tangent} = D = \tan \delta = \frac{1}{2\pi f C_p R_p} \quad (21.6)$$

where δ = loss angle, or as power factor = $\cos \phi$ = [mean power dissipated in condenser/voltage \times current (r.m.s. values)] = $D/\sqrt{1 + D^2}$, where $\phi = (\pi/2) - \delta$ = phase angle. Table 21.1 shows the values of these quantities for pure capacitance and resistance; with real materials, the values lie between these limits.

An alternative method of expressing the properties of the material is in terms of a complex permittivity, ϵ , with the vector diagram of Fig. 21.4(d). We have:

Table 21.1 Dielectric properties

	Vector diagram	Power factor	Dissipation factor	Loss angle	Phase angle
Pure capacitance	$\uparrow j \cdot 2\pi f C_p$	0	0	0	$\pi/2$
Pure resistance	$\rightarrow 1/R_p$	1	∞	$\pi/2$	0

$$\epsilon = \epsilon' - j\epsilon'' \quad (21.7)$$

It can be shown that real part of permittivity = $\epsilon' = \epsilon$, as defined above, and imaginary part of permittivity = loss factor = $\epsilon'' = 1/2\pi f C_p R_p$ and dissipation factor = $\tan \delta = \epsilon''/\epsilon'$.

21.3 Measurement

21.3.1 Experimental methods

To measure the dielectric properties, the material must be placed between the plates of a condenser and the impedance measured. For measurements on material in the form of film, a simple parallel plate condenser, with the plates fitting closely to the film, can be used. Fibres are less easy to handle. Balls [1] used parallel plates and carefully packed cotton fibres either perpendicular or parallel to the plates. Hearle [2] used conical electrodes. A layer of yarn, about 2 mm thick, was wound on the inner cone, and the outer cone was then pressed on it. With this arrangement, densities of packing of about 80% by volume were obtained with continuous-filament yarns, and of about 50% with staple-fibre yarns.

The method of measurement of impedance depends on the frequency being used for the test¹. At audio-frequencies (from about 50 Hz to 100 kHz), a bridge method is suitable. Resonance methods can be used up to about 100 MHz. The condenser is connected in series with an inductance L in a resonant circuit, with the current measured by a high-impedance voltmeter across the condenser. At the resonant frequency f_0 , the current has a maximum value. The capacitance $C = L/(2\pi f_0)^{1/2}$ and $\tan \delta = \Delta f/f_0$, where Δf = difference in frequency between the two values for which the current is $1/\sqrt{2}$ times the maximum value. Circuit-magnification meters, or Q-meters, can be used for this method. At very high frequencies (10 GHz), Shaw and Windle [3] used a cavity resonator. If a small dielectric specimen is placed along the axis of the cavity parallel to the electric field, the resonant frequency of the cavity is given by:

$$f = f_e \left[1 - 1.86 (\epsilon_r - 1) \frac{v_s}{v_e} \right] \quad (21.8)$$

where f_e = resonant frequency of empty resonator, v_s = volume of specimen and v_e = volume of cavity.

¹The methods noted here are those used for the data in this chapter. Subsequent advances in electronics have changed the details of the technology, but not the principles.

At optical frequencies, the dielectric properties can be obtained from a study of refraction and absorption in the fibres by using the equations:

$$\epsilon_r = n^2(1 - k^2) \quad (21.9)$$

$$\tan \delta = \frac{2k}{(1 - k^2)} \quad (21.10)$$

where n = refractive index and k = absorption index, defined by: $2\pi k = \lambda/x_0$, where λ = wavelength, and x_0 = distance in which amplitude decreases to $1/\exp(x)$ times its original value.

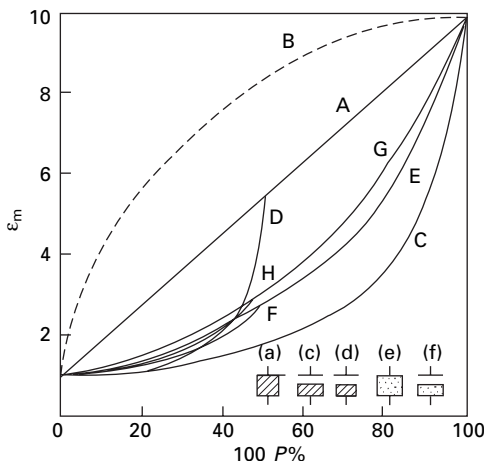
21.3.2 Evaluation of results for an air-fibre mixture

The main difficulty in dealing with fibres is the interpretation of results found with a mixture of air and fibre in order to obtain the properties of the fibrous material itself. Depending on the particular assumptions used, different formulae can be obtained, and it is not easy to see how closely they should fit particular experimental conditions. Some of these relations are described below and shown in Fig. 21.5. We define ϵ_r as the relative permittivity of the fibre material (taken as 10 for the curves in Fig. 21.5), ϵ_m as the effective relative permittivity of the mixture, and P as the volume fraction of fibre between the plates of the condenser.

- If the material is assumed to occupy only a fraction of the total area, but to be continuous between the plates, Fig. 21.5(a), and it is assumed that there is no distortion of the field, we have the parallel mixture law, Fig. 21.5A:

$$\epsilon_m = 1 + (\epsilon_r - 1) P \quad (21.11)$$

Balls [1] used this formula for fibres lined up perpendicular to the plates, but it



21.5 Theoretical curves for the variation of relative permittivity with density of packing.

seems unlikely that, under these conditions, one can neglect the distortion of the electric field. Owing to the high surface/volume ratio in fibres, there will be a large edge effect. The lines of force will concentrate on the region of high relative permittivity and increase the capacity above its expected value. Some curve such as Fig. 21.5B will be obtained.

- If the material is assumed to occupy the whole area, but only a fraction of the distance between the plates, Fig. 21.5(c), we have the series mixture law, Fig. 21.5C:

$$\frac{1}{\epsilon_m} = (1 - P) + \frac{P}{\epsilon_r} \quad (21.12)$$

- A combination of the above two cases, with α as the fraction of area occupied and β as the fraction of the distance between the plates (Fig. 21.5(d)), presents the problems of averaging referred to in Section 20.3.2 in relation to a mixture of mechanical properties. One model gives the following equation:

$$\epsilon_m = \frac{\alpha}{[(1 - \beta) + \beta/\epsilon_r]} + (1 - \alpha) = \frac{\alpha^2}{[(\alpha - p) + P/\epsilon_r]} + (1 - \alpha) \quad (21.13)$$

With $\alpha = 0.5$, this gives Fig. 21.5 D.

- If molar polarisations are additive, the following equation holds [4]:

$$\frac{\epsilon_m - 1}{\epsilon_m + 2} = P \frac{\epsilon_r - 1}{\epsilon_r + 2} \quad (21.14)$$

This system is indicated in Fig. 21.5(e) and gives the curve Fig. 21.5E. It is not valid for large particles owing to the failure of the assumption on which it is based that the Lorentz internal field holds at all places. It has been shown to be a good approximation for small values of P [5]. Various improvements on this formula for particular conditions have been suggested [6–8], and Polder and van Santen [9] have discussed the problem more generally.

If ϵ_r is very nearly equal to 1, so that the difference between $\epsilon_m + 2$ and $\epsilon_r + 2$ is negligible. Equation (21.14) reduces to:

$$\epsilon_m - 1 = P(\epsilon_r - 1) \quad (21.15)$$

which is the same as equation (21.11) leading to Fig. 21.5A.

This is valid for a mixture of gases but would not be expected to be so for fibres, though it was used by Balls [1] for fibres arranged with their axes parallel to the plates.

- A combination of (C) and (E), illustrated in Fig. 21.5(f), would give the curve Fig. 21.5F.
- Licktecker [10] proposed a logarithmic relation, which, for a mixture with one component having unit relative permittivity, reduces to Fig. 21.5G:

$$\log \epsilon_m = P \log E_r \quad (21.16)$$

This has been applied, with experimental support, by Shaw and Windle [3] to the transverse relative permittivity of fibres wound solenoidally.

- A combination of (C) and (G) gives Fig. 21.5H. Hearle [2] obtained curves similar to, but not in quantitative agreement with, this when the density of packing between cones was varied by altering the pressure applied to the outer cone. Different curves, corresponding to different densities in the bulk of the material, can be obtained by using staple-fibre and continuous-filament yarns and by varying the winding tension. An example is given in Fig. 21.6.

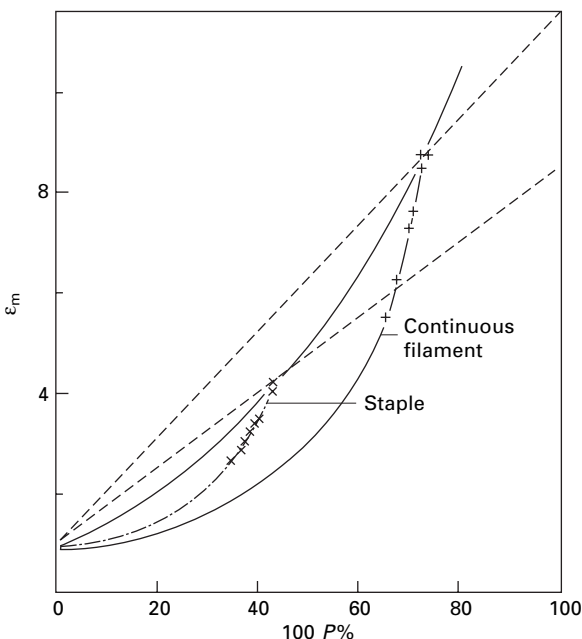
Where the experimental arrangement approximates closely to one of the above models, it may be possible to obtain an accurate extrapolation formula, but, in general, the problem has not been solved.

For dry fibres having a comparatively low permittivity, Errera and Sack [11] overcame the problem by immersing the fibres in a mixture of liquids and adjusting the mixture until the introduction of the fibres made no difference. The permittivities of fibre and liquid were then equal.

21.4 The effect of frequency

21.4.1 General

Frequency has a most important influence on dielectric properties, in a way similar to its influence on dynamic mechanical properties. Owing to their inertia, and to restraints in the structure, the dipoles take a certain time to reverse direction. This is characterised as their relaxation time. At low frequency, the dipoles line up in the



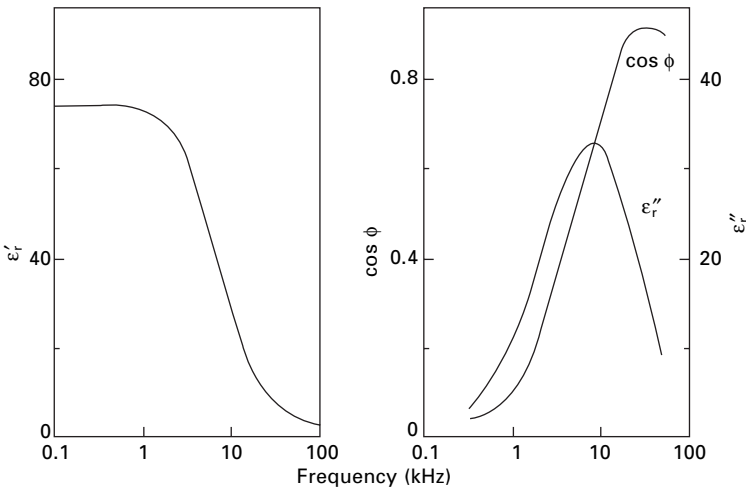
21.6 Practical variation of relative permittivity of viscose rayon with density of packing [2].

field, reverse direction when the field reverses, and so contribute to a high permittivity. At high frequencies, the dipoles will not follow the changes at all, and there will be no contribution to the permittivity. At intermediate, transitional frequencies the reversals of field take place at intervals comparable to the relaxation time, the response of the dipoles is sluggish, which gives a phase difference between voltage and current, and energy is dissipated due to internal friction. Different types of dipole will have different relaxation times, so that, as the frequency is raised, the permittivity drops in steps and the dielectric loss peaks. When the theory is worked out exactly, it is found that the maximum in ϵ'' occurs at the same frequency as the maximum rate of decrease of ϵ' ; the maximum of $\cos \phi$ is displaced to a slightly higher frequency.

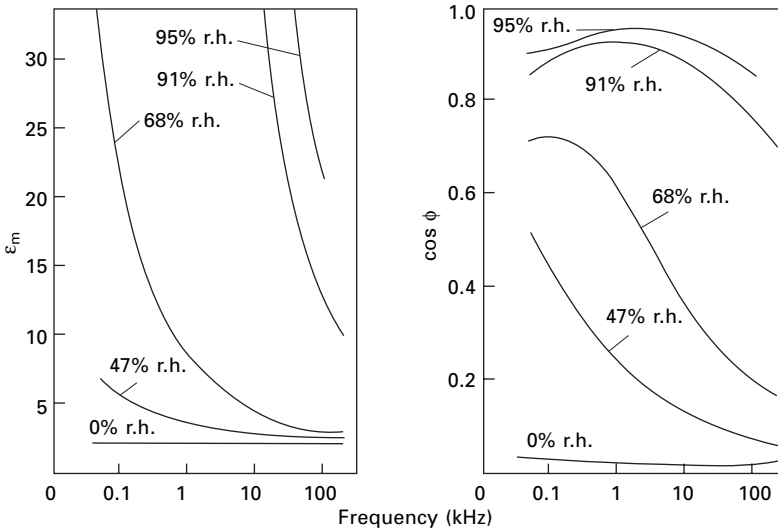
The general behaviour is illustrated by the results for water and ice. At low frequencies, the dipolar water molecules line up in the field, to give a relative permittivity of about 80. At higher frequencies, the permittivity drops in a step, and there is a maximum in the power factor. For ice, (Fig. 21.7), in which the considerable restraints in the structure limit the movement of the dipoles, this occurs at about 10 kHz; but, for liquid water, in which the molecules are less restrained, the permittivity remains constant up to about 1 GHz, and then drops rapidly and passes half its low-frequency value at about 20 GHz. Above these frequencies, there will still be electronic polarisation, but at high enough frequencies this will cease, and there will be a further decrease in permittivity.

21.4.2 Fibres

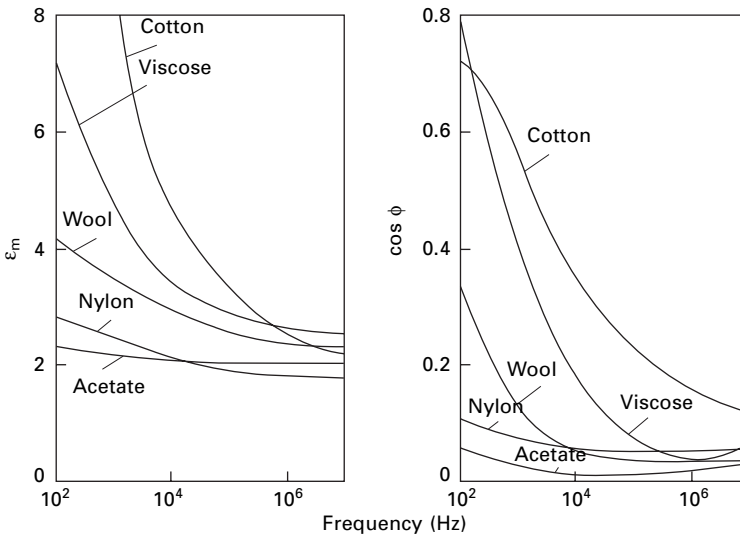
Figures 21.8 and 21.9 show results obtained by Hearle [2, 12] for cotton, viscose rayon, acetate, wool and nylon over the range of frequencies between 50 Hz and 10 MHz. Other values are included in the summary given later in Table 21.4. These results show the great influence of frequency on the dielectric properties, an influence



21.7 Dielectric properties of ice.



21.8 Dielectric properties of cotton yarn in cone condenser [2]. Cotton 44%; air 56%.



21.9 Variation of dielectric properties with frequency for various fibre-air mixtures at 65% r.h. [2, 12].

that becomes more marked the damper the specimen. The changes occur gradually and not in steps, which indicates that a range of relaxation times is involved.

Above 5 kHz, the permittivity decreases in a manner similar to that in ice, but, below 5 kHz, the permittivity curve does not flatten out, as does that of ice, but continues to increase as the frequency decreases. This must correspond to a comparatively large-scale polarisation phenomenon with a long relaxation time. The

maximum in the power factor for damp cotton at 50–100 Hz indicates that there must be a dominant relaxation time of the order of 1/100 second. These effects are probably due to a polarisation of the ion distribution in microscopic or sub-microscopic regions of the fibre structure, or possibly even across the whole fibre. This is the same as the Maxwell–Wagner effect, or interfacial polarisation, which occurs when there are heterogeneities in the conductivity and permittivity of a material between the plates of a condenser.

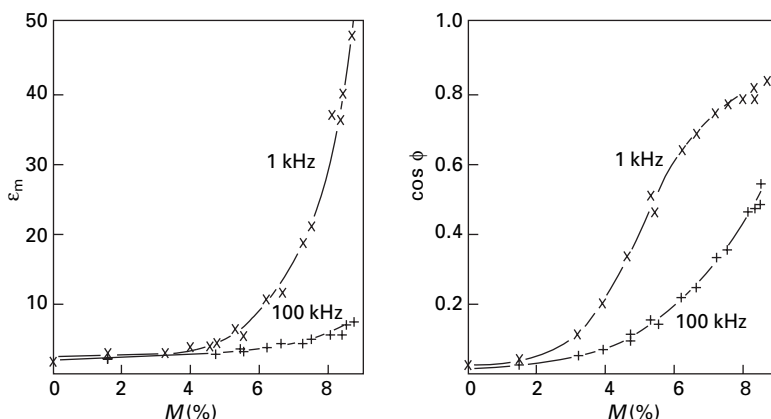
In several types of fibre (viscose rayon, acetate, fairly dry cotton), the power factor begins to increase with an increase in frequency in the region of 1 MHz. These results suggest that, at some frequency greater than 10 MHz, there will be a maximum in the power factor and a corresponding drop in the permittivity. The way in which the curves for viscose rayon and acetate at various humidities come together suggests that this effect is independent of the presence of water. It is probably associated with the lining-up of polar groups within the fibre.

In wool, Windle and Shaw [13, 14] found a decreasing power factor as the frequency increased from 3 to 26 GHz. This indicated the presence of a maximum in the power factor at some frequency below this. This is probably essentially the same effect as that which is suggested for viscose rayon, acetate and cotton by tests at lower frequencies.

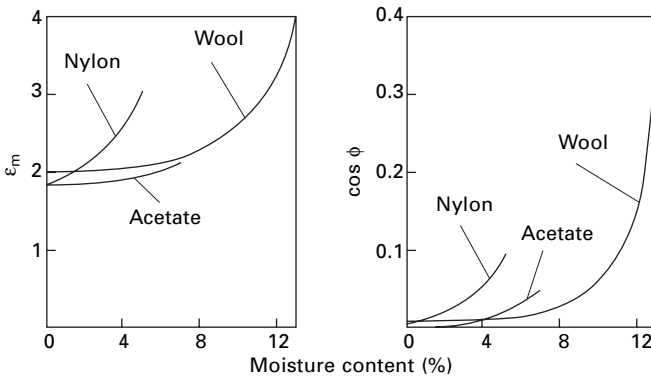
It is interesting to notice that relaxation effects occur in the mechanical behaviour of fibres at similar frequencies to those found in the dielectric properties (see [Section 16.5](#)).

21.5 The effect of moisture

As would be expected, moisture has a marked effect on the dielectric properties; this is illustrated for cotton, acetate, wool and nylon in Figs 21.10 and 21.11. At the higher frequencies, the dielectric properties of the cellulosic fibres are consistent with the assumption that the water molecules are restrained in a manner similar to that in ice. For wool, the permittivity is lower, which indicates that the absorbed water molecules are more tightly held and cannot line up in the field. This behaviour



21.10 Variation with moisture content M of dielectric properties of cotton [2].



21.11 Variation with moisture content of dielectric properties of various fibres at 1 kHz [2].

is particularly marked at low moisture contents and is consistent with Speakman's suggestion (see [Section 12.2.1](#)) that the water first absorbed by wool is firmly bound to hydrophilic groups in the side chains of the keratin molecule. At the lower frequencies, in some materials (notably cotton, in which the permittivity reaches very high values), the effect of water becomes greater than it would be even if it were acting with a relative permittivity of 80, which indicates its importance in freeing other units in the structure so that they can polarise.

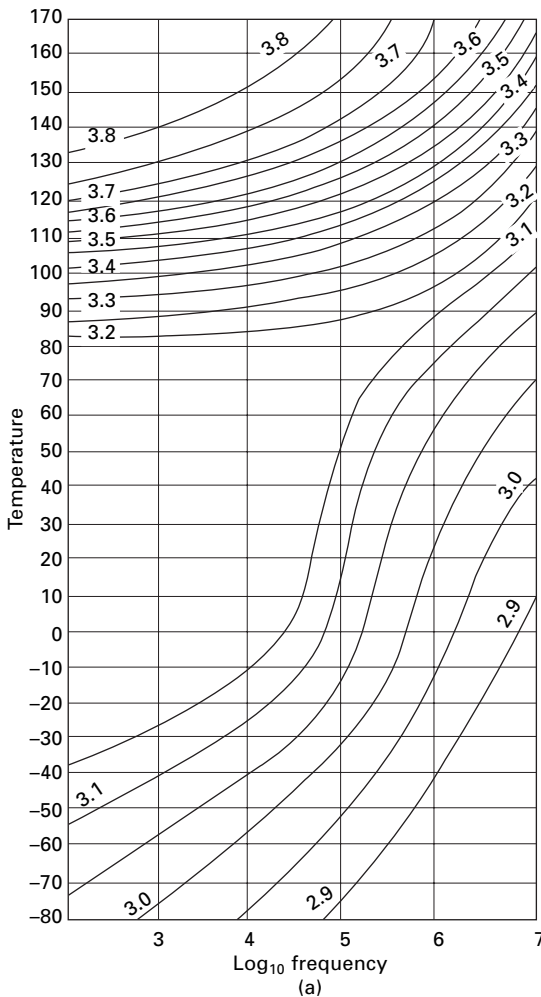
Windle and Shaw [14] have explained their results for wool at very high frequencies in terms of a three-phase theory of moisture absorption. The components of the system were regarded as dry wool, with experimentally determined properties; localised absorbed water, in which the molecules cannot rotate; intermediate absorbed water, in which the molecules are very little restricted; and mobile absorbed water, in which the molecules are as free as in liquid water. Using expressions for the dielectric properties of a mixture of dielectrics, assigning values for the dielectric properties of each component, and dividing up the absorbed water in proportions found theoretically, they obtained a good agreement between experiment and theory.

Of the non-absorbing fibres, polyester (PET) and polyvinylidene chloride (*Saran*) showed no variation in dielectric constant, and only a small change in power factor between 0 and 65% r.h. Polyvinyl chloride (*Vinyon*) and glass (*Fiberglas*) showed a marked change at low frequencies, which was presumably due to surface effects. In general, the effect of additives will have a major effect when the dielectric properties are not dominated by moisture absorption.

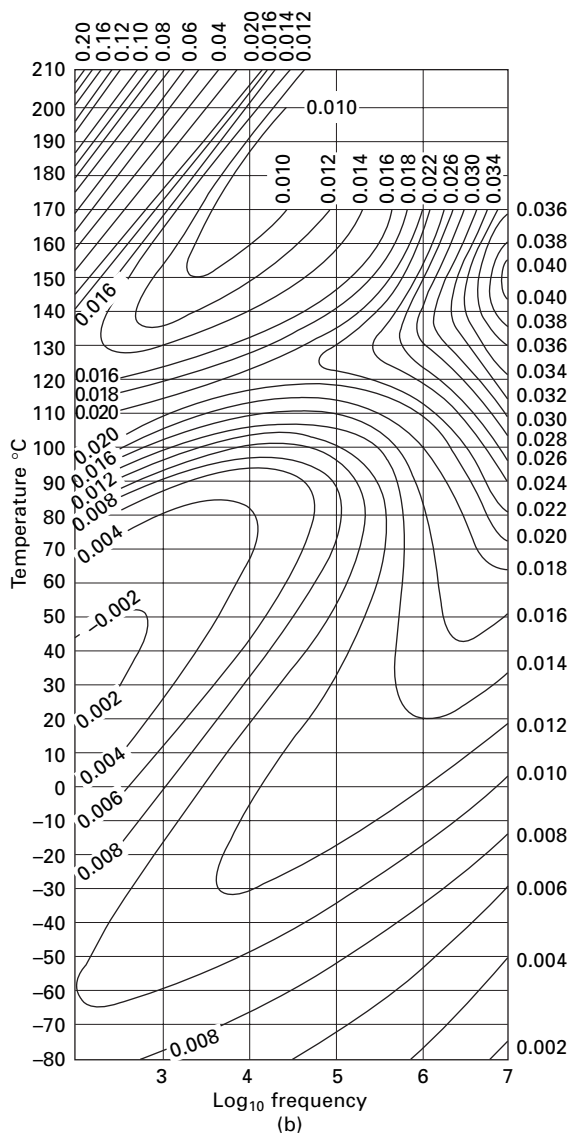
21.6 The effect of temperature

A rise in temperature, reducing the restraints on the dipoles, causes an increase in permittivity in solid materials. (In liquids and gases, where the intermolecular restraints are small, an increase of temperature causes a greater disorganisation, a less regular alignment of the dipoles, and thus a lower permittivity.) As for dynamic mechanical properties, the effects of temperature and frequency are often similar. This is shown

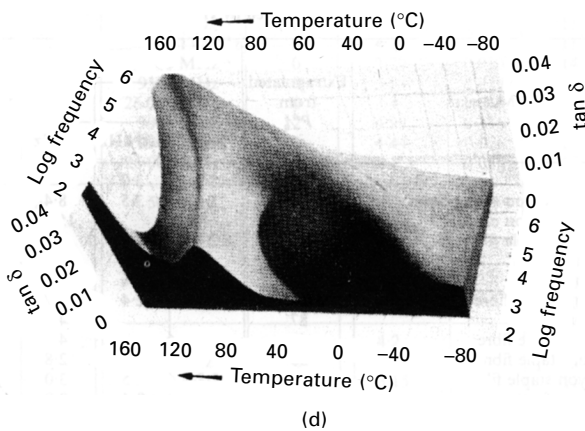
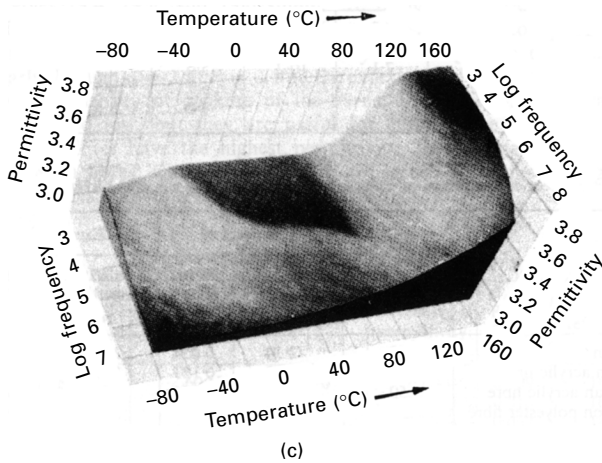
by Reddish's results [15] for polyethylene terephthalate (*Terylene*) film (Fig. 21.12). To include the effect of both variables, contour maps and solid models are used. It will be seen that there is a maximum in $\tan \delta$, occurring at about 1 MHz at room temperature and moving to lower frequencies at lower temperatures; this would correspond to the maximum suggested earlier Section (21.4.2) as being likely in the high-frequency region. At higher temperatures, there is another sharper maximum. These two ridges in $\tan \delta$ in the 3D models correspond to the peaks in mechanical loss shown in Fig. 21.13. Corresponding to the maxima in $\tan \delta$, there are rapid dips in the values of the permittivity. Note that the permittivity plots are the inverse of dynamic modulus plots and would correspond to compliance plots. There is another



21.12 Influence of temperature and frequency on dielectric properties of polyester (*Terylene*) film: (a) relative permittivity contour map; (b) dissipation factor contour map; (c) relative permittivity solid model; (d) dissipation factor solid model. After Reddish [15].



21.12 (Continued)

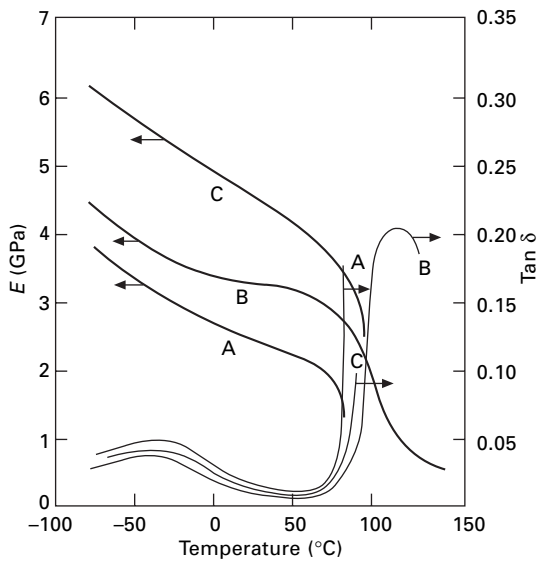


21.12 (Continued)

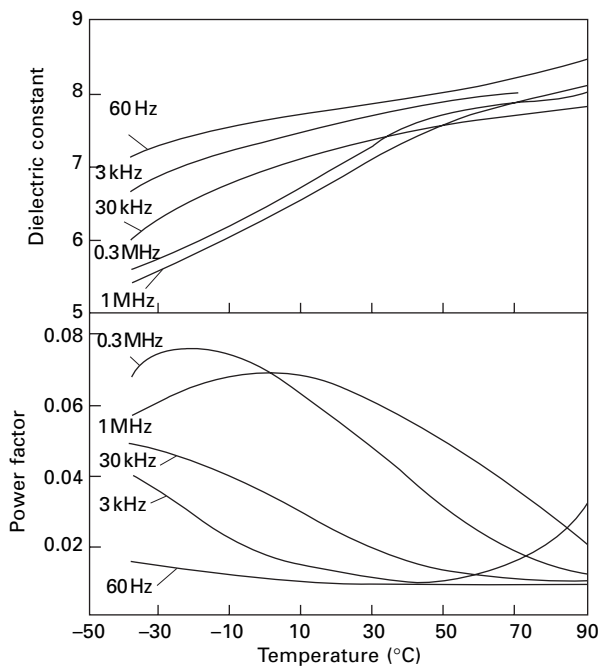
interesting feature: an increase in $\tan \delta$ at low frequency at 160 °C. Although there is no observable maximum, this may indicate another transition at a higher temperature but below the melting point. This may be associated with permanent setting of polyester fibres. Figure 21.14 shows the results obtained by Stoops [17] for dry cellulose film (Cellophane). These also include a low-temperature maximum and, at 60 Hz, indications of a high-temperature maximum. Baker and Yager [18] obtained somewhat similar results with dry nylon 6.10. Table 21.2 shows values of the relative permittivity of nylon and keratin film at 25 and 40 °C at various moisture regains.

21.7 The effect of other factors

The permittivity of an anisotropic material, such as a fibre, would be expected to vary with the direction in which the electric field is applied. The results obtained by Balls [1] for cotton fibres indicate that the axial permittivity is about twice the transverse permittivity, but, as is indicated above Section (21.3.2), the extrapolation on which



21.13 Dynamic mechanical modulus and $\tan \delta$ of poly(ethylene terephthalate) as measured by Kawaguchi [16] at about 100 Hz: A, undrawn, 2% crystallinity; B, undrawn, 50% crystallinity; C, drawn 5x, 25% crystallinity.



21.14 Variation of dielectric properties of cellophane. After Stoops [17].

Table 21.2 Effect of temperature on permittivity of nylon and keratin films [19]

Moisture regain (%)	Relative permittivity			
	Nylon film		Keratin film	
	25 °C	40 °C	25 °C	40 °C
0	4.2	4.5	4.7	4.8
1.8	5.0	6.0		
3.6	7.1	10.2	5.0	5.3
7.2			5.7	6.5
10.8			7.0	8.6

Table 21.3 Effect of extraction on dielectric properties at 65% r.h. and 1 kHz [2]

Material	Density of packing (%)	Unextracted		Extracted	
		Relative permittivity ϵ_m	Power factor $\cos \phi$	Relative permittivity ϵ_m	Power factor $\cos \phi$
Nylon	50	2.34	0.054	2.43	0.063
Acrylic fibre <i>Orlon</i>	40	2.28	0.123	1.73	0.0044
Acrylic fibre <i>Acrilan</i>	50	2.00	0.076	1.94	0.043
Polyester fibre <i>Dacron</i>	50	39.4	0.773	1.66	0.007

these results are based is of doubtful validity. At 3 GHz, Shaw and Windle [3] found that the relative permittivity of dry wool fibres was 3.88 ± 0.15 with the electric field parallel to the fibre axis and 4.41 ± 0.11 with the electric field perpendicular to the fibre axis.

The presence of impurities would be expected to alter the dielectric properties; in particular, ionic impurities would probably have a considerable effect at low frequencies. Table 21.3 shows the effect of the removal of surface dressings from some synthetic fibres by extraction in methanol and benzene. Only with the polyester fibre was there a large change, which was probably due to the removal of an anti-static finish, in the values obtained.

21.8 Summary of results for various materials

Tables 21.4, 21.5 and 21.6 summarise results for various materials at frequencies ranging from supply frequencies (50 Hz) to optical frequencies (10^{15} Hz). The figures given by Hearle [2] are extrapolated linearly through $\epsilon_r = 1$ at $P = 0$, and the experimental point is found with maximum density of packing of the yarns, $P\%$: this will give values that are too low, but they are useful for comparative purposes. The cellulosic fibres have the highest permittivity, these being followed by the protein fibres, with the synthetic non-hygroscopic fibres having the lowest values. The power factors follow a similar order.

Table 21.4 Permittivities obtained by Hearle [2]

Material	Extrapolated from <i>P</i> %	Relative permittivity			
		0% r.h.		65% r.h.	
		1 kHz	100 kHz	1 kHz	100 kHz
Cotton	44	3.2	3.0	18	6.0
Viscose rayon staple fibre	44	3.6	3.5	8.4	5.3
Viscose rayon c.f.	73			15	7.1
Acetate staple fibre	45	2.6	2.5	3.5	3.3
Acetate c.f.	79			4.0	3.7
Wool	53	2.7	2.6	5.5	4.6
Nylon staple fibre	53	2.5	2.4	3.7	2.9
Nylon c.f.	87			4.0	3.2
Acrylic staple fibre <i>Orlon</i>	42	2.8	2.3	4.2	2.8
Acrylic staple fibre <i>Orlon</i> (extracted)	38			2.8	2.5
PVC staple fibre <i>Vinyon</i>	46	2.7	2.5	3.0	2.6
PCVD <i>Saran</i> c.f.	70	2.9	2.4	2.9	2.4
Polyester staple fibre <i>Dacron</i> (extracted)	48	2.3	2.3	2.3	2.3
Glass <i>fiberglass</i> c.f.	63	3.7	3.4	4.4	3.6

c.f. = Continuous-filament yarn

Table 21.5 Other values of dielectric properties

Material	Frequency	Moisture regain (%)	Relative permittivity	Power factor	Reference
Cellophane film	60 Hz	0	7.7	0.009	15
	10 kHz	0	7.3	0.016	15
	1 MHz	0	6.7	0.062	15
	3000 MHz	0	4.04		3
Wool	8 kHz	0	5.4		11
	60 kHz	0	4.4		11
	120 kHz-13 MHz	0	4.2		11
	3000 MHz	0	3.70	0.030	13
	9300 MHz	0	3.54	0.019	13
	26 000 MHz	0	3.4	0.015	14
	3000 MHz	12	4.99	0.146	13
	9300 MHz	12	4.44	0.076	13
	26 000 MHz	12	4.1	0.068	14
Keratin film	500 Hz	0	5		20
	11 kHz	0	4.5		20
	1 MHz	0	4		20
	500 Hz	12	9		20
	11 kHz	12	7.5		20
	1 MHz	12	5.5		20
Nylon	10 kHz	0	4.2		11
	500 kHz	0	3.26		11
	10 MHz	0	3.15		11
	3000 MHz	2	3.13		3
Nylon film	11 kHz	0	4		21
	11 kHz	4	8		21

Table 21.6 Relative permittivity at optical frequencies

Fibre	$\epsilon_r = 2$ with light vibration:	
	Parallel to fibre axis	Perpendicular to fibre axis
Cotton	2.50	2.34
Viscose rayon	2.37	2.31
Acetate	2.19	2.16
Wool	2.40	2.37
Casein	2.37	2.37
Nylon	2.50	2.31
Polyester fibre <i>Terylene</i>	2.96	2.37
Acrylic fibre <i>Orlon</i>	2.25	2.25
Polyethylene	2.43	2.28
Glass	2.40	2.40

* From refractive indices in [Table 24.3](#)

21.9 References

1. W. L. Balls. *Nature*, 1946, **158**, 9.
2. J. W. S. Hearle. *Text. Res. J.*, 1954, **24**, 307.
3. T. M. Shaw and J. J. Windle. *J. Appl. Phys.*, 1950, **21**, 956.
4. C. J. F. Böttcher. *Theory of Electric Polarization*, Amsterdam, Netherlands, 1942, p. 415.
5. J. W. Rayleigh. *Phil. Mag.*, 1892, **34**, 481.
6. C. J. F. Böttcher. *Res. Trav. Chim.*, 1945, **4**, 47.
7. E. Stöcker. *Z. Physik.*, 1920, **2**, 236.
8. O. Wiener. *Abhandl. math. phys. – Klasse sachs. Akad. Wiss. Leipzig.*, 1912, **32**, 509.
9. D. Polder and J. H. van Santen. *Physica*, 1946, **12**, 257.
10. K. Lickteneker. *Physik. Z.*, 1926, **27**, 115.
11. J. Errera and H. S. Sack. *Industr. Engng Chem.*, 1943, **35**, 712.
12. J. W. S. Hearle. *Text. Res. J.*, 1956, **26**, 108.
13. J. J. Windle and T. M. Shaw. *J. Chem. Phys.*, 1954, **22**, 1752.
14. J. J. Windle and T. M. Shaw. *J. Chem. Phys.*, 1956, **25**, 435.
15. W. Reddish. *Trans. Faraday Soc.*, 1950, **46**, 459.
16. T. Kawaguchi. *J. Polymer Sci.*, 1958, **32**, 417.
17. W. N. Stoops. *J. Amer. Chem. Soc.*, 1934, **56**, 1480.
18. W. O. Baker and W. A. Yager. *J. Amer. Chem. Soc.*, 1942, **64**, 2171.
19. G. King and J. A. Medley. *J. Colloid Sci.*, 1949, **4**, 9.
20. G. King. *Trans. Faraday Soc.*, 1947, **43**, 601.
21. G. King. *J. Colloid Sci.*, 1947, **2**, 551.

22.1 Introduction

When electricity was first intentionally conducted from one place to another (from an electrified tube to an ivory ball) by Stephen Gray in 1729, the material used as the conductor was hempen pack-thread. Gray eventually covered distances of up to 233 m along the corridors of his house. In order to do this, he had to support the pack-thread and, after an abortive attempt in which fine copper wires were used, he suspended the thread by silk filaments. Thus both the conductor and the insulator were textile fibres. Soon afterwards, Du Fay found that pack-thread was a better conductor when it was wet. Then, in 1734, Gray discovered metallic conductors, and, apart from some use for insulating purposes, interest in the electrical resistance of fibres did not revive for nearly 200 years [1].

22.2 Definitions

The electrical resistance of a specimen, i.e. the voltage across the specimen divided by the current through it, is determined both by the properties of the material and the dimensions of the specimen. For most substances, the property of the material is best given by the specific resistance ρ (in $\Omega \text{ m}$), which is defined as the resistance between opposite faces of a 1 m cube, but, as with mechanical properties (see [Section 13.3.1](#)), it is more convenient with fibres to base a definition on linear density (mass per unit length) than on area of cross-section. A *mass-specific resistance* R_s is therefore defined as the resistance in ohms between the ends of a specimen 1 m long and of mass 1 kg, giving units of $\Omega \text{ kg/m}^2$. The two quantities are related as follows:

$$R_s = \rho d \quad (22.1)$$

where d = density of material in kg/m^3 .

In practice, it is more convenient to express R_s in $\Omega \text{ g/cm}^2$, when the numerical values for most fibres will differ by less than 50% from the values of ρ expressed in $\Omega \text{ cm}$. With these units, the resistance R of an arbitrary specimen is given by the relation

$$R = R_s \frac{l}{NT} \times 10^5 \quad (22.2)$$

where l = distance between the ends of the specimen in cm, N = number of ends of yarn or fibre and T = linear density of yarn or fibre in tex.

Because of the wide range of resistance values, results are frequently expressed in terms of the logarithm of resistance.

22.3 Methods of measurement

22.3.1 Measurement of resistance

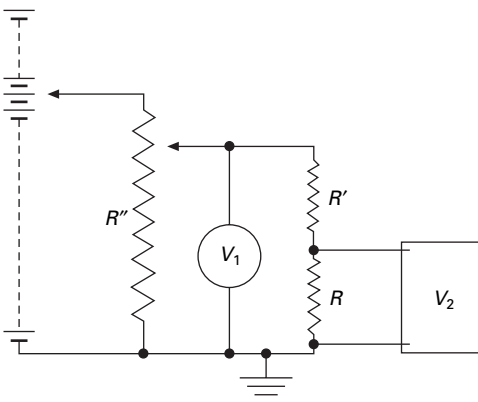
Ideally, the resistance should be measured accurately, instantaneously and at a constant voltage. The difficulties of doing this are increased by the high values of resistance that have to be measured and the wide range that is covered. A variety of methods has been used [1].

The simplest method of measurement is the use of an ammeter in series and a voltmeter across the resistance. This can be done when the resistance of the material is low. With a sensitive galvanometer, the method has been used for resistances up to $10^9 \Omega$, but the time taken for the galvanometer to come to rest may be a disadvantage. Wheatstone bridge methods may also be used for fairly low resistances. The charging or discharging of a capacitor through the resistance is a method of measurement of high resistance. The general relation for the charge Q on a capacity C to which a voltage V_0 has been applied through a resistance R for a time t is:

$$Q = V_0 C (1 - e^{-t/CR}) \quad (22.3)$$

For the capacity discharging, $Q = V_0 C e^{-t/CR}$. Various arrangements may be used to apply these relations, but they all suffer from the defects that the test must last for a measurable time and that the voltage varies during the test.

With high-resistance stable resistors, comparison methods can be used. Fig. 21.1 shows the circuit used by Hearle [2]. The voltage V_1 can be measured by a low-resistance voltmeter. The voltage V_2 must be measured by a voltmeter whose resistance is much greater than that of the unknown resistance R . The resistance to be measured is given in terms of the standard resistance R' by the relation



22.1 Circuit for measurement of high resistances.

$$R = R' \left(\frac{V_2}{V_1 - V_2} \right) \quad (22.4)$$

By this method, high resistances can be measured quickly with a known voltage V_2 adjustable by the potentiometer R' across the specimen. Hersh and Montgomery [3] used a slightly more complicated circuit in a null method, which does not require such a high-resistance detector.

In measuring high resistances, great care must be taken to avoid the pick-up of stray voltages, which necessarily take a long time to discharge.

22.3.2 Arrangement of specimens

Many different arrangements of the material to be tested have been used [1]. The resistance has been measured along single fibres, along many fibres in parallel, along single ends of yarn, along many ends in parallel, parallel to the weft and parallel to the warp in cloth, across yarn and across cloth, and with special electrodes, such as those of the Shirley Moisture Meter (see [Section 7.3.5](#)).

In most of his experiments, Hearle [2, 4] used yarn wound on a polythene former and then held between bulldog clips, lined with tinfoil, 1 cm apart. Hersh and Montgomery [3] stuck fibres or pieces of yarn onto brass tabs with silver conducting paint.

The specimens must be conditioned by being placed in a suitable atmosphere. A simple conditioning chamber is satisfactory for work at constant temperature. Hearle [2] used a glass jar containing saturated salt solutions to control humidity. Leads were brought out through a tight-fitting stopper. A sample of the fibre was suspended in the jar and removed to measure moisture content. Alternatively, the resistance may be measured immediately after removal of the specimen from the conditioning atmosphere.

Securing constant moisture conditions at different temperatures is more difficult. The most satisfactory method is to enclose the specimen in a space so small that no appreciable evaporation can take place, which thus keeps the moisture content constant. Hearle [5] sealed specimens between sheets of rubber, brought out fine copper leads, and immersed the whole in a bath of paraffin.

22.4 Results of experiments

22.4.1 The influence of moisture

Moisture is the most important factor in determining the resistance of most textile materials and causes a variation over a range of at least 10^{10} times. Even the difference between 10 and 90% r.h. will cause a million-fold difference of resistance, namely, a tenfold decrease in resistance for every 13% increase in relative humidity.

For most hygroscopic textile fibres between 30 and 90% r.h., relations of the following form hold:

$$\log R_s = -n \log M + \log K \quad (22.5)$$

$$R_s \cdot M^n = K \quad (22.6)$$

where M = moisture content (%), and n and K are constants.

When plotted over a wider range of moisture conditions, a sigmoidal relation between $\log R_s$ and $\log M$ is obtained (Fig. 22.2). At low moisture contents (below 3.5% for cotton, 7% for viscose rayon and 4% for wool and silk), the following form fits the results:

$$\log R_s = -n' M + \log K' \quad (22.7)$$

where n' and K' are constants. A relation of this form was also found to fit the results for acetate and some specimens of nylon [6].

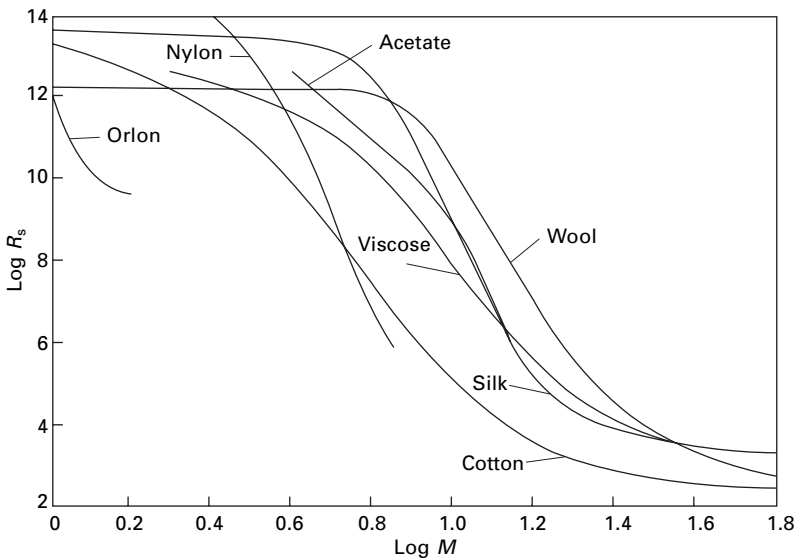
The resistance of a specimen at constant temperature has been found to be a single-valued function of moisture content, no hysteresis being detectable. It follows that there must be hysteresis between resistance and humidity. Nevertheless, for a given part of the hysteresis loop, relations of the following form are found to fit the experimental data fairly well:

$$\log R_s = -aH + b \quad (22.8)$$

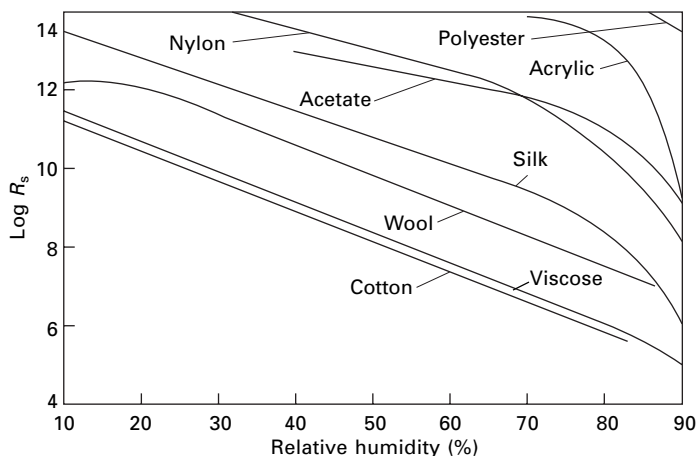
where H = relative humidity, and a and b are constants.

22.4.2 Comparison of different materials

Figure 22.2 shows results for various materials plotted in terms of moisture content; Fig. 22.3 shows them in terms of relative humidity. Table 22.1 gives values of $\log R_s$ at 65% r.h., and of n and $(\log K - n)$. The latter quantity, which is equal to the value of $\log R_s$ at $M = 10\%$, is more useful for comparative purposes than the value of \log



22.2 Variation of resistance of fibres with moisture content [2, 6].



22.3 Variation of resistance of fibres with relative humidity [2, 7].

Table 22.1 Electrical resistance results, along yarn [2, 6, 7]

Material	n	$(\log K - n) = \log R_s$ at $M = 10\%$	$\log R_s$ at 65% r.h.	r.h. % for $R_s = 10^{10} \Omega \text{ g/m}^2$
Cotton	11.4	5.3	6.8	30
Washed cotton	10.7	6.0	7.2	30
Mercurised cotton	10.5	6.8	7.2	30
Flax	10.6	6.8	6.9	30
Viscose rayon	11.6	8.0	7.0	30
Washed viscose rayon	12.0	9.0	7.5	30
Acetate		9.0	11.7	85
Silk	17.6	9.0	9.8	65
Wool	15.8	10.4	8.4	55
Washed wool	14.7	11.9	9.9	60
Nylon			9–12	85
Orlon acrylic fibre (as received)			8.7	85
Purified Orlon acrylic fibre			14	95
Terylene polyester fibre (as received)			8.0	85
Purified Terylene polyester fibre			14	95

K , which has to be obtained by extrapolation and is greatly affected by any error in the value chosen for n . Table 22.2 gives values of n' and $\log K'$ obtained at low moisture contents.

The values of n for the different cellulosic fibres are very nearly the same. Hearle [2] found that they can all be fitted with reasonable accuracy by the relation:

$$\log R_s = -11.2 \log M + \log K \quad (22.9)$$

where the value of $\log K$ can be found by measuring the resistance at one moisture content.

Table 22.2 Electrical resistance results: low moisture contents [8]

Material	n'	$\log K'$	Upper limit of relation, $M\%$	Lower limit of tests, $M\%$
Cotton	1.90	16.0	3.5	1.3
Viscose rayon	0.47	13.6	7	2.2
Wool	0	12.7	4	0
Silk	0.15	13.9	4	1.4
Acetate [6]	0.72	16.5	> 12	4

Within the limits of experimental error, Hearle found no difference between 12 different cottons (two American, five Pakistani, two Egyptian, Brazilian, Tanguis and Uganda). A comparison of the results for cotton and viscose rayon shows that they are in reasonable agreement with the assumption that the conduction is in the non-crystalline region of the fibre, which will have a resistance determined by its own moisture content. Cellulose acetate shows a rather high resistance when considered in terms of either moisture content or relative humidity.

The protein fibres have larger values of n (between 16 and 18 in most cases), and, except at very low moisture contents, they have a much higher resistance than the cellulosic fibres. The change in resistance with moisture content at low moisture contents becomes very small, and in wool it is almost non-existent.

There is a wide variation, depending on their history and the presence of additives, in the resistance of different specimens of nylon. Nylon has a high resistance at a given humidity, but, when plotted against moisture content, the resistance values fall below those of viscose rayon. The curves of $\log R_s$ against $\log M$ show no linear portion. It has been shown by Sharman *et al.* [9] that the resistance of nylon increases as the draw-ratio increases; they consider that the change is greater than would be explained by a change of regain.

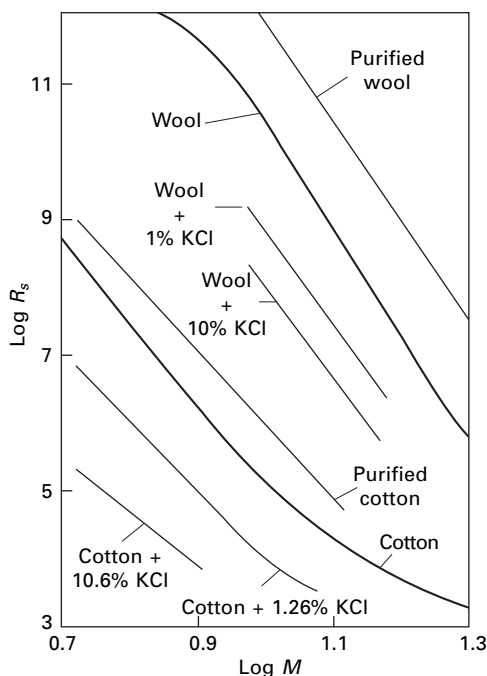
The acrylic fibres show a low resistance at a given moisture content, and at a given relative humidity they may even have a resistance as low as that of wool.

Fibres such as polyester or vinyl fibres, which absorb little water, all have very high resistances. Their resistances decrease at a rate of about ten times for every 10% increase in relative humidity up to about 80% r.h.; above this humidity, the resistance decreases more rapidly. However, for these fibres, anti-static finishes are commonly applied to lower the resistance, as indicated by the million-fold increase in the resistance on removing finish from the polyester fibre in Table 22.1.

The high-modulus, high-tenacity (HM-HT) polymer fibres are inherently good insulators, though there is some effect of moisture in aramid fibres. Glass and ceramic fibres are also good insulators. Surface finishes can, of course, cause a modification of properties. Carbon fibres are fairly good conductors of electricity, with a resistivity of about $15 \Omega \text{ m}$.

22.4.3 Effect of impurities

The resistance of the hygroscopic fibres depends on their electrolyte content, as is illustrated by the results for cotton and wool in Fig. 22.4. The addition of a salt such



22.4 Resistance of wool and cotton as received, purified, and with added electrolyte [2].

as potassium chloride lowers the resistance. At low salt contents, the evidence indicates that conductivity is approximately proportional to electrolyte content, but, at high salt contents (greater than 1%), O'Sullivan [10] found that the resistance of cellulose film at a given moisture content was independent of the nature or amount of salt present.

Washing in distilled water increases the resistance, and a further increase may be obtained by washing in calcium sulphate solution. Walker and Quell's results [11] show the increase in resistance between raw cotton (0.4% of sodium and potassium salts) and washed cotton:

	R_s , $M\Omega \text{ g/cm}^2$
raw cotton	0.5
after washing 200 g in 5 litres distilled water	14
after washing 200 g in 40 litres distilled water	12–25
after washing in CaSO_4 solution followed by distilled water	18–37

The action of the calcium sulphate solution is to replace the monovalent ions left behind after washing in distilled water by less conducting bivalent ions (see [Section 22.5.3](#)). The residual ions are probably associated with ionic groups in the fibre molecule, for example, carboxyl ($-\text{COO}-$) groups present as impurities in cellulose molecules. Church [12] found that, when hydrogen ions were replaced by calcium ions in paper, the resistance increased six times.

Any wet processing, such as bleaching or dyeing, that alters the electrolyte content will alter the electrical resistance. The resistance of the synthetic fibres is much affected by the presence of surface finishes. For example, Hayek and Chromey [13] found a reduction of 10 000 times by a suitable anti-static agent.

Boyd and Bulgin [14] have shown that, when about 30% of carbon black is included in viscose rayon fibres, their specific resistance at 0% r.h. falls from between 10^{14} and $10^{15} \Omega \text{ cm}$ to less than $10^6 \Omega \text{ cm}$. This must be due to the presence of a continuous conducting path of carbon black. With increase of humidity, the resistance increases slightly, presumably owing to a greater dispersion of the carbon black. There is also a change with humidity in the critical concentration of carbon black at which the resistance begins to drop markedly: this rises from 26% carbon black in the dry state to 30% at saturation.

22.4.4 Effect of temperature

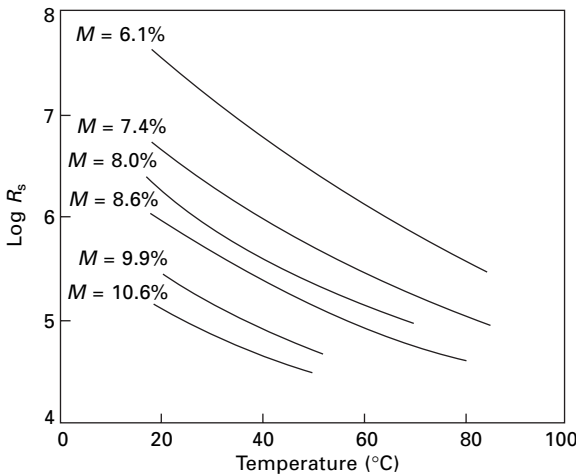
The resistance of fibres decreases as the temperature increases, a rise of 10°C causing a fall of the order of five times. A typical set of results is shown for cotton in Fig. 22.5.

For cotton, viscose rayon and wool, Hearle [5] found that the rate of change of $\log R$ with temperature varied separately with moisture content M and temperature $\theta^\circ \text{C}$.

$$\frac{-d(\log R)}{d\theta} = a - bM - c\theta \quad (22.10)$$

where a , b and c are constants for a given material. Values of a , b and c are given in Table 22.3. The value of a gives the rate of change of $\log R$ with temperature under dry conditions at 0°C , and the values of b and c give the change of $d(\log R)/d\theta$ with moisture content and temperature, respectively.

Clark and Preston [15] have found that the same equation fits the results for

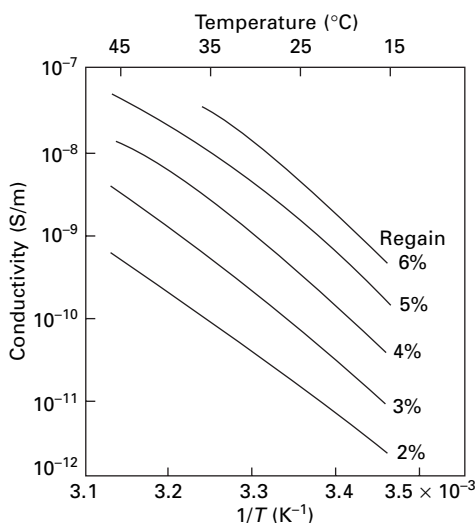


22.5 Variation of resistance of cotton with temperature [5].

Table 22.3 Values of a , b and c [5]

Material	a (per deg C)	b (per deg C per unit moisture content)	c (per deg C per deg C)
Cotton	0.0863	0.005 35	0.000 35
Viscose rayon	0.0707	0.001 86	0.000 37
Wool	0.0960	0.002 12	0.000 57
Acetate*	0.0528	0.000 80	0.000 25
Silk [†]	0.0934	0.002 87	0.000 82

*Only tested over small range.

[†]Near 20 °C and 10% moisture content.

22.6 Variation of conductivity of drawn nylon with temperature [9].

viscose rayon at 24.5% regain down to -60°C . For silk, a relation of the above form is not strictly accurate. For nylon at 20°C and 6% moisture content, it was found that $d(\log R)/d\theta = 0.05$ per $^{\circ}\text{C}$. Sharman *et al.* [9] found that curves of \log (conductivity) against the reciprocal of temperature were approximately parallel at different regains, as is shown in Fig. 22.6.

22.4.5 Arrangement of specimen

One would expect the specific resistance of fibres to vary with the direction of measurement, but, owing to the experimental difficulties, no values for the transverse specific resistance of fibres are available. O'Sullivan [10] found that the resistance of cellulose film parallel to the direction of extrusion was 0.8 times that perpendicular to the direction of extrusion. Hearle and Jones [16] found that the ratios of resistances with three different electrode systems varied with the material and the moisture

content, which indicated that the ratios of specific resistances in different directions varied with these factors.

All the results in the literature, except for those in one paper [17], indicate that the experimentally obtained specific resistance of fibres is independent of the dimensions and form of the specimen. In other words, there is no composite specimen effect, and the resistance of a specimen is proportional to its length and inversely proportional to its area of cross-section (or mass per unit length). This relation will break down if the contact resistance between electrode and specimen becomes comparable with the resistance of the specimen.

Hersh and Montgomery [3] tested nylon specimens ranging in linear density from 3 to 340 den (from 0.33 to 38 tex) and showed that they all gave the same specific resistance. Hearle [4] found only a very small change in resistance when cotton and viscose rayon were subjected to tensions up to near their breaking point.

22.4.6 Polarisation and related effects

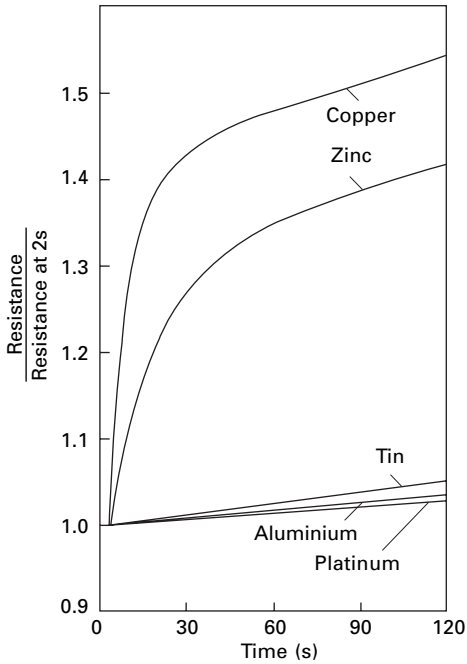
If polarisation, whether electrolytic or electrostatic, causes a back electromotive force (e.m.f.) to occur, it will be detectable in three ways: the resistance will increase with time as the back e.m.f. develops; the resistance will decrease with voltage; and the back e.m.f. will be present, dying away, after the applied voltage has been removed.

Several workers have found that the variation of resistance with time is undetectable or very slight, except at low and high humidities. For raw cotton with tin electrodes, Hearle [4] obtained a significant variation of resistance with time only above 90% r.h. At 17.4% moisture content, the resistance doubled in 30 s. With cotton containing added potassium chloride, the resistance increased with time down to below 50% r.h. With one specimen of wool, the resistance remained constant even at 27% moisture content, but, with another specimen, there was an increase of 7% per minute at 17% moisture content. The nature of the electrodes is an important factor in polarisation effects. The curves in Fig. 22.7 show that, at 9.3% moisture content, the resistance of cotton between copper and zinc electrodes increases rapidly with time, but that, with tin, aluminium, or platinum electrodes, it changes only very slowly. Jones [18] found that a large stainless-steel anode was most effective in eliminating polarisation. On ashing polarised cotton fibres, Williams and Murphy [19] found most of the ash near the electrodes.

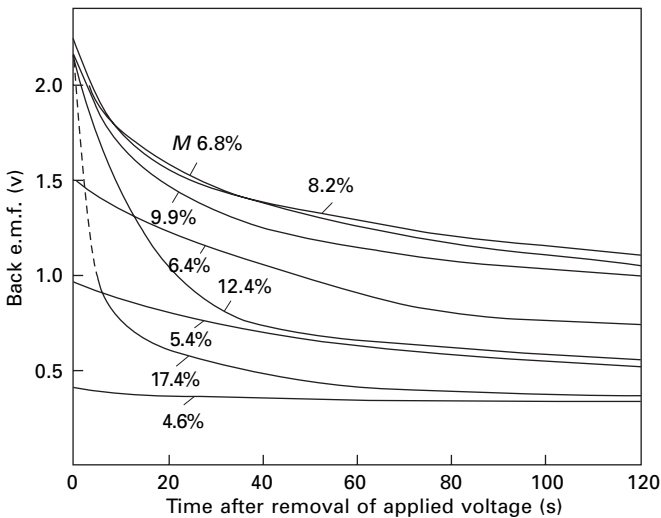
The above effects are typical of polarisation as it occurs in electrolytic solutions, when it is most marked if there is a rapid discharge of ions at the electrodes. It is due to the prevention of the rapid attainment of equilibrium by a slow process at the electrode and is much affected by the nature of the electrodes.

Other effects, such as heating, which will change the temperature and may cause drying, and the transport of water or ions in the specimen, have been suggested as a cause of variation of resistance with time. Although it is likely that these effects may be appreciable in some conditions, they have never been definitely observed.

Back e.m.f. of the order of 2 V has been found by Hearle [4] and others. A set of results for cotton is shown in Fig. 22.8. At low moisture contents, there is only a small back e.m.f. As the moisture content increases, the back e.m.f. also increases



22.7 Variation of resistance of cotton with time for various electrodes [4]. Moisture content = 9.3%.



22.8 Back e.m.f.s in cotton, at various moisture contents, after applying 122 V for 1 min [4].

and reaches a value of about 2 V at 7% moisture content. At higher moisture contents, the back e.m.f. remains the same, but above 9% moisture content it dies away more rapidly after the removal of the applied voltage. The value of the back e.m.f. was found to be different with electrodes of different metals.

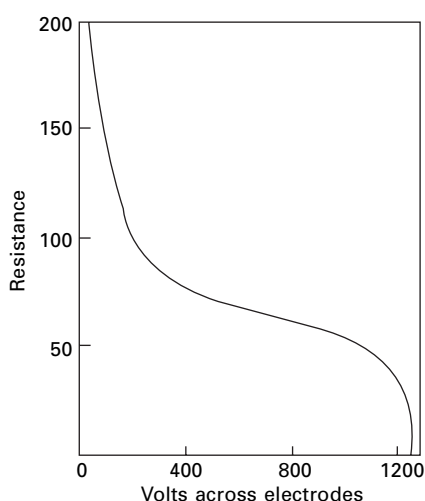
Polarisation effects have also been reported below 25% r.h. for cotton and wool. Murphy [20], working with cotton, found that, under these conditions, the back e.m.f. varied with the applied voltage, and he obtained values of over 100 V. This behaviour indicates electrostatic polarisation.

The variation of resistance with voltage in fibres was observed by Evershed [21] in 1913. Fig. 22.9 shows a typical result for cotton. The decrease of resistance with voltage up to 50 V is adequately explained by the presence of a back e.m.f. of the order of 2 V (Fig. 22.10). Similar effects are observed with other fibres, though with wool the resistance does not vary with voltage below 80% r.h.

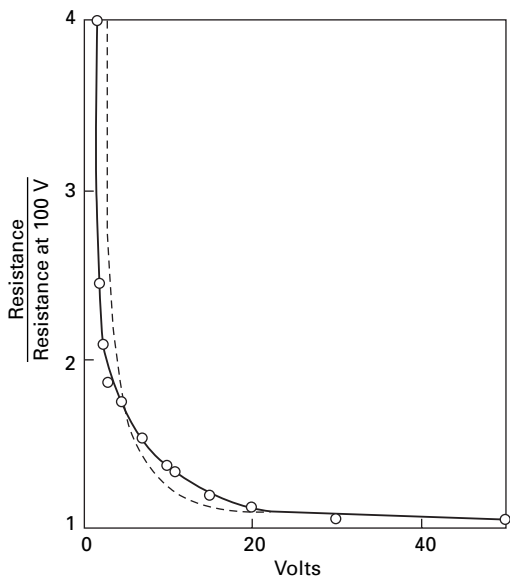
The continuing decrease at higher voltages found by Evershed and others is greater than that due to a small back e.m.f. By testing specimens of various lengths, Hearle [4] showed (Fig. 22.11) that the specific resistance depended on the average field strength (or what comes to the same thing, the current density) rather than on the actual applied voltage.

Hersh and Montgomery [3] have found the resistance of cotton yarns to be ohmic in the range 50–2000 V. However, Cusick and Hearle [22] have suggested that this is because they allowed some time to elapse before measuring the resistance, and consequently an increase of resistance with time fortuitously masked the decrease with voltage. In a later comment, Hersh and Montgomery [23] have suggested that the change in resistance is due to a heating of the specimen. This would be influenced by the air velocity in the neighbourhood of the specimen.

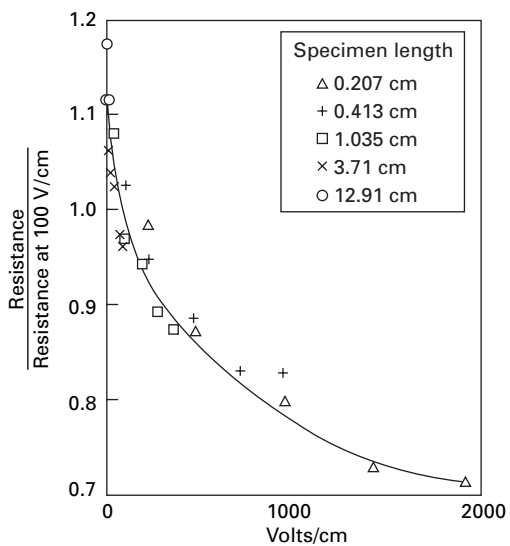
Cusick and Hearle [22] also found that the rate of change of resistance of cotton with time increased as the voltage increased, as shown in Fig. 22.12. When the specimen is left with no voltage applied, the resistance recovers at a similar rate to its previous increase.



22.9 Variation of resistance of cotton with applied voltage. After Evershed [21].



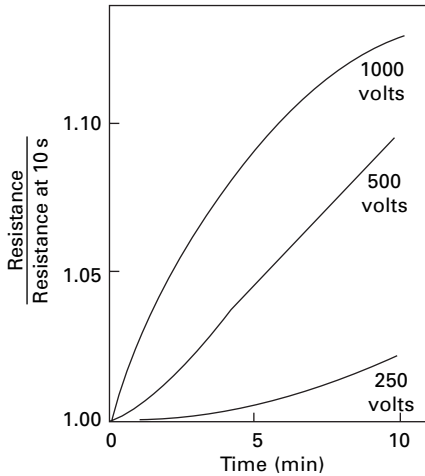
22.10 Variation of resistance of cotton (moisture content = 6.4%) with applied voltage up to 50 V. The dotted line is the theoretical curve for a back e.m.f. of 2 V [4].



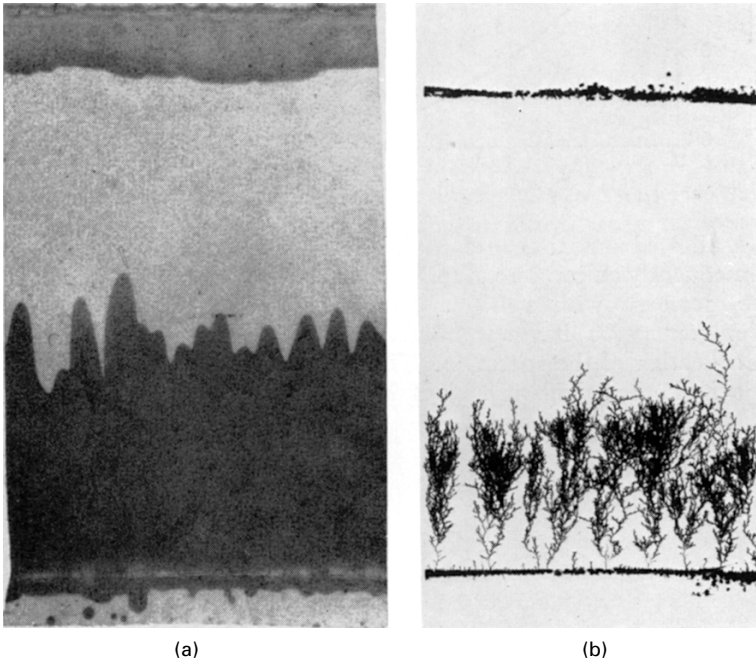
22.11 Variation of resistance with field strength. The points are four specimens of various lengths [4].

22.4.7 Electrolytic effects

During conduction in cellulose film impregnated with salts, O’Sullivan [24] observed phenomena similar to those occurring in the electrolysis of salt solutions. When the film is soaked in sodium chloride, an acid region develops at the anode and an



22.12 Effect of voltage on change of resistance of cotton with time [22].



22.13 Electrolytic effects during conduction in cellulose film. (a) Film impregnated with sodium chloride and an indicator, showing acid and alkaline regions at electrodes. (b) Film impregnated with silver nitrate, showing deposition of silver at cathode and entry of copper at anode.

alkaline region at the cathode. Figure 22.13(a). With silver nitrate in the film, ‘treeing’ occurs (Fig. 22.13(b)) as the silver is deposited at the cathode. The conditions are just those which would cause ‘treeing’ in electroplating (high potential gradient, unstirred bath and low conductivity) and, as in electroplating, it may be avoided by using potassium silver cyanide instead of silver nitrate.

King and Medley [25] measured the amount of hydrogen liberated during conduction in keratin film and found that it was about 90% of that expected from the quantity of electricity passed. There were also small quantities of oxygen and carbon dioxide from the anode reactions.

O'Sullivan [26, 27] measured the bulk mobilities of ions in cellulose film. Typical results are given in Table 22.4.

22.4.8 Resistance noise

Owing to the arrival of current in discrete charges, there is a variable component in direct current. This gives rise to resistance noise, which is one of the factors limiting the amplification of small signals. The magnitude of these random fluctuations has been worked out by Schottky [28] for current carried by electronic charges.

Boyer [29], working with films of various polymers, including cellulose and nylon, has found that the noise level is much higher than that given by Schottky's formula and that the noise has a frequency distribution characteristic of the particular polymer. He concludes that this is due to the arrival of ions at the electrodes in 'avalanches', owing to their being held up at places in the polymer until some movement of the structure allows them to continue to flow.

22.5 Theoretical

22.5.1 Nature of the conduction

In a consideration of the mechanism of conduction of electricity, the first questions to be answered are: 'Where is the current flowing?' and 'What is carrying the current?' Both of these problems have to be solved mainly by circumstantial evidence.

Hersh and Montgomery [3] have shown that for nylon filaments the resistance is inversely proportional to the area of cross-section. This indicates that conduction is predominantly a volume effect, with the current flowing through the bulk of the material. If conduction had been a surface effect, the resistance would have been inversely proportional to the circumference (i.e. the square root of the area or cross-

Table 22.4 Bulk mobility of ions in cellulose film [26, 27]

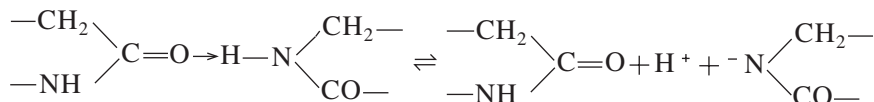
Ion	Mobility in $\text{cm}^2 \text{s}^{-1} \text{V}^{-1}$ at moisture content of:			
	10%	20%	30%	40%
H^+	3×10^{-8}	4×10^{-6}	2.5×10^{-5}	8×10^{-5}
OH^-	1.6×10^{-8}	1.6×10^{-6}	8×10^{-6}	2.5×10^{-5}
K^+	3×10^{-6}	6×10^{-7}	3×10^{-6}	6×10^{-6}
Ag^+	1.6×10^{-7}	4×10^{-6}	1.3×10^{-5}	2.5×10^{-5}
Cl^-	3×10^{-9}	8×10^{-7}	8×10^{-6}	2×10^{-5}
Fe^{2+}		2.5×10^{-7}	1.3×10^{-6}	1×10^{-5}
Cu^{2++}		2.5×10^{-8}	1×10^{-6}	5×10^{-6}
$\text{SO}_4^{2--}, \text{CrO}_4^{2--}$		2×10^{-7}	2.5×10^{-6}	1×10^{-5}
Ca^{2++}				5×10^{-7}

section). Different types of cotton also have the same specific resistance, though here the range of fineness covered is smaller; different qualities of wool differ to an appreciable extent only at low moisture contents, when the influence of impurities is great. Indirect evidence that conduction is a volume effect is provided by the lack of hysteresis between resistance and moisture content (which is a volume, not a surface, quantity), despite the hysteresis between moisture content and relative humidity. Thus, in the hygroscopic fibres, it appears that volume conduction is the dominant effect, surface conduction being negligible in comparison.

Both the close association between resistance and moisture content and the relation between the resistances of cotton and viscose rayon indicate that the current will be flowing in the non-crystalline regions of the fibre. Indeed, the ordered arrangements of cellulose molecules in a crystalline region would be expected to be highly insulating.

In the synthetic fibres, with higher resistance and negligible moisture absorption, surface conduction is likely to be more important and may be the dominant mechanism. Certainly when conducting surface finishes are applied, the current will be almost entirely on the surface.

Current may be carried either by electrons or by ions. Baxter [30], in 1943, put forward a theory that conduction in wool was by electrons, the water molecules acting as impurity centres in an electronic semiconductor, but most workers have assumed that conduction is by ions. Where the products of electrolysis have been directly observed by O'Sullivan [24], using cellulose film, and by King and Medley [25], using keratin film, the current must be ionic. The variation of resistance with electrolyte content and the polarisation effects also support this view. Thus, where there is evidence, it indicates that conduction is ionic, but, where there is no special evidence (for example, at low moisture contents), it cannot be definitely stated that conduction is not electronic. A specialised mechanism that Baker and Yager [31] have suggested for the polyamides is the mobility of hydrogen atoms (protons) from hydrogen bonds. This can, however, be regarded as equivalent to other forms of ionic conduction, since it is essentially an ionisation at the hydrogen bond:



With the possible exceptions noted above, the general picture is of ionic conduction taking place through the bulk of the material. The next step is to consider theories that will explain the enormous variation of resistance with moisture content, the large variation with temperature, and other effects, such as the higher resistance of protein fibres and the low conductivity of bivalent ions. There are two possible causes of variation of resistance: there may be changes in the number of ions available for conduction or there may be changes in the rate at which the ions move through the material under a given applied voltage.

For a specimen having ν ions per unit length available for conduction, with z as the valency of the ions and e as the electronic charge, and on the assumption that the ions move with an average velocity u under a potential difference V between the ends of the specimen, the current I and resistance R are given by:

$$I = vzeu \quad (22.11)$$

$$R = \frac{V}{I} = \frac{V}{vzeu} \quad (22.12)$$

For further study, it is convenient to separate the factors by taking logarithms:

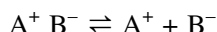
$$\log R = \log V - \log v - \log ze - \log u \quad (22.13)$$

22.5.2 Influence of permittivity on dissociation of ion pairs

There has been no success in attempting to explain the enormous changes of resistance with moisture content on the basis of changes in rate of ion movement. The most likely theory, proposed by O'Sullivan [32] and based on breaks in conducting water paths, was shown by Hearle [33] to be impossible because of the polarisation that would occur. For a successful theory, we must look to changes in the number of available ions.

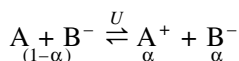
Strong electrolytes are completely ionised, and the ions can be held together in molecules only by electrostatic forces. In solutions in liquids of high permittivity, such as water, these forces are so weak that there is no close association of ions, but even weak inter-ionic forces prevent the ions from acting as completely free particles.

If the permittivity of the solvent is lower, the electrostatic forces will be stronger, and we may consider an equilibrium between ion pairs and free ions

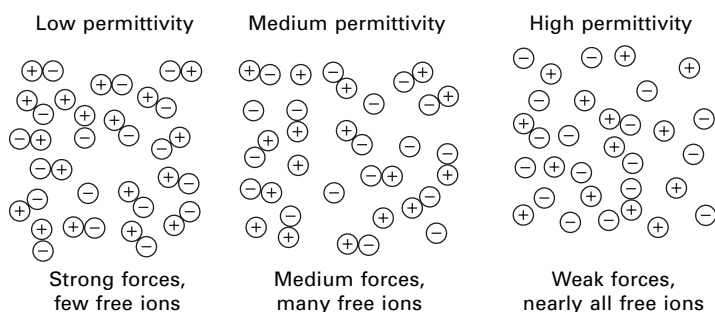


The variation in this equilibrium offers a possible explanation of variations in resistance. A rise in permittivity would cause more dissociation, making more free ions available for conduction and consequently lowering the resistance. This is illustrated diagrammatically in Fig. 22.14.

A simplistic theory, which applies macroscopic ideas to molecular phenomena and does not take account of the interaction of all the ions present, has been put forward by Hearle [33]. Let α be the degree of dissociation of the ion-pairs:



It can be shown that, as a consequence of the Law of Mass Action:



22.14 Effect of permittivity on association of ions.

$$\frac{\alpha^2}{1-\alpha} = A e^{-U/kT} \quad (22.14)$$

where U = the energy of dissociation, k = Boltzmann's constant, T = absolute temperature and A = a constant, of the order of the ratio of the total volume to the volume occupied by ions.

The energy needed to separate two electrostatic charges in a medium of relative permittivity ϵ_r is given by:

$$U = \frac{U_0}{\epsilon_r} \quad (22.15)$$

where U_0 = the energy needed to separate the ions in a medium of unit relative permittivity and is thus a constant. Hence:

$$\frac{\alpha^2}{1-\alpha} = A e^{-U_0/\epsilon_r kT} \quad (22.16)$$

If $\alpha \ll 1$, that is when most of the ions are associated in pairs:

$$\frac{\alpha^2}{1-\alpha} \approx \alpha^2 \quad (22.17)$$

Hence:

$$\alpha = A^{1/2} e^{-U_0/2\epsilon_r kT} \quad (22.18)$$

But, if v_0 is the total number of electrolyte molecules per unit length of specimen, then the number of ions available for conduction is given by:

$$v = 2 \alpha v_0 \quad (22.19)$$

and, substituting in equation (22.13), we get:

$$\begin{aligned} \log R &= \log \frac{V}{u z e} - \log \alpha - 2 \log v_0 \\ &= \log \frac{V}{2 A^{1/2} u z e v_0} + \frac{U_0 \log e}{2 k T} \frac{1}{\epsilon_r} \end{aligned} \quad (22.20)$$

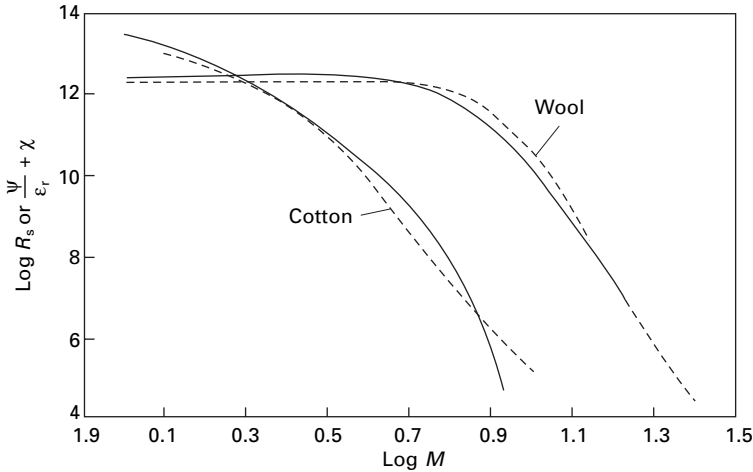
This may be written:

$$\log R = \frac{\Psi}{\epsilon_r + \chi} \quad (22.21)$$

where $\Psi = (U_0 \log e)/(2 k T)$ and $\chi = \log (V/2 A^{1/2} u z e v_0)$.

After suitable values for Ψ and χ have been chosen, equation (22.21) can be tested with experimental results. Figure 22.15 shows a comparison of Hearle's values of resistance with theoretical predictions in which Balls's values [34] of the permittivity of cotton and King's values [35] of the permittivity of keratin film have been used. For cotton, there is a good fit with $\Psi = 76.8$ and $\chi = 1.1$ and for wool with $\Psi = 42.2$ and $\chi = 3.6$. The coincidence of the bending-over of the curve for wool is particularly striking.

From the value chosen for Ψ , the values of U_0 can be calculated. With $\Psi = 76.8$



22.15 comparison of experimental (full lines) and theoretical (dotted lines) curves for variation of resistance of cotton and wool with moisture content [33]. The theoretical expressions are:

$$\text{Cotton:} \quad \text{Log } R_s = \frac{76.8}{\epsilon_r} + 1.1$$

$$\text{Wool:} \quad \text{Log } R_s = \frac{42.2}{\epsilon_r} + 3.6$$

and at room temperature, $T \approx 300 \text{ K}$, this gives $U_0 \approx 1.5 \times 10^{-18} \text{ J}$. This may be compared with the energy required to separate two electronic charges, initially at a distance apart equal to the ionic diameter, i.e. of the order of $5 \times 10^{-10} \text{ m}$, which gives $U_0 \approx 5 \times 10^{-18} \text{ J}$. Thus the chosen value of Ψ proves to be of the right order of magnitude.

This theory will explain the high resistance of multivalent ions. If the ions have valencies z_1 and z_2 , then, considering isolated charges separated by a distance X , we have

$$U = \frac{z_1 z_2 U_0}{\epsilon_r} \approx \frac{z_1 z_2 e^2}{\epsilon_r X} \quad (22.22)$$

where U_0 is assumed to be the value for monovalent ions.

Equation (22.21) therefore becomes:

$$\log R = \frac{z_1 z_2 \Psi}{\epsilon_r + \chi} \quad (22.23)$$

The value of $\log R$ is thus increased by an amount $(z_1 z_2 - 1) \Psi / \epsilon_r$ compared with the value with the same number of monovalent ions present. Some values of this quantity are given in Table 22.5. These figures, being differences in $\log R$, give the number of powers of 10 by which the resistance with multivalent ions would be greater than the resistance with monovalent ions. It will be seen that, in almost all cases, conduction by multivalent ions would be negligible.

Although the constants Ψ and χ would not be expected to be exactly the same for different materials, Hearle [36, 37] has shown that, when values of $\log R_s$ are plotted

Table 22.5 Values of $(z_1 z_2 - 1) \Psi / \epsilon_r$ [33]

ϵ_r	$\Psi = 76.8$		$\Psi = 42.2$	
	$z_1 z_2 = 2$	$z_1 z_2 = 4$	$z_1 z_2 = 2$	$z_1 z_2 = 4$
1	76.8	229	42.9	126
5	15.4	46	8.4	25
10	7.7	23	4.2	13
15	5.1	15	2.8	8
20	3.8	11	1.1	3

against values of $1/\epsilon_r$ (all determined under the same conditions), the straight lines do group closely together. In particular, the differences in their permittivities explain the differences in resistance between cellulosic and protein fibres under similar moisture conditions.

22.5.3 Conduction at high moisture contents

At high moisture contents, when the permittivity becomes high, the condition $\alpha \ll 1$ will break down, and dissociation will become almost complete. Equation (22.21) will then cease to apply, and the effect of the permittivity will be small. Theoretical estimates, based on the value of A , and experimental results for the dissociation of electrolytes in liquids both indicate that α becomes near to unity for permittivities greater than 20. Under these conditions, an alternative mechanism will be limiting the conduction. The theory of breaks in conduction paths would also break down at high moisture contents, when breaks become negligible.

At high moisture contents, the ions will be moving along water paths and their speed will be limited by viscous hindrance to their flow. If the paths are narrow and the water is moving with the ions, Poiseuille's equation for the flow of liquids along tubes should apply to the velocity u of the ions, to give:

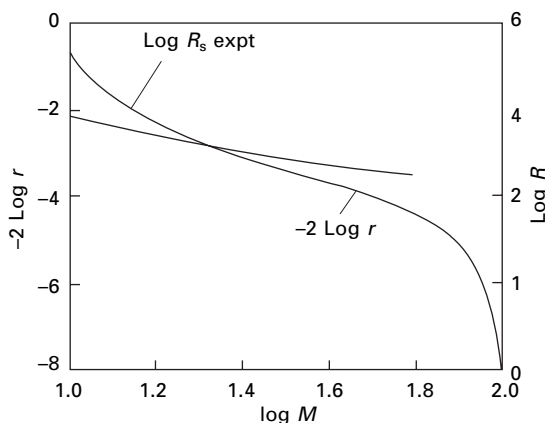
$$u \propto (\text{radius of tube})^4 \propto (\text{volume of water})^2 \propto (\text{regain})^2$$

Note that it is regain r (mass of water per mass of fibre), which tends to infinity as a maximum, and not moisture content M (mass of water per mass of water + fibre), which tends to 1, that is the relevant quantity.

Thus, from equation (22.13):

$$\log R = \log(\text{constant}) - 2 \log r = \log(\text{constant}) - 2 \log M + \log (1 - M) \quad (22.24)$$

As shown in Fig. 22.16, an equation of this form does have approximately the right slope for a plot of $\log R$ against $\log M$ over a range of about 15–30% moisture content for cotton, when the experimental plot starts to level off. Equation (22.24) then has a rapid fall as $\log(1 - M)$ tends to minus infinity. However, at high moisture contents, the tubes become much wider, the ions would effectively be moving through an infinite medium, and the velocity would tend to a constant value, determined by Stokes' equation and giving a constant resistance.



22.16 Comparison of variation of $\log R_s$ and $(-2 \log r)$ with moisture content [33].

22.5.4 An alternative theory

Baxter's [30] theory for wool was that conductance C was due to electrons jumping between absorbed water molecules, so that the decrease in resistance as moisture regain r increased was due to the reduction in distance between absorbed water molecules. His result given below can be transformed into an expression for resistance R :

$$C = A \exp\left(\frac{-B}{r^{1/3}}\right) \quad (22.25)$$

$$\log R = \frac{b}{r^{1/3} - a} \quad (22.26)$$

where r = regain and A , B , a and b are constants.

Christie and coworkers [38, 39] argue that conduction is by mobile protons. Since Baxter's model is independent of the charge carrier, they adapt his equation. For cellulose fibres [38], they find that it is necessary to offset the regain by an amount r_0 , for which they offer possible explanations. The equations become:

$$C = A \exp\left[\frac{-B}{(r - r_0)^{1/3}}\right] \quad (22.27)$$

$$\log R = \frac{b}{(r - r_0)^{1/3} - a} \quad (22.28)$$

This equation gives good agreement with the experimental results for cotton over the measured range to 20% regain. For viscose rayon there is agreement up to 40% regain, but then the conductance levels off.

In order to fit data for wool and silk [39], it was necessary to introduce extra terms to allow for conductivity at zero regain C_0 and for strongly and weakly bonded water:

$$C = C_0 + A_s \exp[-B_s/(r_s)^{1/3}] + A_w \exp[-B_w/(r_w)^{1/3}] \quad (22.29)$$

This accords with two-phase theories of moisture absorption (see [Chapter 12](#)). Although the model could be interpreted as defining the rate at which protons move through the material, it can also be related to the numbers available to jump in a given time, which fits the dissociation model. Introduction of the dependence of dielectric constant on regain might show that there was less difference between the theories than is first apparent.

22.6 References

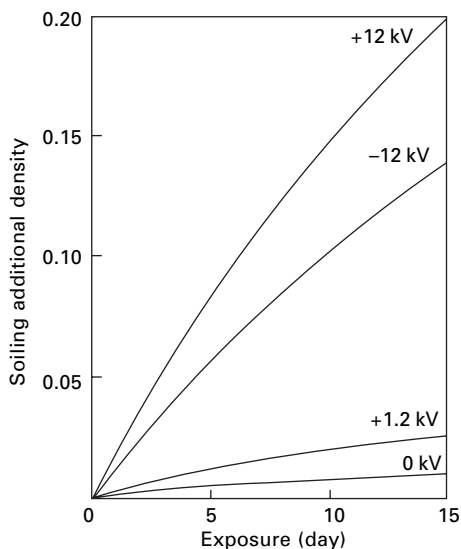
1. J. W. S. Hearle. *J. Text. Inst.*, 1952, **43**, P194 (review of literature).
2. J. W. S. Hearle. *J. Text. Inst.*, 1953, **44**, T117.
3. S. P. Hersh and D. J. Montgomery. *Text. Res. J.*, 1952, **22**, 805.
4. J. W. S. Hearle. *J. Text. Inst.*, 1953, **44**, T155.
5. J. W. S. Hearle. *J. Text. Inst.*, 1953, **44**, T144.
6. G. E. Cusick and J. W. S. Hearle. *J. Text. Inst.*, 1955, **46**, T699.
7. G. E. Cusick and J. W. S. Hearle. *J. Text. Inst.*, 1955, **46**, T369.
8. E. J. Murphy and A. C. Walker. *J. Phys. Chem.*, 1928, **32**, 1761.
9. E. P. Sharman, S. P. Hersh and D. J. Montgomery. *Text. Res. J.*, 1953, **23**, 793.
10. J. B. O'Sullivan. *J. Text. Inst.*, 1947, **38**, T271.
11. A. C. Walker and M. H. Quell. *J. Text. Inst.*, 1933, **24**, T123.
12. H. F. Church. *J. Soc. Chem. Industr.*, 1947, **66**, 221.
13. M. Hayek and F. C. Chromey. *Amer. Dyest. Rep.*, 1951, **40**, 164.
14. J. Boyd and D. Bulgin. *J. Text. Inst.*, 1957, **48**, P66.
15. J. F. Clark and J. M. Preston. *Text. Res. J.*, 1955, **25**, 797.
16. J. W. S. Hearle and E. H. Jones. *J. Text. Inst.*, 1949, **40**, T311.
17. F. Weidmann. *Kunststoffe*, 1939, **29**, 133.
18. E. H. Jones. *J. Sci. Instrum.*, 1940, **17**, 55.
19. R. R. Williams and E. J. Murphy. *Bell Syst. Tech. J.*, 1929, **8**, 225.
20. E. J. Murphy. *J. Phys. Chem.*, 1929, **33**, 200.
21. S. Evershed. *J. Instn Elect. Engrs*, 1913, **52**, 51.
22. G. E. Cusick and J. W. S. Hearle. *Text. Res. J.*, 1955, **25**, 563.
23. S. P. Hersh and D. J. Montgomery. *Text. Res. J.*, 1955, **25**, 566.
24. J. B. O'Sullivan. *J. Text. Inst.*, 1947, **38**, T285.
25. G. King and J. A. Medley. *J. Colloid Sci.*, 1949, **4**, 1.
26. J. B. O'Sullivan. *J. Text. Inst.*, 1947, **38**, T291.
27. J. B. O'Sullivan. *J. Text. Inst.*, 1947, **38**, T298.
28. S. Schottky. *Ann. der. Phys.*, 1918, **57**, 541.
29. R. F. Boyer. *J. Appl. Phys.*, 1950, **21**, 469.
30. S. Baxter. *Trans. Faraday Soc.*, 1943, **39**, 207.
31. W. O. Baker and W. A. Yager. *J. Amer. Chem. Soc.*, 1942, **64**, 2171.
32. J. B. O'Sullivan. *J. Text. Inst.*, 1948, **39**, T268.
33. J. W. S. Hearle. *J. Text. Inst.*, 1953, **44**, T177.
34. W. L. Balls. *Nature*, 1946, **158**, 9.
35. G. King. *Trans. Faraday Soc.*, 1947, **43**, 601.
36. J. W. S. Hearle. *Text. Res. J.*, 1954, **24**, 307.
37. J. W. S. Hearle. *J. Text. Inst.*, 1957, **48**, P40.
38. J. H. Christie and I. M. Woodhead. *Textile Res. J.*, 2002, **72**, 273.
39. J. H. Christie, I. M. Woodhead, S. Krenek and J. R. Sedcole. *Textile Res. J.*, 2002, **72**, 303.

23.1 Introduction

Some of the effects of static electricity were described by Thales in about 600 BC, and the first understanding of the nature of electricity came from the study of the phenomenon of static electricity in the 18th century. After the discovery of current electricity, however, the study of static electricity, with all its experimental difficulties, was neglected, but the increasing amount of trouble in industry that is due to static, resulting from the introduction of new materials, particularly synthetic fibres, led to a revived interest in it [1–3]. Holme *et al.* [4] have published a more recent review. Through its effects, static causes a variety of troubles in textile materials and processing.

Similar charges repel one another. This causes difficulty in handling materials. The filaments in a charged warp will bow out away from one another. There will be ‘ballooning’ of a bundle of slivers. Cloth will not fold down neatly upon itself when it comes off a finishing machine and so on. Unlike charges attract one another. This has caused difficulty in the opening of parachutes. It will also cause two garments, oppositely charged, to stick to one another, and in movement one garment may ride up on the other and cause embarrassment to the wearer. Another consequence is the attraction to a charged material of oppositely charged particles of dirt and dust from the atmosphere (Fig. 23.1). After 15 days, the soiling of a cotton fabric held at +1.2 kV was over twice as severe as at 0 kV. At –12 kV it was 13 times worse, but at +12 kV it was 19 times worse owing to the preponderance of negatively charged dirt particles in the atmosphere [5]. This fine dirt adheres so firmly that it is difficult to remove and causes serious soiling. When this occurs on the portion of cloth in a loom that is left exposed overnight, it is known as ‘fog-marking’. The effects of attraction and repulsion were described by Robert Symmer in 1759, who used to wear two pairs of stockings, white worsted for comfort and black silk for appearance: on separating the stockings: ‘the repulsion of those of the same colour, and the attraction of those of different colour, throws them into an agitation that is not unentertaining’.

Charged bodies are attracted to uncharged bodies. Consequently, fibres will stick to earthed parts of machines; this happens particularly in carding. When a charged yarn is passing through a guide, the extra-normal force due to this attraction may notably increase the friction. Another consequence is that uncharged particles in the atmosphere will be attracted to a charged material.



23.1 Effect of potential on soiling of cotton fabric. After Rees [5].

When high enough fields occur, discharge in air will take place with accompanying sparks. This is easily noticeable on taking off charged clothing. The noise of the discharge may be a nuisance in some special cases, for example in the fur hoods worn in arctic conditions. There is also a risk of fire or explosion owing to the sparks. This is a danger in the textile industry only in exceptional circumstances, but sparks from clothing are a source of danger where inflammable vapours are present, as in the operating theatres of hospitals. Shocks will be given to people coming into contact with static charges. These are only serious where a large insulated conductor (for example, a machine on an insulating floor) has become charged up. The remedy is to earth the machine. More commonly, individuals act as condensers with a large capacity. Walking on a carpet or sliding off a car seat can lead to accumulation of a large charge. On touching metal, a door handle or whatever, the discharge gives a nasty shock.

As discussed below, the limiting condition for high static charges, and hence the susceptibility to troubles in use, has been shown to depend on the resistance of the material. Low-resistance materials such as cotton and viscose rayon will rarely give static troubles; higher-resistance materials such as wool, silk and acetate will give trouble more often; and the very high-resistance synthetic fibres will give most trouble. The speed of the process is also important: thus, to avoid fog-marking in weaving, dissipation in 10 minutes, needing a total current of $0.003 \mu\text{A}$, is adequate, but, to avoid trouble in carding, dissipation must take place in 0.1 s, which needs $0.07 \mu\text{A}$; to avoid trouble in warping, it must take place in 0.01 s, which needs $5 \mu\text{A}$.

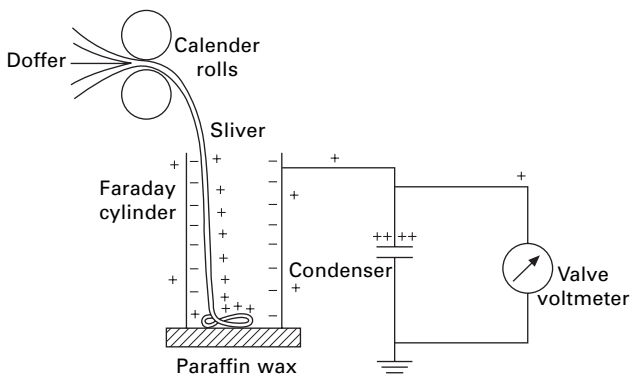
Methods of getting rid of static charges depend upon increasing the leakage by lowering the resistance of either the material or the air, or by providing a conducting liquid at the separation. The resistance of the material may be lowered by raising the humidity or by moistening it. The resistance of the air may be lowered by ionising it,

either by using a high-voltage static eliminator or by the presence of a radioactive material. Safe concentrations of the latter are only sufficient to cause a slow discharge. The use of electrostatic eliminators in the textile industry has been described by Henry [6]. The use of anti-static agents is discussed by Sagar [7], Götze *et al.* [8] and Holme *et al.* [4]. Unfortunately, the hygroscopic salts that are the most effective anti-static agents are usually unsuitable for other reasons.

23.2 Measurement of static

The methodology can be illustrated by methods used in the earlier studies of textile charging. The principles remain the same, but advances in electronics have changed the devices used in electrical measurements [9]. The amount of static present should be expressed by the magnitude of the charge on the material. This may be measured by the use of a Faraday cylinder. Figure 23.2 shows the apparatus used by Keggin *et al.* [10] to measure the charge on card sliver after carding. The charged material in the cylinder induces an equal opposite charge on the inside of the cylinder (since there can be no net charge inside a closed conductor), and this leaves an equal charge, of the same sign as that on the material, to be shared between the outside of the cylinder and a condenser, which give a total capacitance C . The potential V is measured by a voltmeter and the charge Q can be calculated from the usual expression $Q = CV$.

When the specimen cannot be surrounded, even approximately, by a conductor, the potential to which a neighbouring conductor, the 'probe' electrode, comes may be used as a measure of the charge on the specimen. Unless the geometry is simple enough for the induction coefficients to be calculated, this can give only an arbitrary value. However, when the position, size, shape and charge distribution of the specimen remain constant, it is a useful method for obtaining relative values under different conditions. Some authors have replaced the specimen by a conductor of the same size and shape and, by raising this to known potentials, have obtained a calibration for what they refer to as 'the potential of the specimen'. It is, however, meaningless to



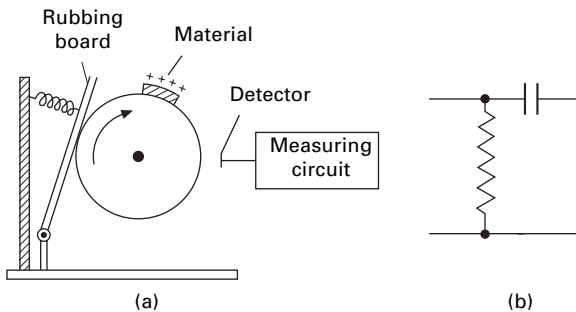
23.2 Measurement of charge by means of a Faraday cylinder. After Keggin *et al.* [10].

talk about the potential of an insulator, since only conductors come to an equal potential at all points.

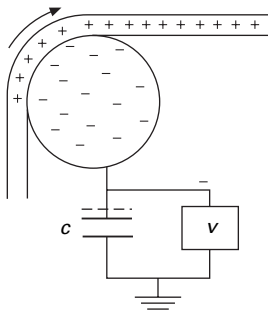
The potential of the probe electrode may be measured either with a d.c. electrometer or by converting it into an alternating potential. Hayek and Chromey's method [11] (Fig. 23.3(a)), illustrates the latter technique. When the specimen, which has been charged by contact with the paddle, passes the probe electrode, an impulse is transmitted to the measuring circuit. The reading of the detector gives an arbitrary measure of the charge on the specimen. Since the input acts as a resistance/capacity differentiating circuit (Fig. 23.3(b)), it is important that the speed of the drum should be constant.

Another method of obtaining the charge on a specimen, which has been used by Medley [12] and by Gonsalves and van Dongeren [13], is to measure the charge remaining on the conductor from which the specimen is separated. This is illustrated in Fig. 23.4. The potential difference between the rod and earth is indicated on the electrometer, V . From a knowledge of the total capacity to earth, the charge left on the rod and the condenser can be calculated. It will be equal and opposite to the charge on the material, provided that no leakage has occurred to other points. If the capacity to earth is large, the rod will remain close to earth-potential but measurable during a test.

The use of electrostatic field meters and voltmeters to measure surface charge distributions is discussed by Seaver [14] and Durkin [15]. Ellison [16] describes a robotic method.



23.3 (a) Intermittent detection by probe electrode. After Hayek and Chromey [11]. (b) Effective input circuit.



23.4 Measurement of charge remaining on conductor.

23.3 Results

23.3.1 Formation of charge

It was once thought that the conditions necessary for charges to appear were a difference between the nature of the surfaces and rubbing between them. It is now clear that either of these conditions by itself is sufficient. The mere separation of two unlike surfaces has been shown to result in a separation of charge, and Henry [17] and others have shown that the asymmetric rubbing of two identical surfaces results in a transfer of charge.

A familiar idea is that of an electrostatic series, in which materials can be arranged in an order such that, on the separation of any two materials, the higher on the list will be positively charged and the lower negatively charged. However, many workers have produced series that are inconsistent with one another, or have found it impossible to produce self-consistent lists. Henry [17] has shown that, provided that care is taken to minimise non-equilibrium effects due to friction, a series of ten materials could be placed in order with no significant inconsistencies. If the equilibrium charge separations at contact could be measured, not only should they be self-consistent in sign, but the magnitude of the charges should also be additively related to one another. Leakage usually prevents the testing of such a relation, but Harper [18] has shown that it holds for a number of metals. Hersh and Montgomery [19] also found a correlation of the magnitude of the charge generated when metals were rubbed on insulators with the work function¹ of the material and the position of the insulator in the series. Arridge [20] confirmed the correlation with the work function of the metal in experiments on nylon.

Table 23.1 gives the series found in three investigations. Polyamides and wool, which both contain $\text{—CO}\cdot\text{NH—}$ groups, are at the positive end; cellulose, acrylics and similar materials are in the middle; and the more inert polymers are at the negative end. Cohen [23] suggested that, on the separation of two materials, the one with the high permittivity would become positive; this rule is not of universal validity but may apply to a limited class of materials.

Reversals of the signs of charges owing to very slight (and sometimes undetected) changes of conditions have often been reported. These reversals must be associated with a change in the mechanism of charge transfer. Gonsalves and van Dongeren [13] frequently found a change from positive to negative, as shown later in Fig. 23.9(B)), on an insulator rubbed against a metal as the pressure increased, but they did not find the reverse change.

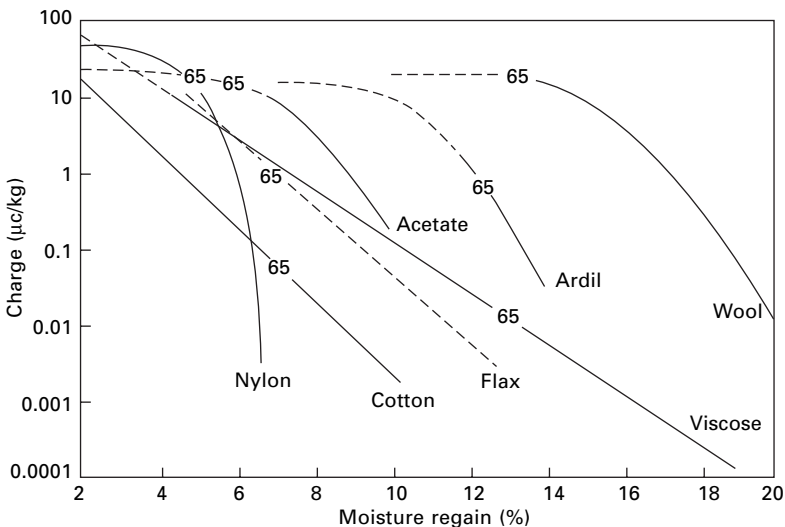
Martin [24] found that, when a wool fibre was pulled out by the root end from a bundle of wool fibres, all lying in the same direction, it became positively charged, whereas when it was pulled out by the tip end, it became negatively charged.

Owing to slight differences in the surface or the asymmetry in the rubbing, charges may easily be generated by inter fibre contact between apparently identical fibres.

¹The work function of a metal is the energy needed by an electron in order to free itself from the metal.

Table 23.1 Electrostatic series

	Smith <i>et al.</i> [21]	Tsuji and Okada [22]	Hersh and Montgomery [19]
Positive (+)	Wool Hercosett wool Nylon 6.6 Nylon 6 Silk Regenerated cellulose Cotton Poly(vinyl alcohol) (PVA) Chlorinated wool Cellulose triacetate Calcium alginate Acrylic Cellulose acetate Polytetrafluoroethylene (PTFE) Polyethylene Polypropylene Poly(ethyleneterephthalate) Poly(1,4-butylene terephthalate) Modacrylic	Glass Nylon 6.6 Nylon 6 Wool Silk Viscose Vinylon (PVAlc) Acrilan (acrylic) Steel Cotton Orlon (acrylic) Acetate Dynel (VC/AN) Saran (PVDC) Rhovyl (PVC) Rubber	Wooll Nylon Viscose Cotton Silk Acetate Lucite (PMMA) PVAlc Dacron (polyester) Orlon (acrylic) PVC Dynel (VC/AN) Velon (VDC/VC) Polyethylene Teflon (PTFE)
Negative (–)	Chlorofibre		



23.5 Charge left on sliver after carding, marking 65% at r.h. level. After Keggin *et al.* [10].

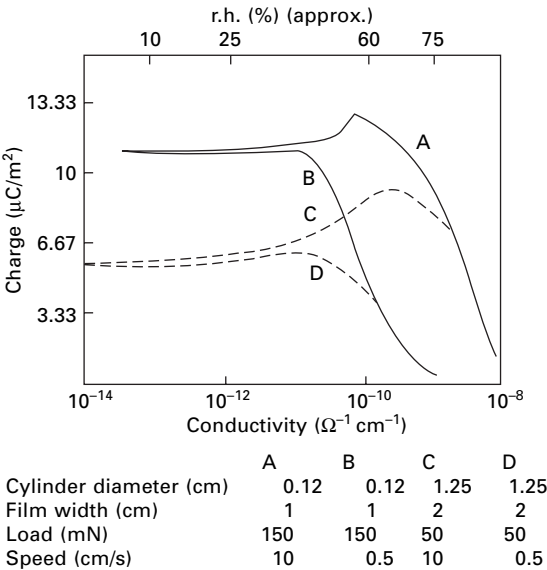
23.3.2 Magnitude of charge

Figure 23.5 shows the charges remaining on the sliver emerging from a card as measured by Keggin *et al.* [10]. It will be seen that at low regains all the materials acquire approximately the same charge. This charge remains constant as the regain

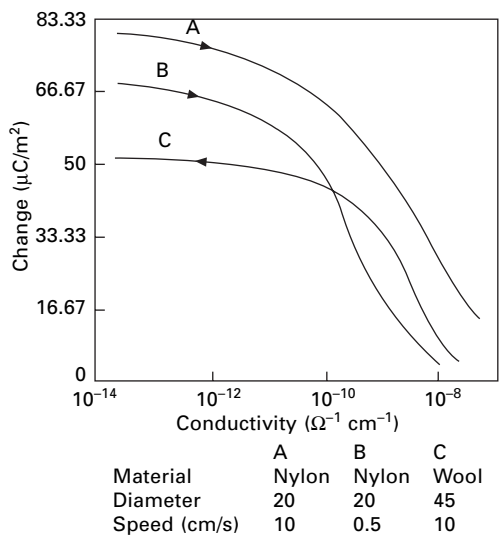
increases until a certain value is reached, and it then drops rapidly for further increases of regain. The points corresponding to 65% r.h. have been marked on the graph, and they illustrate the susceptibility of different fibres to static under the same atmospheric conditions. The amount of static necessary to cause processing difficulties varies from one material to another and is affected by the amount of crimp in the fibre.

Results similar to these have been obtained by Gonsalves and van Dongeren [13] and Medley [12, 25, 26]. The most convenient way of expressing the results is as surface-charge density in microcoulombs per square metre ($\mu\text{C}/\text{m}^2$). Figure 23.6 shows the charge on nylon film and Fig. 23.7 the charge on single fibres, drawn over platinum rods. It appears that, when the conductance is above a certain value, the charge observed falls rapidly as the conductance increases. A similar result (Fig. 23.8) is obtained when a wool roving that has been coated with a surface-conducting agent emerges from between rollers. The conductance necessary for the rapid drop in charge to start is affected by the speed with which the material is passing through the rollers; the higher the speed, the greater is the conductance necessary. This is shown by the results in Table 23.2. In practice, it is found that the cellulosic fibres are least troubled by static charges; wool and silk are intermediate; and acetate, nylon, polyester, acrylic and other synthetic fibres are most affected. This accords with their electrical resistances as given in Chapter 22.

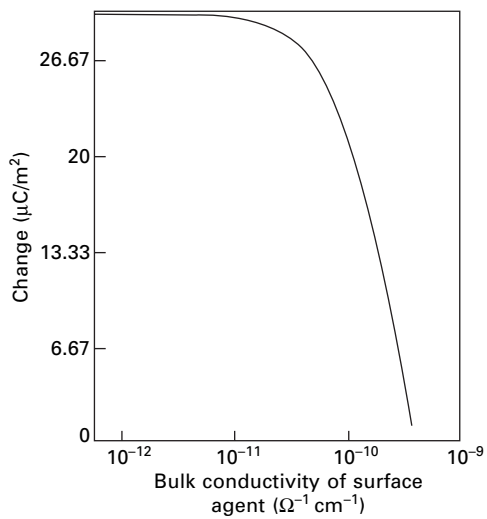
Medley [26] found that the charge increased with the pressure applied to the rollers, probably owing to an increase in the true area of contact. Gonsalves and van Dongeren [13] found similar results (Fig. 23.9) when the contact pressure for rayon and nylon threads wrapped round a cylinder was increased by increasing either the pre-tension or the angle of wrap. The unfinished rayon thread is an example of the sign change with pressure mentioned earlier (Section 23.3.1). In his experiments



23.6 Charge developed on nylon film pulled over platinum cylinder [12].



23.7 Charge developed on single fibres pulled over 0.1 cm diameter platinum cylinder [12].



23.8 Electrification of wool roving coated with surface-conducting agent, on pulling through rollers at 10 cm/s [26].

with material emerging from rollers, Medley [26] also measured the charge lost to neighbouring conductors. When charged roving was passed through a small metal loop, its charge was reduced to less than $0.67 \mu\text{C}/\text{m}^2$: a metal wire held 5 mm below the roving and a metal sheet held 5 cm below it were less effective in discharging the roving.

Lowering the atmospheric pressure reduces the charges that are obtained, as is shown in Fig. 23.10, except at low pressures. In a high vacuum large charges are

Table 23.2 Critical conditions for electrostatic charges (after Medley [25])

(a) Without surface-conducting agents

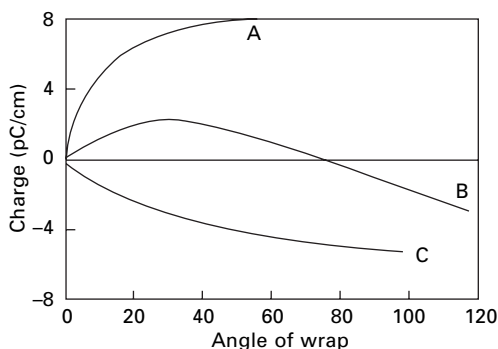
Material	Rollers	Speed (cm/s)	Charge halved at:		$\frac{kt}{\epsilon_0 v}$ or $\frac{ka}{2\epsilon_0 v}$ (see Section 23.5.2) ($\Omega^{-1} \text{ m}^{-1} \text{ s}$)
			r.h. (%)	conductance	
Woollen taffeta	Steel	5.0	40	$1.2 \times 10^{-12*}$	2.8
		2.0	75	$0.4 \times 10^{-12*}$	2.1
		11.0	75	$1.6 \times 10^{-12*}$	1.6
Filter paper	Steel	11.0	40	$1.7 \times 10^{-12*}$	1.8
		15.0	40	$3.4 \times 10^{-12†}$	2.0
Wool roving $a = 0.2 \text{ cm}$	Cork	11.0	70	$3.6 \times 10^{-12†}$	2.9
		1.25	70	$0.6 \times 10^{-12†}$	4.0

* Ω^{-1} for 1 cm length and breadth equals kt .† Ω^{-1} for 1 cm length, equals $2\pi a (ka)$.

‡ KC1-treated.

(b) For wool roving with surface-conducting agent. Cork rollers

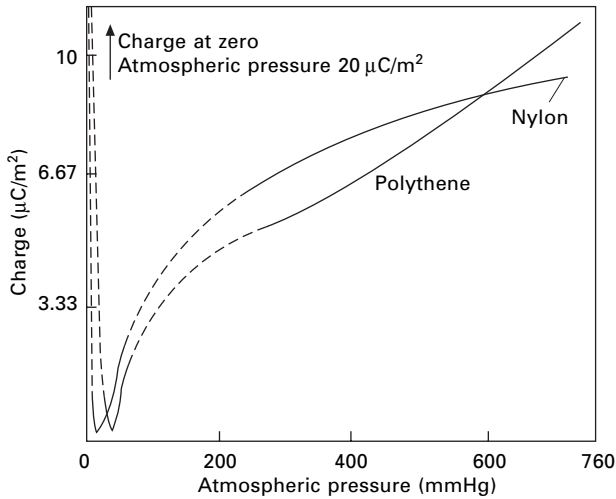
Aerosol OT in combing oil (%)	Bulk conductivity of agent ($\Omega^{-1} \text{ cm}^{-1}$)	Speed at which charge reduced to $12 \mu\text{C}/\text{m}^2$ (cm/s)
0	2×10^{-12}	Unobtainable
1	1×10^{-10}	3
3	2.5×10^{-10}	10



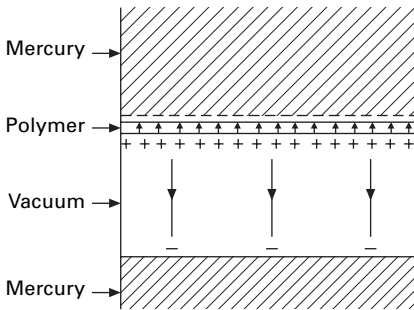
23.9 Effect of wrap on charge on yarn rubbed over steel rod [13]: A, finished rayon; B unfinished rayon; C nylon (approximately 20% r.h.).

obtained. Medley [25] found that, when the air was saturated with carbon tetrachloride, the charge on nylon film increased by 50%. On the other hand, ionising the air reduces the charges that can be obtained.

The maximum charge densities obtained by Medley were about $30 \mu\text{C}/\text{m}^2$ on films, cloth, and roving and about $160 \mu\text{C}/\text{m}^2$ on single fibres. Other workers have also found limiting values of about this amount. However, by an ingenious technique,

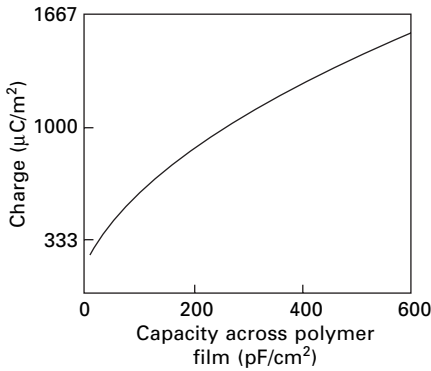


23.10 Effect of atmospheric pressure on charge left on films pulled over platinum wire [12].

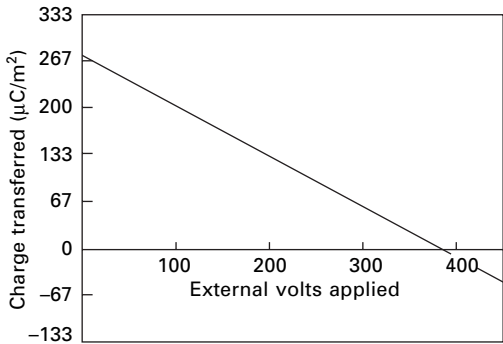


23.11 Charge distribution after separation of mercury from lower surface of polymer.

designed to reduce leakage, Medley [27] was able to obtain much higher values. He separated mercury from a thin layer of polymer, which had another layer of mercury on its opposite side. The whole experiment was carried out in a vacuum. After separation, the charge distribution and electric field will be as shown in Fig. 23.11. The almost equal charge induced on the adjacent layer of mercury after separation can be measured by the usual arrangement of an electrometer and condenser. As soon as the separation has become large compared with the thickness of the polymer, the field in the vacuum will be very small, so that leakage will be negligible. Leakage is possible when the separation is still small, but, under these conditions, the dielectric strength is greater and the insulation is very good. The larger the capacity of the polymer film, the smaller is the chance of leakage. Figure 23.12 shows the results of the experiments. Values of up to $1500 \mu\text{C}/\text{m}^2$ were obtained, and it appears that higher values still are possible. If an external electric field is applied, there will be a charge transfer due to the field superimposed on the charge transfer due to the



23.12 Charge left after separating polymer film from zinc amalgam [27].



23.13 Effect of applied field on electrification of a nylon film [27].

difference in the two surfaces. According to the direction of the field, this may increase or reduce the charge transfer, and, if large enough, it can even reverse it (Fig. 23.13).

23.3.3 Anti-static treatments

The presence of oil on the surface will influence the charge obtained, as is shown in Table 23.3. Insulating oils may increase the charge, but conducting oils will decrease it. Table 23.4 gives some practical results for various types of anti-static agent. Values for the best and worst material of each type are included. For continued efficacy, finishes must not be lost by washing or wear.

Permanent anti-static behaviour is achieved by the use of conducting fibres. Fibres with moderate conductivity can be used instead of regular fibres in a product, but it is more common to use more highly conducting fibres in small quantities in a blend with other fibres. The inclusion of carbon black to give a conducting path, provided the particles are close enough together, was referred to in Section 22.4.3. However, this has the disadvantage of making the material black. Conductivity can be increased by incorporating hydrophilic groups by copolymerisation or by co-extrusion with a

Table 23.3 Effect of insulating and conducting oil [12]

Insulating oil – liquid paraffin Cowtail fibre – 140 μm diameter Platinum cylinder – 0.123 cm diameter				Conducting oil (180 μm fibre)		
Load on fibre (MPa)	Rubbing	Charge ($\mu\text{C}/\text{m}^2$) on:		Conductivity of oil ($\Omega^{-1} \text{cm}^{-1}$)	Rubbing speed (cm/s)	Charge (arbitrary units)
		clean fibre	oiled fibre			
0	Single	0	0	7.5×10^{-13}	5	28
1	Single	13	17	3×10^{-11}	5	8.4
5	Single	25	47	6×10^{-11}	5	1.8
0	Continued	0	0	7.5×10^{-13}	10	30
1	Continued	32	72	3×10^{-11}	10	15
5	Continued	47	94	6×10^{-11}	10	6.8

Table 23.4 Effect of various classes of anti-static agent [8]

Material treated with	Static charge (arbitrary units) 50% r.h.; winding at 180 m/min		
	Viscose rayon	Acetate	Nylon
(Untreated)	47	60	128
Hygroscopic salts	17–38	0–29	3–19
Polyalcohols	45–46	22–33	92–98
Soaps	35–48	21–32	64–88
Sulphonated fatty compounds	34–52	16–32	32–85
Non-ionogenic products	31–42	18–43	22–78
Cation-active products	32–54	15–38	31–62

conducting polymer. For example *DuPont* incorporated streams of colourless polymer in their anti-static nylon carpet fibres. Metal fibres, e.g. *Bekinox* stainless steel fibres, which are made with diameters from 2 to 22 μm , have high conductivity.

A more extensive discussion of the chemistry, effectiveness and durability of the many ways of reducing static is given by Holme *et al.* [4].

23.4 Generation of charge

Henry [28–30] has summarised the chief hypotheses that have been put forward to explain the separation of charge on materials in contact. None of them has been convincingly proved to be the sole mechanism, and he suggests that probably all the mechanisms operate to varying degrees in different cases. Whenever two surfaces are brought into contact, it is likely that some charge transfer across the surface will occur, but the conditions that affect it need to be worked out. Some of the charge transfer will result from the equilibrium distribution of charged particles between the surfaces and some from kinetic effects due to such transient influences as temperature differences. It may be noted that the highest observed charges ($1500 \mu\text{C}/\text{m}^2$) would be explained by the transfer of relatively few charges: one electronic charge for every

100 nm^2 ($10\text{ nm} \times 10\text{ nm}$) would be sufficient. This area would cover many hundreds of atoms.

It is therefore a general rule that, unless the electrical states of two materials are extremely well balanced, there will be a large transfer of charge when their surfaces are brought in contact. The theories discussed below as a justification for this generalisation suggest that charge densities of $10^5\text{ }\mu\text{C/m}^2$ would be commonplace. These values are far in excess of what is observed in practice, where the charge levels are reduced by leakage after separation of the surfaces. It is very difficult to get two surfaces in perfect electrical balance, and, even if it were achieved, the balance would be very easily disturbed by the slightest change of conditions. Charge generation is therefore very difficult to avoid.

There is one possible exception to this rule. Charge separation does require the *movement* of some free charges (electrons or ions). If, in an extremely good insulator, there are no mobile ions or electrons at all, then the charge separation will not occur, although charges may be deposited on the material. This may explain why polypropylene fibres appear to cause fewer static problems than some other synthetic fibres, despite their very high resistance.

The various possible mechanisms of charge transfer, which were discussed in more detail in previous editions of this book, are as follows:

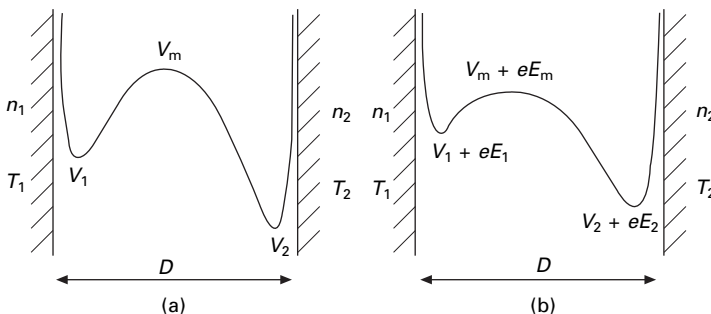
1. Difference in contact potential between two metals in contact, due to difference in energy levels of electrons.
2. Difference in energy levels involving insulators, complicated by the presence of forbidden bands and extra levels on the surface [31, 32].
3. Activation by pressure making lower energy levels accessible and leading to charge reversal from positive to negative [32], as in [Fig. 23.9](#). The reverse is not observed.
4. Presence of mobile cations on an acidic surface or mobile anions on a basic surface. Medley [33] observed this effect due to salt linkages, $\text{R}-\text{COO}^-\text{H}_3\text{N}^+$, in keratin. On treatment with HCl , this changes to $\text{R}-\text{COOH}\text{Cl}^-\text{H}_3\text{N}^+$, giving a mobile Cl^- ion. Treatment with NaOH gives $\text{R}-\text{COO}^-\text{Na}^+\text{H}_2\text{N} + \text{H}_2\text{O}$, with a mobile Na^+ ion. On separating keratin from filter paper, the charge reversed depending on the treatment.
5. Asymmetric rubbing leads to thermal gradient, due to action being distributed along a length of one surface and at one place on the other. Charged mobile particles will move from hot to cold.
6. Symmetrical rubbing may give local asymmetry due to high spots on the surfaces. This is illustrated by a distribution of opposite charges over the surface of a polyethylene sheet when it is rubbed against another sheet [17]. In another example, different charges are found when a fibre is drawn from a lock of wool with or against the scales [24].
7. A double layer on a surface may be rubbed off on to another surface.
8. Piezo-electric polarisation due to pressure may lead to charge separation. In wool, pressure leads to the root end becoming negative and the tip end positive, which Martin [24] suggests may be the cause of the charging of wool withdrawn from a lock.

9. A pyro-electric effect at hot spots. Martin [24] found that wool became negatively charged at the root end on immersion in liquid air.

Henry [28–30] combines the first three mechanisms in an instructive example, which is simplified in that it considers the transfer of only one type of particle and uses classical mechanics, which will not be valid if electrons are involved. For electrons, quantum mechanics should be used. A charged particle between two surfaces is repelled by short-range forces when it is very near one of the surfaces, but it is attracted to the surface by the induced ‘image’ electrostatic forces when it is at a greater distance away. The combination of these forces results in the potential energy diagram shown in Fig. 23.14(a).

We consider unit area with n_1 ions on the first surface, which is at a temperature T_1 , and n_2 ions on the second surface at a temperature T_2 . The number of ions crossing the barrier $(V_m - V_1)$ per unit area per unit time will be proportional to $n_1 T_1^\lambda \exp[-(V_m - V_1)/k T_1]$. The index λ varies according to the particular theory in statistical mechanics employed and need not be specified here. Quantum mechanics would give a less simple energy term, owing to the possibility of the passage of particles through the barrier by means of the tunnel effect. There will be a similar loss of ions from the second surface over the barrier $(V_m - V_2)$. The difference in transfer rates will cause a separation of charge and will give rise to an electrostatic field, which will change the potential energy diagram. This will continue until the electrostatic field is such as to equalise the rates of transfer from each side. If E_1 and E_2 are then the electrostatic potentials at the surfaces, and E_m that at the position of maximum total energy, and if V_m is also now taken at this position (Fig. 23.14(b)) the rate changes to $n_1 T_1^\lambda \exp\{[-(V_m - V_1) + e(E_m - E_1)]/k T_1\}$, where e is the charge on the ion. There is an analogous expression for the reverse direction. Equilibrium will occur when the two rates are equal. An external electric field F , which also changes the height of the barrier, can be added to the model.

The analysis continues so as to predict the charge densities $\pm Q$ on surfaces separated by a distance D . We write $(V_1 - V_2) = (W_2 - W_1) = \Delta W$, where W_1 and W_2 are the amounts of work needed to remove the type of ion concerned from the surfaces into a vacuum and $V + eE = U$. The value of Q is given by:



23.14 Potential energy of charged particles between two surfaces: (a) in absence of electrostatic field; (b) at equilibrium, with electrostatic field.

$$4\pi eDQ = -\Delta W + kT \log_e \left(\frac{n_2}{n_1} \right) + \Delta T/T \left(\lambda kT + U_m - \frac{U_1 + U_2}{2} \right) - eDF \quad (23.1)$$

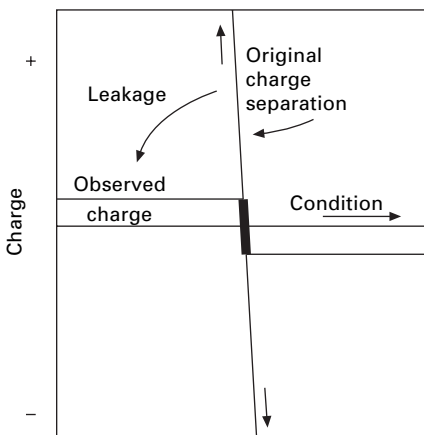
In this expression, $-\Delta W$ represents the difference in energy levels, that is, the contact potential of mechanisms 1 and 2. The second term represents the effect of the different concentrations, n_1 and n_2 , on the two surfaces, that is, mechanism 3. The third term gives the effect of the difference in temperature, ΔT , between the two surfaces, that is, mechanisms 4 and 5. Of this term, the first part within the brackets is an effect similar to thermal diffusion, while the other terms derive from the potential energy 'hump' that has to be overcome. The final term in the expression represents the effect of an external field, which gives rise to an additional charge density sufficient to produce an equal and opposite field. This example illustrates how the various effects combine together. The other mechanisms listed may also come in as additional effects.

Charges as great as those which would be predicted on these theories, amounting to more than $10^5 \mu\text{C}/\text{m}^2$, are rarely observed in practice. Leakage, through either the air or the material, usually occurs and limits the observable charge. This fact makes experimental investigation of charge generation difficult. Leakage also explains the absence of a difference in magnitude of the charge obtained from the distance apart in the electrostatic series and the apparent abruptness with which reversals of charge occur. Whereas the original charge separation may vary continuously from a high positive to a high negative value as conditions change, the observed charge will drop in a step from a constant positive value to a constant negative value, as is illustrated in Fig. 23.15.

23.5 Leakage of charge

23.5.1 Leakage in air

As discussed above, the inherent magnitude of charge separation is much greater than observed charges, unless the two surfaces are almost perfectly balanced. The

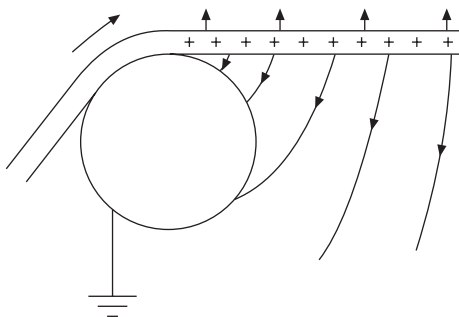


23.15 Original and observed charge separation.

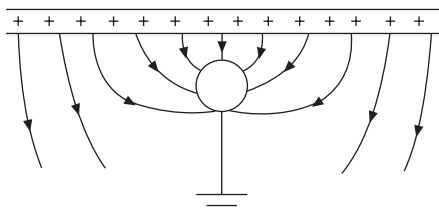
observed charges depend primarily on the extent to which the charge can leak away and this can happen in a variety of ways.

When the material is completely non-conducting, leakage through the air is the only factor that limits the static charge and it is an important factor in materials with low conductivity. The breakdown potential of air at atmospheric pressure is 30 kV/cm, and this means that the maximum charge which can exist on a plane surface is about $30 \mu\text{C}/\text{m}^2$. For a sheet with two surfaces, $60 \mu\text{C}/\text{m}^2$ should be possible, but, in fact, uneven charging and irregularity of the surface usually prevent more than half this amount from being observed. If the material is passing over a rod, the leakage will occur through the air back to the rod, as shown in Fig. 23.16. The presence of other neighbouring conductors may cause a concentration of lines of force, as shown in Fig. 23.17, resulting in a discharge to the conductor and leaving a smaller charge density on the material. This has been found by Medley [26], who has discussed the conditions necessary to cause the greatest discharge. The field strength will also be influenced by the shape of the specimen and by the presence of neighbouring charges. For example, single fibres can support high surface charges (about $150 \mu\text{C}/\text{m}^2$) owing to the rapid decrease of field strength as the lines of force diverge from the fibre. Where fibres are grouped together, as in a roving, however, such high fibre-surface charges are not possible, since the combined field at the outside of the roving would then exceed the dielectric strength of the air.

It is the limitation of charge by conduction in air that results in the constant portion of the curves of charge versus relative humidity or conductance of the material. There may even be a slight increase (as in Fig. 23.6) since, under some conditions, the dielectric strength of air is greater at a higher humidity. Near atmospheric pressure,



23.16 Electrostatic field causing leakage through air back to rod.



23.17 Concentration of lines of force due to neighbouring conductor.

the dielectric strength of air decreases as the pressure drops, which results in a decrease in the observed charge (Fig. 23.10), but in a good vacuum the dielectric strength is high and the observed charges are high. The particular advantage of Medley's technique [27] of backing a thin film of polymer with mercury (see Section 23.3.2) is that the field due to the charge decreases rapidly as the separation of the surfaces increases. In a sufficiently narrow gap, the ions present cannot accelerate enough for ion multiplication by collision to occur; consequently, the breakdown strength increases. At atmospheric pressure, this increase in dielectric strength occurs when the gap is reduced to a few microns, but at low pressures it occurs at greater thicknesses. Thus in the initial stages of the separation, while the field is high, the dielectric strength is also high.

Anything that increases the dielectric strength of the atmosphere, such as saturation with carbon tetrachloride, results in an increase of the limiting charge that can be obtained. Conversely, lowering the resistance of the air by ionising it reduces the limiting charge. Static eliminators, which apply a high voltage to metal points, work on this principle. Alternatively, radioactive material will ionise the air.

To make a complete quantitative analysis of the charge left on the separated material after leakage has occurred, one would need to work out the distribution of electric field in the system and the currents that would flow as a result of the electric field. Working out the field is a complex problem owing to the disturbing influence of dielectrics and conductors in the system. The mathematical difficulty is further increased when current flows, since this alters the charge distribution and consequently alters the electric field producing the current.

The electric fields are determined not only by the charge on the insulator but by image charges in the neighbouring conductor. Medley [12], neglecting the effect of the dielectric constant of the material and using an approximate image system, worked out the field due to an approximately uniform charge distribution on a thin sheet of material separated from a conducting cylinder and parallel to a conducting plane. It can then be seen where the dielectric strength of the air is exceeded. By analysis or successive approximation, a modified charge distribution, taking account of the leakage in air, can be worked out.

In practice, an approximate value can be obtained by assuming that just beyond the point of separation, or just beyond a conductor whose influence is being considered, the charge density is reduced to a uniform value, σ_a , giving a field equal to the dielectric strength of air, E_{crit} . For a plane surface, by the application of Gauss's theorem, this gives:

$$\sigma_a = \frac{2 \epsilon E_{\text{crit}} \cos \theta}{\alpha} \quad (23.2)$$

where ϵ = permittivity of air \approx permittivity of vacuum, α = ratio of the normal flux density to the average normal flux density on both sides of the surface, and θ = angle between lines of force and the normal to the surface.

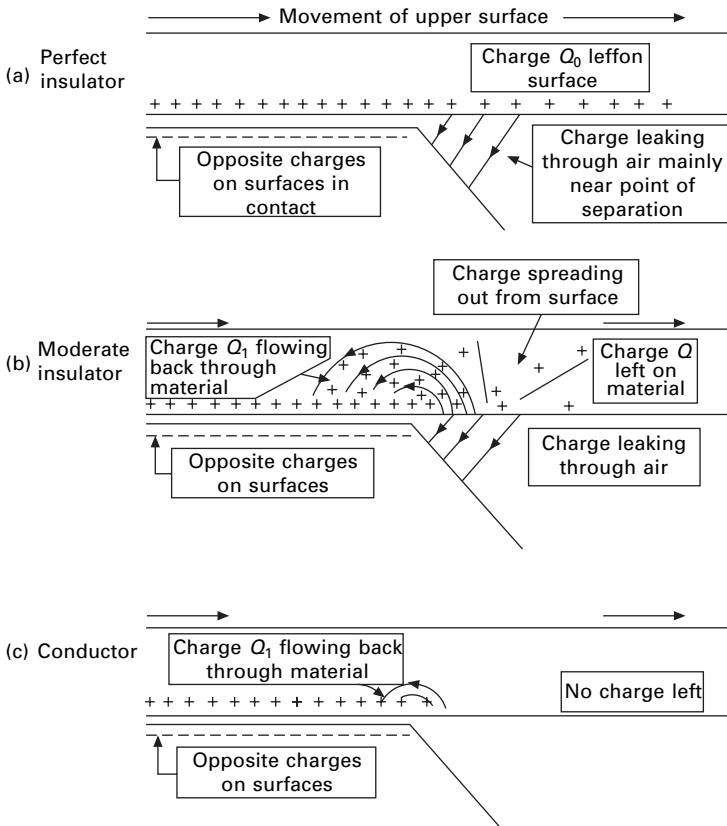
High values of θ will be dominant, giving $\cos = 1$ at 90° . The ratio α will be limited to values between 0 and 2, and, unless there are marked disturbing effects due to dielectrics or conductors near the charged surface, it will be approximately equal

to 1. Thus $(\cos\theta/\alpha) \sim 1$. With $\epsilon_0 = 8.85 \text{ pF}$ and $E_{\text{crit}} \sim 4 \text{ MV/m}$, this indicates a maximum charge density of the order of $10 \mu\text{C/m}^2$ in accord with the usual observations. It will be lower when the electric field is concentrated and higher when special precautions are taken to limit the discharge.

23.5.2 Leakage in the material

As soon as the resistance of the material becomes low enough for appreciable current to flow through it, the observed charge starts to decrease. Since a small increase in humidity causes a large increase in conductance, the curve of charge against relative humidity then drops rapidly, as is shown in Figs 23.6–23.8.

Once again, exact analysis is difficult, but the influence of the material may be illustrated diagrammatically. In a perfect insulator (Fig. 23.18(a)), no current flows through the material and a charge, limited by air leakage, remains on the surface. In a moderate insulator (Fig. 23.18(b)), the charge left after leakage through the air can spread out from the surfaces where it first appears. This gives an electric field acting back along the material, since at a distance the effect of the double layer is negligible.



23.18 Leakage of charge in (a) perfect insulator, (b) moderate insulator and (c) conductor.

Some charge will flow back behind the point of separation and become a source of charge for the double layer at the surfaces in contact. In a good conductor (Fig. 23.18(c)), there will be a large backward current and the charge will never get far beyond the point of separation but will, in effect, be circulating near the surfaces in contact, and never penetrating deeply into the material.

The currents will flow in the reverse direction to the movement of the material that is carrying charge forward. Consequently, the greater the speed of the material, the smaller will be the reduction of charge for a given conductance. This means that the higher the speed of a process, the more likely is the occurrence of static charges.

If we consider unit width of material (Fig. 23.19), of thickness t and conductivity k , moving with a velocity v , and having a charge per unit area σ (not necessarily all on the surface), then the rate of transport of charge past a given point owing to the movement of the material is σv . If there is an electric field E , with a component ($E \sin \phi$) in the opposite direction to the motion, the current flowing will be $(E \sin \phi \cdot kt)$. The net rate of transfer of charge is therefore $(\sigma v - E \sin \phi \cdot kt)$.

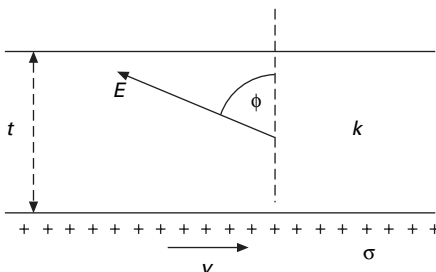
In the steady state, this must be equal at all points along the material, and a relation between σ and $E \sin \phi$ is thus established. If σ' is the limiting charge per unit area left on the material at a long distance from the point of separation, we must have:

$$\sigma' v = \sigma v - E \sin \phi \cdot kt \quad (23.3)$$

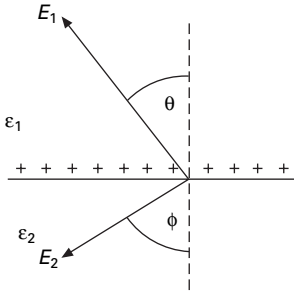
$$\sigma' = \sigma - E \sin \phi \frac{kt}{v} \quad (23.4)$$

Using this relation, and deriving values of E from the approximate image system, Medley [12] worked out, by successive approximations, the charge distribution in the steady state for material coming off a cylinder of unit diameter. This shows that, owing to the influence of the induced charge on the cylinder, a maximum in the charge on the material occurs some distance beyond the point of separation and thus most of the current will finally reach the cylinder by discharge across the gap, rather than by conduction behind the point of separation. This effect is less marked when the ratio of thickness of material to diameter of cylinder is greater.

We may obtain an approximate expression for σ' in the following way. For surface charge on a dielectric material remote from conductors, the field in the dielectric is $(\sigma/2 \epsilon_r \epsilon_0)$. We may therefore put $E \sin \phi = \Phi \sigma/2 \epsilon_0$, where it follows from the geometry of Fig. 23.20 that $\Phi = (2 - \alpha) \tan \phi/\epsilon_r$ and is a dimensionless function



23.19 Field in specimen.



23.20 Effect of surface charge. If σ is the surface density of charge and E_1 and E_2 are electric fields making angles θ and ϕ with the surfaces of two media of permittivity ϵ_1 and ϵ_2 , then by Gauss's theorem: $\epsilon_1 E_1 \cos \phi + \epsilon_2 E_2 \cos \phi = \sigma$. Hence:

$$\begin{aligned}\phi &= \frac{\epsilon_1 E_1 \cos \theta}{\frac{1}{2}(\epsilon_1 E_1 \cos \theta + \epsilon_2 E_2 \cos \phi)} = \frac{2 \epsilon_1 E_1 \cos \theta}{\phi} \\ &= 2 \epsilon_r \epsilon_0 E_1 \cos \theta / \sigma,\end{aligned}$$

where ϵ_r is the relative permittivity of medium 1 and ϵ_0 is the permittivity of a vacuum.

depending on the relative permittivity and the field distribution in the particular system.

Substituting in equation (23.3), we get:

$$\sigma' = \sigma \left(1 - \frac{\Phi k t}{2 \epsilon_0 v} \right) \quad (23.5)$$

Near the point of separation, σ will drop to the value σ_a , limited by air discharge given by equation (23.2), and we have²:

$$\sigma' = \sigma_a \left(1 - \frac{\Phi k t}{2 \epsilon_0 v} \right) = \frac{2 \epsilon_0 E_{\text{crit}} \cos \theta}{\alpha} \left(1 - \frac{\Phi k t}{2 \epsilon_0 v} \right) \quad (23.6)$$

It follows from this equation that the charge remaining on the material is a fraction of the maximum value determined for different systems by the value of (kt/v) . It can be noted that kt is the conductance (reciprocal of resistance) per unit width per unit length. The charge will drop to half the maximum value when $(kt/\epsilon_0 v)$ equals $1/\Phi$. Considering that values of (kt/v) cover a range of at least a million to one, the results given in [Tables 23.2](#) and [23.5](#) support this view and indicate that $1/\Phi$ lies between 1 and 7.

²The various expressions quoted here will only be correct in a consistent set of units. In SI units, this means that the conductivity k should be in $\Omega^{-1} \text{ m}^{-1}$, the thickness t in m, and the velocity v in m/s. The permittivity ϵ_0 is in the usual units (F/m or $\text{kg}^{-1} \text{ m}^{-3} \text{ s}^4 \text{ A}^2$) and has the value 8.85×10^{-12} F/m. The product (kt/v) will have the units $\Omega^{-1} \text{ m}^{-1} \text{ s}$, which also, as should be the case, are equal to $\text{kg}^{-1} \text{ m}^{-3} \text{ s}^4 \text{ A}^2$. We may note that $kt/2v$ will have the same units if k is expressed in $\Omega^{-1} \text{ cm}^{-1}$ and t in cm, with v in m/s.

Table 23.5 Critical conditions for reduction of charge [12]

$\frac{kt}{v}$ or $\frac{ka}{2v}$ ($\Omega^{-1} \text{ m}^{-1} \text{ s}$)	Values of fraction of maximum charge for systems below						
	A	B	C	D	E	F	G
1.3					0.71	0.56	0.67
1.6	0.91	0.80	0.96	0.91			
6.3	0.45	0.52	0.67	0.65			
12.6	0.30	0.30			0.24	0.25	0.19

System	25 μm Nylon strip on platinum cylinder			
	Width (cm)	Load (mN)	Cylinder diameter (cm)	Speed (cm/s)
A	1	150	0.12	0.5
B	1	150	0.12	10
C	2	50	1.25	0.5
D	2	50	1.25	10

Single fibres, 0.1 cm platinum cylinder

	Material	Diameter (μm)	Speed (cm/s)
E	Nylon	20	0.5
F	Nylon	20	10
G	Wool	45	10

Equation (23.6) will cease to hold when kt/v becomes large, and the expression approaches zero and then becomes negative. The derivation is only valid when the current flow is relatively small.

As ϵ_r increases, the line of force would tend to concentrate in the dielectric material, which would increase ϕ . So, as a rough approximation, $\tan \phi = \epsilon_r \tan \theta$, which indicates that $\Phi \approx (2 - \alpha) \tan \theta$. For $\theta = 20^\circ$ and $\alpha = 1$, this would make $1/\Phi$ equal to 2.8, in agreement with the experimental results.

For a cylindrical specimen of radius a , equation (23.5) changes to:

$$\sigma' = \sigma \left(1 - \frac{\Phi ka}{4\epsilon_0 v} \right) \tag{23.7}$$

23.5.3 An alternative leakage equation

The expression $E \sin \phi = \Phi \sigma / 2\epsilon_0$ above (21.11) is an approximation because the charge causing the electric field E will be not the unreduced value σ but some average of values between σ , near to the point of separation, and σ' , at a remote position. This is the source of error in the derivation, which makes the equation invalid for large values of kt/v . If we adopt the other extreme possibility, we put $E \sin \phi = 2\pi\sigma'\Phi$. This leads to:

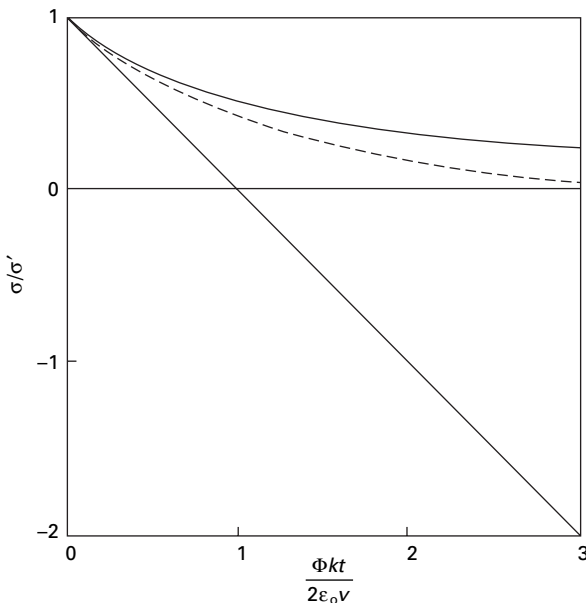
$$\sigma' = \sigma \left(1 + \frac{\Phi k t}{2 \epsilon_0 v} \right)^{-1} \quad (23.8)$$

A comparison of the predictions of the two equations (23.5) and (23.8) is shown in Fig. 23.21. The actual behaviour should lie between the predictions of the two equations, as indicated by the dotted lines.

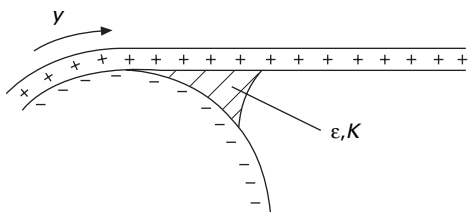
23.5.4 The action of a surface coating

It has already been mentioned that, when the material is a good conductor, the leakage does not penetrate deeply into the material. Consequently, a thin permanent conducting layer on the surface of a fibre would reduce static charges, but Medley [12] has pointed out that the action of a surface dressing may be slightly different from this.

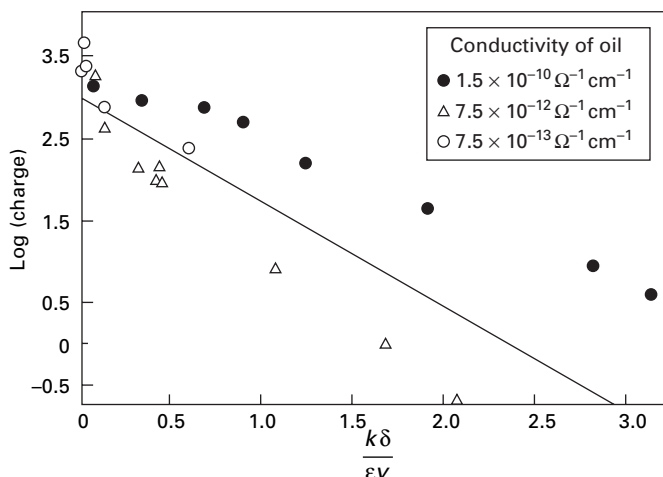
A liquid dressing may not separate the two materials but may instead form a wedge-shaped film at the point at which they diverge from one another, as shown in Fig. 23.22. This liquid will act as a leaky dielectric, and dissipation of charge will occur owing to current flow across it. The time constant of a condenser is independent of its size and shape, and the decay of charge is given by the relation $\sigma = \sigma_0 \exp(-tk/\epsilon)$ where σ_0 is the initial charge density, σ is the charge density at time t , ϵ is the permittivity of the liquid, and k is its conductivity. If v is the speed of the material and δ the length of the wedge, the time for a given portion of material to pass the liquid is δ/v , and therefore:



23.21 Comparison of prediction of equations (23.5) and (23.8), with indication (dotted) of likely real relation.



23.22 Wedge-shaped film at point of separation.



23.23 Reduction of charge on wool fibre due to conducting oils [12]. The line represents equation (23.10). Charge is in arbitrary units.

$$\sigma = \sigma_0 e^{-k\delta/\epsilon\nu} \quad (23.9)$$

$$\log_e \frac{\sigma}{\sigma_0} = -\frac{k\delta}{\epsilon\nu} \quad (23.10)$$

Figure 23.23 shows an experimental check of this relation for varying rubbing speeds and three different mixtures of liquid paraffin and Lubrol MO.

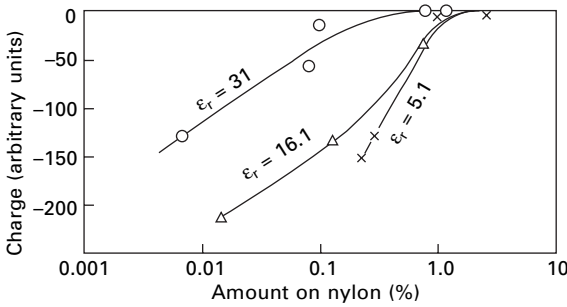
It will be seen from equation (23.9) that the condition for marked reduction of electrification is $\epsilon\nu < k\delta$. It may be noted that the quantity $k\delta/\epsilon\nu$, equal to $k\delta/\epsilon_r\epsilon_0\nu$, is a dimensionless parameter.

It follows from this view of the action of an anti-static agent that it need not be present on the fibres but can be present on the guide or roller in order to give the wedge-shaped film. Medley [12] found that a porous cast-iron roller, impregnated with *Empilan A* (conductivity of $10^{-7} \Omega^{-1} \text{cm}^{-1}$), produced negligible static in worsted drawing, in contrast to the behaviour of an ordinary roller. This procedure does not, of course, meet the need for a permanent anti-static dressing to prevent the troubles due to static in use.

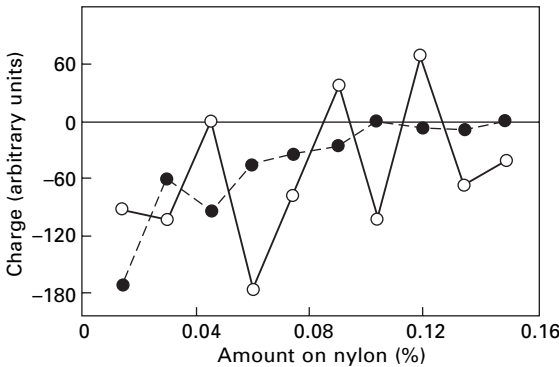
If the liquid is not a conductor, leakage will not occur, and the observed charges may even increase (as in Table 23.3), owing to the greater dielectric strength of the

liquid than that of air. This will reduce discharge in the region near the point of separation where the field is greatest.

Graham [34] has taken a rather different view of the action of anti-static agents. Figures 23.24 and 23.25 show the effect of five liquids on the charge given when nylon is rubbed over brass. He suggests that if it is thick enough, the liquid film prevents the contact potential between the two surfaces from becoming effective and that, if separation then occurs within the film, no charge will result. He associates the more effective action of the liquids with the higher dielectric constants to their greater degree of shielding. For this mechanism to be effective, the liquid film must be reasonably isotropic. With the surface-active agents, Fig. 23.25, the molecules are regularly oriented, and reversals in their effect occur as increasing amounts are applied. The reversals correspond to successive monomolecular layers and will be associated with the surfaces changing from polar to inert groups and vice versa. With triethanolammonium oleate, the regularity breaks down with larger amounts, but it persists to thick layers with potassium oleate.



23.24 Effect of relative permittivity ϵ_r of surface dressing on charge. After Graham [34].



23.25 Effect of surface activity on charge: ○ potassium oleate; ● Dotted line: triethanolammonium oleate. After Graham [34].

23.6 References

1. *Brit. J. Appl. Phys.*, 1953, Supplement No. 2: 'Static Electrification' (report of Conference).
2. *J. Text. Inst.*, 1957, **48**, P4: 'Static Electricity in Textiles' (report of Conference).
3. D. F. Arthur. *J. Text. Inst.*, 1955, **46**, T721 (review of literature).
4. I. Holme, J. E. McIntyre and Z. I. Shen *Textile Progress*, **28**, No. 1, 1998.
5. W. H. Rees. *J. Text. Inst.*, 1954, **45**, P612.
6. P. S. H. Henry. *Brit. J. Appl. Phys.*, 1953, Suppl. No. 2, S78.
7. H. Sagar. *J. Text. Inst.*, 1954, **45**, P206.
8. K. Götze, W. Brasseler and F. Hilgers. *Melliand Textilber.*, 1953, **34**, 141, 220, 349, 451, 548, 658, 768.
9. P. E. Secker and J. N. Chubb. *J. Electrostatics*, 1984, **16**, 1.
10. J. F. Keggin, G. Morris and A. M. Yuill. *J. Text. Inst.*, 1949, **40**, T702.
11. M. Hayek and F. C. Chromey. *Amer. Dyest. Rep.*, 1951, **40**, 164.
12. J. A. Medley. *J. Text. Inst.*, 1954, **45**, T123.
13. V. E. Gonsalves and B. J. van Dongeren. *Text. Res. J.*, 1954, **24**, 1.
14. A. E. Seaver. *J. Electrostatics*, 1995, **35**, 231.
15. W. J. Durkin. *J. Electrostatics*, 1995, **35**, 215.
16. M. S. Ellison. *J. Textile Inst.*, 1991, **82**, 512.
17. P. S. H. Henry. *Brit. J. Appl. Phys.*, 1953, Suppl. No. 2, S31.
18. W. R. Harper. *Proc. Roy. Soc.*, 1951, **A205**, 83.
19. S. P. Hersh and D. J. Montgomery. *Text. Res. J.*, 1955, **25**, 279.
20. R. G. C. Arridge. *Brit. J. Appl. Phys.*, 1967, **18**, 1311.
21. P. A. Smith, G. C. East, R. C. Brown and D. Wade. *J. Electrostatics*, 1988, **21**, 81.
22. W. Tsuji and N. Okada. Cited by I. Skurada in *Handbook of Fiber Science and Technology*, Vol. IV, *Fiber Chemistry*, M. Lewin and E. M. Pearce (Editors), Marcel Dekker, New York, USA, 1985, p. 580.
23. A. Cohen. *Ann. Phys.*, 1898, **64**, 217.
24. A. J. P. Martin. *Proc. Phys. Soc.*, 1941, **53**, 186.
25. J. A. Medley. *Nature*, 1950, **166**, 524.
26. J. A. Medley. *Brit. J. Appl. Phys.*, 1953, Suppl. No. 2, S23.
27. J. A. Medley. *Brit. J. Appl. Phys.*, 1953, Suppl. No. 2, S28.
28. P. S. H. Henry, *Brit. J. Appl. Phys.*, 1953, Suppl. No. 2, S6.
29. P. S. H. Henry, *Sci. Prog.*, 1953, No. 164, 617.
30. P. S. H. Henry. *J. Text. Inst.*, 1957, **48**, P5.
31. F. A. Vick. *Brit. J. Appl. Phys.*, 1953, Suppl. No. 2, S1.
32. V. E. Gonsalves. *Text. Res. J.*, 1953, **23**, 711.
33. J. A. Medley. *Nature*, 1953, **171**, 1077.
34. G. W. Graham. *Nature*, 1951, **168**, 871.

24.1 Introduction

When light falls on a fibre, it may be partly transmitted, absorbed or reflected. Its behaviour in each of these three respects determines the visual appearance of the fibre, although the appearance of fibres in the mass may be considerably modified by the way in which particular arrangements influence the combination of effects in each fibre. The optical properties of fibres are also a useful source of information about their structure. In particular, the orientation of the polymer molecules can be estimated from differences in the refractive indices and in the absorption of light polarised in different directions relative to the fibre axis.

Rigorous analysis of the optical properties of fibres is a very complex subject and, whereas it is of great importance in studies of fibre structure, it does not justify a detailed discussion in a book primarily concerned with practical properties of fibres. The present chapter will be limited to a general account of the subject, particularly in its practical aspects.

24.2 Refraction

24.2.1 Refractive index and birefringence

The velocity with which light is transmitted varies with the medium through which it is passing. In isotropic materials, this property may be used to give the most fundamental definition of refractive index n namely, the ratio of the velocity of light in a vacuum to the velocity of light in the material. The study of this subject, and its consequence, is a well-known branch of physics. One particular result is that the direction of travel of light is refracted or bent on passing from one medium to another. This leads to an alternative definition: refractive index $n = \text{sine of angle of incidence} / \text{sine of angle of refraction}$.

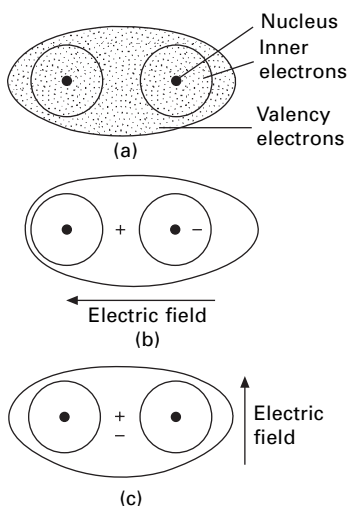
The lower velocity of the waves means that the light waves are retarded on passing through a medium of high refractive index. If they are then combined with a beam that has passed through a different medium, various interference phenomena occur, and these may be utilised in the measurement of refractive index. In general, the refractive index of a material varies with the temperature and with the wavelength of

the light being transmitted. The usual standard conditions of measurement involve the use of monochromatic sodium light, with a wavelength of 589 nm, at 20 °C.

Light is composed of electromagnetic waves, and the change in velocity is associated with the electric polarisation that occurs under the influence of the electric field. The frequency of the waves is very high, so that only the polarisation of the electron distribution round the nuclei of atoms (i.e. the relative displacement of positive and negative charge) is important. Larger-scale effects, such as the rotation of permanent dipoles, cannot take place rapidly enough. The outer electrons, which are taking part in covalent bonds, are those affected, since electrons in the inner complete shells are not easily displaced: this is illustrated in Fig. 24.1. It is therefore possible to assign a polarisability to each chemical bond, although this is influenced to some extent by other atoms nearby. For example, there will be a small difference between the behaviour of a C—H bond in a —CH₂— group in a chain and that of a C—H bond in a terminal —CH₃ group. The polarisability will also vary with the direction of the electric field, as illustrated in Fig. 24.1(b) and (c): it is usually greatest when the field is directed along the line joining the atoms. However, in many simple materials, the molecules are arranged in all directions at random, so that the refractive index is the same in all directions and can be calculated from an appropriate summation of the polarisabilities of each bond in the molecule.

In anisotropic materials, such as textile fibres, the molecules are lined up in certain preferred directions, and the refractive index will therefore vary with the direction of the electric field, being usually greatest when the field is parallel to the axis of the molecules.

The direction of the electric field in an electromagnetic wave is known as the *vibration direction*. In ordinary light, there are vibrations in all directions at right



24.1 (a) Schematic representation of electron distribution around a pair of atoms linked by a covalent bond. (b) Distortion of distribution by an electronic field, acting along line between atoms, showing centres of positive and negative charge. (c) Effect of electric field perpendicular to line of atoms.

angles to the direction of transmission. When light is passed through an anisotropic material with uniaxial symmetry, the light splits up into two rays moving with different speeds corresponding to the components of the electric field parallel and perpendicular to the line of atoms: these are called the *ordinary* and *extraordinary* rays. They will be refracted differently and so may give rise to two separate images of an object viewed through the material. In appropriate circumstances, they may also interfere with one another because of the difference in retardation and cause the appearance of interference colours [1]. It is possible, by passing light through a Nicol prism or a sheet of polaroid, to polarise¹ the light so that it is vibrating in one direction only, the components in the perpendicular direction being completely eliminated. This enables one to study the variation in refractive index with the direction of vibration.

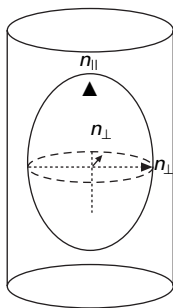
In general, an anisotropic material will have three principal refractive indices, but fibres are usually axially symmetrical so that the refractive indices perpendicular to the fibre axis are all the same. The principal refractive indices, shown in Fig. 24.2, are thus n_{\parallel} for light polarised parallel to the fibre axis, and n_{\perp} for light polarised perpendicular to it. In general, calculation of the refractive indices in other directions is complicated [2].

The refractive index of an isotropic fibre, n_{iso} , is given by the mean of the refractive indices of an oriented fibre in the three principal directions. That is:

$$n_{\text{iso}} = 1/3(n_{\parallel} + 2n_{\perp}) \quad (24.1)$$

The difference ($n_{\parallel} - n_{\perp}$) between the principal refractive indices is known as the *birefringence* of the fibre.

The above discussion refers to the intrinsic birefringence of a fibre due to the orientation of the crystal axes in the crystalline regions and of the individual molecules in the non-crystalline regions. However, Wiener [3] has shown that, if non-spherical particles which are smaller than the wavelength of light are embedded with a preferred orientation in a medium of different refractive index, then birefringence results. This happens even if each material is itself isotropic, and it is called form birefringence.



24.2 Principal refractive indices of a fibre.

¹The word 'polarise' has more than one meaning. Polarisation of light is the limitation of the electric vibrations to one direction (the magnetic field is at right angles to this). Polarisation of atoms (or of a dielectric) implies the orientation or induction of dipoles (permanent or induced).

This type of birefringence may occur in fibres in which crystalline regions may be regarded as embedded in non-crystalline regions of different refractive index.

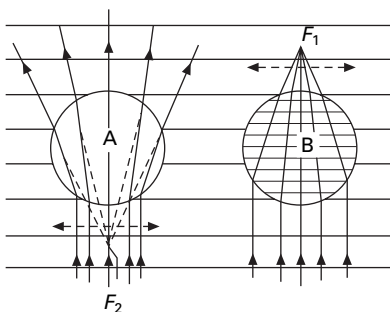
24.2.2 Measurement of refractive indices

If a fibre is immersed in a liquid of the same refractive index as itself, then its boundary ceases to be visible. By trial and error with a series of liquid mixtures of varying composition, the observation of this effect may be used as a means of measuring the refractive index of the fibre. It is, of course, necessary to use polarised light so that only one refractive index is concerned.

There are certain optical manifestations that may be used as aids in experiments of this sort. If the refractive indices of the fibre and the liquid are different, a bright line (the Becke line) can be seen at the boundary between them [4]. When the objective of the microscope is raised, this line moves towards the medium of higher refractive index. Another technique, which is simpler but less sensitive, is described by Heyn [5]. This makes use of the fact that a circular (or roughly lenticular) fibre acts rather like a convex lens and will focus a beam of light (Fig. 24.3). If parallel light comes from below, and the fibre has a higher refractive index than the immersion liquid, an image will form above the fibre. This may be observed as a bright band in the centre of the fibre when the microscope is focused above it. Conversely, if the refractive index of the fibre is less than that of the liquid, a virtual image will be formed below the fibre. The bright band will then be observed on lowering the microscope below the position where the fibre itself is in focus.

The above methods demand the rather tedious process of mounting the fibre in a large number of liquids. Frey-Wyssling [6] has adopted the technique of varying the wavelength of the light with which the fibre is observed in the liquid until the fibre outline disappears. On repetition of the process with a number of liquids, the dispersion curve (refractive index plotted against wavelength) can be found for the fibre. It is necessary to use a monochromator giving a high intensity of light.

Preston and Freeman [7] have used the same principle in a self-contained instrument. Rapid measurements can be made with this *fibre refractometer*. A prism and an associated optical system cast a spectrum onto a calibrated screen at one end of the



24.3 Formation of bright line in Heyn's method: (a) below the fibre at F_2 when the fibre refractive index is lower and (b) above the fibre at F_1 when it is higher.

apparatus. A glass cell, containing the appropriate liquid immersing a glass plate carrying the fibres, is placed in the path of the light dispersed by the prism. At the wavelength for which the refractive indices of liquid and fibres are equal, the light passes straight through and appears brightly on the screen. For other wavelengths it is scattered, and these parts of the spectrum do not appear focused on the calibrated screen. The wavelength of equal refractive indices can thus be read off directly on the scale. By variation of the temperature, equality of refractive indices can be achieved at various wavelengths, and, if suitable corrections are applied, the dispersion curve of the fibre may be found.

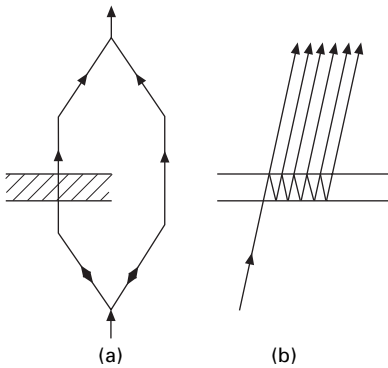
A somewhat similar modification has been introduced by de Vries [8]. If several ends of yarn, wound parallel to one another on a frame, are immersed in a liquid, they will act as a phase-grating and give a diffraction pattern if the refractive indices of fibre and liquid are different. If the refractive indices are the same, diffraction will not occur. In order to make use of this, de Vries observed the first-order diffraction spectrum through a spectrometer. Where the diffraction was absent, a dark band occurred on the spectrum observed in the spectrometer. Thus the wavelength at which the refractive indices were coincident could be found.

It should be noted that the various methods so far described may give different results because they measure the refractive indices of different parts of the fibre. It has been suggested that the Becke line gives the refractive index of the surface layers of the fibre, whereas Heyn's method of central illumination, Frey-Wyssling's method and Preston's refractometer give the refractive index of the bulk of the fibre. However, the problem is more complex than this, and detailed analysis is necessary before changes in refractive index across a fibre can be estimated. A full account of the subject has been given by Faust [9].

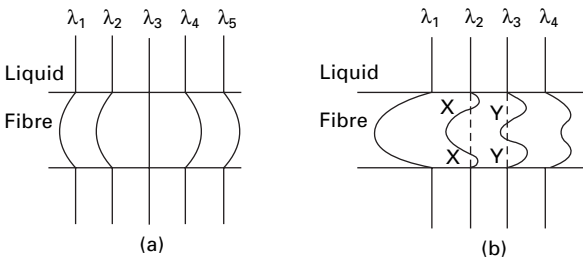
Variations in refractive index across a fibre are better investigated by interference techniques. In the interference microscope, differences in refractive index are transformed into colour changes if white light is used, or into dark and light fringes with monochromatic light. Heyn [10] has described how to use the method in the examination of fibre cross-sections.

Both double-beam and multiple-beam interference techniques have been used by Faust [11–14]. In the first method, Fig. 24.4(a), the light is split into two beams, one of which passes through the specimen, while the other bypasses it. The two are then combined and give an interference pattern. In the second method, Fig. 24.4(b), the specimen is placed between two partly silvered mirrors. A series of beams, which have passed through the specimen for a differing number of times, depending on the number of reflections, are transmitted by the system and combine to give the interference pattern.

There are various ways in which these techniques may be applied. For example, white light, with the interfering wavefronts parallel to one another, may be used. If this falls on a uniform specimen, such as a liquid in a cell, the condition for reinforcement of the interfering beams will be satisfied only at certain wavelengths. Consequently, if it is dispersed by a spectrometer, a series of bright and dark fringes at varying wavelengths will be observed. If a uniform fibre is immersed in the liquid, it will distort the fringes, as illustrated in Fig. 24.5(a). Where the fringe is in one straight



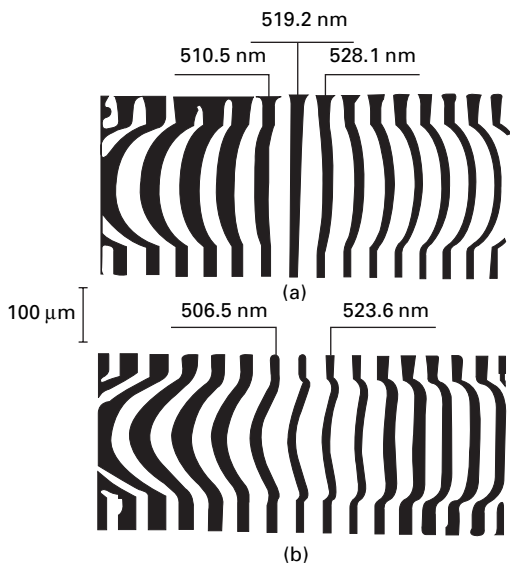
24.4 Schematic representation of (a) double-beam interferometry and (b) multiple-beam interferometry (the beam is inclined for the sake of clarity: it would actually be normal to the specimen, and the reflections would be back and forth along the same line).



24.5 (a) Distortion of fringes with a uniform fibre. At wavelength λ_3 , the indices are equal. (b) Distortion of fringes with a non-uniform fibre. The mean fibre indices are equal to the liquid indices at points X and Y for wavelengths λ_2 and λ_3 , respectively.

line, the refractive indices of fibre and liquid must be equal. For other wavelengths, the fringe is curved owing to the varying thickness of fibre through which the light passes. An example of this is shown in Fig. 24.6(a), where the fringe for 519.2 nm is straight, which indicates that the indices are equal at this wavelength. However, if the fibre is not uniform in refractive index, the fringes will have a more complicated form, such as that shown in Fig. 24.5(b), and none will be straight. The mean refractive index at any position in the fibre can be found by observing the point at which the curved fringe in the fibre crosses the line of the fringes in the liquid. An example of this is illustrated in Fig. 24.6(b). If the dispersion of fibre and liquid is known, the variation in mean refractive index across the fibre, for a constant wavelength, can be calculated.

In two other methods, monochromatic light is used. With parallel light, the field in the liquid is uniform, and it is necessary to match the intensity in part of the fibre with that in the liquid. Alternatively, with the interfering wavefronts inclined to one another, wedge fringes are observed. Where these are in line with fibre and liquid, the indices are equal.



24.6 Interference fringes of varying wavelength, observed with an unstretched viscose rayon model filament immersed in a liquid of similar refractive index. Light vibration (a) parallel and (b) perpendicular to fibre axis. Wavelengths indicated in nm. After Faust [13].

24.2.3 Measurements of birefringence

The birefringence of a fibre is often determined by measuring the two principal refractive indices and subtracting one from the other. It can also be measured directly, however, by determining the retardation, or difference in optical path length, of the one principal ray relative to the other. Since the optical path length equals the product of the refractive index and the thickness of the specimen through which the light passes, it follows that retardation $= (N + \delta N)\lambda = (n_{\parallel} - n_{\perp})t$, where $N + \delta N$ is the number of wavelengths λ for which the light is retarded, and t is the thickness.

In order to find the retardation, it is necessary to measure both the whole number of wavelengths N and the fraction δN : the latter is usually easier to determine than the former.

When a fibre is viewed between crossed Nicol prisms, interference phenomena are observed. In the absence of a specimen, the field of view with crossed Nicols is dark because the polariser will pass only light polarised in one direction, and the analyser will pass only light polarised in a perpendicular direction. If a specimen is present with a principal direction parallel to the axis of either of the prisms, the field is still dark because the component of the light passed by the polariser will be transmitted without change by the specimen and stopped by the analyser. The four perpendicular directions for which this occurs are the extinction positions. If the specimen is at some other angle, however, for example with its principal direction at 45° to the axis of the prisms, the light passed by the polariser will be split by the specimen into two components X and Y , corresponding to the vibration directions of the light, and these will be transmitted at different speeds. When this light reaches the analyser, the

components of X and Y in the vibration direction passed by the analyser will be transmitted, so that the field will not, in general, appear dark, but, because of the differing velocity of transmission through the specimen, one component will be retarded relative to the other, and interference can occur. If there is a retardation of half a wavelength (or an odd multiple of half-wavelengths) the dark field between the crossed Nicols is changed into a bright one. Consequently, for a uniform circular fibre, viewed in monochromatic light, a series of light and dark bands will be seen parallel to the fibre axis, at thicknesses corresponding to retardations of odd and even numbers of half-wavelengths, respectively. In this way, the retardation, and hence the birefringence at various positions across the fibre, can be determined [15, 16].

When viewed in white light, only certain wavelengths satisfy the conditions for interference at a given place in the fibre, and thus interference colours are observed. By comparison with a standard colour chart, the retardation and birefringence can be deduced from these colours [4].

These two methods do not give results that are completely unambiguous. With the colours, the order of interference has to be estimated, and with monochromatic fringes it is not always easy to count close fringes, nor is it always certain that the retardation in a heterogeneous fibre is continuously increasing from fringe to fringe towards the centre. There are experimental dodges that can be used to overcome these difficulties, but a more accurate method of measuring birefringence is to use a compensator.

Compensators superimpose a known, but variable, retardation on that produced by the specimen. The simplest form is a calibrated quartz wedge, but there are other types, such as the Babinet and Berek compensators. If the retardation introduced by the compensator is equal and opposite to that introduced by the specimen, conditions are the same as if neither compensator nor specimen was present and so the field appears dark. The compensator can be adjusted until this condition is satisfied in order to determine the retardation at any point in the fibre, either by the use of white light or, if a more accurate setting is needed, by the use of monochromatic light. A full discussion of the difficulties involved in determining the retardation without ambiguity has been given by Faust and Marrinan [17].

Mortimer and Peguy [18] describe on-line measurement of birefringence.

24.2.4 Refractive index, density and swelling

Since the refractive index of a material is determined by an appropriate summation of the polarisabilities of the bonds present in each of its molecules, it is to be expected that the refractive index will increase as the number of molecules present increases, i.e. as the density increases. In many materials, the relation between the two is given by Gladstone and Dale's law, $(n - 1)/\rho = \text{constant}$, where ρ = density.

This relation is an approximate form of the theoretical Lorentz-Lorenz expression. Hermans [19] has shown experimentally that the law applies to each of the refractive indices of cellulose fibres, although it does not necessarily apply to all anisotropic materials. If the average refractive index is used, the value of the constant is 0.3570.

A similar relation applies to mixtures. If v_m and n_m are the volume and refractive

indices, respectively, of a mixture, and $v_1, v_2, v_3 \dots$ and $n_1, n_2, n_3 \dots$ are the corresponding quantities for the individual components, the relation is:

$$v_m(n_m - 1) = v_1(n_1 - 1) + v_2(n_2 - 1) + v_3(n_3 - 1) + \dots \quad (24.2)$$

For the two components cellulose and water, with the refractive index of water taken as 1.333, this expression reduces to:

$$v_r(n_r - 1) = v_0(n_0 - 1) + 0.333r \quad (24.3)$$

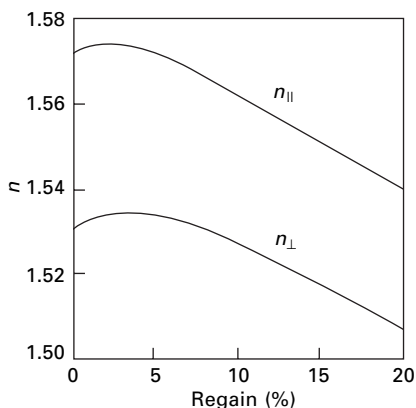
where v_0 is the volume of 1 gram of dry cellulose, v_r is the volume of the same specimen at a fractional regain r , and n_0 and n_r are the refractive indices of the dry and swollen cellulose, respectively.

Hermans [19] found that this relation, which is illustrated in Fig. 24.7, fitted the experimental results for cellulose. The rise in the curve at low regains corresponds to the increase in density that occurs as empty space is filled up (see Section 12.1.6).

Equation (24.3) applies to both the refractive indices n_{\parallel} and n_{\perp} . If we substitute these in turn and subtract one equation from the other, we find how the birefringence varies with the swelling of the fibres:

$$v_r(n_{\parallel} - n_{\perp})r = v_0(n_{\parallel} - n_{\perp}) \quad (24.4)$$

This equation fits in with the experimental results up to regains of about 15%, and this is thought to indicate that the absorbed water is not preferentially oriented. If it were, it might be expected to add to the birefringence. Above 15% regain, the birefringence gradually becomes greater than the value given by equation (24.3). A possible explanation is that this is due to an increasing amount of form birefringence, arising from the arrangement of the crystalline regions within the non-crystalline regions. At low moisture contents, the differences in the refractive indices of the two regions are so small that the form birefringence would be negligible. At high moisture contents, however, since the moisture absorption takes place almost entirely in the non-crystalline regions, the differences are greater and may have an appreciable effect.



24.7 Variation of refractive indices of cellulose with regain. After Hermans [19].

24.2.5 Birefringence and orientation

We have seen that the difference in the refractive indices depends on the relation between the direction of polarisation of the light and the direction of alignment of the molecular chain. It is therefore to be expected that the birefringence will be greatest when the molecules are all lined up parallel to the fibre axis and that it will be zero when they are randomly directed.

Hermans [19] has defined an optical orientation factor f as the ratio of the birefringence of the fibre to that of an ideal fibre in which the molecules are perfectly oriented parallel to the fibre axis. Strictly, the expression should be corrected for differences in density by dividing each birefringence by the corresponding value of the density.

It is desirable to relate this factor to some geometrical measure of orientation, and Hermans has used the average angle of inclination of the molecules ϕ . This is defined as the angle of inclination in an imaginary fibre in which all the molecules are arranged at the same angle and which has the same birefringence as the actual fibre. He has shown that:

$$f = \frac{n_{\parallel} - n_{\perp}}{n'_{\parallel} - n'_{\perp}} \quad (24.5)$$

where n'_{\parallel} and n'_{\perp} refer to the ideally oriented fibre.

In a perfectly oriented fibre, $f = 1$ and $\phi = 0$. In an isotropic fibre, in which there is no birefringence, $f = 0$, so that $\sin^2 \phi = 2/3$ and ϕ is approximately 55° . It follows from equation (24.1) that:

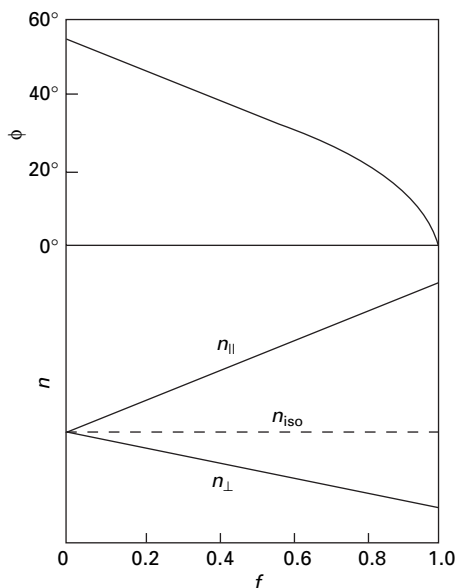
$$n_{\text{iso}} = \frac{1}{3}(n_{\parallel} + 2n_{\perp}) = \frac{1}{3}(n'_{\parallel} + 2n'_{\perp}) \quad (24.6)$$

Consequently, the refractive indices vary with orientation in the way shown in Fig. 24.8. As an example, Table 24.1 gives some comparative values for cellulose fibres of varying degrees of orientation. As expected, the values of n_{iso} calculated from equation (24.6) are the same for differently oriented fibres, except for small differences in the third decimal place.

In cotton and other natural cellulose fibres, the birefringence is reduced, not because of random departure from a parallel orientation in the fibre, but because the molecules form a helix around the fibre axis. The index ellipsoid is thus placed at an angle to the fibre axis, as is shown in Fig. 24.9.

From measurements on highly oriented flax and ramie fibres, Meredith [20] deduced values of $n'_{\parallel} = 1.595$ and $n'_{\perp} = 1.531$; then, from measurements of n_{\parallel} , he calculated values of the spiral angle θ in 36 different cottons. Since the Becke-line method was used, he assumed that the values of refractive index and spiral angle were those of the outside of the fibre. Examples of his results are given in Table 24.2. The longer cottons have higher values of n_{\parallel} and birefringence and a smaller helix angle.

In the above discussion, it has been tacitly assumed that there is no preferred orientation in the directions perpendicular to the fibre axis. This is not necessarily so. Even in a cylindrical fibre with axial symmetry, there may be a preferred orientation of crystallites in either of the two ways shown in Fig. 24.10. This will show up as birefringence when fibre cross-sections are observed, and between crossed polarisers



24.8 Variation of n and ϕ with f .

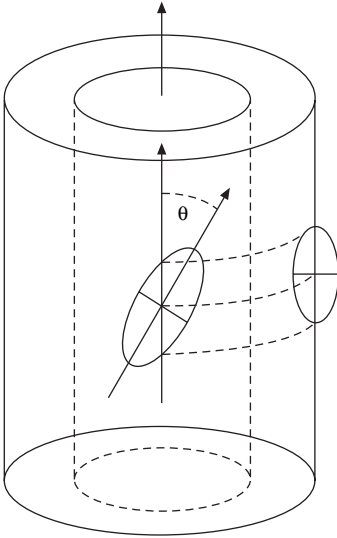
Table 24.1 Refractive indices, and related quantities, of cellulose fibres of varying degrees of orientation (reduced to a density of 1.52) (after Hermans [19])

Fibre	$n_{ }$	n_{\perp}	$(n_{ } - n_{\perp})$	f	ϕ	n_{iso}
Ramie	1.588	1.519	0.069	0.97	8°	1.542
Viscose rayon						
10% stretch	1.560	1.533	0.027	0.53	34°	1.542
80% stretch	1.568	1.531	0.037	0.74	25°	1.543
120% stretch	1.573	1.528	0.045	0.88	16°	1.542
Model filaments						
oriented	1.572	1.531	0.041	0.82	20°	1.544
isotropic	—	—	0	0	55°	1.544

interference colours will appear, except in the extinction directions of the polarisers. The resulting pattern will be a black cross on an illuminated ground. This is characteristic of radial orientation. In some fibres, it is apparent in the whole fibre; in others, such as some forms of regenerated cellulose, it appears only in the skin. In many viscose rayon fibres, the situation is somewhat more complex, as an original circular skin collapses to give a serrated outline. The type of orientation occurring is discussed in Section 1.5.2, and the polarisation effects observed are illustrated in Fig. 1.39.

24.2.6 Comparative values

Table 24.3 gives some values for the refractive indices of various textile fibres. All the values lie within the range 1.5 to 1.6, with the exception of the values for acetate, which fall below it, and the value of $n_{||}$ for Terylene polyester fibre, which is 1.725.

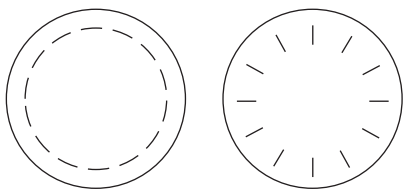


24.9 Index ellipsoid, and principal refractive indices, in a fibre with spiral orientation of chain molecules.

Table 24.2 Refractive indices, birefringence and spiral angle of cotton [20]

Cotton	Refractive indices			Birefringence of fibre ($n_{ } - n_{\perp}$)	Spiral angle θ
	$n_{ }$	n_{\perp}	n_{iso}		
St Vincent	1.581	1.530	1.556	0.052	27°
Montserrat	1.578	1.529	1.553	0.049	30°
Sakel	1.580	1.532	1.556	0.048	29°
Giza	1.579	1.530	1.554	0.049	29°
Tanguis	1.575	1.530	1.554	0.044	34°
Uganda	1.576	1.532	1.554	0.044	32°
Uppers	1.576	1.530	1.555	0.046	32°
Punjab-American 289F	1.577	1.530	1.553	0.047	31°
Brazilian	1.574	1.531	1.552	0.044	34°
Memphis	1.575	1.532	1.554	0.044	33°
Texas	1.575	1.532	1.554	0.044	33°
Oomras	1.574	1.532	1.552	0.043	34°
Bengals	1.574	1.531	1.551	0.043	34°

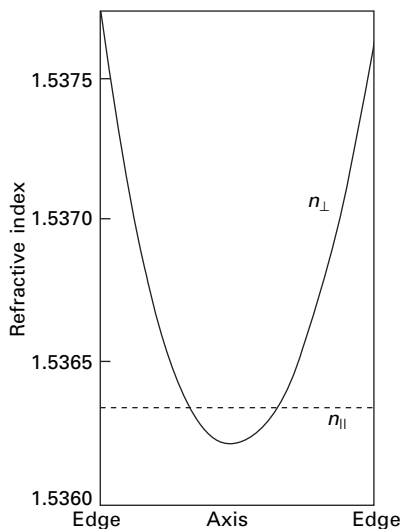
It is necessary to appreciate that the values given in Table 24.3 are only typical examples. Fibres are variable materials and their properties differ somewhat among the fibres in a sample, and to a greater extent between different varieties of the same type of fibre. The refractive index may also vary through a fibre cross-section. For example, Fig. 24.11 shows the variation across the fibre in the mean refractive indices of an unstretched viscose rayon model filament. The value of $n_{||}$ is almost constant, but n_{\perp} is a minimum at the centre. These values were calculated by Faust [13] from the interference fringes shown in Fig. 24.6.



24.10 Two forms of orientation in the cross-section of a fibre with axial symmetry.

Table 24.3 Refractive indices of fibres

Fibre	$n_{ }$	n_{\perp}	$(n_{ } - n_{\perp})$	Ref.
Cotton	1.578	1.532	0.046	[21]
Ramie and flax	1.596	1.528	0.068	[21]
Viscose rayon	1.539	1.519	0.020	[21]
Secondary acetate	1.476	1.470	0.006	[22]
Triacetate	1.474	1.479	-0.005	[22]
Wool	1.553	1.542	0.010	[22]
Silk	1.591	1.538	0.053	[22]
Casein	1.542	1.542	0.000	[23]
<i>Vicara</i> (zein)	1.536	1.536	0.000	[4]
Nylon	1.582	1.519	0.063	[4]
<i>Terylene</i> polyester fibre	1.725	1.537	0.188	[24]
<i>Orlon</i> acrylic fibre	1.500	1.500	0.000	[4]
<i>Acrilan</i> acrylic fibre	1.520	1.524	-0.004	[4]
Polyethylene	1.556	1.512	0.044	[24]
Glass	1.547	1.547	0.000	[4]



24.11 Variation in the mean refractive of an unstretched viscose rayon model filament [13].

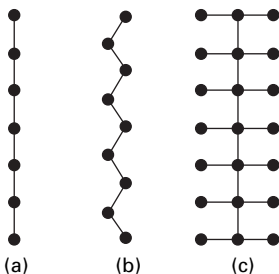
The magnitude of the birefringence, which ranges from -0.005 for triacetate to 0.188 for polyester, depends on two factors: the degree of orientation of the molecules, as discussed in the last section, and the degree of asymmetry of the molecules themselves.

If all the atoms in a molecule are arranged in a straight chain (Fig. 24.12(a)), and if, as usually happens, the bond polarisabilities are greatest along the line joining the atoms, then, for the reasons discussed earlier, a high birefringence will be expected. However, the actual molecules in fibres do not have this form and their birefringence will be reduced for two reasons. Firstly, most main chains have a zigzag form (Fig. 24.12(b)) but, provided that the bonds diverge from the main axis by less than about 55° , this still gives a positive birefringence. The coiling of the keratin molecule will have a similar effect in wool. Secondly, there will be side groups attached to the main chain, as in Fig. 24.12(c), and these will have the effect of providing atomic bonds at right angles to the main axis. This will increase the value of n_\perp and reduce the birefringence. In triacetate and acrylic fibres, the side groups have a greater effect than the main chain, and the birefringence is negative.

A detailed study of the chemical structure of the molecules will account for the differences in the birefringence of perfectly oriented fibres. In polyester, the presence of a benzene ring in the main chain causes a great increase in the birefringence. If the orientation is not perfect, the birefringence will be reduced. This is shown up by the low values of birefringence of the regenerated protein fibres and by a comparison of the values for viscose rayon, cotton and ramie. Experiments on model viscose rayon filaments with varying degrees of orientation confirm this.

If the individual crystallites of a fibre could all be aligned in exactly the same orientation, with all their faces parallel, it would be possible to measure the three principal refractive indices of the polymer crystals. This cannot be done exactly, but Bunn and Garner [25] examined flattened nylon fibres, in which the crystallites are roughly parallel, and found the following refractive indices: 1.580 along axis of chain molecule, 1.565 normal to the flat sheets of the nylon crystal and 1.475 in the plane of the sheets and perpendicular to the fibre axis.

Gupta and Rao [26] report measurements of the birefringence of wool, which decreases with moisture regain and increases with stretching.



24.12 (a) Straight chain. (b) Zigzag chain. (c) Chain with side groups.

24.3 Absorption and dichroism

In addition to changing the velocity of light that is being transmitted, the interaction of electromagnetic waves and matter may also result in the absorption of the radiation. When this happens selectively in the visual region of the spectrum, it results in the materials appearing coloured when viewed in white light. Most textile fibres are either colourless or only slightly coloured in neutral shades. The absorption in the fibre itself is comparatively unimportant. In order to produce colours, the fibre must be dyed, but this subject is chiefly outside the range of this book. There is, however, one feature that is of physical interest. This is the variation in the absorption by the dye with the direction of polarisation of the light, the phenomenon known as *dichroism*, which may result in differences in the depth of shade or even in the actual colour. For this to happen, there are three requirements that must be satisfied. Firstly, the dye molecule must be asymmetrical, so that its absorption varies with the direction of the electric field exciting the characteristic vibrations. Secondly, the dye molecule must be absorbed into the fibre molecule in a particular direction, so that all the dye molecules make the same angle (or a limited range of angles) with the axis of the chain molecules. Thirdly, the chain molecules must be preferentially oriented.

When the first two conditions are satisfied, the magnitude of the dichroism may be used as a measure of the orientation of the molecules in the fibre.

The absorption of light in a material is given by Lambert's Law: $I = I_0 \exp(-kd)$, where I is the intensity of light after passing for a distance d through a material with an absorption coefficient k , and I_0 is the intensity of the incident light. This may also be written:

$$\log \frac{I}{I_0} = -kd(\log e) \quad (24.7)$$

For a material exhibiting dichroism, it is necessary to separate the light polarised parallel and perpendicular to the fibre axis, and we can substitute in equation (24.7) intensities I_{\parallel} and I_{\perp} and absorption coefficients k_{\parallel} and k_{\perp} . Dividing one equation so obtained by the other, we get:

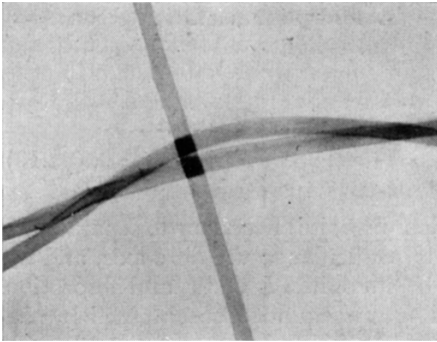
$$\frac{\log I_{\parallel}/I_0}{\log I_{\perp}/I_0} = \frac{k_{\parallel}}{k_{\perp}} = \phi \quad (24.8)$$

The quantity ϕ has been called the *dichroic* or *dichroitic ratio* or *constant* [27]. It has been found to be independent of the concentration of dye and may be used as a measure of orientation in the fibre. Values of the dichroic constant vary from unity in an isotropic material to infinity in a perfectly oriented fibre. Some typical values are given in Table 24.4.

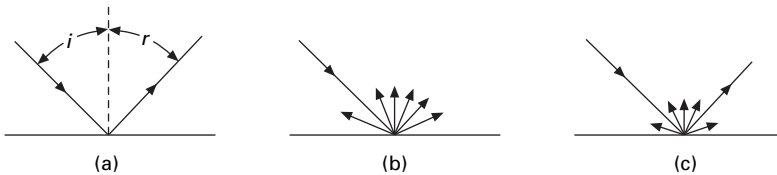
Figure 24.13 illustrates one consequence of dichroism, namely that, when light passes through two dichroic fibres, there is a greater total absorption if they are crossed than there is if they are parallel. The reason is fairly obvious. If the fibres are crossed, the first fibre absorbs a large part of one component and the second fibre absorbs a large part of the perpendicular component, but if the fibres are parallel, the same component is absorbed by both fibres, and the perpendicular component is transmitted through both with little absorption.

Table 24.4 Dichroic constants for direct dyes on cellulose [27]

Material	Dichroic constant
Ramie	9
Viscose rayon	1.4–3.3
Cellophane	1.5



24.13 Exhibition of dichroism by cuprammonium rayon filaments dyed with chlorazol pink Y. The perpendicular crossed filaments appear darker than the nearly parallel ones. After Preston and Tsien [28].



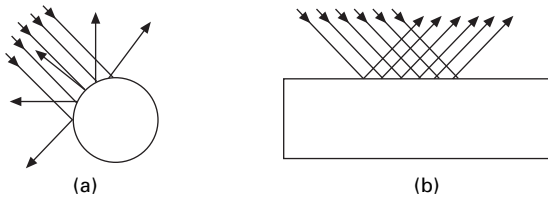
24.14 (a) Specular reflection. (b) Diffuse reflection. (c) Combination of specular and diffuse reflections After Buck and McCord [29].

24.4 Reflection and lustre

Lustre is an important aesthetic property of textile fabrics. If a beam of light falls on a surface, it may be reflected specularly, along the angle of reflection as in Fig. 24.14(a); diffusely, in varying intensity over a hemisphere as in Fig. 24.14(b); or in a combination of both as in Fig. 24.14(c). The reflection may vary with the angle of incidence and with the colour and polarisation of the light. The total visual appearance resulting from these reflections determines the lustre of the material. Lustre is thus easily observed subjectively but is extremely complex to characterise objectively.

This fact, together with the great importance of fibre arrangement in yarns or fabrics, has limited investigations of reflection and lustre from single fibres. Some general comments can, however, be made.

If a fibre behaved as a perfectly reflecting circular cylinder, it would reflect light as shown in Fig. 24.15. It is clear from this diagram that, if the light falls across the fibre, it is reflected at various angles, whereas if it falls along the fibre it is predominantly



24.15 Reflection of light from a circular cylinder [29]: (a) axis normal to incident plane; (b) axis in incident plane.

Table 24.5 Lustre of a range of cottons

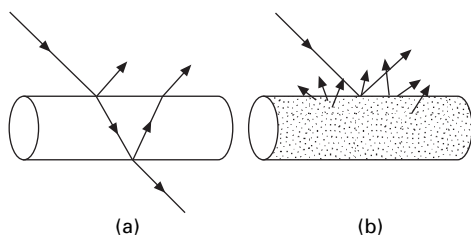
Type of cotton	Ratio of axes or cross-section, a/b	Lustre (arbitrary units)	Convolutions per cm, c
American FGM	3.07	5.7	31.3
Peruvian	2.62	6.7	30.0
Sakel S	2.37	7.1	29.8
St Kitts Sea Island	2.23	7.7	30.6
Surat	2.37	7.8	21.1
US 12, Sea Island	2.15	7.9	32.6
Abassi	2.21	8.0	30.9
Texas	2.22	8.1	29.3
Barbados Sea Island	2.17	8.2	31.4
Sakel CR	2.07	8.8	29.8
Egyptian, grown in Peru	2.11	9.0	30.5
Antigua Sea Island	1.91	10.7	29.9
Mercurised A	1.60	12.2	
B	1.64	12.9	
C	1.47	13.9	

reflected at a constant angle. This is a basic feature of textile lustre and shows the importance of causing the fibres to lie parallel to one another in a lustrous yarn or fabric.

Textile fibres depart from this ideal model in various ways. As was discussed in Section 3.3.3, finer fibres have a lustre which differs from that shown by coarse fibres. Irregularities on the surface of the fibre and in its cross-sectional shape will cause light to be reflected in various directions and will reduce the lustre. To secure the type of reflection shown in Fig. 24.15(b), it is essential that the fibre should be uniform along its length. For this reason, lustre is greatest in regular filaments, such as those of silk and the manufactured fibres.

Fibre shape is itself an important factor. The particular types of lustre associated with nylon, rayon and silk must be due partly to the influence on the pattern of light reflection of their respective circular, serrated and triangular shapes. In melt-spinning, shaped spinnerets can be used to make fibres with multilobal or other shapes, which become somewhat rounded as the molten material tends to a circular shape. This gives fibres with various lustre behaviour.

In cotton, Adderley [30] found a high degree of correlation between lustre and fibre ellipticity, as given by the ratio a/b between two axes taken, respectively, along



24.16 (a) Reflection, transmission and internal reflections in a fibre. (b) Scattering of transmitted light in delustred fibre [29].

the longest possible line through the fibre cross-section and perpendicular to this line at the mid-way position. Values for various types of cotton fibre are reported in [Table 24.5](#), arranged in order of increasing lustre. Mercerisation, which swells the fibres and makes them rounder, increases the lustre of the fibres. Adderley found no connection between lustre and fibre length, linear density, diameter or the number of convolutions. However, in a theoretical investigation, Foster [31] found that for fibres with an elliptic cross-section, the lustre should be proportional to $[(a^2/b^2 + 1)/(a^2/b^2 - 1)]/ac$, where c is the number of convolutions per unit length. This relation gave reasonable agreement with the experimental results. The lustre of cotton is thus essentially due to a flat cross-section, of which the direction changes along the length of the fibre. If there were no convolutions, the light would be more regularly reflected, and the lustre would be different. The failure to observe any correlation between the number of convolutions and the lustre is due to the fact that the variations in c are not great, and their influence is marked by the much greater effect of the differences in a/b . It may, however, be noted that the Surat and US 12 cottons in Table 24.5, which show particularly high and low values of lustre for their values of a/b , are, respectively, the fibres with the lowest and highest values of c .

Not all the light falling on a fibre is reflected at its surface: much of it is transmitted through the fibre. Some of this transmitted light will be reflected from the internal surfaces, and will reinforce the light reflected from the first surface, as is shown in Fig. 24.16(a). If the fibre contains small particles (e.g. of titanium dioxide) or cavities, as in Fig. 24.16(b), these will scatter the transmitted light at varying angles and cause it to emerge as apparently diffuse reflection. This masks the specular reflection and may be used to delustre manufactured fibres.

It is a consequence of the effects of transmission and internal reflection that lustre will be influenced by variations in refractive index with the direction of polarisation of the light and with the position in the fibre. Once again, irregularities diminish lustre.

24.5 References

1. C. W. Bunn. *Chemical Crystallography*, Oxford University Press, London, 1946, Chapter III, p. 67 *et seq.*
2. N. H. Hartshorne and A. Stuart. *Crystals and the Polarizing Microscope*, Arnold, London, 2nd edition, 1950.

3. O. Wiener. *Abh. Sachs. Akad. d. Wiss. Math. Phys. Kl.*, 1912, **32**, 507, 604.
4. A. N. J. Heyn. *Text. Res. J.*, 1952, **22**, 513.
5. A. N. J. Heyn. *Text. Res. J.*, 1953, **23**, 246.
6. A. Frey-Wyssling. *Helv. Chim. Acta*, 1936, **19**, 900.
7. J. M. Preston and K. Freeman. *J. Text. Inst.*, 1943, **34**, T19.
8. H. de Vries. *Ann. Sci. Text. Belg.*, 1955, No. **4**, 286.
9. R. C. Faust. *Proc. Phys. Soc.*, 1951, **B68**, 1081.
10. A. N. J. Heyn. *Text. Res. J.*, 1957, **27**, 449.
11. R. C. Faust. *Proc. Phys. Soc.*, 1952, **B65**, 48.
12. R. C. Faust. *Proc. Phys. Soc.*, 1954, **B67**, 138.
13. R. C. Faust. *Quart. J. Micr. Sci.*, 1956, **97**, 569.
14. R. C. Faust. *Proc. Roy. Soc.*, 1952, **A211**, 240.
15. R. D. Andrews. *J. Appl. Phys.*, 1954, **25**, 1223.
16. R. D. Andrews and J. F. Rudd. *J. Appl. Phys.*, 1956, **27**, 990, 996.
17. R. C. Faust and H. J. Marrinan. *Brit. J. Appl. Phys.*, 1955, **6**, 351.
18. S. A. Mortimer and A. A. Peguy. *Textile Res. J.*, 1994, **64**, 544.
19. P. H. Hermans. *Physics and Chemistry of Cellulose Fibres*, Elsevier, Amsterdam, Netherlands, 1949, pp. 214 et seq.
20. R. Meredith. *J. Text. Inst.*, 1946, **37**, T205.
21. J. M. Preston. *Trans. Faraday Soc.*, 1933, **29**, 65.
22. J. M. Preston. *Modern Textile Microscopy*, Emmott, London, 1933.
23. G. L. Roger and C. Maresh. *Text. Res. J.*, 1947, **17**, 477.
24. C. W. Bunn. In *Fibres from Synthetic Polymers*, R. Hill (Editor), Elsevier, Amsterdam, Netherlands, 1953, Chapter 10, p. 269.
25. C. W. Bunn and E. V. Garner. *Proc. Roy. Soc.*, 1947, **A189**, 39.
26. V. B. Gupta and D. R. Rao. *Textile Res. J.*, 1991, **61**, 510.
27. J. M. Preston. *J. Soc. Dyers Col.*, 1931, **47**, 312.
28. J. M. Preston and P. C. Tsien. *J. Soc. Dyers Col.*, 1946, **62**, 368.
29. G. S. Buck and F. A. McCord. *Text. Res. J.*, 1949, **19**, 715.
30. A. Adderley. *J. Text. Inst.*, 1924, **15**, T195.
31. G. A. R. Foster. *J. Text. Inst.*, 1927, **17**, T77.

25.1 Introduction

25.1.1 Historical development

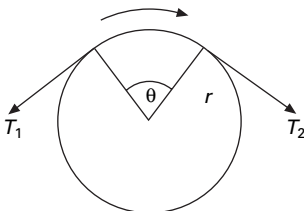
The study of the friction of materials is based on the two classical ‘laws’ of friction, probably understood by Leonardo da Vinci, but rediscovered by Amontons in 1699. These laws state that the frictional force is independent of the area of contact between the two surfaces and is proportional to the normal force between them. They were verified by Coulomb in 1781. He also pointed out the distinction between static friction, the force that must be overcome in order to start sliding, and kinetic friction, the force resisting continued sliding. He observed that kinetic friction was independent of the speed of sliding; this is sometimes called the third law of friction. Mathematically, Amontons’ law is expressed as:

$$F = \mu N \quad (25.1)$$

where F = frictional force acting parallel to the surface in a direction opposing relative movement. μ = coefficient of friction and N = force normal to the surfaces in contact.

When a yarn passes round a guide, as shown in Fig. 25.1, its tension must be increased by an amount necessary to overcome the frictional resistance. It follows from Amontons’ law¹ that:

$$T_2 = T_1 \exp(\mu\theta) \quad (25.2)$$



25.1 Values of $T_2/T_1 = e^{\mu\theta}$.

¹Note deviations from equation (25.2) due to bending, discussed in Section 25.2.2.

where T_2 = leaving tension, T_1 = incoming tension and θ = angle of contact.

In reality, these are not universal laws. The study of fibre friction has largely been the experimental observation of departures from the laws, the reasons for such departures, and their consequences. One of the earliest records is of the discovery by Monge in 1790 that the friction of wool depended on the direction in which the fibres were sliding.

25.1.2 Technological effects

The dualistic nature of the influence of friction on textile processing is illustrated by W. L. Balls's paradox: 'up to the front mule roller, cotton must be slippery; afterwards it must be sticky' [1]. Friction is the force that holds together the fibres in a spun yarn and the interlacing threads in a fabric. If the friction is too low, the yarn strength will fall, and the dimensional stability of cloth will be reduced. Here high friction is an advantage, enabling a greater proportion of the strength of the individual fibres to be utilised.

In many other places, however, fibre friction is a nuisance. If a yarn passes over a number of guides, the angle θ in equation (25.2) becomes the sum of the individual angles of contact. The figures in Table 25.1 show how rapidly the tension may increase in these circumstances. If excessive breaks are to be avoided, and the yarn is not to be permanently damaged by overstraining, it is essential to maintain the frictional resistance at as low a value as possible.

In the stitching of fabrics, high friction causes trouble for two reasons: the needle may become red-hot, and the threads will not slide over one another in order to allow the needle to pass between them. This causes many more threads to be broken; for example, in a particular unlubricated mineral khaki dyed cloth, there were nearly 20 cut threads per 100 needle punctures, but after lubrication the number of cut threads was insignificant [2].

Apart from these examples, where friction is clearly an advantage or a disadvantage, there are many other aspects of textile technology that are influenced by the frictional characteristics of the fibres: the handle and wear resistance of fabrics; the behaviour of fibres during drafting; and, especially in wool, the process of felting.

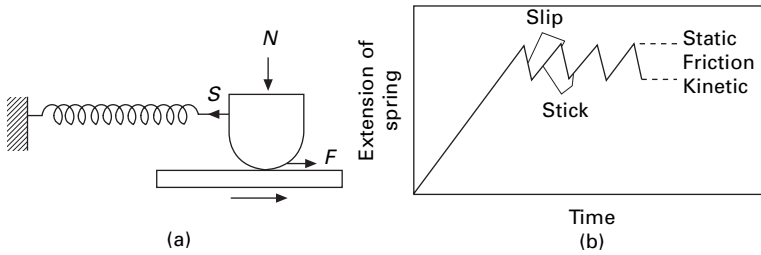
25.2 Measurement of fibre friction

25.2.1 Methods for fundamental studies

The apparatus developed by Bowden and Leben [3] is the best general method for the fundamental study of friction. [Figure 25.2\(a\)](#) illustrates its mode of operation. A

Table 25.1 Values of $T_2/T_1 = e^{\mu\theta}$

	$\theta = \pi/2$	$\theta = \pi$	$\theta = 2\pi$	$\theta = 4\pi$
$\mu = 0.2$	1.4	1.9	3.5	12.3
$\mu = 0.5$	2.2	6.0	22.9	525
$\mu = 1.0$	6.0	22.9	525	270 000



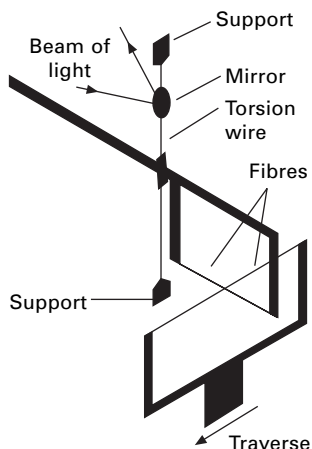
25.2 (a) Basic principle of Bowden and Leben's apparatus [3]. (b) Record of trace.

slider, under a load N , presses on a lower plate, which is moving past it at a constant velocity. The force of friction drags the slider along with the lower plate until the force S exerted by a spring fixed to the slider just balances the frictional force F . The extension of the spring is thus a measure of F . In practice, static friction F_s , the force opposing the start of slippage, is usually greater than kinetic friction F_k . Hence, once the slider has started to slip, it will be accelerated back until the tension in the spring has been reduced from a value equal to the force of static friction to that of the force of kinetic friction. The slider will continue to slip back for a further distance before it has decelerated and come to rest. It then moves forward again with the lower plate under the force of static friction. A record of the extension of the spring will give the 'stick-slip' trace shown in Fig. 25.2(b). If the damping is small, it can be shown that the force of kinetic friction is equal to the mean force exerted by the spring during the slip. Consequently, values of both F_s and F_k can be calculated when the characteristics of the spring are known.

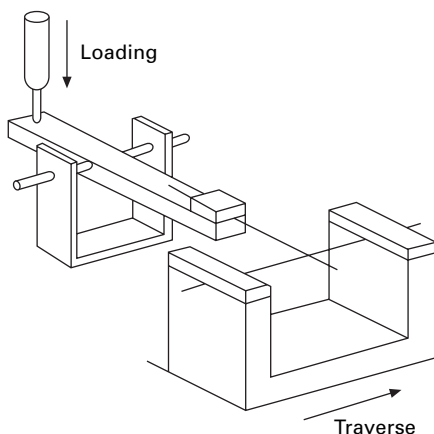
In one practical form of this instrument [4, 5], suitable for loads between 5 mg and 100 g, the spring is a stiff wire beam, deflected horizontally by the movement of the slider, and deflected vertically to apply the load. The slider is carried on a turntable. For heavier loads [4, 5] of up to several kilograms, another form of the apparatus is used, with spring loading of the specimen and with the force opposing the drag of the specimen being applied by means of the rotation of a loaded bifilar suspension.

With these forms of apparatus, measurements of the friction of pads of fibres rubbing against solid surfaces may be made, and polymeric materials, of which fibres are made, may also be investigated, but for work on single fibres modifications are needed. The fibres may be mounted on frames under light tension and then pressed against one another, as is shown in Fig. 25.3. One fibre with its frame is then traversed along, and, in one form of the apparatus, the movement of the other is restrained by a leaf spring. The deflection of the spring may be recorded graphically with a stylus, or photographically by reflection from a mirror mounted on the spring, and gives a stick-slip trace from which the static and kinetic friction can be calculated. This method has been used by Mercer and Makinson [7]. In the similar instrument illustrated in Fig. 25.3 and used by Guthrie and Oliver [6], the 'stationary' fibre is suspended in a frame on a torsion wire, which rotates until the force is sufficient to cause slippage.

An ingenious development of this method for use with very light loads has been described by Pascoe and Tabor [8]. In their apparatus, shown in Fig. 25.4, the sliding



25.3 Essential features of Guthrie and Oliver's apparatus [6].



25.4 Measurement of fibre friction under very low loads [8].

fibre is mounted at one end only. The other end rests on the second fibre, which can be traversed along in a frame. The upper fibre acts as a cantilever. Its displacement in the vertical plane gives the load, and its displacement in the horizontal plane gives the force opposing the frictional drag. The displacements are determined by microscopical observation of the free end of the fibre.

The principles of these methods are still applicable for fundamental studies of fibre friction, but advances in transducers and detectors will lead to differences in detail.

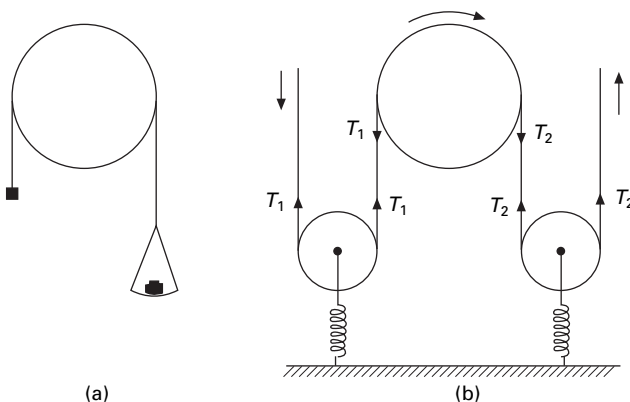
25.2.2 Rapid methods

Whereas the above methods are the most suitable for fundamental investigations, they are less convenient for the rapid technical evaluation of frictional resistance. For

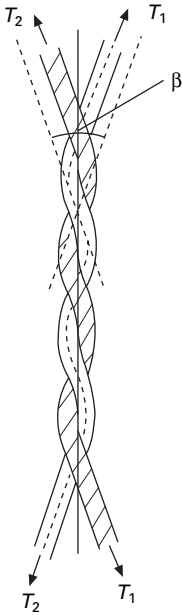
this purpose, there are advantages in the capstan method, which involves measurement of the excess tension needed to pull yarn over a guide. The basic feature of the apparatus is that shown in Fig. 25.1, and the coefficient of friction, assumed to be constant, can be calculated from the relation: $T_2/T_1 = \exp(\mu\theta)$. A static form of the method is illustrated in Fig. 25.5(a). A loop of fibre is placed over the guide and a small load placed on one side. The load on the other side is then decreased until slippage commences. Alternatively, a dynamic method may be used, with the yarn running continuously over the guide. Abbott and Grosberg [9] have described a version of the method suitable for use with an Instron Tensile Tester. Buckle and Pollitt [10] invented a mechanical tester in which the tensions operate in such a way that the coefficient of friction can be directly indicated by a pointer on a scale. However, this has been displaced by advances in electronic tension meters.

A typical modern instrument will have a means of pulling yarn over a guide, with tension meters on either side, as indicated schematically in Fig. 25.5(b). The springs are, in reality, stiff force transducers connected to a computer.

The simple derivation of equation (25.2) assumes that the yarn is perfectly flexible and does not take account of bending stiffness. As discussed in Section 19.5.4 in relation to flex fatigue testing, the form shown in Fig. 25.1 would have a discontinuity in bending moment at the point where it leaves the pin. In reality there will be a zone of changing curvature. An analysis by Jung *et al.* [11] also shows that the forces in the contact region are influenced by fibre stiffness. Equation (25.2) is a good approximation when the yarn or fibre radius is small compared with the pin radius, but Jung *et al.* [11] show that there are appreciable differences when a yarn passes over a guide at an angle. In a typical example, the value of T_2/T_1 increased by 20% in going from zero deviation to a 45° inclination. Another error in equation (25.2) results from bending hysteresis. Energy is dissipated not only in overcoming friction but also in the cycle of bending and unbending, which is undergone by each portion of material. The work done to provide this energy will appear to be a frictional loss and will cause the measured friction to be too large. Grosberg and Plate [12] have discussed the problem and shown that the error may be as high as 2.5%. The contribution



25.5 (a) Static capstan method. (b) Dynamic capstan method.



25.6 Measurement of inter-fibre friction [13].

to the frictional force is found to equal $\Delta M/r$, where ΔM is the difference in bending moment in bending and recovery and r is the radius of curvature of the capstan. The error may therefore be made negligible by using large cylinders.

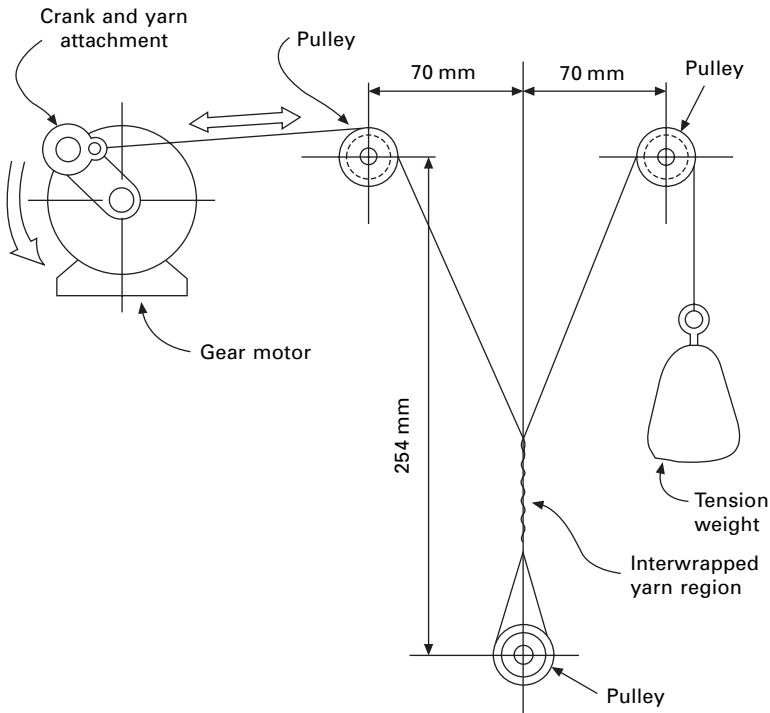
For the measurement of inter-fibre friction, Lindberg and Gralén [13] introduced a method in which the two fibres are twisted together as shown in Fig. 25.6. If the difference between the tensions applied to the opposite ends of each fibre is increased, the fibres will eventually slip over one another. It is shown that:

$$\mu = \log_e \frac{T_2/T_1}{\pi n \beta} \quad (25.3)$$

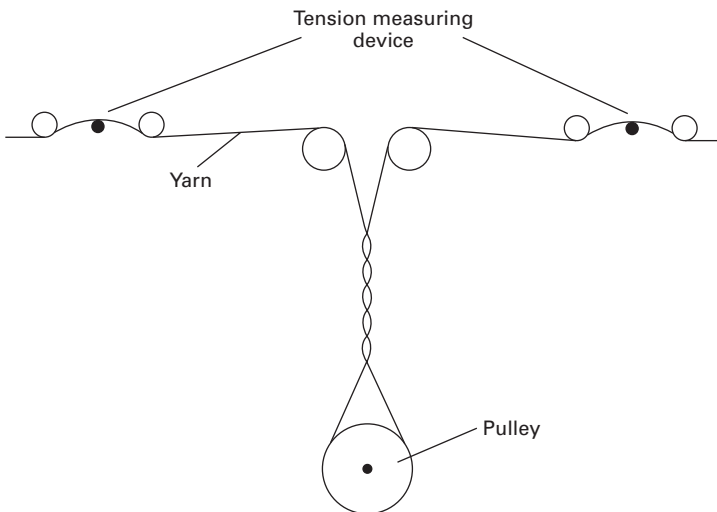
where T_2 and T_1 are the tensions in the fibres, n is the number of turns of twist and β is the angle between the fibre axes and the axis of the twisted element.

The yarn-on-yarn abrasion tester shown in Fig. 25.7 can be adapted to measure friction in this way by adding tension meters or, as shown in Fig. 25.8, measurements can be made on a running yarn. Another variant of the method was used by Gupta and coworkers [14] to measure friction of sutures and hair [15]. This was adapted by Moghazy and Gupta [16] for testing in liquid.

Another technique that has been used to investigate fibre friction is the measurement of the force necessary to remove a single fibre from a mass of fibres under pressure [17], or to pull apart two interlocking fringes of fibres [18]. A convenient version of the latter method in which one fringe of fibres is pulled over another on an apparatus fitted to an Instron Tensile Tester is described by Hearle and Husain [19]. These measurements will be related to the practical behaviour of fibres in drafting and in yarns. Moghazy and Broughton [20] describe a method of using an Instron tester to pull a beard of cotton fibres from between metal plates.



25.7 Yarn-on-yarn abrasion tester.



25.8 Measurement of yarn-on-yarn friction on a running yarn.

A very simple means of measuring friction is the inclined plane method [21]. Several turns of yarn are wound as a bow over a bridge and rested on a horizontal plate of the other material. This plate is gradually inclined. The coefficient of friction is equal to the tangent of the angle of inclination at which slippage starts. Howell and

Mazur [22] have used a similar method for studying the friction between single fibres. A lightly loaded loop of fibre is allowed to rest on another stretched fibre, which is mounted in a frame. The frame is initially horizontal and is then rotated until the loop of fibre just begins to slide down.

25.3 Empirical results

25.3.1 Friction, load and area of contact

The ratio of frictional force F to normal load N for fibres is found to decrease as the load is increased. In other words, Amontons' law is not obeyed. Some typical examples are given in Fig. 25.9. Among the various mathematical relations that have been used to fit the experimental data are the following:

$$F = \mu_0 N + \alpha S \quad (25.4)$$

$$\frac{F}{N} = A - B \log N \quad (25.5)$$

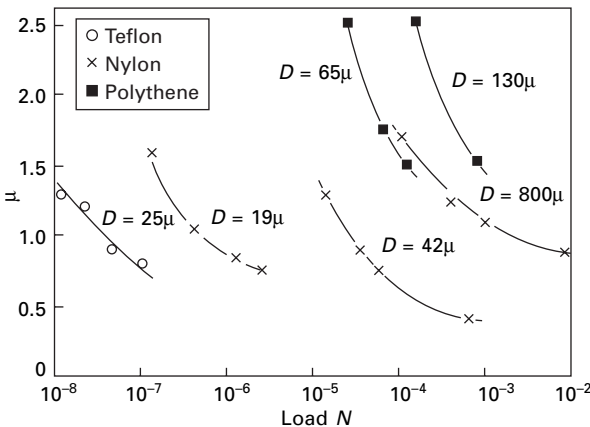
$$F = aN + bN^c \quad (25.6)$$

where S = area of contact, and μ_0 , α , A , B , a , b and c are constants. The most successful relation has, however, been:

$$F = aN^n \quad (25.7)$$

where a and n are constants. This is a form of equation previously found by Bowden and Young [23] to apply to some non-metals: it was first applied to fibres by Lincoln [24] and by Howell and Mazur [22]. The value of the index n generally lies between $2/3$ and 1 , some typical values being given in Table 25.2.

If this relation holds, we can work out the effect of the areas of surfaces in



25.9 Variation of coefficient of friction of fibres with load (D = fibre diameter) [8].

Table 25.2 Values of n

(a) Results by Mazur [25] for single fibres crossed at right angles (fibre in vertical column sliding on fibre in horizontal column)

	Acetate	Nylon	Viscose rayon	Terylene polyester fibre	Wool*
Acetate	0.94	0.89	0.90	0.86	0.92
Nylon	0.86	0.81			
Viscose rayon	0.89	0.88	0.91	0.88	0.87
Polyester fibre Terylene	0.88				
Wool*	0.88	0.86	0.92	0.86	0.90

*Mean values, 'with' and 'against' scales.

(b) Other results

	n
Nylon monofil pulled over glass cylinder [26]	0.91
Acetate yarn pulled over chromium-plated cylinder [27]	0.8
Wool pulled over serge cylinder [28, 29]	0.75
Viscose rayon fibres crossed at right angles [30]	
static friction – normal finish	0.80–1.02†
– extracted	0.75–0.98
kinetic friction – normal finish	0.77–0.94
– extracted	0.64–0.99

† Value varying with filament linear density.

contact². For a load N on an area A_1 , the frictional force is $F_1 = aN^n$. For the same load on an area A_2 , equal to xA_1 , we may consider the total frictional force F_2 to be made up of the sum of the individual frictional forces f on x portions, each of area A_1 , under loads N/x . But, from equation (25.7), it follows that:

$$f = a(N/x)^n \quad (25.8)$$

Therefore:

$$F_2 = \sum f = xa(N/x)^n \quad (25.9)$$

$$\frac{F_2}{F_1} = \frac{xa(N/x)^n}{aN^n} = x^{(1-n)} = \left(\frac{A_2}{A_1}\right)^{(1-n)} \quad (25.10)$$

The two classical laws of friction are thus replaced by the relations: $F = aN^n$, for constant apparent surface area in contact and $F = bA^{(1-n)}$, for constant load, where a

²The more detailed understanding of the nature of frictional force (discussed in Section 25.4.2) shows that the real determining factor is the number of points of true contact between the surfaces. For extensive apparent areas of contact, this number will be proportional to the overall geometric area of contact. This will not hold, however, for crossed fibres making a single-point contact, or for parallel fibres making contact along a line. It also follows that the friction is influenced by the roughness of the surface.

and b are constants, dependent on the area and load, respectively. It should be noted that a and b are not dimensionless and will thus vary with the units used. The parameter n should be a fundamental property of the materials, independent of geometry, although Guthrie and Oliver [30] have found an indication that it increases with filament linear density in staple-fibre rayon. The classical laws of friction will occur as the special case: $n = 1$.

Viswanathan [31] found experimentally that the parameter a is correlated with n to a fairly high degree over a wide range of fibres, and even better within a given fibre type. The values of a decrease approximately linearly from about 3 for $n = 0.6$ to 0.5 at $n = 0.9$. However, it must be remembered that a has the dimensions of $(\text{force})^{(1-n)}$, so that the results would look different in other units. There are theories that suggest reasons, and even equations, for the correlation.

Howell [29] has shown that, if equation (25.7) holds, then equation (25.2), relating the tensions in a yarn or fibre passing round a guide, is modified and becomes:

$$T_2^{(1-n)} = T_1^{(1-n)} + (1 - n)a\theta r^{(1-n)} \quad (25.11)$$

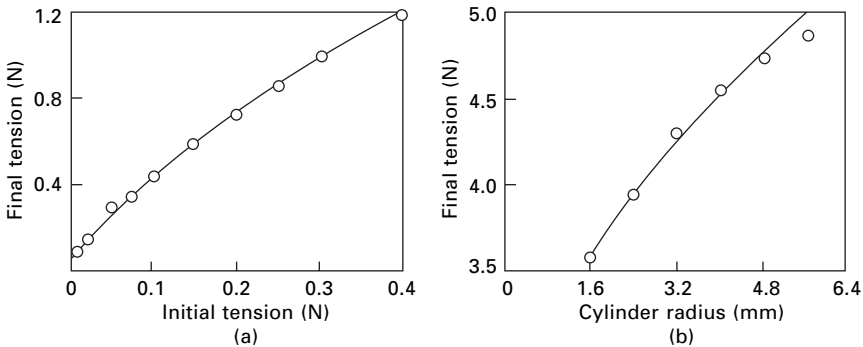
where r is the radius of the cylinder. In the limit, as n approaches 1, this equation reduces to:

$$T_2 = T_1 e^{a\theta(r/T_1)^{(1-n)}} \quad (25.12)$$

This form obviously reduces to the classical form when $n = 1$. Figure 25.10 shows a check of equation (25.11) for varying initial tensions and cylinder radii.

25.3.2 Static and kinetic friction: speed of sliding

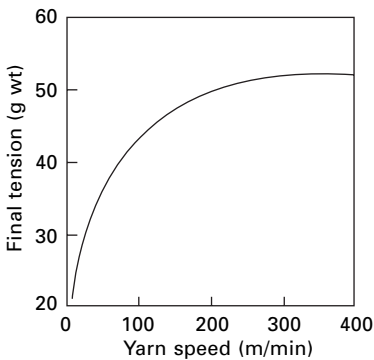
The kinetic friction μ_k is usually less than the static friction μ_s . Some typical examples are given in Table 25.3. The difference affects the feel of the material. If it is large, the material is ‘scroopy’, that is, it will have a coarse, crunchy feel and will give a



25.10 Check of equation (25.11) for (a) varying initial tension and (b) varying cylinder radius. The lines are the theoretical curves, and the points are experimental values for acetate yarn. For curve (a), $n = 0.8$, $a = 1.18$; for curve (b) $n = 0.8$, $a = 1.15$ [27].

Table 25.3 Static and kinetic friction [32]

	Static μ_s	Kinetic μ_k
Rayon on rayon	0.35	0.26
Nylon on nylon	0.47	0.40
Wool on wool		
with scales	0.13	0.11
against scales	0.61	0.38
fibres in same direction	0.21	0.15
Wool on rayon		
with scales	0.11	0.09
against scales	0.39	0.35
Wool on nylon		
with scales	0.26	0.21
against scales	0.43	0.35
Rayon on rayon [30]	0.22	0.14



25.11 Variation of final tension after acetate yarn has passed over a guide at varying speeds [27] (50 g wt = 0.49 N).

fabric that rustles like silk, owing to the marked 'stick-slip' motion. This tendency will be reduced by any finish or lubricant that reduces the differences between μ_s and μ_k . The handle will then be softer.

At low speeds, going from 2 to 90 cm/min, Röder [33] noted a decrease in the friction, but at much higher speeds other workers have found that the friction increases as the speed increases. A typical result is shown in Fig. 25.11. It therefore seems likely that the frictional force passes through a minimum at around 1 m/min, due to mechanisms shown later in Fig. 25.25. The variation of friction with speed will have a considerable influence on the behaviour of fibres in drafting.

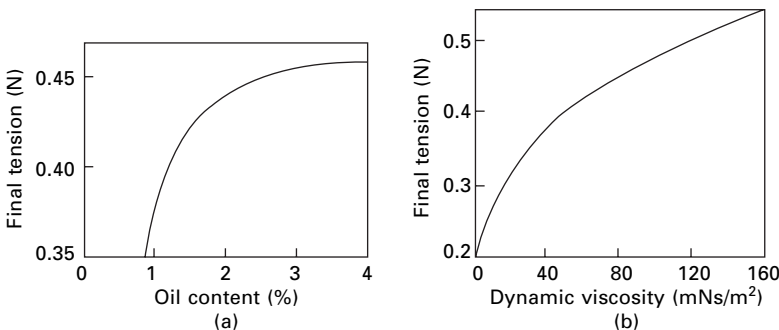
Cotton is exceptional in that even at low speeds the coefficient of friction increases with the speed of sliding. For example, Merkel [34] found that the coefficient of friction of single cotton fibres against cotton-covered cylinders increased steadily

with speed. Under medium-load conditions, the coefficient of friction was 0.23 at 3.6 cm/min, but it increased to 0.25 at 200 cm/min and to 0.39 at 4500 cm/min. One consequence of this is that the slippage of cotton, for example, in the deformation of needled fabrics, occurs more smoothly without the stick–slip effect characteristic of other fibres.

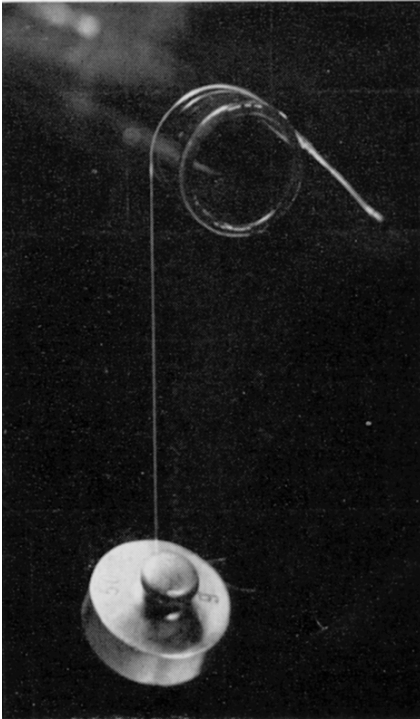
25.3.3 The state of the surface

The frictional force is changed if the surface is lubricated, either naturally, e.g. by waxes in cotton, or artificially, or by contamination with dirt or impurities. Figure 25.12 shows that, for acetate yarn with more than 1% of oil applied, the frictional force increases both as the oil content is increased and as the viscosity of the oil increases. However, fibres from which all traces of lubricant have been removed show high values of friction; thus, in one experiment [2], raw cotton on steel gave $\mu = 0.25$, whereas scoured cotton on steel gave $\mu = 0.7$, and lubricated scoured cotton on steel gave values of μ ranging from 0.14 to 0.35.

Bradbury and Reicher [35] have found that extremely high values of friction are obtained between flat continuous-filament yarns and glass if excessive precautions are taken to ensure the cleanliness of both surfaces. With nylon, the value of μ was at least 8, and a 50 gram weight could be supported on a short length of yarn looped over a glass rod, as shown in Fig. 25.13. This high value of friction was not found if the yarns were twisted, or if the glass surface was roughened by grinding: this suggests that the effect is associated with a high true area of contact (see Section 25.4.2). A similar effect was observed by King [36], who found a reduction in the friction of wool fibres on various materials when the surface was roughened. Values obtained are given in Table 25.4. The dependence on the physical state of the surface is also shown by the results in Table 25.5 for moulded and machined nylon. The newly moulded surface shows the highest coefficient of friction. Taylor and Pollet [38] have investigated the low force friction of several fabrics against engineering surfaces.



25.12 Variation of final tension after passage of acetate yarn over guide, for (a) varying amounts of oil on yarn and (b) varying viscosity of oil [25].



25.13 Demonstration of very high friction with clean nylon and glass [35].

Table 25.4 Effect of surface roughness: Values of μ for wool rubbed on various materials [36]

Material	Polished surface		Rough surface	
	With scales	Against scales	With scales	Against scales
Casein	0.58	0.59	0.47	0.57
Ebonite	0.60	0.62	0.50	0.61
Sheep's horn	0.62	0.63	0.52	0.63
Cow's horn	0.49	0.54	0.42	0.53

Table 25.5 Values of μ for moulded nylon [37]

	As received	Aged 30 min at 170 °C	Aged 5 months at 20 °C
Cold-moulded	0.70	0.45	0.55
Hot-moulded	0.65	0.45	0.55
Machined	0.45	0.40	0.45

25.3.4 Effect of water

The frictional force usually increases as the regain of the fibres is raised. Typical results are given in Fig. 25.14. Moghazy and Gupta [16] found that friction was higher in wet polypropylene and acrylic yarns than in dry ones.

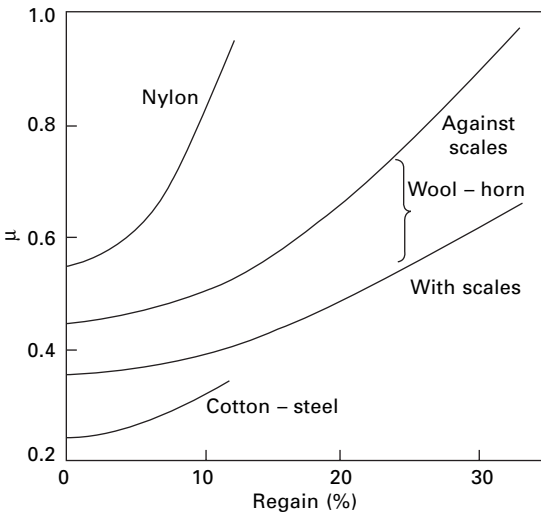
25.3.5 Typical values of $\mu = F/N$

Although fibres do not have a true, constant coefficient of friction, it is useful to quote values of $\mu = F/N$ to express the magnitude of the friction under particular conditions. However, because this value of μ varies with so many of the experimental conditions (load, speed, area and geometry of contact, humidity, etc.) and because it is so dependent on the exact state of the surface, only typical values found in particular experiments can be quoted. Some examples are given in Table 25.6. They cannot be expected to have validity in other circumstances.

In general, values of μ for fibres and plastics range between 0.1 and 0.8, although, under extremely clean conditions, as described in Section 25.3.3, much higher values of fibre friction are found. Another exception is PTFE (known as *Teflon* in fibre form), which has an extremely low coefficient of friction, often less than 0.05, except at the very low loads shown in Fig. 25.9.

Table 25.7 gives values of coefficient of friction of yarns used in high-performance ropes [40]. High-modulus polyethylene (HMPE) fibres have an inherently low coefficient of friction, but the others will have special marine finishes, which reduce inter-fibre abrasion.

Behary *et al.* [41] studied the tribology of sized glass fibres and found wide variations in friction. One fibre had a unimodal distribution for μ ranging from 0.1 to 10 with scattered values up to 15, a peak at 3.5, a mean of 5 and a standard deviation



25.14 Change of coefficient of friction with regain for nylon on nylon, wool on horn [36] and cotton on steel [39].

Table 25.6 Typical values of μ (a) between fibres; (b) for yarns passing over guides [10]

(a)

	Crossed fibres [6]	Parallel fibres [32]
Nylon	0.14–0.6	0.47
Silk	0.26	0.52
Viscose rayon	0.19	0.43
Acetate	0.29	0.56
Cotton	0.29, 0.57	0.22
Glass	0.13	–
Jute	–	0.46
Casein	–	0.46
<i>Saran</i>	–	0.55
<i>Terylene</i> polyester fibre	–	0.58
Wool, with scales	0.20–0.25	0.11
Wool, against scale	0.38–0.49	0.14

(b)

	Hard steel	Porcelain	Fibre pulley	Ceramic
Viscose rayon	0.39	0.43	0.36	0.30
Acetate, bright	0.38	0.38	0.19	0.20
Acetate, dull	0.30	0.29	0.20	0.22
Grey cotton	0.29	0.32	0.23	0.24
Nylon	0.32	0.43	0.20	0.19
Linen	0.27	0.29	0.19	–

Table 25.7 Yarn-on-yarn friction results. From Noble Denton and National Engineering Laboratory [40]

	Load range (g)	Coefficient of friction μ		
		Mean sliding	Mean static	Maximum
<i>Aramid</i>				
<i>Kevlar</i> 29 (961)	100–1600		0.157	0.167
<i>Kevlar</i> 29 (960)	100–1500		0.137	0.150
<i>Twaron</i> 1000	100–1200		0.165	0.180
<i>Twaron</i> 1020	100–2500		0.131	0.138
<i>Technora</i>	100–2200	0.117		
<i>LCP</i>				
<i>Vectran</i>	100–2700		0.144	0.151
<i>HMPE</i>				
<i>Spectra</i> 1000	200–4500	0.058		0.063
<i>Dyneema</i> SK60	2000–6000	0.061		0.064
<i>Polyester</i>				
<i>Diolen</i> 855TN	100–1500		0.092	0.099
<i>Trevira</i> 785	100–2500		0.060	0.064
<i>Seagard</i> IW81	100–1900		0.02	0.096

of 1.7. Another fibre with a different finish had a bimodal distribution with peaks at 1.25 and 6.25 and values from 0.25 to 9. They used atomic force microscopy to observe the fibre surfaces and related the frictional behaviour to the nature of the contacts between fibres. In another paper [42], they report on stick-slip behaviour.

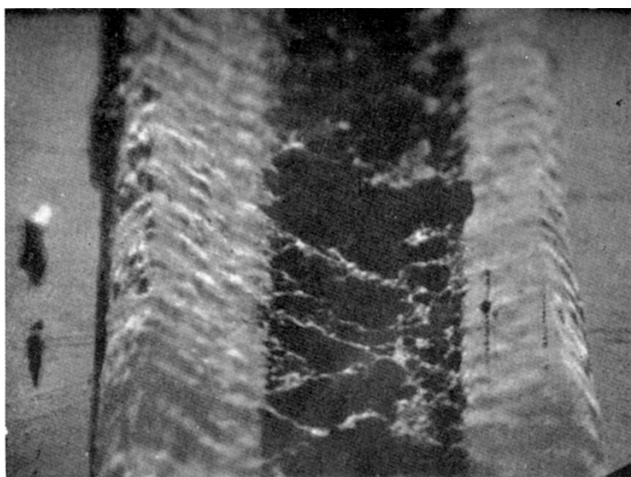
Moghazy and Gupta [16] found that triangular and trilobal polypropylene monofilament had lower friction than circular monofilaments.

25.3.6 Surface damage on rubbed fibres

The nature of the damage to the surface of fibres when they are subject to friction is of intrinsic interest and also leads to an understanding of the nature of the frictional force. Figure 25.15 shows a nylon filament that has been rubbed with a platinum



(a)



(b)

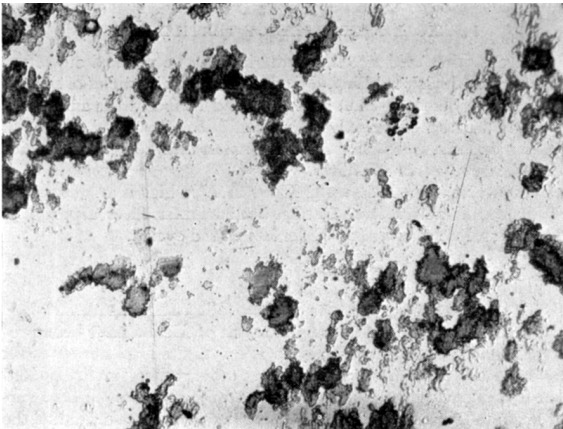
25.15 Effect of friction by platinum slider on nylon monofilament [43]: (a) low load, 0.39 N; (b) high load, 2.8 N.

slider under various loads, viewed by reflection electron microscopy. At low loads, there is a narrow track in which the fibre is slightly flattened, but at higher loads there is a marked deformation, and severe tearing of the surface occurs at the centre of the track. The concave shape of the track is probably due to reduced elastic recovery in the centre, where the deformation is greatest. Other examples of surface damage are shown in the electron micrographs of the surface of acetate fibres that have passed over guides (Fig. 25.16).

There is other evidence that material may be plucked out of the fibre surface during rubbing. Figure 25.17 shows particles of acetate (after dyeing) that were left on a glass rod rubbed with an acetate fibre, under the excessively clean conditions



25.16 Acetate fibre abraded by passing over a ceramic guide at 300 m/min. Damage is due to fibre sticking to a guide and then breaking away [4].



25.17 Particles of acetate left on glass rod, after rubbing with acetate fibre [35].

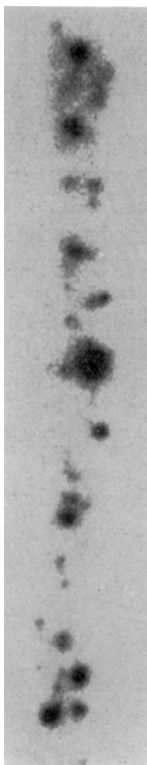
described in Section 25.3.3. Similar deposits were observed with nylon and polyester fibres, but not with viscose rayon or silk fibres. The reverse effect is shown in Fig. 25.18, which is an autoradiograph of radioactive silver that has been transferred to a PVC surface after a silver slider has passed over it.

25.4 The nature of friction

25.4.1 General theory

Over the centuries, many explanations of friction have been proposed. Amontons suggested that it was due to the force needed to lift one surface over the irregularities in the other; others have suggested that it is due to attractive forces between the atoms on the two surfaces, or to electrostatic forces. These theories all assume that the surfaces remain separate and, although they may sometimes play some part, the work of Bowden and Tabor [5, 44] showed that the predominant effects are usually an actual union, or welding, of the two surfaces at points of real contact, and the breaking of these junctions when sliding starts.

The surfaces of most materials are irregular if studied on a small enough scale: only in exceptional cases (for example, the cleavage planes of a crystal of mica) will they be smooth on the molecular scale. Bringing two surfaces into contact is therefore



25.18 Radioactive silver left on polyvinyl chloride surface after rubbing [43].

like ‘turning Switzerland upside down and putting it on top of Austria. Contact only occurs at the tips of the peaks’ [44]. If a load is applied, the pressure at the few points of real contact is very great, and they squash down until the area in contact is adequate to support the load.

The nature and extent of the deformation will depend on the mechanical properties of the materials. Metals flow plastically under high loads, and the flow will continue until the pressure at the points of contact is reduced to the yield pressure, when it will support the load without further deformation. The condition for equilibrium is shown graphically in Fig. 25.19. If A is the total area of real contact, we have:

$$p_y = N/A \quad (25.13)$$

$$A = N/p_y \quad (25.14)$$

where N = applied load and p_y = yield pressure.

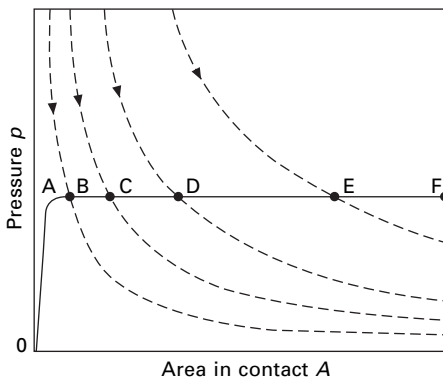
Thus the area of real contact is proportional to the applied load. Under the intense pressure, and an accompanying temperature rise, the junctions weld together, as illustrated in Fig. 25.20. In order to allow sliding, these junctions must be broken by shearing. The resistance to this, which is the frictional force F , will be given by:

$$F = SA \quad (25.15)$$

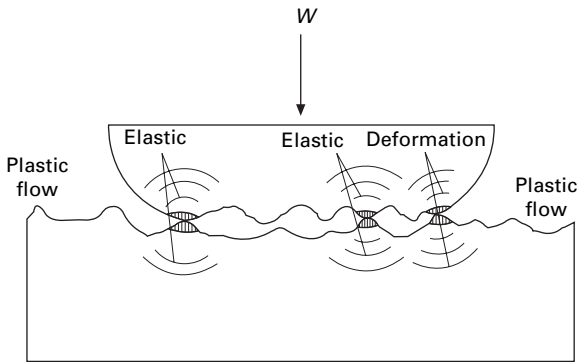
where S = shear strength of the weaker material. But, on substituting from equation (25.13), this gives:

$$F = \frac{S}{p_y} N = \mu N \quad (25.16)$$

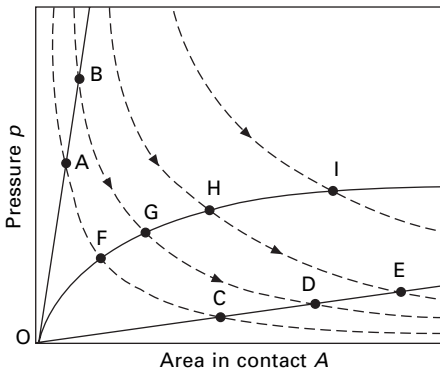
Since S and p_y are both constants, being mechanical properties of the materials, this is Amontons’ law with $\mu = S/p_y$. As the relation between load and contact area is linear, the total area in real contact will be independent of the number of points of contact. This explains the classical law that friction is independent of the overall area



25.19 Deformation of metal contacts. The full line represents the load-deformation curve of the metal, with a elastic region, OA, and a region of plastic flow, AF. The dotted lines are pressure–area curves for constant loads. Equilibrium occurs at the intersections, B, C, D, E, of the full and dotted lines.



25.20 Deformation at points of real contact, showing welded junctions. After Bowden and Tabor [44].



25.21 Deformation of elastic and viscoelastic materials. OB is the line for a hard elastic material, such as diamond; OE is the line for a soft elastic material, rubber; and OI is the curve for a viscoelastic material. Equilibrium occurs at the points of intersection with the pressure–area curves (dotted).

of contact. Bowden and his colleagues have produced a great deal of evidence in support of this theory in its application to metals: the values of μ agree with the above expression; the damage to the surface, the portions of metal plucked up, the metal transferred from one surface to the other, the evidence of strains below the surface, and the form of the track left after sliding show that welding and shearing must have occurred. They have found that, if one surface is much harder than the other, an additional force is needed to plough out a track in the soft metal for the asperities on the hard surface. This force will also contribute to the friction.

They have applied similar theories to non-metals. For brittle solids, such as rock salt, Amontons' law is obeyed, and the behaviour is similar to that in metals, but, in solids that are either very hard, such as diamond, or have a very large elastic deformation, such as rubber, the behaviour is different. With these materials, the deformation within the elastic range is sufficient to give support to the load. This is illustrated in Fig. 25.21. In neither case is the yield pressure reached. The relation between load

and area of real contact under conditions of elastic deformation depends on the geometry of the contacts and has been studied by Hertz [45].

For spheres in contact, $A \propto N^{2/3}$. Since we should still have $F = SA$, this would give $F \propto N^{2/3}$, a result that agrees with experimental results for diamond and rubber. This condition would be expected to apply approximately to the contact between asperities on an extended surface. However, the number of points of contact will affect the proportion of the load borne by each contact, and, since the relation between load and area is non-linear, this will affect the total area of contact. Thus the magnitude of the frictional force will depend on the roughness of the surface and on the overall area of contact.

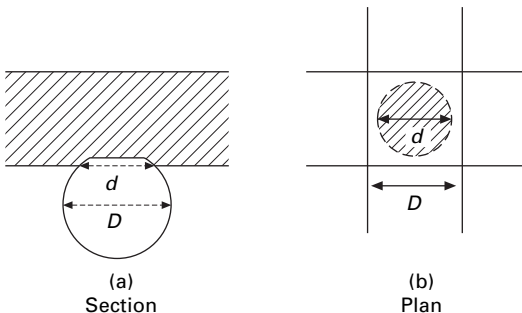
For two cylinders at right angles, the Hertz formulae give $A \propto N^{2/3}$, and for two cylinders in contact along a line they give $A \propto N^{1/2}$.

25.4.2 Application to fibres

The damage to the surfaces of fibres and plastics during sliding shows that there has been a marked deformation of the surface and welding together at points of contact. The essential mechanism of friction is thus the same as that for the other materials discussed in the last section. The friction will depend on the force needed to shear the junctions, and, in general, calculations of shear strength of plastics from friction measurements, by means of equation (25.15), have shown reasonable agreement with bulk measurements of shear strength.

Experimentally, the frictional force is given by $F \propto N^n$, where the index n is less than 1 but is usually greater than that to be expected from a purely elastic deformation. The index will depend on the viscoelastic properties of the material, which determine the shape of the curve relating deformation to pressure. Figure 25.21 includes an example of a curve, not unlike typical fibre stress–strain curves, that would give values intermediate between the elastic deformation, also shown in Fig. 25.21, and the plastic flow of Fig. 25.19.

The relations will also depend on the geometry of the system. Pascoe and Tabor [8] have investigated the effect of the diameter of crossed fibres that make contact at a single point and deform as shown in Fig. 25.22. Working on a large scale with



25.22 Deformation of crossed fibres under load.

Perspex cylinders 1 cm in diameter, they found that the diameter d of the circle of contact fitted the following relation over a wide load range:

$$N \propto d^{2.7} \quad (25.17)$$

Similar results were obtained with steel spheres pressed on various polymers.

The only parameter defining the shape of the deformation is the ratio d/D , where D is the diameter of the cylinder. This parameter will determine the distribution of strains, and hence of stresses, in the cylinders. Consequently, the mean pressure must be a function of d/D , that is:

$$\frac{N}{\pi d^2/4} = f\left(\frac{d}{D}\right) \quad (25.18)$$

If the function is assumed to be a power function, we can put:

$$\frac{N}{d^2} = K\left(\frac{d}{D}\right)^x \quad (25.19)$$

$$N = K \frac{d^{2+x}}{D^x} \quad (25.20)$$

Comparison with the experimental results given by the relation (25.17) shows that $x = 0.7$, so that we have:

$$ND^{0.7} = Kd^{2.7} \quad (25.21)$$

This equation fits the experimental results on cylinders of different diameters.

The frictional force is given by:

$$F = S A = S (\pi d^2/4) \quad (25.22)$$

But from the general relation, equation (25.20), we see that:

$$d^2 = \left(\frac{N D^x}{K} \right)^{2/(2+x)} \quad (25.23)$$

Therefore, in general:

$$F = kN^{2/(2+x)} D^{2x/(2+x)} \quad (25.24)$$

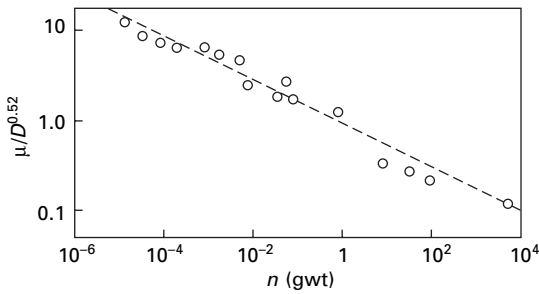
In the special case, with $x = 0.7$, this gives:

$$F = kN^{0.74} D^{0.52} \quad (25.25)$$

$$\mu = \frac{F}{N} = kN^{-0.26} D^{0.52} \quad (25.26)$$

Figure 25.23 shows that this relation fits the experimental results for nylon.

The dependence of friction on the force needed to shear the material in the region of welded junctions does not apply when the strength of the weld is itself very low. This happens with the inert material PTFE, which shows very poor adhesion to other



25.23 Check of equation (25.25) for nylon in the form of fibre, bristles and spheres [8], $\mu/D^{0.52}$ being plotted against N on logarithmic coordinates. The straight line has a slope of -0.26 ($1 \text{ g wt} = 9.81 \text{ m N}$).

surfaces, and is the cause of its low coefficient of friction.

Gupta and Moghazy [46] have made a detailed study of the interaction of asperities on fibre surfaces. They derive the following expression for the empirical equation (25.7) with specific shear strength appearing as in equation (25.16):

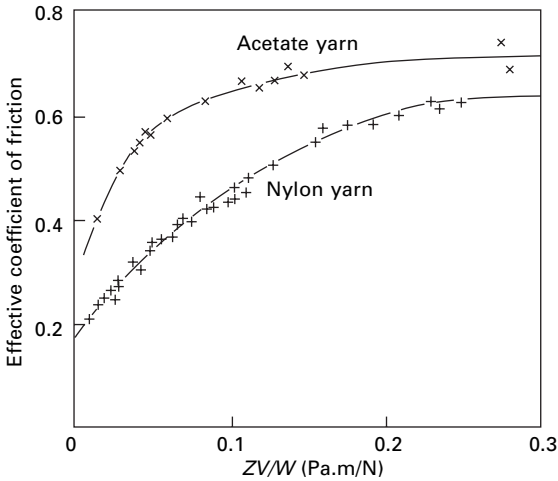
$$F = S [C_M K^{-n} m^{1-n}] N^n \quad (25.27)$$

where C_M depends on the distribution of normal load in the contact area, K is related to the hardness of the areas in contact, given by the relation between pressure P and area A , $P = K A^{(1-n)/n}$ and m = number of asperities in contact. The index n depends on the deformation behaviour of the material as discussed above. This model has been applied to the frictional behaviour of polypropylene, acrylic and cotton fibres [16, 20].

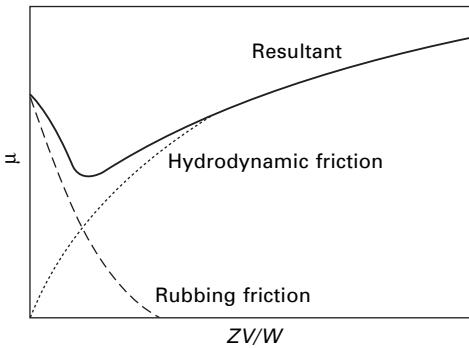
25.4.3 Lubricated conditions

Compared with its effect on metals, where it may reduce the value of μ from 1 to 0.05, lubrication has comparatively little effect on the friction of fibres and will not usually reduce the value of μ below about 0.2. The behaviour is usually thought of as boundary lubrication in which the layer of lubricant is not sufficiently thick to mask the asperities on the surface. Under these conditions, a good lubricant acts by forming monolayers on the surface and preventing the adhesion of the two surfaces at points of contact. There are then very few contacts between the materials, and most of the friction results from the force needed to shear the lubricant film itself.

If greater quantities of lubricant are present, then we may have conditions of hydrodynamic lubrication, in which there is a comparatively thick film of fluid between the surfaces and the friction results from the viscous resistance to flow. In conventional bearing lubrication under hydrodynamic conditions, the coefficient of friction is found to be a single-valued function of ZN/P , where Z is the viscosity of the oil, N is the angular velocity of the journal and P is the nominal pressure on the bearing. The analogous quantity for a yarn passing over a guide is ZV/W , where V is the yarn velocity and W is the load on the guide. Hansen and Tabor [47] have analysed Lyne's data [27], and more of their own, and found, as shown in Fig. 25.24,



25.24 Effective coefficient of friction plotted against ZV/W for acetate yarn and nylon yarn on steel, lubricated with white mineral oils. The point cover variations in speed, pin radius, pre-tension and oil viscosity.



25.25 Combination of rubbing friction and hydrodynamic friction.

that the coefficient of friction is a single-valued function of ZV/W . They conclude that, for moderately high values of ZV/W (high speed, low loads), hydrodynamic lubrication is the dominant factor.

At low speeds (or high loads), an oil film would not be maintained between the surfaces, and rubbing friction would be dominant. This decreases with increased speed. Consequently, a combination of rubbing friction at low speeds and hydrodynamic friction at high speeds would give a minimum in the friction, as is shown in Fig. 25.25. This is in agreement with the experimental results.

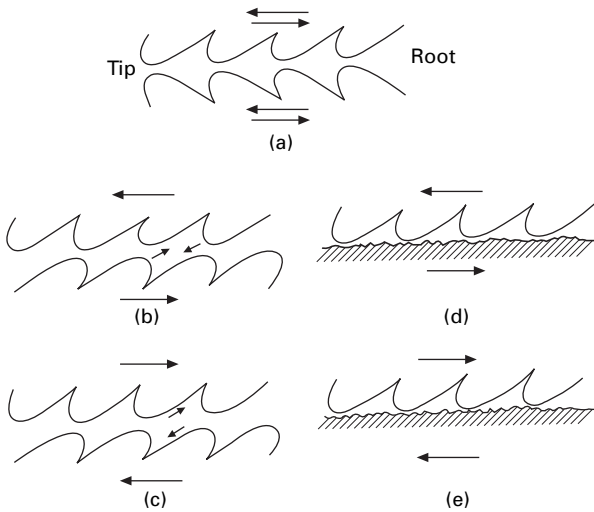
25.5 The friction of wool

25.5.1 Experimental

The friction of the wool fibre depends on the direction in which it is pulled: the

resistance is greater when it is pulled against the scales than when it is pulled with them. This is known as the *directional frictional effect* (DFE), and the various combinations that can occur are illustrated in Fig. 25.26. This effect has important technical consequences, since it means that, in a mass of wool, individual fibres will show preferential movement in one direction and will continually entangle themselves with the remaining fibres: this is the process of felting.

Some experimental values for the directional frictional effects of wool are given in Table 25.8. It has been shown that the effect persists, though to a reduced extent, when the fibres are lubricated or coated with thin films of gold or silver [48]. In



25.26 Directional friction in wool: (a) between fibres placed in same direction; (b) between fibres against scales; (c) between fibres with scales; (d) on plane surface, against scales; (e) on plane surface, with scales.

Table 25.8 Directional friction in wool

	Value of μ	
	With scales	Against scales
Dry wool (twisted fibres) 13	0.11	0.14
Wool in water (twisted fibres) 13	0.15	0.32
Wool unswollen on ebonite swollen in benzene [36]	0.58	0.79
Wool swollen in water on ebonite unswollen [36]	0.62	0.72
Wool swollen in water on ebonite swollen in benzene [36]	0.65	0.88
Wool on horn, dry [41]	0.3	0.5
Wool on horn, wet pH 4.0 [49]		
untreated	0.3	0.6
chlorine-treated	0.1	0.1
alcoholic-caustic-potash-treated	0.4	0.6
sulphuryl-chloride-treated	0.6	0.7

Other values are included in [Tables 25.3](#), [25.4](#) and [25.6](#).

water, or other swelling agents, the difference in the coefficients of friction is greater than it is in air. On the other hand, the difference is less after mechanical abrasion or chemical treatments, designed to reduce shrinkage, which attack the outer layer of the wool fibre.

25.5.2 Theory of the directional frictional effect

The occurrence of directional friction has almost invariably been ascribed to the geometric form of the scales. Other explanations, such as Martin's view [50] that there was an asymmetrical molecular field at the surface of the fibre, appear far-fetched and are not supported by the experimental evidence. The various theories have been reviewed by Makinson [51].

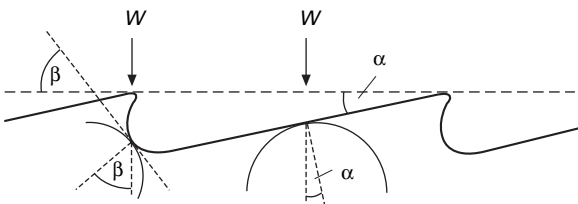
The simplest geometrical theory is that the wool fibre acts as a ratchet, with the scales interlocking with one another or catching against asperities on another surface. Motion against the scales would be strongly resisted, since it would involve rupture or deformation of the scales. Makinson [51] regards this as an effective explanation, and indicates that a ploughing mechanism would also be effective. Lincoln [52] has given a more sophisticated geometrical theory, which applies the general idea that friction is due to the shearing of real areas of contact.

Figure 25.27 shows the contact between an idealised wool scale structure and asperities on another surface. The scale surfaces are assumed to be inclined at an angle α , so that a tangent through the point of contact between an asperity and the scale surface makes an angle α with a line parallel to the axis of the wool fibre. Contact may also occur between an asperity and the scale edge, with the tangent at the contact making an angle β with the fibre axis. For slippage to occur, there must be shearing parallel to the tangents at each point of contact. We must therefore consider the relations between the forces when contact occurs at an angle, as shown in Fig. 25.28.

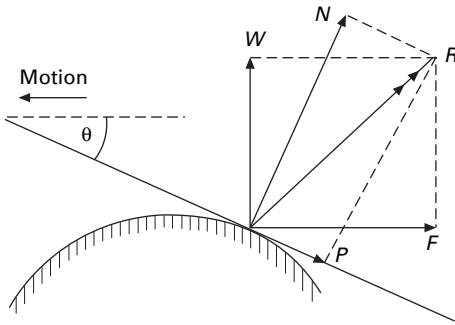
The resultant force R acting at the contact may be resolved either into components W and F acting perpendicular and parallel to the direction of motion, or into components N and P acting perpendicular and parallel to the tangent at the contact. If the angle between these directions is θ , we must have:

$$N = W \cos \theta + F \sin \theta \quad (25.28)$$

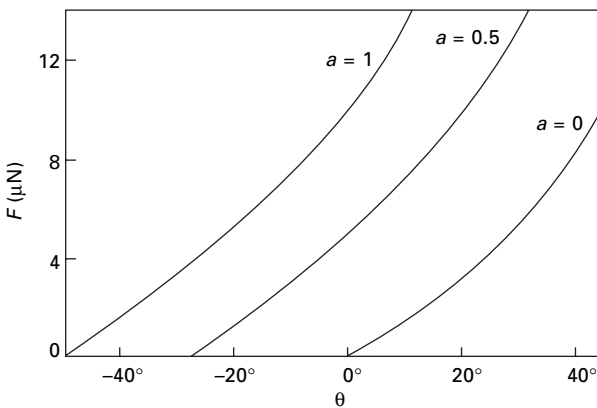
$$P = F \cos \theta - W \sin \theta \quad (25.29)$$



25.27 Contact between scale structure and asperities on a surface.



25.28 Geometry of contact.


 25.29 Variation of F with θ , with $n = 2/3$ (after Lincoln [52]).

For slippage to occur, the junction must be sheared. The force necessary to do this will be given by the general frictional relation $P = aN^n$.

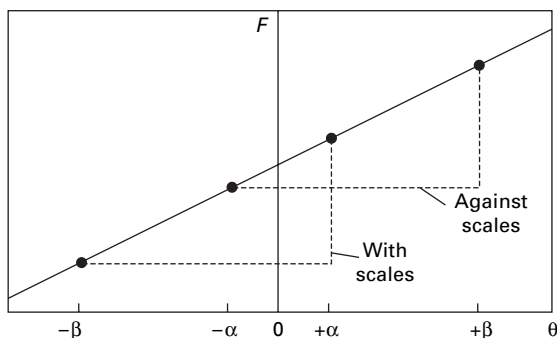
Substituting from equations (25.28 and 25.29), we have

$$F \cos \theta - W \sin \theta = a(W \cos \theta + F \sin \theta)^n \quad (25.30)$$

Lincoln gives a graphical solution of this equation, showing values of F for various values of a and θ , when $n = 2/3$. This value of n is applicable to elastic deformation at the junction. Figure 25.29 is taken from this graph and shows the variation of F with θ . The resistance to motion decreases as the value of θ decreases. When θ is positive, there will be resistance to motion even if $a = 0$, that is, if the friction is zero. It should be noted that negative values of θ correspond to motion in the reverse direction to that shown in Fig. 25.28.

We can now consider the application of this result to the contact between two surfaces. If the asperities on the surfaces are completely random, then large and small, positive and negative, values of θ will be equally likely for motion in any direction and there will be no directional effect.

In wool, however, there is a regular arrangement of asperities, the scale structure. Figure 25.27 shows that, for motion against the scales, the two types of contact will



25.30 Combination of values of α and β , for motion with and against scales.

have values of θ equal to $+\beta$ and $-\alpha$, whereas for motion with the scales the values will be $-\beta$ and $+\alpha$. From the combination of these values, shown in Fig. 25.30, it would appear obvious that the frictional force would be greater against the scales.

There are, however, complications, which have the effect that the frictional force is not a simple mean of the two values of F . Firstly, there are more α contacts than β contacts, since there is a greater length of scale surface than of scale edge. Secondly, the geometry of the contacts will be different and will influence the value of α and the distribution of the load. Thirdly, the values of α depend on the range of values of the scale angle, and the values of β may range up to $\pi/2$, depending on the position of the contact round the scale edge, though the effective negative values of β will be limited by the condition: $F \geq 0$. These factors will reduce the difference in the friction by causing the net force to be nearer that given by the β contacts than that given by the α contacts. In principle, it may even cause a reversal of the directional effect, but the detailed analysis given by Lincoln, considering the three-dimensional view of fibre contacts, shows that this would not happen.

25.6 References

1. W. L. Balls. *Studies of Quality in Cotton*, Macmillan, London, 1928, p. 80.
2. E. Moss. *Brit. J. Appl. Phys.*, 1951, **2**, Suppl. No. 1, 19.
3. F. P. Bowden and L. Leben. *Proc. Roy. Soc.*, 1939, **A169**, 371.
4. V. Peck and W. Kaye. *Text. Res. J.*, 1954, **24**, 295.
5. F. P. Bowden and D. Tabor. *The Friction and Lubrication of Solids*, Oxford University Press, London, 1950; revised reprint, 1954.
6. J. C. Guthrie and P. H. Oliver. *J. Text. Inst.*, 1952, **43**, T579.
7. E. H. Mercer and K. R. Makinson. *J. Text. Inst.*, 1947, **38**, T227.
8. M. W. Pascoe and D. Tabor. *Proc. Roy. Soc.*, 1956, **A235**, 210.
9. G. M. Abbott and P. Grosberg. *Text. Res. J.*, 1966, **36**, 928.
10. H. Buckle and J. Pollitt. *J. Text. Inst.*, 1948, **39**, T199.
11. J. H. Jung, T. J. Kang and J. R. Youn. *Textile Res. J.*, 2004, **74**, 1085.
12. P. Grosberg and D. E. A. Plate. *J. Text. Inst.*, 1971, **62**, 116.
13. J. Lindberg and N. Gralén. *Text. Res. J.*, 1948, **18**, 287.
14. B. S. Gupta, K. W. Wolf and R. W. Postlethwint. *Surg. Gynec. Obst.*, 1985, **161**, 12.
15. N. Fair and B. S. Gupta. *J. Soc. Cosmetic Chem.*, 1982, **33**, 229.

16. Y. E. El Moghazy and B. S. Gupta. *Textile Res. J.*, 1993, **63**, 219.
17. D. S. Taylor. *J. Text. Inst.*, 1955, **46**, P59.
18. E. Lord. *J. Text. Inst.*, 1955, **46**, P41.
19. J. W. S. Hearle and A. K. M. M. Husain. *J. Text. Inst.*, 1971, **62**, 83.
20. Y. E. El Moghazy and R. M. Broughton. *Textile Res. J.*, 1993, **63**, 465.
21. J. B. Speakman and E. Stott. *J. Text. Inst.*, 1931, **22**, T339.
22. H. G. Howell and J. Mazur. *J. Text. Inst.*, 1953, **44**, T59.
23. F. P. Bowden and J. E. Young. *Proc. Roy. Soc.*, 1951, **A208**, 444.
24. B. Lincoln. *Brit. J. Appl. Phys.*, 1952, **3**, 260.
25. J. Mazur. *J. Text. Inst.*, 1955, **46**, T712.
26. H. G. Howell. *J. Text. Inst.*, 1954, **45**, T575.
27. D. G. Lyne. *J. Text. Inst.*, 1955, **46**, P112.
28. A. J. P. Martin and R. Mittelman. *J. Text. Inst.*, 1946, **37**, T269.
29. H. G. Howell. *J. Text. Inst.*, 1953, **44**, T359.
30. J. C. Guthrie and P. H. Oliver. *J. Text. Inst.*, 1952, **43**, T579.
31. A. Viswanathan. *J. Text. Inst.*, 1966, **57**, T30.
32. B. Olofsson and N. Gralén. *Text. Res. J.*, 1950, **20**, 467.
33. H. L. Röder. *J. Text. Inst.*, 1955, **46**, P84.
34. R. S. Merkel. *Text. Res. J.*, 1963, **33**, 84.
35. E. Bradbury and A. Reicher. *J. Text. Inst.*, 1952, **43**, T350.
36. G. King. *J. Text. Inst.*, 1950, **41**, T135.
37. D. Summers-Smith. *Research*, 1955, **8**, S17.
38. P. M. Taylor and D. M. Pollet. *J. Textile Inst.*, 2000, **91**, Part 1, 1.
39. J. A. Morrow. *J. Text. Inst.*, 1931, **22**, T425.
40. Noble Denton and National Engineering Laboratory. Fibre Tethers 2000, Final Report, Noble Denton, London, quoted in H. A. McKenna, J. W. S. Hearle and N. O'Hear, *Handbook of Fibre Rope Technology*, Woodhead Publishing, Cambridge, UK, 2004, p. 70.
41. N. Behary, C. Caze, A. Perwuelz and A. El Achari. *Textile Res. J.*, 2000, **70**, 700.
42. N. Behary, C. Caze, A. Perwuelz and A. El Achari. *Textile Res. J.*, 2001, **71**, 187.
43. J. A. Chapman, M. W. Pascoe and D. Tabor. *J. Text. Inst.*, 1955, **46**, P3.
44. F. P. Bowden and D. Tabor. *Friction and Lubrication*, Methuen, London, 1956.
45. H. Hertz. *J. Reine Angew. Math.*, 1881, **92**, 156.
46. B. S. Gupta and Y. E. El Moghazy. *Textile Res. J.*, 1991, **61**, 547.
47. W. W. Hansen and D. Tabor. *Text. Res. J.*, 1957, **27**, 300.
48. H. M. S. Thompson and J. B. Speakman. *Nature*, 1946, **157**, 804.
49. E. H. Mercer. *Nature*, 1945, **155**, 573.
50. A. J. P. Martin. *J. Soc. Dyers Col.*, 1944, **60**, 325.
51. K. R. Makinson. *Wool Sci. Rev.*, 1972, No. **42**, 2.
52. B. Lincoln. *J. Text. Inst.*, 1954, **45**, T92.

Appendix I

Units

AI.1 Introduction

In most of physics and engineering, size and shape are specified by linear measures as three-dimensional solids, with mass (weight) added when necessary. Textiles are a mixture of solid fibres and space between and are mostly one-dimensional yarns and cords or two-dimensional fabrics. Thickness and volume depend on the methods of measurement and are ill-defined. Mass-based measures, linear or areal density, are more useful. Even for fibres, although area of cross-section and, for simple shapes, thickness, are well defined, linear density is much easier to measure.

AI.2 Fineness

The preferred unit of linear density is *tex* = g/km, which was introduced in the 1950s. The strict SI unit is kg/m = megatex, Mtex, but this is too large a unit, except for ropes. Historically, microgram/inch has been used for cotton. The silk industry used *denier* = gram per 9000 m and this was adopted in the early days of manufactured fibres. Because the numbers are close to those in denier, *decitex*, dtex = gram per 10 000 m is now widely used.

AI.3 Stress and specific stress

Unfortunately tensions and other applied forces can be normalised in a great many ways. Many different units are found in the older literature and several appear in current publications.

There is a primary distinction:

- Conventional stress, force per unit area, is normal in physics and engineering and is commonly used by researchers from an engineering or materials science background. The strict SI unit is Pa = N/m². GPa and MPa are convenient sizes.
- Specific stress, force per unit linear density, is more useful for fibres and is the usual mode in the textile community. The strict SI unit is N/(kg/m). N/tex and m N/tex are convenient sizes.

Numerical values of the two quantities are related by a relation, specific stress =

stress/density, which is valid without numerical factors in strict SI units, N m/kg, Pa, kg/m³, or in the combination of N/tex, GPa, g/cm³.

However, in both categories, many other units are found for the following reasons:

- Equivalence of quantities. Specific stress = energy per unit mass, e.g. kJ/g. Specific modulus = (wave velocity)², e.g. (km/s)². Tenacity is equivalent to breaking length (length failing under its own weight), e.g. km or strictly kmf (kilometer-force).
- Unit system. The SI system is based on metre-kilogram-second (MKS). The older CGS (centimetre-gram-second) includes dyne for force. There are former British Imperial units, which are still widely used in the United States.
- Inertial (unit mass × unit acceleration), e.g. newton, or gravitational. (unit mass × acceleration due to gravity), e.g. gram-force, gf, also called gram-weight, g wt.
- Unit of fineness, e.g. tex or denier.
- Heat units for energy, e.g. cal/g.
- Multiples and sub-multiples.
- Modes of expression, e.g. N/mm² or MPa.
- Abbreviations.

Table A1.1 lists units with conversion factors. It is convenient to note that nylon and polyester fibres can have strengths up to near 1 N/tex. Polymer fibres have densities between 1 and 1.5 g/cm³, so that values in GPa are up to 33% lower than in N/tex.

Table A1.1 Unit conversions for stress and specific stress

Specific stress		Stress: density in g/cm ³ times	
1	<ul style="list-style-type: none"> – N/tex, kJ/g, GPa/g cm⁻³, (km/s)² – 10 c N/dtex, 10.2 gf/dtex, 11.3 gf/den – 102 gf/tex, kmf, kg mm⁻²/g cm⁻³ – 239 cal/g, 430 BTU/lb 	1	<ul style="list-style-type: none"> – GPa, J/mm³ – – 102 kg/mm² 145 ksi
10 ³	<ul style="list-style-type: none"> – mN/tex, J/g, MPa/g cm⁻³ – – 145 000 psi/g cm⁻³ 	10 ³	<ul style="list-style-type: none"> – MPa, N/mm² – 10⁴ bar, 9869 atm – 145 000 psi – (psi = lbf/in²)
*10 ⁶	<ul style="list-style-type: none"> – N/kg m⁻¹, J/kg, Pa/kg m⁻³ – 3.94 × 10⁶ inchf, psi/(lb/cu in) 	10 ⁶	<ul style="list-style-type: none"> – 7.5 × 10⁶ mm Hg
10 ⁹	<ul style="list-style-type: none"> – – 10¹⁰ dyn/g cm⁻¹, erg/g 	*10 ⁹	<ul style="list-style-type: none"> – Pa, N/m², J/m³, kg m⁻¹ s⁻¹ – 10¹⁰ dyn/cm²

*Strict SI units.

Other multiples are also used.

Gravitational units, written above as gf etc. are also found in forms such as: g, e.g. g/den, gm, or g wt; lb or lb wt; km, km wt or Rkm.

Appendix II

Fibre names

All.1 Introduction

Apart from the oddity that flax becomes linen when made into yarns and fabrics, there is no uncertainty in assigning names to natural fibres. With manufactured fibres there are problems. Much of the early literature on the first generation of regenerated and synthetic fibres identifies them by trade names that may no longer be current. For the newer fibres, trade names are more easily recognised by many people. The alternatives are various chemical names, generic fibre names, abbreviations, etc. In this book, all the above forms are used, depending on what is most likely to be informative.

The account below, which includes names mentioned in the text, is simplified. For formal definitions, see Denton and Daniels [1]. Types that are no longer made are included in braces { }. ISO generic names and codes are underlined. The term ‘manufactured fibres’ is now preferred to ‘man-made fibres’.

All.2 Regenerated fibres

- **Rayon** The US generic definition covers manufactured fibres of regenerated cellulose or with less than 15% of substitutions for —OH groups. Viscose CV (cellulose xanthate route), modal CMD (high-wet-modulus viscose), cupro CUP (cuprammonium route), lyocell CLY (organic solvent route). At one time and in some countries, rayon included all manufactured cellulosic fibres, including acetate fibres. *Polynosic* was another name for a modal fibre. Trade names include *Fibro* (Courtaulds staple viscose fibre), *Tenasco* (Courtaulds high-tenacity viscose), {*Durafil*} (high-tenacity staple fibre), {*Fortisan*} (high strength, regenerated from acetate), *Tencel* (lyocell).
- **Acetate** Acetate fibre CA, cellulose ethanoate (acetate), <92% and >74% of —OH groups acetylated. Also known as *secondary acetate*; *Dicel* was a trade name. If >92%, triacetate CTA; *Tricel* was a trade name; in the United States included in acetate.
- **Alginate** Alginate ALG, fibres of metallic salts of alginic acid.
- **Regenerated proteins** {*Lanital*, *Fibrolane*} (milk casein), {*Ardil*} (groundnut protein), {*Vicara*} (corn zein protein).

All.3 Synthetic fibres of linear macromolecules

- **Nylon** (introduced by Du Pont, but not a trade name) Polyamide PA, nylon, >85% amide groups attached to aliphatic groups. *Nylon* is generic in the United States. Different nylons are named by numbers of carbon atoms in repeat units. e.g., nylon 6 for $[-(\text{CH}_2)_5\cdot\text{CO}\cdot\text{NH}-]_n$ and nylon 66 for $[-\text{CO}\cdot\text{NH}\cdot(\text{CH}_2)_6\cdot\text{NH}\cdot\text{CO}\cdot(\text{CH}_2)_4-]_n$. Also see **Aramid**.
- **Polyester** Polyester PES, with >85% of an ester of a diol and benzene-1,4-dicarboxylic acid (terephthalic acid). The trade names *Terylene* (ICI) and *Dacron* (Du Pont) were often used in the earlier scientific literature. Common usage is polyethylene terephthalate, PET or 2GT. In the United States, and in this book, polyester is more widely used and includes: *polybutylene terephthalate*, polytrimethylene-terephthalate, PBT or 3GT; *polyethylene naphthalate*, PEN. Note that the chemical definition of *polyester* is much broader. *Polyester resins* are cross linked polymers used in reinforced plastics.
- **Polyolefin** Polypropylene PP, isotactic $[-\text{CH}_2\cdot\text{CH}(\text{CH}_3)-]_n$. Polyethylene PE, $[-\text{CH}_2-]_n$, see also **HMPE**.
- **Acrylic** Acrylic PAN, with >85% of cyanethene (acrylonitrile) groups. Polyacrylonitrile PAN is also used. Modacrylic MAC, with >35%, <85% acrylonitrile.
- **Vinyl and vinylidene** Includes: chlorofibre CLF, with >50% of chloroethene (vinyl chloride) PVC or 1,1-dichloroethene (vinylidene chloride) PVDC, >65% if rest of chain is acrylonitrile, *Vinyon* is US generic for PVC fibre; vinylal PVAL, polyethenol (polyvinyl alcohol) with differing levels of acetylation, *vinal* is US generic.
- **Fluoro** Fluorofibre PTFE, usually polytetrafluorethylene, but also other aliphatic fluorocarbons.
- **Elastomeric fibres** Elastane EL, with >85% segmented polyurethane. US generic is *spandex*. *Lycra* is a trade name. Elastodiene ED, natural (rubber) or synthetic polyisoprene and other diene–vinyl copolymers.
- **Thermally, chemically resistant** A number of thermally and/or chemically resistant fibres are referred to in the text.

All.4 High-modulus, high-tenacity (HM–HT) linear polymer fibres

- **Aramid** Aramid AR with >85% amide groups attached to two aromatic groups (50% imide groups may be substituted). *Para-aramids* have benzene rings joined in opposite 1,4 positions; trade names include *Kevlar* and *Twaron*. *Technora* is an aramid copolymer. *Meta-aramids* have benzene rings joined in next nearest 1,3 positions; *Nomex* is a trade name.
- **Aromatic polyesters** *Vectran* (trade name) is a fully aromatic co-polyester fibre produced by a melt-spinning route. This type may be referred to as *liquid crystal polymer (LCP) fibres* though many other types are made by a liquid crystal route), *thermotropic liquid crystal polymer (TLCP) fibres* or *liquid crystal aromatic polyester (LCAP) fibres*.

- **PBO** *Polybenzoxazole*, poly(*p*-phenylene benzibisoxazole, fibres are commonly referred to as PBO. *Zylon* is a trade name.
- **M5** *M5* is the development name for a poly(2,6-dimidazo[4,5-*b*:4',5'-*e*]pyridinylene-1,4-(2,5-dihydroxy)phenylene} PIPD fibre.
- **HMPE** High-modulus polyethylene, HMPE or HPPE, gel-spun, highly oriented, high molecular weight polyethylene. *Spectra* and *Dyneema* are trade names.

All.5 Carbon fibres

- **Carbon** Carbon CF, >90% carbon by controlled pyrolysis. Fully carbonised and processed at high temperature are often referred to as graphite fibres. Also thermally resistant, partially carbonised fibres.

All.6 Inorganic fibres

- **Glass** *Glass GF*.
- **Ceramic** Various ceramic fibres are referred to in the text.

All.7 Reference

1. M. J. Denton and P. N. Daniels. *Textile Terms and Definitions*, 11th edition, Textile Institute, Manchester, 2002.

Appendix III

Standard test methods

The following is a selection of some relevant test methods for the study of the physical properties of fibres, particularly the dimensional and other properties that determine the assessment of fibre quality.

ISO and British Standard	ASTM	IWTO Standard (<i>Italics</i> for drafts)
COTTON HVI TESTING		
	ASTM D5867-05 Standard test methods for measurement of physical properties of cotton fibers by high volume instruments	
Sampling procedures		
ISO 1130:1975 Textile fibres – Some methods of sampling for testing		IWTO 7 Sub-sampling staples from grab Samples
BS EN 12751:1999 Textiles. Sampling of fibres, yarns and fabrics for testing		IWTO 38 Method of grab sampling greasy wool from bales
Fibre fineness		
ISO 2403:1972 Textiles – Cotton fibres – Determination of micronaire value	ASTM D1448-05 Standard test method for Micronaire reading of cotton fibers	IWTO 6 Method of test for the determination of the mean fibre diameter of wool fibres in combed sliver using the airflow apparatus
ISO 1136:1976 Wool – Determination of mean diameter of fibres – Air permeability method	ASTM D1282-05 Standard test method for resistance to airflow as an indication of average fiber diameter of wool top, card sliver, and scoured wool	IWTO 8 Method of determining fibre diameter distribution parameters and percentage medullated fibres in wool and other animal fibres by the projection microscope
ISO 137:1975 Wool – Determination of fibre diameter – Projection microscope method	ASTM D5867-05 Standard test methods for measurement of physical properties of cotton fibers by high volume instruments	IWTO 12 Measurement of mean & distribution of fibre diameter using the Sirolan-Laserscan fibre diameter analyser

ISO and British Standard	ASTM	IWTO Standard (<i>Italics for drafts</i>)
BS EN ISO 10306:1995 Textiles. Cotton fibres. Evaluation of maturity by the air flow method	ASTM D1282-05 Standard test method for resistance to airflow as an indication of average fiber diameter of wool top, card sliver, and scoured wool	IWTO 28 Determination by the airflow method of the mean fibre diameter of core samples of raw wool
BS 3085:1981, ISO 4912:1981 Method for evaluation of the maturity of cotton fibres (microscopic method) BS 3181:1968 Method for the determination of cotton fibre fineness by the airflow method	ASTM D7025-04ae1 Standard test method for assessing clean flax fiber fineness ASTM D1577-07 Standard test methods for linear density of textile fibers	IWTO 47 Measurement of the mean & distribution of fibre diameter of wool using an Optical Fibre Diameter Analyser (OFDA) <i>IWTO DTM 62 Determination of fibre length, length distribution, mean fibre diameter and fibre diameter distribution of wool top and slivers by OFDA4000</i>
BS 2016:1973 Methods for the determination of the linear density of textile fibres: gravimetric methods	ASTM D1442-06 Standard test method for maturity of cotton fibers (sodium hydroxide swelling and polarized light procedures)	
Fibre length ISO 4913:1981 Textiles – Cotton fibres – Determination of length (span length) and uniformity index	ASTM D5867-05 Standard test methods for measurement of physical properties of cotton fibers by high volume instruments	<i>IWTO DTM 1 Method of determining barbe & hauteur of wool fibres using a comb sorter</i>
BS ISO 6989:1981 Textiles fibres. Determination of length and length distribution of staple fibres (by measurement of single fibres) BS 6176:1981, ISO 6989-1981 Method for determination of length and length distribution of staple fibres by measurement of single fibres BS 5182:1975, ISO 2646-1974 Method for the measurement of the length of wool fibres processed on the worsted system, using a fibre diagram machine.	ASTM D1234-85(2001) Standard test method of sampling and testing staple length of grease wool ASTM D1440-07 Standard test method for length and length distribution of cotton fibers (array method) ASTM D1575-90 (2001) Standard test method for fiber length of wool in scoured wool and in card sliver	<i>IWTO DTM 5 Method of determining wool fibre length distribution of fibres from yarn or fabric using a single length measuring machine</i> <i>IWTO DTM 16 Method of test for wool fibre length using a WIRA fibre diagram machine</i>
		IWTO 17 Determination of fibre length and distribution parameters

BS 4044:1989 Methods for determination of fibre length by comb sorter diagram

Moisture absorption

BS 4784-1:1988, ISO 6741-1:1987 Methods for determination of commercial mass of consignments of textiles. Mass determination and calculations

BS 1051:1992, ISO 6348:1980 Glossary of terms relating to the mass determination of textiles

Tensile testing

ISO 3060:1974 Textiles – Cotton fibres – Determination of breaking tenacity of flat bundles

BS EN ISO 5079:1996 Textiles. Fibres. Determination of breaking force and elongation at break of individual fibres

BS 4029:1978 Method of test for the determination of tensile elastic recovery of single fibres and filaments (constant-rate-of-extension machines)

BS 3411:1971 Method for the determination of the tensile

ASTM D5103-07 Standard test method for length and length distribution of manufactured staple fibers (single-fiber test)
ASTM D519-04 Standard test method for length of fiber in wool top

ASTM D1576-90 (2001) Standard test method for moisture in wool by oven-drying

ASTM D2495-07 Standard test method for moisture in cotton by oven-drying

ASTM D5867-05 Standard test methods for measurement of physical properties of cotton fibers by high volume instruments
ASTM D2524-95 (2003) Standard test method for breaking tenacity of wool fibers, flat bundle method – 1/8-in. (3.2-mm) Gage Length
ASTM D2653-07 Standard test method for tensile properties of elastomeric yarns (CRE type tensile testing machines)

ASTM D3217-07 Standard test methods for breaking tenacity of

IWTO 30 Determination of staple length and staple strength

IWTO DTM 62 Determination of fibre length, length distribution, mean fibre diameter and fibre diameter distribution of wool top and slivers by OFDA4000

IWTO 33 Method for the determination of oven-dry mass, calculated invoice mass & calculated merchandisable mass of scoured or carbonised wool

IWTO 34 Determination of the oven-dry mass, calculated invoice mass & calculated merchandisable mass of wool tops
IWTO 41 Determination of the invoice mass of scoured or carbonised wool tops or noils by the capacitance method

IWTO 30 Determination of staple length and staple strength

IWTO 32 Determination of the bundle strength of wool fibres

ISO and British Standard	ASTM	IWTO Standard (<i>Italics for drafts</i>)
properties of individual textile fibres	manufactured textile fibers in loop or knot configurations	
BS 5116:1974 Method of test for determination of breaking tenacity of flat bundles of cotton fibres	ASTM D3822-07 Standard test method for tensile properties of single textile fibers ASTM D1294-05 Standard test method for tensile strength and breaking tenacity of wool fiber bundles 1-in. (25.4-mm) gage length ASTM D1445-05 Standard test method for breaking strength and elongation of cotton fibers (flat bundle method)	